

AWARD NUMBER: **W81XWH-15-1-0415**

TITLE: Noninvasive Urine Markers of Interstitial Cystitis

PRINCIPAL INVESTIGATOR: **JAYOUNG KIM, PhD**

CONTRACTING ORGANIZATION: **Cedars-Sinai Medical Center**

REPORT DATE: **OCTOBER 2021**

TYPE OF REPORT: Final Report

PREPARED FOR: U.S. Army Medical Research and Materiel Command
Fort Detrick, Maryland 21702-5012

DISTRIBUTION STATEMENT: Approved for Public Release;
Distribution Unlimited

The views, opinions and/or findings contained in this report are those of the author(s) and should not be construed as an official Department of the Army position, policy or decision unless so designated by other documentation.

REPORT DOCUMENTATION PAGE

Form Approved
OMB No. 0704-0188

Public reporting burden for this collection of information is estimated to average 1 hour per response, including the time for reviewing instructions, searching existing data sources, gathering and maintaining the data needed, and completing and reviewing this collection of information. Send comments regarding this burden estimate or any other aspect of this collection of information, including suggestions for reducing this burden to Department of Defense, Washington Headquarters Services, Directorate for Information Operations and Reports (0704-0188), 1215 Jefferson Davis Highway, Suite 1204, Arlington, VA 22202-4302. Respondents should be aware that notwithstanding any other provision of law, no person shall be subject to any penalty for failing to comply with a collection of information if it does not display a currently valid OMB control number. **PLEASE DO NOT RETURN YOUR FORM TO THE ABOVE ADDRESS.**

1. REPORT DATE October 2021		2. REPORT TYPE FINAL		3. DATES COVERED 08SEP2015- 07SEP2021	
4. TITLE AND SUBTITLE Noninvasive Urine Markers of Interstitial Cystitis				5a. CONTRACT NUMBER	
				5b. GRANT NUMBER W81XWH-15-1-0415	
				5c. PROGRAM ELEMENT NUMBER	
6. AUTHOR(S) Jayoung Kim Email: Jayoung.Kim@cshs.org				5d. PROJECT NUMBER	
				5e. TASK NUMBER	
				5f. WORK UNIT NUMBER	
7. PERFORMING ORGANIZATION NAME(S) AND ADDRESS(ES) CEDARS-SINAI MEDICAL CENTER Los Angeles, CA 90048				8. PERFORMING ORGANIZATION REPORT NUMBER	
9. SPONSORING / MONITORING AGENCY NAME(S) AND ADDRESS(ES) U.S. Army Medical Research and Materiel Command Fort Detrick, Maryland 21702-5012				10. SPONSOR/MONITOR'S ACRONYM(S)	
				11. SPONSOR/MONITOR'S REPORT NUMBER(S)	
12. DISTRIBUTION / AVAILABILITY STATEMENT Approved for Public Release; Distribution Unlimited					
13. SUPPLEMENTARY NOTES					
14. ABSTRACT Interstitial cystitis/painful bladder syndrome (IC) is a debilitating condition that presents with a confusing array of symptoms, including bladder pain, urinary urgency, frequency, nocturia, and small voided volumes in the absence of other identifiable symptoms. Currently, the diagnosis of IC is largely dependent on subjective parameters, leading to extreme difficulties in accurately phenotyping patients. There is no gold standard for IC diagnosis. In general, it takes approximately 4-5 years from the first office visit to obtain a definitive diagnosis of IC. Thus, differentiating IC from other conditions is still a diagnostic challenge, and objective diagnostic markers are urgently needed to improve prospects for clinical care. In this study, we will assess whether these promising biomarkers can segregate IC patients from control subjects, and whether they are potentially involved in bladder pain.					
15. SUBJECT TERMS Nothing listed					
16. SECURITY CLASSIFICATION OF:			17. LIMITATION OF ABSTRACT	18. NUMBER OF PAGES	19a. NAME OF RESPONSIBLE PERSON
a. REPORT	b. ABSTRACT	c. THIS PAGE			19b. TELEPHONE NUMBER (include area code)
U	U	U	UU	504	USAMRMC

Table of Contents

1. INTRODUCTION	3
2. KEYWORDS	3
3. ACCOMPLISHMENTS	
Achievement 1	7
Achievement 2	17
Achievement 3	17
Achievement 4	18
Achievement 5	18
Achievement 6	21
Achievement 7	31
Achievement 8	36
Achievement 9	41
Achievement 10	44
Achievement 11	47
Achievement 12	53
Achievement 13	63
Achievement 14	71
Achievement 15	78
Achievement 16	81
4. IMPACT	86
5. CHANGES/PROBLEMS	92
6. PRODUCTS	92
7. PARTICIPANTS & OTHER COLLABORATING ORGANIZATIONS	104
8. APPENDIX	105

Annual Technical Progress Report

1. INTRODUCTION:

Interstitial cystitis (IC)/painful bladder syndrome is a debilitating condition that presents itself as a confusing array of symptoms. These include bladder pain, urinary urgency, frequent urination, nocturia, and small voided volumes. Currently, there is no gold standard for diagnosing IC and it is largely dependent on subjective parameters; thereby, leading to extreme difficulties in accurately phenotyping patients. In general, it takes approximately 4-5 years from the first office visit to obtain a definitive diagnosis of IC. Thus, differentiating IC from other conditions remains to be an important clinical challenge and identifying objective diagnostic markers would improve prospects for all patients. In this study, we will assess whether our promising biomarkers can segregate IC patients from control subjects, and whether they are potentially involved in bladder pain.

2. KEYWORDS:

Interstitial cystitis/painful bladder syndrome
Biomarkers
Diagnosis and prognosis
Chronic bladder pain

3. ACCOMPLISHMENTS:

3.1. What were the major goals of the project?

The overall goal of this study is to improve the methodology of diagnosis for IC and to develop new insight into the underlying mechanisms that trigger this condition. To achieve this goal, this project focuses on identifying urinary species and assessing their clinical significance to IC. Our hypothesis is that DNA methylation of CNR2 and urinary levels of tyramine can segregate IC patients from controls while also risk-stratifying patients with severe clinical symptoms. Research plan of this proposal included assembly of the Cedars-Sinai Medical Center (CSMC) cohort and the targeted metabolomics analysis, which are completed or almost finalized. In the extended funding period, we have the detail plan to complete the planned metabolomics analyses on our candidate targets.

Approved SOW

Subtask 1. CONTINUATION OF CSMC IC COHORT

- CSMC cohort for Aim 1 and 2
(300 cases in total, patients and controls)

Subtask 2. BIOINFORMATICS ANALYSIS

- Establishing pipeline for computational analysis
- Calculation to test the correlation with clinical symptoms
- Network/pathway analysis

Subtask 3. COMPUTATIONAL ANALYSIS

- Data preprocessing
- Quality control (QC)
- Normalization
- Generation of models
- Calculation of classifier scores
- Biostatistical analysis to determine the correlation of DNA methylation levels with bladder

dysfunction and associated pain

Subtask 4. PUBLICATION AND PATENT APPLICATION

- Paper preparation
- Data report and presentation at scientific meetings
- Patent application

In our 3rd funding year, we have focused on (1) identification on baseline of urine collection, (2) expansion of database for better urine biomarker discovery, (3) technology application to further identify metabolites associated with IC, and (4) continuation of CSMC IC cohort construction.

3.2. What was accomplished under these goals?

(1) Major activities

- CSMC IC cohort

(2) Specific objectives

- **Goal:** Construction of CSMC IC cohort
- CSMC cohort for Aim 1 and 2 (301 cases in total, patients and controls)
- We continued recruiting IC patients and collecting specimens through additional urologists at CSMC.
 - Dr. Brian Benway
 - Dr. Timothy Daskivich
 - Dr. Stephen Freedland
 - Dr. Hyung Kim
 - Dr. Howard Kim
 - Dr. Amit Gupta
- We opened our study to the public and amended our IRB to promote recruitment.
- Since initiation of the study to today (December 1, 2021), we have collected 301 urine specimens from healthy controls and IC patients.
- Milestone Achieved: Our subject recruitment is being successfully achieved.
- In this funding period, we had the negative impacts on our research activities caused by COVID-19 pandemic. It influenced the major laboratory-based experiments and clinical research activities. Since late March 2020, core facilities stopped accepting samples and data analyses. Lab investigators and study coordinators could not access to laboratory and started working remotely. In addition, we had issues to ship out samples to other collaborators since their facilities were started to stop sample acceptance. However, we will resume shipping samples as soon as COVID-19-related issues are resolved.

(3) Significant results or key outcomes

- We were able to optimize the DNA methylation assay and gene expression assay, which were designed for the high throughput screening (HTS) purpose.
 - To perform a quantitative targeted mass spectrometry-based metabolomics analysis (Dr. Kim, Dr. Fiehn, Dr. Yang, Dr. Van Eyk)

- To set up and perform the enzyme-reaction based biochemical assay (Dr. Kim)
 - Primer design and protocol set up (Dr. Kim, Dr. Weisenberger)
 - Pyrosequencing or MethyLight assay optimization (Dr. Kim, Dr. Liang)
 - To construct an IC rat model and to quantify TAAR in IC model rats and sham controls (Dr. Kim, Dr. Knudsen)
 - To measure the association with bladder dysfunction (symptoms and urodynamic profile) (Dr. Kim, Dr. Lee): **Experimental data was submitted for paper publication (submitted paper was attached in the APPENDICES).**
-
- Since last funding period, we have been focused on the optimization of metabolic profiling. More updated state-of-the-art mass spectrometry technologies were applied to identify additional and previously unknown IC biomarker metabolite candidates. We found several biologically relevant biomarker candidates from new approaches and these experimental results were reported in recently published manuscript (*Scientific Reports*)
 - To identify the sex difference in metabolic profiling, we were able to assemble the sub-cohort for pilot study. This cohort consisted of urine specimens from healthy female (n=60) and healthy male (n=60). This project is now being processed at the Dr. Fiehn's metabolomics core at UC Davis. We got the initial results in late August 2017. The data analysts at UC Davis are fine tuning the bioinformatical analysis. We anticipate updating this data in the next progress report and submitting a full research paper for publication.
 - To elucidate the epigenetic modulation in IC, we performed the global proteomics analysis with and without treatment of decitabine (DNA methyltransferase (DNMT) inhibitor). Although we are still in the preliminary phase of data analysis, we found two interesting proteins that were significantly altered by decitabine treatment in normal human bladder cells. In this funding period, we found that decitabine treatment significantly suppressed the protein expression of IC-biomarker candidates such as CNR2.
 - Given the fact that tyramine is a well-known neuromodulator, we speculate that urinary tyramine may affect central and peripheral nervous systems. In our second funding period, we determined expression levels of TAAR1 in normal and IC rat bladder tissue to assess the function of inhibitory small molecule candidates in TAAR1 signaling.
 - Our digitalized and quantitative IHC analysis revealed that protein expression of CNR2 increased in the rat IC model. Our DNA methylation assay also showed that the promoter region of CNR2 was hypo-methylated, compared to the control rat model.
 - We optimized metabolic profiling of urine samples. Updated state-of-the-art mass spectrometry technology was applied to identify additional previously unknown IC biomarker metabolites. We found several biologically relevant candidates from this new approach and our experimental results were recently published.
 - Using a metabolomics approach to capture odor compounds in urine samples of IC patients and healthy controls, we found that urinary menthol levels were significantly lower in IC urine. Further biochemical and functional analyses revealed that urinary menthol may suppress the inflammatory response of immune cells that have infiltrated the bladder epithelium. These findings suggest that the decreased levels of urinary menthol may explain the chronic inflammation in IC bladders.

- Many lipids and lipid metabolites are still not properly annotated nor functionally characterized, which hinders the diagnostic potential of lipid profiling. Our research team actively worked to address this discrepancy and has since developed numerous software and databases that can aid in the lipid structure elucidation process.
- We made significant key scientific outcomes since the previous funding period. Several full research papers and review articles were published in this funding period. **Please refer to the APPENDICES.**
- We were able to optimize the DNA methylation and gene expression assays, which were designed for high-throughput screening (HTS). Using this optimized assay system, we found that an IC-specific metabolite marker, alpha-oxoglutarate, regulates DNA methylation and can turn on an epigenetic switch through ARID1A, a chromatin remodeler in normal bladder epithelial cells.
 - To perform a quantitative targeted mass spectrometry-based metabolomics analysis (Dr. Kim, Dr. Fiehn, Dr. Yang, Dr. Van Eyk)
 - To set up and perform the enzyme-reaction based biochemical assay (Dr. Kim)
 - Primer design and protocol set up (Dr. Kim, Dr. Berman, Dr. Weisenberger)
 - Pyrosequencing or MethyLight assay optimization (Dr. Kim, Dr. Liang)
- We were able to optimize the DNA methylation and gene expression assays, which were designed for high-throughput screening (HTS). Using this optimized assay system, we found that an IC-specific metabolite marker, alpha-oxoglutarate, regulates DNA methylation and can turn on an epigenetic switch through ARID1A, a chromatin remodeler in normal bladder epithelial cells.
- We optimized metabolic profiling of urine samples. Updated state-of-the-art mass spectrometry technology was applied to identify additional previously unknown IC biomarker metabolites. We found several biologically relevant candidates from this new approach and our experimental results were recently published.
- Using a metabolomics approach to capture odor compounds in urine samples of IC patients and healthy controls, we found that urinary menthol levels were significantly lower in IC urine. Further biochemical and functional analyses revealed that urinary menthol may suppress the inflammatory response of immune cells that have infiltrated the bladder epithelium. These findings suggest that the decreased levels of urinary menthol may explain the chronic inflammation in IC bladders.
- Many lipids and lipid metabolites are still not properly annotated nor functionally characterized, which hinders the diagnostic potential of lipid profiling. Our research team actively worked to address this discrepancy and has since developed numerous software and databases that can aid in the lipid structure elucidation process.
- We established new collaboration with a big metabolomics group at our own institute for further validation of target candidates. While our preliminary are based on small numbers and require validation in a large dataset, they nonetheless demonstrate the feasibility of the current study and provide strong support to the fact that we are likely to identify many clinically and biological important linkages with IC and the various IC phenotypes within this study. Also, our concentrated efforts focused on subject recruitment and collection of urine samples.
- Our recent review paper summarized the underlying mechanisms that induce the chronic pain associated with IC and vulvodynia and explain why these two conditions often coexist.

We also developed a statistical model to determine whether the biosignatures to be enhanced by additional systemic changes, such as widespread pain or associated clinical depression.

- Our new collaboration with a big metabolomics group at our own institute for further validation of target candidates has been worked well. We also established an additional pilot collaboration with a Boston-based metabolomics company. We are thinking to use these additional resources for expanding our findings using a larger cohort in near future. These new collaborators will be used for validation of our data as well.
- It is widely believed that ML applications into big healthcare data will lead to extraordinary revolutions. Our group developed a machine learning (ML)-based method for diagnosing IC and assess its performance using metabolomics profiles obtained from a prior study.
- Our recent review paper summarized the underlying mechanisms that induce the chronic pain associated with IC and vulvodynia and explain why these two conditions often coexist. We also developed a statistical model to determine whether the biosignatures to be enhanced by additional systemic changes, such as widespread pain or associated clinical depression.
- Since last report, we were able to reach to potential participants to recruit more for this proposed study. **Mainly due to the COVID-19 pandemic** and its negative effects on clinical trials. We have urine specimens from controls and patients (n=301).

In the following sections, we will update our achievements in detail for your reference.

Optimize the DNA methylation assay and gene expression assay

(1) We initiated experiments to identify DNA methylome and transcriptome associated with interstitial cystitis:

- As an approach to seek the molecular biomarker of IC, we previously performed DNA methylation profiling in urine sediments from IC patients and controls in our pre-existing Inha cohort, which consists of IC patients and age-matched controls under collaboration with Inha University in South Korea (Inha IRB# 10-0751). Given this exciting data, ***we hypothesized that a DNA methylation biomarker panel segregates IC patients from controls.***
- To optimize the experimental conditions, we leveraged pre-existing collaborations between investigators, urine sample collections and accompanying clinical data that have been collected for the Discovery Cohort with approved Institutional Review Board protocol.

(2) We established assay system to identify promoter DNA methylation profiles of the most hypomethylated genes selected from our preliminary data in IC in urine samples from cases and controls:

- Using MethyLight technology, we will examine urine specimens collected from cases, including IC patients and matched healthy subjects, to demonstrate their feasibility as biomarkers of IC in urine. Experimental results from our study will determine whether epigenetic markers in urine are reliable targets for IC diagnosis and whether these epigenetic biomarkers show clinical utility.

- We will begin evaluating the top five genes (*CNR2*, *PR2Y14*, *GRM6*, *F2R* and *CHRM3*), for which MethyLight assays have been designed during this funding period. We will subsequently evaluate the DNA methylation levels of the 20 most hypomethylated genes from preliminary work. Given that multiple marker combinations will be able to improve the sensitivity and specificity of DNA methylation biomarkers, we will perform receiver operator curve (ROC) analysis to determine the sensitivity and specificity of the 20-gene panel dataset. Bisulfite conversion of DNA and following PCR analysis will be conducted as described⁹. We have designed over 1,000 MethyLight assays to date, and have considerable experience performing MethyLight-based assays for DNA methylation measurements.

GENESYM	REFGENE	chromosome	CGsite	strand	SNP & RP	FDR	FC
CNR2	NM_00184	chr1	24239979	-	0	0.003149	-5.0938
P2RY14	NM_01487	chr3	1.51E+08	+	0	0.003657	-4.9635
CTSG	NM_00191	chr14	25046121	-	0	0.010844	-3.9986
DRD4	NM_00079	chr11	640606	-	0	0.01947	-3.564
CTSG	NM_00191	chr14	25046117	-	0	0.014815	-3.8083
S1PR2	NM_00423	chr19	10332165	-	0	0.009565	-4.2056
ADORA3	NM_00108	chr1	1.12E+08	+	0	0.014617	-3.8727
F2R	NM_00199	chr5	76010472	+	0	0.005868	-4.6472
ADORA2A	NM_00067	chr22	24823519	+	0	0.026083	-3.6295
GRM6	NM_00084	chr5	1.78E+08	-	0	0.003261	-4.9346
S1PR4	NM_00377	chr19	3178844	-	0	0.022164	-3.6598
ADORA2A	NM_00067	chr22	24823514	-	0	0.027151	-3.2781
S1PR4	NM_00377	chr19	3179828	-	0	0.031237	-3.3369
P2RY14	NM_01487	chr3	1.51E+08	-	0	0.011163	-4.1008
S1PR4	NM_00377	chr19	3180035	+	0	0.030184	-3.427
CTSG	NM_00191	chr14	25045625	-	0	0.017061	-3.454
ADORA1D	NM_00067	chr20	4202378	+	0	0.004515	-4.4515
F2R	NM_00199	chr5	76010444	-	0	0.020646	-3.541
F2R	NM_00199	chr5	76012827	-	0	0.011762	-3.76
GRM6	NM_00084	chr5	1.78E+08	+	0	0.012732	-3.4133
S1PR4	NM_00377	chr19	3179545	-	0	0.033521	-2.7891
CCKBR	NM_17687	chr11	6292896	-	0	0.008788	-3.6119
P2RX4	NM_00256	chr12	1.22E+08	-	0	0.010372	-3.8145

Table 1. Experimental design for DNA methylation assay

(3) We established collaboration with NanoString to quantify target gene expression in urine samples from IC cases and controls:

- In this funding period, we were able to initiate an active collaboration with an industrial partner, NanoString. We will utilize *NanoString gene expression analysis*, a novel digital technology that is based on direct multiplexed quantification of nucleic acids and offers high levels of precision and sensitivity, in this proposal. NanoString technology employs molecular “barcodes” and single molecule imaging to detect and count target gene expression in a single reaction. The NanoString nCounter provides highly reproducible digital counting capability over 5 logs of dynamic range and does not require any amplification steps that may introduce data bias. We have constructed code probes for the 20 most hypomethylated genes in collaboration with the Nanostring research team (see support letter). After RNA extraction from urine sediments obtained from patients and matched controls, we will quantify gene expression of the panel of 20 most hypomethylated genes using NanoString nCounter analysis in this proposal, and will correlate these data to the DNA methylation data set to identify epigenetically-regulated gene expression in IC.

nCounter™ CodeSet Design Report - Isoform Coverage

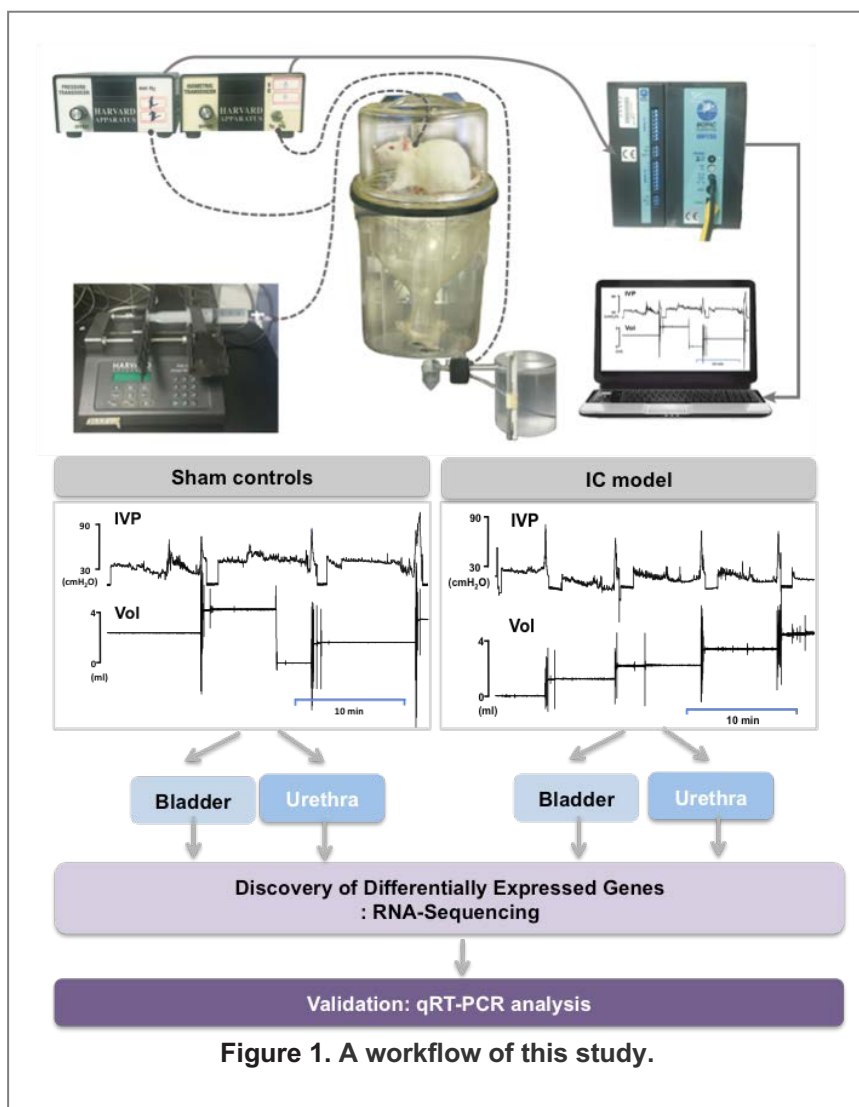
								RefSeq Version:	123015
Customer Name	HUGO Gene	Probe NSID	Tot Isoforms	Isoforms Hit By Probe	# Hit	Isoforms Not Hit By Probe	# Not Hit		
ACTB	ACTB	NM_001101.2:1010		2 NM_001101.3;XM_006715	2		0		
ADORA2A	ADORA2A	NM_000675.3:1095		7 NM_001278500.1;NR_103	7		0		
ADORA3	ADORA3	NM_000677.3:1725		3 NM_000677.3;NM_001302	3		0		
ADRA1D	ADRA1D	NM_000678.2:1135		1 NM_000678.3	1		0		
CCKBR	CCKBR	NM_176875.2:1555		4 NM_176875.3;NM_001318	4		0		
CHRM3	CHRM3	NM_000740.2:1345	10	XM_011544045.1;XM_0115	10		0		
CHRM4	CHRM4	NM_000741.2:0		1 NM_000741.3	1		0		
CNR2	CNR2	NM_001841.1:1570		5 XM_005245736.3;XM_0115	5		0		
CTSG	CTSG	NM_001911.2:160		2 XM_011536499.1;NM_0019	2		0		
DRD4	DRD4	NM_000797.2:990		1 NM_000797.3	1		0		
F2R	F2R	NM_001992.2:985		2 NM_001311313.1;NM_0019	2		0		
F2RL3	F2RL3	NM_003950.2:1425		2 XM_005260139.2;NM_0039	2		0		
GALR1	GALR1	NM_001480.2:1560		1 NM_001480.3	1		0		
GAPDH	GAPDH	NM_002046.5:1041		4 NM_001256799.2;NM_001	5		0		
GRIN2D	GRIN2D	NM_000836.2:1893		2 XM_011526872.1;NM_0008	2		0		
GRM6	GRM6	NM_000843.2:4530		1 NM_000843.3	1		0		
MLNR	MLNR	NM_001507.1:880		1 NM_001507.1	1		0		
P2RX4	P2RX4	NM_001256796.1:316		9 NM_001261397.1;NM_001	9		0		
P2RY14	P2RY14	NM_014879.2:205		5 XM_005247922.3;XM_0115	5		0		
S1PR2	S1PR2	NM_004230.2:185		2 XM_011528425.1;NM_0042	2		0		
S1PR4	S1PR4	NM_003775.2:495		1 NM_003775.3	1		0		
SSTR1	SSTR1	NM_001049.2:2575		1 NM_001049.2	1		0		
TUBB	TUBB	NM_178014.2:1955		7 NM_001293213.1;NM_001	7		0		

Table 2. Collaboration with NanoString for further verification of gene expression

(4) We have constructed IC rat model for mechanistic studies:

- Animals and study design.** A total of 13 female Sprague-Dawley rats (Orient Bio Inc., Gyeonggi-do, South Korea), weighing 200-250 g, were used in the present study. In seven rats, LPS was instilled intravesically, following the intravesical administration of PS. In six rats, the saline was instilled into the bladder and served as the sham group. Continuous cystometry was performed in all of the rats under awake conditions, one month following intravesical instillation of LPS or saline. After cystometry, rats were sacrificed by cervical dislocation. Following laparotomy, the bladder and urethra were obtained en bloc from all rats, separated at the level of the bladder neck, and the bladder was weighed. All experimental animal procedures were conducted in accordance with the Guide for the Care and Use of Laboratory Animals of the National Institutes of Health (Bethesda, MD, USA) and were approved by the INHA Institutional Animal Care and Use Committee at the Inha University Medical School (Incheon, South Korea; approval ID: INHA 140731-321-1). The rats were maintained under a 12-h light:dark photoperiod and normal laboratory conditions, with free access to food pellets and tap water except during the experiments.
- Surgical procedures.** The rats were anesthetized with ketamine (Ketamine; Yuhan Corp., Seoul, Korea; 75 mg kg⁻¹ intraperitoneally) and xylazine (Rompun; Bayer Korea Corp, Seoul, Korea; 15 mg kg⁻¹ intraperitoneally) mixture, during the surgical procedures. Through a lower abdominal midline incision, the bladder and the proximal urethra were approached.
- Induction of cystitis.** Cystitis was induced by the intravesical instillation of LPS following PS, as described previously⁸. Briefly, a 31-gauge needle attached to a syringe (Insulin syringe, SUNGSHIM MEDICAL CO., LTD, Gyeonggi-do, Korea) was inserted into the bladder dome, after the bladder was exposed. The bladder was then emptied by aspiration of urine, and then an appropriate volume of PS (10 mg ml⁻¹) was instilled into the bladder. Twenty minutes later, the bladder was emptied, washed with phosphate-buffered saline (PBS) and then filled with the same volume of LPS (750 µg/ml) for another 20 min. The sham group was instilled with normal saline of the same volume.
- Procedures for intra-vesical catheter implantation.** Three days before cystometry, the catheterization for intravesical pressure (IVP) recordings was done, as described previously^{25,26}. Briefly, after the bladder exposed, a polyethylene catheter (PE-50; Becton-Dickinson, Parsippany, NJ, USA) with a cuff was inserted into the dome of the bladder and held in place with a purse-string suture to record IVP. The

catheter was tunneled through the subcutaneous space, exited through the back of the animals and anchored to the skin of the back with a silk ligature. The free end of the catheter was sealed. After surgery, the animals were caged individually and maintained in the same manner.



- Functional evaluation.** Cystometrograms were performed under unanesthetized, unrestrained conditions in metabolic cages. The external portion of the catheter, implanted into the bladder of the rat, was connected to a two-way valve that was connected via a T-tube to a pressure transducer (Research Grade Blood Pressure Transducer; Harvard Apparatus, Holliston, MA, USA) and a microinjection pump (PHD22/2000 pump; Harvard Apparatus). This was used to record the IVP on the condition of continuous injection. Room-temperature saline was infused into the bladder by microinjection pump at a rate of 10 ml h⁻¹. The micturition volume (MV) was recorded by means of a fluid collector connected to a force displacement transducer (Research Grade Isometric Transducer; Harvard Apparatus). IVP and MV were continuously recorded using Acq Knowledge 3.8.1 software and an MP150 data acquisition system (Biopac Systems, Goleta, CA, USA) at a sampling rate of 50 Hz. The mean values from three reproducible micturition cycles were used for evaluation of cystometric parameters.
- Investigation of cystometric parameters.** Cystometric parameters consisted of pressure and volume parameters of the model, including the lowest bladder pressure during filling phase (BP), bladder pressure immediately before micturition (TP), maximum bladder pressure during the micturition phase (MP), MV, remaining urine after micturition (RV), MV+RV (BC) and intervals between maximum micturition contractions (MI).

	BP (cmH ₂ O)	TP (cmH ₂ O)	MP (cmH ₂ O)	BC (mL)	MV (mL)	RV (mL)	MI (min)
Sham	16.14 ± 1.16	32.16 ± 2.04	74.49 ± 5.71	1.86 ± 0.18	1.86 ± 0.18	0	9.99 ± 0.91
IC	18.87 ± 2.89	38.10 ± 3.76	60.90 ± 4.68	1.31 ± 0.14*	1.17 ± 0.10*	0.15 ± 0.09	6.22 ± 0.83*

Table 2. BP, basal pressure; TP, threshold pressure; MP, micturition pressure; BC, bladder capacity; MV, micturition volume; RV, residual volume; MI, micturition interval; IC, interstitial cystitis; Results are expressed as the mean ± standard error. Pressure parameters were expressed by intravesical pressure. *p<0.05

- **RNA-Sequencing analysis identified the differentially expressed genes, which are specific to bladder or urethra.** To understand the molecular responses associated with IC, we attempted to perform the next generation RNA sequencing analysis and to get the expression profile of the bladder and urethra in response to PS and LPS stimulation, and those of sham controls. Comparison of RNA-Sequencing status between raw and filtered reads was performed as follows.

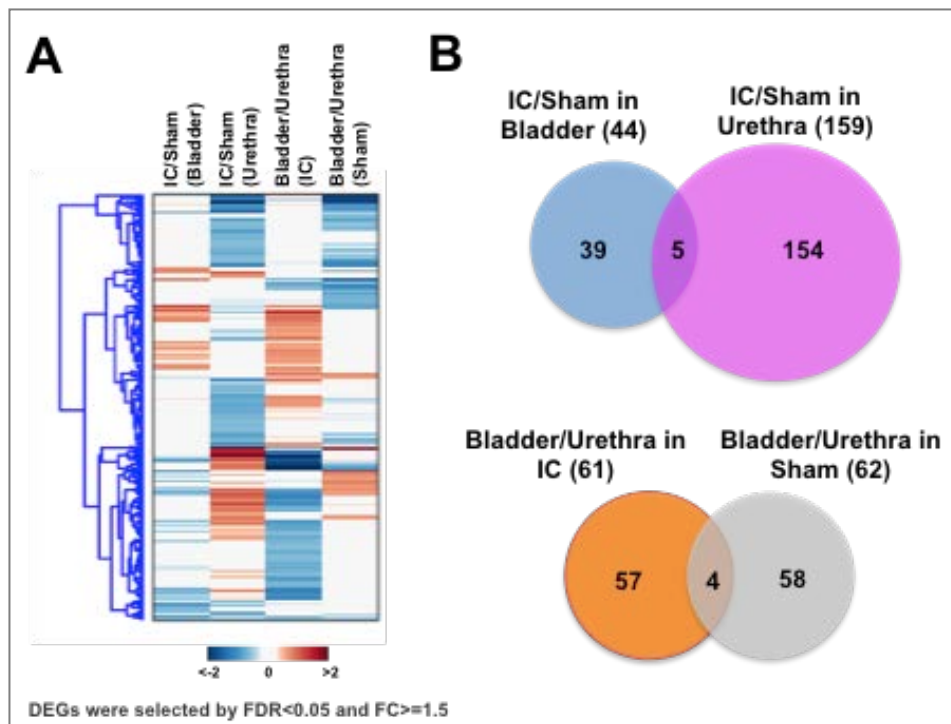


Figure 2. Identification of differentially expressed genes (DEGs) in bladder or urethra obtained from IC rats compared to sham controls. (A) A heatmap showing DEGs **(B)** Diagrams indicating IC-specific DEGs in bladder or urethra (upper), and bladder- or urethra-specific DEGs associated with IC (bottom).

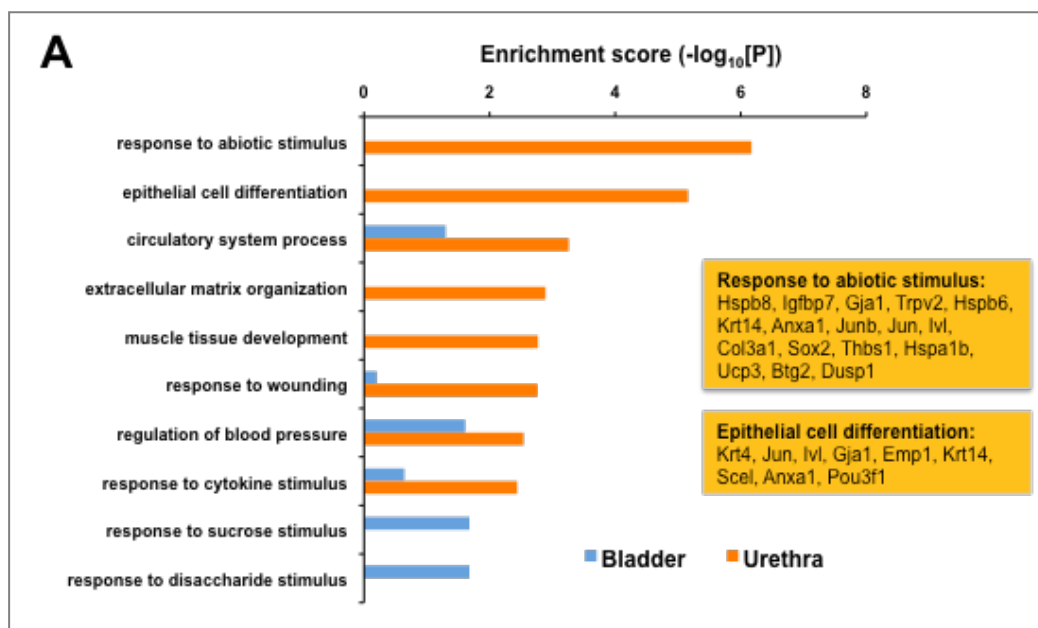
Based on raw sequence data, the filtering processes were performed based on the following criteria; (i) position 1 to 15 base were removed because of hexamer-primed 2nd strand synthesis, (ii) reads with mean base quality ≤ 20 and total base quality (≥ 20) ≤ 80% were removed, and (iii) redundant reads (identical sequences) were collapsed into one read. Further calculation of expression level from the finally filtered reads was done as follows: based on the finally filtered reads and gene expression levels, which were calculated by following procedures; (i) tophat for human genome (hg18), and (ii) cufflinks for human

reference genes (hg18). We compared FPKM (Fragments Per Kilobase of transcript per Million fragments mapped) values across samples based on the merged transcript annotation from human refGene hg18 & CuffLinks.

- The differentially expressed genes in bladder and/or urethra in IC model vs. sham control.** We identified differentially expressed genes (DEGs) with a false discovery rate (FDR)<0.05. A heatmap shown in **Figure 2A** revealed that approximately three-fold more DEGs were perturbed in urethra in comparison of the bladder. Forty-four DEGs were significantly perturbed in bladder tissues obtained from IC rat model, compared to those from control group (**Figure 2B**). The gene expression of 159 DEGs was significantly altered in urethras in the IC rat model (**Figure 2B**). Only five genes were commonly altered both in the bladder and urethra, suggesting that the gene expression of bladder and urethra were distinct (**Figure 2B**).

These five genes include collagen type VII alpha 1 (Col7a1), integrin alpha 7 (Itga7), Serpin Family A Member 3 (Serpina3n), Solute Carrier Family 25 Member 24 (Slc25a24) and Slit Guidance Ligand 3 (Slit3) (**Table 2A**). We also found sixty-one IC-specific (**Figure 2C**) or sixty-two Sham-specific genes (**Figure 2C**). Four commonly perturbed genes in bladder - compared to urethra - included Flavin Containing Monooxygenase 5 (Fmo5), Integrin Subunit Alpha 7 (Itga7), Lymphocyte Cytosolic Protein 1 (Lcp1), and Methyltransferase Like 7B (Mettl7b) (**Figure 2C**).

- Enriched cellular processes perturbed in IC model and the differentially enriched cellular processes in bladder and urethra.** We next attempted to understand the biological and mechanistic meaning of these DEGs by examining the biological pathways over-represented by the genes. The comparison between bladder and urethra revealed that responses of bladder or urethra induced IC model by PS and LPS treatment were different. GOBP and KEGG pathway enrichment analysis demonstrated that the altered genes in bladder tissues of IC model were mainly involved in response to disaccharide stimulus, response to sucrose stimulus, and regulation of blood pressure (**Blue bars, Figure 3A**). The most enriched cellular processes in urethra in IC model included the response to abiotic stimulus, epithelial cell differentiation, extracellular matrix organization and response to wounding et al. (**Orange bars, Figure 3A**). We also found that the cellular processes (e.g., intracellular signaling cascade, cardiac muscle tissue development, and second-messenger-mediated signaling) were enriched in IC-specific DEGs (**Green bars, Figure 3B**).



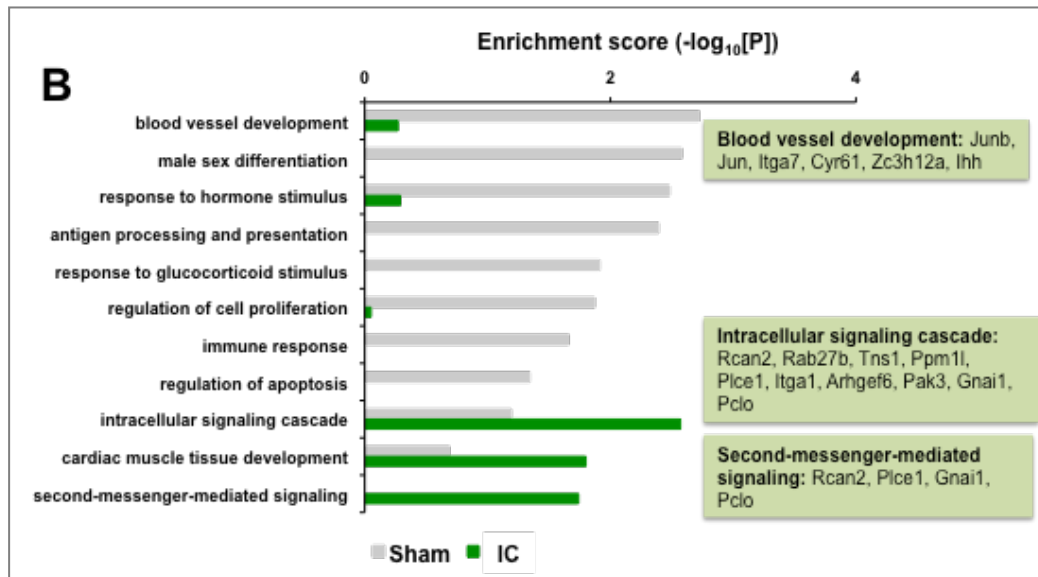


Figure 3. (A) Enriched cellular processes perturbed in IC rats by PS and LPS treatment. Representative DEGs of “response to abiotic stimulus” and “epithelial cell differentiation” were indicated in orange boxes. Blue, bladder specific; Orange, urethra-specific DEGs. **(B)** Differentially enriched cellular processes changed sham or IC specifically. Gray, sham control specific; Green, IC specific DEGs.

- Differentially expressed genes in IC model suggest the bladder specific or urethra specific DEGs.** This pathway analysis could allow us to focus on the gene list of the greatest interest. We chose five genes whose expression levels were significantly increased in bladder, but not in urethra, of IC model for further validation. They were *Fras1* (Fraser syndrome 1), *Adipoq* (adiponectin, C1Q and collagen domain containing), *Tnfaip2* (tumor necrosis factor, alpha-induced protein 2), *Ace2* (angiotensin I converting enzyme 2), and *Frem2* (Fras1 related extracellular matrix protein 2). The fold changes of gene expression in IC model, compared to sham control, were presented in **Figure 4A**.

Additionally we selected five more genes whose expression was significantly increased only in the urethra of IC model. They were *Ceacam1* (carcinoembryonic antigen-related cell adhesion molecule 1, biliary glycoprotein), *Sox2* (SRY, sex determining region Y)-box 2), *Ido1* (indoleamine 2,3-dioxygenase 1), *Ccl21* (chemokine (C-C motif) ligand 21), and *Atf3* (activating transcription factor 3) (**Figure 4B**). **Figure 4C** shows the fold changes of ten genes' gene expression levels in bladder or urethra in IC condition (fold change).

To validate the expression levels and to challenge the importance of these candidates as major modulators of important cellular processes, we performed qRT-PCR analysis using independent bladder (n=3) or urethra (n=3) tissues obtained from IC model (n=3) or sham controls (n=3). In total the top ten genes, which were already selected based on our interest and representativeness of organ that they were belonged to, were analyzed (**Figure 5**).

In summary, we have identified the perturbed gene expression associated with the defected urodynamics in IC mimic animal model, thereby exhibiting the dysfunction of the urinary bladder. A comprehensive analysis based on the next generation RNA-sequencing method combined with a bioinformatics analysis was performed. Our experimental results revealed that the perturbed alterations in gene expression in bladder and urethra are distinct, along with different structure and anatomy, are functionally associated with extracellular matrix organization, wound healing, intracellular signaling cascade and second-messenger-mediated signaling. Further study of the effects on lower urinary tract function may suggest novel therapeutic strategies.

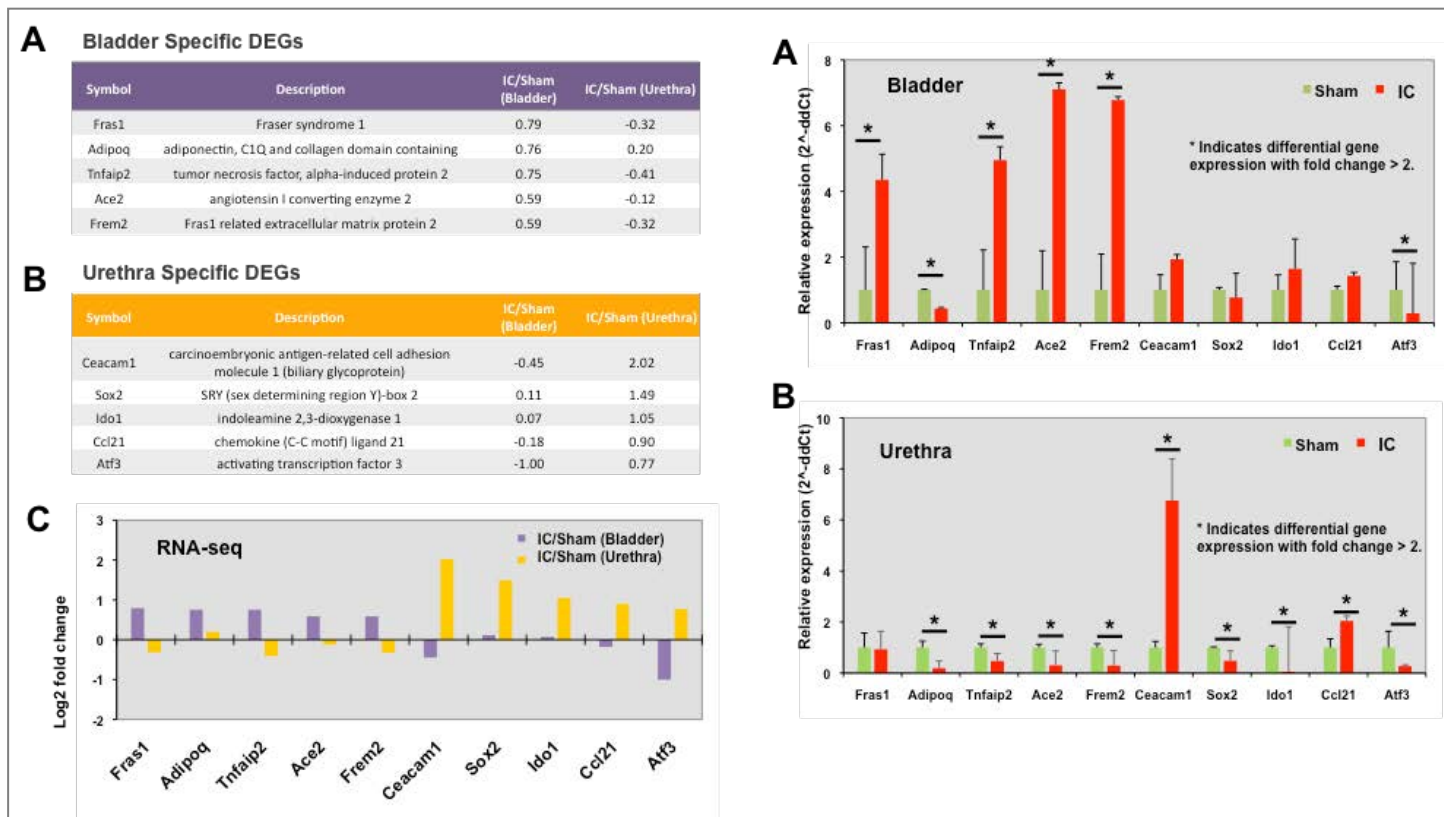


Figure 4. (A) Bladder specific DEGs, (B) Urethra specific DEGs, (C) Expression patterns obtained from RNA-Sequencing data of ten genes.

Figure 5. Further validation using qRT-PCR analysis.

(5) We sought to substantially widen coverage and allow confirmation of metabolites detected in our previous NMR-based study:

To achieve our goals, we performed mass spectrometry (MS)-based metabolomics analysis. Our goal here was to identify non-invasive biomarker candidates and to gain new insight into disease mechanisms. Previous global metabolomics profiling of urine from IC patients suggests the exciting possibility that a urinary metabolic signature for IC can be detected using an additional metabolomics platform, MS.

- **GC-MS analysis of urine specimens from IC patients and controls.** We investigated the metabolite profile of the individual urine samples using GS-MS spectroscopy. Our analysis and data requisition resulted in a total of 490 metabolites detected.

To center the data, the auto scaling method, division of the mean-centered data by the standard deviation, was used. The scores plot for partial least squares (PLS) components showed differentiation of the IC samples from controls with good separation and dispersion (**Figure 6A**). We assessed the accuracy of our predictive model using the leave-one-out cross-validation method as well as the randomized permutation (**Figure 6B**). The observed statistic of this analysis using MetaboAnalyst 3.0 software¹ was significant ($p = 5e-04$), suggesting that these signatures may significantly differentiate patients from healthy controls. A heatmap also showed the distinct expression patterns of metabolites between IC and controls (**Figure 6C**). These metabolites are responsible for the significant difference between IC and controls with fold change either greater than 1.20 or less than 0.83 and p-value less than 0.1.

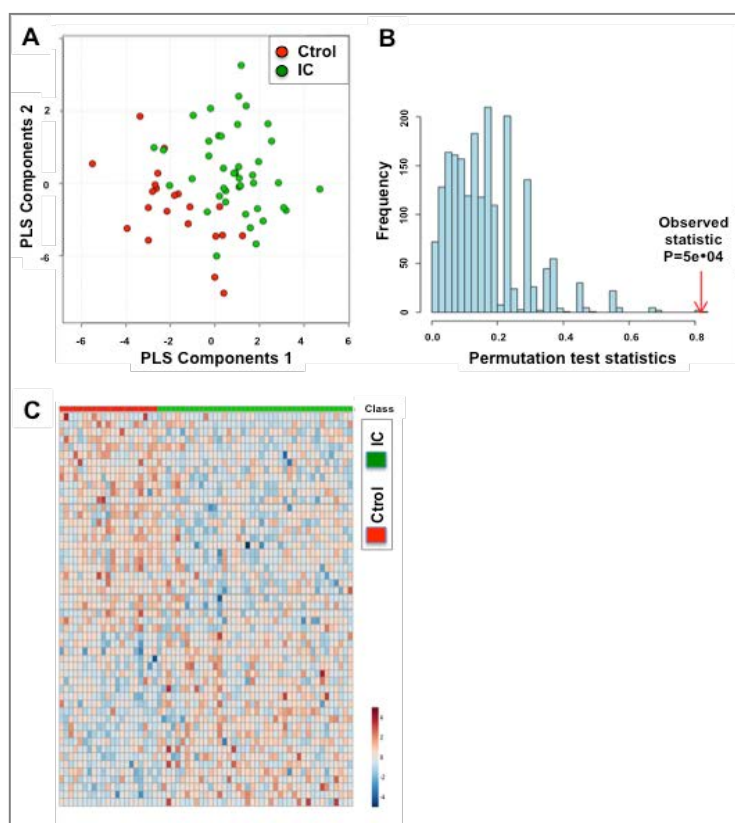


Figure 6. Differentiation of IC patients and healthy control groups using multivariate analysis. (A) Partial least square-discriminant analysis (PLS-DA) score plot of the IC and control groups. PLS-DA plot showed a clear separation of metabolites between patients and matched control subjects. Red: control samples; Green: IC patient samples. The model was established using three principal components. **(B)** For model evaluation, the class prediction results based on cross model validation predictions of the original labeling compared to the permuted data assessed using the separation distance. Histogram shows distribution of separation distance based on permuted data. Red arrow indicates observed statistic ($P = 5e-04$). **(C)** A heatmap of 52 differentially expressed metabolites in IC and control groups. Among 490 detected metabolites in total, 52 metabolites, including both annotated and unannotated metabolites, were significantly altered in IC patients compared to controls ($FC > 1.20$ or $FC < 0.83$ and $P < 0.1$).

To further confirm the identified potential metabolic markers, tenfold cross-validation was applied to evaluate performance based on the identified potential metabolic markers, while SVM regression was used as a classifier. The ROC curve obtained with our significant metabolites 22 annotated metabolites among 52 candidates annotated or unannotated. The AUC (0.8968) of the SVM classifier indicates that the identified candidate metabolic markers perform well to differentiate IC patients and healthy controls.

- Identification of differentially expressed metabolites in urine of IC patients.** Given 490 detected metabolites, we identified 52 differentially expressed metabolites, including both annotated and unannotated metabolites. In the volcano plot (**Figure 7A**), annotated metabolites are presented as log2 fold change against the $-\log_{10}(p)$ of the differential expression between IC patients and healthy controls. 22 annotated differentially expressed metabolites above the threshold ($FC > 1.20$ or $FC < 0.83$, and $P < 0.1$) are marked and presented. Erythronic acid and histidine, were the most upregulated metabolites in the IC patient group compared to that in control, while tartaric acid were the most downregulated as shown in **Figure 7B**.
- Network modeling derived from IC-associated metabolites.** We also performed analysis the histidine-associated differential module (subnetwork) using multilevel local graphical model.
- Collectively,** our GC-MS analysis suggested metabolite candidates associated with IC. This new classification method may provide novel opportunities for better diagnosis and clinical management of IC, particularly in a non-invasive manner. A major clinical challenge remains the early diagnosis of IC. Given that these current findings from this study, although it is out of scope of this study, however we will aim to test whether abnormal metabolism is a key hallmark of IC as a next step. We anticipate that metabolic phenotype. Our multiplex metabolic biomarker panel provides the prospect for assisting predictive factor to determine severity of urinary symptoms and pain/discomfort of IC patients.

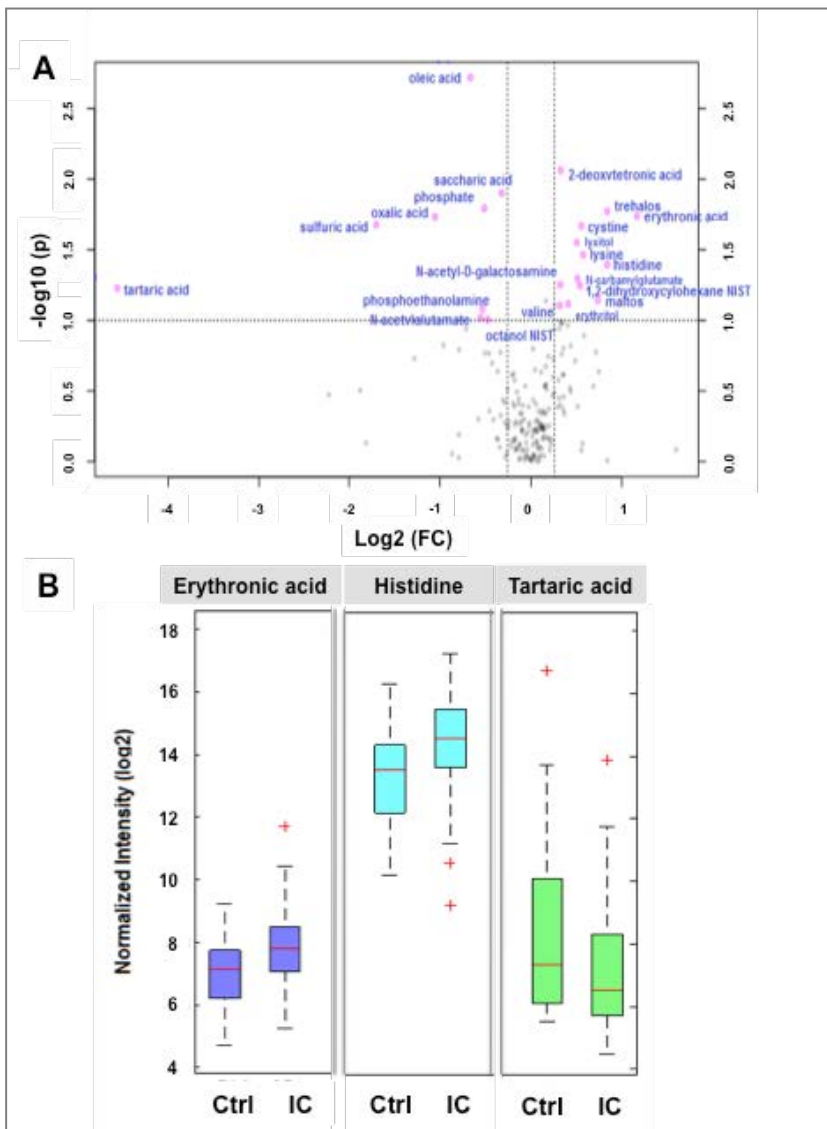


Figure 7. A volcano plot showing differentially expressed metabolites in IC patients. (A) 22 annotated metabolites were significantly altered in IC patients compared to controls ($FC > 1.20$ or $FC < 0.83$ and $P < 0.1$). The red dots represent metabolites above the threshold. The further the metabolite's position away from the (0, 0), the more significant the metabolite is. **(B)** A boxplot showing up-regulated and down-regulated metabolites that could be used to differentiate IC patients from normal subjects. The candidate metabolites, erythronic acid and histidine, were significantly increased in IC patients compared to that in controls, while tartaric acid was significantly decreased. All metabolites show statistical significance with p -value < 0.1 .

DNA methylome and transcriptome associated with IC

In an effort to find molecular biomarkers for IC, we previously performed DNA methylation profiling in the urine sediments of IC and control patients of our pre-existing Inha cohort, which consisted of IC patients and age-matched controls (Inha IRB# 10-0751). Given this exciting data, we ***hypothesized that a DNA methylation biomarker panel segregates IC patients from controls.***

In order to optimize experimental conditions, we leveraged pre-existing collaborations among investigators and utilized urine sample collections with the accompanying clinical data that was collected for the discovery cohort along with approval from the IRB.

Using MethyLight technology, we examined DNA methylation levels of CNR2 in a pilot set of urine specimens collected from cases, including IC patients and matched healthy subjects.

For our next funding period, we anticipate that the experimental results from our study will determine whether epigenetic markers in urine are reliable targets for IC diagnosis and whether they show clinical utility. We will also begin designing primers and evaluating DNA methylation levels of for our other four top genes (*PR2Y14*, *GRM6*, *F2R* and *CHRM3*). We will subsequently evaluate the DNA methylation levels of the 20 most hypomethylated genes from preliminary work. Given that multiple marker combinations will be able to improve the sensitivity and specificity of DNA methylation biomarkers, we will perform receiver operator curve (ROC) analysis to determine the sensitivity and specificity of the 20-gene panel dataset. Bisulfite conversion of DNA and following PCR analysis will be conducted as described¹. Our research team has designed over 1,000 MethyLight assays to date and have considerable experience performing MethyLight-based assays for DNA methylation measurements.

We constructed and characterized an IC-mimic rat model

Animals and study design

A total of 13 female Sprague-Dawley rats (Orient Bio Inc., Gyeonggi-do, South Korea), weighing 200-250 g, were used in the present study. In seven rats, PS and LPS were instilled intravesically in order to induce IC-like symptoms. The six other rats served as the sham group and were instilled with saline. Continuous cystometry was performed in all of the rats under awake conditions, one month following intravesical instillation of LPS or saline. After cystometry, rats were sacrificed by cervical dislocation. Following laparotomy, the bladder and urethra were obtained en bloc from all rats, separated at the level of the bladder neck, and the bladder was weighed.

All experimental animal procedures were conducted in accordance with the Guide for the Care and Use of Laboratory Animals of the National Institutes of Health (Bethesda, MD, USA) and were approved by the INHA Institutional Animal Care and Use Committee at the Inha University Medical School (Incheon, South Korea; approval ID: INHA 140731-321-1). The rats were maintained under a 12-h light:dark photoperiod and normal laboratory conditions, with free access to food pellets and tap water except during the experiments.

Surgical procedures

The rats were anesthetized with a ketamine (Ketamine; Yuhan Corp., Seoul, Korea; 75 mg kg⁻¹ intraperitoneally) and xylazine (Rompun; Bayer Korea Corp, Seoul, Korea; 15 mg kg⁻¹ intraperitoneally) mixture during the surgical procedures. The bladder and proximal urethra were approached through a lower abdominal midline incision.

Induction of cystitis

Cystitis was induced by the intravesical instillation of LPS following PS, as described previously². This procedure involved exposing the bladder and inserting a 31-gauge needle attached to a syringe into the bladder dome. The bladder was then emptied by aspiration of urine and an appropriate volume of PS (10 mg ml⁻¹) was instilled into the bladder. Twenty minutes later, the bladder was emptied, washed with phosphate-buffered saline (PBS), and

then filled with the same volume of LPS (750 µg/ml) for another 20 min. The sham group was instilled with normal saline of the same volume.

Procedures for intra-vesical catheter implantation

Three days before cystometry, the catheterization for intravesical pressure (IVP) recordings was done, as described previously^{3,4}. Briefly, after the bladder exposed, a polyethylene catheter (PE-50; Becton-Dickinson, Parsippany, NJ, USA) with a cuff was inserted into the dome of the bladder and held in place with a purse-string suture to record IVP. The catheter was tunneled through the subcutaneous space, exited through the back of the animals, and anchored to the skin of the back with a silk ligature. The free end of the catheter was sealed. After surgery, the animals were caged individually and maintained in the same manner.

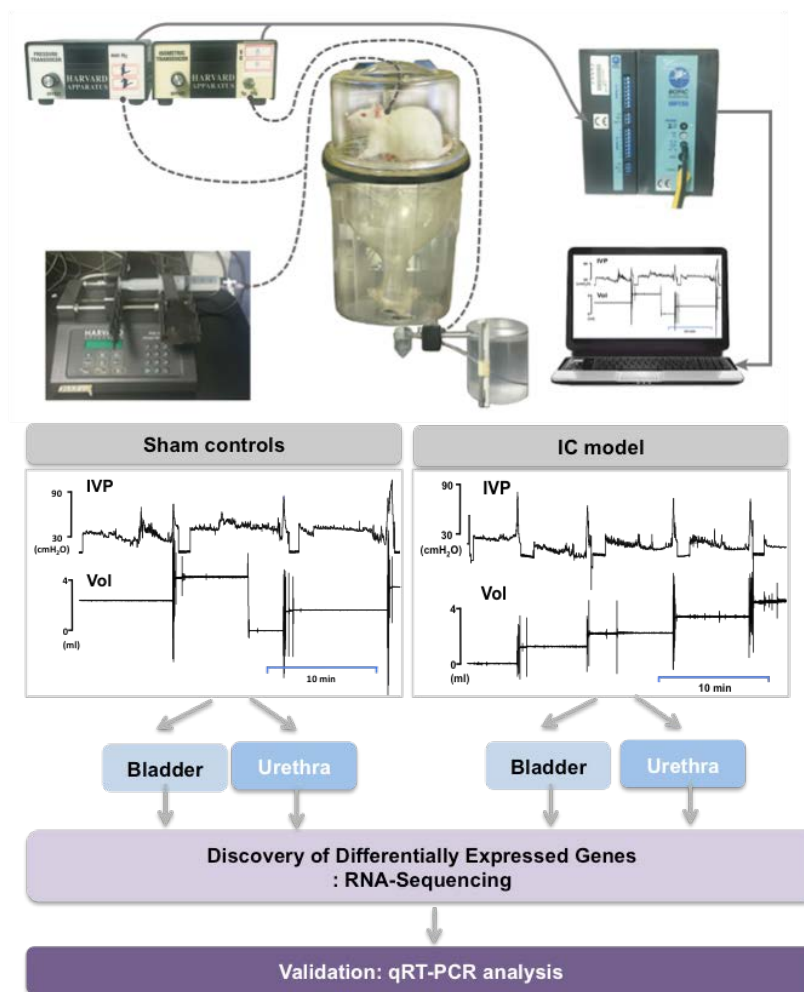


Figure 1. A workflow of this study.

Functional evaluation

Cystometrograms were performed under unanesthetized, unrestrained conditions in metabolic cages. The external portion of the catheter was implanted into the bladder of the rat and connected to a two-way valve that was connected via a T-tube to a pressure transducer (Research Grade Blood Pressure Transducer; Harvard Apparatus, Holliston, MA, USA) and a microinjection pump (PHD22/2000 pump; Harvard Apparatus). This was used to record the IVP on the condition of continuous injection. Room-temperature saline was infused into the bladder by microinjection pump at a rate of 10 ml h⁻¹. The micturition volume (MV) was recorded by means of a fluid collector connected to a force displacement transducer (Research Grade Isometric Transducer; Harvard Apparatus). IVP and MV were continuously recorded using Acq Knowledge 3.8.1 software and an MP150 data acquisition system (Biopac Systems, Goleta, CA, USA) at a sampling rate of 50 Hz. The mean values from three reproducible micturition cycles were used for evaluation of cystometric parameters.

We successfully assessed function of inhibitory small compound candidates in TAAR1 signaling using IC animal model. Our hypothesis in the proposed study, TAAR1-modulating antagonists may be useful for relief the symptoms of IC, was tested.

Rationale

Our preliminary results show that TAAR1 exists in bladder, whose signaling can be blocked by potential TAAR1 antagonists. Given the fact that tyramine is a well-known neuromodulator, we speculated that urinary tyramine may affect central and peripheral nervous systems. Our goals in Aim 2 include determining the expression levels of TAAR1 in the normal bladder tissue of mice, rats, and humans (Aim 2a).

To identify and test TAAR1 inhibitory small molecules

We obtained preliminary evidence that tyramine levels are greater in the urine of IC patients, suggesting that tyramine and TAAR1 may play a role in IC. Based on this information, we hypothesized that tyramine-TAAR1 signaling is associated with the symptoms of IC. We speculated that TAAR1-modulating antagonists may be useful in relieving the symptoms of IC/PBS by blocking signaling.

We tried to get an idea of TAAR1's potential inhibitors by quick searching potential small chemical compounds similar in structure to tyramine and capable of antagonizing TAAR1. Tyramine analogues would be good candidates since drug candidates should bind to TAAR1 with high affinity and competitively inhibit tyramine signaling. Our preliminary efforts searching candidates suggested a list of potential inhibitory small compounds.

Investigation of cystometric parameters

Cystometric parameters consisted of pressure and volume parameters of the model, including the lowest bladder pressure during filling phase (BP), bladder pressure immediately before micturition (TP), maximum bladder pressure during the micturition phase (MP), MV, remaining urine after micturition (RV), MV+RV (BC) and intervals between maximum micturition contractions (MI). Unfortunately, our comprehensive investigation on these cystometric parameters of IC animal model with and without TAAR inhibitory compounds did not show significant symptom relief.

We found that inhibition of DNA methylation suppressed the IC-associated increase of CNR2 protein expression

IHC analysis results of four different rat models

Using IHC analysis of the IC rat model, we investigated protein expression levels of CNR2 between bladder epithelial cells obtained from sham controls (Sham) and those of IC-induced (LPS).

The slides were annotated and characterized by the use of Leica Tissue IA 2.0 software (Copyright 2012 by SlidePath Ltd.) for quantification of digitalized images. For quality control measures, Hematoxylin and Eosin (H&E) stained slides were used during the annotation. The ACSS2 slide was viewed with its corresponding H&E slide in order to ensure the annotation was done on the bladder tumor epithelium only. Stromal and structural tissues were cut off from annotation.

The minimum number of cells measured per slide was 100,000. Following annotations, the "measure stained cells algorithm" option was selected. Color definition preferences were defined and algorithm input parameters were optimized by using several stained images of slides. The optimized algorithm was used for the analysis of all slides. Haematoxylin was set as the nuclear counter stain, and 3,3'Diaminobenzidine (DAB) was set as the nuclear, cytoplasmic, and membrane marker.

Parameters in the software are based on a grayscale. 0 is the minimum intensity (black) and 255 is the maximum intensity (white). We set the maximum threshold at 170 and 80 being the threshold for positive and negative staining respectively. The max nuclear window size radius was set to default and the nuclear area threshold was set to 0 – 500 μm^2 (any nuclei or cells out of these range were cut off). The minimum % of stained area in a nucleus was set to 20%. The threshold for cytoplasm staining was set higher, 160 – 220 due to the presence of antibodies. The minimum % of stained area was set to 75%. After the annotation analysis, data regarding the nuclear h-score, % of positive nuclei, % of positive nuclear area, the cellular cytoplasmic h-score, % of positive cytoplasmic staining was collected and visualized into box plots.

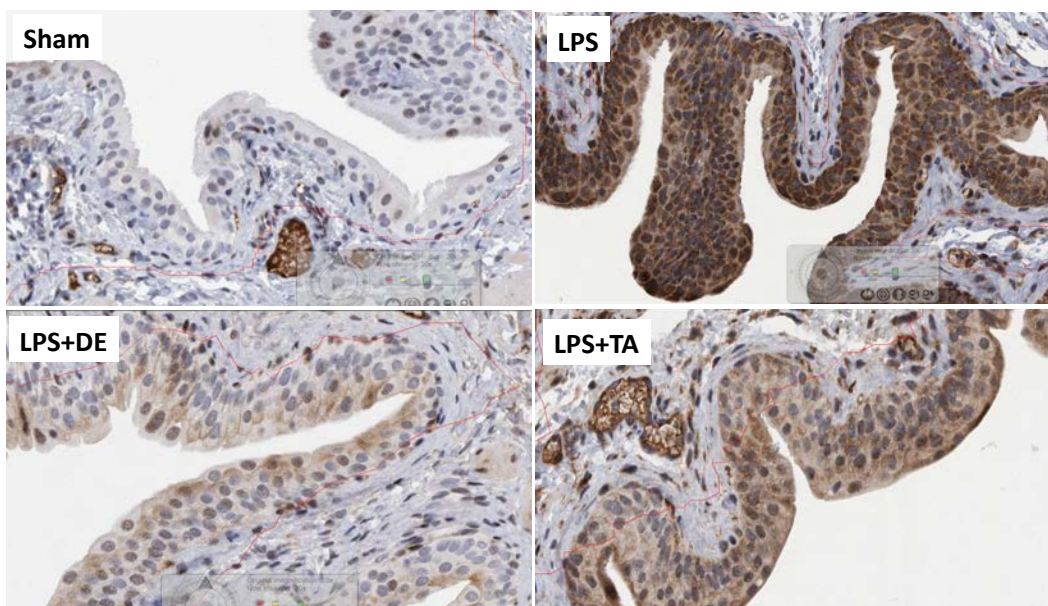


Figure 2. Representative IHC images from four experimental conditions. Sham, sham control model; LPS, IC model; LPS+DE, treatment of DNA methyltransferase (DNMT) inhibitors-treated IC model; LPS+TA, trace amine-associated receptor 1 (TAAR1) inhibitor-treated IC model.

Monitoring the % of positive nuclei showed that CNR2 protein expression increased approximately four fold in the IC model compared to sham controls. CNR2 expression in the TA model was two folds greater compared to the DE condition (treatment of DNA methyltransferase (DNMT) inhibitors-treated IC model), suggesting efficient suppression activity of DNMT inhibitors. However, TAAR1 inhibition could not block CNR2 stimulation in the IC model (TA, trace amine-associated receptor 1 (TAAR1) inhibitor-treated IC model).

The results of the area of positively stained nuclei in the tissue were also consistent with the results discussed above (Figure 3). The H-score of IC model was seven times greater than sham controls, indicating a great protein expression. The H-score of the DNMT inhibitor treated model was 1/7th of the TA model, indicating significantly different CNR2 expression. The H-score for cytoplasmic staining as well as the percentage of positive cytoplasm was significantly higher in the TA model compared to the DE model, suggesting the highly efficient inhibiting function of drug A in the IC rat model. % positive nuclei (Figure 3).

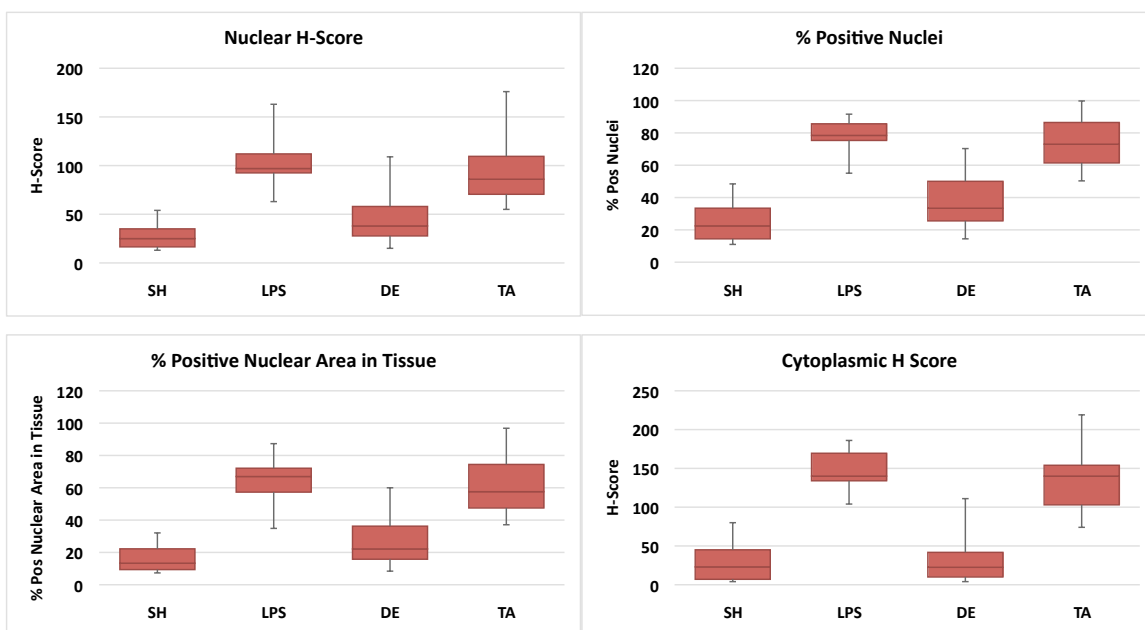


Figure 3. IHC scores of four experimental conditions

Our global metabolomics analysis using state-of-the art mass spectrometry was able to identify new additional metabolite candidates

Characteristics of the study subjects

A clinical diagnosis of IC was made by two independent urologists according to NIDDK criteria (e.g. frequency, urgency, bladder pain, discomfort and the presence of glomerulations during cystoscopic hydrodistention), before any treatment or medication was given. In total, we enrolled 63 female subjects (42 IC patients and 21 normal subjects) with a mean age of 51. Population-based, age-matched controls were recruited from one clinic using the same standard operating procedures (SOPs) during the same research period (2010-2013).

Subjects and urine specimen collection

IC patients and healthy control subjects were diagnosed and recruited from an outpatient urology clinic at Inha University Hospital. Work-up included symptom assessment, cystoscopic evaluation, physical examination, urodynamics, and/or urine culture. Patients with a history of other diseases (such as any types of cancer, inflammation, or diabetes, etc.) were excluded. All subjects were of Asian female descent residing in South Korea. To avoid possible contamination with vaginal or urethral cells, first morning urine specimens were obtained using clean catch methods in a sterile environment. The de-identified specimens were sent to clinical laboratory and were centrifuged to remove cell debris. Supernatants were processed into individual aliquots of 1ml/tube, before storage at -80°C until further analysis.

GC-MS analysis of urine

Gas-chromatography/mass-spectrometry (GC-MS) analysis was performed^{5,6}. Normally, 10ul of urine are dissolved in 1ml -20°C cooled acetonitrile, isopropanol and water (3:3:2 v/v) mixture at pH 7. In this case the urine volume was adjusted between 2 and 10ul to externally measured creatinine levels using a linear calibration curve. Then the solution was vortexed at 4°C for 5 minutes in 1.5ml Eppendorf tubes. Samples were centrifuged for 2min at 14,000 rcf and 500ul were aliquoted. The aliquot was the evaporated in a Labconco Centrivap cold trap to complete dryness. The methoximation step was performed with 10ul of a solution of 40 mg/ml O-methylhydroxylamine hydrochloride (CAS: [593-56-6]; Formula $\text{CH}_5\text{NO.HCl}$) and 90 minutes shaking at 30°C . Then 90ul of N-methyl-N-trimethylsilyltrifluoroacetamide (MSTFA) was added and shaken at 37°C for 30 min. Then a mix of 1ul fatty acid methyl esters (FAME) retention time markers was added. The mixture was transferred to amber crimp autosampler vials. Measurements were performed on a Leco Pegasus IV TOF coupled to an Agilent 6890GC with Agilent 6890 split/splitless injector. The column was a Restek RTX-5Sil MS (95% dimethyl/5% diphenyl polysiloxane) with 30m length, 0.25 mm i.d. and 0.25 um film thickness with 10 m guard column. Injection volume was 1ul at 250°C . The GC parameters were set to 1 ml/min constant flow Helium and an oven ramp of 50°C (1 min hold) to 330°C at $20^{\circ}\text{C}/\text{min}$, 5 min hold before cool-down. The transfer line temperature was 280°C and spectra were recorded in electron ionization mode at 70 eV with a filament temperature of 250°C TOF and scan range of 85-500 u.

Annotation and ID of compounds

The peak and compounds detection or deconvolution was performed with the Leco ChromaTOF software. Spectra were matched against the FiehnLib [3] mass spectral and retention index library. Post-curation and peak replacements were performed with the in-house developed BinBase software and the sample matrix with all known and unknown compounds exported to a Microsoft EXCEL sheet. A total of 490 compounds were detected. 200 compounds were annotated as known compounds by retention index and mass spectral matching and 290 compounds were unknown.

Data processing. For preprocessing of MS data, the data in urine samples from IC patients and healthy subjects were preprocessed as previously described. We excluded one subject from the IC patient group and three subjects from controls because their spectra were outliers based on PCA analysis. Fourier transformation and phase and baseline correction of time domain data were manually performed. The resulting frequency domain data was binned at a 0.002ppm interval. The signals were normalized against total integration values and 0.025% TSP. The region corresponding to water (4.6–5.0ppm) was removed from all spectra. Data pre-treatment including baseline correction, chromatogram alignment, time-window setting, hierarchical multivariate curve resolution, H-MCR, and normalization were performed in MATLAB [version 7.3] using custom scripts. Analysis of NMR spectra was performed using a VNMR500 (Varian Inc.). The metabolites were identified by a data base

search, based on spectra using Chemomx (Spectral database; Edmonton, Alberta, Canada) by fitting the experimental spectra to those in the database.

Identification of metabolic marker candidates

In order to identify potential metabolites as marker candidates that can discriminate IC patients from healthy subjects, we applied the following steps. First, a Student's t-test was performed to extract significant metabolites from the normalized GC-MS data. The volcano plot shows the fold change and the significance of each annotated metabolite. Significant metabolites were selected on the volcano plot if they had a fold change threshold > 1.20 (or < 0.83) and t-tests p -value threshold < 0.1 . Second, the resultant profiles, which contain profiles of 22 annotated differentially expressed metabolites, were imported into MetaboAnalyst version 3.0¹. Log transformation and mean-centered with auto scaling were performed prior to multivariate statistical analysis. Partial least square discriminant analysis (PLS-DA) was performed, and model evaluation with permutation strategy was carried out according to a published protocol⁷. Finally, in order to further confirm the potential metabolic markers, a support vector machine (SVM)-based classifier was built to distinguish IC patients from controls using the identified significant metabolites in MATLAB (R2014a). Tenfold cross-validation was applied to evaluate the performance.

GC-MS analysis of urine specimens from IC patients and controls

We investigated the metabolite profile of the individual urine samples using GS-MS spectroscopy. Our analysis and data requisition resulted in a total of 490 metabolites detected.

To center the data, the auto-scaling method, which divides the mean-centered data by the standard deviation, was used. The scores plot for partial least squares (PLS) components showed differentiation of the IC samples from controls with good separation and dispersion (**Figure 4A**).

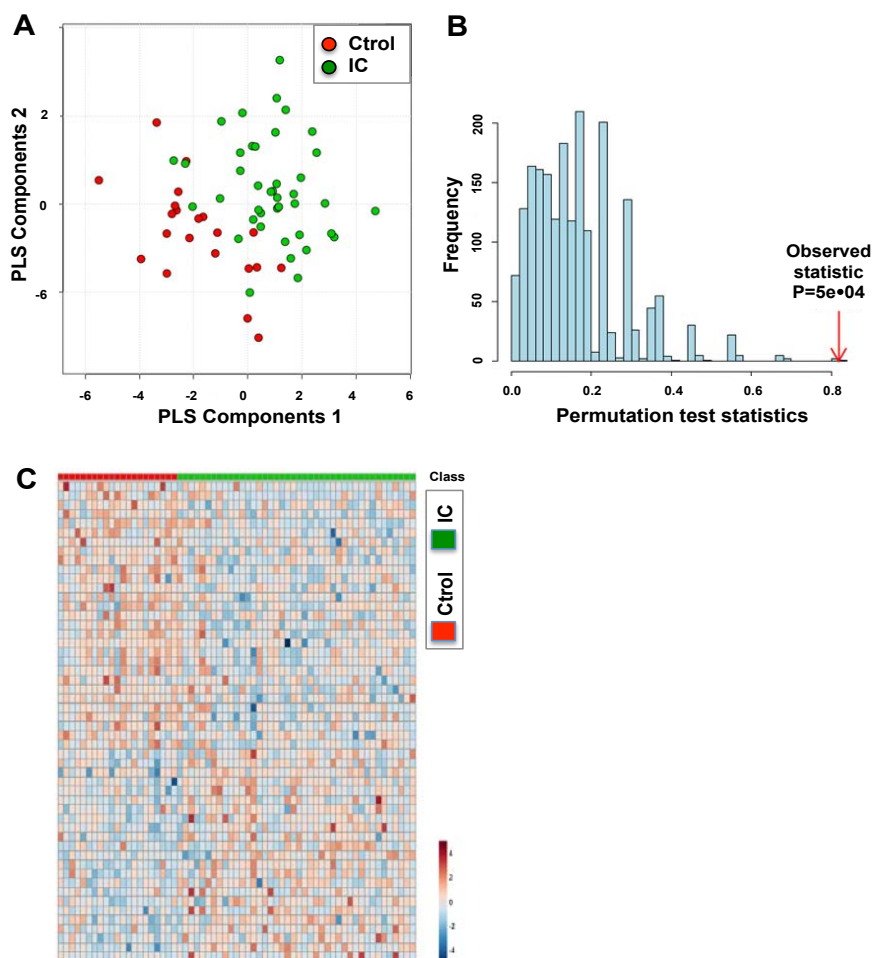


Figure 4. Differentiation of IC patients and healthy control groups using multivariate analysis. (A) Partial least square-discriminant analysis (PLS-DA) score plot of the IC and control groups. PLS-DA plot showed a clear separation of metabolites between patients and matched control subjects. Red: control samples; Green: IC patient samples. The model was established using three principal components. **(B)** For model evaluation, the class prediction results based on cross model validation predictions of the original labeling compared to the permuted data assessed using the separation distance. Histogram shows distribution of separation distance based on permuted data. Red arrow indicates observed statistic ($P = 5e-04$). **(C)** A heatmap of 52 differentially expressed metabolites in IC and control groups. Among 490 detected metabolites in total, 52 metabolites, including both annotated and unannotated metabolites, were significantly altered in IC patients compared to controls ($FC > 1.20$ or $FC < 0.83$ and $P < 0.1$).

We further assessed the accuracy of our predictive model using the leave-one-out cross-validation method as well as the randomized permutation (**Figure 4B**). The observed statistic of this analysis using MetaboAnalyst 3.0 software¹ was significant ($p = 5e-04$), suggesting that these signatures may significantly differentiate patients from healthy controls. A heatmap also showed the distinct expression patterns of metabolites between IC and controls (**Figure 4C**). These metabolites are responsible for the significant difference between IC and controls with a fold change either greater than 1.20 or less than 0.83 and p-value less than 0.1.

To confirm the identified potential metabolic markers, tenfold cross-validation was applied to evaluate performance based on the identified potential metabolic markers, while SVM regression was used as a classifier. **Figure 5** shows the ROC curve obtained with our significant metabolites 22 annotated metabolites among 52 candidates annotated or unannotated. The AUC (0.8968) of the SVM classifier indicates that the identified candidate metabolic markers perform well to differentiate IC patients and healthy controls.

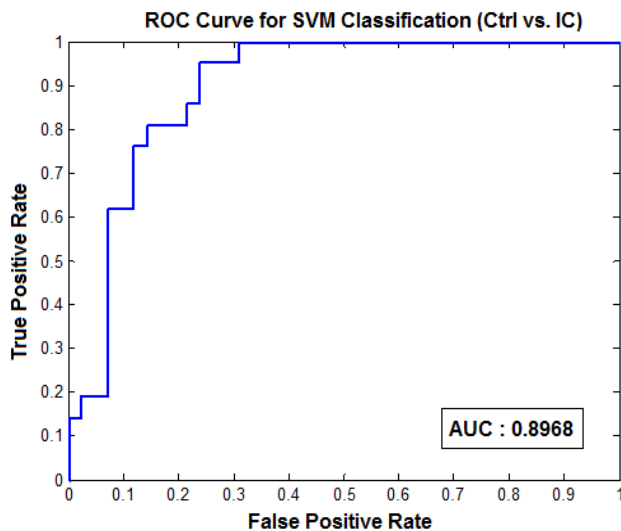


Figure 5. ROC curve of support vector machine (SVM) classification with 10 fold cross-validation (AUC: 0.8968). The ROC curve was obtained with 22 annotated differentially expressed metabolites. The performance of the SVM classifier indicates the distinguish power of the identified metabolic markers.

Identification of differentially expressed metabolites in urine of IC patients

Given 490 detected metabolites, we identified 52 differentially expressed metabolites, including both annotated and unannotated metabolites. In the volcano plot (**Figure 6A**), annotated metabolites are presented as log₂ fold change against the $-\log_{10}(p)$ of the differential expression between IC patients and healthy controls. 22 annotated differentially expressed metabolites above the threshold ($FC > 1.20$ or $FC < 0.83$, and $P < 0.1$) are marked and presented. Erythronic acid and histidine were the most upregulated metabolites in the IC patient group compared to that in control. Tartaric acid was the most downregulated as shown in **Figure 6B and Table 1**.

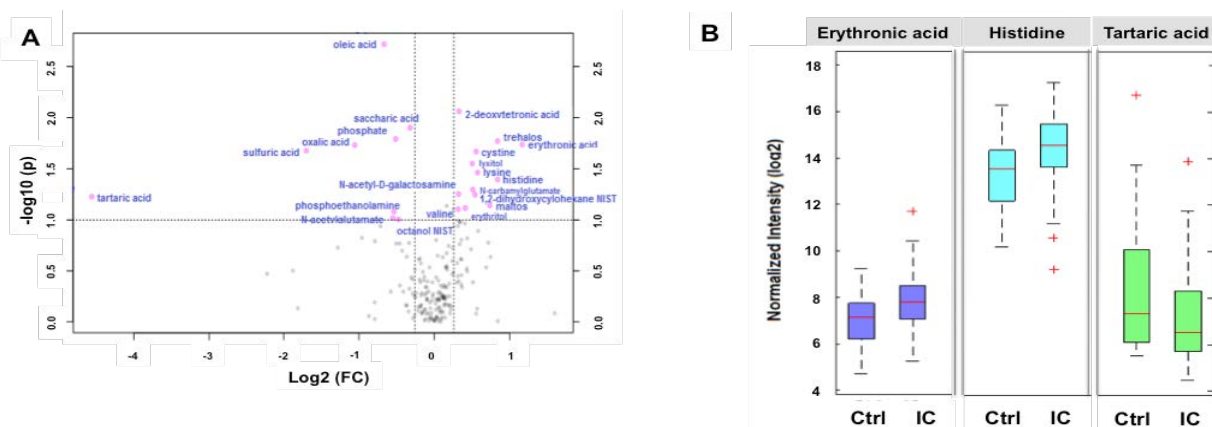


Figure 6. A volcano plot showing differentially expressed metabolites in IC patients. (A) 22 annotated metabolites were significantly altered in IC patients compared to controls ($FC > 1.20$ or $FC < 0.83$ and $P < 0.1$).

The red dots represent metabolites above the threshold. The further the metabolite's position away from the (0, 0), the more significant the metabolite is. **(B)** A boxplot showing up-regulated and down-regulated metabolites that could be used to differentiate IC patients from normal subjects. The candidate metabolites, erythronic acid and histidine, were significantly increased in IC patients compared to that in controls, while tartaric acid was significantly decreased. All metabolites show statistical significance with p-value < 0.1.

Metabolite	Fold Change	p-value
oleic acid	0.63	0.00
2-deoxytetronic acid	1.26	0.01
saccharic acid	0.80	0.01
phosphate	0.70	0.02
trehalose	1.79	0.02
erythronic acid	2.25	0.02
oxalic acid	0.48	0.02
sulfuric acid	0.31	0.02
cystine	1.47	0.02
lyxitol	1.42	0.03
lysine	1.49	0.03
histidine	1.79	0.04
N-carbamylglutamate	1.43	0.05
N-acetyl-D-galactosamine	1.25	0.06
1,2-dihydroxycyclohexane NIST	1.46	0.06
tartaric acid	0.04	0.06
maltose	1.67	0.07
erythritol	1.33	0.08
valine	1.25	0.08
phosphoethanolamine	0.69	0.08
N-acetylglutamate	0.68	0.10
octanol NIST	0.72	0.10

Table 1. A list of metabolites differentially expressed in IC, compared to controls. Recent advances in next generation DNA sequencing (NGS) have revealed that human organs and body surfaces form habitats for an enormous web of interacting microbial communities of great diversity and complexity. In comparison with other organ sites, the microflora of the lower urinary tract has not been extensively studied. This study looks at the composition of fungal communities that reside in the human urine, which was once believed to represent a sterile environment, using state-of-the art NGS technology. Our data from catheterized urine samples suggest that the human urinary tract harbors a unique cellular mycobiota and contains a rich fungal community, which has a richer diversity that may be masked in voided urine abundant with contamination from common skin or GI microbes. We also have found that mycoflora in urine is more diverse than those in colon communities. This finding is new and could open up a new frontier of study that could now pave the way to gain a deeper understanding on urine mycobiome, reflecting the urinary tract mycobiota.

Network modeling derived from IC-associated metabolites

We performed analysis on the histidine-associated differential module (subnetwork) using a multilevel local graphical model⁸ (**Figure 7**). The differential network represents the changes of correlation structure in IC when compared to the background network. Levels of two metabolites, valine and histidine (red circle), are increased in IC. The interactions (correlations) among metabolites indicate that those metabolites may biologically function together. Generally, the variations of interactions among metabolites under different clinical conditions are associated with IC status. The sparse local graphical model⁹ is used to construct both the common and differential metabolite networks simultaneously. In turn, treating each metabolite as a response variable and the remaining annotated metabolites as predictors and running the sparse regression built the network.

Cytoscape (www.cytoscape.org/) was used for differential network visualization and subnetwork identification. The proposed approach identified the IC associated differential network efficiently (**Figure 7**).

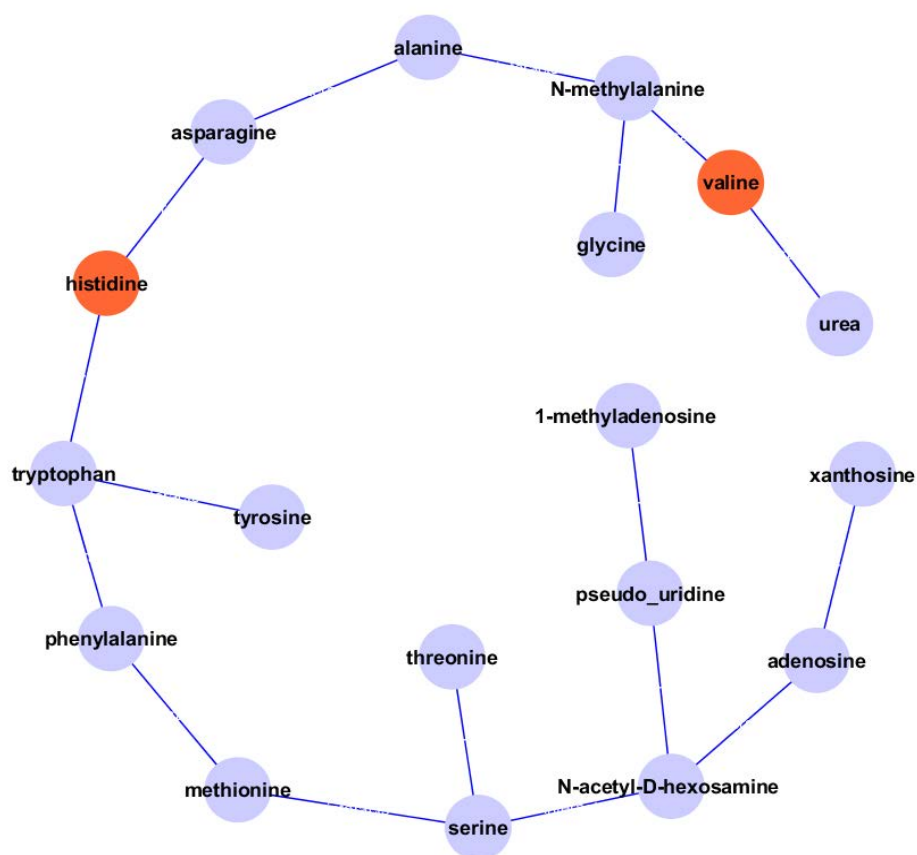


Figure 7. Network modeling derived from IC-associated metabolites. Histidine associated differential module (subnetwork) is shown on Figure 7, where the red nodes indicate upregulated metabolites and light blue nodes represents non-differentiated metabolites.

To further understand our metabolite signature, MetaboAnalyst software was used for functional enrichment analysis. Metabolite enrichment analysis allows us to study the corresponding biological pathways of IC with metabolites on the differential network. We performed Metabolite Set Enrichment Analysis (MSEA) with the 18 metabolites, which were derived from data in figure 4. We found that those 18 metabolites are highly enriched in Protein Biosynthesis and Ammonia Recycling with the FDR of 0.0000136 and 0.00557, respectively (**Figure 8**).

Metabolite Sets Enrichment Overview

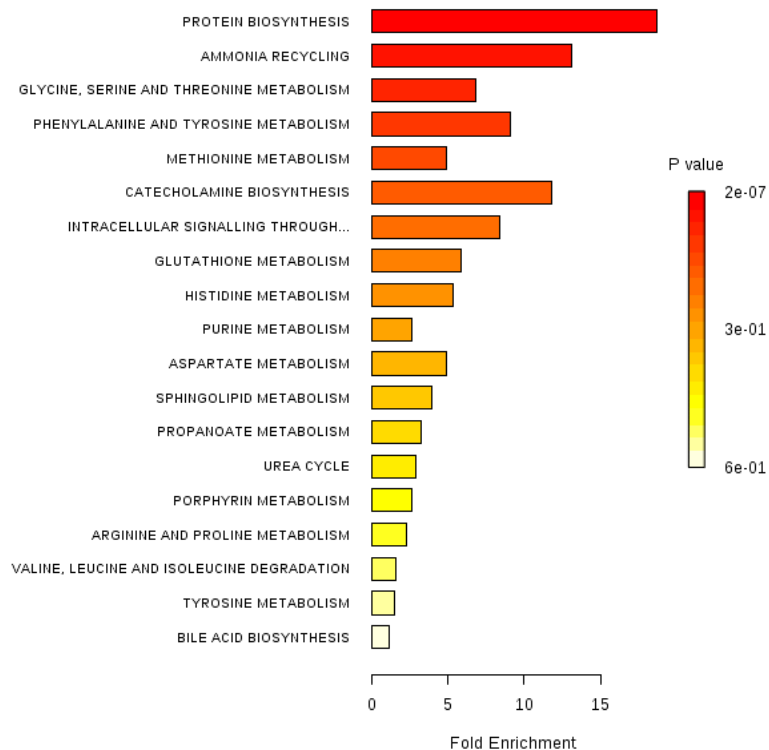


Figure 8. Differential network in IC is identified with multilevel local graphical model (Liu et al. 2015). The differential network represents the changes of correlation structure in IC when compared to the background network.

Collectively, in this study, we proposed novel biomarker candidates that are detectable in human urine specimens for IC diagnosis based on metabolomics analysis using GC-MS. Metabolites including histidine, erythronic acid, and tartaric acid were found to be specific to IC. Although the present report has provided evidence that metabolic fingerprints can predict IC patients, it remains to be determined whether these metabolites might have biological and mechanistic meanings. The relatively small number of subjects is also a limiting factor. These initial findings furthermore require validation with additional cohorts.

An IC-specific urinary metabolite may change DNA methylation in bladder epithelial cells

Although sex disparities are noted in the field of gender medicine, the biological, cellular, and molecular bases of these gender biases remain elusive in the context of IC. One theory is that sex hormones are possibly associated with noted variations in metabolism. This is evident in numerous other diseases. For example, it has been reported that the prevalence of autoimmune disease is three to four times higher among women¹⁻³. Another study suggested that male and female multiple sclerosis patients showed distinct gene signatures⁴. Heart failure and cardiovascular disease (CVD) are also associated with sex differences⁵⁻⁹. In females, hypertension is more common and is often the cause of heart failure. However, females also have a better prognosis than males with heart failure. For CVD, blood pressure and glucose metabolism play more important roles in females, whereas male CVD is affected mostly by cholesterol. The average starting age of CVD incidence in males is around the mid-30s and gradually increases; while in females, CVD usually occurs much later, around 50 years of age. Furthermore, the plasma lipid profiles of younger-aged females are generally better than similarly aged males, which may explain why females have a lower risk for CVD. In an effort to examine these sex-biases, mammalian animal models have been used to explore how males and females develop diseases differently and identify potential therapeutic targets. A study in female and male Sprague–Dawley rat models showed that hearts from female rats have better cardioprotection than male rats. Phosphorylation of mitochondrial proteins in female rats were altered, leading to less reactive oxygen species generation and oxidative metabolism¹⁰. While research into sex differences in other diseases has progressed, the same cannot be said for IC. Therefore, there is a need for more effort in examining the relationships between sex-specific risk factors, metabolic rewiring, prevalence, and symptom severity in IC.

Urine analysis for IC diagnosis. Urine is a critical biological fluid that is filtered through the kidneys and stored in the bladder. It contains the expression of many metabolic properties. It was only recently that urine has been recognized as a potential biological source of disease-associated biomarkers. Prior to this, urine was just considered a voided bodily waste product. While the composition of urine may be less complex than that of serum or tissue, it can nevertheless contain a multitude of biomarkers for medical disorders and state³⁰⁻³³. Considering that bodily fluids most proximal to a disease site provides a wealth of informative biomarkers³⁴⁻³⁶, urine analysis could prove to be tremendously beneficial for bladder diseases³⁷. In addition, assays of urine components are noninvasive and can easily be repeated, even by the patients themselves.

Finding IC urinary biomarkers via unbiased metabolomics profiling. Metabolic profiling can provide global chemical fingerprints regarding the physiology and metabolism of cells. Additionally, nuclear magnetic resonance (NMR) spectroscopy can supply information concerning the physiological and pathological states of biological samples³⁸⁻³⁹. To search for soluble metabolites that can diagnostically segregate female IC patients, we constructed the Inha cohort under a collaboration with Dr. Tack Lee (IRB #10-0751) at Inha University Hospital (Incheon, South Korea). Using a metabolomics approach on urine samples, we identified a list of candidate urinary biomarkers. Further analysis with NMR and lipid chromatography-mass spectrometry (LC-MS) showed substantial differences in the metabolic profiles of urine between female IC patients and healthy controls⁴⁰ (**Fig. 1A/B**). Notably, α -oxoglutarate (α -OG, also known as α -ketoglutarate), a key Krebs cycle intermediate and regulator of cellular redox states¹¹, was one of the key IC-associated urine metabolites.

α -OG perturbs the epigenetic architecture and biology of bladder epithelial cells.

α -OG has been reported to function in epigenetic regulation, indirectly contributing to metabolic reprogramming and macrophage activation^{11,12}. Based on this, we tested our hypothesis that the global DNA methylome of normal human bladder epithelial cells is altered in response to α -OG¹². To assess whether the DNA methylome is changed by α -OG, an EPIC array was performed (**Fig. 2**). Our analysis and data requisition identified a list of differentially methylated genes (DMGs) in response to α -OG. Following the QC steps within minfi, methylation data for 836,329 CpGs were analyzed. The volcano plots show the differentially methylated probes present between the α -OG treatment and control conditions. Significantly hypermethylated probes are shown in orange, while hypomethylated probes are shown in blue (**Fig. 2**).

Figure 1. Urinary levels of α -OG were significantly increased in female IC patients compared to that in controls. (A) Significantly increased levels of two NMR peaks, 3.0157 and 3.0212 ppm indicating α -OG. *FDR < 0.05 (B) LC-MS analysis showing an increased α -OG levels in urine from female IC patients compared with those from healthy female controls. Statistical analysis was performed using student's t-test, and the resulting p-values are indicated. Error bars represent standard error.

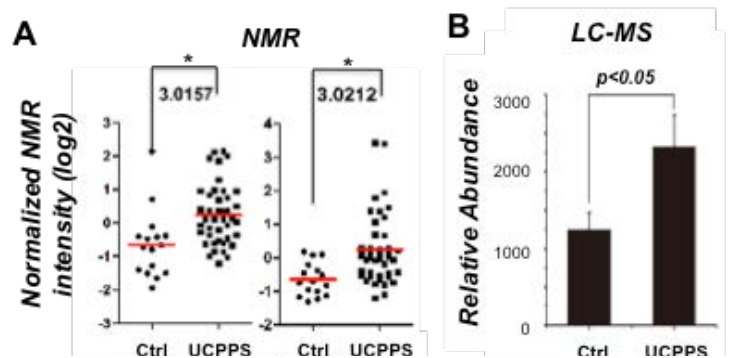
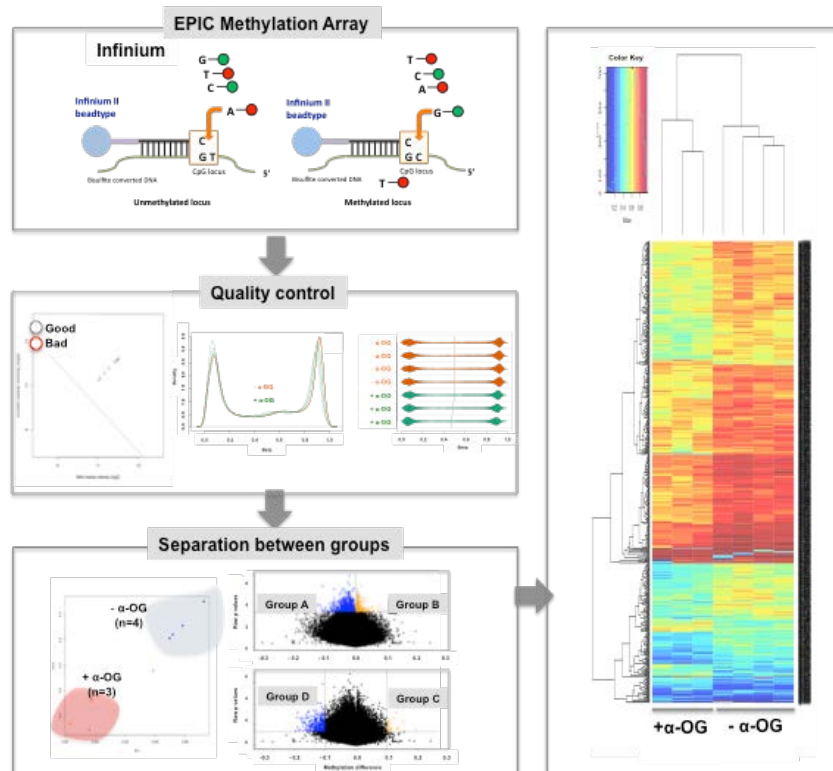


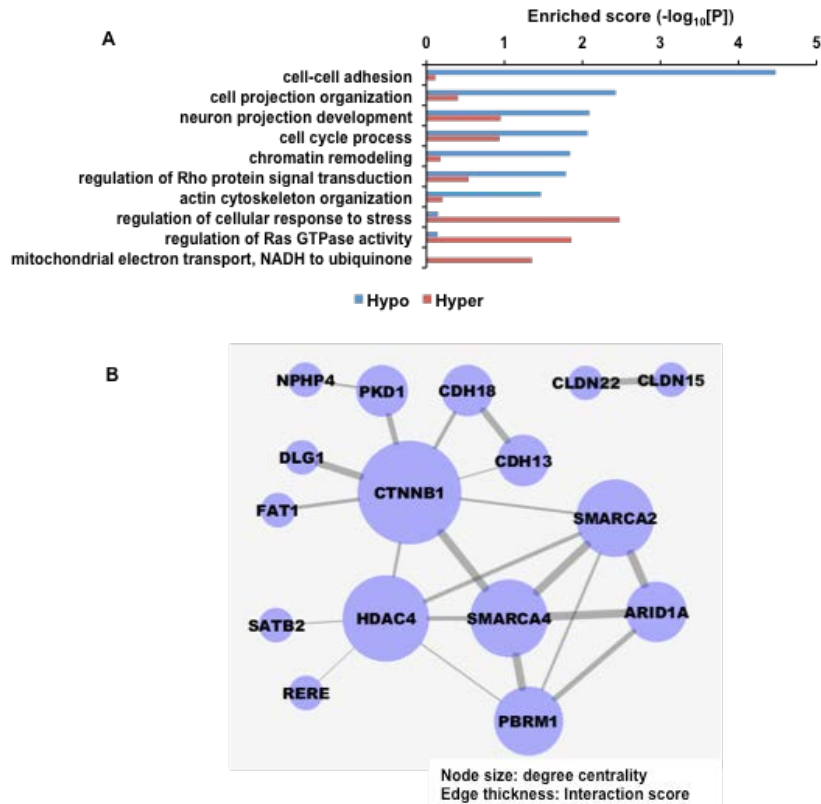
Figure 2. Reprogrammed DNA methylation architecture due to α -OG treatment. Experimental scheme describing EPIC DNA methylation profiling and the following bioinformatics analysis. Volcano plot highlighting differentially methylated probes.



Next, in order to explore the contribution of DNA methylation signatures in IC, we performed functional enrichment analysis and network modeling on the DMGs. Enriched cellular processes and biological pathways perturbed by α -OG treatment were identified using the DAVID software¹³. Hypomethylated genes were found to be enriched for cell-cell adhesion, cell projection organization, neuron projection development, cell-cycle processes, chromatin remodeling, and regulation of Rho protein signal transduction. Hypermethylated genes were found to be enriched for cellular responses to stress, Ras GTPase activity, and transport of NADH to ubiquinone in the mitochondrial electron transport chain (**Fig. 3A**). To further understand the mechanistic connection of perturbed DMGs due to α -OG treatment, a network model was constructed using protein-protein interaction information from the STRING database⁴⁵. This network model consisted of B-CATENIN (CTNNB1), PKD1 (polycystin 1), CDH18 (cadherin 18), SMARCA5 (SWI/SNF related, matrix associated, actin dependent regulator of chromatin, subfamily A, member 4), HDAC4 (histone deacetylase 4), ARID1A (AT-rich interactive domain 1A), PBRM1 (Polybromo-1, a component of the PBAF (Polybromo-associated-BRG1- or BRM-associated factors), chromatin remodeling complex et al. (**Fig. 3B**).

α -OG suppresses cell proliferation in human bladder epithelial cells. In light of our previous global metabolomics data linking α -OG to cell cycle arrest and proliferation suppression¹⁴, we further investigated the effects of α -OG in bladder epithelial cells. Cell cycle transition and proliferation were measured in TRT-HU1 human bladder cells treated with or without 10 mM of α -OG. We found that levels of key cell cycle and proliferation regulators, such as p53 and p21, significantly increased, and the cell proliferation rate was significantly suppressed in response to α -OG (**Fig. 4**).

Figure 3. Enriched biology perturbed by α -OG. (A and B) Enriched cellular processes (A) and KEGG pathways (B). Bar plot represents scores of enrichments by hyper- and hypo-methylated genes. (C) Network model describes cell-cell adhesion and chromatin remodeling genes that were hypo-methylated by α -OG treatment.

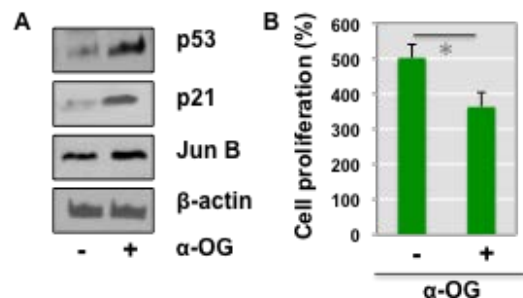


Collectively, in this preliminary study, we examined the biological impact of increased levels of urinary α -OG on the bladder epithelium. Given that our previous global metabolomics profiling of female IC urine suggested the possibility of finding non-invasive metabolic signatures, this study focused on gaining new insight into the mechanism of IC by investigating the biological meaning of upregulated α -OG. In addition, our Infinium Methylation EPIC profiling revealed that the bladder DNA methylome is responsive to α -OG. Our findings provide evidence suggesting that **α -OG may change the physiology of bladder epithelial cells at the epigenetic and metabolic levels.**

Sex-associated differences in baseline urinary metabolites of healthy adults.

In our preliminary work, we hypothesized that the products of metabolism in healthy females and males are distinct. To determine the base levels of urinary metabolites in healthy controls, we attempted to compare urinary metabolomic profiles using state-of-the art untargeted global gas chromatography time-of-flight mass spectrometry (GC-TOF MS) profiling combined with comprehensive bioinformatics analysis. In total, we enrolled 60 females and 60 males for this study. All participants were >2 months free of treatment and/or medication. In order to compare the metabolite profiles of urine samples from healthy females and males, individual urine samples were analyzed using GC-TOF MS. We found that 77% of all compounds yielded a non-normality distribution. Hence, a nonparametric univariate method, the Mann-Whitney U test, was performed to measure and discover significantly changed metabolites. Additionally, we adopted the Benjamini-Hochberg false discovery rate (FDR) correction procedure to deal with the multiple comparison problem and ensure the

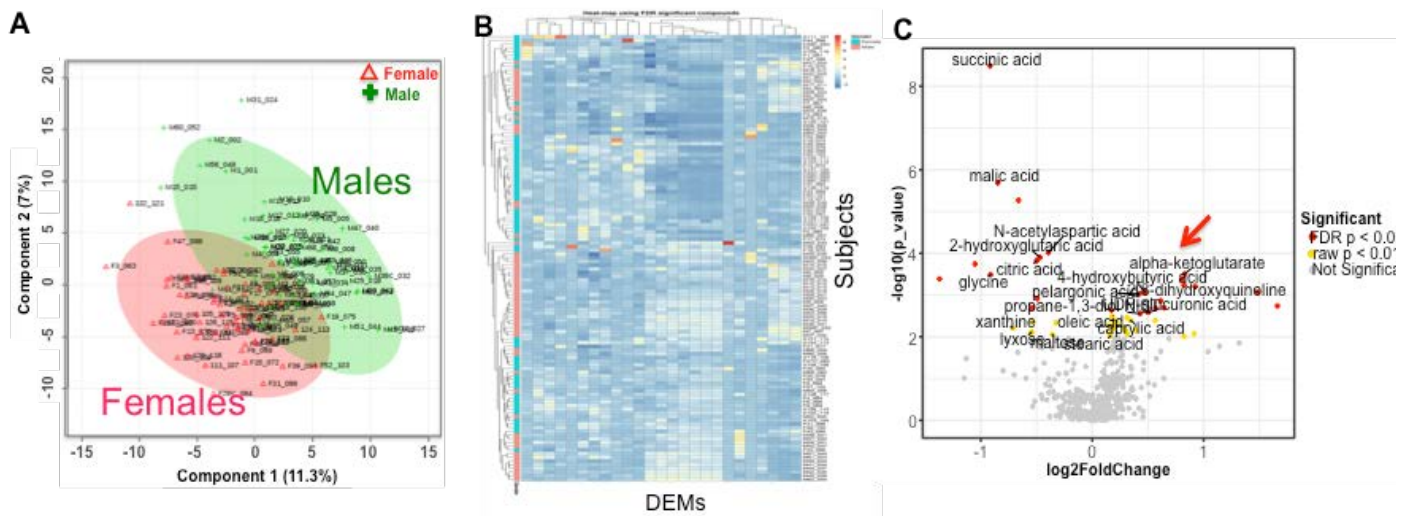
Figure 4. Anti-proliferative effects of α -OG on bladder epithelial cells. (A) Representative western blot showed the reduced levels of p53 and p21 expression in TRT-HU1 normal bladder epithelial cells treated with 10mM of α -OG for 72 hrs. β -actin was used for protein normalization. (B) Proliferation assay was performed. *P<0.05 (two-sided Student's t-test) compared with the control group.



reproducibility of our significant metabolites detection. Metabolites responsible for differences in multivariate metabolic phenotypes between male and female urine were obtained based on variable importance in projection (VIP) from a 10-fold cross-validated partial least-square discriminant analysis (PLS-DA) model. The PLS-DA model achieved a 48.5% rate of discrimination for Q2 and 89.1% for R2. In addition, the model was further validated with a permutation test on prediction accuracy and had a significant result ($p < 0.05$), indicating that the model was robust and results were not obtained by chance. Significantly altered metabolites distinguishing male and female urine were acquired based on conditions of $p < 0.05$, fold-change < 0.8 or > 1.2 , and VIP > 1 (Fig. 5A).

Hierarchical clustering analysis (Euclidean distance and complete method) and constructed heatmaps of the significant metabolites (corrected FDR $p < 0.05$) depicted the relatively disturbed and unbalanced metabolism states between male and female samples (Fig. 5B). Next, we performed the Mann-Whitney U test and Benjamini-Hochberg FDR correction on each compound to compare them between males and females. There were 25 significantly different compounds after FDR correction and 94 without FDR correction. The volcano plot shows the fold change and significance of each annotated metabolite. Significant metabolites in the volcano plot had a fold-change threshold > 1.20 or < 0.83 with a t-test p-value < 0.05 (Fig. 5C). The differentially expressed metabolites (DEMs) were identified based on their p-values, FDR p-values, fold-changes of male vs. female, and PLS-DA VIP values. Of note, **levels of α -OG (male/female fold-change, 2.29) were found to be higher in healthy males compared to females.** In contrast, levels of succinic acid, malic acid, or glycine greatly decreased in males compared to females.

Figure 5. Distinctive urinary metabolic profiles between healthy males and females. (A) Partial least squares-discriminant analysis (PLS-DA) scores plot. It depicted obvious differences between male and female urine samples, with PC1 (11.3%) and PC2 (7%). (B) Heat map showed the distribution of DEMs, which were significantly different (FDR adjusted p value < 0.05) between male and female urine samples. (C) In volcano plot, a total of 50 peaks were significantly changed (Mann-Whitney U test p value < 0.01) in urine samples. Red dots represent 25 significant peaks with FDR adjusted p value < 0.05 . Red arrow represents α -OG.



Summary:

(1) In an effort to understand the molecular mechanism of sex-associated biochemical correlates of IC, our preliminary systematic examination focused on and found distinct urinary metabolite signatures between healthy females and males. **Our urinary metabolomics data clearly suggests that sex differences should be considered in future laboratory and clinical studies.**

(2) Our preliminary data revealed that α -OG, which was abundantly detected in the urine of female IC patients, regulates gene expression epigenetically and contributes to slowed proliferation in bladder epithelial cells. This experimental data provides clues regarding the underlying biology of IC and suggests potential diagnostic and therapeutic targets.

To this date, metabolomics is considered to be one of the major “omics” tools, with the great potential for application in personalized medicine and health¹⁵. Over the last decade, metabolomics has become an integral part of clinical laboratories worldwide for targeted analysis. However, untargeted metabolomics is still widely used as it provides comprehensive insights into complex metabolomes and allows for biomarker discovery. While untargeted metabolomics can be powerful, its main challenge is its low identification rates^{16,17}. Since there is no single platform capable of capturing the entire metabolome of urine, we have employed two platforms most suited for untargeted urine analysis: (1) hydrophilic interaction chromatography (HILIC), for polar metabolite profiling, and (2) charged surface hybrid (CSH) technology, for lipidomics profiling. Through this integration of lipidomics and intensive systems biology, our experimental results provided a comprehensive list of lipid species and biogenic amines in human urine. Lipidomics, a lipid-targeting subarea of metabolomics, involves studying the unique structure and functional roles of cellular lipids in biological systems. Recent technological advancements in high-resolution MS have made comprehensive lipid metabolic profiling of clinical specimens and biofluids, including urine, possible. As important structural components of cellular membranes, lipids play key biological roles in various diseases. However, clinical application of lipidomics profiling still remains a challenge due to the limited databases available for data interpretation. Many lipids and lipid metabolites are still not properly annotated nor functionally characterized. Our group is actively working to address this issue by developing software and databases that can aid in lipid identification. The biologically active metabolites in urine can be identified through global metabolomics profiling and can provide an unbiased chemical fingerprint of the metabolism in the human body. The urinary metabolome in particular is associated with urological diseases, including bladder dysfunctions such as IC¹⁸⁻²⁰. IC is characterized by chronic bladder and/or pelvic pain, as well as nocturia and an increase in urinary frequency and urgency.^{21,22} For our work, we sought to derive urinary metabolomic signatures from IC patients using newly developed comprehensive annotation tools²³ on all five levels of annotation, as defined by the Metabolomics Standards Initiative (MSI). The objective of this work is to provide insight into increasing compound annotation levels in the clinical setting by utilizing a variety of freely available software tools and databases.

EXTRACTION

Subjects, urine specimen collection, and clinical and pathological features of subjects were described in a previous paper from our team. De-identified urine samples were stored at -80°C until further analysis. Urinary lipids were extracted with methanol and methyl tert-butyl ether containing a cocktail of lipid standards. Water was subsequently added for phase separation. This extraction protocol extracts all main lipid classes in urine with high recoveries, specifically phosphatidylcholines (PC), sphingomyelins (SM), phosphatidylethanolamines (PE), lysophosphatidylcholines (LPC), ceramides (Cer), cholesteryl esters (CholE), and triacylglycerols (TG).²⁴ Lipid standards were purchased from Avanti Polar lipids (Alabaster, USA). Polar metabolite extraction was done by taking the polar phase of the lipid extraction procedure. Samples were dried in a centrivap prior to a clean-up step of 50% acetonitrile and dried again. Samples were then reconstituted in 80:20 acetonitrile and water solution containing internal standards from Sigma and CDN Isotopes.

INSTRUMENTATION

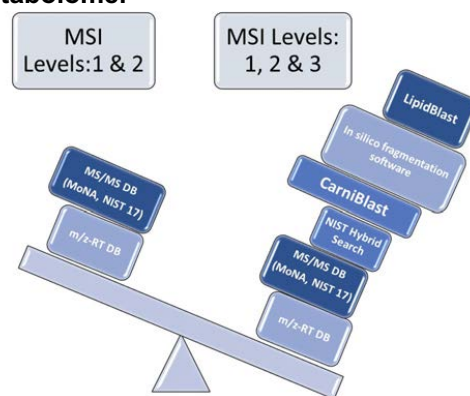
For lipids, all measurements were carried out on a Thermo Q Exactive Hybrid Quadrupole-Orbitrap Mass Spectrometer. Briefly, 1 μL of diluted samples were separated on a Waters Acquity Ultra-Performance LC (ULPC) CSH C18 column (100 \times 2.1 mm; 1.7 μm) coupled to an Acquity UPLC CSH C18 VanGuard Precolumn (5 \times 2.1 mm; 1.7 μm). The column was maintained at 65°C with a flow rate of 0.6 mL/min. The positive ionization mobile phases consisted of (A) acetonitrile:water (60:40, v/v) with ammonium formate (10 mM) and formic acid (0.1%) and (B) 2-propanol:acetonitrile (90:10, v/v) with ammonium formate (10 mM) and formic acid (0.1%). The negative ionization mobile phases consisted of (A) acetonitrile:water (60:40, v/v) with ammonium formate (10 mM) and (B) 2-propanol:acetonitrile (90:10, v/v) with ammonium formate (10 mM). The separation was conducted under the following gradient: 0 min 15% B; 0–2 min 30% B; 2–2.5 min 48% B; 2.5–11 min 82% B; 11–11.5 min 99% B; 11.5–12 min 99% B; 12–12.1 min 15% B; 12.1–15 min 15% B. The Thermo Q Exactive Hybrid Quadrupole-Orbitrap Mass Spectrometer was operated using electrospray ionization (ESI CSH) in positive mode used the following parameters: mass range, 120–1200 m/z; sheath gas flow rate, 60; aux gas flow rate, 25; sweep gas flow rate, 2; spray voltage (kV) 3.6; capillary temp, 300°C ; S-lens radio frequency level, 50; aux gas heater temp, 370°C . The full MS parameters were set as follows: resolution, 60,000; automatic gain control

(AGC) target, 1e6; maximum IT, 100ms; spectrum data type, centroid. Data dependent tandem MS parameters: resolution, 15,000; AGC target 1e5; maximum IT, 50 ms; loop count, 4; TopN, 4; isolation window, 1.0 m/z; fixed first mass, 70.0 m/z; (N)CE / stepped (N)CE, 20, 30, 40; spectrum data type, centroid. For HILIC, all measurements were carried out on the same Thermo Q Exactive Mass Spectrometer. Briefly, 1 μ L of diluted samples were separated on an Waters Acquity UPLC Ethylene Bridged Hybrid (BEH) Amide Column (150 \times 2.1 mm; 1.7 μ m) coupled to an Acquity UPLC BEH Amide VanGuard Precolumn (5 \times 2.1 mm; 1.7 μ m). The column was maintained at 45°C with a flow rate of 0.4 mL/min. The mobile phases consisted of (A) water with ammonium formate (10 mM) and formic acid (0.125%) and (B) acetonitrile:water (95:5, v/v) with ammonium formate (10 mM) and formic acid (0.125%). The separation was conducted under the following gradient: 0 min 100% B; 0–2 min 100% B; 2–7.7 min 70% B; 7.7–9.5 min 40% B; 9.5–10.25 min 30% B; 10.25–12.75 min 100% B; 12.75–17 min 100% B. The Thermo Q Exactive MS instrument was operated using ESI HILIC in positive mode with the following parameters: mass range, 60–900 m/z; sheath gas flow rate, 60; aux gas flow rate, 25; sweep gas flow rate, 2; spray voltage (kV) 3.6; capillary temp, 300°C; S-lens RF level, 50; aux gas heater temp, 370°C. Full MS parameters: microscans, 1; resolution, 60,000; AGC target, 1e6; maximum IT, 100ms; number of scans, 1; spectrum data type, centroid. Data dependent MS2 parameters: microscans, 1; resolution, 15,000; AGC target, 1e5; maximum IT, 50 ms; loop count, 4; multiplexing (MSX) count, 1; TopN, 4; isolation window, 1.0 m/z; isolation offset 0.0 m/z; (N)CE / stepped (N)CE, 20, 30, 40; spectrum data type, centroid.

DATA PROCESSING AND IDENTIFICATION

The LC-MS/MS data was analyzed using MS-DIAL software.²⁵ Detailed parameter settings are listed in Supplemental Tables 1 and 2 (HILIC and lipidomics data processing settings). Accurate masses, retention times, and peak heights were then exported, and further analysis was performed in R Studio and our in-house developed software for statistical analysis, Metabox.²⁶ Automated annotation of metabolites was performed separately for polar metabolites and lipids. Table 1 lists libraries, methods, and software used for each platform. Metabolite annotations were done with the help of our in-house developed library containing >600 authentic lipid standards of different classes and >800 standards of polar metabolites. Next, MS/MS database matching was performed with freely available MS/MS spectra obtained from Mass Bank of North America (MoNA), National Institute of Standard and Technology (NIST) 17, LipidBlast, and the NIST Hybrid Library.^{27–29} Workflow summarizing all the tools, software and databases are shown in Figure 5.

Figure 5. Workflow summarizing tools, software, and databases used for completing annotation of urine metabolome.



RESULTS AND DISCUSSION

m/z-RT and MS/MS databases

Untargeted lipidomics analysis in the positive ionization mode resulted in 112 identified lipids encompassing several lipid classes. The same sample set was also analyzed using HILIC chromatography. Using the established in-house library, we identified 117 metabolites, which consisted of amino acids, biogenic amines, and derivatives. These annotations are level 1 according to MSI, meaning that the experimental data was compared to authentic standards measured under the same instrumental conditions. Chemical standards (n= 874) were analyzed on two instrument types: quad time-of-flight (QToF) and orbitrap in positive ionization mode. These standards provide several orthogonal parameters: accurate mass (m/z), retention time (RT), and MS/MS. This level of annotation is laboratory/chromatography specific and is clearly a limitation if used exclusively. It takes both time and money to develop and establish such a chromatography. In our own experience, two skilled researchers require two years of work to create and validate a chromatographic run with 1000 metabolites measured on it robustly. It is a common practice in metabolomics research to use MS/MS libraries and perform mass spectral similarity searches in order to increase the annotation rate, as fragmentations are not chromatography specific. Those libraries contain mass spectra of authentic standards from a variety of instrumentation and chromatography (this metadata is available in .msp/.mgf formats), and this level of compound ID is described as level 2. Users can use freely available databases, such as MoNA, or can opt for

commercially available MS/MS databases such as NIST17. We combined two mass spectral databases, MoNA and NIST17, and used the merged .msp within MS-DIAL software for mass spectral similarity matching. Meta-data such as dot product, reverse dot product scores, number of matching ions, and MS-DIAL calculated MS2 similarity have been taken into account.

Table 1.

Chromatography and databases	Type of matching	MSI level of annotation	Number of annotations accomplished
HILIC	m/z, RT and MS/MS	1	117
Lipidomics	m/z, RT, MS/MS, in silico MS/MS	1	72
Lipidomics: CarniBlast	m/z , in silico MS/MS	2	18
HILIC: MoNA+NIST14	m/z and MS/MS	2	440
HILIC: CarniBlast	m/z and in silico MS/MS	2	107
Lipidomics: mzRT lookup	m/z	3	96
Hybrid search	MS/MS (hybrid)	3	Sample depending: 4000-8000
In silico fragmentation software: CSI:FingerID	MS1 and in silico MS/MS	3	Sample depending: 4000-8000

M/Z Lookup Table in LipidBlast

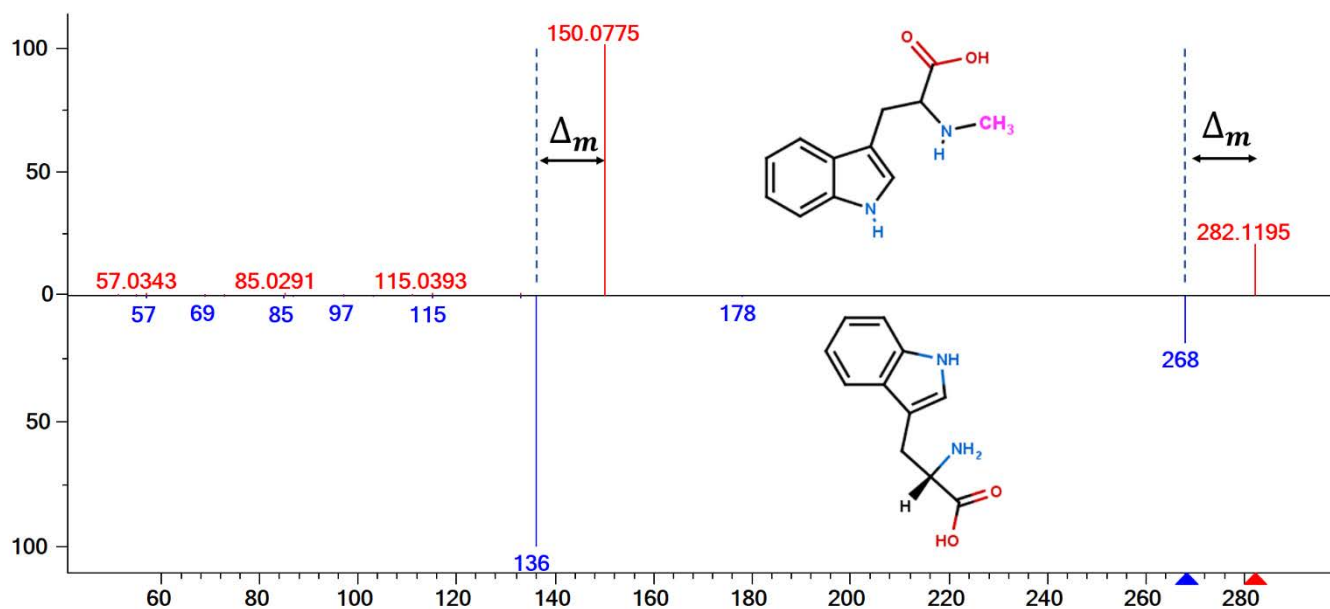
This essentially stand-alone tool can be used in addition to LipidBlast. It provides an automated approach for lipid annotations based on their accurate masses and/or chromatographic RT. Additional structure information of the lipids and their side chains (sn1, sn2, sn3) cannot be made using accurate mass alone. For comprehensive structure elucidation, another orthogonal parameter like MS/MS is needed. We extracted m/z precursor information from the MS-DIAL output in positive ionization mode and used the M/Z Lookup Macro to assign additional lipid annotations. Mass tolerance for lipid assignments was calculated based on the mass accuracy of the Thermo Q Exactive instrument and the internal standards, 0.005 Da. This way, an additional 96 lipid annotations were obtained from the lipidomics data set in positive ionization mode.

CarniBlast

The process of lipid degradation (β -oxidation) in human cells occurs in the mitochondria. This allows for the direct coupling of fatty acid degradation to energy generation via the citric acid cycle and respiratory electron transport chain localized in the inner mitochondrial membrane. For the corresponding import process, fatty acids of different chain lengths and saturation are esterified to L-carnitine with the formation of acylcarnitines.³⁰ L-carnitine can be *de novo* synthesized from *N*-trimethyl-lysine with butyrobetaine as an intermediate in a multi-step pathway. However, most carnitine comes from dietary intake. Fatty acids destined for degradation are first activated via thioesterification into coenzyme A (CoA). Then, three types of carnitine acyltransferases with different chain-length specificities (short, medium, long) transfer fatty acids via transesterification to carnitine with the release of CoA. These are carnitine acyltransferase, carnitine octanoyltransferase, and carnitine palmitoyltransferase. Next, a transport system consisting of carnitine palmitoyltransferase I (outer membrane), carnitine-acylcarnitine translocase, and carnitine palmitoyltransferase II (both inner membrane) transfer the acylcarnitines into the lumen of the mitochondria, where transesterification with CoA regenerates the acyl-CoAs and carnitine.^{31,32} Carnitine then leaves the mitochondria via the above outlined transport complex. During β -oxidation, the fatty acids are cleaved between C2 and C3 with the release of a C₂-unit of acetyl-CoA. A *trans*-2 double bond is formed between C2 and C3, hydrated, oxidized, and finally cleaved by the action of four enzymes. Odd chain and unsaturated fatty acids require additional enzymes.³³ The described overall process is an essential part of the lipid homeostasis which covers all fatty acids of different lengths and saturation. Consequently, diseases that disturb this described lipid homeostasis ultimately increase acylcarnitines in the blood and the urine. Therefore, acylcarnitines can be biomarkers for diseases, including heart failure³⁴, obesity and diabetes³⁵, chronic kidney disease³⁶, chronic psychiatric illness³⁷, migranes³⁸, and endometrial cancer.³⁹ Acylcarnitines in urine serve as biomarkers for bladder cancer⁴⁰, diabetic nephropathy⁴¹, obesity⁴² and human kidney cancer.⁴³ It is well documented that carnitine and its esters can be found in almost every bodily fluid, yet

the chemical standards are severely limited and/or nonexistent. To overcome this obstacle, we used an in-house developed *in silico* database of acylcarnitines as they, like many lipid species, fragment in a predictable manner. We exported the .msp files from both polar and lipidomics profiling and matched them against an *in silico* database of acylcarnitines. Some of the acylcarnitines were already present in our m/z-RT libraries, so using CarniBlast for the lipidomics .msp resulted in only three additional annotations. However, when HILIC .msp was used for the CarniBlast search, it resulted in an additional 793 annotations of acylcarnitines. This number suggests that there are far more carnitines present in urine than previous reports suggest.⁴⁴ This increase in annotation rates of acylcarnitines is important due to their role in lipid metabolism and various metabolic diseases. Interestingly, a majority of acylcarnitines couldn't be annotated with any other software or database.

Figure 6. Head-to-tail comparison of an MS/MS spectra of an amino acid shows distinct shift in the spectrum: methylated vs. non-methylated.

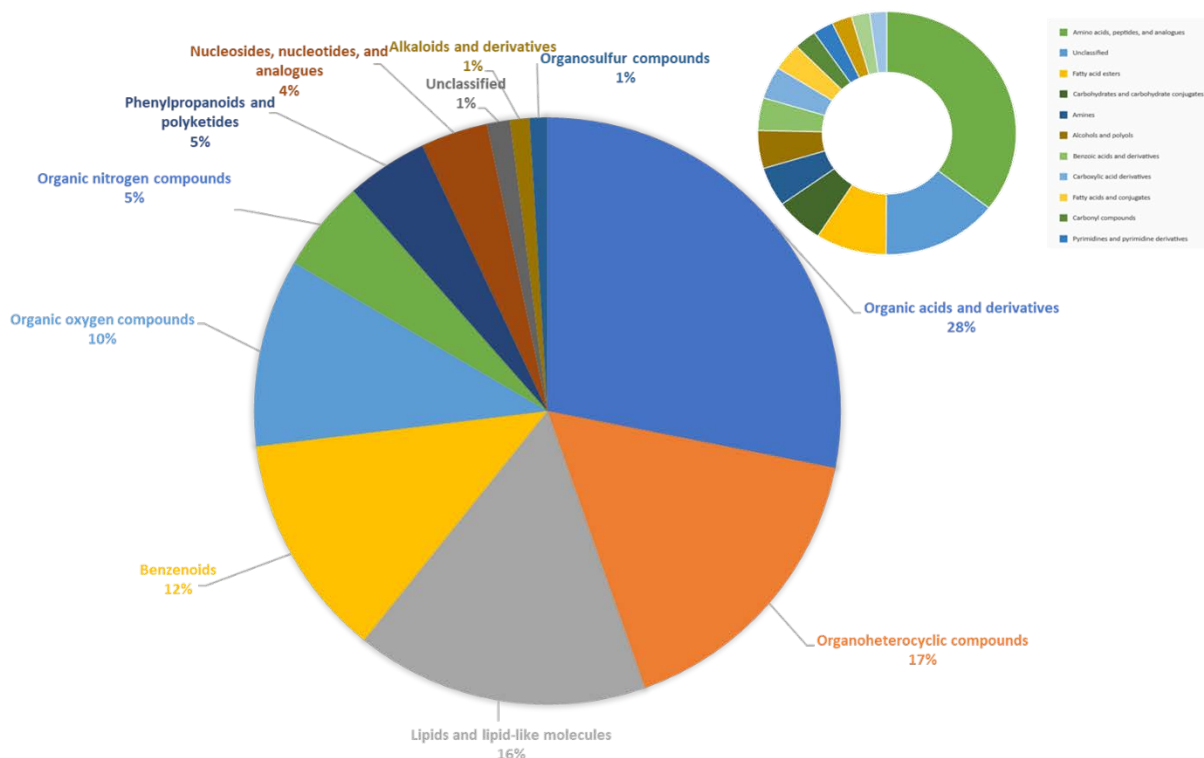


***In silico* fragmentation software**

For the compounds that are not present in our m/z-RT library and have collected MS/MS spectra that cannot be matched in mass spectral libraries, software tools, like MS-FINDER, Sirius, and CFM-ID, are of great value.⁴⁵⁻⁴⁷ We used the latest Sirius software with CSI:FingerID Interface (Sirius 4.0 built 19) to assign molecular identities to acquired MS/MS spectra.⁴⁸ We selected Sirius with CSI:FingerID because it has consistently scored very high during the latest Critical Assessment of Small Molecule Identification (CASMI) challenges. Furthermore, the current version has been improved in accuracy and speed. The MS/MS spectra were exported as a Mascot Generic Format (MGF) file from each raw file using the MSConvert. The MGF file largest in size contained the most MS/MS data and was therefore used for further analysis. A standard MGF file with 6482 MS/MS spectra was imported and 6447 features were available in the software. Formula assignment in positive ionization mode was performed with 10 ppm while retaining the 10 best formula candidates. Processing time was 2 minutes on a 16 CPU machine and the software was capable to assign formulas to a total of 6184 features. Fingerprint matching with CSI:FingerID via a webservice was subsequently performed to annotate isomer structures. Through this, 728 MS/MS peaks could be assigned when searching bio-databases and 1557 features could be assigned when querying the much larger PubChem database. The search time was around 5 minutes. The results, isomer structures, and their scores are presented in the Graphical User Interface (GUI) software. Additionally, results can be exported to CSV files. For the biodatabase search, up to 130 results were obtained per MS/MS scan, while the PubChem fingerprint research resulted in up to 10,000 candidates per MS/MS spectrum searched. Here individual and time-consuming investigations have to be performed to investigate the correctness of the found structures. In order to show the accuracy of CSI:FingerID we also performed a search on compounds that were annotated by our in-house database. Sirius 4.0 and CSI:FingerID with 5ppm mass accuracy and search in bio-databases correctly identified 41 compounds as a top hit. Approximately 52% of the

known compounds were correctly assigned within the top 3. The median rank for all 103 compounds was one and the average rank ten. Considering its excellent search speed and accuracy, CSI:FingerID should be considered a useful annotation tool for the identification of unknown compounds. The associated results can be found in the supplement. In our previous work, we have shown that it is possible to combine the outputs (results) of multiple software to create a new ranking system based on the accuracy of each software and rank the correct structure as the top hit in 93% of the cases.⁴⁹ However, this approach is not easily applicable as it requires both compound database boosting as well as thorough software comparison for the defined sample set.

Figure 7. Structural classification of metabolites present in the urine of 12 patients diagnosed with IC



NIST Hybrid search coupled with ClassyFire

Epimetabolites are defined as regulatory metabolites that have been removed from their classical functions by modification (for example, methylation or acetylation) but often remain chemically similar to their canonical counterparts.⁵⁰ NIST recently introduced a fantastic mass spectral library-based method to annotate MS/MS spectra that contain the aforementioned modifications. It is described as a “hybrid” method because it combines matching fragments but not the m/z of the precursor (to allow for modification calculations that are then reflected).⁵¹ Such a tool is of great assistance in structure elucidation of unknown metabolites, as it mimics the knowledge and experience of a well-trained chemist.⁵² The hybrid search comparison is shown in Figure 2, where the head-to-tail comparison of an amino acid shows a distinct shift in the spectrum, methylated versus non-methylated. We exported the .msp files from MS-DIAL to the NIST pepSearch GUI, activated the hybrid search function, and ran it against the MS/MS hybrid libraries. As a result of the hybrid search, every MS/MS spectra are now associated with an annotation and a variety of scores. Results of the hybrid search for both HILIC and CSH data are presented in Supplemental Table 5. The advantage of using NIST Hybrid search is that it supports batch processing, offers restrictions in terms of which MS/MS spectra should be included or excluded, and allows users to quickly get a snapshot of the metabolome they are measuring. The result list contains a lot of meta-data, such as chemical name, International Chemical Identifier (InChI) key, simplified molecular-input line-entry system (SMILES), probability score, etc. Those annotations should be treated with caution as they do not represent an identification but rather a “nearest known neighbor” to the unknown molecule. Next, the result list of NIST hybrid search was coupled with a fully automated, comprehensive chemical classification tool that utilizes a well-defined chemical hierarchy system - ClassyFire. ClassyFire successfully annotated and classified

thousands of molecules from various libraries, including DrugBank, LIPID MAPS, HMDB, ChEBI, and PubChem.⁵³ We used ClassyFire Batch by Fiehn Lab (<http://cfb.fiehnlab.ucdavis.edu/>), a user-friendly web application capable of batch classifications directly from InChIKeys.

Figure 7 shows complexity of urine metabolome based on the superclass and subclass classifications as defined by Classyfire. Results of classifications are organized into Kingdom, Superclass, Class, Subclass, and two parent levels. Subsets of those results is shown in Supplemental Table 6. We can imagine that such combinatorial approach becomes of importance in personalized medicine or health research in general, since it is evident from Supplemental Tables that the metabolic profile of urine varies from patient to patient. While biomarker discovery focuses on the shared metabolites between patients, it is also important to recognize and investigate differences due to diet, exposure, genetics, and other factors.

Summary

Metabolomics reports and data should be annotated with confidence levels for clarity and reproducibility purposes. Sharing the MS/MS data with the community will directly improve not only other researchers' work but will also help the development of tools that aid structure elucidation process. Hopefully this work provides a comprehensive overview of some of the best freely available tools and databases for metabolomics research and will be of use to analysts when annotating unknown metabolites.

Caffeine-perturbed proteomic profiles in normal bladder epithelial cells

It is estimated that by the end of 2018, 2.3 billion individuals will be affected by at least one lower urinary tract symptom (LUTS)⁵⁴. These symptoms include urinary storage problems, such as urgency, frequency, nocturia, or voiding problems. LUTS also weighs heavily on overall quality of life; patients report significantly higher mental health issues, lower work productivity, and diminished general health status⁵⁵. The current standard treatment for LUTS involves α -blockers, 5 α -reductase inhibitors, and antimuscarinics⁵⁶. However, these are mainly palliative and require consistent maintenance. Consequently, there is a substantial economic burden associated with LUTS⁵⁷.

Previous reports have demonstrated that diet and stress play important factors in the development and progression of LUTS⁵⁸. In particular, caffeine, a naturally occurring compound, has been reported to be a potential dietary risk factor in developing LUTS⁵⁹. Caffeine is ubiquitously found in many plants, including cocoa beans, tea leaves, and coffee beans. It is a stimulatory drug that is widely used to prevent sleepiness and can be found in over-the-counter medications, such as some pain remedies. It has also been observed that caffeine may aggravate or worsen urinary symptoms in patients who already have some form of LUTS⁶⁰. In recent years, caffeinated drinks have become a staple of the average diet; more than 85% of adults in the U.S. regularly consume caffeine⁶¹. A longitudinal study of caffeine intake in young healthy volunteers found that subjects who regularly drank coffee had significant increases in urinary urgency and frequency⁶². Additionally, a separate study observed that greater coffee intake raised the odds of LUTS progression in men and women more than carbonated or citrus beverages⁶³. The effects of caffeine have also been studied in the context of bladder cancer (BC); however, rather than finding a negative risk, there have been reported benefits. A case-control study of BC patients in Italy found no causal relationship between caffeine and BC⁶⁴. A separate study found that caffeine may actually benefit BC patients by making cells more susceptible to chemotherapy and apoptosis⁶⁵. Mechanistically, this has been reported to be mediated through caffeine's effects on the tumor suppressor protein, p53⁶⁶.

Despite the potential link between caffeine and LUTS, research into causative mechanisms and functions is lacking. One prior study suggested that caffeine may be facilitating bladder instability and frequent urination by enhancing the activation of neuronal micturition centers through increased expression of transcription factor c-Fos and nerve growth factor⁶⁷. While informative, this study focused primarily on the bladder muscles with little attention on the bladder epithelium, which is more anatomically exposed to urine and its biological/chemical contents. A separate study using a mouse model found that oral caffeine administration resulted in detrusor overactivity and increased bladder sensory signaling⁶⁸. Further studies found similar effects on the detrusor

muscle in humans⁶⁹. However, the direct effects of caffeine, its delivery into cells, and its mechanisms remain unestablished.

Our present study sought to examine the cellular effects of caffeine on the bladder epithelium without any pathological conditions. Quantitative and global proteomics analysis found that caffeine can perturb the whole proteome, possibly through the regulation of chromatin assembly in normal bladder epithelial cells.

Quantitative proteomic analysis of normal bladder epithelial cells

Due to the lack of knowledge regarding the effects of caffeine on biological and proteomic perturbations in the normal bladder epithelium, this study aimed to examine the whole proteome alterations caused by caffeine consumption. To gain insight on the underlying mechanism of caffeine on the bladder epithelium, we treated normal bladder epithelial cells with caffeine and performed tandem mass tag (TMT)-based quantitative proteomic analysis, as outlined in **Figure 8**.

Based on previous literature, we opted to use caffeine concentrations within normal physiological consumption^{65,70}. Whole-cell lysates in biological duplicates were digested with trypsin. Using LC-MS/MS followed by bioinformatic analyses, we identified 44,597 peptides corresponding to 5,832 proteins with more than 2 peptides in more than two sets of pooled lysates from at least three biological samples per condition. The caffeine-treated group had 5,821 identified proteins with high expression, while the control group had 5,808. We then performed functional categorization of the proteins to check whether our quantitative proteomic analysis was biased by any cellular compartments or biological process-related proteins using Panther software⁷¹. All the identified proteins can be categorized into 14 cellular processes, including cellular process, metabolic process, cellular component organization of biogenesis, localization, biological regulation, response to stimulus, developmental process, multicellular organismal process, biological adhesion, immune system process, locomotion, reproduction, growth, and cell killing, indicating that this proteome reveals major biological functions of bladder epithelial cells in normal physiology. In addition to this, we examined the cellular localization of the detected proteins, which showed the significant enrichment of 8 cellular compartments, including cell part, organelle, macromolecular complex, membrane, extracellular region, cell junction, synapse, and extracellular matrix. **Collectively**, our quantitative proteomic analysis identified a comprehensive list of proteins in all cellular components and illustrated the cellular functions of highly expressed proteins in normal bladder epithelial cells.

Figure 8. Unbiased proteomics analysis identified proteins in TRT-HU1 cells. Experimental scheme describing unbiased global proteomics profiling and bioinformatics analysis.

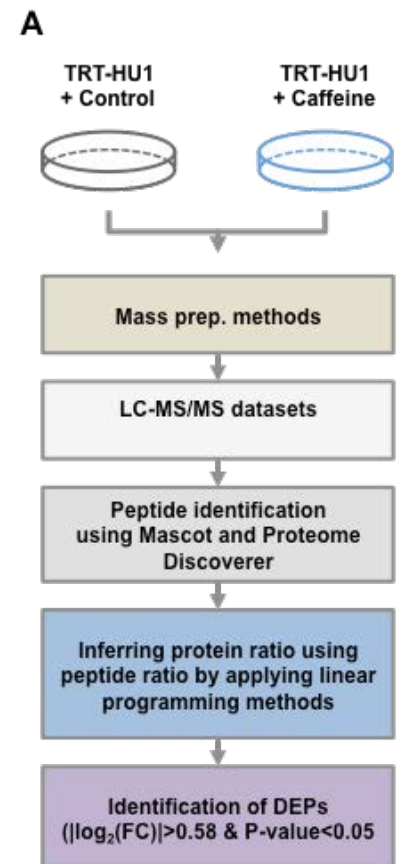


Table 2. List of upregulated proteins in bladder epithelial cells perturbed by caffeine treatment.

Symbol	Full name	Fold change (log2)	P-value
S100A8	S100 calcium binding protein A8	4.17759	0.000112
ST13	ST13, Hsp70 interacting protein	3.918705	0.000224
SERPINB3	serpin family B member 3	3.553147	0.000559
SERPINB4	serpin family B member 4	3.553147	0.000559
WASH3P	WAS protein family homolog 3 pseudogene	2.327444	0.001342
POTEKP	POTE ankyrin domain family member K, pseudogene	2.210099	0.001565
RBMS1	RNA binding motif single stranded interacting protein 1	2.032904	0.001789
KPRP	keratinocyte proline rich protein	1.526693	0.002124
S100A7	S100 calcium binding protein A7	1.4274	0.002236

TGM1	transglutaminase 1	1.214751	0.002572
MYH7B	myosin heavy chain 7B	0.970592	0.003131
MYH3	myosin heavy chain 3	0.970592	0.003131
MYH1	myosin heavy chain 1	0.970592	0.003131
MYH7	myosin heavy chain 7	0.970592	0.003131
MYH8	myosin heavy chain 8	0.970592	0.003131
MYH2	myosin heavy chain 2	0.970592	0.003131
MYH13	myosin heavy chain 13	0.970592	0.003131
MYH4	myosin heavy chain 4	0.970592	0.003131
MYH7B	myosin heavy chain 7B	0.970537	0.004025
MYH3	myosin heavy chain 3	0.970537	0.004025
MYH1	myosin heavy chain 1	0.970537	0.004025
MYH7	myosin heavy chain 7	0.970537	0.004025
MYH8	myosin heavy chain 8	0.970537	0.004025
MYH2	myosin heavy chain 2	0.970537	0.004025
MYH13	myosin heavy chain 13	0.970537	0.004025
MYH4	myosin heavy chain 4	0.970537	0.004025
H2BFS	H2B histone family member S	0.895712	0.005255
S100A9	S100 calcium binding protein A9	0.871394	0.005367
UVRAG	UV radiation resistance associated	0.738812	0.00559
SULT1A4	sulfotransferase family 1A member 4	0.665067	0.005814
SULT1A1	sulfotransferase family 1A member 1	0.665067	0.005814
UCHL1	ubiquitin C-terminal hydrolase L1	0.622981	0.006261
MAGI3	membrane associated guanylate kinase, WW and PDZ domain containing 3	0.615023	0.006373
KRT74	keratin 74	0.598941	0.006485
KRT73	keratin 73	0.598941	0.006485
ACTA2	actin, alpha 2, smooth muscle, aorta	0.598824	0.006708
LRRRC8E	leucine rich repeat containing 8 VRAC subunit E	0.594574	0.00682
KRT74	keratin 74	0.594473	0.006932
KRT73	keratin 73	0.594473	0.006932
KRT74	keratin 74	0.594472	0.007156
KRT73	keratin 73	0.594472	0.007156
FLCN	folliculin	0.592834	0.007379
KRT74	keratin 74	0.589943	0.007491
KRT73	keratin 73	0.589943	0.007491
CPNE6	copine 6	0.587267	0.007715
CPNE4	copine 4	0.587267	0.007715

Whole proteome in bladder epithelial cells perturbed by caffeine treatment. We determined which proteins were differentially expressed after caffeine treatment. Differentially expressed proteins (DEPs) were selected for if they had an absolute \log_2 fold-change greater than 0.58 and p-value less than 0.05. In total, we identified 32 upregulated and 25 downregulated proteins between the control vs. caffeine groups (**Table 2**). As shown in the volcano plot, some DEPs, including PSMC6 (proteasome 26S subunit ATPase 6), RUFY1 (RUN and FYVE domain containing 1), IARS (isoleucyl-tRNA synthetase), MCU (mitochondrial calcium uniporter), NAV1 (neuron navigator 1), RARG (retinoic acid receptor, gamma), and etc, significantly increased with caffeine treatment, while ST13P4 (ST13, Hsp70 interacting protein pseudogene 4), EIF5AL1 (eukaryotic translation initiation factor 5A-like 1), WASH2P (WAS protein family homolog 2 pseudogene), RBMS3 (RNA binding motif single stranded interacting protein 3), and etc. decreased.

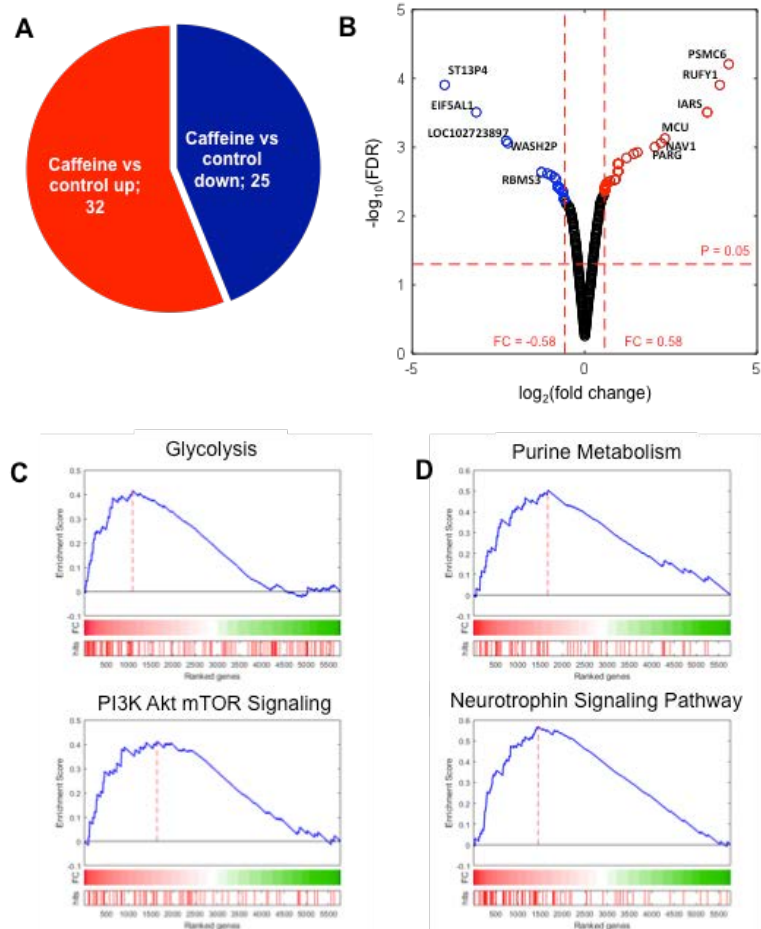
Next, to understand the function of the perturbed proteins, we performed gene set enrichment analysis (GSEA) using the hallmark gene sets from the Molecular Signature Database (MSigDB)⁷². As a result, we found that the “glycolysis” and “PI3K/AKT/MTOR” signaling gene sets were significantly enriched for DEGs due to caffeine treatment (**Figure 9**). We also checked the enrichment of Kyoto Encyclopedia of Genes and Genomes (KEGG) pathways in the same context and found that the “neurotrophin signaling pathway” and “purine metabolism” were significantly enriched for in the caffeine-treated condition (**Figure 9**). These results suggest that caffeine may be stimulating the bladder epithelium by altering the activation of the PI3K/AKT/MTOR pathway, neurotrophin signaling, and purine metabolism.

For this, we conducted separate functional enrichment analyses on each of the 32 up- and 25 downregulated proteins using DAVID¹³. The results suggest that upregulated DEPs were significantly enriched for “actin-myosin filament sliding”, “muscle contraction”, “purine nucleotide metabolic process”, “ATP metabolic process”, “autophagy”, “response to external biotic stimulus”, and “response to other organism”. Downregulated DEPs were significantly enriched for “chromatin assembly”, “DNA packaging”, and “cellular macromolecular complex assembly” (**Figure 10A**). We extracted a list of the significantly upregulated DEPs belonging to “purine nucleotide metabolic process”, “autophagy”, “muscle contraction”, “response to external biotic stimulus”, and “chromatin assembly”. For the downregulated DEPs, we extracted those belonging to “chromatin assembly” (**Figure 10B and 10C**).

Summary

The aim of this study was to evaluate if caffeine consumption is associated with changes to protein expression in the normal bladder using semi-quantitative proteomic analysis. Although there are some reports about anti-lipid accumulation via gene expression suppression of proliferator activated receptor (PPAR) γ and CCAAT/enhancer binding protein (C/EBP) α in 3T3-L1 adipocytes⁷³, or apoptosis induction in various cell lines, the direct effects of caffeine on the bladder remains elusive. Although the amount of caffeine in a cup of coffee varies, it is typically 300-600 mg. Using caffeine levels equivalent to 1-2 cups of coffee, we treated bladder epithelial cells and performed unbiased proteomic analysis using LC-MS/MS. Through this, we identified 32 upregulated and 25 downregulated DEPs (\log_2 fold-change > 0.58; p-value < 0.05). These DEPs were enriched for functions such as actin-myosin filament sliding, muscle contraction, and chromatin assembly. Alterations to the cytoskeleton and the proteins that interact with it have been linked to a wide range of diseases⁷⁴. Caffeine

Figure 9. Differentially expressed proteins (DEPs) perturbed by caffeine treatment. (A) Pie chart showing the DEPs in presence of caffeine. (B) A volcano plot showing the up- or downregulated DEPs due to caffeine in bladder epithelial cells. Up- or down-regulated DEPs are marked as red or blue dot. (C) Enriched biological processes and cellular compartment of the DEPs. (D) Bar plot depicts enrichment of KEGG pathways by DEPs.



has similar actions with AMP-activated protein kinase (AMPK), an enzyme whose roles include contraction during energy deprivation in skeletal muscles⁷⁵. Among the proteins involved in the enriched cellular functions, ACTG2, also known as alpha smooth muscle actin, is associated with multiple functions in cell motility, structure, integrity, and intercellular signaling⁷⁶. However, caffeine did not change any of the muscle associated stabilizing proteins which regulate the number, or the length, of microtubules⁷⁷. This suggests that increased expression of ACTG2 by caffeine in the bladder may enhance the contractility of bladder and may also be associated with urinary symptoms. Our experimental data suggested that these proteins, such as ACTG2 and HIST1H2BM, become more redundant in bladder epithelial cells upon exposure to caffeine. Although the function of HIST1H2BM as a regulator of caffeine and its effects has not been studied thoroughly, it is originally known to be associated with epigenetic regulation in response to DNA methylation⁷⁸.

Figure 10. Differential enrichment of cellular processes by up- and downregulated proteins perturbed by caffeine. (A) Bar plot showing enriched cellular processes in up- or downregulated DEPs. **(B)** List of proteins involved in the enriched cellular processed by upregulated DEPs. Proteins reported with cancer are in bold. **(C)** List of proteins involved in the enriched cellular processed by downregulated DEPs.

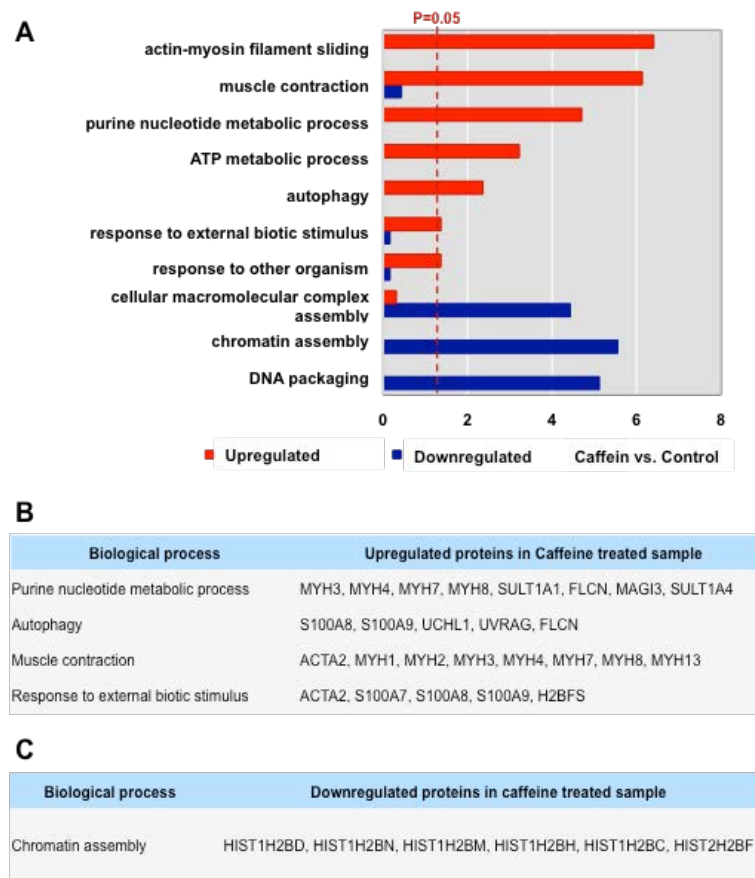


Table 3. List of downregulated proteins in bladder epithelial cells treated with caffeine.

Symbol	Full name	Fold-change (log2)	P-value
ST13P4	ST13, Hsp70 interacting protein pseudogene 4	-4.06184	0.000224
EIF5AL1	eukaryotic translation initiation factor 5A-like 1	-3.14456	0.000559
LOC102723897-		-2.27955	0.001453

WASH2P	WAS protein family homolog 2 pseudogene	-2.27955	0.001453
RBMS3	RNA binding motif single stranded interacting protein 3	-2.22487	0.001565
POTEI	POTE ankyrin domain family member I	-1.25276	0.004137
POTEJ	POTE ankyrin domain family member J	-1.25276	0.004137
HIST1H2BM	histone cluster 1 H2B family member m	-1.07852	0.00436
DES	desmin	-0.97497	0.004584
TENM1	teneurin transmembrane protein 1	-0.87939	0.004919
ACTG2	actin, gamma 2, smooth muscle, enteric	-0.82627	0.005255
HIST1H2BD	histone cluster 1 H2B family member d	-0.78302	0.006708
HIST1H2BC	histone cluster 1 H2B family member c	-0.78302	0.006708
HIST2H2BF	histone cluster 2 H2B family member f	-0.78302	0.006708
HIST1H2BH	histone cluster 1 H2B family member h	-0.78302	0.006708
HIST1H2BN	histone cluster 1 H2B family member n	-0.78302	0.006708
RPL29	ribosomal protein L29	-0.73583	0.007044
RNF175	ring finger protein 175	-0.71108	0.007267
TFAP2B	transcription factor AP-2 beta	-0.65122	0.007715
DLG2	discs large MAGUK scaffold protein 2	-0.64864	0.007826
RAB3A	RAB3A, member RAS oncogene family	-0.62645	0.00805
ZDHC13	zinc finger DHC-type containing 13	-0.60304	0.009951
EPHA6	EPH receptor A6	-0.60218	0.010063
PRC1	protein regulator of cytokinesis 1	-0.59503	0.010174
MRPL34	mitochondrial ribosomal protein L34	-0.5944	0.010286

Urinary menthol suppresses chronic inflammation in the bladder

Urine has long been one of the most uninvestigated biomarker sources for IC. Previous studies of urine have mainly focused on its chemical composition, as opposed to its metabolic properties, as indicative sources for medical disorders ⁷⁹. Urine is an extremely important biological fluid that is secreted from the kidneys. Urination is the primary route through which the body eliminates water-soluble waste products. The resulting urine contains the expression of many metabolites, such as urea (from amino acid metabolism), inorganic salts (chloride, sodium, and potassium), creatinine, ammonia, organic acids, various water-soluble toxins, and pigmented products of hemoglobin breakdown, including urobilin – which gives urine its characteristic color. Collection of urine is also simpler and provides a relatively larger volume of sample compared to other biological fluids. Although the complexity of sources within metabolites creates many obstacles in urine analysis, progress in the field has been promising and this may ultimately prove to be tremendously beneficial.

Odor consists of various volatile organic chemical compounds (VOCs), which can be identified through mass spectrometry. VOCs generally have a relatively lower molecular weight and higher vapor pressure. For cancer detection, there have been several studies on using gas chromatography mass spectrometry (GC-MS) for detecting odor in skin, tissue, breath, feces, and bodily fluids, such as urine and sweat ⁸⁰. Several previous studies showed that well-trained dogs are capable of detecting specific VOCs and were able to classify cancer patients from healthy controls ⁸¹⁻⁸³. For instance, VOCs from urine can be used to assist in the diagnosis of lung cancer ⁸⁴. Electronic noses capable of detecting odor signatures have been developed and successfully applied in discriminating prostate cancer patients from normal control ^{83,85}. In general, urinary symptoms, such as incontinence and urgency, have a negative impact on women's sexual life. This is mainly due to urinary odor and leakage ⁸⁶. A significantly common issue among IC patients is a foul urine odor. Given our previous findings that IC patients may have a distinct metabolism ^{87,88}, we hypothesized that the urine from IC patients may contain a distinguishing VOC profile and volatile odor signature reflective of disease condition.

In our present volatolomic study, we tested the hypothesis that urinary volatiles differ between IC patients and healthy controls. We analyzed VOCs obtained from the urine headspace and extracted them via solid-phase micro-extraction (SPME). GC-MS analysis was employed to profile samples of patients with IC symptoms from

those who did not have any urinary pain symptoms. The aim of this study was to identify IC-associated VOCs and further analyze their biological meaning in the bladder epithelium. Using comprehensive and unbiased metabolomics analysis, we found menthol as a novel compound involved in IC inflammation. Our analysis found that urinary menthol is decreased in the urine specimens of IC patients and that these reduced levels are potentially linked to chronic inflammation, a symptom that is commonly observed in IC.

Subjects and Urine Specimen Collection.

Patients and healthy control subjects were recruited from an outpatient urology clinic at Inha University Hospital. All subjects were Asian females. Subjects were instructed to avoid tobacco, nicotine, chemical compounds, alcohol, herbal foods, caffeine, and medication 24 hrs before their urine collection. Recruitment was conducted following the National Institute of Diabetes and Digestive and Kidney Diseases (NIDDK) guidelines. Workup included symptom assessment, cystoscopic evaluation, physical examination, urodynamics, and/or urine culture. Patients with a history of other diseases, including cancer, chronic inflammation, diabetes, et al., were excluded.

To minimize possible contamination with vaginal, rectal, or urethral cells, first morning urine specimens were obtained using clean catch methods in a sterile environment. The de-identified specimens were sent to laboratory and were centrifuged for 10 minutes to remove cell debris. Urine supernatants were then processed into individual aliquots, and stored in 15 ml tubes at -80°C until further analysis.

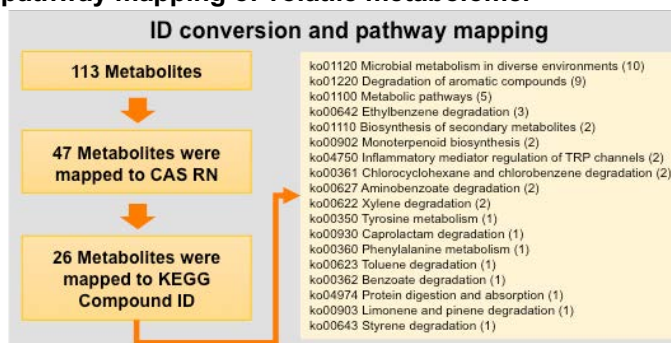
Volatile metabolomics profile reveals menthol levels are significantly reduced in urine specimens derived from interstitial cystitis patients compared to healthy controls. We sought to determine the volatile urinary odor composition by performing volatile metabolite profiling through SPME-GC-TOF-MS using healthy and IC urine samples. We used fatty acid methyl esters (FAMES) as internal standards for quality control (including injections) and for retention index corrections. The procedure used for untargeted profiling of urine headspace volatiles was based on the method developed by Robinson⁸⁹. From the raw data, automatic peak detection and deconvolution were conducted using ChromaTOF software.

After data cleaning and pre-processing, a total of 113 peaks were identified and quality assessment of quantification result was done after quantile normalization⁹² (Supplementary Figure 1). Peak intensities were summed for all identified metabolites (mTIC). Each peak was then normalized to the sample's total volatile metabolome.

We then investigated association of these peaks with known metabolic pathways. For this, we first selected 47 peaks annotated with a CAS registry number and then identified 26 peaks that can be mapped to at least one KEGG Compound ID. Using DAVID software¹³, we found that 26 metabolites are associated with 26 pathways as shown in Figure 11. We next performed differential analysis to identify significantly altered metabolites between IC patients and healthy controls. 76 peaks with quantification of more than half of the samples in each condition were included for this hypothesis testing, resulting in 12 peaks identified with a $\text{FDR} < 0.1$. FDR was calculated using the integrated hypothesis testing method⁹⁰. Among them, menthol (CAS RN: 89-78-1) was identified as significantly different between healthy control and IC urine samples with a $\text{FDR} = 0.024$ and \log_2 fold-change = -1.467. We only observed authentic volatile compounds, not chemicals or metabolites that could come from degradation processes.

Given the lower menthol levels in IC urine and prior knowledge from literature, we speculated that reduced levels of menthol may influence bladder health. Our hypothesis was that the urine of IC patients contains reduced levels of anti-inflammatory metabolites, particularly menthol, which leads to increased IC-associated cytokines. To test this hypothesis, we sought to evaluate whether the anti-inflammatory effect of menthol can suppress lipopolysaccharide (LPS)-induced inflammation events in immune cells. In order to determine the biological

Figure 11. Analysis workflow of ID conversion and pathway mapping of volatile metabolome.

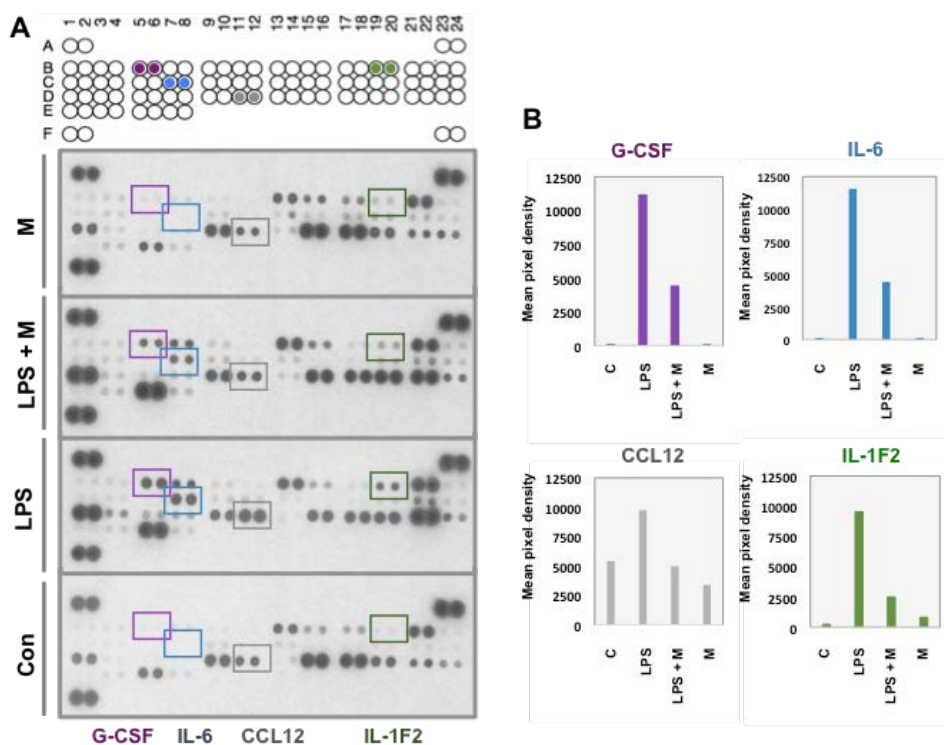


effects of menthol on inflammation, we decided to use two independent approaches: (i) mesoscale cytokine profiling, and (ii) gene expression microarray analysis.

In order to characterize the effect of menthol on macrophages, comprehensive microarray analysis was conducted on mouse RAW 264.7 macrophage cells. Cells were treated with menthol or control vehicle for 1 hr. The macrophages were stimulated with LPS treatment (100ng/ml) for the following 6 hrs. Three groups of gene expression profiles were defined: control vs menthol (C vs M), control vs LPS (C vs LPS) and menthol vs LPS (M vs LPS).

Cytokine profiling revealed that menthol down-regulated the LPS-induced production of inflammatory cytokines in RAW 264.7 cells

Figure 12. Reduced production of LPS-induced inflammatory cytokines by menthol in RAW 264.7 cells (cell lysates) (A) Inflammatory cytokine array analysis of CCL3, CXCL10 and TNF- α . The expression of these inflammatory cytokines is highly induced by LPS, but down-regulated by menthol. (B) Quantification of array band intensity of CCL3, CXCL10 and TNF- α with image-analysis software.

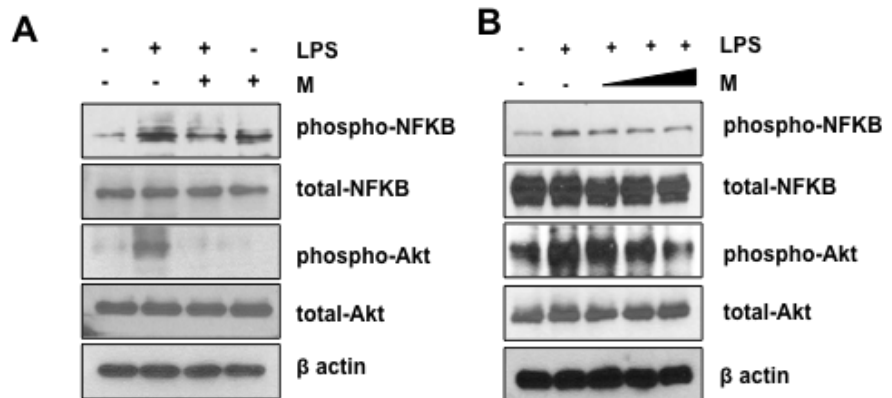


An inflammatory cytokine array was used to identify the specific cytokines that were produced and secreted into the conditioned surrounding medium by the RAW 264.7 macrophage cells. To determine whether the presence of menthol inhibits the production and release of inflammatory cytokines, RAW 264.7 cells were treated with LPS (100 ng/mL) with or without menthol (500 μ mol/mL) for 6 hrs. Cells were pretreated with menthol or control (vehicle only) for 1 hr and by induced with LPS (100ng/ml) for 6 hrs after. The expression of each inflammatory cytokine was subsequently measured. The cytokine profiler data showed that a series of cytokines, including C-C motif chemokine ligand 3 (CCL3), C-X-C motif chemokine ligand 10 (CXCL10), and tumor necrosis factor alpha (TNF- α), were induced by LPS treatment (Figure 12A, LPS condition). The addition of menthol significantly downregulated the production of CCL3, CXCL10, and TNF- α , compared to just LPS alone (Figure 12A, LPS +M compared to LPS). In figure 12B, ImageJ analysis software was used to measure values from scan dots according to the intensity of the cytokine array panel. This data suggests that menthol is involved in downregulating the LPS-induced production of inflammatory cytokines in macrophages.

Signaling pathways involved in anti-inflammatory effect of menthol

We next speculated that the specific signaling pathways involved in LPS-stimulated cytokine perturbation are modulated by menthol treatment. To determine the signaling pathways associated with the production and secretion of inflammatory cytokines, we screened the activation of key signaling pathways, which include nuclear factor- κ B (NF- κ B), Akt, and other main MAPK pathways. The presence of LPS induced phosphorylation of NF- κ B and Akt in RAW 264.7 macrophages. The phosphorylation levels of NF- κ B and Akt, but not those of Erk1/2 (data were not shown), were significantly attenuated by menthol pretreatment (LPS+M compared to LPS) (Figure 13A). LPS-induced phosphorylation of NF- κ B and Akt was significantly reduced by menthol treatment in a dose-dependent manner (Figure 13B). This data suggests that menthol inhibits LPS-induced inflammatory cytokines via the Akt-NF- κ B signaling pathway.

Figure 13. Anti-inflammatory effects of menthol are mediated via the Akt-NF- κ B pathway. (A) Phosphorylation levels of NF- κ B and Akt were reduced by menthol treatment. (B) Phosphorylation of NF- κ B and Akt were suppressed by menthol treatment in dose-dependent manner. β -actin was used as the loading control in western blot analysis.



Sexual Pain and IC/BPS in Women

Female sexual dysfunction (FSD) and interstitial cystitis/bladder pain syndrome (IC/BPS) are important factors affecting women's health. A study conducted on the association between sexual and general well-being found that women reported better quality of life (QoL) with higher sexual satisfaction, regardless of age and/or menopausal status.¹ Both FSD and IC/BPS significantly impairs women's abilities to pursue and enjoy sexual relations. Approximately 40-50% of women experience FSD and 0.5-12% experience IC/BPS. Considering these incidence rates in the general population, both these diseases become serious challenges for patients and clinicians.²⁻⁶

Chronic pain deteriorates not only personal health and wellness, but also quality of life. Chronic pain can induce sexual dysfunction, such as arousal disorder and relationship problems.⁷ Furthermore, studies have shown that significantly more women with chronic pelvic pain (CPP) showed FSD compared to those without CPP. Women with CPP and FSD had various types of FSD, such as hypoactive sexual desire disorder, sexual arousal disorder, orgasmic disorder, and sexual pain disorder.⁸

The symptoms of IC/BPS, such as urinary frequency, urgency, and pelvic pain, have a negative impact on sexual activity and life quality.⁹ Women with overactive bladder (OAB) frequently have a risk for sexual dysfunction.¹⁰ In the postmenopausal group, women with scores indicating severe OAB had worse sexual function, mainly in the arousal, lubrication, orgasm, pain, and total domains.¹¹ Despite the known association of sexual dysfunction with bladder diseases, contributing risk factors have yet to be explored. Evaluating the impact of duration, severity, pain localization, sexual trauma history, anxiety, and depression on sexual dysfunction may help elucidate risk factors. Increasing our knowledge about sexual dysfunction as it relates to bladder diseases may aid in clinical diagnoses and play a major role in treatment strategies and overall symptom improvement in this patient population. This review will provide an overview of studies that address FSD in women with IC/BPS.

PAIN IN FSD

FSD is classified as hypoactive sexual desire dysfunction, female sexual arousal dysfunction, female orgasmic dysfunction, female-genital-pelvic pain dysfunction, persistent genital arousal disorder, postcoital syndrome, hypohedonic orgasm, or painful orgasm through consensus by the 4th International Consultation on Sexual Medicine (ICSM).^{2, 12} Guidelines from the 4th ICSM defines pain-associated FSD as female-genital-pelvic pain dysfunction and includes all conditions that inhibit sexual intercourse and induce negative effects on sexual functions. Female-genital-pelvic pain dysfunction is different from the previous classification noted pain associated with FSD as sexual pain disorder including dyspareunia and vaginismus.¹³ In the 4th ICSM, female-genital-pelvic pain dysfunction includes persistent or recurrent difficulties with at least one of the following: (1) vaginal penetration during intercourse, (2) marked vulvovaginal or pelvic pain during genital contact, (3) marked fear or anxiety about vulvovaginal or pelvic pain in anticipation of, during, or as a result of genital contact, or (4) marked hypertonicity or overactivity of pelvic floor muscles with or without genital contact.¹⁴ Painful orgasm is also considered and means the occurrence of genital and/or pelvic pain during or shortly after orgasm.² These recent new definitions reflect the evolving concept behind pain-associated FSD as it also now includes pain in the vulvovaginal and pelvic area and pelvic floor hypertonicity. The new categorization of female-genital-pelvic pain dysfunction has broadened the view on pain-associated FSD and has differentiated it from its previous classification that confined symptoms to each organ or single disease. This recent change in classification by the ICSM considers pain-associated FSD as a complex condition influenced by psychological and physical factors and supports the general thought that FSD is multifactorial.

Previously, vulvodynia had been generalized under chronic vulvar pain and there was no precise discrimination for it. However, recent consensus has redefined chronic vulvar pain as vulvar pain associated with specific diseases, such as inflammation, neoplasm, and/or injury. This was conducted at a conference with the International Society for the Study of Vulvovaginal Disease, the International Society for the Study of Women's Sexual Health, and the International Pelvic Pain Society.¹⁵ Vulvodynia is reported with diverse pain characteristics; therefore, pain-based classification helps in identification, diagnosis, and treatment. Vulvodynia can be characterized as either general (entire vulva) or localized (parts of the vulva) according to the location of pain. Additionally, based on the situation of the pain, vulvodynia can be classified as either provoked (triggered by physical contact) or unprovoked (spontaneous occurrence without specific triggers).¹⁶ Women of all ages can experience vulvodynia and provoked vulvodynia is the most commonly diagnosed.^{17,18} Provoked vulvodynia is thought to be more widely diagnosed than unprovoked because its symptoms can be better recognized by doctors. Therefore, there is an important need to better identify these patients.

SEXUAL PAIN AND IC/BPS

IC/BPS is a disorder that induces chronic pain or discomfort in the bladder and surrounding pelvic organs.^{19,20} At present, IC/BPS is not a disease confined to just the bladder and pelvic area; it is a complex disease that includes outside the genitourinary tract. There is a study that reflects these pain characteristics. Tripp et al.²¹ investigated the pain characteristics of IC/BPS using whole-body diagram pain locators. They found that women with IC/BPS reported significantly more pain all over their body, compared to healthy women without. Fifty two of the 193 IC/BPS diagnosed women (27%) presented pain restricted to the bladder and pelvic area. Moreover, various comorbidities are found in IC/BPS patients. Diseases such as irritable bowel syndrome, fibromyalgia, vulvodynia, chronic pelvic pain, endometriosis, OAB, allergies and chronic fatigue syndrome often coexist in IC/BPS patients.²²⁻²⁸

In addition, there are several reports that IC/BPS can increase the risk for or worsen other diseases, including FSD. A population based study found higher prevalence of FSD in women with IC/BPS.²⁹ Moreover, FSD increased depending on the severity of IC/BPS symptoms, suggesting that FSD is a factor worsening IC/BPS. In regards to the pain associated with FSD, vulvodynia may be contributing to flare-ups of IC/BPS symptoms and could be the reason why IC/BPS patients avoid sexual activity.^{9,30}

FSD AND IC/BPS: BE GENERALIZED AS ONE DISEASE?

Diseases with lower urinary tract symptoms (LUTS) in female such as incontinence and OAB are known to have negative impact on female sexual function over all domains-arousal, orgasm, pain, and satisfaction. Symptoms of IC/BPS also deteriorate patient's sexual activities and life quality. Significant numbers of IC/BPS patients avoid

sexual activity because of pain. In addition, FSD and IC/BPS share similar clinical characteristics and comorbidities, making it difficult to discriminate between the two.³¹⁻³³ As mentioned previously, there are many clinical reports presenting the association between IC/BPS and vulvodynia, particularly from various conditions of FSD.

Although the mechanisms of these correlations are unclear, visceral nerve cross-talking and the anatomic relationship between genital organs and the bladder offer a simple proximity explanation for the relationship between IC/BPS and vulvodynia. Another possible mechanism to explain the association between IC/BPS and vulvodynia is abnormal pain hypersensitivity induced by peripheral and central sensitization. The abnormal pain response frequently observed in vulvodynia patients is caused by central or peripheral maladaptive pain processing due to local insult, injury, or trauma (Figure 1).

Role of Peripheral Sensitization in the Pain Hypersensitivity of Vulvodynia and IC/BPS

Exposure of nociceptors to repetitive pain stimulation reduces the pain threshold and amplifies the responsiveness of nociceptors. Therefore, peripheral transduction of sensitivity can abnormally increase and peripheral pain hypersensitivity can develop.³⁴⁻³⁶ The potential underlying mechanism of peripheral pain hypersensitivity noted in both vulvodynia and IC/BPS could be sensory nerve upregulation. Previous studies have shown that sensory nerve density is significantly increased in vulva vestibule and bladder. Compared to the normal population, patients with vulvodynia were found to have increased nociceptors in their vulvar vestibule.³⁷⁻⁴⁰ Consequentially, this increased density of peripheral nociceptors results in increased sensitivity. It was also found that transient receptor potential V1 (TRPV1) exists in these nociceptive nerve endings and enhances pain signaling.^{37,41,42} Pukall CF et al.⁴³ and Giesecke J et al.⁴⁴ reported increased peripheral tactile, pressure, and pain sensitivity in the patients with vulvodynia and confirmed histologic and molecular changes of peripheral nociceptors is associated with clinical manifestations. Similarly with vulvodynia, upregulation of sensory innervation and TRPV1 in the bladder is reported in patients with IC/BPS.⁴⁵⁻⁴⁷

Role of Central Sensitization in the Pain Hypersensitivity of Vulvodynia and IC/BPS

Central sensitization is an important mechanism underlying various conditions associated with chronic pain and induces pain hypersensitivity through pathologically enhanced pathways that are not normally associated with nociception; for example, the low-threshold A δ fiber that is mostly used for temperature and pressure signaling. Chronic pain induced by central sensitization is persistent even after the initiating and peripheral cause has gone.⁴⁸ Studies have shown that the pain characteristics of central sensitization can be found in patients with vulvodynia. Foster DC et al.⁴⁹ observed that vulvar vestibulitis syndrome patients experienced hyperalgesia and allodynia more often than normal controls after intradermal foot and forearm capsaicin injections. In addition, pelvic organ crosstalk has an important role in central sensitization because pelvic organs, such as, the bladder, colon and vulva, are controlled by same neural pathway.⁵⁰ Thus, afferent signals from other pelvic organs provoked pain through neural crosstalk even though initiating and peripheral causes of vulvodynia and IC/BPS disappeared. Therefore, central sensitization plays an important role in the chronic pain observed in vulvodynia and IC/BPS. Clinically, similar manifestation of vulvodynia and IC/BPS has also existed. Moreover, recently, there has been an attempt to categorize various pain associated conditions due to central sensitization as central sensitivity syndrome (CSS). Vulvodynia and IC/BPS are considered subgroups of CSS.⁵¹ Previous studies on clinical findings support the notion that the same mechanism associated with central sensitization is involved in the pain behind vulvodynia and IC/BPS.⁵²⁻⁵⁴

Recently, evidence supporting central sensitization using functional and structural brain imaging were reported in vulvodynia and IC/BPS. Previously, Pukall et al.⁵⁵ showed that increased perception and activation of pain-related brain regions were observed in women with vulvar vestibulitis syndrome, compared to normal women, after tactile stimulation of the vulvar vestibule. Other studies have reported that patients with vulvodynia showed increased grey matter density in pain-modulating and stress-related regions of the brain as well as alterations in the intrinsic connectivity of regions comprising the sensorimotor, salience, and default mode resting state networks.^{56,57} Similarly, women with IC/BPS showed alterations of oscillation frequency and functional connectivity of brain regions previously reported in other chronic pain conditions⁵⁸ and various white matter (right anterior thalamic radiation, left forceps major, and right longitudinal fasciculus, right superior and bilateral inferior longitudinal fasciculi) abnormalities that correlated with severity of pain, urinary symptoms, and impaired quality

of life.⁵⁹ Figure 2 shows common therapeutic approaches and points of divergence among the these IC, IC+vulvodynia, and vulvodynia patient groups.

APPROACH AND MANAGEMENT FO VULVODYNIA AND IC/BPS PATIENTS

Clinically, vulvodynia and IC/BPS often coexists and differentiation between the two is not easy, especially when the patient reports of LUTS combined with pain. A majority of patients also seek medical care after relatively longer periods of initially feeling pain, leading to central sensitization that has is firmly established. Furthermore, clinical manifestations of chronic pain found in various other comorbidities can mask vulvodynia and IC/BPS, making it confusing and difficult to officially diagnose.

Many previous studies have revealed the close correlation between LUTS and impaired sexual function; IC/BPS is not an exception. Besides, it is not uncommon to have trouble differentiating sexual pain and IC-BPS-related genital pain in women. Unfortunately, there is a lack of comprehensive studies regarding sexual dysfunction and IC/BPS despite the growing population of affected individuals (Table 1). Clinicians should take more concern regarding sexual dysfunction and pain in IC/BPS patients and more randomized controlled studies should be conducted to better understand correlations and diagnostic differentiations.

CONCLUSION

Both vulvodynia and IC/BPS are common and irritable conditions that disrupt normal life and reduce QoL in women. Vulvodynia also manifests itself along with IC/BPS and there are several reports supporting the association between the two diseases. Unfortunately, knowledge concerning vulvodynia and IC/BPS is inadequate when considering the clinical impact and importance of these two conditions. Therefore, there is an essential need for further studies that delve into discovering the features of vulvodynia and IC/BPS.

Complete compound annotation of all mass spectra from untargeted urine metabolomics

To this date, metabolomics is considered to be one of the major “omics” tools, with the great potential for application in personalized medicine and health¹. Over the last decade, metabolomics has become an integral part of clinical laboratories worldwide for targeted analysis. However, untargeted metabolomics is still widely used as it provides comprehensive insights into complex metabolomes and allows for biomarker discovery. While untargeted metabolomics can be powerful, its main challenge is its low identification rates^{2,3}. Since there is no single platform capable of capturing the entire metabolome of urine, we have employed two platforms most suited for untargeted urine analysis: (1) hydrophilic interaction chromatography (HILIC), for polar metabolite profiling, and (2) charged surface hybrid (CSH) technology, for lipidomics profiling. Through this integration of lipidomics and intensive systems biology, our experimental results provided a comprehensive list of lipid species and biogenic amines in human urine. Lipidomics, a lipid-targeting subarea of metabolomics, involves studying the unique structure and functional roles of cellular lipids in biological systems. Recent technological advancements in high-resolution MS have made comprehensive lipid metabolic profiling of clinical specimens and biofluids, including urine, possible. As important structural components of cellular membranes, lipids play key biological roles in various diseases. However, clinical application of lipidomics profiling still remains a challenge due to the limited databases available for data interpretation. Many lipids and lipid metabolites are still not properly annotated nor functionally characterized. Our group is actively working to address this issue by developing software and databases that can aid in lipid identification. The biologically active metabolites in urine can be identified through global metabolomics profiling and can provide an unbiased chemical fingerprint of the metabolism in the human body. The urinary metabolome in particular is associated with urological diseases, including bladder dysfunctions such as IC⁴⁻⁶. IC is characterized by chronic bladder and/or pelvic pain, as well as nocturia and an increase in urinary frequency and urgency.^{7,8} For our work, we sought to derive urinary metabolomic signatures from IC patients using newly developed comprehensive annotation tools⁹ on all five levels of annotation, as defined by the Metabolomics Standards Initiative (MSI). The objective of this work is to provide insight into increasing compound annotation levels in the clinical setting by utilizing a variety of freely available software tools and databases.

EXTRACTION

Subjects, urine specimen collection, and clinical and pathological features of subjects were described in a previous paper from our team. De-identified urine samples were stored at -80°C until further analysis. Urinary lipids were extracted with methanol and methyl tert-butyl ether containing a cocktail of lipid standards. Water was subsequently added for phase separation. This extraction protocol extracts all main lipid classes in urine with high recoveries, specifically phosphatidylcholines (PC), sphingomyelins (SM), phosphatidylethanolamines (PE), lysophosphatidylcholines (LPC), ceramides (Cer), cholesteryl esters (CholE), and triacylglycerols (TG).¹⁰ Lipid standards were purchased from Avanti Polar lipids (Alabaster, USA). Polar metabolite extraction was done by taking the polar phase of the lipid extraction procedure. Samples were dried in a centrivap prior to a clean-up step of 50% acetonitrile and dried again. Samples were then reconstituted in 80:20 acetonitrile and water solution containing internal standards from Sigma and CDN Isotopes.

INSTRUMENTATION

For lipids, all measurements were carried out on a Thermo Q Exactive Hybrid Quadrupole-Orbitrap Mass Spectrometer. Briefly, $1\ \mu\text{L}$ of diluted samples were separated on a Waters Acquity Ultra-Performance LC (ULPC) CSH C18 column ($100 \times 2.1\ \text{mm}$; $1.7\ \mu\text{m}$) coupled to an Acquity UPLC CSH C18 VanGuard Precolumn ($5 \times 2.1\ \text{mm}$; $1.7\ \mu\text{m}$). The column was maintained at 65°C with a flow rate of $0.6\ \text{mL}/\text{min}$. The positive ionization mobile phases consisted of (A) acetonitrile:water (60:40, v/v) with ammonium formate (10 mM) and formic acid (0.1%) and (B) 2-propanol:acetonitrile (90:10, v/v) with ammonium formate (10 mM) and formic acid (0.1%). The negative ionization mobile phases consisted of (A) acetonitrile:water (60:40, v/v) with ammonium formate (10 mM) and (B) 2-propanol:acetonitrile (90:10, v/v) with ammonium formate (10 mM). The separation was conducted under the following gradient: 0 min 15% B; 0–2 min 30% B; 2–2.5 min 48% B; 2.5–11 min 82% B; 11–11.5 min 99% B; 11.5–12 min 99% B; 12–12.1 min 15% B; 12.1–15 min 15% B. The Thermo Q Exactive Hybrid Quadrupole-Orbitrap Mass Spectrometer was operated using electrospray ionization (ESI CSH) in positive mode used the following parameters: mass range, 120–1200 m/z; sheath gas flow rate, 60; aux gas flow rate, 25; sweep gas flow rate, 2; spray voltage (kV) 3.6; capillary temp, 300°C ; S-lens radio frequency level, 50; aux gas heater temp, 370°C . The full MS parameters were set as follows: resolution, 60,000; automatic gain control (AGC) target, $1\text{e}6$; maximum IT, 100ms; spectrum data type, centroid. Data dependent tandem MS parameters: resolution, 15,000; AGC target $1\text{e}5$; maximum IT, 50 ms; loop count, 4; TopN, 4; isolation window, 1.0 m/z; fixed first mass, 70.0 m/z; (N)CE / stepped (N)CE, 20, 30, 40; spectrum data type, centroid. For HILIC, all measurements were carried out on the same Thermo Q Exactive Mass Spectrometer. Briefly, $1\ \mu\text{L}$ of diluted samples were separated on an Acquity UPLC Ethylene Bridged Hybrid (BEH) Amide Column ($150 \times 2.1\ \text{mm}$; $1.7\ \mu\text{m}$) coupled to an Acquity UPLC BEH Amide VanGuard Precolumn ($5 \times 2.1\ \text{mm}$; $1.7\ \mu\text{m}$). The column was maintained at 45°C with a flow rate of $0.4\ \text{mL}/\text{min}$. The mobile phases consisted of (A) water with ammonium formate (10 mM) and formic acid (0.125%) and (B) acetonitrile:water (95:5, v/v) with ammonium formate (10 mM) and formic acid (0.125%). The separation was conducted under the following gradient: 0 min 100% B; 0–2 min 100% B; 2–7.7 min 70% B; 7.7–9.5 min 40% B; 9.5–10.25 min 30% B; 10.25–12.75 min 100% B; 12.75–17 min 100% B. The Thermo Q Exactive MS instrument was operated using ESI HILIC in positive mode with the following parameters: mass range, 60–900 m/z; sheath gas flow rate, 60; aux gas flow rate, 25; sweep gas flow rate, 2; spray voltage (kV) 3.6; capillary temp, 300°C ; S-lens RF level, 50; aux gas heater temp, 370°C . Full MS parameters: microscans, 1; resolution, 60,000; AGC target, $1\text{e}6$; maximum IT, 100ms; number of scans, 1; spectrum data type, centroid. Data dependent MS2 parameters: microscans, 1; resolution, 15,000; AGC target, $1\text{e}5$; maximum IT, 50 ms; loop count, 4; multiplexing (MSX) count, 1; TopN, 4; isolation window, 1.0 m/z; isolation offset 0.0 m/z; (N)CE / stepped (N)CE, 20, 30, 40; spectrum data type, centroid.

DATA PROCESSING AND IDENTIFICATION

The LC-MS/MS data was analyzed using MS-DIAL software.¹¹ Detailed parameter settings are listed in Supplemental Tables 1 and 2 (HILIC and lipidomics data processing settings). Accurate masses, retention times, and peak heights were then exported, and further analysis was performed in R Studio and our in-house developed software for statistical analysis, Metabox.¹² Automated annotation of metabolites was performed separately for polar metabolites and lipids. Table 1 lists libraries, methods, and software used for each platform. Metabolite annotations were done with the help of our in-house developed library containing >600 authentic lipid standards of different classes and >800 standards of polar metabolites. Next, MS/MS database matching was performed with freely available MS/MS spectra obtained from Mass Bank of North America (MoNA), National Institute of Standard and Technology (NIST) 17, LipidBlast, and the NIST Hybrid Library.^{13–15} Workflow summarizing all the tools, software and databases are shown in Figure 5.

RESULTS AND DISCUSSION

m/z-RT and MS/MS databases

Untargeted lipidomics analysis in the positive ionization mode resulted in 112 identified lipids encompassing several lipid classes. The same sample set was also analyzed using HILIC chromatography. Using the established in-house library, we identified 117 metabolites, which consisted of amino acids, biogenic amines, and derivatives. These annotations are level 1 according to MSI, meaning that the experimental data was compared to authentic standards measured under the same instrumental conditions. Chemical standards (n= 874) were analyzed on two instrument types: quad time-of-flight (QToF) and orbitrap in positive ionization mode.

These standards provide several orthogonal parameters: accurate mass (m/z), retention time (RT), and MS/MS. This level of annotation is laboratory/chromatography specific and is clearly a limitation if used exclusively. It takes both time and money to develop and establish such a chromatography. In our own experience, two skilled researchers require two years of work to create and validate a chromatographic run with 1000 metabolites measured on it robustly. It is a common practice in metabolomics research to use MS/MS libraries and perform mass spectral similarity searches in order to increase the annotation rate, as fragmentations are not chromatography specific. Those libraries contain mass spectra of authentic standards from a variety of instrumentation and chromatography (this metadata is available in .msp/.mgf formats), and this level of compound ID is described as level 2. Users can use freely available databases, such as MoNA, or can opt for commercially available MS/MS databases such as NIST17. We combined two mass spectral databases, MoNA and NIST17, and used the merged .msp within MS-DIAL software for mass spectral similarity matching. Metadata such as dot product, reverse dot product scores, number of matching ions, and MS-DIAL calculated MS2 similarity have been taken into account.

Figure 5. Workflow summarizing tools, software, and databases used for completing annotation of urine metabolome.

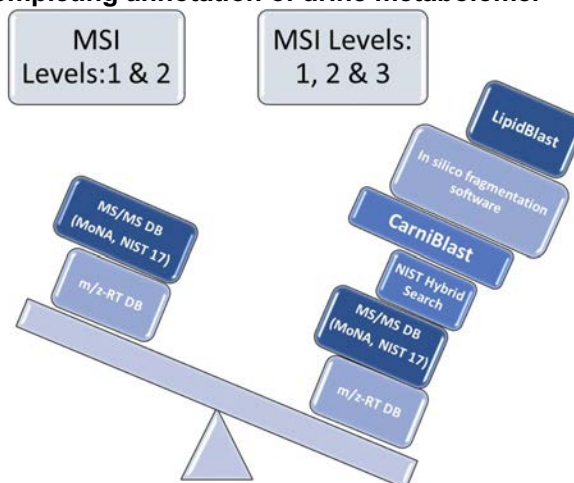


Table 1.

Chromatography and databases	Type of matching	MSI level of annotation	Number of annotations accomplished
HILIC	m/z , RT and MS/MS	1	117
Lipidomics	m/z , RT, MS/MS, in silico MS/MS	1	72
Lipidomics: CarniBlast	m/z , in silico MS/MS	2	18
HILIC: MoNA+NIST14	m/z and MS/MS	2	440
HILIC: CarniBlast	m/z and in silico MS/MS	2	107
Lipidomics: mzRT lookup	m/z	3	96
Hybrid search	MS/MS (hybrid)	3	Sample depending: 4000-8000
In silico fragmentation software: CSI:FingerID	MS1 and in silico MS/MS	3	Sample depending: 4000-8000

M/Z Lookup Table in LipidBlast

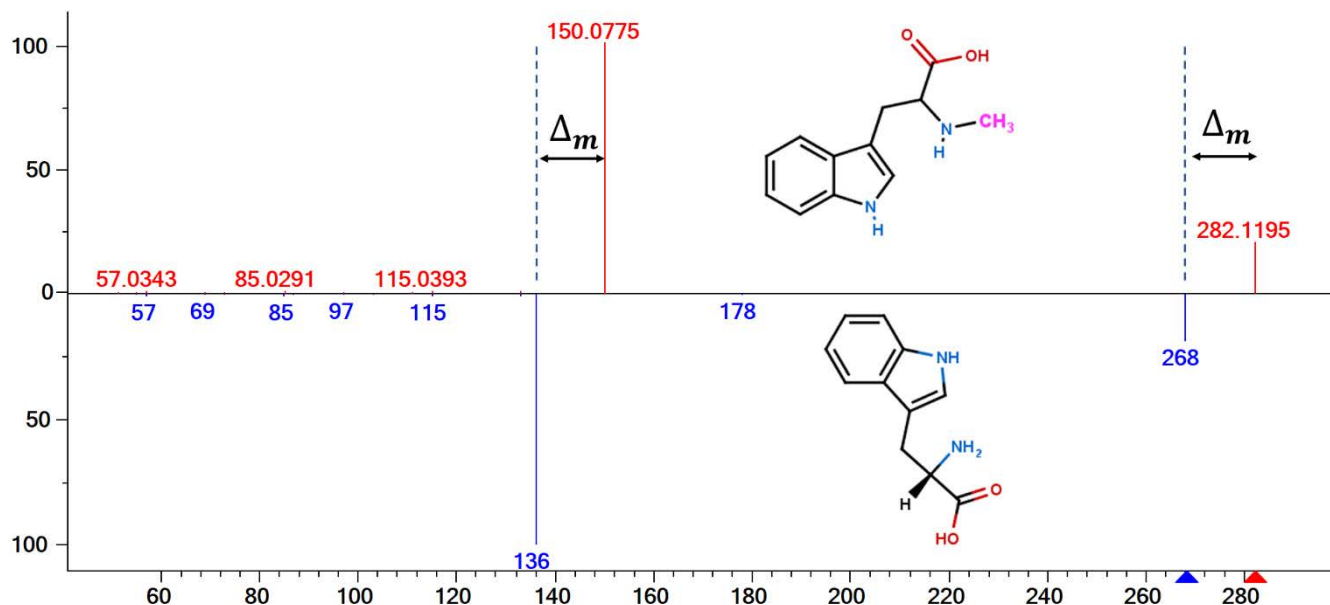
This essentially stand-alone tool can be used in addition to LipidBlast. It provides an automated approach for lipid annotations based on their accurate masses and/or chromatographic RT. Additional structure information of

the lipids and their side chains (sn1, sn2, sn3) cannot be made using accurate mass alone. For comprehensive structure elucidation, another orthogonal parameter like MS/MS is needed. We extracted m/z precursor information from the MS-DIAL output in positive ionization mode and used the M/Z Lookup Macro to assign additional lipid annotations. Mass tolerance for lipid assignments was calculated based on the mass accuracy of the Thermo Q Exactive instrument and the internal standards, 0.005 Da. This way, an additional 96 lipid annotations were obtained from the lipidomics data set in positive ionization mode.

CarniBlast

The process of lipid degradation (β -oxidation) in human cells occurs in the mitochondria. This allows for the direct coupling of fatty acid degradation to energy generation via the citric acid cycle and respiratory electron transport chain localized in the inner mitochondrial membrane. For the corresponding import process, fatty acids of different chain lengths and saturation are esterified to L-carnitine with the formation of acylcarnitines.¹⁶ L-carnitine can be *de novo* synthesized from *N*-trimethyl-lysine with butyrobetaine as an intermediate in a multi-step pathway. However, most carnitine comes from dietary intake. Fatty acids destined for degradation are first activated via thioesterification into coenzyme A (CoA). Then, three types of carnitine acyltransferases with different chain-length specificities (short, medium, long) transfer fatty acids via transesterification to carnitine with the release of CoA. These are carnitine acyltransferase, carnitine octanoyltransferase, and carnitine palmitoyltransferase. Next, a transport system consisting of carnitine palmitoyltransferase I (outer membrane), carnitine-acylcarnitine translocase, and carnitine palmitoyltransferase II (both inner membrane) transfer the acylcarnitines into the lumen of the mitochondria, where transesterification with CoA regenerates the acyl-CoAs and carnitine.^{17,18} Carnitine then leaves the mitochondria via the above outlined transport complex. During β -oxidation, the fatty acids are cleaved between C2 and C3 with the release of a C₂-unit of acetyl-CoA. A *trans*-2 double bond is formed between C2 and C3, hydrated, oxidized, and finally cleaved by the action of four enzymes. Odd chain and unsaturated fatty acids require additional enzymes.¹⁹ The described overall process is an essential part of the lipid homeostasis which covers all fatty acids of different lengths and saturation. Consequently, diseases that disturb this described lipid homeostasis ultimately increase acylcarnitines in the blood and the urine. Therefore, acylcarnitines can be biomarkers for diseases, including heart failure²⁰, obesity and diabetes²¹, chronic kidney disease²², chronic psychiatric illness²³, migranes²⁴, and endometrial cancer.²⁵ Acylcarnitines in urine serve as biomarkers for bladder cancer²⁶, diabetic nephropathy²⁷, obesity²⁸ and human kidney cancer.²⁹ It is well documented that carnitine and its esters can be found in almost every bodily fluid, yet the chemical standards are severely limited and/or nonexistent. To overcome this obstacle, we used an in-house developed *in silico* database of acylcarnitines as they, like many lipid species, fragment in a predictable manner. We exported the .msp files from both polar and lipidomics profiling and matched them against an *in silico* database of acylcarnitines. Some of the acylcarnitines were already present in our m/z-RT libraries, so using CarniBlast for the lipidomics .msp resulted in only three additional annotations. However, when HILIC .msp was used for the CarniBlast search, it resulted in an additional 793 annotations of acylcarnitines. This number suggests that there are far more carnitines present in urine than previous reports suggest.³⁰ This increase in annotation rates of acylcarnitines is important due to their role in lipid metabolism and various metabolic diseases. Interestingly, a majority of acylcarnitines couldn't be annotated with any other software or database.

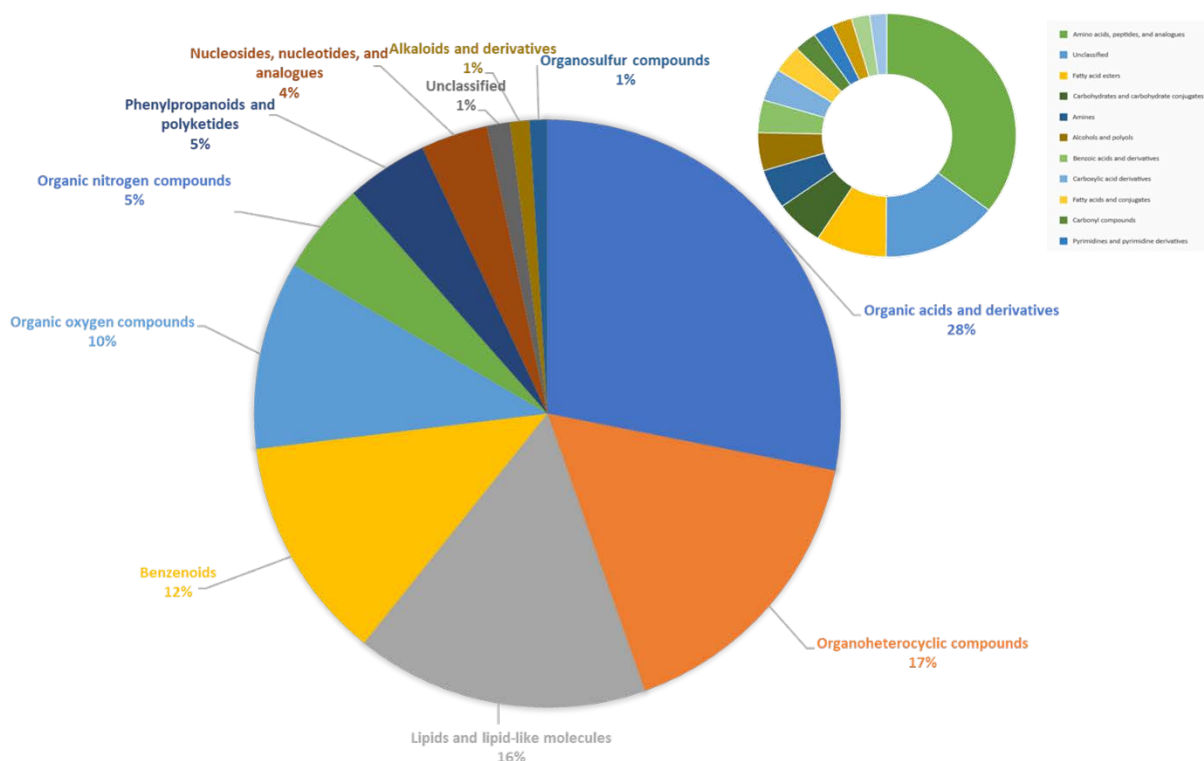
Figure 6. Head-to-tail comparison of an MS/MS spectra of an amino acid shows distinct shift in the spectrum: methylated vs. non-methylated.



***In silico* fragmentation software**

For the compounds that are not present in our m/z-RT library and have collected MS/MS spectra that cannot be matched in mass spectral libraries, software tools, like MS-FINDER, Sirius, and CFM-ID, are of great value.³¹⁻³³ We used the latest Sirius software with CSI:FingerID Interface (Sirius 4.0 built 19) to assign molecular identities to acquired MS/MS spectra.³⁴ We selected Sirius with CSI:FingerID because it has consistently scored very high during the latest Critical Assessment of Small Molecule Identification (CASMI) challenges. Furthermore, the current version has been improved in accuracy and speed. The MS/MS spectra were exported as a Mascot Generic Format (MGF) file from each raw file using the MSConvert. The MGF file largest in size contained the most MS/MS data and was therefore used for further analysis. A standard MGF file with 6482 MS/MS spectra was imported and 6447 features were available in the software. Formula assignment in positive ionization mode was performed with 10 ppm while retaining the 10 best formula candidates. Processing time was 2 minutes on a 16 CPU machine and the software was capable to assign formulas to a total of 6184 features. Fingerprint matching with CSI:FingerID via a webservice was subsequently performed to annotate isomer structures. Through this, 728 MS/MS peaks could be assigned when searching bio-databases and 1557 features could be assigned when querying the much larger PubChem database. The search time was around 5 minutes. The results, isomer structures, and their scores are presented in the Graphical User Interface (GUI) software. Additionally, results can be exported to CSV files. For the biodatabase search, up to 130 results were obtained per MS/MS scan, while the PubChem fingerprint research resulted in up to 10,000 candidates per MS/MS spectrum searched. Here individual and time-consuming investigations must be performed to investigate the correctness of the found structures. In order to show the accuracy of CSI:FingerID we also performed a search on compounds that were annotated by our in-house database. Sirius 4.0 and CSI:FingerID with 5ppm mass accuracy and search in bio-databases correctly identified 41 compounds as a top hit. Approximately 52% of the known compounds were correctly assigned within the top 3. The median rank for all 103 compounds was one and the average rank ten. Considering its excellent search speed and accuracy, CSI:FingerID should be considered a useful annotation tool for the identification of unknown compounds. The associated results can be found in the supplement. In our previous work, we have shown that it is possible to combine the outputs (results) of multiple software to create a new ranking system based on the accuracy of each software and rank the correct structure as the top hit in 93% of the cases.³⁵ However, this approach is not easily applicable as it requires both compound database boosting as well as thorough software comparison for the defined sample set.

Figure 7. Structural classification of metabolites present in the urine of 12 patients diagnosed with IC



NIST Hybrid search coupled with ClassyFire

Epimetabolites are defined as regulatory metabolites that have been removed from their classical functions by modification (for example, methylation or acetylation) but often remain chemically similar to their canonical counterparts.³⁶ NIST recently introduced a fantastic mass spectral library-based method to annotate MS/MS spectra that contain the aforementioned modifications. It is described as a “hybrid” method because it combines matching fragments but not the m/z of the precursor (to allow for modification calculations that are then reflected).³⁷ Such a tool is of great assistance in structure elucidation of unknown metabolites, as it mimics the knowledge and experience of a well-trained chemist.³⁸ The hybrid search comparison is shown in Figure 2, where the head-to-tail comparison of an amino acid shows a distinct shift in the spectrum, methylated versus non-methylated. We exported the .msp files from MS-DIAL to the NIST pepSearch GUI, activated the hybrid search function, and ran it against the MS/MS hybrid libraries. As a result of the hybrid search, every MS/MS spectra are now associated with an annotation and a variety of scores. Results of the hybrid search for both HILIC and CSH data are presented in Supplemental Table 5. The advantage of using NIST Hybrid search is that it supports batch processing, offers restrictions in terms of which MS/MS spectra should be included or excluded, and allows users to quickly get a snapshot of the metabolome they are measuring. The result list contains a lot of meta-data, such as chemical name, International Chemical Identifier (InChI) key, simplified molecular-input line-entry system (SMILES), probability score, etc. Those annotations should be treated with caution as they do not represent an identification but rather a “nearest known neighbor” to the unknown molecule. Next, the result list of NIST hybrid search was coupled with a fully automated, comprehensive chemical classification tool that utilizes a well-defined chemical hierarchy system - ClassyFire. ClassyFire successfully annotated and classified thousands of molecules from various libraries, including DrugBank, LIPID MAPS, HMDB, ChEBI, and PubChem.³⁹ We used ClassyFire Batch by Fiehn Lab (<http://cfb.fiehnlab.ucdavis.edu/>), a user-friendly web application capable of batch classifications directly from InChIKeys.

Figure 7 shows complexity of urine metabolome based on the superclass and subclass classifications as defined by Classyfire. Results of classifications are organized into Kingdom, Superclass, Class, Subclass, and two parent levels. Subsets of those results is shown in Supplemental Table 6. We can imagine that such combinatorial

approach becomes of importance in personalized medicine or health research in general, since it is evident from Supplemental Tables that the metabolic profile of urine varies from patient to patient. While biomarker discovery focuses on the shared metabolites between patients, it is also important to recognize and investigate differences due to diet, exposure, genetics, and other factors.

Summary

Metabolomics reports and data should be annotated with confidence levels for clarity and reproducibility purposes. Sharing the MS/MS data with the community will directly improve not only other researchers' work but will also help the development of tools that aid structure elucidation process. Hopefully this work provides a comprehensive overview of some of the best freely available tools and databases for metabolomics research and will be of use to analysts when annotating unknown metabolites.

Pioglitazone Alters the Proteomes of Normal Bladder Endothelial Cells but Shows No Tumorigenic Effects

Thiazolidinediones (TZDs), such as pioglitazone and rosiglitazone, are currently the only oral drugs with a confirmed antihyperglycemic impact in type 2 diabetes mellitus (T2DM) patients. As agonists of peroxisome proliferator-activated receptor γ (PPAR γ), TZDs are known to positively influence insulin sensitivity and β -cell function and potentially alter lipid profiles. Pioglitazone is a synthetic ligand of PPAR γ and is used as a therapeutic treatment for patients with T2DM. PPAR γ , a ligand-activated transcription factor, is expressed in white and brown adipose tissues as well as in the urinary bladder⁴⁰. Pioglitazone has also been shown to reduce macrophage infiltration through the activation of PPAR γ and induction of apoptotic cell death⁴¹, which can lead to decreased numbers of macrophages in adipose tissues⁴². To examine the impact of PPAR γ on bladder cell function, several studies analyzed the expression of PPAR γ in normal bladder and bladder cancer (BC) mucosal samples. They observed different rates of cell migration and invasion in various BC cell lines that express PPAR γ . In addition, prior studies have shown that vascular endothelial growth factor A (VEGF-A), a primary proangiogenic factor, is positively regulated by PPAR γ ⁴³. PPAR γ can also exert its functions via the activation of signaling pathways, interaction with Wnt/ β -catenin, and induction of signaling pathways involved in proliferation and survival, such as IGF-I/PI3K/AKT/mTOR and MAPK⁴⁴. Furthermore, PPAR γ can regulate the inflammatory response of macrophages through TLR4/NF- κ B signaling⁴⁵.

There have been contradictory reports on the potential association between diabetes mellitus (DM) and elevated risk of BC^{46,47}. Studies have demonstrated that pioglitazone can have adverse effects that exaggerate the risk of BC. DM patients, particularly males, on long-term, high doses of pioglitazone, are at a higher risk of developing BC^{48,49}. The Kaiser Permanente Northern California (KPNC) study determined that inflated dose and length of pioglitazone treatment correlated to increased rates of BC⁴³. Currently, the U.S. Food and Drug Administration (FDA) allows the use of pioglitazone in patients with special caution to those with a prior history or active BC⁵⁰. A potential reason for this observation could be that PPAR γ signaling in BC cells may provide a tumor microenvironment that allows for de novo lipogenesis of lipids that can be utilized in increasing tumor mass and energy usage⁵¹. However, other studies have shown that TZDs posed no risk on survival in BC patients who underwent radical cystectomy⁵². A recent meta-analysis found no difference in BC incidence among users of pioglitazone and nonusers⁵³. These inconsistencies between studies have led to questions in the legitimacy of studies and the actual dangers of continued pioglitazone use. Due to the inherent difficulty of accurately assessing the link between TZDs and BC, the association between the two is still in controversy.⁵⁴

The goal of our study was to determine whether TZDs have any negative or positive effects on the healthy bladder epithelium. Since pathophysiological changes require the actions of a series of key proteins, global proteomic analysis of protein alterations using state-of-the-art mass spectrometry is ideal for acquiring unbiased biological information regarding molecular mechanisms. Using such a method, this study aimed to understand the mechanistic meanings of proteome perturbations in the normal bladder due to TZD treatment. We sought to examine the effects of pioglitazone specifically, being that is the most widely used TZD. Our global quantitative proteomic analyses found that pioglitazone alters the proteome and biological networks in normal human bladder cells without tumorigenic effects.

MATERIALS AND METHODS

Cell culture. Immortalized normal human bladder epithelial cells, TRT-HU1, were established and characterized as described previously⁵⁵. Cell lines that were initially established, frozen, and under a passage number of 10 were used in this study. Culture media was changed after one day of subculturing and cells were passed again when there was 70-80% confluence. All cells were negative for mycoplasma contamination, and this was tested for monthly via PCR. Cells were maintained in Dulbecco's modified Eagle's medium (DMEM) supplemented with 10% fetal bovine serum (FBS) (Invitrogen), 1% penicillin/streptomycin, and 1% L-glutamine (Sigma-Aldrich Corp., St. Louis, MO, USA) under a humidified atmosphere of 5% CO₂ at 37 °C.

Antibodies and reagents. Antibodies against various proteins were obtained from the following sources: ACTG2 (ab189385), MYH3 (ab124205), OXPHOS (ab110413) from Abcam; phospho-NF- κ B (3033), phospho-HER2/ErbB2 (2247), phospho-PAK1 (2601), phospho-GSK-3 β (9336), Snail (3879), N-cadherin (13116), Slug (9585), β -catenin (8480), E-cadherin (14472), Tight Junction Antibody Kit (8683) from Cell Signaling Technology, and β -actin (A1978) from Sigma. Commercially available horseradish peroxidase (HRP)-conjugated secondary antibodies (7074, 7076) were obtained from Cell Signaling Technologies. All other chemical reagents were procured from Sigma Chemical Corp.

Quantitative proteomics. For quantitative proteomics, the tandem mass tagging (TMT)-based method was performed, as previously described^{56,57}. In brief, cellular proteins from 25 μ M pioglitazone-treated and control TRT-HU1 cells were extracted using a 4% SDS-containing buffer. The protein concentration was then determined from each sample using the Pierce 660nm Assay Kit (Thermo Fisher Scientific). The kit was carried out using 60 μ g of protein from each sample, which was digested with trypsin via filter-aided sample preparation (FASP) and labeled with TMT6plex reagents in parallel.

After TMT-labeling, the peptides were reconstituted and desalted via C18 spin columns (Thermo Scientific) and separated by high-pH reversed-phase liquid chromatography (RPLC) using an Ultimate 3000 XRS System (Thermo Scientific). For high-pH RPLC, 50 μ g of TMT-labeled peptides were injected onto a 100-mm Hypersil GOLD C₁₈ column (2.1 mm inner diameter, 3 μ m particle size, 175 Å pore size) (Thermo Scientific) and eluted for 3 min with a flow rate of solvent A, which consisted of 10 mM ammonium formate at pH10. Peptides were then separated with a 7 min linear gradient of 0-40% solvent B, which consisted of 10 mM ammonium formate and 95% acetonitrile at pH10. The labeled peptides were then separated into 24 fractions, concentrated into 12 fractions, and dried down through a SpeedVac (Thermo Scientific). Peptides in each fraction were rehydrated with 0.2% formic acid, and liquid chromatography-tandem mass spectrometry (LC-MS/MS) analysis was performed using an EASY-nLC 1000 connected to an LTQ Orbitrap Elite Mass Spectrometer (Thermo Scientific). Briefly, peptides were loaded onto a 2-cm trap column (PepMap 100 C18, 75 μ m inner diameter, 3 μ m particles, 100 Å pore size) and separation was done using a 50-cm EASY-Spray column (PepMap RSLC C₁₈, 75 μ m inner diameter, 2 μ m particles, 100 Å pore size) heated up to 55°C. To separate low-pH peptides, RPLC was employed using a mobile phase that consisted of either 0.1% formic acid in water (phase A) or acetonitrile (phase B). The LC gradient was 4-24% B over 200 min, 24-50% B over 20 min, and 50-100% B over 5 min at a flow rate of 150 nL/min, which was then followed by 100% B over 15 min at a flow rate of 300 nL/min.

Mass spectra were acquired in a data-dependent manner, selecting up to the 15 most abundant precursor ions for higher-energy collisional dissociation. No further data processing, such as smoothing, de-isotoping, and/or filtering, was carried out. The mass resolution for precursor and fragment ions were set to 120,000 and 30,000, respectively. The isolation width was set to 1.5 and the normalized collision energy was set to 40. Database searching and protein quantification was performed by Proteome Discoverer (v2.1) using the SEQUEST algorithm. The acquired raw data were searched against the human Uniprot Protein Sequence Database (released on 01/22/2016, containing 20,985 protein sequences). Several parameters were set as follows: trypsin, up to two missed tryptic cleavages were allowed; precursor ion tolerance of 10 ppm, fragment ion tolerance of 0.02 Da; followed by numerous modifications: carbamidomethylation of cysteines and TMT6plex alteration of lysines. The N-terminal of peptides was set as fixed variations; while the acetylation of protein N-term, oxidation of methionine, and deamination of asparagines and glutamines were variable modifications. To identify peptides

identifications and proteins, a standard false discovery rate (FDR) of 1% was applied to filter peptide-spectrum matches (PSMs).

To quantify proteins, peptides with >30% precursor ion interference were excluded to minimize inaccurate quantifications caused by precursor ion interference. PSM level information was extracted using Proteome Discoverer⁵⁸. After quantifying each PSM intensity, the peptide intensities were summarized, as previously described⁵⁹. In brief, this was done in 4 steps: 1) the normalized log₂ intensity of the PSMs matched to each peptide by the substrate mean PSM from each reporter intensity was centered, 2) outliers were detected using Dixon's Q-test and generalized electrostatic discharge (ESD) test, 3) the mean intensity without outliers was taken, and 4) the grand mean intensities of the three highest abundant PSMs were added before being mean-centered. Bipartite graphs of peptides and protein groups were generated according to the information of the aligned peptides. Among the protein group, we defined the representative protein that had the largest number of peptides or unique peptide⁶⁰. When there was more than one protein with the same number of peptides in the same protein group, we selected the protein that had the highest sequence coverage. We then computed the relative intensity of the protein group using a linear-programming formulation, as previously described⁶¹.

Identification of differentially expressed proteins (DEPs). To identify DEPs, we first selected proteins that have more than two non-redundant peptides in each sample. We then performed a one sample t-test using the log₂ fold-changes to compute the significance. For hypothesis testing, an empirical null distribution, which means that a protein is not differentially expressed, was estimated through the following steps: 1) we applied 100,000 random permutations of the samples, 2) we computed t-values using log₂ fold-changes of randomly permuted samples, and 3) we applied the Gaussian kernel density estimation method to t statistics. FDRs of each protein for the one sample t-test were then calculated using Storey's correction method⁶². Proteins were identified as DEPs if they had FDR<0.05 and absolute log₂ fold-change ≥0.58 (1.5 fold). Functional enrichment analysis of DEPs was performed using DAVID (Ver. 6.8)⁶³. Significantly enriched cellular processes were selected for if they had an enrichment p-value<0.05. Functional classification analysis was performed using PANTHER (Ver. 11)⁶⁴.

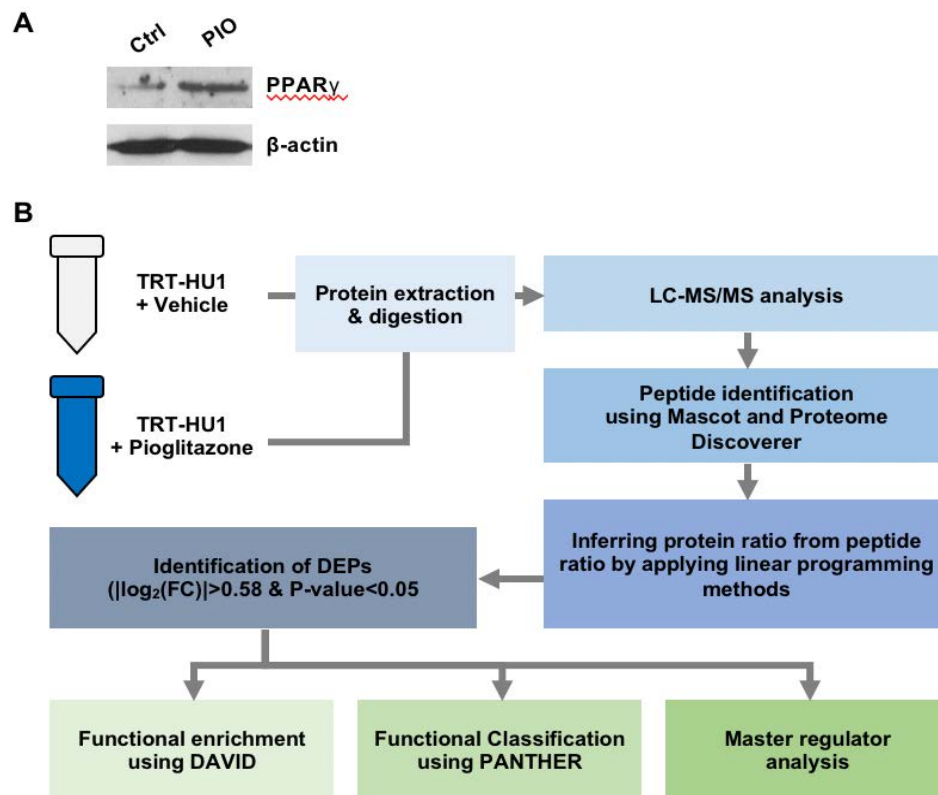
Master regulator analysis (MRA). To identify master regulators, we discerned each DEP and counted their individual partners. The protein-protein interaction information was obtained from six interactome databases: the Biological General Repository for Interaction Datasets (BioGRID)⁶⁵, the Database of Interacting Proteins (DIP)⁶⁶, High confidence protein-protein interactions (HitPredict)⁶⁷, the IntAct molecular interaction database (IntAct)⁶⁸, the Molecular INTERaction database (MINT)⁶⁹, and the STRING database⁷⁰. We then computed the enrichment p-values using Fisher's exact test. Finally, we selected proteins with p-values lower than 0.01 and prioritized the DEPs based on the number of interaction partners.

Western blot analysis. Whole-cell lysates were prepared as previously described⁷¹. Briefly, cells were seeded onto 10 cm plates and exposed to 25 μM concentrations of pioglitazone for 72 h. Control and treated cells were then collected, lysed with RIPA buffer (20 mM Tris, 150 mM NaCl, 1% Nonidet, P-40, 0.1 mM EDTA) (Pierce, ThermoFisher) supplemented with a phosphatase inhibitor cocktail (ThermoFisher), homogenized, and centrifuged at 13,000 g and 4°C for 20 min to obtain whole-cell lysates. Using 25 μg of extracted protein, we separated the proteins using a 4-15% SDS-PAGE gel and transferred them onto a polyvinylidene fluoride (PVDF) membrane. The membranes were then blocked with either 5% bovine serum albumin (BSA) or 5% nonfat milk in Tris-buffered saline with 0.1% Tween 20 (TBST [2.42 g/L Tris-HCl, 8 g/L NaCl, and 1 mL/L Tween 20 (pH 7.6)]) for 1 h at room temperature. All primary antibodies incubations were done at 4°C overnight followed by 3 X 10 min washes with TBST. HRP-conjugated secondary antibody incubations were done at room temperature for 1 h and followed by 3 X 10 min washes with TBST. β-actin was used as an internal control. All western blot experiments were run in at least triplicates for each antibody and analyzed from different lysates using standard procedures.

Measurement of Reactive Oxygen Species (ROS). Intracellular ROS levels were measured with 2',7'-dichlorofluorescein diacetate (DCF-DA) using fluorescence-activated cell sorting (FACS) analysis as previously described⁷². Cells were loaded with 20 μM of DCF-DA and fluorescence was measured with a flow cytometer (FACSCalibur, Becton-Dickinson, Franklin Lakes, NJ). The mean DCF fluorescence intensity was measured with maximum excitation and emission spectra of 495 nm and 529 nm, respectively.

Cell proliferation assay. To determine cell growth during exposure to pioglitazone, TRT-HU1 cells were seeded at a density of 5×10^4 cells/well in six-well plates. Cells were then incubated with standard growth medium and treated with varying doses of pioglitazone (0, 25, 50, or 100 μM) (E6910, Sigma-Aldrich Corp.) or vehicle. Cell numbers were evaluated after 24, 48, and 72 h by removing the medium, incubating cells with trypsin/EDTA for 5 min, adding trypan blue, and counting the suspended live cells using a hemocytometer. The formula averages of each count were used as the total density of the well after each time point. For crystal violet staining, the medium was removed and replaced by 200 μl of a 0.05% solution of crystal violet. After incubation at room temperature for 15 min, the dye was removed, and the wells were washed thoroughly with phosphate buffered saline (PBS). Later, the cells were fixed with 4% paraformaldehyde at room temperature for 5 min. The cells were then washed with tap water and dried out on filter paper. For quantitative analysis, the stained cells were

Figure 1. **Overview of global proteomics workflow for data generation and analysis.** (A) Western blot analysis shows the effects of pioglitazone treatment on PPAR γ expression. (B) Proteomics analysis workflow for this study.



dissolved in 10% acetic acid and subjected to absorbance measurements at 570-590 nm⁷³. Each assay condition was run in triplicates, and the data are representative of three independent trials.

Statistical analysis. Student's t-tests were performed to evaluate differential expression of the proteins between two groups. Variables with normal distribution were expressed as mean \pm standard deviation (SD). All reported p-values are two-tailed, with $p < 0.05$ being considered as statistically significant.

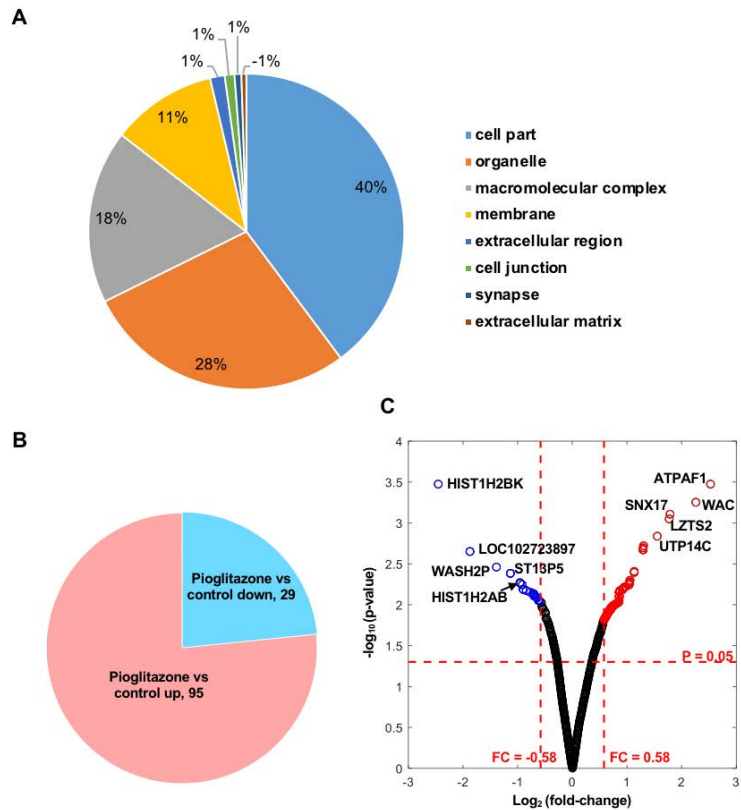
RESULTS

Pioglitazone perturbs the whole proteome in bladder epithelial cells. Labeled LC-MS/MS proteomic analysis was conducted to identify the global proteomes TRT-HU1 bladder cells treated with or without 25 μM of pioglitazone. We found that pioglitazone treatment increased PPAR γ protein expression (Figure 1A). Our proteomics analysis workflow is summarized in Figure 1B.

We detected 5,769 proteins in total, including proteins from the cell part (n=2,375), organelle (n=1,663), macromolecular complex (n=1,060), membrane (n=643), extracellular region (n=88), cell junction (n=61), synapse (n=43), and extracellular matrix (n=29) (**Figure 2A**). To identify DEPs between the control vs. pioglitazone groups, we performed a statistical hypothesis test using an empirical null model (see Methods). Among the 5,769 proteins, 124 DEPs (including 95 upregulated and 29 downregulated proteins) were found to have absolute log₂ fold-changes ≥ 0.58 and p-values < 0.05 . Approximately 70% of the DEPs (n=95) showed increased expression due to pioglitazone treatment (**Figure 2B**).

Volcano plot displays DEPs between control and pioglitazone groups. The top 5 most significantly up- or downregulated proteins were highlighted with their official symbol (**Figure 2C**). HIST1H2BK (histone cluster 1 H2B family member K), ST13P5 (ST13, Hsp70 interacting protein pseudogene 5), and WASH2P (WAS Protein Family Homolog 2 Pseudogene) were the most significantly downregulated by pioglitazone treatment. ATPAF1 (ATP Synthase Mitochondrial F1 Complex Assembly Factor 1), SNX17 (Sorting Nexin 17), LZTS2 (Leucine Zipper Tumor Suppressor 2), and UTP14C (UTP14C, Small Subunit Processome Component) were the most upregulated in response to pioglitazone. **Supplementary Table S1** shows the list of DEPs that were altered in response to pioglitazone along with the transcriptional targets of PPAR γ and test statistics. This data suggest that pioglitazone may induce transcriptional programming through PPAR γ , which contributes to increased protein expression.

Figure 2. Total proteins and differentially expressed proteins (DEPs) perturbed by pioglitazone treatment. (A) Pie chart depicts the cellular location of the detected DEPs. **(B)** Pie chart shows proportion of up- and downregulated DEPs in cells treated with pioglitazone. **(C)** Volcano plot showing the up- or downregulated DEPs in bladder epithelial cells treated with pioglitazone. Up- and downregulated DEPs are marked as red or blue, respectively. Protein symbol of the top 5 up- or downregulated proteins are presented in the volcano plot.



Functional enrichment analysis reveals that pioglitazone modulates key biological processes. To check the function of proteins perturbed by pioglitazone, we performed functional enrichment and classification using DAVID and PANTHER, respectively^{63,64}. Muscle filament sliding, actin-mediated cell contraction, cellular oxidant detoxification, cell adhesion, purine nucleoside monophosphate metabolic process, ATP metabolic process, and cytoskeleton organization were enriched by upregulated DEPs. However, chromatin silencing, gene silencing, and regulation of gene expression were enriched by downregulated DEPs (**Figure 3A**). We listed the DEPs belonging to actin-mediated cell contraction, cellular oxidant detoxification, cell adhesion, purine nucleoside monophosphate metabolic process, and chromatin silencing (**Table 1**).

Table 1. Enriched biological processes and corresponding proteins in upregulated (A) and downregulated proteins (B).

A.

GO term	Gene	P-value	Z Score
Muscle filament sliding	MYH2, MYH3, MYH4, MYH7, MYH8, MYL1, MYL3	3.84E-08	7.41
Actin-mediated cell contraction	MYH2, MYH3, MYH4, MYH7, MYH8, MYL1, MYL3	1.29E-05	4.89
Cellular oxidant detoxification	SOD1, TXN, CCS, PARK7, TXNDC17, SRXN1	7.75E-05	4.11
Cell adhesion	ARHGDIB, DSG1, S100A11, SOD1, PCDHGB4, PCDHGA8, CCS, PARK7, PCDHGA12, PYCARD, PCDHGC5, PCDHGC4, PCDHGB3, PCDHGA9, PCDHGA6, PCDHGA5, PCDHGA4, PCDHGA3, PCDHGA2, PCDHGA1	0.000906	3.04
Cytoskeleton organization	ARHGDIB, CFL1, KRT5, KRT9, KRT16, MYH3, SOD1, PHPT1, PYCARD, SH3BGL3, KRT74, MTPN, WASH3P	0.014298	1.84

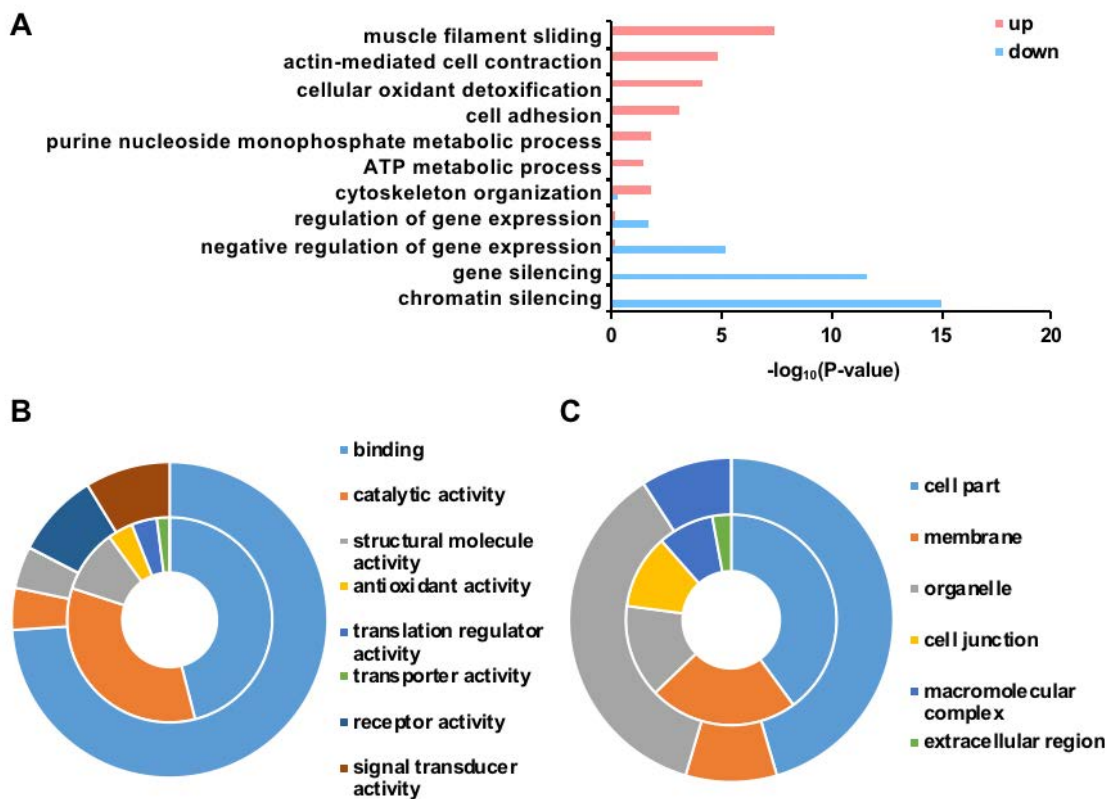
B.

GO term	Gene	P-value	Z Score
Negative regulation of gene expression	BMI1, HIST1H2AD, HIST1H2AJ, HIST1H2AC, HIST1H2AB, HIST2H2AA3, HIST2H2AC, HIST1H4A, HIST1H2AG, H2AFJ, HIST1H2AH, HIST3H2A	5.9895E-06	5.22
Regulation of gene expression	ACTG2, BMI1, HIST1H2AD, HIST1H2AJ, HIST1H2AC, HIST1H2AB, HIST2H2AA3, HIST2H2AC, HIST1H4A, HIST1H2AG, H2AFJ, HIST1H2AH, HIST3H2A	0.021575	1.66
Chromatin silencing	HIST1H2AD, HIST1H2AJ, HIST1H2AC, HIST1H2AB, HIST2H2AA3, HIST2H2AC, HIST1H4A, HIST1H2AG, H2AFJ, HIST1H2AH, HIST3H2A	1.13049E-15	14.94
Gene silencing	HIST1H2AD, HIST1H2AJ, HIST1H2AC, HIST1H2AB, HIST2H2AA3, HIST2H2AC, HIST1H4A, HIST1H2AG, H2AFJ, HIST1H2AH, HIST3H2A	2.35734E-12	11.63

Interestingly, the classified molecular functions of the DEPs include binding, catalytic activity, structural molecule activity, antioxidant activity, translation regulator activity, transporter activity, receptor activity, and signal transducer activity (**Figure 3B**). Binding function was the largest portion of both the upregulated and downregulated DEPs. Catalytic, antioxidant, translation regulator, and transporter activity were the major molecular functions in the upregulated DEPs. However, receptor and signal transducer activity were the major functions in downregulated DEPs. The classified cellular compartments of the DEPs were cell part, membrane, organelle, cell junction, macromolecular complex, and extracellular region (**Figure 3C**). Membrane, cell junction, and extracellular region were the major cellular compartments in upregulated DEPs. Organelle and macromolecular complex are major cellular compartments in the outer circle.

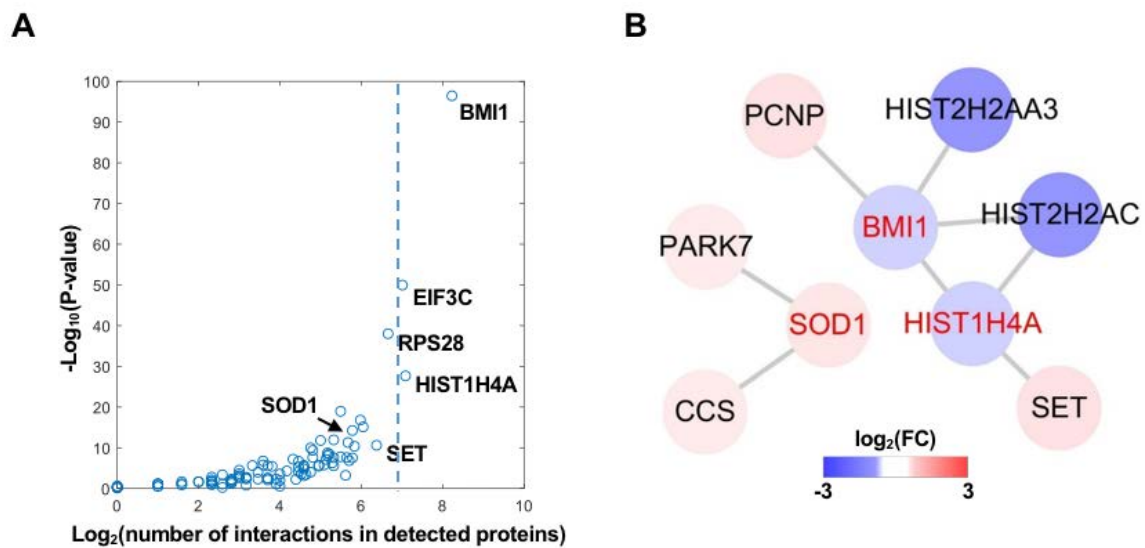
Identification of protein interaction networks regulated by pioglitazone treatment. Our present study revealed a large set of proteins (n=5,769) with relevant levels of abundance in normal bladder epithelial cells. These proteins actively participate in various cellular processes, including actin regulation and chromatin remodeling (**Figure 3A**). Pioglitazone perturbs and modulates these cellular processes by affecting protein-protein interactions. We therefore performed MRA using all the proteins detected in our global proteomic analysis to identify key proteins that can be major nodes in the protein-protein interaction networks. To select key proteins, we first identified proteins with a large number of interactions from those detected. We then determined the top 5 proteins with the largest number of interactions and the most significant p-values (**Figure 4A and Supplementary Table S2**).

Figure 3. Functional enrichment and classification of the DEPs. (A) Bar plot shows biological processes enriched by the up- and downregulated DEPs. (B) Top molecular functions of upregulated (inner circle) and downregulated (outer circle) proteins. (C) Top cellular compartments of upregulated (inner circle) and downregulated (outer circle) proteins.



To reconstruct the network model, top 3 proteins were then used. Of note, B lymphoma Mo-MLV insertion region 1 homolog (BMI1), HIST1H4A, and superoxide dismutase 1 (SOD1) were found to be the top 3 regulators, with p-values <0.01 and large target counts. The network model describes the interactions among the top 3 regulators and their interactors with significant differential expression when treated with pioglitazone. Pioglitazone treatment downregulated expression of BMI1, which was found to interact mainly with histone proteins, such as HIST2AH2AA3, HIST2H2AC, HIST1H4A (**Figure 4B**). Expression of SOD1 increased with pioglitazone treatment and it was found to interact with two other upregulated proteins, PARK7 (parkinsonism associated deglycase) and CCS (copper chaperone for superoxide dismutase). Interestingly, downregulation of BMI1 and its interacting histone proteins in the network model suggests potential epigenetic regulation by pioglitazone, which is consistent with functional enrichment data indicating “chromatin silencing” (**Figure 3A**).

Figure 4. Potential master regulators suggested by master regulator analysis (MRA). (A) Scatter plot displays distribution of detected proteins by number of interactions and level of significance driven by MRA. (B) Network model describing the interactions of the top 3 master regulators and their interacting DEP partners. Red font denotes the top 3 master regulators.

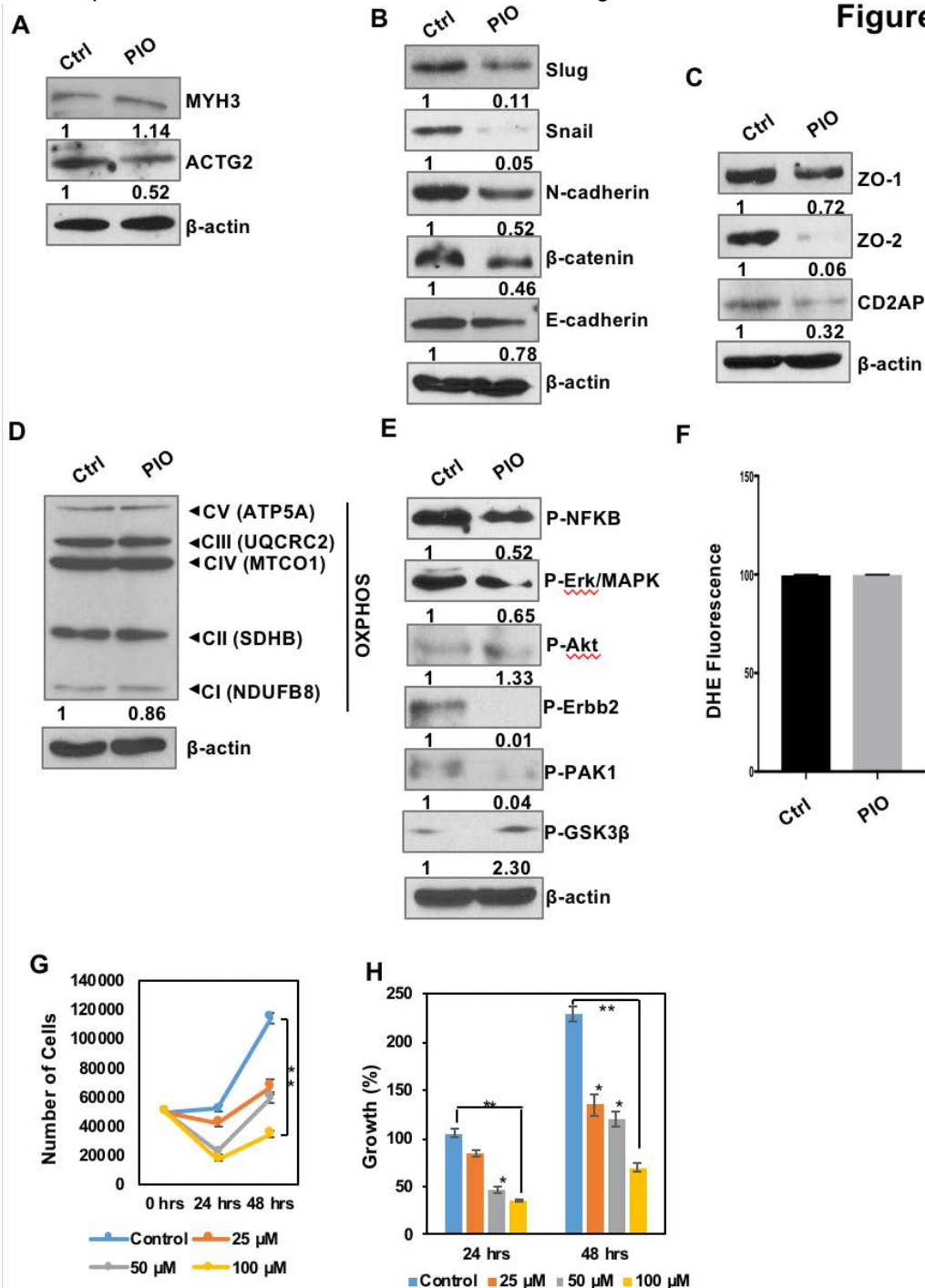


Biological effects of pioglitazone on immortalized normal bladder epithelial cells. To further validate the DEPs between the control vs. pioglitazone groups, proteins were selected for based on functional enrichment analyses. Additional western blot analysis demonstrated that expression of MYH3 (myosin heavy chain 3) was upregulated, while expression of ACTG2 (actin gamma 2) was downregulated in cells treated with 25 μM of pioglitazone (**Figure 5A**). Consistent with morphological changes in pioglitazone-treated cells, we found that protein expression of mesenchymal cell markers, including N-cadherin, Snail, Slug, and β -catenin, were significantly reduced in pioglitazone-treated cells, compared to control cells (**Figure 5B**). In addition, tight junction proteins, including zonula occludens (ZO) 1 and 2 and CD2AP (CD2-associated protein), that are involved in cell-cell contact regions⁷⁴ were greatly reduced in pioglitazone-treated cells (**Figure 5C**).

To determine whether pioglitazone regulates mitochondrial quantity or metabolic respiration-associated proteins, a series of mitochondrial oxidative phosphorylation (OXPHOS) proteins⁷⁵ were measured via western blot analysis. The expression levels of OXPHOS subunits, such as C I subunit (NDUFB8), C II subunit [SDHB (succinate dehydrogenase)], C III core protein 2 [UQCRC2 (ubiquinol- cytochrome C reductase core protein 2)], C IV subunit [MTCO1 (Mitochondrially Encoded Cytochrome C Oxidase I)], and C V alpha subunit [ATP5A (ATP synthase subunit alpha)], did not change by pioglitazone treatment (**Figure 5D**). To profile the phosphorylation events in normal bladder cells, human TRT-HU1 cells were treated with or without pioglitazone. We performed a series of western blot analyses between the control and pioglitazone-treated groups and found that several phosphorylation events of specific signaling pathways were regulated by pioglitazone. The phosphorylation levels of NF- κ B, Erk/MAPK, ERBB2 and p21 activated kinase 1 (PAK1) decreased. On the contrary, only the phosphorylation levels of GSK3 β increased. Additionally, studies have shown that the activation of PPAR γ through agonists reduces diabetic myocardial fibrosis via regulation of the TGF- β /ERK pathway and EMT⁷⁶, which were both found to be upregulated in pioglitazone-treated cells compared to controls (**Figure 5E**).

To further elucidate on the role of pioglitazone on oxidative stress, cells were treated with pioglitazone for 72 h, and the resulting ROS levels were measured and analyzed. Levels of ROS were unchanged between the control and pioglitazone groups (**Figure 5F**). In addition to our proteomic analysis, we assessed whether pioglitazone affects cell proliferation. After incubating TRT-HU1 cells in varying concentrations of pioglitazone (25, 50, or 100 μM) for 24 and 48 h, we found that the cell proliferation rates of cells treated for 48 h were significantly suppressed, compared to controls (**Figure 5G-H**).

Figure 5. Effects of pioglitazone treatment on THT-HU1 cells. Cells were incubated in DMEM supplemented with 25 μ M of pioglitazone for 72 h before cell lysates were immunoblotted with various antibodies as indicated. **(A)** Immunoblot analyses were performed to validate the expression levels of identified DEPs. The protein expression levels of MYH3 and ACTG2 significantly decreased with pioglitazone treatment (PIO), compared to controls (Ctrl). **(B)** Several EMT markers, including Slug, Snail, N-cadherin, β -catenin, and E-cadherin, were measured by immunoblot analysis. **(C)** Cell junction markers (ZO-1, ZO-2, and CD2AP) were also measured by immunoblot analysis. β -actin was used as the loading control. **(D)** Levels of mitochondrial oxidative phosphorylation (OXPHOS) markers were compared between Ctrl and PIO groups. No significant changes were observed in response to pioglitazone treatment. **(E)** Western blot analysis of key signal transduction proteins, including phospho-NF- κ B, phospho-Erk/MAPK, phospho-HER2/ErbB2, phospho-PAK1 and phospho-GSK-3 β . β -actin was used as an internal control. **(F)** ROS production levels were compared between Ctrl and PIO groups. NS, nonsignificant. **(G)** Cell proliferation rate was measured by counting with trypan blue staining. *, $P < 0.01$; **, $P < 0.005$; NS, nonsignificant. **(H)** Dose- and time-dependent cell growth rates were measured in an independent set of experiments. *, $P < 0.01$; **, $P < 0.005$; NS, nonsignificant.



DISCUSSION

There are many discrepancies surrounding the link between TZD usage and side effects on bladder function. Diabetic bladders can have several dysfunctions, ranging from bladder overactivity to impaired contractility, which represent a wide spectrum of clinical symptoms. The widespread pathophysiology of bladder dysfunction in diabetic patients is associated with multiple factors, including neuronal dysfunction, smooth muscle dysfunction, and urothelial impairment⁷⁷. In patients, diabetes has been shown to be a significant predictor of death from cancer, including BC⁷⁸. Evidence from a meta-analysis study has linked the use of pioglitazone to increased BC risk as well⁵³. The tumorigenic effect of pioglitazone is thought to be due to signaling modifications in the PPAR pathway⁷⁹. However, it is still unclear whether the long-term use of pioglitazone increases the chances of developing bladder dysfunctions or disease.

PPAR γ is part of the PPAR subfamily that consists of two other subunits, alpha and beta/delta. As the most extensively studied subunit, the functions of PPAR γ have been linked to several crucial biological processes, including glucose metabolism, lipid biosynthesis, and anti-inflammatory response⁸⁰. The association of PPAR γ to diabetes is based on its role in lipid and glucose metabolism⁸¹. It has been shown that patients with dominant negative mutations of PPAR γ have severe hypoglycemia, insulin resistance, and DM⁸². This means that there is a significant genetic link between both PPAR γ and DM. Treatment with TZDs has proven to substantially decrease insulin resistance in diabetes and possibly induces transcription of adipose cell differentiation, which generates smaller insulin-sensitive adipocytes⁸³. However, despite their beneficial effects in patients with diabetes, TZDs are known to have adverse effects. This includes weight gain, fluid retention, bone mineral density reduction, and excess myocardial infarction⁸⁴. The fluid retention induced by TZDs has also been proven to significantly increase urine volume and excretion of sodium⁸⁵. Because of this, there is some controversy surrounding the safety of long-term TZD usage to treat diabetes.

In addition to the documented roles of PPAR γ in lipid metabolism and DM, there has been growing research on its functions in both BC and interstitial cystitis (IC). Approximately 20-25% of human BC is driven by hyperactive PPAR signaling that is due to either PPAR γ gene amplification or RXRA hot-spot mutations⁸⁶. Furthermore, it was found that the PPAR γ transcription pathway can be a tumor-intrinsic mechanism for immune evasion in muscle-invasive BC⁸⁷. Along with this immune escape, it has been proposed that PPAR γ cooperates with the FOXA1 (forkhead box protein A1) and GATA3 (GATA binding protein 3) networks to drive transdifferentiation of basal BC cells into luminal types⁸⁸. PPAR γ has also been identified to be associated with IC. Mahal A et al. found that treating their IC rat model with PPAR γ agonists improved bladder function and urinary health⁸⁹. Based on the complex relationship of PPAR γ with diabetes and urological malignancies, it would be compelling to better understand how patients who routinely take TZDs are affected.

This study revealed that BMI1 is a master node in pioglitazone-regulated networks. A recent study showed that overexpression of BMI1 repressed transcripts of PPAR γ in mesenchymal stem cells (MSCs)⁹⁰. Our proteomic profiling of BMI1 exhibited significant downregulation in normal bladder epithelial cells treated with pioglitazone, suggesting a potential inverse relationship between PPAR γ and BMI1. One possible hypothesis for our future study is that PPAR γ signaling induced by pioglitazone may cause loss of BMI1 expression in bladder cells. Expression of telomere maintenance proteins including HIST1H4A, HIST2H2AA3 and HIST2H2AC, which interact with BMI1, are downregulated as well. The presence of an upregulated telomere maintenance mechanism is a hallmark of cancer, and it is interesting to note that HIST2H2AA3 and HIST2H2AC were identified as genes upregulated, differentially expressed in BC⁹¹. This may signify a stage shift, by pioglitazone treatment, from developing cancer. PPAR γ agonism has also been shown to increase the antitumor effects of histone deacetylase inhibitors in multiple myeloma cells.⁸⁵

Most notably, in our study, we found a series of contractile and cytoskeleton proteins, such as myosin light polypeptides, myosin heavy polypeptides, keratins, and ACTG2, as being significantly up- or downregulated in TRT-HU1 bladder epithelial cells treated with pioglitazone. Myosin is a particularly important structural component of muscles that interacts with actin filaments and plays a vital role in actin filament contraction, bundling, motor action, and binding. Furthermore, our network modeling revealed that these actin-binding proteins comprise the central hub. These results suggest the potential pathophysiological mechanisms of pioglitazone's effects.

Our data demonstrated that the activation of PPAR γ signaling pathways inhibits the proliferation of bladder epithelial cells. Interestingly, these findings are consistent with clinical observations that the IC bladder has thinner epithelial layers⁹² and that IC bladder cells exhibit reduced proliferation due to cell cycle arrest⁹³. Our epigenetic remodeling study supports this mechanistic link between IC and defective cell proliferation.⁹⁴ Furthermore, previous reports suggest that the anti-proliferative role of PPAR γ is through the upregulation of PTEN expression in various cancers, which leads to decreased PI-3K activity⁹⁵. It is currently known that PPAR γ agonists promote cell cycle arrest by downregulating cyclin D1 in several tumor lines; thereby, inhibiting cyclin D1/CDK-mediated retinoblastoma (pRb) phosphorylation and maintaining its active form to prevent the G1 to S phase transition⁹⁶. Activation of PPAR γ via agonists in normal human urothelial cells has been shown to induce expression of gene/protein markers associated with late/terminal urothelial differentiation, including uroplakins, cytokeratins, and tight junction constituents^{97,98}.

In summary, although pioglitazone is widely used among T2DM patients, its effects on the bladder are still in controversy. While there have been studies examining the effects of pioglitazone on healthy bladder cells, there is no conclusive evidence. Through unbiased quantitative proteomic profiling, our report comprehensively characterized the proteome of normal bladder epithelial cells treated with pioglitazone. We observed suppressed cell proliferation, which may be explained by the decreased expression of tight junction proteins. Taken together, our study provides no experimental evidence to support a tumorigenic effect of pioglitazone on the bladder. This proteomic approach will be useful for examining any potential side effects of the one of the most commonly used drugs.

Advances in Urinary Biomarker Discovery in Urological Research

Why we care about bladder cancer and other benign bladder diseases?

The bladder is a hollow, soft muscular organ located in the lower abdomen, which stores urine until it is ready to excrete. In urological diseases, the incidence of bladder diseases is quite high. The common bladder diseases include bladder cancer, bladder dysfunction (cystitis, urinary incontinence, overactive bladder, etc.) and other bladder problems. Bladder cancer (BC) is the sixth most common cancer in the United States, accounting for 4.7% of cancer cases¹. About 45,000 men and 17,000 women in the United States are diagnosed as BC every year.

Interstitial cystitis (IC) is the most common disease in bladder dysfunction. According to the International Continence Society, the definition of IC is "the complaint of suprapubic pain related to bladder filling, accompanied by other symptoms such as increased daytime and nighttime frequency, in the absence of proven urinary infection or other obvious pathology."² The morbidity of IC in the general population is 0.26-12.6%^{3,4}. The estimated morbidity of IC in women is 45/100.000, which is 4-5 times than that in men, with the morbidity of 8/100.000⁵. In the United States, 3.3 million women are diagnosed as IC every year⁶. At present, one of the most important methods to diagnose bladder diseases is cystoscopy, but this technique is invasive and may lead to urinary tract infection. Compared to cystoscopy, urine testing is easier to perform in clinical practice. Urine can be obtained non-invasively and shows increased stability over serum or blood, which allows for easy multiple sampling. With the direct contact between urine and bladder diseases, the use of urinary biomarkers detection in bladder diseases becomes more and more important.

Will it be useful the urine-based diagnostic biomarkers to detect and monitor the bladder diseases?

Urinary biomarkers are particularly attractive due to the direct contact of the urine with the urothelial tumor cells and the ease of sample collection. Urine-based diagnostic biomarkers are reviewed in our paper from the following aspects: gene mutations and gene expression-based biomarkers, proteomic biomarkers (**Table 1**), metabolomic biomarkers (**Table 2**), and DNA methylation biomarkers (**Table 3**).

Gene mutations associated with BC

The exact cause of BC is still unclear. There are several risk factors related to BC, including environment, smoking, toxic industrial chemicals and gases, bladder inflammation, and gene mutations. As a noninvasive method, detecting mutant genes in urine plays an important role in the diagnosis of BC.

A study of Zhu et al.⁷ indicated 14 important mutation genes related to BC by searching the COSMIC database. The mutation genes included P53, Fibroblast Growth Factor Receptor 3 (FGFR3), TSC Complex Subunit 1 (TSC1), Stromal Antigen 2 (STAG2), **HRas** Proto-Oncogene (HRAS), Phosphatidylinositol-4,5-Bisphosphate 3-Kinase Catalytic Subunit Alpha (PIK3CA), Erb-B2 Receptor Tyrosine Kinase 3 (ERBB3), Neurofibromatosis type 1 (NF1), Erb-B2 Receptor Tyrosine Kinase 2 (ERBB2), **Fibroblast Growth Factor Receptor 1** (FGFR1), **cyclin-dependent kinase Inhibitor 2A** (CDKN2A), AT-Rich Interaction Domain 1A (ARID1A), Histone-lysine N-methyltransferase 2D (KTM2D), and CREB Binding Protein (CREBBP). Several studies showed that the development of BC is associated with the mutations of P53 gene⁸⁻¹¹. Sidransky et al.¹² first described the mutations of P53 gene in the urine of BC patients in 1991. They found that alterations in P53 gene were associated with poor differentiation, advanced urothelial cell carcinoma and poor prognosis^{8,9}. Traczyk-Borszynska et al.¹³ showed that the mutations of P53 gene were more common in clinically and histologically advanced carcinoma, and were the negative prognostic factor in BC. FGFR3 mutations also participated in the development of BC. A study showed that mutations of the FGFR3 gene were surrogate markers for the detection of genome stable bladder tumors¹⁴. Another study indicated that FGFR3 mutations were the feature of well-differentiated BC but not the prognostic marker in BC¹³. In other studies, Van Rhijn et al.¹⁵ showed that the combination of FGFR3 with MIB-1 (Ki67) had a more accurate prediction of the progression and survival in BC. Ploussard et al.¹⁶ found that the progression and recurrence of FGFR3 mutations in disease depended on allele loss of 9p22. Also, Rebouissou et al.¹⁷ found that the progression of FGFR3 mutations in non-muscle-invasive disease depended on the homozygous deletion of 9p21. HRAS is a proto-oncogene, which may promote tumorigenesis in several organs including the bladder. HRAS gene mutations in bladder cells were associated with BC, but the mutation rate was low. A study showed that the mutation rate of HRAS gene varies greatly in BC (0-30%)¹⁸. Beukers et al.¹⁹ indicated that HRAS gene mutations were more likely to occur in young BC patients (<20 years) compared with older patients. It suggested that mosaicism of oncogenic HRAS mutations may increase the risk of developing BC at a young age.

Several studies showed that TSC1 had inactive point mutations on 9q34 in 10-15% of BC patients, resulting in complete loss of function of TSC1²⁰⁻²². Also, the deletion of a single TSC1 allele may promote the growth of bladder epithelial cells and therefore promote the development of BC²³. Stromal Antigen 2 (STAG2) mutations were recently identified in BC patients. However, the significance of STAG2 mutations remains controversial. Solomon et al.²⁴ showed that loss of STAG2 promoted the lymph node metastases in BC and increased the risk of recurrence and mortality. However, different subtypes of BC may exhibit different mutations²⁵. In several studies, loss of STAG2 was reported to be associated with BC in low stage and low grade²⁶⁻²⁸.

Alana et al.²⁹ found that STAG2 mutations were much more common in non-muscle invasive BC (32%) than in muscle invasion BC (12%). These studies suggested that STAG2 could be a potentially useful biomarker for predicting recurrence and progression in non-muscle invasive BC. BRCA1 Associated Protein 1 (BAP1) is a nuclear ubiquitin carboxy-terminal hydrolase or deubiquitinating enzyme which can regulate several cellular functions, including cell cycle, differentiation, proliferation, and DNA damage response³⁰. The recent research indicated that BAP1 mutations were related to BRCA pathway alterations in bladder cancer. Lin et al.³¹ indicated that patients carrying BAP1 genetic variant alleles of rs12163565 had an increased risk of developing BC, although the increased risk was not statistically significant (OR=1.17, P=0.070). There were studies showed that PIK3CA gene alterations, including mutations, copy gains or amplifications, were associated with non-muscle invasive BC^{32,33}.

Duenas et al.³³ showed that PIK3CA gene alterations were frequent and associated with low recurrence and low progression in non-muscle invasive BC, which indicated that PIK3CA may be a potential biomarker for predicting recurrence and progression in non-muscle invasive BC. Collectively, many genes mutations have been found in BC patients. Further studies are required to discover more gene mutations and new biomarkers in BC before they can be used in clinical practice.

Gene expression-based BC biomarkers

Gene expression-based urinary biomarkers have good sensitivity and specificity in the detection of BC. They are less likely to be affected by inflammatory and other benign conditions. Several important genetic changes in BC have been identified in the past two decades. Based on the technology of rapid nucleic acid extraction and the proven stability of DNA and RNA in urine, gene expression-based biomarkers play an important role in the detection of BC.

A study from Beukers et al. showed that FGFR3, Telomerase Reverse Transcriptase (TERT), and Orthodenticle Homeobox 1 (OTX1) were significant in the diagnosis of BC³⁴. They acted as a urinary biomarker combination with a sensitivity of 57% in low grade primary BC patients and 83% in pT1 or muscle invasive BC. In a study of Holyoake et al.³⁵, the researchers used microarray data from BC patients and healthy controls to generate a panel of genes that were differentially expressed in various stages and grades of BC patients and normal controls. They tested the markers in voided-urine samples to generate an mRNA panel, including Cyclin-dependent kinase-1 (CDK1; also known as *CDC2*), Midkine (MDK), Insulin Like Growth Factor Binding Protein 5 (IGFBP5), and Homeobox A3 (HOXA3), which could predict the presence of BC with a sensitivity of 48%-100% and a specificity of 85%. Park et al.³⁶ examined Aurora kinase A (AURKA) gene amplification in exfoliated cells in urine samples. They concluded that AURKA could be a biomarker for the detection of BC with a specificity of 96.6% and a sensitivity of 87%, and the degree of gene amplification was also associated with high grade BC. Urquidi et al.³⁷ used Affymetrix arrays of 92 patients (52 BC and 40 controls) and derived a 14 gene panel that could predict the presence of BC, with high sensitivity and specificity (90% and 100%, respectively) and AUC (area under the receiver operating curve) of 0.98. The 14 genes were: carbonic anhydrase 9 (CA9), Transmembrane Protein 45A (TMEM45A), C-C Motif Chemokine Ligand 18 (CCL18), Matrix Remodeling Associated 8 (MXRA8), Matrix metalloproteinase 9 (MMP9), Semaphorin 3D (SEMA3D), erb-b2 receptor tyrosine kinase 2 (ERBB2), Vascular Endothelial Growth Factor A (VEGFA), desmocollin 2 (DSC2), Ras-related protein Rab-1A (RAB1A), angiotensinogen (AGT), Synaptogyrin 1 (SYNGR1), Deleted in malignant brain tumors 1 (DMBT1), Angiogenin (ANG). The first seven genes were upregulated and the last seven genes were down-regulated in the urines of BC patients. Bongiovanni et al.³⁸ found that the expression levels of Septin 4 (SEPT4) were up-regulated in the urine of BC patients, with a sensitivity of 93%, a specificity of 65%, and AUC of 0.798. All these studies have shown promise in the diagnosis of BC. However, the majority of them remain in the discovery phase.

MicroRNAs (miRNAs) are a class of small, endogenous, noncoding RNA. They regulate gene expression by affecting mRNA translation and stability or by modulating promoter activity of their target genes. In oncology, miRNAs are considered as promising biomarkers for early diagnosis, prognosis evaluation and therapeutic response prediction of the tumor. A large number of studies showed that miRNAs acted as diagnostic biomarkers in urine samples of BC patients^{36,39-42}. Some miRNAs were down-regulated such as miR-125b, miR-140-5p, miR-141, miR-200a, miR-200c, and others were up-regulated such as miR-18a, miR-92a, miR-96. Other studies indicated that miR126, miR152, miR222, and miR452 were up-regulated in BC⁴³⁻⁴⁵. However, miR-200 family, miR-155, miR-192, miR-205, and miR-143 were found to be down-regulated in studies^{44,46}. Eissa et al.⁴⁷ found that the levels of miR-324-5p, miR4738-3p, and FOSB mRNA were up-regulated in the urine of BC patients, whereas lncRNA miR497-HG and RCAN1 mRNA were down-regulated in BC patients, compared with patients with benign lesions and healthy controls. The sensitivities and accuracies of the RNAs were significantly higher than those of cytology. In the urinary ceRNA: lncRNA-miRNA-mRNA network, 2 mRNAs (FOS B and RCAN1) displayed the highest accuracy for the diagnosis of BC. A study of Chen et al.⁴⁸ showed that MiR-101 was decreased in BC patients, and was negatively associated with aggressive clinical characteristics, with a sensitivity of 82.0% and a specificity of 80.9% in BC.

Most of the studies on miRNAs were different in methodology, with little overlap, and no results were fully validated. At present, there are no valid conclusions about urinary miRNAs in the detection of BC patients. Multicenter prospective validation studies in large clinical settings are needed in the future.

Proteomics profiling revealed urinary biomarkers for BC

The urinary proteome enriched in proteins reflects the development and invasion of the tumor through direct contact with BC. The study of urinary proteomic biomarkers has been mainly used to help diagnose primary and recurrent BC and to assess the aggressiveness of the disease.

Nuclear matrix protein 22 (NMP22) is one urinary biomarker approved by the U.S. Food and Drug Administration (FDA) using ELISA test and BladderChek point-of-care (POC) test^{49,50}. However, in a meta-analysis of 19 studies for the detection of BC, the sensitivity of NMP22 was 52-59% and the specificity was 87-89%, with an AUC of 0.83⁵¹. Another biomarker approved by FDA is the bladder tumor antigen (BTA), also known as human complement factor H related protein (hCFHrp). In a meta-analysis of 13 studies using BTA STAT test, the sensitivity of BTA was 64-69% and the specificity was 73-77%⁵². In a meta-analysis of 5 studies using BTA STAT test, the sensitivity of BTA was 62-71% and the specificity was 45-81%⁵³. Both of the two markers above were not good in sensitivities and specificities.

An ideal protein biomarker should be the one with high sensitivity, specificity, positive predictive value (PPV), negative predictive value (NPV), and AUC values⁵⁴. Several studies showed that Apo-A1, BLCA-4, and hyaluronidase in urine were independently validated in BC with high sensitivities and specificities⁵⁵⁻⁶⁰. Apo-A1 is the primary protein component of high-density lipoprotein, which may improve tumor angiogenesis through kinase activation^{61,62}. But the association between lipoproteins and BC progression is still not very clear. Studies showed that Apo-A1 was independently validated in BC with the sensitivity of 89-95% and the specificity of 85-92%⁵⁵⁻⁵⁷. BLCA-4 is a nuclear transcription factor found in the early stages of BC. Cai et al.⁵⁸ found that BLCA-4 was independently validated with the sensitivity of 93% and the specificity of 97% through an analysis of nine studies. Hyaluronidase could improve cellular proliferation and motility through hyaluronic acid [63]. Studies of Eissa et al.⁵⁹ and Pham et al.⁶⁰ showed the sensitivity and specificity of Hyaluronidase ranged from 87-100% and 89-98% respectively. Besides the three proteins, there were several additional urine proteins that exhibited with high sensitivities and specificities, but they have not yet been independently validated, including angiogenin (ANG), apolipoprotein E (APOE), carbonic anhydrase 9 (CA-9), interleukin-8 (IL-8), matrix metalloproteinase-9 (MMP-9), matrix metalloproteinase-10 (MMP-10), plasminogen activator inhibitor 1 (PAI-1), vascular endothelial growth factor (VEGF)^{63,64}. Goodison et al.⁶³ found that the eight-biomarker panel above achieved a sensitivity of 92% and a specificity of 97%, while the BTA TRAK ELISA test achieved a sensitivity of 78% and a specificity of 83% in the same cohort for BC detection. Another study of Urquidi et al.⁶⁵ showed that urine CCL18 achieved a sensitivity of 88% and a specificity of 86%, while BTA TRAK ELISA achieved a sensitivity of 80% and a specificity of 84% in the same cohort for BC detection. All of the biomarkers above had better sensitivities and specificities than BTA. These head-to-head studies compared the biomarkers with the FDA-approved test in the same patient cohort, increasing the validity of the studies.

Proteomics profiling revealed urinary biomarkers for IC

IC/BPS is the most common disease in bladder dysfunction. At present, the etiology of IC/BPS is still not fully understood. There are several possible mechanisms, including infection, inflammation, toxic substances absorption, mucus layer with deficient glycosaminoglycan, hypoxia, and genetics. So far there are no gold standards in the diagnosis of IC/BPS. Some invasive testing including biopsy, urodynamic, and cystoscopy are applied to help diagnose the disease. However, there is still a lack of tools to facilitate accurate diagnosis and objective follow-up. Therefore, it is significant to investigate urinary biomarkers that can be used in clinical practice.

A study by Thais et al.⁶⁶ reviewed the urinary biomarkers associated with IC/BPS. They found potential biomarkers investigated in urine specimens included macrophage inhibitory factor (MIF), nerve growth factor (NGF), methylhistamine, histamine, interleukin-6 (IL-6), APF, epithelial growth factor (EGF), HB-EGF, glycoprotein G5P1, and a chemokine profile. Tonyali et al.⁶⁷ detected urinary NGF and nerve density in the bladder mucosa. They found that urinary NGF/Cr was significantly increased in IC/BPS patients comparing to control groups, which was similar to nerve density. Corcoran et al.⁶⁸ assessed both urine samples and bladder biopsy samples to determine the profile of 23 chemokines in 10 IC/BPS patients and 10 controls. The results indicated that univariate analysis showed no significant differences in any of the urinary proteins assessed, but multivariate analysis showed that VCAM-1 and ICAM-1 in urine were significantly different between IC/BPS and controls. A study of Vera et al.⁶⁹ studied urinary MIF concentrations in subgroups of BPS with and without

Hunner lesions and control groups. They verified that urinary MIF was significantly higher in BPS patients with Hunner lesion compared with patients without Hunner and with controls, with a sensitivity of 74.4%, a specificity of 71.8%, and AUC 0.718. For the urinary MIF/Cr ratio, the sensitivity was 47%, the specificity was 91% and AUC was 0.730 in identifying patients with IC/BPS and Hunner lesions. Lamale et al.⁷⁰ investigated urinary histamine, IL-6, and methylhistamine in IC/BPS patients and controls. They found that urinary concentrations of histamine and IL-6 were increased in IC/BPS patients. However, methylhistamine levels had no significant differences between IC/BPS patients and controls. Further logistic regression analysis demonstrated that the best predictor for IC/BPS was a combined model with IL-6 and methylhistamine, with an AUC of 0.788. Furthermore, Keay et al.⁷¹ found that APF was increased in IC/BPS patients compared to controls, but HB-EGF concentrations were decreased in IC/BPS patients. Byrne et al.⁷² demonstrated that glycoprotein G5P1 concentration in urine was lower in IC/BPS patients than that in controls.

In general, urine proteomic biomarkers of bladder diseases have great promise, but the best biomarkers with the highest clinical utility remain to be discovered. There is still a need for more comprehensive screening of urine proteomic markers through extensive multi-institution validation. **Table 1** shows the urinary biomarkers suggested for BC and IC diagnosis.

Table 1. Proteomics-based Urinary Biomarkers

Bladder Diseases	Biomarkers	Study	Sample size	Method	Sensitivity	Specificity	AUC	Notes
BC	NMP22	Wang 2017 [50]	5291 patients total (Meta-analysis of 19 studies)	NMP22 BladderChek, ELISA	52%-59%	87%-89%	0.83	FDA-approved
	BTA	Guo 2014 [51]	3462 patients total (Meta-analysis of 13 studies)	BTA stat test	64%-69%	73%-77%	0.75	FDA-approved
	BTA	Glas 2003 [52]	829 patients total (Meta-analysis of 5 studies)	BTA TRAK test	62%-71%	45%-81%	NO	FDA-approved
	Apo-A1	Li 2011 [54]	107 BC and 49 OUC	ELISA	83.7%-91.6%	85.7%-89.7%	0.875-0.928	
		Li 2014 [55]	223 BC and 153 controls	ELISA	89%	85%	0.948	
		Chen 2010 [56]	126 specimens	ELISA	95%	92%	0.982	
	BLCA-4	Cai 2015 [57]	1119 subjects total (Meta-analysis of 9 studies)	ELISA (8 studies) qPCR (1 study)	93%	97%	0.9607	
	Hyaluronidase	Eissa 2015 [58]	94 BC, 60 OUC, and 56 HC	Zymography	89%	91%	0.948	PPV = 89%
		Pham 1997 [59]	22 G1 BC, 9 G2 BC, 40 G3 BC, 48 OUC, and 20 HC	ELISA-like assay	100%	89%	NO	
		ANG, APOE, CA-9, IL-8, MMP- 9, MMP-10, PAI-1, VEGF	Goodison 2012 [62]	64 BC and 62 HC	ELISA	92%	97%	NO
	CCL18	Urquidí 2012 [64]	64 BC and 63 controls	ELISA	88%	86%	0.919	PPV = 86%, NPV = 87%
IC/BPS	NGF	Tonyali 2018 [66]	15 women with BPS, 18 male and female controls	ELISA	NO	NO	NO	NGF/Cr was increased (p < 0.001)
	VCAM-1, ICAM-1 and MCP-3	Corcoran 2013 [67]	10 men and women with BPS, 10 male and female controls	Immuno-assay	NO	NO	NO	VCAM-1 and ICAM-1 was increased; MCP-3 was decreased (p < 0.05)
	MIF	Vera 2018 [68]	55 women with BPS without Hunner lesions, 43 women with BPS with Hunner lesions, and 100 female controls	ELISA	MIF 74.4%, MIF/Cr 47%	MIF 71.8%, MIF/Cr 91%	MIF 0.718, MIF/Cr 0.730	MIF, MIF/Cr was increased in BPS with Hunner lesion
	Histamine, IL-6, and Methyl-histamine	Lamale 2006 [69]	40 women with BPS, and 29 female controls	RIA, ELISA	70.00%	72.40%	0.788	Histamine and IL-6 was increased (p < 0.05). Best predictor: combined model with IL-6 and methylhistamine
	APF and HB-EGF	Keay 2004 [70]	24 men with BPS 36 male controls	3H-thymidine incorporation in cell cultures, ELISA	94%	95%	NO	APF was increased, HB-EGF was decreased (P < 0.00001)
	G5P1	Byrne 1999 [71]	36 patients with BPS and 23 controls	ELISA	NO	NO	NO	G5P1/Cr was decreased (p < 0.0001)

OUC= controls with other urinary conditions; HC= healthy controls. ELISA= enzyme-linked immunosorbent assay ; AUC= area under the receiver operating curve; PPV= positive predictive value; NPV= negative predictive value; FDA= U.S. Food and Drug Administration; NO= not reported.

Metabolomic biomarkers for BC

At present, urinary metabolomic biomarker studies are primarily conducted either by NMR-based or mass spectrometry (MS)-based identification. Three metabolites (2,5-furandicarboxylic acid, ribitol, and ribonic acid) were found to be lower in the urine of BC patients than in healthy controls⁷³⁻⁷⁵. Taurine is the metabolite known as a free-radical scavenger that can prevent cell damage. Studies showed that taurine was elevated in the urine of BC patients than in healthy controls^{75,76}. Several studies showed that urinary citrate, succinate, and hippurate were reduced in BC patients compared with control groups, which suggested that citrate changes were related to an altered tricarboxylic acid (TCA) cycle in BC metabolism⁷³⁻⁷⁷. On the study of glycolysis-related metabolites,

decreased fructose levels and increased lactate levels were showed in BC patients ^{73,75}. Urinary acetylcarnitine and adipate in BC patients were elevated, which were the results of disturbed fatty acid transportation, altered mitochondrial TCA cycle, and energy metabolism processes or an excess of acetyl- CoA production ^{74,75,77}.

Wittmann et al. ⁷⁵ identified between 178 and 233 discriminating metabolites (depending on the respective comparison) in a retrospective MS study. They compared current BC patients with three different control groups: patients with haematuria, controls with BC in the past but without the current disease, and a mixed group of patients with haematuria, those with BC in the past and some healthy subjects. They found that 3-hydroxybutyrate and gluconate were the most highly increased in BC patients, while anserine, 3-hydroxyphenylacetate and pyridoxate showed the lowest values in BC patients. In another high-resolution LC-MS study, glycolysis and acylcarnitines were increased in BC than a combined control group (patients with haematuria and healthy controls) ⁷⁸. Besides, amino acid metabolism and fatty acid oxidation were also important factors in BC pathology. A study showed that the acylcarnitines, decanoylcarnitine, decenoylcarnitine, hydroxynonanoylcarnitine and hydroxybutyrylcarnitine were all increased in BC patients ⁷⁹. These urinary metabolomic biomarkers may have potential significance in the diagnosis of BC.

Metabolomic biomarkers for IC

In the research of IC/BPS, Parker et al. ⁸⁰ used liquid chromatography-MS in urine samples of 40 women with IC/BPS and 40 controls to determine metabolomic profiles. They found six metabolites were closely associated with IC/BPS. One of them was etiocholan-3 α -ol-17-one (Etio-S). The elevated Etio-S was a good predictor of IC/BPS, with a sensitivity of 91.2%, a specificity of 87.4%, and AUC of 0.92. Longitudinal analysis of women in this cohort showed that the differences in Etio-S persisted, indicating that these changes could last long.

The results from these early studies on metabolomic biomarkers suggest that urine may act as a potential tool on screening or monitoring bladder diseases in the clinical field, but it is still in the discovery phase. More large multicenter studies with independent validation cohorts are needed to advance the field. **Table 2** shows the urinary biomarkers suggested for IC diagnosis.

Table 2. Metabolomics Urinary Biomarkers

Bladder Diseases	Biomarkers	Study	Sample size	Method	Sensitivity	Specificity	AUC	Notes
BC	2,5-furandicarboxylic aci, Ribitol, and Ribonic acid	Pasikanti 2013 [72]	38 BC and 61 controls	G \times G \times C-TOFMS	71%	100%	NO	Decreased
		Pasikanti 2010 [73]	24 BC and 51 controls	GC-TOFMS	100%	NO	0.9	Decreased
		Wittmann 2014 [74]	95 BC and 345 controls	UHPLC-MS/MS and GC-MS	NO	NO	NO	Increased
	Taurine	Srivastava 2010 [75]	33 BC and 37 healthy	1H NMR spectroscopy	NO	NO	NO	Increased
		Pasikanti 2013 [72]	38 BC and 61 controls	G \times G \times C-TOFMS	71%	100%	NO	Decreased
		Pasikanti 2010 [73]	24 BC and 51 controls	GC-TOFMS	100%	NO	0.9	Decreased
	Citrate	Pasikanti 2010 [73]	24 BC and 51 controls	GC-TOFMS	100%	NO	0.9	Decreased
		Pasikanti 2010 [73]	24 BC and 51 controls	GC-TOFMS	100%	NO	0.9	Decreased
	Succinate and Hippurate	Huang 2011 [76]	27 BC and 32 controls	LC-MS	92.60%	68.80%	0.867(Hippurate)	Decreased
		Pasikanti 2013 [72]	38 BC and 61 controls	G \times G \times C-TOFMS	71%	100%	NO	Fructose Decreased and Lactate Increased
	Acetylcarnitine and Adipate	Pasikanti 2010 [73]	24 BC and 51 controls	GC-TOFMS	100%	NO	0.9	Increased
		Huang 2011 [76]	27 BC and 32 controls	LC-MS	NO	NO	0.598(acetylcarnitine)	Increased
	Component I and Carnitine C9:1	Huang 2011 [76]	27 BC and 32 controls	LC-MS	90.50%	96.90%	0.9 and 0.88, respectively	Increased
	3-hydroxybutyrate and Gluconate	Wittmann 2014 [74]	95 BC and 345 controls	UHPLC-MS/MS and GC-MS	NO	NO	NO	Increased
	Anserine, 3-hydroxyphenylacetate and Pyridoxate	Wittmann 2014 [74]	95 BC and 345 controls	UHPLC-MS/MS and GC-MS	NO	NO	NO	Decreased
Glycolysis and Acylcarnitines	Jin 2014 [77]	138 BC, 52 haematuria, and 69 healthy	high-resolution LC-MS	85%-91.3%	85%-92.5%	0.937	Increased	
Acylcarnitines, Decanoylcarnitine, Decenoylcarnitine, Hydroxynonanoylcarnitine and Hydroxybutyrylcarnitine	Liu 2018 [78]	53 BC, 6 benign lesions, and 203 healthy controls	high-resolution LC-MS	NO	NO	0.8	Increased	
IC/BPS	Etio-S	Parker 2016 [79]	40 women with BPS and 40 controls	liquid chromatography-MS	91.20%	87.40%	0.92	Increased

G \times G \times C-TOFMS= two-dimensional gas chromatography time-of-flight mass spectrometry; UHPLC-MS/MS=Ultrahigh-performance liquid chromatography/tandem mass spectrometry; GC-MS= gas chromatography- mass spectrometry; LC-MS= liquid chromatography-mass spectrometry; NO= not reported.

DNA methylation biomarkers for BC

DNA methylation has been recognized to be important in developmental biology and cancer etiology⁸¹. Aberrant DNA methylation is a major characteristic of BC and it plays an important role in tumor occurrence and progression⁸²⁻⁸⁴. Compared to RNA or protein, DNA is inherently stable, so it is more powerful in cancer detection. Chan et al.⁸⁵ examined the DNA methylation of seven genes (The retinoid acid receptor- β (RAR β), Death Associated Protein Kinase 1 (DAPK), E-cadherin, cyclin-dependent kinase inhibitor 2A (p16), p15^{INK4b} (p15), Glutathione S-Transferase Pi 1 (GSTP1), and O-6-Methylguanine-DNA Methyltransferase (MGMT)) in voided urine of BC patients and age- and sex-matched controls. Four biomarkers (Death-associated protein kinase 1 (DAPK), The retinoid acid receptor- β (RAR β), E-cadherin, and p16) achieved a sensitivity of 91% and a specificity of 76% for detecting BC. And cytology achieved a sensitivity of 46% and a specificity of 100% by comparison. Friedrich et al.⁸⁶ examined DNA methylation of apoptosis-associated genes (Death Associated Protein Kinase 1 (DAPK), Telomerase Reverse Transcriptase (TERT), and Apoptosis Regulator (BCL2)) in the urine of BC patients. They found that combined methylation analyses achieved both high sensitivity and specificity (78% and 100%, respectively) for detecting BC. In another study, Hoque et al.⁸⁷ examined the DNA methylation of nine genes (Adenomatous polyposis coli (APC), ARF tumor suppressor (p14ARF), Cadherin-1 (CDH1), GSTP1, O-6-Methylguanine-DNA Methyltransferase (MGMT), cyclin dependent kinase inhibitor 2A (CDKN2A), Retinoic Acid Receptor Beta (RARb2), ras association domain family member 1 (RASSF1A), and TIMP Metalloproteinase Inhibitor 3 (TIMP3)). They found that combined methylation analysis based on four genes (CDKN2A, p14ARF, MGMT, and GSTP1) achieved a sensitivity of 69% and a specificity of 100%. Recently there were some studies on Twist Family BHLH Transcription Factor 1 (TWIST1) and Nidogen 2 (NID2) genes. Renard et al.⁸⁸ reported that TWIST1 and NID2 genes were frequently methylated in BC patients in a total of 496 urine samples collected from three urology clinical sites. The sensitivity of this 2-gene panel was significantly better than that of cytology (90% and 48%, respectively), with the specificity of 93% and 96%, respectively. The positive predictive value and negative predictive value of the 2-gene panel was 86% and 95%, respectively. Yegin et al.⁸⁹ also found the high sensitivity of TWIST1 and NID2 genes for detecting BC (87.5% and 95.8%, respectively). However, the sensitivities of these two genes were poor in the studies of Abern et al.⁸⁹ and Fantony et al.⁹⁰. In other studies, Reinert et al.⁹¹ found a 4-marker panel (zinc finger protein 154 (ZNF154), Homeobox protein Hox-A9 (HOXA9), POU Class 4 Homeobox 2 (POU4F2), and eomesodermin (EOMES) achieved a sensitivity of 84% and a specificity of 96% for detecting BC in urine samples from 119 BC patients and 59 controls. Another study of Reinert et al.⁹² found a 6-marker panel (EOMES, HOXA9, POU4F2, TWIST1, Vimentin (VIM), and Zinc Finger Protein 154 (ZNF154)) had a sensitivity of 82%–89% and a specificity of 94%–100% for detecting BC in urine samples from 184 BC patients and 35 controls.

In a study of 368 urine samples collected from 90 non-muscle invasive BC patients, Su et al.⁹³ reported that a panel of 3 markers (SRY-box transcription factor 1 (SOX1), Interleukin 1 Receptor Associated Kinase 3 (IRAK3), and L1-MET) discriminated between patients with recurrence and with no recurrence, with a sensitivity of 86% and a specificity of 89% of patients with recurrence, compared with the sensitivity of 80% and specificity of 97% of patients with no recurrence in validation sets. The results demonstrated that the combination of SOX1, IRAK3, and L1-MET could detect disease recurrence with high sensitivity and specificity. Another study selected seven DNA methylation biomarkers (CDH13, Cystic fibrosis transmembrane conductance regulator (CFTR), Nidogen 2 (NID2), spalt like transcription factor 3 (SALL3), Transmembrane Protein With EGF Like And Two Follistatin Like Domains 2 (TMEFF2), TWIST1, and VIM2) from four recently published BC studies^{81,94-96}. They found that the best possible combination to discriminate against BC from controls was the combination CFTR, SALL3, and TWIST1⁹⁷. The three-gene methylation classifier achieved an AUC of 0.874, with a sensitivity of 85% and a specificity of 68%. The discovery of highly sensitive methylation biomarkers may allow us to lower the number of follow-up cystoscopies in patients with BC, which can improve the life quality of the patients.

DNA methylation biomarkers for IC

In the research of IC/BPS, Thais et al.⁶⁶ concluded that DNA methylation in urine samples was associated with IC/BPS. Bradley et al.⁹⁸ determined DNA methylation profiles in IC/BPS and controls. After Bonferroni correction, there was no genome-scale significantly different methylation in CpG sites. Among the methylated CpG sites, the most prominent enrichment pathway was the mitogen-activated protein kinase (MAPK) pathway. This pathway had 86% of sites with hypomethylation in IC/BPS patients compared to the controls.

There is evidence that DNA methylation biomarkers are more sensitive than cytology although there were biomarkers tested on cohorts that varied between studies. and some markers showed specificity comparable with that of cytology. A highly selective panel of methylation biomarkers may increase the sensitivity and specificity of urine analysis in the clinical studies⁹⁹. Standardized assays and cutoff values should be used in a large and well-designed cohort in future studies. **Table 3** summarizes urine epigenetics-based biomarkers for BC and IC.

Table 3. Epigenetic Urinary Biomarkers

Bladder Diseases	Biomarkers	Study	Sample size	Method	Sensitivity	Specificity	AUC	Notes	
BC	A combination of FGFR3, TERT, and OTX1	Beukers 2017 [34]	977 BC	RT-PCR	57%-83%	59%	NO		
	A combination of CDC2, MDK, IGFBP5, and HOXA3	Holyoake 2008 [35]	75 BC and 77controls	RT-PCR	48%-100%	85%	NO		
	AURKA	Park 2008 [36]	23 BC and 7 controls	FISH	87%	96.60%	0.939		
	A 14 gene panel: CA9, TMEM45A, CCL18, MXRA8, MMP9, SEMA3D, ERBB2, VEGFA, DSC2, RAB1A, AGT, SYNGR1, DMBT1, ANG	Urquidi 2012 [37]	52 BC and 40 controls	Affymetrix arrays	90%	100%	0.98	The first 7 genes were upregulated and the last 7 genes were downregulated	
	SEPT4	Bongiovanni 2012 [38]	41 BC and 17 controls	RT-PCR	93%	65%	0.798	upregulated	
	miR126 and miR152	Hanke 2010 [43]	18 BC and 18 controls	RT-qPCR	72%(the RNA ratio of miR-126:miR-152)	82%(the RNA ratio of miR-126:miR-152)	0.768(the RNA ratio of miR-126:miR-152)	upregulated	
	miR222 and miR452	Puerta-Gil 2012 [44]	37 BC and 57 controls	RT-qPCR			0.718 and 0.848	upregulated	
	miR96 and miR183	Yamada 2011 [45]	100 BC and 498 controls	RT-qPCR	71% and 74%	89.2% and 77.3%	0,831 and 0.817	upregulated	
	miR-200 family, miR-155, miR-192, miR-205	Wang 2012 [46]	51 BC and 24 controls	RT-qPCR	NO	NO	NO	downregulated	
	miR-324-5p, miR4738-3p, and FOSB mRNA	Eissa 2019 [47]	98 BC, 48 benign diseases, and 50 controls	RT-qPCR	87.7%, 84.7%, and 99%	86.7%, 80.6%, and 98.9%	NO	upregulated	
	lncRNA miR497-HG and RCAN1 mRNA	Eissa 2019 [47]	98 BC, 48 benign diseases, and 50 controls	RT-qPCR	90.5% and 99%	83% and 98.9%	NO	downregulated	
	DNA methylation biomarkers								
		DAPK, RAR β , E-cadherin, and p16	Chan 2002 [84]	22 BC and 17 controls	MSP	91%	76%	NO	
		DAPK, TERT, and BCL2	Friedrich 2004 [85]	37 BC and 20 controls	MSP	78%	100%	NO	
	CDKN2A, p14ARF, MGMT, and GSTP1	Hoque 2006 [86]	160 BC and 94 controls	qMSP	69%	100%	NO		
	TWIST1 and NID2	Renard 2010 [87]	496 urine samples	qMSP	90% and 48%, respectively	93% and 96%, respectively	NO		
		Abern 2014 [88]	111 patients	qMSP	79% (a combination)	63% (a combination)	NO		
		Fantony 2015 [89]	209 patients	qMSP	67% (a combination)	69% (a combination)	NO		
	A 4-marker panel (ZNF154, HOXA9, POU4F2, and EOMES)	Reinert 2011 [90]	119 BC and 59 controls	MSP	84%	96%	NO		
	A 6-marker panel (EOMES, HOXA9, POU4F2, TWIST1, VIM, and ZNF154)	Reinert 2012 [91]	184 BC and 35 controls	MS-HRM	82%–89%	94%–100%	NO		
	A 3-marker panel(SOX1, IRAK3, and L1-MET)	Su 2014 [92]	90 non-muscle invasive BC	MSP	86% in BC with recurrence and 80% in BC with no recurrence	89% in BC with recurrence and 97% in BC with no recurrence	NO		
	A combination of CFTR, SALL3, and TWIST1	van der Heijden 2018 [96]	111 BC and 57 controls	MSP	85%	68%	0.874		
IC/BPS	CpG-sites, MCP-3, G5P1, and HB-EGF	Magalhaes 2019 [65]	478 records total	A systematic review	NO	NO	NO	hypomethylation	
	CpG sites	Bradley 2018 [97]	19 IC BPS and 17 controls	Illumina Infinium MethylationEPIC BeadChip	NO	NO	NO	86% of MARK pathway sites with hypomethylation	

FISH= fluorescence in situ hybridization; RT-PCR= reverse transcriptase-polymerase chain reaction; RT-qPCR= quantitative reverse transcriptase-polymerase chain reaction; MSP= methylation-specific polymerase chain reaction; qMSP = specific high-resolution melting; MS-MLPA = methylation-specific multiplex ligation-dependent probe amplification; MS-HRM= methylation-specific high-resolution melting; NO= not reported.

Application of potential urinary biomarkers in clinical setting?

In conclusion, many studies have shown that urinary-based biomarkers have high sensitivity and specificity in the diagnosis of bladder diseases (such as BC and IC), which confirms the feasibility of using urinary exfoliated epithelium as an analyzer to diagnose bladder diseases. As shown in **Table 4**, commercially available biomarker kits for diagnosis of bladder disease such as BC have been introduced in market. If this method is accurate and reliable enough, it can be used not only for the diagnosis of bladder diseases but also for the screening of diseases in the population. However, further researches are needed to apply urinary biomarkers to clinical practice. More efforts should be made to improve and validate the biomarker panel and promote the progress of urine-based biomarker analysis, which will be applied to clinical work as soon as possible.

Table 4. Commercially Available Biomarker Kits for BC Diagnosis

Biomarker Kits	Study	Sensitivity	Specificity	Notes
Cytology	Liou 2006 [99]	16-89%	81-100%	FDA-approved
Hematuria dipstick	Liou 2006 [99]	40-93%	51-97%	FDA-approved
NMP22	Wang 2017 [50]	52-59%	87-89%	FDA-approved
BTA stat test	Guo 2014 [51]	64-69%	73-77%	FDA-approved
BTA TRAK test	Glas 2003 [52]	62-71%	45-81%	FDA-approved
Immuno Cyt	Liou 2006 [99]	39-100%	73-84%	approved only for BC surveillance
FGFR3	Beukers 2017 [34]	57-83%	59-82.7%	FDA-approved

Summary

A disease-specific biomarker (or biomarkers) is a characteristic reflecting a pathological condition in human body, which can be used as a diagnostic or prognostic tool for the clinical management. A urine-based biomarker(s) may provide a clinical value as attractive tools for clinicians to utilize in the clinical setting in particular to bladder diseases including bladder cancer and other bladder benign dysfunctions. Urine can be easily obtained by patients with no preparation or painful procedures required from patients' side. Currently advanced omics technologies and computational power identified potential omics-based novel biomarkers. An unbiased profiling based on transcriptomics, proteomics, epigenetics, metabolomics approaches et al. found that expression at RNA, protein, and metabolite levels are linked with specific bladder diseases and outcomes. In this chapter, we will discuss about the urine-based biomarkers reported by many investigators including us and how these biomarkers can be applied as a diagnostic and prognostic tool in clinical trials and patient care to promote bladder health. Furthermore, we will discuss how these promising biomarkers can be developed into a smart medical device and what we should be cautious about toward being used in real clinical setting.

Classification of the Urinary Metabolome Using Machine Learning and Potential Applications to Diagnose Interstitial Cystitis

Summary

With the advent of artificial intelligence (AI) in biostatistical analysis and modeling, machine learning can potentially be applied into developing diagnostic models for interstitial cystitis (IC). In the current clinical setting, urologists are dependent on cystoscopy and questionnaire-based decisions to diagnose IC. This is a result of a lack of objective diagnostic molecular biomarkers. The purpose of this study was to develop a machine learning-based method for diagnosing IC and assess its performance using metabolomics profiles obtained from a prior study. To develop the machine learning algorithm, two classification methods, support vector machine (SVM) and logistic regression (LR), set at various parameters, were applied to 43 IC patients and 16 healthy controls. There were 3 measures used in this study: accuracy, precision (positive predictive value), and recall (sensitivity). Individual precision and recall (PR) curves were drafted. Since the sample size was relatively small, complicated deep learning could not be done. We achieved a 76-86% accuracy with cross validation depending on the method and parameters set. The highest accuracy achieved was 86.4% using SVM with a polynomial kernel degree set to 5, but a larger area under the curve (AUC) from the PR curve was achieved using LR with a l_1 -norm regularizer. The AUC was greater than 0.9 in its ability to discriminate IC patients from controls, suggesting that the algorithm works well in identifying IC, even when there is a class distribution imbalance between the IC and control samples. This finding provides further insight into utilizing previously identified urinary metabolic biomarkers in developing machine learning algorithms that can be applied in the clinical setting.

Interstitial cystitis (IC), also known as painful bladder syndrome or bladder pain syndrome, is a chronic visceral pain syndrome of unknown etiology that presents itself as a constellation of symptoms, including bladder pain, urinary frequency, urgency, and small voided volumes, in the absence of other identifiable diseases(1-3). Urine is in direct contact with the bladder epithelial cells that could be giving rise to IC; as a result, metabolites released from bladder cells may be enriched in urine(4).

The urinary metabolome was previously investigated by our group for potential IC diagnostic biomarkers (5-7). We attempted to identify IC-associated metabolites from urine specimens obtained from IC patients and controls using nuclear magnetic resonance (NMR). Our findings provided preliminary evidence that metabolomics analysis of urine can potentially segregate IC patients from controls. We sought to capture the most differentially detected NMR peaks and discern if there was a significant difference in the peak distribution between IC and control specimens. Based on multivariate statistical analysis, principal component analysis (PCA) suggested that the urinary metabolome of IC patients and controls were clearly different; 140 NMR peaks were significantly altered in IC patients (FDR < 0.05) compared to controls (5).

Machine learning (ML), originally described as a program that learns to perform a task or make decisions based on data, is a valuable and increasingly necessary tool for modern healthcare (8). However, this definition is broad and could cover nearly any form of data-driven needs. ML is not a magical approach that can turn data in immediate benefits, even though many news outlets imply that it can. Rather, it is natural extension to traditional statistical approaches. In our present study, we utilized ML and automated performance metrics to evaluate the clinical value of our 140 identified NMR peaks. We used ML algorithms examine the relationship between metabolic expression and disease. We applied logistic regression (LR) (9) and support vector machine (SVM) (10, 11), which are traditionally known to work well even with small sample sizes, to our metabolomics signatures and used this data together with patient clinicopathological features to diagnose IC. We used our dataset of 59 cases to train, test, and validate the model. The results showed that our ML-based algorithms were able to successfully identify IC patients from healthy subjects.

This study aimed to address the question of, “Does utilizing metabolic data in ML play a role in diagnosing IC?”. ML is a form of artificial intelligence (AI) and learns from past data in order to predict the future. Our NMR-based ML algorithm was able to collectively distinguish the IC patient urinary profile from that of controls.

MATERIALS AND METHODS

Ethics Statement

For this paper, we used the deposited dataset derived from the published data. This study used the publicly deposited data, which does not need IRB approval.

Dataset

There are 59 samples in total in the IC dataset. In order to acquire IC-associated metabolites, urine samples were collected from 43 IC patient group and 16 healthy control group. Each urine specimen was analyzed using nuclear magnetic resonance (NMR) and biomarkers were identified with 140 NMR peaks. The 140 NMR peak feature was utilized to apply the dataset to ML algorithms for classification of IC patients in this paper (5).

Machine Learning

Method.

Due to limited sample size, we adopted two machine learning algorithms, i.e., Support Vector Machine (SVM) (10, 11) and Logistic Regression (LR)(9), that are traditional but work well even with small number of samples. These are supervised learning algorithms, where each data sample is represented by a number of features and comes with a label that tells which group the sample belongs to.

When data is represented as scattered data points in a feature space that consists of two clusters representing individual groups, SVM finds a decision boundary (either linear or non-linear) that separates the different groups. Training an SVM optimizes the decision boundary to maximize the margin between the clusters, and it requires a kernel function train a kernel SVM that learns a non-linear decision boundary, i.e., a non-linear classifier (12). The model contains a user parameter known as ‘slack variable’ that controls the width of the margin.

LR is also a classifier that learns via a linear model. By feeding a set of training samples with a number of features, it learns specific weights associated with features. When a data sample is input into to a LR model, a classification is made by a linear combination between the weights and the data; together with a sigmoid function, the combined value is mapped to a probability between 0 and 1. The predicted label is assigned according to the probability, and by minimizing the classification error (usually formulated using cross-entropy) in the training

dataset, the weights are learned. One can add additional regularization terms in the model, such as l_1 or l_2 -norm of the weights, where l_1 -norm controls the sparsity of the weights (13), which will select the most important features, while l_2 -norm controls the smoothness of the weights to make the model more robust (13, 14).

Both SVM and LR were implemented using the sklearn package in Python.

Training.

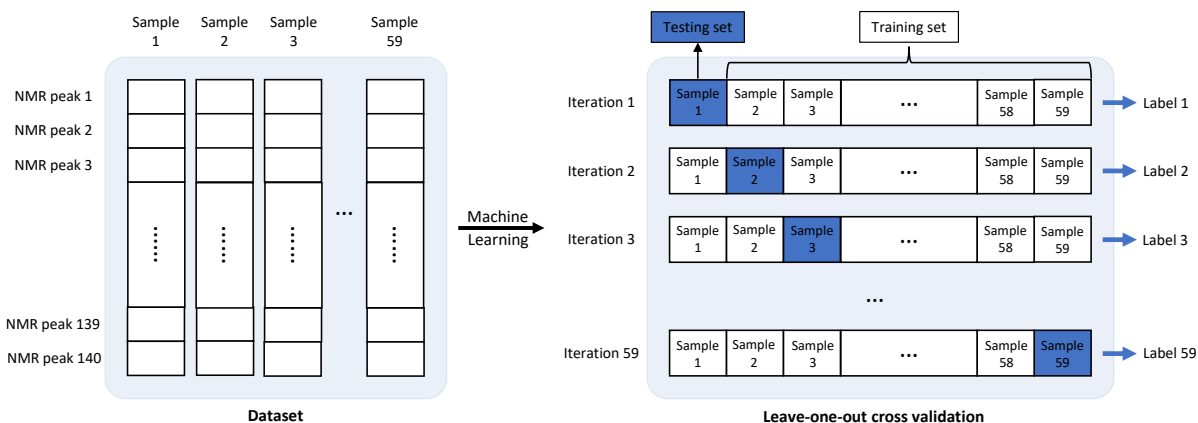
Because the sample size was very small, the leave-one-out cross validation (CV) (15) method was utilized to make full use of the data set and to obtain unbiased result from the classifiers. With leave-one-out, we picked one sample as a testing set while using the rest of samples as a training set to train and test the model. The same process was iterated for every sample in the dataset. An illustration of the leave-one-out CV workflow is given in the **Figure 1**.

For SVM, we performed a set of experiments with a linear model, radial basis function (RBF) kernel, polynomial kernel with degree being 3, 5, 7. The slack variable was set to 1 for all cases. For LR, we tried l_1 and l_2 penalties with different strengths; i.e. the inverse of regularization strength C was set to 1, 5, and 10.

Evaluation.

After repeating training and testing the model 59 times with leave-one-out CV, each sample was assigned a predicted label. By comparing these 59 predicted labels with the true labels, we constructed a confusion matrix by counting numbers of True Positive (TP), True Negative (TN), False Positive (FP) and False Negative (FN). From these numbers, accuracy, precision and recall were calculated to evaluate the performances of the models. Receiver operating characteristic (ROC) curve and precision-recall (PR) curve are plotted, and their area under the curve (AUC) are reported in the result section. Especially when the distribution of labels in the dataset is skewed, the AUC of the PR curve is a suitable measure for evaluating to account for the imbalance.

Figure 1. IC classification experimental scheme with leave-one-out cross validation



RESULTS

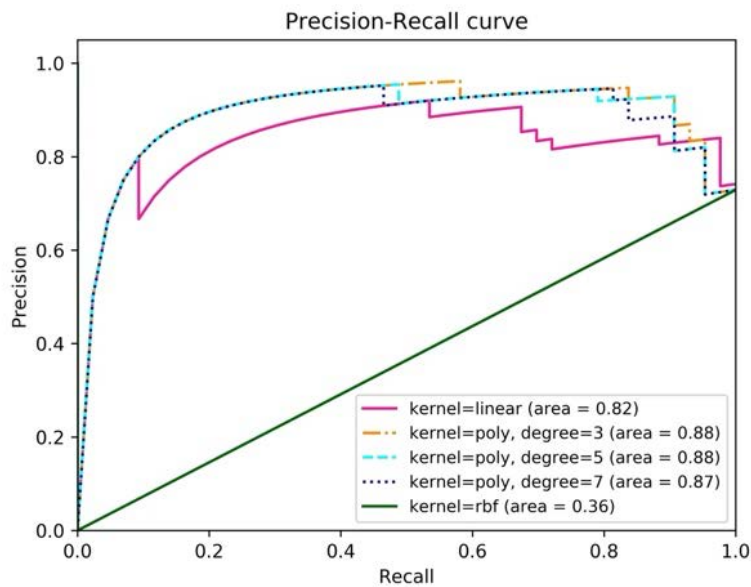
Classification of IC Samples with SVM.

SVM was applied to the IC dataset with the leave-one-out CV scheme to classify IC samples from controls. The result varied depending on user parameters (i.e., kernel type and kernel parameters) as shown in **Figure 2** and **Table 1**. Comparing the numbers, it was found that SVM with polynomial kernel resulted in the best performance when the degree of the polynomial kernel was 3 with 86.4% accuracy, 0.88 AUC of PR curve, and 0.85 AUC of ROC curve. Although the accuracy was the highest when the degree was 5, the AUCs of ROC and PR curves with degrees set to 3 was the highest. Moreover, the degree equal to 3 has less chance of overfitting than a degree of 5.

Here, the usage of linear kernel did not perform well. It may be because the data were not linearly separable or simply the sample size (N=59) was too small compared to the dimension of the data (i.e., 140 features). Performance of RBF kernel was also poor; looking at the accuracy using RBF kernel with SVM shown in **Table 1** (i.e., 72.9%), it was the same as the proportion of IC samples in the dataset (i.e., 43 IC subjects out of 59 subjects) and its recall was 1. This means that the classifier was simply predicting that all the samples belong to IC group and was not able to handle the class distribution imbalance problem.

Figure 2. Classification result evaluation curves using SVM. (a) the Precision-Recall curve, (b) ROC curve. The values of AUC are calculated for each curve and larger values indicate better performance.

(a)



(b)

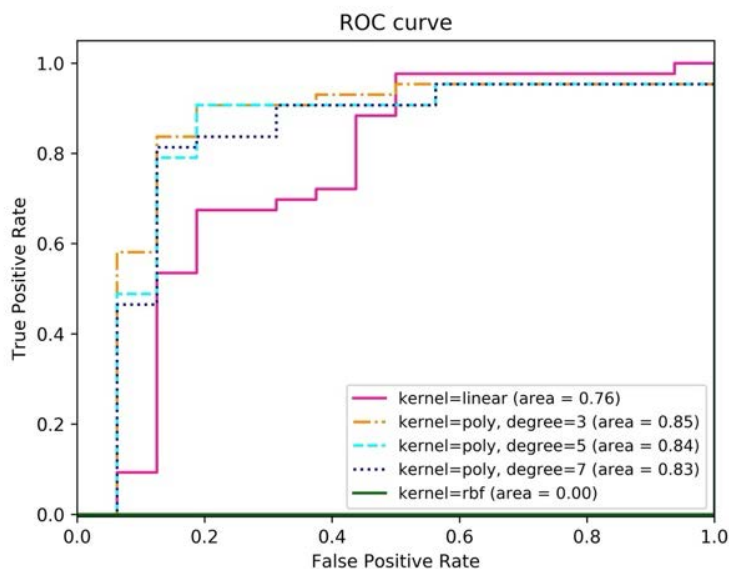


Table 1. The comparison of results from SVM with different set of parameters. TP: True Positive, TN: True Negative, FP: False Positive, and FN: False Negative.

Parameters	TP	TN	FP	FN	Accuracy	Precision	Recall	AUC of PR	AUC of ROC
kernel=linear	36	9	7	7	0.763	0.837	0.837	0.82	0.76
kernel=poly, degree=3	39	11	5	4	0.847	0.886	0.907	0.88	0.85
kernel=poly, degree=5	39	12	4	4	0.864	0.907	0.907	0.88	0.84
kernel=poly, degree=7	39	11	5	4	0.847	0.886	0.907	0.87	0.83
kernel=rbf	43	0	16	0	0.729	0.729	1.000	0.36	0.00

Classification of IC Samples with LR.

In addition to SVM experiment, LR was used to classify IC samples and the results are shown in **Figure 3** and **Table 2** with different user parameter settings. LR with l_1 -penalty yielded the best performance when its penalty parameter was set to 10 with 84.7% accuracy, 0.91 for AUC of PR curve and 0.86 for the AUC of ROC curve, which was slight better than the results from SVM. These numbers are the best among several trials because of its randomness with the initial weights being trained, and the results from other trials did not differ much from those reported in **Figure 3** and **Table 2**.

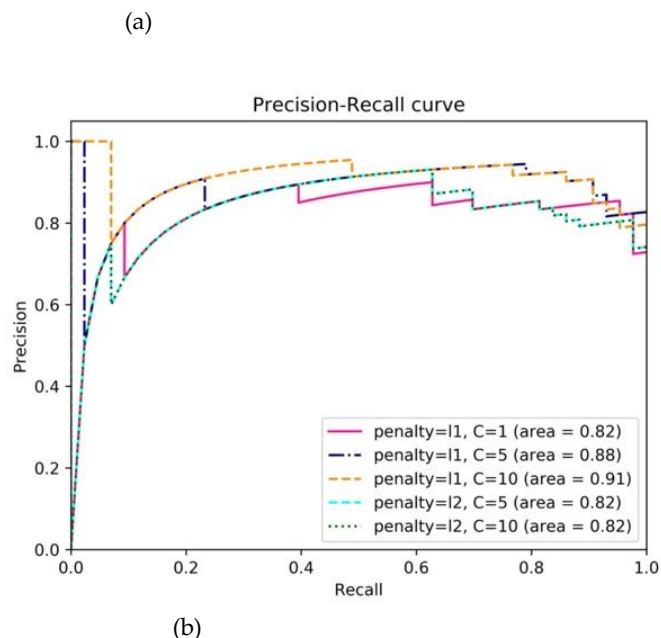
Table 2. The comparison of results from LR with different set of parameters. TP: True Positive, TN: True Negative, FP: False Positive, and FN: False Negative.

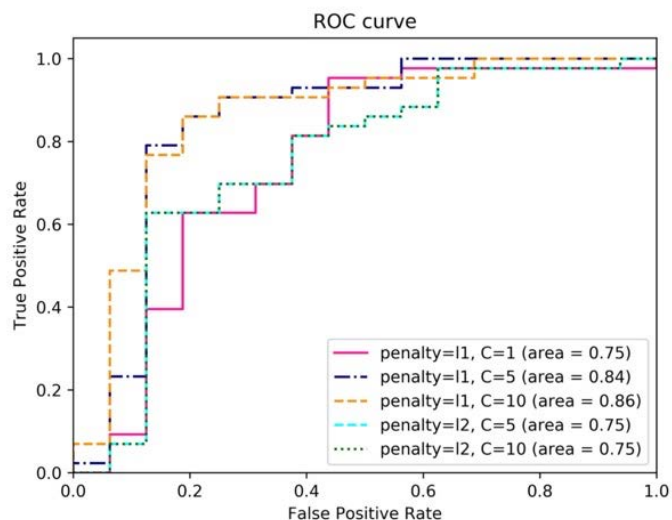
LR	TP	TN	FP	FN	Accuracy	Precision	Recall	AUC of PR	AUC of ROC
penalty=l1, C=1	39	9	7	4	0.814	0.848	0.907	0.82	0.75
penalty=l1, C=5	39	10	6	4	0.831	0.867	0.907	0.88	0.84
penalty=l1, C=10	38	12	4	5	0.847	0.905	0.884	0.91	0.86
penalty=l2, C=5	38	7	9	5	0.763	0.809	0.884	0.82	0.75
penalty=l2, C=10	38	7	9	5	0.763	0.809	0.884	0.82	0.75

It was observed that LR worked well despite being a linear model. Notice that the performance of linear SVM was poor in **Table 1**; this is because of the l_1 -norm penalty applied to the trained parameter imposing sparsity and behaving as a natural feature selector. When we checked the trained weight of features, most of the weights converged to 0 (a very small number on average of absolute values across the leave-one-out process). When the penalty parameter was 10, the average weights of 133 features was less than or equal to 0.1. This means that we only need a few critical features to predict correct label. In our experiment, feature id = 73, 4, 129, and 35 were the most dominant features with the highest weights regardless of the random initialization. In other words, they were the four most useful NMR features. We have performed further statistical group analysis on these four NMR peaks using two-sample t-test, which resulted in p -values of 0.003, 0.001, 0.057, and 0.036 respectively. It was interesting to see that there were many other NMR peaks with even lower p -values and the peak ID=129 had a p -value greater than 0.05. While these statistical tests are performed independently, our classification results were derived by taking all the peaks at the same time for the analysis and it demonstrates that a linear combination of the features can be more powerful to distinguish IC from controls.

The l_2 -norm constraint did not contribute much in these experiments. This is because the model can robustly operate even without the l_2 -norm regularizer, which typically degrades performance of models in exchange for model robustness. Especially with the l_1 -norm regularizer significantly lowering the dimension of the data (with 133 redundant features), the sample size ($N=59$) was sufficient to make robust and correct predictions for IC samples.

Figure 3. Classification result evaluation curves using LR. (a) the Precision-Recall curve, (b) ROC curve. The values of AUC are calculated for each curve and larger values indicate better performance.





DISCUSSION

It comes with no surprise that medicine is awash with claims that ML applications into big healthcare data will create extraordinary revolutions(8, 16, 17). Recent examples have demonstrated how big data and ML can create algorithms that can perform on par with human physicians. AI is one ML approach without prerequisites. Various AI techniques already exist, and successful metabolomics analysis has been reported in previous studies(18-20). Conventional statistical analysis and AI-based methods were used to assess the discrimination capability of quantified metabolites. A multiple logistic regression (MLR) model, alternative decision tree (ADTree), neurofuzzy modelling (NFM), artificial neural network (ANN), and SVM machine learning methods were used(21, 22).

Modern advancements in computational and data science, with its most popular implementation in ML, has facilitated novel complex data-driven research approaches. Combined with biostatistics, ML aims at learning from data. It accomplishes this by optimizing the performance of algorithms with immediate previous knowledge. ML can be applied in either a supervised or unsupervised fashion. Supervised learning entails monitoring of the algorithm while it is being trained to learn a correct class assignment from a set of parameters, such as how to make a correct diagnosis from clinical and laboratory information(18).

Current biomarkers for IC diagnosis and prognosis are insufficiently robust for clinical practice using AI. Instead, we used AI to identify IC-related metabolites in an NMR metabolomics dataset from our previous study (5), which was able to collectively distinguish IC patient urinary profiles from that of healthy controls. The development of diagnostic tools using ML may be useful for more accurately identifying IC patients. AI has the potential to manage the imprecision and uncertainty that is common in clinical and biological data. AI or ML-based algorithms can take several different forms. The icons in the presented figures in this paper represent typical ML methods. These include multilayer neuronal networks, decision tree-based algorithms, SVM, and related algorithms that separate classes by placing hyperplanes between them, and prototype-based algorithms, such as k-nearest neighbors that compare feature vectors carried by a case with those carried by other cases and assign classes based on similarities. ML-based algorithms are not being actively applied to IC research. Such applications could lead to a better understanding and deeper knowledge of metabolomics data, which would then provide insights into biomarker discovery.

Although this is out of scope for this study, AI algorithms can be used to predict IC progression or therapeutic responses, too(23, 24). Patient clinicopathological features are commonly used to train AI algorithms to predict patient outcomes in other diseases, such as cancer(25-27). For instance, Wong et al. developed a prostate

cancer patient-specific ML algorithm based on clinicopathological data to predict early biochemical recurrence after prostatectomy (28). The resulting 3 ML algorithms were trained using 338 patients and achieved an accuracy of 95-98% and AUC of 0.9-0.94. When compared to traditional Cox regression analysis, the 3 ML algorithms had superior prediction performance. This study demonstrated how AI algorithms, trained with clinicopathological data, imaging radiomic features, and genomic profiling, outperformed the prediction accuracy of D'Amico risk stratification, single clinicopathological features, and multiple discriminant analysis, a type of conventional multivariate statistics (28). There is also a role for AI in selecting effective drugs for cancer treatment(29). Using an ML-based algorithm, Saeed et al. quantified the phenotypes of castration-resistant prostate cancer cells and tested their response to over 300 emerging and established clinical cancer drugs (30).

We are aware that one of the limitations of this study includes the novelty of using crowdsourcing in medical biomarker development. To our knowledge, there is no previous reference for comparison. Additionally, this study was limited to participants in South Korea and to a 1-time point collection. A major problem associated with medical datasets is a small sample size(5). Given that sufficiently large datasets are important when creating classification schemes for disease modeling, a relatively larger dataset can result in reasonable validation due to sufficient partitioning of training and testing sets. On the contrary, a smaller training dataset can lead to misclassifications and may result in unstable or biased models. For our study, a major problem was the small sample size. However, the reason for this is that it takes an immense amount of time, effort, and cost to collect a larger amount of medical research data. Furthermore, medical research data is often inconsistent, incomplete, or noisy in nature; thereby, reducing sample sizes even more. Such small sample size for high-dimensional data often leads to 'curse of dimensionality', i.e., failing to properly estimate necessary parameters due to lack of samples, which we also faced with only 59 samples for 140 NMR features. In this work, we have used SVM and LR as classifiers. For SVM, when casting its objective function as a dual form using Lagrangian multiplier, the optimization problem seeks for a sparse solution that identifies a few 'support vectors' and thus greatly reduces the dimension of problem. For the LR, we used two different regularizers on the parameters to estimate, i.e., L1 and L2-norms, to avoid curse of dimensionality and obtain feasible solutions. As demonstrated in the results, as L1-norm constraint behaved as a data-driven feature selector reducing the dimension of the problem, the classifier avoided the curse of dimensionality. Although we were able to stay away from the curse of dimensionality in this study, poor analysis may lead to data overfitting and irreproducible results. ML-based algorithms may be manipulated by datasets containing dominant but irrelevant features when the sample number is limited. Also, AI cannot be used as an end-all solution to any question. There are instances where traditional statistics has outperformed AI or where additional AI does not improve results.

In summary, we have found that ML-based algorithms can be applied to developing diagnostic models for IC patients. In the current clinical setting, urologists are generally dependent on cystoscopy and questionnaire-based decisions to diagnose IC due to a lack of objective molecular biomarkers. The purpose of this study was to develop machine learning methods for diagnosing IC and assess their performance using metabolomics data. Considering how ML techniques for analyzing omics data can play a role in predicting the diagnosis and prognosis of diseases, future studies should integrate use of a larger multidimensional and heterogenous dataset, application of more accurate validation results, and use of different techniques for classifying and selecting features to pave a promising way toward clinical applications.

BRINGING MACHINE LEARNING TO PICK OUT HIDDEN CLINICAL VALUES FROM BIG DATA IN UROLOGY

Suppose you are asked to select one the most important information technology revolution of our time that can give your decision-making processes a massive upgrade. Many of us will choose machine learning (ML). A definition of ML is "gives computers the ability to learn without being explicitly programmed." The main premise of ML is to introduce algorithms that ingest input data, apply computer analysis to predict output values within an acceptable range of accuracy, identify patterns and trends within the data and finally learn from previous experience. ML is often applied to complicated, poorly understood phenomena in nature, such as complex biological systems, climate change, astronomy, or particle physics.

Let us tell you the mathematics and methodological of ML. The two major pathways in machine learning are supervised learning and unsupervised learning. In supervised learning, an algorithm is often provided with data $X_{N \times P}$ (N samples with P features) related to the learning objective and a desired target measure y . The goal is to train a classifier (i.e., learn a decision function) f that can perform prediction on the target y for unseen data X , i.e., $f(X) = y$, and identify links between the features and the target measures. Supervised learning primarily deals with classification and regression problems. In unsupervised learning, an algorithm is provided with data X without any class label / annotation to find any latent patterns, sometimes producing both answers and questions that may not have been conceived by the investigators. Unsupervised learning typically deals with clustering and dimensionality reduction problems. The patterns identified in unsupervised learning often need to be evaluated for utility either by human interrogation or via application within a supervised learning task.

While validation of unsupervised algorithm can only be performed based on a dataset with ground truth that is hidden during the training process, the performance of a supervised learning algorithm can be evaluated by various metrics based on the objective of a task. For supervised learning algorithms, a dataset is typically divided into two independent sets, i.e., training set and testing set, where training of an algorithm is performed using the training set and then the trained model is evaluated using the testing set. In order to remove any bias that may have been introduced in a single division of training and testing sets, Cross Validation (CV) is often used to evaluate a supervised learning algorithm. CV divides a dataset into k subsets, also known as k -folds, and iterates through k number of training and testing phases that use i -th subset as a testing set and the rest of subsets for training. Such iterations yields k different results with different training-testing set pairs and aggregating the results let us avoid those cases that may have performed successfully or poorly by bias or coincidence.

The performance of a supervised learning algorithm is often measure by accuracy, precision and recall. While accuracy being the main measure of interest, it does not consider class distribution imbalance in a dataset which is quite common in many biomedical studies. For example, when a dataset consists of two class, e.g., positive and negative, where the number of normal subjects dominates, then simply predicting all samples in a testing set as normal will yield high accuracy with significant false-positives. That is why one needs to consider precision and recall together, where precision measures how precise the prediction made by a trained model is and recall measures how much of the total positive examples in the testing set the trained model can predict as true positive. F1-score is also a common measure, which accounts for both precision and recall simultaneously.

How ML is applied to develop precision medicine for us?

Many of us may agree with this statement - "big data will transform medicine". In recent years, a large amount of data has been accumulated in big omics studies of genomes, epigenomes, transcriptomes, proteomes, metabolomes and other sources. This big data needs to be analyzed, interpreted and manipulated to provide the biological meaning. Where ML shines is in handling enormous numbers of predictors. ML has become ubiquitous and indispensable for solving complex problems in most sciences. ML will become an indispensable tool for clinicians seeking to truly understand their patients. Yet, we are aware that ML has shortcomings in dealing with big data[1]. First, algorithms might "overfit" predictions to spurious correlations in the data; multicollinear, correlated predictors could produce unstable estimates. Second, ML algorithms often require millions of observations to reach acceptable performance levels. Third, biases in data collection can substantially affect both performance and generalizability. Finally, ML does not solve any of the fundamental problems of causal inference in observational data sets.

Precision medicine is one of the important developments in current medicine. It helps doctors with early intervention by using advanced diagnostic procedures and customizes reasonable and better personalized treatment methods for patients. Many scientists and physicians are convinced by the importance of information technology and ML for the implementation of precision medicine, which includes data storage and analysis for determining the association between disease outcome, identification of patient characteristics and optimal treatment. Utilizing ML approaches for pattern recognition and development of statistical models, creating a knowledge base of all existing phenotype categories and disease, organization of clinical datasets of population size and open software platform development for statistical analysis of high-dimensional healthcare and multi-omics data are crucial for practical realization of precision medicine.

As you can imagine, ML will have a huge impact in disease (especially cancer) diagnostics and prognostics, specifically on the development of novel computational tools for stratification, grading, and prognostication of patients with the goal of improving patient care. There are many different ML techniques and algorithms, which have been widely used in disease prediction, diagnosis and prognosis. A series of studies show how ML could improve diagnostic performance and prediction accuracy in clinically relevant patient cohorts[2]. A study demonstrates how ML can improve well established standards such as the Gleason, thus yielding to more precise prognostication. Another study developed a ML system to predict Microsatellite instability (MSI) in patients with gastrointestinal cancer and endometrial cancers, both accuracies are higher than the prediction of molecular markers. Some studies have shown that ML can get higher accuracy of drug response prediction. ML methods have become a popular tool for medical researchers, which is able to effectively predict future outcomes of disease.

So how ML is involved in current clinical research? For digitalized pathology field, various applications incorporating ML are being developed to assist the process of pathologic diagnosis. Major applications that have been studied so far include detection of specific objects such as cancer cells, cell nuclei, cell divisions, ducts, and blood vessels, classification and grading of tumors, and quantitative evaluation of immunostaining. The major obstacle facing ML of pathological images is inadequate image dataset annotation. At present, many technologies have been developed [3]. For example, generative adversarial networks (GAN), the techniques for learning and generating color tones using “generative model” technology, is used for pathological data analysis to automatically prepare image datasets necessary for subsequent DL. Pathologists are looking forward to a gold standard technology to process pathological images.

ML applications in radiology are designed to help computers identify medical imaging data and support diagnosis by associating with clinical data, such as treatment or outcome. These radiomics techniques can predict diseases with higher accuracy than human eyes. Using ML to recognize and analyze image data will fundamentally change our understanding of disease risk and treatment. ML can also use the image information that human eyes can't recognize, so as to find new disease patterns and predictive markers.

At present, it is very popular to find cancer biomarkers through omics research. Because of the large data set, people need to use advanced information technology (such as machine learning technology) to analyze and understand the data. ML has been applied to mass spectrometry (MS) data from different biological disciplines, particularly for various cancers. ML can be useful in determining which proteins, from MS data, could be used as biomarkers to differentiate between samples of different classes. Metabolomics can also be considered as a method complementary to proteomics. ML is the most useful for the interpretation of large genomic data sets and has been used to annotate a wide variety of genomic sequence elements, in the process, to identify potentially valuable disease biomarkers.

Then, how about ML application in urological research?

For prostate cancer (PC) many technology platforms for diagnosis, prognosis, and treatment demonstrated the potential benefits of ML. In diagnostic imaging, ML can read cross-sectional radiographic images reproducibly and rapidly to make a diagnosis. The ML methods described for diagnostic imaging can be extended to treatment planning and interventions by augmenting the surgeon's display with information such as cancer localization and other image-guided interventions. Computer-assisted diagnosis of PC in histopathological slides could be achieved by ML in order to optimize accuracy. ML method is also used in genomics research. By identifying specific genes or genes, we can develop diagnostic and risk stratification tools, determine the best individualized treatment methods and generate targeted drug treatment schemes.

ML can read radiological / pathological images of bladder cancer to provide diagnostic, treatment and prognostic information. Some studies have shown that by using ML model to analyze MRI data of bladder cancer, low-grade and high-grade bladder cancer can be identified before operation, with an accuracy of 83%. ML-based methods have been further applied to accurately quantify tumor buds from immunofluorescence-labeled slides of muscle-invasive bladder cancer (MIBC) patients. ML algorithms have been employed to create recurrence and survival predictive models from imaging and operative data. ML algorithms used to identify genes at initial presentation

that are most predictive of recurrence can be applied as molecular signatures to predict the risk of recurrence within 5 years after TURB[4].

More and more ML technology has been used to analyze the clinical and imaging data of renal cell carcinoma to provide doctors with disease diagnosis, prognosis information and help to make treatment plans. Previous studies have shown that ML model can accurately distinguish high-grade and low-grade renal clear cell carcinoma by analyzing CT image features [4]. In recent years, identifying biomarkers and multiple gene expression-based signatures by ML have been developed to predict survival and disease prognosis in ccRCC. Moreover, some studies have demonstrated that noninvasive ML and DL models constructed from radionics features have comparable performance to percutaneous renal biopsy in predicting the International Society of Urological Pathology (ISUP) grading.

ML has been also applied in various modalities of urinary stone therapy. Computer-assisted detection using image features can support radiologists in identifying stones. With multiple layers on large datasets, artificial neural networks (ANN) can predict outcomes after various forms of endourologic intervention. ANN has been used to differentiate ureteral stones from phleboliths in thin slice CT volumes due to their similarity in shape and intensity. ANN also can be used for the early detection of kidney stone type and most influential parameters to provide a decision-support system. The model resulted in 97.1% accuracy for predicting kidney stone type. Recently, ML algorithms have been used to predict treatment success after a single-session shock wave lithotripsy (SWL) in ureteral stone patients.

Furthermore, ML can be applied to benign bladder diseases, such as overactive bladder (OAB) syndrome[5]. A ML model using a random forest-based algorithm was studied to identify patients for whom anticholinergic medications are likely to fail. A validated ML prediction model can predict the treatment failure of a 3 months standard anticholinergic treatment experiment, and the accurate rate is more than 80%.

How ML will be evolved in tomorrow's urology?

In today's fast-moving technologically enhanced world, ML is still in its evolution. The steps needed to integrate ML into the clinic are still unknown. How the new algorithms will influence the diagnosis and management of our patients remains our decision. Future research should focus on the construction of larger medical databases and further development of AI techniques. The predictive precision of ML will continue to provide and enhance personalized medicine with the further inclusion of data and model retraining. There are limitless future applications for artificial intelligence in the field of urology.

Metabolomic and Lipidomic Approaches to Identify Biomarkers for Bladder Cancer and Interstitial Cystitis

INTERSTITIAL CYSTITIS

IC is a chronic condition of unknown etiology with long-term notable pelvic/suprapubic pain and urinary storage symptoms, such as urgency, nocturia, and frequency (21). The advent of cystoscopy led to major findings in IC, including bladder glomerulations during hydrodistention and Hunner's lesions (22). Although the epidemiology of IC is difficult to monitor owing to its plethora of symptoms, recent studies have suggested an estimated prevalence of 100–300 per 100,000 women. The prevalence rate is about 10–20% lower in men (23).

IC is generally diagnosed through exclusion; however, several attempts have been made to define standard diagnostic criteria. Recent guidelines set by the European Society for the Study of Interstitial Cystitis and the American Urological Association are currently being used worldwide to treat IC (24). Although treatment options for IC are limited and included hydrodistention, several oral pharmaceutical drugs have been approved by the US Food and Drug Administration, including pentosan polysulfate (Elmiron), antihistamines, tricyclic antidepressants, and immune modulators (25).

Owing to its unknown etiology and large variability in sites of occurrence and symptom severity, IC is difficult to subtype. However, there is still an urgent need for a well-established and precise subtyping system. According to the International Society for the Study of Bladder Pain Syndrome, Hunner's lesions are a clear symptom in IC with bladder pain. A recent study found that IC with Hunner's lesions displayed completely different histology, gene expression, and prognoses compared to other forms of IC (26). IC can also be defined as a distinct non-inflammatory disorder characterized by preservation of the urothelium layer and symptom spread beyond the bladder without lesions (27).

METABOLOMICS AND LIPIDOMICS

Metabolomics

Metabolomics is defined as the large-scale study of small molecules and metabolites involved in the regulation of metabolic pathways and their networks. Compared to genomics and proteomics, metabolomics is more closely linked to phenotypes; therefore, it can detect subtle changes in biological pathways under different physiological conditions and abnormal pathological processes. For the purposes of this review, we will focus on the application of metabolomics and lipidomics to BC.

The aim of precision medicine is to create novel approaches to prevent disease and update clinical strategies to take into account each individual's variability in terms of environment, lifestyle, genetics, and molecular phenotypes (28). Metabolomics holds much promise for precision medicine and can be used to measure all metabolites in biological specimens (29). Metabolomics presents significant analytical challenges over both genomics and proteomics; it aims to measure molecules that range in polarity, from organic water-soluble acids to nonpolar lipids, which have disparate physical properties (30). As a complement to other omics techniques, metabolomics serves as a critical component of systems biology. Moreover, the study of metabolites and molecules is closely related to phenotypes and can improve our understanding of intracellular metabolic alterations (29). The main aim of metabolomics is to identify altered metabolic pathways and biomarkers (31). Recent developments in metabolomics and statistical capabilities have boosted our ability to investigate cancer metabolism and better understand cancer-related changes in metabolism, such as the conversion of glucose into the macromolecules needed for tumor cell proliferation and vascularization (32-34).

Lipidomics

Lipids are essential building blocks in the body that play several critical cellular functions and can provide a snapshot of ongoing lipid metabolism. The lipidome is the total lipid content in a cell (35). The emergence of lipidomics now allows for the complete characterization of the cellular metabolome. Lipidomics is the potential key to many metabolic diseases and can be utilized in several research areas, as well as in the development of diagnostic tools, drugs, and therapeutic strategies (36). Lipidomics combined with bioinformatics can serve as a powerful tool for better understanding the biochemical mechanisms underlying lipid-related diseases by quantifying changes in the levels of individual lipids, subclasses, and molecular species, and identifying alterations in pathways and networks (35). The emergence of metabolomics and lipidomics has enabled us to better define differential metabolites in pathological conditions. Over the past two decades, both metabolomics and lipidomics have seen significant advances, facilitated by rapid developments in novel analysis strategies, approaches, instruments, and techniques (37).

EMERGING TECHNOLOGIES

Current Development of Methodologies

The physicochemical properties of all metabolites add additional complexity to metabolomics studies. To overcome these restrictions, various methods have been applied to overcome this complexity/challenges. MS and nuclear magnetic resonance (NMR) are the most frequently applied analytical approaches in metabolomics studies.

NMR Spectroscopy

NMR is a nondestructive, nonbiased, easily quantifiable, fast, and reproducible spectroscopy technique based on the principle that nuclei absorb and emit electromagnetic signals based on changes in the external magnetic field. NMR has several unique advantages in metabolomics (38). Metabolomics profiling by NMR is a powerful tool that can be used to diagnose a variety of diseases. NMR is based on the fact that nuclei, such as ^1H , ^{13}C , and ^{31}P , have nuclear spins and are able to exist at different energy levels in a magnetic field. Thus, these nuclei can generate valuable and identifiable information about metabolites. When analyzing biological samples, hydrogen, carbon, and phosphorus are the good targets. ^1H NMR is the most commonly used technique in metabolomics since ^1H is naturally abundant in biological samples. ^{13}C and ^{31}P NMR are used less frequently but can provide additional information on specific metabolites.

Mass Spectrometry

MS-based metabolomics offers quantitative analysis of metabolites, ranging from measurement of a single molecule to thousands, with high selectivity and sensitivity. The combination of MS with separation techniques reduces the complexity of mass spectra by separating metabolites based on time, providing isobar separation, and delivering additional information regarding physicochemical properties. To calculate the mass-to-charge ratio (m/z), MS acquires spectral data and relative intensity of the measured compounds. One potential drawback of MS-based techniques is the need for sample preparation, which can lead to potential loss of metabolites, changes in experimental conditions, discrimination of specific metabolite classes, and other consequences.

MS can effectively analyze small molecules separated by techniques, such as gas chromatography (GC), liquid chromatography (LC), and capillary electrophoresis (CE). LC-MS and GC-MS can provide huge amounts of chemical information for metabolomics studies. GC-MS uses the gaseous phase and achieves better metabolite separation than LC. However, unlike LC, GC typically requires chemical derivatization of the metabolic species prior to analysis. GC-MS is widely used in metabolomics studies as it can detect a wide range of intact metabolites with no need for chemical modification. For the separation of nonpolar to slightly polar molecules, traditional reverse-phase chromatography is used. Hydrophilic interaction LC (HILIC) is the technique of choice for separating strongly to slightly polar metabolites.

Advantages and Disadvantages

For metabolomics studies, each analytical technique has its own advantages and limitations. No single instrument or method can detect all metabolites accurately. Thus, multiple methods and instruments are recommended to detect the greatest number of metabolites. For instance, the Phenome Centre Birmingham utilizes both LC-MS and NMR spectroscopy for metabolomic profiling and is able to detect a higher number of metabolites than using a single method alone (<https://www.birmingham.ac.uk>). Owing to the complexity of the metabolome, no single analytical method can fully discern the metabolome. NMR and MS each have their own strengths and weaknesses.

APPLYING METABOLOMICS AND LIPIDOMICS TO IC

Applying Metabolomics to IC

Chronic bladder pain is a hallmark of IC. Metabolomics studies can be used to analyze the characteristics of the disease state and identify novel approaches for reducing symptoms (54). Kind et al. performed global metabolomics profiling using various platforms, including NMR and LC-MS. Utilizing urine from IC patients, they profiled 490 metabolites, including histidine, erythronic acid, and tartaric acid, and identified those with the highest fold changes. The identified metabolites were found to be associated with IC, suggesting its possible clinical use in urinary IC diagnosis (55). Using an MS-based metabolomics approach, the Multidisciplinary Approach to the Study of Chronic Pelvic Pain (MAPP) Research Network's central clinical protocol, the Trans-MAPP Epidemiology and Phenotyping discovered urinary biomarkers in female IC patients who underwent extensive urologic and non-urologic phenotyping (56). Parker et. al used LC-MS to identify molecular correlates of IC from urine obtained from female patients. This study identified a novel biomarker, etiocholan-3 α -ol-17-one

sulfate (Etio-S), a steroid metabolite, as being associated with a phenotypic subgroup of highly symptomatic IC (57).

There are no reports in the literature involving the use of lipidomics to identify lipid compounds associated with IC.

HUMAN SPECIMENS-BASED METABOLOMICS MARKERS IN IC

IC can present as a long continuum of mild to severe symptoms. In recent years, new metabolomics techniques have been applied to gain a better understanding of disease mechanisms and uncover novel biomarkers (71). One study applied UPLC-MS-based metabolomics to examine urine samples from 10 IC patients and 10 healthy controls. Phenylacetylglutamine (PAGN) was identified as a urinary marker of IC and was found to be elevated in the urine of mild-to-moderate IC patients (72). In a separate study, Parker et al. used LC-MS to profile the metabolomes of urine samples from 40 IC patients and matched controls. They identified six metabolites as being closely associated with IC pathogenesis; one of which was etiocholan-3 α -ol-17-one (Etio-S). Further analysis found that elevated Etio-S was a good predictor of IC, with sensitivity of 91.2%, specificity of 87.4%, and area under the curve (AUC) of 0.92. Longitudinal analysis of women in this cohort showed that the differences in Etio-S persisted, indicating that these changes were long-lasting.

Taking an untargeted comprehensive metabolomic profiling approach, Kind et al. performed GC-MS analysis on urine specimens from IC patients and healthy donors and identified a total of 490 differentially expressed metabolites (55). Another study by Lamale et al. used urine samples from 40 women with IC and 29 healthy controls collected within a 24-hour time frame. They discovered higher expression of three inflammatory markers, histamine, methylhistamine, and IL-6, in IC patients compared to controls (73). In our biomarker discovery study, we applied NMR-based global metabolomics analysis to urine samples obtained from female IC patients and matched healthy controls. The levels of tyramine and 2-oxoglutarate were significantly elevated in the IC urine specimens (71). We also performed comprehensive solid-phase microextraction-gas chromatography-time-of-flight-mass spectrometry (SPME-GC-TOF-MS) profiling combined with bioinformatic analysis and found that levels of volatile urinary metabolites, including menthol, were significantly reduced in IC patients compared to normal (74).

Table 2 summarizes metabolomics-based IC biomarker candidates reported previously.

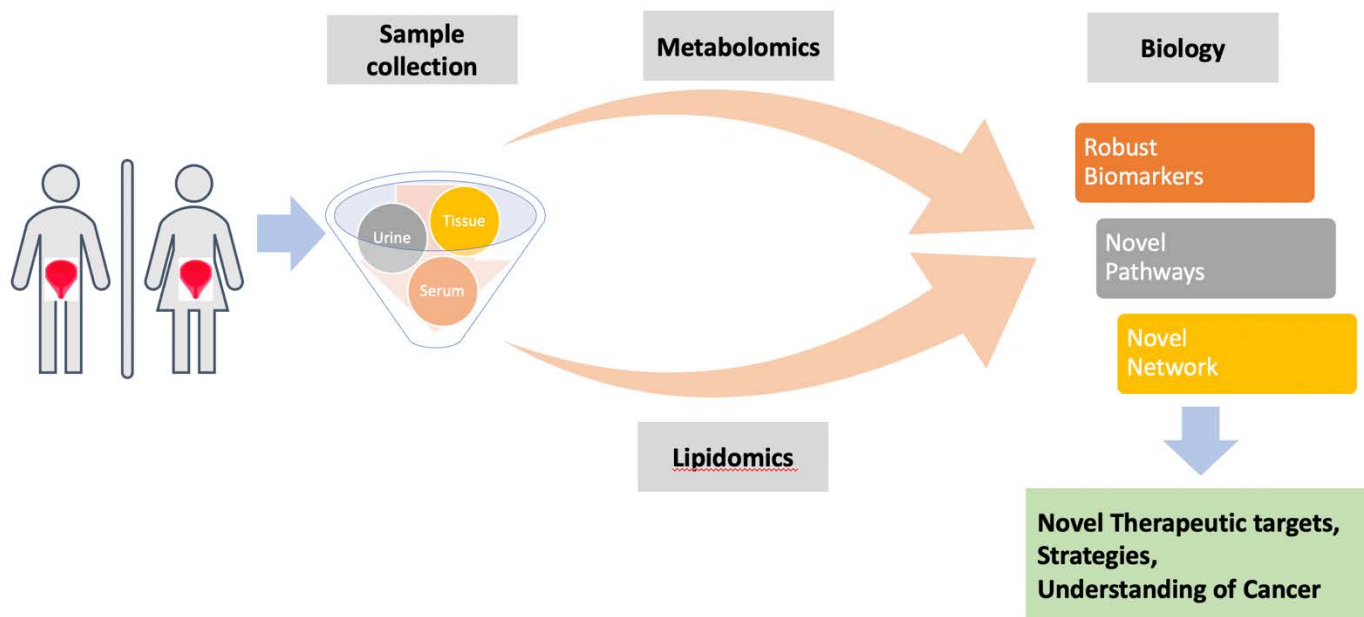
CONCLUSIONS AND PERSPECTIVES

Investigation of potential biomarkers of BC and IC based on pathophysiology, metabolomics, and lipidomics has progressed in recent decades. However, these technologies are still evolving. This review systematically outlined and reviewed the specific processes and results of metabolomic and lipidomic studies on BC and IC in recent years (**Figure 1**). Biomarkers detected by metabolomics can give great insight into cancer biology and, if utilized correctly, can lead to new strategies for diagnosis and therapeutic discovery. Unfortunately, current biomarker research in IC is lagging owing to the time required for validation, testing, and approval of assays. Additionally, the lack of standardization for urine and tissue biopsy collection can lead to invalid results. Well-structured clinical studies that satisfy rigorous criteria are needed to qualify clinical biomarkers for bladder diseases. Thus, a lot of work still needs to be done with regards to IC biomarkers, but significant progress has been made to date. As techniques and methods continue to expand and improve, omics may prove to be the key to tackling these diseases.

Biomarker discovery in the clinical setting.

The field of metabolomics and lipidomics has advanced with respect to technology development. Large-scale datasets can help paint a systems-scale picture of diseases with inputs from metabolomics- and lipidomics-based analyses, which provide insightful biological data. This data can lead to robust and valid individual specific biomarkers for novel disease-specific pathways and networks. The application of new (analytical) technologies

in omics studies should provide new information about attractive drug therapeutics and improve our understanding of the diseases.



Summary

The discovery/introduction/clinical use of prognostic and diagnostic biomarkers significantly improved outcomes for patients with various illnesses, including bladder cancer (BC) and other bladder-related diseases, such as benign bladder dysfunction and interstitial cystitis (IC). Several sensitive and noninvasive clinically relevant biomarkers for BC and IC have been identified. Metabolomic- and lipidomic-based biomarkers have incredible clinical potential in improving treatment outcomes for cancer patients; however, there are also some noted limitations. This review article provides a short and concise summary of the literature on metabolomic and lipidomic biomarkers for BC and IC, focusing on the possible clinical utility of profiling metabolic alterations in BC and IC.

3.3. What opportunities for training and professional development has the project provided?

This project was not intended to provide training and professional development opportunities.

"Nothing to Report."

3.4. How were the results disseminated to communities of interest?

Although this project was not originally proposed to enhance public awareness for communities of interest, I was able to provide several talks through media and outreach activities that were undertaken to reach members of communities who are not usually aware of these project activities. I have also provided scientific seminars on IC research to the science and medical community, focusing on post-doctoral fellows, medical students, nurses, and urologists. I believe these talks and educational campaigns greatly enhance public understanding, which then increases interest in learning and encourages careers in science, technology, and the humanities.

3.5. What do you plan to do during the next reporting period to accomplish the goals?

- Number of patients completed/ original planned target: 301/300. We will continue with our efforts to build upon the CSMC IC cohort for Specific Aims 1 and 2, as planned.
- We will complete all planned analyses using this cohort.
- The experimental data is to be published, submitted, or will be submitted for peer-reviewed publications.
- Most of our research results were presented in major scientific conferences and talks. New data will be submitted into the 2021 conferences.

4. IMPACT:

4.1. What was the impact on the development of the principal discipline(s) of the project?

This study will have significant ***clinical impact*** because the results may lead to novel clinical methods that can increase diagnostic accuracy and an improved understanding of the molecular origins of IC and its relationship with other urological conditions that share overlapping symptoms. In the long term, we seek to validate viable drug targets for therapeutic strategies using the expertise of our research team (urology, molecular and cell biology, chemical analysts, pathology, and biomarker development). We also believe that these findings can promote the adoption of effective and proven tests for IC diagnosis.

There have been many prior efforts attempting to identify unique and directly quantitative biomarkers associated with IC. However, these studies have overlooked the potential impact of gender on IC biomarkers. The biological basis of gender variability among IC states is not well established and there has been little advancement in investigating gender-related metabolomic differences in urine specimens. This underlies the misconception that risk factors and treatment regimens should be the same for both males and females. Considering that the composition of urine reflects the generation of metabolic by-products in the body, a urine metabolomics approach would be a great scientific tool for better understanding IC metabolism. Urine metabolite profiles provide a window of opportunity to study the global chemical fingerprints associated with physiological and pathological states. However, the discovery of biologically active metabolites in urine has raised questions on the clinical value and biological role of urine in IC.

We previously reported that our urine metabolomics profiling identified α -oxoglutarate (α -OG) as a female-specific IC biomarker. Our preliminary EPIC DNA methylation profiling and mechanistic preliminary studies on human bladder epithelial cells revealed the potential role of α -OG in epigenetic remodeling, through its effects on ARID1A in the bladder. Interestingly, an additional independent preliminary study conducted by our group found ***sex-associated differences in baseline urinary metabolites in healthy adults***. In other preliminary studies, comprehensive metabolomics profiling combined with bioinformatic analyses on urine samples from healthy males and females revealed biologically meaningful and sex-related baseline characteristics.

Interestingly, we found that levels of a series of metabolites, including α -OG, were greater in male samples. Recently established chemical similarity enrichment analysis further revealed that differentially expressed metabolites were significantly related to gender. These findings indicate that there are baseline sex-related differences in urinary metabolites, which should be considered for biomarker discovery, diagnosis, development of therapeutic strategies, and treatment options.

4.2. What was the impact on other disciplines?

Nothing to Report

4.3. What was the impact on technology transfer?

Nothing to Report

4.4. What was the impact on society beyond science and technology?

(1) Enhancing public awareness through broadcasting and media:

I moved to Los Angeles from Boston to continue my academic career as an Associate Professor of Surgery at CSMC and University of California Los Angeles. I immediately involved myself in a local Korean community-based radio broadcasting career and developed a rapidly growing base of listeners. Since 1989, I have been a primary interviewer, a reporter, and a scripter for two major media outlets in South Korea. I have covered many of the biggest local stories on business, education, and science, either at the anchor desk or as a frontier reporter. I have also hosted an hour-long educational quiz show on a weekly basis for three years.

Since this Department of Defense (DoD) research project started in 2015, I have worked closely with my Korean radio show and have hosted the daily "*Health and Science Story*" column series.

- Woori Broadcasting, USA, Afternoon Radio Program, Talk Show on the Education, Science and Health in formal talk show setting. April 30, 2015. Talked about the interstitial cystitis symptoms.
- Woori Broadcasting, USA. Hosting the Daily Column on the Science and Health entitled "Health and Science Story", since June 2015 to present (daily basis talk show). Produced ten topics related to bladder study and interstitial cystitis diagnosis.
- Woori Broadcasting, USA, Afternoon Radio Program, Talk Show on how to prepare the competition for Science in formal talk show setting. May 17, 2016
- TvK TV Medical and Science Show—"Modern Medicine" Desk, producing and anchor, starting on-air August 2016 and distributing through USA
- Invited Guest, Talk Show, September 2017

I believe that these outreach activities will improve public knowledge, attitudes of physicians and other health providers, social, economic, and environmental conditions of patients and their family members.

(2) Enhancing public awareness by community health educational lecture (only selected from very recent events)

I always seek chances to enhance public awareness of IC. Here are some examples of health lectures I have done for the local community. I believe that these outreach activities will improve public knowledge, attitudes of physicians and other health providers, social, economic, and environmental conditions for patients and their family members.

June 5, 2018
CSMC Health Fair, Koreatown Senior Center, Los Angeles, CA

August 15, 2018
Korea Senior Center in Koreatown, Los Angeles, CA

September 9, 2018
Oriental Mission Church, Los Angeles, CA

September 22, 2018
Free Prostate Cancer Screening Day, Cedars-Sinai Medical Center, CA

September 24, 2018
Health Lecture Series
Young Nak Church, Evergreen College, Celebration Chapel, Los Angeles, CA

October 19, 2018
Korean Health Fair (Free Flu Vaccine)
Young Nak Church, Evergreen College, Celebration Chapel, Los Angeles, CA

December 1, 2018
KSEA-KWISE STEM FAIR
Santa Monica College, Los Angeles, CA

May 4, 2019
KWISE Westcoast Annual Conference
Biola University, CA

January 12, 2019
Ygnit 2019 Conference
Renaissance Los Angeles Airport Hotel, CA

April 12, 2019
Health Lecture Series
Young Nak Church, Evergreen College, Celebration Chapel, Los Angeles, CA

April 13, 2019
KSEA-KWISE Math Competition, Chair
Harvey Mudd College, CA

April 27, 2019
KSEA SWRC (South West Regional Conference)
Speaker
Chapman University School of Pharmacy, Irvine, CA

May 10, 2019
Health Lecture Series
Young Nak Church, Evergreen College, Celebration Chapel, Los Angeles, CA

October 1, 2019
Breast Cancer Awareness Initiative
Khier Clinic, Los Angeles, CA

October 15, 2019

Working for “press release” in Korean community

Active committee member of Korean American Health Coalition (KAHC) and the Korean American Graduate Medical Association (KAGMA). KAHC is a coalition of over 20 Korean American and mainstream organizations committed to making a measurable impact on the health disparities in Korean Americans. KAGMA, a non-profit 501c3, is one of the largest Korean American physician organizations in California, with its primary mission to improve healthcare outcomes in the Korean American and Asian American community (www.kukminusa.com/news/view.php?gisa_id...)

Health and Science Seminar Series for Korean community:
(ny.koreatimes.com/article/20170609/1060500)

Speaker and Interview at National Breast Cancer Awareness Month event "Call to Action". Please click, below, to links to Korean-media news coverage of this event.

[TV] SBS International (Circulation 130,000)
Headline: Korean’s screening rate is low “Call to action for sign-in free screening”
Youtube Link: <https://youtu.be/i2Qq7vYEG0>
Website: <https://www.sbs-int.com/copy-of-news?lang=en>

[TV] KBS America (Circulation 1,500,000)
Headline: Incident rate of Breast cancer is top 1, screening rate is low
Youtube Link: <https://youtu.be/VWRSJbbxD7Q>

[Newspaper] Korea Daily (Circulation 80,000)
Headline: Koreans “I don’t feel sick” neglect regular cancer screening”
http://www.koreadaily.com/news/read.asp?art_id=7647482

[Newspaper] Korea Times (Circulation 70,000)
Headline: Korean's cancer screening rate is lower than other ethnic group
<http://www.koreatimes.com/article/20191002/1272034>

[Newspaper] Koreatown Daily (Circulation 40,000)
Headline: “I don’t get a breast cancer screening since I don’t feel sick?”

[Newspaper] Chosun Daily LA (Circulation 40,000)
Headline: “Call to action for breast cancer screening”

[Newspaper] Woori1230 (Circulation 60,000)
<http://www.radiok1230.com/news/articleView.html?idxno=505194>

[Radio] Radio Seoul (Circulation 70,000)
J. Kim CV 9
Headline: Cancer incidence rate among Koreans is increasing, screening rate is low

[Radio] Woori1230 (Circulation 60,000)
Headline: First step to starting cancer prevention movement for Koreans

<http://www.radiok1230.com/news/articleView.html?idxno=505194>

Professional Service by Broadcasting and Media Coverage:

Worked closely with the Korean broadcasting and has hosted the daily “*Health and Science Story*” column series at two prominent Korean Broadcasting Station.

Guest speaker of the “*Information Plus Show*” since 2015 (refer this stream: <https://soundcloud.com/radiok1230/04302015-2a>).

Producer of a series of TV shows focusing on the science and health issues this summer.

Strongly Connected with Korean American mass media (newspapers, magazine, cable, and TV channels)—LA Korea Times, Radio Korea, TV K24, Korea Herald, Korea Daily, LA18, Korean American, MBC American, YTN, Kook Min Ilbo, and Christian Today et al.

Hosting two radio shows at Korea Town-based Broadcasting Stations (Radio Korea and Woori Broadcasting)—daily health talks

Speaker for Education Podcasts

Woori Broadcasting, USA, Afternoon Radio Program, Talk Show on the Education, Science and Health in formal talk show setting. April 30, 2015

Woori Broadcasting, USA. Hosting the Daily Column on the Science and Health entitled “Health and Science Story”, since June 2015 to present (daily basis talk show)

Woori Broadcasting, USA, Afternoon Radio Program, Talk Show on how to prepare the competition for Science in formal talk show setting. May 17, 2016

Woori Broadcasting, USA, TV Health and Science Column, hosting since July, 2016.

TvK TV Medical and Science Show—“Modern Medicine” Desk, producing and anchor, starting on-air Summer 2017 and distributing through USA

Radio Korea Broadcasting, USA. Hosting the Weekly Radioshow to enhance the public awareness on health issues focused on cancer, since October 2016

Interview articles in newspaper (Korea Daily and LA Korea Times, July 2017)

Interviewed for Korean community health (LA Korea Times, Korea Daily, tvK, Radio Korea, Woori Broadcasting, January-February 2018)

Interviewed for Korean education (Korea Daily, January 14, 2019)

Interviewed for STEAM Education (Radio Seoul, May 1, 2019)

Interviewed for Health and Science (Radio Seoul, Health and Morning, May 13, 2019)

Interview articles in newspaper (Korea Daily and LA Korea Times, February 2020)

Los Angeles-based Korean Community Cancer Lecture Series (only selected from very recent events):

April 27, 2018

Young Nak Church, Evergreen College, Celebration Chapel, Los Angeles, CA

May 11, 2018

Young Nak Church, Evergreen College, Celebration Chapel, Los Angeles, CA

May 18, 2018

Korean CEO Forum, Los Angeles, CA

June 5, 2018

CSMC Health Fair, Koreatown Senior Center, Los Angeles, CA

August 15, 2018

Korea Senior Center in Koreatown, Los Angeles, CA

September 9, 2018

Oriental Mission Church, Los Angeles, CA

September 22, 2018

Free Prostate Cancer Screening Day, Cedars-Sinai Medical Center, CA

September 24, 2018

Health Lecture Series

Young Nak Church, Evergreen College, Celebration Chapel, Los Angeles, CA

October 19, 2018

Korean Health Fair (Free Flu Vaccine)

Young Nak Church, Evergreen College, Celebration Chapel, Los Angeles, CA

December 1, 2018

KSEA-KWISE STEM FAIR

Santa Monica College, Los Angeles, CA

May 4, 2019

KWISE Westcoast Annual Conference

Biola University, CA

January 12, 2019

Ygnit 2019 Conference

Renaissance Los Angeles Airport Hotel, CA

April 12, 2019

Health Lecture Series

Young Nak Church, Evergreen College, Celebration Chapel, Los Angeles, CA

April 13, 2019

KSEA-KWISE Math Competition, Chair

Harvey Mudd College, CA

April 27, 2019

KSEA SWRC (South West Regional Conference)

Speaker, Chapman University School of Pharmacy, Irvine, CA

May 10, 2019
Health Lecture Series
Young Nak Church, Evergreen College, Celebration Chapel, Los Angeles, CA

January 15, 2020
Health Lecture Series
Korea Town Senior Center, Los Angeles, CA

October 10, 2020
Community Education Lecture
Korean American Virtual Conference/ Forum

October 23, 2020
Community Education Lecture – Statistics and COVID 19
Hosted student science video competition
Korean American Virtual Conference/ Forum

5. CHANGES/PROBLEMS:

5.1. Changes in approach and reasons for change

Nothing to Report

5.2. Actual or anticipated problems or delays and actions or plans to resolve them

Nothing to Report

5.3. Changes that had a significant impact on expenditures

Nothing to Report

5.4. Significant changes in use or care of human subjects, vertebrate animals, biohazards, and/or select agents

Nothing to Report

5.5. Significant changes in use or care of human subjects

Nothing to Report

5.6. Significant changes in use or care of vertebrate animals.

Nothing to Report

5.7. Significant changes in use of biohazards and/or select agents

Nothing to Report

6.PRODUCTS:

6.1. Publications, conference papers, and presentations

Publications Published During the Funding Period

Acknowledged DoD grant support

Acknowledgement of DoD support (yes)

Please see attached paper

1. Yun SJ, Jeong P, Kang HW, Shinn HK, Kim YH, Yan C, Choi YK, Kim D, Ryu

- DH, Ha YS, Kim TH, Kwon TG, Kim JM, Suh SH, Kim SK, Kim SY, Kim ST, Kim WT, Lee OJ, Moon SK, Kim NH, Kim IY, **Kim J**, Cha HJ, Choi YH, Cha EJ, Kim WJ (2016) Increased Expression of Herpes Virus-Encoded hsv1-miR-H18 and hsv2-miR-H9-5p in Cancer-Containing Prostate Tissue Compared to That in Benign Prostate Hyperplasia Tissue. *Int Neurourol J.* 20(2):122-30. PMID:27377944 PMCID: PMC4932644
2. Kind T, Cho E, Park T, Deng N, Liu Z, Lee T, Fiehn O, **Kim J** (2016) Interstitial Cystitis-Associated Urinary Metabolites Identified by Mass-Spectrometry Based Metabolomics Analysis, *Scientific Reports*, 6:39227, PMID: 27976711
 3. Chen Z, **Kim J.** (2016) Urinary proteomics and metabolomics studies to monitor bladder health and urological diseases, *BMC Urology*, 16(1):11, PMID: 27000794
 4. **Kim J.** (2016) Immune Checkpoint Blockade Therapy for Bladder Cancer Treatment, *Investigative and Clinical Urology*; 57 Suppl 1: S98-S105.
 5. Moon J, Choi M, **Kim J** (2016) Metabolic Profiling of Cholesterol and Sex Hormones to Monitor Urological Diseases. *Endocrine-Related Cancer* 23(10): R455-67 PMID: 27580660
 6. **Kim J** (2016) Are We Ready to Use the Omics Strategies for Precision Medicine? *Int Neurourol J*, 20(Suppl 2):S65-67. PMID: 27915470, PMCID: PMC5169089, DOI: 10.5213/inj.1620edi007
 7. Yun SJ, Kim S-K, **Kim J**, Cha E-J, Kim J-S, Kim S-J, Ha Y-S, Kim Y-H, Jeong P, Kang HW, Kim J-H, Park J-L, Choi Y-K, Moon S-K, Choi Y-H, Kim S-Y, Kim W-J. (2017) Transcriptomic features of primary prostate cancer and their prognostic relevance to castration-resistant prostate cancer, *Oncotarget*, 2017, Vol. 8, (No. 70), pp: 114845-114855
 8. Choi B-H, You S, Park C-S, Cho E-H, Park TD, Kim S, Kim Y-J, Lee T, Kim J. (2017) Differential perturbation of the interstitial cystitis-associated genes of bladder and urethra in rat model, *Cell Cycle*, 16(8), 749–758, PMID: **28278053**, PMCID: [PMC5405721](https://pubmed.ncbi.nlm.nih.gov/PMC5405721/), DOI: [10.1080/15384101.2017.1295184](https://doi.org/10.1080/15384101.2017.1295184)
 9. Kim WJ, **Kim J** (2017) Looking to the Metabolic Landscapes for Prostate Health Monitoring, *Prostate International*, 5(3), 85-88
 10. **Kim J.** (2018) Era of the Fourth Industrial Revolution and the Urologists' Journey to Navigating Big Omics Data, *International Neurourology Journal*. 22(Suppl 2):S101-102, PMID: 30068072
 11. Shahid M, Yeager N, Yeon A, Cho E, Bae J, Sairam V, Kim M, Yoon H, Berman B, **Kim J.** (2018) Alpha-oxoglutarate inhibits the proliferation of immortalized normal bladder epithelial cells via an epigenetic switch involving ARID1A, *Scientific Reports*, 14;8(1):4505. doi: 10.1038/s41598-018-22771-2. PMID: 29540744, **Publications with *University of California Students (SRP program, CSMC Research Interns)**
 12. Shahid M, Lee MY, Yeon A, Cho E, Sairam V, You S, **Kim J.** (2018) Menthol, a Unique Urinary Volatile Compound Associated with Chronic Inflammation in Interstitial Cystitis, *Scientific Reports*, 8(1):10859. PMID: 30022124, **Publications with *University of California Students (SRP program, CSMC Research Interns)**
 13. Fan S, Yeon A, Shahid M, Anger JT, Eilber KS, Fiehn O, **Kim J.** (2018) Sex-associated differences in baseline urinary metabolites of healthy adults, *Scientific Reports*, 8(1):11883. PMID:30089834

14. Piao X-M, Byun YJ, Kim WJ, **Kim J.** (2018) Unmasking molecular profiles of bladder cancer, *Investigative and Clinical Urology*, 2018 Mar;59(2):72-82. doi:10.4111/icu.2018.59.2.72.
15. **Kim J.** (2018) Biological characterization and implications of TRMP7, a calcium channel, in renal cell carcinoma, Editorial Comment, *Investigative and Clinical Urology*, 59:263-274.
16. Wen H, Lee S, Zhu W-G, Lee O-K, Yun SJ, **Kim J***, Park S*. (2018) Glucose-derived Acetate and ACSS2 as Key Players in Cisplatin Resistance in Bladder Cancer, *Biochimica et Biophysica Acta - Molecular and Cell Biology of Lipids*, S1388 -1981(18) 30126-4. PMID: 29883801
17. Yeon A, You S, Kim M, Gupta A, Park MH, Weisenberger D, Liang G, **Kim J.** (2018) Rewiring of cisplatin-resistant bladder cancer cells through epigenetic regulation of genes involved in amino acid metabolism, *Theranostics*, 8(16):4520-4534 PMID:30214636
18. Shahid M, Yeon A, Cho E, Bae J, Park RJ, **Kim J.** (2018) Language and Culture Appropriate Approaches Needed to Improve Health Education to Reduce Disparities among Korean American Immigrants Living in Los Angeles Area. (*International Journal of Innovative Research in Medical Science*, Volume 03 Issue 08. **Publications with *University of California Students (SRP program, CSMC Research Interns)** DOI: <https://doi.org/10.23958/ijirms/vol03-i08/02>
19. Jung JH, You S, Oh JW, Yeon A, Shahid M, Cho E, Sairam V, Park TD, Kim KP, **Kim J.** (2018) Integrated proteomic and phosphoproteomic analyses of cisplatin-sensitive and resistant bladder cancer cells reveal CDK2 network as a key therapeutic target, *Cancer Letters*, 437:1-12. PMID: 30145203, **Publications with *University of California Students (SRP program, CSMC Research Interns)**
20. Shahid M, Kim M, Yeon A, Andres AM, You S, **Kim J.** Quantitative Proteomic Analysis Reveals Caffeine-Perturbed Proteomic Profiles in Normal Bladder Epithelial Cells, *Proteomics*, e1800190. PMID: 30232827
21. Mansour AM, Abdulreheem M, Laymon M, Elsherbeeney M, Sultan M, Shokeir A, Mosbah A, Abol-Enein H, Cho E, Sairam V, Park TD, Shahid M, **Kim J** (2018) Epidermal Growth Factor Expression as a Predictor of Chemotherapeutic Resistance in Muscle-Invasive Bladder Cancer, *BMC Urology*, 18(1):100. PMID:30413194, **Publications with *University of California Students (SRP program, CSMC Research Interns)**
22. Shahid M, Andreas A, Li P, Yeon A, Lee M, Yang W, Zhou B, Cho E, Bae J, Wang Y, Kim M, Kim HL, **Kim J.** (2018) Centromere protein F (CENPF), a microtubule binding protein, modulates cancer metabolism by regulating pyruvate kinase M2 phosphorylation signaling, *Cell Cycle* doi: 10.1080/15384101.2018.1557496. [Epub ahead of print] PMID: 30526248, **Publications with *University of California Students (SRP program, CSMC Research Interns)**
23. Blaženović I, Kind T, Vaniya A, Wancewicz B, Roberts BS, Lee T, Song H, Ji J, Roselius L, Biedendieck R, Jahn M, Schauer N, Jahn D, **Kim J***, Fiehn O*. (2019) Structure annotation of all mass spectra in untargeted metabolomics, *Analytical Chemistry*, doi: 10.1021/acs.analchem.8b04698. [Epub ahead of print], PMID:30608141, ***co-corresponding authors**
24. Kim S, Yeon A, Cho E, Shahid M, **Kim J** (2019) Effectiveness of a Tailored Colorectal Cancer Educational Seminar in Enhancing the Awareness, Knowledge, and Behavior of Korean Americans Living in the Los Angeles Koreatown Area, *Diversity & Equality in Health and Care*,

16(1): 1-8, **Publications with *University of California Students (SRP program, CSMC Research Interns)** PMID: 31019695

25. Kim W-J, **Kim J.** (2019) Innovative technologies for the smart E-Healthcare system *Investig Clin Urol.* 60(1):1-3. PMID:30637354
26. Myung NV, Jung S, **Kim J.** (2019) Application of low-cost, easy-to-use, portable biosensor systems for diagnosing bladder dysfunctions. *International Neurourology Journal.* 23(1):86-87, PMID:30943698
27. Shahid M, You S, Lee MY, Yeon A, Bae J, **Kim J.** (2019) Downregulation of CENPF Remodels Prostate Cancer Cells and Alters Cellular Metabolism, *Proteomics*, 2019 Apr 8:e1900038. PMID:30957416
28. Kim SJ, **Kim J***, Yoon H*. (2019) Sexual Pain and IC/BPS in Women, *BMC Urology*, 19(1):47, PMID:31170952 ***co-corresponding authors**
29. **Kim J.** (2019) Looking into Clinical Application of CD47-targeted Near-Infrared Photoimmunotherapy for Human Bladder Cancer Treatment, *Translational Andrology and Urology*, 8(Suppl 3): S322-S324, PMID: 31392158
30. Kim W-J, Jin P, Kim WH, **Kim J** (2020) Utilizing machine learning to discern hidden clinical values from big data in urology, *Investig Clin Urol*, 61(3):239-241. PMID: 32377598, PMCID: PMC7189104, DOI: 10.4111/icu.2020.61.3.239
31. Park H, **Kim J**, Jung S (2020) Development of Non-invasive Biosensor Device Development for Detection of Bladder Cancer in Urine, *Clinical Oncology & Research*, 3(6): 2-4, DOI: [10.31487/j.COR.2020.06.11](https://doi.org/10.31487/j.COR.2020.06.11)
32. **Kim J**, Kim WT, Kim W-J. (2020) Advances in urinary biomarker discovery in urological research, *Investigative and Clinical Urology*, 61(Suppl 1):S8-S22.
33. Jung S, **Kim J.** (2020) Biomarker Discovery and Beyond for Diagnosis of Bladder Diseases. *Bladder*, 7(1):e40, **Selected as a Cover Image**
34. Fan S, Shahid M, Jin F, Asher A, **Kim J.** (2020) Identification of Metabolic Alterations in Breast Cancer Using Mass Spectrometry-based Metabolomic Analysis, *Metabolites*, 10(4). pii: E170. doi: 10.3390/metabo10040170. PMID:32344578
35. **Kim J**, Jin P, Kim WH, Kim W-J. (2020) Bringing Machine Learning to Pick Out Hidden Clinic Values from Big Data in Urology, *Investigative and Clinical Urology*, 61:239-24, PMID: 32377598
36. Shahid M, Kim M, Jin P, Zhou B, Wang Y, Yang W, You S, **Kim J.** (2020) S-Palmitoylation as a Functional Regulator of Proteins Associated with Cisplatin Resistance in Bladder Cancer, *International Journal of Biological Sciences*, 16(14):2490-2505, PMID: **32792852**,
37. Tang F, Shahid M, Peng J, Jung S, Kim WH, **Kim J.** (2020) Classification of the urinary metabolome using machine learning and potential applications to diagnosing interstitial cystitis, *Bladder*, 7(2):e43; DOI: 10.14440/bladder. 2020.815
38. Park H, **Kim J**, Jung S (2020) Non-invasive Biosensor Device Development for Detection of Bladder Cancer in Urine, *Clinical Oncology & Research*, 3(6): 2-4, DOI: [10.31487/j.COR.2020.06.11](https://doi.org/10.31487/j.COR.2020.06.11)

39. **Kim J**, Gewertz B (2020) Teleurology and digital health app in COVID-19 pandemic, *Investigative and Clinical Urology*, 61(4):333-334, PMID: 32665988
40. **Kim J** (2020) Equality, Inclusion, and Diversity in Healthcare During the COVID-19 Pandemic, *International Neurourology Journal*, 24(2):1-2, doi:10.5213/inj.2040198.099
41. Shahid M, Yeon A, **Kim J**, (2020) Metabolomic and Lipidomic Approaches to Identify Biomarkers for Bladder Cancer and Interstitial Cystitis, *Molecular Medicine Report*, 22: 5003-5011, DOI: 10.3892/mmr.2020.11627
42. **Kim J**, Jin P, Yang W, Kim W-J (2020) Proteomic Profiling of Bladder Cancer for Precision Medicine in the Clinical Setting: A Review for the Busy Urologist, *Investigative and Clinical Urology*, 61(6):539-554, PMID: 33135400 – * **Video Interview of Author**, <https://youtu.be/iYVoLYkE7j8>
43. Jin P, Park H, Jung S, **Kim J** (2021) Challenges in Urology During COVID-19 Pandemic, *Urologia Internationalis*, 23;1-14, PMID: 33227808, DOI: 10.1159/000512880
44. Shahid M, **Kim J** (2020) Exercise Effects on Post-treatment symptoms relief and Metabolism of Breast Cancer Patients. *Metabolites*, 10(9), 377, PMID: [32962184](https://pubmed.ncbi.nlm.nih.gov/32962184/)
45. Park H, Jin P, Jung S, **Kim J** (2021) Quick Overview of Diagnostic Kits and Smartphone Apps for Urologists During the COVID-19 Pandemic, *Translational Andrology and Urology*, 10(2):939-953, PMID: 33718094, PMCID: PMC7947436, DOI: 10.21037/tau-20-1042
46. **Kim J**, Yeon A, Parks S, Shahid M, Thiombane A*, Cho E*, You S, Emam H, Kim D-G, Kim M (2021) Alendronate-induced Perturbation of the Bone Proteome and Microenvironmental Pathophysiology, *International Journal of Medical Sciences*, 18(14):3261-3270. PMID: 34400895, PMCID: PMC8364444, DOI: 10.7150/ijms.61552, * **UCLA mentees**

Research Papers (Peer-Reviewed, in revision)

Acknowledged DoD grant support

1. Cho H, Tong F, You S, Jung S, Kim WH, **Kim J** (2021) Prediction of Response to Immunotherapy in Bladder Cancer Patients, *IEEE Access*, in press
2. **Kim J***, Yeon A, Kim W-K, Kim K-H, Ohn T. (2021) Stress-Induced Accumulation of HnRNP K into Stress Granules, *Apoptosis*, in review, * **corresponding author**
3. **Kim J***, Yeon A, Ahmed KT, Zhang W, Kim W-K, Kim K-H (2021) Upregulation of Apoptosis and Alteration of the Microenvironment is Mediated by Lipid Raft Microdomains in Bladder Epithelial Cells Exposed to Candida, in review, * **corresponding author**

6.2. Books or other non-periodical, one-time publications.

Book Chapter

Acknowledged DoD grant support

1. Jin F, Shahid M, Kim J. (2021) Research Progress of Urine Biomarkers in the Diagnosis, Treatment, and Prognosis of Bladder Cancer, Springer Nature Switzerland AG 2021, H. M. Baptista Carreira dos Santos (ed.), *Translational Urinomics*, Advances in Experimental Medicine and Biology

Other non-periodical, one-time publications.

1. Genetic Engineering & Biotechnology News (GEN)
 - i. Metabolomics in Precision Medicine
 - ii. <http://www.genengnews.com/gen-articles/metabolomics-in-precision-medicine/5502/?kwrd=jayoung%20kim#gsaccess>
 - iii. Acknowledgement of federal support (no)
2. UroToday
 - i. UroToday since 2003, has established itself as a global leader in the delivery of quality, clinically relevant content.
3. Metabolomics insights into pathophysiological mechanisms of interstitial cystitis,
 - i. <http://www.urotoday.com/recent-abstracts/pelvic-health-reconstruction/interstitial-cystitis/79104-metabolomics-insights-into-pathophysiological-mechanisms-of-interstitial-cystitis-beyond-the-abstract-by-jayoung-kim-phd.html>
 - ii. Acknowledgement of federal support (no)
4. Metabolic Pathway Signatures Associated with Urinary Metabolite Biomarkers Differentiate Bladder Cancer Patients from Healthy Controls.
 - i. <http://www.urotoday.com/recent-abstracts/urologic-oncology/bladder-cancer/88889-metabolic-pathway-signatures-associated-with-urinary-metabolite-biomarkers-differentiate-bladder-cancer-patients-from-healthy-controls.html>
 - ii. Acknowledgement of federal support (no)
5. Commentary articles on IC and painful sex
<https://www.urotoday.com/recent-abstracts/pelvic-health-reconstruction/interstitial-cystitis/113380-what-we-know-about-sexual-pain-and-ic-bps-in-women-beyond-the-abstract.html>

This article was well received by science community. There was a lot of requests of talk and phone calls from physicians and patients.

6.3. Other Publications, Conference papers, and Presentations

Conference Papers

1. Wen H, Lee T, You S, Park S-H, Song H, Eilber KS, Anger JT, Freeman MR, Park S, **Kim J.** Noninvasive Biomarker Candidates of Interstitial Cystitis, SUFU 2015 Winter Meeting, February 24 - 28, 2015 , Scottsdale, AZ
2. You S, Lee T, Keay S, Anger J, Freeman MR, **Kim J.** Signal Network of Interstitial Cystitis-Associated Antiproliferative Peptide, SUFU 2015 Winter Meeting, February 24 - 28, 2015, Scottsdale, AZ
3. You S, **Kim J,** Freeman MR. Prostate Cancer Classification Using a Transcriptome Atlas. AACR Joint Conference, Translation of the Cancer Genome. Computational and Systems Biology of Cancer. February 7-11, 2015. The Fairmont San Francisco San Francisco, CA

4. Wen H, Lee T, You S, Park S-H, Song H, Eilber KS, Anger JT, Freeman MR, Park S, **Kim J**. Urinary Biomarker Candidates of Interstitial Cystitis, The Annual Conference US HUPO, March 15-18, 2015, Tempe, AZ
5. **Kim J**. Non-invasive Biomarker Metabolites of Interstitial Cystitis. Metabolomics-2015, April 27-29, Philadelphia, PA
6. **Kim J**. Interstitial Cystitis Metabolic Biomarkers. 11th Annual International Conference of the Metabolomics Society, June 29-July 2, 2015, San Francisco, CA
7. **Kim J**. Cholesterol Metabolism in Prostate Cancer. Androgen Today, July 10, 2015, Seoul, Korea
8. You S, Knudsen BS, Erho N, Alshalalfa M, Takhar M, Ashab HA, Davicioni E, Karnes J, Klein EA, Den RB, Garraway IP, **Kim J**, Freeman MR. Three intrinsic subtypes of prostate cancer with distinct pathway activation profiles differ in prognosis and treatment response, Prostate Cancer Foundation (PCF) Retreat, October 8-10, 2015, Washington DC
9. You S, Knudsen BS, Erho N, Alshalalfa M, Takhar M, Ashab HA, Davicioni E, Karnes J, Klein EA, Den RB, Garraway IP, **Kim J**, Freeman MR. Three intrinsic subtypes of prostate cancer with distinct pathway activation profiles differ in prognosis and treatment response, SBUR, November 12-16, 2015, Florida
10. An epigenomic pathway from cholesterol to intracrine androgen. The Western Section American Urological Association (AUA) Meeting, 2015, held in Palm Springs, California
11. Ackerman AL, Anger JT, Tang J, Eilber K, Funari V, **Kim J**, Freeman MR. Identification of a diverse fungal community (mycobiome) in the normal female human lower urinary track. SUFU 2016 Winter Meeting (**Best Poster Award**)
12. Ackerman AL, Anger JT, Tang J, Eilber K, Funari V, **Kim J**, Freeman MR. Identification of a diverse fungal community (mycobiome) in the normal female human lower urinary track. 2016 American Urological Association (AUA), San Diego, CA
13. You S, Knudsen BS, Erho N, Alshalalfa M, Takhar M, Ashab HA, Davicioni E, Karnes J, Klein EA, Den RB, Garraway IP, **Kim J**, Freeman MR. Three intrinsic subtypes of prostate cancer with distinct pathway activation profiles differ in prognosis and treatment response, AACR Annual Meeting 2016 in New Orleans, Louisiana, April 16-20, 2016
14. Kim WT, Yun SJ, Yan C, Jeong P, Kim Y-J, Lee S-C, Park S, Moon S-K, Choi Y-H, Choi YD, **Kim J***, Kim W-J*, Metabolic pathways associated with urinary metabolite biomarkers differentiate bladder cancer patients from healthy controls, AACR Annual Meeting 2016 in New Orleans, Louisiana, April 16-20, 2016
15. You S, Knudsen BS, Erho N, Alshalalfa M, Takhar M, Ashab HA, Davicioni E, Karnes J, Klein EA, Den RB, Garraway IP, **Kim J**, Freeman MR. Three intrinsic subtypes of prostate cancer with distinct pathway activation profiles differ in prognosis and treatment response, AUA 2016 in San Diego, May 2016
16. Kind T, Cho E, Park T, Deng N, Liu Z, Lee T, Fiehn O, **Kim J**, Interstitial Cystitis-Associated Urinary Metabolites Identified by Mass-Spectrometry Based Metabolomics Analysis, The 1st International Electronic Conference on Metabolomics, Section: Metabolomics in Human Diseases, November 1-30, 2016
17. **Kim J**, Interstitial Cystitis-Associated Urinary Metabolites, International Society for Computational Biology (ISCB), The RSG-DREAM 2016 conference, Phoenix, AZ, November 6-9, 2016.

18. Shahid M, Kim SS, **Kim J**, The Prognostic Gene Signature Predicting Chemosensitivity of Non-Small Cell Lung Cancer, Cedars-Sinai Research Day, January 2017
19. **Kim J**, Research and Outreach Activities on Korean and Korean-American in Los Angeles, Cedars-Sinai Research Day, January 2017
20. Skove SL, Howard LE, Senechal J, De Hoedt A, Bresee C, **Kim J**, Freedland SJ, Anger JT, The Misdiagnosis of Interstitial Cystitis/Painful Bladder Syndrome, AUA 2017, Boston, April 2017
21. Lee T, Song HS, **Kim J**, Interstitial Cystitis-Associated Urinary Metabolites Identified by Mass-Spectrometry Based Metabolomics Analysis, Annual Meeting of Korean Urology Association, Seoul, Korea, May 2017
22. Lee T, Song HS, **Kim J**, Differential Perturbation of the Interstitial Cystitis-Associated Genes of Bladder and Urethra in Rat Model, Annual International Continence Society, Florence, Italy, September 12-15, 2017
23. Lee MY, Yeon Y, Shahid M, Cho E, Sairam V, Figlin R, Kim K-H, **Kim J** (2017) Reprogrammed Lipid Metabolism in Bladder Cancer with Cisplatin Resistance, Intelligent Systems for Molecular Biology and 16th European Conference on Computational Biology (ISMC/ECCB 2017), Prague, Czech Republic, July 21-July 25, 2017
24. Nickel JC, Stephens A, Landis JR, Mullins C, Bokhoven A, Anger J, Ackerman AL, **Kim J**, Freeman MR, Sutcliffe S, Ehrlich G, Urinary Fungi Associated with Urinary Symptom Severity but not Flares or Pain Severity among Women in the MAPP Network Study with Interstitial Cystitis/Bladder Pain Syndrome (IC/BPS), 2018 American Urological Association (AUA) Annual Conference, San Francisco, California, May 18 – May 21, 2018
25. Skove SL, Howard LE, Senechal J, Hoedt AD, Bresee C, Cunningham T, **Kim J**, Freedland SJ, Anger JT, The Misdiagnosis of Interstitial Cystitis/Bladder Pain Syndrome (IC/BPS), 2018 American Urological Association (AUA) Annual Conference, San Francisco, California, May 18 – May 21, 2018
26. Anger J, Ackerman AL, Spivia W, van den Broek I, Crear D, Eilber K, Freeman M, **Kim J**, Fu Q, Van Eyk J. Differential protein expression in patients with UCPPS: A MAPP study, SUFU 2018 Winter Meeting, Austin, TX, February 27 – March 3, 2018
27. **Kim J**, Urine Odormics Profiling Revealed Menthol level is Associated with Interstitial Cystitis, The 16th Urological Association of Asia (UAA) Congress 2018 Kyoto, Japan, April 17 - April 21, 2018
28. **Kim J**, Reprogrammed Lipid Metabolism in Cisplatin Resistance in Aggressive Bladder Cancer, The 16th Urological Association of Asia (UAA) Congress 2018, Kyoto, Japan, April 17 – April 21, 2018
29. **Kim J**, Interstitial Cystitis-Associated Urinary Metabolites Identified by Mass-Spectrometry Based Metabolomics Analysis, The 16th Urological Association of Asia (UAA) Congress 2018, Kyoto, Japan, April 17 – April 21, 2018
30. **Kim J**, Proteomic Signatures Predictive of Cisplatin Resistance in Bladder Cancer, The 16th Urological Association of Asia (UAA) Congress 2018 Kyoto, Japan, April 17- April 21, 2018
31. **Kim J**, Urine odor profiling for diagnosis of interstitial cystitis, Annual Conference of Experimental Biology (EB)/American Society for Biochemical and Molecular Biology (ASBMB), San Diego, CA, USA, April 21- April 25, 2018
32. Van Den Broek I, Mouapi KN, Mastali M, Holewinski R, Venkatraman V, Fu Q, Ackerman AL, **Kim J**,

Freeman M, Anger JT, Millis K, Percy A, Van Eyk JE. A stable-isotope labeled protein and peptide mixture for global normalization in targeted and data-independent quantitative bottom-up proteomics, American Society for Mass Spectrometry (ASMS), San Diego, CA, USA, June 3 – June 7, 2018

33. Shahid M, Lee MY, Yeon A, Cho E, Sairam V, You S, **Kim J**. Menthol, a Unique Urinary Volatile Compound Associated with Chronic Inflammation in Interstitial Cystitis, The CSMC Research Day, February 16, 2018
34. Yeon Y, Lee MY, Shahid M, Cho E, Sairam V, Figlin R, Kim K-H, **Kim J**. Reprogrammed Lipid Metabolism in Bladder Cancer with Cisplatin Resistance, The CSMC Research Day, February 16, 2018, **Best post award**
35. Anger J, Spivia W, van den Broek I, Crear D, Venkatraman V, Ackerman AL, Eilber K, Freeman M, **Kim J**, Fu Q, Van Eyk J. Differential protein expression in patients with UCPPS: A MAPP study, 2018 American Urological Association (AUA) Annual Conference, San Francisco, California, May 18 – May 21, 2018
36. Kim M, Yoon J, **Kim J**, Freeman MR, You S. Facilitating Biological and Clinical Discoveries Using The Prostate Cancer Transcriptome Atlas. 2018 American Urological Association (AUA) Annual Conference, San Francisco, California, May 18 – May 21, 2018
37. Junhee Yoon J, Kim M, Erho N, Alshalalfa M, Takhar M, Al-deen Ashab H, Davicioni E, **Kim J**, Freeman MR, You S. A Systematic Comparison of the Prostate Cancer PCS and PAM50 Classification Schemes. 2018 American Urological Association (AUA) Annual Conference, San Francisco, California, May 18 – May 21, 2018
38. Shahid M, Lee MY, Yeon A, Cho E, Sairam V, You S, **Kim J**. Urinary Volatile Compound Associated with Chronic Inflammation in Interstitial Cystitis, Immunology LA 2018, California, June 15, 2018
39. Yeon Y, Lee MY, Shahid M, Cho E, Sairam V, Figlin R, Kim K-H, **Kim J**. Reprogrammed Lipid Metabolism in Bladder Cancer with Cisplatin Resistance, Immunology LA 2018, California, June 15, 2018
40. Laden BF, Hoedt AD, Scharfenberg A, Saxena R, Senechal JF, Barbour KE, **Kim J**, Freedland SJ, Anger JT, Comorbid Conditions in a Nationwide, Heterogenous Population of Patients with Interstitial Cystitis/Bladder Pain Syndrome, 2019 American Urological Association (AUA) Annual Conference, 2019
41. The Serum Proteome Correlates with Clinical Phenotypes of UCPPS: A MAPP Study, 2019 Annual Meeting of the American Urological Association, Chicago, Illinois, May 3-6, 2019
42. Rewiring of cisplatin-resistant bladder cancer cells through epigenetic regulation of genes involved in amino acid metabolism, 2019 Keystone Symposia Conference, Cancer Metastasis: The Role of Metabolism, Immunity and the Microenvironment, Firenze Fiera- Fortezza da Basso, Florence, March 15-19, 2019
43. Wen H, Lee S, Zhu W-G, Lee O-J, Yun SJ, Kim J, Park S, Glucose-derived Acetate and ACS2 as Key Players in Cisplatin Resistance in Bladder Cancer, AACR Annual Meeting 2019, March 30-April 3, 2019
44. Epigenetic remodeling of cancer metabolisms in cisplatin resistant bladder cancer, AACR Bladder Cancer: Transforming the Field Special Conference, taking place May 18–21, 2019, in Denver, Colorado

45. Acetate metabolism mediated by Acetyl-CoA synthetase 2 in cisplatin resistant bladder cancer, AACR Bladder Cancer: Transforming the Field Special Conference, taking place May 18–21, 2019, in Denver, Colorado
46. Characterization of the global proteome and phosphoproteome in cisplatin resistant bladder cancers revealed the CDK2 network as a potential therapeutic target, AACR Bladder Cancer: Transforming the Field Special Conference, taking place May 18–21, 2019, in Denver, Colorado
47. **Kim J**, Integrated phosphoproteomic biosignatures in cisplatin resistant bladder cancer, 108th Annual Meeting of the Japanese Urological Association (oral presentation), April 23-26, 2020, Kobe, Japan. – Reschedule in Dec 22-24, 2020
48. **Kim J**, A Potential Biomarker of Interstitial Cystitis, Alpha-Oxoglutarate, Perturbates Epigenetic Landscapes and Biology of Bladder Epithelial Cells, 108th Annual Meeting of the Japanese Urological Association (oral presentation), April 23-26, 2020, Kobe, Japan. – Reschedule in Dec 22-24, 2020
49. Tholemeier VN, Wiggins E, Dallas KB, Bresee CT, De Hoedt A, Senechal JF, Barbour KE, **Kim J**, Freedland SF, Anger JT, Variation in symptoms experienced by women with Interstitial Cystitis/Bladder Pain Syndrome, American Urogynecologic Society (AUGS) Pelvic Floor Disorders (PFD) Week, October 6-10, 2021, Vancouver, Canada
50. **Kim J**, Kim M, Emam H, Kim D-G, Clinicopathology and Mechanisms in *Bisphosphonate*-induced Osteonecrosis of the Jaw, 2021 IADR/AADR/CADR General Session, Virtual, July 21-24, 2021
51. Lior, Bresee C, **Kim J**, De Hoedt A, Freedland S, Anger JT. Urodynamic Findings in a Heterogenous Population with Interstitial Cystitis: The Bladder Remains an Unreliable Witness, 2021 American Urogynecologic Society (AUGS), October 12-15, 2021 Phoenix, Arizona
52. Tholemeier LN, Dubinskaya A, Erickson T, De Hoedt AM, Kim J, Freedland SJ, Anger JT. Black race, prior depression, and PTSD are associated with increased pain and depression symptoms in a cohort of women with Interstitial Cystitis/Bladder Pain Syndrome, PFD Week 2021, Annual scientific meeting of AUGS, 10/12/2021 to 10/15/2021, Phoenix, Arizona
53. Tholemeier LN, Bresee C, De Hoedt AM, Kim J, Freedland SJ, Anger JT. Do bladder instillation patterns in a cohort of women with Interstitial Cystitis/Bladder Pain Syndrome follow treatment guidelines? PFD Week 2021, Annual scientific meeting of AUGS, 10/12/2021 to 10/15/2021, Phoenix, Arizona
54. Tholemeier LN, Bresee C, De Hoedt AM, Kim J, Freedland SJ, Anger JT. Do medication prescription patterns follow guidelines in a cohort of women with Interstitial Cystitis/Bladder Pain Syndrome? PFD Week 2021, Annual scientific meeting of AUGS, 10/12/2021 to 10/15/2021, Phoenix, Arizona
55. Lee RJ, Madan RA, Kim J, Posadas EM, Yu EY. Disparities in cancer care and the Asian American population. UKC 2021, December 15-18, Los Angeles, CA

Presentation and Seminar

1. Keynote Speaker, The Steroid Today-2015, Seoul, Korea, “Cholesterol Metabolism in Prostate Cancer”, 2015
2. Keynote Speaker, State-of -the-Art-Lecture, Annual Korean Bladder Dysfunction Society Conference, September 3-4, 2016, Seoul, Korea

3. Invited Speaker, Kyung Hee University, MRC Seminar Series for Graduate Students, “Unmasking Interstitial Cystitis”, May 31, 2016, Seoul, Korea
4. Invited Speaker, Ewha Women’s University, Urology Grand Round Seminar Series for Medical Students and Clinical Fellows, “Current and Future Research Aspects on Interstitial Cystitis”, June 3, 2016, Seoul, Korea
5. Invited Guest Speaker, Gachon University, INITIATIVE for Interstitial Cystitis Network, “Interstitial Cystitis and Beyond”, June 14-15, 2016, Incheon, Korea
6. Invited Speaker, the US-Egypt Science and Technology Development Fund Symposium held in Cairo, Egypt, October 24-25, 2016
7. Visiting Lecture, Mansoura University, Mansoura, Egypt, “Omics Approaches to understand Urological Diseases”, October 23, 2016
8. Workshop Organizer and Speaker, Mansoura University, Egypt, “Molecular Biology Lab Initiative”, October 23, 2016
9. “Distinguished Women in Science Series” guest speaker, Women in Science (AWIS) Talk, Cedars-Sinai Medical Center, 2016
10. “Unmasking interstitial cystitis” CDC-sponsored seminar series, Cedars-Sinai Medical Center, 2016
11. Invited Speaker, Medical Education Department, Simulation Center, Cedars-Sinai Medical Center, 2017
12. Invited Speaker, Community outreach, Meeting with Korean community journalists and media, Cedars-Sinai Medical Center, 2017
13. Invited Guest Speaker, Golden Age Lions Club, 2017
14. Speaker and Organizer, Webinar Series in Molecular Biology in Mansoura University, Egypt, March 27, 2017
15. Speaker and Organizer, Webinar Series in Molecular Biology in Mansoura University, Egypt, August, 2017
16. Keynote Speaker, Inha Medical Research Center, Incheon, South Korea, August 10, 2017
17. Keynote Speaker, Gacheon Medical Center and Inha University Annual Conference, Incheon, South Korea, August 11-12, 2017
18. Invited Speaker, Ewha Women’s University School of Medicine, Seoul, South Korea, August 14-15, 2017
19. Invited Speaker, Urology Symposium, Seoul, South Korea, August 13, 2017
20. Invited Speaker, Korea Institute of Science and Technologies (KIST), October 24, 2017
21. Invited Speaker, Korea Institute of Science and Technologies (KIST), Seoul, South Korea, March 28, 2018
22. Invited Speaker, Catholic University, Seoul, South Korea, March 29, 2018

23. Keynote Speaker, Seoul National University, Seoul, South Korea, March 30, 2018
24. Invited Speaker, International US-Korea Conference (UKC) 2018, St. Johns, August 2- 5, 2018
25. Invited Speaker, the US-Egypt Science and Technology Development Fund Symposium held in Cairo, Egypt, November 5-7, 2018
26. Keynote Speaker, Ain Shams University, Egypt, November 8-9, 2018
27. Invited Speaker, Korean Women in Science and Engineering (KWise) 12nd West Coast Annual Conference
28. Invited panelist, Ygnite Conference 2019, "Future of Research & New Challenges & Emerging Trends", 2019
29. Speaker, University of Texas Arlington, Department of Electrical Engineering, March 7-9, 2019
30. Invited Speaker, The 29th Annual South West Regional Conference, The Southern California Chapter of Korean-American Scientists and Engineers Association, '*data driven real world problem solving*', April 27, 2019
31. Invited Speaker, University of Texas Arlington, Department of Electrical Engineering, March 7-9, 2019
32. Invited Speaker, University of East Virginia Medical School, March 28, 2019
33. Invited Speaker, UKC 2019, Chicago, August 15-18, 2019
34. Forum panel, UKC 2019, Chicago, August 15-18, 2019
35. Keynote Speaker, Urinomics 2019, Caparica, Portugal, September 2-4, 2019
36. Keynote Speaker, Ewha Urology Symposium, Seoul, Republic of Korea, September 19-21, 2019
37. Invited Speaker, Chapman University School of Pharmacy, Irvine, October 24, 2019
38. Invited Speaker, West Regional Conference (WRC) 2019 "Smart Science, Engineering and Technology", Seattle, November 2, 2019
39. Speaker, Panel and Chair of KWise-KOWFST Women's Forum at UKC 2020 Virtual, December 15-18, 2020
40. Speaker, Panel and Chair of KWSE-KWise Forum UKC 2020 Virtual, December 15-18, 2020
41. Speaker, Panel and Chair of GBIHN Biomedical Global Talent Nurturing Program Networking Forum UKC 2020 Virtual, December 15-18, 2020
42. Invited Speaker, Los Angeles KWise Seminar Series, March 13, 2021
43. Panel and Speaker, The **Conversations For All, By All- Celebrating Asian American Pacific Islander** Month, May 18, 2021
44. Keynote Speaker, 13th Aslla Symposium, July 1, 2021

45. Invited Panel and Speaker, ACS Los Angeles ResearchHERS Launch Event (to raise funds and also highlight the research being done at CSMC), July 22, 2021
46. Keynote Speaker, The Brain Korea Kangwon National Univeristy International Conference, August 23, 2021
47. Keynote Speaker, 2021 The 26th Annual Meeting of the Korean Continece Society & The 12th Practitioner Workshop September 10-11, 2021, Cheongju, South Korea

6.3.4. Website(s) or other Internet site(s)

Please refer the above section

6.3.5. Technologies or techniques

Nothing to report

6.3.6. Inventions, patent applications, and/or licenses

Nothing to report

6.3.7. Other Products

Daily radio shows to enhance public awareness through broadcasting and media
(Please refer the above section)

7. PARTICIPANTS & OTHER COLLABORATING ORGANIZATIONS

7.1. What individuals have worked on the project?

No change
Jayoung Kim

7.2. Has there been a change in the active other support of the PD/PI(s) or senior/key personnel since the last reporting period?

Nothing to Report

7.3. What other organizations were involved as partners?

Nothing to Report

8. SPECIAL REPORTING REQUIREMENTS

8.1. COLLABORATIVE AWARDS: Nothing to Report

8.2. QUAD CHARTS: Nothing to Report

9. APPENDICES:

Original copies of journal articles with reprints of manuscripts are attached.
Only published with acknowledgment of this funding

DEBATE

Open Access

Virus encoded circulatory miRNAs for early detection of prostate cancer



Jayoung Kim^{1,2,3*}, Seok Joong Yun⁴ and Wun-Jae Kim^{4*}

Abstract

Background: Prostate cancer (PCa) is the most commonly diagnosed cancer and kills about 28,000 American men annually. Although progress has been made in understanding the molecular features of different forms of the disease, PCa is considered incurable when it becomes resistant to standard therapies. Prostate specific antigen (PSA) test has been a gold standard of diagnosis for PCa, however, it can result in lead to the unnecessary biopsies and treatment of indolent cancers due to the low specificity. Thus, the limitations of PSA screening for PCa have prompted much focus on strategies how to enhance the accuracy of PSA for distinction between aggressive and indolent cancers.

Discussion: Studies of miRNAs in PCa patients have suggested differentially expressed miRNAs between healthy controls and those with PCa, providing potential biomarker candidates using body fluids including urine and blood. Virus infection has been considered to associate with PCa incidence. Virus infected PCa cells may shed extracellular vesicles and communicate with neighboring cells, which were not infected yet, however, no mechanistic approaches were performed to understand the biology. The miRNAs composition in the shedding extracellular vesicles, and its role in PCa are completely undefined. In the near future, new insights to connect between the viral derived miRNAs and PCa progression might provide an opportunity to diagnose, risk prediction and therapeutic strategies.

Summary: The goal of this debate article is to provide a short review on miRNAs, virus infection and viral encoded miRNAs in PCa, with a primary focus on circulating miRNAs as potential non-invasive biomarkers for PCa patients.

Keywords: miRNAs, Virus, Extracellular vesicles, Prostate cancer

Background

Prostate cancer (PCa) remains one of the most commonly diagnosed malignant tumor in men and the second leading cause of death from cancer [1–3]. Several new drugs including Radium-223, Cabazitaxel, Sipuleucel-T, Abiraterone, and Enzalutamide have shown significantly improved survival in castration-resistant metastatic disease (CRPC) patients in Phase 3 trials [4–8]. For early detection of PCa, urologists rely on serum prostate-specific antigen (PSA) testing or digital rectal examination (DRE) [9]. Serum PSA testing has successfully achieved a dramatic increase of PCa detection, however, PSA testing has a low specificity because an increase of PSA level is not a PCa-specific event.

Serum PSA levels are also elevated in men with benign prostatic hyperplasia and prostatitis. Limitations of DRE for the early detection derived from its low accuracy and the dependence on highly trained clinicians. Such a lack of PCa-specific early detection tool leads to create unnecessary biopsies or severe treatments for indolent PCa [2]. Development of methods of prebiopsy risk stratification and more simple, noninvasive, sufficiently sensitive and specific tests for PCa diagnosis would allow the stratification of PCa patients who are at the very early stage of disease [1, 10]. Current efforts to improve the accuracy of PSA and develop new biomarkers for PCa may hold the promise of improving the screening, diagnosis, and monitoring of prostate cancer. PCA3, a non-coding and large chain RNA that is significantly overexpressed in PCa compared to non-tumorous prostate cells, was introduced as a biomarker for PCa to show high sensitivity (52 % to 58 %) and specificity (72 % to 87 %) [11–16]. The US FDA approved PCA3 as a risk assessment tool for PCa to guide prostatic biopsy

* Correspondence: Jayoung.Kim@cshs.org; wjkim@chungbuk.ac.kr

¹Departments of Surgery and Biomedical Sciences, Cedars-Sinai Medical Center, 8700 Beverly Blvd., Davis Room 5071, Los Angeles, CA 90048, USA

⁴Department of Urology, Chungbuk National University College of Medicine, 62 Kaeshin-dong, Heungduk-gu, Cheongju 361-763, Republic of Korea
Full list of author information is available at the end of the article

among men with negative previous prostate biopsies. Urinary PCA3 assay combined with TMPRSS2:ERG is reported to improve the diagnostic accuracy [17, 18]. Recently reported studies suggested that these requirements could be fulfilled using the diagnostic approach based on analysis of urine, which has become the future for non-invasive biomarker testing [10, 19].

This brief debate article is to discuss and seek to characterize the circulating microRNAs (miRNAs) in urine with regard to PCa. We aim to provide our audience the current knowledge, in particular, focused on clinical implication as a liquid biopsy with a clinically satisfactory degree of sensitivity and specificity.

Discussion

MicroRNAs in prostate cancer

What are microRNAs?

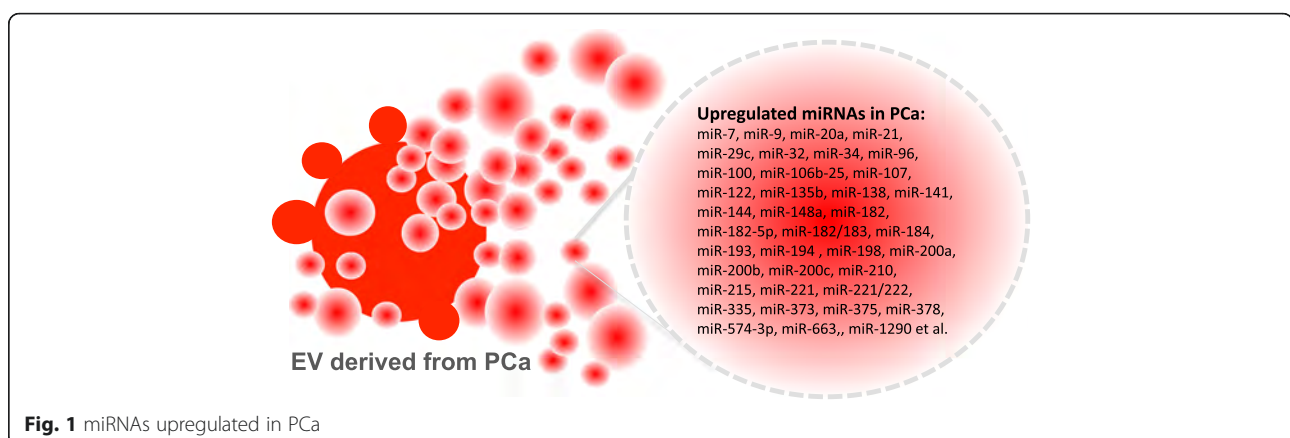
Small non-coding microRNA (miRNA) molecules are known as post-transcriptional regulators involved in the regulation of gene and protein expression by interfering in the post-transcriptional level, resulting in the degradation and translation inhibition of mRNAs. Approximately more than 2,000 mature human miRNAs have been reported so far. These miRNAs are short (19–24 nt) and low molecular weight RNAs. miRNAs are derived from hairpin-like precursor transcripts (pre-miRNAs) and taken out of nucleus by a mediator protein, exportin 5. Pre-miRNA is then cleaved by Dicer (a ribonuclease III enzyme) to excise the mature miRNAs in the form of siRNA-like duplexes and asymmetrical assembling of the mature miRNA strands. Since miRNAs interact with multiple messenger RNAs by binding the pairing of bases of the mRNAs and repress target gene expression, and regulate mRNA cleavage and mRNA decay initiated by the miRNA-guided rapid deadenylation, miRNAs have a wide variety of functions contributing to various pathological conditions including prostate cancer [20].

How miRNAs are connected with PCa development and progression cancer?

Many of miRNAs play roles in cell proliferation and apoptosis processes, thus miRNA expression profiles can be considered as useful biomarkers monitoring many types of cancer progression and treatment responses [21]. Previous studies have suggested several miRNA biomarker candidates associated with PCa [22]. miR-548c-3p was found significantly overexpressed in CRPC. Expression levels of miR-548c-3p negatively correlated with recurrence-free survival. miR-375 was significantly downregulated in 83.5 % of PC patients compared to BPH controls. Metastatic CRPC patients with chemotherapy-resistant had the higher miR-21 levels compared with those with hormone dependent primary PCa. A combined diagnostic testing of miR-21 and PSA could stratify patients effectively. miR-21 was introduced as one of miRNAs of a multiple diagnostic profile, which includes miR-21, miR-141, and miR-221. miR-141 was independently identified as a biomarker of CRPC. Another combination panel of PSA and expression levels of let-7c, miR-30c, miR-141, and miR-375 was suggested as diagnostic biomarkers for PCa screening outperforming the PSA testing alone. Some PCa-specific miRNAs were identified from mouse PCa model. A set of 46 miRNAs in the serum of transgenic mice with advanced adenocarcinoma PCa were identified. Among those, miR-141, miR-298, and miR-375 were found to be elevated in the serum of metastatic CRPC patients. In particular, miR-141 and miR-375 showed a correlation with disease outcome. Diagrammatic representation of miRNAs associated with PCa is shown in Fig. 1.

What can be the target genes or pathways of miRNAs in PCa?

In the accumulated literature the roles of miRNAs in the pathobiology of PCa were found in cell cycle, apoptosis, epithelial to mesenchymal transition (EMT) and



mesenchymal to epithelial transition (MET) states, invasion and metastasis, PCa stem cell, and androgen receptor (AR) pathway. PTEN-PI3 Kinase-AKT, EGFR and AR pathways are considered as the most important signaling pathways in PCa. Upregulation of miR-221/-222 in PCa suggest a mechanistic link to PCa since miR-221/-222 plays a role in AR pathway regulation, c-kit, PTEN, and TIMP3 et al. miR-124 was characterized to have a direct targeting of AR thereby inducing down-regulation of miR-125b and up-regulation of p53. When miR-125b is suppressed miR-125b effectors (p52, Puma, Bak1, and p14ARF) were downregulated. The regulation of miR-125b on apoptotic proteins (mitochondrial cytochrome C and Caspase-3) and NCOR2 (a co-repressor of AR) was well known. Another PCa-associated miRNA, miR-let-7c regulates AR pathway and involves in the conversion of hormone dependent PCa to CRPC.

Urinary microRNAs as prostate cancer biomarkers

Several cancer-associated miRNAs were found in circulating body fluids such as urine, which make it possible to develop non-invasive biomarkers mainly due to their ease of access and stability. Only few studies for PCa-associated miRNA in urine were reported. Five of the miRNAs that were differentially quantified in PCa patients compared to controls (miR-107, miR-574-3p, miR375, miR200b and miR-141) were successfully quantified in urine of men with cancer, which were much higher in PCa patients than that of healthy volunteers. Such reports provide evidence that circulating miRNAs might be a next-generation biomarker and contribute to cancer screening in non-invasive liquid biopsy. Two additional promising miRNAs, miR-141 and miR-375 were found in the patient blood. In particular, data from this study showed that metastatic PCa patients have approximately 50 fold higher miR-141 levels, compared to the healthy individuals.

Virus infection and prostate cancer

Among the various viruses, herpes virus is one of the viruses most commonly related to carcinogenesis. Several epidemiological studies evaluated the association between herpes virus infection and prostate cancer risk, although results were inconsistent. Herpes virus plays an important role in the pathogenesis of cancer via the inhibition of cell apoptosis and stimulation of DNA synthesis, which may ultimately lead to PC. Previous meta-analysis indicated that infection by herpes simplex virus type 2 (HSV-2) or human herpesvirus 8 (HHV-8) may be associated with a higher prostate cancer risk. However, there has not been a study to elucidate the potential mechanism of HSV-2 infection

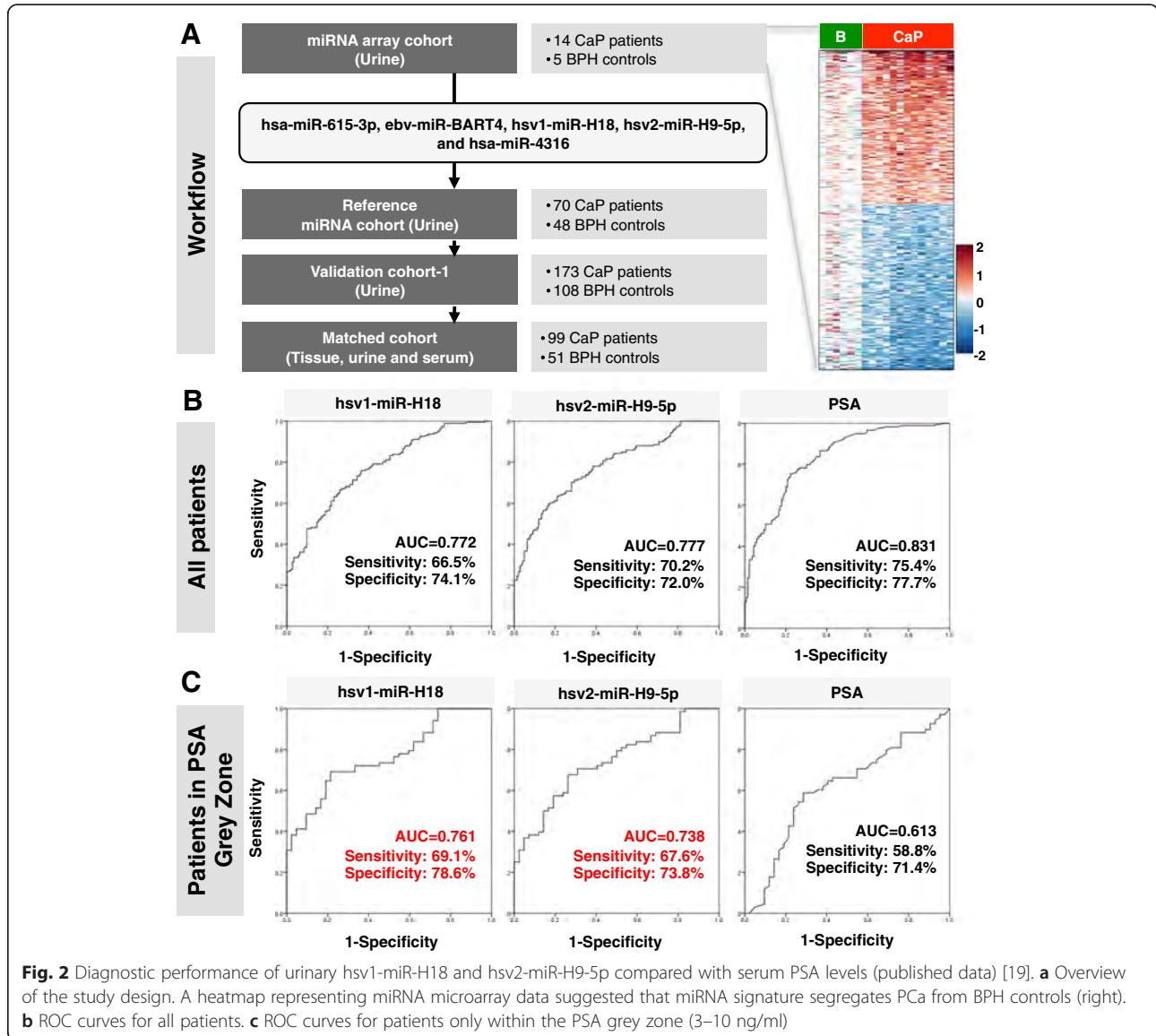
underlying viral PC carcinogenesis. A potential link between HPV infection and PCa risk was attempted to study the causal role of HPV-16 in prostate carcinogenesis. A significant increase of PCa risk related with HPV-16 infection was observed. However, this is still contradictory since other epidemiological studies could not find same association [23–25]. Therefore, an elaborate and comprehensive demonstration of the association between herpes virus infection and prostate cancer risk is of significance [24]. Further investigations and large-sample studies are required to and the relationship between herpes virus infection and prostate cancer risk.

Our recent findings demonstrated the overexpression of herpes virus-encoded miRNAs in urine samples from prostate cancer patients, compared to those of control subjects [19]. Interestingly, hsv1-miR-H18 and hsv2-miR-H9-5p detected in urine samples showed better diagnostic performance than tPSA levels in patients within the PSA grey zone. A recent meta-analysis showed that HSV infection is associated with an increased PCa risk, however, it remains puzzling how these two particular vir-miRNAs contribute to PCa. To better understand the biological contribution of hsv1-miR-H18 and hsv2-miR-H9-5p to PCa, the geographic distribution, gender difference and socioeconomic variation of virus infection and their possible impact on prostate cancer should be considered to investigate (Fig. 2).

Viral miRNAs circulating through biofluids

Viruses also encode their own sets of miRNAs, which they use to control the expression of either the host's genes and/or their own. In the past few years' evidence of the presence of cellular miRNAs in extracellular human body fluids such as serum, plasma, saliva, and urine has been accumulated [26, 27]. Furthermore, it has been also demonstrated that miRNAs secreted by virus-infected cells are transferred to and act in uninfected recipient cells [19].

The first viral-encoded miRNAs was found in cells infected with EBV [27, 28]. The majority of natural viruses found to encode miRNAs. In DNA viruses (such as herpes virus, polyomavirus, ascovirus, baculovirus, iridovirus, and adenovirus families), a DNA component to replication cycle can exploit the initiating host miRNA biogenesis machinery in the nucleus, where they replicate and cause long-term persistent infections. Among DNA viruses, which account for the majority of known virus-encoded miRNAs, 95 % of viral miRNAs known today are of herpes virus origin. However, little has been identified about the role of circulating miRNAs from the virus-infected cells.



Extracellular vesicles and their biological role of EV in prostate cancer

Cells can release different types of vesicles, which have been difficult to categorize in a definitive manner. The transmission of vesicles from cancer cells to other cell types has been the subject of intensive studies in recent years. It is a process that can make it possible a sophisticated form of cellular communication through the delivery of highly complex and dynamic cargo. As a delivery vehicle between cells, extracellular vesicles (EV) have been considered as a molecular cargo mediating a communication between cells in the microenvironment. Although EV were originally considered to be a means for exclusion of garbage molecules from cells, it is now clear that EV alter signaling pathways and have a biological influence in neighboring cells [29].

Also, since EV have the bioactivity of their molecular cargo and can be readily isolated from multiple biological fluids (e.g., urine, serum, plasma, pleural effusion, saliva), EV has been considered as a non-invasive biomarker candidate [30–32].

There are multiple types of EV, the small sealed membrane vesicles that are produced from cells differing in size, biology, contents, and secretory mechanisms. Exosomes and microparticles (MPs) are two distinct groups of EV. Exosomes are originated from the inward budding of the limiting membrane of multivesicular bodies (MVBs), while MPs are in bigger size vesicles formed by the outward membrane budding. Vesicles that are produced from cells during cell death are apoptotic bodies.

It is known that PCa patients had higher levels of urinary exosomes than the healthy donors. The membranes

of exosomes are resistant to the osmolytic and proteolytic activity of urine, indicating that exosomes are quite stable in urine. PC cell-derived EV can deliver various genetic factors such as nucleic acids, including DNA, mRNA, miRNA, and small non-coding RNAs, as well as oncoproteins and metabolites, leading to the horizontal transfer of oncogenic information to neighboring immune cells, vessel cells, or cancer cells [33, 34]. EV-mediated RNA transfer provides benefits as a communication [35–37]. However, little is known how EV-mediated transfer of these molecules enters into recipient cells, and how specific miRNA species can be sorted into EV. Our series of publications in this field suggest that EV shedding can influence on microenvironment of PCa by modulating immune cell proliferation and activation [38].

EV influence immune response in prostate cancer

Role of immune response caused/mediated by miRNA was suggested by a series of studies showing that EV-derived miRNAs participate in the regulation of inflammatory responses. A recent report from our group demonstrated that EV derived from amoeboid phenotype of prostate cell may influence the immune response of the tumor microenvironment. A tritiated thymidine (^3H -thymidine) incorporation assay revealed that EV contain miRNAs (e.g., miR-125a), which are transferred to tumor microenvironment leading to proliferative inhibition of immune cells. Other interesting findings suggest immune response may be mediated by miRNAs regulating Toll-like receptors (TLRs), which play an important role in immune response and inflammation including tissue repair and tissue injury-induced inflammation. In PCa cell lines, several miRNAs (e.g., has-miR-29b, -29c, -148b, and -152) were upregulated by TLR3 activation, leading to antitumoral effects on PCa. EV derived from dendritic cells contain miR-155 (a promoter of inflammatory responses) and miR-146a (a mediator of immune suppression), which are known as important players to regulate inflammation, alter the gene expression of inflammation related targets and reprogram the response to endotoxin [39, 40].

EV released from virus-infected cells

In virology field, biology of extracellular vesicles are well understood compared to cancer mainly because virus should be enveloped to be released from infected host. The accumulating evidence suggests that viruses, such as retroviruses, hepatitis C virus, herpes simplex virus, Epstein-Barr virus, Coxsackie virus B3 (CVB3), utilize the cellular vesiculation pathway for budding and assembly, immune evasion, and intercellular communication. It is also well known that many virally infected cells secrete vesicles (most of cases, exosomes) containing various viral proteins and genetic materials such as RNAs. Studies on herpes simplex virus-infected cells demonstrated that

virus communicate via vesicles. In the case of Epstein-Barr virus, recent reports suggested that herpes virus utilizes exosomes, one kind of extracellular vesicles, as a mechanism of cell-to-cell communication and transfers signaling competent proteins and functional miRNAs to uninfected neighbor cells. For example, exosomes released from infected cells have been shown to contain co-receptors for HIV, which can enhance virus entry into cells. Proteins in the secreted exosomes from virus-infected cells can induce apoptosis in CD4 T cells, and contribute innate immune response.

EV as cargoes to deliver viral miRNAs

EV-mediated communication would allow the virus to respond to the cellular microenvironment. Virus-infected cells continuously shed and transfer EV to uninfected neighboring cells. Throughout EV shedding and secretion to extracellular space, the virus-encoded miRNAs were delivered to other cells, leading to alteration of miRNA-mediated gene repression and intercellular communication. Thus, the presence of viral-encoded miRNAs in EV suggests that virus-infected cells perturb gene expression in the surrounding tissue, resulting in destruction of the immune system. Exosomes secreted from HIV-infected alveolar macrophages have been identified to carry viral miRNA (vir-miRNA) such as vmiR88, vmiR99, and vmiR-TAR. It has not been clearly identified how vir-miRNA composition is decided and recruited to EV. Vir-miRNAs might have a role in cancer initiation by blocking of major tumor suppressors (e.g., p53) or acceleration of cancer development by evading cellular immune response (e.g., mi17-92).

These findings still raise a number of exciting questions. Does virus-infected prostate cells secrete miRNAs using EV as a cargo? What are the target genes of the abundantly secreted viral miRNAs? Are extracellular vesicles shed only in the absence of viral replication? Is there any evidence for functional miRNA delivery in vivo? If so, what's the biological mechanism? In addition, the detail mechanism is currently lacking whether virus infection promotes miRNAs sorting into EV, or whether this secretion is a selective and specific process.

Conclusions

In PCa biomarker development, the greatest unmet need remains: a biomarker that stratifies men at risk of aggressive PCa or a biomarker that identify the early stage of patients who need active surveillance, eventually leading to a reduction of unnecessary interventions. Although miRNAs might have many useful clinical applications for patients with PCa, many additional studies are warranted to clarify their function and regulation during tumorigenesis and tumor progression. The

studies to determine the role of circulating miRNAs during PCa progression would have the potential that PCa patients can be molecularly stratified based on their miRNAs profile in urine samples. In addition, the studies could uncover important clues about underlying disease mechanisms.

Urine analyses have great potential to be adapted in clinical practice, based on its non-invasiveness. Identification of non-invasive clinical indicators of PCa would be one of the most important advances achievable in this field. Our current mechanistic understanding of shedding vesicle biology and function, especially in the context of virus infection and communication with host, is not mature enough. Identification of potential candidates of the circulating miRNAs signature in patient urine samples would have significant implications for an alternative and/or supportive diagnostic tool for PCa.

Unnecessary diagnostic procedures would be minimized for patients with early stage of PCa, contributing to the easier diagnostic assessment and to the reducing associated public health and economic burden to patients. In addition, the studies to understand role and biology of the circulating miRNAs have significant clinical relevance to public health since it will improve accuracy of predicting patient survival, identifying responsiveness candidates of PCa patients. Furthermore, we envision that this study will also provide the mechanistic data to address the long-term goal of the PCa field identifying new treatments tailoring more specific and effective therapies for PCa, thus it holds great promise for the treatment of high risk PCa patients.

Abbreviations

PCa: Prostate cancer; CRPC: Castration-resistant metastatic disease; PSA: Prostate-specific antigen; DRE: Digital rectal examination; miRNAs: MicroRNAs; EMT: Mesenchymal transition; MET: Mesenchymal to epithelial transition; AR: Androgen receptor; HSV-2: Herpes simplex virus type 2; HHV-8: Human herpesvirus 8; EV: Extracellular vesicles; MPs: Microparticles; MVBs: Multivesicular bodies; CVB3: Coxsackie virus B3.

Competing interests

The authors have stated that they have no conflicts of interest.

Authors' contributions

JK, SY and WK participated in the design of the study and performed the analysis of references. JK and WK supervised study design and led obtaining funding. JK drafted the manuscript, and SY and WK participated critical revision of the manuscript. All authors read and approved the final manuscript.

Acknowledgements

This work was supported by the National Research Foundation of Korea (NRF) grant funded by the Korea government (MSIP) (No. NRF-2014R1A2A1A09006983), the Ministry of Education, Science and Technology (2012R1A1A4A01008753 and 2013R1A1A2004740) (to W-J.K.), NIH grants 1R01DK100974-01, [DoD W81XWH-15-1-0415](#), U24 DK097154, NIH NCATS UCLA CTSI UL1TR000124, IMAGINE NO IC Research Grant, the Steven Spielberg Discovery Fund in Prostate Cancer Research Career Development Award, Interstitial Cystitis Association (ICA) Pilot Grant, and a Fishbein Family IC Research Grant by ICA, New York Academy of Medicine; Boston Children's Hospital Faculty Development (to J.K.).

Author details

¹Departments of Surgery and Biomedical Sciences, Cedars-Sinai Medical Center, 8700 Beverly Blvd., Davis Room 5071, Los Angeles, CA 90048, USA.

²Departments of Medicine, University of California, Los Angeles, CA, USA.

³Department of Surgery, Harvard Medical School, Boston, MA, USA.

⁴Department of Urology, Chungbuk National University College of Medicine, 62 Kaeshin-dong, Heungduk-gu, Cheongju 361-763, Republic of Korea.

Received: 4 August 2015 Accepted: 18 November 2015

Published online: 26 November 2015

References

- Attard G, Parker C, Eeles RA, Schroder F, Tomlins SA, Tannock I, et al. Prostate cancer. *Lancet*. 2015.
- Behesnilian AS, Reiter RE. Risk stratification of prostate cancer in the modern era. *Curr Opin Urol*. 2015;25(3):246–51.
- Siegel RL, Miller KD, Jemal A. Cancer statistics, 2015. *CA Cancer J Clin*. 2015;65(1):5–29.
- Hoy SM. Abiraterone acetate: a review of its use in patients with metastatic castration-resistant prostate cancer. *Drugs*. 2013;73(18):2077–91.
- McGann S, Horton ER. Radium-223 dichloride: a novel treatment option for castration-resistant prostate cancer patients with symptomatic bone metastases. *Ann Pharmacother*. 2015;49(4):469–76.
- Mukherji D, Omlin A, Pezaro C, Shamseddine A, de Bono J. Metastatic castration-resistant prostate cancer (CRPC): preclinical and clinical evidence for the sequential use of novel therapeutics. *Cancer Metastasis Rev*. 2014;33(2–3):555–66.
- Vuong W, Sartor O, Pal SK. Radium-223 in metastatic castration resistant prostate cancer. *Asian J Androl*. 2014;16(3):348–53.
- Zustovich F, Fabiani F. Therapeutic opportunities for castration-resistant prostate cancer patients with bone metastases. *Crit Rev Oncol Hematol*. 2014;91(2):197–209.
- Smith RA, Manassaram-Baptiste D, Brooks D, Doroshenko M, Fedewa S, Saslow D, et al. Cancer screening in the United States, 2015: a review of current American cancer society guidelines and current issues in cancer screening. *CA Cancer J Clin*. 2015;65(1):30–54.
- Trock BJ. Circulating biomarkers for discriminating indolent from aggressive disease in prostate cancer active surveillance. *Curr Opin Urol*. 2014;24(3):293–302.
- Birnbaum JK, Feng Z, Gulati R, Fan J, Lotan Y, Wei JT, et al. Projecting benefits and harms of novel cancer screening biomarkers: a study of PCA3 and prostate cancer. *Cancer Epidemiol Biomarkers Prev*. 2015;24(4):677–82.
- Day JR, Jost M, Reynolds MA, Groskopf J, Rittenhouse H. PCA3: from basic molecular science to the clinical lab. *Cancer Lett*. 2011;301(1):1–6.
- Hessels D, Klein Gunnewiek JM, van Oort I, Karthaus HF, van Leenders GJ, van Balken B, et al. DD3(PCA3)-based molecular urine analysis for the diagnosis of prostate cancer. *Eur Urol*. 2003;44(1):8–15. discussion 15–16.
- Loeb S. Prostate cancer: Predicting prostate biopsy results—PCA3 versus phi. *Nat Rev Urol*. 2015;12(3):130–1.
- Marks LS, Fradet Y, Deras IL, Blase A, Mathis J, Aubin SM, et al. PCA3 molecular urine assay for prostate cancer in men undergoing repeat biopsy. *Urology*. 2007;69(3):532–5.
- Wei JT, Feng Z, Partin AW, Brown E, Thompson I, Sokoll L, et al. Can urinary PCA3 supplement PSA in the early detection of prostate cancer? *J Clin Oncol*. 2014;32(36):4066–72.
- Sidaway P. Prostate cancer: Urinary PCA3 and TMPRSS2:ERG reduce the need for repeat biopsy. *Nat Rev Urol*. 2015.
- Tomlins SA, Day JR, Lonigro RJ, Hovelson DH, Siddiqui J, Kunju LP, et al. Urine TMPRSS2:ERG Plus PCA3 for Individualized Prostate Cancer Risk Assessment. *Eur Urol*. 2015.
- Yun SJ, Jeong P, Kang HW, Kim YH, Kim EA, Yan C, et al. Urinary MicroRNAs of prostate cancer: virus-encoded hsv1-miRH18 and hsv2-miR-H9-5p could be valuable diagnostic markers. *Int Neurourol J*. 2015;19(2):74–84.
- Ayub SG, Kaul D, Ayub T. Microdissecting the role of microRNAs in the pathogenesis of prostate cancer. *Cancer Genet*. 2015.
- Lin XJ, Chong Y, Guo ZW, Xie C, Yang XJ, Zhang Q, et al. A serum microRNA classifier for early detection of hepatocellular carcinoma: a multicentre, retrospective, longitudinal biomarker identification study with a nested case-control study. *Lancet Oncol*. 2015;16(7):804–15.
- Korzeniewski N, Tosev G, Pahernik S, Hadaschik B, Hohenfellner M, Duensing S. Identification of cell-free microRNAs in the urine of patients with prostate cancer. *Urol Oncol*. 2015;33(1):16 e17–22.

23. Heidegger I, Borena W, Pichler R. The Role of Human Papilloma Virus in Urological Malignancies. *Anticancer Res.* 2015;35(5):2513–9.
24. Ge X, Wang X, Shen P. Herpes simplex virus type 2 or human herpesvirus 8 infection and prostate cancer risk: A meta-analysis. *Biomed Rep.* 2013;1(3):433–9.
25. Caini S, Gandini S, Dudas M, Bremer V, Severi E, Gherasim A. Sexually transmitted infections and prostate cancer risk: a systematic review and meta-analysis. *Cancer Epidemiol.* 2014;38(4):329–38.
26. Meckes Jr DG, Shair KH, Marquitz AR, Kung CP, Edwards RH, Raab-Traub N. Human tumor virus utilizes exosomes for intercellular communication. *Proc Natl Acad Sci U S A.* 2010;107(47):20370–5.
27. Qi P, Han JX, Lu YQ, Wang C, Bu FF. Virus-encoded microRNAs: future therapeutic targets? *Cell Mol Immunol.* 2006;3(6):411–9.
28. Qureshi A, Thakur N, Monga I, Thakur A, Kumar M. VIRmiRNA: a comprehensive resource for experimentally validated viral miRNAs and their targets. *Database (Oxford).* 2014;2014.
29. Minciaccchi VR, Freeman MR, Di Vizio D. Extracellular vesicles in cancer: exosomes, microvesicles and the emerging role of large oncosomes. *Semin Cell Dev Biol.* 2015;40:41–51.
30. Hessels D, Schalken JA. Urinary biomarkers for prostate cancer: a review. *Asian J Androl.* 2013;15(3):333–9.
31. Webber J, Yeung V, Clayton A. Extracellular vesicles as modulators of the cancer microenvironment. *Semin Cell Dev Biol.* 2015;40:27–34.
32. Kim J, Morley S, Le M, Bedoret D, Umetsu DT, Di Vizio D, et al. Enhanced shedding of extracellular vesicles from amoeboid prostate cancer cells: potential effects on the tumor microenvironment. *Cancer Biol Ther.* 2014;15(4):409–18.
33. Hessvik NP, Sandvig K, Llorente A. Exosomal miRNAs as Biomarkers for Prostate Cancer. *Front Genet.* 2013;4:36.
34. Greening DW, Gopal SK, Mathias RA, Liu L, Sheng J, Zhu HJ, et al. Emerging roles of exosomes during epithelial-mesenchymal transition and cancer progression. *Semin Cell Dev Biol.* 2015;40:60–71.
35. Tetta C, Ghigo E, Silengo L, Deregibus MC, Camussi G. Extracellular vesicles as an emerging mechanism of cell-to-cell communication. *Endocrine.* 2013;44(1):11–9.
36. Yanez-Mo M, Sijlander PR, Andreu Z, Zavec AB, Borrás FE, Buzas EI, et al. Biological properties of extracellular vesicles and their physiological functions. *Journal of extracellular vesicles.* 2015;4:27066.
37. Yoon YJ, Kim OY, Gho YS. Extracellular vesicles as emerging intercellular comunicasomes. *BMB Rep.* 2014;47(10):531–9.
38. Choi DY, You S, Jung JH, Lee JC, Rho JK, Lee KY, et al. Extracellular vesicles shed from gefitinib-resistant nonsmall cell lung cancer regulate the tumor microenvironment. *Proteomics.* 2014;14(16):1845–56.
39. Alexander M, Hu R, Runtsch MC, Kagele DA, Mosbrugger TL, Tolmachova T, et al. Exosome-delivered microRNAs modulate the inflammatory response to endotoxin. *Nat Commun.* 2015;6:7321.
40. Galli R, Paone A, Fabbri M, Zanesi N, Calore F, Cascione L, et al. Toll-like receptor 3 (TLR3) activation induces microRNA-dependent reexpression of functional RARbeta and tumor regression. *Proc Natl Acad Sci U S A.* 2013;110(24):9812–7.

Submit your next manuscript to BioMed Central
and we will help you at every step:

- We accept pre-submission inquiries
- Our selector tool helps you to find the most relevant journal
- We provide round the clock customer support
- Convenient online submission
- Thorough peer review
- Inclusion in PubMed and all major indexing services
- Maximum visibility for your research

Submit your manuscript at
www.biomedcentral.com/submit



SCIENTIFIC REPORTS



OPEN

Interstitial Cystitis-Associated Urinary Metabolites Identified by Mass-Spectrometry Based Metabolomics Analysis

Received: 22 August 2016
Accepted: 18 November 2016
Published: 15 December 2016

Tobias Kind¹, Eunho Cho², Tae-eun D. Park³, Nan Deng⁴, Zhenqiu Liu⁴, Tack Lee⁵, Oliver Fiehn^{1,6} & Jayoung Kim^{2,4,7,8}

This study on interstitial cystitis (IC) aims to identify a unique urine metabolomic profile associated with IC, which can be defined as an unpleasant sensation including pain and discomfort related to the urinary bladder, without infection or other identifiable causes. Although the burden of IC on the American public is immense in both human and financial terms, there is no clear diagnostic test for IC, but rather it is a disease of exclusion. Very little is known about the clinically useful urinary biomarkers of IC, which are desperately needed. Untargeted comprehensive metabolomic profiling was performed using gas-chromatography/mass-spectrometry to compare urine specimens of IC patients or health donors. The study profiled 200 known and 290 unknown metabolites. The majority of the thirty significantly changed metabolites before false discovery rate correction were unknown compounds. Partial least square discriminant analysis clearly separated IC patients from controls. The high number of unknown compounds hinders useful biological interpretation of such predictive models. Given that urine analyses have great potential to be adapted in clinical practice, research has to be focused on the identification of unknown compounds to uncover important clues about underlying disease mechanisms.

More than 3–8 million women and 1–4 million men are diagnosed with Interstitial Cystitis (IC), also known as Painful Bladder Syndrome, in the US annually¹. IC impacts health-related qualities of life immensely, and in some instances can be more debilitating than end-stage renal disease^{2,3}. In spite of an increase in the number of diagnosed cases, objective diagnostic criteria are not consistently applied in general practice⁴. Some lower urinary tract symptoms, such as overactive bladder (OAB), have symptoms in common with IC, further complicating the diagnosis. Diagnosis of the disease has been dependent on clinical parameters (e.g. pain, urgency, and frequency) due to the lack of proper conventional markers (e.g. PSA for prostate cancer diagnosis)^{3,5}. Diagnostic tests include urinalysis, urine culture, cystoscopy, bladder biopsy and hydrodistention of the bladder. Nonetheless, we still lack definite criteria for the disease. Estimates of the prevalence and natural history of IC still fluctuate widely because of different diagnostic standards, populations evaluated, and challenges inherent in following patients over time⁶. Thus, the identification of sensitive and non-invasive biomarkers has the potential to greatly improve the accuracy of an IC diagnosis. However, our current understanding of mechanisms involving pelvic pain is also unclear and fragmented.

Urinary metabolites represent a signature of a subject's metabolic state and may convey critical information about the pathophysiology of disease. This may be especially true for pelvic disorders because urine is the body fluid most proximal to the urinary tract. Because metabolites vary in size, chemistry and physicochemical properties, a single platform has only a limited capacity to interrogate the entire metabolome in a given body fluid. Use of more than one platform spanning different technologies is the preferred means of performing comprehensive

¹West Coast Metabolomics Center, University of California, Davis, Davis, CA, USA. ²University of California Los Angeles, CA, USA. ³University of California, Berkeley, CA, USA. ⁴Samuel Oschin Comprehensive Cancer Institute, Cedars-Sinai Medical Center, Los Angeles, CA, USA. ⁵Department of Urology, Inha University College of Medicine, Incheon, South Korea. ⁶King Abdulaziz University, Jeddah, Saudi Arabia. ⁷Departments of Surgery and Biomedical Sciences, Cedars-Sinai Medical Center, Los Angeles, CA, USA. ⁸Department of Medicine, University of California Los Angeles, Los Angeles, CA, USA. Correspondence and requests for materials should be addressed to J.K. (email: Jayoung.Kim@cshs.org)

metabolome analyses. Urine excretions represent a snapshot of many metabolic endpoints including those from food, drugs, nutrients and bacterial transformations. This renders urine analysis very challenging due to the complexity, sources and numbers of metabolites.

In this study, we performed gas-chromatography time of flight mass spectrometry (MS)-based metabolomics analysis. Our goal here was to increase coverage of known metabolites that may play a role in IC and to gain new insight into disease mechanisms. Previous global metabolomics profiling of urine from IC patients suggests that a urinary metabolic signature for IC can be detected using platforms such as Nuclear Magnetic Resonance (NMR) and Liquid chromatography–mass spectrometry (LC-MS). The experimental results from this paper suggest that candidate metabolites were found to be associated with IC, and that the IC metabolic signature can be identified in patient urine. Using multiparametric models such partial least squares discriminant analysis IC metabolic signature can stratify patients from control subjects.

Results

Characteristics of the study subjects. A clinical diagnosis of IC was made by two independent urologists, according to NIDDK criteria (e.g. frequency, urgency, bladder pain, discomfort and the presence of glomerulations during cystoscopic hydrodistention), before any treatment or medication was given. Only subjects of >2 month “free of treatment or medication” were included. In total, we enrolled 63 female subjects (42 IC patients and 21 normal controls) with a mean age of 51. Given that most of patients (over 80%) are women, we recruited only female patients for this particular study to seek potential sex-specific urine biomarkers for female IC patients. Population-based, age-matched controls were recruited from one clinic using the same standard operating procedures (SOPs) during the same research period (2010–2013).

GC-TOF MS analysis of urine specimens from IC patients and controls. We investigated the metabolite profile of the individual urine samples using GC-TOF mass spectrometry. Our analysis and data requisition resulted in a total of 490 metabolites detected (200 known and 290 unknown metabolites).

Data were autoscaled and mean-centered. The scores plot for partial least squares (PLS) components showed differentiation of the IC samples from controls with good separation and dispersion (Fig. 1A). We assessed the accuracy of our predictive model using the leave-one-out cross-validation method as well as the randomized permutation (Fig. 1B). The observed statistic of this analysis using MetaboAnalyst 3.0 software¹ was significant at $p = 0.005$, suggesting that the model significantly differentiate patients from healthy controls. A heat map also showed the distinct expression patterns of metabolites between IC and controls (Fig. 1C). These metabolites are responsible for the significant difference between IC and controls with fold change either greater than 1.20 or less than 0.83 and p -value less than 0.1.

Identification of differentially expressed metabolites in urine of IC patients. Given 490 detected metabolites, we investigated 52 differentially expressed metabolites, including both annotated and unannotated metabolites. In the volcano plot (Fig. 2A), annotated metabolites are presented as \log_2 fold change against the $-\log_{10}(p)$ of the differential expression between IC patients and healthy controls. 22 annotated differentially expressed metabolites above the threshold ($FC > 1.20$ or $FC < 0.83$, and $P < 0.1$) are marked and presented. Erythronic acid and histidine, were the most upregulated metabolites in the IC patient group compared to that in control, while tartaric acid were the most downregulated as shown in Fig. 2B and Table 1.

Network modeling derived from IC-associated metabolites. We performed analysis the histidine-associated differential module (subnetwork) using multilevel local graphical model⁷ (Fig. 3). The differential network represents the changes of correlation structure in IC when compared to the background network. Levels of two metabolites, valine and histidine (in red circle), are increased in IC. The interactions (correlations) among metabolites indicate that those metabolites may biologically function together. Generally, the variations of interactions among metabolites under different clinical conditions are associated with IC status. Sparse local graphical model⁸ is used to construct both common and differential metabolite networks simultaneously. Treating each metabolite, in turn, as the response variable and the remaining annotated metabolites as predictors, and running the sparse regression built the network. In such an approach, for each metabolite x_i , the regression model is defined as

$$x_i = X_{-i}\alpha_i + yX_{-i}\beta_i + \varepsilon_i,$$

where X_{-i} are the metabolite expression values except for metabolite x_i , and y (1/0) represents IC (1) or control (0). The common and differential networks are formed by collecting all of the α_i s and β_i s, respectively. Parameters (α_i) determine the direct correlations between metabolite x_i and the remaining metabolites, and $\alpha_{ij} \neq 0$ indicate there is a partial correlation (edge) between metabolites x_i and x_j , giving the remaining metabolites. Moreover, β_i measure y dependent associations and differential correlations across different clinical condition. Parameter $\beta_{ij} \neq 0$ indicates that there is a differential interaction between metabolites x_i and x_j in IC and control.

Cytoscape (www.cytoscape.org/) was used for differential network visualization and subnetwork identification. The proposed approach identified the IC associated differential network efficiently (Fig. 3). For further understanding on our metabolite signature, software MetaboAnalyst was used for functional enrichment analysis. Metabolite enrichment analysis allows us to study the corresponding biological pathways of IC with metabolites on the differential network. We performed Metabolite Set Enrichment Analysis (MSEA) with the 18 metabolites, which were derived from data in Fig. 3. We found that those 18 metabolites are highly enriched in Protein Biosynthesis and Ammonia Recycling with the FDR of 0.0000136 and 0.00557, respectively (Fig. 4).

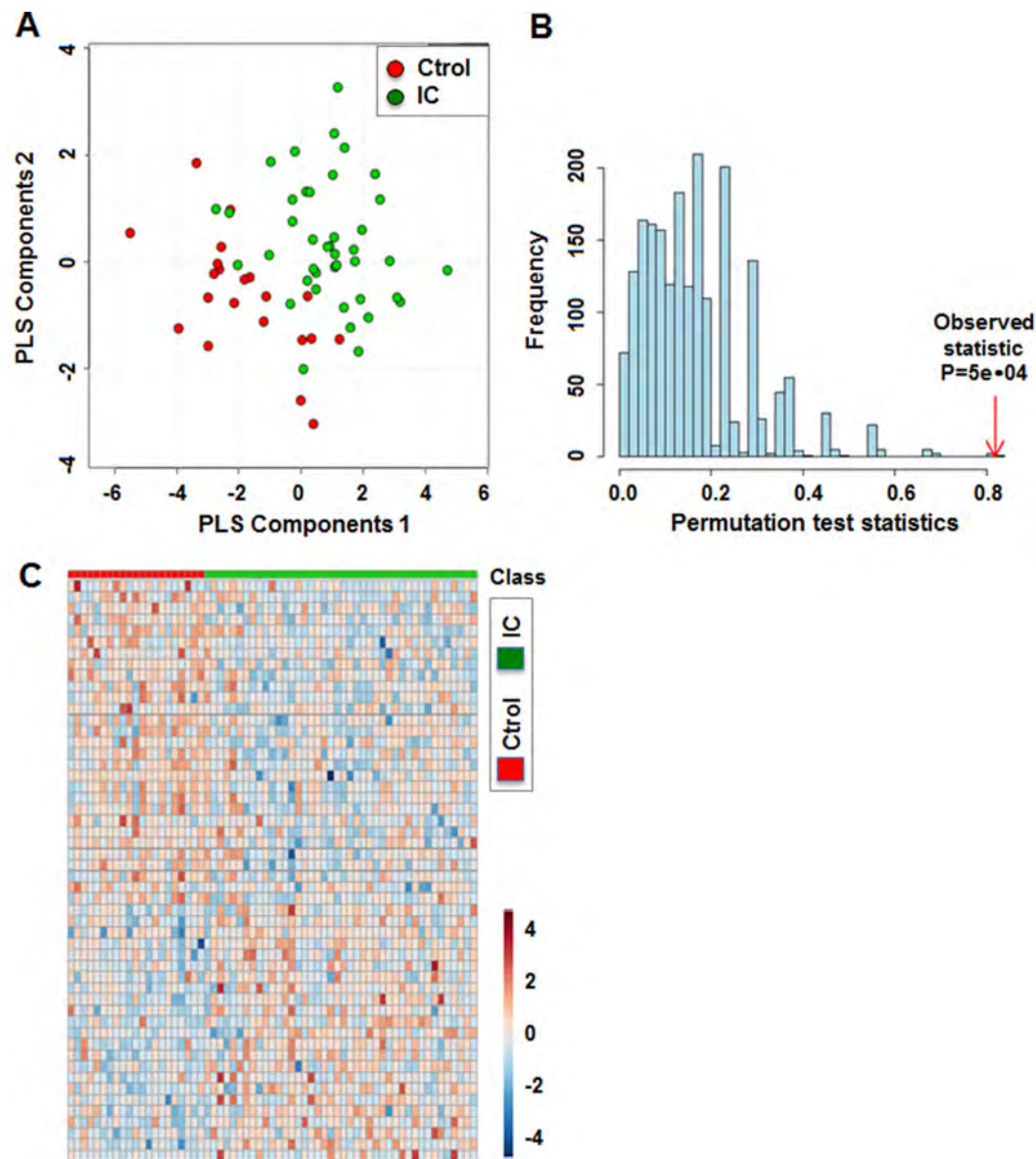


Figure 1. Differentiation of IC patients and healthy control groups using multivariate analysis. (A) Partial least square-discriminant analysis (PLS-DA) score plot of the IC and control groups. PLS-DA plot showed a clear separation of metabolites between patients and matched control subjects. Red: control samples; Green: IC patient samples. The model was established using three principal components. (B) For model evaluation, the class prediction results based on cross model validation predictions of the original labeling compared to the permuted data assessed using the separation distance. Histogram shows distribution of separation distance based on permuted data. Red arrow indicates observed statistic ($P = 5e-04$). (C) A heatmap of 52 differentially expressed metabolites in IC and control groups. Among 490 detected metabolites in total, 52 metabolites, including both annotated and unannotated metabolites, were significantly altered in IC patients compared to controls ($FC > 1.20$ or $FC < 0.83$ and $P < 0.1$).

Discussion

In this study we profiled 490 metabolites in human urine specimens for IC diagnosis using GC-TOF MS. Metabolites including histidine, erythronic acid, and tartaric acid were found to have the highest fold-changes. Power analysis and false discovery rate correction (FDR, Benjamini-Hochberg) suggests that the study sample size has to be increased to validate any findings. The present report has provided evidence that metabolic fingerprints can predict IC patients using multiparametric models such as PLS-DA, however it remains to be determined whether these metabolites might have biological and mechanistic meanings. Especially the large number of unknown compounds is challenging (59% in this study), because without structural annotation, unknown metabolites can only be partly assigned to larger biochemical modules through mass spectral similarity analysis. Some unknowns may even ultimately prove to be chemical contaminants and should be excluded from multiparametric models. One solution to increase mass spectral library coverage is to use quantum chemical simulations

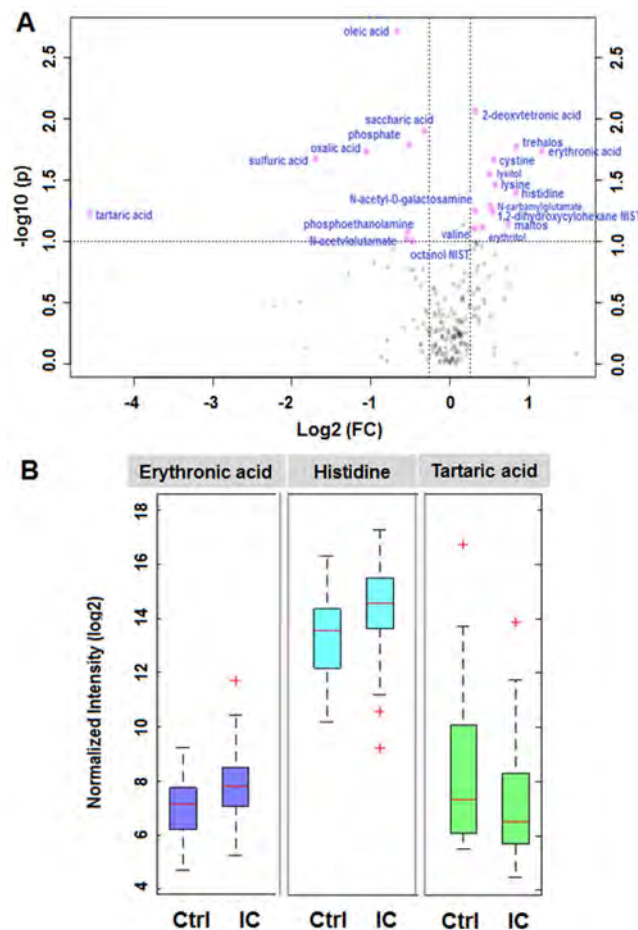


Figure 2. A volcano plot showing differentially expressed metabolites in IC patients. (A) 22 annotated metabolites were significantly altered in IC patients compared to controls ($FC > 1.20$ or $FC < 0.83$ and $P < 0.1$). The red dots represent metabolites above the threshold. The further the metabolite's position away from the (0, 0), the more significant the metabolite is. (B) A boxplot showing up-regulated and down-regulated metabolites that could be used to differentiate IC patients from normal subjects. The candidate metabolites, erythronic acid and histidine, were significantly increased in IC patients compared to that in controls, while tartaric acid was significantly decreased. All metabolites show statistical significance with p -value < 0.1 .

predict electron ionization mass spectra⁹ or to utilize novel machine learning methods to improve compound identification¹⁰. This can also include novel metabolic compounds that can be expected to exist from known metabolic transformations¹¹.

Histidine, one of essential amino acids in humans, is a known precursor of the neurotransmitter histamine. Increased histidine level leads to increase of histamine level in blood, brain and possibly bladder, suggesting the possibility that histidine may have many other possible functions affecting human bladder sensory system. Previous work using IC rat model demonstrated that overexpression of monocyte chemo-attractant protein-1 (MCP-1) in bladder tissues contributes histamine production and IC¹². More recently, findings from animal model suggest that mast cell-derived histamine mediates IC-associated pain. Authors showed that histamine receptors 1 and 2 modulate pelvic pain and antihistamines attenuate bladder pain in their animal model. We believe the simplest explanation for this finding is that an increased secretion of histamine and histidine (precursor of histamine) may be associated with IC symptoms mediated by mast cells infiltrated in bladder. Other candidate metabolites from our study are summarized in Table 1.

Previous studies have suggested a series of IC biomarker candidates, including antiproliferative factor¹³, phenylacetylglutamine¹⁴, interleukin-6, histamines¹⁵, nerve growth factor *et al.* Our laboratory also found tyramine and 2-oxoglutarate as urinary biomarkers for IC diagnosis¹⁶. More recently, the Multidisciplinary Approach to the Study of Chronic Pelvic Pain (MAPP) Research Network identified Etio-S (etiocholan-3 α -ol-17-one sulfate) to discriminate IC patients from healthy controls¹⁷. This urinary sulfometabolome profiling study was performed using Liquid Chromatography–Mass Spectrometry (LC–MS) in female subjects who had high symptom scores as well as high pelvic pain/pressure/discomfort scores.

Metabolic fingerprints shown in a heatmap (Fig. 1C) consist of 22 annotated metabolites among 52 metabolites shown in a heatmap (Fig. 1C) including histidine, valine, tartaric acid, and erythronic acid *et al.* These

Num	Name	Fold-change	p-value	FDR
1	Unknown BB_31554	2.56	0.000132	0.064576
2	Unknown BB_34163	0.55	0.000514	0.12586
3	oleic acid	0.63	0.001933	0.315675
4	2-deoxytetronic acid	1.26	0.008732	0.571396
5	Unknown BB_17651	0.66	0.009136	0.571396
6	saccharic acid	0.80	0.012642	0.571396
7	Unknown BB_17140	1.44	0.015588	0.571396
8	phosphate	0.70	0.016252	0.571396
9	trehalose	1.79	0.017026	0.571396
10	Unknown BB_5900	0.81	0.017487	0.571396
11	erythronic acid	2.25	0.018393	0.571396
12	Unknown BB_109809	0.56	0.018576	0.571396
13	oxalic acid	0.48	0.018665	0.571396
14	Unknown BB_34027	0.44	0.019904	0.571396
15	Unknown BB_1704	0.63	0.020865	0.571396
16	sulfuric acid	0.31	0.021197	0.571396
17	Unknown BB_23635	0.69	0.02138	0.571396
18	cystine	1.47	0.021607	0.571396
19	Unknown BB_3029	0.70	0.022156	0.571396
20	Unknown BB_12330	2.19	0.02596	0.614149
21	Unknown BB_31549	0.37	0.026702	0.614149
22	lyxitol	1.42	0.028288	0.614149
23	Unknown BB_31756	1.74	0.028827	0.614149
24	lysine	1.49	0.034624	0.706901
25	histidine	1.79	0.040576	0.743323
26	Unknown BB_31359	0.81	0.043988	0.743323
27	Unknown BB_5121	0.64	0.045462	0.743323
28	Unknown BB_100869	1.58	0.046685	0.743323
29	Unknown BB_3294	1.37	0.046907	0.743323
30	Unknown BB_31764	1.33	0.048566	0.743323

Table 1. A list of metabolites differentially expressed in IC, compared to controls (p-level = 0.005, FDR (Benjamini Hochberg)).

metabolites are listed in Table 1. This metabolic fingerprint might be applicable to segregate IC patients from healthy controls in the clinical setting, although it is out of scope of this study.

Urine analysis is certainly challenging due to its high biological variance, because urine is a sink for all water soluble metabolites coming from food sources, the microbiome, drugs, chemicals and generally the exposome. However urine can be collected non-invasively, across all age ranges and in large quantities compared to blood, it is also an excellent matrix for personalized clinical profiles.

For robust statistical analysis many confounding factors such as age, race, geographical location or food intake have to be considered. Subject meta-data may be collected through questionnaires at time of sample collection in the clinic, but it can also be assessed through thorough chemical profiling analyses, called exposome screening (e.g. for pharmaceutical agents or food biomarkers). For example the compound 2-furoylglycine can be used to diagnose fatty acid beta-oxidation disorders, but is also found in food prepared by strong heating (<http://www.hmdb.ca/metabolites/HMDB00439>). Cotinine is a known marker for exposure to cigarette smoke, and other metabolites are known food markers such as caffeine and theobromine for coffee consumption. Such markers can be easily collected along with metabolomic analyses and could be used to stratify patient cohorts or to adjust for exposure parameters during data analysis.

Urine metabolite levels are currently collected from published reports¹⁸. However individual urinary metabolite levels are currently not collected in large databases. Therefore it is difficult to determine minimum, mean, maximum levels of specific metabolites or to perform correlations to dietary intake, which would affect the validity of certain biomarkers. Here efforts have to be undertaken to collect such profiles, similar to personalized efforts that will sequence individual humans or collect individual metabolic profiles from blood.

In summary, our GC-TOF MS analysis suggested a number of metabolite candidates associated with IC. Large cohorts have to be utilized to validate predictive biomarkers or models. This method may provide novel opportunities for better diagnosis and clinical management of IC, particularly in a non-invasive manner. A major clinical challenge remains the early diagnosis of IC. Given that these current findings from this study, although it is out of scope of this study, however we will aim to test whether abnormal metabolism is a key hallmark of IC as a next step. Our metabolic biomarker panel provides the prospect for assisting predictive factor to determine severity of urinary symptoms and pain/discomfort of IC patients.

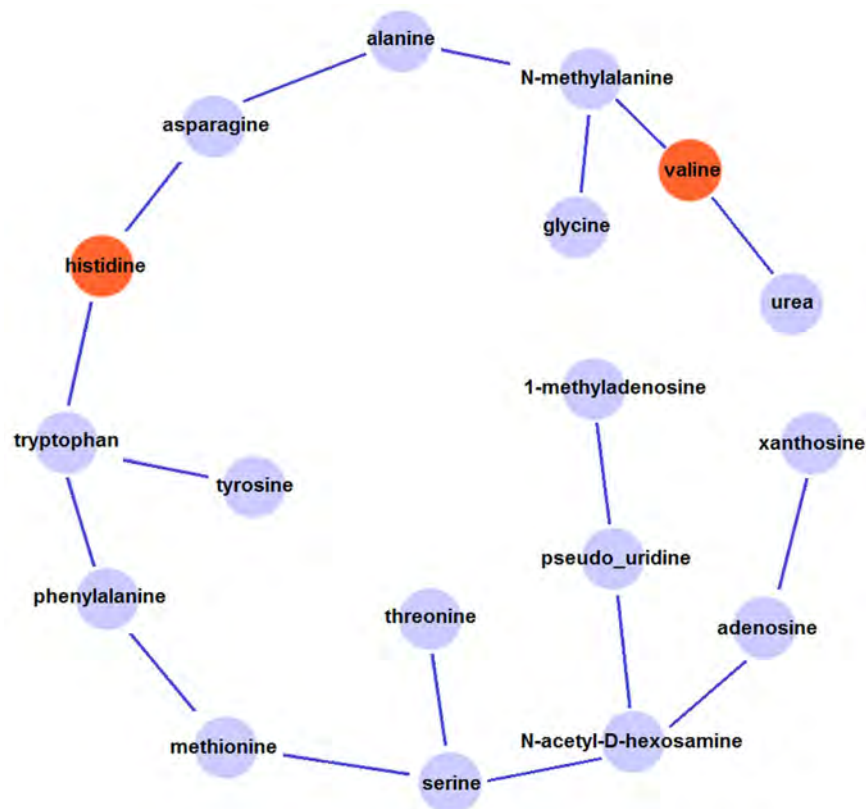


Figure 3. Network modeling derived from IC-associated metabolites. Histidine associated differential module (subnetwork) is shown, where the red nodes indicate upregulated metabolites and light blue nodes represents non-differentiated metabolites.

Materials and Methods

Ethics statement. The Ethics Committee of Inha University Hospital in South Korea approved this study. The Institutional Review Board of Inha University Hospital approved collection, curation and analysis of all samples. All subjects participated in this study provided written informed consent, and all experiments were performed in accordance with relevant guidelines and regulations.

Subjects and urine specimen collection. IC patients and healthy control subjects were diagnosed and recruited from an outpatient urology clinic at Inha University Hospital. Work-up included symptom assessment, cystoscopic evaluation, physical examination, urodynamics, and/or urine culture. Patients with a history of other diseases (such as any types of cancer, inflammation, or diabetes, etc.) were excluded. All subjects were of Asian female descent resident in South Korea. To avoid possible contamination with vaginal or urethral cells, first morning urine specimens were obtained using clean catch methods in a sterile environment. The de-identified specimens were sent to clinical laboratory and were centrifuged to remove cell debris. Supernatants were processed into individual aliquots of 1 ml/tube, before storage at -80°C until further analysis.

GC TOF-MS analysis of urine. The gas-chromatography/mass-spectrometry (GC-MS) analysis was performed^{19,20}. Normally, 10 μl of urine are dissolved in 1 ml -20°C cooled acetonitrile, isopropanol and water (3:3:2 v/v) mixture at pH 7. In this case the urine volume was adjusted between 2 and 10 μl to externally measured creatinine levels using a linear calibration curve. Then the solution was vortexed at 4°C for 5 minutes in 1.5 ml Eppendorf tubes. Samples were centrifuged for 2 min at 14,000 rcf and 500 μl were aliquoted. The aliquot was the evaporated in a Labconco Centrivap cold trap to complete dryness. The methoximation step was performed with 10 μl of a solution of 40 mg/ml O-methylhydroxylamine hydrochloride (CAS: [593-56-6]; Formula $\text{CH}_5\text{NO} \cdot \text{HCl}$) and 90 minutes shaking at 30°C . Then 90 μl of N-methyl-N-trimethylsilyltrifluoroacetamide (MSTFA) was added and shaken at 37°C for 30 min. Then a mix of 1 μl fatty acid methyl esters (FAME) retention time markers was added. The mixture was transferred to amber crimp autosampler vials. Measurements were performed on a Leco Pegasus IV TOF coupled to an Agilent 6890GC with Agilent 6890 split/splitless injector. The column was a Restek RTX-5Sil MS (95% dimethyl/5% diphenyl polysiloxane) with 30 m length, 0.25 mm i.d. and 0.25 μm film thickness with 10 m guard column. Injection volume was 1 μl at 250°C . The GC parameters were set to 1 ml/min constant flow Helium and an oven ramp of 50°C (1 min hold) to 330°C at $20^{\circ}\text{C}/\text{min}$, 5 min hold before cool-down. The transfer line temperature was 280°C and spectra were recorded in electron ionization mode at 70 eV with a filament temperature of 250°C TOF and scan range of 85–500 u. All the raw data was deposited to the Metabolomics Workbench repository under study ID ST000381.

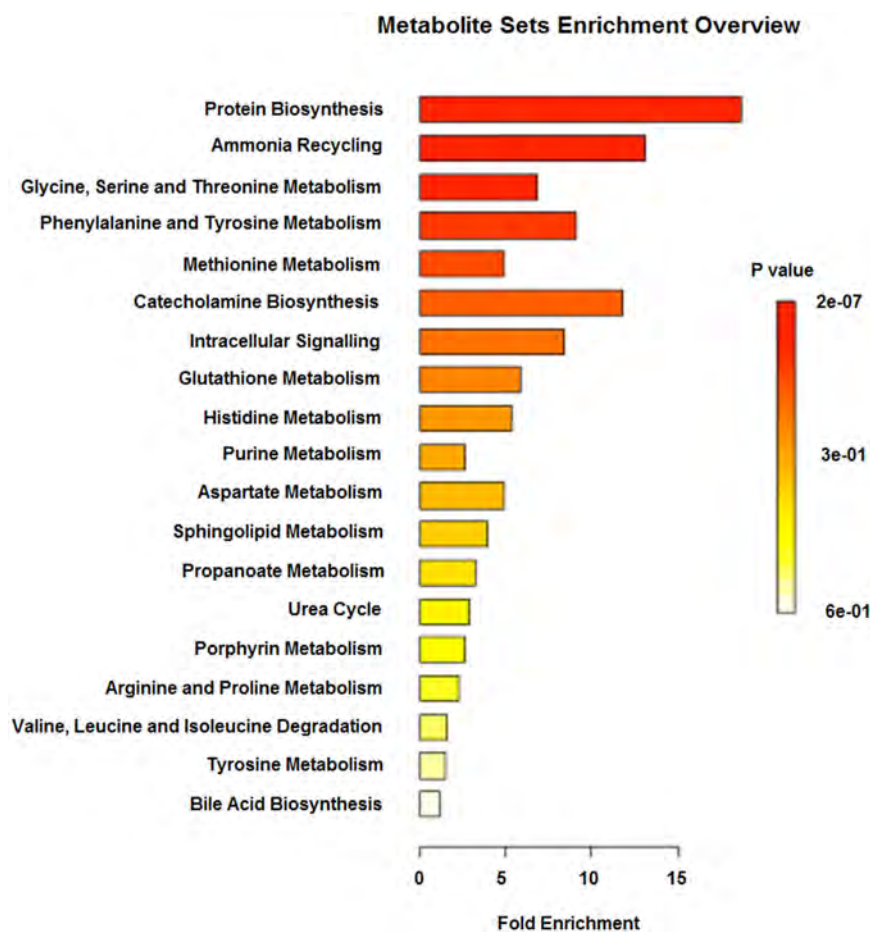


Figure 4. Differential network in IC is identified with multilevel local graphical model⁷. The differential network represents the changes of correlation structure in IC when compared to the background network. Two metabolites (in red) are also upregulated in IC. The interactions (correlations) among metabolites indicate those metabolites may function together biologically. Metabolite Set Enrichment Analysis (MESA) with the 18 metabolites shows that those metabolites are highly enriched in Protein Biosynthesis and Ammonia Recycling with the FDR of 0.0000136 and 0.00557, respectively. The following is the result of MSEA.

Annotation and ID of compounds. The peak and compounds detection or deconvolution was performed with the Leco ChromaTOF software. Spectra were matched against the FiehnLib mass spectral and retention index library²⁰. Post-curation and peak replacements were performed with the in-house developed BinBase software and the sample matrix with all known and unknown compounds exported to a Microsoft EXCEL sheet. A total of 490 compounds were detected. 200 compounds were annotated as known compounds by retention index and mass spectral matching and 290 compounds remain unknown.

Data processing. We excluded one subject from the IC patient group and three subjects from controls because their spectra were outliers based on PCA analysis. To identify potential metabolites as marker candidates that can discriminate IC patients from healthy subjects, we applied the following steps. Data was normalized and the t-test was applied on the log₂ of the processed data. The Student's t-test was performed to extract significant metabolites from the normalized GC-MS data. 30 metabolites had levels of *p*-value threshold <0.05. Twelve of these were known metabolites, the remainder unknown metabolites. After false positive correction (FDR) using Benjamini–Hochberg procedure none of the *p*-values remained significant on the chosen level of 0.05.

The volcano plot shows the fold change and the significance of each annotated metabolite. The significant metabolites were selected by volcano plot with fold change threshold >1.20 (or <0.83) and t-tests *p*-value threshold <0.1. Second, the resultant profiles, which contain profiles of 22 annotated differentially expressed metabolites, were imported into MetaboAnalyst version 3.0¹. Log transformation and mean-centered with auto scaling were performed prior to multivariate statistical analysis. Partial least square discriminant analysis (PLS-DA) was performed, and model evaluation with permutation strategy was carried out according to a published protocol²¹.

References

- Berry, S. H. *et al.* Prevalence of symptoms of bladder pain syndrome/interstitial cystitis among adult females in the United States. *The Journal of urology* **186**, 540–544, doi: 10.1016/j.juro.2011.03.132 (2011).
- Hanno, P. M. *et al.* AUA guideline for the diagnosis and treatment of interstitial cystitis/bladder pain syndrome. *The Journal of urology* **185**, 2162–2170, doi: 10.1016/j.juro.2011.03.064 (2011).
- Winters, J. C. *et al.* Urodynamic studies in adults: AUA/SUFU guideline. *The Journal of urology* **188**, 2464–2472, doi: 10.1016/j.juro.2012.09.081 (2012).
- Hanno, P., Keay, S., Moldwin, R. & Van Ophoven, A. International Consultation on IC - Rome, September 2004/Forging an International Consensus: progress in painful bladder syndrome/interstitial cystitis. Report and abstracts. *International urogynecology journal and pelvic floor dysfunction* **16** Suppl 1, S2–S34, doi: 10.1007/s00192-005-1301-x (2005).
- Clemens, J. Q. *et al.* Validation of a modified National Institutes of Health chronic prostatitis symptom index to assess genitourinary pain in both men and women. *Urology* **74**, 983–987, quiz 987 e981–983, doi: 10.1016/j.urology.2009.06.078 (2009).
- Stephens-Shields, A. J. *et al.* Symptom Variability and Early Symptom Regression in the MAPP Study: A Prospective Study of Urological Chronic Pelvic Pain Syndrome. *The Journal of urology* **196**, 1450–1455, doi: 10.1016/j.juro.2016.04.070 (2016).
- Liu, Z. *et al.* Suboptimal cytoreduction in ovarian carcinoma is associated with molecular pathways characteristic of increased stromal activation. *Gynecologic oncology* **139**, 394–400, doi: 10.1016/j.ygyno.2015.08.026 (2015).
- Liu, Z., Sun, F., Braun, J., McGovern, D. P. & Piantadosi, S. Multilevel regularized regression for simultaneous taxa selection and network construction with metagenomic count data. *Bioinformatics* **31**, 1067–1074, doi: 10.1093/bioinformatics/btu778 (2015).
- Grimme, S. Towards first principles calculation of electron impact mass spectra of molecules. *Angewandte Chemie* **52**, 6306–6312, doi: 10.1002/anie.201300158 (2013).
- Allen, F., Pon, A., Greiner, R. & Wishart, D. Computational Prediction of Electron Ionization Mass Spectra to Assist in GC/MS Compound Identification. *Analytical chemistry* **88**, 7689–7697, doi: 10.1021/acs.analchem.6b01622 (2016).
- Jeffryes, J. G. *et al.* MINEs: open access databases of computationally predicted enzyme promiscuity products for untargeted metabolomics. *Journal of cheminformatics* **7**, 44, doi: 10.1186/s13321-015-0087-1 (2015).
- Lv, J. *et al.* MCP-1-induced histamine release from mast cells is associated with development of interstitial cystitis/bladder pain syndrome in rat models. *Mediators of inflammation* **2012**, 358184, doi: 10.1155/2012/358184 (2012).
- Erickson, S. *et al.* Interferon-alpha inhibits Stat5 DNA-binding in IL-2 stimulated primary T-lymphocytes. *European journal of biochemistry/FEBS* **269**, 29–37 (2002).
- Fukui, Y., Kato, M., Inoue, Y., Matsubara, A. & Itoh, K. A metabonomic approach identifies human urinary phenylacetylglutamine as a novel marker of interstitial cystitis. *Journal of chromatography. B, Analytical technologies in the biomedical and life sciences* **877**, 3806–3812, doi: 10.1016/j.jchromb.2009.09.025 (2009).
- Lamale, L. M., Lutgendorf, S. K., Zimmerman, M. B. & Kreder, K. J. Interleukin-6, histamine, and methylhistamine as diagnostic markers for interstitial cystitis. *Urology* **68**, 702–706, doi: 10.1016/j.urology.2006.04.033 (2006).
- Wen, H. *et al.* Urinary metabolite profiling combined with computational analysis predicts interstitial cystitis-associated candidate biomarkers. *Journal of proteome research* **14**, 541–548, doi: 10.1021/pr5007729 (2015).
- Parker, K. S. *et al.* Urinary Metabolomics Identifies a Molecular Correlate of Interstitial Cystitis/Bladder Pain Syndrome in a Multidisciplinary Approach to the Study of Chronic Pelvic Pain (MAPP) Research Network Cohort. *EBioMedicine* **7**, 167–174, doi: 10.1016/j.ebiom.2016.03.040 (2016).
- Bouatra, S. *et al.* The human urine metabolome. *PLoS one* **8**, e73076, doi: 10.1371/journal.pone.0073076 (2013).
- Kind, T., Tolstikov, V., Fiehn, O. & Weiss, R. H. A comprehensive urinary metabolomic approach for identifying kidney cancer. *Analytical biochemistry* **363**, 185–195, doi: 10.1016/j.ab.2007.01.028 (2007).
- Kind, T. *et al.* FiehnLib: mass spectral and retention index libraries for metabolomics based on quadrupole and time-of-flight gas chromatography/mass spectrometry. *Analytical chemistry* **81**, 10038–10048, doi: 10.1021/ac9019522 (2009).
- Xia, J., Sinelnikov, I. V. & Wishart, D. S. MetAT: a web-based metabolomics tool for analyzing time-series and two-factor datasets. *Bioinformatics* **27**, 2455–2456, doi: 10.1093/bioinformatics/btr392 (2011).

Acknowledgements

The authors acknowledge support from National Institutes of Health (1U01DK103260, 1R01DK100974, U24DK097154, NIH NCATS UCLA CTSI UL1TR000124), Department of Defense (W81XWH-15-1-0415), Centers for Disease Controls and Prevention (1U01DP006079), IMAGINE NO IC Research Grant, the Steven Spielberg Discovery Fund in Prostate Cancer Research Career Development Award, the U.S.-Egypt Science and Technology Development Fund by the National Academies of Sciences, Engineering, and Medicine (all to J.K.), and Inha University Research grant (INHA-50487 (to T.L.)). J.K. is former recipient of Interstitial Cystitis Association Pilot Grant, a Fishbein Family IC Research Grant, New York Academy of Medicine, and Boston Children's Hospital Faculty Development. Funding for T.K. and O.F. was supported by NSF MCB1139644, NSF MCB1611846, NIH P20HL113452 and U24DK097154. Additional funding for T.K. was provided by the American Heart Association 15SDG25760020 and NIH 2R01HL091357-05. The funders had no role in the design, data collection and analysis, decision to publish or preparation of the manuscript.

Author Contributions

J.K., O.F., and T.L. designed the study, led obtaining funding, and overviewed the literature analysis and drafting the manuscript. T.K., E.C., and T.D.P. performed metabolomics analysis and sample preparation. N.D., and Z.L. performed data analysis and visualize the data. T.K., E.C., T.D.P., N.D., and Z.L. helped writing the manuscript. All authors read and approved the final manuscript.

Additional Information

Competing financial interests: The authors declare no competing financial interests.

How to cite this article: Kind, T. *et al.* Interstitial Cystitis-Associated Urinary Metabolites Identified by Mass-Spectrometry Based Metabolomics Analysis. *Sci. Rep.* **6**, 39227; doi: 10.1038/srep39227 (2016).

Publisher's note: Springer Nature remains neutral with regard to jurisdictional claims in published maps and institutional affiliations.



This work is licensed under a Creative Commons Attribution 4.0 International License. The images or other third party material in this article are included in the article's Creative Commons license, unless indicated otherwise in the credit line; if the material is not included under the Creative Commons license, users will need to obtain permission from the license holder to reproduce the material. To view a copy of this license, visit <http://creativecommons.org/licenses/by/4.0/>

© The Author(s) 2016

REVIEW

Open Access



Urinary proteomics and metabolomics studies to monitor bladder health and urological diseases

Zhaohui Chen¹ and Jayoung Kim^{2,3,4*}

Abstract

Background: Assays of molecular biomarkers in urine are non-invasive compared to other body fluids and can be easily repeated. Based on the hypothesis that the secreted markers from the diseased organs may locally release into the body fluid in the vicinity of the injury, urine-based assays have been considered beneficial to monitoring bladder health and urological diseases. The urine proteome is much less complex than the serum and tissues, but nevertheless can contain biomarkers for diagnosis and prognosis of diseases. The urine metabolome has a much higher number and concentration of low-molecular metabolites than the serum or tissues, with a far lower lipid concentration, yet informs directly about dietary and microbial metabolism.

Discussion: We here discuss the use of mass spectrometry-based proteomics and metabolomics for urine biomarker assays, specifically with respect to the underlying mechanisms that trigger the pathological condition.

Conclusion: Molecular biomarker profiles, based on proteomics and metabolomics studies, reliably distinguish patients from healthy controls, stratify sub-populations with respect to treatment options, and predict therapeutic response of patients with urological disease.

Keywords: Urinary biomarkers, Proteomics, Metabolomics, Bladder diseases

Background

Personalized medicine aims for a customized healthcare for each patient to match treatments with the right patients at the perfect timing. Gene-specific data (SNP genotyping as well as epigenetics) is too static to enable such timed treatments. It is therefore essential to collect variable biomarker, along with other clinical information, data to achieve accurate diagnostic assessment for individual patients [1–3]. Multi-omic readouts of cellular and organ phenotypes (RNA-Seq, proteomics and metabolomics) will be indispensable in the era of personalized medicine. Only through a combination of exact genotypic and molecular phenotypic information we will improve the development of custom and precision therapies [4–6]. Sub-grouping of patients is necessary to

define the evidence-based protocol for matching treatments to the right patients with appropriate timing [5, 7]. The necessity of compiling molecular information and clinical outcomes in personalized medicine prompted us to believe that the use of multi-omic data in conjunction with clinical outcome data is ever more important not only at the time of medical intervention, but throughout patients' lives. The need for and possibilities associated with big data approach to gain insight into biological processes driving diseases and to identify novel diagnostics is enlarging. In this review, we will discuss how far metabolomic and proteomic approaches have come to aid in this long-term goal.

Urological diseases including urological cancers and benign bladder dysfunctions are complex in nature and require powerful, precise treatments. Tests to find patient candidates for a specific or combination of therapy and to identify biomarkers are incredibly challenging to determine [6, 8, 9]. Urine contains information not only from the urinary track, but also from other organs, providing biomarkers for bladder and other systemic

* Correspondence: Jayoung.Kim@cshs.org

²Department of Surgery, Cedars-Sinai Medical Center, 8700 Beverly Blvd, Los Angeles, CA 90048, USA

³Department of Biomedical Sciences, Cedars-Sinai Medical Center, 8700 Beverly Blvd, Los Angeles, CA 90048, USA

Full list of author information is available at the end of the article



diseases [10–12]. Looking at urine data in conjunction with other available patient clinical data may enable us to understand the molecular signature, which helps monitor the stages of the diseases and responses to therapies. This is particularly true in urological diseases, where urine samples provide the primary window for diagnosis and drug behavior observation [13].

A common definition of the proteome is the entire set of proteins expressed by a cell, tissue or organism at a certain time. Since proteomics is the large-scale study of proteome, it can contribute to expanding the understanding of biological systems and functions in cells or organs. Proteomes are directly responsible for cell functions, and therefore, abnormal protein expression is an indication of cellular disruption due to the pathological conditions [14, 15]. Current global proteomic technologies may provide a comprehensive understanding of urological diseases, characteristics of the disease's state, and novel approaches to relieve the clinical symptoms [16–18].

Metabolomics provides a global chemical fingerprint of the metabolism of cells and indicates physiological and pathological states of biological samples [19–21]. Thus, the power of metabolomics opens up an unparalleled opportunity to query the molecular mechanisms of the disease. Metabolites are not merely the end products of gene/protein expression, rather, they are the result of the interactions of the genome and proteome with their environment in the cells. They play as powerful mediators of cellular events both in long-distance actions (e.g. hormones), stress and physiological actors (e.g. oxylipins) [22] and as cell-internal mediators (e.g. α -ketoglutarate in pluripotency) [23]. Thus, analyzing metabolic differences between pathological and normal conditions could provide undiscovered insights into the underlying disease pathology.

In addition to the advancements in multi-omics data acquisitions, novel bioinformatics methods enable an integrated view to identify the combined action of biomarkers as well as to develop drugs [24–27]. A significant volume of data with various omics data, including genetic, epigenetic, transcriptomic, proteomic, metabolomic and clinical outcome data, provides researchers with the capability to see a broader perspective and make discoveries that couldn't previously be delivered [28–31]. Integrative approaches have become the essential part of experimental designs aimed at better understanding the biology of bladder diseases.

The main goal of this article is to provide the reader with an up-to-date summary of the main molecular variations taking place in biofluids with respect to various urological diseases including urological cancers (e.g., prostate cancer (hereafter PCa) and bladder cancer (BCa)) and benign bladder dysfunctions (e.g., benign prostatic hyperplasia (BPH), interstitial cystitis/pelvic

bladder syndrome, bladder pain syndrome (IC)), as well as of the analytical strategies employed to unveil urinary biomarkers.

We here focus on mainly two omics analyses—proteomics and metabolomics—and associated data integration strategies. These approaches enable researchers to: (a) identify unknown molecular mechanisms; (b) select molecular markers that can be used for drug discovery, preclinical, and clinical drug development; (c) develop diagnostic tools. First, we present a short review on the urine-based studies. Second, we discuss analytical techniques that are used in urinary omics analyses, including computational methods for data processing. Next, we present studies that have used proteomics or metabolomics approaches to reveal the fingerprints of urological diseases. Finally, we discuss the future research directions and prospective how to apply to diagnosis and precision medicine for patients to summarize the review.

Discussion

Urine-based biomarkers for diagnosis, prognosis, or monitoring the treatment efficiency

A concerted effort bridging basic biology and clinical research is needed to identify high quality predictive biomarkers [31]. Discovery and validation of predictive biomarkers should be an integral part of clinical trials. In the clinical setting, the best diagnostic value is given by noninvasive biomarker tests that have both high sensitivity and specificity. A non- or minimally invasive diagnostic method using biofluids (e.g., urine, blood, saliva, fecal extract, and sputum specimens) may play a significant role in urological diseases with regard to early detection, diagnosis, prognosis, drug development, and sensitivity prediction to clinical treatments [12, 32–34].

So far the most attractive biofluids for biomarker discovery in bladder health and urological diseases are serum and urine [32–34]. Serum is a relatively accessible, stable and informative biofluid, making it ideal for early detection of systemic alteration in a wide range of diseases [35, 36]. Monitoring of serum has several advantages mainly due to its stability and minimum dilution effect. Proteomic and metabolic profiles of serum can be regarded as important indicators of physiological and pathological states and may aid in the understanding of the mechanism behind disease occurrence and progression [37–39]. However, blood samples pose certain disadvantages. During blood sample collection, proteases are often activated, which degrades proteins quickly and introduces a range of variability. On the other hand, 20 highly abundant proteins in the blood, which correspond to 99 % of the proteins, may hinder the identification of other less abundant, potentially important, proteins [40–43]. This feature makes it challenging to develop

plasma or serum based assays and often analytes enrichment or protein depletion is needed.

Urine definitely is not a waste in regards to gaining patients' diagnostics and therapeutic information [18, 44, 45]. However, it is still in debate whether urine plays an active role in regulating bladder biology. Urine's composition is 95 % of water with small amounts of ammonia, sulfate, and other constituents. Total protein concentration in urine from healthy donor is very low (<100 mg/L) and urinary proteome contains over 100,000 different peptides [18, 32, 44, 46, 47]. Approximately 1500 proteins have been shown to constitute the urinary proteome, of which large proportions are extra cellular proteins, plasma membrane proteins, and lysosomal proteins [18, 48]. The Human Kidney and Urine Proteome Project by the Human Proteome Organization (HUPO) suggested that urine is an ultra filtration of the blood in the body, since urine and blood samples share the proteome profile [49–51]. Approximately 30 % of the proteins in normal human urine are plasma proteins, while the other 70 % are proteins derived from the kidney and genitourinary tract [49, 50].

Urine samples usually need special treatments to meet the requirements of reproducible measurements after sample collections. To obtain reliable and consistent profiles of urine, first, urine must be collected in a sterile bag or plastic container, because urinary bacteria metabolism significantly interferes on the urine proteome and metabolome. Secondly, urine samples must be properly processed (e.g., pH adjustment and/or removal of cell debris) and frozen at -80°C immediately after collection, until analysis [40, 46]. In addition, analysis of urine samples poses several analytical challenges for profiling owing to wide variations in the ionic strength, pH, and osmolality, particularly under conditions of physiological stress, diet, exercise, medication, health condition, and environmental exposure [46, 52, 53]. Furthermore, urine samples typically have a huge dynamic range of metabolite and protein concentrations. Another potential problem is the presence of proteolytic activity in the urine by urokinase and other enzymes [54]. Proteases found in stored urine degrade urinary albumin to a substantial degree. However, the extent to which proteases affect biomarkers in the urine is still unclear.

Despite all these shortcomings, urine is still an attractive source for studying bladder diseases. To monitor bladder condition, urine-based assays present the most attractive strategy, among other biofluids-based methods, given that the body fluids that are most proximal to a disease site often can provide a source of informative biomarkers. Urine is readily obtained and available with no required preparations by the patient and it is less complex than other body fluids. The ease of collection allows for serial sampling to monitor disease and therapeutic responses.

Care must be taken in interpreting urine-based proteomics and metabolomics data. The main disadvantage of urine is the variation in protein concentration due to differences in fluid consumption during the day, which can be countered by normalizing with creatinine. However, although creatinine is the best possible internal standard for correcting urine volume effects, creatinine levels can vary due to dietary intake and pathological conditions. Computational approaches for data normalization methods can be applied to reduce artifacts due to sample variability using currently developed probabilistic quotient- and median-fold changes in normalization strategies [55].

Analytical techniques and databases for urine-based omics for bladder diseases

With the latest advances in high-throughput technologies, the pace of advances in the “omics” field accelerated the rate of novel biomarker discovery and therapeutic targets for various bladder diseases. Various omics technologies for personalized medicine are shown in Fig. 1, and ideal applications and workflow of urine-based biomarkers in clinical settings are shown in Fig. 2.

Proteomic technology has made a dramatic progress in the overall quality and information content over the past 5 years [56]. When computationally matching identified proteins (or metabolites) against knowledge-based databases, proteomics or metabolomics profiles today provide direct insights for biological interpretation of molecular perturbations unique in patients with urological diseases [47, 57, 58]. In this section, we review the current proteomic and metabolomic techniques and analytical tools/software that are used to identify signatures of urological diseases.

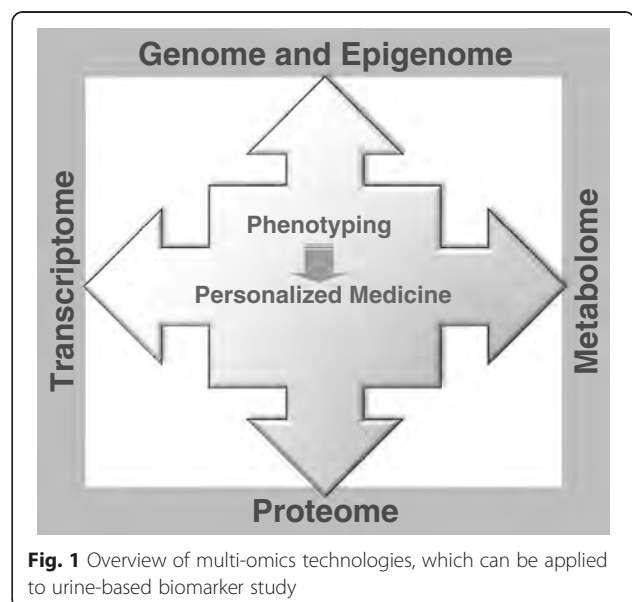
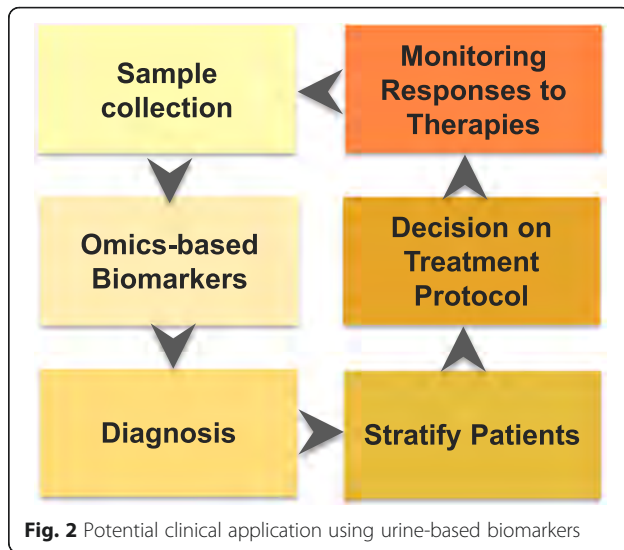


Fig. 1 Overview of multi-omics technologies, which can be applied to urine-based biomarker study



Urinary proteomics studies

Proteins are the major players influencing a person's health, since proteins frequently have the greatest clinical significance for the diagnosis of diseases. Studies in the field of proteomics aim to elucidate proteomes and understand the identity, quantity, modification, localization, interaction, and function of all proteins in a given cell type or tissue. A number of powerful proteomic technologies were developed, demonstrating that proteomic approaches have wide utility [59, 60]. Proteomics profiling enabled the comparing of protein differences between patients suffering from a wide range of ailments and healthy controls to discover biomarkers for diagnosis and monitoring treatment response [49, 56]. Further developments to understand the post-translational modifications (PTMs) in tissues and biological fluids from patients have been achieved through the development of mass spectrometry instrumentation with increasing sensitivity [61, 62]. Established protocols for PTM enrichment and pipelines for high-throughput assays for clinical specimens may provide the potential of automated and large-scale identification and quantification of PTM-ome and its biological role in diseases [63].

For urine proteomics, many mass spectrometry techniques, such as 2D PAGE-mass spectrometry (MS), liquid chromatography-mass spectrometry (LC-MS/MS), capillary electrophoresis-mass spectrometry (CE-MS), surface-enhanced laser desorption/ionization time-of-flight mass spectrometry (SELDI-TOF MS), matrix assisted laser desorption/ionization time-of-flight (MALDI-TOF) MS and nano-liquid chromatography-tandem mass spectrometry (Nano-MALDI-MS) have been used with some advantages and limitations [64–68]. We described here only a few analytical tools that highlight the usefulness of it for urinary proteomics research. Briefly, 2D PAGE-MS is time

consuming and technically challenging but very effective for large molecules. LC-MS is also time-consuming but pretty sensitive. CE-MS is cheap and good for biomarker discovery. MALDI-TOF MS is relatively simple, inexpensive, and, thus, a good option for fast screening. In general, nano-MALDI-MS is known to be much more sensitive than MALDI-TOF MS [64].

The gel-based 2-DE method enables urinary proteins to be resolved based on their molecular weight and isoelectric point. Several tools for image noise subtraction, protein spot detection, spot quantification, and spot matching can be used for 2-DE analysis including *Melanie*, *ImageMaster2D*, and *PDQuest* et al. The main steps in differential analysis of 2DE gels involve and statistical analysis. Often, the 2-DE method is coupled with MALDI-TOF MS or LC-MS/MS. Peptides from protein spots of interest are mixed with a matrix (e.g., α -cyano-4-hydroxycinnamic acid) solution and are spotted onto a MALDI plate and analyzed with a MALDI-TOF MS to identify a peptide-mass fingerprint. These peptides can also be analyzed with nanoLC-MS/MS to sequence each peptide and thus identify the protein.

Besides identification and characterization, urine proteins can also be quantified. Today, label-free proteomics is the primary approach to relative quantifications of the human urinary proteome [69, 70]. A major advantage of label-free quantification is that this method is cheaper, simpler and involves less complicated data analysis than isotope-labeled approaches. Data processing is often performed by softwares such as *Decyder MS*, *Protein Lynx*, *SIEVE*, and *skyline* [71]. However, label-free quantification is limited by its lower quantification accuracy (especially for spectral counting in data dependent scan methods), and label-free data dependent acquisition quantifications are generally results in the identifications of less proteins and poor reproducibility. Currently SWATH and other data independent mass spectrometry acquisition methods and several computational algorithms are tested in their potential to overcome these limitations [59, 69, 70, 72].

The use of the most advanced proteomics mass spectrometry technologies has allowed discovering and verifying several urinary biomarkers of bladder diseases. In a large proteomics study, 407 patient urine samples were analyzed using MALDI-TOF MS. Two markers, uromodulin and semenogelin, could distinguish PCa versus BPH with 71.2 % sensitivity and 67.4 % specificity [9]. In another study on prostate cancer (PCa), capillary electrophoresis was coupled with MS detection of proteins and was able to identify and validate 12 novel urinary biomarkers for PCa [73]. This report suggested that collecting mid-stream urine samples was uninformative, but that first void urine was able to identify patients with PCa with 91 % sensitivity and 69 % specificity [73]. Due to its

limited size, this study certainly requires additional validation in a larger cohort. In general, it can be assumed that a panel of biomarkers will most likely achieve an overall high level of specificity and robustness than using a single urinary protein biomarker. Further development of quantitative proteomics and selective or multiple reaction monitoring (SRM/MRM) methods [74–76] may allow the protein-quantification data to stand by their own without redundant validation using traditional protein quantification methods such as Western blot and ELISA. In many cases, there is no antibody available, and the capability of measuring multiple biomarkers in a panel for immune-based assays is very limited.

Urinary metabolomics studies

Metabolomic profiling, or metabolomics, is the systemic study of the unique small chemical fingerprints in a biological sample, and is the collection of small-molecule profiles that represent the end products of cellular processes in biological systems (e.g., cells, tissues, or organs) [20, 77]. As little as 5 μ l of plasma or urine allows the characterization of hundreds of metabolites that provide a functional readout of the metabolic state. A recent effort to characterize the metabolomes of human urine has completed to identify and annotate approximately 2500 urinary metabolites using nuclear magnetic resonance spectroscopy (NMR, in most cases ^1H -NMR), gas chromatography mass spectrometry (GC-MS), direct flow injection mass spectrometry (DFI/LC-MS/MS), inductively coupled plasma mass spectrometry (ICP-MS) and high performance liquid chromatography (HPLC) [78]. The detailed information of metabolite structures, concentrations, related literature references and disease associations is publically available via an online database (<http://www.urinemetabolome.ca>) [77]. Urinary metabolite levels are usually standardized by creatinine concentrations. Endogenous substrate levels in normal healthy subjects can inform on the status of each subject's metabolizing enzyme activities. The comparison of urinary metabolite levels of patients vs. healthy controls, and responders vs. non-responders to a particular drug should facilitate the development of useful biomarkers to diagnose the disease or to predict the response, respectively. Also, understanding of urinary metabolome in healthy condition may help the titration of drug dose and monitoring drug response [18, 77].

Metabolomic studies typically begin with sample collection followed by sample analysis. A number of analytical techniques including NMR spectroscopy, GC-MS, and liquid chromatography-mass spectrometry (LC-MS) are used as methods of analysis [19]. NMR spectroscopy has proven to be particularly good for urine metabolomics analysis, because the technique is highly reproducible, requires minimal sample handling, and is straightforward to

implement [79]. While the reproducibility, quantitative ability, and structure information derived from the NMR methods are big advantages, the relatively lower sensitivity and less straightforward identification methods are disadvantages of the NMR method [79]. MS-based metabolomics is considered more sensitive, providing greater coverage, and to be more cost-efficient than NMR-based applications. Given that the coverage varies with different technologies and instruments, the combination of different metabolomic approaches may provide a broad range of information that covers the metabolite profile and may maximize the capability of metabolomics analysis [19–21].

For metabolomics data processing, several statistical tools are currently used to analyze NMR and MS-based metabolomics datasets (e.g., MS-DIAL [80], XCMS, MZmine, MetAlign, MathDAMP, and LCMStats) [81, 82]. As metabolite databases, the Human Metabolome Database (HMDB), Madison Metabolomics Consortium Database, METLIN, and LipidMaps are generally used. To further understand the biology of the identified metabolites, HMDB (<http://www.hmdb.ca/>), METLIN (<http://metlin.scripps.edu/>), MassBank (<http://www.massbank.jp/>), PubChem (<https://pubchem.ncbi.nlm.nih.gov/>) and KEGG (<http://www.genome.jp/kegg/>) can be used.

There is an increasing awareness of standardization or careful accounting in experimental design of urinary metabolomics study. To overcome possible limitations and pitfalls of the metabolomics approach, specific recommendations for urine collection, sample handling, storage, data acquisition, and statistical validation are also needed [78].

Urinary extracellular vesicle-derived omics studies

Most cells including cancer cells shed different types of vesicles into extracellular environment [83]. These vesicles are so-called extracellular vesicles (EV) including microvesicles, exosomes, and oncosomes, which are named based mainly on their size and characteristics [84]. EV have an increasing attention in the field of biomarker discovery. Given that EV are membrane bound structures, the components should be protected from degradation by extracellular proteases, DNase and RNase. A possibly selective package process during EV formation and shedding may lead to the reduced complexity of the contents [83, 84].

EV were originally considered a cleaning system to trash away the unnecessary molecules from cells. However, accumulated evidence demonstrates that EV influence their microenvironments by altering signaling pathways and delivering genetic information to other cells within close proximity [85–88]. Today, EV are accepted as potent mediators of cellular communication and as selectively packed delivery vehicle, which can provide clues to EV biogenesis, targeting, and cellular

effects [87–89]. EV may also be used as a source of biomarkers for disease diagnosis, prognosis and response to treatment [89, 90]. Since EV can be readily isolated from multiple biological fluids (e.g., urine, serum, plasma, pleural effusion and saliva et al.), they have been considered to contain non-invasive biomarker candidates. In some pathological conditions including urological cancers, EV are easily secreted into the urine, and the urinary EV contain rich molecular information specific to the disease conditions such as cytoplasmic RNAs, miRNAs, metabolites and proteins [91]. Several disease-associated proteome were identified in urine from patients. Since EV-based urinary biomarkers are cell-free and do not rely on the presence of shed cells, urine provides a promise for the easy detection of bladder diseases [92, 93].

Unfortunately, there is no gold-standard technique for enriching and isolating EV in the clinical practice [94]. Nevertheless, several techniques have been developed to enrich and isolate urinary EV. This section discusses the different methods used to isolate urinary EV. Before isolating EV, it is advised to remove well-known abundant proteins in urine (e.g., uromodulin) [95]. Step-wise differential ultracentrifugation including low speed and high-speed centrifugation, and immuno-affinity and peptide-based isolation methods can be applied. The so-called Vn-96 peptide, based on surface marker of EV, was introduced to capture EV from biological fluids including urine. ExoQuick-TC™, Exospin™, and miRCURY™ EX isolation kits are based on aggregating agents followed by a low-speed centrifugation. Size-exclusion chromatography was also introduced to fractionate urine samples and isolate EV. Exochip™, a microfluidic-based method, has been recently shown to isolate EV. In particular, the hydrostatic dialysis method is efficient to enrich EV from highly diluted samples with molecular weight cut-off of 1000 kDa [94]. After omics analysis is done using EV isolated from urine samples, data can be analyzed using three major publically accessible EV-associated databases, EVpedia, ExoCarta, and Vesiclepedia [71, 96].

Because the variable results have been obtained with different isolation techniques, further discussion on the standard protocols for EV isolation, and normalization problem, which are major obstacles for the quantitative omics studies of EV, will be needed to apply this interesting biological resource into clinical practice.

Computational approaches to integrate data for better knowledge extraction

Using all information available from a wide variety of sources, including behavioral, genomic and life-style data has been coined “Big Data”. In clinical research, Big Data approaches show promise to connect information for

individualized therapy approaches, called Personalized Medicine, once Big Data Initiative has been shown to lead to new scientific insights to better understand the biology [4]. Omics studies generate long lists of interconnected genes, proteins and metabolites, which may be integrated in clinical settings via computational approaches [18, 21, 28, 75]. The systems approach, integrating multi-omics, data will increase the reliability of discovering biomarkers and development therapeutic strategies for bladder diseases.

Currently available tools for integrating omics data can be categorized (i) to identify parameters of disease-associated biological networks and (ii) to identify pathway-based targets. Computational methods and tools for identification of important molecular targets and biomarker candidates are summarized. The major network-based visualization tools include VANTED (<https://immersive-analytics.infotech.monash.edu/vanted/>), VisAnt (visant.bu.edu/), Metscape2 (metscape.ncibi.org/metscape2/), Arena3D (arena3d.org/) and MetaMapR [97]. In order to construct a disease-perturbed network, several softwares and integrative querying systems for interaction information (PSICQUIC), network modeling and analysis tools (STRING [98] and Cytoscape [99]), and pathway analysis (KEGG [100]) might be useful. Commercial tools (e.g., GeneGo and Ingenuity Pathway Analysis (IPA)) are also helpful to construct a network. For pathway visualization, various tools are available, including Pathguide (www.pathguide.org/), KEGG-based pathway visualization tool (www.genome.jp/kegg/pathway.html), Paintomics (www.paintomics.com/), ProMeTra (<https://www.cebitec.uni-bielefeld.de/polyomics/index.php/comics-software/75-prometra/>), KaPPa-View (kpv.kazusa.or.jp/), MapMan (mapman.gabipd.org/), MAYDAY, and PaVESy (pavesy.m-pimp-golm.mpg.de/). Based on the biochemical activities extracted from experimental datasets, interactive pathways can be constructed [101].

Importantly, in order to extract biological knowledge and to perform successful data integration across multiple resources, it is always essential to understand the context of the biology. Most current approaches, maybe with the exception of the Ingenuity Pathway analysis, are ignorant of disease etiologies and common pathological information that are very well known to clinical scientists. Hence, it is critical that scientists using pathway or genomic software are aware of this pitfall and use such network analyses only as additional tool to structure data and information, but not to expect immediate understanding. Only under careful interpretation of clinical knowledge and scientific literature can Omics data and software provide new hypotheses on undiscovered biological pathways and processes, eventually allowing us to personalized care and therapies on bladder diseases.

Potential biomarkers of bladder diseases

Next, we review the current state of proteomics and metabolomics in conjunction with recent technical advances in mass spectrometry in this section. The key applications and achievements by urinary proteomics and metabolomics in clinical biomarker research are discussed. Focus will be given to PCa, BCa, BPH and IC among other urological diseases. Examples of urine-based biomarkers suggested by previous studies are shown in Fig. 3.

Urinary biomarkers for prostate cancer

As the second most prevalent cancer in men, PCa's incidence reaches 899,000 new cases and 258,000 deaths per year [102]. One of the gold standard diagnostic tools for PCa progression detection is the measurement of prostate specific antigen (PSA) in serum [102].

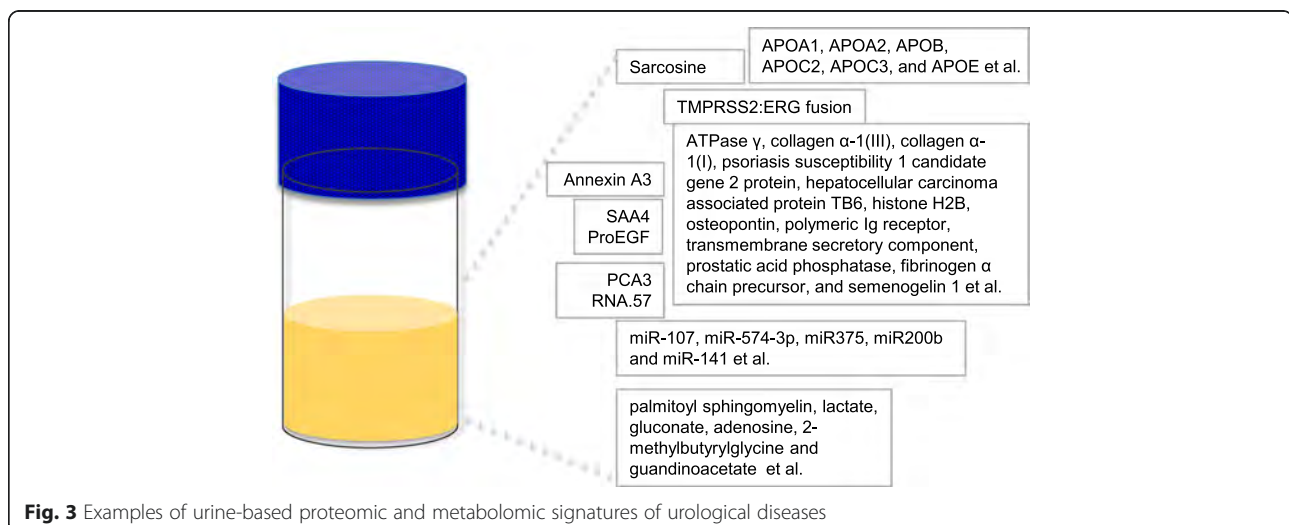
There have been many proteomic approaches to identify the urine-based biomarkers of PCa. For example, a large study using urine samples from 591 patients reported Annexin A3, a calcium-binding protein that plays a role in the regulation of cellular growth and in signal transduction pathways, as a novel urine-based biomarker for early PCa detection when used in conjunction with PSA [103]. Using CE-MS, 12 urinary biomarkers for PCa, including sodium/potassium-transporting ATPase γ , collagen α -1(III), collagen α -1(I), psoriasis susceptibility 1 candidate gene 2 protein, hepatocellular carcinoma associated protein TB6, histone H2B, osteopontin, polymeric Ig receptor, transmembrane secretory component, prostatic acid phosphatase, fibrinogen α chain precursor, and semenogelin 1, were identified and validated (91 % sensitivity and 69 % specificity) [104].

These findings strongly suggest that the use of a panel of biomarkers for disease diagnosis rather than a stand-alone biomarker, which may not be as specific, would

benefit to diagnostic precision. However, unfortunately, currently none of these urinary protein biomarkers have been introduced into clinical practice, since current diagnostic biomarkers are suboptimal and of poor utility for low-grade disease and surveillance. To become routine tests, these biomarker candidates should be carefully tested in multicenter clinical trials and should be measured in biological fluids by robust, standardized analytical methods.

For development of metabolite markers, both LC-MS and GC-MS methods were applied to profile various clinical samples (including tissues, urine, and plasma) from PCa patients and identified 87 metabolites that distinguished PCa from normal subjects [105]. This study suggested that an interesting urinary metabolite, sarcosine (N-methylglycine), associates with PCa progression to metastasis with significant predictive value [105]. A following nested case control study showed that urinary sarcosine (and cysteine) levels were significantly higher in 54 PCa patients who had a recurrence after treatment [106]. However, another follow-up study done using an independent cohort of 106 PCa patients failed to reproduce the ability of urinary sarcosine (normalized to creatinine) as a PCa biomarker [107]. It is certainly possible that sarcosine may serve only as cell-internal signal, and not be excreted or shed into biofluids.

In addition, several cell-free and exosome-derived urinary microRNAs were suggested as PCa biomarkers [43]. The following reports provided evidence that circulating miRNAs might be a next-generation biomarker and contribute to cancer screening in non-invasive liquid biopsy. Only few studies for PCa-associated miRNA in urine were reported. Five of the miRNAs were differentially quantified in PCa patients compared to controls (miR-107, miR-574-3p, miR375, miR200b and miR-141) in urine of men with cancer, compared to that of healthy



volunteers [108]. Among them, two miRNAs (miR-141 and miR-375) were also found higher in the PCa patient blood [108]. In the case of miR-141, the urinary levels were approximately 50 fold higher in metastatic PCa patients, compared to the healthy controls. Nilsson et al. found that exosomes were carriers for the TMPRSS2:ERG fusion, which is an early molecular event associated with PCa invasion, and PCA3 RNA.57, which were originally found as PCa biomarkers in prostate tissues [108].

Recently we also found interesting urinary miRNAs including virus-encoded miRNAs, which are specific to PCa, suggesting that this miRNA panel can be usable for the clinical setting [88]. This miRNA panel showed much better specificity and sensitivity to PSA for the early PCa patients whose serum PSA levels are undetectable [88]. In addition to RNA detection, proteomic profiling of exosomes and EV in human urine is underway and may lead to new biomarker development for a variety of diseases, including urological cancers and other benign diseases, with a hope of the potential use of EV as reservoirs of disease biomarkers.

Urinary biomarkers for bladder cancer

Urinary bladder cancer (BCa), the fourth most common cancer worldwide, is a significant cause of morbidity and mortality with a high recurrence rate [109]. For a follow-up surveillance, the diagnostic methods have been mostly instrumental in approaches including cystoscopy and cytology, which are painful and invasive. Thus, the molecular assays in a non-invasive fashion are needed for BCa patient surveillance at an early stage. High-throughput proteomic profiling technologies will identify molecular signatures that are associated with BCa, and will provide us understanding on bladder cancer biology, eventually leading to the development of targeted therapeutics [57, 110].

The complementary techniques of high-resolution MS and Western blotting/dot blot were able to quantify the urinary proteome specific to NMIBC. 29 proteins had a significantly higher abundance ($p < 0.05$) in urine samples of NMIBC compared with matched controls [111]. Another MS analysis using a Bruker Ultraflex extreme MALDI-TOF-MS revealed that the urine peptidome was associated with MIBC [57, 112]. Using hexapeptide-based library beads and an antibody-based affinity column using the iTRAQ technique, six apolipoproteins (APOA1, APOA2, APOB, APOC2, APOC3, and APOE) were suggested as BCa-associated urine proteins [112]. In this study, SAA4 and ProEGF were also significantly altered in BCa subgroups [112]. The combined signatures of SAA4 and ProEGF were demonstrated to have a good diagnostic capacity (AUC = 0.80 and $p < 0.001$) on BCa [112]. The other urine proteomic study using 2-DE MS demonstrated the increased level of urinary

apolipoprotein-A1 (Apo-A1) in BCa patients compared to control subjects. Additional validation assays ($n = 379$) supported that Apo-A1 could be used as a BCa biomarker with a sensitivity and specificity of 89.2 and 84.6 %, respectively [113].

An unbiased global metabolomic profiling using high-performance liquid chromatography-quadrupole time-of-flight mass spectrometry (HPLC-QTOFMS) profiled urine metabolites of BCa patients and controls. Comprehensive data analyses suggested 12 differential metabolites that contributed to the distinction between the BCa and control groups with a great sensitivity (91.3 %) and specificity (92.5 %) (AUC = 0.937) [114]. Interestingly, BCa-associated urinary metabolomes are enriched in glycolysis and beta-oxidation [114]. Recent urine metabolic profiling was performed on two subject cohorts with and without BCa in three independent platforms, which include ultrahigh-performance liquid chromatography/tandem mass spectrometry (UHPLC-MS/MS) in the negative ion mode, UHPLC-MS/MS in the positive ion mode, and GC-MS. As a set of candidate biomarkers for bladder cancer, 6 biomarkers (palmitoyl sphingomyelin, lactate, gluconate, adenosine, 2-methylbutyrylglycine and guanidinoacetate) were suggested [115].

There is no study on urine exosome-derived miRNA signature associated with BCa, however, exosome proteomics studies demonstrated exosomes were highly purified from cultured BCa cells. Using ultracentrifugation on a sucrose cushion, Western blotting and flow cytometry of exosome-coated beads, 18 urine exosome proteins (e.g., basigin, galectin-3, and trophoblast glycoprotein (5 T4) et al.) were identified and validated [116], suggesting that exosomes in urine are a highly stable resource of biomarkers for BCa.

Urinary biomarkers for BPH

Incidence of benign prostatic hyperplasia (BPH), the most common benign disease among men, is known to be associated with age. Since BPH patients have similar symptoms to those of PCa patients, there have been diagnostic challenges in clinical settings.

The urine proteome-based method for discrimination of BPH from high-grade prostatic intraepithelial neoplasia or PCa was developed through testing 407 patient samples using MALDI-TOF [73]. Recently performed urinary proteome profiling of men with BPH vs. PCa using iTRAQ LC/LC/MS/MS have identified 25 proteins that were differentially expressed in urines [73]. Three proteins, β 2M, PGA3, and MUC3, were further validated by western blot analysis. The combination of these three proteins showed an AUC of 0.710 (95 % CI: 0.631–0.788, $P < 0.001$) and enhanced a diagnostic accuracy when combined with PSA (AUC = 0.812, 95 % CI:

0.740–0.885, $P < 0.001$), suggesting a useful biomarker candidate panel segregating BPH from PCa [9].

Urinary biomarkers for IC

IC is a chronic bladder syndrome with bladder pain, urinary frequency/urgency, pressure, discomfort, and nocturia, which cause the suppressed physical function and social activity and adverse impact on the quality of life [117–119]. Approximately 1 out of 77 people in the United States have been diagnosed with IC. There is no gold standard for IC diagnosis. Objective diagnostic markers are urgently needed to improve prospects for clinical care. Etiologies of IC remain unknown. Prescription of medications has not been clearly suggested in clinical settings. Thus, there is a clear clinical need for the identification of biomarkers of IC.

The urine-based omics approaches to identify IC diagnostic markers have been employed. A small glycosylated peptide, antiproliferative factor (APF) was found in urine samples derived from IC patients [120]. Urinary APF bioactivity could segregate IC patients from controls (94 % sensitivity and 95 % specificity). The following global and unbiased quantitative proteomics combined with bioinformatics analysis performed by our group has enabled us to reveal the *in vitro* APF signaling network [121, 122]. Additional proteomics profiles associated with IC were suggested by studies using various technologies. Using 2-DE and MALDI-TOF, urine samples from 9 IC patients and 9 asymptomatic controls were analyzed, and the proteins such as uromodulin, kininogens (precursors of kinin) and inter- α -trypsin inhibitory heavy chain H4 were significantly altered in urine samples of IC patients [123]. A study by Kuromitsu et al. suggested that neutrophil elastase is significantly higher in IC subset with bladder pain and small bladder capacity than in other IC patients and healthy controls by using the 2D-DIGE nanoLC-MS/MS [124]. Another urinary proteome identified by Goo et al. revealed that α -1B-glycoprotein, orosomucoid-1, transthyretin and hemopexin were altered in 60 % of IC patients compared to controls [125].

A few attempts to use metabolomics analysis to identify an IC signature have suggested promising metabolite signatures specific to IC. Fukui et al. used ultra-performance liquid chromatography-mass spectrometry (UPLC-MS) and found that the urinary ratio of phenylacetylglutamine to creatinine can be correlated to the clinical grade of IC (e.g. mild to severe based on symptoms) [126]. A report from Van et al. has suggested that IC patients exhibited distinct MS and NMR spectral patterns from non-IC patients [127]. With follow-up studies in a larger cohort, global metabolite profiling combined with multivariate statistical and bioinformatics analysis may validated some of these compounds as important biomarker metabolites contributing to the biological

responses, such as the drug-induced toxicity, or response as metabolic biomarkers.

Conclusion: concluding remarks and perspectives

In this short review, we have provided information on the current state of ‘omics’ studies and available data sets relevant to bladder health and pathological condition, and presents opportunities for new research directed at understanding the pathogenesis of this complex condition. We believe that the ultimate goals of urine profiling of proteome and metabolome should be (i) to identify non-invasive diagnostic and prognostic biomarkers of bladder diseases, (ii) to better understand the biology of bladder diseases, and (iii) to determine the therapeutic strategies targeting the critical pathways of various bladder diseases. Recent efforts in the generation of large genomics, transcriptomics, proteomics, metabolomics, and other types of ‘omics’ data sets have provided a series of urinary biomarker candidates of bladder diseases. In spite of much efforts to identify candidate urinary biomarkers, it is still required to validate such markers in larger numbers of urine samples using targeted proteomics and metabolomics analyses in a prospective way.

Diagnostic and treatment modalities, even subjective diagnostic tools, are largely unavailable. As described here, our attempts to perform a systematic review and to build a pooled database using existing public ‘omics’ data associated with bladder health and various pathological conditions revealed the significant limitations and challenges facing investigators in the field. Many reports have suggested that natural diversity of patient population clearly plays a role in the difficulty of validating urine biomarkers. Expanding tests to include the general population often leads to loss or decrease in sensitivity. However, if tests are used for patients presenting specific symptoms in the clinic, and not for the general population, to inform about prognosis or treatment options, the pitfalls of general-population based urinary biomarkers may be alleviated. However, the cost of developing and validating a clinical grade assay is clearly beyond regular laboratory funding and would require concerted efforts by health agencies.

Collectively, despite these numerous pitfalls, urine is an interesting source of biomarkers for monitoring the bladder health. Rather than a single urinary molecular biomarker, a panel of biomarkers may be required to achieve the overall high level of specificity needed, so the trend is shifting towards implementing a panel of biomarkers, which may increase specificity. In order to translate potential biomarkers to clinical practice, vigorous validation must be pursued, with input from industry or large collaborative studies. Computational approaches combined with high quality ‘omics’ data could provide new insights in the field, essential molecular details about regulatory

mechanisms and perturbations leading to bladder diseases, and essential information if we are to offer improved diagnostic capability and treatment strategies for patients.

Availability of data and materials

All the data supporting your findings is contained within the manuscript.

Abbreviations

APF: antiproliferative factor; BCa: bladder cancer; BPH: benign prostatic hyperplasia; DEPs: differentially expressed proteins; DFI/LC-MS/MS: direct flow injection mass spectrometry; EV: extracellular vesicles; GC-MS: gas chromatography mass spectrometry; HMDB: human metabolome database; HPLC: high performance liquid chromatography; IC: interstitial cystitis/pelvic bladder syndrome/bladder pain syndrome; ICP-MS: inductively coupled plasma mass spectrometry; iTRAQ: isobaric tags for relative and absolute quantitation; LC-MS: liquid chromatography-mass spectrometry; MALDI-TOF: matrix assisted laser desorption/ionization time-of-flight; MIBC: muscle invasive bladder cancer; MS: mass spectrometry; nano-MALDI-MS: nano-liquid chromatography-tandem mass spectrometry; NMIBC: non-muscle invasive bladder cancer; NMR: nuclear magnetic resonance spectroscopy; PCa: prostate cancer; PTMs: posttranslational modifications; SELDI-TOF: surface-enhanced laser desorption/ionization time-of-flight; SILAC: stable-isotope labeling by amino acids; SRM/MRM: selective or multiple Reaction monitoring.

Competing interests

The authors declare that they have no competing interests.

Authors' contributions

ZC and JK participated in the design of the study and performed the analysis of references. JK led obtaining funding and drafted the manuscript. All authors read and approved the final manuscript.

Acknowledgements

The authors would like to thank Dr. Oliver Fiehn (UC Davis) for careful review and editing the manuscript.

Funding

The authors acknowledge support from National Institutes of Health grants (1U01DK103260, 1R01DK100974, U24 DK097154, NIH NCATS UCLA CTSI UL1TR000124 (to J.K.)), Department of Defense grants (PR140285 (to J.K.)), Centers for Disease Control and Prevention (1U01DP006079 (to J.K.)), IMAGINE NO IC Research Grant, the Steven Spielberg Discovery Fund in Prostate Cancer Research Career Development Award. J.K. is former recipient of Interstitial Cystitis Association Pilot Grant, a Fishbein Family IC Research Grant, New York Academy of Medicine, and Boston Children's Hospital Faculty Development.

Author details

¹Advanced Clinical Biosystems Research Institute, Cedars-Sinai Medical Center, Los Angeles, CA, USA. ²Department of Surgery, Cedars-Sinai Medical Center, 8700 Beverly Blvd, Los Angeles, CA 90048, USA. ³Department of Biomedical Sciences, Cedars-Sinai Medical Center, 8700 Beverly Blvd, Los Angeles, CA 90048, USA. ⁴Department of Medicine, University of California, Los Angeles, CA, USA.

Received: 30 September 2015 Accepted: 10 March 2016

Published online: 22 March 2016

References

- Roper N, Stensland KD, Hendricks R, Galsky MD. The landscape of precision cancer medicine clinical trials in the United States. *Cancer Treat Rev*. 2015; 41(5):385–90.
- Roychowdhury S, Chinnaiyan AM. Advancing precision medicine for prostate cancer through genomics. *J Clin Oncol*. 2013;31(15):1866–73.
- Rubin MA. Toward a prostate cancer precision medicine. *Urol Oncol*. 2015; 33(2):73–4.
- Garay JP, Gray JW. Omics and therapy - a basis for precision medicine. *Mol Oncol*. 2012;6(2):128–39.
- Robinson PN. Deep phenotyping for precision medicine. *Hum Mutat*. 2012; 33(5):777–80.
- Zhao Y, Polley EC, Li MC, Lih CJ, Palmisano A, Sims DJ, Rubinstein LV, Conley BA, Chen AP, Williams PM et al. GeneMed: an informatics hub for the coordination of next-generation sequencing studies that support precision oncology clinical trials. *Cancer Informat*. 2015;14 Suppl 2:45–55.
- Wei WQ, Denny JC. Extracting research-quality phenotypes from electronic health records to support precision medicine. *Genome Med*. 2015;7(1):41.
- Meric-Bernstam F, Johnson A, Holla V, Bailey AM, Brusco L, Chen K, Routbort M, Patel KP, Zeng J, Kopetz S et al. A decision support framework for genomically informed investigational cancer therapy. *J Natl Cancer Inst*. 2015;107(7). doi: 10.1093/jnci/djv098.
- Yang J, Roy R, Jedinak A, Moses MA. Mining the human proteome: biomarker discovery for human cancer and metastases. *Cancer J*. 2015;21(4): 327–36.
- Antunes-Lopes T, Cruz CD, Cruz F, Sievert KD. Biomarkers in lower urinary tract symptoms/overactive bladder: a critical overview. *Curr Opin Urol*. 2014; 24(4):352–7.
- Kamat AM, Vlahou A, Taylor JA, Hudson ML, Pesch B, Ingersoll MA, Todenhofer T, van Rhijn B, Kassouf W, Barton Grossman H et al. Considerations on the use of urine markers in the management of patients with high-grade non-muscle-invasive bladder cancer. *Urol Oncol*. 2014;32(7): 1069–77.
- Kuo HC. Potential urine and serum biomarkers for patients with bladder pain syndrome/interstitial cystitis. *Int J Urol*. 2014;21 Suppl 1:34–41.
- Pedroza-Diaz J, Rothlisberger S. Advances in urinary protein biomarkers for urogenital and non-urogenital pathologies. *Biochimica Medica*. 2015;25(1): 22–35.
- Filip S, Zoidakis J, Vlahou A, Mischak H. Advances in urinary proteome analysis and applications in systems biology. *Bioanalysis*. 2014;6(19):2549–69.
- Mendez O, Villanueva J. Challenges and opportunities for cell line secretomes in cancer proteomics. *Proteomics Clin Appl*. 2015;9(3–4):348–57.
- Anderson L. Six decades searching for meaning in the proteome. *J Proteome*. 2014;107:24–30.
- Iliuk AB, Arrington JV, Tao WA. Analytical challenges translating mass spectrometry-based phosphoproteomics from discovery to clinical applications. *Electrophoresis*. 2014;35(24):3430–40.
- Zou L, Sun W. Human urine proteome: a powerful source for clinical research. *Adv Exp Med Biol*. 2015;845:31–42.
- Naz S, Moreira dos Santos DC, Garcia A, Barbas C. Analytical protocols based on LC-MS, GC-MS and CE-MS for nontargeted metabolomics of biological tissues. *Bioanalysis*. 2014;6(12):1657–77.
- Weckwerth W, Morgenthal K. Metabolomics: from pattern recognition to biological interpretation. *Drug Discov Today*. 2005;10(22):1551–8.
- Zhang A, Sun H, Yan G, Wang P, Wang X. Metabolomics for biomarker discovery: moving to the clinic. *BioMed Res Int*. 2015;2015:354671.
- Hou Q, Ufer G, Bartels D. Lipid signalling in plant responses to abiotic stress. *Plant Cell Environ*. 2015. doi: 10.1111/pce.12666.
- Carey BW, Finley LW, Cross JR, Allis CD, Thompson CB. Intracellular alpha-ketoglutarate maintains the pluripotency of embryonic stem cells. *Nature*. 2015;518(7539):413–6.
- Benjamin DI, Cravatt BF, Nomura DK. Global profiling strategies for mapping dysregulated metabolic pathways in cancer. *Cell Metab*. 2012;16(5):565–77.
- Di Girolamo F, Del Chierico F, Caenaro G, Lante I, Muraca M, Putignano L. Human serum proteome analysis: new source of markers in metabolic disorders. *Biomark Med*. 2012;6(6):759–73.
- Fischer R, Bowness P, Kessler BM. Two birds with one stone: doing metabolomics with your proteomics kit. *Proteomics*. 2013;13(23–24):3371–86.
- Zhang A, Sun H, Wang P, Han Y, Wang X. Recent and potential developments of biofluid analyses in metabolomics. *J Proteome*. 2012;75(4):1079–88.
- Alyass A, Turcotte M, Meyre D. From big data analysis to personalized medicine for all: challenges and opportunities. *BMC Med Genet*. 2015;8:33.
- Boja ES, Rodriguez H. Proteogenomic convergence for understanding cancer pathways and networks. *Clin Proteomics*. 2014;11(1):22.
- Stransky B, Barrera J, Ohno-Machado L, De Souza SJ. Modeling cancer: integration of "omics" information in dynamic systems. *J Bioinforma Comput Biol*. 2007;5(4):977–86.
- Goossens N, Nakagawa S, Sun X, Hoshida Y. Cancer biomarker discovery and validation. *Translat Cancer Res*. 2015;4(3):256–69.

32. Dijkstra S, Mulders PF, Schalken JA. Clinical use of novel urine and blood based prostate cancer biomarkers: a review. *Clin Biochem*. 2014;47(10-11): 889–96.
33. Hessels D, Schalken JA. Urinary biomarkers for prostate cancer: a review. *Asian J Androl*. 2013;15(3):333–9.
34. Sorio C, Mauri P, Pederzoli P, Scarpa A. Non-invasive cancer detection: strategies for the identification of novel cancer markers. *IUBMB Life*. 2006; 58(4):193–8.
35. Kumar A, Baycin-Hizal D, Shiloach J, Bowen MA, Betenbaugh MJ. Coupling enrichment methods with proteomics for understanding and treating disease. *Proteomics Clin Appl*. 2015;9(1–2):33–47.
36. Stastna M, Van Eyk JE. Secreted proteins as a fundamental source for biomarker discovery. *Proteomics*. 2012;12(4–5):722–35.
37. Deutsch EW, Eng JK, Zhang H, King NL, Nesvizhskii AI, Lin B, Lee H, Yi EC, Ossola R, Aebersold R. Human Plasma PeptideAtlas. *Proteomics*. 2005;5(13): 3497–500.
38. Nanjappa V, Thomas JK, Marimuthu A, Muthusamy B, Radhakrishnan A, Sharma R, Ahmad Khan A, Balakrishnan L, Sahasrabudhe NA, Kumar S et al. Plasma Proteome Database as a resource for proteomics research: 2014 update. *Nucleic Acids Res*. 2014;42(Database issue):D959–65.
39. Omenn GS. Data management and data integration in the HUPO plasma proteome project. *Methods Mol Biol*. 2011;696:247–57.
40. Lygirou V, Makridakis M, Vlahou A. Biological sample collection for clinical proteomics: existing SOPs. *Methods Mol Biol*. 2015;1243:3–27.
41. Roobol MJ, Carlsson SV. Risk stratification in prostate cancer screening. *Nat Rev Urol*. 2013;10(1):38–48.
42. Stovsky M, Ponsky L, Vourganti S, Stuhldreher P, Siroky MB, Kipnis V, Fedotoff O, Mikheeva L, Zaslavsky B, Chait A et al. Prostate-specific antigen/ solvent interaction analysis: a preliminary evaluation of a new assay concept for detecting prostate cancer using urinary samples. *Urology*. 2011;78(3): 601–5.
43. Trock BJ. Circulating biomarkers for discriminating indolent from aggressive disease in prostate cancer active surveillance. *Curr Opin Urol*. 2014;24(3): 293–302.
44. Emwas AH, Luchinat C, Turano P, Tenori L, Roy R, Salek RM, Ryan D, Merzaban JS, Kaddurah-Daouk R, Zeri AC et al. Standardizing the experimental conditions for using urine in NMR-based metabolomic studies with a particular focus on diagnostic studies: a review. *Metabolomics*. 2015; 11(4):872–94.
45. Rolfo C, Castiglia M, Hong D, Alessandro R, Mertens I, Baggerman G, Zwaenepoel K, Gil-Bazo I, Passiglia F, Carreca AP et al. Liquid biopsies in lung cancer: the new ambrosia of researchers. *Biochim Biophys Acta*. 2014; 1846(2):539–46.
46. Thomas CE, Sexton W, Benson K, Sutphen R, Koomen J. Urine collection and processing for protein biomarker discovery and quantification. *Cancer Epidemiol Biomark Prev*. 2010;19(4):953–9.
47. Wood SL, Knowles MA, Thompson D, Selby PJ, Banks RE. Proteomic studies of urinary biomarkers for prostate, bladder and kidney cancers. *Nat Rev Urol*. 2013;10(4):206–18.
48. Hortin GL, Sviridov D. Diagnostic potential for urinary proteomics. *Pharmacogenomics*. 2007;8(3):237–55.
49. Farrah T, Deutsch EW, Omenn GS, Sun Z, Watts JD, Yamamoto T, Shteynberg D, Harris MM, Moritz RL. State of the human proteome in 2013 as viewed through PeptideAtlas: comparing the kidney, urine, and plasma proteomes for the biology- and disease-driven Human Proteome Project. *J Proteome Res*. 2014;13(1):60–75.
50. Yamamoto T. The 4th Human Kidney and Urine Proteome Project (HKUPP) workshop. 26 September 2009, Toronto, Canada. *Proteomics*. 2010;10(11): 2069–70.
51. Yamamoto T, Langham RG, Ronco P, Knepper MA, Thongboonkerd V. Towards standard protocols and guidelines for urine proteomics: a report on the Human Kidney and Urine Proteome Project (HKUPP) symposium and workshop, 6 October 2007, Seoul, Korea and 1 November 2007, San Francisco, CA, USA. *Proteomics*. 2008;8(11):2156–9.
52. Court M, Selevsek N, Matondo M, Allory Y, Garin J, Masselon CD, Domon B. Toward a standardized urine proteome analysis methodology. *Proteomics*. 2011;11(6):1160–71.
53. Drake RR, White KY, Fuller TW, Igwe E, Clements MA, Nyalwidhe JO, Given RW, Lance RS, Semmes OJ. Clinical collection and protein properties of expressed prostatic secretions as a source for biomarkers of prostatic disease. *J Proteome*. 2009;72(6):907–17.
54. Cho YT, Chen CW, Chen MP, Hu JL, Su H, Shiea J, Wu WJ, Wu DC. Diagnosis of albuminuria by tryptic digestion and matrix-assisted laser desorption/ionization/time-of-flight mass spectrometry. *Clin Chim Acta*. 2013;420: 76–81.
55. Dieterle F, Ross A, Schlotterbeck G, Senn H. Probabilistic quotient normalization as robust method to account for dilution of complex biological mixtures. Application in 1H NMR metabonomics. *Anal Chem*. 2006;78(13):4281–90.
56. Hathout Y. Proteomic methods for biomarker discovery and validation. Are we there yet? *Expert Rev Proteomics*. 2015;12(4):329–31.
57. Bauca JM, Martinez-Morillo E, Diamandis EP. Peptidomics of urine and other biofluids for cancer diagnostics. *Clin Chem*. 2014;60(8):1052–61.
58. Bechis SK, Otsetov AG, Ge R, Olumi AF. Personalized medicine for the management of benign prostatic hyperplasia. *J Urol*. 2014;192(1):16–23.
59. Muntel J, Xuan Y, Berger ST, Reiter L, Bachur R, Kentsis A, Steen H. Advancing urinary protein biomarker discovery by data-independent acquisition on a quadrupole-orbitrap mass spectrometer. *J Proteome Res*. 2015;14(11):4752–62.
60. Ovrehus MA, Zurbig P, Vikse BE, Hallan SI. Urinary proteomics in chronic kidney disease: diagnosis and risk of progression beyond albuminuria. *Clin Proteomics*. 2015;12(1):21.
61. Ordureau A, Munch C, Harper JW. Quantifying ubiquitin signaling. *Mol Cell*. 2015;58(4):660–76.
62. Weissinger EM, Mischak H. Application of proteomics to posttransplantational follow-up. *Methods Mol Med*. 2007;134:217–28.
63. Schwammle V, Verano-Braga T, Roepstorff P. Computational and statistical methods for high-throughput analysis of post-translational modifications of proteins. *J Proteome*. 2015;129:3–15.
64. Gopal J, Muthu M, Chun SC, Wu HF. State-of-the-art nanoplateform-integrated MALDI-MS impacting resolutions in urinary proteomics. *Proteomics Clin Appl*. 2015;9(5–6):469–81.
65. Heemskerck AA, Deelder AM, Mayboroda OA. CE-ESI-MS for bottom-up proteomics: Advances in separation, interfacing and applications. *Mass Spectrom Rev*. 2014. doi: 10.1002/mas.21432.
66. Hellstrom M, Jonmarker S, Lehtio J, Auer G, Egevad L. Proteomics in clinical prostate research. *Proteomics Clin Appl*. 2007;1(9):1058–65.
67. Robledo VR, Smyth WF. Review of the CE-MS platform as a powerful alternative to conventional couplings in bio-omics and target-based applications. *Electrophoresis*. 2014;35(16):2292–308.
68. Whelan LC, Power KA, McDowell DT, Kennedy J, Gallagher WM. Applications of SELDI-MS technology in oncology. *J Cell Mol Med*. 2008;12(5A):1535–47.
69. Collier TS, Muddiman DC. Analytical strategies for the global quantification of intact proteins. *Amino Acids*. 2012;43(3):1109–17.
70. Matzke MM, Brown JN, Gritsenko MA, Metz TO, Pounds JG, Rodland KD, Shukla AK, Smith RD, Waters KM, McDermott JE et al. A comparative analysis of computational approaches to relative protein quantification using peptide peak intensities in label-free LC-MS proteomics experiments. *Proteomics*. 2013;13(3–4):493–503.
71. Kim DK, Kang B, Kim OY, Choi DS, Lee J, Kim SR, Go G, Yoon YJ, Kim JH, Jang SC et al. EVpedia: an integrated database of high-throughput data for systemic analyses of extracellular vesicles. *J Extracell Vesicles*. 2013;2. doi: 10.3402/jev.v2i0.20384.
72. Gillet LC, Navarro P, Tate S, Rost H, Selevsek N, Reiter L, Bonner R, Aebersold R. Targeted data extraction of the MS/MS spectra generated by data-independent acquisition: a new concept for consistent and accurate proteome analysis. *Mol Cell Proteomics*. 2012;11(6):O111.016717.
73. Jedinak A, Curatolo A, Zurakowski D, Dillon S, Bhasin MK, Libermann TA, Roy R, Sachdev M, Loughlin KR, Moses MA. Novel non-invasive biomarkers that distinguish between benign prostate hyperplasia and prostate cancer. *BMC Cancer*. 2015;15:259.
74. Colangelo CM, Chung L, Bruce C, Cheung KH. Review of software tools for design and analysis of large scale MRM proteomic datasets. *Methods*. 2013; 61(3):287–98.
75. Harlan R, Zhang H. Targeted proteomics: a bridge between discovery and validation. *Expert Rev Proteomics*. 2014;11(6):657–61.
76. Shi T, Su D, Liu T, Tang K, Camp 2nd DG, Qian WJ, Smith RD. Advancing the sensitivity of selected reaction monitoring-based targeted quantitative proteomics. *Proteomics*. 2012;12(8):1074–92.
77. Bouatra S, Aziat F, Mandal R, Guo AC, Wilson MR, Knox C, Bjorn Dahl TC, Krishnamurthy R, Saleem F, Liu P et al. The human urine metabolome. *PLoS One*. 2013;8(9):e73076.

78. Khamis MM, Adamko DJ, El-Aneed A. Mass spectrometric based approaches in urine metabolomics and biomarker discovery. *Mass Spectrom Rev*. 2015. doi: 10.1002/mas.21455.
79. Zheng C, Zhang S, Ragg S, Raftery D, Vitek O. Identification and quantification of metabolites in (1)H NMR spectra by Bayesian model selection. *Bioinformatics*. 2011;27(12):1637–44.
80. Tsugawa H, Cajka T, Kind T, Ma Y, Higgins B, Ikeda K, Kanazawa M, VanderGheynst J, Fiehn O, Arita M. MS-DIAL: data-independent MS/MS deconvolution for comprehensive metabolome analysis. *Nat Methods*. 2015; 12(6):523–6.
81. Krumsiek J, Suhre K, Evans AM, Mitchell MW, Mohnhey RP, Milburn MV, Wägele B, Romisch-Margl W, Illig T, Adamski J et al. Mining the unknown: a systems approach to metabolite identification combining genetic and metabolic information. *PLoS Genet*. 2012;8(10):e1003005.
82. Zhou B, Wang J, Rössler HW. MetaboSearch: tool for mass-based metabolite identification using multiple databases. *PLoS One*. 2012;7(6):e40096.
83. Coleman BM, Hill AF. Extracellular vesicles—Their role in the packaging and spread of misfolded proteins associated with neurodegenerative diseases. *Semin Cell Dev Biol*. 2015;40:89–96.
84. Yanez-Mo M, Sijlender PR, Andreu Z, Zavec AB, Borrás FE, Buzas EI, Buzas K, Casal E, Cappello F, Carvalho J et al. Biological properties of extracellular vesicles and their physiological functions. *J Extracellular Vesicles*. 2015;4: 27066.
85. Choi DY, You S, Jung JH, Lee JC, Rho JK, Lee KY, Freeman MR, Kim KP, Kim J. Extracellular vesicles shed from gefitinib-resistant nonsmall cell lung cancer regulate the tumor microenvironment. *Proteomics*. 2014;14(16):1845–56.
86. Jung JH, Lee MY, Choi DY, Lee JW, You S, Lee KY, Kim J, Kim KP. Phospholipids of tumor extracellular vesicles stratify gefitinib-resistant nonsmall cell lung cancer cells from gefitinib-sensitive cells. *Proteomics*. 2015;15(4):824–35.
87. Kim J, Morley S, Le M, Bedoret D, Umetsu DT, Di Vizio D, Freeman MR. Enhanced shedding of extracellular vesicles from amoeboid prostate cancer cells: potential effects on the tumor microenvironment. *Cancer Biol Ther*. 2014;15(4):409–18.
88. Yun SJ, Jeong P, Kang HW, Kim YH, Kim EA, Yan C, Choi YK, Kim D, Kim JM, Kim SK et al. Urinary MicroRNAs of prostate cancer: virus-encoded hsv1-miR118 and hsv2-miR-H9-5p could be valuable diagnostic markers. *Int Neurourol J*. 2015;19(2):74–84.
89. Astro V, de Curtis I. Plasma membrane-associated platforms: dynamic scaffolds that organize membrane-associated events. *Sci Signal*. 2015;8(367):re1.
90. Robbins PD, Morelli AE. Regulation of immune responses by extracellular vesicles. *Nat Rev Immunol*. 2014;14(3):195–208.
91. Schey KL, Luther JM, Rose KL. Proteomics characterization of exosome cargo. *Methods*. 2015;87:75–82.
92. Gonzalez E, Falcon-Perez JM. Cell-derived extracellular vesicles as a platform to identify low-invasive disease biomarkers. *Expert Rev Mol Diagn*. 2015; 15(7):907–23.
93. Duijvesz D, Luider T, Bangma CH, Jenster G. Exosomes as biomarker treasure chests for prostate cancer. *Eur Urol*. 2011;59(5):823–31.
94. Pitto M, Corbetta S, Raimondo F. Preparation of urinary exosomes: methodological issues for clinical proteomics. *Methods Mol Biol*. 2015;1243: 43–53.
95. Hiemstra TF, Charles PD, Hester SS, Karet FE, Lilley KS. Uromodulin exclusion list improves urinary exosomal protein identification. *J Biomol Tech*. 2011; 22(4):136–45.
96. Kalra H, Simpson RJ, Ji H, Aikawa E, Altevogt P, Askenase P, Bond VC, Borrás FE, Breakefield X, Budnik V et al. Vesiclepedia: a compendium for extracellular vesicles with continuous community annotation. *PLoS Biol*. 2012;10(12):e1001450.
97. Grapov D, Wanichthanarak K, Fiehn O. MetaMapR: pathway independent metabolomic network analysis incorporating unknowns. *Bioinformatics*. 2015;31(16):2757–60.
98. von Mering C, Huynen M, Jaeggi D, Schmidt S, Bork P, Snel B. STRING: a database of predicted functional associations between proteins. *Nucleic Acids Res*. 2003;31(1):258–61.
99. Shannon P, Markiel A, Ozier O, Baliga NS, Wang JT, Ramage D, Amin N, Schwikowski B, Ideker T. Cytoscape: a software environment for integrated models of biomolecular interaction networks. *Genome Res*. 2003;13(11): 2498–504.
100. Ogata H, Goto S, Sato K, Fujibuchi W, Bono H, Kanehisa M. KEGG: Kyoto Encyclopedia of Genes and Genomes. *Nucleic Acids Res*. 1999;27(1):29–34.
101. Fiehn O, Kim J. Metabolomics insights into pathophysiological mechanisms of interstitial cystitis. *Int Neurourol J*. 2014;18(3):106–14.
102. Hayes JH, Barry MJ. Screening for prostate cancer with the prostate-specific antigen test: a review of current evidence. *JAMA*. 2014;311(11):1143–9.
103. Schostak M, Schwall GP, Poznanovic S, Groebe K, Muller M, Messinger D, Miller K, Krause H, Pelzer A, Horninger W et al. Annexin A3 in urine: a highly specific noninvasive marker for prostate cancer early detection. *J Urol*. 2009; 181(1):343–53.
104. Theodorescu D, Schiffer E, Bauer HW, Douwes F, Eichhorn F, Polley R, Schmidt T, Schofer W, Zurbig P, Good DM et al. Discovery and validation of urinary biomarkers for prostate cancer. *Proteomics Clin Appl*. 2008;2(4): 556–70.
105. Sreekumar A, Poisson LM, Rajendiran TM, Khan AP, Cao Q, Yu J, Laxman B, Mehra R, Lonigro RJ, Li Y et al. Metabolomic profiles delineate potential role for sarcosine in prostate cancer progression. *Nature*. 2009;457(7231):910–4.
106. Stabler S, Koyama T, Zhao Z, Martinez-Ferrer M, Allen RH, Luka Z, Loukachevitch LV, Clark PE, Wagner C, Bhowmick NA. Serum methionine metabolites are risk factors for metastatic prostate cancer progression. *PLoS One*. 2011;6(8):e22486.
107. Jentzmik F, Stephan C, Miller K, Schrader M, Erbersdobler A, Kristiansen G, Lein M, Jung K. Sarcosine in urine after digital rectal examination fails as a marker in prostate cancer detection and identification of aggressive tumours. *Eur Urol*. 2010;58(1):12–8. discussion 20–11.
108. Bryant RJ, Pawlowski T, Catto JW, Marsden G, Vessella RL, Rhee B, Kuslich C, Visakorpi T, Hamdy FC. Changes in circulating microRNA levels associated with prostate cancer. *Br J Cancer*. 2012;106(4):768–74.
109. Noon AP, Catto JW. Bladder cancer in 2012: Challenging current paradigms. *Nat Rev Urol*. 2013;10(2):67–8.
110. Bansal N, Gupta A, Sankhwar SN. Proteometabolomics of bladder cancer: current and future prospects. *Cancer Biomark*. 2015;15:339–48.
111. Linden M, Lind SB, Mayrhofer C, Segersten U, Wester K, Lyutvinskiy Y, Zubarev R, Malmstrom PU, Pettersson U. Proteomic analysis of urinary biomarker candidates for nonmuscle invasive bladder cancer. *Proteomics*. 2012;12(1):135–44.
112. Chen CL, Lin TS, Tsai CH, Wu CC, Chung T, Chien KY, Wu M, Chang YS, Yu JS, Chen YT. Identification of potential bladder cancer markers in urine by abundant-protein depletion coupled with quantitative proteomics. *J Proteome*. 2013;85:28–43.
113. Li C, Li H, Zhang T, Li J, Liu L, Chang J. Discovery of Apo-A1 as a potential bladder cancer biomarker by urine proteomics and analysis. *Biochem Biophys Res Commun*. 2014;446(4):1047–52.
114. Jin X, Yun SJ, Jeong P, Kim IY, Kim WJ, Park S. Diagnosis of bladder cancer and prediction of survival by urinary metabolomics. *Oncotarget*. 2014;5(6): 1635–45.
115. Wittmann BM, Stirdivant SM, Mitchell MW, Wulff JE, McDunn JE, Li Z, Dennis-Barrie A, Neri BP, Milburn MV, Lotan Y et al. Bladder cancer biomarker discovery using global metabolomic profiling of urine. *PLoS One*. 2014;9(12):e115870.
116. Welton JL, Khanna S, Giles PJ, Brennan P, Brewis IA, Staffurth J, Mason MD, Clayton A. Proteomics analysis of bladder cancer exosomes. *Mol Cell Proteomics*. 2010;9(6):1324–38.
117. Clemens JQ, Mullins C, Kusek JW, Kirkali Z, Mayer EA, Rodriguez LV, Klumpp DJ, Schaeffer AJ, Kreder KJ, Buchwald D et al. The MAPP research network: a novel study of urologic chronic pelvic pain syndromes. *BMC Urol*. 2014; 14:57.
118. Lai HH, Krieger JN, Pontari MA, Buchwald D, Hou X, Landis JR, Network MR. Painful Bladder Filling and Painful Urgency Are Distinct Characteristics in Men and Women with Urologic Chronic Pelvic Pain Syndromes - A MAPP Research Network Study. *J Urol*. 2015;194:1634–41.
119. Landis JR, Williams DA, Lucia MS, Clauw DJ, Naliboff BD, Robinson NA, van Bokhoven A, Sutcliffe S, Schaeffer AJ, Rodriguez LV et al. The MAPP research network: design, patient characterization and operations. *BMC Urol*. 2014;14:58.
120. Keay SK, Szekeley Z, Conrads TP, Veenstra TD, Barchi Jr JJ, Zhang CO, Koch KR, Michejda CJ. An antiproliferative factor from interstitial cystitis patients is a frizzled 8 protein-related sialoglycopeptide. *Proc Natl Acad Sci U S A*. 2004;101(32):11803–8.
121. Yang W, Chung YG, Kim Y, Kim TK, Keay SK, Zhang CO, Ji M, Hwang D, Kim KP, Steen H et al. Quantitative proteomics identifies a beta-catenin network as an element of the signaling response to Frizzled-8 protein-related antiproliferative factor. *Mol Cell Proteomics*. 2011;10(6):M110.007492.

122. Yang W, Kim Y, Kim TK, Keay SK, Kim KP, Steen H, Freeman MR, Hwang D, Kim J. Integration analysis of quantitative proteomics and transcriptomics data identifies potential targets of frizzled-8 protein-related antiproliferative factor in vivo. *BJU Int.* 2012;110(11 Pt C):E1138–46.
123. Canter MP, Graham CA, Heit MH, Blackwell LS, Wilkey DW, Klein JB, Merchant ML. Proteomic techniques identify urine proteins that differentiate patients with interstitial cystitis from asymptomatic control subjects. *Am J Obstet Gynecol.* 2008;198(5):553.e1–6.
124. Kuromitsu S, Yokota H, Hiramoto M, Morita S, Mita H, Yamada T. Increased concentration of neutrophil elastase in urine from patients with interstitial cystitis. *Scand J Urol Nephrol.* 2008;42(5):455–61.
125. Goo YA, Tsai YS, Liu AY, Goodlett DR, Yang CC. Urinary proteomics evaluation in interstitial cystitis/painful bladder syndrome: a pilot study. *Int Braz J Urol.* 2010;36(4):464–78. discussion 478–469, 479.
126. Fukui Y, Kato M, Inoue Y, Matsubara A, Itoh K. A metabonomic approach identifies human urinary phenylacetylglutamine as a novel marker of interstitial cystitis. *J Chromatogr B Anal Technol Biomed Life Sci.* 2009; 877(30):3806–12.
127. Van QN, Klose JR, Lucas DA, Prieto DA, Luke B, Collins J, Burt SK, Chmurny GN, Issaq HJ, Conrads TP et al. The use of urine proteomic and metabonomic patterns for the diagnosis of interstitial cystitis and bacterial cystitis. *Dis Markers.* 2003;19(4–5):169–83.

Submit your next manuscript to BioMed Central and we will help you at every step:

- We accept pre-submission inquiries
- Our selector tool helps you to find the most relevant journal
- We provide round the clock customer support
- Convenient online submission
- Thorough peer review
- Inclusion in PubMed and all major indexing services
- Maximum visibility for your research

Submit your manuscript at
www.biomedcentral.com/submit



Immune checkpoint blockade therapy for bladder cancer treatment

Jayoung Kim^{1,2}

¹Departments of Surgery and Biomedical Sciences, Cedars-Sinai Medical Center, Los Angeles, CA, ²Department of Medicine, University of California, Los Angeles, CA, USA

Bladder cancer remains the most immunogenic and expensive malignant tumor in the United States today. As the 4th leading cause of death from cancer in United States, Immunotherapy blocking immune checkpoints have been recently been applied to many aggressive cancers and changed interventions of urological cancers including advanced bladder cancer. The applied inhibition of PD-1–PD-L1 interactions can restore antitumor T-cell activity and enhance the cellular immune attack on antigens. The overall goals of this short review article are to introduce current cancer immunotherapy and immune checkpoint inhibitors, and to provide new insight into the underlying mechanisms that block immune checkpoints in tumor microenvironment. Furthermore, this review will address the preclinical and clinical trials to determine whether bladder cancer patients could benefit from this new cancer therapy in near future.

Keywords: Immune checkpoint; PD-1; PD-L1; Bladder cancer; Immune therapy

This is an Open Access article distributed under the terms of the Creative Commons Attribution Non-Commercial License (<http://creativecommons.org/licenses/by-nc/4.0>) which permits unrestricted non-commercial use, distribution, and reproduction in any medium, provided the original work is properly cited.

INTRODUCTION

Cancer immuno-therapeutics or tumor immunotherapy in essence can be viewed as anticancer therapies to spark the body's immune system to help fight against cancer [1,2]. In the last several years, new insights into tumor immunology have lead to the development of a new class of drugs termed “immune checkpoint inhibitors”– several of which have demonstrated impressive antitumor responses in several malignancies, including melanoma, non-small cell lung cancer (NSCLC), and renal cell carcinoma (RCC). The personalized cancer immunotherapy (PCI) aims to provide each patient with a treatment tailored to harness his or her own immune system to fight cancer [3,4].

Currently, two representative tumor immunotherapies

are in use in various cancer types–T-cell therapy and immune checkpoint blockade. The T-cell therapy is based on the specialized T cells produced by the immune system to target cancer cells, while immune checkpoint inhibition targets immune regulatory mechanisms and enhancing the immune system to attack cancer cells. These therapies are effective for some portion of patients with metastatic cancer. By blocking the PD-1–PD-L1 pathway, cancer cells become exposed and the immune system becomes triggered to send out the alerting messages and launch a system-wide attack on cancer cells [3,5].

Bladder cancer (BC) is the second most common urological malignancy in humans. There are an estimated 76,960 new cases of cancer in the urinary bladder every year in the United States (US). In 2016, there are expected to be

Received: 1 April, 2016 • **Accepted:** 1 May, 2016

Corresponding Author: Jayoung Kim

Departments of Surgery and Biomedical Sciences, Cedars-Sinai Medical Center, 8700 Beverly Blvd., Los Angeles, CA 90048, USA
TEL: +1-310-423-7168, FAX: +1-310-967-3809, E-mail: Jayoung.Kim@cshs.org

16,390 deaths resulting from BC, with the 5-year survival rate failing to improve significantly in the last 10 years. The clinico-pathologic feature classifies BC into 2 groups; nonmuscle invasive bladder cancer (NMIBC) and muscle-invasive bladder cancer (MIBC). MIBC is the main cause of cancer-specific deaths in BC patients [6,7]. NMIBC shows better survival than other malignancies, however, 30%–50% of patients with NMIBC will experience frequent recurrence after removing the primary tumor, and among them 10%–20% will progress to MIBC [8,9]. Therefore, frequent recurrence and eventual progression to MIBC have been challenges to patients and physicians. Unfortunately, there have been no new U.S. Food and Drug Administration (FDA)-approved therapies for those who cannot tolerate or fail to respond to cisplatin-based chemotherapy, a current gold standard treatment for BC [10,11].

BC is highly immunogenic cancer type with a higher rate of mutations, due to the fact that more mutations associate with a higher chance of tumor antigens triggering the correct immune response. The immune response of host to tumor cells is based on their interactions within the cancer microenvironment. There has been reported various types of tumor-infiltrating immune cells in BC, and how the signaling pathways between tumor and tumor-infiltrating immune cells. Immunotherapy has been used as a treatment for BC in the past. A portion of patients with moderate to high-grade BC—not those with muscle invasive BC—have been given intravesical immunotherapy with bacillus Calmette-Guérin (BCG) [12-14]. BCG is the first U.S. FDA-approved immunotherapy in the US and reduces the risk of BC recurrence by stimulating an immune response. Resultantly, approximately 70% of BC patients go into remission after BCG therapy. Thus, the continued development of checkpoint inhibiting immunotherapies may provide a new treatment for advanced BC. Since the FDA granted atezolizumab (MPDL3280A, the anti-PD-L1 antibody) “breakthrough” status for the advanced and metastatic BC treatment in 2014, a couple of large immunotherapy clinical trials are on going for patients with BC. By blocking inhibitory molecules or, alternatively, activating stimulatory molecules, these treatments are designed to improve pre-existing anticancer immune responses. Currently, there are a number of additional immune-based BC treatments using immune checkpoint inhibitors (such as pembrolizumab or atezolizumab) in development, which include nonmuscle invasive disease with BCG (clinical trial NCT02324582) as well as neo-adjuvant or adjuvant therapy after cystectomy (NCT02451423, NCT02450331). Numerous ongoing studies are expected to establish the worth of PD-1 pathway inhibitors

in other tumor types as well as in combinations with approved agents.

In summary, this short review article will provide a general overview of the classical and current immune therapies for various cancer types. We will also discuss the clinical significance and impacts of immune checkpoint blockage for future BC management and treatment. Finally we will summarize the clinical trials currently on going for BC patients and potential side effects.

CANCER IMMUNOLOGY AND IMMUNE CHECKPOINTS

Cancer immunology is the study interaction between the immune system and cancer cells, contributing to the development of immuno-therapies such as vaccine or antibody therapies. The ultimate purpose of this study is the prevention of cancer initiation and disease progression [15-17]. Immune therapy modulates and boosts the patient's immune response of the tumor leading to an anticancer response. Cancer immuno-surveillance and immuno-editing have been proposed as mechanisms by which tumors escape control through the development of tumor immunogenicity by the body's own immune system [15,18].

BCG has been widely used to treat BC, in particular to NMIBC, as a standard-of-care. The American Urological Association and European Association of Urology guidelines suggest that the first-line of treatment in the management of intermediate or high-risk NMIBC should complete transurethral resection of the tumor followed by BCG intravesical therapy [12-14]. BCG therapy sparks the body's immune system and shows some positive effects, however, approximately 40% of patients show recurrence within 2 years. Population based studies also showed that BCG therapy remains suboptimal and unsuccessful [19-23].

There are several inhibitory immune checkpoints between antigen presenting cells (APCs), T cells, cancer cells, and normal cells et al. T cells enter the active state when T-cell receptors bind to the major histocompatibility complex (MHC)-peptide complex on APCs or tumor cells. Several inhibitory checkpoints interact with their cognate ligands expressed on each respective tumor cell. When T cells encounter an antigen presented by MHC class I molecules on a cancer cell, the cancer cell expresses cognate ligands to interact with inhibitory checkpoints expressed on T cell. In general the immune checkpoint proteins are cell surface molecules on tumor-specific lymphocytes. There have been many advances in cancer immunology with immune checkpoint blockers against cytotoxic T

lymphocyte-associated antigen-4 (CTLA-4) and programmed death receptor ligand (PD-L1) et al. In next sections, we will further discuss immune therapies targeting these immune checkpoints.

TARGETING THE CYTOTOXIC T LYMPHOCYTE-ASSOCIATED ANTIGEN-4 (CTLA-4, CD152) CHECKPOINT

To evade the host immune system, tumors use multiple strategies. In order to engage the immune system against tumors, the interactions between the checkpoint proteins and their ligands can be used to inhibit the proliferation and function of cancer cells. Antibodies targeting and blocking these immuno-inhibitory interactions have been suggested as a new immune therapy. Structurally homologous to the costimulatory molecule CD28, CTLA-4 exerts its inhibitory role by binding to the same ligands, B7.1 (CD80) and B7.2 (CD86) as CD28 does, but with a much higher affinity than CD28 [24-26]. This competitive binding inhibits CD28-induced T-cell activation and decreases cytokine production and cell cycle transition. CTLA-4 is expressed by Tregs, which plays an important role in peripheral tolerance via suppressive activity on cytotoxic T cells.

In 2011, the FDA approved ipilimumab (also called as Yervoy, an immune checkpoint blocking monoclonal antibody to target the CTLA-4) for metastatic melanoma patients [27-29]. As one of the most well-known and well-studied members of the B7 super-family, ipilimumab is used as an adjuvant therapy in patients with melanoma in the skin and lymph nodes or patients whose diseases cannot be removed by surgery. Ipilimumab showed a prolonged survival in patients with advanced melanoma. Although ipilimumab can produce durable long-term responses in patients with advanced melanoma, it showed significant immune-related toxicities [18]. This therapeutic effect of CTLA-4 is being studied [30], not only in melanoma, but also in the treatment of other cancers, such as glioblastoma [31-33]. Antitumor activity by enhancing naturally or vaccine induced T cells was also observed in animal studies, which provided the evidence that the transgenic adenocarcinoma of the mouse prostate-C1 is implantable in the tumor line. Furthermore, these findings led to testing whether CTLA-4 blockade effectively enhances immune response to reject tumors in men with prostate cancer in a clinical setting [34-36].

TARGETING THE IMMUNE CHECKPOINT PROGRAMMED DEATH-1 (PD-1, CD279)

Recent efforts demonstrated that antibodies blocking the PD-1 and PD-L1 pathway could have anti-tumor effects in the tumor microenvironment [37,38]. PD-1 is a surface protein in the activated T cells, and is integral in basic protein function throughout the body. When PD-L1 or PD-L2 (ligands) binds to PD-1, the T cells become inactivated (Fig. 1). PD-L1 and the PD-1 pathway is involved in the T-cell immune evasion through the induction of T-cell apoptosis, anergy, functional exhaustion, or interleukin-10 (IL-10) production.

PD-1 is a type I transmembrane receptor member of the immunoglobulin superfamily, expressed by activated T cells, and binds to two ligands, PD-L1 (B7-H1, CD274) and PD-L2 (B7-DC, CD273)—both of which are part of the B7 immunoglobulin superfamily [39-41]. PD-L1 is highly expressed in tumor cells, APCs, T lymphocytes, epithelial cells, or fibroblasts. PD-L1 secreted from PD-L1-overexpressing tumor cells protects them from CD8⁺ T-cell-mediated tumor cell lysis. Antibodies targeting either PD-1 or PD-L1 pathways reinvigorating the immune system showed clinically meaningful antitumor activity in patients with melanoma and NSCLC, RCC, BC and head and neck cancers. These antibodies showed the less immune-related toxicities, compared to ipilimumab. PD-1 targeting drugs include nivolumab (MDX-1106, BMS-936558, ONO-4538), pembrolizumab (MK-3475), and pidilizumab (CT-011) et al—all of which block PD-L1 from binding to PD-1, resulting in the T cell to continue active.

Nivolumab, which was approved by the FDA in Decem-

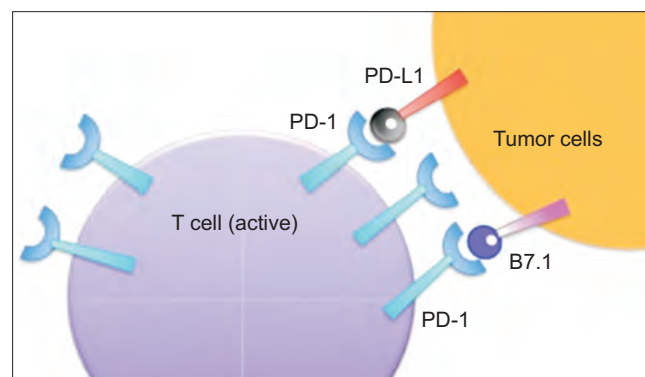


Fig. 1. Tumor cells or tumor-infiltrating immune cells overexpress PD-L1 on their plasma membrane surface. PD-L1 binds to T-cell receptors (B7.1 or PD-1) in active T cells, deactivates cytotoxic T cells. Preventing PD-L1 from binding to its receptors on T cells makes T cells to remain active in tumor microenvironment.

ber 2014, is a representative human IgG4 subtype anti-PD-1 monoclonal antibody that blocks ligand activation of the PD-1 receptor on activated T cells specific for tumor antigens. In the phase I studies, nivolumab was used with a single dose (0.3–10 mg/kg) for patients who no longer responded to other drugs. These treatment-refractory solid tumors include melanoma, colorectal cancer, castration-resistant prostate cancer, NSCLC, and RCC. The serum half-life of nivolumab ranged from 12 to 20 days. Nivolumab can be used alone or with other drugs such as ipilimumab and/or BRAF inhibitors for the patients with resectable or metastatic melanoma if they have no *BRAF* mutation. Advanced LSCLC or RCC patients who failed from cisplatin chemotherapy or angiogenesis inhibitor therapies along with patients suffering from Hodgkin's lymphoma, can be treated by nivolumab. Common treatment-related side effects such as pneumonitis, mild fatigue, diarrhea, pruritus, anorexia, rash, nausea, and decreased appetite were reported. Single-agent trials of nivolumab are ongoing or planned across a spectrum of tumor types including lymphomas, NSCLC, melanoma after progression on anti-CTLA-4 antibody, and hepatocellular carcinoma in multiple clinical trials including NCT02038946, NCT02038933, NCT01721759, NCT02066636, NCT02156804, and NCT01658878.

Pembrolizumab is a humanized monoclonal IgG4 antibody targeting PD-1 receptor. In the preclinical setting, antitumor activity of pembrolizumab was demonstrated in animal models of multiple tumor types. Being initially used to treat melanoma patients, pembrolizumab was approved in September 2014 by the FDA. Pembrolizumab was tested for treatment of advanced melanoma patients containing a BRAF mutation with ipilimumab and a BRAF inhibitor. The phase I study showed that the half-life of pembrolizumab is 13.6–21.7 days. This trial also showed the 37%–38% response rate in patients with advanced melanoma and an overall response rate of 26% in patients who had progressive disease after treatment with ipilimumab [42].

Phase II clinical trials of pembrolizumab were for NSCLC in patients with oligometastatic disease. Ongoing trials of pembrolizumab monotherapy are being conducted in patients with advanced solid tumors (NCT01295827), NSCLC (NCT01840579) and hematologic malignancies (NCT01953692). Randomized trials comparing pembrolizumab to standards of care are ongoing in PD-L1-positive NSCLC patients in comparison to combination chemotherapy (NCT02142738). Single-agent docetaxel in ipilimumab-treatment-naive patients with melanoma are also being tested in comparison to ipilimumab and ipilimumab-refractory patients with melanoma.

Pidilizumab is a humanized IgG1k recombinant anti-PD-1 monoclonal antibody usable for the treatment of cancer and infectious diseases. In preclinical mouse cancer models as well as phase I study in patients with advanced hematologic cancers, pidilizumab has showed antitumor activity. The half-life of pidilizumab was observed very short with range of 217–410 hours. Phase II studies for diffuse large B-cell lymphoma, relapsed follicular lymphoma, or advanced melanoma, showed good results. However, the response rate of the solid tumor appeared to be less than those reported with the other anti-PD-1 inhibitors. Currently, the action mechanism of pidilizumab remains elusive.

TARGETING THE IMMUNE CHECKPOINT PD-L1 (B7-H1, PD-L1 LIGAND, CD274)

Another approach to targeting the PD-1 pathway is through antibodies that bind to and prevent the activity of PD-L1—which is a 40 kDa-transmembrane protein expressed on activated T cells, B cells, and myeloid cells. PD-L1 binding to PD-1 contributes to T-cell inactivation through regulation of signaling pathways (e.g., NF- κ B signaling). In animal models, a blockade of PD-1 has been tested for urine pancreatic carcinoma, B16 melanoma, squamous cell carcinoma, and CT26 colon carcinoma. PD-L1 targeting drugs such as BMS-936559, MPDL3280A, and MEDI-4736 et al. have been developed and applied to patients.

BMS-936559 is a fully humanized IgG4 antibody that inhibits binding of PD-L1 to PD-1 and CD80 with high affinity. MPDL3280A is also a human IgG1 antibody that targets PD-L1. A significant response rate was noted in patients with metastatic melanoma, RCC, NSCLC, or advanced BC in recent phase I studies using MPDL3280A. In particular, clinical trials for BC patients suggested that the PD-L1 expression in tumor-infiltrating immune cells was correlated with a response rate. As biomarkers were identified with treatment response, circulating interferon- γ , IL-18 and activated CD8+ T cells were suggested. Large scale phase II trial in patients with advanced BC is ongoing (NCT02108652) and supported by the FDA. We will address these efforts in the next session in great detail.

In addition to the targeting on PD-1/PD-L1 pathway, recent efforts blocking some of negative immune regulators have been accumulated to pursue the clinical application. These immune regulators include *LAG-3* (lymphocyte-activation gene 3) [43,44], TIM-3 (T-cell immunoglobulin and mucin containing protein-3) [45,46], B7-H3 (B7 homolog 4, B7S1, B7x, VTCN1) [41,47,48] and B7-H4/B7-Hx (V domain Ig suppressor of T-cell activation, B7-H5 or PD-1

Homolog) et al. [41,49-51]. Proteins such as CEACAM1 (carcinoembryonic antigen-related cell adhesion molecule 1 CD66a)—a transmembrane glycoprotein that negatively regulates cytotoxic T-cell proliferation—have been targeted. In melanoma, CEACAM1 monoclonal antibody blocks CEACAM1 homophilic interactions and inhibits cancer cells response to T cell mediated lysis [52-54].

Examples of PD-1–PD-L1 pathway and other immune checkpoint inhibitors in clinical development were summarized in Fig. 2.

PRECLINICAL WORK AND CLINICAL TRIALS FOR BLADDER CANCER PATIENTS

Advanced BC after recurrence is considered as one of the most difficult cancer types, with very low survival rates. No new treatment options for them have been suggested in the last 30 years (since 1998). The standard of care remains

cisplatin-based chemotherapy, however, not all patients are eligible for this treatment. Cisplatin-based systemic chemotherapy administered in the neoadjuvant or adjuvant setting, often combined with radiotherapy, has decreased the morbidity and mortality from recurrent BC. Although these approaches are considered as a current gold standard for metastatic BC, treatment failure frequently occurs due to acquired chemoresistance. The ACS estimates that only 5%–15% 5 years survival rate was found after recurrence in people with advanced BC (stage IV), while approximately 88% of 5-year survival was shown when they were diagnosed in early phase (stage I).

In particular to BC, there are ongoing and planned trials of single-agent or combined inhibitors targeting multiple checkpoints as briefly described in the previous section. In an early-stage phase I trial, atezolizumab—which is designed to target PD-L1 expressing BC and tumor-infiltrating immune cells and inhibit the T-cell activation [55,56]—achieved impressive results. There was an approximately 25% overall response rate in patients with PD-L1-positive metastatic BC (as confirmed to have high levels of PD-L1 expression [e.g., score 2 or 3] by immunohistochemistry [IHC] analysis). Results in this study include that PD-L1 expressions were positively associated with better responses to atezolizumab. In order to evaluate PD-L1 expression on tumor cells and tumor-infiltrating immune cells, the investigational IHC test was developed by Roche Diagnostics. More than half of the patients with high levels of PD-L1 expression experienced tumor shrinkage at 12 weeks and survived at least one year after their treatment. Two of these patients (20%) had a complete response, with no signs of cancer after therapy. Notably, atezolizumab showed the favourable toxicity profile with no renal toxicity in BC patients who are generally old and have a higher incidence of renal impairment [57,58].

Following the success of atezolizumab early trial, a randomized phase III study is ongoing to compare

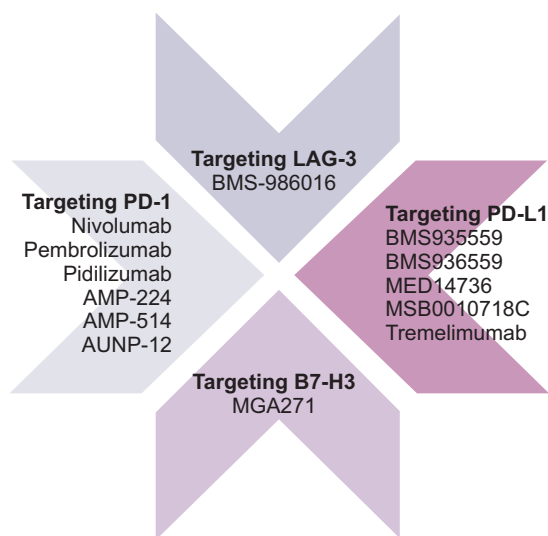


Fig. 2. Examples of immune checkpoint blockade drugs for cancer treatment in development.

Table 1. Immune checkpoint inhibitor-based immunotherapies for bladder cancer

Clinical trial	Phase	Agents
NCT02302807	II	MPDL3280A Pembrolizumab
NCT02324582	III	Pembrolizumab/BCG
NCT02308943	I	Nivolumab, Ipilimumab
NCT02308943	I	Nivolumab, Cabozantinib, Ipilimumab
NCT01693562	I	MED14736
NCT102013804	I	AMP-514
NCT01943461	I	MSB001071BC
NCT01391143	I	MGA271

BCG, bacillus Calmette-Guérin.

atezolizumab with standard-of-care chemotherapy in BC patients with relapse. Another study is used to compare atezolizumab effects in early-stage MIBC patients with high PD-L1 expression and BC patients are at risk for recurrence. All studies include the evaluation of an IHC test to determine PD-L1 expression status.

A recent Lancet paper reported results performed a by a single-arm, multicentre, phase 2 trial [59], which suggested that atezolizumab is effective in heavily pretreated patients with locally advanced or metastatic BC, and that response rates were significantly higher in patients with a greater expression of PD-L1 in tumor-infiltrating immune cells. This was the first report suggesting that the The Cancer Genome Atlas molecular subtypes are associated with atezolizumab response, and that mutation load is important to predict response to atezolizumab in advanced BC. These findings imply that genomic, molecular, and immunological factors are involved in the response rate, and support the idea that PD-L1 can be applicable as a biomarker to subclassify BC patients who are most likely to benefit when treated with atezolizumab or a combination of atezolizumab and another medicine. Table 1 summarizes the clinical trials.

CONCLUDING REMARKS AND PERSPECTIVES

More recent efforts have accumulated on the activation of antitumor immunity of tumor microenvironment using antibodies blocking the PD-1–PD-L1 pathway. In this short review article, we tried to address and summarize early stage clinical studies and clinical trials in various cancer types including advanced BC. There have been much efforts to develop combination regimens using PD-1 blockade as a backbone in unison with other chemotherapeutic drugs. Combination therapies to treat BC involving cytotoxic chemotherapy, antiangiogenic agents, alternative immune-checkpoint inhibitors, immuno-stimulatory cytokines and cancer vaccines are currently under clinical investigation. The combination treatment with checkpoint blockade and small molecule inhibitors is an attractive strategy since it would increase tumor antigen presentation.

For the PCI, another important research topic would be how to monitor the responses to immune therapy in patients. Possibly noninvasive (or minimally invasive) and accurate biomarkers should be urgently needed. However, we currently do not have gold standard biomarkers to predict the likelihood of response for each patient for immune checkpoint inhibitors. Efforts should be focused on identification of predictive biomarkers of responses, which

may lead to advances in BC treatment and control.

CONFLICTS OF INTEREST

The author has nothing to disclose.

ACKNOWLEDGMENTS

The authors acknowledge support from National Institutes of Health grants (1U01DK103260, 1R01DK100974, U24 DK097154, NIH NCATS UCLA CTSI UL1TR000124 [to J.K.], Department of Defense grants (PR140285 [to J.K.]), Centers for Disease Control and Prevention (1U01DP006079 [to J.K.]), and US-Egypt Science and Technology Joint Fund. IMAGINE NO IC Research Grant, the Steven Spielberg Discovery Fund in Prostate Cancer Research Career Development Award (to J.K.). J.K. is former recipient of Interstitial Cystitis Association Pilot Grant, a Fishbein Family IC Research Grant, New York Academy of Medicine, and Boston Children's Hospital Faculty Development.

REFERENCES

1. Dunn GP, Old LJ, Schreiber RD. The three Es of cancer immunoeediting. *Annu Rev Immunol* 2004;22:329-60.
2. Finn OJ. Immuno-oncology: understanding the function and dysfunction of the immune system in cancer. *Ann Oncol* 2012;23 Suppl 8:viii6-9.
3. Yuan J, Hegde PS, Clynes R, Foukas PG, Harari A, Kleen TO, et al. Novel technologies and emerging biomarkers for personalized cancer immunotherapy. *J Immunother Cancer* 2016;4:3.
4. Hammerich L, Binder A, Brody JD. In situ vaccination: cancer immunotherapy both personalized and off-the-shelf. *Mol Oncol* 2015;9:1966-81.
5. Nirschl CJ, Drake CG. Molecular pathways: coexpression of immune checkpoint molecules. Signaling pathways and implications for cancer immunotherapy. *Clin Cancer Res* 2013;19:4917-24.
6. Kaufman DS, Shipley WU, Feldman AS. Bladder cancer. *Lancet* 2009;374:239-49.
7. Parkin DM, Bray F, Ferlay J, Pisani P. Global cancer statistics, 2002. *CA Cancer J Clin* 2005;55:74-108.
8. Messing E. Markers of detection. *Urol Oncol* 2007;25:344-7.
9. Quan C, Cha EJ, Lee HL, Han KH, Lee KM, Kim WJ. Enhanced expression of peroxiredoxin I and VI correlates with development, recurrence and progression of human bladder cancer. *J Urol* 2006;175:1512-6.
10. Bellmunt J, Pons F, Orsola A. Molecular determinants of response to cisplatin-based neoadjuvant chemotherapy. *Curr*

- Opin Urol 2013;23:466-71.
11. Galluzzi L, Senovilla L, Vitale I, Michels J, Martins I, Kepp O, et al. Molecular mechanisms of cisplatin resistance. *Oncogene* 2012;31:1869-83.
 12. Lenis AT, Chamie K. Bladder cancer in 2014: from the genomic frontier to immunotherapeutics. *Nat Rev Urol* 2015;12:74-6.
 13. Macleod LC, Ngo TC, Gonzalzo ML. Complications of intravesical bacillus calmette-guerin. *Can Urol Assoc J* 2014;8(7-8):E540-4.
 14. Steinberg RL, Thomas LJ, Nepple KG. Intravesical and alternative bladder-preservation therapies in the management of non-muscle-invasive bladder cancer unresponsive to bacillus Calmette-Guerin. *Urol Oncol* 2016 Jan 14 [Epub]. <http://dx.doi.org/10.1016/j.urolonc.2015.12.004>.
 15. Pardoll DM. The blockade of immune checkpoints in cancer immunotherapy. *Nat Rev Cancer* 2012;12:252-64.
 16. Chen DS, Mellman I. Oncology meets immunology: the cancer-immunity cycle. *Immunity* 2013;39:1-10.
 17. Lesterhuis WJ, Haanen JB, Punt CJ. Cancer immunotherapy: revisited. *Nat Rev Drug Discov* 2011;10:591-600.
 18. Zitvogel L, Tesniere A, Kroemer G. Cancer despite immunosurveillance: immunoselection and immunosubversion. *Nat Rev Immunol* 2006;6:715-27.
 19. Kamat AM, Sylvester RJ, Bohle A, Palou J, Lamm DL, Brausi M, et al. Definitions, end points, and clinical trial designs for non-muscle-invasive bladder cancer: recommendations from the international bladder cancer group. *J Clin Oncol* 2016 [Epub]. <http://dx.doi.org/10.1200/JCO.2015.64.4070>.
 20. Liu S, Hou J, Zhang H, Wu Y, Hu M, Zhang L, et al. The evaluation of the risk factors for non-muscle invasive bladder cancer (NMIBC) recurrence after transurethral resection (TURBt) in Chinese population. *PLoS One* 2015;10:e0123617.
 21. Matsumoto K, Gondo T, Hayakawa N, Maeda T, Ninomiya A, Nakamura S. The role of single instillation chemotherapy in patients who receive subsequent bacillus Calmette-Guerin: a retrospective single centre study, and systematic review of the literature. *Can Urol Assoc J* 2015;9(7-8):E411-6.
 22. O'Regan T, Tatton M, Lyon M, Masters J. The effectiveness of BCG and interferon against non-muscle invasive bladder cancer: a New Zealand perspective. *BJU Int* 2015;116 Suppl 3:54-60.
 23. Ahn JJ, Ghandour RA, McKiernan JM. New agents for bacillus Calmette-Guerin-refractory nonmuscle invasive bladder cancer. *Curr Opin Urol* 2014;24:540-5.
 24. Hodi FS. Cytotoxic T-lymphocyte-associated antigen-4. *Clin Cancer Res* 2007;13(18 Pt 1):5238-42.
 25. Leach DR, Krummel MF, Allison JP. Enhancement of antitumor immunity by CTLA-4 blockade. *Science* 1996;271:1734-6.
 26. Mokyr MB, Kalinichenko T, Gorelik L, Bluestone JA. Realization of the therapeutic potential of CTLA-4 blockade in low-dose chemotherapy-treated tumor-bearing mice. *Cancer Res* 1998;58:5301-4.
 27. Hodi FS, O'Day SJ, McDermott DF, Weber RW, Sosman JA, Haanen JB, et al. Improved survival with ipilimumab in patients with metastatic melanoma. *N Engl J Med* 2010;363:711-23.
 28. Li Z, Chen L, Rubinstein MP. Cancer immunotherapy: are we there yet? *Exp Hematol Oncol* 2013;2:33.
 29. Peggs KS, Quezada SA. Ipilimumab: attenuation of an inhibitory immune checkpoint improves survival in metastatic melanoma. *Expert Rev Anticancer Ther* 2010;10:1697-701.
 30. Robert C, Ribas A, Wolchok JD, Hodi FS, Hamid O, Kefford R, et al. Anti-programmed-death-receptor-1 treatment with pembrolizumab in ipilimumab-refractory advanced melanoma: a randomized dose-comparison cohort of a phase 1 trial. *Lancet* 2014;384:1109-17.
 31. Brower V. Early-stage progress on glioma vaccines. *J Natl Cancer Inst* 2011;103:1361-2.
 32. Preusser M, Lim M, Hafler DA, Reardon DA, Sampson JH. Prospects of immune checkpoint modulators in the treatment of glioblastoma. *Nat Rev Neurol* 2015;11:504-14.
 33. Ribas A. Clinical development of the anti-CTLA-4 antibody tremelimumab. *Semin Oncol* 2010;37:450-4.
 34. Kwek SS, Lewis J, Zhang L, Weinberg V, Greaney SK, Harzstark AL, et al. Preexisting levels of CD4 T cells expressing PD-1 are related to overall survival in prostate cancer patients treated with ipilimumab. *Cancer Immunol Res* 2015;3:1008-16.
 35. Reese Z, Straubhar A, Pal SK, Agarwal N. Ipilimumab in the treatment of prostate cancer. *Future Oncol* 2015;11:27-37.
 36. Sobol I, Thompson RH, Dong H, Krco C, Kwon ED. Immunotherapy in prostate cancer. *Curr Urol Rep* 2015;16:34.
 37. Okazaki T, Honjo T. PD-1 and PD-1 ligands: from discovery to clinical application. *Int Immunol* 2007;19:813-24.
 38. Chen DS, Irving BA, Hodi FS. Molecular pathways: next-generation immunotherapy. Inhibiting programmed death-ligand 1 and programmed death-1. *Clin Cancer Res* 2012;18:6580-7.
 39. Dong H, Strome SE, Salomao DR, Tamura H, Hirano F, Flies DB, et al. Tumor-associated B7-H1 promotes T-cell apoptosis: a potential mechanism of immune evasion. *Nat Med* 2002;8:793-800.
 40. Seliger B, Marincola FM, Ferrone S, Abken H. The complex role of B7 molecules in tumor immunology. *Trends Mol Med* 2008;14:550-9.
 41. Zou W, Chen L. Inhibitory B7-family molecules in the tumour microenvironment. *Nat Rev Immunol* 2008;8:467-77.
 42. Tumeh PC, Harview CL, Yearley JH, Shintaku IP, Taylor EJ, Robert L, et al. PD-1 blockade induces responses by inhibiting adaptive immune resistance. *Nature* 2014;515:568-71.

43. Goldberg MV, Drake CG. LAG-3 in cancer immunotherapy. *Curr Top Microbiol Immunol* 2011;344:269-78.
44. Triebel F, Jitsukawa S, Baixeras E, Roman-Roman S, Genevee C, Viegas-Pequignot E, et al. LAG-3, a novel lymphocyte activation gene closely related to CD4. *J Exp Med* 1990;171:1393-405.
45. Ngiow SF, von Scheidt B, Akiba H, Yagita H, Teng MW, Smyth MJ. Anti-TIM3 antibody promotes T cell IFN- γ -mediated antitumor immunity and suppresses established tumors. *Cancer Res* 2011;71:3540-51.
46. Zhu C, Anderson AC, Schubart A, Xiong H, Imitola J, Khoury SJ, et al. The Tim-3 ligand galectin-9 negatively regulates T helper type 1 immunity. *Nat Immunol* 2005;6:1245-52.
47. Roth TJ, Sheinin Y, Lohse CM, Kuntz SM, Frigola X, Inman BA, et al. B7-H3 ligand expression by prostate cancer: a novel marker of prognosis and potential target for therapy. *Cancer Res* 2007;67:7893-900.
48. Suh WK, Gajewska BU, Okada H, Gronski MA, Bertram EM, Dawicki W, et al. The B7 family member B7-H3 preferentially down-regulates T helper type 1-mediated immune responses. *Nat Immunol* 2003;4:899-906.
49. Seliger B, Quandt D. The expression, function, and clinical relevance of B7 family members in cancer. *Cancer Immunol Immunother* 2012;61:1327-41.
50. Zang X, Loke P, Kim J, Murphy K, Waitz R, Allison JP. B7x: a widely expressed B7 family member that inhibits T cell activation. *Proc Natl Acad Sci U S A* 2003;100:10388-92.
51. Zang X, Thompson RH, Al-Ahmadie HA, Serio AM, Reuter VE, Eastham JA, et al. B7-H3 and B7x are highly expressed in human prostate cancer and associated with disease spread and poor outcome. *Proc Natl Acad Sci U S A* 2007;104:19458-63.
52. Gray-Owen SD, Blumberg RS. CEACAM1: contact-dependent control of immunity. *Nat Rev Immunol* 2006;6:433-46.
53. Kuespert K, Pils S, Hauck CR. CEACAMs: their role in physiology and pathophysiology. *Curr Opin Cell Biol* 2006;18:565-71.
54. Thies A, Moll I, Berger J, Wagener C, Brummer J, Schulze HJ, et al. CEACAM1 expression in cutaneous malignant melanoma predicts the development of metastatic disease. *J Clin Oncol* 2002;20:2530-6.
55. Taylor RC, Patel A, Panageas KS, Busam KJ, Brady MS. Tumor-infiltrating lymphocytes predict sentinel lymph node positivity in patients with cutaneous melanoma. *J Clin Oncol* 2007;25:869-75.
56. Sharma P, Shen Y, Wen S, Yamada S, Jungbluth AA, Gnjatic S, et al. CD8 tumor-infiltrating lymphocytes are predictive of survival in muscle-invasive urothelial carcinoma. *Proc Natl Acad Sci U S A* 2007;104:3967-72.
57. Fenner A. Bladder cancer: could MPDL3280A offer a therapeutic breakthrough in metastatic bladder cancer? *Nat Rev Urol* 2015;12:61.
58. Powles T, Eder JP, Fine GD, Braithel FS, Loriot Y, Cruz C, et al. MPDL3280A (anti-PD-L1) treatment leads to clinical activity in metastatic bladder cancer. *Nature* 2014;515:558-62.
59. Rosenberg JE, Hoffman-Censits J, Powles T, van der Heijden MS, Balar AV, Necchi A, et al. Atezolizumab in patients with locally advanced and metastatic urothelial carcinoma who have progressed following treatment with platinum-based chemotherapy: a single-arm, multicentre, phase 2 trial. *Lancet* 2016 Mar 4 [Epub]. [http://dx.doi.org/10.1016/S0140-6736\(16\)00561-4](http://dx.doi.org/10.1016/S0140-6736(16)00561-4).

Metabolic profiling of cholesterol and sex steroid hormones to monitor urological diseases

Ju-Yeon Moon¹, Man Ho Choi¹ and Jayoung Kim^{2,3}

¹Molecular Recognition Research Center, Korea Institute of Science and Technology, Seoul, Korea

²Departments of Surgery and Biomedical Sciences, Cedars-Sinai Medical Center, Los Angeles, California, USA

³Department of Medicine, University of California, Los Angeles, California, USA

Correspondence should be addressed to M H Choi or J Kim
Email
mh_choi@kist.re.kr or
Jayoung.Kim@cshs.org

Abstract

Cholesterol and sex steroid hormones including androgens and estrogens play a critical role in the development and progression of urological diseases such as prostate cancer. This disease remains the most commonly diagnosed malignant tumor in men and is the leading cause of death from different cancers. Attempts to understand the role of cholesterol and steroid metabolism in urological diseases have been ongoing for many years, but despite this, our mechanistic and translational understanding remains elusive. In order to further evaluate the problem, we have taken an interest in metabolomics; a discipline dedicated to the systematic study of biologically active metabolites in cells, tissues, hair and biofluids. Recently, we provided evidence that a quantitative measurement of cholesterol and sex steroid metabolites can be successfully achieved using hair of human and mouse models. The overall goal of this short review article is to introduce current metabolomic technologies for the quantitative biomarker assay development and also to provide new insight into understanding the underlying mechanisms that trigger the pathological condition. Furthermore, this review will place a particular emphasis on how to prepare biospecimens (e.g., hair fiber), quantify molecular profiles and assess their clinical significance in various urological diseases.

Key Words

- ▶ steroid
- ▶ cholesterol
- ▶ biomarkers
- ▶ mass spectrometry
- ▶ metabolomics
- ▶ urological cancers
- ▶ prostate diseases

Endocrine-Related Cancer
(2016) **23**, R455–R467

Introduction

Urological health conditions have become increasingly prevalent in the world, affecting individuals spanning a multitude of ages. Prostate cancer (PC) is one such condition that has seen an exponential rise in the number of cases, with over 220,000 new cases having been recorded in 2015 alone. The effects of PC can even be seen outside of the USA, as it is the most common cancer among men in all developed countries. However, not all urological health problems are related to cancer, and the most common of these include the common occurrence of urinary tract infection, kidney stones,

incontinence and benign prostatic hyperplasia (BPH). These diseases pose both a financial and physiological burden, indicating the need for further research in the prevention and study of these urological conditions. The use of biomarkers for early diagnosis in patients would be valuable in reducing the recurrence and progression of these urological health problems. As an example, there are clinical needs for biomarkers to identify PC patients who have aggressive disease and are more likely to experience disease progression, which could help increase the ability to manage patients with urological disease.

Research has indicated that high levels of cholesterol and sex steroid hormones are risk factors of urological disease (Allott & Hursting 2015). A correlation has been studied, relating a typical Western diet to an increase in the risk of urological disease (Ito 2014, YuPeng *et al.* 2015). Western diet normally features a high intake of red meat and dairy products, providing a high intake of cholesterol and calories to individuals consuming such foods (Ito 2014, YuPeng *et al.* 2015). These studies have also provided evidence that patients with a metabolic syndrome (e.g., obesity, impaired fasting glucose tolerance, high blood pressure, hypertension, dyslipidemia, type 2 diabetes and cardiovascular diseases) were more likely to have great prostate volume increase (Gacci *et al.* 2015), suggesting a high concentration of cholesterol within urological disease. Hypercholesterolemia, an obesity-associated co-morbidity, influences approximately 20% of the US population (Fryar *et al.* 2010). Furthermore, cholesterol-lowering drugs such as statins may reduce the risk of PC (Nielsen *et al.* 2012).

Sex steroids and their receptors play a crucial role in the determination of urological disease development. Androgen and its derivatives including dihydrotestosterone (DHT) are vital in not only male development but also the development of PC and BPH. Following androgen binding, androgen receptors undergo a multi-step process involving dimerization, phosphorylation and translocation to the nucleus. Once localized, the receptor acts as a transcription factor and binds to androgen receptor elements (AREs) in order to begin assembling a transcription complex of co-activators and co-repressors (Dehm & Tindall 2007). These complexes are key oncogenic risk factors associated with the increased risk of PC and BPH.

In order to better understand the metabolism and internal mechanisms underlying urological diseases, several resources have been studied. Metabolomic fingerprints have been analyzed in addition to the use of non-invasive biomarkers such as urine or blood-based assays. Hair-based metabolomic profiles could be useful in confirming the correlation between cholesterol and sex steroid hormones with urological diseases. Using human and animal hair samples in order to study the metabolite process specific to urological disease, our research group established the novel mass spectrometry-based protocols for steroid metabolomics with the goal of monitoring hormone levels, which can be used for drug treatment of PC and BPH patients.

This short review article aims to provide support for the claim that a correlation exists between cholesterol and steroid sex hormones with urological diseases. By specifically

examining PC and BPH, we discuss the significance of cholesterol and steroid sex hormones associated with these health conditions, while also introducing current technologies that can be used to measure the amount of cholesterol and sex steroid hormones in various sources throughout the body (tissues, urine, blood and hair). The final topic deals with the use of hair metabolomics to identify potential biomarkers for PC and BPH.

Metabolism of cholesterol and sex steroid hormones

Cholesterol is a crucial component of mammalian cell membranes, as it serves diverse cellular functions – including the modulation of membrane permeability and fluidity (Maxfield & Tabas 2005). Cholesterol synthesis pathways are shown in Fig. 1. Cholesterol is also the precursor of all steroid hormones and bile acids and plays important roles in membrane trafficking, transmembrane signaling processes as well as cell proliferation (Goedeke & Fernandez-Hernando 2012). Cholesterol is made from the conversion of citrate, derived from the tricarboxylic acid (TCA) cycle in the mitochondria. Here, acetyl coenzyme A (acetyl-CoA) is formed and followed by the mevalonate pathway. This combination of reactions is primarily regulated by a rate-limiting step catalyzed by 3-hydroxy-3-methylglutaryl-coenzyme A (HMG-CoA) reductase, an integral membrane protein of the smooth endoplasmic reticulum, which converts HMG-CoA to a six-carbon intermediate mevalonate. This intermediate is then metabolized via a series of isoprenoid intermediates to squalene (the polymerization of six five-carbon isoprene units to form the 30-carbon linear structure of squalene). The cyclization of squalene reacted by squalene cyclase and one molecule of O₂ forms the four fused rings of the steroid nucleus, which results in the synthesis of lanosterol as a cholesterol precursor.

Cholesterol in tissues and blood is metabolized as follows. First, it can be fatty acylated to form cholesteryl esters (CEs) through sterol O-acyltransferase (also called acyl-CoA cholesterol acyltransferase or simple ACAT) or lecithin-cholesterol acyltransferase (LCAT, also called phosphatidylcholine-sterol O-acyltransferase). The CEs then serve as a major form of transporter as plasma lipoproteins, or as storage units in the form of lipid droplets (Kraemer 2007). Secondly, cholesterol can be oxidized to form oxygenated derivatives of cholesterol, termed oxysterols, by enzymatic (hydroxylase, cytochrome P450 (CYP) families) or non-enzymatic hydroxylations at the C-4, C-7, C-19, C-20, C-24, C-25 and C-27 positions

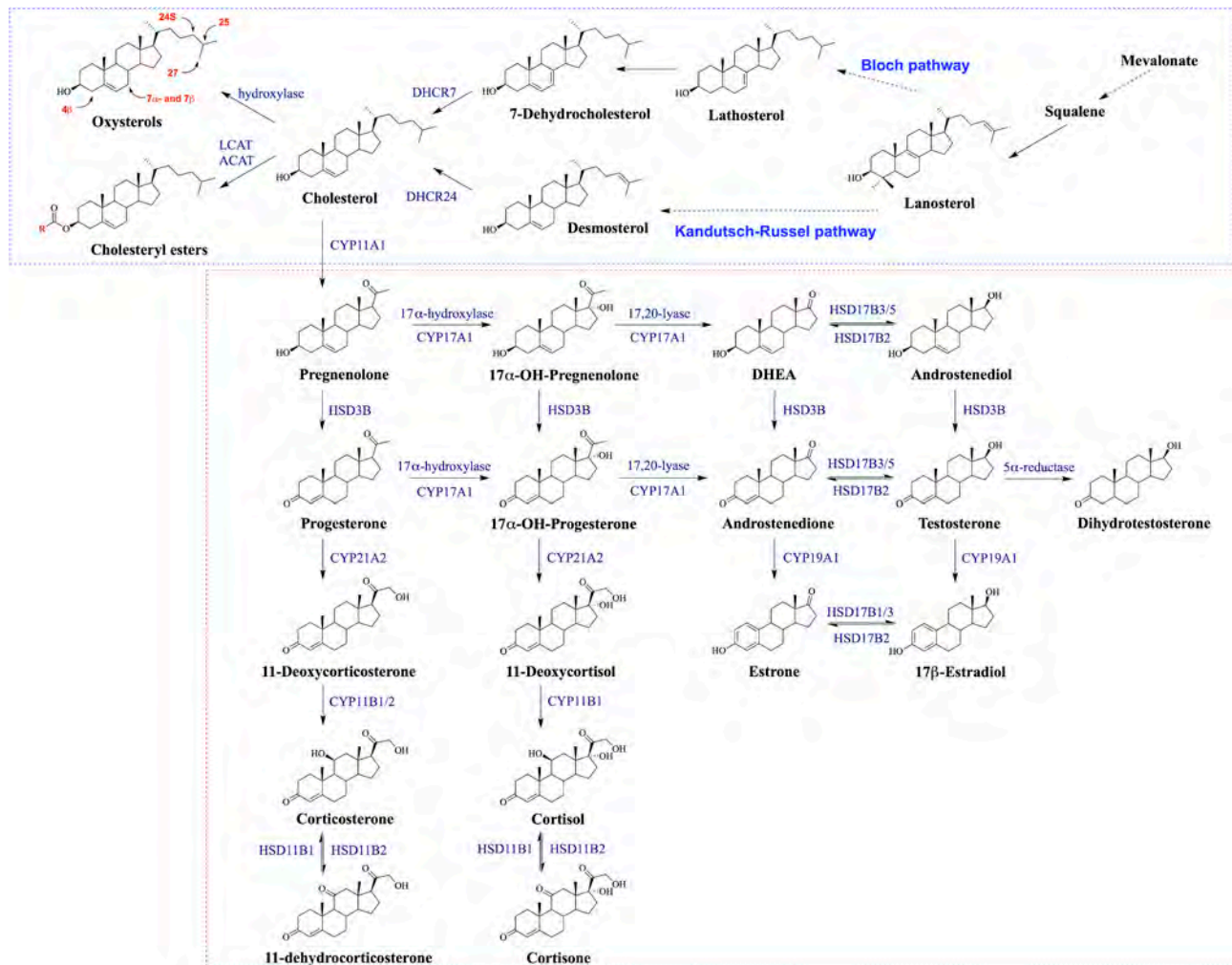


Figure 1
Overview of cholesterol and steroid hormone pathways.

(Pikuleva 2006, Son *et al.* 2014, Seo & Choi 2015). Oxysterols serve as regulators of cholesterol homeostasis, allowing cells to manage large cholesterol loads rapidly and avoid triggering cytotoxic events (Bjorkhem 2002, Bielska *et al.* 2012). For example, cholesterol activates 7 α -hydroxylase (CYP7A1), which produces 7 α -hydroxycholesterol as the major pathway for elimination of cholesterol from the body (Bjorkhem 2002). In addition, the most important oxysterols (as transport forms of cholesterol) are side chain-oxidized oxysterols at the C-24 or 27 position by CYP46 and CYP27, respectively, which flow continuously from peripheral tissues to the liver and become further oxidized into bile acids or other water-soluble metabolites (Nielsen *et al.* 2012). 4 β -hydroxycholesterol catalyzed by CYP 3A4 may indicate slow elimination when its levels are high in the blood (Bodin *et al.* 2002). In addition,

the 25-hydroxycholesterol that is produced and secreted by macrophages can regulate interleukin-1 β , a potent cytokine, facilitating cross talk between cholesterol metabolism and the immune system (Simon 2014).

Cholesterol is also metabolized to steroid hormones, which regulate physiological and pharmacological processes in the body (Falkenstein *et al.* 2000). Steroidogenic enzymes are responsible for the biosynthesis of cholesterol from various steroid hormones including corticoids, progestins, androgens and estrogens. These are generally synthesized in the adrenal cortex, gonads (testes and ovaries), brain, placenta and adipose tissue (Falkenstein *et al.* 2000, Payne & Hales 2004). In biosynthetic pathways of steroid hormones, two major types of enzymes are involved: cytochrome P450 enzymes (CYPs) and hydroxysteroid dehydrogenases (HSDs).

Initially, steroid hormones start with the conversion of cholesterol to pregnenolone by rate-limiting enzyme CYP11A (cholesterol side-chain cleavage), which is bound to the inner membrane of the mitochondrion in all steroidogenic tissues. This acute regulation is mediated by the steroidogenic acute regulatory protein (StAR) on the outer membrane, which facilitates the rapid influx of cholesterol into mitochondria (Payne & Hales 2004, Miller 2008).

Cholesterol and sex steroid hormones in prostate health

Cholesterol, a critical component of the cellular plasma membrane, contributes to the maintenance of plasma membrane fluidity. Also, cholesterol is an important component of lipid raft micro-domains on plasma membrane and regulates intracellular signaling processes (Krycer & Brown 2013). Cholesterol is also the precursor for endogenous sex steroid biosynthesis, suggesting that elevated serum cholesterol levels might be somehow linked to the increased risk of prostate cancer (Fagherazzi *et al.* 2010). Steroid biosynthesis may be an important mechanism linking cholesterol and prostate cancer and BPH.

StAR and CYP11A are involved in converting cholesterol into pregnenolone and progesterone, which are sequentially converted to DHEA and androstenedione by CYP17A. DHEA is then converted to form testosterone and then DHT via HSD3B, HSD17B3 (or AKR1C3) and SRD5A. The 5 α -androstenedione pathway leads to produce DHEA, androstenedione and then testosterone. There are multiple enzymes, which actively play roles in cholesterol and sex steroid hormone synthesis. AKR1C1 converts DHT to 5 α -androstane-3,17-diol (3 α -androstenediol or 3 α -diol) and AKR1C2 converts DHT to 5 α -androstane-3,17-diol (3 β -diol). UGT2B15 and UGT2B17 irreversibly inhibit androgen signaling by glucuronidation, which is the known rate-limiting step of androgen signaling.

Prostate epithelial cells have higher cholesterol content, compared with other organs, and cholesterol levels increase during progression of normal healthy prostate into PC or BPH (Krycer & Brown 2013), suggesting that cholesterol accumulation may benefit prostate cancer or BPH progression. Accumulating evidence demonstrates that elevated cholesterol is a risk factor of more aggressive PC – in terms of recurrence or mortality (Platz *et al.* 2008, 2009, Farwell *et al.* 2011, Mondul *et al.* 2011, Shafique *et al.* 2012). Our previous studies also support the hypothesis that cholesterol promotes PC growth *in vitro* and *in vivo*

(Zhuang *et al.* 2002). Cholesterol-lowering drugs (e.g., statins, zetia or combination of both) also lowered serum as well as intratumoral androgen levels, leading to the arrest of tumor growth (Mostaghel *et al.* 2012). Statins have been used for patients with cardiovascular diseases (Ridker & Cook 2013). There are a series of epidemiological studies suggesting that statins could reduce cancer risk (Farwell *et al.* 2008), chronic inflammation and angiogenesis (Demierre *et al.* 2005, Pelton *et al.* 2012). However, several meta-analyses have also reported a null association between statin use and risk of prostate cancer recurrence (Mass *et al.* 2012, Park *et al.* 2013, Scosyrev *et al.* 2013), suggesting that they remain contradictory in the field.

Analytical techniques for sex steroid metabolome

Tissue- and biofluid-based metabolite profiling

As the most common specimens used in biomarker discovery, tissues and biological fluids have been used for metabolite profiling. Both formalin-fixed, paraffin-embedded (FFPE) and fresh-frozen tissue specimens can be used for the tissue-based metabolomic studies. Metabolite extraction from FFPE tissues includes de-paraffinization steps with xylene, homogenization in MeOH:H₂O solution (1:1 v/v), vortexing and sonication.

Biofluids such as urine and serum have a great advantage of being the easiest samples to work with, urine being the most common and accessible samples for metabolomic analyses. Metabolome in urine can be greatly influenced by age, occupation, environmental factors, different diets, hormones and lifestyle such as exercise, and urine specimens should be immediately stored within a few hours after sample collection at –80°C until further analysis.

In order to identify the steroid signatures and to suggest steroid metabolism-associated enzyme activities through profiling of tissues or biofluid-derived metabolites, we can use quantitative mass spectrometry combined with gas or liquid chromatographic separation techniques (GC–MS or LC–MS) for steroid profiling. Our previous studies to develop the quantitative steroid signatures using GC–MS (Ha *et al.* 2009, Moon *et al.* 2009) demonstrated that we could measure concentrations of over 65 endogenous steroids and cholesterols in plasma or urine samples at a time. In addition, LC–MS-based steroid profiling enables to quantify 21 endogenous corticoids including urinary glucocorticoids and mineralocorticoids (Cho *et al.* 2009). Both GC–MS and LC–MS urinary steroid signatures were

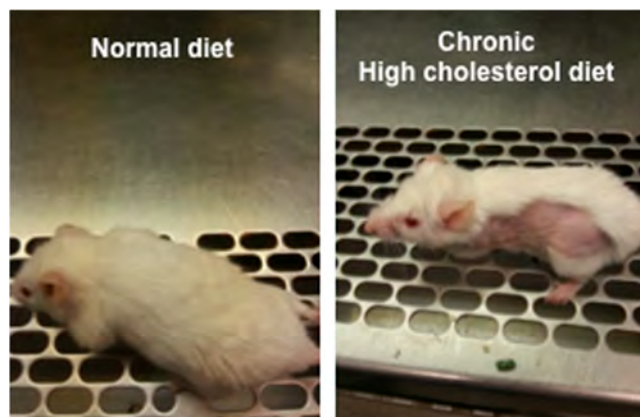


Figure 2
Our metabolomic profile showing the distinct patterns between prostate cancer and healthy controls.

applied into the samples obtained from patients with PC or BPH from age- and gender-matched healthy subjects.

As a good example, our GC–MS analysis data showed that urinary cholesterol levels in BPH patients were significantly increased in those with healthy controls ($P=0.015$) (Fig. 2A). First morning urine samples obtained from 59 BPH patients (age: 65.3 ± 8.2 years) and 41 healthy male subjects (age: 56.7 ± 7.1 years) were used for this analysis. We screened various cholesterol and sex hormones and found that cholesterol level could segregate BPH patients from healthy controls (AUC, 0.66) (Fig. 2B).

Hair metabolomics for hair-based metabolite profile

Although urine and blood are widely used to measure sex steroid hormones in many clinical and toxicological studies (Wudy et al. 2000, Choi et al. 2011, Choi & Chung 2015, Son et al. 2015), their concentrations fluctuate on a daily basis. Additionally, careful handling of biological fluids is required for sample collection, handling, processing, storage and transport to the laboratory (Two Roger & Hankinson 2006) under controlled circumstances. In contrast, hair grows about 1 cm per month (Wennig 2000). Thus, it can offer the possibility of reflecting and revealing historical information of exposure to drug abuse, environmental toxins and endogenous or exogenous hormones over several months (Villain et al. 2004). Moreover, hair sampling is non-invasive and the storage and processing of it is much simpler than plasma or serum (Sulek et al. 2014). Therefore, hair analysis has been used in chemical toxicology, forensic science, doping control and clinical applications (Cho et al. 2010, Pichini et al. 2012, Choi et al. 2013, Gray et al. 2013,

Pereg et al. 2013, Chan et al. 2014, Veldhorst et al. 2014, Son et al. 2016).

Sample preparation: extraction from hair fiber

Hair analysis in steroid research is mainly coupled with solubilization or digestion of the hair matrix after cutting (Choi et al. 2001a, 2013, Cho et al. 2010). In general, androgens and sterols are extracted from the hair matrix by alkaline hydrolysis involving the complete digestion of hair (Choi & Chung 1999, Choi et al. 2000, Ryu et al. 2006), whereas corticoids are unstable under these conditions. Hence, ultrasonication with an organic solvent was also tested for steroid profiling including androgens, sterols, corticoids and progestins, which enables the profiling of hair steroids (Jung et al. 2011). A mixed solvent of methanol and dichloromethane is an effective solvent for lipid extraction from biological samples (Folch et al. 1957). However, absolute methanol was chosen as the extraction solvent to decrease sample complexity and simplify the sample purification steps. The hair strands were washed with isopropyl alcohol to prevent contamination and were then obtained simply by cutting the specific lengths from the proximal part of the vertex scalp (Jung et al. 2011). Thirty milligrams of chopped hair were incubated with 0.5 mL methanol in an ultrasonic bath for 1 h at 50°C. After cooling to room temperature, a methanolic solution was diluted with 5.5 mL sodium acetate buffer (pH 5.2) to less than 8% methanol. The samples were loaded directly onto the Oasis HLB™ (divinylbenzene and *N*-vinylpyrrolidone) solid-phase extraction (SPE) cartridge, which is preferable for the sample purification of steroidal compounds (Moon et al. 2009, Choi & Chung 2015). The SPE procedure removed more effective interference from the hair matrix and gave a lower matrix background than liquid–liquid extraction (LLE) (Mondul et al. 2011). However, these extraction processes require a relatively large amount of hair matrix and extensive, time-consuming pretreatment procedures.

Recently, the pulverization method has been used to highly disintegrate hair components and has allowed for efficient extraction (Miyaguchi et al. 2007, Kim et al. 2011, Son et al. 2016). Compared with our previous techniques (Ryu et al. 2006, Jung et al. 2011), this method enables increased extractable surface area of the hair matrix through the destruction of the cuticle layer and thereby the permeation of an extraction solvent into the hair. The pulverization of hair using a ball mill such as zirconia beads was achieved for improved extraction yields of steroids and sterols and therefore can reduce sample preparation

times as well as sample amounts significantly. Therefore, hair steroid analysis has been successfully applied in clinical applications using sampling of 100–150 strands of hair and extraction from a minimum of 10 mg (Choi *et al.* 2013). Hair sterols were measured in only two strands of 3 cm hair segments, corresponding roughly to a period of recent 3 months.

The sample preparation technique is also required for the removal of endogenous matrix components from lipid-rich samples. In particular, phospholipids are extremely abundant in hair as well as blood (Singh & Gershbein 1967). The use of hybrid precipitation/SPE plates for selective removal of phospholipids and precipitated proteins has been increasing over the past few years (Bylda *et al.* 2014). The hybrid SPE-precipitation cartridge (H-PPT) applies to reduce the phospholipid-based matrix effect, which is a superior purification method for sterol analysis (Pucci *et al.* 2009, Son *et al.* 2014) relative to membrane filtration (Miyaguchi *et al.* 2007). The H-PPT specifically retains phospholipids by Lewis acid–base interactions between the zirconia-coated silica particles bonded to the stationary phase and the phosphate group of the phospholipids, which provides simple yet rapid selective removal of interference (Bylda *et al.* 2014). When the extraction recoveries of the sterols were compared at different pulverization times (1, 2, 5, 10, 15 and 20 min) and different frequencies (10, 15, 20, 25 and 30 Hz), 10 min at 25 Hz was chosen as the optimized extraction method (Son *et al.* 2016). To facilitate sterol extraction, two strands of 3 cm-long hair samples were pulverized in 0.5 mL methanol using a TissueLyser for 10 min at 25 Hz in a 2 mL Safe-Lock tube containing three zirconia beads (3.0 mm I.D.). Bead-assisted liquid–liquid extraction via the addition of methanol and then centrifugation can be achieved simultaneously with pulverization, extraction and protein precipitation (Son *et al.* 2016). Samples were then loaded into H-PPT cartridges and eluted three times with 0.5 mL methanol. The matrix background such as proteins and phospholipids was easily removed and finally hair sterols were collected.

Sample pretreatment: chemical derivatization In GC separation, derivatization of steroid molecules is a prerequisite step to generate compounds with better volatility, thermal stability and thereby improved chromatographic properties (Marcos & Pozo 2015). The common reactions used in GC analysis are silylation, acylation and alkylation (Choi & Chung 2015), depending on the individual properties of the steroid

and the detection system. Silylation is the most widely used derivatization reaction in steroid analysis, and trimethylsilyl (TMS) derivatization is extensively used for most functional groups on steroid backbone, including aliphatic and phenolic alcohols, and carbonyl and amine groups. The purpose of this is to increase volatility as well as MS characteristics for GC–MS (Choi *et al.* 2002, Moon *et al.* 2009, Marcos & Pozo 2015). The most common reagents are *N,O*-bis (trimethylsilyl)-trifluoroacetamide (BSTFA) and the more volatile *N*-methyl-*N*-trimethylsilyl trifluoroacetamide (MSTFA) as a powerful trimethylsilyl (TMS) donor in the derivatization procedure (Shareef *et al.* 2006, Marcos & Pozo 2015). One of the most reported derivatization techniques in steroid profiling is the application of a mixture of MSTFA/ammonium iodide (NH₄I)/dithioerythritol (DTE) in a ratio of 500:4:2 (v/w/w) (Moon *et al.* 2009, 2010, Jung *et al.* 2011, Son *et al.* 2015). Most steroids were monitored using their molecular ions as base peaks.

For the profiling of 18 sterols, including cholesterol, six CEs, three cholesterol precursors and eight OHCs Cholesterol and cholesterol precursors have a hydroxyl group at the C-3 position, and OHCs have two polar functional groups: one is a hydroxyl group at the C-3 position and the other is a hydroxyl or ketone group at the C-4, C-7, C-19, C-20, C-24, C-25 or C-27 position. In TMS derivatization, both hydroxyl and carbonyl ketone groups were derivatized with TMS, whereas CEs were unaffected by TMS agents because they do not have polar groups in their chemical structures. The characteristic ions of cholesterol were observed at m/z 458 [M]⁺, m/z 443 [M–15; M–CH₃]⁺, m/z 368 [M–90; M–OTMS]⁺, m/z 353 [M–90–15; M–OTMS–CH₃]⁺, m/z 329 [M–129; M–TMS–O⁺=CHCH=CH₂]⁺ and m/z 129 [TMS–O⁺=CHCH=CH₂]⁺, which are in accordance with a general mass spectral interpretation. Among these fragments, the m/z 368 ion was chosen as the quantitative ion. All CEs generated a base peak at m/z 368 by cleavage of the ester bond, regardless of the fatty acid moiety (Jung *et al.* 2009). The quantitative ion of desmosterol was selected to be the m/z 343 ion that was formed by the loss of the side chain and two nuclear hydrogens. The quantitative ions of lathosterol and lanosterol were selected to be m/z 458 [M]⁺ and m/z 393 [M–90–15]⁺, respectively. In addition, OHCs showed different fragmentation patterns depending on the –OH positions (Moon *et al.* 2014). These results may provide useful information about the chemical structures of cholesterol and its metabolites.

For chemical transformation of multi-functional steroids

Mixed derivatization is performed to improve physical and chemical properties and mass spectral characteristics. Sensitive and selective quantification of eight steroids related to androgen biosynthesis in human hair was achieved by a combination of TMS and pentafluorophenyltrimethylsilylation (flop-hemesyl-TMS) (Choi & Chung 1999). The spectra of flop-hemesyl derivatives generally display intense molecular ions under electron impact ionization, resulting in enhanced chromatographic selectivity and mass spectral information with sensitive detection (Choi et al. 2001a, Choi & Chung 2015). Recently, the enhanced GC-MS analytical selectivity and sensitivity were allowed for quantitative analysis of estrogen metabolites in urine samples obtained from the postmenopausal female patients with osteoporosis (Moon et al. 2011b). It was successfully achieved by two-phase extractive ethoxycarbonylation (EOC) and subsequent pentafluoropropionyl (PFP) derivatization. In case of estrogen profiling, the ultra-sensitive LC-MS analytical method has been conducted with a novel chemical derivatization procedure, which formed analytes as pre-ionized N-methyl pyridinium-3-sulfonyl (NMPS) derivatives (Wang et al. 2015).

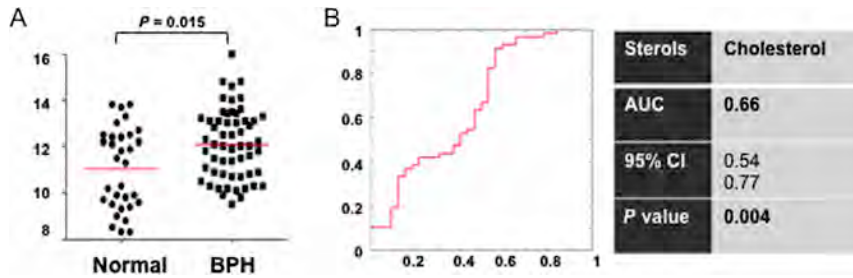
Analytical instrumentation Although radio-immunoassay (RIA) or enzyme immunoassays (EIA) are widely used to evaluate the quantification of steroid molecules (Thomson et al. 2009, Musshoff et al. 2012, Chan et al. 2014), the specificity of these methods is relatively low, which may result in an overestimation of the actual steroid content in samples. Furthermore, only single enzymes are estimated at a single time (Spiehler 2000, Hsing et al. 2007, Wood et al. 2008), making the method even more inaccurate. In contrast, mass spectrometry-based quantification has better reproducibility and generates multi-targeted profiling analysis (Cho et al. 2009, Ha et al. 2009, Jung et al. 2009, 2011, Moon et al. 2009, Son et al. 2015).

Several mass spectrometric methods for the measurement of steroids and sterols from various biological matrices have been proposed, coupled to GC (Ahmida et al. 2006, Ryu et al. 2006, Moon et al. 2009, 2011b, 2014, Choi et al. 2011, 2013, Son et al. 2014, 2015) or LC (Lembcke et al. 2005, Griffiths et al. 2008, DeBarber et al. 2008, Honda et al. 2009, Karu et al. 2011). The LC-MS methods based on electrospray and atmospheric pressure chemical ionization techniques have been conducted with a good sensitivity and chromatographic resolution of estrogens (Falk et al. 2008, Penning et al. 2010,

Wang et al. 2015), sterols and oxysterols (Burkard et al. 2004, Karuna et al. 2009, McDonald et al. 2012). However, the method often requires sample derivatization with dansyl chloride (Falk et al. 2008), pentafluorobenzyl chloride (Penning et al. 2010), Girard P hydrazine (Griffiths et al. 2006), picolinyl esterification (Yamashita et al. 2007, Honda et al. 2009) and NMPS (Wang et al. 2015) to improve ionization efficiencies and detection sensitivity. These methods enable to quantify the analytes in the low pg/mL ranges but are time-consuming because they require derivatization (Yamashita et al. 2007, Honda et al. 2009) and a long analytical run (Xu et al. 2007). Girard P derivatization can be seen in more detailed structure information due to MS³ (MS/MS/MS) applicability, but it appeared more laborious than GC-MS-based methods (Griffiths et al. 2006).

In particular, GC-MS with electron impact ionization is used widely for the measurement of steroid hormones with good analytical efficiencies as well as structural information. Initially, eight steroids related to androgen biosynthesis and two main estrogens (estrone and 17 β -estradiol) were determined in hair (Choi et al. 2000, Choi & Chung 2015). In 2011, the simultaneous quantification of hair steroids, including androgens, progestins, corticoids and sterols by GC-MS method in selected ion monitoring (SIM) mode, was successfully validated to evaluate the concentrations of individual steroids as well as the activities of the enzymes responsible for steroidogenesis in hair follicles and sebaceous glands (Jung et al. 2011). This can synthesize many steroids from cholesterol or locally convert circulating steroids with a range of metabolic enzymes (Chen et al. 2002, Ohnemus et al. 2006). For hair steroid profiling, 62 steroids were analyzed on an Ultra-1 capillary column (25 m \times 0.2 mm i.d., 0.33 μ m film thickness), and only 20 hair steroids, including eight androgens, three progestins, five sterols and four corticoids, were detectable (Jung et al. 2011).

Compared with the conventional GC-MS techniques using a fused silica capillary column (Ahmida et al. 2006), high-temperature gas chromatography-mass spectrometry (HTGC-MS) with a thermally stable stainless steel capillary column is described as an alternative technique for the analysis of lipophilic compounds (Son et al. 2014). In previous studies, it successfully achieved good chromatographic properties for the analysis of lipid molecules including cholesterol (Jung et al. 2009, 2010), as well as estrogens with two-phase extractive EOC and subsequent PFP derivatization (Moon et al. 2011a,b). Results showed that lower bleeding achieved results in better detectability with a short analytical run compared with

**Figure 3**

High cholesterol, high sex steroids and hair loss were observed in mice with chronic high-cholesterol diet. Line within the value represents the median.

a fused silica GC column. The present HTGC-MS-based quantitative cholesterol signatures of 18 sterols including cholesterol, six cholesteryl esters (CEs), three cholesterol precursors and eight oxysterols have been conducted with H-PPT purification and GC separation through a HTGC column separation. All analytes were successfully separated and detected without any interference within a 27-min chromatographic run. The oven temperature was held initially at 260°C for 3 min, ramped to 320°C at 10°C/min, increased to 330°C at 2°C/min (held for 8 min) and finally increased to 380°C at 30°C/min and then held for 3 min. Cholesterol, three cholesterol precursors (desmosterol, lathosterol and lanosterol) and eight OHCs were eluted within 7 min, while six CEs were eluted in the order of the number of carbons in the hydrocarbon chain: cholesteryl laurate (CE 12:0), myristate (CE 14:0), palmitate (CE 16:0), oleate (CE 18:1), linoleate (CE 18:2) and stearate (CE 18:0) (Son et al. 2014).

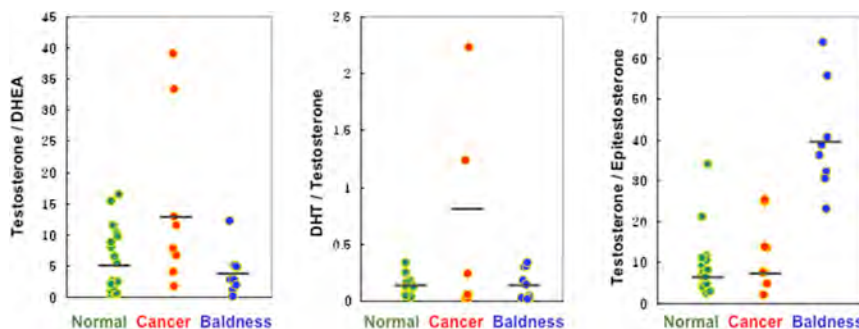
Hair metabolomics for monitoring potential biomarkers of urological diseases

Although the acute monitoring for drug efficacy is not applicable with hair analysis, hair steroid analysis still gives us the valuable information to confirm the 5 α -reductase inhibition after dutasteride administration (Jung et al. 2011). With the same pathological events, the biochemical mechanism of male pattern baldness (MPB) was clearly confirmed with hair steroid analysis (Choi et al. 2001b), and mode of actions of sex steroids in

MPB hair samples was differentiated between Caucasian and Korean (Choi et al. 2013). In addition to the androgen actions, the cortisol metabolic alteration can be monitored as a biochemical marker of chronic stress, which is an excessive symptom that causes cumulative negative impacts on health outcomes (Lee et al. 2015). The detection of cortisol in biological fluids, even saliva, has still been questionable. The increased levels of hair cortisol were observed in childhood obesity, which were also linked to long-term activation of HPA axis (Veldhorst et al. 2014), and the risk of cardiovascular disease (Manenschijn et al. 2013). Recently, our research team was able to successfully establish the analytical method for the profiling of cholesterol precursors and metabolites (e.g., 7 β -hydroxylation of cholesterol).

In the laboratory setting, we have observed that high circulating cholesterol in blood could be associated with high levels of androgens and hair loss in male mice (Fig. 3). Nude mice were grouped ($n=5$ /each group) and fed with high-cholesterol diet or normal chow for 2 months. No weight changes or liver function or dysfunction was observed. Levels of cholesterol and androgen were increased in all mice of high-cholesterol group (five out of five mice). Interestingly, three out of five mice in high-cholesterol group showed hair loss (Fig. 3).

Although increased androgen levels have been associated with both PC and MPB (Demark-Wahnefried et al. 1997), no studies have shown an association in hair samples. In establishing a proof of concept, our pilot study showed the increased levels of DHEA, testosterone

**Figure 4**

Metabolic ratios of hair androgens in patients with prostate cancer and male pattern baldness compared with healthy control subjects. Line within the value represents the median.

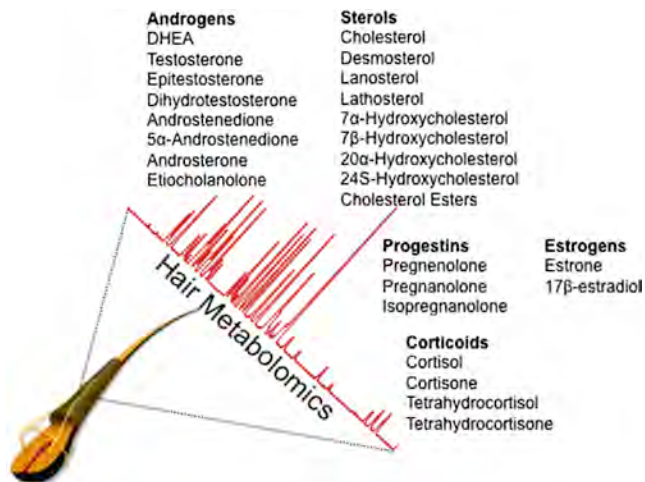


Figure 5

The clinically applicable hair metabolomic approaches to monitor cholesterol and steroid hormone levels in urological diseases.

and DHT in hair samples obtained from both PC and MPB subjects compared with those of age-/sex-matched control subjects. In particular, the metabolic ratios of testosterone:DHEA and DHT:testosterone in PC group tended to increase against the other two groups, whereas a metabolic ratio of testosterone:epitestosterone was significantly increased in MPB group (Fig. 4). This is in accordance with our previous findings (Manenschijn *et al.* 2013). These results suggest that the altered metabolic ratios of androgens combined with the higher levels of androgens might serve as the potential biomarkers for PC and MPB.

Concluding remarks and perspectives

PC and BPH are characterized by alterations of steroidogenic genes, which are important in synthesis of androgens from cholesterol, or genes converting adrenal androgens to DHT or DHT to inactive metabolites. In this short review article, we summarized these cholesterol and sex steroid metabolic pathways during progression of PC and BPH. Given the evidence derived from our and others' laboratories, hair metabolomics could be used for monitoring lipoidal hormones, such as cholesterol and sex steroids as well as corticoids. Both synthesis and metabolism of sex steroids with intracrine or paracrine actions are expressed locally in skin, which serve as a target for various steroid hormones including cholesterol (Słominski 2005). Hair as the adnexal structure of the skin contains the entire biochemical apparatus necessary for the production of steroid hormones either

from precursors of systemic origin or, alternatively, through the conversion of steroid precursors. Thus, hair metabolomics could therefore be a promising technique for the retrospective assessment of physiological changes in many clinical events including urological diseases. Figure 5 shows important lipid metabolites that our laboratory has successfully established, with the optimized quantitative analysis methods to measure cholesterol and sex steroid hormones for monitoring, using hair metabolomics.

Declaration of interest

The authors declare that there is no conflict of interest that could be perceived as prejudicing the impartiality of this review.

Funding

The authors acknowledge the support from the Korea Institute of Science and Technology Institutional Program (Project No. 2E26110 (to M H C)), National Institutes of Health grants (1U01DK103260, 1R01DK100974, U24 DK097154, NIH NCATS UCLA CTSI UL1TR000124 (to J K)), Department of Defense grants (PR140285 (to J K)), Centers for Disease Control and Prevention (1U01DP006079 (to J K)), IMAGINE NO IC Research Grant, the Steven Spielberg Discovery Fund in Prostate Cancer Research Career Development Award, and U.S. – Egypt Science and Technology Development Fund by the National Academies of Sciences, Engineering, and Medicine. J K is the former recipient of Interstitial Cystitis Association Pilot Grant, a Fishbein Family IC Research Grant, New York Academy of Medicine, and Boston Children's Hospital Faculty Development.

Authors' contribution statement

M H C and J K designed the study, led obtaining funding and overviewed the literature analysis and drafting the manuscript. J Y M performed the analysis of references and assisted in writing the manuscript. All authors read and approved the final manuscript.

Acknowledgements

The authors would like to thank Mr Taeun Daniel Park for careful review and editing the manuscript.

Availability of data and materials

All the data supporting the findings here is contained within the manuscript.

References

- Allott EH & Hursting SD 2015 Obesity and cancer: mechanistic insights from transdisciplinary studies. *Endocrine-Related Cancer* **22** R365–R386. (doi:10.1530/ERC-15-0400)
- Ahmida HS, Bertucci P, Franzo L, Massoud R, Cortese C, Lala A & Federici G 2006 Simultaneous determination of plasmatic phytosterols and cholesterol precursors using gas chromatography-mass spectrometry (GC-MS) with selective ion monitoring (SIM). *Journal of Chromatography B* **842** 43–47. (doi:10.1016/j.jchromb.2006.05.024)

- Bielska AA, Schlesinger P, Covey DF & Ory DS 2012 Oxysterols as non-genomic regulators of cholesterol homeostasis. *Trends in Endocrinology and Metabolism* **23** 99–106. (doi:10.1016/j.tem.2011.12.00)
- Bjorkhem I 2002 Do oxysterols control cholesterol homeostasis? *Journal of Clinical Investigation* **110** 725–730. (doi:10.1172/JCI16388)
- Bodin K, Andersson U, Rystedt E, Ellis E, Norlin M, Pikuleva I, Eggertsen G, Bjorkhem I & Diczfalusy U 2002 Metabolism of 4 beta-hydroxycholesterol in humans. *Journal of Biological Chemistry* **277** 31534–31540. (doi:10.1074/jbc.M201712200)
- Burkard I, Rentsch KM & von Eckardstein A 2004 Determination of 24S- and 27-hydroxycholesterol in plasma by high-performance liquid chromatography-mass spectrometry. *Journal of Lipid Research* **45** 776–781. (doi:10.1194/jlr.D300036-JLR200)
- Bylda C, Thiele R, Kobold U & Volmer DA 2014 Recent advances in sample preparation techniques to overcome difficulties encountered during quantitative analysis of small molecules from biofluids using LC-MS/MS. *Analyst* **139** 2265–2276. (doi:10.1039/c4an00094c)
- Chan J, Sauve B, Tokmakejian S, Koren G & Van Uum S 2014 Measurement of cortisol and testosterone in hair of obese and non-obese human subjects. *Experimental and Clinical Endocrinology and Diabetes* **122** 356–362. (doi:10.1055/s-0034-1374609)
- Chen W, Thiboutot D & Zouboulis CC 2002 Cutaneous androgen metabolism: basic research and clinical perspectives. *Journal of Investigative Dermatology* **119** 992–1007. (doi:10.1046/j.1523-1747.2002.00613.x)
- Cho HJ, Kim JD, Lee WY, Chung BC & Choi MH 2009 Quantitative metabolic profiling of 21 endogenous corticosteroids in urine by liquid chromatography-triple quadrupole-mass spectrometry. *Analytica Chimica Acta* **632** 101–108. (doi:10.1016/j.aca.2008.10.059)
- Cho SH, Choi MH, Sim WY, Lee WY & Chung BC 2010 Metabolic alterations of DHEA and cholesterol sulphates in the hair of patients with acne measured by liquid chromatography-mass spectrometry. *Experimental Dermatology* **19** 694–696. (doi:10.1111/j.1600-0625.2010.01094.x)
- Choi MH & Chung BC 1999 GC-MS determination of steroids related to androgen biosynthesis in human hair with pentafluorophenyltrimethylsilyl-trimethylsilyl derivatisation. *Analyst* **124** 1297–300. (doi:10.1039/a903912k)
- Choi MH & Chung BC 2015 Bringing GC-MS profiling of steroids into clinical applications. *Mass Spectrometry Reviews* **34** 219–236. (doi:10.1002/mas.21436)
- Choi MH, Kim KR & Chung BC 2000 Determination of estrone and 17 beta-estradiol in human hair by gas chromatography-mass spectrometry. *Analyst* **125** 711–714. (doi:10.1039/a909107f)
- Choi MH, Kim KR, Kim IS, Lho DS & Chung BC 2001a Increased hair polyamine levels in patients with Alzheimer's disease. *Annals of Neurology* **50** 128. (doi:10.1002/ana.1086)
- Choi MH, Yoo YS & Chung BC 2001b Biochemical roles of testosterone and epitestosterone to 5 alpha-reductase as indicators of male-pattern baldness. *Journal of Investigative Dermatology* **116** 57–61. (doi:10.1046/j.1523-1747.2001.00188.x)
- Choi MH, Hahm JR, Jung BH & Chung BC 2002 Measurement of corticoids in the patients with clinical features indicative of mineralocorticoid excess. *Clinica Chimica Acta* **320** 95–99. (doi:10.1016/S0009-8981(02)00050-5)
- Choi MH, Moon JY, Cho SH, Chung BC & Lee EJ 2011 Metabolic alteration of urinary steroids in pre- and post-menopausal women, and men with papillary thyroid carcinoma. *BMC Cancer* **11** 342. (doi:10.1186/1471-2407-11-342)
- Choi MH, Kim SJ, Lew BL, Sim WY & Chung BC 2013 Hair steroid profiling reveals racial differences in male pattern baldness between Korean and Caucasian populations. *Journal of Investigative Dermatology* **133** 822–824. (doi:10.1038/jid.2012.349)
- DeBarber AE, Lutjohann D, Merckens L & Steiner RD 2008 Liquid chromatography-tandem mass spectrometry determination of plasma 24S-hydroxycholesterol with chromatographic separation of 25-hydroxycholesterol. *Analytical Biochemistry* **381** 151–153. (doi:10.1016/j.ab.2008.05.037)
- Dehm SM & Tindall DJ 2007 Androgen receptor structural and functional elements: role and regulation in prostate cancer. *Molecular Endocrinology* **21** 2855–2863. (doi:10.1210/me.2007-0223)
- Demark-Wahnefried W, Lesko SM, Conaway MR, Robertson CN, Clark RV, Lobaugh B, Mathias BJ, Strigo TS & Paulson DF 1997 Serum androgens: associations with prostate cancer risk and hair patterning. *Journal of Andrology* **18** 495–500. (doi:10.1002/j.1939-640.1997.tb01964.x)
- Demierre MF, Higgins PD, Gruber SB, Hawk E & Lippman SM 2005 Statins and cancer prevention. *Nature Reviews Cancer* **5** 930–942. (doi:10.1038/nrc1751)
- Fagherazzi G, Fabre A, Boutron-Ruault MC & Clavel-Chapelon F 2010 Serum cholesterol level, use of a cholesterol-lowering drug, and breast cancer: results from the prospective E3N cohort. *European Journal of Cancer Prevention* **19** 120–125. (doi:10.1097/CEJ.0b013e3283354918)
- Falk RT, Xu X, Keefer L, Veenstra TD & Ziegler RG 2008 A liquid chromatography-mass spectrometry method for the simultaneous measurement of 15 urinary estrogens and estrogen metabolites: assay reproducibility and interindividual variability. *Cancer Epidemiology of Biomarkers and Prevention* **17** 3411–3418. (doi:10.1158/1055-9965.EPI-08-0355)
- Falkenstein E, Tillmann HC, Christ M, Feuring M & Wehling M 2000 Multiple actions of steroid hormones – a focus on rapid, nongenomic effects. *Pharmacological Review* **52** 513–556.
- Farwell WR, Scranton RE, Lawler EV, Lew RA, Brophy MT, Fiore LD & Gaziano JM 2008 The association between statins and cancer incidence in a veterans population. *Journal of National Cancer Institute* **100** 134–139. (doi:10.1093/jnci/djm286)
- Farwell WR, Lourenco C, Holmberg E, Hall RB, D'Avolio L, Lawler EV & Michael Gaziano J 2011 The association between height and prostate cancer grade in the Early Stage Prostate Cancer Cohort Study. *Cancer Causes and Control* **22** 1453–1459. (doi:10.1007/s10552-011-9820-x)
- Folch J, Lees M & Sloane Stanley GH 1957 A simple method for the isolation and purification of total lipides from animal tissues. *Journal of Biological Chemistry* **226** 497–509.
- Fryar CD, Hirsch R, Eberhardt MS, Yoon SS & Wright JD 2010 Hypertension, high serum total cholesterol, and diabetes: racial and ethnic prevalence differences in U.S. adults, 1999–2006. *NCHS Data Brief* **36** 1–8.
- Gacci M, Corona G, Vignozzi L, Salvi M, Serni S, De Nunzio C, Tubaro A, Oelke M, Carini M & Maggi M 2015 Metabolic syndrome and benign prostatic enlargement: a systematic review and meta-analysis. *BJU International* **115** 24–31. (doi:10.1111/bju.12728)
- Goedeke L & Fernandez-Hernando C 2012 Regulation of cholesterol homeostasis. *Cellular and Molecular Life Sciences* **69** 915–930. (doi:10.1007/s00018-011-0857-5)
- Gray BP, Viljanto M, Bright J, Pearce C & Maynard S 2013 Investigations into the feasibility of routine ultra high performance liquid chromatography-tandem mass spectrometry analysis of equine hair samples for detecting the misuse of anabolic steroids, anabolic steroid esters and related compounds. *Analytica Chimica Acta* **787** 163–172. (doi:10.1016/j.aca.2013.05.058)
- Griffiths WJ, Wang Y, Alvelius G, Liu S, Bodin K & Sjoval J 2006 Analysis of oxysterols by electrospray tandem mass spectrometry. *Journal of the American Society for Mass Spectrometry* **17** 341–362. (doi:10.1016/j.jasms.2005.10.012)
- Griffiths WJ, Wang Y, Karu K, Samuel E, McDonnell S, Hornshaw M & Shackleton C 2008 Potential of sterol analysis by liquid chromatography-tandem mass spectrometry for

- the prenatal diagnosis of Smith-Lemli-Opitz syndrome. *Clinical Chemistry* **54** 1317–1324. (doi:10.1373/clinchem.2007.100644)
- Ha YW, Moon JY, Jung HJ, Chung BC & Choi MH 2009 Evaluation of plasma enzyme activities using gas chromatography-mass spectrometry based steroid signatures. *Journal of Chromatography B* **877** 4125–4132. (doi:10.1016/j.jchromb.2009.11.010)
- Honda A, Yamashita K, Hara T, Ikegami T, Miyazaki T, Shirai M, Xu G, Numazawa M & Matsuzaki Y 2009 Highly sensitive quantification of key regulatory oxysterols in biological samples by LC-ESI-MS/MS. *Journal of Lipid Research* **50** 350–357. (doi:10.1194/jlr.D800040-JLR200)
- Hsing AW, Stanczyk FZ, Belanger A, Schroeder P, Chang L, Falk RT & Fears TR 2007 Reproducibility of serum sex steroid assays in men by RIA and mass spectrometry. *Cancer Epidemiology, Biomarkers and Prevention* **16** 1004–1008. (doi:10.1158/1055-9965.EPI-06-0792)
- Ito K 2014 Prostate cancer in Asian men. *Nature Reviews Urology* **11** 197–212. (doi:10.1038/nrurol.2014.42)
- Jung HJ, Lee WY, Chung BC & Choi MH 2009 Mass spectrometric profiling of saturated fatty acid esters of steroids separated by high-temperature gas chromatography. *Journal of Chromatography A* **1216** 1463–1468. (doi:10.1016/j.chroma.2008.12.059)
- Jung HJ, Lee WY, Yoo YS, Chung BC & Choi MH 2010 Database-dependent metabolite profiling focused on steroid and fatty acid derivatives using high-temperature gas chromatography-mass spectrometry. *Clinica Chimica Acta* **411** 818–824. (doi:10.1016/j.cca.2010.02.068)
- Jung HJ, Kim SJ, Lee WY, Chung BC & Choi MH 2011 Gas chromatography/mass spectrometry based hair steroid profiling may reveal pathogenesis in hair follicles of the scalp. *Rapid Communications in Mass Spectrometry* **25** 1184–1192. (doi:10.1002/rcm.4975)
- Karu K, Turton J, Wang Y & Griffiths WJ 2011 Nano-liquid chromatography-tandem mass spectrometry analysis of oxysterols in brain: monitoring of cholesterol autoxidation. *Chemistry and Physics of Lipids* **164** 411–424. (doi:10.1016/j.chemphyslip.2011.04.011)
- Karuna R, von Eckardstein A & Rentsch KM 2009 Dopant assisted-atmospheric pressure photoionization (DA-APPI) liquid chromatography-mass spectrometry for the quantification of 27-hydroxycholesterol in plasma. *Journal of Chromatography B* **877** 261–268. (doi:10.1016/j.jchromb.2008.12.033)
- Kim JY, Cheong JC, Lee JI & In MK 2011 Improved gas chromatography-negative ion chemical ionization tandem mass spectrometric method for determination of 11-nor-Delta9-tetrahydrocannabinol-9-carboxylic acid in hair using mechanical pulverization and bead-assisted liquid-liquid extraction. *Forensic Science International* **206** e99–e102. (doi:10.1016/j.forsciint.2011.01.013)
- Kraemer FB 2007 Adrenal cholesterol utilization. *Molecular and Cellular Endocrinology* **265–266** 42–45. (doi:10.1016/j.mce.2006.12.001)
- Krycer JR & Brown AJ 2013 Cholesterol accumulation in prostate cancer: a classic observation from a modern perspective. *Biochimica et Biophysica Acta* **1835** 219–229. (doi:10.1016/j.bbcan.2013.01.002)
- Lee DY, Kim E & Choi MH 2015 Technical and clinical aspects of cortisol as a biochemical marker of chronic stress. *BMB Reports* **48** 209–216. (doi:10.5483/BMBRep.2015.48.4.275)
- Lembcke J, Ceglarek U, Fiedler GM, Baumann S, Leichtle A & Thiery J 2005 Rapid quantification of free and esterified phytosterols in human serum using APPI-LC-MS/MS. *Journal of Lipid Research* **46** 21–26. (doi:10.1194/jlr.C400004-JLR200)
- Manenschijn L, Schaap L, van Schoor NM, van der Pas S, Peeters GM, Lips P, Koper JW & van Rossum EF 2013 High long-term cortisol levels, measured in scalp hair, are associated with a history of cardiovascular disease. *Journal of Clinical Endocrinology and Metabolism* **98** 2078–2083. (doi:10.1210/jc.2012-3663)
- Marcos J & Pozo OJ 2015 Derivatization of steroids in biological samples for GC-MS and LC-MS analyses. *Bioanalysis* **7** 2515–2636. (doi:10.4155/bio.15.176)
- Mass AY, Agalliu I, Laze J & Lepor H 2012 Preoperative statin therapy is not associated with biochemical recurrence after radical prostatectomy: our experience and meta-analysis. *Journal of Urology* **188** 786–791. (doi:10.1016/j.juro.2012.05.011)
- Maxfield FR & Tabas I 2005 Role of cholesterol and lipid organization in disease. *Nature* **438** 612–621. (doi:10.1038/nature04399)
- McDonald JG, Smith DD, Stiles AR & Russell DW 2012 A comprehensive method for extraction and quantitative analysis of sterols and secosteroids from human plasma. *Journal of Lipid Research* **53** 1399–1409. (doi:10.1194/jlr.D022285)
- Miller WL 2008 Steroidogenic enzymes. *Endocrine Development* **13** 1–18. (doi:10.1159/000134751)
- Miyaguchi H, Kakuta M, Iwata YT, Matsuda H, Tazawa H, Kimura H & Inoue H 2007 Development of a micropulverized extraction method for rapid toxicological analysis of methamphetamine in hair. *Journal of Chromatography A* **1163** 43–48. (doi:10.1016/j.chroma.2007.06.017)
- Mondul AM, Weinstein SJ, Virtamo J & Albanes D 2011 Serum total and HDL cholesterol and risk of prostate cancer. *Cancer Causes and Control* **22** 1545–1552. (doi:10.1007/s10552-011-9831-7)
- Moon JY, Jung HJ, Moon MH, Chung BC & Choi MH 2009 Heat-map visualization of gas chromatography-mass spectrometry based quantitative signatures on steroid metabolism. *Journal of the American Society for Mass Spectrometry* **20** 1626–1637. (doi:10.1016/j.jasms.2009.04.020)
- Moon JY, Ha YW, Moon MH, Chung BC & Choi MH 2010 Systematic error in gas chromatography-mass spectrometry-based quantification of hydrolyzed urinary steroids. *Cancer Epidemiology, Biomarkers and Prevention* **19** 388–397. (doi:10.1158/1055-9965.EPI-09-0581)
- Moon JY, Kang SM, Moon MH, Hong J, Kim KT, Jeong DH, Kim YN, Chung BC & Choi MH 2011a Extractive ethoxycarbonylation in high-temperature gas chromatography-mass spectrometry based analysis of serum estrogens. *Journal of Chromatography B* **879** 3742–3748. (doi:10.1016/j.jchromb.2011.10.024)
- Moon JY, Kim KJ, Moon MH, Chung BC & Choi MH 2011b A novel GC-MS method in urinary estrogen analysis from postmenopausal women with osteoporosis. *Journal of Lipid Research* **52** 1595–1603. (doi:10.1194/jlr.D016113)
- Moon JY, Moon MH, Kim KT, Jeong DH, Kim YN, Chung BC & Choi MH 2014 Cytochrome P450-mediated metabolic alterations in preeclampsia evaluated by quantitative steroid signatures. *Journal of Steroid Biochemistry and Molecular Biology* **139** 182–191. (doi:10.1016/j.jsmb.2013.02.014)
- Mostaghel EA, Solomon KR, Pelton K, Freeman MR & Montgomery RB 2012 Impact of circulating cholesterol levels on growth and intratumoral androgen concentration of prostate tumors. *PLoS ONE* **7** e30062. (doi:10.1371/journal.pone.0030062)
- Musshoff F, Kirschbaum KM, Graumann K, Herzfeld C, Sachs H & Madea B 2012 Evaluation of two immunoassay procedures for drug testing in hair samples. *Forensic Science International* **215** 60–63. (doi:10.1016/j.forsciint.2011.03.030)
- Nielsen SF, Nordestgaard BG & Bojesen SE 2012 Statin use and reduced cancer-related mortality. *New England Journal of Medicine* **367** 1792–1802. (doi:10.1056/NEJMoa1201735)
- Ohnemus U, Uenal M, Inzunza J, Gustafsson JA & Paus R 2006 The hair follicle as an estrogen target and source. *Endocrine Reviews* **27** 677–706. (doi:10.1210/er.2006-0020)
- Park HS, Schoenfeld JD, Mailhot RB, Shive M, Hartman RI, Ogembo R & Mucci LA 2013 Statins and prostate cancer recurrence following radical prostatectomy or radiotherapy: a systematic review and

- meta-analysis. *Annals of Oncology* **24** 1427–1434. (doi:10.1093/annonc/mdt077)
- Payne AH & Hales DB 2004 Overview of steroidogenic enzymes in the pathway from cholesterol to active steroid hormones. *Endocrine Reviews* **25** 947–970. (doi:10.1210/er.2003-0030)
- Pelton K, Freeman MR & Solomon KR 2012 Cholesterol and prostate cancer. *Current Opinion in Pharmacology* **12** 751–759. (doi:10.1016/j.coph.2012.07.006)
- Penning TM, Lee SH, Jin Y, Gutierrez A & Blair IA 2010 Liquid chromatography-mass spectrometry (LC-MS) of steroid hormone metabolites and its applications. *Journal of Steroid Biochemistry and Molecular Biology* **121** 546–555. (doi:10.1016/j.jsmb.2010.01.005)
- Pereg D, Chan J, Russell E, Berlin T, Mosseri M, Seabrook JA, Koren G & Van Uum S 2013 Cortisol and testosterone in hair as biological markers of systolic heart failure. *Psychoneuroendocrinology* **38** 2875–2882. (doi:10.1016/j.psyneuen.2013.07.015)
- Pichini S, De Luca R, Pellegrini M, Marchei E, Rotolo MC, Spoletini R, D'Aloja P, Pacifici R, Mortali C & Scaravelli G 2012 Hair and urine testing to assess drugs of abuse consumption in couples undergoing assisted reproductive technology (ART). *Forensic Science International* **218** 57–61. (doi:10.1016/j.forsciint.2011.10.011)
- Pikuleva IA 2006 Cholesterol-metabolizing cytochromes P450. *Drug Metabolism and Disposition* **34** 513–520. (doi:10.1124/dmd.105.008789)
- Platz EA, Clinton SK & Giovannucci E 2008 Association between plasma cholesterol and prostate cancer in the PSA era. *International Journal of Cancer* **123** 1693–1698. (doi:10.1002/ijc.23715)
- Platz EA, Till C, Goodman PJ, Parnes HL, Figg WD, Albanes D, Neuhaus ML, Klein EA, Thompson IM Jr & Kristal AR 2009 Men with low serum cholesterol have a lower risk of high-grade prostate cancer in the placebo arm of the prostate cancer prevention trial. *Cancer Epidemiology, Biomarkers and Prevention* **18** 2807–2813. (doi:10.1158/1055-9965.EPI-09-0472)
- Pucci V, Di Palma S, Alfieri A, Bonelli F & Monteagudo E 2009 A novel strategy for reducing phospholipids-based matrix effect in LC-ESI-MS bioanalysis by means of HybridSPE. *Journal of Pharmaceutical and Biomedical Analysis* **50** 867–871. (doi:10.1016/j.jpba.2009.05.037)
- Ridker PM & Cook NR 2013 Statins: new American guidelines for prevention of cardiovascular disease. *Lancet* **382** 1762–1765. (doi:10.1016/S0140-6736(13)62388-0)
- Ryu HK, Jung BH, Kim KM, Yoo EA, Woo JT & Chung BC 2006 Determination of cholesterol in human hair using gas chromatography-mass spectrometry. *Biomedical Chromatography* **20** 999–1003. (doi:10.1002/bmc.615)
- Scosyrev E, Tobis S, Donsky H, Wu G, Joseph J, Rashid H & Messing E 2013 Statin use and the risk of biochemical recurrence of prostate cancer after definitive local therapy: a meta-analysis of eight cohort studies. *BJU International* **111** E71–E77. (doi:10.1111/j.1464-410X.2012.11527.x)
- Seo HS & Choi MH 2015 Cholesterol homeostasis in cardiovascular disease and recent advances in measuring cholesterol signatures. *Journal of Steroid Biochemistry and Molecular Biology* **153** 72–79. (doi:10.1016/j.jsmb.2015.04.014)
- Shafique K, McLoone P, Qureshi K, Leung H, Hart C & Morrison DS 2012 Cholesterol and the risk of grade-specific prostate cancer incidence: evidence from two large prospective cohort studies with up to 37 years' follow up. *BMC Cancer* **12** 25. (doi:10.1186/1471-2407-12-25)
- Shareef A, Angove MJ & Wells JD 2006 Optimization of silylation using N-methyl-N-(trimethylsilyl)-trifluoroacetamide, N,O-bis-(trimethylsilyl)-trifluoroacetamide and N-(tert-butyl-dimethylsilyl)-N-methyltrifluoroacetamide for the determination of the estrogens estrone and 17 α -ethynylestradiol by gas chromatography-mass spectrometry. *Journal of Chromatography A* **1108** 121–128. (doi:10.1016/j.chroma.2005.12.098)
- Simon A 2014 Cholesterol metabolism and immunity. *New England Journal of Medicine* **371** 1933–1935. (doi:10.1056/NEJMcibr1412016)
- Singh EJ & Gershbein LL 1967 Phospholipids of human hair lipids. *Journal of Chromatography* **31** 20–27. (doi:10.1016/S0021-9673(01)86020-9)
- Slominski A 2005 Neuroendocrine system of the skin. *Dermatology* **211** 199–208. (doi:10.1159/000087012)
- Son HH, Moon JY, Seo HS, Kim HH, Chung BC & Choi MH 2014 High-temperature GC-MS-based serum cholesterol signatures may reveal sex differences in vasospastic angina. *Journal of Lipid Research* **55** 155–162. (doi:10.1194/jlr.D040790)
- Son HH, Kim SH, Moon JY, Chung BC, Park MJ & Choi MH 2015 Serum sterol profiling reveals increased cholesterol biosynthesis in childhood obesity. *Journal of Steroid Biochemistry and Molecular Biology* **149** 138–145. (doi:10.1016/j.jsmb.2015.02.012)
- Son HH, Lee DY, Seo HS, Jeong J, Moon JY, Lee JE, Chung BC, Kim E & Choi MH 2016 Hair sterol signatures coupled to multivariate data analysis reveal an increased 7 β -hydroxycholesterol production in cognitive impairment. *Journal of Steroid Biochemistry and Molecular Biology* **155** 9–17. (doi:10.1016/j.jsmb.2015.09.024)
- Spiehler V 2000 Hair analysis by immunological methods from the beginning to 2000. *Forensic Science International* **107** 249–259. (doi:10.1016/S0379-0738(99)00168-1)
- Sulek K, Han TL, Villas-Boas SG, Wishart DS, Soh SE, Kwek K, Gluckman PD, Chong YS, Kenny LC & Baker PN 2014 Hair metabolomics: identification of fetal compromise provides proof of concept for biomarker discovery. *Theranostics* **4** 953–959. (doi:10.7150/thno.9265)
- Thomson S, Koren G, Van Steen V, Rieder M & Van Uum SH 2009 Testosterone concentrations in hair of hypogonadal men with and without testosterone replacement therapy. *Therapeutic Drug Monitoring* **31** 779–782. (doi:10.1097/FTD.0b013e3181c004f1)
- TwoRoger SS & Hankinson SE 2006 Collection, processing, and storage of biological samples in epidemiologic studies: sex hormones, carotenoids, inflammatory markers, and proteomics as examples. *Cancer Epidemiology, Biomarkers and Prevention* **15** 1578–1581. (doi:10.1158/1055-9965.EPI-06-0629)
- Veldhorst MA, Noppe G, Jongejan MH, Kok CB, Mekic S, Koper JW, van Rossum EF & van den Akker EL 2014 Increased scalp hair cortisol concentrations in obese children. *Journal of Clinical Endocrinology and Metabolism* **99** 285–290. (doi:10.1210/jc.2013-2924)
- Villain M, Cirimele V & Kintz P 2004 Hair analysis in toxicology. *Clinical Chemistry and Laboratory Medicine* **42** 1265–1272. (doi:10.1515/CCLM.2004.247)
- Wang Q, Rangiah K, Mesaros C, Snyder NW, Vachani A, Song H & Blair IA 2015 Ultrasensitive quantification of serum estrogens in postmenopausal women and older men by liquid chromatography-tandem mass spectrometry. *Steroids* **96** 140–152. (doi:10.1016/j.steroids.2015.01.014)
- Wennig R 2000 Potential problems with the interpretation of hair analysis results. *Forensic Science International* **107** 5–12. (doi:10.1016/S0379-0738(99)00146-2)
- Wood L, Ducroq DH, Fraser HL, Gillingwater S, Evans C, Pickett AJ, Rees DW, John R & Turkes A 2008 Measurement of urinary free cortisol by tandem mass spectrometry and comparison with results obtained by gas chromatography-mass spectrometry and two commercial immunoassays. *Annals of Clinical Biochemistry* **45** 380–388. (doi:10.1258/acb.2007.007119)
- Wudy SA, Hartmann M & Homoki J 2000 Hormonal diagnosis of 21-hydroxylase deficiency in plasma and urine of neonates using

- benchtop gas chromatography-mass spectrometry. *Journal of Endocrinology* **165** 679–683. (doi:10.1677/joe.0.1650679)
- Xu X, Keefer LK, Ziegler RG & Veenstra TD 2007 A liquid chromatography-mass spectrometry method for the quantitative analysis of urinary endogenous estrogen metabolites. *Nature Protocol* **2** 1350–1355. (doi:10.1038/nprot.2007.176)
- Yamashita K, Okuyama M, Watanabe Y, Honma S, Kobayashi S & Numazawa M 2007 Highly sensitive determination of estrone and estradiol in human serum by liquid chromatography-electrospray ionization tandem mass spectrometry. *Steroids* **72** 819–827. (doi:10.1016/j.steroids.2007.07.003)
- YuPeng L, YuXue Z, PengFei L, Cheng C, YaShuang Z, DaPeng L & Chen D 2015 Cholesterol levels in blood and the risk of prostate cancer: a meta-analysis of 14 prospective studies. *Cancer Epidemiology, Biomarkers and Prevention* **24** 1086–1093. (doi:10.1158/1055-9965.EPI-14-1329)
- Zhuang L, Lin J, Lu ML, Solomon KR & Freeman MR 2002 Cholesterol-rich lipid rafts mediate akt-regulated survival in prostate cancer cells. *Cancer Research* **62** 2227–2231.

Received in final form 29 July 2016

Accepted 4 August 2016



Editorial

Int Neurorol J 2016;20 Suppl 2:S65-67
<https://doi.org/10.5213/inj.1620edi007>
pISSN 2093-4777 · eISSN 2093-6931



Are We Ready to Use the Omics Strategies for Precision Medicine?

Jayoung Kim  <http://orcid.org/0000-0002-3683-4627>

Guest Editor

Cedars-Sinai Medical Center, University of California, Los Angeles, CA, USA
E-mail: Jayoung.Kim@csmc.edu



It was nearing the end of summer on a rainy day when the editorial board members of the *International Neurourology Journal* (INJ) met and discussed publishing a special issue. We decided to introduce and summarize recent advances in multiomic approaches to better understand bladder diseases and beyond.

The recently implemented “Precision Medicine Initiative” has enabled great advances in personalized healthcare. In recent years, the explosive growth of individual whole genomes has led to a greater systematic understanding of the variety of important and essential factors in cellular mechanics, such as transcriptomes, proteomes, and metabolomes. With all of this information, what then is the promise of precision medicine? We have found that it will allow us to deepen our biological understanding of a patient’s background and needs at the molecular level. This will allow us to tailor our care to provide more proactive, predictive, and precise treatments at a highly targeted level for individuals.

Qualified biomarkers revealed by multiomic approaches are part of a more concentrated effort to provide “personalized advice” with respect to monitoring the severity, progression, and prediction of therapies of diseases. As scientists and physicians, our long-term goals include determination of disease specific biomarkers for accurate diagnosis, continuing improvement of our understanding of the biological basis of disease, and identification of new strategies for patient care. The advanced approaches and expertise we have described here are meant to bring the new capabilities of precision medicine to a wider range of areas through cutting edge technology and novel strategies.

In this special issue, which is titled “Omic Approaches to

Understand Bladder Diseases and Beyond,” our goals are (1) to update our readers with the current progress of relevant cutting-edge technologies, and (2) to describe the scientific and clinical impacts resulting from these new discoveries.

Of the various proteomic-based technologies in biomedical research, mass spectrometry (MS)-based platforms are one of best for unbiased and targeted proteomic analyses. The first paper in this volume is a review titled “Urine Proteomics in the Era of Mass Spectrometry” by Dr. Ashely Beasley-Green [1] at the National Institute of Standards and Technology (Gaithersburg, MD, USA). It explains a number of advantageous features of MS-based technologies on individual biomarker identification along with their effectiveness when applied to renal disease diagnosis. Urine albumin is a major, biologically noninvasive component used in multiple renal disease measurement technologies. It is shown from this review that amazing results have been achieved in protein identification using multiplexed candidate reference measurement procedures that utilize mass spectrometry and multiple reaction monitoring. These tools permit qualitative assessment of biomarker candidates.

The second article [2] is an informative review by Dr. Sang Tae Park, who was a former trainee at Harvard Medical School and the current CEO and CSO of the MacroGen Clinical Laboratory, MacroGen Corporation (Rockville, MD, USA). It provides a general understanding of next-generation sequencing (NGS) such as the following questions: What types of NGS technologies and platforms are being used? How can NGS be applied in understanding human genetics and genomics? What we can expect in a new era of whole genome sequencing (WGS)?



This is an Open Access article distributed under the terms of the Creative Commons Attribution Non-Commercial License (<http://creativecommons.org/licenses/by-nc/4.0/>) which permits unrestricted non-commercial use, distribution, and reproduction in any medium, provided the original work is properly cited.

NGS applications allow for epigenetic studies, whole genome methylation sequencing, and chromatin immunoprecipitation followed by sequencing. He explains these important issues point-by-point and discusses how these technologies can be applied to personalized precision medicine.

Dr. Gangning Liang, Professor of Research in the Department of Urology at the University of Southern California (Los Angeles, CA, USA), who has 20 years of hands-on experience in the field of epigenetics, then talks about his experience in characterizing the roles of DNA methyltransferases and microRNAs during tumorigenesis. His discussion delves into how we can develop novel methods of characterizing epigenetic changes and how to monitor these changes in patients. His article [3] includes detailed information on current research, ranging from somatic genetic aberrations to various epigenetic regulations such as DNA methylation, histone modifications, microRNA regulation, and nucleosome positioning. He also provides evidence suggesting genetic and epigenetic alterations as possible therapeutic targets.

We then switch gears a little bit to the specific diseases that our INJ audience is interested in learning about. The second section answers our questions as to how these cutting edge technologies can be applied to aspects of translation. We invited several more experts in benign urological diseases, such as interstitial cystitis and bladder pain syndrome (IC/BPS), lower urinary tract dysfunction (LUTD), prostate cancer, and gastric cancer.

Dr. Hann-Chorng Kuo et al. at the Buddhist Tzu Chi General Hospital and Tzu Chi University (Hualien, Taiwan) introduces the accumulated efforts to identify potential biomarkers targeting IC/BPS, which is an irritating bladder syndrome and is usually characterized by frequent nocturia as well as bladder pain in patients. He summarized the pathomechanisms of IC/BPS by mapping the heterogeneity of the disease and the concentrated efforts on the potential serum and urinary biomarkers of the disease [4].

Dr. Akihiro Kanematsu, a former trainee at Harvard Medical School/Boston Children's Hospital and a current Associate Professor and a pediatric urologist at Hyogo College of Medicine (Hyogo, Japan), provides a comprehensive review of translational research aimed at elucidating the pathophysiology of pediatric LUTD [5].

In "Racial Differences of Diagnosis and Treatment for Prostate Cancer," Dr. Jong Y. Park, an associate member at the Moffitt Cancer Institute (Tampa, FL, USA), discusses how new gen-

eration omic tools have been adapted for the field of molecular epidemiology. Prostate cancer is the second most common cancer in the U.S. Recent statistics from the American Cancer Society state that an estimated 26,120 deaths will occur in 2016 due to prostate cancer alone. Interestingly, the incident rates and mortality rates of different ethnic groups in the U.S. vary greatly. The causes of these disparities are numerous. In his review, Dr Jong Y. Park et al. compare inequalities at diagnosis and treatment while also considering the genetic susceptibility of different ethnic groups who are affected by prostate cancer. According to his study, there is a positive correlation between high socioeconomic status and survival rate in both African American and Caucasian groups; socioeconomically wealthier groups had more of a chance of detecting prostate cancer at an earlier age with a higher survival rate. In terms of therapy/treatment, it is important to note the relationship between the lower survival rate of African Americans and the fact that African Americans experience treatment delays and postoperative complications more often than Caucasians. The authors also suggest that we need to expand these variables, which affect the differences, in order to better understand the factors of these disparities [6].

It is widely accepted that early prostate cancer detection and treatment can result in a higher survival rate for a patient, but, occasionally might lead to overdiagnosis and overtreatment. The development of precision medicine is therefore a novel tool that enables us to lower the chances of false negatives and false positives while also improving therapies for diseases. A review titled "How Precisely Can Prostate Cancer Be Managed?" by Dr. Liyan Zhung et al. [7], at Lahey Hospital and Medical Center, Tufts University School of Medicine (Burlington, MA, USA) responds to the following questions: who will need a biopsy? a re-biopsy? who are candidates for active surveillance? and who needs adjuvant radiation or hormonal therapy after prostatectomy? In addition to answering these questions, the paper introduces a number of useful diagnostic tools based on genomic screening to give us a better understanding of current tools. It also helps us understand the precision medicine that has been applied to prostate cancer and other cancer treatments.

Dr. Samuel J. Klempner et al. at the Angeles Clinic and Research Institute, and Samuel Oschin Comprehensive Cancer Institute, Cedars-Sinai Medical Center (Los Angeles, CA, USA) discuss the current research being developed on phosphatidylinositol-3-kinase (PI3K) pathway signaling in gastric cancer, the most common cancer among men in Korea [8].

This collection of 8 review articles in this special issue are all

tied together by one common and simple mission: to close our knowledge gap for better patient care. While this gap will not close overnight, it is time to think of basic science, molecular epidemiology, and clinical translation science as utilizing multi-omic approaches as strong tools with a mission that can be combined to make greater advances in healthcare.

- **Fund/Grant Support:** The author acknowledges support from the National Institutes of Health grants (1U01DK103260, 1R01DK100974, U24 DK097154, NIH NCATS UCLA CTSI UL1TR000124), Department of Defense grants (W81XWH-15-1-0415), Centers for Disease Control and Prevention (1U01DP006079), IMAGINE NO IC Research Grant, the Steven Spielberg Discovery Fund in Prostate Cancer Research Career Development Award, the U.S.-Egypt Science and Technology Development Fund by the National Academies of Sciences, Engineering, and Medicine. Dr. Kim is a former recipient of the Interstitial Cystitis Association Pilot Grant, a Fishbein Family IC Research Grant, New York Academy of Medicine, and Boston Children's Hospital Faculty Development. The funders had no role in the design, data collection and analysis, decision to publish or preparation of the manuscript.
- **Conflict of Interest:** No potential conflict of interest relevant to this article was reported.

REFERENCES

1. Beasley-Green A. Urine proteomics in the era of mass spectrometry. *Int Neurourol J* 2016;20(Suppl 2):S70-5.
2. Park ST, Kim J. Trends in next-generation sequencing and a new era for whole genome sequencing. *Int Neurourol J* 2016;20(Suppl 2):S76-83.
3. Li HT, Duymich CE, Weisenberger DJ, Liang G. Genetic and epigenetic alterations in bladder cancer. *Int Neurourol J* 2016;20(Suppl 2):S84-94.
4. Jhang JF, Kuo HC. Pathomechanism of interstitial cystitis/bladder pain syndrome and mapping the heterogeneity of disease. *Int Neurourol J* 2016;20(Suppl 2):S95-104.
5. Kanematsu A. Translational research for pediatric lower urinary tract dysfunction. *Int Neurourol J* 2016;20(Suppl 2):S105-11.
6. Di Pietro G, Chornokur G, Kumar N, Davis C, Park JY. Racial differences in the diagnosis and treatment of prostate cancer. *Int Neurourol J* 2016;20(Suppl 2):S112-9.
7. Zhuang L, Johnson MT. How precisely can prostate cancer be managed? *Int Neurourol J* 2016;20(Suppl 2):S120-30.
8. Tran P, Nguyen C, Klempner SJ. Targeting the phosphatidylinositol-3-kinase pathway in gastric cancer: can omics improve outcomes? *Int Neurourol J* 2016;20(Suppl 2):S131-40.

REPORT

Differential perturbation of the interstitial cystitis-associated genes of bladder and urethra in rat model

Bo-Hwa Choi^a, Sungyong You^b, Chang-Shin Park^a, Eun-Ho Cho^{b,c}, Taeun D. Park^{b,d}, Sungsoo Kim^e, Young-Ju Kim^{a,f}, Tack Lee^f, and Jayoung Kim^{b,c}

^aDepartment of Pharmacology, Hypoxia-Related Disease Research Center, Inha Research Institute for Medical Sciences, Inha University College of Medicine, Incheon, South Korea; ^bDepartments of Surgery and Biomedical Sciences, Cedars-Sinai Medical Center, Los Angeles, CA, USA; ^cUniversity of California, Los Angeles, CA, USA; ^dUniversity of California, Berkeley, CA, USA; ^eDepartment of Biochemistry and Molecular Biology, Medical Research Center for Bioreaction to Reactive Oxygen Species and Biomedical Science Institute, School of Medicine, Kyung Hee University, Seoul, South Korea; ^fDepartment of Urology, Inha University College of Medicine, Incheon, South Korea

ABSTRACT

Interstitial cystitis (IC) is a chronic bladder dysfunction characterized as urinary frequency, urgency, nocturia, and pelvic pain. The changes in urethra may wind up with the bladder changes in structure and functions, however, the functions of the urethra in IC remains elusive. The aim of this study was to understand the perturbed gene expression in urethra, compared with urinary bladder, associated with the defected urodynamics. Using female IC mimic rats, a comprehensive RNA-sequencing combined with a bioinformatics analysis was performed and revealed that IC-specific genes in bladder or urethra. Gene ontology analysis suggested that the cell adhesion or extracellular matrix regulation, intracellular signaling cascade, cardiac muscle tissue development, and second messenger-mediated signaling might be the most enriched cellular processes in IC context. Further study of the effects of these bladder- or urethra-specific genes may suggest underlying mechanism of lower urinary tract function and novel therapeutic strategies against IC.

ARTICLE HISTORY

Received 15 December 2016
Revised 25 January 2017
Accepted 8 February 2017

KEYWORDS

bladder; gene expression;
interstitial cystitis; rat model;
RNA-Sequencing; urethra

Introduction

Interstitial cystitis (IC) is a chronic noninfectious inflammatory disease of the bladder wall, characterized by recurring discomfort or pain possibly related to the bladder symptoms such as urinary frequency, urgency, nocturia.⁸ Increasingly clinical important issues include significant negative impacts on the quality of life and social function as well as high prevalence in the general population.^{1,6} Given that IC affects approximately 3.3 million women in the United States, IC is a major health issue largely affecting the quality of everyday life of patients—approximately 50% of those diagnosed with IC have difficulties working full-time, while approximately 70% of patients have trouble sleeping. Additionally, 75% of patients report dyspareunia.¹⁵ Multimodality therapy has become a standard treatment of IC, because of no notable responses to therapy as a single agent.⁷ This suggests that there are multiple underlying factors involved in the etiology of IC, and all of which have a direct impact on the symptom characteristics, disease course and variable responses to therapy. Many causative factors of IC have been documented, however, our current understanding of the causation still clings to the assumption of a leaky urothelium to toxic substances, allergens or bacteria from the urine. This may be the primary step on the inflammatory process of the deeper bladder wall layer.¹⁰ Although it is plausible, additional

understanding of mechanisms involved in this theoretical mechanism may be required to clarify the mechanisms behind this devastating disease.

Various rodent models for IC study have been introduced to phenotype (a) nociception to bladder distention, (b) pelvic nociception, and/or (c) urinary frequency. IC animal models include the bladder injury rat model that mimics IC in which protamine sulfate (PS) and the endotoxin lipopolysaccharide (LPS) are administered intravesically to Sprague-Dawley rats. PS treatment destroys the bladder glycosaminoglycan (GAGs) layer, leading to enhancement of the LPS action. Animal models including ours bear 3 similarities to currently known pathophysiologic steps of human IC.^{4,28} At first, PS damaged the bladder mucus, and then urothelium was injured by bacterial toxins such as LPS.⁴ Following these steps, the injured mucus and urothelium are exposed to rat's urine for an additional one month to give enough time for inducing chronic inflammation into the injured bladder wall by the toxins from urine. Our previous findings in this rat model demonstrated the involvement of degranulated mast cells, which was consistent with observation in the human bladder affected with IC. Over 50% of patients have mast cells in lamina propria.^{4,26} Mast cells have been considered to play key pathophysiological roles in the initiation and propagation of inflammation, by the production

CONTACT Tack Lee  lee.tack33@gmail.com  Department of Urology, Inha University College of Medicine, 5th Floor Jung-Suk Building, 7-241, 3-Ga, Shinheung-Dong, Jung-Gu, Incheon 400-712, South Korea; Jayoung Kim  Jayoung.Kim@cshs.org  Departments of Surgery and Biomedical Sciences, Cedars-Sinai Medical Center, 8700 Beverly Blvd., Davis Research Building 5071, Los Angeles, CA 90048, USA.

Color versions of one or more of the figures in the article can be found online at www.tandfonline.com/kccy.

proinflammatory mediators, neurotrophic factors and immunoregulatory cytokines.²⁵ Mast cells also secrete nerve growth factor (NGF) leading to the neuropathic pain, one of IC characteristics.²⁶

Another hypothesis for the etiology of IC is that an initial insult to the bladder such as urinary tract infection triggers neurogenic inflammation. Several studies have shown that there is an increase in the number and sensitivity of nerve fibers in the bladders of patients with IC.^{19,22} A central role of this inflammation has been suggested in the pathogenesis of interstitial cystitis.⁹ The etiology of the IC is obscure, and some studies have been attributed to an anatomic problem such as bladder outlet obstruction (BOO) in LUT dysfunction, regardless of sex difference.⁵ Chronic prostatitis/chronic pelvic pain syndrome (CP/CPPS) is a condition that is similar to IC in men.²⁷ Many men who are categorized as having CP/CPPS have urodynamically proven BOO.²⁰ Some evidence shows that the female paraurethral glands in the distal urethra are homologous to the prostate, and the inflammation in these glands may be related to the pathophysiology of IC.²⁸ There may be a wind-up of urethral changes in structure and function with these bladder changes without any clear mechanistic explanation.

The urinary bladder and urethra are the 2 most relevant organs to understand the regulatory mechanism of IC. The normal function of the lower urinary tract is to store and periodically evacuate the urine, which is delicately regulated by the opposing actions of the bladder and the urethra during each phase of storage and voiding. The urethra, a tube through which urine is excreted from the urinary bladder inside the body for elimination to outside the body in urination, allows voluntary control over urination. In males, the urethra carries urine as well as semen. In females, it is much shorter than those in males, and is used only for urination. As the urinary bladder and urethra work together as a functional unit, the changes in bladder function are closely related to those of the urethral function.

In this study, we hypothesized that urethra and urinary bladder have different molecular signatures and regulatory mechanisms in IC patients. In this study using the IC rat model and comparable sham control model, we sought to understand the urethra- or bladder-specific gene signatures and the differences of biologic functions.

Results

The goal of this study was to identify the differentially expressed genes specifically in the bladder or urethra within the IC model, compared with the control. A workflow describing our analytic procedures for the construction of our IC rat model, measurement of cystometric parameters, harvests and extractions of bladder and urethra from animal model, and RNA-Sequencing down in this study were shown in Fig. 1.

Body weight, bladder weight and ratio were not changed in rat model

First, we wondered if there were any general health issues in IC rats compared with sham control rats. There was no significant

difference in the body weight between the sham group (477.6 ± 10.5 g) and the IC group (495.6 ± 13.0 g), one month after intravesical instillations of PS and LPS or saline. The bladder weight did not differ significantly between the sham (0.22 ± 0.01 mg) and IC group (0.24 ± 0.02 mg). Although the bladder weight was normalized to body weight, there was no significant difference between the 2 groups (Sham; 0.47 ± 0.03 , IC; 0.49 ± 0.04).

The cystometric parameters between the sham controls and IC rats were assessed

Rats of the IC group did not show any significant difference to sham rats in any pressure parameters - including BP, TP, and MP. However, all volume parameters except the RV (BC, MV and MI) decreased in IC rats comparing to sham, showing the features of IC. Although the value of RV did not show any significance between sham and IC, 57.1% (4 among 7 rats) of rats in IC group showed RV. However, no rats in the sham group showed RV (Table 1 and Fig. 1).

RNA-Sequencing analysis identified the differentially expressed genes, which are specific to bladder or urethra

To understand the molecular responses associated with IC, we attempted to perform the next generation RNA sequencing analysis and to get the expression profile of the bladder and urethra in response to PS and LPS stimulation, and those of sham controls. Comparison of RNA-Sequencing status between raw and filtered reads was performed as follows.

Based on raw sequence data, the filtering processes were performed based on the following criteria; (i) position 1 to 15 base were removed because of hexamer-primed 2nd strand synthesis, (ii) reads with mean base quality ≤ 20 and total base quality (≥ 20) $\leq 80\%$ were removed, and (iii) redundant reads (identical sequences) were collapsed into one read. Further calculation of expression level from the finally filtered reads was done as follows: filtered reads were aligned with the UCSC rn5 build of the *Rattus-norvegicus* genome using the Subread aligner.¹⁶ Gene-wise counts were obtained using the featureCounts.¹⁷ We compared normalized read count values across samples based on the annotation from UCSC rn5 build.

The differentially expressed genes in bladder and/or urethra in IC model vs. sham control

We identified differentially expressed genes (DEGs) with a false discovery rate (FDR) < 0.05 . A heatmap shown in Fig. 2A revealed that approximately 3-fold more DEGs were perturbed in urethra in comparison of the bladder. Forty-four DEGs were significantly perturbed in bladder tissues obtained from IC rat model, compared with those from control group (Fig. 2B and Supplementary Table 1A).

The gene expression of 159 DEGs was significantly altered in urethras in the IC rat model (Fig. 2B and Supplementary Table 1B). Only 5 genes were commonly altered both in the bladder and urethra, suggesting that the gene expression of bladder and urethra were distinct (Fig. 2B). These 5 genes include collagen type VII α 1 (Col7a1), integrin α 7 (Itga7),

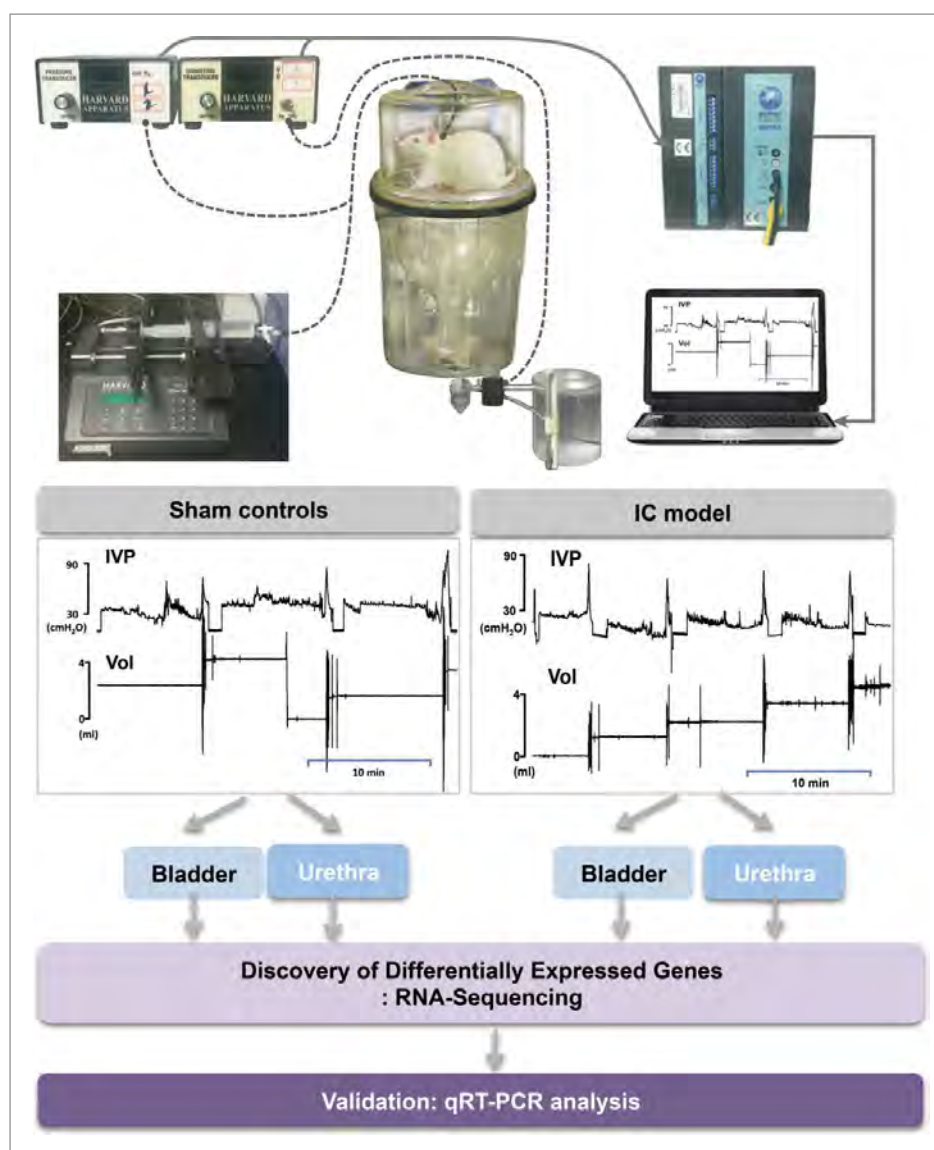


Figure 1. A workflow of this study.

Serpin Family A Member 3 (Serpina3n), Solute Carrier Family 25 Member 24 (Slc25a24) and Slit Guidance Ligand 3 (Slit3) (Table 2A). We also found 61 IC-specific (Fig. 2C and Supplementary Table 2A) or 62 Sham-specific genes (Fig. 2C and Supplementary Table 2B). Four commonly perturbed genes in bladder - compared with urethra - included Flavin Containing Monooxygenase 5 (Fmo5), Integrin Subunit α 7 (Itga7), Lymphocyte Cytosolic Protein 1 (Lcp1), and Methyltransferase Like 7B (Mettl7b) (Fig. 2C and Table 2B).

Enriched cellular processes perturbed in IC model and the differentially enriched cellular processes in bladder and urethra

We next attempted to understand the biologic and mechanistic meaning of these DEGs by examining the biologic pathways over-represented by the genes. The comparison between bladder and urethra revealed that responses of bladder or urethra induced IC model by PS and LPS treatment were different. GOBP and KEGG pathway enrichment analysis demonstrated

Table 1. Cystometric parameters in conscious, unrestrained Sprague-Dawley rats in the sham and IC groups. Table 1. Cystometric parameters (including pressure and volume parameters) in awake rats subjected to sham-operation or intravesical PS/LPS-treated rats (IC rats).

	BP (cmH ₂ O)	TP (cmH ₂ O)	MP (cmH ₂ O)	BC (mL)	MV (mL)	RV (mL)	MI (min)
Sham	16.14 ± 1.16	32.16 ± 2.04	74.49 ± 5.71	1.86 ± 0.18	1.86 ± 0.18	0	9.99 ± 0.91
IC	18.87 ± 2.89	38.10 ± 3.76	60.90 ± 4.68	1.31 ± 0.14*	1.17 ± 0.10*	0.15 ± 0.09	6.22 ± 0.83*

BP, basal pressure; TP, threshold pressure; MP, micturition pressure; BC, bladder capacity; MV, micturition volume; RV, residual volume; MI, micturition interval; IC, interstitial cystitis; Results are expressed as the mean ± standard error. Pressure parameters were expressed by intravesical pressure.

*p < 0.05,

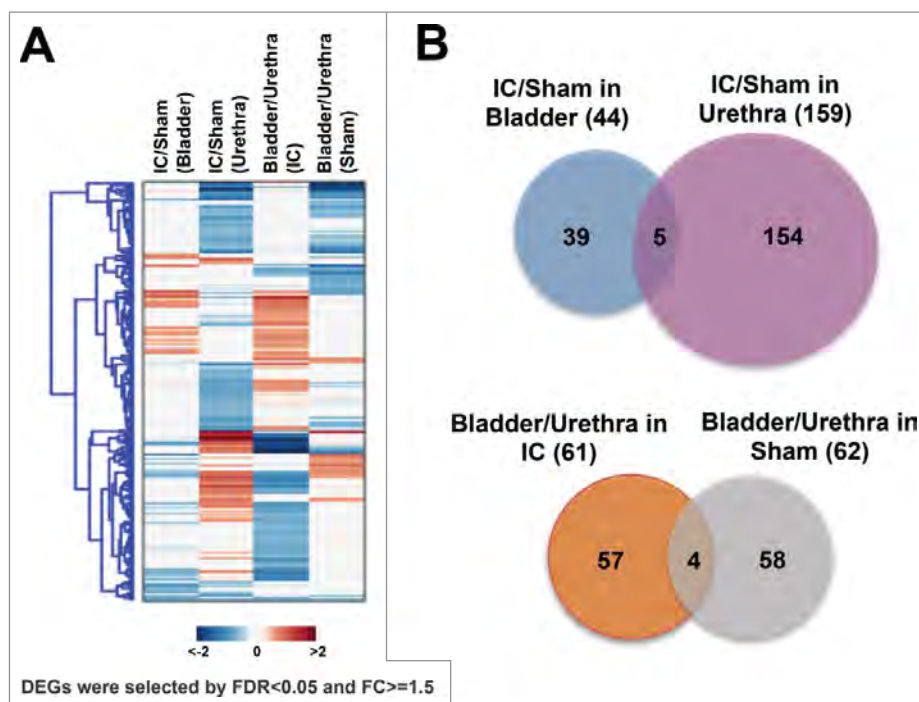


Figure 2. Identification of differentially expressed genes (DEGs) in bladder or urethra obtained from IC rats compared with sham controls. (A) A heatmap showing DEGs (B) Diagrams indicating IC-specific DEGs in bladder or urethra (upper), and bladder- or urethra-specific DEGs associated with IC (bottom).

that the altered genes in bladder tissues of IC model were mainly involved in response to disaccharide stimulus, response to sucrose stimulus, and regulation of blood pressure (Blue bars, Fig. 3A). The most enriched cellular processes in urethra in IC model included the response to abiotic stimulus, epithelial cell differentiation, extracellular matrix organization and response to wounding et al. (Orange bars, Fig. 3A). We also found that the cellular processes (e.g., intracellular signaling cascade, cardiac muscle tissue development, and second-messenger-mediated signaling) were enriched in IC-specific DEGs (Green bars, Fig. 3B).

Differentially expressed genes in IC model suggest the bladder specific or urethra specific DEGs

This pathway analysis could allow us to focus on the gene list of the greatest interest. We chose 5 genes whose expression levels

were significantly increased in bladder, but not in urethra, of IC model for further validation. They were *Fras1* (Fraser syndrome 1), *Adipoq* (adiponectin, C1Q and collagen domain containing), *Tnfaip2* (tumor necrosis factor, α -induced protein 2), *Ace2* (angiotensin I converting enzyme 2), and *Frem2* (*Fras1* related extracellular matrix protein 2). The fold changes of gene expression in IC model, compared with sham control, were presented in Fig. 4A.

Additionally we selected 5 more genes whose expression was significantly increased only in the urethra of IC model. They were *Ceacam1* (carcinoembryonic antigen-related cell adhesion molecule 1, biliary glycoprotein), *Sox2* (SRY, sex determining region Y)-box 2), *Ido1* (indoleamine 2,3-dioxygenase 1), *Ccl21* (chemokine (C-C motif) ligand 21), and *Atf3* (activating transcription factor 3) (Fig. 4B). Fig. 4C shows the fold changes of 10 genes' gene expression levels in bladder or urethra in IC condition (fold change).

Table 2. (A) List of 5 common genes in the comparison of IC vs. Sham controls, (B) List of 4 common genes in the comparison of bladder vs. urethra.

A		IC/Sham (Bladder)	IC/Sham (Urethra)
Symbol	Description		
<i>Col7a1</i>	collagen, type VII, α 1	-0.65	-0.97
<i>Itga7</i>	integrin, α 7	0.81	-0.6
<i>Serpina3n</i>	serine (or cysteine) peptidase inhibitor, clade A, member 3N	-0.88	-0.74
<i>Slc25a24</i>	solute carrier family 25 (mitochondrial carrier, phosphate carrier), member 24	0.7	1.14
<i>Slit3</i>	slit homolog 3 (<i>Drosophila</i>)	-0.86	0.99
B		Bladder/Urethra (Sham)	Bladder/Urethra (IC)
Symbol	Description		
<i>Fmo5</i>	flavin containing monooxygenase 5	0.77	0.99
<i>Itga7</i>	integrin, α 7	-0.75	0.67
<i>Lcp1</i>	lymphocyte cytosolic protein 1	0.73	0.84
<i>Mettl7b</i>	methyltransferase like 7B	-0.84	0.76

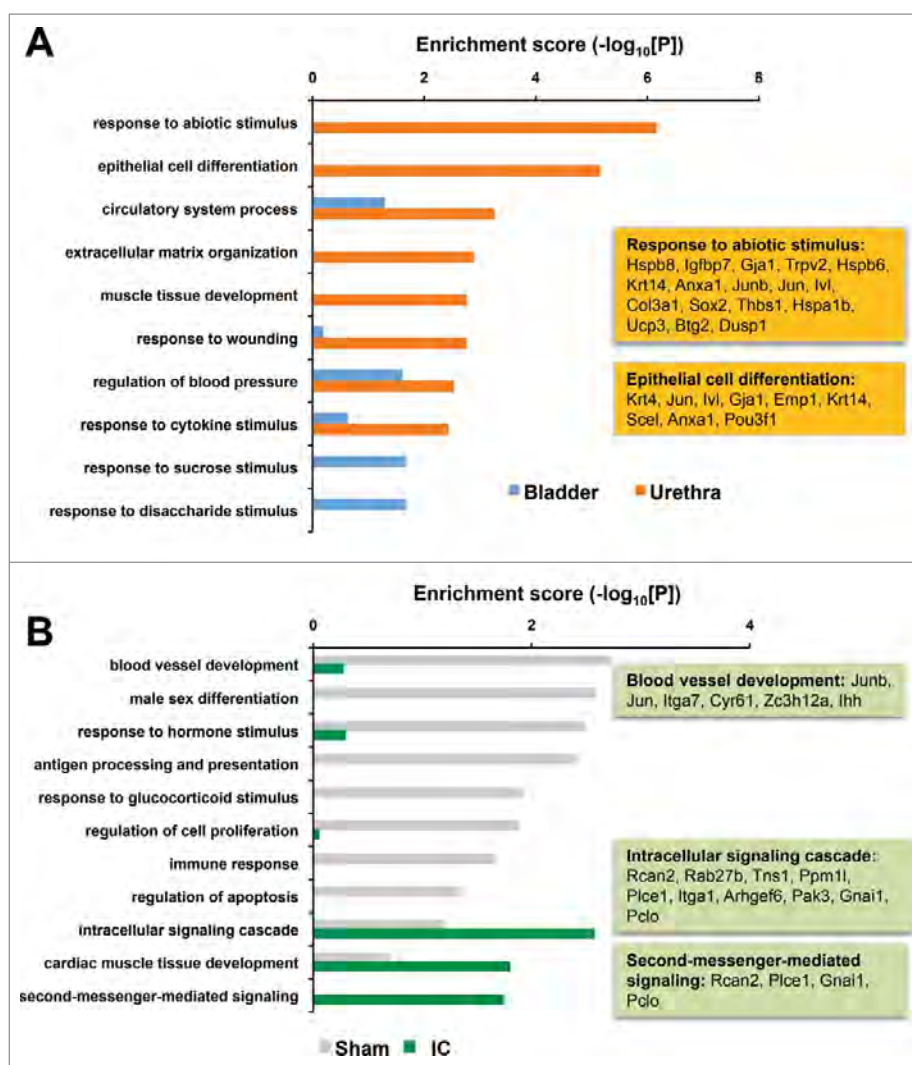


Figure 3. (A) Enriched cellular processes perturbed in IC rats by PS and LPS treatment. Representative DEGs of “response to abiotic stimulus” and “epithelial cell differentiation” were indicated in orange boxes. Blue, bladder specific; Orange, urethra-specific DEGs. (B) Differentially enriched cellular processes changed sham or IC specifically. Gray, sham control specific; Green, IC specific DEGs.

To validate the expression levels and to challenge the importance of these candidates as major modulators of important cellular processes, we performed qRT-PCR analysis using independent bladder ($n = 3$) or urethra ($n = 3$) tissues obtained from IC model ($n = 3$) or sham controls ($n = 3$). In total the top 10 genes, which were already selected based on our interest and representativeness of organ that they were belonged to, were analyzed (Fig. 5). Consistent with the expression levels quantified in the RNA-sequencing analysis, we found gene expression of *Fras1*, *Tnfaip2*, *Ace2*, and *Frem2* were increased in IC model, and expression of *Adipoq* and activating transcription factor 3 (*Atf3*) was decreased in IC model, compared with sham controls (Fig. 6A). In the urethra, expression of genes such as *Ceacam1*, *Ido1*, and *Ccl21* was increased in IC group, while gene expression of *Adipoq*, *Tnfaip2*, *Ace2*, *Frem2*, *SRY*, and *Atf3* was significantly decreased (Fig. 6B).

Discussion

In this study, we sought to understand the functional mechanism associated with the altered gene expression in our IC rat

model. Our global RNA profile using a comprehensive RNA-sequencing analysis identified genes whose expression levels were significantly altered in Sprague-Dawley rats by intravesical instillations of LPS following PS. Animal models are useful tools, in particular to study the symptom-driven human disorders of unknown etiology such as IC.² Although IC is not an infectious disease, LPS - an endotoxin from *E. coli* - is commonly used as an acute precipitating factor in animal models of IC.²⁹ Our previous series of animal experiments in Sprague-Dawley rats by intravesical instillations of LPS following PS demonstrated that this chronic rat model exhibited the uninhibited detrusor contractions proved by simultaneous intra-abdominal pressure (detrusor overactivity; DO) during the filling phase and the characteristic degranulated mast cells in their histologic appearance.⁴

Our study took a systems approach to overview the enriched biologic pathways of these DEGs, and to identify an IC-regulatory bladder or urethra specific gene set. This approach provides a testable hypothesis that the bladder of IC patients may be different from the urethra of these same patients. We also performed independent biochemical validation experiments, which revealed

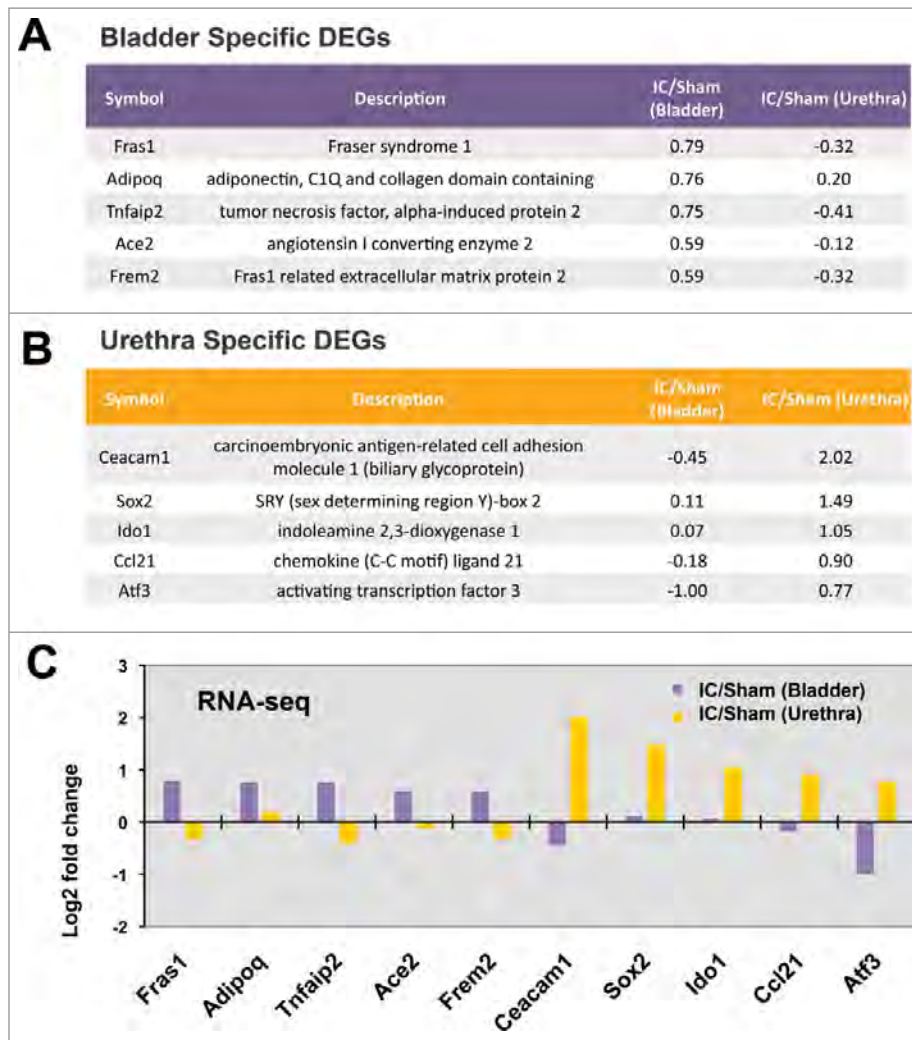


Figure 4. (A) Bladder specific DEGs, (B) Urethra specific DEGs, (C) Expression patterns obtained from RNA-Sequencing data of 10 genes.

the 10 most altered genes in bladder vs. urethra. These findings suggest the molecular mechanism in bladder or urethra tissues of IC patients may be distinct, leading to different responses to therapeutic approaches of IC patients, by regulating downstream gene sets, and the understanding of the difference would benefit patient treatment.

A central observation of the present study was that chronic IC with similar characteristics to the human disease was induced in rat model by intravesical instillations of LPS following PS.²⁸ All rats in this chronic model except one exhibited degranulated mast cells, which was crucial evidence for the successful establishment of a model resembling the human disease. All rats demonstrated DO during the filling phase. These findings are similar to those of a previous rat model of IC induced by intravesical administration of HCl.¹³ Previous population-based studies on IC reported a prevalence of urodynamically verified DO ranging from 14–30% in IC patients.

Urine is a liquid-by-product of the body, which is made up of 95 percent water and 5 percent dissolved urinary toxic solutes including urea, chloride, sodium and potassium ions. These poisonous or toxic materials are always subject to invading into the bladder wall, which is protected in normal conditions by the tight junction of the umbrella cells and

bladder mucus composed of GAGs and proteoglycans. This layer is known as a critical regulator of the bladder's permeability to water and urinary solutes, and is deficient in many patients with IC.²³ The lower urinary tract (LUT) dysfunction results from simultaneous opposing interactions between the bladder and urethra, such as bladder relaxation and urethral contraction during storage, and bladder contraction and active urethral relaxation during micturition. These continuously changing intravesical environments make the bladder wall more susceptible to these toxins. If there were an initial insult such as LPS, the toxic urine results in urothelial hyperplasia and alterations of the LUT functions, forming a vicious cycle. According to the urodynamic study, obstruction is common in male or female patients with IC, which was postulated to be primarily due to pelvic floor dysfunction.^{3,24} This may be caused by bladder wall inflammation. However, these alterations that affect these interactions and result in voiding dysfunction in IC patients have not yet been fully elucidated.

Among 10 identified IC-specific DEGs from our female IC rats, we found that at least 3 of the DEGs (Fras1, Frem2, and Ceacam1) were related to cell adhesion or extracellular matrix regulation. Further GO analysis suggested that the

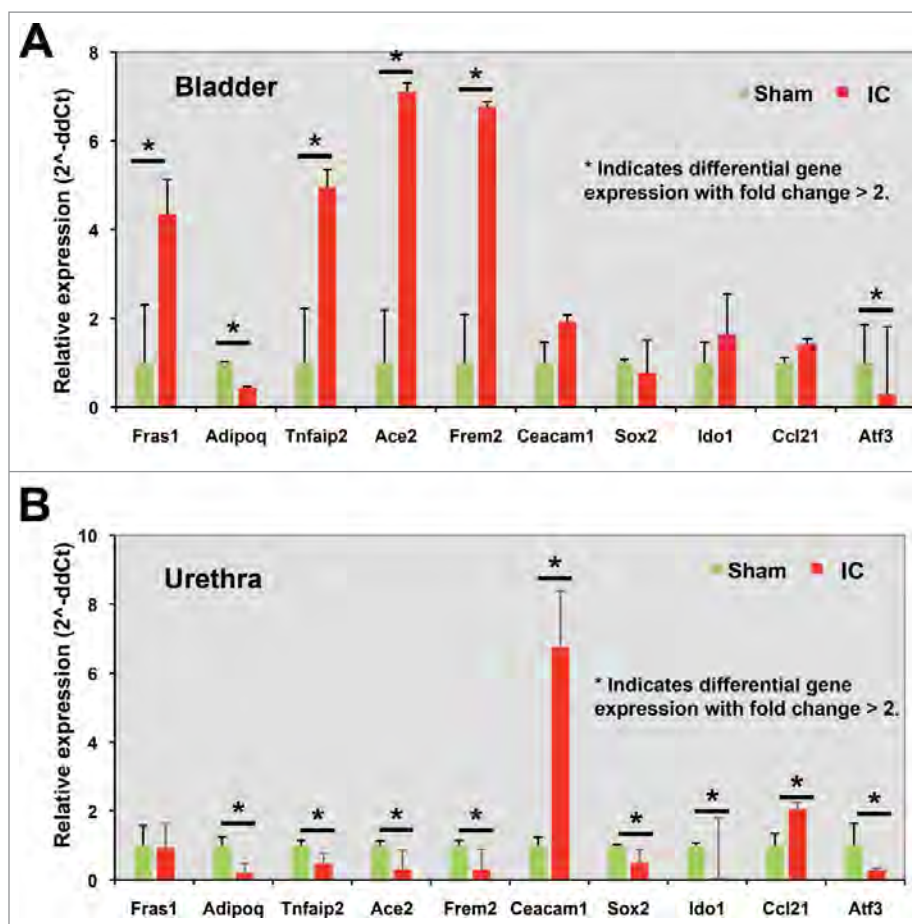


Figure 5. Further validation using qRT-PCR analysis.

intracellular signaling cascade, cardiac muscle tissue development, and second messenger-mediated signaling were the most enriched cellular processes in bladder and urethra of IC group. Experimental data from quantitative RT-PCR analysis for further validation showed the patterns of gene expression in bladder and urethral cells were quite different. Expression of *Tnfaip2*, *Ace2*, and *Frem2* was significantly changed but in the opposite way (Fig. 5). These findings strongly suggest that perturbed genes in IC context are significantly different in the bladder and urethra. In contrast, expression of *Atf3* and *Adipoq* was both significantly down-regulated both in bladder and urethra of IC rats, compared with sham controls. Although the biologic function of *Atf3* in bladder or urethra remain unknown, a previous study suggested that *Atf3* as a player involving in the growth of the detrusor muscle and its motor innervation following infravesical outlet obstruction,³⁰ suggesting the possibility that *Atf3* downregulation may cause bladder dysfunction observed in IC. Adiponectin, an adipose tissue-secreted adipocytokine, was reported to associate with bladder contraction, through *PKC α* signaling pathway and calcium sensitivity. Downregulation of *Adipoq* found in our study suggests a potential functional link to bladder contraction allowing proper voiding pattern - although this speculation should be tested in future work. We also found *Ccl21* was significantly increased only in urethra, not in bladder tissues of IC rats. A previous study using 15 women with IC and 15

control subjects with stress urinary incontinence without bladder pain suggested that *Ccl21* may be correlated significantly with clinical outcomes through an increased nociceptive signaling by *Ccl21*.²¹

In summary, we have identified the perturbed gene expression associated with the defected urodynamics in IC mimic animal model, thereby exhibiting the dysfunction of the urinary bladder. A comprehensive analysis based on the next generation RNA-sequencing method combined with a bioinformatics analysis was performed. Our experimental results revealed that the perturbed alterations in gene expression in bladder and urethra are distinct, along with different structure and anatomy, are functionally associated with extracellular matrix organization, wound healing, intracellular signaling cascade and second-messenger-mediated signaling. Further study of the effects on lower urinary tract function may suggest novel therapeutic strategies.

Materials and methods

Animals and study design

A total of 13 female Sprague-Dawley rats (Orient Bio Inc., Gyeonggi-do, South Korea), weighing 200–250 g, were used in the present study. In 7 rats, LPS was instilled intravesically, following the intravesical administration of PS. In 6 rats, the saline was instilled into the bladder and served as the sham group. To

avoid potential leak of drugs during *instillation of PS and LPS to the bladder, which might cause epithelial damage and subsequent inflammation*, we were careful not to overflow the capacity of the individual bladders while the rats were anesthetized. In addition, the drugs were injected to ensure that the fluid does not flow to the urethra and were injected only into the bladder dome. The normal urethra is closed during the storage phase and anesthesia.

Continuous cystometry was performed in all of the rats under awake conditions, one month following intravesical instillation of LPS or saline. After cystometry, rats were killed by cervical dislocation. Following laparotomy, the bladder and urethra were obtained en bloc from all rats, separated at the level of the bladder neck, and the bladder was weighed. All experimental animal procedures were conducted in accordance with the Guide for the Care and Use of Laboratory Animals of the National Institutes of Health (Bethesda, MD, USA) and were approved by the INHA Institutional Animal Care and Use Committee at the Inha University Medical School (Incheon, South Korea; approval ID: INHA 140731-321-1). The rats were maintained under a 12-h light:dark photoperiod and normal laboratory conditions, with free access to food pellets and tap water except during the experiments.

Surgical procedures

The rats were anesthetized with ketamine (Ketamine; Yuhan Corp., Seoul, Korea; 75 mg kg⁻¹ intraperitoneally) and xylazine (Rompun; Bayer Korea Corp, Seoul, Korea; 15 mg kg⁻¹ intraperitoneally) mixture, during the surgical procedures. Through a lower abdominal midline incision, the bladder and the proximal urethra were approached.

Induction of cystitis

Cystitis was induced by the intravesical instillation of LPS following PS, as described previously.²⁸ Briefly, a 31 gauge needle attached to a syringe (Insulin syringe, SUNGSHIM MEDICAL CO., LTD, Gyeonggi-do, Korea) was inserted into the bladder dome, after the bladder was exposed. The bladder was then emptied by aspiration of urine, and then an appropriate volume of PS (10 mg ml⁻¹) was instilled into the bladder. Twenty minutes later, the bladder was emptied, washed with phosphate-buffered saline (PBS) and then filled with the same volume of LPS (750 µg/ml) for another 20 min. The sham group was instilled with normal saline of the same volume.

Procedures for intra-vesical catheter implantation

Three days before cystometry, the catheterization for intravesical pressure (IVP) recordings was done, as described previously^{12,14} Briefly, after the bladder exposed, a polyethylene catheter (PE-50; Becton-Dickinson, Parsippany, NJ, USA) with a cuff was inserted into the dome of the bladder and held in place with a purse-string suture to record IVP. The catheter was tunneled through the subcutaneous space, exited through the back of the animals and anchored to the skin of the back with a silk ligature. The free end of the catheter was sealed. After surgery, the animals were caged individually and maintained in the same manner.

Functional evaluation

Cystometrograms were performed under unanesthetized, unrestrained conditions in metabolic cages. The external portion of the catheter, implanted into the bladder of the rat, was connected to a 2-way valve that was connected via a T-tube to a pressure transducer (Research Grade Blood Pressure Transducer; Harvard Apparatus, Holliston, MA, USA) and a micro-injection pump (PHD22/2000 pump; Harvard Apparatus). This was used to record the IVP on the condition of continuous injection. Room-temperature saline was infused into the bladder by microinjection pump at a rate of 10 ml h⁻¹. The micturition volume (MV) was recorded by means of a fluid collector connected to a force displacement transducer (Research Grade Isometric Transducer; Harvard Apparatus). IVP and MV were continuously recorded using Acq Knowledge 3.8.1 software and an MP150 data acquisition system (Biopac Systems, Goleta, CA, USA) at a sampling rate of 50 Hz. The mean values from 3 reproducible micturition cycles were used for evaluation of cystometric parameters.

Investigation of cystometric parameters

Cystometric parameters consisted of pressure and volume parameters of the model, including the lowest bladder pressure during filling phase (BP), bladder pressure immediately before micturition (TP), maximum bladder pressure during the micturition phase (MP), MV, remaining urine after micturition (RV), MV+RV (BC) and intervals between maximum micturition contractions (MI).

Next generation RNA-Sequencing analysis

RNA-Sequencing analysis identified the differentially expressed genes, which are specific to the bladder or urethra. To understand the molecular responses associated with IC, we attempted to perform the next generation RNA sequencing analysis and to get the expression profile of bladder and urethra in response to PS and LPS stimulation, and also those of sham controls. Comparison of RNA-Sequencing status between raw and filtered reads was performed as follows.

Bladder (n = 3) and urethra tissues (n = 3) were harvested from Sham controls (n = 6 in total) or IC rat model (n = 6 in total), and total RNA from the urine sediments were purified using the miRNeasy mini kit according to the manufacturer's instruction (Qiagen). Concentration and yield of RNA samples was determined using a NanoDrop ND-1000 Spectrophotometer (NanoDrop Technologies). RNA integrity was determined by analysis on an Agilent 2100 Bioanalyzer (Agilent Technologies) following the manufacturer's recommendations. Only samples with a RIN score greater than 7.0 were used for the subsequent molecular analysis. Nugen Ovation RNA-Seq System V2 kit was used to generate the double-stranded cDNA using a mixture of random and poly (T) priming. cDNA library was prepared using commercial kits and following manufacturer's protocols. Kapa LTP library kit was used to make the sequencing library. The workflow consists of fragmentation of double stranded cDNA, end repair to generate blunt ends, A-tailing, adaptor ligation and PCR amplification. Different adaptors were used for multiplexing samples in one lane.

Sequencing was performed on Illumina NextSeq 500 for a single read 75 run. Data quality check was done on Illumina SAV. Demultiplexing was performed with Illumina CASAVA 1.8.2.

The quality of sequence reads was assessed using the FastQC tool (Babraham Bioinformatics, Cambridge, UK). The few low-quality bases were trimmed from read extremities using Short-Read (version 1.30.0) package from R bioconductor (version 3.3). More than 30×10^6 reads were generated for each replicate and were aligned with the UCSC rn5 build of the *Rattus norvegicus* genome, through the use of the Subread aligner.¹⁶ Gene-wise counts were obtained with the featureCounts program.¹⁷ Genes were filtered out and excluded from downstream analysis if they failed to achieve raw read counts of at least 2 across all the libraries. DESeq2¹⁸ (version 1.6.1) was used for calculating normalized data count data by regularized log transformation and conducting differential gene expression analyses. Differentially expressed genes (DEGs) were determined with false discovery rate (FDR) < 0.05 and fold change ≥ 1.5 . If certain conditions didn't have replicate to estimate dispersion of the IC model versus Sham control in Urethra tissue and IC Bladder vs. IC Urethra, DEGs were determined by only using fold change of more than 1.5 folds due to no replicate in the IC model from Urethra tissue. Finally, to identify cellular processes represented by the DEGs, the enrichment analysis was performed using the DAVID software.¹¹ Specifically enriched cellular processes between up- and downregulation was selected with enrichment $P < 0.05$. Bar graphs were used to represent the level of significance of each cellular process with enrichment score ($-\log_{10} [P]$).

Reverse transcription and PCR analysis

Total RNA was separately purified from bladder ($n = 3$) or urethra tissues ($n = 3$) from the Sham controls ($n = 6$ in total) and IC model rats ($n = 6$ in total) using a QiagenRNeasy tissue extraction kit (Qiagen Inc., Valencia, California). RNA concentration was measured using a Nanodrop ND-1000 spectrophotometer (Thermo Scientific, Wilmington, DE). Primers for RT-PCR were designed based on sequence information suggested from RNA-sequencing data.

Statistical analysis

All results were analyzed using SigmaStat 2.0 (SPSS Inc., Chicago, USA). The results are presented as the mean values \pm standard error of the mean. The Shapiro-Wilk W-test confirmed normal distributions. Statistical significance was determined by paired or unpaired t-tests. Unpaired t-tests were used to determine the statistical significance to detect differences in urodynamic parameters and histological data between the sham and IC groups. For multiple comparisons, one-way analysis of variance with Tukey's test was used to detect differences. Statistical significance was considered at $p < 0.05$. All calculations were made on the basis of n , which denoted the number of animals.

Disclosure of potential conflicts of interest

No potential conflicts of interest were disclosed.

Funding

This study was supported by Basic Science Research Program through the National Research Foundation of Korea (NRF) funded by the Ministry of Education (NRF-2016R1D1A1B03932278 (to T.L.)) and National Research Foundation of Korea (NRF) grant funded by the Korea government (MSIP) (NRF-2014R1A5A2009392 (to C.S.P., B.H.C.)). The authors acknowledge support from National Institutes of Health grants (1U01DK103260, 1R01DK100974, U24 DK097154, NIH NCATS UCLA CTSI UL1TR000124 (to J.K.)), Department of Defense grants ((W81XWH-15-1-0415) (to J.K.)), Centers for Disease Controls and Prevention (1U01DP006079 (to J.K.)), IMAGINE NO IC Research Grant, the Steven Spielberg Discovery Fund in Prostate Cancer Research Career Development Award, and US-Egypt Science and Technology Development Fund by the National Academies of Sciences, Engineering, and Medicine. J.K. is former recipient of Interstitial Cystitis Association Pilot Grant, a Fishbein Family IC Research Grant, New York Academy of Medicine, and Boston Children's Hospital Faculty Development. The funders had no role in the design, data collection and analysis, decision to publish or preparation of the manuscript.

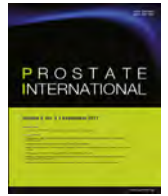
Author contributions

JK, TL and SK designed the study, led obtaining funding, and overviewed the literature analysis and drafting the manuscript. BHC and CSP performed animal experiments. YJK, EC, and TDP performed data analysis and organized sample collection. SY performed the analysis of gene expression data. SK, YJK, and TDP assisted writing the manuscript. All authors read and approved the final manuscript.

References

- Berry SH, Elliott MN, Suttrop M, Bogart LM, Stoto MA, Eggers P, Nyberg L, Clemens JQ. Prevalence of symptoms of bladder pain syndrome/interstitial cystitis among adult females in the United States. *J Urol* 2011; 186:540-44; PMID:21683389; <http://dx.doi.org/10.1016/j.juro.2011.03.132>
- Bjorling DE, Wang ZY, Bushman W. Models of inflammation of the lower urinary tract. *Neurourol Urodyn* 2011; 30:673-82; PMID:21661012; <http://dx.doi.org/10.1002/nau.21078>
- Cameron AP, Gajewski JB. Bladder outlet obstruction in painful bladder syndrome/interstitial cystitis. *Neurourol Urodyn* 2009; 28:944-48; PMID:19301413; <http://dx.doi.org/10.1002/nau.20729>
- Choi BH, Jin LH, Kim KH, Han JY, Kang JH, Yoon SM, Park CS, Lee T. Mast cell activation and response to tolterodine in the rat urinary bladder in a chronic model of intravesical protamine sulfate and bacterial endotoxin-induced cystitis. *Mol Med Rep* 2014; 10:670-76; PMID:24859757; <http://dx.doi.org/10.3892/mmr.2014.2262>
- Dmochowski RR. Bladder outlet obstruction: Etiology and evaluation. *Rev Urol* 2005; 7(Suppl 6):S3-S13; PMID:16986027
- El Khoudary SR, Talbott EO, Bromberger JT, Chang CC, Songer TJ, Davis EL. Severity of interstitial cystitis symptoms and quality of life in female patients. *Journal Women's Health* 2009; 18:1361-68; PMID:19743907; <http://dx.doi.org/10.1089/jwh.2008.1270>
- Evans RJ. Treatment approaches for interstitial cystitis: Multimodality therapy. *Rev Urol* 2002; 4(Suppl 1):S16-20; PMID:16986029
- Gillenwater JY, Wein AJ. Summary of the national institute of arthritis, diabetes, digestive and kidney diseases workshop on interstitial cystitis, national institutes of health, Bethesda, Maryland, August 28-29, 1987. *J Urol* 1988; 140:203-6; PMID:3379688
- Grover S, Srivastava A, Lee R, Tewari AK, Te AE. Role of inflammation in bladder function and interstitial cystitis. *Ther Adv Urol* 2011; 3:19-33; PMID:21789096; <http://dx.doi.org/10.1177/1756287211398255>
- Hohlbrugger G. Leaky urothelium and/or vesical ischemia enable urinary potassium to cause idiopathic urgency/frequency syndrome and urge incontinence. *Int Urogynecol J Pelvic Floor Dysfunct* 1996; 7:242-55; PMID:9127181; <http://dx.doi.org/10.1007/BF01901246>
- Huang da W, Sherman BT, Lempicki RA. Systematic and integrative analysis of large gene lists using DAVID bioinformatics resources.

- Nat Protoc 2009; 4:44-57; PMID:19131956; <http://dx.doi.org/10.1038/nprot.2008.211>
- [12] Jin LH, Park CS, Kim D, Choi BH, Park SH, Yoon SM, Lee T. Flow starting point and voiding mechanisms measured by simultaneous registrations of intravesical, intra-abdominal, and intraurethral pressures in awake rats. *Int Neurourol J* 2014; 18:68-76; PMID:24987559; <http://dx.doi.org/10.5213/inj.2014.18.2.68>
- [13] Jin LH, Shin HY, Kwon YH, Park CS, Yoon SM, Lee T. Urodynamic findings in an awake chemical cystitis rat model observed by simultaneous registrations of intravesical and intraabdominal pressures. *Int Neurourol J* 2010; 14:54-60; PMID:21120177; <http://dx.doi.org/10.5213/inj.2010.14.1.54>
- [14] Kim KH, Jung HB, Choi DK, Park GH, Cho ST. Does methylphenidate affect cystometric parameters in spontaneously hypertensive rats? *Int Neurourol J* 2015; 19:67-73; PMID:26126435; <http://dx.doi.org/10.5213/inj.2015.19.2.67>
- [15] Koziol JA. Epidemiology of interstitial cystitis. *Urol Clin North Am* 1994; 21:7-20; PMID:8284848
- [16] Liao Y, Smyth GK, Shi W. The subread aligner: Fast, accurate and scalable read mapping by seed-and-vote. *Nucleic Acids Res* 2013; 41:e108; PMID:23558742; <http://dx.doi.org/10.1093/nar/gkt214>
- [17] Liao Y, Smyth GK, Shi W. featureCounts: An efficient general purpose program for assigning sequence reads to genomic features. *Bioinformatics* 2014; 30:923-30; PMID:24227677; <http://dx.doi.org/10.1093/bioinformatics/btt656>
- [18] Love MI, Huber W, Anders S. Moderated estimation of fold change and dispersion for RNA-seq data with DESeq2. *Genome Biol* 2014; 15:550; PMID:25516281; <http://dx.doi.org/10.1186/s13059-014-0550-8>
- [19] Marchand JE, Sant GR, Kream RM. Increased expression of substance P receptor-encoding mRNA in bladder biopsies from patients with interstitial cystitis. *Br J Urol* 1998; 81:224-28; PMID:9488063; <http://dx.doi.org/10.1046/j.1464-410X.1998.00507.x>
- [20] Mayo ME, Ross SO, Krieger JN. Few patients with "chronic prostatitis" have significant bladder outlet obstruction. *Urology* 1998; 52:417-21; PMID:9730453; [http://dx.doi.org/10.1016/S0090-4295\(98\)00202-7](http://dx.doi.org/10.1016/S0090-4295(98)00202-7)
- [21] Offiah I, Didangelos A, Dawes J, Cartwright R, Khullar V, Bradbury EJ, O'Sullivan S, Williams D, Chessell IP, Pallas K, et al. The expression of inflammatory mediators in bladder pain syndrome. *Eur Urol* 2016; 70:283-90; PMID:26965559; <http://dx.doi.org/10.1016/j.eururo.2016.02.058>
- [22] Pang X, Marchand J, Sant GR, Kream RM, Theoharides TC. Increased number of substance P positive nerve fibres in interstitial cystitis. *Br J Urol* 1995; 75:744-50; PMID:7542136; <http://dx.doi.org/10.1111/j.1464-410X.1995.tb07384.x>
- [23] Parsons CL. The role of the urinary epithelium in the pathogenesis of interstitial cystitis/prostatitis/urethritis. *Urology* 2007; 69:9-16; PMID:17462486; <http://dx.doi.org/10.1016/j.urology.2006.03.084>
- [24] Payne C. Urodynamics for the evaluation of painful bladder syndrome/interstitial cystitis. *J Urol* 2010; 184:15-16; PMID:20478598; <http://dx.doi.org/10.1016/j.juro.2010.04.026>
- [25] Sant GR, Kempuraj D, Marchand JE, Theoharides TC. The mast cell in interstitial cystitis: Role in pathophysiology and pathogenesis. *Urology* 2007; 69:34-40; PMID:17462477; <http://dx.doi.org/10.1016/j.urology.2006.08.1109>
- [26] Sant GR, Theoharides TC. The role of the mast cell in interstitial cystitis. *Urol Clin North Am* 1994; 21:41-53; PMID:8284844
- [27] Schaeffer AJ, Datta NS, Fowler JE, Jr., Krieger JN, Litwin MS, Nadler RB, Nickel JC, Pontari MA, Shoskes DA, Zeitlin SI, et al. Overview summary statement. Diagnosis and management of chronic prostatitis/chronic pelvic pain syndrome (CP/CPPS). *Urology* 2002; 60:1-4; PMID:12521576
- [28] Stein PC, Pham H, Ito T, Parsons CL. Bladder injury model induced in rats by exposure to protamine sulfate followed by bacterial endotoxin. *J Urol* 1996; 155:1133-38; PMID:8583579; [http://dx.doi.org/10.1016/S0022-5347\(01\)66406-1](http://dx.doi.org/10.1016/S0022-5347(01)66406-1)
- [29] Uchida K, Samma S, Rinsho K, Warren JR, Oyasu R. Stimulation of epithelial hyperplasia in rat urinary bladder by escherichia coli cystitis. *J Urol* 1989; 142:1122-26; PMID:2677413
- [30] Xu A, Frederiksen H, Kanje M, Uvelius B. Partial urethral obstruction: ATF3 and p-c-Jun are involved in the growth of the detrusor muscle and its motor innervation. *Scand J Urol Nephrol* 2011; 45:30-38; PMID:20969496; <http://dx.doi.org/10.3109/00365599.2010.521188>



Review Article

Looking to the metabolic landscapes for prostate health monitoring

Wun-Jae Kim ^{a, *}, Jayoung Kim ^{b, c, *}^a Department of Urology, Chungbuk National University College of Medicine, Cheongju, South Korea^b Departments of Surgery and Biomedical Sciences, Cedars-Sinai Medical Center, Los Angeles, CA, USA^c Department of Medicine, University of California Los Angeles, CA, USA

ARTICLE INFO

Article history:

Received 4 March 2017

Accepted 14 March 2017

Available online 18 March 2017

ABSTRACT

Abnormal metabolism is a widely accepted biological signature of prostatic diseases, including prostate cancer and benign prostate hyperplasia. Recently accumulated epidemiological and experimental evidence illustrate that the metabolic syndrome, impaired mitochondrial function, and prostatic pathological conditions intersect. The perturbed metabolism and metabolic mediates influence key signaling pathways in various prostatic pathological conditions. This short review article aids to highlight recent findings on metabolism, metabolic mechanisms, and mitochondrial metabolism as a possible route to finding a cure for prostate diseases, including prostate cancer. The effort to better understand the role that mitochondria plays in cancer metabolism and the biological meaning of defective and/or deleted mitochondrial DNA in cancer will also be discussed.

© 2017 Asian Pacific Prostate Society, Published by Elsevier Korea LLC. This is an open access article under the CC BY-NC-ND license (<http://creativecommons.org/licenses/by-nc-nd/4.0/>).

1. Metabolism, metabolic syndrome, and prostate health

The definition of metabolism is the set of life-sustaining chemical transformations within the cells of living organisms.¹ Metabolic syndrome (MetS) is a common and complex cluster of clinical conditions. It includes abdominal obesity, hypertension, hypertriglyceridemia, hyperglycemia, and low high-density lipoprotein cholesterol. MetS is a risk factor of cardiovascular and metabolic complications; which is associated with several medical conditions such as type 2 diabetes, cardiovascular diseases, and nonalcoholic fatty liver disease.^{1–3}

A series of epidemiological evidence suggests that MetS is also associated with various prostatic diseases; which include hypogonadism, erectile dysfunction, infertility, and bladder and prostate dysfunctions, such as benign prostate hyperplasia (BPH) and lower urinary tract symptoms (LUTS). Recent studies demonstrated that MetS is associated with an enlarged prostate size, suggesting metabolic reprogramming in prostatic diseases.⁴ Moreover, MetS is associated with prostatic inflammation.⁵ Epidemiological studies

showed that LUTS and BPH are associated with obesity and prostatic inflammation. Recently, a series of urinary chemokines associated with obesity and prostatic inflammation were measured in BPH/LUTS patients and healthy controls. The levels of these cytokines (e.g., CXCL-8, CXCL-10, and sIL-1ra) were increased in BPH/LUTS patients, suggesting a significant association between obesity, inflammation, and BPH/LUTS.⁶

MetS has also been proposed to be associated with prostate cancer (PC), which is the sixth leading cause of cancer death among the male population. Consistent with accumulating epidemiological evidence, MetS plays a role in PC. Abnormal metabolism in MetS is linked with the alteration of signaling networks (e.g., insulin and insulin-like growth factor-1), and the modification of sex steroid pathways (e.g., testosterone and estradiol).^{7,8} Consistent with findings from BPH/LUTS, MetS-related cytokines, growth factors, leptin, and adiponectin are increased significantly in patients with PC.^{9,10}

2. Cancer metabolism

Altered metabolism has been widely accepted as a cancer hallmark.¹¹ The Nobel Laureate, Otto H. Warburg, who demonstrated that cancer cells have an altered energy metabolism, first postulated the Warburg effect. He found a fundamental difference in the metabolism between normal and cancer cells is the ratio of glycolysis to respiration.^{12,13} Instead of using an oxidative breakdown of pyruvate in mitochondria, cancer cells convert glucose into

* Corresponding authors. Department of Urology, Chungbuk National University, College of Medicine, Chungdae-ro 1, Seowon-Gu, Cheongju, Chungbuk 28644, South Korea (W.-J. Kim); Departments of Surgery and Biomedical Sciences, Cedars-Sinai Medical Center, 8700 Beverly Boulevard, Los Angeles, CA 90048, USA (J. Kim).

E-mail addresses: wjkim@chungbuk.ac.kr (W-J Kim), jayoung.kim@cshs.org (J Kim).

lactate and primarily use glycolysis to synthesize ATP, even in the presence of high oxygen tension. Thus, aerobic glycolysis can produce ATP at a high rate, which is an aggressive metabolic phenotype and is the dominant metabolism in cancer cells. The Warburg effect has been found in a series of cancer cells that exhibit a much higher rate of glucose uptake, consumption, and lactate production; leading to a higher volume of amino acid and fatty-acid synthesis that is needed for rapid cell proliferation.

More recently, the Warburg effect has been more defined in the context of metabolic reprogramming, which is specifically observed in cancer cells, not normal cells. Oncogenic signals can be triggered by activation of oncogenes (e.g., BRAF mutant V600E and c-Myc), loss of tumor suppressors (e.g., p53), and/or activation of metabolic signaling pathways (e.g., mTORC1).^{6,8,14–18} These can all contribute to metabolic rewiring or reprogramming. BRAF V600E increases 3-hydroxy-3-methylglutaryl-CoA lyase, intracellular levels of acetoacetate, and MEK1 phosphorylation, suggesting that there is crosstalk between metabolic pathways and cell-signaling networks.^{14,19}

In glioma and acute myeloid leukemia, cancer associated mutants of isocitrate dehydrogenases 1 and 2 produce an oncometabolite, 2-hydroxyglutamate, and inhibit DNA repair process.^{20–22} As MYC is a key driver of cell-cycle entry and progression, the MYC-dependent cell growth is linked to impairment of mitochondrial function through the mitochondrial serine hydroxymethyltransferase. A previous comprehensive profile of mitochondrial targets of MYC revealed approximately 400 mitochondrial genes,²³ the functions of which are associated with mitochondrial transcription, translation, protein import, and complex assembly. It has become evident that the impairment of mitochondrial biogenesis by MYC overexpression leads to the Warburg effect in cancer through the stimulation of oxidative metabolism, fatty acid metabolism, and production of acetyl-CoA as a source of energy and chemical intermediates for biosynthesis.²⁴ MYC overexpression also increases the expression of glucose transporter 1, pyruvate kinase muscle isozyme M2 (PKM2) and lactate dehydrogenase, and cell division cycle 25A (CDC25A), which are all important glycolytic genes. In addition, mutant of p53, a well-known tumor suppressor, also stimulates the Warburg effect through the RhoA/ROCK/ glucose transporter 1 signaling pathway that controls cell metabolism.²⁵

Lastly, in the epidermal growth factor receptor-promoted tumorigenesis we can observe another example suggesting that altered metabolism influences cell signaling networks. epidermal growth factor receptor activates the c-Src-mediated CDC25A phosphorylation, which allows the interaction of CDC25A with PKM2. Upon binding, CDC25A can dephosphorylate PKM2, leading to β -catenin activation.²⁶

Being a double-edged regulator of cancer cell metabolism, 5' AMP-activated protein kinase (AMPK) plays a role in tumor initiation, progression, metastasis, etc. Although AMPK is a well-known tumor suppressor and negative modulator of cancer formation and growth, recent findings demonstrate that AMPK activation enhances tumor growth in a specific cell environment.²⁷ However, the underlying mechanism that decides the fate of AMPK still remains unclear.

3. Mitochondria and mitochondrial DNA in cancer metabolism

Mitochondria, as a main source of energy and biosynthesis, play a decisive role in cancer metabolism.²⁸ Mitochondria is the location of ATP production and its intermediates; contributing to the reprogramming of bioenergetics metabolism by regulating the biosynthesis of amino acids, lipids, nucleic acids, etc.^{29,30} Mitochondria have a well-recognized role in the activation of signaling pathways and in the mediation of cell apoptosis, proliferation,

differentiation, stemness, tumorigenesis, etc.^{31,32} Given that the mitochondria senses stimuli and makes cells respond accordingly to microenvironment changes, mitochondrial metabolism has been considered as a potential cancer therapeutic strategy.

Mitochondria have their own genome containing approximately 16,000+ base pairs of double-stranded and circular DNA molecules, mitochondrial DNA (mtDNA). MtDNA encodes for polypeptides of the mitochondrial respiratory chain, transfer RNAs, and ribosomal RNAs. In cancer cells, modification, reduction, or depletion of mtDNA has been identified; which is often linked to those in the nuclear genome and biological outcomes, such as chemo-resistance and tumorigenesis.³³ The relevance of metabolic reprogramming in conferring drug resistance could be explained through the biological effects of mtDNA defects.³⁴

MtDNA depletion or defects have been observed in various key cancer types, such as lung, gastric, colorectal, prostate, and breast cancer. At the molecular level, defected mtDNA in cancer cells results in increased cell invasion, metastasis, epithelial-to-mesenchymal transition, and stemness.^{35,36} Furthermore, several studies in different cancer cell types showed that mtDNA depletion leads to the activation of key antiapoptotic signaling pathways, which allow cancer cells to be more resistant to therapies.^{25,37,38}

The role of mitochondrial dysfunction in promoting chemo-resistance has been suggested in previous literature.³⁷ MtDNA depletion made human myelogenous leukemia cells to be resistant to TNF-induced cell apoptosis.^{37,39} The mtDNA-defected hepatocarcinoma cells became resistant to the reactive oxygen species-inducing cell apoptosis by increasing expression of antioxidant enzymes, such as glutathione peroxidase and manganese superoxide dismutase.⁴⁰ Transfer of mtDNA from aggressive breast cancer phenotypes was able to provide metastatic characteristics in NIH3T3 cells. Cisplatin-sensitive ovarian cancer cells showed an increased mitochondrial membrane potential and higher basal oxygen consumption compared to its cisplatin-resistant derivative. Depletion of mtDNA in cisplatin-sensitive ovarian cancer cells resulted in resistance to cisplatin.^{41,42} When mtDNA was depleted, androgen-dependent LNCaP prostate cancer cells became resistant to paclitaxel, a chemotherapy agent.^{43,44} The mtDNA depleted PC-3 prostate cancer cells became more invasive, cancer-stem like, and resistant to chemotherapy as well as radiotherapy.

Recently, mitochondrial RNA has been shown to play a role in cancer progression and chemo-resistance through the horizontal mitochondrial transfer mechanism; which is the cell-to-cell transfer of mitochondria through intercellular bridges of tube-like structures, called tunneling nanotubes.^{45–50} This horizontal mitochondrial transfer was observed not only between cancer cells but also between endothelial cells and cancer cells, contributing to chemoresistance to doxorubicin treatment.^{41,51}

There are several reports on the alternative delivery mechanisms of the horizontal transfer of mtDNA, one of which is proposed to be through exosomes, a type of membrane vesicle that originates from the endosomal and plasma membrane. Glioblastoma and astrocytes cells released exosomes containing mtDNA.^{52,53} MtDNA-containing exosomes were found in the serum and tumors obtained from prostate cancer patients. These recent findings collectively suggest that targeting mitochondria in cancer cells may offer a novel strategy for cancer treatment.

4. Concluding remarks and perspectives

Collectively, accumulating evidence based on research in the laboratory and clinical settings implicates that metabolic rewiring through mitochondrial bioenergetics, biosynthesis and crosstalk with activated signaling pathways are critical for cancer initiation, progression, metastasis, and chemo-resistance. However, there is

still a missing piece of the puzzle in the field. We still have to continue emerging studies to assess how to reverse the reprogrammed metabolism in cancer, how to deal with the perturbed heterogeneous metabolism in patients, and when the best timing is to add antimetabolic approaches to get maximized and synergistic benefits during chemotherapy for patients.

Conflicts of interest

The authors declare that there is no conflict of interest that could be perceived as prejudicing the impartiality of this review.

Funding

The authors acknowledge support from the International Science and Business Belt Program through the Ministry of Science, ICT and Future Planning (2016K000297) (to W.-J. K.), National Institutes of Health grants (1U01DK103260), Department of Defense grants (W81XWH-15-1-0415), Centers for Disease Control and Prevention (1U01DP006079), the Steven Spielberg Discovery Fund in Prostate Cancer Research Career Development Award, and U.S.-Egypt Science and Technology Development Fund by the National Academies of Sciences, Engineering, and Medicine (to J.K.).

Authors' contributions

WK and JK designed the study, led obtaining funding, and overviewed the literature analysis and drafting the manuscript. All authors read and approved the final manuscript.

Acknowledgments

The authors would like to thank Mr. Taeun Daniel Park and Mr. Austin Yeon for careful review and editing the manuscript.

Availability of data and materials

All the data supporting the findings here are contained within the manuscript.

References

- Clemmensen C, Muller TD, Woods SC, Berthoud HR, Seeley RJ, Tschoop MH. Gut-brain cross-talk in metabolic control. *Cell* 2017;168:758–74.
- Aguilar-Olivos NE, Almeda-Valdes P, Aguilar-Salinas CA, Uribe M, Mendez-Sanchez N. The role of bariatric surgery in the management of nonalcoholic fatty liver disease and metabolic syndrome. *Metabolism* 2016;65:1196–207.
- Heinl RE, Dhindsa DS, Mahlof EN, Schultz WM, Ricketts JC, Varghese T, et al. Comprehensive cardiovascular risk reduction and cardiac rehabilitation in diabetes and the metabolic syndrome. *Can J Cardiol* 2016;32:S349–57.
- Gacci M, Corona G, Vignozzi L, Salvi M, Serni S, De Nunzio C, et al. Metabolic syndrome and benign prostatic enlargement: a systematic review and meta-analysis. *BJU Int* 2015;115:24–31.
- Gacci M, Vignozzi L, Sebastianelli A, Salvi M, Giannessi C, De Nunzio C, et al. Metabolic syndrome and lower urinary tract symptoms: the role of inflammation. *Prostate Cancer Prostatic Dis* 2013;16:101–6.
- Tyagi P, Motley SS, Kashyap M, Pore S, Gingrich J, Wang Z, et al. Urine chemokines indicate pathogenic association of obesity with BPH/LUTS. *Int Urol Nephrol* 2015;47:1051–8.
- Han JH, Choi NY, Bang SH, Kwon OJ, Jin YW, Myung SC, et al. Relationship between serum prostate-specific antigen levels and components of metabolic syndrome in healthy men. *Urology* 2008;72:749–54. discussion 54–5.
- Zhang PL, Rosen S, Veeramachaneni R, Kao J, DeWolf WC, Buble G. Association between prostate cancer and serum testosterone levels. *Prostate* 2002;53:179–82.
- De Nunzio C, Aronson W, Freedland SJ, Giovannucci E, Parsons JK. The correlation between metabolic syndrome and prostatic diseases. *Eur Urol* 2012;61:560–70.
- Gacci M, Russo GI, De Nunzio C, Sebastianelli A, Salvi M, Vignozzi L, et al. Meta-analysis of metabolic syndrome and prostate cancer. *Prostate Cancer Prostatic Dis* 2017. <http://dx.doi.org/10.1038/pcan.2017.1> [Epub ahead of print].
- Vander Heiden MG, DeBerardinis RJ. Understanding the intersections between metabolism and cancer biology. *Cell* 2017;168:657–69.
- Otto AM. Warburg effect(s)—a biographical sketch of Otto Warburg and his impacts on tumor metabolism. *Cancer Metab* 2016;4:5.
- Lu J, Tan M, Cai Q. The Warburg effect in tumor progression: mitochondrial oxidative metabolism as an anti-metastasis mechanism. *Cancer Lett* 2015;356:156–64.
- Kang HB, Fan J, Lin R, Elf S, Ji Q, Zhao L, et al. Metabolic rewiring by oncogenic BRAF V600E links ketogenesis pathway to BRAF-MEK1 signaling. *Mol Cell* 2015;59:345–58.
- Martinelli E, Morgillo F, Troiani T, Ciardiello F. Cancer resistance to therapies against the EGFR-RAS-RAF pathway: The role of MEK. *Cancer Treat Rev* 2017;53:61–9.
- Perri F, Pisconti S, Della Vittoria Scarpati G. P53 mutations and cancer: a tight linkage. *Ann Transl Med* 2016;4:522.
- Villar VH, Nguyen TL, Delcroix V, Teres S, Bouche-careilh M, Salin B, et al. mTORC1 inhibition in cancer cells protects from glutaminolysis-mediated apoptosis during nutrient limitation. *Nat Commun* 2017;8:14124.
- Zhang C, Liu J, Liang Y, Wu R, Zhao Y, Hong X, et al. Tumour-associated mutant p53 drives the Warburg effect. *Nat Commun* 2013;4:2935.
- Penman CL, Faulkner C, Lowis SP, Kurian KM. Current understanding of BRAF alterations in diagnosis, prognosis, and therapeutic targeting in pediatric low-grade gliomas. *Front Oncol* 2015;5:54.
- Dang L, White DW, Gross S, Bennett BD, Bittinger MA, Driggers EM, et al. Cancer-associated IDH1 mutations produce 2-hydroxyglutarate. *Nature* 2009;462:739–44.
- Green A, Beer P. Somatic mutations of IDH1 and IDH2 in the leukemic transformation of myeloproliferative neoplasms. *New Engl J Med* 2010;362:369–70.
- Mardis ER, Ding L, Dooling DJ, Larson DE, McLellan MD, Chen K, et al. Recurring mutations found by sequencing an acute myeloid leukemia genome. *New Engl J Med* 2009;361:1058–66.
- Kim J, Lee JH, Iyer VR. Global identification of Myc target genes reveals its direct role in mitochondrial biogenesis and its E-box usage *in vivo*. *PLoS One* 2008;3:e1798.
- Edmunds LR, Sharma L, Kang A, Lu J, Vockley J, Basu S, et al. c-Myc programs fatty acid metabolism and dictates acetyl-CoA abundance and fate. *J Biol Chem* 2014;289:25382–92.
- Liang J, Cao R, Zhang Y, Xia Y, Zheng Y, Li X, et al. PKM2 dephosphorylation by Cdc25A promotes the Warburg effect and tumorigenesis. *Nat Commun* 2016;7:12431.
- Morrish F, Hockenbery D. MYC and mitochondrial biogenesis. *Cold Spring Harb Perspect Med* 2014;4. pii: a014225.
- Kim WJ. Is 5'-AMP-activated protein kinase both Jekyll and Hyde in bladder cancer? *Int Neurolog J* 2015;19:55–66.
- Shoshan M. On mitochondrial metabolism in tumor biology. *Curr Opin Oncol* 2017;29:48–54.
- Guo JY, White E. Autophagy, metabolism, and cancer. *Cold Spring Harbor Symp Quant Biol* 2017. pii: 030981. [Epub ahead of print].
- Danhier P, Banski P, Payen VL, Grasso D, Ippolito L, Sonveaux P, et al. Cancer metabolism in space and time: beyond the Warburg effect. *Biochim Biophys Acta* 2017. pii: S0005-2728(17)30023-3. [Epub ahead of print].
- Corbet C, Feron O. Cancer cell metabolism and mitochondria: Nutrient plasticity for TCA cycle fueling. *Biochim Biophys Acta* 2017;1868:7–15.
- Tomasetti M, Lee W, Santarelli L, Neuzil J. Exosome-derived microRNAs in cancer metabolism: possible implications in cancer diagnostics and therapy. *Exp Mol Med* 2017;49:e285.
- Hardie RA, van Dam E, Cowley M, Han TL, Balaban S, Pajic M, et al. Mitochondrial mutations and metabolic adaptation in pancreatic cancer. *Cancer Metab* 2017;5:2.
- Reznik E, Wang Q, La K, Schultz N, Sander C. Mitochondrial respiratory gene expression is suppressed in many cancers. *Elife* 2017;6. pii: e21592.
- Berridge MV, Dong L, Neuzil J. Mitochondrial DNA in tumor initiation, progression, and metastasis: role of horizontal mtDNA transfer. *Cancer Res* 2015;75:3203–8.
- Tan AS, Baty JW, Dong LF, Bezawork-Geleta A, Endaya B, Goodwin J, et al. Mitochondrial genome acquisition restores respiratory function and tumorigenic potential of cancer cells without mitochondrial DNA. *Cell Metab* 2015;21:81–94.
- Guerra F, Arbini AA, Moro L. Mitochondria and cancer chemoresistance. *Biochim Biophys Acta* 2017. pii: S0005-2728(17) 30020-8.
- Amoedo ND, Obre E, Rossignol R. Drug discovery strategies in the field of tumor energy metabolism: limitations by metabolic flexibility and metabolic resistance to chemotherapy. *Biochim Biophys Acta* 2017. pii: S0005-2728(17) 30027-0. [Epub ahead of print].
- Suzuki S, Naito A, Asano T, Evans TT, Reddy SA, Higuchi M. Constitutive activation of AKT pathway inhibits TNF-induced apoptosis in mitochondrial DNA-deficient human myelogenous leukemia ML-1a. *Cancer Lett* 2008;268:31–7.
- Park SY, Chang I, Kim JY, Kang SW, Park SH, Singh K, et al. Resistance of mitochondrial DNA-depleted cells against cell death: role of mitochondrial superoxide dismutase. *J Biol Chem* 2004;279:7512–20.
- Catanzaro D, Gaude E, Orso G, Giordano C, Guzzo G, Rasola A, et al. Inhibition of glucose-6-phosphate dehydrogenase sensitizes cisplatin-resistant cells to death. *Oncotarget* 2015;6:30102–14.
- Montopoli M, Bellanda M, Lonardoni F, Ragazzi E, Dorigo P, Froidi G, et al. “Metabolic reprogramming” in ovarian cancer cells resistant to cisplatin. *Curr Cancer Drug Targets* 2011;11:226–35.

43. Moro L, Arbini AA, Marra E, Greco M. Mitochondrial DNA depletion reduces PARP-1 levels and promotes progression of the neoplastic phenotype in prostate carcinoma. *Cell Oncol* 2008;30:307–22.
44. Li X, Zhong Y, Lu J, Axcrone K, Eide L, Syljuasen RG, et al. MtDNA depleted PC3 cells exhibit Warburg effect and cancer stem cell features. *Oncotarget* 2016;7:40297–313.
45. Lu J, Zheng X, Li F, Yu Y, Chen Z, Liu Z, et al. Tunneling nanotubes promote intercellular mitochondria transfer followed by increased invasiveness in bladder cancer cells. *Oncotarget* 2017;8:15539–52.
46. Wang X, Gerdes HH. Transfer of mitochondria via tunneling nanotubes rescues apoptotic PC12 cells. *Cell Death Differ* 2015;22:1181–91.
47. Thayanithy V, Dickson EL, Steer C, Subramanian S, Lou E. Tumor-stromal cross talk: direct cell-to-cell transfer of oncogenic microRNAs via tunneling nanotubes. *Transl Res* 2014;164:359–65.
48. Las G, Shirihai OS. Miro1: new wheels for transferring mitochondria. *EMBO J* 2014;33:939–41.
49. Pasquier J, Guerrouahen BS, Al Thawadi H, Ghiabi P, Maleki M, Abu-Kaoud N, et al. Preferential transfer of mitochondria from endothelial to cancer cells through tunneling nanotubes modulates chemoresistance. *J Transl Med* 2013;11:94.
50. Omsland M, Bruserud O, Gjertsen BT, Andresen V. Tunneling nanotube (TNT) formation is downregulated by cytarabine and NF-kappaB inhibition in acute myeloid leukemia (AML). *Oncotarget* 2017;8:7946–63.
51. Desir S, Dickson EL, Vogel RI, Thayanithy V, Wong P, Teoh D, et al. Tunneling nanotube formation is stimulated by hypoxia in ovarian cancer cells. *Oncotarget* 2016;7:43150–61.
52. Guescini M, Genedani S, Stocchi V, Agnati LF. Astrocytes and Glioblastoma cells release exosomes carrying mtDNA. *J Neural Transm (Vienna)* 2010;117:1–4.
53. Barteneva NS, Maltsev N, Vorobjev IA. Microvesicles and intercellular communication in the context of parasitism. *Front Cell Infect Microbiol* 2013;3:49.



Letter

Int Neurourol J 2018;22:72-73

<https://doi.org/10.5213/inj.1836032.016>

pISSN 2093-4777 · eISSN 2093-6931



Response to Current Pharmacologic Approaches in Painful Bladder Research: An Update

Jayoung Kim^{1,2,3,4,5}

Departments of ¹Surgery, ²Biomedical Sciences, and ³Samuel Oschin Comprehensive Cancer Institute, Cedars-Sinai Medical Center, Los Angeles, CA, USA

⁴Department of Medicine, University of California Los Angeles, CA, USA


⁵Department of Urology, Ga Cheon University College of Medicine, Incheon, Korea



To the editor,

I read, with great interest, the article “Current Pharmacologic Approaches in Painful Bladder Research: An Update” published by Karl-Erik Andersson and Lori Birder in *Int Neurourol J* on December 2017 [1], and would like to commend on the authors on their review article. The aim of this short review was to summarize the accumulating literature on interstitial cystitis/bladder pain syndrome (IC/BPS) and suggest ways that experimental findings could be applied to preclinical and clinical research. This article discussed several currently developed treatments that focus on systemic and pharmacological intervention and are being used in the clinical setting. I believe that this topic was clinically relevant and the timing was perfect. The recently implemented Multidisciplinary Approach to the Study of Chronic Pelvic Pain (MAPP) research network has made great advances in understanding the phenotypes of IC/BPS patients and the molecular basis that underlie this disease [2,3]. There has also been growing interest toward understanding whether symptoms related to IC/BPS are bladder-based, outside the bladder (systemic), or both. However, this remains discrepant. In this review article, the authors discussed a series of research activities and clinical trials that are focused on pharmaceutical blocking of nerve growth factor (e.g., tanezumab and fulranumab), tumor necrosis factor- α (e.g., adalimumab), P2X3 receptor (e.g., AF-219), and α 1-adrenoceptor (e.g., prazosin). The SHIP1 activating drug, AQX-1125, is a known negative regulator of the PI3K network and inflammatory signaling pathways, and has also been considered and tested as a potential systemic treat-

ment for IC/BPS. The authors further provided reasoning on why current systemic pharmacological treatments have shown only limited success. This may be caused by: (1) the lack of current knowledge on how to accurately phenotype and subgroup individual IC/BPS patients for certain treatments, and/or (2) the low efficacy of systemic drug treatments, themselves. Additionally, the writers debated on the important role of local treatment options in overcoming the lower effectiveness of systemic pharmaceutical treatments and concluded that more efforts should be focused on investigating local treatment approaches. Research strategies, including the blocking of toll-like receptor 7 (e.g., hydroxychloroquine) and intravesical liposomes should be tested against IC/BPS in large well-designed cohorts. Successful phenotyping could stratify patient groups who are suffering from localized disease from those suffering from a systemic disorder and provide efficient treatment options. While bladder-specific or systemic-based differences are certainly useful, we would also like to bring up sex differences to the attention of readers. While sex-determined disparities are evident and well-documented in numerous other diseases [4,5], the biological, cellular, and molecular basis of gender biases remain elusive in context of IC/BPS. One potential hypothesis would be that the biological role of sex hormones, such as estrogen, testosterone, et al., create variations in the metabolic rewiring of female and male IC/BPS patients [6]. However, we understand that there are still many areas lacking in this field. Consideration of sex differences in preclinical work and clinical trials will give a better picture of the disease to esteemed readers of

Corresponding author: Jayoung Kim  <https://orcid.org/0000-0002-3683-4627>
Departments of Surgery and Biomedical Sciences, Cedars-Sinai Medical Center
8700 Beverly Blvd., Davis Room 5071, Los Angeles, CA 90048, USA
E-mail: kayoing.kim@csmc.edu / Tel: +1-310-423-7168 / Fax: +1-310-967-3809
Submitted: February 1, 2018 / **Accepted after revision:** February 7, 2018



This is an Open Access article distributed under the terms of the Creative Commons Attribution Non-Commercial License (<http://creativecommons.org/licenses/by-nc/4.0/>) which permits unrestricted non-commercial use, distribution, and reproduction in any medium, provided the original work is properly cited.

this article. We hope investigators in this field will continue to conduct studies assessing how to deal with sex disparities and their effects on heterogeneous metabolism in female and male patients. Hopefully, in the near future, merged knowledge will enable us to find the best timing to apply a systemic, local, or combination treatment against IC/BPS to get maximized and synergistic benefits for patients.

• **Grant/Fund Support:** The author acknowledges support from National Institutes of Health grants (1U01DK103260, 1R01DK100974, U24 DK097154, NIH NCATS UCLA CTSI UL1TR000124), Department of Defense grants (W81XWH-15-1-0415), Centers for Disease Controls and Prevention (1U01DP006079), IMAGINE NO IC Research Grant, the Steven Spielberg Discovery Fund in Prostate Cancer Research Career Development Award, the U.S.-Egypt Science and Technology Joint Fund (to J.K.). J.K. is former recipient of Interstitial Cystitis Association Pilot Grant, a Fishbein Family IC Research Grant, New York Academy of Medicine, and Boston Children's Hospital Faculty Development. The funders had no role in the design, data collection and analysis, decision to publish or preparation of the manuscript. In addition, this article is derived from the Subject Data funded in whole or part by NAS and USAID. Any opinions, findings, conclusions, or recommendations expressed in this article are those of the authors alone, and do not necessarily reflect the views of USAID or NAS.

• **Conflict of Interest:** No potential conflict of interest relevant to this article was reported.

REFERENCES

1. Andersson KE, Birder L. Current pharmacologic approaches in painful bladder research: an update. *Int Neurourol J* 2017;21:235-242.
2. Clemens JQ, Mullins C, Kusek JW, Kirkali Z, Mayer EA, Rodríguez LV, et al. The MAPP research network: a novel study of urologic chronic pelvic pain syndromes. *BMC Urol* 2014;14:57. <https://doi.org/10.1186/1471-2490-14-57>.
3. Landis JR, Williams DA, Lucia MS, Clauw DJ, Naliboff BD, Robinson NA, et al. The MAPP research network: design, patient characterization and operations. *BMC Urol* 2014;14:58. <https://doi.org/10.1186/1471-2490-14-58>.
4. Carrero JJ, Hecking M, Chesnaye NC, Jager KJ. Sex and gender disparities in the epidemiology and outcomes of chronic kidney disease. *Nat Rev Nephrol* 2018 Jan 22 [Epub]. <https://doi.org/10.1038/nrneph.2017.181>.
5. Santilli F, D'Ardes D, Guagnano MT, Davi G. Metabolic syndrome: sex-related cardiovascular risk and therapeutic approach. *Curr Med Chem* 2017;24:2602-27.
6. Wen H, Lee T, You S, Park SH, Song H, Eilber KS, et al. Urinary metabolite profiling combined with computational analysis predicts interstitial cystitis-associated candidate biomarkers. *J Proteome Res* 2015;14:541-8.



Letter

Int Neurourol J 2018;22(Suppl 2):S101-102

<https://doi.org/10.5213/inj.1836170.085>

pISSN 2093-4777 · eISSN 2093-6931



Era of the Fourth Industrial Revolution and the Urologists' Journey to Navigating Big Omics Data

Jayoung Kim^{1,2,3}

¹Division of Cancer Biology and Therapeutics, Departments of Surgery and Biomedical Sciences, Samuel Oschin Comprehensive Cancer Institute, Cedars-Sinai Medical Center, Los Angeles, CA, USA

²Department of Medicine, University of California Los Angeles, Los Angeles, CA, USA

³Department of Urology, Gachon University College of Medicine, Incheon, Korea



Have you ever had at least one wearable internet technology or downloaded a health-related app on your mobile device for monitoring your health status? Beyond providing you with real-time health information, your wearable technologies can create a cloud of big personal data. This is not just limited to your health apps; usage of search engines, social media, and entertainment, such as Google, Youtube, Alibaba, Instagram, Facebook, Netflix, Amazon, and Twitter, creates vast amounts of data about “you.” In addition, advancement of sensor-equipped technologies will accelerate data collection on the ways we live, work, and who we are. According to Klaus Schwab, the founder and executive chairman of the World Economic Forum, this is just one part of the technological revolution that will be brought forth by the fourth industrial revolution.


In the business world, all this big data enables us to perform better predictions on consumer needs. Big data refers to the large quantities of information collected through careful observations of repeating patterns. It is an essential component for artificial intelligence, which utilizes deep machine learning algorithms to digest big data. More data will also result in better prediction outcomes. For instance, this principle can be clearly applied to the insurance industry. Data associated with health and driving habits can be collected and used for determining insurance charges and guiding decisions on policies.

How about big data and the field of medicine? This powerful analytics tool can be used to enhance the quality of healthcare, which may include the development of diagnostic subgrouping

and predictive biomarkers for various therapeutic options. Big data can also be applied to the management of clinical information. Systems for electronic medical record (EMR) are being implemented in the hope of yielding timely and clinically valuable data from a patient's clinical chart without repetitive chart review [1]. This wealth of data will allow for clinicians to have the tools needed to make appropriate clinical decisions. It could be even greater if we have cost-effective and maximized capabilities to retrieve necessary clinical data from multicenter EMR in real-time.

In the current health care system, there has been accumulating efforts to optimize precision medicine, also known as personalized medicine, across all medical specialties, including urology. A patient's omics signature, which is retrieved from genomics, epigenetics, proteomics, transcriptomics, and/or metabolomics profiles, can independently or jointly identify different patient phenotypes. By combining clinical and medical information, Big data-based signatures can support physicians on deciding therapeutic plans unique to individual patients.

Recently, our integrated classification of prostate cancer using a large cohort of 1,321 human prostate cancer transcriptome profiles from 38 different cohorts revealed that pathway activation signatures can be a new classification system for subgrouping prostate cancer into 3 different types (PCS1, PCS2, and PCS3). This subtyping is based on distinct gene expression patterns. Our study further showed that these 3 different prostate cancer phenotypes had different clinical outcomes; PCS1 tu-

Corresponding author: Jayoung Kim  <https://orcid.org/0000-0002-3683-4627>
Departments of Surgery and Biomedical Sciences, Cedars-Sinai Medical Center, 8700 Beverly Blvd., Los Angeles, CA 90048, USA
E-mail: Jayoung.Kim@cshs.org / Tel: +1-310-423-7168 / Fax: +1-310-967-3809
Submitted: July 13, 2018 / **Accepted after revision:** July 17, 2018



This is an Open Access article distributed under the terms of the Creative Commons Attribution Non-Commercial License (<http://creativecommons.org/licenses/by-nc/4.0/>) which permits unrestricted non-commercial use, distribution, and reproduction in any medium, provided the original work is properly cited.

mors progressed more rapidly to metastatic disease in comparison to PCS2 or PCS3 [2]. Subtyping has also been applied to other cancers as well. Molecular subtypes of bladder cancer have been identified using comprehensive genomic data from The Cancer Genome Atlas, which is a massive coordinated gene data bank with contributions from all over the world. Specific DNA mutations and/or copy number aberrations were found to be unique to each molecular bladder cancer subtype, suggesting that personalized management of patients is possible [3]. This is just some of the many examples on how big omics data can be used to provide personalized medicine. However, in order to enhance the utilization of big data in medicine, improved accessibility to robust, well-annotated, and interactive human omics data is a critical departing point [4]. Development of deep machine learning pipelines is also a crucial step for interpreting data. Machine learning can provide pattern recognition of information from patient charts, medical records, and clinical trials. It can produce accurate disease prediction better than traditional statistical regression models [5]. If successful, these tools can broaden scientific insight and arm clinicians with the knowledge on how to deliver personalized care.

The ultimate goal of big data is to access accurate and meaningful material regarding patient symptoms and family history, and use that data to provide real-time information about patients, their clinical outcomes, and the quality of care needed. However, there are some issues and problems that can arise from this technology. Big data is still elusive—How can individual privacy be protected? How can such rich data be interpreted? How can this information be explained to patients and caregivers who do not have a scientific background? Strategies on addressing big data are fully dependent on how the next generation of researchers and physicians are trained for analysis and interpretation. We are currently limited by this need for those specialized in communicating big data to physicians and patients. Currently, many medical schools have initiated establishing an extensive educational curriculum to foster specialists in this fourth industrial revolution era [6]. There is a potential meaningful use for big data in the future ahead and the possibilities are exciting, but getting there is the challenge.

So...are we ready for the next big shift?

- **Grant/Fund Support:** The author acknowledges support from National Institutes of Health grants (1U01DK103260, 1R01DK100974, U24 DK097154, NIH NCATS UCLA CTSI UL1TR000124), Department of Defense grants (W81XWH-15-1-0415), Centers for Disease Controls and Prevention (1U01DP006079), IMAGINE NO IC Research Grant, the Steven Spielberg Discovery Fund in Prostate Cancer Research Career Development Award, and the U.S.-Egypt Science and Technology Development Fund by the National Academies of Sciences, Engineering, and Medicine (to JK). JK is former recipient of Interstitial Cystitis Association Pilot Grant, a Fishbein Family IC Research Grant, New York Academy of Medicine, and Boston Children's Hospital Faculty Development. The funders had no role in the design, data collection and analysis, decision to publish, or preparation of the manuscript.
- **Conflict of Interest:** No potential conflict of interest relevant to this article was reported.

REFERENCES

1. Telenti A, Steinhubl SR, Topol EJ. Rethinking the medical record. *Lancet* 2018;391:1013.
2. You S, Knudsen BS, Erho N, Alshalalfa M, Takhar M, Al-Deen Ashab H, et al. Integrated classification of prostate cancer reveals a novel luminal subtype with poor outcome. *Cancer Res* 2016;76:4948-58.
3. Choi W, Ochoa A, McConkey DJ, Aine M, Höglund M, Kim WY, et al. Genetic alterations in the molecular subtypes of bladder cancer: illustration in the cancer genome atlas dataset. *Eur Urol* 2017;72:354-65.
4. Beane J, Campbell JD, Lel J, Vick J, Spira A. Genomic approaches to accelerate cancer interception. *Lancet Oncol* 2017;18:e494-e502.
5. Buzdin A, Sorokin M, Garazha A, Sekacheva M, Kim E, Zhukov N, et al. Molecular pathway activation - new type of biomarkers for tumor morphology and personalized selection of target drugs. *Semin Cancer Biol* 2018 Jun 20 [Epub]. pii: S1044-579X(18)30043-9. <https://doi.org/10.1016/j.semcancer.2018.06.003>.
6. Chahine S, Kulasegaram KM, Wright S, Monteiro S, Grierson LEM, Barber C, et al. A call to investigate the relationship between education and health outcomes using big data. *Acad Med* 2018;93:829-32.

SCIENTIFIC REPORTS



Correction: Author Correction

OPEN

Alpha-oxoglutarate inhibits the proliferation of immortalized normal bladder epithelial cells via an epigenetic switch involving ARID1A

Muhammad Shahid¹, Nicole Gull², Austin Yeon², Eunho Cho³, Joeun Bae³, Hyun Seok Yoon⁴, Sungyong You¹, Hana Yoon⁴, Minjung Kim⁵, Benjamin P. Berman² & Jayoung Kim^{1,3,6,7}

Interstitial cystitis (IC) is a chronic urinary tract disease that is characterized by unpleasant sensations, such as persistent pelvic pain, in the absence of infection or other identifiable causes. We previously performed comprehensive metabolomics profiling of urine samples from IC patients using nuclear magnetic resonance and gas-chromatography/mass spectrometry and found that urinary α -oxoglutarate (α -OG), was significantly elevated. α -OG, a tricarboxylic acid (TCA) cycle intermediate, reportedly functions to suppress the proliferation of immortalized normal human bladder epithelial cells. Here, we identified AT-rich interactive domain 1A (ARID1A), a key chromatin remodeler, as being hypomethylated and upregulated by α -OG treatment. This was done through EPIC DNA methylation profiling and subsequent biochemical approaches, including quantitative RT-PCR and western blot analyses. Furthermore, we found that α -OG almost completely suppresses ten-eleven translocation (TET) activity, but does not affect DNA methyltransferase (DNMT) activity. Altogether, our studies reveal the potential role of α -OG in epigenetic remodeling through its effects on ARID1A and TET expression in the bladder. This may provide a new possible therapeutic strategy in treating IC.

Urine is a critical biological fluid that is filtered through the kidneys and stored in the bladder. It contains the expression of many metabolites, such as urea (from amino acid metabolism), inorganic salts (chloride, sodium, and potassium), creatinine, ammonia, organic acids, various water-soluble toxins, and pigmented products from hemoglobin breakdown. Because urination is also the primary route through which the body eliminates water-soluble waste and extra unnecessary products, urine has long been considered as an expendable composite. However, more recently, urine has been acknowledged as an uninvestigated biomarker source with great potential use for disease diagnosis. While previous studies of urine have mainly focused on its chemical composition, new focus is being placed on its metabolic properties as indicative sources for medical disorders. Although the complexity of sources within metabolites creates many obstacles in urine analysis, progress in the field has been promising. Urine analysis could prove to be tremendously beneficial¹.

Interstitial cystitis/bladder pain syndrome (IC/BPS, hereafter IC) is a debilitating urological dysfunction that presents itself as a constellation of symptoms, including bladder pain, urinary urgency, frequency, nocturia, and small voided volumes, in the absence of other identifiable etiologies^{2–7}. The prevalence of IC in the United States is 3–6% in women and 2–4% in men^{8,9}. IC patients experience substantial decline in physical activity, social

¹Departments of Surgery and Biomedical Sciences, Cedars-Sinai Medical Center, Los Angeles, CA, USA. ²Center for Bioinformatics and Functional Genomics, Department of Biomedical Sciences, Cedars-Sinai Medical Center, Los Angeles, California, USA. ³University of California Los Angeles, Los Angeles, CA, USA. ⁴Department of Urology, School of Medicine, Ewha Womans University, Seoul, Republic of Korea. ⁵Department of Molecular Oncology, Moffitt Cancer Center, Tampa, Florida, USA. ⁶Samuel Oschin Comprehensive Cancer Institute, Cedars-Sinai Medical Center, Los Angeles, CA, USA. ⁷Department of Urology, Ga Cheon University College of Medicine, Incheon, Republic of Korea. Muhammad Shahid and Nicole Gull contributed equally to this work. Correspondence and requests for materials should be addressed to J.K. (email: Jayoung.Kim@cshs.org)

interaction, and quality of life, mainly due to chronic pelvic pain, frequent urination, and other symptoms^{10–12}. Despite the considerable burden of IC on public health, there is no diagnostic gold standard for IC. Urologists currently use the American Urological Association guidelines for diagnosing IC in the absence of other identifiable causes for symptoms (e.g., urinary tract infection and cancer). Therefore, clearer disease indicators and studies involving larger populations are needed to further our understanding of the molecular and cellular mechanisms behind IC. Current treatment options also remain suboptimal. Because so little is known regarding IC, palliative care is the only option available to patients.

In an effort to identify IC biomarkers, we have been keen on examining urine as a bio-resource; mainly because bodily fluid most proximal to a disease site provides a wealth of informative biomarkers^{13–15}. A series of our studies involving metabolic profiling revealed a list of candidate urinary biomarkers associated with IC. Previously, we used nuclear magnetic resonance (NMR) and liquid chromatography–mass spectrometry (LC–MS) to show substantial differences between the metabolic profiles of urine from IC patients and those of healthy control subjects¹⁶. We found that α -oxoglutarate (α -OG) was significantly increased in IC patients. α -OG, also known as α -ketoglutarate, is a key Krebs cycle intermediate and regulator of cellular redox states¹⁷. More recently, α -OG has been reported to function in epigenetic regulation, contributing to metabolic reprogramming and macrophage activation^{17,18}. Treatment with α -OG in bladder epithelial cells suppressed cell proliferation and was consistent with previous observations by other groups that found α -OG inhibited cell cycle transitions through the up or downregulation of p21^{Waf1/Cip1}, p27^{Kip1}, cyclin D1, and Rb. However, no functional impacts or mechanisms of urinary α -OG have been proposed in the setting of bladder wall abnormalities or diseases and no correlations have been previously described.

In this study, we examined the biological impact of increased levels of α -OG. Given that our previous global metabolomics profiling of IC patient urine suggested the possibility of finding non-invasive metabolic signatures, this study focused on gaining new insight into the mechanism of IC through investigating the biological meaning of upregulated α -OG. Here, our Infinium MethylationEPIC profiling revealed the bladder DNA methylome as being responsive to α -OG. Our findings provide evidence suggesting that α -OG may change the physiology of bladder epithelial cells at the epigenetic and metabolic levels.

Materials and Methods

Cell Culture and Proliferation Assay. Immortalized normal human bladder epithelial cells, TRT-HU1, were maintained as described previously¹⁹. The TRT-HU1 cell line was constructed and extensively characterized in previously published papers. Cells were cultured in Dulbecco's modified Eagle's medium (DMEM), containing 10% fetal bovine serum (FBS, Invitrogen), 1% penicillin/streptomycin, and 1% L-glutamine (Sigma, St. Louis, MO) in a 37 °C humidified incubator with 5% CO₂. TRT-HU1 cells were seeded in 10 cm culture plates at a density of 1×10^6 cells in standard growth medium. When the cells reached approximately 80% confluence, they were treated and incubated with 10 mM of α -OG or vehicle for 72 h. For the crystal violet staining cell proliferation assay, cells were stained with 0.5% crystal violet (Sigma-Aldrich Corp., St. Louis, MO, USA) in 30% ethanol for 10 minutes at room temperature. The cells were lysed in a 1% SDS solution. The absorbance of the solution was measured using a microplate spectrophotometer at a wavelength of 595 nm.

Epigenome-wide DNA methylation. Methylation profiles were obtained using the Illumina Infinium HumanMethylationEPIC BeadChip kit, which assayed approximately 850,000 methylation sites per sample at a single nucleotide resolution²⁰. Methylation scores were computed as β -values, which took into account the ratio of methylated probe intensities and the overall probe intensities (methylated and un-methylated plus a constant, $C = 100$). β -values are between 0 and 1. Assays and validations were performed according to the manufacturer's recommendations.

Bioinformatic analysis. A data analysis pipeline was established using a combination of R Studio and Bioconductor. Illumina HumanMethylationEPIC data (IDAT files) were imported into the Bioconductor minfi package. Extension of minfi package to support EPIC arrays is described in previous literature²¹. Background in the data was corrected using PreprocessNoob²². No normalization was done. Data was mapped to the genome according to standards outlined by minfi. Annotations were added using IlluminaMethylationManifest, a class built within the minfi package. Volcano plots were constructed using the Bioconductor package, TCGAbiolinks²³. Heatmaps were created using the Bioconductor package, ComplexHeatmap²⁴. Differentially methylated genes (DMGs) were identified using a simple T-test comparing treated and un-treated groups. Additionally, we compared the mean β -values of two groups and only included probes that had a difference of 10%. Using the DAVID software (Ver. 6.8)²⁵, we performed functional enrichment analysis of the DMGs to identify cellular processes and pathways perturbed by α -OG treatment.

Network analysis. From the functional enrichment analysis, we identified the hypo-methylated genes as those involved in cellular processes, including cell-cell adhesion and chromatin remodeling. We then searched for interactions among the hypo-methylated genes using the STRING database²⁶. A network model was reconstructed with the interactions between these genes and visualized using Cytoscape (Ver. 3.4)²⁷. Node size represents degree centrality, which is the number of interactions in the network model, and edge thickness represents interaction scores, which are combined scores obtained from the STRING database²⁶. These combined scores were computed by adding the probabilities from different evidence of interactions in the database and correcting for the probability of randomly observing an interaction.

Quantitative RT-PCR. Total RNA was purified using the MagNA Pure Compact RNA isolation kit, according to the manufacturer's instructions (Roche). cDNA was synthesized using the iScript cDNA Synthesis Kit (Bio-Rad). Q-PCR was carried out with iTaq universal SYBR green supermix (BioRad) on a 7500 Fast Real-Time

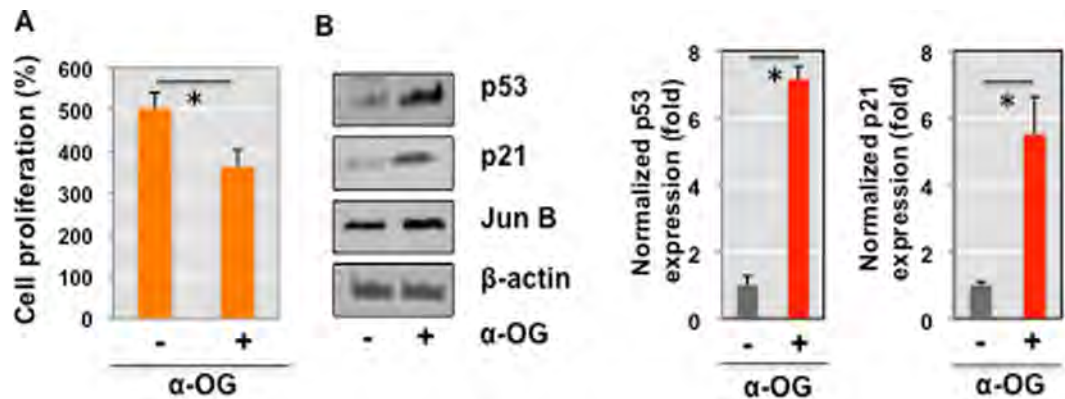


Figure 1. Cell proliferation was suppressed in response to α -OG treatment. (A) TRT-HU1, immortalized normal bladder epithelial cells were treated with 10 mM of α -OG for 72 h and then proliferation assay was performed as described in Methods. * $P < 0.05$ (two-sided Student's t-test) compared with the control group. (B) Representative western blot showed the reduced levels of p53 and p21 expression in TRT-HU1 cells treated with α -OG. β -actin was used for protein normalization.

PCR system (Life Technologies). The annealing temperature for the qPCR was set to 60 °C and the total cycle number was 40. Actb was used as internal control for gene expression normalization. Primers used for qRT-PCR assay are described in Supplementary Table 1.

Western blot analysis. Total cell lysates were prepared in lysis buffer (Bio-Rad) with protease inhibitors (Thermo Fisher). Protein levels were measured and 25 μ g of cell lysates per condition were used for SDS-PAGE gel running. After transferring proteins to nitrocellulose membranes, western blot analysis was performed using antibodies specific for p53 (1:1000; sc-126; Santa Cruz), p21 (1:1000; 2947; Cell Signaling Technology), JunB (1:1000; 3746; Cell Signaling Technology), ARID1A (1:1000; 12354; Cell Signaling Technology), HDAC4 (1:1000; 5392; Cell Signaling Technology), PKD (1:1000; 2052; Cell Signaling Technology), β -catenin (1:1000; 8480; Cell Signaling Technology), PBRM1 (1:1000; 91894; Cell Signaling Technology), SMARCA2 (1:1000; 11966; Cell Signaling Technology), and β -actin (1:2000; A1978; Sigma-Aldrich). These were incubated overnight and followed by anti-specie-specific HRP-conjugated secondary antibodies (1:5000; 7074, 7076; Cell Signaling Technology) and then chemiluminescent detection. Some blots were stripped using Restore (Thermo Fisher) and detected using other primary antibodies.

DNA Methyltransferase (DNMT) and ten-eleven translation (TET) activity assay. Cells were seeded 24 h before experiments and incubated with α -OG-containing media for 20 h. A commercially available EpiQuik™ DNMT Activity/Inhibition Assay Ultra Kit (Epigentek, Farmingdale) was used to determine DNMT enzymatic activity as per the manufacturer's instruction. For the TET activity assay, the Epigenase™ 5mC-Hydroxylase TET Activity/Inhibition Assay Kit (Colorimetric) was used, as per the manufacturer's instructions. This sandwich-based 5hmC ELISA reads the conversion of methylated products to hydroxymethylated products through the presence of TET enzymes in samples.

Ethics statement. The Ethics Committee of Ewha Womans University Hospital (Seoul, Republic of Korea) approved this study. The Institutional Review Board of Ewha University Hospital approved collection, curation and analysis of all samples. All subjects participated in this study provided written informed consent, and all experiments were performed in accordance with relevant guidelines and regulations.

Subjects and biopsy tissue collection. Subjects, including IC patients (mean age, 52.5 \pm 10.1) and healthy controls (mean age, 54.2 \pm 9.3), were Asian-descent female residents in South Korea who were enrolled at their initial evaluation, before any treatments or procedures. They were diagnosed and recruited by two independent urologists, Drs. Hana Yoon and Hyun Seok Yoon, who have extensive clinical expertise in IC at an outpatient urology clinic at Ewha Womans University Hospital. Careful clinical diagnosis was done using clinical criteria in the AUA guidelines^{28,29}, "An unpleasant sensation (pain, pressure, discomfort) perceived to be related to the urinary bladder, associated with lower urinary tract symptom(s) of more than 6 weeks duration, in the absence of infection or other identifiable causes" (<http://www.auanet.org/education/guidelines/ic-bladder-pain-syndrome.cfm>). Diagnostic criteria included persistent or recurrent chronic pelvic pain, pressure or discomfort perceived to be related to the urinary bladder accompanied by at least one other urinary symptom such as an urgent need to void or urinary frequency in the absence of any identifiable pathology. Work-up included symptom assessment, cystoscopic evaluation, physical examination, urodynamics, and/or urine culture. Patients with a history of other diseases (such as any types of cancer, inflammation, or diabetes, etc.) were excluded. Patients who were under any active treatment or medication were clearly excluded. Only subjects >2 months "free of treatment, therapy, or any medications", such as hormone use, pentosan polysulphate, or intravesical instillation therapy, were included. Staging was done based on symptoms, bladder pain, and quality of life. Matched controls were carefully selected

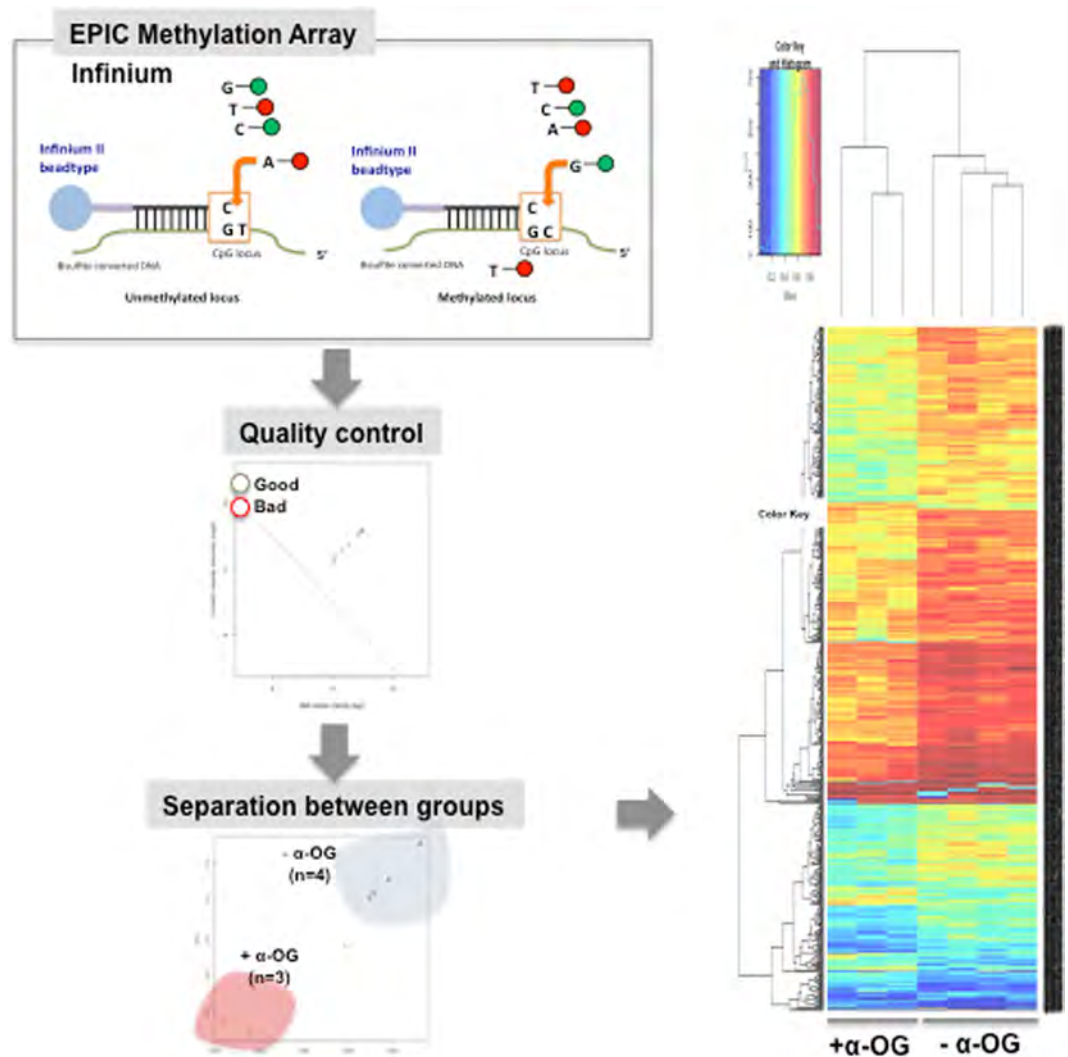


Figure 2. Experimental scheme describing EPIC DNA methylation profiling and the following bioinformatics analysis.

considering age, menopausal status, hormone use *et al.* Bladder biopsies were performed before procedures such as hydrodistention or fulguration. Biopsy sites included lateral walls, dome, posterior wall of bladder wall, but not from trigone, for both IC patients and controls.

ARID1A immunohistochemistry (IHC) and scoring system. IHC analysis for ARID1A expression was performed on 5- μ m slides using a polyclonal rabbit anti-ARID1A antibody (1:250, HPA005456; Sigma-Aldrich). Antigen retrieval was performed by submerging the tissue sections in citrate buffer (pH 6.0) and then in a steamer for 10 minutes. The sections were then incubated with the rabbit antibody at a dilution of 1:200 at 4°C overnight. A positive reaction was detected by the EnVision + System (Dako).

Statistics. All data were generated from experiments performed at least three times and expressed as mean \pm standard deviation (SD). The student's *t*-tests were used to determine the statistical significance of differences between samples treated under different conditions. Differences were considered statistically significant when $p < 0.05$ (*), $p < 0.01$ (**), or $p < 0.001$ (***)

Results

α -OG, an IC-associated metabolite, suppresses cell proliferation in immortalized normal human bladder-derived epithelial cells. In light of our previous global metabolomics data linking α -OG to cell cycle arrest and proliferation suppression¹⁶, we first investigated the effects of α -OG in immortalized normal bladder epithelial cells. Cell cycle transition and proliferation were measured in TRT-HU1 cells treated with or without 10 mM of α -OG. Consistent with previous reports, we observed significant suppression of cell proliferation in response to α -OG (Fig. 1A). Western blot analysis was performed to ascertain the involvement of several key cell cycle and proliferation regulators. We found that levels of p53 and p21 significantly increased while levels of JunB modestly increased in the presence of α -OG (Fig. 1B).

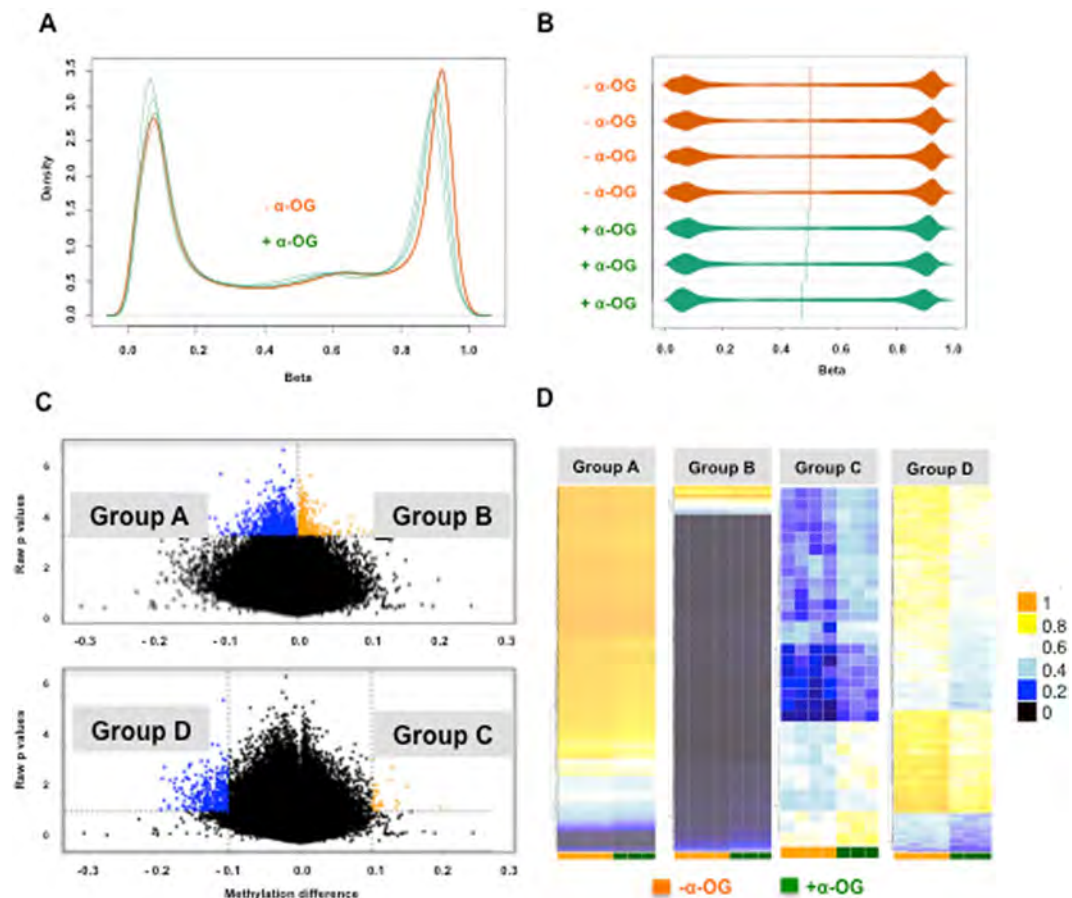


Figure 3. Reprogrammed DNA methylation architecture by α -OG treatment. **(A)** QC (density plots) of probes for DNA methylation levels (β -values). The orange group represents untreated samples, which show a slight hypermethylation pattern. The green group, α -OG-treated samples, shows a more even distribution of beta values across probes. **(B)** Density Bean Plot of probes for β -values in two experimental samples. Distribution of β -values across each sample (orange, untreated; green, α -OG-treated) was shown. **(C)** Volcano Plots indicates differentially methylated probes between untreated and treated samples. Each dot represents a single CpG probe on the array, with hypomethylated probes colored blue and hypermethylated probes colored orange. The upper plot defines differential methylation based on statistical significance alone (Group A – hypomethylated probes: $p < 0.0005$, Group B – hypermethylated probes: $p < 0.0005$). The lower plot shows the exact same volcano plot, but defines differential methylation based on both statistical significance and β -value difference (Group C – hypermethylated probes: $p < 0.05$ and β -value difference > 0.1 , Group D – hypomethylated probes: $p < 0.05$ and β -value difference > 0.1). **(D)** Sample-specific β -values are shown as heatmaps for the probes in Groups A-D. Group A: 873 probes, Group B: 382 probes, Group C: 32 probes, Group D: 366 probes.

α -OG perturbed the epigenetic architecture of immortalized normal bladder epithelial cells.

Given previous reports demonstrating that α -OG modulates epigenetic regulation, we next tested our hypothesis that the global DNA methylome is altered in response to α -OG in immortalized normal human bladder epithelial cells¹⁸. In order to assess whether the DNA methylome is changed by α -OG, EPIC array was performed. Our workflow is described in Fig. 2. Our analysis and data requisition resulted in differentially methylated genes (DMGs) in response to α -OG (Supplementary Table 2–4).

Using the results from the quality control (QC) test, density plots for probes were constructed for DNA methylation levels (β -values) in control and α -OG treated conditions. Untreated control samples (in orange) showed a slight hypermethylation pattern. The α -OG-treated samples (in green) showed a more even distribution of β values across probes (Fig. 3A). Density bean plots for probes (Fig. 3B) shows the DNA methylation levels (β -values) among different samples.

Following the QC steps within minfi (Fig. 3A, B), methylation data for 836,329 CpGs were analyzed. Because we were unable to use minfi's stringent cutoffs to identify Differentially methylated regions (DMRs) with BumpHunter and dmpFinder, we opted to do our analysis using quantitative cutoffs, splitting into four groups of probes. The resulting volcano plots show the differentially methylated probes present between α -OG treatment and control conditions. Significantly hyper-methylated probes are shown in orange, while hypo-methylated probes are shown in blue. First, the most statistically robust CpGs were selected using a p-value cutoff of 0.0005. Unexpectedly, the most significant probes had the smallest differences in methylation β -values ($\beta < 0.1$). These

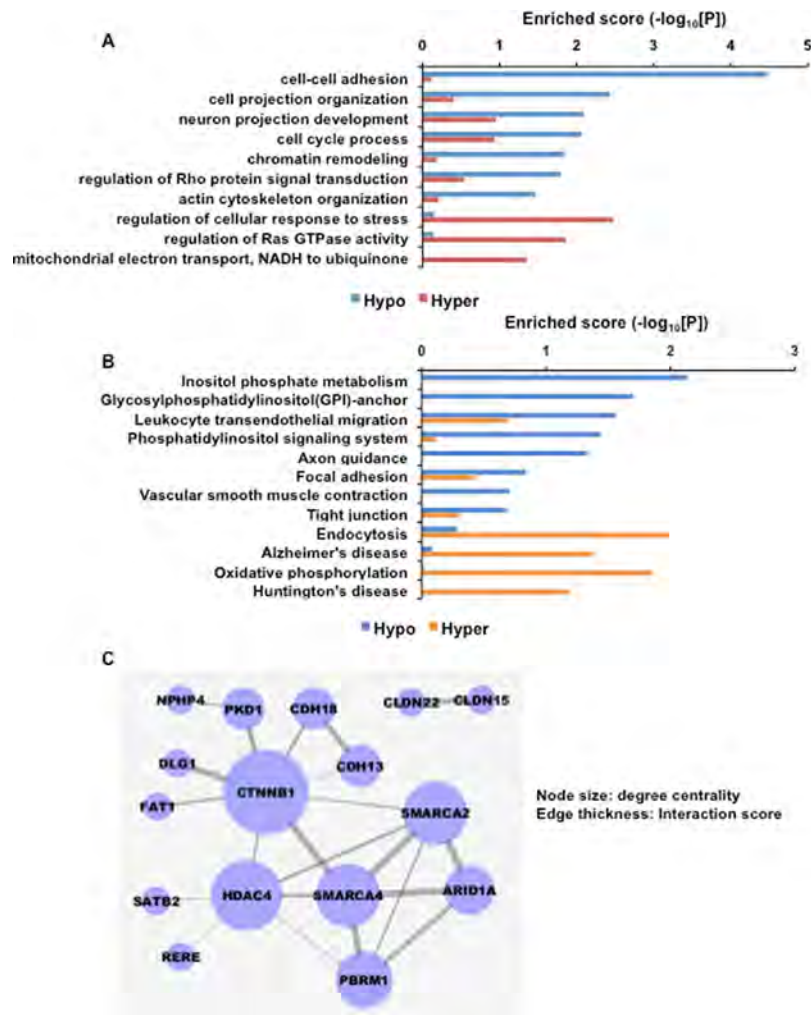


Figure 4. Enriched biology perturbed by α -oxoglutarate. (A and B) Enriched cellular processes (A) and KEGG pathways (B). Bar plot represents scores of enrichments by hyper- and hypo-methylated genes. (C) Network model describes cell-cell adhesion and chromatin remodeling genes that were hypo-methylated by α -OG treatment.

two cutoffs yielded two groups, Group A and B, shown in Fig. 3C, as having 873 and 382 probes, respectively. The other two groups (C and D) were identified by looking at the largest difference in β -values present, $\beta > 0.1$. These probes were less statistically significant, with a p -value < 0.05 . Group C only had 32 probes while Group D had 366. Overall, our analysis of probes that were most statistically significant and had the greatest magnitude of change showed a general shift towards increased global hypo-methylation. Based on these results, we opted to further analyze the groups that had the largest changes in β -values, focusing mostly on group D due to the limited number of probes in group C.

Gene tables for the groups with the largest numbers of identified probes, group A, B, and D, can be found in Supplementary Tables 2, 3, and 4, respectively). Heatmaps of all four groups of probes are shown in Fig. 3D. The heatmaps demonstrate a trend of increased hypo-methylation in probes of cells treated with α -OG, particularly in Group D.

Biological meanings of DMGs responsive to α -oxoglutarate. In order to explore the contribution of DNA methylation signatures in IC, we performed functional enrichment analysis and network modeling on the DMGs. Enriched cellular processes and biological pathways perturbed by α -OG treatment were identified by using DAVID software³⁵. Hypo-methylated genes were enriched for cell-cell adhesion, cell projection organization, neuron projection development, cell cycle processes, chromatin remodeling, and Rho protein signal transduction regulation, while cellular responses to stress, Ras GTPase activity, and transport of NADH to ubiquinone in the mitochondrial electron transport chain were enriched for by hyper-methylated genes (Fig. 4A). We also found that KEGG pathways. inositol phosphate metabolism, glycosylphosphatidylinositol-anchor biosynthesis, leukocyte trans-endothelial migration, phosphatidylinositol signaling were enriched for by hypo-methylated genes and endocytosis, Alzheimer's disease, oxidative phosphorylation, Huntington's disease were enriched for by hyper-methylated genes (Fig. 4B). Table 1 shows the related DMGs for each of the enriched cellular processes.

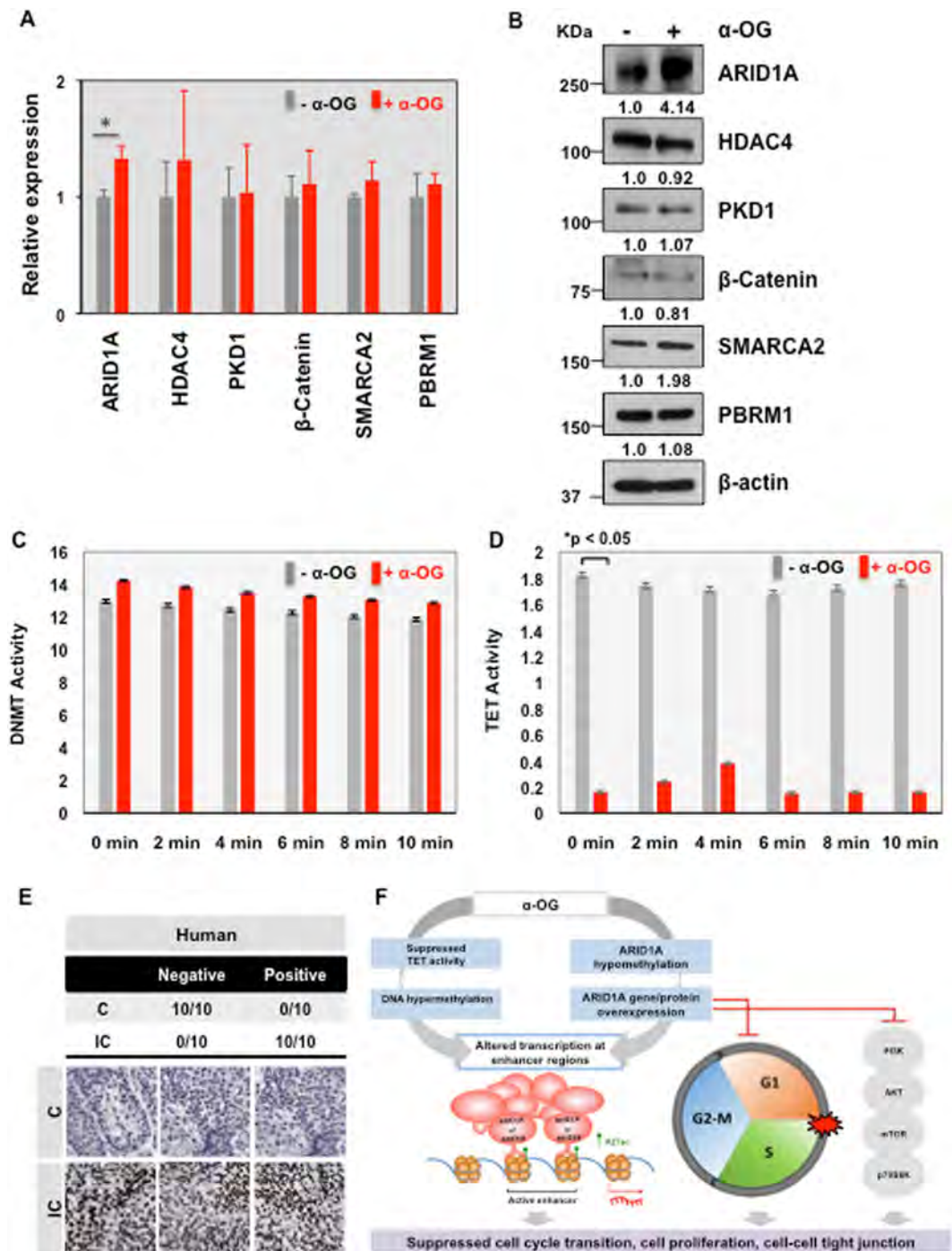


Figure 5. The expression levels of ARID1A were significantly increased in α -OG treated condition. (A) Quantification result from RT-PCR analysis to measure the gene expression levels of six candidate genes (ARID1A, HDAC4, PKD1, β -CATENIN, SMARCA2, and PBRM1) in the presence or absence of α -OG. * $P < 0.05$ (two-sided Student's t-test). (B) Representative western blot show the levels of candidates (ARID1A, HDAC4, PKD1, β -CATENIN, SMARCA2, and PBRM1) and β -actin. (C) DNMT and (D) TET activity were measured in response to α -OG treatment. * $P < 0.05$ (two-sided Student's t-test). (E) Representative Immunohistochemical stain showed ARID1A expression in bladder tissues obtained from IC patients (IC) and healthy donors (C). (F) A diagram showing the potential mechanism that redundant α -OG in urine may regulate bladder epithelial cells and contribute to suppression of cell proliferation.

Our previous study on RNA-sequencing analysis of a IC rat mimic model revealed significant association of cell adhesion and IC context³⁰. In addition, gene expression changes of chromatin remodeling genes were identified in human bladder epithelial cells from patients with IC³⁰. We thus focused on cell-cell adhesion and

Term	Hypo-methylated genes	Hyper-methylated genes
cell-cell adhesion	PCDHGA9, PCDHGA8, PCDHGA7, PCDHGA6, PCDHGA5, PCDHGA4, PCDHGA3, PCDHGA2, CTNNB1, PCDHGA1, CLDN15, PCDHGB1, NPHP4, FAT1, COL6A2, PKD1, DLG1, PCDHGA12, PCDHGA10, PCDHGA11, PCDHGB7, CLDN22, PCDHGB6, PCDHGB3, CERCAM, PCDHGB2, PCDHGB5, PCDHGB4, CDH13, CDH18	CDK5R1, PARD3, EZR, CTNND2, PTPRT
cell projection organization	ADORA2A, PAX6, GRIN3A, TPM1, EPHB1, VCL, DFN31, IGF1R, HOXA2, ATXN10, BCL11B, NUMB, DCLK1, PRKCA, MCF2, BAIAP2L1, BAIAP2, RXRA, NUP85, WWTR1, CDH13, TSC1, CYFIP1, MAPK8IP3, EFNA5, APBB2, APBB1, DST, NGF, MYH10	PPP1R9B, PARD6B, CDK5R1, PARD3, ILK, NUMB, SIAH1, LMX1A, FEZ1
neuron projection development	PRKCA, ADORA2A, MCF2, BAIAP2, RXRA, PAX6, GRIN3A, EPHB1, IGF1R, HOXA2, ATXN10, BCL11B, NUMB, MAPK8IP3, CYFIP1, EFNA5, APBB2, APBB1, DST, DCLK1, MYH10, NGF	PPP1R9B, PARD6B, CDK5R1, PARD3, ILK, NUMB, SIAH1, LMX1A, FEZ1
cell cycle process	MAD1L1, FZR1, KIF25, TSG101, POLA1, CETN1, CDC34, CDC16, TCF7L2, CTNNB1, PLAGL1, PSMF1, CUL2, RAD51L1, PSMD1, PBRM1, PKD1, HBP1, PSMD5, TCF3, ZW10, PSMD9, NFATC1, RAD52, WEE1, FOXN3, PPM1G, MNAT1, PPM1D, NOLC1, CUL4A, SYCP3, CDK2AP1, CDK11B, HORMAD1, CHFR, APBB2, APBB1, DST, MYH10	KIFC1, KIF22, DAXX, TCF7L2, CENPJ, DDTIT3, PPP1R9B, KIF2C, CUL5, CUL4A, ILK, SKA2, PSMD4, MAPRE1, MAP9, DHCR24
chromatin remodeling	HDAC4, SATB2, SYCP3, PBRM1, ARID1A, SMARCA2, RERE, SMARCA4	BAZ1B, SUPT5H
regulation of Rho protein signal transduction	OBSCN, BCR, PLEKHG1, ABR, TSC1, PLEKHG7, MCF2, ARHGEF16, TRIO, ABRA, FARP1	PREX2, BCL6, MLST8, ARHGEF11
actin cytoskeleton organization	FMNL2, SHROOM3, TNXB, SSH1, CALD1, CYTH2, MYO9B, DAAM2, TPM1, ARHGAP26, NPHP4, SCIN, GRID2IP, DST, LCP1, MYH10, CDC42BPB, DLG1	PPP1R9B, EZR, BCL6, FHDC1, ARHGEF11
regulation of cellular response to stress	SH3RF1, MAP3K9, MAP3K10, MAPK8IP3, PKN1	FGF19, ERCC6, AIDA, POLH, EEF1E1, HIPK3, DAXX, SPP1
regulation of Ras GTPase activity	TBC1D2B, TSC1, TBC1D14, RABGAP1L, AGAP1	RABGAP1L, ASAP1, BCL6, EVI5L, MLST8, TBC1D20, AGAP2
mitochondrial electron transport, NADH to ubiquinone		NDUFS7, NDUFB10, NDUFA10, NDUFS1

Table 1. Lists of DMGs for each of the enriched cellular processes.

chromatin remodeling. To this end a network model describing the interactions of the hypo-methylated genes involved in cell-cell adhesion and chromatin remodeling were reconstructed with protein-protein interaction information from the STRING database²⁶. This network model consisted of β -CATENIN (CTNNB1), PKD1 (polycystin 1), CDH18 (cadherin 18), SMARCA4 (SWI/SNF related, matrix associated, actin dependent regulator of chromatin, subfamily A, member 4), HDAC4 (histone deacetylase 4), ARID1A (AT-rich interactive domain 1A), PBRM1 (Polybromo-1, a component of the PBAF (Polybromo-associated-BRG1- or BRM-associated factors) chromatin remodeling complex) *et al.* Of note, CTNNB1 and SMARCA4 are valid candidates regulating cell adhesion and chromatin remodeling in this system (Fig. 4C).

ARID1A expression significantly increased with α -OG treatment. ARID1A, HDAC4, PKD1, β -CATENIN, SMARCA2, and PBRM1 were suggested in our network model for IC and were selected for further validation. These genes were all hypo-methylated in response to α -OG treatment. To ascertain that α -OG treatment modifies the DNA methylome in TRT-HU1 cells, we next quantified the levels of DNA methylation and gene expression of the targeted candidate genes. Using quantitative RT-PCR analysis with customized primers (Supplementary Table 1), we found the mRNA expression levels of all candidate genes as being slightly elevated. Gene expression of ARID1A was significantly increased in the α -OG treated condition ($p = 0.018$) (Fig. 5A). The Protein expression levels of ARID1A and SMARCA2 increased; however, those of HDAC4, PDK, β -CATENIN, and PBRM1 did not (Fig. 5B).

α -OG treatment altered the activity of ten-eleven translation (TET) hydroxylase but not DNA methyltransferase (DNMT). To further elaborate on the effects of α -OG on epigenetic regulation in immortalized normal bladder epithelial cells, we measured the activity of two DNA methylation regulators, DNMT and TET, in the presence of α -OG (Fig. 5C). In our experiments, α -OG treatment suppressed TET activity almost completely; however, there was no influence on DNMT activity (Fig. 5D).

On histological examination, we found that ARID1A expression greatly increased in IC patients. IHC analysis of bladder tissue samples obtained from 10 IC patients and 10 normal controls showed 100% positive staining in IC tissue for ARID1A, while none of the control tissue showed any staining (Fig. 5E). A hypothetical diagram suggesting epigenetic modulation on ARID1A by α -OG is shown in Fig. 5F.

Discussion

Our previous reports provided evidence showing that bladder cell metabolism is altered in IC and suggested several urinary metabolites, including α -OG, as candidate biomarkers¹⁶. However, it is still unclear whether these metabolic biomarkers are biologically active in urine and how they contribute to bladder pathogenesis and homeostasis. The metabolic changes in the IC bladder are largely speculated to be associated with the microenvironment, resulting in altered oxygen states and metabolites. As products of this perturbed metabolism, these metabolites may be what are mediating the epigenetic alteration seen in the IC bladder. Here, our experimental results demonstrate that a novel IC biomarker, α -OG, directly reduces TET activity. α -OG also simultaneously

causes DNA hypo-methylation of ARID1A and cell cycle transition arrest in immortalized normal bladder epithelial cells (Fig. 5F). These findings are consistent with clinical observations in patients; one characteristic of IC is thin bladder epithelium layers^{31,32}. Previous mechanistic studies have shown that bladder epithelial cells derived from IC patients have suppressed proliferation and cell cycle arrest^{31,33}. Based on these previous observations and our findings, α -OG may not only be a novel urinary metabolite associated with IC, but may also have an active biological function.

Altering the methylation status of DNA promoters and enhancers are widely linked to reductions in gene transcription. There are two main processes that orchestrate DNA methylation of key epigenetic regulators; these involve 5-methylcytosine (5mC) and 5-hydroxymethylcytosine (5hmC), which are located on the CpG islands of gene promoters and enhancers. Currently, the most well-studied process of covalent DNA modification is methylation through the addition of methyl groups to produce 5mC. Active DNA methyltransferases, such as DNMT1 and DNMT3A/B, use S-adenosylmethionine as methyl donors and are required for establishing and maintaining DNA methylation patterns. DNA demethylation is another important epigenetic mechanism and is mediated by TET, which converts 5mC to 5hmC and further to 5-carboxylcytosine (5-caC) through its hydroxylase activity.

In the context of IC, perturbed epigenetic architectures, such as DNA methylation and demethylation, in the bladder epithelium have not been carefully investigated. However, given that our encouraging data shows suppressed TET activity as a potential IC biomarker, it may be clinically significant to elaborate on the potential role of TET and its targets as diagnostic markers and/or therapeutic targets. It is not known how these changes in TET and 5hmC profiles are related to IC and how TET can be reactivated. What is known so far is that the TET family (TET1, TET2, and TET3) plays an important role in hydroxymethylating and demethylating 5mC in IC. It is still unclear how these changes in TET and 5hmC profiles are related to IC and how TET can be reactivated. Unfortunately, due to the lack of commercially available TET activators, we could not perform any tests to see if TET stimulation can reverse bladder dysfunction.

Our results also suggest the possible physiological role of ARID1A in maintaining normal homeostasis in the bladder epithelium through controlling chromatin remodeling. ARID1A and SMARCA2, both are subunits of the SWI/SNF chromatin-remodeling complex, were suggested as key players of α -OG signaling pathway in our network model. Although modest, the expression of SMARCA2 also increased upon α -OG treatment (Fig. 5B). This finding is consistent with previously published microarray analyses of IC primary culture cells and controls. The gene expression of both IC patient-derived primary culture cells and APF (anti-proliferative factor, an urinary IC biomarker)-treated cells suggested a less proliferative phenotype, with increased expression of SMARCA2³⁴.

ARID1A sustains chromatin accessibility through H3K27me3 and H3k27ac in the enhancer regions^{35,36}. ARID1A is also a well-known bona fide tumor suppressor that is frequently inactivated by mutations or reduced in expression due to promoter hyper-methylation³⁷. Along with p21, cyclins, and E2F-responsive genes, ARID1A is essential for normal cell cycle arrest; thus, inactivation of ARID1A results in tumor transformation, metastasis, and/or drug resistance^{38,39}. However, the biological function of ARID1A is context dependent. In bladder cancer, increased ARID1A expression is generally correlated with higher tumor grade; however, there is some variation based on the cancer type^{40,41}. Detailed information regarding the mechanism and physiological roles of ARID1A and its co-factors has been lacking. Based on our study, we propose that ARID1A can be regulated through α -OG, contributing to an impaired cell proliferation in IC. We believe that additional attempts to validate the epigenetic regulation of α -OG on ARID1A in clinical samples may provide novel insight into the etiology of IC and identify metabolites that can serve as IC biomarkers for clinical application.

In summary, evidence from our EPIC DNA methylation profiling suggests that α -OG, a potential IC biomarker candidate, regulates ARID1A epigenetically. Modification of the promoter for ARID1A contributes to increased expression at both the mRNA and protein levels, leading to suppressed proliferation in the bladder epithelial cells. These findings indicate that urinary metabolites in the bladder can lead to epigenetic reprogramming. Given our observations, we may have defined the epigenetic regulatory mechanisms of ARID1A and TET activity in the anti-proliferative axis in immortalized normal bladder epithelial cells.

References

- Pflumm, M. Animal instinct helps doctors ferret out disease. *Nature medicine* **17**, 143, <https://doi.org/10.1038/nm0211-143> (2011).
- Hanno, P., Keay, S., Moldwin, R. & Van Ophoven, A. International Consultation on IC - Rome, September 2004/Forging an International Consensus: progress in painful bladder syndrome/interstitial cystitis. Report and abstracts. *International urogynecology journal and pelvic floor dysfunction* **16**(Suppl 1), S2–S34, <https://doi.org/10.1007/s00192-005-1301-x> (2005).
- Hanno, P. et al. Diagnosis of interstitial cystitis. *The Journal of urology* **143**, 278–281 (1990).
- Ness, T. J., Powell-Boone, T., Cannon, R., Lloyd, L. K. & Fillingim, R. B. Psychophysical evidence of hypersensitivity in subjects with interstitial cystitis. *The Journal of urology* **173**, 1983–1987, <https://doi.org/10.1097/01.ju.0000158452.15915.e2> (2005).
- Nordling, J. et al. Primary evaluation of patients suspected of having interstitial cystitis (IC). *European urology* **45**, 662–669, <https://doi.org/10.1016/j.eururo.2003.11.021> (2004).
- Warren, J. W. & Keay, S. K. Interstitial cystitis. *Current opinion in urology* **12**, 69–74 (2002).
- Anger, J. T. et al. Treatment choice, duration, and cost in patients with interstitial cystitis and painful bladder syndrome. *International urogynecology journal* **22**, 395–400, <https://doi.org/10.1007/s00192-010-1252-8> (2011).
- Berry, S. H. et al. Prevalence of symptoms of bladder pain syndrome/interstitial cystitis among adult females in the United States. *The Journal of urology* **186**, 540–544, <https://doi.org/10.1016/j.juro.2011.03.132> (2011).
- Suskind, A. M. et al. The prevalence and overlap of interstitial cystitis/bladder pain syndrome and chronic prostatitis/chronic pelvic pain syndrome in men: results of the RAND Interstitial Cystitis Epidemiology male study. *The Journal of urology* **189**, 141–145, <https://doi.org/10.1016/j.juro.2012.08.088> (2013).
- Berry, S. H. et al. Development, validation and testing of an epidemiological case definition of interstitial cystitis/painful bladder syndrome. *The Journal of urology* **183**, 1848–1852, <https://doi.org/10.1016/j.juro.2009.12.103> (2010).
- Clemens, J. Q. et al. Validation of a modified National Institutes of Health chronic prostatitis symptom index to assess genitourinary pain in both men and women. *Urology* **74**, 983–987, quiz 987 e981–983, <https://doi.org/10.1016/j.urology.2009.06.078> (2009).
- Bogart, L. M., Berry, S. H. & Clemens, J. Q. Symptoms of interstitial cystitis, painful bladder syndrome and similar diseases in women: a systematic review. *The Journal of urology* **177**, 450–456, <https://doi.org/10.1016/j.juro.2006.09.032> (2007).

13. Zhang, A., Sun, H. & Wang, X. Serum metabolomics as a novel diagnostic approach for disease: a systematic review. *Analytical and bioanalytical chemistry* **404**, 1239–1245, <https://doi.org/10.1007/s00216-012-6117-1> (2012).
14. Gebregiorgis, T. & Powers, R. Application of NMR metabolomics to search for human disease biomarkers. *Combinatorial chemistry & high throughput screening* **15**, 595–610 (2012).
15. Serkova, N. J. & Brown, M. S. Quantitative analysis in magnetic resonance spectroscopy: from metabolic profiling to *in vivo* biomarkers. *Bioanalysis* **4**, 321–341, <https://doi.org/10.4155/bio.11.320> (2012).
16. Wen, H. *et al.* Urinary Metabolite Profiling Combined with Computational Analysis Predicts Interstitial Cystitis-Associated Candidate Biomarkers. *Journal of proteome research*. <https://doi.org/10.1021/pr5007729> (2014).
17. Vatrinet, R. *et al.* The alpha-ketoglutarate dehydrogenase complex in cancer metabolic plasticity. *Cancer & metabolism* **5**, 3, <https://doi.org/10.1186/s40170-017-0165-0> (2017).
18. Xu, T. *et al.* Metabolic control of TH17 and induced Treg cell balance by an epigenetic mechanism. *Nature* **548**, 228–233, <https://doi.org/10.1038/nature23475> (2017).
19. Kim, J. *et al.* An hTERT-immortalized human urothelial cell line that responds to anti-proliferative factor. *In vitro cellular & developmental biology. Animal* **47**, 2–9, <https://doi.org/10.1007/s11626-010-9350-y> (2011).
20. Zhou, W., Laird, P. W. & Shen, H. Comprehensive characterization, annotation and innovative use of Infinium DNA methylation BeadChip probes. *Nucleic acids research* **45**, e22, <https://doi.org/10.1093/nar/gkw967> (2017).
21. Fortin, J. P., Triche, T. J. Jr. & Hansen, K. D. Preprocessing, normalization and integration of the Illumina HumanMethylationEPIC array with minfi. *Bioinformatics* **33**, 558–560, <https://doi.org/10.1093/bioinformatics/btw691> (2017).
22. Triche, T. J. Jr., Weisenberger, D. J., Van Den Berg, D., Laird, P. W. & Siegmund, K. D. Low-level processing of Illumina Infinium DNA Methylation BeadArrays. *Nucleic acids research* **41**, e90, <https://doi.org/10.1093/nar/gkt090> (2013).
23. Colaprico, A. *et al.* TCGAAbiolinks: an R/Bioconductor package for integrative analysis of TCGA data. *Nucleic acids research* **44**, e71, <https://doi.org/10.1093/nar/gkv1507> (2016).
24. Gu, Z., Eils, R. & Schlesner, M. Complex heatmaps reveal patterns and correlations in multidimensional genomic data. *Bioinformatics* **32**, 2847–2849, <https://doi.org/10.1093/bioinformatics/btw313> (2016).
25. Huang da, W., Sherman, B. T. & Lempicki, R. A. Systematic and integrative analysis of large gene lists using DAVID bioinformatics resources. *Nature protocols* **4**, 44–57, <https://doi.org/10.1038/nprot.2008.211> (2009).
26. Szklarczyk, D. *et al.* The STRING database in 2017: quality-controlled protein-protein association networks, made broadly accessible. *Nucleic acids research* **45**, D362–D368, <https://doi.org/10.1093/nar/gkw937> (2017).
27. Shannon, P. *et al.* Cytoscape: a software environment for integrated models of biomolecular interaction networks. *Genome research* **13**, 2498–2504, <https://doi.org/10.1101/gr.1239303> (2003).
28. Hanno, P. M. *et al.* AUA guideline for the diagnosis and treatment of interstitial cystitis/bladder pain syndrome. *The Journal of urology* **185**, 2162–2170, <https://doi.org/10.1016/j.juro.2011.03.064> (2011).
29. Hanno, P. M., Erickson, D., Moldwin, R., Faraday, M. M. & American Urological, A. Diagnosis and treatment of interstitial cystitis/bladder pain syndrome: AUA guideline amendment. *The Journal of urology* **193**, 1545–1553, <https://doi.org/10.1016/j.juro.2015.01.086> (2015).
30. Choi, B. H. *et al.* Differential perturbation of the interstitial cystitis-associated genes of bladder and urethra in rat model. *Cell cycle* **16**, 749–758, <https://doi.org/10.1080/15384101.2017.1295184> (2017).
31. Kim, J., Keay, S. K., Dimitrakov, J. D. & Freeman, M. R. p53 mediates interstitial cystitis antiproliferative factor (APF)-induced growth inhibition of human urothelial cells. *FEBS letters* **581**, 3795–3799, <https://doi.org/10.1016/j.febslet.2007.06.058> (2007).
32. Tomaszewski, J. E. *et al.* Biopsy features are associated with primary symptoms in interstitial cystitis: results from the interstitial cystitis database study. *Urology* **57**, 67–81 (2001).
33. Keay, S., Zhang, C. O., Shoenfelt, J. L. & Chai, T. C. Decreased *in vitro* proliferation of bladder epithelial cells from patients with interstitial cystitis. *Urology* **61**, 1278–1284 (2003).
34. Keay, S., Seillier-Moiseiwitsch, F., Zhang, C. O., Chai, T. C. & Zhang, J. Changes in human bladder epithelial cell gene expression associated with interstitial cystitis or antiproliferative factor treatment. *Physiological genomics* **14**, 107–115, <https://doi.org/10.1152/physiolgenomics.00055.2003> (2003).
35. Hodges, C., Kirkland, J. G. & Crabtree, G. R. The Many Roles of BAF (mSWI/SNF) and PBAF Complexes in Cancer. *Cold Spring Harbor perspectives in medicine* **6**, <https://doi.org/10.1101/cshperspect.a026930> (2016).
36. Wilson, B. G. & Roberts, C. W. SWI/SNF nucleosome remodellers and cancer. *Nature reviews. Cancer* **11**, 481–492, <https://doi.org/10.1038/nrc3068> (2011).
37. Wu, J. N. & Roberts, C. W. ARID1A mutations in cancer: another epigenetic tumor suppressor? *Cancer discovery* **3**, 35–43, <https://doi.org/10.1158/2159-8290.CD-12-0361> (2013).
38. Shain, A. H. *et al.* Convergent structural alterations define SWItch/Sucrose NonFermentable (SWI/SNF) chromatin remodeler as a central tumor suppressive complex in pancreatic cancer. *Proceedings of the National Academy of Sciences of the United States of America* **109**, E252–259, <https://doi.org/10.1073/pnas.1114817109> (2012).
39. Wang, K. *et al.* Exome sequencing identifies frequent mutation of ARID1A in molecular subtypes of gastric cancer. *Nature genetics* **43**, 1219–1223, <https://doi.org/10.1038/ng.982> (2011).
40. Faraj, S. F. *et al.* ARID1A immunohistochemistry improves outcome prediction in invasive urothelial carcinoma of urinary bladder. *Human pathology* **45**, 2233–2239, <https://doi.org/10.1016/j.humpath.2014.07.003> (2014).
41. Li, J., Lu, S., Lombardo, K., Monahan, R. & Amin, A. ARID1A alteration in aggressive urothelial carcinoma and variants of urothelial carcinoma. *Human pathology* **55**, 17–23, <https://doi.org/10.1016/j.humpath.2016.04.006> (2016).

Acknowledgements

The authors acknowledge support from Florida Department of Health, Bankhead-Coley Cancer Research Program (5BC03) (to M.K.), National Institutes of Health grants (1U01DK103260, 1R01DK100974, U24DK097154, NIH NCATS UCLA CTSI UL1TR000124), Department of Defense grants (W81XWH-15-1-0415), Centers for Disease Controls and Prevention (1U01DP006079), IMAGINE NO IC Research Grant, the Steven Spielberg Discovery Fund in Prostate Cancer Research Career Development Award, the U.S.-Egypt Science and Technology joint Fund (to J.K.). J.K. is former recipient of Interstitial Cystitis Association Pilot Grant, a Fishbein Family IC Research Grant, New York Academy of Medicine, and Boston Children's Hospital Faculty Development. The funders had no role in the design, data collection and analysis, decision to publish or preparation of the manuscript. In addition, this article is derived from the Subject Data funded in whole or part by NAS and USAID. Any opinions, findings, conclusions, or recommendations expressed in such article are those of the authors alone, and do not necessarily reflect the views of USAID or NAS.

Author Contributions

M.S. and A.Y. involved and performed most of the experiments. N.Y., S.Y., and M.K. performed DNA methylation analysis and helped to draft paper. A.Y., E.C., H.S.Y., and J.B. performed immunohistochemical works. M.S.,

A.Y., and E.C. performed biochemical and functional analysis *in vitro*. H.Y. and M.K. provided IHC images and provided clinical insights. B.B. supported EPIC data interpretation and provided scientific comments on project. J.K. designed and conceived the study and wrote the paper. All authors discussed the results and commented on the manuscript at all stages, and read and approved the manuscript.

Additional Information

Competing Interests: The authors declare no competing interests.

Publisher's note: Springer Nature remains neutral with regard to jurisdictional claims in published maps and institutional affiliations.



Open Access This article is licensed under a Creative Commons Attribution 4.0 International License, which permits use, sharing, adaptation, distribution and reproduction in any medium or format, as long as you give appropriate credit to the original author(s) and the source, provide a link to the Creative Commons license, and indicate if changes were made. The images or other third party material in this article are included in the article's Creative Commons license, unless indicated otherwise in a credit line to the material. If material is not included in the article's Creative Commons license and your intended use is not permitted by statutory regulation or exceeds the permitted use, you will need to obtain permission directly from the copyright holder. To view a copy of this license, visit <http://creativecommons.org/licenses/by/4.0/>.


© The Author(s) 2018

SCIENTIFIC REPORTS



OPEN

Menthol, a unique urinary volatile compound, is associated with chronic inflammation in interstitial cystitis

Muhammad Shahid¹, Min Young Lee², Austin Yeon¹, Eunho Cho³, Vikram Sairam³, Luis Valdiviez⁴, Sungyong You¹  & Jayoung Kim^{1,3,5,6}

Chronic inflammation is a potential systemic risk factor for many bladder dysfunctions, including interstitial cystitis (IC). However, the underlying mechanism through which a healthy bladder protects itself from inflammatory triggers remains unknown. In this study, we identified odor compounds in urine obtained from IC patients and healthy controls. Using comprehensive solid-phase microextraction-gas chromatography-time-of-flight-mass spectrometry (SPME-GC-TOF-MS) profiling and bioinformatics, we found that levels of urinary volatile metabolites, such as menthol, were significantly reduced in IC patients, compared to healthy controls. In an attempt to understand the mechanistic meaning of our volatile metabolites data and the role of menthol in the immune system, we performed two independent experiments: (a) cytokine profiling, and (b) DNA microarray. Our findings suggest that lipopolysaccharide (LPS)-stimulated inflammatory events, such as the production and secretion of inflammatory cytokines (e.g., TNF- α , IL-6, and IL-1 β) and the activation of NF- κ B and associated proteins within a large signaling network (e.g., Akt, TLR1, TNFAIP3, and NF- κ B), are suppressed by the presence of menthol. These findings broaden our knowledge on the role of urinary menthol in suppressing inflammatory events and provide potential new strategies for alleviating both the odor and inflammation associated with IC.

Interstitial cystitis (IC) is a clinical condition that presents itself as sensory hypersensitivity of unknown cause and is characterized by frequent urination, bladder discomfort, and pelvic pain¹. IC occurs in both women and men over a broad age range and across ethnic/racial groups². In the United States, more than 3–8 million women and 1–4 million men are diagnosed with IC annually³. The prevalence estimates of IC vary substantially because of differences in source populations and case ascertainment⁴. Current diagnostic techniques include cystoscopy, potassium sensitivity tests, hydrodistension *et al.* However, these procedures are not only invasive, painful, and inconvenient, but also extremely costly, complicated, and minimally informative. In addition to these complications with diagnosis, the lack of consensus regarding the cause of IC has resulted in difficulties determining effective and specific therapies.

Although there has been immense progress in the fields of genomics and proteomics, further research into the biological end points of human diseases is needed for improved disease diagnosis, prognosis, and therapeutic development. In recent years, metabolomic profiling, also known as metabolomics, has been viewed as a promising technique in disease diagnosis. Metabolomics focuses on utilizing and analyzing metabolites and biomarkers as signals for cellular states. These biological biomarkers have been used to understand the metabolic changes that occur over time in a variety of diseases⁵. In particular, clinical samples, such as tissues and biofluids (e.g. serum, plasma, urine, and saliva), have proven to be valuable sources for diagnostic purposes. For instance, human plasma proteins originate from a variety of cells and various medical studies have shown that these proteins reflect

¹Departments of Surgery and Biomedical Sciences, Cedars-Sinai Medical Center, Los Angeles, CA, USA. ²Institute for Systems Biology, Seattle, WA, USA. ³University of California Los Angeles, Los Angeles, CA, USA. ⁴West Coast Metabolomics Center, UC Davis, Davis, CA, 95616, USA. ⁵Samuel Oschin Comprehensive Cancer Institute, Cedars-Sinai Medical Center, Los Angeles, CA, USA. ⁶Department of Urology, Ga Cheon University College of Medicine, Incheon, South Korea. Correspondence and requests for materials should be addressed to J.K. (email: Jayoung.Kim@cshs.org)

human physiological and pathological states. Therefore, they can potentially be utilized to increase diagnostic efficiency and prognostic efficacy⁶. Other biological fluids have been quantitatively determined in regards to their metabolic composition through procedures such as gas chromatography, high-pressure liquid chromatography, mass spectrometry.

Urine contains a multitude of water-soluble waste products filtered through the kidneys and eliminated from the body via micturition. It contains many metabolites, such as urea (from amino acid metabolism), inorganic salts (chloride, sodium, and potassium), creatinine, ammonia, organic acids, water-soluble toxins, and urobilin. While this complexity can make urine analysis difficult, the potential information that can result will be very beneficial, and progress in the field has been promising. Additionally, collection of urine is simpler and provides a relatively larger volume of sample compared to other biological fluids.

Odor consists of various volatile organic chemical compounds (VOCs), which can be identified through mass spectrometry. Compared to other organic compounds, VOCs generally have a lower molecular weight and higher vapor pressure. Many prior studies have applied VOCs into cancer research. For cancer detection, there have been several studies on using gas chromatography-mass spectrometry (GC-MS) to detect certain odor compounds in skin, tissue, breath, feces, and bodily fluids, such as sweat and urine⁷⁻⁹. VOCs can also be used to assist in the diagnosis of lung and prostate cancer¹⁰. Electronic noses capable of detecting odor signatures have been developed and successfully applied in discriminating prostate cancer patients from healthy controls^{9,11}. In terms of IC, perturbed VOCs may underlie the commonly reported changes in urine odor. IC is known to negatively impact overall quality of life through its effects on urinary odor and leakage; many patients often report foul smelling urine¹². Given our previous findings that IC patients may have a distinct metabolism^{13,14}, we hypothesized that urine from IC patients might contain a distinguishing VOC signature that is reflective of disease conditions.

In our present volatile metabolomics study, we tested the hypothesis that urinary VOCs differ between IC patients and healthy controls. Using urinary samples from the urine headspace of IC patients and healthy controls. We extracted VOCs via solid-phase micro-extraction and analyzed them using GC-MS. The aim of this study was to identify IC-associated VOCs and further examine their biological meaning in the bladder epithelium. From our comprehensive and unbiased metabolomics analysis, we found menthol to be a novel compound involved in IC-associated inflammation. We discovered that urinary menthol decreased in IC patients and that these reduced levels are potentially linked to the chronic inflammation commonly observed in IC.

Materials and Methods

Cell Line. The mouse macrophage cell line, RAW 264.7, was obtained from Sigma Cells (St. Louis, MO, USA) and was cultured in Dulbecco's Modified Eagle Medium (DMEM) supplemented with 10% fetal bovine serum (FBS). The cells were kept in humidified incubators with 5% CO₂ at 37 °C. The medium was replaced every day and the cells were passed every two to three days to maintain logarithmic growth.

Reagents. Menthol and bacterial lipopolysaccharide (LPS) (*Escherichia coli*, 0111: B4) were purchased from Sigma (USA). Mass spectrometry grade reagents (column, buffer *et al.*) were all purchased from Sigma (USA). The Mouse Proteome Profiler Array was purchased from R&D Systems (USA). The antibodies used were CCL3 (ab25128, Abcam, USA), IL-6 (12912; Cell Signaling Technology, USA), TNF- α (11948S; Cell Signaling Technology, USA), p-NF- κ B (3033; Cell Signaling Technology, USA), NF- κ B (8242; Cell Signaling Technology, USA), p-Akt (4051; Cell Signaling Technology, USA), Akt (9272; Cell Signaling Technology, USA), TLR1(2209; Cell Signaling Technology, USA), TNFAIP3 (5630; Cell Signaling Technology, USA), IFIT1 (14769; Cell Signaling Technology, USA), viperin (13996; Cell Signaling Technology, USA), IL-1 β (AF-401-NA, R&D Systems, USA), and β -actin (A1978; Sigma-Aldrich, USA). HRP-conjugated secondary antibodies were obtained from Cell Signaling Technologies (7074, 7076; USA).

Ethics Statements. The ethics committee at Inha University Hospital (Incheon, South Korea) approved this study. Written informed consent was obtained from all subjects. The Institutional Review Board of Inha University Hospital approved collection, curation, and analysis of all samples (IRB #10-0751)^{13,14}. All methods were performed in accordance with the relevant guidelines and regulations.

Subjects and Urine Specimen Collection. Patients and healthy control subjects were recruited from an outpatient urology clinic at Inha University Hospital. All subjects were Asian females. Subjects were instructed to avoid tobacco, nicotine, chemical compounds, alcohol, herbal foods, caffeine, and medication 24 hrs before their urine collection. Recruitment was conducted following the National Institute of Diabetes and Digestive and Kidney Diseases (NIDDK) guidelines. Workup included symptom assessment, cystoscopic evaluation, physical examination, urodynamics, and/or urine culture. Patients with a history of other diseases, including cancer, chronic inflammation, or diabetes, were excluded.

To minimize possible contamination with vaginal, rectal, or urethral cells, first morning urine specimens were obtained using clean catch methods in a sterile environment. The de-identified specimens were sent to laboratory and centrifuged for 10 mins to remove cell debris. Urine supernatants were then processed into individual aliquots and stored in 15 ml tubes at -80 °C until further analysis.

Availability of data and materials. All the data supporting the findings here is contained within the manuscript.

Volatile Metabolomics

Sample preparation. Metabolomics analysis was performed using urine samples obtained from IC diagnosed ($n = 10$) and healthy age-matched controls ($n = 10$). Urine samples were prepared in triplicates in 20 ml amber headspace vials with magnetic screw caps and silicone/PTFE septa. Urine samples (10 ml) were added to a vial containing 2.5 g of sodium chloride that had been dried at 100–150 °C for at least 2 hrs prior to weighing. The solution was capped, vortexed, and loaded onto an autosampler tray. No more than 18 samples were prepared at a time; this was done to minimize the length of time the last sample in the batch sat at ambient laboratory temperature prior to extraction and analysis. Quality control experiments were performed as described in a previous paper¹⁵.

Solid-phase microextraction (SPME) and GC-TOF-MS analysis. A LECO Pegasus III Time-of-Flight Mass Spectrometer (LECO, St. Joseph, MI, USA) equipped with an Agilent 6890 Gas Chromatograph (Agilent Technologies, Santa Clara, CA, USA) was used for analysis. ChromaTOF (ver. 4.50.8.0, LECO) was used for raw data processing, including automatic peak detection and deconvolution, as described in a previous paper¹⁵.

Urine GC-MS data pre-processing. We performed data cleaning and pre-processing using Excel and R Studio¹⁵. A two-way analysis of variance comparing the first and last four samples did not show any differences in false discovery rate (FDR) corrected significance levels for peak abundances.

Differential expression analysis for volatile metabolite profiles. To identify differentially expressed metabolites between the urines of IC patients and controls, we applied the integrative hypothesis testing method¹⁶. The t-test, log₂-median-ratio test, and Wilcoxon rank sum test were also performed. For the t-test and log₂-median-ratio test, an empirical distribution of the null hypothesis (the means of the metabolite intensity levels are not different) was estimated using random permutations of the samples. For each metabolite, a p-value was computed by performing a two-tailed test on the empirical distributions. The three p-values were combined using Stouffer's method to compute the adjusted p-values. The FDR was computed from the adjusted p-value using Storey's method¹⁷. We identified 12 metabolites with a FDR < 0.1.

Western blot analysis. Cells were lysed with a RIPA buffer (20 mM Tris, 150 mM NaCl, 1% Nonidet, P-40, 0.1 mM EDTA) (Pierce, ThermoFisher) that was supplemented with a phosphatase inhibitor cocktail (ThermoFisher). The protein concentration of each sample was measured using the Bradford Protein Assay Kit, according to the manufacturer's protocol (Pierce, ThermoFisher). Equal amounts of extracts were separated by SDS-PAGE and transferred onto a PVDF membrane. The membranes were then blocked with 5% bovine serum albumin or 5% nonfat milk in tris-buffered saline with tween 20 (TBST) [2.42 g/L Tris-HCl, 8 g/L NaCl, and 1 mL/L Tween 20 (pH 7.6)] and incubated overnight at 4 °C with specific primary antibodies in TBST. Following this first incubation, the membranes were washed and incubated again with horseradish peroxidase-conjugated secondary antibodies. β -actin was used as an internal control.

Cytokine array. Cell lysates and conditioned media were collected and analyzed using a cytokine array from R&D Systems (USA). They were then diluted and mixed with a cocktail of biotinylated detection antibodies. The sample/antibody mixture was then incubated with the mouse cytokine array membrane. Any cytokine or detection antibody complex was bound to its cognate immobilized capture-antibody on the membrane. Following a wash to remove unbound material, streptavidin-HRP and chemiluminescent detection reagents were added sequentially. Light was produced at each spot in proportion to the amount of cytokine bound. For data quantification ImageJ was used.

RNA preparation for DNA microarray analysis. Total RNA was extracted from RAW 264.7 macrophage cells that were treated with LPS and/or menthol, using a Qiagen RNEasy Mini Kit (Qiagen Inc., Valencia, CA, USA). The RNA concentration of the samples and quality controls was measured using the Bioanalyzer 2100 and Nanodrop 8000a (ThermoScientific, Wilmington, DE, USA).

Microarrays and data analysis. Total RNA (200 ng) was transcribed to double-stranded cRNA using the MessageAmp Primer RNA Amplification Kit (Life Technologies, Carlsbad, CA, USA) with an oligo(dT) primer, according to the manufacturer's instructions. After fragmentation, 11 μ g of biotin-labeled cRNA was hybridized for 16 hrs at 45 °C on the Affymetrix Mouse Genome 430 Plus 2.0 Array (Affymetrix, Santa Clara, CA, USA). GeneChips were then washed and stained in the Affymetrix Fluidics Station 450 and scanned using the Affymetrix GeneChip Scanner 3000 G7 (Affymetrix). Quality control was performed with the Affymetrix Expression Console software (Affymetrix version 1.3). The raw data was normalized using the gcrma package (version 2.10.0) in R 2.6.1. The log₂ GC-RMA signals were then exported and used for differential expression analysis. Both the CEL files and normalized data discussed here are deposited and available at Gene Expression Omnibus (<http://www.ncbi.nlm.nih.gov/geo/>) under the accession number GSE98933.

To identify differentially expressed genes (DEGs), we used a two-tailed Welch's t-test. DEGs were identified as genes with a p-value < 0.05 and fold-change ≥ 1.5 . In order to reduce unreliable detection and false positives, probe sets with average expression levels higher than the average of all probe sets in the data were also considered for further analysis. To identify biological processes affected by LPS or menthol, we performed functional enrichment analysis of Gene Ontology Biological Processes (GOBPs) using DAVID¹⁸. Those with p-values < 0.05 and DEGs ≥ 3 were selected as significantly represented GOBPs.

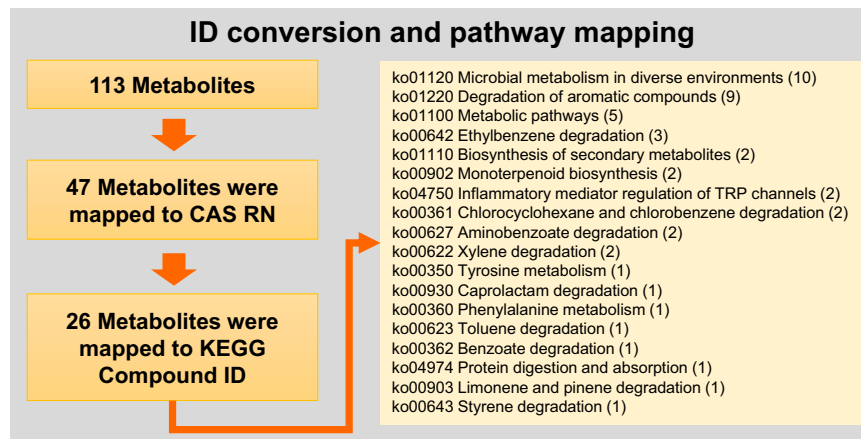


Figure 1. The analysis workflow of volatile metabolome identification, conversion to KEGG IDs, and pathway mapping.

Statistical analysis. The mean of more than three replicates was used as the average. For simple comparisons, *p*-values were calculated using a standard unpaired Student's *t*-test. Statistical significance was considered as *p* < 0.05.

Results

Volatile metabolomics profiling revealed that menthol levels are significantly reduced in the urine specimens of IC patients. We sought to determine the VOC composition of urine in IC and healthy patients by performing volatile metabolite profiling using SPME-GC-TOF-MS. We used fatty acid methyl esters (FAMES) as internal standards for quality control (including in injections) and for retention index corrections. The method used for untargeted profiling was based on the method developed by Robinson¹⁹, with some added modifications (see materials and methods). The ChromaTOF software was used for automatic peak detection and deconvolution of the raw data. After data cleaning and pre-processing, a total of 113 peaks were identified. Quality assessment of these quantification results was done after quantile normalization²⁰ (Supplementary Fig. 1). Peak intensities were summed for all identified metabolites (mTIC). Each peak was then normalized to the sample's total volatile metabolome.

We then investigated the association of these peaks with known metabolic pathways. To do this, we first selected 47 peaks that were annotated with a CAS registry number and then identified 26 peaks that can be mapped to at least one Kyoto Encyclopedia of Genes and Genomes (KEGG) compound ID. Using the DAVID software¹⁸, we found that 26 metabolites were associated with 26 pathways (Fig. 1). We next performed differential analysis to identify which metabolites were significantly altered between IC patients and healthy controls. The analysis included 76 peaks, with quantification of more than half of the samples in each condition. This resulted in 12 peaks that were identified with a FDR < 0.1 (Table 1). The FDR was calculated using the integrated hypothesis testing method (see materials and methods)¹⁶. Among them, menthol (CAS RN: 89-78-1) was identified to be significantly different, with a FDR of 0.024 and log₂ fold-change of -0.1467. We observed only authentic VOCs, not chemicals or metabolites that could come from degradation processes.

Given our results demonstrating reduced menthol levels in the urine of IC patients and prior knowledge from literature, we speculated that menthol may be influencing bladder health. We hypothesized that the urine of IC patients contains reduced levels of anti-inflammatory metabolites, particularly menthol, which leads to an increase in IC-associated cytokines. To test this hypothesis, we sought to evaluate whether the anti-inflammatory effects of menthol could suppress LPS-induced inflammatory events in immune cells. We decided to use two independent approaches: (i) mesoscale cytokine profiling, and (ii) gene expression microarray analysis.

In order to characterize the effects of menthol on macrophages, comprehensive microarray analysis was conducted on RAW 264.7 cells under various conditions. Cells were treated with menthol or control vehicle for 1 hr. The macrophages were then stimulated with LPS treatment (100 ng/ml) for the following 6 hrs. Three groups of gene expression profiles were defined: control vs menthol (C vs M), control vs LPS (C vs LPS), and menthol vs LPS (M vs LPS).

Cytokine profiling revealed that menthol downregulated the LPS-induced production of inflammatory cytokines in RAW 264.7 macrophages. An inflammatory cytokine array was used to identify the specific cytokines that were produced and secreted into the surrounding medium by the RAW 264.7 cells. To determine whether the presence of menthol affects the production and release of cytokines, RAW 264.7 cells were pretreated with menthol (500 μmol/ml) or control for 1 hr and then induced with LPS (100 ng/ml) for 6 hrs. The expression of each inflammatory cytokine was subsequently measured. The cytokine profiling data showed that a series of cytokines, including C-C motif chemokine ligand 3 (CCL3), C-X-C motif chemokine ligand 10 (CXCL10), and tumor necrosis factor alpha (TNF-α), were induced by LPS (Fig. 2A, LPS condition).

Compared to treatment with LPS alone, the addition of menthol significantly downregulated the production and secretion of these cytokines (Fig. 2A, LPS+M compared to LPS). ImageJ analysis software was used

Name	CAS Registry Number	KEGG	Retention Time	FDR	FC	SD
Benzaldehyde,3,5-dimethyl-	5779-95-3	NA	540.902	0.005	5.246	3.261
Cyclohexanol, 5-methyl-2-(1-methylthyl)-, (1a,2a,5a)-(n)-	89-78-1	C00400	520.734	0.024	-1.467	1.381
t-Butyl ethyl ether2	1634-04-4	C11344	228.028	0.026	-0.539	0.597
yy054	NA	NA	526.908	0.027	-1.092	0.767
yy088	NA	NA	773.515	0.046	0.332	0.278
yy003	NA	NA	193.042	0.049	-0.574	1.109
Benzene, (1-methyl-1-butenyl)-	53172-84-2	NA	527.026	0.053	-0.974	0.737
yy032	NA	NA	455.642	0.063	0.383	0.372
2-Pentanone	107-87-9	C01949	295.78	0.074	-0.718	1.006
yy082	NA	NA	708.541	0.085	0.429	0.671
Benzene, (2-isothiocyanatoethyl)-	2257-09-2	NA	643.92	0.092	1.445	1.298
yy010	NA	NA	366.443	0.096	0.770	0.995

Table 1. Differentially expressed metabolites in urine specimens obtained from IC patients compared to health controls (FDR < 0.1). Menthol (KEGG compound ID: C00400) was expressed less in IC patients, compared to controls. The CAS registry numbers of the identified metabolites were mapped to their KEGG compound IDs. The FDR indicates the false discovery rate, which was computed using Storey's method. FC is log₂ fold change between IC and control. SD represents standard deviation. Positive and negative FC values indicate up- and downregulation of the metabolite in IC urine, compared to control (NA meaning not available).

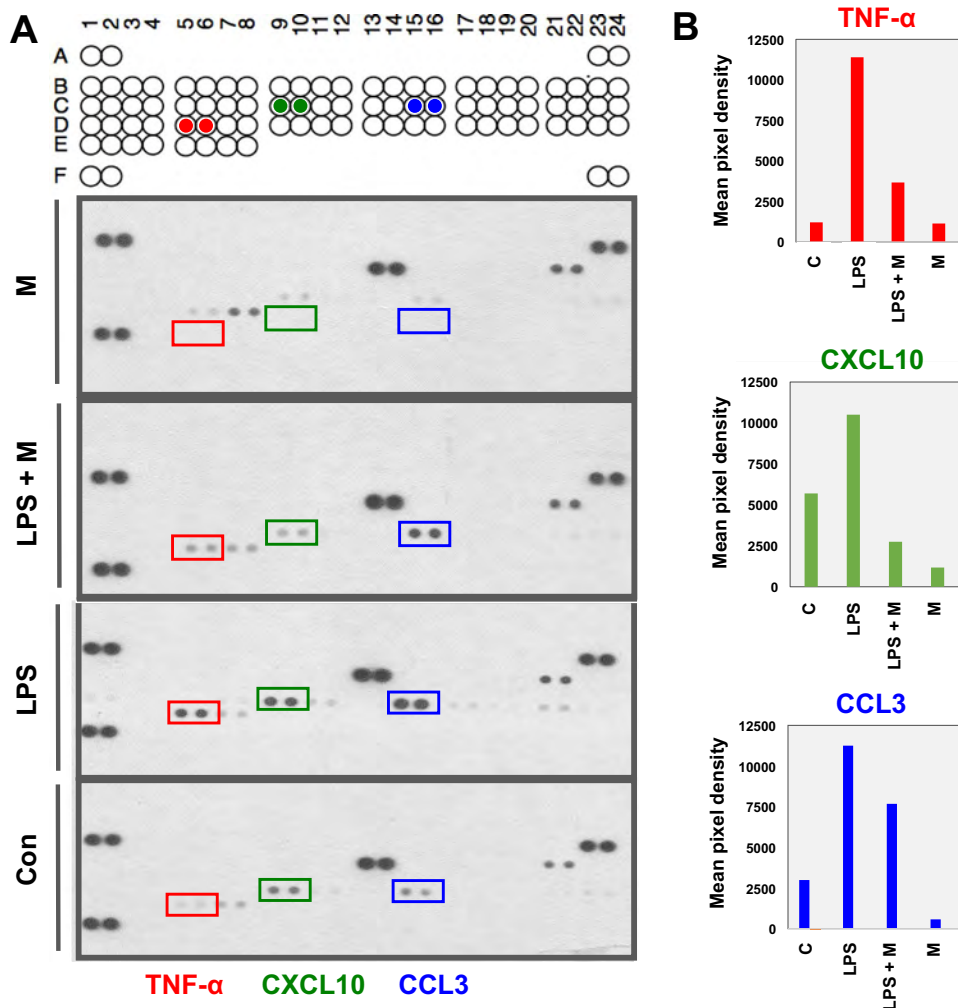


Figure 2. Reduced production of LPS-induced inflammatory cytokines by menthol in RAW 264.7 cells (cell lysates) (A) Inflammatory cytokine array analysis of CCL3, CXCL10 and TNF- α . The expression of these inflammatory cytokines is highly induced by LPS, but downregulated by menthol. (B) Quantification of array band intensity of CCL3, CXCL10 and TNF- α with ImageJ-analysis software.

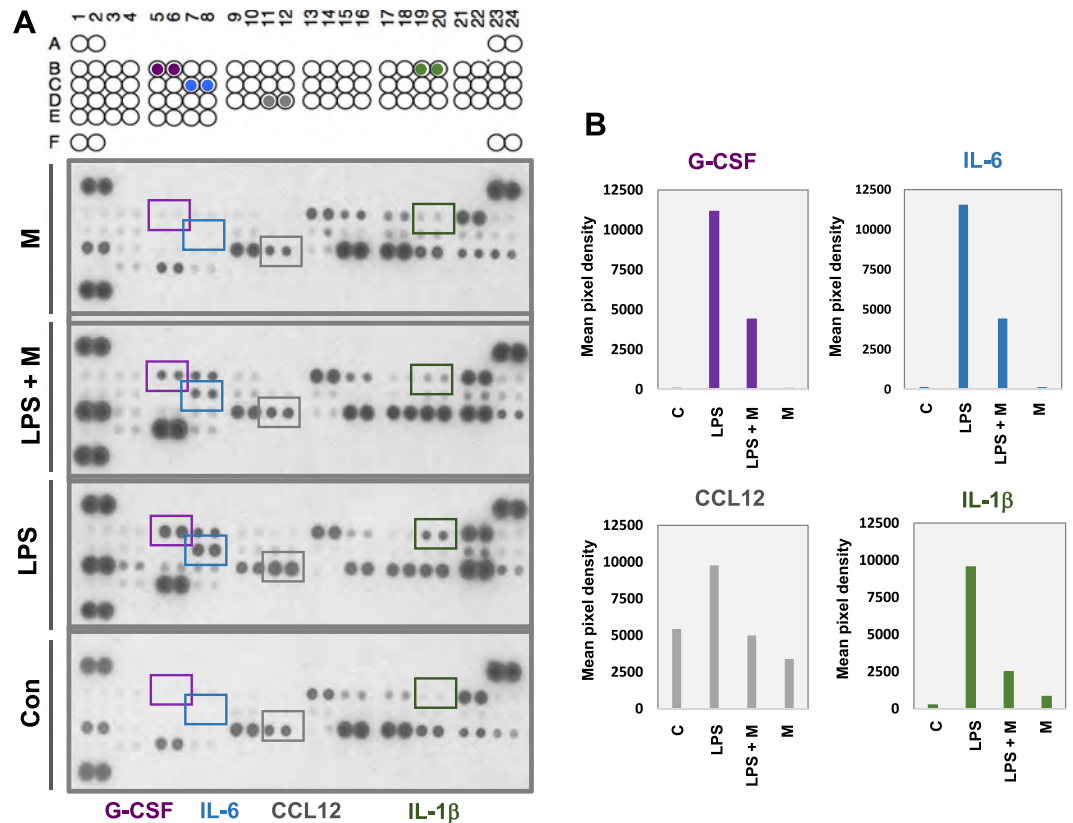


Figure 3. Decreased secretion of LPS-induced inflammatory cytokines by menthol in RAW 264.7 cells (conditioned media) (A) Inflammatory cytokine array analysis of IL-1 β , IL-6, CCL5, CCL12 and G-CSF. The expression of these inflammatory cytokines is highly induced by LPS, but downregulated by menthol. (B) Quantification of array band intensity of IL-1 β , IL-6, IL-1 and G-CSF with imageJ-analysis software.

to measure of the values of the scan dots, according to their intensity on the cytokine array panel (Fig. 2B). These results suggested that menthol is involved in downregulating the production of LPS-induced inflammatory cytokines.

We also carried out the inflammatory cytokine array to identify which cytokines were secreted into the RAW 264.7 cell culture media. We detected increased secretion of inflammatory cytokines, including interleukin 1 β (IL-1 β), interleukin 6 (IL-6), C-C motif chemokine ligand 5 (CCL5), C-C motif chemokine ligand 12 (CCL12), and granulocyte colony stimulating factor (G-CSF), in the LPS-treated condition (Fig. 3A). We also found that pretreatment with menthol significantly downregulated the secretion of these cytokines, compared to LPS alone (Fig. 3A, LPS+M compared to LPS). The dot intensities of each inflammatory cytokine were quantified using ImageJ software, as described in the Methods (Fig. 3B).

The cytokine profile array results were independently tested again with western blot analysis. The RAW 264.7 cells used for this analysis underwent the same LPS and menthol treatment as the ones used for the cytokine arrays. Western blot data revealed that cells pre-treated with menthol had significantly reduced expression of TNF- α , CCL3, IL-6, and IL-1 β (Fig. 4A). We next decided to use western blot analysis to examine if the effects of menthol were dose-dependent. RAW 264.7 cells were first pretreated with LPS (100 ng/ml) or control for 3 hrs. They were then incubated with varying concentrations of menthol (50, 100, 500 μ mol/ml) for 6 hrs. Our results validated that menthol did indeed affect macrophages in a dose-dependent manner (Fig. 4B).

Gene expression altered by menthol treatment. Further analysis using nucleotide microarrays validated our previous results showing that menthol mitigates LPS-induced inflammation in RAW 264.7 macrophage cells. Genes that were considered to be differentially expressed in C vs M, C vs LPS, and M vs LPS were selected, if they had a fold change >1.5 and p-value < 0.05. Figure 5A shows the number of upregulated and downregulated genes in each of the different groups. Figure 5B shows the list of DEGs for each group that were upregulated with menthol treatment; (C vs M) Trem1, MBP1, and TES; (C vs LPS) CD52, CD40, SEPT11, and MRP152; (M vs LPS) SEPT11, RIOK3, and MRP152. We also annotated downregulated DEGs for each group; (C vs M) WDR43, WWP1, and XYLT2; (C vs LPS) YPE13, ZDHHC14, and ZFP408; (M vs LPS) GCNT1, GORASP2, and MLER3.

To better understand the biological processes affected by menthol, we performed functional enrichment analyses based on GOBPs. DEGs were classified into different functional categories according to their GOBPs. Genes upregulated from LPS treatment were significantly associated with biological processes relating to inflammatory response (GO: 0006954) and response to lipopolysaccharides (GO: 0032496) (Fig. 5C). Genes downregulated by menthol treatment were those significantly involved in immune system processes (GO: 0002376) and the

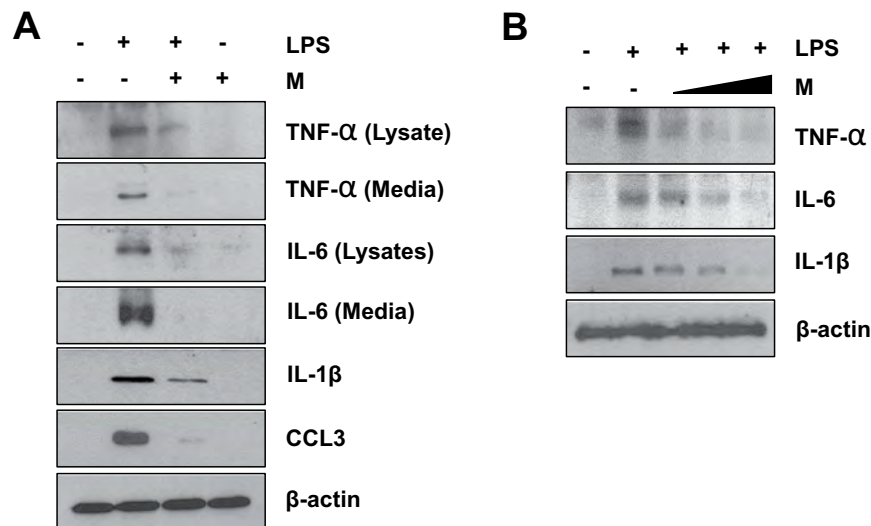


Figure 4. Menthol inhibits LPS-induced cytokine production in RAW 264.7 cells. (A) RAW 264.7 cells were pretreated with menthol, followed by stimulation with LPS for 6 hrs. Expression level of TNF- α , IL-6, IL-1 β and CCL3 were induced by LPS and reduced in LPS+M compared to LPS. (B) Pretreatment of LPS (100 ng/mL) or control for 3 hrs and followed by induction with different concentration of menthol (50, 100 and 500 μ mol/mL) for 6 hrs. Expression level of TNF- α , IL-6 and IL-1 β were reduced by menthol treatment in a dose-dependent manner. β -actin was used as a loading control for western blot analysis.

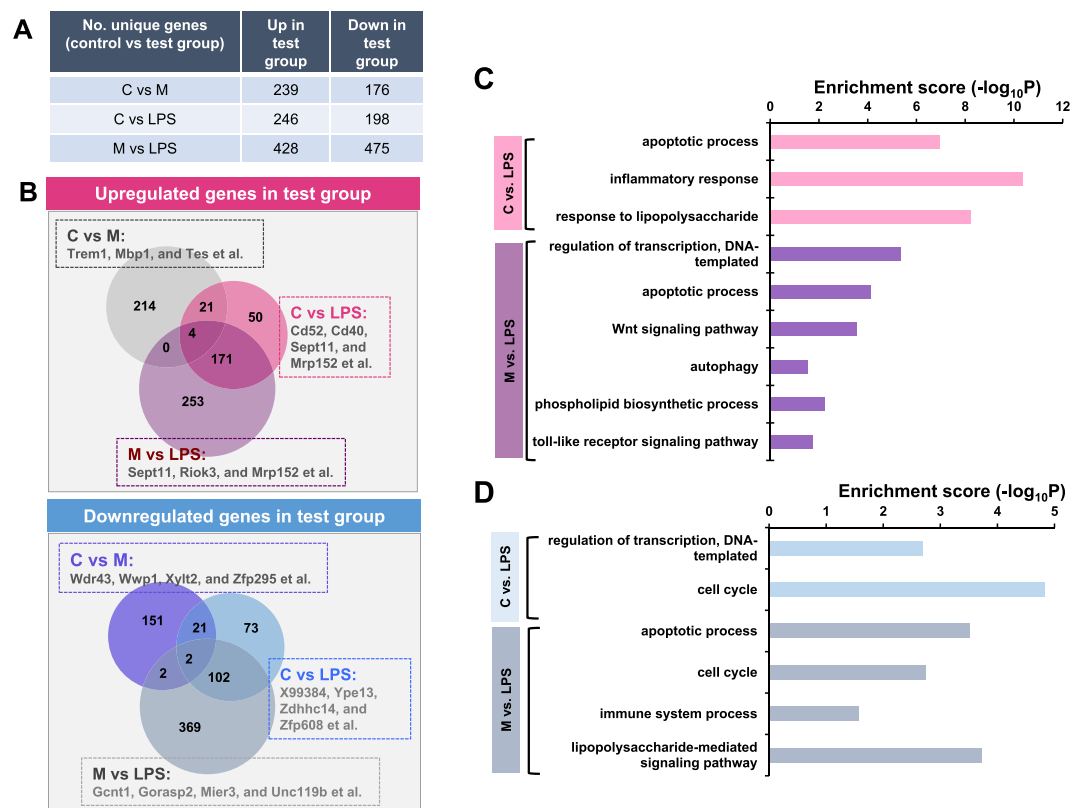


Figure 5. Differentially expressed genes in LPS, LPS+Menthol (LPS+M), and menthol (M) only conditions. (A) The number of DEGs perturbed by LPS or menthol treatment. (B) Venn diagram depicts shared and different DEGs. (C,D) Gene Ontology analysis suggested functional annotations (biological process) that were associated with up- (C) and downregulated (D) genes. Bar graph shows significantly enriched biological processes, which were up- and downregulated genes in test group. The inflammation events induced by LPS were inhibited by menthol in LPS mediated signaling pathway.

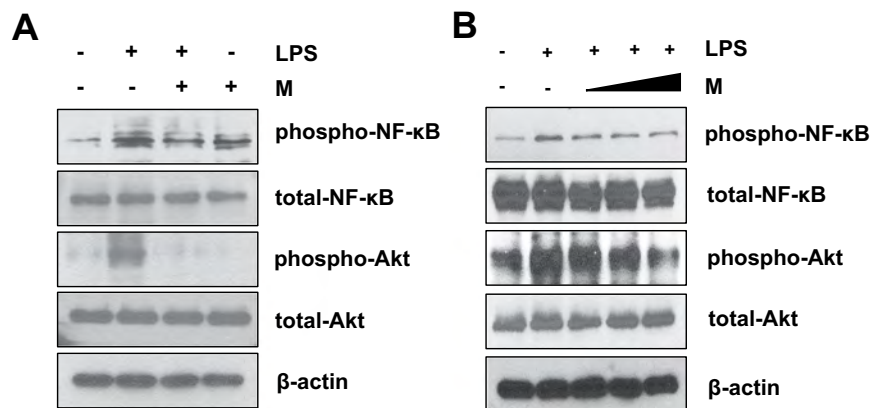


Figure 6. Menthol inhibits LPS-induced activation of NF- κ B and Akt signaling pathways. **(A)** Phosphorylation levels of NF- κ B and Akt were reduced by menthol treatment. **(B)** Phosphorylation of NF- κ B and Akt were suppressed by menthol treatment in dose-dependent manner. β -actin was used as the loading control in western blot analysis.

lipopolysaccharide-mediated signaling pathways of different groups (GO: 0031663) (Fig. 5D). These results indicate the LPS-driven inflammatory responses can be modulated by menthol treatment, suggesting that low levels of menthol may be associated with higher levels of inflammation from immune stimulants, such as LPS.

Signaling pathways involved in the anti-inflammatory effects of menthol. We next wondered if the specific signaling pathways involved in LPS-stimulated cytokine perturbation can be modulated by menthol treatment. To determine the signaling pathways associated with the production and secretion of inflammatory cytokines, we screened the activation of key signaling pathways, including those of nuclear-factor- κ B (NF- κ B), Akt, and Erk1/2 MAPK. We found that the added presence of LPS induced phosphorylation of NF- κ B and Akt in RAW 264.7 macrophage cells. Pretreatment with menthol significantly attenuated the phosphorylation levels of NF- κ B and Akt, but not those of Erk1/2 MAPK (Fig. 6A, LPS+M compared to LPS). In addition, menthol treatment significantly reduced LPS-induced phosphorylation of NF- κ B and Akt in a dose-dependent manner (Fig. 6B). This data suggest that menthol potentially inhibits LPS-induced inflammatory cytokines via the NF- κ B and Akt signaling pathways.

Nucleotide microarray analysis consistently showed that menthol affects production of LPS-induced cytokines in RAW 264.7 macrophage cells. We next sought to identify DEGs in cells exposed to LPS with or without menthol via microarray analysis (Fig. 7A). Approximately 30% of the DEGs showed increased expression patterns when stimulated by LPS alone and decreased when treated additionally with menthol. Those DEGs included: C3, CCL2, CCL3, CCL4, CCL5, CCL9, CCL12, CXCL2, CXCL10, NFKB1A, toll-like microbial pattern recognition receptor 1 (TLR1), TNF- α induced protein 3 (TNFAIP3) *et al.* (Fig. 7A, box). Mapping of genes and protein expression from our study suggested that menthol suppresses the TLR pathway. The gene expression of interferon-induced protein with tetratricopeptide repeats 1 (IFIT1), TNFAIP3, TLR1, and viperin increased in response to LPS and decreased in response to menthol. To further validate the perturbed DEGs, western blot analysis was carried out. Protein levels of IFIT1, TNFAIP3, TLR1, and viperin changed consistent to gene expression changes (Fig. 7B).

Collectively, these experimental results propose a potential pathway through which TNF- α production and secretion is stimulated. This consequently leads to the activation of TLR1, TNFAIP3-NF- κ B signaling, and inflammation of the bladder. These results also lead us to suggest that menthol could suppress IC-associated inflammation by blocking the activation of our hypothetical pathway (Fig. 7C).

Discussion

Our GC-MS peak resolution and compound identification revealed unique urinary VOC profiles between IC patients and healthy controls. Based on these results, we further sought to understand the biological function of menthol, an identified IC-associated urinary metabolite. We identified this novel compound through recently improved data processing that could annotate unknown VOCs. These developments include database analysis tools, such as BinBase Database²¹, AMDIS²², SpectConnect (<http://spectconnect.mit.edu>), MZmine²³, TagFinder²⁴, MetAlign 3.0, and MetAlignID^{25,26}. For this study, we used BinBase; this tool can be assessed by the public at <http://vocBinBase.fiehnlab.ucdavis.edu>.

Cytokines and chemokines associated with IC. Although IC affects millions of people every year, the etiology of this disease remains elusive. The bladders of IC patients exhibit various pathophysiological alterations in the urothelium barrier lining, sensory nervous system, recruitment of immune cells, and activation of major signaling pathways. The inflammation that is associated with IC is potentially a result of inflammatory or bacterial agents. One such agent is LPS, a component of the bacterial outer membrane, which is known to bind to TLR4 and stimulate inflammation through upregulating the release of cytokines. Consequently, this increased

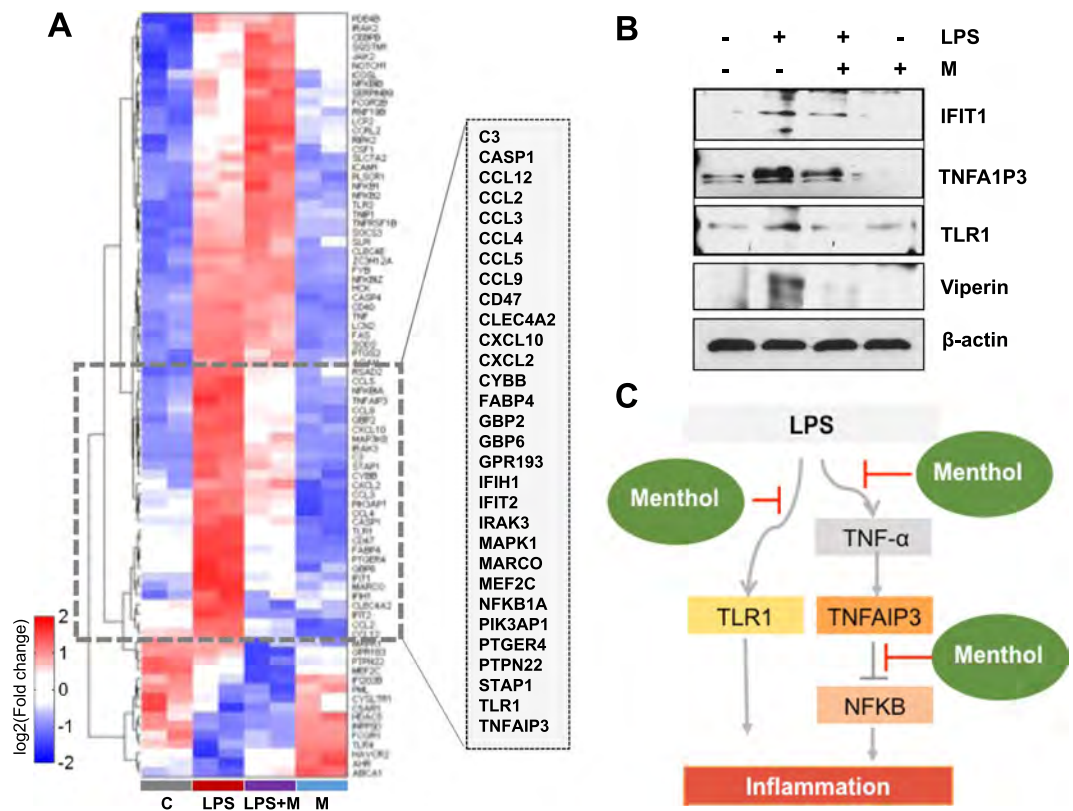


Figure 7. Menthol regulates the LPS-induced inflammatory response. **(A)** Heatmap image of DNA microarray data. RAW 264.7 cells were treated with LPS (100 ng/mL) with or without menthol (500 μ mol/mL) for 6 hrs. The list of the genes in the enlarged box was sorted in order of gene symbol. **(B)** Cells were treated with LPS (100 ng/mL) with or without menthol (500 μ mol/mL) for 6 hrs. Few candidates from (Figure A, Box): IFIT1, TNFAIP3, TLR1, and viperin were repressed by menthol treatment. **(C)** Hypothetical diagram showing how menthol may be attenuating the activation of the TLR1 and TNFAIP3-NF- κ B signaling pathways; thereby, reducing downstream cytokine expression.

production and secretion of cytokines leads to bladder inflammation, which induces an immune response and may be associated with additional urinary symptoms, such as hyper-excitability and pain^{27,28}.

There have been a series of previous reports suggesting the use of inflammatory cytokines as IC biomarkers. They demonstrate that levels of cytokines, such as TNF- α , IL-2, IL-6, IL-8, and IL-1 β , increase in the bladder and urine of IC patients. In our present study, we were able to observe elevated gene and protein expression levels of TNF- α , IL-6, IL-1 β , and NF- κ B in LPS-stimulated RAW 264.7 macrophage cells. TNF- α is a well-known pro-inflammatory cytokine that leads to the activation of inflammation, induces the expression of adhesion molecules, and contributes to the development of pain sensation. Prior studies have shown that pharmaceutical inhibition of TNF- α signaling or addition of neutralizing antibodies against TNF- α reduced the development of nociception in animal models. Collectively, the experimental data from our current study and preceding reports suggest that the hypersensitivity and/or inflammation seen in IC bladders may be treated by targeting inflammatory cytokines²⁸.

Menthol and IC-associated inflammation. Our VOC metabolomics analysis revealed that menthol expression is significantly less abundant in the urine of IC patients. Menthol, an aromatic and cyclic terpene alcohol, is a compound that is commonly used in a wide variety of products. Its main use is in relieving local inflammation, pain (e.g. joint aches), noxious heat, sensory hypersensitivity, sore throat *et al.* The analgesic and anti-inflammatory effects of menthol may be attributed to the fact that it is a TRPM8 agonist^{29,30}. However, the underlying mechanisms of menthol's biological effects remain obscure. Because of its mitigating effects, menthol was a particularly interesting compound in the context of IC. Chronic inflammation is typical in the pathogenesis of IC³¹, and higher levels of pro-inflammatory cytokines, such as macrophage-derived chemokines³² or urinary nerve growth factors, are reported to be associated with the disease^{33,34}.

Given its anti-inflammatory effects, ability to suppress respiratory irritation, and association with pain relief, menthol is widely used for medicinal purposes^{35,36}. Our study investigated the effectiveness of menthol on LPS-induced cytokine production and secretion. Interestingly, we found that levels of various inflammatory cytokines were suppressed by menthol. This was done through DNA microarrays and cytokine profiling; the results were verified through additional independent western blot analysis. We observed that menthol significantly reduced levels of TNF- α , IL-1 β , IL-6, and CCL3 in LPS-stimulated RAW 264.7 macrophage cells. Previous

literature has suggested that histamine release from mast cells is inhibited by menthol^{37,38}. Furthermore, by regulating the NF- κ B signaling pathway, menthol decreases carrageenan-induced inflammation processes³⁹. Our results were also in accordance with these past findings and were similar to outcomes observed in menthol treatment of ulcerative colitis⁴⁰ and ethanol-induced gastric ulcers⁴¹.

TNF- α is a pro-inflammatory cytokine involved in regulating a wide spectrum of biological processes, including cell differentiation, apoptosis, coagulation, and lipid metabolism. It is associated with a number of diseases, including autoimmune diseases, insulin resistance, and, most notably, cancer. NF- κ B is protein complex responsible for DNA transcription, cytokine production, and basic survival in almost all animal cells⁴². Toll-like microbial pattern recognition receptors (TLRs) represent a non-self-recognition system that is hardwired to trigger inflammation⁴³. In our present study, LPS-induced TLR1 was downregulated by menthol treatment. TNFAIP3, a protein whose expression is rapidly induced by TNF- α , is a ubiquitin-centered enzyme and has been shown to constrain NF- κ B activation. The encoded protein is involved in most cytokine-mediated inflammatory responses; this is likely due to the presence of both ubiquitin ligase and deubiquitinase within the enzyme. Because of this, TNFAIP3 serves as a negative feedback regulator of NF- κ B activation when TNF is present⁴⁴. Our results provide new insights in LPS-induced inflammation, suggesting that it can be regulated by menthol via its suppression of TNF- α , TLR1, and/or TNFAIP3 and subsequent regulation of NF- κ B activation. Altogether, this study indicates the potential placating role of menthol in IC patients.

Although further studies are warranted to ascertain the mechanistic basis of menthol's observed anti-inflammatory effects, it would be interesting to investigate whether menthol can suppress any inflammation or sensory hypersensitivity in IC patients in the pre-clinical or clinical setting. Our discoveries provide potential therapeutic strategies; potent agonists of TNF- α , TLR1, TNFAIP3, and/or the NF- κ B network may benefit IC patients through anti-hyperalgesic and anti-inflammatory effects.

Accession numbers. The metabolomics data have been deposited in the Metabolomics Workbench Public Repository with the study ID number ST000603. The microarray data was deposited and is available at the Gene Expression Omnibus (<http://www.ncbi.nlm.nih.gov/geo/>), under the accession number GSE98933.

References

- Dasgupta, J. & Tincello, D. G. Interstitial cystitis/bladder pain syndrome: an update. *Maturitas* **64**, 212–217, <https://doi.org/10.1016/j.maturitas.2009.09.016> (2009).
- Clemens, J. Q. *et al.* Prevalence of painful bladder symptoms and effect on quality of life in black, Hispanic and white men and women. *The Journal of urology* **177**, 1390–1394, <https://doi.org/10.1016/j.juro.2006.11.084> (2007).
- Berry, S. H. *et al.* Prevalence of symptoms of bladder pain syndrome/interstitial cystitis among adult females in the United States. *The Journal of urology* **186**, 540–544, <https://doi.org/10.1016/j.juro.2011.03.132> (2011).
- Hanno, P. M., Erickson, D., Moldwin, R., Faraday, M. M. & American Urological, A. Diagnosis and treatment of interstitial cystitis/bladder pain syndrome: AUA guideline amendment. *The Journal of urology* **193**, 1545–1553, <https://doi.org/10.1016/j.juro.2015.01.086> (2015).
- Duan, H. *et al.* Identification of biomarkers for melamine-induced nephrolithiasis in young children based on ultra high performance liquid chromatography coupled to time-of-flight mass spectrometry (U-HPLC-Q-TOF/MS). *Journal of chromatography. B, Analytical technologies in the biomedical and life sciences* **879**, 3544–3550, <https://doi.org/10.1016/j.jchromb.2011.09.039> (2011).
- Thadikkaran, L. *et al.* Recent advances in blood-related proteomics. *Proteomics* **5**, 3019–3034, <https://doi.org/10.1002/pmic.200402053> (2005).
- Kahn, N., Lavie, O., Paz, M., Segev, Y. & Haick, H. Dynamic Nanoparticle-Based Flexible Sensors: Diagnosis of Ovarian Carcinoma from Exhaled Breath. *Nano letters* **15**, 7023–7028, <https://doi.org/10.1021/acs.nanolett.5b03052> (2015).
- Phillips, M. *et al.* Prediction of breast cancer using volatile biomarkers in the breath. *Breast cancer research and treatment* **99**, 19–21, <https://doi.org/10.1007/s10549-006-9176-1> (2006).
- Sun, X., Shao, K. & Wang, T. Detection of volatile organic compounds (VOCs) from exhaled breath as noninvasive methods for cancer diagnosis. *Analytical and bioanalytical chemistry* **408**, 2759–2780, <https://doi.org/10.1007/s00216-015-9200-6> (2016).
- Matsumura, K. *et al.* Urinary volatile compounds as biomarkers for lung cancer: a proof of principle study using odor signatures in mouse models of lung cancer. *PLoS one* **5**, e8819, <https://doi.org/10.1371/journal.pone.0008819> (2010).
- Peled, N. *et al.* Volatile fingerprints of cancer specific genetic mutations. *Nanomedicine: nanotechnology, biology, and medicine* **9**, 758–766, <https://doi.org/10.1016/j.nano.2013.01.008> (2013).
- Nilsson, M., Lalos, O., Lindkvist, H. & Lalos, A. How do urinary incontinence and urgency affect women's sexual life? *Acta obstetrica et gynecologica Scandinavica* **90**, 621–628, <https://doi.org/10.1111/j.1600-0412.2011.01120.x> (2011).
- Wen, H. *et al.* Urinary metabolite profiling combined with computational analysis predicts interstitial cystitis-associated candidate biomarkers. *Journal of proteome research* **14**, 541–548, <https://doi.org/10.1021/pr5007729> (2015).
- Kind, T. *et al.* Interstitial Cystitis-Associated Urinary Metabolites Identified by Mass-Spectrometry Based Metabolomics Analysis. *Scientific reports* **6**, 39227, <https://doi.org/10.1038/srep39227> (2016).
- Sherman, E. *et al.* Reference samples guide variable selection for correlation of wine sensory and volatile profiling data. *Food Chemistry*, <https://doi.org/10.1016/j.foodchem.2017.10.073> (2017).
- Hwang, D. *et al.* A data integration methodology for systems biology. *Proceedings of the National Academy of Sciences of the United States of America* **102**, 17296–17301, <https://doi.org/10.1073/pnas.0508647102> (2005).
- Storey, J. D. & Tibshirani, R. Statistical significance for genomewide studies. *Proceedings of the National Academy of Sciences of the United States of America* **100**, 9440–9445, <https://doi.org/10.1073/pnas.1530509100> (2003).
- Huang da, W., Sherman, B. T. & Lempicki, R. A. Systematic and integrative analysis of large gene lists using DAVID bioinformatics resources. *Nature protocols* **4**, 44–57, <https://doi.org/10.1038/nprot.2008.211> (2009).
- Robinson, A. L., Boss, P. K., Heymann, H., Solomon, P. S. & Trengove, R. D. Development of a sensitive non-targeted method for characterizing the wine volatile profile using headspace solid-phase microextraction comprehensive two-dimensional gas chromatography time-of-flight mass spectrometry. *Journal of chromatography. A* **1218**, 504–517, <https://doi.org/10.1016/j.chroma.2010.11.008> (2011).
- Bolstad, B. M., Irizarry, R. A., Astrand, M. & Speed, T. P. A comparison of normalization methods for high density oligonucleotide array data based on variance and bias. *Bioinformatics* **19**, 185–193 (2003).
- Skogerson, K., Wohlgenuth, G., Barupal, D. K. & Fiehn, O. The volatile compound BinBase mass spectral database. *BMC bioinformatics* **12**, 321, <https://doi.org/10.1186/1471-2105-12-321> (2011).

22. Mastrangelo, A., Ferrarini, A., Rey-Stolle, F., Garcia, A. & Barbas, C. From sample treatment to biomarker discovery: A tutorial for untargeted metabolomics based on GC-(EI)-Q-MS. *Analytica chimica acta* **900**, 21–35, <https://doi.org/10.1016/j.aca.2015.10.001> (2015).
23. Katajamaa, M., Miettinen, J. & Oresic, M. MZmine: toolbox for processing and visualization of mass spectrometry based molecular profile data. *Bioinformatics* **22**, 634–636, <https://doi.org/10.1093/bioinformatics/btk039> (2006).
24. Luedemann, A., Strassburg, K., Erban, A. & Kopka, J. TagFinder for the quantitative analysis of gas chromatography-mass spectrometry (GC-MS)-based metabolite profiling experiments. *Bioinformatics* **24**, 732–737, <https://doi.org/10.1093/bioinformatics/btn023> (2008).
25. Lommen, A. & Kools, H. J. MetAlign 3.0: performance enhancement by efficient use of advances in computer hardware. *Metabolomics: Official journal of the Metabolomic Society* **8**, 719–726, <https://doi.org/10.1007/s11306-011-0369-1> (2012).
26. Lommen, A. *et al.* metAlignID: a high-throughput software tool set for automated detection of trace level contaminants in comprehensive LECO two-dimensional gas chromatography time-of-flight mass spectrometry data. *Journal of chromatography. A* **1263**, 169–178, <https://doi.org/10.1016/j.chroma.2012.09.056> (2012).
27. Rosen, J. M. & Klumpp, D. J. Mechanisms of pain from urinary tract infection. *International journal of urology: official journal of the Japanese Urological Association* **21**(Suppl 1), 26–32, <https://doi.org/10.1111/iju.12309> (2014).
28. Yoshimura, N. *et al.* Bladder afferent hyperexcitability in bladder pain syndrome/interstitial cystitis. *International journal of urology: official journal of the Japanese Urological Association* **21**(Suppl 1), 18–25, <https://doi.org/10.1111/iju.12308> (2014).
29. Patel, R. *et al.* Anti-hyperalgesic effects of a novel TRPM8 agonist in neuropathic rats: a comparison with topical menthol. *Pain* **155**, 2097–2107, <https://doi.org/10.1016/j.pain.2014.07.022> (2014).
30. McEntire, D. M. *et al.* Pain transduction: a pharmacologic perspective. *Expert review of clinical pharmacology* **9**, 1069–1080, <https://doi.org/10.1080/17512433.2016.1183481> (2016).
31. Yang, W. *et al.* Integration analysis of quantitative proteomics and transcriptomics data identifies potential targets of frizzled-8 protein-related antiproliferative factor *in vivo*. *BJU international* **110**, E1138–1146, <https://doi.org/10.1111/j.1464-410X.2012.11299.x> (2012).
32. Abernethy, M. G. *et al.* Urinary Microbiome and Cytokine Levels in Women With Interstitial Cystitis. *Obstetrics and gynecology* **129**, 500–506, <https://doi.org/10.1097/AOG.0000000000001892> (2017).
33. Qu, H. C., Zhang, W., Yan, S., Liu, Y. L. & Wang, P. Urinary nerve growth factor could be a biomarker for interstitial cystitis/painful bladder syndrome: a meta-analysis. *PloS one* **9**, e106321, <https://doi.org/10.1371/journal.pone.0106321> (2014).
34. Sheng, W., Zhang, H. & Ruth, K. H. Could urinary nerve growth factor be a biomarker for overactive bladder inverted question mark A meta-analysis. *Neurourology and urodynamics*. <https://doi.org/10.1002/nau.23210> (2017).
35. MacDougall, J. M., Fandrick, K., Zhang, X., Serafin, S. V. & Cashman, J. R. Inhibition of human liver microsomal (S)-nicotine oxidation by (–)-menthol and analogues. *Chemical research in toxicology* **16**, 988–993, <https://doi.org/10.1021/tx0340551> (2003).
36. Cortright, D. N., Krause, J. E. & Broom, D. C. TRP channels and pain. *Biochimica et biophysica acta* **1772**, 978–988, <https://doi.org/10.1016/j.bbadis.2007.03.003> (2007).
37. Cho, Y. *et al.* TRPM8 mediates cold and menthol allergies associated with mast cell activation. *Cell calcium* **48**, 202–208, <https://doi.org/10.1016/j.ceca.2010.09.001> (2010).
38. Bromm, B., Scharein, E., Darsow, U. & Ring, J. Effects of menthol and cold on histamine-induced itch and skin reactions in man. *Neuroscience letters* **187**, 157–160 (1995).
39. Liu, Z. *et al.* Chemopreventive efficacy of menthol on carcinogen-induced cutaneous carcinoma through inhibition of inflammation and oxidative stress in mice. *Food and chemical toxicology: an international journal published for the British Industrial Biological Research Association* **82**, 12–18, <https://doi.org/10.1016/j.fct.2015.04.025> (2015).
40. Ghasemi-Pirbaluti, M., Motaghi, E. & Bozorgi, H. The effect of menthol on acute experimental colitis in rats. *European journal of pharmacology*. <https://doi.org/10.1016/j.ejphar.2017.03.003> (2017).
41. Rozza, A. L., Meira de Faria, F., Souza Brito, A. R. & Pellizzon, C. H. The gastroprotective effect of menthol: involvement of anti-apoptotic, antioxidant and anti-inflammatory activities. *PloS one* **9**, e86686, <https://doi.org/10.1371/journal.pone.0086686> (2014).
42. Lawrence, T. The nuclear factor NF-kappaB pathway in inflammation. *Cold Spring Harbor perspectives in biology* **1**, a001651, <https://doi.org/10.1101/cshperspect.a001651> (2009).
43. Leifer, C. A. & Medvedev, A. E. Molecular mechanisms of regulation of Toll-like receptor signaling. *Journal of leukocyte biology* **100**, 927–941, <https://doi.org/10.1189/jlb.2MR0316-117RR> (2016).
44. Song, H. Y., Rothe, M. & Goeddel, D. V. The tumor necrosis factor-inducible zinc finger protein A20 interacts with TRAF1/TRAF2 and inhibits NF-kappaB activation. *Proceedings of the National Academy of Sciences of the United States of America* **93**, 6721–6725 (1996).

Acknowledgements

We thank our long-term collaborator, Dr. Oliver Fiehn, for providing guidance on this project, and the members of his lab for discussions. This work was supported by the National Institutes of Health grants (DK097154 (to O.F.), 1U01DK103260, 1R01DK100974, NIH NCATS UCLA CTSI UL1TR000124), Department of Defense grants (W81XWH-15-1-0415), Centers for Disease Controls and Prevention (1U01DP006079), Interstitial Cystitis Association (ICA) Research Grant, the Steven Spielberg Discovery Fund in Prostate Cancer Research Career Development Award, the U.S.-Egypt Science and Technology Joint Fund (to J.K.). J.K. is former recipient of Interstitial Cystitis Association Pilot Grant, a Fishbein Family IC Research Grant, New York Academy of Medicine, and Boston Children's Hospital Faculty Development. The funders had no role in the design, data collection and analysis, decision to publish or preparation of the manuscript. In addition, this article is derived from the Subject Data funded in whole or part by National Academies of Sciences, Engineering, and Medicine (NAS) and The United States Agency for International Development (USAID). Any opinions, findings, conclusions, or recommendations expressed in this article are those of the authors alone, and do not necessarily reflect the views of USAID or NAS.

Author Contributions

J.K. designed the study, led the obtainment of funding, and overviewed the analysis of literature and drafting of the manuscript. L.V. performed metabolomics analysis and data interpretation. M.L. and S.Y. performed computational analyses of metabolomics data. M.S., A.Y., E.C. and V.S. performed biochemical and functional experiments in the cell culture system. M.S., M.L., A.Y. and S.Y. carried out the analysis of references and drafted the manuscript. All authors read and approved the final manuscript.

Additional Information

Supplementary information accompanies this paper at <https://doi.org/10.1038/s41598-018-29085-3>.

Competing Interests: The authors declare no competing interests.


Publisher's note: Springer Nature remains neutral with regard to jurisdictional claims in published maps and institutional affiliations.



Open Access This article is licensed under a Creative Commons Attribution 4.0 International License, which permits use, sharing, adaptation, distribution and reproduction in any medium or format, as long as you give appropriate credit to the original author(s) and the source, provide a link to the Creative Commons license, and indicate if changes were made. The images or other third party material in this article are included in the article's Creative Commons license, unless indicated otherwise in a credit line to the material. If material is not included in the article's Creative Commons license and your intended use is not permitted by statutory regulation or exceeds the permitted use, you will need to obtain permission directly from the copyright holder. To view a copy of this license, visit <http://creativecommons.org/licenses/by/4.0/>.

© The Author(s) 2018

SCIENTIFIC REPORTS



OPEN

Sex-associated differences in baseline urinary metabolites of healthy adults

Sili Fan¹, Austin Yeon², Muhammad Shahid², Jennifer T. Anger³, Karyn S. Eilber³, Oliver Fiehn^{1,4} & Jayoung Kim^{5,6,7,8}

The biological basis for gender variability among disease states is not well established. There have been many prior efforts attempting to identify the unique urine metabolomic profiles associated with specific diseases. However, there has been little advancement in investigating the metabolomic differences associated with gender, which underlies the misconception that risk factors and treatment regimens should be the same for both male and female patients. This present study aimed to identify biologically-meaningful baseline sex-related differences using urine samples provided by healthy female and male participants. To elucidate whether urinary metabolic signatures are globally distinct between healthy males and females, we applied metabolomics profiling of primary metabolism with comprehensive bioinformatics analyses on urine samples from 60 healthy males and females. We found that levels of α -ketoglutarate and 4-hydroxybutyric acid increased 2.3-fold and 4.41-fold in males compared to females, respectively. Furthermore, chemical similarity enrichment analysis revealed that differentially expressed metabolites, such as saturated fatty acids, TCA, and butyrates, were significantly related to the gender effect. These findings indicate that there are baseline sex-related differences in urinary metabolism, which should be considered in biomarker discovery, diagnosis, and treatment of bladder diseases, such as interstitial cystitis.

Interstitial cystitis (IC), also known as painful bladder syndrome (PBS), is a chronic pain disorder with no known etiology¹. Due to the limited amount of objective diagnostic tools for IC^{2,3}, there is great need to identify sensitive and non-invasive biomarkers that can vastly improve the accuracy of IC diagnoses⁴. Unfortunately, current understanding of the basic mechanisms behind pelvic pain are also fragmented^{5,6}. One area of interest that may provide a wealth of information is the impact of gender on IC. Epidemiological studies have consistently demonstrated a sex-based dimorphism in IC prevalence rates⁷⁻¹¹. It is generally accepted that the female to male ratio is approximately 8:2 or 9:1⁷⁻¹². However, the reasons for this difference are currently not well understood.

One suggestion for the stark discrepancy between male and female IC prevalence rates is sexual dimorphism. Moreover, there are sex-determined differences when diseases start and develop. Although these disparities are well-noted, the biological, cellular, and molecular basis of these gender biases remain elusive. One theory is that sex hormones are possibly associated with noted variations in metabolism. This is evident in other diseases. For example, it has been reported that female cases of autoimmune disease are three to four times higher than that of males¹³⁻¹⁵. Another study suggested that multiple sclerosis (MS) patients showed distinct gene signatures between females and males¹⁶.

In addition to the aforementioned diseases, heart failure and cardiovascular disease (CVD) have been reported to be associated with sex differences¹⁷⁻²¹. In females, hypertension is more common and is often the cause of heart failure. However, females also have a better prognosis than males with heart failure. For CVD, blood pressure and glucose metabolism play more important roles in females, whereas male CVD is affected mostly by cholesterol. The average starting age of CVD incidence in males is around the mid-30s and gradually increases; while

¹West Coast Metabolomics Center, University of California, Davis, Davis, CA, USA. ²Departments of Surgery, Cedars-Sinai Medical Center, Los Angeles, CA, USA. ³Division of Urology, Department of Surgery, Cedars-Sinai Medical Center, Los Angeles, CA, USA. ⁴King Abdulaziz University, Jeddah, Saudi Arabia. ⁵Departments of Surgery and Biomedical Sciences, Cedars-Sinai Medical Center, Los Angeles, CA, USA. ⁶Samuel Oschin Comprehensive Cancer Institute, Cedars-Sinai Medical Center, Los Angeles, CA, USA. ⁷University of California Los Angeles, Los Angeles, CA, USA. ⁸Department of Urology, Ga Cheon University College of Medicine, Incheon, Republic of Korea. Correspondence and requests for materials should be addressed to J.K. (email: Jayoung.Kim@cshs.org)

in females, CVD usually occurs much later, around 50 years of age. Furthermore, the plasma lipid profiles of younger-aged females are generally better than similarly aged males, which may explain why females have lower risk for CVD. In an effort to examine these sex-biases, mammalian animal models have been used to explore how males and females develop diseases differently and identify potential therapeutic targets. A study in female and male Sprague–Dawley rat models showed that hearts from female rats have better cardioprotection than male rats. Phosphorylation of mitochondrial proteins in female rats were altered, leading to less reactive oxygen species (ROS) generation and oxidative metabolism²².

Despite the numerous metabolic studies on various types of diseases in animal models^{23,24}, gender bias in metabolic signatures has not been mechanistically investigated in the healthy human setting. One study used a metabolomics approach to identify specific urinary markers for major depressive disorder (MDD). The authors reported that male and female MDD patients showed very distinct metabolomic signatures²⁵. More recently, in the cross-sectional KarMeN (Karlsruhe Metabolomics and Nutrition) study, the metabolite profile of healthy human urine was reported to be capable of predicting age and sex²⁶. While research into sex differences in other diseases has progressed, the same cannot be said for lower urinary tract symptoms, such as IC or overactive bladder (OAB). The biological mechanisms underlying sex variation in various bladder dysfunctions are still not fully understood. Further investigation into the relationships among sex-specific risk factors, metabolic rewiring, IC prevalence, and symptom severity are essential for explaining these sex-related differences.

In this study, our first aim was to determine the base levels of urinary metabolites in healthy controls. We additionally attempted to test whether urinary metabolomic profiles were globally different between females and males. To achieve these goals, we performed untargeted global gas chromatography-time-of-flight-mass spectrometry (GC-TOF-MS) profiling of primary metabolism and comprehensive bioinformatics analysis. Our metabolomic profiles showed distinct patterns of differentially expressed metabolites (DEMs) and suggested an interesting list of DEMs specific to healthy females and males. Given that sex influences some of the biomarkers reported, our findings provide evidence showing that baseline gender-related differences should be considered when developing urine-based strategies for metabolomic biomarkers.

Materials and Methods

Ethics statement. The Ethics Committee and the Institutional Review Board of Cedars-Sinai Medical Center (CSMC) approved recruitment, sample collection, curation, and analysis of metabolomics profiling data for this study (IRB# Pro00040261). All subjects who participated in this study provided written informed consent, and all experiments were performed in accordance with relevant guidelines and regulations.

Participants and urine collection. Healthy participants were recruited from an outpatient urology clinic at CSMC. Subjects with a history of any chronic diseases (such as any types of cancer, inflammatory conditions, diabetes, etc.) were excluded. We enrolled 60 females and 60 age-matched males in this study. All participants were >2 months “free of treatment or medication” (2015–2016).

To minimize possible contamination with vaginal or urethral cells, urine was collected using the clean catch method in a sterile environment. The de-identified samples were assigned with new identification numbers by laboratory staff in a double-blinded manner. To remove cell debris, samples were then centrifuged at 2500 rpm for 10 min.

GC-TOF-MS analysis of urine. *Sample pre-processing and preparation.* We investigated the metabolite profiles of the individual urine samples via gas-chromatography/mass-spectrometry (GC-MS) analysis^{27,28}. The Gerstel CIS4—with dual MPS Injector and Agilent 6890 GC-Pegasus III TOF MS was used for this analysis.

First, 10 μ l of urine was dissolved in a 1 ml –20 °C mixture of acetonitrile, isopropanol, and water (3:3:2 v/v) at a pH of 7.0. The urine volume was adjusted between 2–10 μ l to match externally measured creatinine levels based on a linear calibration curve. The solution was then vortexed at 4 °C for 5 min in 1.5 ml centrifuge tubes. Samples were additionally centrifuged for 2 min at 14,000 rcf and 500 μ l of the supernatants were aliquoted. Aliquots were evaporated in a Labconco Centrivap cold trap to complete dryness. The methoximation step was done using a 10 μ l solution of 40 mg/ml *o*-methylhydroxylamine hydrochloride (CAS:[593-56-6]; formula $\text{CH}_3\text{NO}\cdot\text{HCl}$) in pyridine (Cas:[11-0-86-1]; formula $\text{C}_5\text{H}_5\text{N}$) and shaken for 90 min at 30 °C. Then, 90 μ l of a *n*-methyl-*n*-trimethylsilyltrifluoroacetamide (MSTFA) and fatty acid methyl esters (FAME) retention time markers mixture (100:1 v/v) was added and the entire solution was shaken for 30 min at 37 °C. The mixture was transferred to amber crimp auto-sampler vials with flat bottom micro-inserts. Measurements were performed on a Leco Pegasus IV TOF coupled to an Agilent 6890GC with an Agilent 6890 split/splitless injector. The column used was a Restek RTX-5Sil MS (95% dimethyl/5% diphenyl polysiloxane) with a 30 m length, 0.25 mm i.d., and 0.25 μ m film thickness with a 10 m guard column. Each injection had a set volume of 0.5 μ l and was done at 50 °C. The GC parameters were set to a 1 ml/min constant flow helium and an oven ramp temperature of 50 °C (1 min hold) that steadily increased to 330 °C at a rate of 20 °C/min, with a 5 min hold before cooling-down. The transfer line temperature was set to 280 °C and the spectra were recorded in the electron ionization mode at 70 eV with a source temperature of 250 °C TOF and scan range of 85–500 u.

Injector conditions. The Agilent 6890 GC was equipped with a Gerstel Automatic Liner Exchange System (ALEX) that included a multipurpose sample (MPS2) dual rail and a Gerstel cold injection system (CIS) (Gerstel, Muehlheim, Germany). The temperature program was set as follows: 50 °C to a final temperature of 275 °C at a rate of 12 °C/sec with a hold for 3 min. Injections were done at a speed of 10 μ l/sec on a splitless injector with a purge time of 25 sec. The liner (Gerstel #011711-010-00) was changed after every 10 samples using the Maestro1 Gerstel software (version 1.1.4.18). Before and after each injection, the 10 μ l injection syringe was washed 3x with 10 μ l of ethyl acetate.

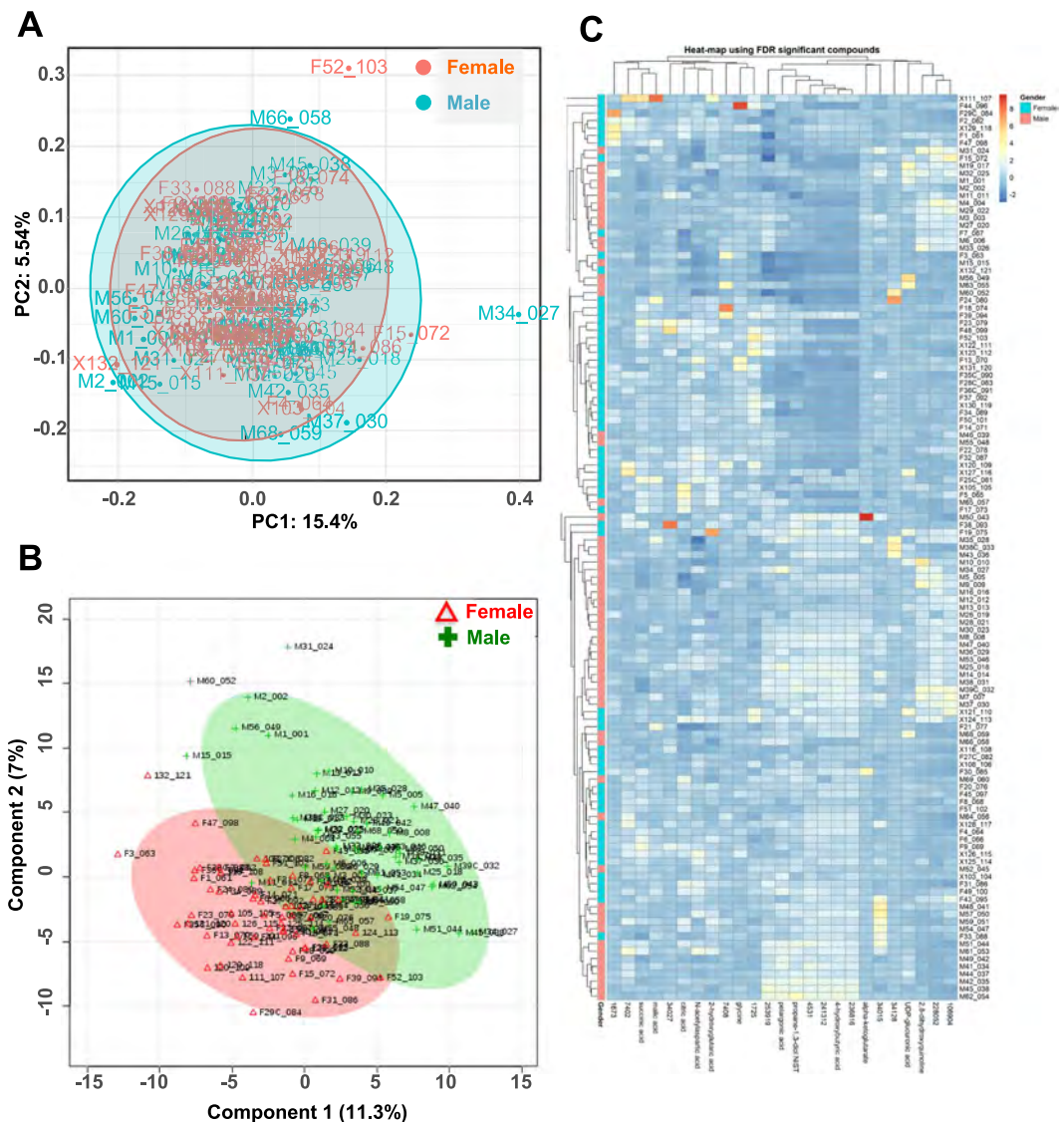


Figure 1. Differentiation of male and female groups using multivariate analysis. **(A)** Score plot of the PCA model distinguishing male and female urine samples. **(B)** PLS-DA scores plot. It depicted obvious differences between male and female urine samples, with PC1 (11.3%) and PC2 (7%). **(C)** Heat map showed the distribution of 25 metabolites, which include 12 annotated ones, that were significantly different (FDR adjusted p -value < 0.05) between male and female urine samples.

Gas chromatography conditions. A 30 m long, 0.25 mm i.d. RTX-5Sil MS column (0.25 μ m, 95% dimethyl 5% diphenyl polysiloxane film) with an additional 10 m integrated guard column was used (Restek, Bellefonte, PA). A constant flow of 1 ml/min 99.99% pure helium, with a built-in purifier, was set. The oven temperature was held at 50 °C for 1 min and then ramped up to 330 °C at a rate of 20 °C/min, where it was then maintained constant for 5 min.

Mass spectrometer settings. A Leco Pegasus IV Time-of-Flight Mass Spectrometer was used and controlled using the Leco ChromaTOF software (vers. 4.1) (St. Joseph, MI). The transfer line temperature between the gas chromatograph and mass spectrometer was set to 280 °C. A 70 V electron impact ionization was employed with an ion source temperature of 250 °C. The acquisition rate was set to 17 spectra/sec, with a scan mass range of 85–500 Da.

Annotation and ID of compounds. The peak and compounds detection or deconvolution was performed with the Leco ChromaTOF software. Spectra were matched against the FiehnLib Mass Spectral and Retention Index Library²⁸. Post-curation and peak replacements were performed with the in-house developed BinBase software and the sample matrix with all known and unknown compounds was exported to an excel sheet. Missing peak intensity data was automatically replaced with the raw extracted ion intensities at the target retention times for each compound, subtracted by adjacent noise levels. This way, only 2 of the 49,680 values were reported with ‘zero’ values, compound BB 109708 and creatinine. These two values were replaced with a value of 1.

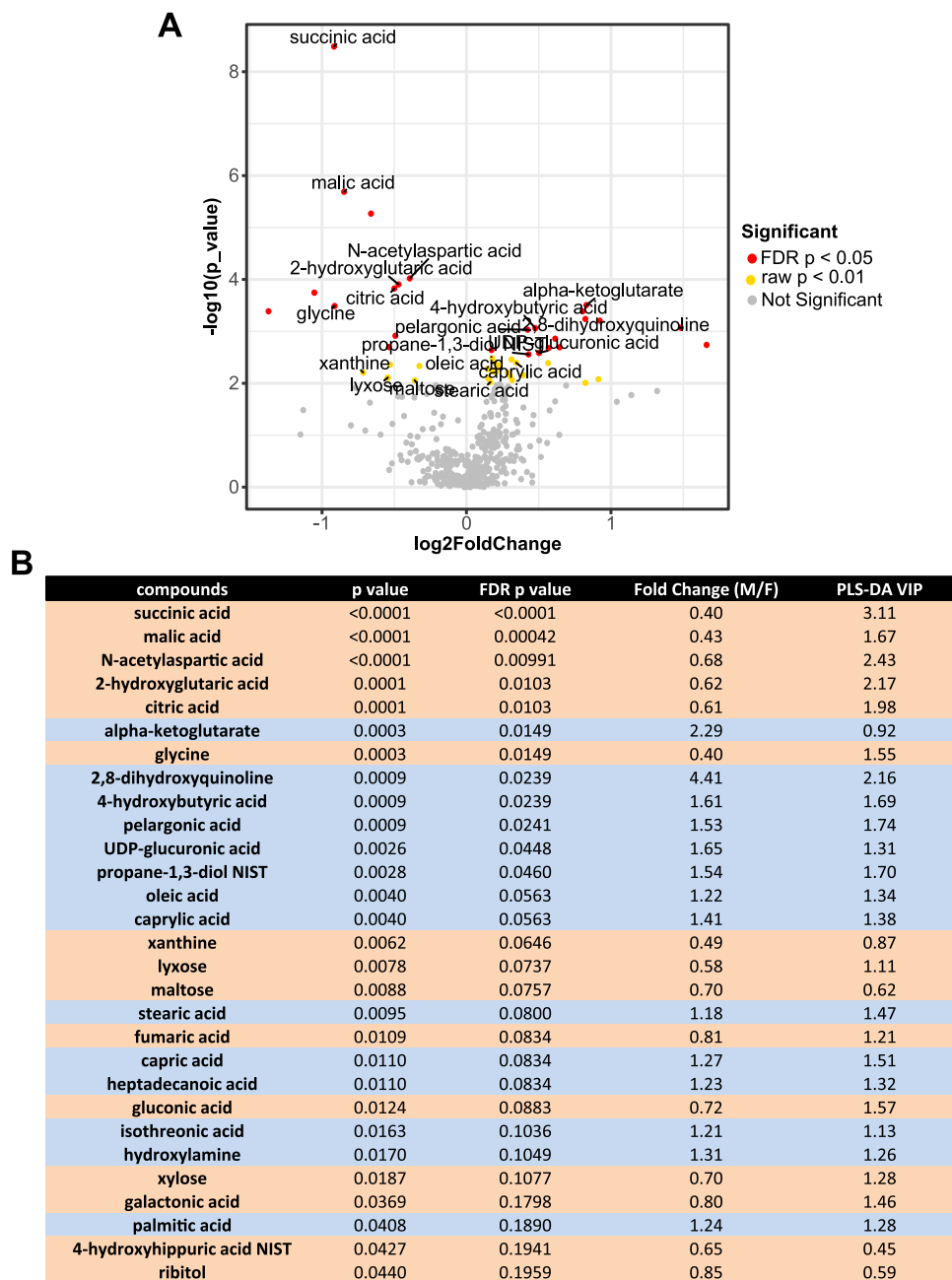


Figure 2. Volcano plot and significant metabolite table. **(A)** In the volcano plot, a total of 50 peaks were significantly changed (Mann-Whitney U test p-value < 0.01) in urine samples. Red dots represent 25 significant peaks with FDR adjusted p-values < 0.05. The annotated significant metabolites are labeled on the plot. **(B)** List of the 21 potential biomarkers in urine samples. P-values were calculated using two-tailed Mann-Whitney U tests. FDR p-values were p-values corrected for the multiple comparison problem using the Benjamini and Hochberg procedure. Fold changes were defined as the ratio of median of male over female for each compound. The variable importance for projection (VIP) reflects the capability of the compounds to explain Y (gender effect).

Missing value replacement method. BinBase was used for post-curation and peak replacements and the sample matrix was exported to an excel sheet. Any missing peak intensity data was automatically replaced by the raw extract ion intensity subtracted by their adjacent noise levels. For each positively detected metabolite, the average retention time was calculated. For each chromatogram and each missing value, the intensity of the quantification ion at this retention time was extracted by seeking its maximum value in a retention time region of 1 sec and subtracting the minimum (local background) intensity in a retention time region of 5 sec around the peak maximum. The resulting report table therefore did not have any missing values²⁹.

The two missing values (*ion intensity* = 0), for compound 109708 and creatinine, were replaced with a value of 1. All peak intensities were normalized to the sum of the peak intensities of all identified metabolites to account

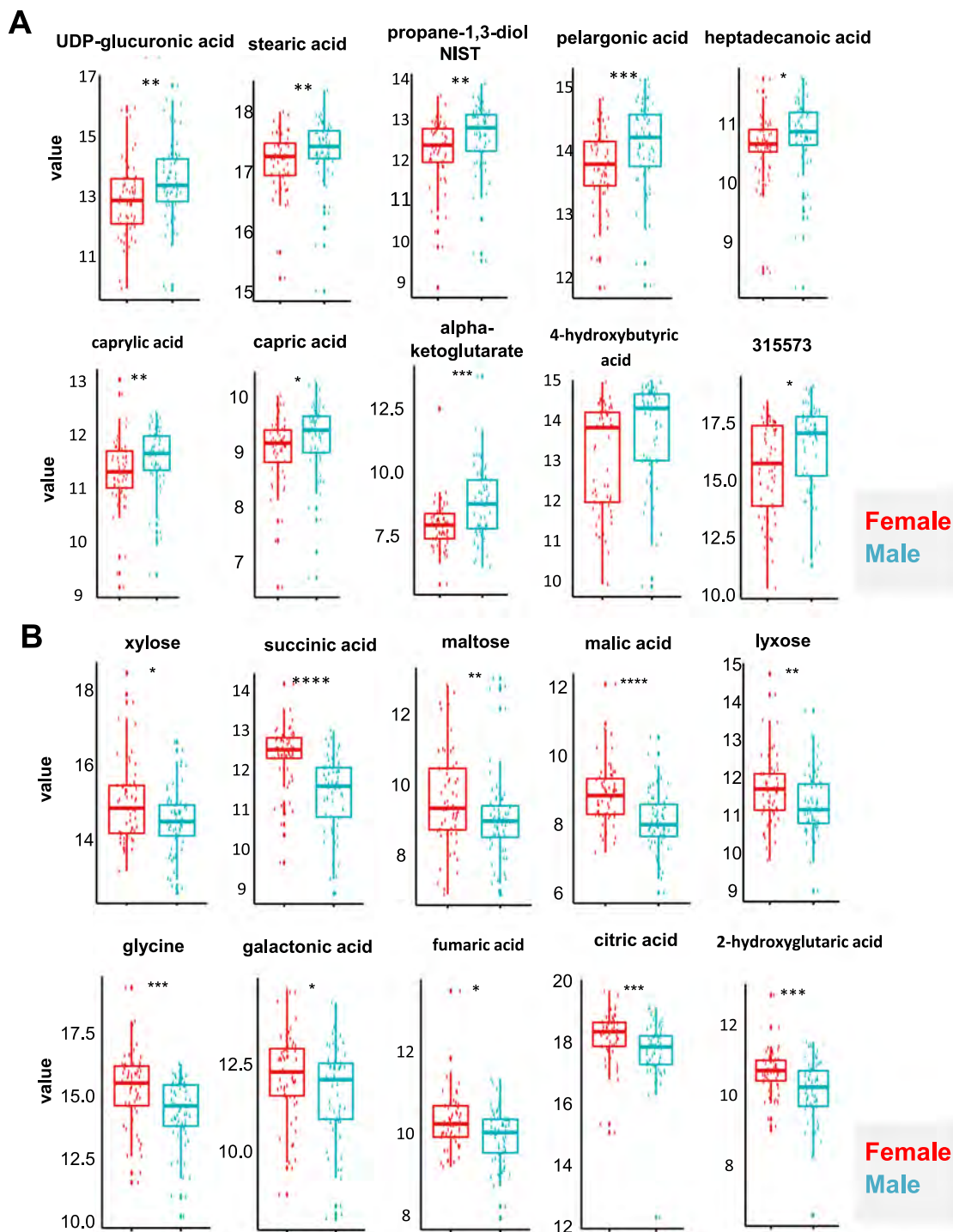


Figure 3. Compound individual boxplots. Boxplots showing upregulated (A) and downregulated (B) metabolites that could be used to differentiate male and female samples. Significance levels were highlighted using * (p value < 0.05), ** ($p < 0.01$), *** ($p < 0.001$), and **** ($p < 0.0001$).

for small errors during extraction or normalization. We found that 77% of all compounds yielded a non-normality distribution. Hence, a nonparametric univariate method, the Mann-Whitney U test, was performed to measure and discover significantly changed metabolites between the male and female urine samples. Additionally, we adopted the Benjamini-Hochberg false discovery rate (FDR) correction procedure to deal with the multiple comparison problem and ensure the reproducibility of our significant metabolites detection. Multivariate statistical analyses, principal component analysis (PCA) and partial least-square discriminant analysis (PLS-DA), were performed to discriminate males and females.

Num	Name	Fold-change	p-value	FDR
1	Unknown BB_31554	2.56	0.000132	0.064576
2	Unknown BB_34163	0.55	0.000514	0.12586
3	oleic acid	0.63	0.001933	0.315675
4	2-deoxytetronic acid	1.26	0.008732	0.571396
5	Unknown BB_17651	0.66	0.009136	0.571396
6	saccharic acid	0.80	0.012642	0.571396
7	Unknown BB_17140	1.44	0.015588	0.571396
8	phosphate	0.70	0.016252	0.571396
9	trehalose	1.79	0.017026	0.571396
10	Unknown BB_5900	0.81	0.017487	0.571396
11	erythronic acid	2.25	0.018393	0.571396
12	Unknown BB_109809	0.56	0.018576	0.571396
13	oxalic acid	0.48	0.018665	0.571396
14	Unknown BB_34027	0.44	0.019904	0.571396
15	Unknown BB_1704	0.63	0.020865	0.571396
16	sulfuric acid	0.31	0.021197	0.571396
17	Unknown BB_23635	0.69	0.02138	0.571396
18	cystine	1.47	0.021607	0.571396
19	Unknown BB_3029	0.70	0.022156	0.571396
20	Unknown BB_12330	2.19	0.02596	0.614149
21	Unknown BB_31549	0.37	0.026702	0.614149
22	lyxitol	1.42	0.028288	0.614149
23	Unknown BB_31756	1.74	0.028827	0.614149
24	lysine	1.49	0.034624	0.706901
25	histidine	1.79	0.040576	0.743323
26	Unknown BB_31359	0.81	0.043988	0.743323
27	Unknown BB_5121	0.64	0.045462	0.743323
28	Unknown BB_100869	1.58	0.046685	0.743323
29	Unknown BB_3294	1.37	0.046907	0.743323
30	Unknown BB_31764	1.33	0.048566	0.743323

Table 1. List of metabolites differentially expressed in IC, compared to controls (p-value = 0.005, FDR (Benjamini Hochberg)).

Statistical analysis. The Mann-Whitney U test was performed on each compound to compare males vs. females. The Benjamini-Hochberg false discovery rate (FDR) correction was utilized to deal with the multiple comparison problem.

Results

GC-TOF-MS analysis of urine specimens from healthy females and males. In total, we enrolled 60 females and 60 age-matched males (age range, 45–65) in this study. All participants were >2 months free of treatment and/or medication. In order to compare the metabolite profiles of urine samples from healthy females and males, individual urine samples were analyzed using GC-TOF mass spectrometry. Multivariate statistical analyses, PCA and PLS-DA, were performed to discriminate males and females (Fig. 1A, B).

Metabolites responsible for the differences in multivariate metabolic phenotypes between male and female urine was obtained based on variable importance in the projection (VIP) from a 10-fold cross-validated PLS-DA model. This model achieved a 48.5% rate of discrimination for Q2 and an 89.1% for R2. In addition, the model was further validated with the permutation test on prediction accuracy and had a significant result ($p < 0.05$), indicating that the model was robust and results were not obtained by chance. Significantly altered metabolites distinguishing male and female urine were acquired based on conditions of $p < 0.05$, fold-change < 0.8 or > 1.2 , and $VIP > 1$ (Fig. 1B). Hierarchical clustering analysis (Euclidean distance and complete method) and constructed heatmaps, using the significant metabolites (corrected FDR $p < 0.05$), depicted the relatively disturbed and unbalanced metabolism states between male and female samples (Fig. 1C).

Distinct urinary metabolite patterns between healthy females and males. Next, we performed the Mann-Whitney U test and Benjamini-Hochberg false discovery rate (FDR) correction on each compound to compare them between males and females. There were 25 significantly different compounds with FDR correction and 94 without (Supplementary Table 1). The volcano plot shows the fold change and significance of each annotated metabolite. Significant metabolites in the volcano plot had a fold-change threshold > 1.20 or < 0.83 with a t-test p-value < 0.05 (Fig. 2A). The 25 significantly different compounds are shown with their p-values, FDR p-values, fold-changes of male vs. female, and PLS-DA VIP values (Fig. 2B). These compounds

label	PubChem	PLS-DA VIP Score	p_value	p_value_adj	Fold Change
xylose	135191	1.28	0.0187	0.1077	0.70
UDP-glucuronic acid	17473	1.31	0.0026	0.0448	1.65
succinic acid	1110	3.11	0.0000	0.0000	0.40
propane-1,3-diol NIST	10442	1.70	0.0028	0.0460	1.54
pelargonic acid	8158	1.74	0.0009	0.0241	1.53
palmitic acid	985	1.28	0.0408	0.1890	1.24
oleic acid	445639	1.34	0.0040	0.0563	1.22
N-acetylaspartic acid	65065	2.43	0.0001	0.0099	0.68
malic acid	525	1.67	0.0000	0.0004	0.43
lyxose	439240	1.11	0.0078	0.0737	0.58
isothreonic acid	151152	1.13	0.0163	0.1036	1.21
hydroxylamine	787	1.26	0.0170	0.1049	1.31
heptadecanoic acid	10465	1.32	0.0110	0.0834	1.23
glycine	750	1.55	0.0003	0.0149	0.40
gluconic acid	6857417	1.57	0.0124	0.0883	0.72
galactonic acid	128869	1.46	0.0369	0.1798	0.80
citric acid	311	1.98	0.0001	0.0103	0.61
caprylic acid	379	1.38	0.0040	0.0563	1.41
capric acid	2969	1.51	0.0110	0.0834	1.27
4-hydroxybutyric acid	10413	1.69	0.0009	0.0239	1.61
2-hydroxyglutaric acid	43	2.17	0.0001	0.0103	0.62
2,8-dihydroxyquinoline	97250	2.16	0.0009	0.0239	4.41

Table 2. List of metabolites with a PLS-DA VIP score > 1, Mann-Whitney U test p-value < 0.05, fold-change (male/female) < 0.8 or > 1.2.

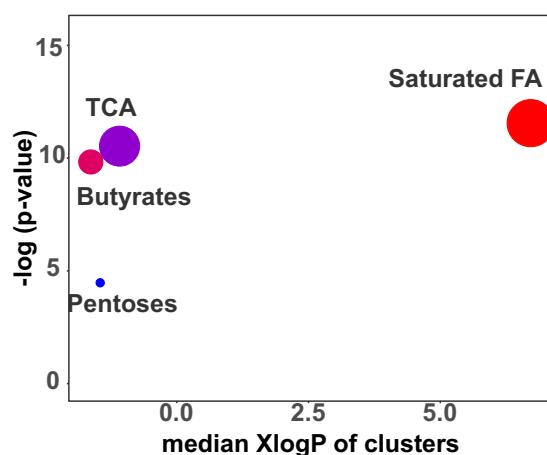


Figure 4. Chemical similarity enrichment analysis results. Y-axis shows the most significantly altered clusters on the top. Cluster color gives the proportion of increased or decreased metabolites (red = increased, blue = decreased, purple = mostly decreased). Chemical enrichment statistics was calculated using Kolmogorov–Smirnov test. Only significantly different enrichment clusters (raw $p < 0.05$) were shown.

include succinic acid, malic acid, N-acetylaspartic acid, 2-hydroxyglutaric acid, citric acid, α -ketoglutarate and others. Among these, α -ketoglutarate (male/female fold-change of 2.29) or 4-hydroxybutyric acid (male/female fold-change 4.41) increased in healthy males compared to females. In contrast, levels of succinic acid (male/female fold-change of 0.40), malic acid (male/female fold-change of 0.43), or glycine (male/female fold-change of 0.40) greatly decreased in males compared to females.

Significantly increased and decreased metabolites in males, compared to females, are shown in Fig. 3A and 3B, respectively. Box-whisker plots were constructed after log₂ transformation. The Mann-Whitney U test was used to determine significance ($*p < 0.05$, $**p < 0.01$, or $***p < 0.005$). All metabolites identified in this study are shown in Supplementary Tables 1 and 2. A few example metabolites whose expression was lower or higher in healthy females compared to healthy males are shown in Fig. 3A and 3B. Expression levels of UDP-glucuronic acid, stearic acid, propane-1,3-diol, pelargonic acid, heptadecanoic acid, caprylic acid, capric acid, α -ketoglutarate, hydroxybutyric acid, and unknown compound BB 315573 were all detected to be considerably lower in urine

Cluster name	Cluster size	p-values	FDR	Increased	Decreased	Increased ratio	Altered Ratio
Saturated FA	10	0.000096	0.00018	6	0	0.6	0.6
TCA	8	0.00027	0.00025	1	5	0.1	0.8
Butyrates	5	0.00054	0.00034	2	0	0.4	0.4
Pentoses	4	0.011	0.054	0	2	0	0.5
Sugar Acids	9	0.26	0.99	0	2	0	0.2
Amino Acids	7	1	1	0	1	0	0.1
Benzoates	3	1	1	0	0	0	0
Cinnamates	3	1	1	0	0	0	0
Dicarboxylic Acids	3	1	1	0	0	0	0
Disaccharides	4	1	1	0	1	0	0.2
Gum Arabic	3	1	1	0	0	0	0
Hexoses	7	1	1	0	0	0	0
Hippurates	3	1	1	0	1	0	0.3
Indoles	4	1	1	0	0	0	0
Phenols	5	1	1	0	0	0	0
Phenylacetates	4	1	1	0	0	0	0
Purinones	3	1	1	0	1	0	0.3
Pyrimidinones	3	1	1	0	0	0	0
Sugar Alcohols	14	1	1	0	1	0	0.07

Table 3. Chemical similarity enrichment analysis. Cluster name is redefined metabolite chemical clusters. Cluster size indicates the size of the cluster. P-values are the result of the Kolmogorov–Smirnov test evaluating how significant difference a metabolite cluster was represented by chance. FDR is the Benjamini–Hochberg corrected p values. The Increase/ratio (Decreased/ratio) shows the numbers/ratio of directions of significant compounds in a cluster.

obtained from healthy females compared to males (Fig. 3A). In contrast, levels of xylose, succinic acid, maltose, malic acid, lyxose, glycine, galactonic acid, fumaric acid, citric acid, and 2-hydroxyglutaric acid were found to be greater in females than in males (Fig. 3B). Table 1 shows a list of metabolites differentially expressed in IC, compared to controls (p-level = 0.005, FDR (Benjamini Hochberg). A list of metabolites with PLS-DA VIP score > 1, Mann-Whitney U test p value < 0.05, and fold change (male/female) < 0.8 or > 1.2 are shown in Table 2.

We speculated that metabolite enrichment analysis may be able to provide the corresponding gender-specific pathways derived from the specific metabolites on their differential networks. We performed metabolite set enrichment analysis (MSEA) with the 29 significant metabolites (Mann-Whitney U test p-value < 0.05). We found that differentially expressed metabolites in female and male groups were highly related to α -ketoglutarate dehydrogenase complex deficiency, with a FDR of 0.00524 (raw p, 0.0000181; Holm p, 0.00524) (Supplementary Fig. 1).

Recently, we published a paper demonstrating that the hypergeometric test could be flawed for metabolomics analyses and should not be used³⁰. We also noted that MSEA may be faulty as well. Thus, in this study, we opted to utilize the newly developed chemical similarity enrichment analysis (ChemRICH)³⁰ instead (<http://chemrich.us>). ChemRICH is a chemical similarity-based statistical enrichment tool with better subsequent enrichment statistics than pathway enrichments and is not dependent on biochemical knowledge annotations. However, it does not provide information regarding enzymes or diseases. To better understand the metabolic signature specific to female and male groups, we performed ChemRICH using the Mann-Whitney U test p-values and median fold-changes of our 140 identified metabolites. ChemRICH was implemented using the Kolmogorov–Smirnov test on the identified clusters to evaluate whether a metabolite cluster was represented more than expected by chance. As a result, we found that saturated fatty acids (FA) (raw p, 0.000096; FDR p, 0.00018), TCA (raw p, 0.00027; FDR p, 0.00025), and butyrates (raw p, 0.00054; FDR p, 0.00034) were significantly related (FDR p < 0.05) to the gender effect (Fig. 4, Table 3).

Discussion

Our objective in this study was to systematically examine sex differences in urine samples obtained from healthy participants. The experimental results from this study provided evidence suggesting that gender influences the global metabolome in healthy female and male subjects. It has been generally accepted that pathogenesis in females may be influenced by metabolic perturbations caused by various hormones, such as estrogen, and other reproductive factors. Although further research is needed, levels of sex hormones may be related to the differences in metabolites detected in the urine of healthy adults.

As proposed in our previously published review articles, monitoring the changes in metabolic landscape, cholesterol, and sex hormones through metabolic profiling can be of immense benefit to patients^{31,32}. Our urinary metabolomics data clearly suggests that sex differences should be considered in future laboratory and clinical studies. Sex has not been heavily considered as an important factor when it comes to identifying druggable targets in diseases, resulting in few biomarker studies that actively look at sex. Since gender is an influencing factor on

pharmacological responses, which in turn is monitored through biomarker changes, careful should be done when consideration should be given when developing effective treatments for males and females.

Levels of urinary metabolites, including UDP-glucuronic acid, α -ketoglutarate, and 2-hydroxyglutaric acid, were found to be higher or lower in females than in males (Fig. 3). We further hypothesized the biology associated with sex-specific metabolites detected in urine samples is linked with sex hormones. Our data suggested the level of UDP-glucuronic acid is higher in healthy males, compared to females. UDP-glucuronic acid is oxidized from UDP-glucose and NAD^+ by UDP-glucose dehydrogenase (UGDH). Considering that the expression of UGDH is known to be stimulated by androgen, a male sex hormone³³, it would be interesting to see if androgen causes the differential levels of UDP-glucuronic acid found in urine samples of female vs. males. In addition, 2-hydroxyglutaric acid (2HG) was found to be greater in females than in males (Fig. 3B). 2HG is known as an oncometabolite that can accumulate in estrogen receptor-negative breast tumors³⁴, suggesting a potential association between increased 2HG levels and estrogen, a female sex hormone.

Previous work from our laboratory and others proposed a series of urinary metabolites as potential IC biomarker candidates^{35–40}. Compared to healthy controls, these metabolites significantly increased or decreased in IC patient urine samples³⁶. One metabolite of interest that we found was α -ketoglutarate, which is an important TCA cycle product and is involved in lipid and acetate metabolism. It is also an epigenetic regulator, controlling transcription and translation of DNA through histone acetylation. Treatment with α -ketoglutarate slowed cell proliferation in normal bladder epithelial cells³⁹. This is consistent with prior clinical observations suggesting that there are thinner layers of bladder epithelium in IC^{41,42}. It was interesting that our current study found higher levels of α -ketoglutarate in healthy males, compared to females. Furthermore, a recent finding from our laboratory suggested the molecular mechanism through which α -ketoglutarate epigenetically regulates bladder epithelial cells⁴³.

Unfortunately, in this current study, we could not provide solid experimental evidence explaining why healthy male urine samples contained these higher levels of α -ketoglutarate. Furthermore, considering that previous results from our group were based only on female participants, expansion of our earlier findings in both sexes would be warranted in the near future.

In summary, our findings suggested that baseline sex-determined differences would be helpful in identifying sex specific biomarkers. Currently, gender differences have not been carefully considered as important confounding factors for biomarker development. Our results provide evidence demonstrating otherwise; drug development and therapies may need more precise and detailed experimental designs that recognize the effects of sex differences on therapeutic efficacy.

References

- Hanno, P., Keay, S., Moldwin, R. & Van Ophoven, A. International Consultation on IC - Rome, September 2004/Forging an International Consensus: progress in painful bladder syndrome/interstitial cystitis. Report and abstracts. *International urogynecology journal and pelvic floor dysfunction* **16**(Suppl 1), S2–S34, <https://doi.org/10.1007/s00192-005-1301-x> (2005).
- Hanno, P. M. *et al.* AUA guideline for the diagnosis and treatment of interstitial cystitis/bladder pain syndrome. *The Journal of urology* **185**, 2162–2170, <https://doi.org/10.1016/j.juro.2011.03.064> (2011).
- Hanno, P. *et al.* Diagnosis of interstitial cystitis. *The Journal of urology* **143**, 278–281 (1990).
- Erickson, D. R. *et al.* A comparison of multiple urine markers for interstitial cystitis. *The Journal of urology* **167**, 2461–2469 (2002).
- Nordling, J. *et al.* Primary evaluation of patients suspected of having interstitial cystitis (IC). *European urology* **45**, 662–669, <https://doi.org/10.1016/j.eururo.2003.11.021> (2004).
- Warren, J. W. & Keay, S. K. Interstitial cystitis. *Current opinion in urology* **12**, 69–74 (2002).
- Berry, S. H. *et al.* Prevalence of symptoms of bladder pain syndrome/interstitial cystitis among adult females in the United States. *The Journal of urology* **186**, 540–544, <https://doi.org/10.1016/j.juro.2011.03.132> (2011).
- Clemens, J. Q., Meenan, R. T., Rosetti, M. C., Gao, S. Y. & Calhoun, E. A. Prevalence and incidence of interstitial cystitis in a managed care population. *The Journal of urology* **173**(discussion 102), 98–102, <https://doi.org/10.1097/01.ju.0000146114.53828.82> (2005).
- Forrest, J. B. & Schmidt, S. Interstitial cystitis, chronic nonbacterial prostatitis and chronic pelvic pain syndrome in men: a common and frequently identical clinical entity. *The Journal of urology* **172**, 2561–2562 (2004).
- Link, C. L. *et al.* Prevalence and psychosocial correlates of symptoms suggestive of painful bladder syndrome: results from the Boston area community health survey. *The Journal of urology* **180**, 599–606, <https://doi.org/10.1016/j.juro.2008.04.009> (2008).
- Parsons, J. K., Kurth, K. & Sant, G. R. Epidemiologic issues in interstitial cystitis. *Urology* **69**, 5–8, <https://doi.org/10.1016/j.urol.2006.05.050> (2007).
- Barry, M. J., Link, C. L., McNaughton-Collins, M. F. & McKinlay, J. B., Boston Area Community Health, I. Overlap of different urological symptom complexes in a racially and ethnically diverse, community-based population of men and women. *BJU international* **101**, 45–51, <https://doi.org/10.1111/j.1464-410X.2007.07191.x> (2008).
- Oertelt-Prigione, S. The influence of sex and gender on the immune response. *Autoimmunity reviews* **11**, A479–485, <https://doi.org/10.1016/j.autrev.2011.11.022> (2012).
- Scotland, R. S., Stables, M. J., Madalli, S., Watson, P. & Gilroy, D. W. Sex differences in resident immune cell phenotype underlie more efficient acute inflammatory responses in female mice. *Blood* **118**, 5918–5927, <https://doi.org/10.1182/blood-2011-03-340281> (2011).
- Weyand, C. M., Schmidt, D., Wagner, U. & Goronzy, J. J. The influence of sex on the phenotype of rheumatoid arthritis. *Arthritis and rheumatism* **41**, 817–822, doi:10.1002/1529-0131(199805)41:5<817::AID-ART7>3.0.CO;2-S (1998).
- Menon, R. *et al.* Gender-based blood transcriptomes and interactomes in multiple sclerosis: involvement of SP1 dependent gene transcription. *Journal of autoimmunity* **38**, J144–155, <https://doi.org/10.1016/j.jaut.2011.11.004> (2012).
- Blenck, C. L., Harvey, P. A., Reckelhoff, J. F. & Leinwand, L. A. The Importance of Biological Sex and Estrogen in Rodent Models of Cardiovascular Health and Disease. *Circulation research* **118**, 1294–1312, <https://doi.org/10.1161/CIRCRESAHA.116.307509> (2016).
- Buoncervello, M. *et al.* Preclinical models in the study of sex differences. *Clinical science* **131**, 449–469, <https://doi.org/10.1042/CS20160847> (2017).
- Santilli, F., D'Ardes, D., Guagnano, M. T. & Davi, G. Metabolic Syndrome: Sex-Related Cardiovascular Risk and Therapeutic Approach. *Current medicinal chemistry* **24**, 2602–2627, <https://doi.org/10.2174/0929867324666170710121145> (2017).
- Mihailidou, A. S. & Ashton, A. W. Cardiac effects of aldosterone: does gender matter? *Steroids* **91**, 32–37, <https://doi.org/10.1016/j.steroids.2014.08.013> (2014).

21. Rosen, S. E., Henry, S., Bond, R., Pearte, C. & Mieres, J. H. Sex-Specific Disparities in Risk Factors for Coronary Heart Disease. *Current atherosclerosis reports* **17**, 49, <https://doi.org/10.1007/s11883-015-0523-8> (2015).
22. Lagranha, C. J., Deschamps, A., Aponte, A., Steenbergen, C. & Murphy, E. Sex differences in the phosphorylation of mitochondrial proteins result in reduced production of reactive oxygen species and cardioprotection in females. *Circulation research* **106**, 1681–1691, <https://doi.org/10.1161/CIRCRESAHA.109.213645> (2010).
23. Garcia-Perez, I. *et al.* Urinary metabolic phenotyping the slc26a6 (chloride-oxalate exchanger) null mouse model. *Journal of proteome research* **11**, 4425–4435, <https://doi.org/10.1021/pr2012544> (2012).
24. Won, E. Y. *et al.* Gender-specific metabolomic profiling of obesity in leptin-deficient ob/ob mice by 1H NMR spectroscopy. *PLoS one* **8**, e75998, <https://doi.org/10.1371/journal.pone.0075998> (2013).
25. Zheng, P. *et al.* Identification of sex-specific urinary biomarkers for major depressive disorder by combined application of NMR- and GC-MS-based metabolomics. *Translational psychiatry* **6**, e955, <https://doi.org/10.1038/tp.2016.188> (2016).
26. Rist, M. J. *et al.* Metabolite patterns predicting sex and age in participants of the Karlsruhe Metabolomics and Nutrition (KarMeN) study. *PLoS one* **12**, e0183228, <https://doi.org/10.1371/journal.pone.0183228> (2017).
27. Kind, T., Tolstikov, V., Fiehn, O. & Weiss, R. H. A comprehensive urinary metabolomic approach for identifying kidney cancer. *Analytical biochemistry* **363**, 185–195, <https://doi.org/10.1016/j.ab.2007.01.028> (2007).
28. Kind, T. *et al.* FiehnLib: mass spectral and retention index libraries for metabolomics based on quadrupole and time-of-flight gas chromatography/mass spectrometry. *Analytical chemistry* **81**, 10038–10048, <https://doi.org/10.1021/ac9019522> (2009).
29. Fiehn, O. *et al.* Quality control for plant metabolomics: reporting MSI-compliant studies. *The Plant journal: for cell and molecular biology* **53**, 691–704, <https://doi.org/10.1111/j.1365-313X.2007.03387.x> (2008).
30. Barupal, D. K. & Fiehn, O. Chemical Similarity Enrichment Analysis (ChemRICH) as alternative to biochemical pathway mapping for metabolomic datasets. *Scientific reports* **7**, 14567, <https://doi.org/10.1038/s41598-017-15231-w> (2017).
31. Kim, W. J. & Kim, J. Looking to the metabolic landscapes for prostate health monitoring. *Prostate international* **5**, 85–88, <https://doi.org/10.1016/j.pnrl.2017.03.004> (2017).
32. Moon, J. Y., Choi, M. H. & Kim, J. Metabolic profiling of cholesterol and sex steroid hormones to monitor urological diseases. *Endocrine-related cancer* **23**, R455–467, <https://doi.org/10.1530/ERC-16-0285> (2016).
33. Wei, Q., Galbenus, R., Raza, A., Cerny, R. L. & Simpson, M. A. Androgen-stimulated UDP-glucose dehydrogenase expression limits prostate androgen availability without impacting hyaluronan levels. *Cancer research* **69**, 2332–2339, <https://doi.org/10.1158/0008-5472.CAN-08-3083> (2009).
34. Terunuma, A. *et al.* MYC-driven accumulation of 2-hydroxyglutarate is associated with breast cancer prognosis. *The Journal of clinical investigation* **124**, 398–412, <https://doi.org/10.1172/JCI71180> (2014).
35. Kind, T. *et al.* Interstitial Cystitis-Associated Urinary Metabolites Identified by Mass-Spectrometry Based Metabolomics Analysis. *Scientific reports* **6**, 39227, <https://doi.org/10.1038/srep39227> (2016).
36. Wen, H. *et al.* Urinary metabolite profiling combined with computational analysis predicts interstitial cystitis-associated candidate biomarkers. *Journal of proteome research* **14**, 541–548, <https://doi.org/10.1021/pr5007729> (2015).
37. Blalock, E. M., Korre, G. S., Stromberg, A. J. & Erickson, D. R. Gene expression analysis of urine sediment: evaluation for potential noninvasive markers of interstitial cystitis/bladder pain syndrome. *The Journal of urology* **187**, 725–732, <https://doi.org/10.1016/j.juro.2011.09.142> (2012).
38. Keay, S. *et al.* Antiproliferative factor, heparin-binding epidermal growth factor-like growth factor, and epidermal growth factor in men with interstitial cystitis versus chronic pelvic pain syndrome. *Urology* **63**, 22–26 (2004).
39. Kuo, H. C. Potential urine and serum biomarkers for patients with bladder pain syndrome/interstitial cystitis. *International journal of urology: official journal of the Japanese Urological Association* **21**(Suppl 1), 34–41, <https://doi.org/10.1111/iju.12311> (2014).
40. Tyagi, P. *et al.* Urinary chemokines as noninvasive predictors of ulcerative interstitial cystitis. *The Journal of urology* **187**, 2243–2248, <https://doi.org/10.1016/j.juro.2012.01.034> (2012).
41. Ratliff, T. L., Klutke, C. G. & McDougall, E. M. The etiology of interstitial cystitis. *The Urologic clinics of North America* **21**, 21–30 (1994).
42. Tomaszewski, J. E. *et al.* Biopsy features are associated with primary symptoms in interstitial cystitis: results from the interstitial cystitis database study. *Urology* **57**, 67–81 (2001).
43. Shahid, M. *et al.* Alpha-oxoglutarate inhibits the proliferation of immortalized normal bladder epithelial cells via an epigenetic switch involving ARID1A. *Scientific reports* **8**, 4505, <https://doi.org/10.1038/s41598-018-22771-2> (2018).

Acknowledgements

The authors acknowledge support from National Institutes of Health (1U01DK103260, 1R01DK100974, U24 DK097154, NIH NCATS UCLA CTSI UL1TR000124), Department of Defense (W81XWH-15-1-0415), Centers for Disease Controls and Prevention (1U01DP006079), IMAGINE NO IC Research Grant, the Steven Spielberg Discovery Fund in Prostate Cancer Research Career Development Award, the U.S.-Egypt Science and Technology Development Fund by the National Academies of Sciences, Engineering, and Medicine (to J.K.). J.K. is former recipient of Interstitial Cystitis Association Pilot Grant, a Fishbein Family IC Research Grant, New York Academy of Medicine, and Boston Children's Hospital Faculty Development. The funders had no role in the design, data collection and analysis, decision to publish or preparation of the manuscript.

Author Contributions

J.K. designed the study, led obtaining funding, and overviewed the literature analysis and drafting the manuscript. S.F., A.Y. and M.S. performed metabolomics analysis and sample preparation. S.F. and O.F. performed data analysis and visualize the data. O.F., S.F., J.A. and K.E. helped writing the manuscript. All authors read and approved the final manuscript.

Additional Information

Supplementary information accompanies this paper at <https://doi.org/10.1038/s41598-018-29592-3>.

Competing Interests: The authors declare no competing interests.

Publisher's note: Springer Nature remains neutral with regard to jurisdictional claims in published maps and institutional affiliations.



Open Access This article is licensed under a Creative Commons Attribution 4.0 International License, which permits use, sharing, adaptation, distribution and reproduction in any medium or format, as long as you give appropriate credit to the original author(s) and the source, provide a link to the Creative Commons license, and indicate if changes were made. The images or other third party material in this article are included in the article's Creative Commons license, unless indicated otherwise in a credit line to the material. If material is not included in the article's Creative Commons license and your intended use is not permitted by statutory regulation or exceeds the permitted use, you will need to obtain permission directly from the copyright holder. To view a copy of this license, visit <http://creativecommons.org/licenses/by/4.0/>.

© The Author(s) 2018



Unmasking molecular profiles of bladder cancer

Xuan-Mei Piao¹, Young Joon Byun¹, Wun-Jae Kim¹, Jayoung Kim^{2,3}

¹Department of Urology, Chungbuk National University College of Medicine, Cheongju, Korea, ²Departments of Surgery and Biomedical Sciences, Cedars-Sinai Medical Center, Los Angeles, CA, ³Department of Medicine, University of California, Los Angeles, CA, USA

Precision medicine is designed to tailor treatments for individual patients by factoring in each person's specific biology and mechanism of disease. This paradigm shifted from a "one size fits all" approach to "personalized and precision care" requires multiple layers of molecular profiling of biomarkers for accurate diagnosis and prediction of treatment responses. Intensive studies are also being performed to understand the complex and dynamic molecular profiles of bladder cancer. These efforts involve looking bladder cancer mechanism at the multiple levels of the genome, epigenome, transcriptome, proteome, lipidome, metabolome etc. The aim of this short review is to outline the current technologies being used to investigate molecular profiles and discuss biomarker candidates that have been investigated as possible diagnostic and prognostic indicators of bladder cancer.

Keywords: Biomarkers; Liquid biopsy; Precision medicine; Urinary bladder neoplasms

This is an Open Access article distributed under the terms of the Creative Commons Attribution Non-Commercial License (<http://creativecommons.org/licenses/by-nc/4.0>) which permits unrestricted non-commercial use, distribution, and reproduction in any medium, provided the original work is properly cited.

INTRODUCTION

Molecular profiling is the global analysis of genomic, epigenetic, transcriptomic, proteomic and metabolomics profiles. It represents a critical pre-requisite for the future success in developing tailored treatment strategies for individual patient [1].

Bladder cancer (BC) is the second most common urological malignancy and requires the most expensive care [2]. Since the time of diagnosis directly influences survival rate, early detection and life-long surveillance of BC is very important. Microhematuria testing and urine cytology are currently the most widely used diagnostic tools for BC; however, these methods are limited due to its costliness and invasiveness [3].

Clinico-pathological features classify BC into two distinct groups; non-muscle invasive bladder cancer (NMIBC) and

muscle-invasive bladder cancer (MIBC). MIBC is the main cause of cancer-specific deaths among BC patients [4,5]. Although NMIBC has better survival than MIBC and other malignancies, 30% to 50% of patients will experience recurrence throughout the remainder of their lives. This rate accounts for cases with surgical resection of the primary tumor and adjuvant therapy. About 10% to 20% of these recurrences will progress to MIBC [6,7]. Therefore, the odds of recurrence and progression in BC have been major challenges for patients and physicians. While the introduction of cisplatin-based chemotherapy has increased the chances of recurrence-free survival, there have been no new U.S. Food and Drug Administration (FDA)-approved therapies for those who cannot tolerate or fail to respond to the treatment [8].

BC is also known as a highly immunogenic cancer type that has a higher rate of mutation than other types

Received: 18 October, 2017 • **Accepted:** 27 December, 2017

Corresponding Author: Jayoung Kim

Departments of Surgery and Biomedical Sciences, Cedars-Sinai Medical Center, 8700 Beverly Blvd., Davis Research Building 5071, Los Angeles, CA 90048, USA
TEL: +1-310-423-7168, FAX: +1-310-967-3809, E-mail: Jayoung.Kim@csmc.edu
ORCID: <http://orcid.org/0000-0002-3683-4627>

of cancer. In BC, various types of tumor-infiltrating immune cells have been reported. The signaling pathways between the tumor and immune cells have been studied. Immunotherapy has been widely accepted as a treatment option for BC and recent new immunotherapies have been studied in various BC clinical trials. New cancer immunotherapies have been tested and applied using clinically immune checkpoints blockers against cytotoxic T lymphocyte-associated antigen-4 (CTLA-4), checkpoint programmed death-1 (PD-1), or programmed death receptor ligand (PD-L1) etc. [9]. A portion of patients with moderate to high-grade NMIBC has been given intravesical immunotherapy with bacillus Calmette-Guérin (BCG) [10-12]. However, this has not been shown to be effective in those with MIBC.

Muscle-invasive disease is managed through cystectomy with or without systemic cisplatin-based chemotherapy. Despite this, it is still not possible to distinguish between patients who will benefit and those who will not from the chemotherapy. It would be tremendously useful and innovative to identify reliable biomarkers that could enable clinicians to distinguish these patients and would provide optimal and personalized treatment plans for each individual case. However, to ensure that the path from discovery to clinical diagnostics continues to be successfully paved, the analytic, diagnostic, and regulatory requirements of a clinical assay need to be understood. Furthermore, active partnerships with industry and effective communication between clinicians and scientists are necessary.

In this short review article, we will provide a general overview of classical and current technologies and molecular findings in BC research. We will also summarize the clinical significance and impacts of these discoveries for future precision medicine in BC patient management and treatment. A simplified diagram shows a series of approaches to precision medicine for BC patients that will be discussed in this short review (Fig. 1).

ESTABLISHED TECHNOLOGY AND RECENT BREAKTHROUGHS IN BLADDER CANCER RESEARCH

Improved understanding of the molecular classification of BC could provide great benefits in the clinical setting. It would serve to bring improved insight and decision-making regarding diagnosis, prognosis, and treatment. The Cancer Genome Atlas (TCGA) includes such comprehensive genomic analyses; such as whole-exome sequencing, mRNA and microRNA (miRNA) sequencing, DNA methylation analysis, and proteomic analysis [13].

Epigenetic modifications include DNA methylation, histone modifications, miRNA, and nucleosome positioning etc. Expression changes and genetic mutations of epigenetic regulatory genes such as DNA methyltransferases, chromatin modifiers and remodelers have been found [14]. Epigenetic alterations contribute to gene expression levels during cancer initiation and progression [14]. As an epigenetic regulator, miRNAs regulate gene expression. For example, miRNAs such as *miR-101*, *miR-21*, *miR-148a*, *miR-126*, *miR-152*, and *miR-29a/29b/29c* etc. can repress epigenetic regulators like EZH2 (H3K27 methyltransferase) [15], DNMT1 (DNA methyltransferase) [16,17], and DNMT3A/3B [18].

For clinical proteomics, there have been a series of mass spectrometry-based techniques used; including liquid chromatography-mass spectrometry (LC-MS/MS), capillary electrophoresis-mass spectrometry (CE-MS), surface-enhanced laser desorption/ionization time-of-flight mass spectrometry, matrix assisted laser desorption/ionization time-of-flight mass spectrometry (MALDI-TOF MS), and nano-liquid chromatography-tandem mass spectrometry (nano-MALDI-MS) [19]. Each of these proteome analytic technologies has their own advantages and disadvantages. LC-MS is sensitive yet expensive, while CE-MS is cheaper than the others. MALDI-TOF MS is relatively cheap and simple; however, nano-MALDI-MS is known more sensitive than MALDI-TOF MS [20-22].

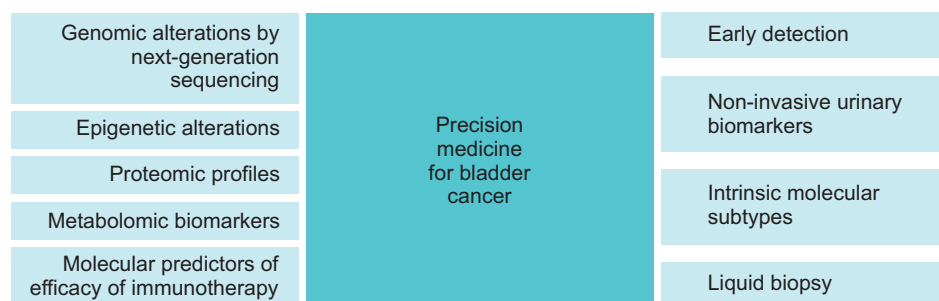


Fig. 1. A diagram showing current translational and clinical approaches to precision medicine for bladder cancer patients.

In order to better understand cancer metabolism, a metabolomics approach has often been utilized. It has since provided information and insight on global chemical fingerprints associated with the physiological and pathological states of cancer [23]. Using various metabolomics technologies, including nuclear magnetic resonance spectroscopy (NMR, also known as, $^1\text{H-NMR}$), gas chromatography mass spectrometry (GC-MS), direct flow injection mass spectrometry, inductively coupled plasma mass spectrometry, and high performance liquid chromatography, possible metabolic fingerprints associated with BC have been tried to be identified.

In addition to analytic technologies, an adequate *ex vivo* BC model, which is currently a major limitation towards identifying predictive biomarkers, is needed to better understand the molecular mechanisms of BC. A series of previous studies have suggested that cancer cells in three dimensional (3D) culture systems respond differently from those in 2D cultures [24,25]. The lack of clinico-physiology of cell line models, and *in vivo* models (e.g., animal and patient-derived xenografts) have greatly limited urological research. However, recent developments of 3D organoids received from patients seem to provide a realistic bladder microenvironment. This pre-clinical BC mimic model has the potential to be used as a method of therapeutic pre-screening for individual patients. Using a rotating wall vessel bioreactor under microgravity conditions, BC organoids have been previously developed from cell line or tissue biopsy samples. Well-constructed 3D organoids play as a functional unit and closely mimic the tissue of origin. 3D organoids are characterized to exhibit 4–6 multiple cell layers, and this amenability allows organoids to be powerful pre-clinical BC models.

Successful construction of BC patient-derived 3D organoids has further broadened our understanding of the molecular mechanisms and drivers that promote BC development. DNA sequencing analysis of patient-derived 3D organoids suggest that these organoids share very similar mutational profiles with those of real tumor samples [26]. Thus, it is speculated that genetic information from patient organoids can be used for personalized drug-prescreening and predicting responses to treatment. While these experimental results need intensive follow-up validation, 3D organoid-based drug response assays seem very promising and will undeniably benefit clinical decisions. If successful, a patient-derived organoid biobank could facilitate personalized medicine in BC research.

APPLICATION TO BLADDER CANCER STUDY

1. Urine biomarkers for early detection of bladder cancer

Molecular profiling methods have been used for phenotyping BC. Recent reports have shown that modern classification of BC into various distinct subtypes is associated with responses to chemotherapy and immune checkpoint inhibitors. There are various commercial BC biomarkers that are currently being used in the clinical setting. They include nuclear-matrix protein 22 (NMP22), UroVysion test, and others. NMP22 levels are shown to be associated with disease recurrence and progression [27]. The UroVysion test is a multicolor fluorescence in situ hybridization (FISH) assay designed to detect aneuploidy of chromosomes 3, 7, or 17, and/or the loss of the 9p21 locus [28]. A series of recent reports showed that utilization of FISH-based assay may be used as an additional tool for sub-classification of patients or determining a treatment option [29-32].

Because it is stored in the bladder before micturition, urine is an attractive non-invasive biomarker resource for BC. As potential urinary BC biomarkers, perturbed levels of urinary miRNAs and DNA methylation have been reported. The most promising urinary BC biomarkers include: *miRNA-96*, *miRNA-138*, *miRNA-126*, *miRNA-182*, *miRNA-143*, *miRNA-222*, *miRNA-21*, *miRNA-133b*, *miRNA-518c-5p*, *miRNA-452*, *miRNA-129*, *miRNA-200c*, *miRNA-99a*, *miRNA-100*, and *miRNA-29c* [33].

The methylation statuses of *SALL3*, *CFTR*, *ABCC6*, *HPRI*, *RASSF1A*, *MT1A*, *ALX4*, *CDH13*, *RPRM*, *MINT1*, and *BRCA1* in the urine samples of BC patients is also shown to be associated with the disease [34]. In other studies, a specific three-gene panel, consisting of *BCL2*, *hTERT*, and *DAPK*, was linked with BC in urine [35]. Seven other genes in urinary cell-free DNA (cfDNA) have also been found to be associated with BC. These include *FGFR3*, *TERT*, *PIK3CA*, *TP53*, *HRAS*, *RXRA*, and *KDM6A* [36]. This report suggested that one of avenues of biomarker detection includes identifying circulating cell-free tumor DNA.

2. Genomic alterations detected by next-generation sequencing in bladder cancer

BC, and in particular MIBC, has one of the largest mutational burdens of all tumor types studied in the TCGA. The key cause of this is believed to be due to smoking, which leads to the production of reactive oxygen species and resultant DNA damage. TCGA analysis has shown

that DNA mutation of the *ERCC2* and *APOBEC3B* genes drives BC genomic heterogeneity and disease progression [37,38]. Inactivation of the *TP53* gene is also a well-known mutation in BC. *TP53* gene mutations were observed in approximately 50% of MIBC cases and 20% of NMIBC cases [39]. *TERT* promoter mutations and chromatin-modifying gene mutations are some of the most frequently altered genes, having frequency rates of 73% and 69%, respectively [40,41]. In addition, amplification of *cyclin D1* and *MYC* has been reported in BC [42]. Approximately 20% of NMIBC and MIBC show *cyclin D1* amplification and 13% of MIBC show *MYC* amplification. Activating mutations, fusions, or amplifications of the *EGFR* family have also been reported [43].

DNA alterations of *EGFR*, *ERBB2*, *ERBB3*, and *ERBB4* have been reported in BC [44,45]. *FGFR3* mutations are common in low-grade and low-stage NMIBC. *FGFR3* mutant tumors are known to be associated with higher risk for intravesical recurrence. Both *ERBB2* and *FGFR3* alterations are present in 57% of high-grade NMIBC tumors in a mutually exclusive pattern [46-48].

In BC, oncogenes or tumor suppressor genes, such as those found in the Ras-MEK-ERK pathway and PI3 kinase-AKT-mTOR pathway, are often mutated. *PIK3CA* and/or PI3k/Akt pathway alterations are associated with favorable disease-specific outcomes, independent of tumor and lymph node stage [49]. For better sensitivity and specificity, *FGFR3* mutation levels are sometimes combined with *PIK3CA* or *CDKN2A* alterations [50].

3. Epigenetic alterations in bladder cancer

In this section, we will discuss the epigenetic alterations in BC. Several epigenetic drugs have been used in the clinical and pre-clinical settings. They include: DNMT inhibitors (5-azacytidine and 5-Aza-2'-deoxycytidine), histone deacetylases inhibitors (SAHA, valproic acid, and romidepsin), and Tazemetostat (an EZH2 inhibitor). These epigenetic drugs are being considered for BC treatment [51].

Modified histone proteins lead to the perturbation of gene expression and other key biological processes [52]. For example, histone modification, such as trimethylation of histone H3 at lysine 4 (H3K4me3), trimethylation on H3 lysine 9 (H3K9me3), lysine 27 (H3K27me3), acetylation on H3 lysine 9 (H3K9Ac), and lysine 27 (H3K27Ac), regulates gene activation [53]. DNA alterations are frequently observed on *histone H3 lysine 27 (H3K27)* in NMIBC and *histone H3 lysine 4 (H3K4)* methyltransferase *MLL2* in MIBC [54].

DNA hypomethylation of *LINE-1* repetitive element has been found often in BC, and this correlates with

activated *MET* oncogene transcription [55]. *RUNX3*-promoter DNA methylation is positively correlated with BC progression and patient survival [56]. It was also reported DNA hypermethylation of *A2BP1*, *NPTX2*, *SOX11*, *PENK*, *NKX62*, *DBC1*, *MYO3A*, *CA10*, *POU4F2*, *HOXA9*, *MEIS1*, *GDF15*, *TMEFF2*, *VIM*, *STK11*, *MSH6*, *BRCA1*, *TBX2*, *TBX3*, *GATA2*, *ZIC4*, *PAX5A*, *MGMT*, and *IGSF4* [57]. DNA hypermethylation of *CDH1*, *FHIT*, *LAMC2*, *RASSF1A*, *DAPK*, *MINT31*, and *SFRP* are also related to BC development and survival [58-60]. Furthermore, DNA methylation signatures of candidate genes were combined and tested to determine if the joint DNA methylation signature shows high sensitivity and specificity in diagnosing BC. The recently identified urinary 3-marker DNA methylation panel (*SOX1*, *IRAK3*, and *LINE-1-MET*) showed an area under the curve (AUC) of 0.90 (95% confidence interval [CI], 0.86–0.92) with sensitivity of 86% (95% CI, 74%–99%) and specificity of 89% (95% CI, 81%–97%) by the 5-fold cross-validation analysis [61].

4. Molecular predictors of efficacy of BCG therapy

BC is known as one of highly immunogenic cancer types [62,63], and cancer immunotherapies aimed to stimulate the body's immune system (e.g., BCG) have been utilized to treat BC patients [9]. In the last ten years, there have been continued drug developments on new classes of immune checkpoint inhibitors. These include Pembrolizumab, Atezolizumab, Nivolumab, Avelumab, Durvalumab, Ipilimumab, and Tremelimumab etc. The current ongoing clinical trial NCT02324582 was designed to test the efficacy of immune checkpoint inhibitors when combined with BCG in NMIBC. Clinical trials for testing neo-adjuvant and adjuvant immune checkpoint therapy following cystectomy were also designed as well (NCT02451423, NCT02450331).

For over forty years, BCG therapy, the first FDA-approved immunotherapy and the most effective intravesical treatment, has been used to reduce the risk of BC recurrence for high-risk disease. However, approximately 70% of BC patients eventually failed to respond to intravesical BCG therapy and experienced remission after treatment [12]. Interestingly, BC patients who did not respond to BCG therapy exhibit the higher PD-L1 expression than those who responded to it. This suggests that PD-L1 could attenuate responses to BCG therapy by neutralizing T cells and possibly infers a biological role for PD-1/PD-L1 interactions [64].

More recent studies on the genomic alterations correlated with recurrence following BCG therapy suggest a possible association between *ARID1A* mutations and BCG outcomes. When compared to the *ARID1A* wild-type,

ARID1A truncating mutations were significantly associated with an increased risk of recurrence following BCG therapy [65]. Further investigation is needed in determining whether inactivation of *ARID1A*, due to its truncating mutation, can be a reliable predictive biomarker of BCG therapy. *ARID1A* inactivation may also be reversed by epigenetic inhibition, which could benefit patients who fail to respond to BCG treatment [66,67].

5. Proteomics in bladder cancer

The scope of this section is to briefly present on the contribution of proteomics towards BC research. Concerted efforts aimed at discovering biomarkers for BC detection and disease monitoring have led to the discovery of many proteomic biomarkers in the urine, tissue, blood etc. [20,21].

Multiple different approaches have been attempted in order to characterize the BC-specific urine proteome landscape. These include using LC-MS/MS, multiple reaction monitoring, and/or CE-MS. These biomarker candidates were also validated using targeted proteomic techniques such as enzyme linked immunosorbent assay (ELISA).

Global urinary glycoproteomic analysis performed by Kreunin et al. [68] revealed the alpha-1B-glycoprotein as a potential biomarker for BC. A different study found increased levels of urinary fibrinogen, lactate dehydrogenase B, Apo-A1, clusterin, and haptoglobin as being associated with BC [69,70]. Higher levels of histone H2B and nuclear interacting factor 1/Zinc finger 335 were detected in the urine and tumor tissue from BC patients. This was further confirmed through independent ELISA and immunohistochemistry (IHC) analyses. ADAM28, midkine, and hepatocyte growth factor activator inhibitor type 1 (HAI-1) were also found to be significantly elevated in the urine of BC patients, compared to controls [71]. Interleukin 8, matrix metalloproteinase 9, and syndecan-1 are additional metabolites discovered to be heightened in a set of urine samples [72]. Moreover, some secreted proteins from isolated exosomes (e.g., calcium-signal transducer 2) were found in the *in vitro* cell culture as well as in the urine specimens of BC patients.

In addition to urine, the BC-specific proteome has also been obtained from tissue and blood specimens. Dynamin and clusterin were identified as potential biomarkers of BC and were further validated via IHC of tissue arrays. It was found that lowered expression of clusterin is associated with MIBC. Dynamin is negatively correlated with adverse outcomes [71]. From these proteomic analyses, differentially expressed proteins were found when comparing MIBC to NMIBC [73]. Cullin-3 and stathmin-1 were found to have

increased expression in BC and are linked with unfavorable outcomes [74]. Differential expression of prelamin-A/C (LMNA), transcription factor AP-1 (JUN), nucleasesensitive element-binding protein 1 (YBOX1), L-selectin (LYAM1), cyclindependent kinase inhibitor 1 (CDN1A), and mothers against decapentaplegic homolog 3 (SMAD3) were reported as tissue-based BC biomarkers. Three proteins, 4F2 cell-surface antigen heavy chain (SLC3A2), stathmin (STMN1) and transgelin-2 (TAGLN2), were revealed as upregulated in BC. The BC-specific blood proteome revealed S100A8 and S100A9 expression as being significantly different between BC and healthy controls (AUC of 0.946) [75].

Evidently, our future research efforts should concentrate on the proper validation of these promising biomarkers through multiple large and independent patient cohorts. Coordinated efforts to utilize existing or developing biorepositories of clinical samples and perform well-designed proteomic profiling should be maintained. BC molecular subtypes should be considered in the proteomics approach of attributing biological significance to proteomic findings.

6. Metabolomics of bladder cancer

Significant progress has been made from current metabolomic techniques to distinguish BC patients from control subjects. Various techniques such as NMR, GC-MS, and LC-MS have contributed to BC metabolomic research. The intermediates of glucose metabolism, including lactic and citric acids, were found to be significantly different in cancer samples [76]. This phenomenon is widely known as the Warburg effect, which states that cancer cells exhibit increased dependence on the glycolytic pathway for ATP generation, giving rise to enhanced lactic acid production [77]. Hence, measuring lactic acid level in biological samples of BC is useful in BC diagnosis. Increased amino acid levels have been demonstrated in the urine, serum and tissue samples of BC patients. Decreased levels of citric acid and fumarate, which are the metabolic intermediates of aerobic oxidation, were also observed in BC samples [76].

A NMR-derived metabolomics study has also proven to be a potential useful avenue for BC diagnosis [23,78,79]. NMR spectroscopy was found to adequately detect hidden biomarkers for the early detection of BC [78]. In a current study with the urinary metabolomics-based diagnostic approach, both high sensitivity and specificity were found [80]. This approach is non-invasive, needs only a small sample of urine, and the diagnosis can be made relatively quickly and objectively. The study showed that patients with BC had elevated levels of urinary acetyl-CoA and carnitine. It also established several acylcarnitines that were found

to differentiate between cancer and control groups [80]. Another study using the targeted mass spectrometry found that it is highly sensitive for detecting metabolic alterations. This provides insight into metabolic pathways that are potentially associated with tumorigenesis and tumor progression [77].

CLINICAL IMPLICATIONS OF MOLECULAR PROFILES

1. Intrinsic molecular subtypes of bladder cancer

Intrinsic molecular subtypes of BC were recently established through many studies based on comprehensive genomic data from TCGA. The relationships between subtypes and their clinical implications have been investigated.

Specific genetic alterations have been found in distinct phenotypes, suggesting distinct disease entities. Most of NMIBC primarily show *FGFR3* mutations, *Ras* activation, and wild-type *TP53* [33,81]. Basal/squamous cell carcinoma (SCC)-like MIBC is the most aggressive phenotype. However, it is also the most sensitive to cisplatin chemotherapy [82]. *RB1* and *NFE2L2* mutations are frequently observed in the basal/SCC-like MIBC phenotype. The p53-like MIBC is characterized as being chemo-resistant. Alterations of *FGFR3* and *KDM6A* are associated in the luminal subtype of p53-like MIBC. Luminal cluster I shows lowered expression of CD8+ effector genes and PD-L1 immune or tumor cells. Meanwhile, luminal cluster II subtypes are linked to activated T-effector cells. The Lund classification currently recognizes five subtypes of BC; urobasal A (uroA), urobasal B (uroB), genomically unstable, and infiltrated/SCC-like [83]. Cancerous cells that can switch between the luminal and basal subtypes has also been found. This suggests that longitudinal studies are critical for understanding subtype changes and the associated responses to various chemotherapies. Collectively, based on these genetic alterations of these different phenotypes, research efforts are now moving to consider clinical strategies that can better the management of BC patients.

2. Liquid biopsy

Liquid biopsies are being considered as a potential applicable non-invasive molecular profiling tool. A number of non-invasive multi-marker tests are currently commercially available for BC. In particular, ImmunoCyt™ is able to measure levels of mucin and carcinoembryonic antigens in urine samples for BC diagnosis [84]. Another urine test, Aura Tek FDP Test™, can detect BC recurrence

[85]. Circulating factors, including circulating tumor cells (CTCs), cfDNAs, RNAs (miRNAs, long non-coding RNAs [lncRNAs], mRNAs), cell-free proteins, peptides, or exosomes et al., are derived from cells in human body. However, it is still elusive where these circulating molecules are coming from.

CTCs of BC were previously detected in the urine and serum from patients with metastatic BC. Rising levels of CTCs were also positively correlated with aggressiveness [86,87]. CTCs derived from BC can be measured by using CTC-specific proteins, such as c-MET and PD-L1 [88-90]. Increased CTC levels were able to predict clinical outcomes, such as recurrence and survival. CellSearch™, an FDA-approved CTC assay kit, is currently being used in the clinical setting for prognostic purposes.

Tumor-derived DNA is released into the body's circulation. Circulating tumor DNA (ctDNA) may reflect the genetic profile of all tumor sub-clones. In most cases, ctDNA has a very small size, usually between 180–200 base pairs. Quantification of ctDNA levels and the integrity status of ctDNA can be of great potential clinical utility for early diagnosis and prognosis of BC. Like other liquid biopsies, ctDNA testing can also be easily and frequently repeated in order to monitor changes during treatment [91]. In addition, genetic alterations can be detected in ctDNA. In the urine specimens of BC patients, *TERT* promoter mutations correlated with recurrence [92], while *KRAS2* mutations were found in the plasma even before BC diagnosis [93].

Circulating RNA classes, which include mRNAs, miRNAs, and lncRNAs, were also found to be potential non-invasive biomarkers [94]. The urinary *CAIX* splice variant mRNA was reported to have high diagnostic performance and value [95]. Urinary *UBE2C* and *hTERT* mRNA are found to be potential markers for early diagnosis and prognosis of BC [96]. Urinary levels of *miR-126* and *miR-146a-5p* were also discovered to be elevated in BC and are associated with tumor grade and invasiveness [97].

The delivery of circulating molecules employs the use of small vesicles, called exosomes. Exosomes transfer biologically active molecules and can be secreted into the urine, blood, and other body fluids [98]. Hence, exosomes are essential mediators of cell-to-cell communication [98]. There is a strong association between heightened exosome levels and BC [99]. In urinary exosomes, significantly increased levels of active molecules (e.g., *TACSTD2*, lncRNAs–*HOTAIR*, *HOX-AS-2*, *ANRIL*, and linc-ROR, et al.) were found to in high-grade MIBC patients [100].

CONCLUDING REMARKS AND PERSPECTIVES

In this short review article, we addressed current concerted efforts on developing molecular profiling focused on BC. Development of high-throughput profiling technologies, including genomics, epigenomics, proteomics, metabolomics, and bioinformatics etc., have accumulated evidence through research in the laboratory and clinical settings. Experimental findings have proposed promising biomarker candidates for clinical application. Subtyping of BC based on molecular signatures associated with clinical outcomes suggest mechanistic clues on how to monitor responses to chemotherapy in patients. However, clinically applicable and personalized biomarkers for early diagnosis and prediction of recurrence, progression, and treatment are unsolved and require more investigation. Focused efforts should continue in order to extract applicable and synergistic benefits from our current findings. This will likely ensure that a clear path from discovery to clinical diagnostics will be successfully paved.

CONFLICTS OF INTEREST

The authors have nothing to disclose.

ACKNOWLEDGMENTS

The authors acknowledge support from the International Science and Business Belt Program through the Ministry of Science, ICT and Future Planning (2016K000297) (to W-J. K.), National Institutes of Health grants (1U01DK103260), Department of Defense grants (W81XWH-15-1-0415), Centers for Disease Control and Prevention (1U01DP006079), the Steven Spielberg Discovery Fund in Prostate Cancer Research Career Development Award, Burroughs Wellcome Fund (BWF) 2017 Collaborative Research Travel Grant (CRTG), Southeast Center for Integrated Metabolomics (SECIM) Pilot and Feasibility Grant, and the U.S.-Egypt Science and Technology (S&T) Joint Fund, funded by the National Academies of Sciences, Engineering, and Medicine and USAID (to J.K.). Any opinions, findings, conclusions, or recommendations expressed in this article are those of the authors alone, and do not necessarily reflect the views of any of the previously mentioned sponsors.

WK and JK designed the study, led obtaining funding, and overviewed the literature analysis and drafting the manuscript. All authors read and approved the final manuscript.

The authors would like to thank Mr. Taeun Daniel Park and Mr. Austin Yeon for careful review and editing the manuscript.

REFERENCES

1. Diamandis M, White NM, Yousef GM. Personalized medicine: marking a new epoch in cancer patient management. *Mol Cancer Res* 2010;8:1175-87.
2. Johnson DC, Greene PS, Nielsen ME. Surgical advances in bladder cancer: at what cost? *Urol Clin North Am* 2015;42:235-52, ix.
3. Burger M, Catto JW, Dalbagni G, Grossman HB, Herr H, Karakiewicz P, et al. Epidemiology and risk factors of urothelial bladder cancer. *Eur Urol* 2013;63:234-41.
4. Kaufman DS, Shipley WU, Feldman AS. Bladder cancer. *Lancet* 2009;374:239-49.
5. Parkin DM, Bray F, Ferlay J, Pisani P. Global cancer statistics, 2002. *CA Cancer J Clin* 2005;55:74-108.
6. Messing E. Markers of detection. *Urol Oncol* 2007;25:344-7.
7. Quan C, Cha EJ, Lee HL, Han KH, Lee KM, Kim WJ. Enhanced expression of peroxiredoxin I and VI correlates with development, recurrence and progression of human bladder cancer. *J Urol* 2006;175:1512-6.
8. Bellmunt J, Pons F, Orsola A. Molecular determinants of response to cisplatin-based neoadjuvant chemotherapy. *Curr Opin Urol* 2013;23:466-71.
9. Kim J. Immune checkpoint blockade therapy for bladder cancer treatment. *Investig Clin Urol* 2016;57 Suppl 1:S98-105.
10. Lenis AT, Chamie K. Bladder cancer in 2014: from the genomic frontier to immunotherapeutics. *Nat Rev Urol* 2015;12:74-6.
11. Macleod LC, Ngo TC, Gonzalgo ML. Complications of intravesical bacillus calmette-guérin. *Can Urol Assoc J* 2014;8:E540-4.
12. Steinberg RL, Thomas LJ, Nepple KG. Intravesical and alternative bladder-preservation therapies in the management of non-muscle-invasive bladder cancer unresponsive to bacillus Calmette-Guérin. *Urol Oncol* 2016;34:279-89.
13. Tomczak K, Czerwińska P, Wiznerowicz M. The Cancer Genome Atlas (TCGA): an immeasurable source of knowledge. *Contemp Oncol (Pozn)* 2015;19:A68-77.
14. Kim WJ, Kim YJ. Epigenetics of bladder cancer. *Methods Mol Biol* 2012;863:111-8.
15. Martínez-Fernández M, Rubio C, Segovia C, López-Calderón FF, Dueñas M, Paramio JM. EZH2 in bladder cancer, a promising therapeutic target. *Int J Mol Sci* 2015;16:27107-32.
16. Wu CT, Lin WY, Chang YH, Lin PY, Chen WC, Chen MF. DNMT1-dependent suppression of microRNA424 regulates tumor progression in human bladder cancer. *Oncotarget*

- 2015;6:24119-31.
17. Lombard AP, Mooso BA, Libertini SJ, Lim RM, Nakagawa RM, Vidallo KD, et al. miR-148a dependent apoptosis of bladder cancer cells is mediated in part by the epigenetic modifier DNMT1. *Mol Carcinog* 2016;55:757-67.
 18. Palmboos PL, Wang L, Yang H, Wang Y, Leflein J, Ahmet ML, et al. ATDC/TRIM29 drives invasive bladder cancer formation through miRNA-mediated and epigenetic mechanisms. *Cancer Res* 2015;75:5155-66.
 19. Chen Z, Kim J. Urinary proteomics and metabolomics studies to monitor bladder health and urological diseases. *BMC Urol* 2016;16:11.
 20. Di Meo A, Pasic MD, Yousef GM. Proteomics and peptidomics: moving toward precision medicine in urological malignancies. *Oncotarget* 2016;7:52460-74.
 21. Thomas S, Hao L, Ricke WA, Li L. Biomarker discovery in mass spectrometry-based urinary proteomics. *Proteomics Clin Appl* 2016;10:358-70.
 22. Frantzi M, Latosinska A, Flühe L, Hupe MC, Critselis E, Kramer MW, et al. Developing proteomic biomarkers for bladder cancer: towards clinical application. *Nat Rev Urol* 2015;12:317-30.
 23. Chan EC, Pasikanti KK, Hong Y, Ho PC, Mahendran R, Raman Nee Mani L, et al. Metabonomic profiling of bladder cancer. *J Proteome Res* 2015;14:587-602.
 24. Deiss F, Mazzeo A, Hong E, Ingber DE, Derda R, Whitesides GM. Platform for high-throughput testing of the effect of soluble compounds on 3d cell cultures. *Anal Chem* 2013;85:8085-94.
 25. Håkanson M, Textor M, Charnley M. Engineered 3D environments to elucidate the effect of environmental parameters on drug response in cancer. *Integr Biol (Camb)* 2011;3:31-8.
 26. Gao D, Vela I, Sboner A, Iaquina PJ, Karthaus WR, Gopalan A, et al. Organoid cultures derived from patients with advanced prostate cancer. *Cell* 2014;159:176-87.
 27. Shariat SF, Savage C, Chromecki TF, Sun M, Scherr DS, Lee RK, et al. Assessing the clinical benefit of nuclear matrix protein 22 in the surveillance of patients with nonmuscle-invasive bladder cancer and negative cytology: a decision-curve analysis. *Cancer* 2011;117:2892-7.
 28. Ho CC, Tan WP, Pathmanathan R, Tan WK, Tan HM. Fluorescence-in-situ-hybridization in the surveillance of urothelial cancers: can use of cystoscopy or ureteroscopy be deferred? *Asian Pac J Cancer Prev* 2013;14:4057-9.
 29. Gomella LG, Mann MJ, Cleary RC, Hubosky SG, Bagley DH, Thumar AB, et al. Fluorescence in situ hybridization (FISH) in the diagnosis of bladder and upper tract urothelial carcinoma: the largest single-institution experience to date. *Can J Urol* 2017;24:8620-6.
 30. Lavery HJ, Zaharieva B, McFaddin A, Heerema N, Pohar KS. A prospective comparison of UroVysion FISH and urine cytology in bladder cancer detection. *BMC Cancer* 2017;17:247.
 31. Liem EIML, Baard J, Cauberg ECC, Bus MTJ, de Bruin DM, Laguna Pes MP, et al. Fluorescence in situ hybridization as prognostic predictor of tumor recurrence during treatment with Bacillus Calmette-Guérin therapy for intermediate- and high-risk non-muscle-invasive bladder cancer. *Med Oncol* 2017;34:172.
 32. Virk RK, Abro S, de Ubago JMM, Pambuccian SE, Quek ML, Wojcik EM, et al. The value of the UroVysion® FISH assay in the risk-stratification of patients with "atypical urothelial cells" in urinary cytology specimens. *Diagn Cytopathol* 2017;45:481-500.
 33. Yoshino H, Seki N, Itesako T, Chiyomaru T, Nakagawa M, Enokida H. Aberrant expression of microRNAs in bladder cancer. *Nat Rev Urol* 2013;10:396-404.
 34. Yu J, Zhu T, Wang Z, Zhang H, Qian Z, Xu H, et al. A novel set of DNA methylation markers in urine sediments for sensitive/specific detection of bladder cancer. *Clin Cancer Res* 2007;13:7296-304.
 35. Vinci S, Giannarini G, Selli C, Kuncova J, Villari D, Valent F, et al. Quantitative methylation analysis of BCL2, hTERT, and DAPK promoters in urine sediment for the detection of non-muscle-invasive urothelial carcinoma of the bladder: a prospective, two-center validation study. *Urol Oncol* 2011;29:150-6.
 36. Ward DG, Baxter L, Gordon NS, Ott S, Savage RS, Beggs AD, et al. Multiplex PCR and next generation sequencing for the non-invasive detection of bladder cancer. *PLoS One* 2016;11:e0149756.
 37. Kim J, Mouw KW, Polak P, Braunstein LZ, Kamburov A, Kwiatkowski DJ, et al. Somatic ERCC2 mutations are associated with a distinct genomic signature in urothelial tumors. *Nat Genet* 2016;48:600-6.
 38. Burns MB, Temiz NA, Harris RS. Evidence for APOBEC3B mutagenesis in multiple human cancers. *Nat Genet* 2013;45:977-83.
 39. Nagata M, Muto S, Horie S. Molecular biomarkers in bladder cancer: novel potential indicators of prognosis and treatment outcomes. *Dis Markers* 2016;2016:8205836.
 40. Zhang X, Zhang Y. Bladder cancer and genetic mutations. *Cell Biochem Biophys* 2015;73:65-9.
 41. Nickerson ML, Witte N, Im KM, Turan S, Owens C, Misner K, et al. Molecular analysis of urothelial cancer cell lines for modeling tumor biology and drug response. *Oncogene* 2017;36:35-46.
 42. Seiler R, Thalmann GN, Rotzer D, Perren A, Fleischmann A. CCND1/CyclinD1 status in metastasizing bladder cancer: a

- prognosticator and predictor of chemotherapeutic response. *Mod Pathol* 2014;27:87-95.
43. Dadhania V, Zhang M, Zhang L, Bondaruk J, Majewski T, Siefker-Radtke A, et al. Meta-analysis of the luminal and basal subtypes of bladder cancer and the identification of signature immunohistochemical markers for clinical use. *EBioMedicine* 2016;12:105-17.
 44. Ross JS, Wang K, Al-Rohil RN, Nazeer T, Sheehan CE, Otto GA, et al. Advanced urothelial carcinoma: next-generation sequencing reveals diverse genomic alterations and targets of therapy. *Mod Pathol* 2014;27:271-80.
 45. Ross JS, Wang K, Gay LM, Al-Rohil RN, Nazeer T, Sheehan CE, et al. A high frequency of activating extracellular domain ERBB2 (HER2) mutation in micropapillary urothelial carcinoma. *Clin Cancer Res* 2014;20:68-75.
 46. Moss TJ, Qi Y, Xi L, Peng B, Kim TB, Ezzedine NE, et al. Comprehensive genomic characterization of upper tract urothelial carcinoma. *Eur Urol* 2017;72:641-9.
 47. Pietzak EJ, Bagrodia A, Cha EK, Drill EN, Iyer G, Isharwal S, et al. Next-generation sequencing of nonmuscle invasive bladder cancer reveals potential biomarkers and rational therapeutic targets. *Eur Urol* 2017;72:952-9.
 48. Choi W, Ochoa A, McConkey DJ, Aine M, Höglund M, Kim WY, et al. Genetic alterations in the molecular subtypes of bladder cancer: illustration in the cancer genome atlas dataset. *Eur Urol* 2017;72:354-65.
 49. Abbosh PH, McConkey DJ, Plimack ER. Targeting signaling transduction pathways in bladder cancer. *Curr Oncol Rep* 2015;17:58.
 50. Christensen E, Birkenkamp-Demtröder K, Nordentoft I, Høyer S, van der Keur K, van Kessel K, et al. Liquid biopsy analysis of FGFR3 and PIK3CA hotspot mutations for disease surveillance in bladder cancer. *Eur Urol* 2017;71:961-9.
 51. Ding XL, Yang X, Liang G, Wang K. Isoform switching and exon skipping induced by the DNA methylation inhibitor 5-Aza-2'-deoxycytidine. *Sci Rep* 2016;6:24545.
 52. Jenuwein T, Allis CD. Translating the histone code. *Science* 2001;293:1074-80.
 53. Kouzarides T. Chromatin modifications and their function. *Cell* 2007;128:693-705.
 54. Gui Y, Guo G, Huang Y, Hu X, Tang A, Gao S, et al. Frequent mutations of chromatin remodeling genes in transitional cell carcinoma of the bladder. *Nat Genet* 2011;43:875-8.
 55. Wolff EM, Byun HM, Han HF, Sharma S, Nichols PW, Siegmund KD, et al. Hypomethylation of a LINE-1 promoter activates an alternate transcript of the MET oncogene in bladders with cancer. *PLoS Genet* 2010;6:e1000917.
 56. Kim EJ, Kim YJ, Jeong P, Ha YS, Bae SC, Kim WJ. Methylation of the RUNX3 promoter as a potential prognostic marker for bladder tumor. *J Urol* 2008;180:1141-5.
 57. Costa-Pinheiro P, Montezuma D, Henrique R, Jerónimo C. Diagnostic and prognostic epigenetic biomarkers in cancer. *Epigenomics* 2015;7:1003-15.
 58. Maruyama R, Toyooka S, Toyooka KO, Harada K, Virmani AK, Zöchbauer-Müller S, et al. Aberrant promoter methylation profile of bladder cancer and its relationship to clinicopathological features. *Cancer Res* 2001;61:8659-63.
 59. Marsit CJ, Karagas MR, Andrew A, Liu M, Danaee H, Schned AR, et al. Epigenetic inactivation of SFRP genes and TP53 alteration act jointly as markers of invasive bladder cancer. *Cancer Res* 2005;65:7081-5.
 60. Catto JW, Azzouzi AR, Rehman I, Feeley KM, Cross SS, Amira N, et al. Promoter hypermethylation is associated with tumor location, stage, and subsequent progression in transitional cell carcinoma. *J Clin Oncol* 2005;23:2903-10.
 61. Su SF, de Castro Abreu AL, Chihara Y, Tsai Y, Andreu-Vieyra C, Daneshmand S, et al. A panel of three markers hyper- and hypomethylated in urine sediments accurately predicts bladder cancer recurrence. *Clin Cancer Res* 2014;20:1978-89.
 62. Ratliff TL, Gillen D, Catalona WJ. Requirement of a thymus dependent immune response for BCG-mediated antitumor activity. *J Urol* 1987;137:155-8.
 63. Sweis RF, Galsky MD. Emerging role of immunotherapy in urothelial carcinoma-immunobiology/biomarkers. *Urol Oncol* 2016;34:556-65.
 64. Donin NM, Lenis AT, Holden S, Drakaki A, Pantuck A, Beldgrun A, et al. Immunotherapy for the treatment of urothelial carcinoma. *J Urol* 2017;197:14-22.
 65. Bitler BG, Aird KM, Garipov A, Li H, Amatangelo M, Koskenkov AV, et al. Synthetic lethality by targeting EZH2 methyltransferase activity in ARID1A-mutated cancers. *Nat Med* 2015;21:231-8.
 66. Balbás-Martínez C, Rodríguez-Pinilla M, Casanova A, Domínguez O, Pisano DG, Gómez G, et al. ARID1A alterations are associated with FGFR3-wild type, poor-prognosis, urothelial bladder tumors. *PLoS One* 2013;8:e62483.
 67. Scott SN, Ostrovnya I, Lin CM, Bouvier N, Bochner BH, Iyer G, et al. Next-generation sequencing of urine specimens: a novel platform for genomic analysis in patients with non-muscle-invasive urothelial carcinoma treated with bacille Calmette-Guérin. *Cancer Cytopathol* 2017;125:416-26.
 68. Kreunin P, Zhao J, Rosser C, Urquidi V, Lubman DM, Goodison S. Bladder cancer associated glycoprotein signatures revealed by urinary proteomic profiling. *J Proteome Res* 2007;6:2631-9.
 69. Li H, Li C, Wu H, Zhang T, Wang J, Wang S, et al. Identification of Apo-A1 as a biomarker for early diagnosis of bladder transitional cell carcinoma. *Proteome Sci* 2011;9:21.
 70. Li F, Chen DN, He CW, Zhou Y, Olkkonen VM, He N, et al.

- Identification of urinary Gc-globulin as a novel biomarker for bladder cancer by two-dimensional fluorescent differential gel electrophoresis (2D-DIGE). *J Proteomics* 2012;77:225-36.
71. Orenes-Piñero E, Barderas R, Rico D, Casal JI, Gonzalez-Pisano D, Navajo J, et al. Serum and tissue profiling in bladder cancer combining protein and tissue arrays. *J Proteome Res* 2010;9:164-73.
 72. Urquidi V, Chang M, Dai Y, Kim J, Wolfson ED, Goodison S, et al. Il-8 as a urinary biomarker for the detection of bladder cancer. *BMC Urol* 2012;12:12.
 73. Srinivasan H, Allory Y, Sill M, Vordos D, Alhamdani MS, Radvanyi F, et al. Prediction of recurrence of non muscle-invasive bladder cancer by means of a protein signature identified by antibody microarray analyses. *Proteomics* 2014;14:1333-42.
 74. Grau L, Luque-Garcia JL, González-Peramato P, Theodorescu D, Palou J, Fernandez-Gomez JM, et al. A quantitative proteomic analysis uncovers the relevance of CUL3 in bladder cancer aggressiveness. *PLoS One* 2013;8:e53328.
 75. Bansal N, Gupta A, Sankhwar SN, Mahdi AA. Low- and high-grade bladder cancer appraisal via serum-based proteomics approach. *Clin Chim Acta* 2014;436:97-103.
 76. Cheng Y, Yang X, Deng X, Zhang X, Li P, Tao J, et al. Metabolomics in bladder cancer: a systematic review. *Int J Clin Exp Med* 2015;8:11052-63.
 77. von Rundstedt FC, Rajapakshe K, Ma J, Arnold JM, Gohlke J, Putluri V, et al. Integrative pathway analysis of metabolic signature in bladder cancer: a linkage to the cancer genome atlas project and prediction of survival. *J Urol* 2016;195:1911-9.
 78. Bansal N, Gupta A, Mitash N, Shakya PS, Mandhani A, Mahdi AA, et al. Low- and high-grade bladder cancer determination via human serum-based metabolomics approach. *J Proteome Res* 2013;12:5839-50.
 79. Cao M, Zhao L, Chen H, Xue W, Lin D. NMR-based metabolomic analysis of human bladder cancer. *Anal Sci* 2012;28:451-6.
 80. Jin X, Yun SJ, Jeong P, Kim IY, Kim WJ, Park S. Diagnosis of bladder cancer and prediction of survival by urinary metabolomics. *Oncotarget* 2014;5:1635-45.
 81. Knowles MA, Hurst CD. Molecular biology of bladder cancer: new insights into pathogenesis and clinical diversity. *Nat Rev Cancer* 2015;15:25-41.
 82. Dyrskjøt L, Zieger K, Kruhøffer M, Thykjaer T, Jensen JL, Primdahl H, et al. A molecular signature in superficial bladder carcinoma predicts clinical outcome. *Clin Cancer Res* 2005;11:4029-36.
 83. Sjö Dahl G, Lauss M, Lövgren K, Chebil G, Gudjonsson S, Veerla S, et al. A molecular taxonomy for urothelial carcinoma. *Clin Cancer Res* 2012;18:3377-86.
 84. Yang M, Zheng Z, Zhuang Z, Zhao X, Xu Z, Lin H. Immuno-CytTM and cytology for diagnosis of bladder carcinoma: a meta analysis. *Chin Med J (Engl)* 2014;127:758-64.
 85. Siemens DR, Morales A, Johnston B, Emerson L. A comparative analysis of rapid urine tests for the diagnosis of upper urinary tract malignancy. *Can J Urol* 2003;10:1754-8.
 86. Naoe M, Ogawa Y, Morita J, Omori K, Takeshita K, Shichijyo T, et al. Detection of circulating urothelial cancer cells in the blood using the CellSearch System. *Cancer* 2007;109:1439-45.
 87. Flaig TW, Wilson S, van Bokhoven A, Varella-Garcia M, Wolfe P, Maroni P, et al. Detection of circulating tumor cells in metastatic and clinically localized urothelial carcinoma. *Urology* 2011;78:863-7.
 88. Qi F, Liu Y, Zhao R, Zou X, Zhang L, Li J, et al. Quantitation of rare circulating tumor cells by folate receptor α ligand-targeted PCR in bladder transitional cell carcinoma and its potential diagnostic significance. *Tumour Biol* 2014;35:7217-23.
 89. Anantharaman A, Friedlander T, Lu D, Krupa R, Premashekharan G, Hough J, et al. Programmed death-ligand 1 (PD-L1) characterization of circulating tumor cells (CTCs) in muscle invasive and metastatic bladder cancer patients. *BMC Cancer* 2016;16:744.
 90. Zhang T, Boominathan R, Foulk B, Rao C, Kemeny G, Strickler JH, et al. Development of a novel c-MET-based CTC detection platform. *Mol Cancer Res* 2016;14:539-47.
 91. Crowley E, Di Nicolantonio F, Loupakis F, Bardelli A. Liquid biopsy: monitoring cancer-genetics in the blood. *Nat Rev Clin Oncol* 2013;10:472-84.
 92. Kinde I, Munari E, Faraj SF, Hruban RH, Schoenberg M, Bivalacqua T, et al. TERT promoter mutations occur early in urothelial neoplasia and are biomarkers of early disease and disease recurrence in urine. *Cancer Res* 2013;73:7162-7.
 93. Gormally E, Vineis P, Matullo G, Veglia F, Caboux E, Le Roux E, et al. TP53 and KRAS2 mutations in plasma DNA of healthy subjects and subsequent cancer occurrence: a prospective study. *Cancer Res* 2006;66:6871-6.
 94. Fernandez-Mercado M, Manterola L, Larrea E, Goicoechea I, Arestin M, Armesto M, et al. The circulating transcriptome as a source of non-invasive cancer biomarkers: concepts and controversies of non-coding and coding RNA in body fluids. *J Cell Mol Med* 2015;19:2307-23.
 95. Malentacchi F, Vinci S, Melina AD, Kuncova J, Villari D, Nesi G, et al. Urinary carbonic anhydrase IX splicing messenger RNA variants in urogenital cancers. *Urol Oncol* 2016;34:292.e9-16.
 96. Xie XY, Yang X, Zhang JH, Liu ZJ. Analysis of hTERT expression in exfoliated cells from patients with bladder transitional cell carcinomas using SYBR green real-time fluorescence quantitative PCR. *Ann Clin Biochem* 2007;44:523-8.
 97. Sasaki H, Yoshiike M, Nozawa S, Usuba W, Katsuoka Y, Aida K, et al. Expression level of urinary MicroRNA-146a-5p is increased in patients with bladder cancer and decreased in those

- after transurethral resection. *Clin Genitourin Cancer* 2016;14:e493-9.
98. Yu S, Cao H, Shen B, Feng J. Tumor-derived exosomes in cancer progression and treatment failure. *Oncotarget* 2015;6:37151-68.
99. Nawaz M, Camussi G, Valadi H, Nazarenko I, Ekström K, Wang X, et al. The emerging role of extracellular vesicles as biomarkers for urogenital cancers. *Nat Rev Urol* 2014;11:688-701.
100. Berrondo C, Flax J, Kucherov V, Siebert A, Osinski T, Rosenberg A, et al. Expression of the long non-coding RNA HO-TAIR correlates with disease progression in bladder cancer and is contained in bladder cancer patient urinary exosomes. *PLoS One* 2016;11:e0147236.



Down-regulation of transient receptor potential melastatin member 7 prevents migration and invasion of renal cell carcinoma cells via inactivation of the Src and Akt pathway

Yun-Sok Ha^{1,2}, Yeon-Yong Kim^{3,4}, Na Hee Yu^{1,2}, So Young Chun^{1,2}, Seock Hwan Choi^{1,2}, Jun Nyung Lee^{1,2}, Bum Soo Kim^{1,2}, Eun Sang Yoo^{1,2}, Tae Gyun Kwon^{1,2}

¹Department of Urology, School of Medicine, Kyungpook National University, Daegu, ²Department of Urology, Kyungpook National University Hospital, Daegu, ³Department of Pharmacology, Kyungpook National University School of Medicine, Daegu, ⁴Immunoregulatory Material Research Center, Korea Research Institute of Bioscience and Biotechnology (KRIBB), Jeongeup, Korea

Purpose: Transient receptor potential melastatin member 7 (TRPM7), an ion channel and serine/threonine protein kinase, has been linked with distinct human malignancies. However, the role of TRPM7 in renal cell carcinoma (RCC) has not been investigated. The aim of this study is to determine whether TRPM7 regulates the migration and invasion of RCC cells. Its relationship with signal transduction pathways was also studied.

Materials and Methods: The human RCC cell lines ACHN and SN12C were chosen for this study. The molecular mechanisms of TRPM7 action were studied using Western blot analysis and small interfering RNA (siRNA)-based knockdown. The effect of TRPM7 knockdown on RCC cells was measured by using Transwell invasion and wound healing migration assays.

Results: siRNA-induced silencing of TRPM7 notably decreased the migration and invasion of ACHN and SN12C RCC cells. The phosphorylation levels of Src in both cells were obviously reduced after TRPM7 silencing compared with that of the control ACHN and SN12C cells. Furthermore, the phosphorylation levels of Akt were greatly decreased in ACHN cells after siRNA-induced knockdown of TRPM7. Additionally, the treatment of cells with Src and Akt inhibitors clearly limited the migration and invasion of RCC cells.

Conclusions: Our data show that TRPM7 regulated ACHN and SN12C RCC cell invasion via the Src/Akt signaling pathway. Therefore, targeting the Src/Akt signaling pathway and/or the expression or function of TRPM7 could be a potential beneficial treatment for patients with RCC.

Keywords: Carcinoma, renal cell; Neoplasm invasiveness; Neoplasm metastasis; Signal transduction

This is an Open Access article distributed under the terms of the Creative Commons Attribution Non-Commercial License (<http://creativecommons.org/licenses/by-nc/4.0>) which permits unrestricted non-commercial use, distribution, and reproduction in any medium, provided the original work is properly cited.

Received: 15 December, 2017 • **Accepted:** 17 April, 2018

See Editorial on page 273

Corresponding Author: Tae Gyun Kwon

Department of Urology, Kyungpook National University Chilgok Hospital, 807 Hoguk-ro, Buk-gu, Daegu 41404, Korea

TEL: +82-53-420-5841, FAX: +82-53-421-9618, E-mail: tgkwon@knu.ac.kr

ORCID: <http://orcid.org/0000-0002-4390-0952>

INTRODUCTION

Renal cell carcinoma (RCC) accounts for 3% of all cancers and 90% of all kidney cancers. RCC is also the third most recurrent urologic tumor [1,2]. At first diagnosis, circa 30% of patients with RCC have metastases. Additionally, 20% of the patients diagnosed with a clinically localized disease will develop metastases, regardless of the use of curative nephrectomy. Therefore, the mean survival of metastatic RCC is only 12 months [3-5]. Furthermore, limited therapeutic options are currently available. For instance, metastatic RCC is insensitive to chemotherapy, and drugs for targeted therapies and immunotherapies are ineffective in the treatment of this disease [6]. Thus, there is an urgent need to explore novel therapeutic agents against metastatic RCC.

Transient receptor potential melastatin member 7 (TRPM7) is a nonselective cation channel. Furthermore, it is a member of the diverse TRPM subfamily and part of the transient receptor potential (TRP) superfamily [7]. A recent study showed the participation of TRP channels in cell homeostasis, including cell proliferation, differentiation, apoptosis [8]. Specifically, TRPM7 is well known as an essential regulator of Mg^{2+} homeostasis and a transporter of other cations [9,10]. Structurally, TRPM7 is comparable to TRPs and possesses six transmembrane domains, which form a hydrophobic central pore or channel. Additionally, TRPM7 transmembrane domains have amino- and carboxyl-terminals (N- and C-terminals) facing the intracellular side of the cell membrane flanking the transmembrane segments [11]. TRPM7 is a bifunctional protein that has the ability to function as an ion channel and a protein kinase, participating in cancer and other diseases. Indeed, some TRP channels have been associated with the growth and development of cancer [12] and recent research has suggested some mechanisms underlying the role of TRPM7 in human cancers. Nonetheless, the functional relationship between TRPM7 and RCC has not been well documented. Moreover, the effect of TRPM7 knockdown on RCC cell migration and invasion and the underlying mechanism have not yet been determined. Hence, we aimed to explore the role of TRPM7 in RCC.

MATERIALS AND METHODS

This study was approved by the Institutional Review Board of Kyungpook National University Chilgok Hospital (approval number: KNUMC 2016-05-021).

1. Cell culture

The ACHN, SN12C, Caki-1, and Caki-2 cell lines were obtained from the Korean Cell Line Bank (Seoul, Korea) and American Type Culture Collection (ATCC, Manassas, VA, USA). All kidney cancer cells were grown in Dulbecco's modified Eagle's medium (DMEM) (Hyclone, Logan, UT, USA) supplemented with penicillin (100 U/mL), streptomycin (100 mg/mL), and 10% fetal bovine serum (FBS) and incubated at 37°C in a humidified atmosphere containing 5% (v/v) CO_2 .

2. TRPM7 small interfering RNA (siRNA) and transfection

AccuTarget Predesigned siRNAs specific for human TRPM7 and scramble siRNAs purchased from Bioneer (Daejeon, Korea) were used to knockdown TRPM7 expression. The sequences for human TRPM7 siRNA were Fwd 5'-GUC UUG CCA UGA AAU ACU CUU-3' and Rev 5'-GAG UAU UUC AUG GCA AGA CUU-3'. For transient transfection, cells were grown to 80% confluence, and Lipofectamine[®] RNAiMAX (13778-150; Invitrogen, Carlsbad, CA, USA) was used. Knockdown efficiency was determined using Western blot analysis.

3. Reverse transcriptase-polymerase chain reaction (PCR)

Total RNA was isolated using the TRIzol reagent. The Revert Aid First strand cDNA synthesis kit (K1621; Thermo Fisher Scientific, Waltham, MA, USA) was used for reverse transcription. PCR was performed by using a Maxime PCR Premix (25025; iNtRON Biotech, Seongnam, Korea). The cycling conditions were as follows: 95°C for 2 minutes and 35 cycles at 94°C for 20 seconds, 56°C for 40 seconds, and 72°C for 90 seconds. The primers for TRPM7 were Fwd 5'-TAG CCT TTA GCC ACT GGA C-3' and Rev 5'-GCA TCT CCT AGA TTT GC-3'. For β -actin, the primers were Fwd 5'-CAT CCT GCG TCT GGA CCT G-3' and Rev 5'-ATC TCC TTC TGC ATC CTG TC-3'.

4. Western blot analysis

Total cell lysates were prepared in lysis buffer (#9803; Cell Signaling Technology, Beverly, MA, USA) and centrifuged at 14,000 $\times g$ for 10 minutes. Proteins (50 μg) were loaded into a sodium dodecyl sulfate-polyacrylamide gel and transferred onto nitrocellulose membranes for immunoblotting analysis. An anti- β -actin antibody (#4967, rabbit polyclonal, 1:1,000; Cell Signaling Technology) was used as an internal loading control. An anti-TRPM7 antibody (ab85016, mouse monoclonal, 1:1,000) was purchased

from Abcam (Cambridge, UK), and the rabbit polyclonal antibodies (1:1,000) against matrix metalloproteinase (MMP)-2 (#4022), MMP-9 (#2270s), Akt (#9272), phospho-Akt (#9271, Ser473), p38 (#9212), phospho-p38 (#9211, Thr180/Tyr182), Src (#2108), phospho-Src (#2105, Tyr527), ERK1/2 (#9102), phospho-ERK1/2 (#9101, Thr202/Tyr204), JNK (#9252), phospho-JNK (#9251, Thr183/Tyr185) were purchased from Cell Signaling Technology. Immunoreactive protein bands were visualized using a chemiluminescent substrate (Thermo Fisher Scientific).

5. Cell proliferation assay

For the cell viability assay, ACHN and SN12C cells were seeded at 1×10^5 cells/mL and cultured for 24 hours before transfection with 50 to 100 pmole/ μ L siRNA for 24 hours. After treatment, 20 μ L/well of MTS from a cell proliferation colorimetric assay kit (K300; BioVision, Milpitas, CA, USA) was added, followed by a 2-hour incubation at 37°C in the dark. Subsequently, the medium was removed, and the formazan precipitate was dissolved in dimethyl sulfoxide (34869; Sigma-Aldrich, St. Louis, MO, USA). The absorbance of the formazan product was measured at 490 nm using an enzyme-linked immunosorbent assay (ELISA) reader (BioTek, Winooski, VT, USA).

6. Wound healing assay

For wound healing assay, the surface of cell monolayers in 6-well plates were scratched with a pipette tip. The wounded cells were washed several times with phosphate-buffered saline to eliminate debris. Subsequently, DMEM containing Lipofectamine (25 pmole) and TRPM7 siRNA (50–100 pmole) were added into the scratched wells. The cells were then incubated for 24 hours at 37°C. The initial wound

and migration of the cells into the scratched area were photographically monitored and imaged at 0 and 24 hours using an Olympus CKX41 inverted microscope coupled with a digital imaging system.

7. In vitro migration assay

A 24-well Transwell plate system (Costar; Corning Inc., Corning, NY, USA) was used to analyze cell migration. Kidney cancer cells were implanted at a density of 5×10^4 cells/well onto 8.0 μ m Transwell inserts. Inserts were filled with 300 μ L of cell suspension, and the lower chamber was filled with 700 μ L of DMEM containing 10% FBS. The cells were incubated for 24 hours or 48 hours at 37°C (5% CO₂). Pictures (at 40 \times magnification) of the membrane were taken in 10 random fields per chamber. After imaging, all Transwell membranes were harvested by incubating the inserts in 100 μ L of DMSO for 20 minutes. An ELISA reader (BioTek) was used to detect the absorbance intensity at 595 nm. Each experiment was performed in triplicate.

8. In vitro invasion assay

Invasion assays were performed as previously described. Briefly, 300 μ L of cell suspensions (5×10^4 cells) in DMEM supplemented with 10% FBS were added into Matrigel-coated invasion chambers (8.0- μ m, 24-well plates, Costar; Corning Inc.) for 2 hours at 37°C. Photographs were taken, and membranes were harvested by incubating the wells in 100 μ L DMSO for 20 minutes. Absorbance was measured at 595 nm on an ELISA reader (BioTek).

9. Inhibitor treatments

Src (ab141987, SKI-606, Bosutinib) and Akt1/2 (#9901, LY294002) inhibitors obtained from Sigma-Aldrich and

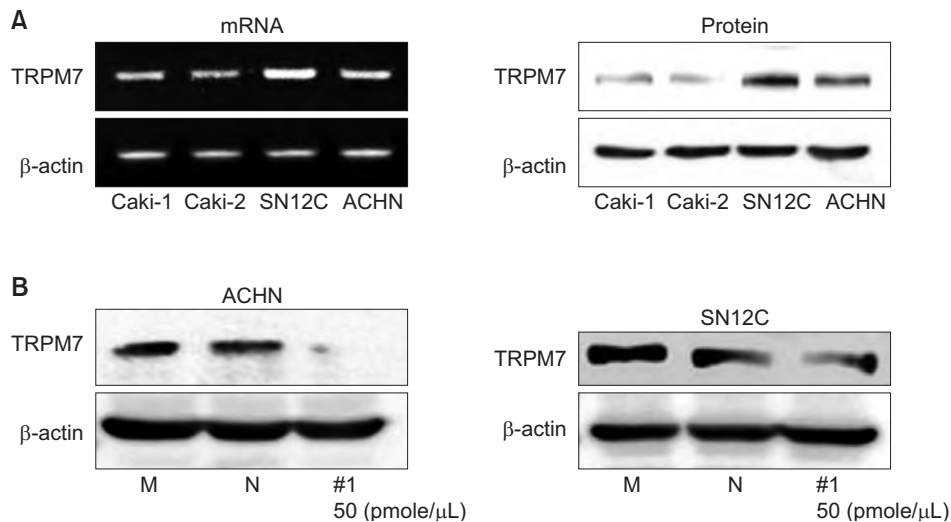


Fig. 1. (A) Differentially expressed mRNA and protein levels of transient receptor potential melastatin member 7 (TRPM7) in various renal cell carcinoma lines. ACHN and SN12C cells were selected for gene silencing experiments because of the higher expression levels of TRPM7. (B) Small interfering RNA-mediated knock-down of TRPM7 in ACHN and SN12C cell lines analyzed by Western blotting. β -actin was used as an internal loading control. The band is a representative of three independent experiments. M, mock; N, negative control.

Abcam, respectively; were used in *in vitro* migration and invasion assays.

10. Statistical analysis

Data were expressed as mean±standard error. Student's t-test and ANOVA were used to compare groups and determine statistical significance. All statistical analyses were performed using the Statistical Package for the Social Sciences with PASW Statistics ver. 18.0 software (IBM Co., Armonk, NY, USA). A p-value <0.05 was considered statistically significant.

RESULTS

1. TRPM7 expression and knockdown

To determine whether TRPM7 is expressed in RCC cell lines, TRPM7 mRNA and protein expression levels were assessed in different RCC cells (Caki-1, Caki-2, SN12C, and ACHN cell lines). As TRPM7 was more highly expressed in ACHN and SN12C cells than in the other cell types, they were selected for knockdown experiments (Fig. 1A). TRPM7 siRNA was used to knockdown its expression, and the efficiency of this knockdown was determined by analysis the protein expression levels of TRPM7 by Western blot. The results show that TRPM7 expression was successfully silenced with TRPM7 siRNA in both ACHN and SN12C RCC cells compared with that in mock and negative control cells (Fig. 1B).

2. Effect of TRPM7 silencing on RCC cell growth

To assess the effects of *TRPM7* gene silencing on RCC

cells, we first analyzed cell viability using the MTS assay. After transfection of ACHN and SN12C cells with TRPM7 siRNA at different doses, silencing of TRPM7 had a weak suppressive effect on ACHN cells, but this effect was not significant. Moreover, silencing of TRPM7 had no effect on SN12C cell viability (Fig. 2).

3. Migration and invasion are suppressed in TRPM7 siRNA-transfected RCC cells

Next, we focused on whether *TRPM7* gene silencing influences the migration and invasion ability of RCC cells. Cells that were 90% confluent were scratched with a pipette tip and incubated with either TRPM7 siRNA, mock siRNA, or negative control (transfection reagent alone) for 24 hours. As demonstrated in Fig. 3, a decrease in cell migration to the scratched area was observed following TRPM7 siRNA treatment. Subsequently, the effect of TRPM7 siRNA on the migration of RCC cells was examined by Transwell assays. As shown in Fig. 4A, knockdown of TRPM7 significantly inhibited the migration ability of ACHN and SN12C cells. Furthermore, the effect of TRPM7 siRNA on the metastatic potential of the RCC cells was examined by using an invasion assay. The invasive rates were reduced by TRPM7 siRNA transfection (Fig. 4), suggesting that silencing TRPM7 expression inhibits the metastatic potential of RCC cells.

4. TRPM7 gene silencing leads to a decrease in the phosphorylation Src and Akt

To determine the mechanism of action by which TRPM7 influences the migration and invasion of RCC cells,

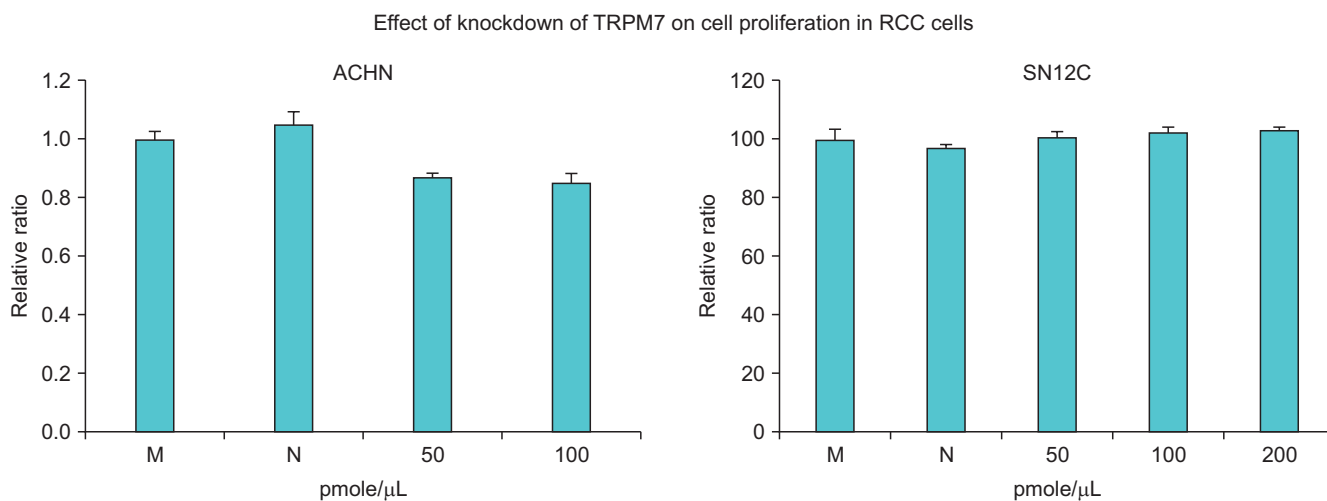


Fig. 2. Effect of the small interfering RNA (siRNA)-mediated knockdown of transient receptor potential melastatin member 7 (TRPM7) on the viability of renal cell carcinoma (RCC) cells. The viability of RCC cells was measured by MTS assay after transfection with TRPM7 siRNA. No significant effect on viability were induced by silencing of TRPM7. M, mock; N, negative control.

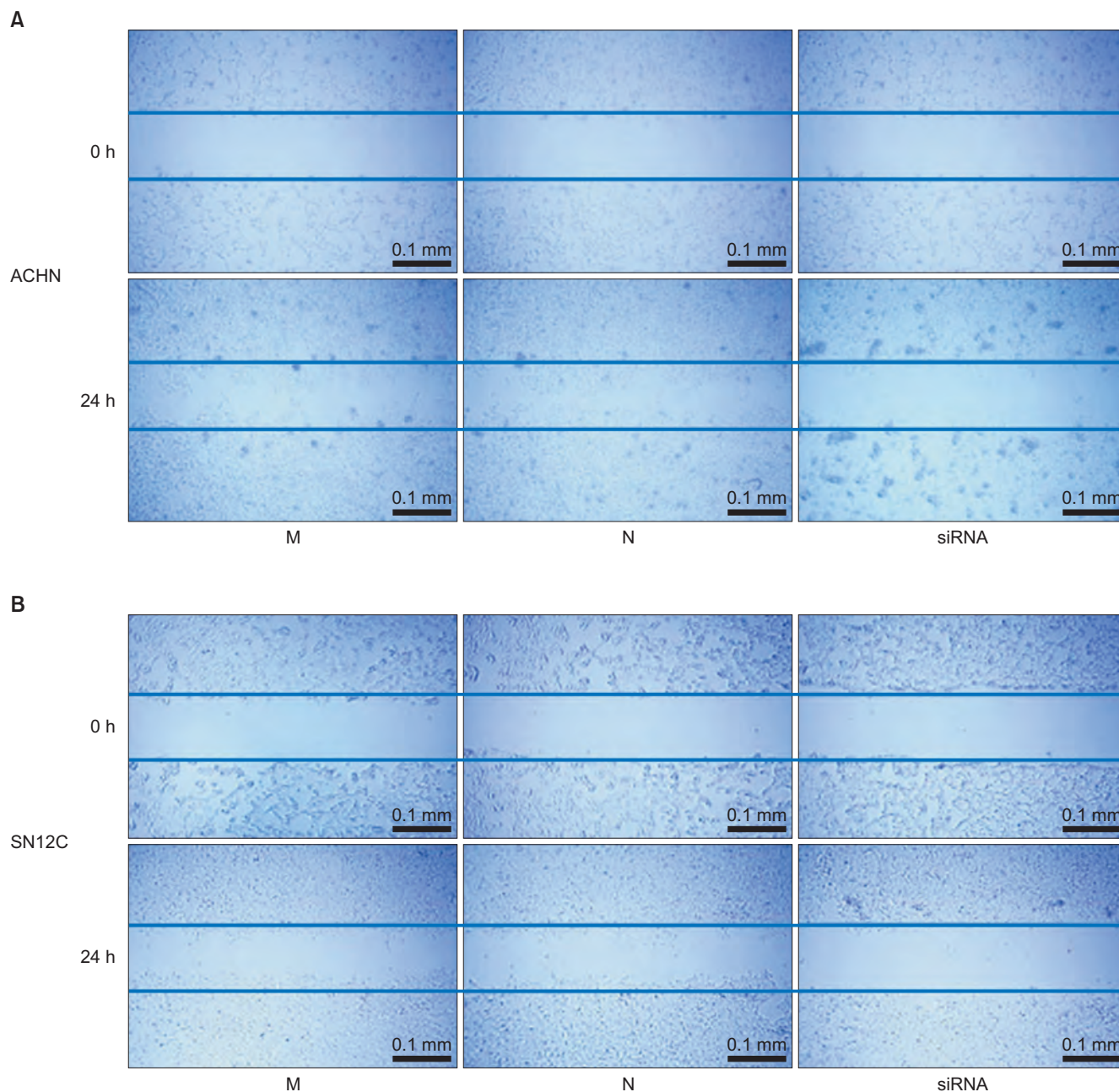


Fig. 3. Effect of transient receptor potential melastatin member 7 (TRPM7) small interfering RNA (siRNA) on cell migration. Wound healing assays reveal a significant decrease in migration of renal cell carcinoma cells after TRPM7 knockdown for 24 hours. (A) ACHN cells. (B) SN12C cells. M, mock; N, negative control.

the phosphorylation of Src, ERK, JNK, p38, and Akt was examined by immunoblotting. After silencing of TRPM7, a considerable decrease in the phosphorylation level of Src was observed compared to that with mock siRNA and negative control (Fig. 5). Similarly, the phosphorylation level of Akt in ACHN RCC cells was reduced considerably after silencing of TRPM7 compared to that with mock siRNA (Fig. 5). To confirm that TRPM7 knockdown-mediated inhibition of migration and invasion is indeed linked to Src

and Akt phosphorylation, the cells were treated with the Src inhibitor SKI-606 and the Akt inhibitor LY294002. Fig. 6A shows that treatment with Akt or Src inhibitor reduced the migration ability of ACHN cells in wound healing assays. Moreover, the Src inhibitor decreased the migration of SN12C cells to the scratched area (Fig. 6B). In Fig. 7A, the Transwell assay showed that the Src inhibitor significantly inhibited the migration ability of ACHN and SN12C cells. In ACHN cells, the Akt inhibitor considerably suppressed

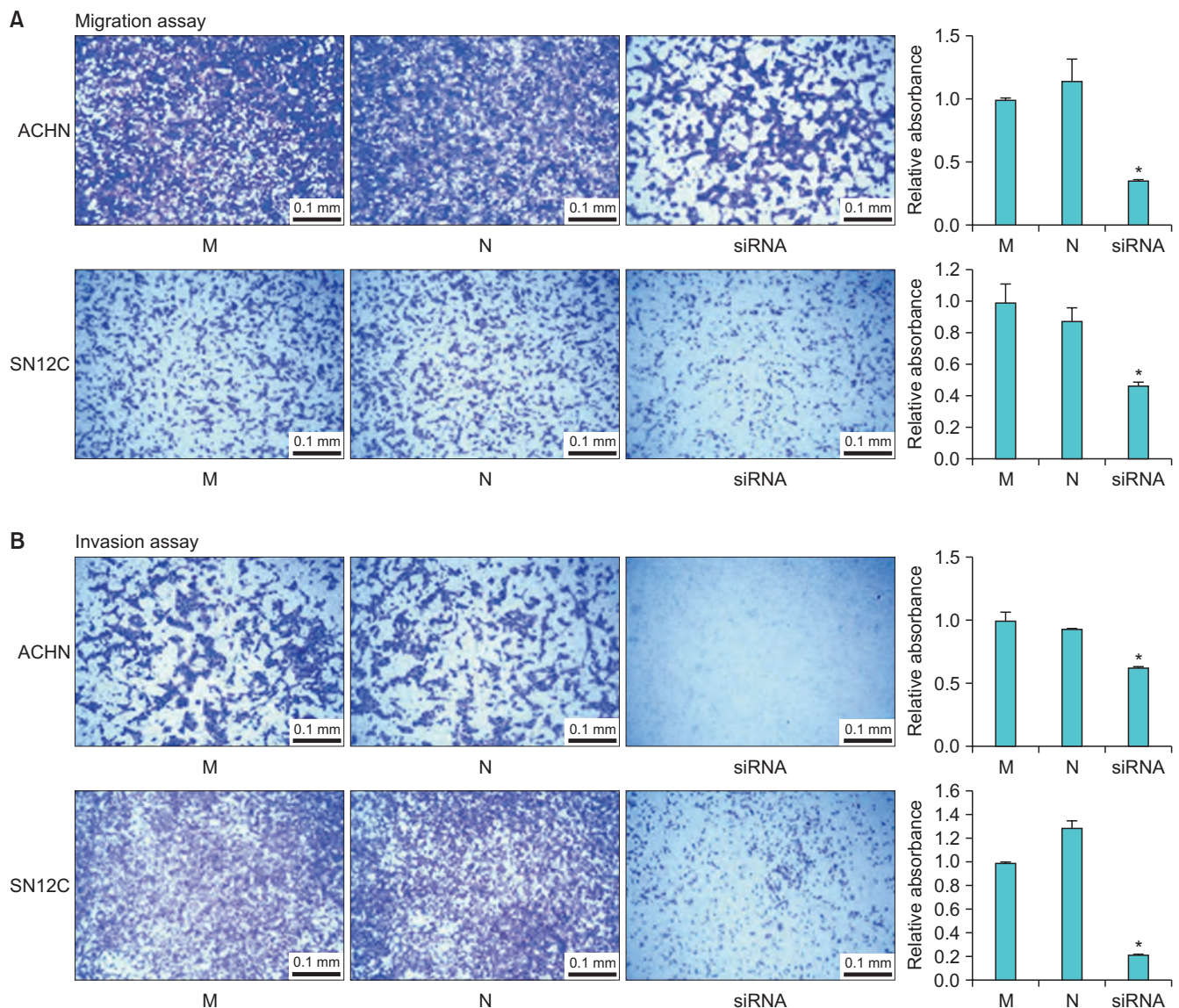


Fig. 4. Effect of small interfering RNA (siRNA)-mediated knockdown of transient receptor potential melastatin member 7 (TRPM7) on the migration and invasion of ACHN and SN12C cells. (A) Effect of TRPM7 siRNA on the migration of renal cell carcinoma (RCC) cells was examined by Transwell assay. The difference in migration was measured as a fold change in absorbance as compared to mock (M) siRNA. The Transwell assay showed that knockdown of TRPM7 significantly inhibited the migration ability of ACHN and SN12C cells. (B) Invasion of RCC cells was investigated by using Matrigel-coated chambers. The number of invading cells was presented as a fold difference relative to M siRNA. The invasion rates were reduced by TRPM7 siRNA transfection, suggesting that silencing of TRPM7 inhibits the metastatic potential of RCC cells. Bar graph shows quantitative analysis of crystal violet extracted from the cells placed under the Transwell. *Significant difference at $p < 0.05$. N, negative control.

cell migration as indicated by the Transwell assay (Fig. 7A). The effect of Src and Akt inhibition on RCC invasion was also examined using an invasion assay. Invasion rates were reduced by inhibition of both Src and Akt, suggesting that TRPM7 silencing inhibits the metastatic potential of RCC cells via inactivation of the Src and Akt signaling pathways (Fig. 7B).

5. TRPM7 knockdown in RCC cells is not linked to MMP-2 and MMP-9 expression

Recently, a study has reported that MMP-9 expression

is associated with migration, invasion, and aggressiveness of tumor cells [13]. Thus, we examined whether TRPM7 knockdown inhibits the expression of MMP-2 and MMP-9 in RCC cells. MMP-2 and MMP-9 were not reduced by TRPM7 siRNA transfection of RCC cells (Fig. 8).

DISCUSSION

To date, kidney cancer remains the ninth most prevalent malignancy among men, with an estimated 1,131 deaths in Korea in 2017 [14]. Kidney cancer progression varies from

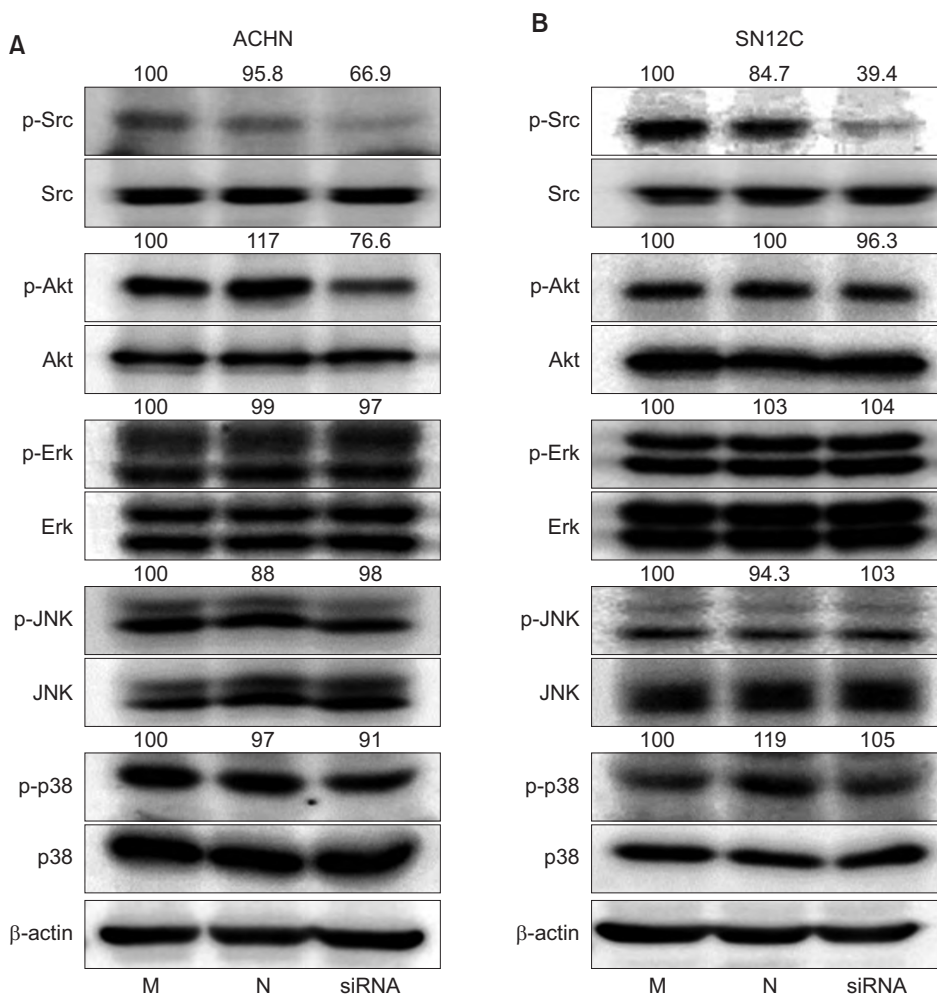


Fig. 5. Effect of transient receptor potential melastatin member 7 (TRPM7) down-regulation on Akt and Src phosphorylation in renal cell carcinoma cells. (A) In ACHN cells, the phosphorylation levels of Akt and Src were significantly reduced by the small interfering RNA (siRNA)-mediated knockdown of TRPM7. (B) Western blot images show decreased phosphorylation of Src in SN12C cells following transfection with TRPM7 siRNA. M, mock; N, negative control.

slow to highly aggressive. When kidney cancer metastasizes, the mean survival of patients is limited. Given the heterogeneity of RCC, the vigorous study of the underlying molecular mechanisms is a sensible approach [15]. Moreover, metastasis of RCC is a significant obstacle for the systemic treatment of this disease [16,17]. Metastasis, the migration of tumor cells from their original site to distant organs, is an intricate multistep mechanism, which involves complex cell adhesion, invasion, and migration [18]. Despite the significance of metastasis to RCC survival and morbidity, little is known on the cellular and molecular mechanisms mediating RCC metastasis.

TRPM7, a well-known member of the TRP protein family, is an ion channel and protein kinase that is ubiquitously expressed in several normal tissues [9]. Recently, TRPM7 has been implicated in cancer metastasis and carcinogenesis [19]. In this study, the evidence collected from wound healing and Transwell assays distinctly shows reduced migration and invasion in ACHN and SN12C RCC cells after the silencing of TRPM7 (Figs. 3, 4). However, cell proliferation remained unaffected (Fig. 2). These results

suggest that TRPM7 plays an important role in the invasion phenotype of ACHN and SN12C RCC cells. A recent study showed that depressing the function of TRPM7 is known to inhibit the migration and invasion of MDA-MB-435 breast cancer cells, which is consistent with our data [19]. Besides, up-regulation of TRPM7 augments the migration of A549 lung cancer cells and vascular smooth muscle cells [20,21].

Although there is a substantial amount of evidence that indicates that TRPM7 is required for controlling cell migration and invasion, the signaling pathways that mediate its action remain largely undiscovered. In the current study, we investigated the expression and activation of various signaling molecules to examine the pathways involved in RCC migration and invasion that are dependent on TRPM7. Akt, the main signal transducer of the phosphoinositide 3-kinase (PI3K) pathway, promotes the progression of tumor cells by inhibiting apoptosis, promoting cell proliferation, and regulating cell migration and invasion [22]. In RCC, the PI3K/Akt pathway is moderately mutated but highly activated. A large number of patients with RCC were recently involved in an extensive integrated

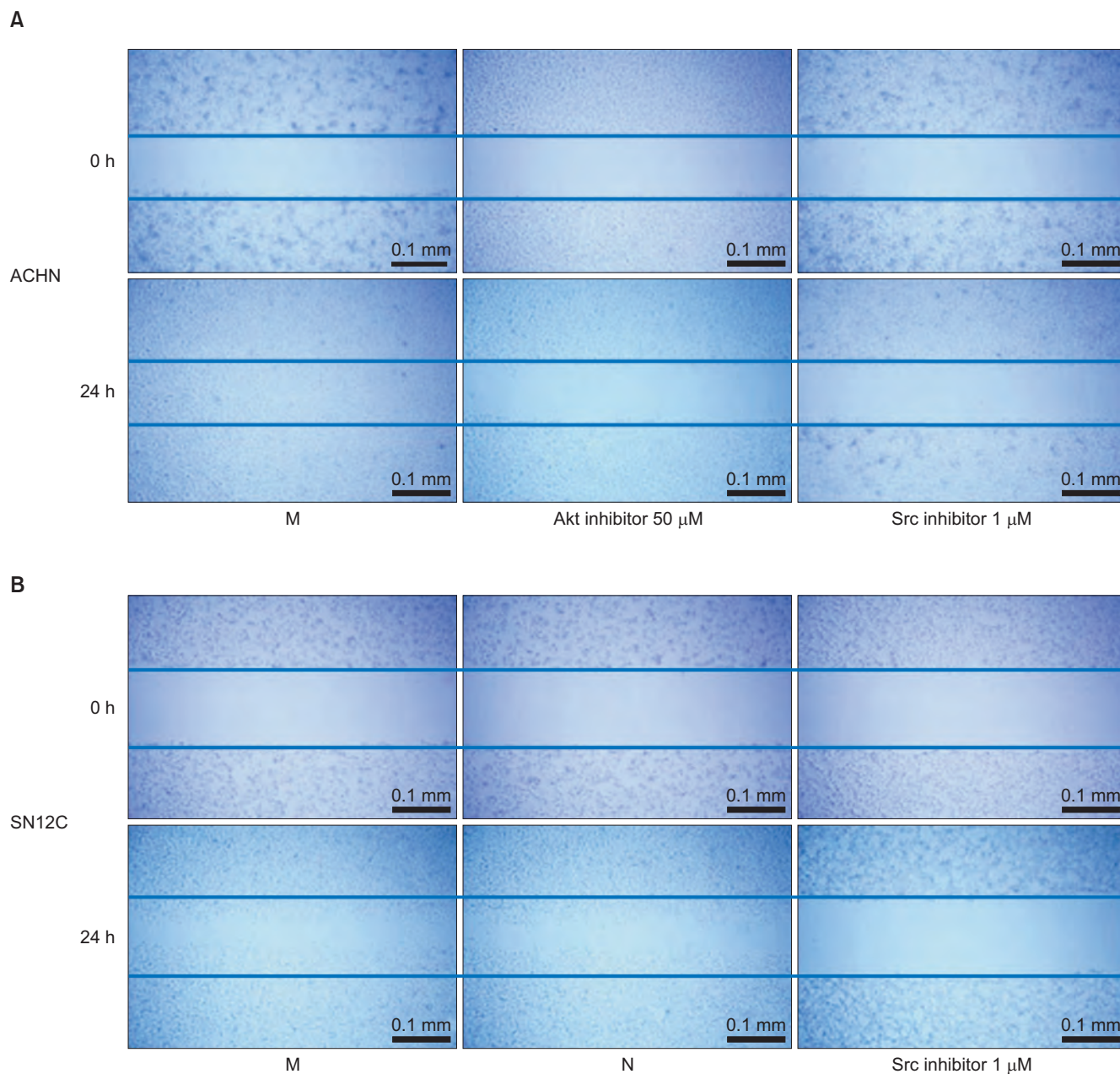


Fig. 6. Effect of Akt and Src inhibition on cell migration. (A) Treatment with Akt or Src inhibitor of ACHN cells reduced cell migration in wound healing assays. (B) In SN12C cells, the Src inhibitor decreased the cell migration to the scratched area. M, mock; N, negative control.

analysis of the PI3K/Akt pathway. The results reiterated the crucial role of the PI3K/Akt pathway in this cancer [23]. Indeed, PI3K pathway inhibitors of the rapalog family have been approved for use in RCC therapy [24]. Our data show that activity of Akt was altered, when the migration and invasion capacity of ACHN cells was decreased by the silencing of TRPM7 (Fig. 5). Moreover, the Akt1/2 inhibitor LY294002 further reinforced the role of Akt in cell migration and invasion of RCC (Figs. 6, 7). Therefore, the conjecture that the TRPM7-mediated migration and invasion of ACHN RCC cells was associated with the Akt

signaling pathway is justified. Nevertheless, these results were not apparent in SN12C cells.

Cancer metastasis generally involves the complex coordination of signal transduction pathways. As these signaling pathways control cancer cell migration, invasion, and the reestablishment of tumors, the potential role of Src and mitogen-activated protein kinase (MAPK) in RCC metastasis was considered and studied. These two signaling pathways are known to regulate crucial occurrences in metastasis, such as cancer cell invasion and migration [25,26]. Indeed, a previous study indicated that a member of

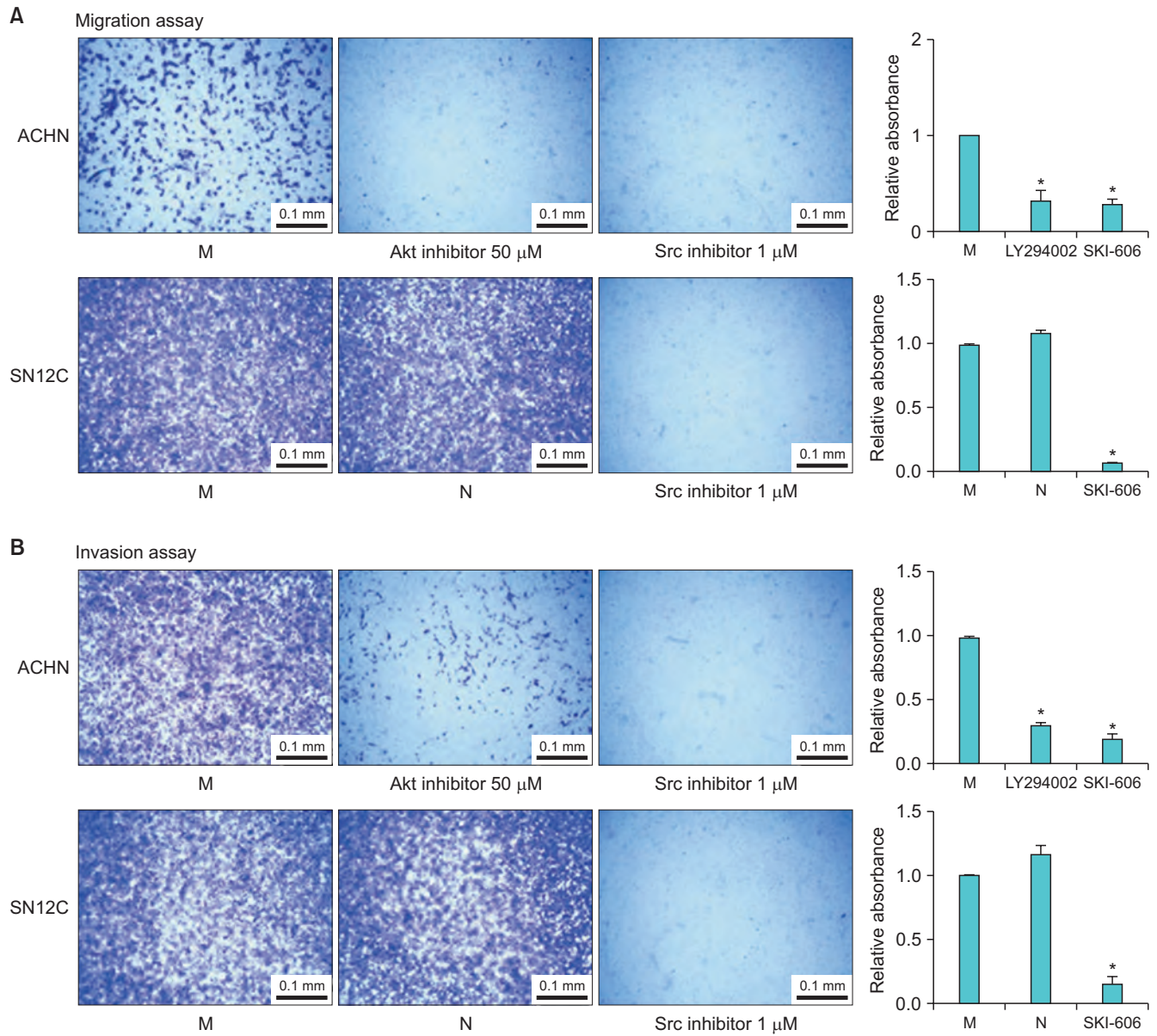


Fig. 7. Effect of Akt and Src inhibition on cell migration and invasion. (A) Transwell assays show that Src inhibition significantly inhibited the migration ability of ACHN and SN12C cells. In ACHN cells, the Akt inhibitor was effective in inhibiting cell migration. (B) The effect of Src and Akt inhibition on the invasion capabilities of renal cell carcinoma (RCC) cells was also examined. Src and Akt inhibitors reduced RCC invasion rates, suggesting that transient receptor potential melastatin member 7 silencing inhibits the metastatic potential of RCC cells via inactivation of the Src and Akt signaling pathways. Bar graph shows quantitative analysis of crystal violet extracted from the cells placed under the Transwell. *Significant difference at $p < 0.05$. M, mock; N, negative control.

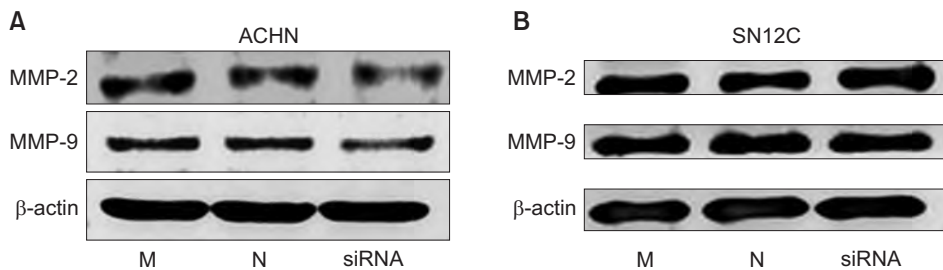


Fig. 8. Effect of transient receptor potential melastatin member 7 (TRPM7) down-regulation on matrix metalloproteinase (MMP)-2 and MMP-9 phosphorylation in ACHN (A) and SN12C renal cell carcinoma (RCC) cells (B). MMP-2 and MMP-9 were not reduced by TRPM7 small interfering RNA (siRNA) transfection of RCC cells. M, mock; N, negative control.

the Src kinase family is associated with a poor prognosis in patients with RCC and could be a potential therapeutic target for RCC [27]. Moreover, a recent study identified that the activation of p38-MAPK signaling was associated with RCC metastasis [28]. Our data demonstrated that the siRNA-mediated silencing of TRPM7 led to a considerable reduction in the migration and invasion capacity of ACHN and SN12C cells and concomitant inactivation of Src (Fig. 5). This suggests that TRPM7 alteration of the migration and invasion of RCC cells involves the Src signaling pathway. To support these findings, ACHN and SN12C cells were treated with the Src inhibitor SKI-606 (Figs. 6, 7). The results indicated that the inhibition of Src reduced the migration and invasion abilities of these cells. Similar results were seen in a previous report in which Src inhibition promoted tumor cell inhibition in RCC [29]. Epithelial-mesenchymal transition in RCC cells is known to involve both the Src and Akt signaling pathways [30]. Notwithstanding, our data indicated that when the migration and invasion capability of RCC cells was reduced by silencing of TRPM7, the activity of MAPKs, including p38, ERK1/2, and JNK1/2, was not affected.

The current study has some limitations. Overexpression experiments should be performed to identify the exact role of TRPM7 in RCC cells. Moreover, TRPM7 expression in human RCC tissues should be measured. To elucidate the precise effects of TRPM7 in RCC, further studies such as expression studies in human tissues are needed.

CONCLUSIONS

To the best of our knowledge, this is the first report to address TRPM7 function and mechanism of action in RCC. We provide compelling evidence that TRPM7 channels play an important role in the migration and invasion of cancer cells in human RCC. There is also significant evidence that the signaling route is through the Akt and Src pathways. In conclusion, TRPM7 down-regulation reduced the migration and invasion activity of RCC cells via inactivation of Src and Akt signaling pathways.

ACKNOWLEDGMENTS

This work was supported by a Biomedical Research Institute grant, Kyungpook National University Hospital (2015).

CONFLICTS OF INTEREST

The authors have nothing to disclose.

REFERENCES

1. Siegel RL, Miller KD, Jemal A. Cancer statistics, 2017. *CA Cancer J Clin* 2017;67:7-30.
2. Compérat E, Camparo P. Histological classification of malignant renal tumours at a time of major diagnostic and therapeutic changes. *Diagn Interv Imaging* 2012;93:221-31.
3. Athar U, Gentile TC. Treatment options for metastatic renal cell carcinoma: a review. *Can J Urol* 2008;15:3954-66.
4. Cohen HT, McGovern FJ. Renal-cell carcinoma. *N Engl J Med* 2005;353:2477-90.
5. Choi JY, Ko YH, Song PH. Clinical significance of preoperative thrombocytosis in patients who underwent radical nephrectomy for nonmetastatic renal cell carcinoma. *Investig Clin Urol* 2016;57:324-9.
6. Duensing S, Hohenfellner M. Adjuvant therapy for renal-cell carcinoma: settled for now. *Lancet* 2016;387:1973-4.
7. Gaudet R. A primer on ankyrin repeat function in TRP channels and beyond. *Mol Biosyst* 2008;4:372-9.
8. Lehen'kyi V, Shapovalov G, Skryma R, Prevarskaya N. Ion channels and transporters in cancer. 5. Ion channels in control of cancer and cell apoptosis. *Am J Physiol Cell Physiol* 2011;301:C1281-9.
9. Runnels LW, Yue L, Clapham DE. TRP-PLIK, a bifunctional protein with kinase and ion channel activities. *Science* 2001;291:1043-7.
10. Ryazanova LV, Rondon LJ, Zierler S, Hu Z, Galli J, Yamaguchi TP, et al. TRPM7 is essential for Mg²⁺ homeostasis in mammals. *Nat Commun* 2010;1:109.
11. Latorre R, Zaelzer C, Brauchi S. Structure-functional intimacies of transient receptor potential channels. *Q Rev Biophys* 2009;42:201-46.
12. Kunzelmann K. Ion channels and cancer. *J Membr Biol* 2005; 205:159-73.
13. Reis ST, Leite KR, Piovesan LF, Pontes-Junior J, Viana NI, Abe DK, et al. Increased expression of MMP-9 and IL-8 are correlated with poor prognosis of bladder cancer. *BMC Urol* 2012;12:18.
14. Jung KW, Won YJ, Oh CM, Kong HJ, Lee DH, Lee KH. Prediction of cancer incidence and mortality in Korea, 2017. *Cancer Res Treat* 2017;49:306-12.
15. Lee JN, Chun SY, Lee HJ, Ha YS, Kim HT, Yoo ES, et al. High Notch1 expression correlates with tumor stage and size in clear cell renal cell carcinoma. *Korean J Urol Oncol* 2016;14:130-7.
16. Wang J, Zhao X, Qi J, Yang C, Cheng H, Ren Y, et al. Eight

proteins play critical roles in RCC with bone metastasis via mitochondrial dysfunction. *Clin Exp Metastasis* 2015;32:605-22.

17. Cho YH, Kim MS, Chung HS, Hwang EC. Novel immunotherapy in metastatic renal cell carcinoma. *Investig Clin Urol* 2017;58:220-7.
18. Gupta GP, Massagué J. Cancer metastasis: building a framework. *Cell* 2006;127:679-95.
19. Meng X, Cai C, Wu J, Cai S, Ye C, Chen H, et al. TRPM7 mediates breast cancer cell migration and invasion through the MAPK pathway. *Cancer Lett* 2013;333:96-102.
20. Gao H, Chen X, Du X, Guan B, Liu Y, Zhang H. EGF enhances the migration of cancer cells by up-regulation of TRPM7. *Cell Calcium* 2011;50:559-68.
21. Callera GE, He Y, Yogi A, Montezano AC, Paravicini T, Yao G, et al. Regulation of the novel Mg²⁺ transporter transient receptor potential melastatin 7 (TRPM7) cation channel by bradykinin in vascular smooth muscle cells. *J Hypertens* 2009;27:155-66.
22. Song G, Ouyang G, Bao S. The activation of Akt/PKB signaling pathway and cell survival. *J Cell Mol Med* 2005;9:59-71.
23. Guo H, German P, Bai S, Barnes S, Guo W, Qi X, et al. The PI3K/AKT pathway and renal cell carcinoma. *J Genet Genomics* 2015;42:343-53.
24. Duran I, Lambea J, Maroto P, González-Larriba JL, Flores L, Granados-Principal S, et al. Resistance to targeted therapies in renal cancer: the importance of changing the mechanism of action. *Target Oncol* 2017;12:19-35.
25. Playford MP, Schaller MD. The interplay between Src and integrins in normal and tumor biology. *Oncogene* 2004;23:7928-46.
26. Reddy KB, Nabha SM, Atanaskova N. Role of MAP kinase in tumor progression and invasion. *Cancer Metastasis Rev* 2003;22:395-403.
27. Roseweir AK, Qayyum T, Lim Z, Hammond R, MacDonald AI, Fraser S, et al. Nuclear expression of Lyn, a Src family kinase member, is associated with poor prognosis in renal cancer patients. *BMC Cancer* 2016;16:229.
28. Li JK, Chen C, Liu JY, Shi JZ, Liu SP, Liu B, et al. Long noncoding RNA MRCCAT1 promotes metastasis of clear cell renal cell carcinoma via inhibiting NPR3 and activating p38-MAPK signaling. *Mol Cancer* 2017;16:111.
29. Lue HW, Cole B, Rao SA, Podolak J, Van Gaest A, King C, et al. Src and STAT3 inhibitors synergize to promote tumor inhibition in renal cell carcinoma. *Oncotarget* 2015;6:44675-87.
30. Yuan H, Meng X, Guo W, Cai P, Li W, Li Q, et al. Transmembrane-Bound IL-15-promoted epithelial-mesenchymal transition in renal cancer cells requires the Src-dependent Akt/GSK-3β/β-catenin pathway. *Neoplasia* 2015;17:410-20.

EDITORIAL COMMENT

Biological characterization and implications of transient receptor potential melastatin member 7, a calcium channel, in renal cell carcinoma

It is estimated that there will be approximately 65,340 new cases (42,680 men and 22,660 women) and 14,970 deaths (10,010 men and 4,960 women) from kidney cancer in 2018. Kidney cancer, also known as renal cell carcinoma (RCC), is widely recognized as the most lethal genitourinary cancer. Metastatic RCC (mRCC) is advanced kidney cancer and occurs when the cancer has spread to the lymph nodes or other organs in the body. The US Food and Drug Administration has approved the use of numerous agents for treating mRCC and most of them are based on scientific understanding of cellular signaling pathways, such as VHL, VEGFR, mTOR, HGF/c-MET, and Wnt/β-catenin. Unfortunately, a number of drugs developed in recent years have shown limited efficacy in treating mRCC.

Given that regulation of cell invasion and migration are critical for tumor metastasis, a research team led by Dr. Tae Gyun Kwon (Kyungpook National University) discovered promising findings suggesting that transient receptor potential melastatin member 7 (TRPM7) kinase, a membrane cation channel, is a central regulator of RCC invasion and migration *in vitro*. Knocking down TRPM7 expression in RCC cell lines impaired their ability to migrate. Furthermore, the investigators were able to demonstrate that TRPM7 controls RCC migration and invasion through the Src/Akt pathway. These experimental results implicate the function of TRPM7 as a sort of sensor that may enable RCC cells to receive signals from the microenvironment and direct cells to metastasize. Although TRPM7 is known to regulate cell adhesion and migration and is a critical determinant of metastasis in several cancer types, such as breast, ovarian, and bladder, it has not been determined if it has an important role in RCC metastasis.

Even though further validation in mRCC mouse models and human patient cohorts are essential, these findings from the Kwon laboratory present evidence suggesting the biological mechanism of TRPM7 in mRCC and its clinical implications. As described in the hypothetical mechanism, TRPM7 may play a role in Src/Akt signaling and metastasis of RCC by epigenetic regulation, perturbed gene expression, and/or key transcriptional factors (Fig. 1). The effects of potent TRPM7 inhibitors on the metastatic capability of RCC could also be easily tested *in vitro* and in the pre-clinical setting. If successful, these experiments will have direct clinical significance since it may identify biomarkers

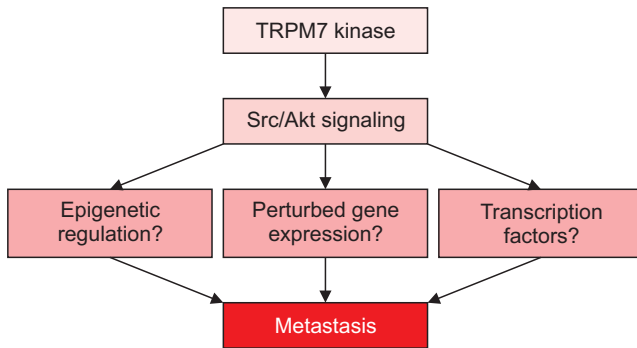


Fig. 1. A diagram suggesting the potential mechanism of transient receptor potential melastatin member 7 (TRPM7) in metastatic renal cell carcinoma.

of mRCC. Additionally, we envision that this study will provide mechanistic data for addressing the long-term goal of identifying new therapeutics for mRCC cases for which current therapeutic options do not exhibit optimal efficacy.

CONFLICTS OF INTEREST

The author has nothing to disclose.

ACKNOWLEDGMENTS

The author acknowledges support from National

Institutes of Health grants (1U01DK103260, 1R01DK100974, U24 DK097154, NIH NCATS UCLA CTSI UL1TR000124), Department of Defense grants (W81XWH-15-1-0415), Centers for Disease Controls and Prevention (1U01DP006079), IMAGINE NO IC Research Grant, the Steven Spielberg Discovery Fund in Prostate Cancer Research Career Development Award, and the U.S.-Egypt Science and Technology Development Fund by the National Academies of Sciences, Engineering, and Medicine (to J.K.). J.K. is former recipient of Interstitial Cystitis Association Pilot Grant, a Fishbein Family IC Research Grant, New York Academy of Medicine, and Boston Children's Hospital Faculty Development. The funders had no role in the design, data collection and analysis, decision to publish, or preparation of the manuscript.

Jayoung Kim^{1,2,3}

ORCID: <http://orcid.org/0000-0002-3683-4627>

¹Department of Surgery, Harvard Medical School, Boston, MA, ²Division of Cancer Biology and Therapeutics, Departments of Surgery and Biomedical Sciences, Samuel Oschin Comprehensive Cancer Institute, Cedars-Sinai Medical Center, Los Angeles, CA, ³Department of Medicine, University of California Los Angeles, Los Angeles, CA, USA
E-mail: Jayoung.kim@csmc.edu



Glucose-derived acetate and ACSS2 as key players in cisplatin resistance in bladder cancer



He Wen^{a,1}, Sujin Lee^{b,1}, Wei-Guo Zhu^a, Ok-Jun Lee^c, Seok Joong Yun^d, Jayoung Kim^{e,f,*}, Sunghyoun Park^{b,**}

^a Guangdong Key Laboratory for Genome Stability and Human Disease Prevention, Department of Biochemistry and Molecular Biology, Shenzhen University School of Medicine, Shenzhen 518060, China

^b College of Pharmacy, Natural Product Research Institute, Seoul National University, Seoul 151-742, South Korea

^c Department of Pathology, College of Medicine and Institute for Tumor Research, Chungbuk National University, Cheongju, Chungbuk 361-711, South Korea

^d Department of Urology, College of Medicine and Institute for Tumor Research, Chungbuk National University, Cheongju, Chungbuk 361-711, South Korea

^e Departments of Surgery and Biomedical Sciences, Cedars-Sinai Medical Center, Los Angeles, CA 90048, USA

^f Department of Medicine, University of California, Los Angeles, CA 90095, USA

ARTICLE INFO

Keywords:

In-cell metabolomics
ACSS2
Acetate
Cisplatin resistance
Bladder cancer

ABSTRACT

Cisplatin is an important chemotherapeutic agent against metastatic bladder cancer, but resistance often limits its usage. With the recent recognition of lipid metabolic alterations in bladder cancers, we studied the metabolic implications of cisplatin resistance using cisplatin-sensitive (T24S) and resistant (T24R) bladder cancer cells. Real-time live metabolomics revealed that T24R cells consume more glucose, leading to higher production of glucose-derived acetate and fatty acids. Along with the activation of general metabolic regulators, enzymes involved in acetate usage (ACSS2) and fatty acid synthesis (ACC) and a precursor for fatty acid synthesis (acetyl-CoA) were elevated in T24R cells. Consistently, metabolic analysis with ¹³C isotope revealed that T24R cells preferred glucose to acetate as the exogenous carbon source for the increased fatty acid synthesis, contrary to T24S cells. In addition, ACSS2, rather than the well-established ACLY, was the key enzyme that supplies acetyl-CoA in T24R cells through glucose-derived endogenous acetate. The relevance of ACSS2 in cisplatin resistance was further confirmed by the abrogation of resistance by an ACSS2 inhibitor and, finally, by the higher expression of ACSS2 in the patient tissues with cisplatin resistance. Our results may help improve the treatment options for chemoresistant bladder cancer patients and provide possible vulnerability targets to overcome the resistance.

1. Introduction

Bladder cancer (BC) usually arises in the bladder epithelial lining, and is the seventh most common cancer for men worldwide [1–3]. A majority of BC cases (~90%) are classified as transitional cell carcinoma (TCC), which can be further categorized as non-muscle invasive (NMIBC) or muscle invasive bladder cancer (MIBC), according to the extent of invasion into the muscular layer. NMIBC exhibits better prognosis and survival rate, but about 20% of those patients progress to MIBC [4, 5]. Radical cystectomy is a standard treatment for MIBC, but about 50% of the patients develop distant metastases within two years. For metastatic BC, cisplatin-based chemotherapy, with or without

radiotherapy, is the current gold standard. Those who do not respond well to this treatment generally have a poor prognosis [6].

It is well established that cisplatin kills rapidly proliferating cancer cells mostly through DNA damages [7]. It generates intra- and inter-strand purine crosslinks that interferes with DNA replication, which eventually lead to apoptosis. The toxicity mechanism, especially for kidney, has also been reported as involving the generation of reactive oxygen species and oxidative stress [8]. However, the biochemical processes underlying its resistance are more complex and may involve various signaling pathways such as p53, PI3K/AKT, and ROS detoxification [9]. In addition, the contribution of these individual mechanisms may differ according to the particular tumors involved.

* Correspondence to: J. Kim, Departments of Surgery and Biomedical Sciences, Cedars-Sinai Medical Center, 8700 Beverly Blvd., Los Angeles, CA 90048, USA.

** Correspondence to: S. Park, College of Pharmacy, Natural Product Research Institute, Seoul National University, Sillim-dong, Gwanak-gu, 151-742 Seoul, South Korea.

E-mail addresses: Jayoung.Kim@cshs.org (J. Kim), psh@snu.ac.kr (S. Park).

¹ These authors contributed equally to this work.

Recent results suggest that not only these well-established cell signaling mechanisms, but also metabolic activities may be involved in cisplatin-induced cell death [10]. For example, differences in succinate dehydrogenase-mediated production of NADPH generation may be responsible for pharmacometabonomic heterogeneity of cisplatin-induced kidney toxicity [11]. In addition, the level of UDP-GlcNAc, the metabolite involved in *N*-acetylglucosamine glycosylation, was shown to correlate with cisplatin sensitivity of cancer cells [12]. As metabolism is increasingly recognized as involved in cancer initiation and progression [13], metabolic study of cisplatin resistance may lead to clues for improving therapies for refractory bladder cancer.

Among key metabolites that fuel cancer cell proliferation, acetate has not drawn as much attention as glucose and glutamine [14]. Recent studies, however, have found acetate to be a key substrate for cancer bioenergetics or macromolecular synthesis [15, 16]. In addition, increased usages of ^{13}C -acetate positron emission tomography in clinics provide proof of concept evidence for the importance of acetate metabolism in cancer [17]. At the heart of acetate utilization in cancer is the enzyme ACS2, responsible for converting acetate to acetyl-CoA. Production of acetyl-CoA is critical for the upkeep of fatty acid synthesis in cancer cells [14]. Fatty acid metabolism is a critical aspect of cancer metabolism, as cancer cell proliferation requires large amount of biomass. It is also interesting to note that bladder cancer may also have alterations in lipid or fatty acid metabolism [18–21]. Despite this interesting relationship among acetate, fatty acid, and cancer metabolism, the exact source of acetate in cancer cells is still debatable due to the low blood concentration of acetate.

In this study, we applied real-time live metabolomics to identify metabolic reprogramming in cisplatin-resistant bladder cancer cells and verified the results in patient-derived tissues. Our findings may reveal a new aspect of the acquired chemoresistance and vulnerabilities to overcome the resistance.

2. Materials and methods

2.1. Chemicals and reagents

The stable isotope labeled D -Glucose ($\text{U-}^{13}\text{C}_6$, 99%) and acetate ($1,2\text{-}^{13}\text{C}$, 99%) were purchased from Cambridge Isotope Laboratories (Andover, MA, USA). The standard compounds, including pyruvate, lactate, alanine, acetate, succinate, glucose, palmitate, glycine, glutamate, isoleucine, valine, leucine, and glutathione(reduced) were obtained from Sigma-Aldrich (St. Louis, MO, USA). The inhibitors for ACS2, 1-(2,3-di(thiophen-2-yl)quinoxalin-6-yl)-3-(2-methoxyethyl) urea, and for ACLY, 3,5-Dichloro-2-hydroxy-*N*-(4-methoxy[1,1'-biphenyl]-3-yl)-benzenesulfonamide (BMS-303141), were purchased from ChemBridge (San Diego, CA, USA) and Bio-Techne (Minneapolis, MN, USA), respectively. The following antibodies, β -Actin (A1978, 1:5000) from Sigma, ACS2 (PA5-52059, 1:1000) from Thermo Fisher Scientific, were used. All other antibodies, ACC (3676, 1:750), FAS (3180, 1:750), EGFR (2232; 1:1000), phospho-EGFR (Tyr1068) (3777; 1:1000), Src (2108; 1:750), phospho-Src (Tyr527) (2105; 1:1000), mTOR (2983; 1:1000), phospho-mTOR (Ser2448) (5536; 1:1000), and HRP-conjugated secondary antibodies (7074, 1:1000; 7076, 1:1000) were obtained from Cell Signaling Technologies.

2.2. Cell culture and biochemical assays

T24S and T24R urothelial carcinoma cells were cultured in DMEM supplemented with 10% FBS, 2 mM *L*-glutamine, and 1% antibiotic solution (all from Invitrogen, Carlsbad, CA). All cells were maintained in a humidified incubator (37 °C and 5% CO_2). Cisplatin-resistant bladder cancer cells (T24R) were obtained through chronic treatments of cisplatin at low doses over six months [22, 23]. Briefly, the final cell viability was < 40% for T24S cells and nearly 100% for T24R cells upon 10 μM cisplatin treatment for 12 h. Cell viability assay was

performed using MTS (Promega, Inc., Madison, WI) according to the manufacturer's protocol. Western blot analysis was performed following routine procedures with actin as normalization control.

2.3. Sample preparation for live NMR metabolomics

Six plates (100 mm) of 70% confluent cultured cells were harvested with centrifugation. After the re-suspension of the cells with 5 mL DPBS, cells were counted, and 3×10^7 cells were moved into a new tube. After centrifugation, the harvested cells were re-suspended with 500 μL glucose-free DMEM media (Gibco, Grand Island, NY, USA) supplemented with 10% dialyzed FBS (Welgene, Daegu, Korea), 25 mM $^{13}\text{C}_6$ -labeled glucose, and 10% D_2O . The cells were spun in an NMR tube with a weak centrifugal force (30g for 100 s) to allow sedimentation, enough to cover the active region of the NMR detection coil. The NMR tubes with the cells were inserted into NMR magnet and the spectra were acquired as usual.

2.4. Isotope incorporation analysis for fatty acids

The T24S and T24R cells were counted (5×10^6) and seeded in 6-well plates. After 24 h adaptation, cells were treated with glucose-free DMEM media (Gibco, Grand Island, NY, USA) supplemented with 10% dialyzed FBS (Welgene, Daegu, Korea), and 5 mM non-labeled glucose.

For the ^{13}C -acetate and ^{13}C -glucose treatment, 0.5 mM [$1,2\text{-}^{13}\text{C}$] acetate and 20 mM [$\text{U-}^{13}\text{C}$] glucose was added, respectively. For the inhibitor treatment, the ACS2 inhibitor (15.6 μM) and the ACLY inhibitor (32 μM) were also added to the cell media. After a 24 h treatment, the fatty acids were extracted from the counted (9.05×10^6) cells using the two-layer methanol-chloroform extraction method as previously described [24].

2.5. NMR measurement

$^1\text{H-}^{13}\text{C}$ Heteronuclear Single Quantum Coherence (HSQC) NMR spectra were measured on a 800-MHz Bruker Avance spectrometer (Bruker BioSpin, Rheinstetten, Germany) equipped with a cryogenic triple resonance probe at Seoul National University, Korea. The dataset comprises 1024×128 points for the direct and indirect dimensions, respectively. The time course spectral measurement was obtained at 310 K for 24 time points, with each experiment lasting for 288 s. Each of the metabolites was identified by spiking the standard compounds. Metabolites were quantified as described previously [25]. Non-uniformly sampled HSQC (NUS-HSQC) were obtained as described previously [26].

2.6. Quantification of acetyl-CoA

The levels of acetyl-CoA were measured from cell lysates using PicoProbe™ Acetyl-CoA Assay Kit (BioVision, Milpitas, CA), following the protocol provided by the manufacturer. Briefly, free CoA was quenched, and then Acetyl-CoA was converted to CoA. The CoA was then reacted to form NADH which interacts with PicoProbe, resulting in the fluorescence. The reading was done with $\text{Ex} = 535/\text{Em} = 587 \text{ nm}$.

2.7. Immunohistochemistry (IHC) analysis

To stain the slides of bladder tumor tissues obtained from BC patients showing complete remission (CR) or progressive disease (PD), the ACS2 antibody (1:100, LifeSpan Biosciences, Inc., Seattle, WA) was utilized. A high pH was used for the antigen retrieval and an Ultraview DAB Detection Kit from Ventana Medical Systems was used for counterstaining. To acquire the digital images, stained slides were scanned using an Aperio Turbo Scanscope AT machine (Leica Biosystems, Buffalo Grove, IL). High-resolution images of each slide were uploaded onto the Leica Biosystems cloud drive for further annotations and

analysis. Digitized images were analyzed with the Tissue IA Optimiser (Leica Biosystems, Buffalo Grove, IL) software installed on the Leica Digital Image Hub. Following pathological annotations, the Measure Stained Cells Algorithm option on the Leica Tissue IA software was used. Each annotated slide had a minimum threshold of 100,000 cells to be analyzed. After analysis, data for the nuclear h-score, % of positive nuclei, and % of positive nuclear area in tissue were collected and used for comparative graphing.

2.8. Routine statistics

All functional validation experiments were repeated at least three times. Data were compared using Student's *t*-tests. $P < 0.05$ was considered to be statistically significant.

3. Results

3.1. Live metabolomics comparison between cisplatin-sensitive and resistant bladder cancer cells

Through several metabolomics studies, it has been found that bladder cancers may have abnormalities in metabolites involved in lipid usages [18, 21]. It has been also suggested that perturbed metabolism may have implication in cancer drug resistance and cancer aggressiveness or progression [27]. We hypothesized that there should be differences in metabolism and metabolism-associated pathways between cisplatin-sensitive and resistant bladder cancer cells. To test the possibility, we applied the live metabolomics approach that we recently developed [24] to isogenic bladder cancer cell lines T24S (cisplatin-sensitive) and T24R (cisplatin-resistant) [22]. The metabolites generated from ^{13}C -glucose tracer were monitored with 2D ^1H - ^{13}C HSQC NMR in real-time (Fig. 1A and B). By spiking the spectra with standard compounds, we obtained the peak assignments for those with significant changes (Supplementary Table S1). Along with the peaks for metabolites involved in glycolysis, pyruvate metabolism and the TCA cycle, those corresponding to fatty acids could be readily identified. This was possible by the live metabolomics, since lipid-soluble fatty acids and water-soluble polar metabolites are usually not quantifiable in a single analysis with conventional cell lysate metabolomics [26].

3.2. Cisplatin resistance may be linked to the increased glucose consumption and acetate production

The time-dependent changes of these metabolites revealed that T24R cells exhibited specific metabolic characteristics in comparison with T24S cells. Glucose consumption was greater in T24R cells, indicating the higher input to glycolysis in T24R cells (Fig. 1C). The level of pyruvate, the last glycolytic metabolite prior to the TCA cycle, became almost the same, just after the brief higher consumption at an early period in T24R cells (Fig. 1D). Lactate, alanine and acetate all exhibited net productions in both cells, but there was an intriguing difference. Lactate and alanine accumulated faster and to higher levels in T24S than T24R cells (Fig. 1E and F), while acetate accumulated much faster and kept the much higher level throughout in T24R cells (Fig. 1G). In addition, despite the higher consumption of glucose in T24R cells, lactate production and excretion was significantly lower, (Fig. 1E and Supplementary Fig. S1). These findings suggest that the preferred metabolic route of the increased glucose consumption in T24R cells is not lactate formation, as occurs in Warburg-type metabolism, but it may be other metabolites generated through acetate. One possible destination may be fatty acids, because the fatty acid level was also higher in T24R cells, as estimated by their mid-chain CH_2 peak intensities (Fig. 1H). For other metabolites, glycine, a possible indicator of one carbon metabolism, and glutamate, an important anaplerotic metabolite to TCA, exhibited no significant difference in the two cells (Fig. 1I and J).

3.3. Two carbon pathway involving acetate leading to fatty acid synthesis is enhanced in the cisplatin-resistant T24 cells

We took notice of the differential patterns of changes of acetate in comparison with lactate and alanine between T24S and T24R cells. These three downstream metabolites from pyruvate exhibited similar patterns of changes in our previous live metabolomics studies with liver cells [24]. In addition, lactate and alanine retain all three carbons from pyruvate, whereas acetate is formed through the loss of one carbon from pyruvate. With these unique characteristics of acetate and the higher ^{13}C -fatty acid level in T24R cells, we hypothesized that there might be an alteration in pathways of fatty acid metabolism involving acetate. To test this hypothesis, we first looked at the levels of the upstream signaling molecules that can affect fatty acid metabolism. Significant increase in the phosphorylated EGFR and mTOR in T24R without much increase in their total levels suggested that cisplatin resistance is associated with the activation of upstream metabolic regulators (Fig. 2A). Then, looking at more downstream enzymes, we found that acetyl-CoA carboxylase (ACC), a key enzyme synthesizing malonyl-CoA from acetyl-CoA, is expressed much higher in T24R cells (Fig. 2B). Malonyl-CoA is a direct substrate of fatty acid synthase (FAS) which was present at similar levels in both cells (Fig. 2B). For the involvement of acetate in the fatty acid synthesis, we measured ACS2 levels, as it is a key enzyme in pathways for incorporating acetate into fatty acids. The ACS2 level was much higher in T24R cells (Fig. 2C), which was also corroborated by the higher level of acetyl-CoA generated from acetate by ACS2 (Fig. 2D). Given that ACC and ACS2 are two major enzymes that incorporate the acetate into fatty acids, our experimental results suggest that T24R may have the enhanced fatty acid synthesis via two carbon metabolism involving acetate.

3.4. Glucose-derived endogenous acetate contributes to the enhanced fatty acid de novo synthesis in T24R cells

The metabolic flux through a particular step can increase significantly even with a constant enzyme level, as long as there is an increased supply of the substrates. We observed activation of the acetate-involving two carbon metabolism leading to the FAS step in T24R cells despite similar FAS levels in T24S and T24R cells (see Fig. 2B). Therefore, we tested if the actual fatty acid de novo synthesis is increased and correlated with the activation of the acetate-involving two carbon metabolism in T24R cells. The de novo fatty acid synthesis was assessed by measuring the splitting of the omega methyl carbon signal arising from ^{13}C - ^{13}C coupling in the HSQC spectra obtained with ^{13}C -glucose tracer. This is possible because ^{13}C labels from a glucose-derived two carbon unit are incorporated into the omega methyl group for de novo fatty acid synthesis (Fig. 3A). In comparison, fatty acid chain elongation starting from a pre-existing fatty acyl chain occurs only at the carboxyl terminal end. The intensities of the splitting doublet of the omega methyl group of fatty acids, derived from the tracer glucose, were much higher in T24R (Fig. 3B), indicating elevated de novo fatty acid synthesis from glucose in T24R. Combined with the above results for the increased acetate production from glucose and higher levels of ACS2, ACC and acetyl-CoA, this indicates that an acetate-involving two carbon unit from glucose should contribute to the enhanced fatty acid synthesis in T24R cells.

Since previous studies emphasized the roles of blood-borne exogenous acetate, not glucose-derived endogenous, in the bioenergetics or lipid biosynthesis [15, 16], we also tested the de novo fatty acid synthesis from exogenous ^{13}C -acetate added to the medium. The incorporation of acetate to the terminal methyl was much lower in T24R cells, indicating that exogenous acetate is not a major source for their increased fatty acid de novo synthesis (Fig. 3C). The lower production of glucose-derived fatty acids in T24S cells is also consistent with the higher excretion of lactate from glucose (See Supplementary Fig. S1). In comparison, the higher consumption of glucose in T24R cells may

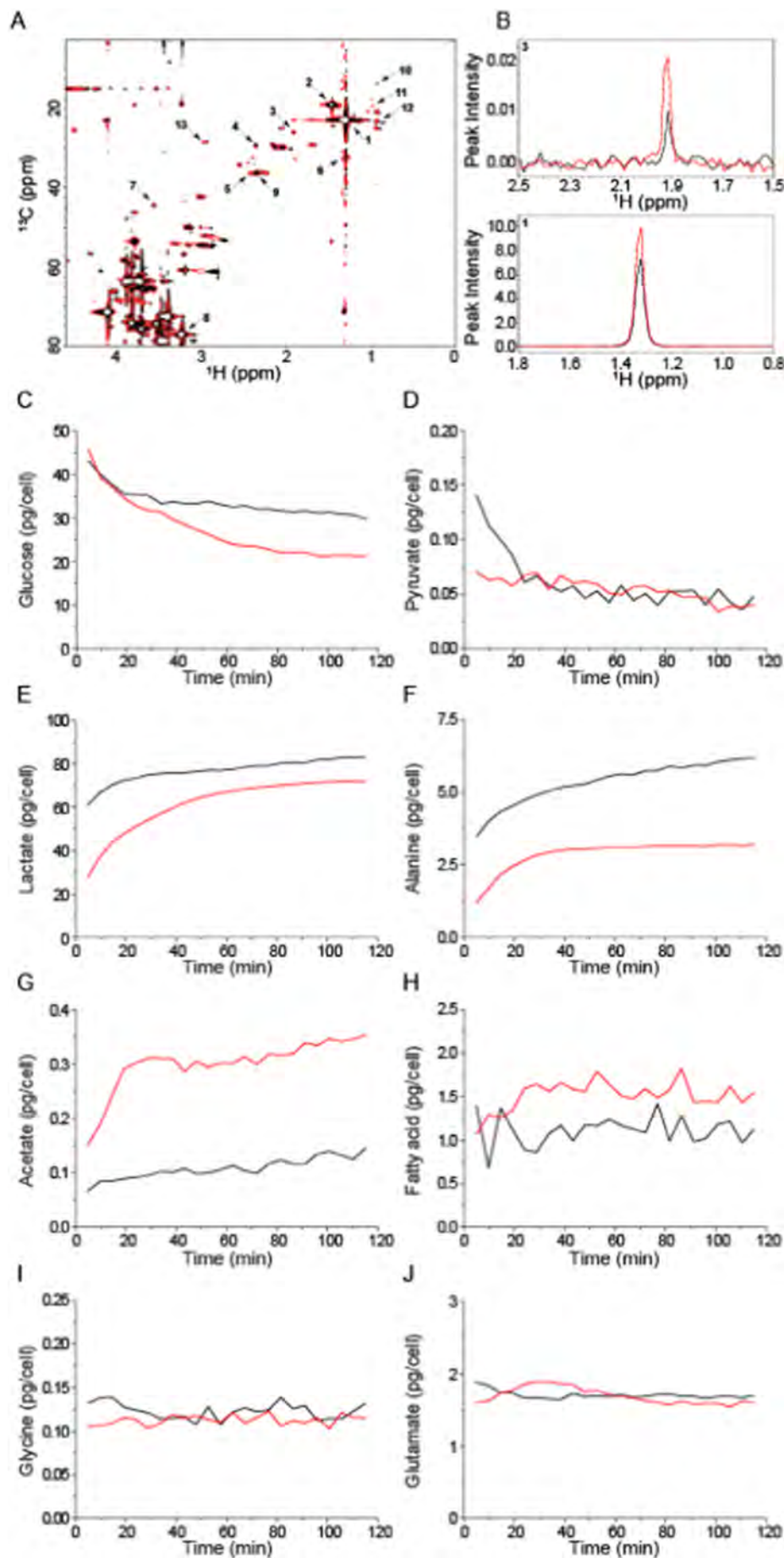


Fig. 1. Live NMR metabolomic comparison between cisplatin-sensitive and resistant cells.

(A) The first (black) and last (red) spectra obtained from cisplatin-sensitive (T24S) cancer cells over 1 h and 56 min after the addition of $^{13}\text{C}_6$ -glucose. (1: lactate, 2: alanine, 3: acetate, 4: pyruvate, 5: succinate, 6: fatty acid, 7: glycine, 8: glucose, 9: glutamate, 10: isoleucine, 11: valine, 12: leucine, 13: glutathione (reduced); see supplementary Table S1). Assignments were obtained by spiking the standard compounds. (B) One-dimensional spectra from two compounds were extracted for comparison (1 and 3). (C through J) Time-dependent metabolic changes between T24S (black) and T24R (red) cells were obtained in real-time with live NMR metabolomics approach. The metabolites were quantified as described previously [24].

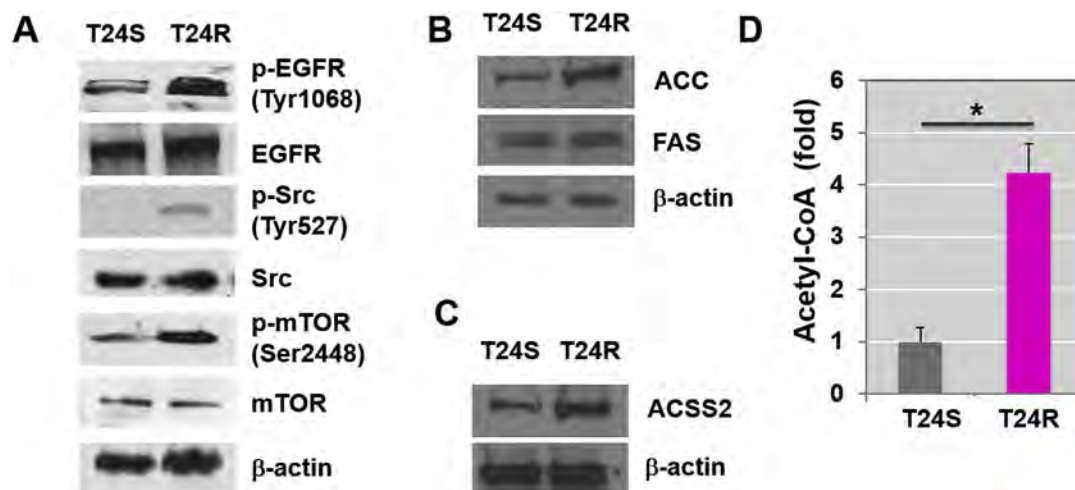


Fig. 2. Expression levels of metabolic regulators and enzymes in T24S and T24R cells.

Western blot analysis of (A) upstream regulators of metabolism (EGFR, Src, and mTOR) and their phosphorylated forms, (B) acetyl-CoA carboxylase (ACC) and fatty acid synthase (FAS) involved in fatty acid synthesis, and (C) acetyl-CoA synthetase 2 (ACSS2) for acetate utilization in T24S and T24R cells. The expression levels of β -actin were used as a loading control for western blot analysis. (D) The acetyl-CoA level was measured as described in the method section. The statistical analysis was performed using Student's *t*-test, and the asterisk indicates $P < 0.05$. The error bars represent the standard deviation ($N = 5$).

contribute to the higher de novo fatty acid synthesis through acetate production.

3.5. ACSS2 Inhibition decreases fatty acid synthesis and cell viability for T24R cells

As the data above collectively suggest a possible link from glucose to fatty acid synthesis through endogenous acetate from glucose, we decided to obtain further details on the pathways. Theoretically, a glucose-derived two carbon unit can be incorporated into fatty acids either via acetate or citrate, with the former mediated by ACSS2 and the latter by ACLY (Fig. 4A). The ACLY-mediated pathway has been considered the major pathway in various cancers [28], whereas the ACSS2-mediated pathway using glucose-derived endogenous acetate has been very little explored. Therefore, we selectively inhibited either of the two pathways using specific inhibitors, and measured the de novo fatty acid synthesis with NMR as above.

Inhibition of the ACSS2 pathway by 1-(2,3-di(thiophen-2-yl)quinoxalin-6-yl)-3-(2-methoxyethyl)urea decreased the de novo synthesis of fatty acid by > 60% in T24R cells, whereas no significant changes were observed in T24S cells (Fig. 4B). In comparison, ACLY inhibition by BMS-303141 led to a decrease in the de novo synthesis in T24S cells without significant effects on T24R cells. Importantly, the same ACSS2 inhibitor led to the growth inhibition of the T24R cells under cisplatin resistance condition (Fig. 4C). As we did not add any acetate in the media, these results confirm that the incorporation of glucose-derived endogenous acetate into fatty acids via ACSS2 is important in the cisplatin-resistance phenotype of T24R. We further obtained consistent data with siRNA approach. ACSS2 siRNA treatment induced a substantial decrease in acetyl-CoA in T24R cells, whereas ACLY siRNA treatment did not change the level (Supplementary Fig. S2A). The data also show that ACSS1 has much smaller role in acetyl-CoA production in T24R cells. Furthermore, ACLY siRNA induced a larger decrease in fatty acid synthesis in T24S than T24R cells (Supplementary Fig. S2B).

3.6. ACSS2 expression is increased in cisplatin-resistant patient tissue

To obtain the relevance of the above results in clinical settings, we tested the implication of ACSS2 with patient tissues. We measured the expression of ACSS2 in bladder tumor tissues obtained from patients who underwent a series of cisplatin-based chemotherapies. Bladder tumor tissues obtained from BC patients with complete remission (CR)

upon chemotherapies exhibited low levels of ACSS2, while those from patients with progressive disease (PD) had much higher levels of ACSS2 expression (Fig. 5A and B). Representative IHC images are also shown in Fig. 5C. These results confirm the relevance of ACSS2 in the cisplatin resistance of bladder cancer. As cisplatin-resistant bladder cancers are often more aggressive, we also performed an immunohistochemistry (IHC) analysis using bladder cancer tissue microarrays (TMA) with varying aggressiveness. The results showed that ACSS2 protein expression level is significantly associated with the aggressiveness of bladder cancers (Supplementary Fig. S3).

4. Discussion

By employing a live metabolomics and biochemical approach, we show that glucose-derived endogenous acetate contributes to fatty acid synthesis in cisplatin-resistant cells. Fatty acids are required components in proliferating cells, just like DNA, and therefore, it may not be surprising that cisplatin-resistant cells can have an alternative machinery to make fatty acids in the presence of the toxic drug. Still, the use of endogenous acetate in fatty acid synthesis may require more explanation. The most well-established pathway for fatty acid synthesis utilizes citrate as an intermediate for acetyl-CoA, whether it is from glucose or glutamine [29]. Citrate formed in mitochondria is lysed in the cytosol by ACLY to give oxaloacetate and acetyl-CoA that can be used for fatty acid synthesis. Another pathway for fatty acid synthesis involves exogenous acetate and requires ACSS2 for generating acetyl-CoA in the cytosol [16]. Although the involvement of ACSS2 is the same for both exogenous and endogenous acetate usage for fatty acid synthesis, we showed that ^{13}C incorporation into fatty acids from exogenous ^{13}C -acetate is much lower in cisplatin-resistant cells. Therefore, endogenous acetate seems to be the preferred source of the two carbon unit needed for fatty acid synthesis for the cisplatin-resistant cancer cells. Actually, the formation of endogenous acetate in cancers is not unprecedented. It was first documented about 80 years ago [30], but its roles in cancer metabolism has been little considered. For general fatty acid synthesis, too, endogenous acetate was proposed as an intermediate about 50 years ago [31], but it has been largely neglected compared to citrate as the main intermediate [14, 29]. Now, our data suggest a novel implication of endogenous acetate from glucose in the fatty acid synthesis in cisplatin-resistant cells. With currently available state-of-the-art analytical techniques, more roles of endogenous acetate in cancer metabolism are expected to be revealed.

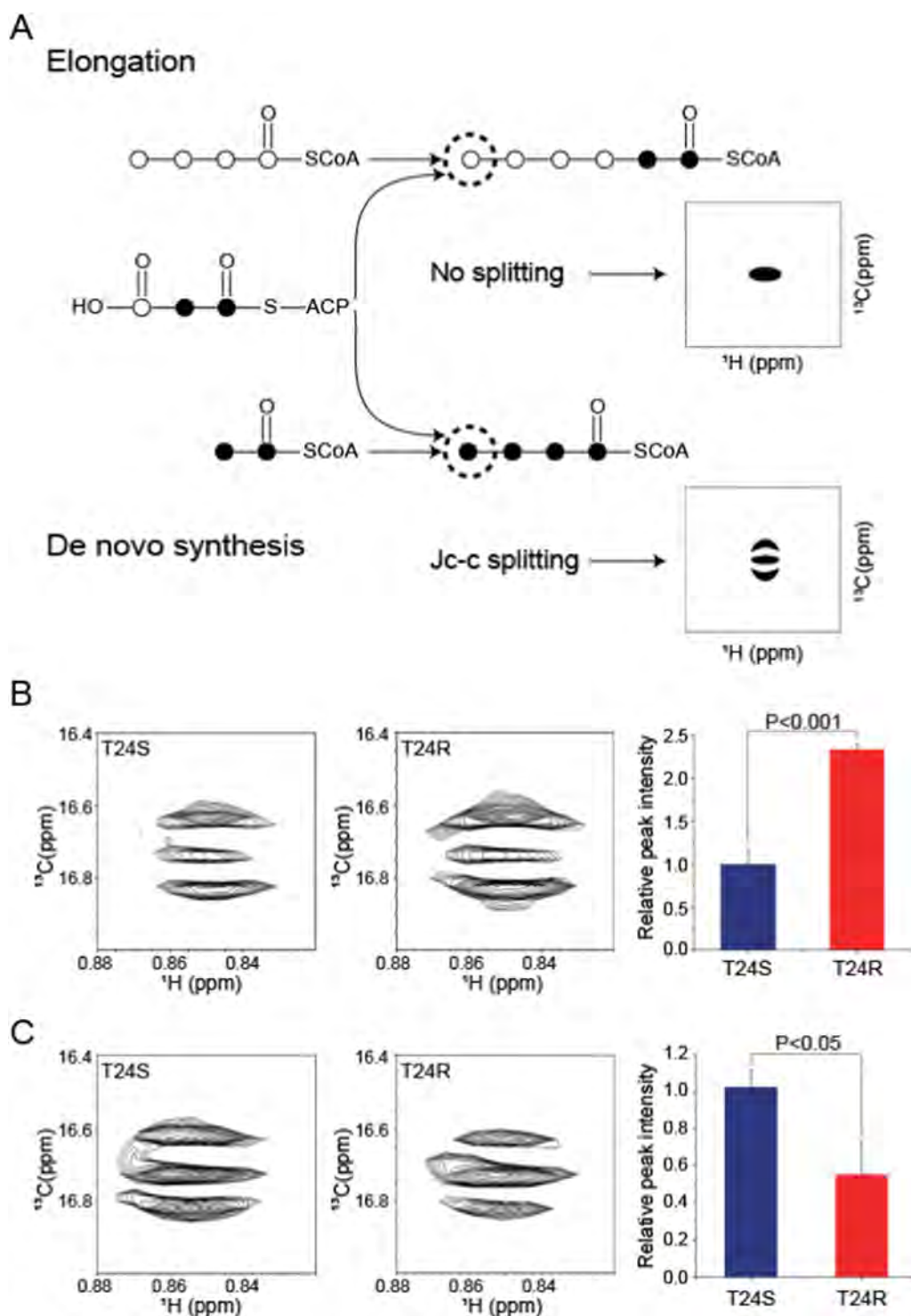


Fig. 3. Fatty acid de novo synthesis from glucose and acetate.

(A) Schematic representation of NMR signal splitting patterns by ^{13}C -acetyl-CoA for fatty acid elongation and de novo synthesis steps. Filled circles represent ^{13}C isotopes whereas open circles represent unlabeled carbons. (B) ^{13}C isotope incorporations in the omega position of the fatty acid alkyl chain with $\text{U-}^{13}\text{C}$ -glucose. Left and Middle, NUS HSQC spectra for the omega carbon in fatty acid alkyl chains from T24S and T24R cells, respectively. Right, The peak area of the doublet of the omega carbon from the spectra. The peak area was normalized by the number of harvested cells. (C) ^{13}C isotope incorporations as in (B) with $\text{U-}^{13}\text{C}$ -acetate. T24S and T24R cells were cultured in the media containing 5 mM non-labeled glucose supplemented with 20 mM ^{13}C -glucose (B) or 0.5 mM ^{13}C -acetate (C) for 24 h. The statistical analysis from three independent experiments was performed using the Student's *t*-test and the resulting *P*-values are indicated. The error bars represent the standard deviation.

Our data suggest that the endogenous acetate is derived from glucose, most probably through pyruvate, and we showed that acetate can be generated from pyruvate in mitochondria [32]. We also observed decrease in acetate production when T24R cells are treated with UK5099, an inhibitor of mitochondrial pyruvate carrier (MPC) (Supplementary Fig. S4). The pyruvate uptake through MPC is lower in some cancer cells, but still many cancers import pyruvate into mitochondria. For example, glioblastoma generates about half of cellular glutamate from glucose-driven TCA cycle that goes through pyruvate [15]. In osteosarcoma cells, glucose-derived citrate through pyruvate accounted for ~60% of total citrate pool [33]. Simultaneous

enhancement of Warburg effect and TCA cycle using glucose-derived pyruvate was also observed in small cell lung cancer [34]. Therefore, despite pronounced Warburg effect that can reduce pyruvate uptake into cancer mitochondria and reduced MPC functions in some cancer cells, pyruvate can still contribute to acetate generation in mitochondria. The higher oxygen consumption rate for T24R cells also supports functional mitochondrial activity in T24R cells. (Supplementary Fig. S5).

An interesting question may be raised as to how the increased fatty acid synthesis affects the cisplatin chemosensitivity. There have been several reports linking fatty acid synthesis and anticancer drug

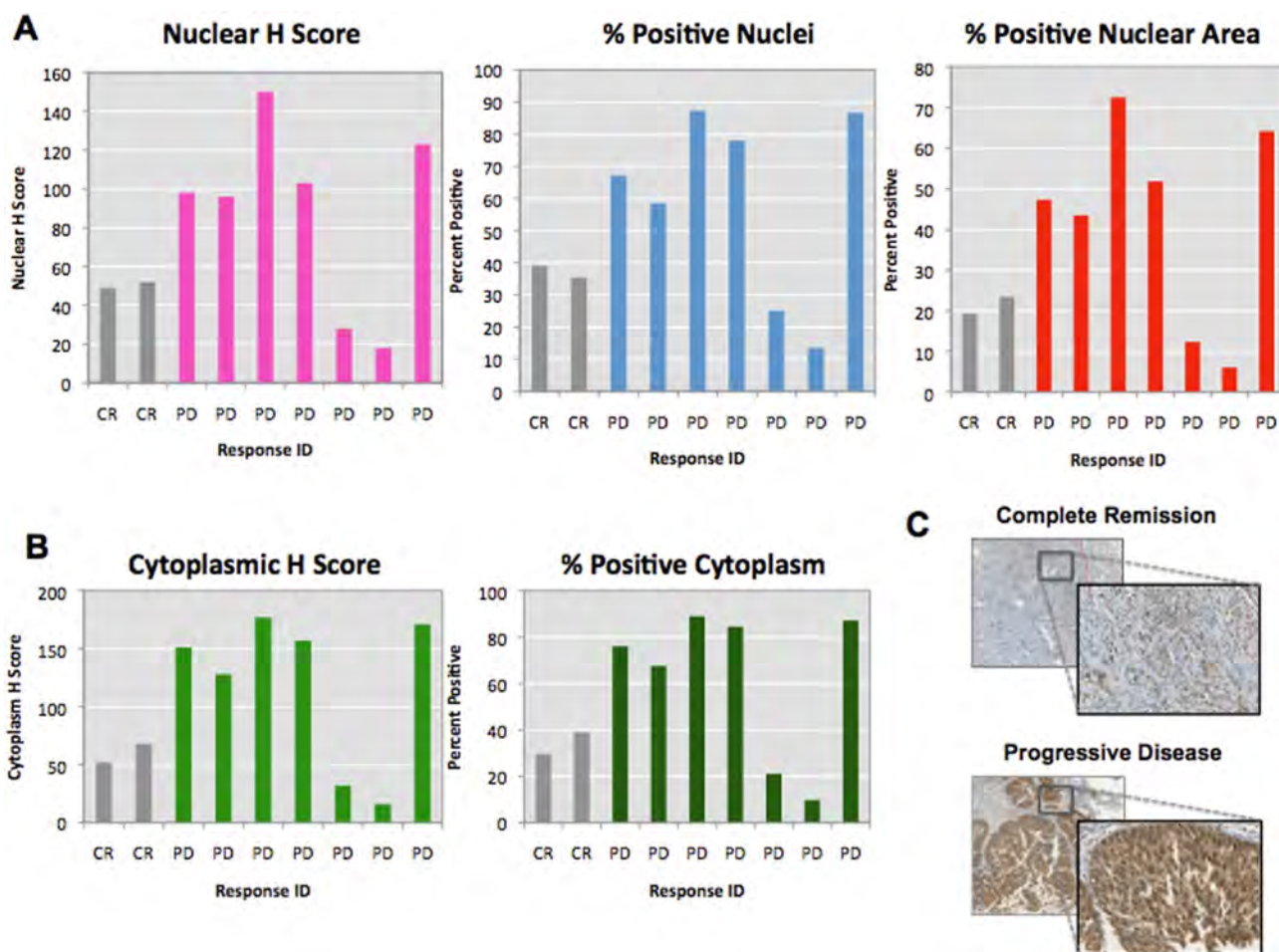


Fig. 5. The expression levels of ACSS2 in the tissues from cisplatin-sensitive and resistant BC patients.

(A) Quantitative analysis of annotated regions of the nucleus from IHC results: the nuclear H-score, percent of positive nuclei, and percent of positive nuclear area in BC tumors are presented. (B) Quantitative analysis of annotated regions of the cytoplasm from IHC results: the cytoplasmic H-score and percent of positive cytoplasm are presented. (C) Representative digitalized immunohistochemistry images. Complete remission (CR; cisplatin-sensitive) or progressive disease (PD; cisplatin-resistant) groups. An anti-ACSS2 antibody was used for IHC staining.

Author contributions

J.K. and SP designed the study. H.W. and S.L. performed metabolomics study and analyzed the data. W.Z. and J.K. performed Western blot and Acetyl-CoA measurement experiments. O.J.L. and S.J.Y. provided patient data and sample, and they performed H&E analysis. J.K., H. W., S.L. and S.P. wrote the manuscript. All authors read and approved the final manuscript.

Transparency document

The Transparency document associated with this article can be found, in online version.

Acknowledgments

The authors acknowledge support from National Institutes of Health grants [1U01DK103260], Department of Defense grants [W81XWH-15-1-0415], Centers for Disease Control and Prevention [1U01DP006079], the Steven Spielberg Discovery Fund in Prostate Cancer Research Career Development Award, Burroughs Wellcome Fund (BWF) 2017 Collaborative Research Travel Grant (CRTG), Southeast Center for Integrated Metabolomics (SECIM) Pilot and Feasibility Grant, and the U.S. - Egypt Science and Technology (S&T) Joint Fund, funded by the National Academies of Sciences, Engineering, and Medicine and USAID

(to J.K.). Any opinions, findings, conclusions, or recommendations expressed in this article are those of the authors alone, and do not necessarily reflect the views of any of the previously mentioned sponsors. This study was also supported by the Basic Science Research Program through the National Research Foundation of Korea funded by the Ministry of Education, Science, and Technology [2014-069340 and NRF-2018R1A3B1052328], and the Bio-Synergy Research Project (NRF-2015M3A9C4075818). This study was also supported by National Key R&D Program of China [2017YFA0503900], Natural Science Foundation of China [31701099], Science and Technology Foundation of Shenzhen City [JCYJ20170302144650949 and JCYJ20170818094707964], Natural Science Foundation of Guangdong Province [2017A030310459], and Natural Science Foundation of SZU [2017085].

Appendix A. Supplementary data

Supplementary data to this article can be found online at <https://doi.org/10.1016/j.bbalip.2018.06.005>.

References

- [1] L.A. Kiemeny, J.A. Witjes, A.L. Verbeek, R.P. Heijbroek, F.M. Debruyne, The clinical epidemiology of superficial bladder cancer. *Dutch South-East Cooperative Urological Group, Br. J. Cancer* 67 (1993) 806–812.
- [2] L.S. Borden Jr., P.E. Clark, M.C. Hall, Bladder cancer, *Curr. Opin. Oncol.* 15 (2003)

- 227–233.
- [3] M.C. Hall, S.S. Chang, G. Dalbagni, R.S. Pruthi, J.D. Seigne, E.C. Skinner, J.S. Wolf Jr., P.F. Schellhammer, Guideline for the management of nonmuscle invasive bladder cancer (stages Ta, T1, and Tis): 2007 update, *J. Urol.* 178 (2007) 2314–2330.
- [4] M. Babjuk, W. Oosterlinck, R. Sylvester, E. Kaasinen, A. Bohle, J. Palou-Redorta, U. European association of, EAU guidelines on non-muscle-invasive urothelial carcinoma of the bladder, *Eur. Urol.* 54 (2008) 303–314.
- [5] A. Stenzl, N.C. Cowan, M. De Santis, M.A. Kuczyk, A.S. Merseburger, M.J. Ribal, A. Sherif, J.A. Witjes, Treatment of muscle-invasive and metastatic bladder cancer: update of the EAU guidelines, *Eur. Urol.* 59 (2011) 1009–1018.
- [6] P.C. Black, C.P. Dinney, Growth factors and receptors as prognostic markers in urothelial carcinoma, *Curr. Urol. Rep.* 9 (2008) 55–61.
- [7] S.M. Cohen, S.J. Lippard, Cisplatin: from DNA damage to cancer chemotherapy, *Prog. Nucleic Acid Res. Mol. Biol.* 67 (2001) 93–130.
- [8] N.A.G. Santos, C.S. Catao, N.M. Martins, C. Curti, M.L.P. Bianchi, A.C. Santos, Cisplatin-induced nephrotoxicity is associated with oxidative stress, redox state unbalance, impairment of energetic metabolism and apoptosis in rat kidney mitochondria, *Arch. Toxicol.* 81 (2007) 495–504.
- [9] Z.H. Siddik, Cisplatin: mode of cytotoxic action and molecular basis of resistance, *Oncogene* 22 (2003) 7265–7279.
- [10] A. Viale, G.F. Draetta, Metabolic features of cancer treatment resistance, *Recent Results Cancer Res.* 207 (2016) 135–156.
- [11] H.N. Kwon, M. Kim, H. Wen, S. Kang, H.J. Yang, M.J. Choi, H.S. Lee, D. Choi, I.S. Park, Y.J. Suh, S.S. Hong, S. Park, Predicting idiopathic toxicity of cisplatin by a pharmacometabonomic approach, *Kidney Int.* 79 (2011) 529–537.
- [12] X. Pan, M. Wilson, L. Mirbahai, C. McConville, T.N. Arvanitis, J.L. Griffin, R.A. Kauppinen, A.C. Peet, In vitro metabolomic study detects increases in UDP-GlcNAc and UDP-GalNAc, as early phase markers of cisplatin treatment response in brain tumor cells, *J. Proteome Res.* 10 (2011) 3493–3500.
- [13] L.B. Sullivan, D.Y. Gui, M.G.V. Heiden, Altered metabolite levels in cancer: implications for tumour biology and cancer therapy, *Nat. Rev. Cancer* 16 (2016) 680–693.
- [14] Z.T. Schug, J. Vande Voorde, E. Gottlieb, The metabolic fate of acetate in cancer, *Nat. Rev. Cancer* 16 (2016) 708–717.
- [15] T. Mashimo, K. Pichumani, V. Vemireddy, K.J. Hatanpaa, D.K. Singh, S. Sirasanagandla, S. Nannepaga, S.G. Piccirillo, Z. Kovacs, C. Foong, Z. Huang, S. Barnett, B.E. Mickey, R.J. DeBerardinis, B.P. Tu, E.A. Maher, R.M. Bachoo, Acetate is a bioenergetic substrate for human glioblastoma and brain metastases, *Cell* 159 (2014) 1603–1614.
- [16] S.A. Comerford, Z. Huang, X. Du, Y. Wang, L. Cai, A.K. Witkiewicz, H. Walters, M.N. Tantawy, A. Fu, H.C. Manning, J.D. Horton, R.E. Hammer, S.L. McKnight, B.P. Tu, Acetate dependence of tumors, *Cell* 159 (2014) 1591–1602.
- [17] Y. Yoshii, T. Furukawa, T. Saga, Y. Fujibayashi, Acetate/acetyl-CoA metabolism associated with cancer fatty acid synthesis: overview and application, *Cancer Lett.* 356 (2015) 211–216.
- [18] X. Jin, S.J. Yun, P. Jeong, I.Y. Kim, W.J. Kim, S. Park, Diagnosis of bladder cancer and prediction of survival by urinary metabolomics, *Oncotarget* 5 (2014) 1635–1645.
- [19] L. Lin, Z. Huang, Y. Gao, Y. Chen, W. Hang, J. Xing, X. Yan, LC-MS-based serum metabolic profiling for genitourinary cancer classification and cancer type-specific biomarker discovery, *Proteomics* 12 (2012) 2238–2246.
- [20] N. Putluri, A. Shojaie, V.T. Vasu, S.K. Vareed, S. Nalluri, V. Putluri, G.S. Thangjam, K. Panzitt, C.T. Tallman, C. Butler, T.R. Sana, S.M. Fischer, G. Sica, D.J. Brat, H. Shi, G.S. Palapattu, Y. Lotan, A.Z. Weizer, M.K. Terris, S.F. Shariat, G. Michailidis, A. Sreekumar, Metabolomic profiling reveals potential markers and bioprocesses altered in bladder cancer progression, *Cancer Res.* 71 (2011) 7376–7386.
- [21] Z. Huang, L. Lin, Y. Gao, Y. Chen, X. Yan, J. Xing, W. Hang, Bladder cancer determination via two urinary metabolites: a biomarker pattern approach, *Mol. Cell. Proteomics* 10 (2011) (M111 007922).
- [22] W.T. Kim, J. Kim, C. Yan, P. Jeong, S.Y. Choi, O.J. Lee, Y.B. Chae, S.J. Yun, S.C. Lee, W.J. Kim, S100A9 and EGFR gene signatures predict disease progression in muscle invasive bladder cancer patients after chemotherapy, *Ann. Oncol.* 25 (2014) 974–979.
- [23] M.Y. Lee, A. Yeon, M. Shahid, E. Cho, V. Sairam, R. Figlin, K.H. Kim, J. Kim, Reprogrammed lipid metabolism in bladder cancer with cisplatin resistance, *Oncotarget* 9 (2018) 13231–13243.
- [24] H. Wen, W.J. Xu, X. Jin, S. Oh, C.H. Phan, J. Song, S.K. Lee, S. Park, The roles of IP3 receptor in energy metabolic pathways and reactive oxygen species homeostasis revealed by metabolomic and biochemical studies, *Biochim. Biophys. Acta* 1853 (2015) 2937–2944.
- [25] H. Wen, Y.J. An, W.J. Xu, K.W. Kang, S. Park, Real-time monitoring of cancer cell metabolism and effects of an anticancer agent using 2D in-cell NMR spectroscopy, *Angew. Chem. Int. Ed. Eng.* 54 (2015) 5374–5377.
- [26] S. Lee, H. Wen, Y.J. An, J.W. Cha, Y.J. Ko, S.G. Hyberts, S. Park, Carbon isotopomer analysis with non-uniform sampling HSQC NMR for cell extract and live cell metabolomics studies, *Anal. Chem.* 89 (2017) 1078–1085.
- [27] N.D. Amoedo, E. Obre, R. Rossignol, Drug discovery strategies in the field of tumor energy metabolism: limitations by metabolic flexibility and metabolic resistance to chemotherapy, *Biochim. Biophys. Acta* 1858 (2017) 674–685.
- [28] N. Zaidi, J.V. Swinnen, K. Smans, ATP-citrate lyase: a key player in cancer metabolism, *Cancer Res.* 72 (2012) 3709–3714.
- [29] F. Rohrig, A. Schulze, The multifaceted roles of fatty acid synthesis in cancer, *Nat. Rev. Cancer* 16 (2016) 732–749.
- [30] K.A. Elliott, M.E. Greig, The metabolism of lactic and pyruvic acids in normal and tumour tissues: the formation of succinate, *Biochem. J.* 31 (1937) 1021–1032.
- [31] M.S. Kornacker, J.M. Lowenstein, Citrate and the conversion of carbohydrate into fat. The activities of citrate-cleavage enzyme and acetate thiokinase in livers of starved and re-fed rats, *Biochem. J.* 94 (1965) 209–215.
- [32] W.J. Xu, H. Wen, H.S. Kim, Y.J. Ko, S.M. Dong, I.S. Park, J.I. Yook, S. Park, Observation of acetyl phosphate formation in mammalian mitochondria using real-time in-organelle NMR metabolomics, *Proc. Natl. Acad. Sci. U. S. A.* 115 (2018) 4152–4157.
- [33] A.R. Mullen, W.W. Wheaton, E.S. Jin, P.H. Chen, L.B. Sullivan, T. Cheng, Y. Yang, W.M. Linehan, N.S. Chandel, R.J. DeBerardinis, Reductive carboxylation supports growth in tumour cells with defective mitochondria, *Nature* 481 (2012) 385–388.
- [34] M. Morita, T. Sato, M. Nomura, Y. Sakamoto, Y. Inoue, R. Tanaka, S. Ito, K. Kurosawa, K. Yamaguchi, Y. Sugiura, H. Takizaki, Y. Yamashita, R. Katakura, I. Sato, M. Kawai, Y. Okada, H. Watanabe, G. Kondoh, S. Matsumoto, A. Kishimoto, M. Obata, M. Matsumoto, T. Fukuhara, H. Motohashi, M. Suematsu, M. Komatsu, K.I. Nakayama, T. Watanabe, T. Soga, H. Shima, M. Maemondo, N. Tanuma, PKM1 confers metabolic advantages and promotes cell-autonomous tumor cell growth, *Cancer Cell* 33 (2018) 355–367 (e357).
- [35] C. Peetla, S. Vijayaraghavalu, V. Labhasetwar, Biophysics of cell membrane lipids in cancer drug resistance: implications for drug transport and drug delivery with nanoparticles, *Adv. Drug Deliv. Rev.* 65 (2013) 1686–1698.
- [36] E. Rysman, K. Brusselmans, K. Scheys, L. Timmermans, R. Derua, S. Munck, P.P. Van Veldhoven, D. Waltregny, V.W. Daniels, J. Machiels, F. Vanderhoydonc, K. Smans, E. Waelkens, G. Verhoeven, J.V. Swinnen, De novo lipogenesis protects cancer cells from free radicals and chemotherapeutics by promoting membrane lipid saturation, *Cancer Res.* 70 (2010) 8117–8126.
- [37] H. Liu, Y. Liu, J.T. Zhang, A new mechanism of drug resistance in breast cancer cells: fatty acid synthase overexpression-mediated palmitate overproduction, *Mol. Cancer Ther.* 7 (2008) 263–270.

Research Paper

Rewiring of cisplatin-resistant bladder cancer cells through epigenetic regulation of genes involved in amino acid metabolism

Austin Yeon¹, Sungyong You^{1,6}, Minhyung Kim¹, Amit Gupta¹, Myung Hee Park², Daniel J. Weisenberger³, Gangning Liang⁴, Jayoung Kim^{1,5,6,7,8}✉

1. Departments of Surgery, Cedars-Sinai Medical Center, Los Angeles, CA, USA
2. National Institute of Dental and Craniofacial Research, National Institutes of Health Bethesda, MD, USA
3. Department of Biochemistry and Molecular Medicine, USC Norris Comprehensive Cancer Center, University of Southern California
4. Department of Urology, Keck School of Medicine, University of Southern California, Los Angeles, CA, USA
5. Departments of Biomedical Sciences, Cedars-Sinai Medical Center, Los Angeles, CA, USA
6. Samuel Oschin Comprehensive Cancer Institute, Cedars-Sinai Medical Center, Los Angeles, CA, USA
7. Department of Medicine, University of California Los Angeles, CA, USA
8. Department of Urology, Ga Cheon University College of Medicine, Incheon, Republic of Korea

✉ Corresponding author: Jayoung Kim, PhD., Departments of Surgery and Biomedical Sciences, Cedars-Sinai Medical Center, 8700 Beverly Blvd., Los Angeles, CA 90048. Tel: +1-310-423-7168; Fax: +1-310-967-3809; E-mail: Jayoung.Kim@cshs.org

© Ivyspring International Publisher. This is an open access article distributed under the terms of the Creative Commons Attribution (CC BY-NC) license (<https://creativecommons.org/licenses/by-nc/4.0/>). See <http://ivyspring.com/terms> for full terms and conditions.

Received: 2018.01.24; Accepted: 2018.07.23; Published: 2018.08.10

Abstract

Alterations in DNA methylation are important epigenetic markers in bladder cancer (BC). These epigenome modifications may drive the mechanisms of aggressive chemo-resistant BC. Clinicopathological biomarkers that indicate chemotherapeutic resistance are critical for better assessing treatment strategies for individual patients. Thus, in this study, we aimed to determine whether DNA methylation of certain metabolic enzymes is significantly altered in cisplatin-resistant BC cells.

Methods: To characterize CpG methylation and nucleosome accessibility in cisplatin-resistant BC cells, the Illumina Infinium HM450 DNA methylation assay was performed. Perturbed gene expression was found to be associated with cisplatin resistance, and the biological roles of spermidine/spermine N¹-acetyltransferase (SAT1) and argininosuccinate synthase 1 (ASS1) were further studied using qRT-PCR analysis and various cell biology assays, including western blot.

Results: *ASS1* and *SAT1*, genes for amino acid and polyamine metabolism catalysts, respectively, were found to be vastly hypermethylated, resulting in greatly downregulated expression. *ASS1* expression is of particular interest because prior studies have demonstrated its potential association with BC stage and recurrence. In regard to chemoresistance, we found that aberrant expression or induced stimulation of *SAT1* restored cisplatin sensitivity in the cell culture system. We also found that the addition of exogenous arginine deiminase through administration of ADI-PEG 20 (pegylated arginine deiminase) increased *ASS1* expression and enhanced cisplatin's apoptotic effects.

Conclusions: Our study demonstrates a novel mechanistic link between the epigenetic perturbation of *SAT1* and *ASS1* and cancer metabolism in cisplatin-resistant bladder cancer cells. These findings suggest potential utility of *SAT1* and *ASS1* as predictive biomarkers in re-sensitizing bladder cancer to chemotherapy and personalizing therapy.

Key words: *SAT1*, *ASS1*, cancer metabolism, metabolomics, DNA methylation, chromatin accessibility, cisplatin resistance

Introduction

Bladder cancer (BC) is the second most common genitourinary malignancy worldwide and the fourth most common cancer in the U.S. [1-3]. Most patients

are diagnosed with treatable cell carcinoma or non-muscle invasive bladder cancer (NMIBC) [4, 5]. However, approximately 20-30% of all NMIBC cases

eventually progress to become muscle-invasive bladder cancer (MIBC). From there, about 50% of these patients develop metastases within two years, even after radical cystectomy [6, 7]. In addition, MIBC patients who do not respond to adjuvant chemotherapy have a worse prognosis [8]. Unfortunately, there are currently no well-defined and available prognostic marker(s) that can identify these higher-risk patients [9-11]. Therefore, in order to develop new diagnostic technologies, a comprehensive molecular understanding of the patient subsets who will acquire chemoresistance is required. The identification of markers capable of predicting the response in patients treated with platinum-based drugs is urgently needed in order to improve the outcomes for those BC patients who are at higher risk of developing resistance.

Epigenetic regulation has been demonstrated to play an important role in bladder tumorigenesis [12-14]. Recently, three separate subtypes of BC patients have been identified through analysis of DNA methylation profiles [14]. Epigenetic dysregulation occurs via cytosine methylation-dependent gene silencing, which is also considered a characteristic of therapeutic-resistance [15]. Cancer-specific DNA methylation mostly occurs on the CpG islands located in the promoter regions of genes and causes silencing of downstream genes [16, 17]. Currently, two DNA methyltransferase (DNMT) inhibitors (5-azacytidine and its variant, 5-aza-CdR) have been approved by the FDA for the treatment of high-risk myelodysplastic syndrome [18] and are also in clinical trials for solid forms of human cancers [19]. In addition to DNA methylation, there are other relevant epigenetic mechanisms that affect gene expression levels, including histone modification and nucleosome positioning. These processes work together to create the epigenetic landscape that directs the process of gene expression. Chromatin structure, which is based on DNA methylation and nucleosome accessibility (occupancy), plays a critical role in the regulation of gene expression at the transcriptional start sites of genes. Recent computational modeling using molecular dynamics simulations revealed the potential effects of epigenetic DNA methylation on nucleosome stability [20] and demonstrated that CpG methylation that contributes to nucleosome positioning can also be DNMT1 independent [21]. These findings suggest that monitoring chromatin accessibility, DNA methylation, and histone modification is crucial for better understanding therapeutic responses in BC [22-24].

Since first observed 90 years ago by Dr. Otto Warburg, metabolic reprogramming has been accepted as a hallmark of cancer [25-28]. Considering

this, targeting cancer-associated amino acid metabolism has been tested as a potential treatment option [29, 30]. Amino acids, such as arginine, proline, and glutamine, play a variety of functional roles in the cell. However, most importantly, they act as essential precursors for the biosynthesis of proteins. Therefore, depletion therapies, such as arginine deiminase (ADI) treatment, are being extensively tested against several cancer types, including ovarian cancer, mesothelioma, and hepatocellular carcinoma [31-35].

In this study, we sought to understand the epigenetic alterations underlying the metabolic reprogramming in cisplatin-resistant BC cells. Our experimental results suggest that cancer-specific epigenetic silencing of two genes encoding for metabolic enzymes, spermidine/spermine N¹-acetyltransferase (*SAT1*) and argininosuccinate synthase 1 (*ASS1*), is closely associated with cisplatin resistance and is epigenetically regulated in T24 BC cells. Both enzymes are related to arginine metabolism: *ASS1* catalyzes the final step in arginine biosynthesis. *SAT1*, on the other hand, catabolizes spermidine and spermine that are derived from arginine in sequential enzymatic steps that involve the conversion of arginine to ornithine, ornithine to putrescine, putrescine to spermidine, and spermidine to spermine [36, 37].

Results

Characterization of CpG methylation and nucleosome accessibility in cisplatin-resistant BC cells

In order to investigate the epigenetic modulation linked to cisplatin resistance in BC, we used two isogenic T24 BC cell lines—one that is cisplatin sensitive (T24S) and one cisplatin resistant (T24R). T24 cells were utilized because the characteristics of these cells have been previously reported by our group [38]. The T24R cell line exhibited much less responsiveness to cisplatin-induced apoptosis compared to T24S cells (**Figure 1A**). In order to understand the epigenetic reprogramming associated with cisplatin resistance, three independent sets of data profiles, namely (1) DNA methylation, (2) nucleosome accessibility, and (3) gene expression, were generated in T24R and T24S cells (**Figure 1B**).

We first performed DNA methylation analysis using the Illumina HumanMethylation450 BeadChip, in which >482,421 CpG sites are queried across the human genome. We identified 118,465 CpG sites as being differentially methylated in T24R cells compared to T24S cells, with a fold change of M-value ≥ 1.0 . Of these 118,465 differentially methylated CpG sites, we identified decreased methylation of 9,014

sites in 4,052 genes and increased methylation of 109,451 sites in 93,068 genes in T24R cells compared to T24S. (Figure S1 and Table S1). These findings suggest that DNA methylation profiles are radically altered in T24R cells and that hypermethylation may be correlated to cisplatin resistance in T24 BC cells.

Given the predominant global DNA hypermethylation pattern in T24R cells, we

speculated that T24R cells also have distinctive chromatin modifications and accessibility alterations that affect gene expression. Chromatin structure, which is organized through DNA methylation and nucleosome accessibility (or occupancy), plays a critical role in regulating gene expression at the transcription start site [39]. Thus, monitoring of chromatin accessibility, DNA methylation, and

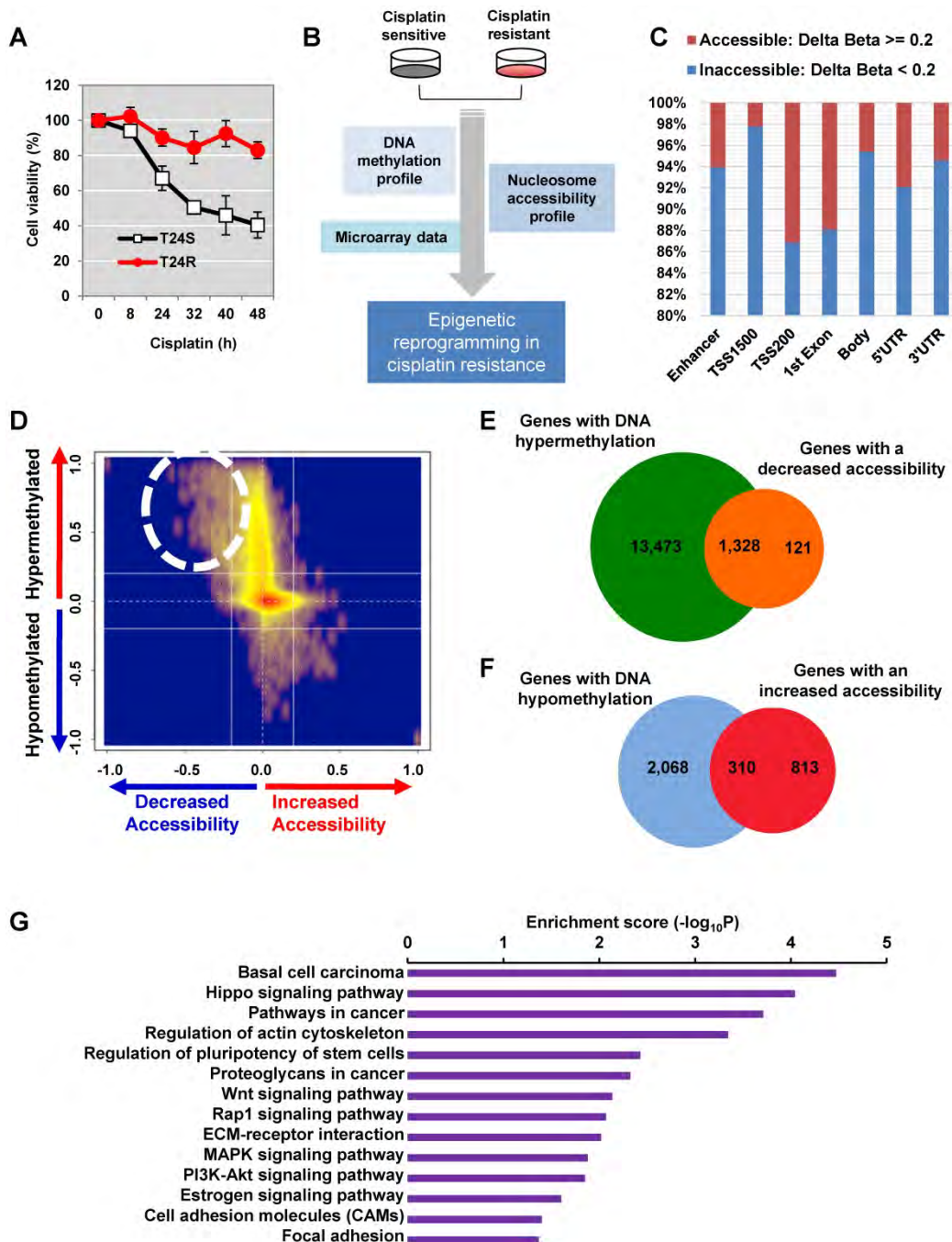


Figure 1. Determination of the epigenetic rewiring in cisplatin-resistant bladder cancer. (A) Cell viability was measured at the indicated times after 10 μM cisplatin treatment. (B) Overall experimental workflow of the investigation of epigenetic regulation associated with cisplatin resistance in this study. (C) Bar graph showing increased and decreased chromatin accessibility in T24R and T24S cells. Selection of the accessible CpG sites was based on delta beta at a threshold value 0.2. The percentage indicates the changes in accessible chromatin upon cisplatin resistance for individual genome features. (D) Chromatin accessibility visualized by Kernel density scatter plot of delta-methylation versus delta-accessibility. Circle depicts the region showing a loss of chromatin accessibility accompanied by DNA hyper-methylation. (E) Venn diagram depicting 14,801 genes with DNA hypermethylation and 1,449 genes with decreased accessibility. (F) Venn diagram showing 2,378 genes with DNA hypomethylation and 1,123 genes with increased accessibility. (G) Bar graph depicting enriched KEGG pathways of 1,328 hypermethylated genes with reduced chromatin accessibility.

histone modification is crucial for understanding disease progression and responses to therapy. Due to its importance in chromatin structuring, we hypothesized that nucleosome accessibility is altered in cisplatin-resistant BC cells, leading to altered DNA methylation.

To test this hypothesis, we used the AcceSss/ble assay [39] to determine nucleosome occupancy and positioning in T24R and T24S cells by probing CpGs using the Illumina HM450 BeadChip [39]. We identified a digital footprint of nucleosome occupancy and positioning in both the CpG-rich islands and CpG-poor regions of T24R and T24S cells. Methylation of nuclei treated with or without M.SssI, a CpG methyltransferase enzyme that methylates CpG sites on nucleosome-depleted unbound DNA, was compared using the Illumina HM450 BeadChip. We then stratified CpG sites with altered nucleosome accessibility (**Figure 1C**). Many genomic regions displayed decreased accessibility, except TSS 200 and the first exon.

Differential DNA methylation plotted against differential chromatin accessibility is shown in the Kernel density scatter plot (**Figure 1D**) with the circle depicting genes with decreased chromatin accessibility and DNA hypermethylation. Interestingly, we observed that nucleosome occupancy was greatly altered in T24R cells compared to the control T24S cells (**Figure S1**). In particular, we identified 1,328 genes with DNA hypermethylation and decreased chromatin accessibility in T24R cells compared to T24S cells (**Figure 1D-E** and **Table S2**). We also identified 310 genes with DNA hypomethylation and increased chromatin accessibility in T24R versus T24S cells (**Figure 1D, F** and **Table S3**). The top 10 genes with hypermethylation and decreased chromatin accessibility and the top 10 genes with hypomethylation and increased accessibility are listed in **Table S4** and **Table S5**. To understand the biological function of these genes, we performed functional enrichment analysis on the 1,328 hypermethylated genes, which revealed significant advancement of cancer-related pathways in T24R cells (**Figure 1G**). These findings provide a finer resolution on the nature of epigenetic mechanisms and broaden our understanding of nucleosome occupancy and DNA methylation changes in cisplatin-resistant BC cells.

Perturbed epigenetic signatures in cisplatin-resistant BC cells may lead to changes in gene expression

The DNA methylation data was integrated with our previously reported gene expression data [40]. According to the gene expression and DNA

methylation pattern, we grouped the genes into 6 clusters (**Figure 2A**). Among these, clusters 1 (up-hypo) and 2 (down-hyper) showed opposite patterns of gene expression and DNA methylation between T24R and T24S cells (**Figure 2A**). Cluster 1 contained genes in T24R cells whose expression was upregulated and DNA methylation was decreased. Cluster 2 consisted of genes in T24R cells whose expression was downregulated and DNA methylation was increased (**Figure 2A**). Follow-up gene ontology bioinformatic analyses of the experimental data further suggested that there is significant epigenetic silencing of genes that regulate arginine and proline metabolism, as well as extracellular matrix receptor interaction, PPAR signaling, adherens junction and focal adhesion, in cisplatin-resistant BC cells [40] (**Figure 2B**). In contrast, genes related to DNA replication were found to be epigenetically upregulated (hypomethylated) (**Figure 2B**).

As a result of this hypomethylation, transcription of genes associated with DNA replication, repair, and pyrimidine metabolism was upregulated. This suggests that there may possibly be a metabolic relationship between amino acid metabolism and DNA repair mechanisms. In an independent effort to explore metabolic perturbation of cisplatin resistance, a Kyoto Encyclopedia of Genes and Genomes (KEGG) metabolic map was constructed that displayed the differential regulation of metabolic pathways between cisplatin-resistant BC cells and controls. This also supported the idea that transcripts for the metabolism of amino acids, such as arginine and proline (down-hyper), and of purine and pyrimidine (up-hypo), are significantly altered in T24R cells (**Figure 2C**). In particular, promoters of genes associated with amino acid metabolism, such as arginine and proline metabolism, were hypermethylated, leading to decreased gene expression levels, as shown in the dotted box in **Figure 2C** and **Figure S2**.

Cisplatin-resistant T24 cells displayed epigenetic silencing (hypermethylation and decreased mRNA expression) of genes associated with arginine and proline metabolism, such as *GLUD2* (glutamate dehydrogenase 2), *ARG2* (arginase 2), *ALDH2* (aldehyde dehydrogenase 2), *P4HA1* (prolyl 4-hydroxylase subunit alpha 1), *ALDH7A1*, (aldehyde dehydrogenase 7 family member A1), *GLUD1* (glutamate dehydrogenase 1), *PYCR1* (pyrroline-5-carboxylate reductase 1), *ASS1* (argininosuccinate synthase 1), *ALDH18A1* (aldehyde dehydrogenase 18 family member A1), *P4HA2* (prolyl 4-hydroxylase subunit alpha 2), *NAGS* (N-acetylglutamate synthase), as well as *SAT1* (spermidine/spermine N1-acetyltransferase), and *CKB* (creatine kinase B) (fold

change ≥ 2 and FDR <0.05 ; Table 1). We identified *SAT1* and *ASS1* as the two most prominently hypermethylated and downregulated genes in T24R cells. The fold change of *SAT1* expression was -6.09 (FDR <0.001), while that of *ASS1* was -5.27 (FDR=0.017). Given that *SAT1* and *ASS1* have not yet been studied in the context of cisplatin resistance in BC, our results suggest new gene targets.

Expression levels of epigenetically regulated genes are associated with clinical outcomes in BC patients

We next speculated if the differentially methylated genes (DMGs) identified in T24R cells could be clinically predictive indicators for recurrence, tumor grade, overall survival, and/or

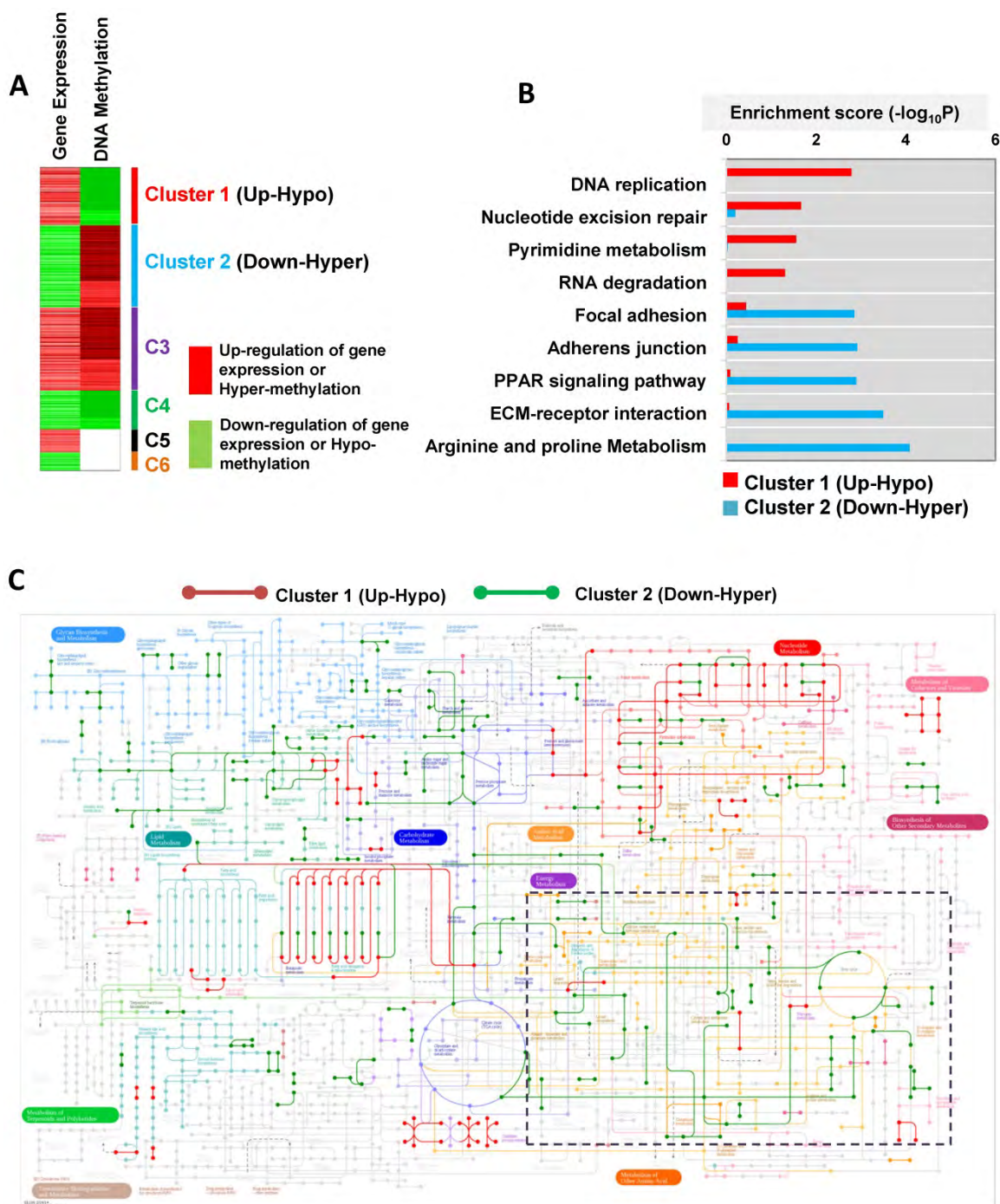


Figure 2. Metabolic pathways directed by differentially expressed and methylated genes. (A) Heatmap depicting differential gene expression and DNA methylation patterns of T24R cells compared to T24S cells. **(B)** The enriched biological processes associated with the upregulated genes with DNA hypomethylation vs. the downregulated genes with DNA hypermethylation. **(C)** Metabolic pathway map displaying the changes seen in cisplatin-resistant BC. The KEGG metabolic map was overlaid with gene expression data. The nodes represent metabolic compounds and edges represent genes involved in the reactions (red lines: upregulated and hypomethylated genes; green lines: downregulated and hypermethylated-genes). The boxes with dotted lines indicate significantly altered pathways, including those for arginine and proline metabolism.

stage. To test this, we performed a series of analyses on the association of the DMGs with clinical outcomes using publicly available gene expression microarray data derived from 103 BC patients [41]. *GLUD1*, *ASS1*, and *ALDH2* were found to be associated with recurrence in BC patients who had already undergone chemotherapy (Figure 3A). *ASS1* was downregulated in BC patients who had recurrence (n=36) compared to those without (n=67) (Figure 3A). BC tumor grades were positively or negatively associated with gene expression levels of our protein panel, which included *GLUD1*, *ARG2*, *TYMS* (thymidylate synthase), and *TK1* (thymidine kinase 1) (Figure 3B). *TYMS* and *TK1* are proteins associated with pyrimidine metabolism and their gene levels were more upregulated and hypomethylated in T24R cells (Figure 2B). Furthermore, gene expression patterns of *GLUD1*, *GLS*, *ALDH2*, *SAT1*, *ASS1*, and *TYMS* distinguished patients who had worse overall survival from those with recurrence-free survival (Figure 3C). Of note, *ASS1* expression was also negatively correlated with BC stage: lower *ASS1* expression was a feature of higher tumor stage (Figure 3D). Collectively, these results suggest that *SAT1* and *ASS1* are hypermethylated in cisplatin-resistant BC cells, thereby resulting in aberrant loss of expression. These defects may be what causes the decrease in recovery efficiency after DNA damage.

Epigenetic landscapes of *SAT1* and *ASS1* in cisplatin-resistant BC cells

We next sought to determine the DNA methylation landscape of *ASS1*, which is located on chromosome 9 and has several CpG islands. The difference in DNA methylation of *ASS1* between T24R and T24S cells was 4.35-fold (log₂) and the gene expression difference was -5.27-fold (log₂) (Figure 4A). *SAT1* and *TYMS* are localized on chromosomes X and 18, respectively. *SAT1* showed 1.33-fold (log₂) increased DNA methylation and 6.09-fold (log₂) decreased gene expression in T24R cells. Individual DNA methylation levels at specific CpG sites in *ASS1*, *SAT1*, and *TYMS* are shown in Figure 4B.

To further assess the causative relationship of *ASS1* and *SAT1* to cisplatin resistance, protein expression levels were compared between T24R and T24S cells (Figure 4C). We also found that *in vitro* addition of decitabin, a DNMT inhibitor, increased protein expression of both *SAT1* and *ASS1* in T24R cells (Figure 4D). Furthermore, two additional cisplatin-resistant BC cells lines, J82R and RT4R, were used to test whether decitabine treatment increases *SAT1* and *ASS1* expression. Experimental results showed that protein expression of both *SAT1* and *ASS1* were significantly enhanced in the presence of

decitabine, which was consistent with data from T24R cells (Figure 5E). Collectively, these findings indicate that downregulation of *SAT1* and *ASS1* may most likely be due to changes in epigenetic regulation (DNA hypermethylation of CpG promoter regions).

Table 1. Comparison of genes in cisplatin-resistant (T24R) and cisplatin-sensitive (T24S) cells. The genes are listed in two categories, DNA replication (pink) or arginine, proline, and polyamine metabolism (blue). The most downregulated (and hypermethylated) genes in cisplatin-resistant cells are those regulating arginine and proline metabolism, which include *ASS1* and *SAT1*.

Pathways	Symbol	Full name	mRNA Fold change	Accessibility
DNA replication	MCM7	minichromosome maintenance complex component 7	2.35	No change
	POLD1	polymerase (DNA directed), delta 1, catalytic subunit	1.54	No change
	POLE4	polymerase (DNA-directed), epsilon 4, accessory subunit	1.52	No change
	POLE	polymerase (DNA directed), epsilon, catalytic subunit	1.48	No change
	RFC3	replication factor C (activator 1) 3, 38kDa	1.36	No change
	RNASEH2C	Ribonuclease H2, subunit C	1.28	No change
	Arginine and proline metabolism	GLUD2	glutamate dehydrogenase 2	-1.12
ARG2		arginase 2	-3.15	No change
ALDH2		aldehyde dehydrogenase 2 family (mitochondrial)	-5.09	Decreased
P4HA1		prolyl 4-hydroxylase, alpha polypeptide I	-1.67	No change
ALDH7A1		aldehyde dehydrogenase 7 family, member A1	-1.27	Decreased
GLUD1		glutamate dehydrogenase 1	-1.09	No change
GLS		glutaminase	-1.88	No change
PYCR1		pyrroline-5-carboxylate reductase 1	-1.14	No change
ASS1		argininosuccinate synthase 1	-5.27	Decreased
ALDH18A1		aldehyde dehydrogenase 18 family, member A1	-1.21	No change
SAT1		spermidine/spermine N1-acetyltransferase 1	-6.09	Increased
P4HA2		prolyl 4-hydroxylase, alpha polypeptide II	-1.31	Decreased
NAGS		N-acetylglutamate synthase	-1.91	No change
CKB	creatine kinase, brain	-1.22	No change	

SAT1 and *ASS1* play critical roles in cisplatin resistance

Western blot analysis data demonstrated that cisplatin-resistant BC cells express little *SAT1*, while cisplatin-sensitive cells exhibit clearly detectable expression. Based on this, we hypothesized that activation or induced expression of *SAT1* could re-sensitize T24R cells. T24R cells were transfected with a FLAG-*SAT1* vector (Figure 5A). We found that induced *SAT1* expression in T24R cells enhanced apoptosis in both the absence and presence of cisplatin (Figure 5B). Upon cisplatin treatment, *SAT1*-overexpressing T24R cells displayed a significant increase in apoptosis, an approximate 3.5-fold of untreated basal levels (Figure 5B). *SAT1* overexpression also led to an estimated 2.3-fold

increase in the production of reactive oxygen species (ROS), which may contribute to the re-sensitization of T24R cells to cisplatin (Figure 5C).

Next, to evaluate the potential interdependence of SAT1 activation and drug sensitivity, we treated T24R cells with a combination of cisplatin and BENSpm (a SAT1 inducing reagent) (Figure 5D). This

resulted in a significant synergistic reduction of cell survival that was greater than treatment with cisplatin or BENSpm alone. Consistent with the findings in T24R cells, additional experiments conducted on J82R (Figure 5E) and RT4R (Figure 5F) cells showed that BENSpm sensitized cisplatin-resistant BC cells.

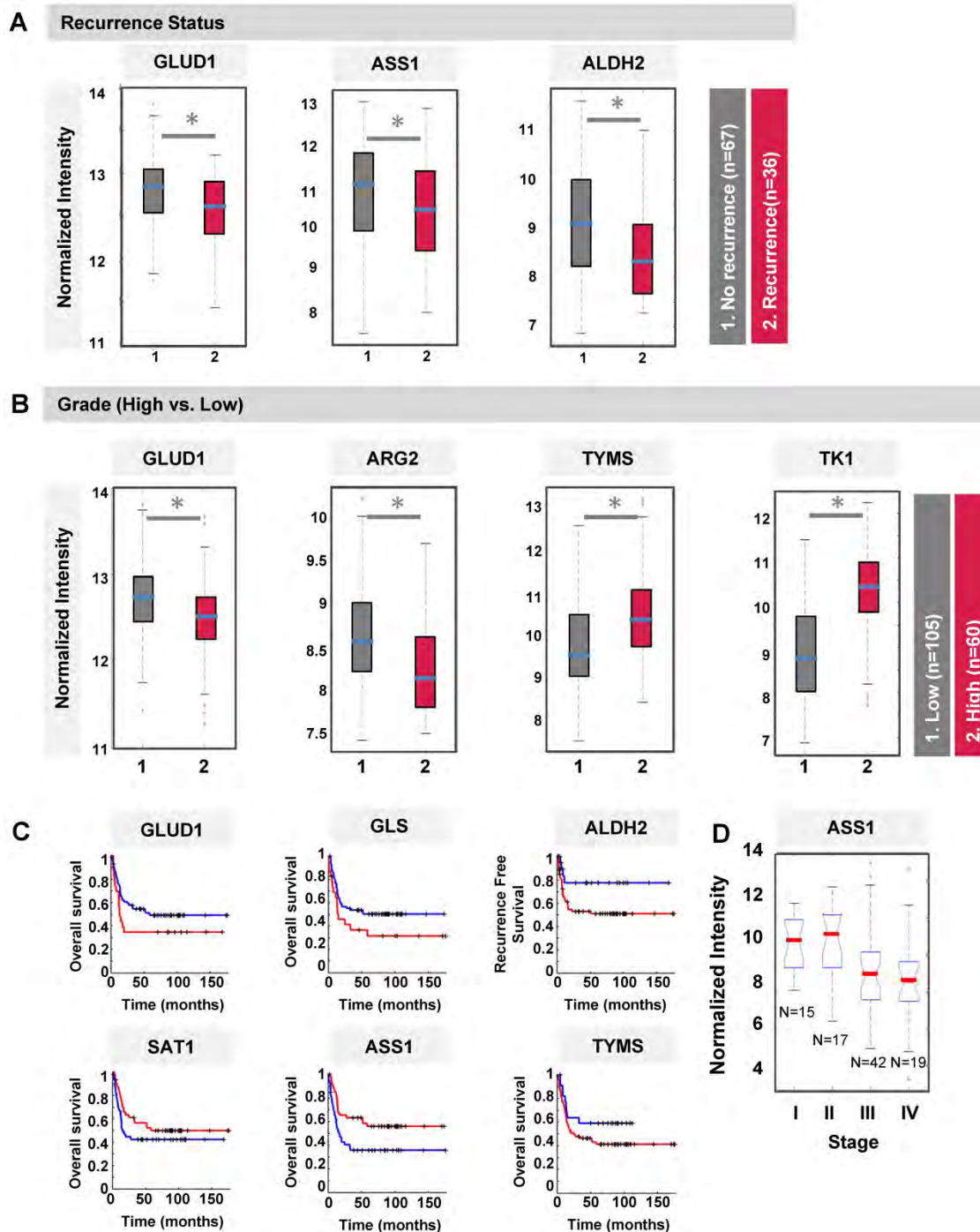


Figure 3. Clinical association of DMGs with differential expression in T24R and T24S cells. (A) Box plot showing recurrence predictability of *GLUD1*, *ASS1*, and *ALDH2*. **(B)** Box plot showing grade predictability of *GLUD1*, *ARG2*, *TYMS*, and *TK1*. **(C)** Overall survival rate graph showing survival predictability of *GLUD1*, *GLS*, and *ALDH2*. **(D)** Box plot showing tumor stage predictability of *ASS1*.

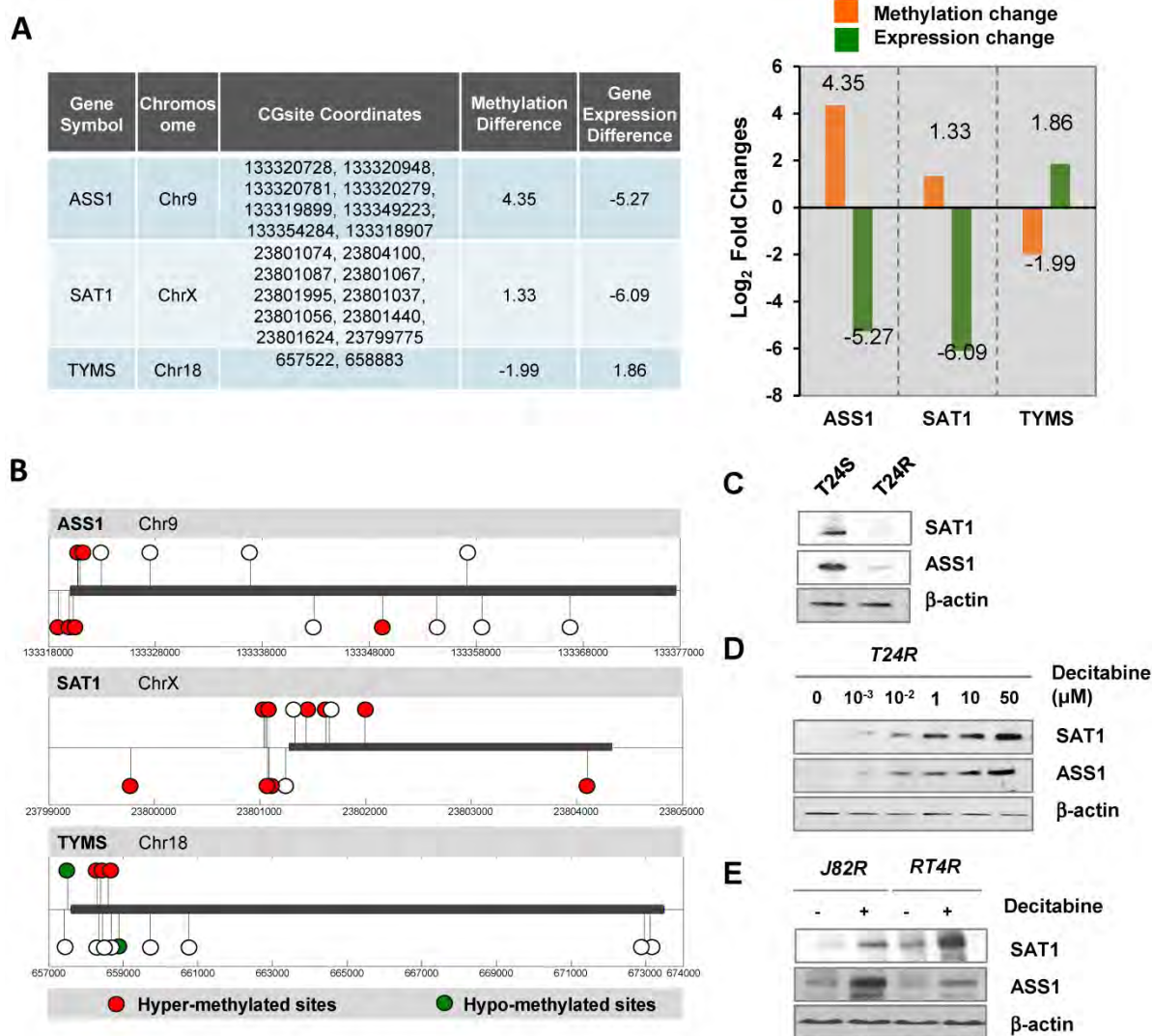


Figure 4. Alteration of DNA methylation landscapes in cisplatin-resistant BC cells. (A) Table showing promoter CpG methylation sites identified by HM450 array, and fold changes in DNA methylation and gene expression of *ASS1*, *SAT1*, and *TYMS*. Fold changes of DNA methylation (orange bars) and gene expression (green bars) of *ASS1*, *SAT1*, and *TYMS* in T24R compared to T24S, are shown. **(B)** Methylation sites on *ASS1*, *SAT1*, and *TYMS* (red circle, hypermethylated sites; green circle, hypomethylated sites; white circle, no changes). **(C)** Downregulation of *SAT1* and *ASS1* protein expression levels in T24R cells compared to T24S. **(D)** Increased protein expression of *SAT1* and *ASS1* in T24R cells upon treatment with decitabine, an inhibitor of DNA methylation. **(E)** Increased protein expression of *SAT1* and *ASS1* in J82R or RT4R cells upon treatment with decitabine.

Our experimental data provided evidence that DNA methylation of *ASS1* is increased and gene expression is decreased in T24R cells (Figure 4A). In addition, arginine metabolism is also shown to be defective in T24R cells. This opens the possibility that this may also hold true for other cisplatin-resistant cancers. During analysis of publicly available human BC data collections, we found that *ASS1* expression is negatively correlated with BC recurrence and grade. Currently, pegylated arginine deiminase (ADI-PEG 20), an arginine-depleting therapy, is under evaluation in clinical trials for many types of cancers, including BC. We found that similar treatment with ADI-PEG 20 increased *ASS1* expression in T24S cells (Figure 5G). In T24R cells, *ASS1* was not expressed up to 72 h following treatment with ADI-PEG 20 (Figure 5G). We also found that *ASS1* was not re-expressed

when T24R cells were treated for 96 h. Given that T24S cells exhibit *ASS1* expression, *ASS1* deficiency will likely be a key factor in selecting patients for clinical trials involving ADI-PEG 20 therapy, which is consistent with previous observations in other cancer types [42].

Next, we determined whether arginine depletion via ADI-PEG 20 could induce apoptosis in T24R cells that do not express *ASS1*. T24R cells were treated under various conditions: (1) cisplatin alone, or (2) combination of cisplatin and ADI-PEG 20 in a dose-dependent manner (1, 10, 100, and 750 ng/mL). Cell survival rates were measured using two independent assays, the MTS (Figure 5H) and crystal violet assay (Figure 5I). The following time-dependent experiments showed consistent results (Figures 5J) (crystal violet assay) and Figure 5K

(MTS assay)). In addition, J82R and RT4R cells were tested with ADI-PEG 20 treatment as well. The results suggested that a combination of cisplatin and ADI-PEG 20 greatly enhances responsiveness to cisplatin in resistant BC cell lines and resulted in approximately 50% and 40% reduction in cell survival rates in J82R and RT4R cells, respectively (Figures 5L-M).

To further supplement evidence for the association of ASS1 and SAT1 with BC, immunohistochemistry (IHC) analysis was performed

using commercial BC tumor microarrays (TMAs). We found that 80% of the tumors (32/40 cores) were negative for SAT1 and ASS1 protein expression (data not shown). These results imply that SAT1 and/or ASS1 silencing are potential indicators of disease. In this regard, patients with little to no expression of SAT1 and ASS1 may be good candidates for combination treatments with ADI-PEG 20 and cisplatin. This is because SAT1 and ASS1 expression may be indicators of clinical benefit from cisplatin chemotherapy and/or arginine deprivation therapy.

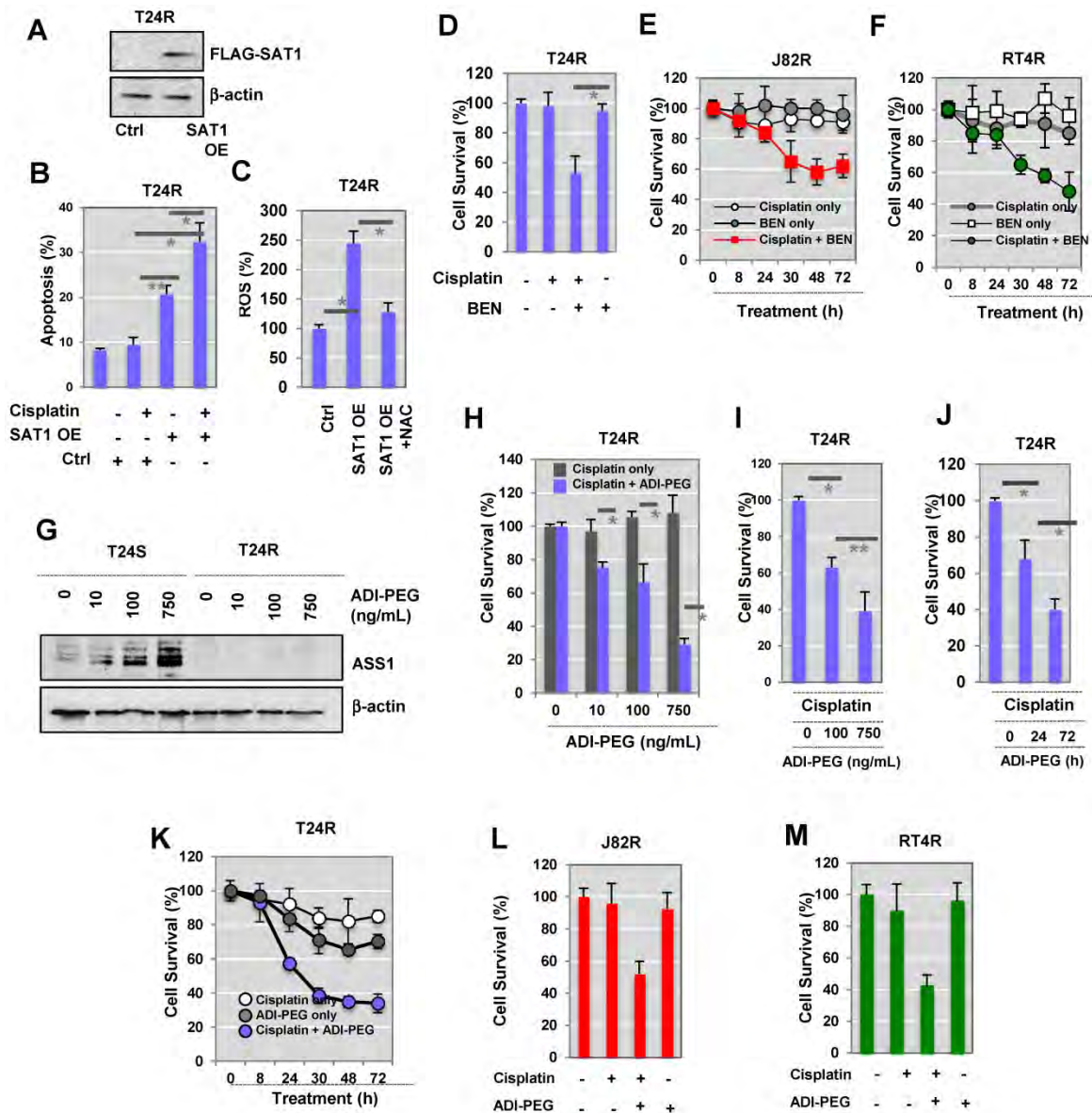


Figure 5. Sensitization of T24R cells to cisplatin-induced apoptosis by overexpression of SAT1 or BENSpm treatment. (A) Overexpression of SAT1 protein in T24R cells transfected with pCMV7.1 3XFLAG-hSAT1 was confirmed by western blot analysis using an anti-flag antibody. **(B)** Sensitization of T24R cells to cisplatin-induced cell apoptosis upon overexpression of SAT1. **(C)** Increase in ROS production through overexpression of SAT1 in T24R cells and reduction of ROS by N-acetylcysteine (NAC). The levels of ROS produced in control cells are set at 100%. Each bar represents the mean ± SD of three independent experiments (*, P<0.05). **(D)** Suppression of survival of cisplatin-treated T24R cells by BENSpm treatment. **(E-F)** Treatment with BENSpm sensitized cisplatin-resistant BC cells, J82R (E) and RT4R (F). **(G)** Restoration of ASS1 expression in T24S cells by ADI-PEG 20 in a dose-dependent manner. Cells were harvested 72 h after treatment. **(H-J)** Enhancement of apoptosis through the combination of cisplatin and ADI-PEG 20 in cisplatin-resistant T24R, but not T24S, cells. Cell survival was determined used **(H)** MTS assay and **(I)** crystal violet assay 72 h after treatment with cisplatin with or without ADI-PEG 20. **(J)** T24R cells were treated with cisplatin alone, ADI-PEG 20 alone, or with cisplatin plus ADI-PEG 20 for 0, 24, or 72 h. Crystal violet assay was performed. **(K)** T24R cells were treated with cisplatin alone, ADI-PEG 20 alone, or with cisplatin plus ADI-PEG 20 for 0, 8, 24, 30, 48, or 72 h. (Blue circle: ADI-PEG 20 plus cisplatin; white circle: cisplatin alone; gray circle: ADI-PEG 20 alone). Cell survival rates were measured using MTS assay. **(L-M)** Cell survival rates increased in J82R or RT4R cells upon treatment with cisplatin and ADI-PEG 20.

Discussion

In this study, we sought to determine if epigenetically regulated metabolic reprogramming is associated with cisplatin resistance in BC, and if *SAT1* and *ASS1* are potential predictive biomarkers for cisplatin resistance. Generally, treatment for recurrent BC involves systemic cisplatin chemotherapy [43]. Although this current standard has decreased morbidity and mortality, failure of treatment frequently occurs due to acquired chemoresistance. This has resulted in a 5-year survival rate of only 5-15% following recurrence [44-46]. Therefore, concerted efforts are necessary to identify markers associated with cisplatin resistance in BC patients. Moreover, identification of markers is key to comprehending the mechanisms of cisplatin resistance that is critically needed in order to develop novel treatment strategies.

In our study, decitabine reestablished cisplatin susceptibility in resistant BC cells by increasing *ASS1* expression. Our experimental results demonstrate the epigenetic regulatory mechanisms of *ASS1* and *SAT1* and their potential contributions to metabolic perturbations that are apparent in the context of drug resistance. This study also provides evidence that therapeutic targeting of metabolic pathways through the use of BENSpm or ADI-PEG 20 may help overcome cisplatin resistance. Furthermore, analysis of tumor tissue samples from BC patients showed that approximately 80% had little to no expression of *ASS1* and *SAT1*, an indication that these genes have profound roles in BC tumorigenesis and development. Although this is out of the scope of this current study, it would be of great interest to evaluate if *ASS1* and/or *SAT1* are predictive indicators of response to adjuvant chemotherapy among assembled BC patient populations.

Global reprogramming of DNA methylation has been linked to the onset and progression of cancer [23, 47]. DNA hypermethylation at promoter regions of tumor suppressor genes often leads to silencing of expression. In contrast, DNA hypomethylation has been reported to induce genome instability and can activate proto-oncogenes [48, 49]. DNA-demethylating agents, such as 2'-deoxy-5-azacitidine/decitabine (DAC) and 5-azacitidine/azacitine (AZA), can induce global DNA demethylation in tumor cells when they are transiently given at low doses [50, 51]. DAC and AZA can also reverse epigenetic silencing and reactivate tumor suppressor gene expression, which might contribute to antitumor effects. In non-cancer diseases, such as myelodysplastic syndrome (MDS), the FDA has approved AZA and DAC as treatment options. Next-generation DNMT inhibitors and oral formulations are also currently

under development. However, epigenetic therapies alone may not be effective in treating human cancers. They are likely best when combined with other modalities, such as chemotherapies or immunotherapies. Thus, there are a series of ongoing clinical trials using DNMT inhibitors in combination with conventional regimens for many cancer types [52].

Our current study further investigated the epigenetic landscape of cisplatin-resistant BC and found that resistance may be associated with modifications in the arginine metabolome via *ASS1*, the rate-limiting enzyme in arginine synthesis. Loss of *ASS1* drives cancer cells to become dependent on extracellular arginine, effectively converting these cells into arginine auxotrophs. *ASS1* deficiency has been observed in various other cancer types, including hepatocellular carcinoma, melanoma, myxofibrosarcoma, mesothelioma, prostate cancer, and renal cancer [53-57]. In terms of BC, *ASS1* deficiency is particularly common in urothelial carcinoma, small cell, and squamous cell carcinoma subtypes [57, 58]. Based on this, ADI-PEG 20 is currently being tested in clinical trials for many cancer types (<https://clinicaltrials.gov>, identifiers NCT01497925, NCT02029690, and NCT02101593, etc.). Given previous findings demonstrating that *ASS1* expression is negatively correlated with the anti-cancer effects of ADI-PEG 20 treatment, loss of or reduced *ASS1* may be a predictive factor that can determine which patients will benefit from treatment.

Our results also showed that *SAT1* overexpression promotes the sensitivity of T24R cells to cisplatin-induced apoptosis. This is consistent with a previous report showing that *SAT1* overexpression can lead to the depletion of spermidine and spermine, while simultaneously increasing polyamine oxidation [59]. This depletion of spermidine and spermine causes apoptosis through a mitochondria-mediated pathway [59]. Since mitochondrial dysfunction and redox imbalance are known to contribute to cancer, it would be interesting to investigate the connection between polyamine metabolism and cisplatin resistance in the context of mitochondrial function, metabolic pathways, and cell signaling. Although we did not delve into this area in our study, we believe that a better understanding of the potential link between nitrogen metabolism and cisplatin resistance in BC may provide supplemental information on epigenetic regulation of metabolism.

In summary, our present study suggests that the epigenetic regulation of certain amino acids and polyamine metabolic enzymes is significantly altered in BC and that this change may play a critical role in BC chemoresistance. The main results from our study are expected to lead to a novel molecular signature

that could potentially be applied in clinical tests for guiding treatment decisions. Thereby, these results could pave a path towards identification of novel drugs that can decrease chemoresistance. Our data also suggests the involvement of polyamine and arginine pathways in BC chemoresistance. The experimental results from this study contribute to a better understanding of the dependence of BC on exogenous polyamine or arginine, which may potentially lead to the capability of accurately distinguishing MIBC patients who will not develop cisplatin resistance. The status of SAT1 or ASS1 expression may be a reliable method of identifying which MIBC patients will or will not develop cisplatin resistance after chemotherapy. Furthermore, this study has significant clinical relevance to public health; it provides pre-clinical evidence that enhancing polyamine catabolism or arginine biosynthesis may overcome cisplatin resistance in aggressive BC.

Methods

Reagents

ADI-PEG 20 was generously provided by Polaris Pharmaceuticals (San Diego, CA). A vector construct encoding FLAG-tagged human SAT1 (pCMV7.1 3XFLAG-hSAT1) was provided by Dr. MH Park [60]. BENSpm, a SAT1 agonist, was a gift from Dr. David Oupicky at the University of Nebraska Medical Center. Decitabine, a DNMT inhibitor, was obtained from Selleckchem (Cat. No. S1200). The following antibodies were purchased, as indicated: β -actin (Sigma, USA), SAT1 (Thermo Fisher Scientific, USA), ASS1 (Cell Signaling Technology, USA), PARP, and cleaved-PARP (Cell Signaling Technology, USA).

Tissue culture

Three human BC cell lines (T24, J82, and RT4) were procured from the American Type Culture Collection (Manassas, VA). Cisplatin-sensitive (T24S, J82S, and RT4S) or resistant (T24R, J82R, and RT4R) cells were constructed and characterized in our laboratory [38]. Experiments were carried out in accordance with approved protocols and all methods adhered to institutional guidelines.

Accessibility assay

The principle of this assay has been described and published prior [39, 61]. Cell pellets were washed twice with ice-cold PBS buffer then resuspended in 1 mL PBS. Lysis buffer (10 mM Tris (pH 7.4), 10 mM NaCl, 3 mM MgCl₂, 0.1 mM EDTA, 0.5% NP-40) was then added and the lysates were centrifuged at 1006 rcf for 5 min at 4 °C. The supernatant was removed and the pellets were suspended in 2 mL of wash

buffer (10 mM Tris (pH 7.4), 10 mM NaCl, 3 mM MgCl₂, 0.1 mM EDTA). This suspension was then divided into two microcentrifuge tubes (no enzyme and M.Sssl reactions) and centrifuged again at 1006 rcf for 5 min at 4 °C. The supernatant was removed and the following was added to each tube: 84.25 μ L 1X NEBuffer 2, 7.5 μ L 10X NEBuffer 2, 45 μ L 1 M sucrose, 1.5 μ L 32 mM S-adenosylmethionine (SAM), and 12.5 μ L 4 U/ μ L M.Sssl (or H₂O for the no enzyme tube). The reaction mixtures were incubated at 37 °C for 15 min. Pre-warmed (37 °C) 300 μ L stop solution (10 mM Tris-HCl (pH 7.9), 600 mM NaCl, 1% SDS, 0.1 mM EDTA) and 6 μ L of Proteinase K were added to each tube, and the reaction mixtures were incubated at 55 °C for 16 h. DNA was then purified via phenol/chloroform extraction and ethanol precipitation, and then redissolved in 20 μ L of ddH₂O for subsequent analyses.

Quality control M.Sssl treatment

In total, 1 μ g of no enzyme or M.Sssl-treated DNA was subjected to bisulfite conversion using the Zymo EZ DNA Methylation Kit (using the Illumina Infinium® Methylation Assay alternative incubation conditions). Bisulfite (BS)-converted DNA was then analyzed by the high-resolution melt (HRM) method using the Bio-Rad Precision Melt Supermix (Catalog #172-5110) (reaction mix: 10 μ L Precision Melt Supermix, 0.8 μ L of 5 μ M primer mix, 1 μ L BS-converted DNA, 8.2 μ L ddH₂O) (PCR protocol: 95 °C for 00:02:00, [95 °C for 00:00:10, 58 °C for 00:00:30, plate read, 72 °C for 00:00:30] \times 60 cycles, 95 °C for 00:00:30, 60 °C for 00:01:00, melt curve 65 °C to 90 °C [00:00:10 and plate read at each degree]). Primer sequences: ACTB: 5'-AGAGGGGGTAAAAAATGT TGTAT-3', 5'-TCGAACCATAAAAAACAACCTTTC-3'; GADPH: 5'-TTTTAAGATTTGGGTTGGGT-3', 5'-CTATCGAACAAAAAACAACAAAAAC-3'; C1D: 5'-TTTTTGGAGAAGAGTTAAGGAGTAGG-3'; 5'-AC TCCAATCTCCCGAAAAAC-3'; RPLP0: 5'-AGGTGG TAGTAGTTTAGAGTAAGTTTT-3', 5'-CGAATACA AACACCATTAAATA-3'. Proper M.Sssl treatment was verified by a shift in melting curves upon methylation. For HM450 analysis, >0.5 μ g of BS-treated DNA samples with verified M.Sssl treatment were submitted.

Infinium® HumanMethylation450 BeadChip assay and data processing

The amount of bisulfite-converted DNA and the completion of bisulfite conversion were determined using a panel of MethyLight-based quality control (QC) tests, as described previously [62]. All the samples that passed the QC tests were subjected to the HM450 assay data production [49].

The HM450 probes interrogate the methylation statuses of ~485,000 CpG sites, which covers 99% of RefSeq genes, 96% of CpG islands, and spans promoters 5' UTRs, first exons, gene bodies, and 3' UTRs. The probe list was then filtered to remove probes with a detection p -value > 0.05 and those located within 15 base pairs of a single-nucleotide polymorphism, mapped to multiple locations, or are on sex chromosomes. The end result is a dataset of corrected beta-values for 385,826 probes that cover ~19,500 genes. The intensities of methylation-specific probes over the signals of unmethylated-specific probes were computed as M values [63]. The M values from the arrays were normalized using the quantile method [64].

Chromatin accessibility analysis

The beta value method with methylation data was used to analyze bisulfite-treated DNA as described in a previous study [39]. Briefly, The accessibility scale was defined as the beta value of M.SssI-treated cells minus the beta value of the no-enzyme control (delta-beta), defined on a 0–1 scale, after removing the probes with delta-beta < 0 . Accessible probes were defined as delta-beta > 0.2 .

Identification of differentially expressed genes

To identify differentially expressed genes (DEGs) between T24S and T24R cells, we performed the integrated hypothesis testing method [65, 66]. Briefly, the T value, \log_2 -median ratios, and Z values for rank-sum differences were computed for each gene. Empirical distributions of the null hypothesis were estimates for the T values, \log_2 -median ratios, and Z values of the genes after permuting the samples. For each gene, adjusted P -values of its observed T -values, \log_2 -median ratios, and rank-sum ratios were computed using their corresponding empirical distributions in a two-tailed test. The individual P -values from the two tests were then combined and the false discovery rate (FDR) was computed using the Stouffer's method [65, 66]. The DEGs were chosen based on their FDR and fold change (FDR < 0.05 and \log_2 -fold-change ≥ 1.0).

Functional enrichment analysis

Enrichment analysis of gene ontology biological processes (GOBPs) and KEGG pathways for the genes listed as DMGs and DEGs was performed using the DAVID software [67].

Construction of a network model

To construct a network model describing cisplatin resistance in BC cells, we first selected the subsets of genes from Clusters 1 and 2 that were involved in metabolic processes. We then collected

the interaction data regarding these genes from the STRING database (Ver. 10.5) and used this information to reconstruct a network model [68]. Finally, the network model was visualized using Cytoscape [69]. The nodes in the network model represent the genes distributed according to the metabolic pathway in which they are involved.

Quantitative RT-PCR analysis

Total RNA was purified using the MagNA Pure Compact RNA Isolation Kit (Roche), according to the manufacturer's instructions. The cDNA was then synthesized using the iScript cDNA Synthesis Kit (Bio-Rad), which was followed by qPCR using iTaq Universal SYBR Green Supermix (Bio-Rad) on an ABI 7500 Fast Real-Time PCR System (Life Technologies). The annealing temperature for qPCR was set to 60 °C and actin-beta (ACTB) was used as an internal control for normalization of gene expression.

Western blot analysis

The collected cells were washed twice with ice-cold PBS and lysed with a whole-cell extract lysis buffer (Bio-Rad) with a protease inhibitor cocktail (Thermo Fisher). Protein levels were measured and cell lysates containing 25 μ g of proteins were used for SDS-PAGE. Proteins were then electrophoretically transferred onto nitrocellulose membranes for further processing. After blocking for 30 min with 5% milk in tris-buffered saline with tween 20 (TBST), the membranes were incubated with a specific primary antibody overnight at 4 °C. Following this step, the membranes were washed and incubated with secondary, species-specific horseradish peroxidase-conjugated antibodies. Immunoreactive proteins were detected via chemiluminescence (Pierce Laboratories) and band intensities were quantified using ImageJ.

Cell survival assay

T24 cell lines were incubated with cisplatin, BENSpm, and/or ADI-PEG 20, as indicated. Cell survival after treatment was determined by measuring cell viability using MTS reagents (Promega Corporation, Madison, WI), according to the company's protocols.

Reactive oxygen species (ROS) measurement

To determine intracellular ROS levels, cells were stained using dichlorofluorescein diacetate (DCF-DA) (Sigma-Aldrich). Cells were seeded into 6-well plates at a density of 2×10^5 cells/well. At 24 h post seeding, DCF-DA was added to the wells under low-light conditions and the plates were incubated in the dark at room temperature for 20 min. The cells were then washed twice with PBS and fluorescence intensities were determined using the FACS Calibur

Flow Cytometer. Data was analyzed using FlowJo software.

Statistical analysis

Statistical analyses were conducted using MATLAB (Ver. 9.2). Data was expressed as mean \pm standard deviation (SD). For most of the biochemical data analyses, Student's *t*-test was used. Differences were considered statistically significant when $*p < 0.05$, or $**p < 0.01$.

Abbreviations

ADI: arginine deiminase; *ALDH18A1*: aldehyde dehydrogenase 18 family member A1; *ALDH2*: aldehyde dehydrogenase 2; *ALDH7A1*: aldehyde dehydrogenase 7 family member A1; *ARG2*: arginase 2; *ASS1*: argininosuccinate synthase 1; *AZA*: 5-azacitidine/azacitine; BC: bladder cancer; *CKB*: creatine kinase B; DAC: 2'-deoxy-5-azacitidine/decitabine DCF-DA: dichlorofluorescein diacetate; DEGs: differentially expressed genes; DMGs: differentially methylated genes; DNMT: DNA methyltransferase; FD: fold-change; FDR: false discovery rate; *GLUD1*: glutamate dehydrogenase 1; *GLUD2*: glutamate dehydrogenase 2; GOBPs: gene ontology biological processes; MDS: myelodysplastic syndrome; MIBC: muscle invasive bladder cancer; NAGS: N-acetylglutamate synthase; NMIBC: non-muscle invasive bladder cancer; PARP: poly-(ADP-ribose)-polymerase; PBS: phosphate-buffered saline; *P4HA1*: prolyl-4-hydroxylase subunit alpha 1; *P4HA2*: prolyl-4-hydroxylase subunit alpha 2; *PYCR1*: pyrroline-5-carboxylate reductase 1; ROS: reactive oxygen species; SD: standard deviation; *SAT1*: spermidine/spermine N¹-acetyltransferase; T24R: cisplatin-resistant T24R cells; T24S: cisplatin-sensitive T24R cells.

Supplementary Material

Supplementary figure and table legends, supplementary figures, supplementary tables 4-5.

<http://www.thno.org/v08p4520s1.pdf>

Supplementary table 1.

<http://www.thno.org/v08p4520s2.xls>

Supplementary table 2.

<http://www.thno.org/v08p4520s3.xls>

Supplementary table 3.

<http://www.thno.org/v08p4520s4.xls>

Acknowledgements

The authors acknowledge support from National Institutes of Health (1U01DK103260, 1R01DK100974, U24 DK097154, NIH NCATS UCLA CTSA UL1TR000124), Department of Defense (W81XWH-15-1-0415), Centers for Disease Controls and

Prevention (1U01DP006079), IMAGINE NO IC Research Grant, the Steven Spielberg Discovery Fund in Prostate Cancer Research Career Development Award, the U.S.-Egypt Science and Technology Development Fund by the National Academies of Sciences, Engineering, and Medicine (to J.K.), the Vicky Joseph Cancer Research Foundation, and Kure it for Cancer Research (to G.L.). J.K. is former recipient of Interstitial Cystitis Association Pilot Grant, a Fishbein Family IC Research Grant, New York Academy of Medicine, and Boston Children's Hospital Faculty Development. The funders had no role in the design, data collection and analysis, decision to publish or preparation of the manuscript.

Authors' Contributions

JK conceptualized and designed the study, led the fund acquisition process, and overviewed the literature analysis and drafting of the manuscript. AY and DJW performed HM450 analysis and nucleosome accessibility analysis. AY contributed to pre-processing of samples. MP, DJW, and GL provided scientific insights to data analyses. SY and MK performed full data analysis and visualization of the data. AG, DJW, and MP assisted in the preparation of the manuscript. All authors read and approved the final manuscript.

Competing Interests

The authors have declared that no competing interest exists.

References

- Kiemeny LA, Witjes JA, Verbeek AL, Heijbroek RP, Debruyne FM. The clinical epidemiology of superficial bladder cancer. Dutch South-East Cooperative Urological Group. British journal of cancer. 1993; 67: 806-12.
- Borden LS, Jr., Clark PE, Hall MC. Bladder cancer. Current opinion in oncology. 2003; 15: 227-33.
- Hall MC, Chang SS, Dalbagni G, Pruthi RS, Seigne JD, Skinner EC, et al. Guideline for the management of nonmuscle invasive bladder cancer (stages Ta, T1, and Tis): 2007 update. The Journal of urology. 2007; 178: 2314-30.
- Kamat AM. Commentary on "Surveillance guidelines based on recurrence patterns after radical cystectomy for bladder cancer: the Canadian Bladder Cancer Network experience." Yafi FA, Aprikian AG, Fradet Y, Chin JL, Izawa J, Rendon R, Estey E, Fairey A, Cagiannos I, Lacombe L, Lattouf JB, Bell D, Saad F, Drachenberg D, Kassouf W. Department of Surgery (Urology), McGill University, Quebec, Canada: BJU Int 2012;110(9):1317-23 [Epub 2012 Apr 13]. Urologic oncology. 2013; 31: 717-8.
- Large MC, Cohn JA, Steinberg GD. Optimal risk-adapted surveillance strategies for NMIBC, including upper tract imaging. The Urologic clinics of North America. 2013; 40: 305-15.
- Babjuk M, Oosterlinck W, Sylvester R, Kaasinen E, Bohle A, Palou-Redorta J. EAU guidelines on non-muscle-invasive urothelial carcinoma of the bladder. European urology. 2008; 54: 303-14.
- Stenzl A, Cowan NC, De Santis M, Kuczyk MA, Merseburger AS, Ribal MJ, et al. Treatment of muscle-invasive and metastatic bladder cancer: update of the EAU guidelines. European urology. 2011; 59: 1009-18.
- Black PC, Dinney CP. Growth factors and receptors as prognostic markers in urothelial carcinoma. Current urology reports. 2008; 9: 55-61.
- Apolo AB, Grossman HB, Bajorin D, Steinberg G, Kamat AM. Practical use of perioperative chemotherapy for muscle-invasive bladder cancer: summary of session at the Society of Urologic Oncology annual meeting. Urologic oncology. 2012; 30: 772-80.
- Schwentner C, Stenzl A, Gakis G. Monitoring high-risk bladder cancer. Current opinion in urology. 2012; 22: 421-6.
- Sompavde G, Sternberg CN. Neoadjuvant chemotherapy for invasive bladder cancer. Current urology reports. 2012; 13: 136-46.

12. Feber A, Dhimi P, Dong L, de Winter P, Tan WS, Martinez-Fernandez M, et al. UroMark-a urinary biomarker assay for the detection of bladder cancer. *Clinical epigenetics*. 2017; 9: 8.
13. Li HT, Duymich CE, Weisenberger DJ, Liang G. Genetic and Epigenetic Alterations in Bladder Cancer. *International neurology journal*. 2016; 20: S84-94.
14. Lopez JJ, Angulo JC, Martin A, Sanchez-Chapado M, Gonzalez-Corpas A, Colas B, et al. A DNA hypermethylation profile reveals new potential biomarkers for the evaluation of prognosis in urothelial bladder cancer. *APMIS : acta pathologica, microbiologica, et immunologica Scandinavica*. 2017; 125: 787-96.
15. Hesson LB, Patil V, Sloane MA, Nunez AC, Liu J, Pimanda JE, et al. Reassembly of nucleosomes at the MLH1 promoter initiates resiliencing following decitabine exposure. *PLoS genetics*. 2013; 9: e1003636.
16. Jimenez-Useche I, Ke J, Tian Y, Shim D, Howell SC, Qiu X, et al. DNA methylation regulated nucleosome dynamics. *Scientific reports*. 2013; 3: 2121.
17. You JS, Jones PA. Cancer genetics and epigenetics: two sides of the same coin? *Cancer cell*. 2012; 22: 9-20.
18. Silverman LR, Greenberg P, Raza A, Olnes MJ, Holland JF, Reddy P, et al. Clinical activity and safety of the dual pathway inhibitor rigosertib for higher risk myelodysplastic syndromes following DNA methyltransferase inhibitor therapy. *Hematological oncology*. 2015; 33: 57-66.
19. Treppendahl MB, Kristensen LS, Gronbaek K. Predicting response to epigenetic therapy. *The Journal of clinical investigation*. 2014; 124: 47-55.
20. Portella G, Battistini F, Orozco M. Understanding the connection between epigenetic DNA methylation and nucleosome positioning from computer simulations. *PLoS computational biology*. 2013; 9: e1003354.
21. Huff JT, Zilberman D. Dnmt1-independent CG methylation contributes to nucleosome positioning in diverse eukaryotes. *Cell*. 2014; 156: 1286-97.
22. Yoo CB, Jones PA. Epigenetic therapy of cancer: past, present and future. *Nature reviews Drug discovery*. 2006; 5: 37-50.
23. Jones PA. Functions of DNA methylation: islands, start sites, gene bodies and beyond. *Nature reviews Genetics*. 2012; 13: 484-92.
24. Kelly TK, Liu Y, Lay FD, Liang G, Berman BP, Jones PA. Genome-wide mapping of nucleosome positioning and DNA methylation within individual DNA molecules. *Genome research*. 2012; 22: 2497-506.
25. Masui K, Cavenee WK, Mischel PS. mTORC2 in the center of cancer metabolic reprogramming. *Trends in endocrinology and metabolism: TEM*. 2014; 25: 364-73.
26. Masui K, Cavenee WK, Mischel PS. mTORC2 dictates Warburg effect and drug resistance. *Cell Cycle*. 2014; 13: 1053-4.
27. Phan LM, Yeung SC, Lee MH. Cancer metabolic reprogramming: importance, main features, and potentials for precise targeted anti-cancer therapies. *Cancer biology & medicine*. 2014; 11: 1-19.
28. Kroemer G, Pouyssegur J. Tumor cell metabolism: cancer's Achilles' heel. *Cancer cell*. 2008; 13: 472-82.
29. Soga T. Cancer metabolism: key players in metabolic reprogramming. *Cancer science*. 2013; 104: 275-81.
30. Ferreira LM, Hebrant A, Dumont JE. Metabolic reprogramming of the tumor. *Oncogene*. 2012; 31: 3999-4011.
31. Phillips MM, Sheaff MT, Szlosarek PW. Targeting Arginine-Dependent Cancers with Arginine-Degrading Enzymes: Opportunities and Challenges. *Cancer research and treatment : official journal of Korean Cancer Association*. 2013; 45: 251-62.
32. Maze I, Noh KM, Soshnev AA, Allis CD. Every amino acid matters: essential contributions of histone variants to mammalian development and disease. *Nature reviews Genetics*. 2014; 15: 259-71.
33. Cheon DJ, Walts AE, Beach JA, Lester J, Bomalaski JS, Walsh CS, et al. Differential expression of argininosuccinate synthetase in serous and non-serous ovarian carcinomas. *The journal of pathology Clinical research*. 2015; 1: 41-53.
34. McAlpine JA, Lu HT, Wu KC, Knowles SK, Thomson JA. Down-regulation of argininosuccinate synthetase is associated with cisplatin resistance in hepatocellular carcinoma cell lines: implications for PEGylated arginine deiminase combination therapy. *BMC cancer*. 2014; 14: 621.
35. Szlosarek PW, Luong P, Phillips MM, Baccharini M, Stephen E, Szyszko T, et al. Metabolic response to pegylated arginine deiminase in mesothelioma with promoter methylation of argininosuccinate synthetase. *Journal of clinical oncology : official journal of the American Society of Clinical Oncology*. 2013; 31: e111-3.
36. Chang X, Monitto CL, Demokan S, Kim MS, Chang SS, Zhong X, et al. Identification of hypermethylated genes associated with cisplatin resistance in human cancers. *Cancer research*. 2010; 70: 2870-9.
37. Pegg AE, Casero RA, Jr. Current status of the polyamine research field. *Methods in molecular biology*. 2011; 720: 3-35.
38. Kim WT, Kim J, Yan C, Jeong P, Choi SY, Lee OJ, et al. S100A9 and EGFR gene signatures predict disease progression in muscle invasive bladder cancer patients after chemotherapy. *Annals of oncology : official journal of the European Society for Medical Oncology*. 2014; 25: 974-9.
39. Pandiyan K, You JS, Yang X, Dai C, Zhou XJ, Baylin SB, et al. Functional DNA demethylation is accompanied by chromatin accessibility. *Nucleic acids research*. 2013; 41: 3973-85.
40. Lee S, Yoon CY, Byun SS, Lee E, Lee SE. The role of c-FLIP in cisplatin resistance of human bladder cancer cells. *The Journal of urology*. 2013; 189: 2327-34.
41. Kim WJ, Kim EJ, Kim SK, Kim YJ, Ha YS, Jeong P, et al. Predictive value of progression-related gene classifier in primary non-muscle invasive bladder cancer. *Molecular cancer*. 2010; 9: 3.
42. Synakiewicz A, Stachowicz-Stencel T, Adamkiewicz-Drozynska E. The role of arginine and the modified arginine deiminase enzyme ADI-PEG 20 in cancer therapy with special emphasis on Phase I/II clinical trials. *Expert opinion on investigational drugs*. 2014; 23: 1517-29.
43. Noon AP, Catto JW. Bladder cancer in 2012: Challenging current paradigms. *Nature reviews Urology*. 2013; 10: 67-8.
44. Kamat AM, Hegarty PK, Gee JR, Clark PE, Svatek RS, Hegarty N, et al. ICUD-EAU International Consultation on Bladder Cancer 2012: Screening, diagnosis, and molecular markers. *European urology*. 2013; 63: 4-15.
45. Gakis G, Efstathiou J, Lerner SP, Cookson MS, Keegan KA, Guru KA, et al. ICUD-EAU International Consultation on Bladder Cancer 2012: Radical cystectomy and bladder preservation for muscle-invasive urothelial carcinoma of the bladder. *European urology*. 2013; 63: 45-57.
46. Sternberg CN, Bellmunt J, Sonpavde G, Siefker-Radtke AO, Stadler WM, Bajorin DF, et al. ICUD-EAU International Consultation on Bladder Cancer 2012: Chemotherapy for urothelial carcinoma-neoadjuvant and adjuvant settings. *European urology*. 2013; 63: 58-66.
47. Baylin SB, Jones PA. A decade of exploring the cancer epigenome - biological and translational implications. *Nature reviews Cancer*. 2011; 11: 726-34.
48. Jones PA, Baylin SB. The epigenomics of cancer. *Cell*. 2007; 128: 683-92.
49. Yang X, Han H, De Carvalho DD, Lay FD, Jones PA, Liang G. Gene body methylation can alter gene expression and is a therapeutic target in cancer. *Cancer cell*. 2014; 26: 577-90.
50. Shen H, Laird PW. In epigenetic therapy, less is more. *Cell stem cell*. 2012; 10: 353-4.
51. Tsai HC, Li H, Van Neste L, Cai Y, Robert C, Rassoul FV, et al. Transient low doses of DNA-demethylating agents exert durable antitumor effects on hematological and epithelial tumor cells. *Cancer cell*. 2012; 21: 430-46.
52. Juergens RA, Wrangle J, Vendetti FP, Murphy SC, Zhao M, Coleman B, et al. Combination epigenetic therapy has efficacy in patients with refractory advanced non-small cell lung cancer. *Cancer discovery*. 2011; 1: 598-607.
53. Khadeir R, Szyszko T, Szlosarek PW. Optimizing arginine deprivation for hard-to-treat cancers. *Oncotarget*. 2017; 8: 96468-9.
54. Kremer JC, Prudner BC, Lange SES, Bean GR, Schultze MB, Brashears CB, et al. Arginine deprivation inhibits the Warburg effect and upregulates glutamine anaplerosis and serine biosynthesis in ASS1-deficient cancers. *Cell reports*. 2017; 18: 991-1004.
55. Ohshima K, Nojima S, Tahara S, Kurashige M, Hori Y, Hagiwara K, et al. Argininosuccinate synthase 1-deficiency enhances the cell sensitivity to arginine through decreased DEPTOR expression in endometrial cancer. *Scientific reports*. 2017; 7: 45504.
56. Panosyan EH, Lin HJ, Koster J, Lasky JL, 3rd. In search of druggable targets for GBM amino acid metabolism. *BMC cancer*. 2017; 17: 162.
57. Sahu D, Gupta S, Hau AM, Nakashima K, Leivo MZ, Searles SC, et al. Argininosuccinate synthetase 1 loss in invasive bladder cancer regulates survival through general control nonderepressible 2 kinase-mediated eukaryotic initiation factor 2 alpha activity and is targetable by pegylated arginine deiminase. *The American journal of pathology*. 2016.
58. Allen MD, Luong P, Hudson C, Leyton J, Delage B, Ghazaly E, et al. Prognostic and therapeutic impact of argininosuccinate synthetase 1 control in bladder cancer as monitored longitudinally by PET imaging. *Cancer research*. 2014; 74: 896-907.
59. Mandal S, Mandal A, Park MH. Depletion of the polyamines spermidine and spermine by overexpression of spermidine/spermine N(1)-acetyltransferase 1 (SAT1) leads to mitochondria-mediated apoptosis in mammalian cells. *The Biochemical journal*. 2015; 468: 435-47.
60. Lee SB, Park JH, Woster PM, Casero RA, Jr., Park MH. Suppression of exogenous gene expression by spermidine/spermine N1-acetyltransferase 1 (SSAT1) cotransfection. *The Journal of biological chemistry*. 2010; 285: 15548-56.
61. Becket E, Chopra S, Duymich CE, Lin JJ, You JS, Pandiyan K, et al. Identification of DNA methylation-independent epigenetic events underlying clear cell renal cell carcinoma. *Cancer research*. 2016; 76: 1954-64.
62. Campan M, Weisenberger DJ, Trinh B, Laird PW. MethyLight. *Methods in molecular biology*. 2009; 507: 325-37.
63. Irizarry RA, Ladd-Acosta C, Carvalho B, Wu H, Brandenburg SA, Jeddleloh JA, et al. Comprehensive high-throughput arrays for relative methylation (CHARM). *Genome research*. 2008; 18: 780-90.
64. Bolstad BM, Irizarry RA, Astrand M, Speed TP. A comparison of normalization methods for high density oligonucleotide array data based on variance and bias. *Bioinformatics*. 2003; 19: 185-93.
65. Huang D, Rust AG, Ramsey S, Smith JJ, Leslie DM, Weston AD, et al. A data integration methodology for systems biology. *Proceedings of the National Academy of Sciences of the United States of America*. 2005; 102: 17296-301.
66. Hwang D, Smith JJ, Leslie DM, Weston AD, Rust AG, Ramsey S, et al. A data integration methodology for systems biology: experimental verification. *Proceedings of the National Academy of Sciences of the United States of America*. 2005; 102: 17302-7.
67. Huang da W, Sherman BT, Lempicki RA. Systematic and integrative analysis of large gene lists using DAVID bioinformatics resources. *Nature protocols*. 2009; 4: 44-57.

68. Szklarczyk D, Morris JH, Cook H, Kuhn M, Wyder S, Simonovic M, et al. The STRING database in 2017: quality-controlled protein-protein association networks, made broadly accessible. *Nucleic acids research*. 2017; 45: D362-D8.
69. Shannon P, Markiel A, Ozier O, Baliga NS, Wang JT, Ramage D, et al. Cytoscape: a software environment for integrated models of biomolecular interaction networks. *Genome research*. 2003; 13: 2498-504.



Original Articles

Integrated proteomic and phosphoproteomic analyses of cisplatin-sensitive and resistant bladder cancer cells reveal CDK2 network as a key therapeutic target

Jae Hun Jung^{a,1}, Sungyong You^{b,e,1}, Jae Won Oh^a, Junhee Yoon^b, Austin Yeon^b, Muhammad Shahid^b, Eunho Cho^{b,c}, Vikram Sairam^{b,c}, Taeun D. Park^{b,d}, Kwang Pyo Kim^{a,**}, Jayoung Kim^{b,c,e,*}

^a Department of Applied Chemistry, College of Applied Science, Kyung Hee University, Yongin, Republic of Korea

^b Department of Surgery and Biomedical Sciences, Cedars-Sinai Medical Center, Los Angeles, CA, USA

^c University of California, Los Angeles, CA, USA

^d University of California, Berkeley, CA, USA

^e Samuel Oschin Comprehensive Cancer Institute, Cedars-Sinai Medical Center, Los Angeles, CA, USA

ARTICLE INFO

Keywords:

Global proteome
Phosphoproteomics
Cisplatin resistance
Bladder cancer
Biological network
Competing interests

ABSTRACT

Background: Cisplatin-based chemotherapy is currently part of the standard of care for bladder cancer (BC). Unfortunately, some patients respond poorly to chemotherapy and have acquired or developed resistance. The molecular mechanisms underlying this resistance remain unclear. Here, we introduce a multidimensional proteomic analysis of a cisplatin-resistant BC model that provides different levels of protein information, including that of the global proteome and phosphoproteome.

Methods: To characterize the global proteome and phosphoproteome in cisplatin-resistant BC cells, liquid chromatography-mass spectrometry/mass spectrometry experiments combined with comprehensive bioinformatics analysis were performed. Perturbed expression and phosphorylation levels of key kinases associated with cisplatin resistance were further studied using various cell biology assays, including western blot analysis.

Results: Analyses of protein expression and phosphorylation identified significantly altered proteins, which were also EGF-dependent and independent. This suggests that protein phosphorylation plays a significant role in cisplatin-resistant BC. Additional network analysis of significantly altered proteins revealed CDK2, CHEK1, and ERBB2 as central regulators mediating cisplatin resistance. In addition to this, we identified the CDK2 network, which consists of CDK2 and its 5 substrates, as being significantly associated with poor survival after cisplatin chemotherapy.

Conclusions: Collectively, these findings potentially provide a novel way of classifying higher-risk patients and may guide future research in developing therapeutic targets.

1. Introduction

Bladder cancer (BC) is a common malignancy of the urinary tract. Resection of the tumor (when possible) and cisplatin-based chemotherapy is the present standard of care. However, resistance to chemotherapy has been a clinical challenge for long-term remission [11]. Chemo-resistance can rapidly develop and a majority of patients ultimately experience disease progression and a poor prognosis [4]. The failure of conventional treatment following remission typically results

in a < 15% chance of 5-year survival [10,18,39]. Therefore, therapeutic strategies that can re-sensitize tumors to chemotherapy would significantly benefit BC patient care. Additionally, a molecular signature panel capable of predicting cisplatin resistance in BC would greatly improve prognostic and clinical outcomes for high-risk patients. Unfortunately, despite multiple independent studies aimed at identifying the subset of patients who will develop chemo-resistance, research on predictive biomarker(s) is still in its infancy [3,36,38].

Overexpression, amplification, or mutations of EGFR family

* Corresponding author. Department of Surgery and Biomedical Sciences, Cedars-Sinai Medical Center, 8700 Beverly Blvd., Los Angeles, CA, 90048, USA.

** Corresponding author. Department of Applied Chemistry, Kyung Hee University, Yongin, Gyeonggi-do, 463-707, Republic of Korea.

E-mail addresses: kimkp@khu.ac.kr (K.P. Kim), Jayoung.Kim@cshs.org (J. Kim).

¹ These authors equally contributed to this manuscript.

members are often observed in BC. This suggests that the proteins involved in the epidermal growth factor receptor (EGFR) signaling pathways may play important roles in the carcinogenesis and maintenance of BC, making them relevant therapeutic targets. Our group had previously established cisplatin-sensitive (T24S) and resistant (T24R) T24 human BC cell lines [21]. The viability of the resistant cells was reduced by inhibition of EGFR kinase activity [21]. Either expression or phosphorylation of the proteins involved in signaling pathways can contribute to alterations of pathway activations. Thus, analyses of the global proteome and phosphoproteome would allow for direct interrogation of the altered activation of signaling pathways and provide comprehensive profiles regarding protein quantification and phosphorylation [6,8,41]. A network model describing such protein alterations in cancer cells could provide novel insights into the molecular mechanisms of resistance and contribute to identifying new biomarkers or therapeutic targets.

To obtain such a systems-level insight into cisplatin-resistance, we used high-resolution mass spectrometry and investigated the temporal changes in protein abundance and phosphorylation in T24S and T24R cells after EGF stimulation. Our comprehensive proteomic analysis identified proteins involved in EGFR signaling that were perturbed in cisplatin-resistant cells. This included substrates of EGF receptors and downstream kinases. Further network analysis of our proteomic and phosphoproteomic data identified downstream kinases of EGFR signaling pathways.

2. Materials and methods

2.1. Reagents

Antibodies against CDK2 (1:1000, Novus Biologicals; Littleton, CO), and β -actin (1:5000, Sigma) were used for this study. The following antibodies: P-CDK2 (Thr160) (2561, 1:1000), P-ERBB2 (Tyr1196) (6942, 1:1500), P-CHEK1 (Ser345) (2348, 1:750), phospho-mTOR (Ser2448) (5536; 1:1000), p-Rb (Ser807/811) (8516, 1:1000), p-tyrosine (P-Tyr-100) (9411, 1:2000), and HRP-conjugated secondary antibodies (7074, 1:1000; 7076, 1:1000) were obtained from Cell Signaling Technologies.

2.2. Cell culture

T24, J82, and RT4 BC cells were obtained and cultured, according to instructions provided by the American Type Culture Collection (ATCC) (Manassas, VA). Media was supplemented with 10% fetal bovine serum, 2% glutamine, and 1% antibiotics (Invitrogen, Carlsbad, CA). Cells were maintained in a humidified incubator with 5% CO₂ at 37 °C [21].

2.3. Protein extraction and quantification

The cell pellets were kept at –80 °C for 30 min. Afterwards, the cells were lysed with RIPA buffer [50 mM Tris-HCl, 150 mM NaCl, 0.1% (w/v) sodium dodecyl sulfate (SDS), 1% (v/v) NP-40, 1 mM PMSF, 1X protease inhibitor cocktail, 1X phosphatase inhibitor cocktail, PhoSTOP] and left on ice for 15 min while undergoing sonication. The cellular lysates were centrifuged at 14,000 g for 15 min at 4 °C. The supernatant was collected and 500 μ g of protein for each cell line was digested using the filter aided sample preparation (FASP) method [43].

2.4. Filter aided sample preparation (FASP)

Proteins were reduced in a sodium dodecyl sulfate (SDS)-lysis buffer (4% (w/v) SDS; 0.1 M Tris/HCl pH 7.6; 0.1 M DTT) at 37 °C for 45 min. The proteins were then boiled at 95 °C for 10 min and then sonicated for 10 min. The solution was transferred to a 30 k membrane filter (Microcon devices, YM-30, Millipore, MA) and centrifuged at 14,000 g

and 20 °C for 60 min. The concentrates were diluted in their filters with 0.2 ml of UA solution (8 M urea in 0.1 M Tris/HCl, pH 8.5) and centrifuged at 14,000 g for 30 min to remove the remaining SDS ($\times 3$). After that, the concentrates were mixed with 0.1 ml of 50 mM indole-3-acetic acid (IAA) in UA solution and incubated in darkness at room temperature for 25 min. Following centrifugation, the resulting product was diluted with 0.2 ml of UA solution and concentrated again. This step was repeated 3 times. Next, the concentrates were washed with 0.2 ml of 100 mM triethyl ammonium bicarbonate (TEAB) and centrifuged at 14,000 g for 30 min ($\times 3$). Subsequently, 10 μ g of trypsin prepared in 0.1 ml of 100 mM TEAB (with the enzyme to protein ratio of 1:50) was added to the filter and the samples were incubated at 37 °C overnight. The second digestion was done using trypsin with an enzyme to protein ratio of 1:100 for 6 h. Peptides were collected by centrifuging the filter units at 14,000 g for 30 min. TEAB (75 μ L, 100 mM) was added to the filter and centrifuged at 14,000 g for 20 min ($\times 3$). Finally, the peptide solutions were dried in a speed vacuum concentrator and stored at –80 °C.

2.5. TMT labeling of peptide

Peptides were labeled with TMT™ Isobaric Mass Tagging Reagent, according to the manufacturer's instructions (ThermoScientific, Foster City, CA). For each sample of 500 μ g peptides, 250 μ l of 200 mM TEAB were added. TMT reagents were resuspended in anhydrous acetonitrile and then added to each sample (126: Cisplatin sensitive/EGF 0 min, 127: Cisplatin sensitive/EGF 10 min, 128: Cisplatin sensitive/EGF 30 min, 129: Cisplatin resistant/EGF 0 min, 130: Cisplatin resistant/EGF 10 min, 131: Cisplatin resistant/EGF 30 min). After 1 h, the reaction was quenched with 5% hydroxylamine. The chemically tagged samples were pooled into one tube and concentrated via speed vacuum centrifugation. The labeled samples were then mid-pH fractionated.

2.6. Mid-pH reversed phase liquid chromatography (RPLC) fractionation

Mid-pH RPLC fractionation was performed to separate peptides based on their hydrophobicity. An Accucore™ 150 C18 LC column (150 \times 2.1 mm, 4 μ m) was used for fractionation with mid-pH buffers A and B; (A) the mobile phase was 10 mM TEAB in water (pH 7.5) and (B) the mobile phase was 10 mM TEAB in 90% CAN (pH 7.5). The samples were then divided into 15 smaller samples using the Agilent 1260 Series HPLC System (Agilent Technologies, Santa Clara, CA). The resultant gradient was 0–10 min, 5% B; 10–70 min, 5–35% B; 70–80 min, 70% B; 80–105 min, 5% B. The separated peptides were collected and dried in a speed vacuum. Each fraction was vacuum dried and stored at –80 °C until liquid chromatography-mass spectrometry/mass spectrometry (LC-MS/MS) experiments.

2.7. Phosphopeptide enrichment using immobilized metal affinity chromatography (IMAC)

IMAC beads were prepared from Ni-NTA magnetic agarose beads. Ni-NTA beads (500 ml) were washed (3 \times) with deionized water (DIW). The beads were then reacted with 100 mM of EDTA (pH 8.0) for 30 min with end-over-end rotation to remove nickel ions. The reacted EDTA solution was eliminated and the beads were washed 3 \times with DIW. The NTA beads were treated with 10 mM of aqueous FeCl₃ solution for 30 min with end-over-end rotation. Iron-chelated IMAC beads were washed ($\times 3$) with DIW. IMAC beads were aliquoted into 10 microcentrifuge tubes and each bead was washed with 400 μ l of 80% acetonitrile (CAN)/0.1% trifluoroacetic acid (TFA). In total, 10 fractions, which were obtained by combining some fractions from 15 (#1 and #11, #2 and #12, #3 and #13, #4 and #14, #5 and #15, #6, #7, #8, #9, #10), were used to enrich for phosphopeptides. The 10 fractionated peptide samples were suspended in 500 μ l of 80% ACN/0.1% TFA and were reacted with IMAC beads again for 30 min with end-over-end

rotation. Phosphopeptides were eluted using 125 μ l of 1:1 ACN/2.5% ammonia in 2 mM phosphate buffer (pH 10) after incubating for 1.5 min. All phosphopeptides were acidified immediately with 10% TFA. The collected phosphopeptides were dried in a speed vacuum and purified in C18 spin columns for LC-MS/MS analysis.

2.8. LC-MS/MS analysis

All peptide samples were separated on an ultra performance liquid chromatography (UPLC) system that was equipped with analytical columns (75 μ m \times 50 cm, C18, 3 μ m, 100 \AA) and trap columns (75 μ m \times 2 cm, C18, 3 μ m, 100 \AA). The temperature of the analytical columns was set to 60 $^{\circ}$ C. The solvents A and B were 0.1% formic acid in water and 0.1% formic acid in acetonitrile, respectively. A gradient made after 180 min (1–40% solvent B for 160 min, 40–80% solvent B for 5 min, 80% solvent B for 10 min, and 1% solvent B for 5 min) was used for global proteome profiling analysis. A gradient made after 134 min (5–40% solvent B for 120 min, 40–80% solvent B for 2 min, 80% solvent B for 10 min, and 1% solvent B for 2 min) was used for phosphoproteome analysis. The flow rate of all experiments was set to 250 nl/min. The eluted peptides from LC were mass-analyzed on a Q Exactive Orbitrap Mass Spectrometer (ThermoScientific, Bremen, Germany). The electric potential of electrospray ionization was kept at 2.0 kV and the temperature of desolvation capillary was set to 250 $^{\circ}$ C. Full MS scans were acquired for a mass range of 400–2000 Th at a resolution of 70,000. The 10 most abundant ions, with charges of 2, 3, 4, and 5, were dynamically selected with an isolation width of 2.0 Th and fragmented with an exclusion duration of 30 s with a normalized collision energy (NCE) of 30 for higher energy collisional dissociation (HCD). The LC-MS/MS scans were acquired at a resolution of 17,500 with a fixed initial m/z of 100 Th. Maximum ion injection times were 120 ms for both the full MS and LC-MS/MS scans. The automated gain control (AGC) target value was set to 1.0×10^6 for both the MS and LC-MS/MS scans.

2.9. Identification of peptides and proteins

MS and MS/MS spectra were converted from Thermo.RAW files into the mzML format using Mconvert (ProteoWizard) and searched with MSGF + against the Universal Protein Resource Human Database (Uniprot released 2016_02, 20,198 entries, <http://www.uniprot.org/>). Search parameters were as follows: 20 ppm tolerance for precursor ion mass error and fixed modification for carbamidomethylation (+57.0214 Da) to cysteine, variable modification for methionine oxidation (+15.994915 Da), phosphorylation (+79.966330 Da) to serine, threonine, tyrosine, TMT (+229.162932) to N-termini and lysine and acetylation (+42.010564) to N-terminal of protein. The peptide identification stringency was set to a maximum of 1% peptide-to-spectrum matches (PSMs) FDR in the target-decoy way. The intensities of all TMT-6 plex reporter ions were extracted using the MAGIC software [27]. When multiple phosphopeptides were assigned to a phosphoprotein, the phosphopeptide that had the largest comparative fold change [44] was used as the representative fold change of the phosphoprotein. The mass spectrometry proteomics data has been deposited to the PRIDE [17] repository with the dataset identifier, PXD005308.

2.10. Identification of proteins with altered expression or phosphorylation

TMT intensities of the peptides were normalized using the quantile normalization method [5]. Protein abundance was estimated by summing all TMT reporter ion intensities of different fully tryptic peptides belonging to the same protein groups. Of these qualified proteins, those with more than 2 non-redundant peptides were chosen for the next analyses. We then identified differentially expressed proteins (DEPs) using an integrative statistical method, as reported previously [14]. Briefly, for each protein, the t -test and \log_2 -median-ratio test were

applied to its abundances for all 3 replicates. An empirical null distribution was estimated by applying the Gaussian Kernel Density Estimation method to \log_2 fold-changes that were obtained after performing all possible permutations on all the TMT labels [1]. Using the distributions for each protein, we computed the adjusted p-values for the two tests. We then combined the p-values to compute the overall p-value using Stouffer's method. Finally, we computed the false discovery rate (FDR) for the overall p-values using Storey's method. We selected DEPs that had a combined FDR < 0.05, fold change ≥ 1.5 , and were detected as proteins in at least 2 of the 3 replicates.

For the phosphoproteome, we applied differential phosphorylation analysis at the peptide level to identify significantly altered phosphopeptides between cell types or time points. For this, the same normalization and statistical testing methods described above were used. Phosphopeptides were selected and considered as significantly altered if they had a FDR < 0.05 and fold-change ≥ 1.5 . Finally, differentially phosphorylated proteins (DPPs) were identified as proteins that contained significantly altered phosphopeptides that were uniquely assigned to the protein. The Phospho-UMC filter was used to localize the site of phosphorylation. This simple method uses unique mass class (UMC) information to differentiate phosphopeptides with different phosphorylation sites [28]. Briefly, MS features within 10 ppm, but emerging over a period of time during their LC elution, were identified and grouped into an UMC. Then, the links between the LC-MS/MS data and the UMCs were made. The resultant LC-MS/MS data were subjected to a database search using the MSGF + engine and peptide identifications within 1% FDR were used.

To explore the cellular processes and subcellular localizations represented by the DEPs and DPPs, functional enrichment analyses of gene ontology biological processes (GOBPs), gene ontology cellular components (GOCCs), and Kyoto Encyclopedia of Genes and Genomes (KEGG) pathways [19] were performed using the DAVID software [13]. The GOBPs, GOCCs, and KEGG pathways represented by DEPs and DPPs were identified as those with $p < 0.05$.

2.11. Reconstruction of cellular network models and identification of key kinases

To identify key kinases regulating DPPs, data for more than 12,000 kinase-substrate interactions (KSI) was collected from the SIGNOR database [34]. For each kinase, the number of targets in the DEPs was calculated using the KSI data. The p-value for the number of substrates was then computed based on a hypergeometric distribution from Fisher's exact test. Of the kinases with $p < 0.05$, those belonging to DEPs or DPPs were selected as key kinases. We estimated an empirical distribution of network density by randomly sampling the same number of proteins in each kinase group with KSIs 100,000 times. Significance levels of the kinases were computed using the right-sided test.

2.12. Western blot analysis

After EGF treatment (10 ng/ml), cells were quickly harvested, flash frozen in liquid nitrogen, and stored at -80° C. Total protein was extracted using a lysis buffer [1% Nonidet P-40, 50 mM Tris (pH 7.4), 10 mM NaCl, 1 mM NaF, 5 mM MgCl_2 , 0.1 mM EDTA, 1 mM phenylmethylsulfonyl fluoride] with a complete protease inhibitor cocktail (Roche Diagnostics GmbH, Mannheim, Germany). The solution was centrifuged at 12,500 \times g for 15 min. After measuring for protein concentration, 25 μ g of protein per line were subjected to SDS-PAGE gel running and then transferred onto nitrocellulose membranes for western blot analysis. After blocking for 1 h with 10% bovine serum albumin (BSA) in phosphate buffered saline with Tween 20 (PBST), the membranes were incubated with specific antibodies in PBST, overnight. β -actin was used as the loading control. The blots were visualized using enhanced chemiluminescence.

2.13. Gene silencing and cell viability assay

For transient cell transfections of siRNA oligonucleotides, T24R cells were grown to 80% confluence in 6-well culture plates and transfected with siRNAs targeting CDK2, CHEK1, ERBB2, and control (ThermoScientific) using Lipofectamine 2000 (Invitrogen), according to the manufacturer's instructions. Cisplatin-resistant BC cells (T24R, J82R, and RT4R) were incubated with cisplatin and/or CDK2 inhibitor for 72 h. Post-treatment cell survival was determined by measuring cell viability using MTS reagents (Promega Corporation, Madison, WI), according to the provided protocols.

2.14. Tissue micro-array (TMA) construction

Patient consent and IRB approval was given prior to tissue collection, and TMA slides were constructed from a cohort of 42 BC patients at Cedars-Sinai Medical Center (IRB #: Pro00044997). Detailed information was not available except that a majority of the patients were male and over 60 years old. Although tumors were pathologically graded prior to tissue collection, the annotations and image analysis were blindly conducted by two trained scientists, including one certified pathologist. Tumor and normal bladder tissue samples were received from all patients. Circular TMA cores 1 mm in diameter were constructed for all tissue samples onto glass slides. In total, there were 82 TMA cores per slide.

2.15. Immunohistochemistry (IHC) analysis

Antibodies against CDK2 (Novus Biologicals; Littleton, CO) were incubated on their respective slides for 32 min. Following antibody incubation, antigen retrieval was done at a high pH for 64 min. Ultraview DAB Detection (Ventana Medical Systems; Tucson, AZ) was used for nuclear and cytoplasmic counterstaining. These slides were scanned and uploaded onto the Leica Biosystems cloud drive.

2.16. Digitalized image analysis

Following staining with both the antibodies of interest and pan-CK, the slides were scanned using the Aperio Turbo Scanscope AT (Leica Biosystems; Buffalo Grove, IL). High resolution images of each slide were uploaded onto the Leica Biosystems cloud drive for annotations and analysis.

Annotation and analysis of slides were done using the Leica Tissue Image Analysis (IA) 2.0 software program (Copyright, 2012 by SlidePath Ltd.). Stromal and structural tissues were not included in the annotations. Although these structures may provide additional insight, the focus of the experiment was based on tumor epithelium only. Each annotated core had a minimum threshold of 100,000 cells to be analyzed. Following annotations, the "Measure Stained Cells Algorithm" option in the Leica Tissue IA software was used. For each antibody slide, color definition preferences were defined and algorithm input parameters were optimized based on several cores. These individualized parameters were used to analyze the annotated regions on each slide.

For the color definition, haematoxylin was set as the nuclear counter stain, and DAB was set as the nuclear, cytoplasmic, and membrane marker. Parameters in the program were based on a numbered greyscale between 0 and 255, with 0 being the minimum intensity (black) and 255 being the maximum (white). The max threshold in our analysis was set to 220, with 180 being the threshold for positive or negative staining. The max nuclear window size radius was set to 37 (default) and the nuclear area threshold was set to be 0–1500 mm²; any nuclei or cells out of these parameters were eliminated from analysis. The minimum percent of stained area in the nucleus to be considered as positive was set to 20%. The threshold for positive identification of cytoplasmic staining was set at a higher threshold for some of the

antibodies due to differences in background and staining. The maximum threshold range was set for cytoplasmic staining detection between 220 and 240, with a minimum percent of stained area set to 70%.

After analysis, data regarding the nuclear h-score, % of positive nuclei, % of positive nuclear area in tissue, cytoplasmic h-score, and % of positive cytoplasm of cells was collected and used for comparative graphing. These scores were chosen to represent the level and intensity of nuclear and cytoplasmic staining in the epithelial cells. Test runs of the analysis were conducted with a pathologist to assure that the program correctly identified and graded the nuclear and cytoplasmic components of epithelial cells.

2.17. Comparative graphing and statistical analysis

R Studio was used for analyzing and graphing the data. Using the ggplot2 package, violin plots were constructed to demonstrate the differences in nuclear h-score, % of positive nuclei, % of positive nuclear area in tissue, cytoplasmic h-score, and % of cells with positive cytoplasmic staining between tumor and normal adjacent to tumor (NAT) cores. Statistical analysis was done via a two-sided Wilcoxon rank-sum test. Statistical significance was defined as $p < 0.05$.

3. Results

3.1. Global proteome and phosphoproteome in cisplatin-resistant BC cells

We sought to understand the molecular mechanisms of cisplatin resistance using a paired cell culture system consisting of T24S and T24R cells. Alterations of EGFR signaling pathways have been frequently observed and reported in various cancer types. It has also been considered a critical module associated with resistance mechanisms against several kinase inhibitors and other drugs, including cisplatin [9,12,15,29]. Based on this knowledge, we applied a multiplexed TMT and LC/LC-MS/MS approach to samples and replicates harvested after 0 min, 10 min, and 30 min of EGF stimulation (10 ng/ml) (Fig. 1A). After a FASP peptide digestion, each conditioned peptide was respectively labeled with 6-plex TMT reagents. For mid-pH fractionation, we used TEAB as a buffer solvent. Several benefits of using TEAB include compatibility with TMT labeling, high volatility (allowing us to skip the desalting step), and low harmful impact on separation columns. After fractionation, 5% of the peptides from each of the 15 fractions were used for global proteome analysis. The remaining 95% of the peptides were subjected to an IMAC enrichment experiment and analyzed using an orbitrap-based high resolution/accurate-mass mass spectrometer (Fig. 1B). This serial enrichment strategy was done to simultaneously observe changes in either global or phosphopeptides from the same peptide pool [32]. We then searched for acquired mass spectra using MS/MS automated selected ion chromatography (MASIC) in the UniProt Human Protein Database (2016) with MSGF + TMT reporter ion extraction [20] (see methods). From the 3 biological replicates of the global proteome, we identified an average of 48,044 non-redundant peptides (9405 protein groups) (Supplementary Table 1 and Fig. 1C). We also identified an average of 13,980 phosphopeptides and 16,700 phosphosites (Supplementary Table 2) belonging to 3939 protein groups (Supplementary Table 3 and Fig. 1D).

3.2. Altered proteins in cisplatin-resistant BC cells

To identify proteins with altered expression and phosphorylation between T24R and T24S cells before any EGF stimulation, we performed separate statistical hypothesis testing for the global proteome and phosphoproteome. From the global proteome, we identified 223 DEPs between T24R and T24S cells (Fig. 2A). When analyzing the phosphoproteome, we identified 899 differentially phosphorylated peptides belonging to 501 DPPs (Fig. 2B). Comparing the list of DEPs and DPPs (Supplementary Table 4), we observed that 33 proteins

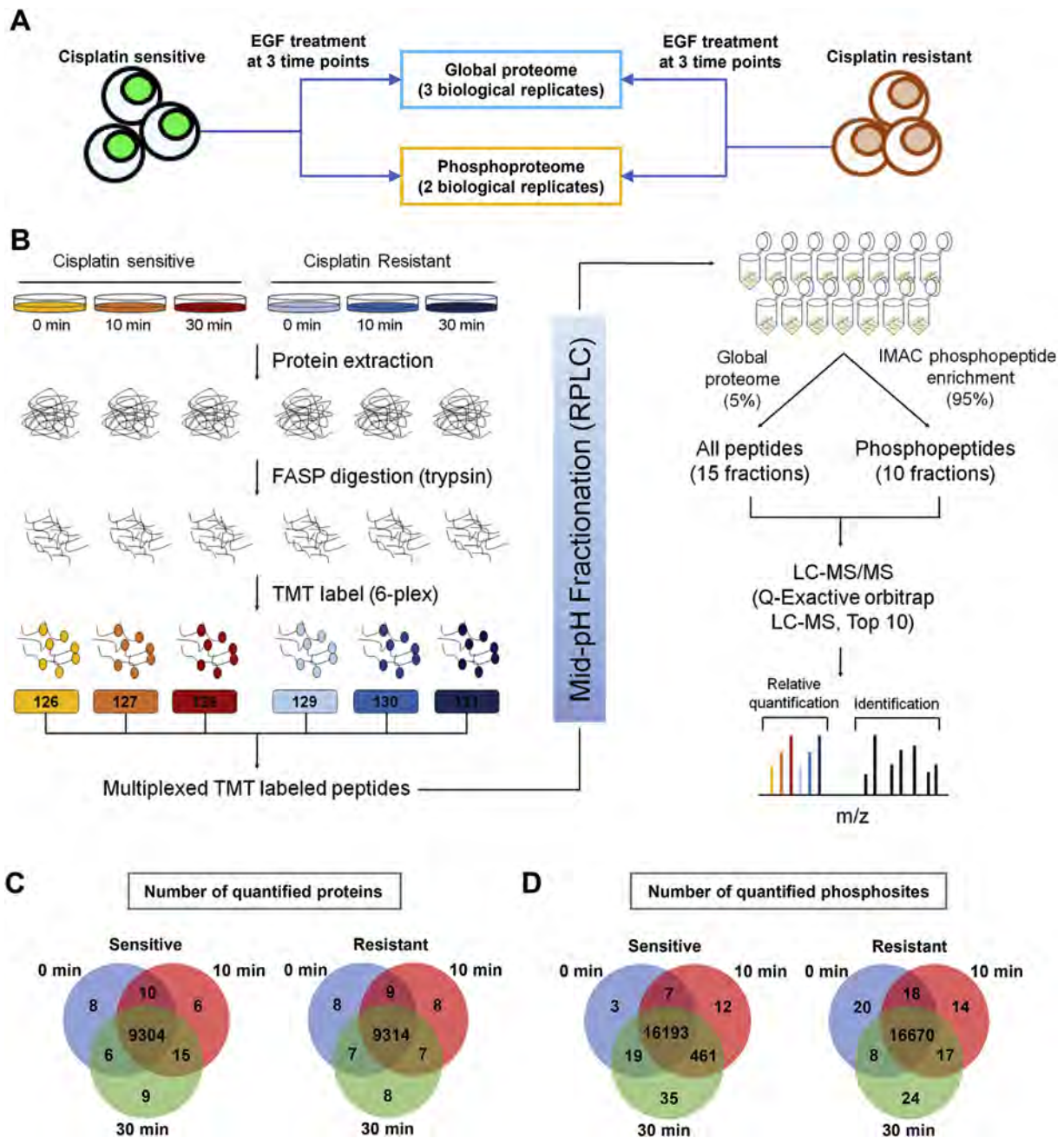


Fig. 1. Quantitative measuring of the proteome and phosphoproteome using TMT labeling. A. Experimental design to study the effects of EGF stimulation across 3 time points. A total of 3 and 2 biological replicates from T24S and T24R cells were analyzed for their global proteome and phosphoproteome, respectively. B. Overall experimental workflow for multiplex TMT labeling and comprehensive profiling of the global proteome and phosphoproteome. Both T24S and T24R cells were treated with EGF (0, 10, or 30 min). Proteins were extracted using RIPA buffer and peptides were FASP digested with trypsin. Peptide samples were derived at 6 different time points, labeled using TMT reagents, mixed, and separated using mid-pH reverse phase chromatography. Fractions were combined in a non-contiguous way into 15 fractions for proteome analysis (5% of total proteins) and 10 fractions for phosphoproteome analysis (95% of total proteins). All peptides and phosphopeptides were analyzed on a Q Exactive Mass Spectrometer. Protein identification and quantification was achieved using the MSGF + search engine and MASIC (reporter ion intensity extractor). C and D. Numbers of identified (C) proteins or (D) phosphopeptides from T24S and T24R cells. Venn diagrams depict the number of common and uniquely identified proteins or phosphopeptides in T24S and T24R cells after 0, 10 and 30 min of EGF stimulation.

exhibited a positive correlation (Spearman's rho = 0.50; P < 0.001), with significant changes at both the phosphorylation and expression levels (Fig. 2C). Functional enrichment analysis, using DAVID [13], showed that DEPs and DPPs were enriched for common and distinct cellular processes (Fig. 2D). DEPs exhibited predominant enrichment for cell adhesion and migration-related processes, including extracellular matrix organization and leukocyte migration. DPPs, on the other hand, displayed direct association with the EGFR signaling pathway and downstream processes, such as small GTPase signal

transduction, mitotic cell cycle, and chromatin organization. Both DEPs and DPPs were enriched for cell survival and proliferation-related processes. These results suggest that DPPs in cisplatin-resistant BC cells represent the activation of EGFR signaling pathways or EGF-driven resistance mechanisms.

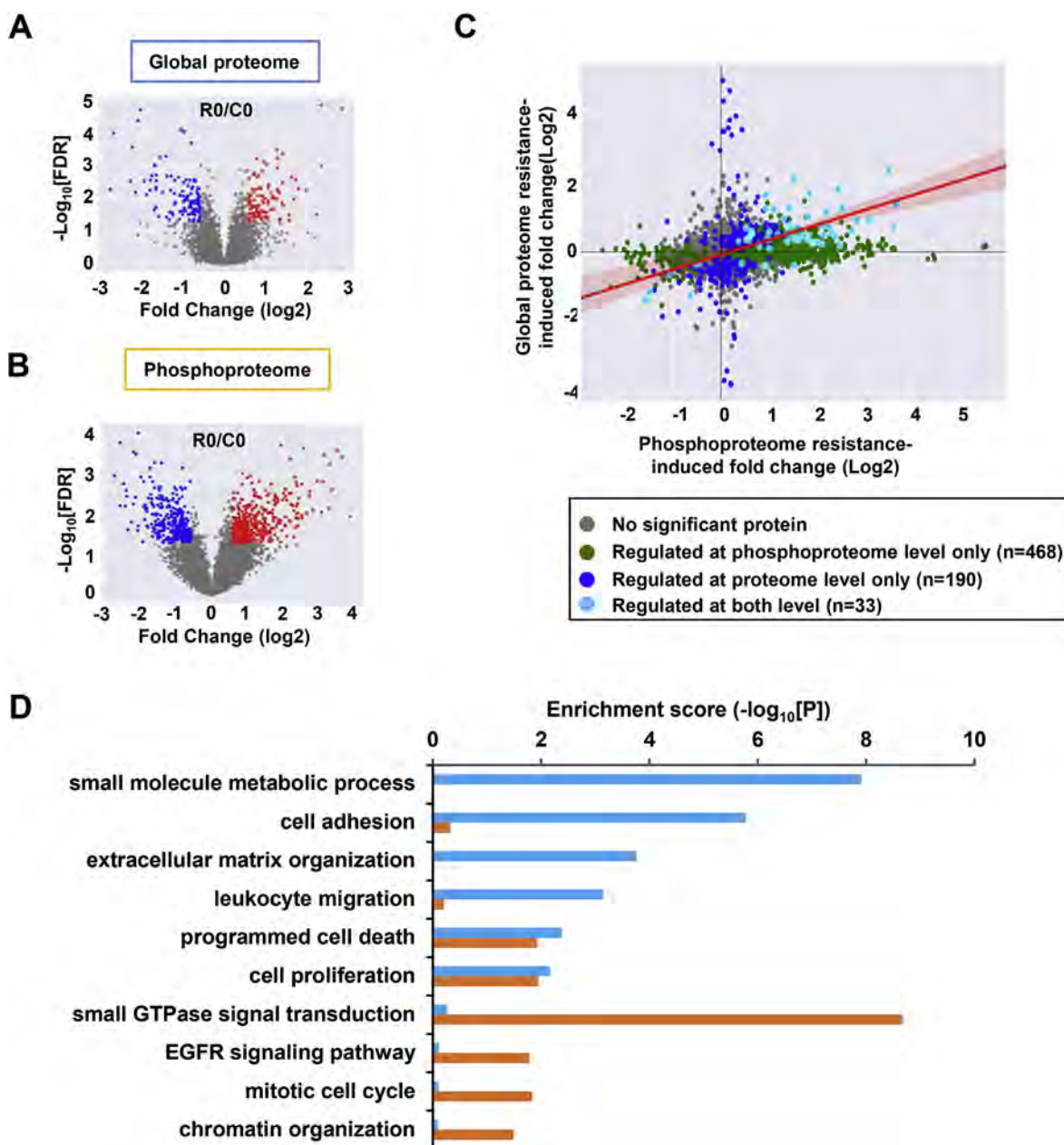


Fig. 2. Altered proteins in the global proteome and phosphoproteome between T24R and T24S cells. **A** and **B**. Volcano plots display differentially expressed (A) proteins or (B) differentially phosphorylated peptides. Red and blue dots represent upregulated and downregulated proteins or peptides, respectively. **C**. Protein expression and phosphorylation levels were compared and represented in the scatterplot. Proteins and phosphorylation sites were considered to be perturbed by cisplatin resistance based on the integrative hypothesis testing method (FDR < 0.05). Comparison between biological replicates of MS-based quantitative proteomic and phosphoproteomic experiments of T24R and T24S cells. Each dot represents one protein. **D**. Enrichment analysis using DAVID software showed that differentially expressed proteins (cyan) and differentially phosphorylated peptides (purple) were enriched for various cellular functions. (For interpretation of the references to color in this figure legend, the reader is referred to the Web version of this article.)

3.3. Altered proteins belonging to the EGFR signaling pathway are involved in cisplatin resistance

Using our global proteome and phosphoproteome data, we next performed differential analyses of EGF stimulation in T24R and T24S cells. For the global proteome in both T24R and T24S cells, only the tails of the density distribution in the log₂ fold change increased with EGF stimulation (Fig. 3A and Supplementary Fig. 1A). In contrast, the global median of the phosphoproteome in T24S cells increased in abundance when stimulated with EGF (Fig. 3B). The largest changes in EGF-induced phosphorylation were observed in T24S cells, which exhibited phosphosite changes of 4% (656) and 5.3% (887) after 10 min

and 30 min of EGF stimulation, respectively. T24R cells were altered less, with the percentage of altered phosphorylation sites being 1.1% and 0.7% after 10 min and 30 min, respectively (Supplementary Fig. 1B). This suggested that the effects of EGF stimulation impacts T24S cells more. Volcano plots for differentially phosphorylated proteins were consistent with the density plots shown in Fig. 3B (Fig. 3C).

We next sought to select altered proteins (APs) that were associated with cisplatin resistance and were part of the EGFR signaling pathway. Both DEPs and DPPs were considered as APs because either protein expression or phosphorylation can reflect alterations in signaling pathways. A total of 749 APs (454 APs at 10 min and 547 APs at 30 min) were identified in T24S cells (Supplementary Table 5). Of these

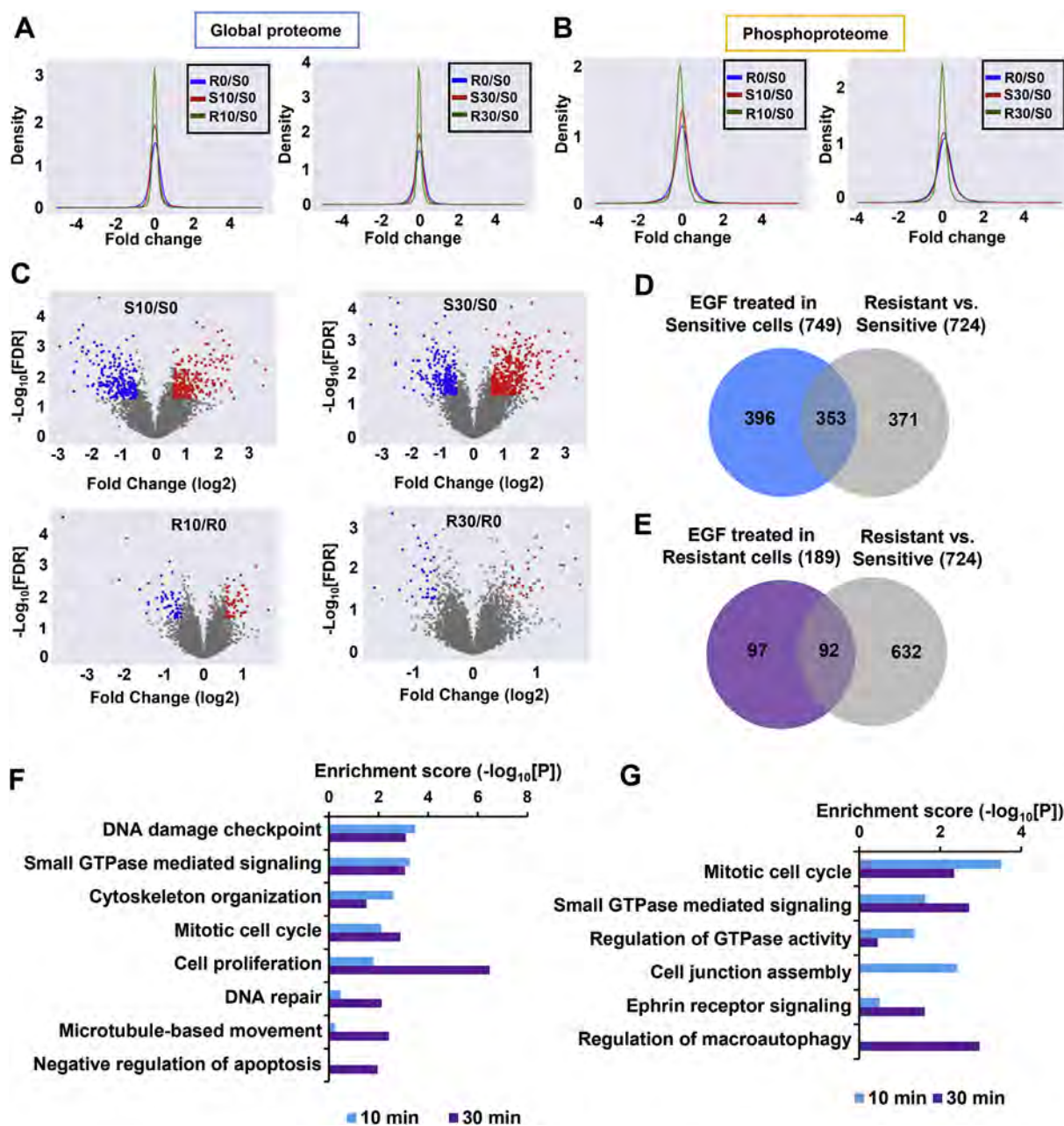


Fig. 3. Distinct protein alteration patterns in T24R and T24S cells after EGF stimulation. A and B. Density plots are shown for the log₂fold changes of the (A) global proteome and (B) phosphoproteome for T24R and T24S cells after 10 min and 30 min of EGF treatment. Only phosphopeptides or proteins quantified in at least two samples were plotted. Log₂ fold changes in T24S cells at 10 min (S10) vs. 0 min (S0) of EGF treatment, T24S cells at 30 min (S30) vs. 0 min (S0) of EGF treatment, T24R cells at 10 min (R10) vs. 0 min (R0) of EGF treatment, T24R cells at 30 min (R30) vs. 0 min (R0) of EGF treatment, and R0 vs. S0 are displayed. C. Volcano plots display differentially expressed phosphopeptides in T24R and T24S cells after 10 min and 30 min of EGF treatment. Red and blue dots indicate up- and down-regulated phosphopeptides, respectively. Only those quantified in at least two samples were plotted. D and E. Number of phosphoproteins associated with cisplatin resistance mechanisms that are involved in EGFR signaling in (D) T24S and (E) T24R cells. Venn diagram depicts the overlapping altered phosphoproteins in (D) T24S or (E) T24R cells with or without EGF treatment. F and G. Enriched cellular functions of the overlapping proteins after 10 min and 30 min of EGF treatment in (F) T24S and (G) T24R cells. (For interpretation of the references to color in this figure legend, the reader is referred to the Web version of this article.)

749 APs, 353 overlapped with the 724 APs identified from T24S vs. T24R cells with no EGF treatment. Interestingly, 49% (353 out of 724) of the APs responsible for cisplatin resistance were regulated by EGF stimulation (Fig. 3D). This suggested that a large proportion of APs are involved in downstream EGFR signaling and are likely to also be associated with cisplatin resistance. In contrast, T24R cells exhibited a relatively smaller number of APs (n = 92) that overlapped with those found between T24R and T24S cells (Fig. 3E). Functional enrichment analysis of the 353 APs (Supplementary Table 6) in T24S cells revealed known associations of cisplatin resistance with DNA damage, repair,

and cell cycle regulation (Fig. 3F). This was replicated with the 92 APs (Supplementary Table 7) found in T24R cells (Fig. 3G). The results were consistent with previous reports demonstrating inherent and persistent downstream EGFR signaling in resistant cells [21].

3.4. Several key kinases involved in cisplatin resistance were identified

Given this total list of 374 APs, 353 from T24S and 92 from T24R (with overlap), we next aimed to identify the key regulators of the observed phosphorylation profiles linked to cisplatin resistance. To this

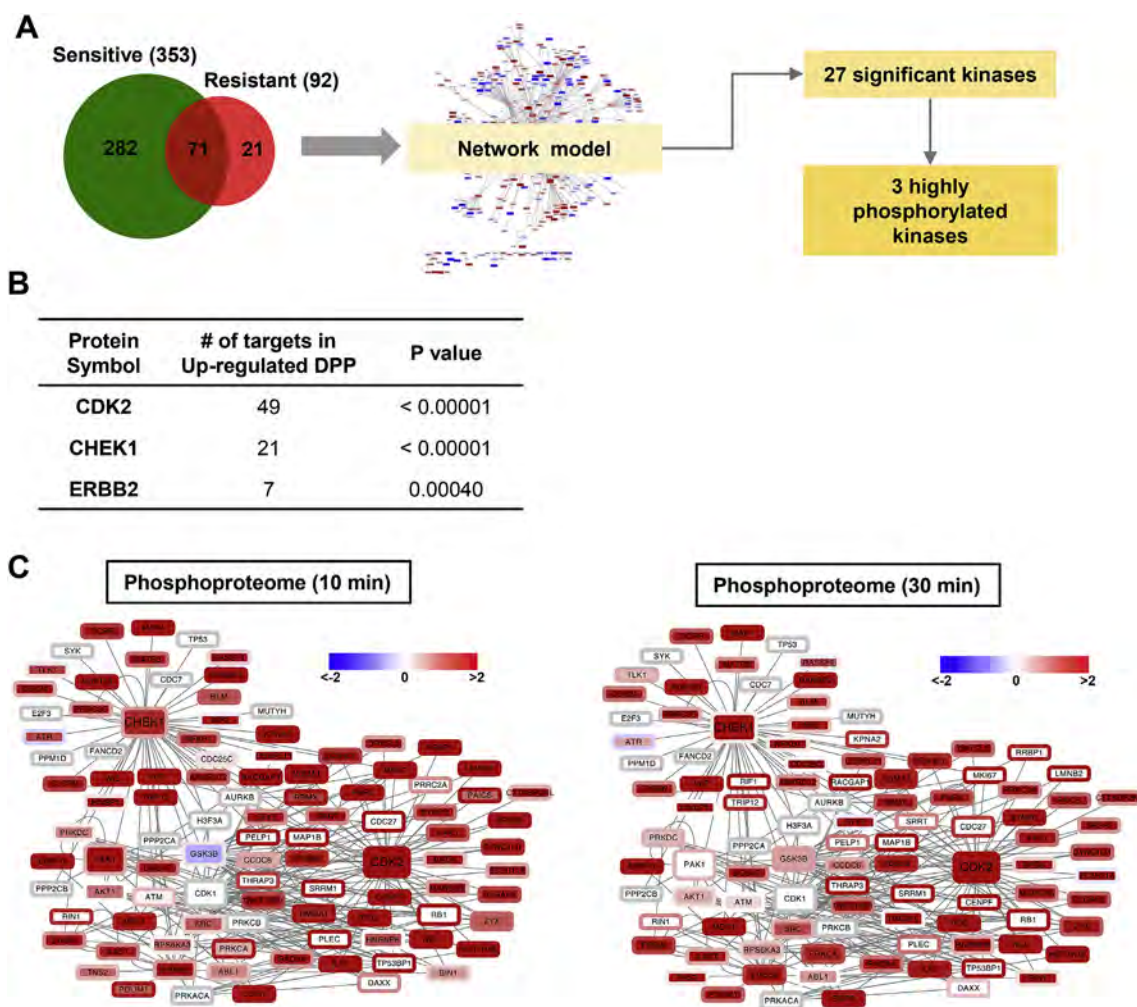


Fig. 4. Identification of key kinases linked to cisplatin resistance through the activation of EGFR signaling. A. Schematic diagram describing the process of reconstructing the networks of proteins significantly altered by EGF stimulation in T24R and T24S cells. Venn diagram depicts number of altered proteins involved in cisplatin resistance in downstream EGFR signaling. Using kinase-substrate interaction information of the significantly altered proteins and their upstream kinases, 27 kinases were initially selected. Of those, 3 kinases were found to be significant altered in either protein expression or phosphorylation after EGF treatment. B. List of the 3 key kinases with the number of significantly altered substrates and number of interactions. C. Network model describing the interactions of the 3 kinases and their substrates. Node and border color represent proteins phosphorylation ratios in T24R vs. T24S cells after 10 min or 30 min of EGF treatment, respectively. Red and green indicate up- and downregulated phosphorylation following EGF treatment, respectively. (For interpretation of the references to color in this figure legend, the reader is referred to the Web version of this article.)

end, we focused on the kinases that can regulate the phosphorylation levels of these differential sites by performing a kinase enrichment analysis. Using kinase-substrate interactions obtained from the SIGNOR database [34], we constructed a network model consisting of 121 kinases and 329 substrates with 893 interactions (Supplementary Fig. 2). Kinase enrichment analysis of the network model identified 3 out of the 27 kinases (Supplementary Table 8), checkpoint kinase 1 (CHEK1), cyclin-dependent kinase 2 (CDK2), and Erb-B2 receptor tyrosine kinase 2 (ERBB2), as having a significant number of interactions with APs when stimulated by EGF (Fig. 4A and B). Based on these 3 key kinases and their substrates, we reconstructed a subnetwork consisting of 101 nodes connected by 265 edges (Fig. 4A). The subnetwork was visualized using Cytoscape [37]. Notably, most of the substrates were highly phosphorylated in T24R, rather than T24S cells (Fig. 4C).

Validation with western blot analysis confirmed that phosphorylation of CDK2, CHEK1, ERBB2, mTOR, AKT, and RB significantly increased in T24R cells after treatment with 10 ng/ml of EGF (Fig. 5A). These results provide potential molecular mechanisms through which these 3 major kinases mediate cisplatin resistance. To further identify genes that have a critical effect on cisplatin resistance, we knocked-down the 3 kinases, CDK2, CHEK1, and ERBB2, in T24R cells using

siRNAs. Western blot analysis was conducted to confirm knockdown of these kinases (Fig. 5B, right). T24R cells were significantly sensitized to cisplatin when CDK2 was knocked-down, suggesting that CDK2 may be important in maintaining resistance (Fig. 5B). We next tested whether a potent and selective inhibitor of CDK2, dinaciclib (SCH 727965) [33], could overcome resistance in three independent cisplatin-resistant human BC cell lines, T24R, J82R, and RT4R (Fig. 5C). Consistent to the data shown in Fig. 5B, inhibition of CDK2 sensitized resistant cells when they were incubated in combination with cisplatin (Fig. 5C).

To further investigate the correlation of high CDK2 expression in BC, IHC analysis was done on BC TMAs. There were statistically significant differences in comparative scores for CDK2 expression between tumor and normal adjacent to tumor (NAT) cores (Fig. 5D). We applied a digital annotation algorithm to the core images in an effort to quantitatively assess this observation. Our image algorithm was set so that nuclear and cytoplasmic staining could be detected as positive at a color spectrum darker than that for typical DAB staining. Using the scores from our digital image analysis, we observed significantly upregulated expression of CDK2 in tumor cores. Comparative images of the tumor to NAT tissue show increased nuclear and cytoplasmic staining in the tumor epithelium (Fig. 5D). Collectively, these results demonstrate that

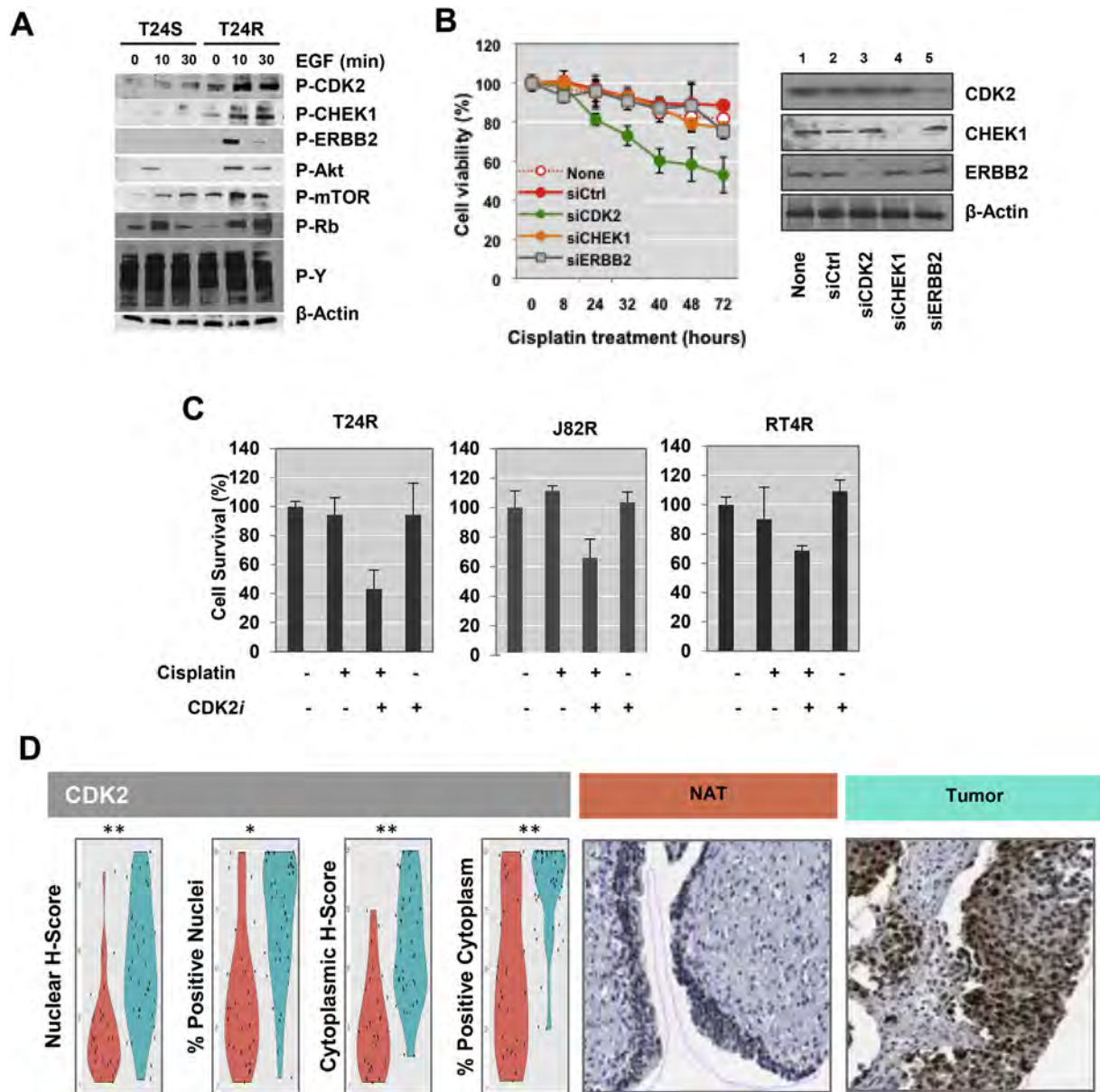


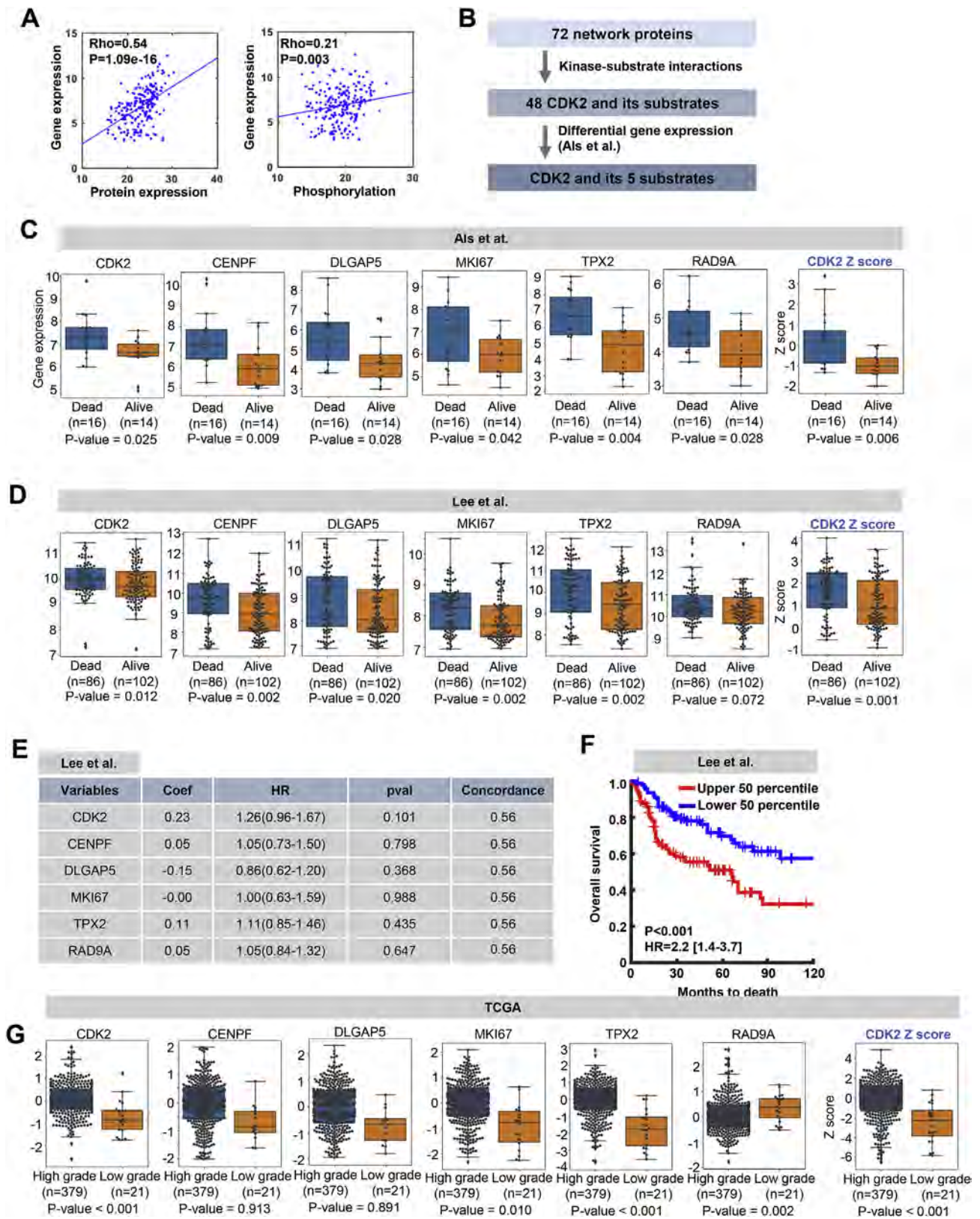
Fig. 5. Functional role of CDK2 associated with cisplatin resistance. A. Western blot analysis of the key protein kinases. After stimulation with 10 ng/ml of EGF treatment for 0, 10, or 30 min, cells were harvested for protein extraction and western blot analysis. Representative western blot images were selected after experiments were repeated at least 3 times. B. Gene silencing of CDK2 enhanced cisplatin sensitivity in T24R cells. T24R cells transiently transfected with siRNAs targeting CDK2, CHEK1, or ERBB2 were incubated in culture medium with 10 μM cisplatin. T24R cells transfected with control siRNAs (siCtrl) were used as controls. The cell viability rate was measured at various time points (0, 8, 24, 32, 40, 48, and 72 h). Experiments were done in triplicate. **p* < 0.05 (Student's t-test). Representative western blot analysis data demonstrated that the levels expression of CDK2, CHEK1, or ERBB2 in these experiments were downregulated by targeting siRNAs. C. Cisplatin resistant BC cell lines (R24R, J82R, or RT4R) were treated with cisplatin alone, CDK2 inhibitor (CDKi), or a combination of both for 72 h. Cell survival rates were quantified as describe in Methods. D. Increased expression levels of CDK2 in BC. IHC analysis was performed to measure the protein expression of CDK2 in bladder tissues from BC patients. Violin plots showing expression of CDK2 in NAT and tumor tissue. Representative images of NAT and tumor cores are shown.

our proteome-driven signature may be a useful predictor of survival for patients who have already undergone cisplatin chemotherapy.

3.5. Clinical implications of the key kinases and their substrates

Based on the significance of CDK2 and its substrates to cisplatin resistance, we examined the association of gene expression of CDK2 and its substrates to clinical outcomes. For this, we utilized the transcriptome dataset (GSE5287) from Als et al. [2], which contains the gene expression profiles of 30 BC patients along with their survival information after cisplatin chemotherapy. We first assessed the

correlation of APs in the global network model in terms of gene expression versus protein expression or phosphorylation levels (Fig. 6A). Significant positive correlations between gene expression versus protein expression (*P* = 1.09e-16) and gene expression versus protein phosphorylation (*P* = 0.003) were observed (Fig. 6A). This suggests that gene expression profiling can reflect protein expression and phosphorylation, supporting the possibility that the gene expression profiles of APs in BC patients can be indicators of dysregulated networks. We then searched for CDK2 substrates from the network model, which resulted in 48 proteins that were selected based on kinase-substrate interaction information from the SIGNOR database (Fig. 6B). For further selection,



(caption on next page)

we examined differential gene expression of the 48 proteins, including CDK2 and its substrates, using the BC dataset from Als et al. (GSE5287) [2]. For this we stratified the samples into those who survived 5 or more years (alive) and those who deceased within 5 years after chemotherapy (dead). This allowed us to identify genes in the CDK2

network that were significantly associated with poor survival after cisplatin chemotherapy (Fig. 6C). As a result, 6 genes out of 72 were found to have higher expression in the dead group. These were CDK2, CENPF, DLGAP5, MKI67, TPX2, and RAD9A.

We further investigated the clinical association of the 6 genes to the

Fig. 6. CDK2 network may have clinical implications in BC. **A.** Correlation of 72 network proteins in levels of gene expression vs. protein expression (left) or phosphorylation (right). Dots on the scatter plot represent proteins and lines represent regression lines. Correlation was measured using the Spearman's rank correlation method. **B.** Selection criteria used to identify the 6 proteins from the 72 network proteins. **C and D.** Box plots display differential gene expression of the selected 6 proteins from the network model using the gene expression datasets from (C) Als et al. and (D) Lee et al. Box plots at the far right display differential representation of CDK2 network scores computed by the Z-score method. Significance levels of differential gene expression between BC patients who were alive and deceased after cisplatin treatment were computed via the Wilcoxon rank-sum test. **E.** Regression coefficient and significance of the 6 genes based on multivariate Cox regression analysis using Lee et al. dataset. **F.** Kaplan-Meier curves for overall survival based on the expression of the CDK2 network genes are shown for the high (upper 50th percentile; n = 97) and low (lower 50th percentile; n = 91) z-score groups from the Lee et al. patient dataset. P-values and hazard ratios (HRs) were taken from a Cox regression analysis. **G.** Box plots display differential expression of the 6 genes in the TCGA BC cohort. Wilcoxon rank-sum test was performed to compute significance of differential expression between high and low grade samples.

CDK2 network using two gene expression datasets from Als et al. (GSE5287) [2] and Lee et al. (GSE13507) [24]. The Als et al. dataset showed significantly higher expression of the 6 genes in the CDK2 network and its summarized score (Z-score) in the dead group (Fig. 6C). The same was true in the Lee et al. dataset (Fig. 6D). Using the Lee et al. dataset, we then examined the association of these 6 CDK2 network genes to recurrence-free survival (RFS) by performing multivariate Cox regression analysis (Fig. 6E). Although individual genes showed no significant correlation with RFS, the summarized score of the 6 genes presented significant association with RFS (Fig. 6F). We further confirmed that expression of the 6 gene and its summarized score in the CDK2 network were significantly segregated high vs low grade BC samples from The Cancer Genome Atlas (TCGA) [35] (Fig. 6G). Collectively, these results suggest that our AP-derived CDK2 network genes may be helpful in predicting prognosis and treatment options for BC patients.

4. Discussion

Our present work characterized the enriched global proteome and phosphoproteome in cisplatin-resistant BC. By characterizing the signaling network alterations associated with cisplatin resistance, we also demonstrated the utility of quantitative phosphoproteomics in highlighting perturbed networks between cisplatin-resistant and sensitive BC cells. This approach revealed a vastly different cellular context between T24R and T24S cells, suggesting that there are potential key regulators modulating the perturbation of signaling networks. Measuring the abundance of proteins and mapping the phosphorylated kinase-substrate interactions facilitated a comprehensive biological interpretation of the complex network context behind cisplatin resistance. Expanded analysis of transcriptome data from BC patients further provided strong evidence that concurrent molecular alterations in gene expression to protein modification can be the core basis of disease.

Our experimental results illustrated that the global phosphoproteomics profile in cisplatin-resistant cells is significantly altered and that several key kinases may be mediating this. These kinases could potentially be used as therapeutic targets for blocking chemo-resilience. We also observed an increase in the phosphorylation of CDK2, CHEK1, and ERBB2 in cisplatin-resistant cells. Our comprehensive proteomics approach revealed many novel phosphorylation sites of CDK2, CHEK1, ERBB2, and their substrates, suggesting new intervention points in cisplatin resistance-specific signaling networks. The experimental results from this study implicate the active involvement of CDK2, CHEK1, and ERBB2 in contributing to resistance against cisplatin-based chemotherapies.

CHEK1 is a serine/threonine kinase that is involved in the checkpoint-mediated control of the cell cycle and the activation of DNA repair in response to DNA damage or the presence of unreplicated DNA. The ATR-CHEK2 signaling pathway was recently proposed to play an important role in regulating the response to cisplatin in BC [16]. Inhibition of the ATR-CHEK2 pathway with selective inhibitors can sensitize cells to cisplatin [7,26]. ERBB2 (HER2), a member of the EGF receptor family of receptor tyrosine kinases, has been known to be associated with aggressive variants of BC. Mutated ERBB2 is well documented as a cancer driver gene and is primarily found in high-risk

tumors. Mutations in ERBB2 have also been found to be independent risk factors associated with death in BC patients [22]. Thus, ERBB2-targeting treatment has been an attractive option in improving clinical outcomes for BC patients.

Our kinase activity-based network modeling suggested that one of the most significantly increased sites of phosphorylation in resistant cells is CDK2. The CDK2 network consists of several putative substrates, including CDC27, DAXX, and CENPF (Fig. 4A). CDK2, a Ser/Thr protein kinase, phosphorylates substrates at the S/TPx(x)R/K consensus motif. CDK2 is originally known to function in cell cycle regulation; increased CDK2 kinase activity is essential for the G1 to S stage transition as well as the phosphorylation of the Rb protein. During the S phase, active CDK2 and cyclin A complexes predominate and phosphorylate E2F [30]. CDK2 inhibitors (e.g., ribociclib, dinociclib, seliciclib et al.), which deregulate E2F, have been suggested as promising pharmacological strategies against various cancer types. However, a comprehensive overview of CDK2 and its substrates has not yet been established and the biological effects or regulatory mechanisms of CDK2 remain elusive.

Our findings suggest that inhibition of CDK2, a key player of cisplatin resistance, could induce cisplatin sensitivity. Therefore, CDK2 may be a potential target in the modulation of cisplatin resistance modulating human BC. This is consistent with previous reports. Alterations of CDK2 that are associated with cisplatin resistance in vitro have been reported in other cancer types, such as ovarian [31,40], oral [25], testicular [23] and cervical [42]. While our results are promising, we are aware of the limitations in our study, mainly owing to a lack in quantity of clinical specimens for phosphoproteomic analysis. Our study was also restricted to cell line-derived signatures; although, it was further validated in the clinical setting. Since this finding was based on a retrospective study from a single institution, the efficacy of the signature could be impaired. Future prospective validation studies using high-throughput assays should be followed up in multiple centers to consolidate our signature's analytical validity and reproducibility in the routine clinical practice setting.

Acknowledgements

The authors acknowledge support from the Bio and Medical Technology Development Program (project no. 2012M3A9B6055305) though the National Research Foundation of Korea funded by the Korean Ministry of Education, Science and Technology. We also appreciate support from the Multiomics Research Program (NRF-2012M3AB9036675), which is funded by the Korean Ministry of Science, ICT, and Future Planning. This work was also supported by the National Institutes of Health grants (1U01DK103260, 1R01DK100974, U24 DK097154, NIH NCATS UCLA CTSI UL1TR000124), Department of Defense (W81XWH-15-1-0415), Centers for Disease Controls and Prevention (1U01DP006079), IMAGINE NO IC Research Grant, Steven Spielberg Discovery Fund in Prostate Cancer Research Career Development Awards, and the U.S.-Egypt Science and Technology Joint Fund (to J.K.). J.K. is a former recipient of the Interstitial Cystitis Association Pilot Grant, Fishbein Family IC Research Grant, New York Academy of Medicine, and Boston Children's Hospital Faculty Development. Any opinions, findings, conclusions, or recommendations expressed in this article are those of the authors alone and do not

necessarily reflect the views of any of the previously mentioned sponsors. In addition, this article is derived from the Subject Data funded in whole or part by National Academy of Sciences, Engineering, and Medicine (NAS) and The United States Agency for International Development. Any opinions, findings, conclusions, or recommendations expressed in this article are those of the authors alone, and do not necessarily reflect the views of USAID or NAS.

Appendix A. Supplementary data

Supplementary data related to this article can be found at <https://doi.org/10.1016/j.canlet.2018.08.014>.

References

- [1] A.W. Bowman, A. Azzalini, *Applied Smoothing Techniques for Data Analysis: the Kernel Approach with S-plus Illustrations*, Clarendon Press; Oxford University Press, Oxford New York, 1997.
- [2] A.B. Als, L. Dyrskjot, H. von der Maase, K. Koed, F. Mansilla, H.E. Toldbod, J.L. Jensen, B.P. Ulhøi, L. Sengelov, K.M. Jensen, T.F. Orntoft, Emmprin and survival predict response and survival following cisplatin-containing chemotherapy in patients with advanced bladder cancer, *Clin. Canc. Res.* 13 (2007) 4407–4414.
- [3] A.B. Apolo, H.B. Grossman, D. Bajorin, G. Steinberg, A.M. Kamat, Practical use of perioperative chemotherapy for muscle-invasive bladder cancer: summary of session at the Society of Urologic Oncology annual meeting, *Urol. Oncol.* 30 (2012) 772–780.
- [4] P.C. Black, C.P. Dinney, Growth factors and receptors as prognostic markers in urothelial carcinoma, *Curr. Urol. Rep.* 9 (2008) 55–61.
- [5] B.M. Bolstad, R.A. Irizarry, M. Astrand, T.P. Speed, A comparison of normalization methods for high density oligonucleotide array data based on variance and bias, *Bioinformatics* 19 (2003) 185–193.
- [6] P. Casado, M. Hijazi, D. Britton, P.R. Cutillas, Impact of phosphoproteomics in the translation of kinase-targeted therapies, *Proteomics* 17 (2017).
- [7] S. Chen, X. Chen, G. Xie, Y. He, D. Yan, D. Zheng, S. Li, X. Fu, Y. Li, X. Pang, Z. Hu, H. Li, W. Tan, J. Li, Cdc6 contributes to cisplatin-resistance by activation of ATR-Chk1 pathway in bladder cancer cells, *Oncotarget* 7 (2016) 40362–40376.
- [8] P.R. Cutillas, Role of phosphoproteomics in the development of personalized cancer therapies, *Proteomics Clin. Appl.* 9 (2015) 383–395.
- [9] N. Eckstein, K. Servan, L. Girard, D. Cai, G. von Jonquieres, U. Jaehde, M.U. Kassack, A.F. Gazdar, J.D. Minna, H.D. Royer, Epidermal growth factor receptor pathway analysis identifies amphiregulin as a key factor for cisplatin resistance of human breast cancer cells, *J. Biol. Chem.* 283 (2008) 739–750.
- [10] G. Gakis, J. Efsthathiou, S.P. Lerner, M.S. Cookson, K.A. Keegan, K.A. Guru, W.U. Shipley, A. Heidenreich, M.P. Schoenberg, A.I. Sagalowsky, M.S. Soloway, A. Stenzl, ICUD-EAU International Consultation on Bladder Cancer 2012: radical cystectomy and bladder preservation for muscle-invasive urothelial carcinoma of the bladder, *Eur. Urol.* 63 (2013) 45–57.
- [11] O.N. Gofrit, Re: long-term outcomes in patients with muscle-invasive bladder cancer after selective bladder-preserving combined-modality therapy: a pooled analysis of radiation therapy oncology group protocols 8802, 8903, 9506, 9706, 9906, and 0233, *Eur. Urol.* 68 (2015) 165–166.
- [12] M.L. Granados, L.G. Hudson, S.L. Samudio-Ruiz, Contributions of the epidermal growth factor receptor to acquisition of platinum resistance in ovarian cancer cells, *PLoS One* 10 (2015) e0136893.
- [13] W. Huang da, B.T. Sherman, R.A. Lempicki, Systematic and integrative analysis of large gene lists using DAVID bioinformatics resources, *Nat. Protoc.* 4 (2009) 44–57.
- [14] D. Hwang, A.G. Rust, S. Ramsey, J.J. Smith, D.M. Leslie, A.D. Weston, P. de Auri, J.D. Aitchison, L. Hood, A.F. Siegel, H. Bolouri, A data integration methodology for systems biology, *Proc. Natl. Acad. Sci. U. S. A.* 102 (2005) 17296–17301.
- [15] M. Inoue, F. Koga, S. Yoshida, T. Tamura, Y. Fujii, E. Ito, K. Kihara, Significance of ERBB2 overexpression in therapeutic resistance and cancer-specific survival in muscle-invasive bladder cancer patients treated with chemoradiation-based selective bladder-sparing approach, *Int. J. Radiat. Oncol. Biol. Phys.* 90 (2014) 303–311.
- [16] M. Isono, M.J. Hoffmann, M. Pinkerneil, A. Sato, M. Michaelis, J. Cinatl Jr., G. Niegisch, W.A. Schulz, Checkpoint kinase inhibitor AZD7762 strongly sensitises urothelial carcinoma cells to gemcitabine, *J. Exp. Clin. Oncol. Res. CR (Clim. Res.)* 36 (2017) 1.
- [17] P. Jones, R.G. Cote, L. Martens, A.F. Quinn, C.F. Taylor, W. Derache, H. Hermjakob, R. Apweiler, PRIDE: a public repository of protein and peptide identifications for the proteomics community, *Nucleic Acids Res.* 34 (2006) D659–D663.
- [18] A.M. Kamat, P.K. Hegarty, J.R. Gee, P.E. Clark, R.S. Svatek, N. Hegarty, S.F. Shariat, E. Xylinas, B.J. Schmitz-Drager, Y. Lotan, L.C. Jenkins, M. Droller, B.W. van Rhijn, P.I. Karakiewicz, ICUD-EAU international consultation on bladder cancer 2012: screening, diagnosis, and molecular markers, *Eur. Urol.* 63 (2013) 4–15.
- [19] M. Kanehisa, S. Goto, Y. Sato, M. Furumichi, M. Tanabe, KEGG for integration and interpretation of large-scale molecular data sets, *Nucleic Acids Res.* 40 (2012) D109–D114.
- [20] S. Kim, P.A. Pevzner, MS-GF+ makes progress towards a universal database search tool for proteomics, *Nat. Commun.* 5 (2014) 5277.
- [21] W.T. Kim, J. Kim, C. Yan, P. Jeong, S.Y. Choi, O.J. Lee, Y.B. Chae, S.J. Yun, S.C. Lee, W.J. Kim, S100A9 and EGFR gene signatures predict disease progression in muscle invasive bladder cancer patients after chemotherapy, *Ann. Oncol.* 25 (2014) 974–979.
- [22] F. Koga, S. Yoshida, M. Tatokoro, S. Kawakami, Y. Fujii, J. Kumagai, L. Neckers, K. Kihara, ErbB2 and NfκB overexpression as predictors of chemoradiation resistance and putative targets to overcome resistance in muscle-invasive bladder cancer, *PLoS One* 6 (2011) e27616.
- [23] R. Koster, A. di Pietro, H. Timmer-Bosscha, J.H. Gibcus, A. van den Berg, A.J. Suurmeijer, R. Bischoff, J.A. Gietema, S. de Jong, Cytoplasmic p21 expression levels determine cisplatin resistance in human testicular cancer, *JCI (J. Clin. Invest.)* 120 (2010) 3594–3605.
- [24] J.S. Lee, S.H. Leem, S.Y. Lee, S.C. Kim, E.S. Park, S.B. Kim, S.K. Kim, Y.J. Kim, W.J. Kim, I.S. Chu, Expression signature of E2F1 and its associated genes predict superficial to invasive progression of bladder tumors, *J. Clin. Oncol.* 28 (2010) 2660–2667.
- [25] M.R. Lee, C. Lin, C.C. Lu, S.C. Kuo, J.W. Tsao, Y.N. Juan, H.Y. Chiu, F.Y. Lee, J.S. Yang, F.J. Tsai, YC-1 induces G0/G1 phase arrest and mitochondria-dependent apoptosis in cisplatin-resistant human oral cancer CAR cells, *Biomedicine* 7 (2017) 12.
- [26] C.C. Li, J.C. Yang, M.C. Lu, C.L. Lee, C.Y. Peng, W.Y. Hsu, Y.H. Dai, F.R. Chang, D.Y. Zhang, W.J. Wu, Y.C. Wu, ATR-Chk1 signaling inhibition as a therapeutic strategy to enhance cisplatin chemosensitivity in urothelial bladder cancer, *Oncotarget* 7 (2016) 1947–1959.
- [27] K.S. Lynn, C.C. Chen, T.M. Lih, C.W. Cheng, W.C. Su, C.H. Chang, C.Y. Cheng, W.L. Hsu, Y.J. Chen, T.Y. Sung, MAGIC: an automated N-linked glycoprotein identification tool using a Y1-ion pattern matching algorithm and in silico MS(2) approach, *Anal. Chem.* 87 (2015) 2466–2473.
- [28] Madar, Reduction of ambiguity in phosphorylation-site localization in large-scale phosphopeptide profiling by data filter using unique mass class information, *Bull. Kor. Chem. Soc.* 35 (2014) 845.
- [29] R. Mandic, C.J. Rodgarkia-Dara, V. Krohn, S. Wiegand, R. Grenman, J.A. Werner, Cisplatin resistance of the HNSCC cell line UT-SCC-26A can be overcome by stimulation of the EGF-receptor, *Anticancer Res.* 29 (2009) 1181–1187.
- [30] D.O. Morgan, Cyclin-dependent kinases: engines, clocks, and microprocessors, *Annu. Rev. Cell Dev. Biol.* 13 (1997) 261–291.
- [31] H. Pan, F. Wang, G.O. Rankin, Y. Rojanasakul, Y. Tu, Y.C. Chen, Inhibitory effect of black tea pigments, theaflavin-3/3'-gallate against cisplatin-resistant ovarian cancer cells by inducing apoptosis and G1 cell cycle arrest, *Int. J. Oncol.* 51 (2017) 1508–1520.
- [32] J.M. Park, J.H. Park, D.G. Mun, J. Bae, J.H. Jung, S. Back, H. Lee, H. Kim, H.J. Jung, H.K. Kim, H. Lee, K.P. Kim, D. Hwang, S.W. Lee, Integrated analysis of global proteome, phosphoproteome, and glycoproteome enables complementary interpretation of disease-related protein networks, *Sci. Rep.* 5 (2015) 18189.
- [33] K. Paruch, M.P. Dwyer, C. Alvarez, C. Brown, T.Y. Chan, R.J. Doll, K. Keertikar, C. Knutson, B. McKittrick, J. Rivera, R. Rossman, G. Tucker, T. Fischmann, A. Hruza, V. Madison, A.A. Nomeir, Y. Wang, P. Kirschmeier, E. Lees, D. Parry, N. Scambellone, W. Seghezzi, L. Schultz, F. Shanahan, D. Wiswell, X. Xu, Q. Zhou, R.A. James, V.M. Paradkar, H. Park, L.R. Rokosz, T.M. Stauffer, T.J. Guzi, Discovery of dinaciclib (SCH 727965): a potent and selective inhibitor of cyclin-dependent kinases, *ACS Med. Chem. Lett.* 1 (2010) 204–208.
- [34] L. Perfetto, L. Briganti, A. Calderone, A. Cerquone Perpetuini, M. Iannuccelli, F. Langone, L. Licata, M. Marinkovic, A. Mattioni, T. Pavlidou, D. Peluso, L.L. Petrilli, S. Pirro, D. Posca, E. Santonico, A. Silvestri, F. Spada, L. Castagnoli, G. Cesareni, SIGNOR: a database of causal relationships between biological entities, *Nucleic Acids Res.* 44 (2016) D548–D554.
- [35] A.G. Robertson, J. Kim, H. Al-Ahmadie, J. Bellmunt, G. Guo, A.D. Cherniack, T. Hinoue, P.W. Laird, K.A. Hoadley, R. Akbani, M.A.A. Castro, E.A. Gibb, R.S. Kanchi, D.A. Gordenin, S.A. Shukla, F. Sanchez-Vega, D.E. Hansel, B.A. Czerniak, V.E. Reuter, X. Su, B. de Sa Carvalho, V.S. Chagas, K.L. Mungall, S. Sadeghi, C.S. Pedamallu, Y. Lu, L.J. Klimczak, J. Zhang, C. Choo, A.I. Ojesina, S. Bullman, K.M. Leraas, T.M. Lichtenberg, C.J. Wu, N. Schultz, G. Getz, M. Meyerson, G.B. Mills, D.J. McConkey, T.R. Network, J.N. Weinstein, D.J. Kwiatkowski, S.P. Lerner, Comprehensive molecular characterization of muscle-invasive bladder cancer, *Cell* 171 (2017) 540–556 e525.
- [36] C. Schwentner, A. Stenzl, G. Gakis, Monitoring high-risk bladder cancer, *Curr. Opin. Urol.* 22 (2012) 421–426.
- [37] P. Shannon, A. Markiel, O. Ozier, N.S. Baliga, J.T. Wang, D. Ramage, N. Amin, B. Schwikowski, T. Ideker, Cytoscape: a software environment for integrated models of biomolecular interaction networks, *Genome Res.* 13 (2003) 2498–2504.
- [38] G. Sonpavde, C.N. Sternberg, Neoadjuvant chemotherapy for invasive bladder cancer, *Curr. Urol. Rep.* 13 (2012) 136–146.
- [39] C.N. Sternberg, J. Bellmunt, G. Sonpavde, A.O. Siefker-Radtke, W.M. Stadler, D.F. Bajorin, R. Dreicer, D.J. George, M.I. Milowsky, D. Theodorou, D.J. Vaughn, M.D. Galsky, M.S. Soloway, D.I. Quinn, ICUD-EAU international consultation on bladder cancer 2012: chemotherapy for urothelial carcinoma-neoadjuvant and adjuvant settings, *Eur. Urol.* 63 (2013) 58–66.
- [40] Y. Sun, L. Jin, J.H. Liu, Y.X. Sui, L.L. Han, X.L. Shen, Interfering EZH2 expression reverses the cisplatin resistance in human ovarian cancer by inhibiting autophagy, *Cancer Biother. Radiopharm.* 31 (2016) 246–252.
- [41] V.M. Tan, L.C. Cheng, J.M. Drake, Complementing genomics and transcriptomics: phosphoproteomics illuminates systems biology in prostate cancer, *Mol. Cell Oncol.* 3 (2016) e1246075.
- [42] B. Zhang, Z. Huang, R. Gao, Z. Zeng, W. Yang, Y. Sun, W. Wei, Z. Wu, L. Yu, Q. Li, S. Wang, F. Li, G. Liu, B. Liu, L. Leng, W. Zhan, Y. Yu, G. Yang, S. Zhou, Expression of long noncoding RNA urothelial cancer associated 1 promotes cisplatin resistance in cervical cancer, *Cancer Biother. Radiopharm.* 32 (2017) 101–110.
- [43] J.R. Wisniewski, A. Zougman, N. Nagaraj, M. Mann, Universal sample preparation method for proteome analysis, *Nat. Methods* 6 (2009) 359–362.
- [44] B. Zhang, M.C. Chambers, D.L. Tabb, Proteomic parsimony through bipartite graph analysis improves accuracy and transparency, *J. Proteome Res.* 6 (2007) 3549–3557.

Quantitative Proteomic Analysis Reveals Caffeine-Perturbed Proteomic Profiles in Normal Bladder Epithelial Cells

Muhammad Shahid, Minhyung Kim, Austin Yeon, Allen M. Andres, Sungyong You, and Jayoung Kim*

Lower urinary tract symptoms (LUTSs) are highly prevalent among the elderly and negatively impact quality of life. Since caffeinated beverages are enjoyed worldwide and the relationship between LUTS and caffeine is still not fully understood, it would be of particular interest to examine the underlying mechanisms that drive caffeine's influence on LUTS development and progression. The aim of this study is to characterize the effects of caffeine on hTert-immortalized normal bladder epithelial cells by investigating whether exposure to caffeine can cause potential changes in the bladder proteome and/or biological pathways. In labeled LC-MS/MS proteomic analysis, 57 proteins are found as being differentially expressed in caffeine-treated bladder epithelial cells, compared to controls; this included 32 upregulated and 25 downregulated proteins. Further functional gene enrichment analysis reveals that caffeine affects major biological pathways, including those for "muscle contraction" and "chromatin assembly." These findings provide new scientific insights that may be useful in future studies investigating the role of caffeine in bladder dysfunctions.

1. Introduction

It is estimated that by the end of 2018, 2.3 billion individuals will be affected by at least one lower urinary tract symptom (LUTS).^[1] These symptoms include urinary storage problems, such as urgency, frequency, nocturia, or voiding problems. LUTS also weighs heavily on overall quality of life; patients report significantly higher mental health issues, lower work productivity, and

diminished general health status.^[2] The current standard treatment for LUTS involves α -blockers, 5 α -reductase inhibitors, and antimuscarinics.^[3] However, these are mainly palliative and require consistent maintenance. Consequently, there is a substantial economic burden associated with LUTS.^[4] Previous reports have demonstrated that diet and stress play important roles in the development and progression of LUTS.^[5] In particular, caffeine, a naturally occurring compound, has been reported to be a potential dietary risk factor in developing LUTS.^[6] Caffeine is ubiquitously found in many plants, including cocoa beans, tea leaves, and coffee beans. It is a stimulatory drug that is widely used to prevent sleepiness and can be found in over-the-counter medications, such as some pain remedies. It has also been observed that caffeine

may aggravate or worsen urinary symptoms in patients who already have some form of LUTS.^[7] In recent years, caffeinated drinks have become a staple of the average diet; more than 85% of adults in the United States regularly consume caffeine.^[8] A longitudinal study of caffeine intake in young healthy volunteers found that subjects who regularly drank coffee had significant increases in urinary urgency and frequency.^[9] Additionally, a separate study observed that greater coffee intake raised the odds of

Dr. M. Shahid, Dr. M. Kim, A. Yeon, Dr. S. You, Dr. J. Kim
Departments of Surgery and Biomedical Sciences
Cedars-Sinai Medical Center
Los Angeles, CA, USA
E-mail: Jayoung.Kim@cshs.org


Dr. A. M. Andres
Department of Medicine
Cedars Sinai Medical Center
Los Angeles, CA, USA

Dr. A. M. Andres
Cedars-Sinai Heart Institute
Los Angeles, CA, USA

Dr. S. You, Dr. J. Kim
Samuel Oschin Comprehensive Cancer Institute
Cedars-Sinai Medical Center
Los Angeles, CA, USA

Dr. J. Kim
University of California Los Angeles
CA, USA

Dr. J. Kim
Department of Urology
Ga Cheon University College of Medicine
Incheon, South Korea

 The ORCID identification number(s) for the author(s) of this article can be found under <https://doi.org/10.1002/pmic.201800190>

DOI: 10.1002/pmic.201800190

LUTS progression in men and women more than carbonated or citrus beverages.^[10] The effects of caffeine have also been studied in the context of bladder cancer (BC); however, rather than finding a negative risk, there have been reported benefits. A case-control study of BC patients in Italy found no causal relationship between caffeine and BC.^[11] A separate study found that caffeine may actually benefit BC patients by making cells more susceptible to chemotherapy and apoptosis.^[12] Mechanistically, this has been reported to be mediated through caffeine's effects on the tumor suppressor protein, p53.^[13]

Despite the potential link between caffeine and LUTS, research into causative mechanisms and functions is lacking. One prior study suggested that caffeine may be facilitating bladder instability and frequent urination by enhancing the activation of neuronal micturition centers through increased expression of transcription factor c-Fos and nerve growth factor.^[14] While informative, this study focused primarily on the bladder muscles with little attention on the bladder epithelium, which is more anatomically exposed to urine and its biological/chemical contents. A separate study using a mouse model found that oral caffeine administration resulted in detrusor overactivity and increased bladder sensory signaling.^[15] Further studies found similar effects on the detrusor muscle in humans.^[16] However, the direct effects of caffeine, its delivery into cells, and its mechanisms remain unestablished.

Our present study sought to examine the cellular effects of caffeine on the bladder epithelium without any pathological conditions. Quantitative and global proteomics analysis found that caffeine can perturb the whole proteome, possibly through the regulation of chromatin assembly in normal bladder epithelial cells.

2. Experimental Section

2.1. Cell Culture and Cell Proliferation Assay

Immortalized normal human bladder epithelial cells, TRT-HU1, were maintained as described previously.^[17] The TRT-HU1 cell line was constructed and extensively characterized in previously published papers. The passage number of each cell line was below ten, and mycoplasma contamination was tested for monthly via PCR analysis. Cells were cultured in Dulbecco's modified Eagle's medium, containing 10% fetal bovine serum (Invitrogen), 1% penicillin/streptomycin, and 1% L-glutamine (Sigma–Aldrich Corp., St. Louis, MO, USA) in a 37 °C humidified incubator with 5% CO₂. To test cell growth during exposure to caffeine, TRT-HU1 cells were seeded onto six-well plates with a density of 5 × 10⁴ cells per well. Cells were then incubated with standard growth medium with varying doses of caffeine at 0, 0.005, 0.05, or 0.1 mM (C6035, Sigma–Aldrich Corp.) or vehicle for 24, 48, or 72 h. Cell proliferation was measured by manually counting cells using a hemocytometer. The averages of each count were used as the total density of the well after each time point. For crystal violet staining, the culture medium was removed, the cells were fixed with 4% paraformaldehyde at room temperature for 5 min and then stained with 0.05% crystal violet for 15 min. The cells were then washed with tap water, after which the water was removed and the cells were dried out on filter paper. The cell plates were

Significance Statement

Caffeine, a methylxanthine that is derived from coffee intake, has been reported to be a potential dietary risk factor in developing lower urinary tract symptoms (LUTS). Despite this known potential link, research into causative mechanisms and functions is lacking. Our unbiased proteomics study revealed that caffeine alters the global proteome in human-immortalized normal bladder epithelial cells and enriches biological pathways related to muscle contraction and chromatin assembly. Our study is clinically significant because it provides the potential mechanisms through which caffeine can provoke LUTS and suggests that the restriction of caffeine intake may be benefit muscle contraction and functional gene expression.

scanned and quantified using 10% acetic acid and measured at an absorbance of 570–590 nm.^[18] All experiments were run in triplicate for each cell line, and the data are representative of three independent trials.

2.2. Antibodies and Reagents

Antibodies against various proteins were obtained from the following sources: ACTG2 (ab189385, Abcam), ACTA2 (ab5694, Abcam), MYH2 (ab124937, Abcam), MYH7B (ab172967, Abcam), HISTH2B (ab52599, Abcam), HIST1H2BM (SAB1301739, Sigma), and β -actin (A1978, Sigma). Commercially available horseradish peroxidase (HRP)-conjugated secondary antibodies (7074 and 7076) were obtained from Cell Signaling Technology. All other chemical reagents were procured from Sigma Chemical Corp.

2.3. Quantitative Proteomics

Tandem mass tagging (TMT)-based quantitative proteomics was performed as previously described.^[19] Briefly, cellular protein was extracted from caffeine-treated and control cells using 4% SDS-containing buffer. The protein concentration was measured using the Pierce 660 nm Assay Kit. From each sample, 60 μ g of protein was digested with trypsin using filter-aided sample preparation and labeled with TMT6plex reagents in parallel.

After TMT labeling, the peptides were merged, desalted with C18 spin columns (Thermo Scientific), and fractionated via high-pH reversed phase liquid chromatography (RPLC) using an Ultimate 3000 XRS System (Thermo Scientific). For high-pH RPLC, about 50 μ g TMT-labeled peptides were loaded onto a 100-mm Hypersil GOLD C₁₈ column (2.1 mm id, 3 μ m particle size, 175 Å pore size; Thermo Scientific), flushed for 3 min with solvent A (10 mM ammonium formate, pH 10), and then separated with a 7-min linear gradient of 0–40% solvent B (10 mM ammonium formate, 95% acetonitrile, pH 10.0). A total of 24 fractions were collected, concentrated into 12 fractions, and dried down in a SpeedVac (Thermo Scientific). Peptides in each fraction were redissolved with 0.2% formic acid and analyzed by LC–MS/MS using an EASY-nLC 1000 connected to an LTQ Orbitrap Elite Mass Spectrometer (Thermo Scientific). Briefly, peptides were loaded

onto a 2-cm trap column (PepMap 100 C18, 75 μm id, 3 μm particles, 100 Å pore size) and separated by a 50-cm EASY-Spray column (PepMap RSLC C₁₈, 75 μm id, 2 μm particles, 100 Å pore size) heated to 55 °C. For low-pH RPLC separation, the mobile phase consisted of 0.1% formic acid in water (phase A) or acetonitrile (phase B). The LC gradient was 4–24% B over 200 min, 24–50% B over 20 min, and 50–100% B over 5 min at a flow rate of 150 nL min⁻¹, followed by 100% B over 15 min at a flow rate of 300 nL min⁻¹.

Mass spectra were acquired in a data-dependent manner, selecting up to the 15 most abundant precursor ions for higher-energy collisional dissociation. The mass resolution for precursor and fragment ions was set to 120 000 and 30 000, respectively. The isolation width was set as 1.5 and the normalized collision energy was set as 40. Database searching and protein quantification was performed by Proteome Discoverer (v2.1), using the SEQUEST algorithm. The acquired raw data were searched against the human Uniprot Protein Sequence Database (released on January 22, 2016, containing 20 985 protein sequences). Searching parameters were set as follows: trypsin, up to two missed cleavage; precursor ion tolerance of 10 ppm and fragment ion tolerance of 0.02 Da; carbamidomethylation of cysteines and TMT6plex modification of lysines and peptide N-term as fixed modifications; and acetylation of protein N-term, oxidation of methionine, and deamidation of asparagines and glutamines as variable modifications. A standard false discovery rate (FDR) of 1% was applied to filter peptide-spectrum matches (PSMs), peptide identifications, and protein identifications.

For protein quantification, peptides with >30% precursor ion interference were excluded to minimize erroneous quantification caused by precursor ion interference. PSM level information was extracted using the Proteome Discoverer.^[20] After quantifying each PSM intensity, the peptide intensities were summarized, as described by Niu et al.^[21] In brief, this was done in four steps: 1) the normalized log₂ intensity of the PSMs matched to each peptide by the substrate mean PSM from each reporter intensity was centered, 2) outliers were detected using Dixon's *Q*-test and generalized electrostatic discharge test, 3) the mean intensity without outliers was taken, and 4) the grand-mean intensities of the three highest abundant PSMs were added before being mean-centered. Bipartite graphs of peptides and protein groups were generated according to the information of the aligned peptides. Among the proteins in the protein group, we defined the representative protein that had the largest number of peptides or unique peptide.^[22] When there were more than proteins with the same number of peptides in the same protein group, we selected the protein that had the higher sequence coverage. We then computed the relative intensity of the protein group using a linear-programming formulation, as previously described.^[23]

2.4. Identification of Differentially Expressed Proteins

To identify the differentially expressed proteins (DEPs), we selected proteins that have more than two nonredundant peptides. For the selected proteins, we then performed an one sample *t*-test using log₂-fold changes to compute the significance of *t*-values. For this statistical test, an empirical distribution of the null hypothesis, a protein is not differentially expressed, was estimated

by following steps: 1) 100 000 random permutations were applied to the samples, 2) *t*-values were computed using the log₂-fold changes of the randomly permuted samples, and 3) the Gaussian kernel density estimation method was applied to *t*-values. The FDRs of each protein from the one sample *t*-tests were then calculated using Storey's method.^[24] The DEPs were identified as those with a FDR < 0.05 and absolute log₂-fold change > 0.58 (1.5 fold). Functional enrichment analysis of DEPs was performed using DAVID software (Ver. 6.8).^[25] Significantly enriched cellular processes were selected for if they had a *p*-value < 0.05.

2.5. Western Blot Analysis

Cells were seeded onto 10-cm plates and exposed to 0.05 mM concentrations of caffeine for 72 h. Cells were lysed with RIPA buffer (20 mM Tris, 150 mM NaCl, 1% Nonidet, P-40, 0.1 mM EDTA; Pierce, ThermoFisher) supplemented with a phosphatase inhibitor cocktail (ThermoFisher). The protein concentration of each sample was measured with the Bradford Protein Kit Assay, according to the manufacturer's instructions (Pierce, ThermoFisher). Equal amounts of protein extract were separated by SDS-PAGE and transferred onto a PVDF membrane. The membranes were then blocked with 5% bovine serum albumin or 5% nonfat milk in Tris-buffered saline with 0.1% Tween 20 (TBST [2.42 g L⁻¹ Tris-HCl, 8 g L⁻¹ NaCl, and 1 mL L⁻¹ Tween 20 (pH 7.6)]) and incubated overnight at 4 °C with specific primary antibodies in TBST. The membranes were then incubated with secondary antibodies conjugated with HRP, as described previously. β -actin was used as an internal control. All western blot experiments were run in at least triplicates for each antibody.

2.6. Seahorse Respirometry Assay

TRT-HU1 cells were seeded onto a 24-well Seahorse culture plate at a density of 50 000 cells per well 24 h before the Seahorse assay. Media was then changed to XF Base Medium (pH 7.4) supplemented with 10 mM glucose, 1 mM sodium pyruvate, and 1 mM sodium glutamine. Cells were equilibrated for 1 h in a non-CO₂ incubator at 37 °C before the assay began. Cells were treated with caffeine at 0.05 mM, or 0.5 mM for experiments. Chemical reagents (Sigma) were used at final concentrations, as follows: 1 μM oligomycin—an ATP synthase inhibitor, 1 μM (FCCP) carbonyl cyanide 4-(trifluoromethoxy) phenylhydrazone—an uncoupling agent, and a mixture of 0.5 μM antimycin A—a cytochrome C reductase inhibitor and 0.5 μM rotenone—a complex I inhibitor. Oxygen consumption rate (OCR) and extracellular acidification rate (ECAR) was monitored during the duration of the assay run. OCR and ECAR were monitored before and after addition of caffeine. Results were normalized to protein concentrations determined by BCA assay (Thermo Scientific).

2.7. Statistical Analysis

Student's *t*-test was performed to confirm differential expression of the proteins between two groups. Variables with normal distribution were presented as mean \pm SD. All reported *p*-values are two-tailed, with *p*-values < 0.05 indicating statistical significance.

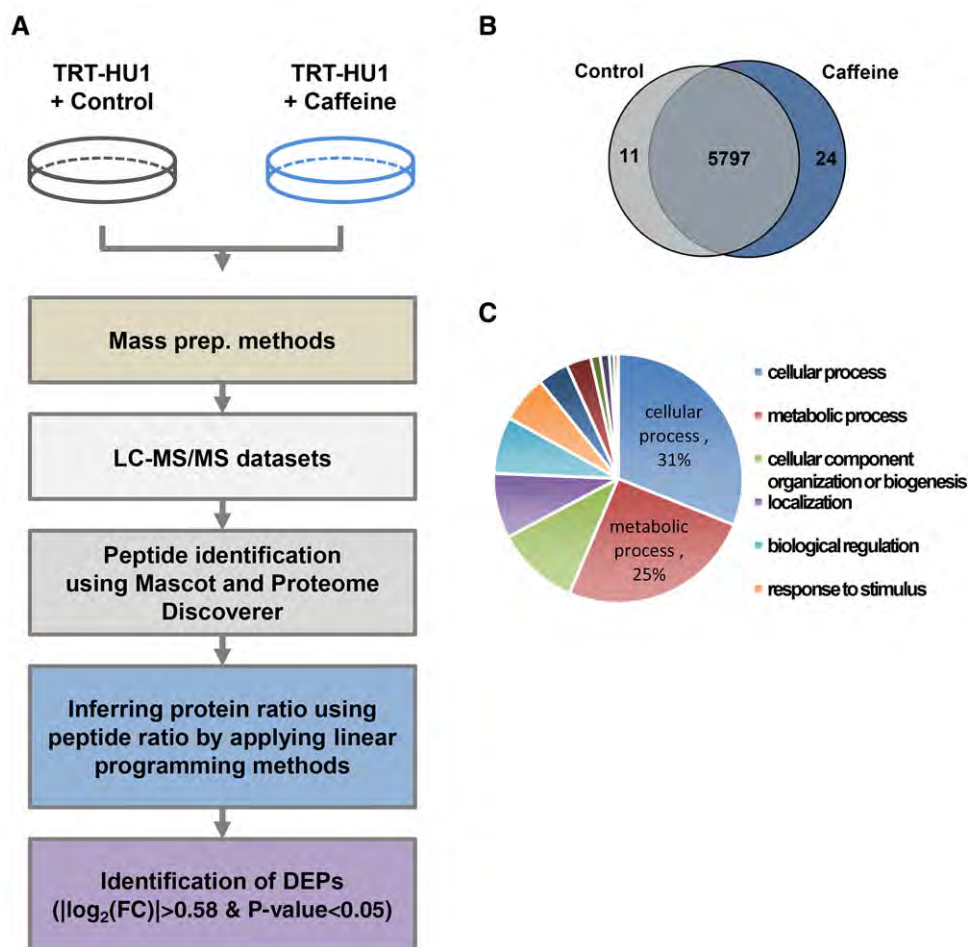


Figure 1. Unbiased proteomics analysis identified proteins in TRT-HU1 cells. A) Experimental scheme describing unbiased global proteomics profiling and bioinformatics analysis. B) Venn diagram depicts number of unique proteins detected in caffeine treated and nontreated normal bladder epithelial cells. C) Pie chart displays functional categories of all the identified proteins.

3. Results

3.1. Quantitative Proteomic Analysis of Normal Bladder Epithelial Cells

Due to the lack of knowledge regarding the effects of caffeine on biological and proteomic perturbations in the normal bladder epithelium, this study aimed to examine the whole proteome alterations caused by caffeine consumption. To gain insight on the underlying mechanism of caffeine on the bladder epithelium, we treated normal bladder epithelial cells with caffeine and performed TMT-based quantitative proteomic analysis, as outlined in **Figure 1A**. Based on previous literature, we opted to use caffeine concentrations within normal physiological consumption.^[12,26] Whole-cell lysates in biological duplicates were digested with trypsin. Using LC-MS/MS and followed by bioinformatic analyses, we identified 44 597 peptides corresponding 5832 proteins with more than two peptides in more than two sets of pooled lysates from at least three biological samples per condition. The caffeine-treated group had 5821 identified proteins with high expression, while the control group had 5808

(**Figure 1B**). We then performed functional categorization of the proteins to check whether our quantitative proteomic analysis was biased by any cellular compartments or biological process-related proteins using Panther software.^[27] All the identified proteins can be categorized into 14 cellular processes, including cellular process, metabolic process, cellular component organization of biogenesis, localization, biological regulation, response to stimulus, developmental process, multicellular organismal process, biological adhesion, immune system process, locomotion, reproduction, growth, and cell killing, indicating that this proteome reveals major biological functions of bladder epithelial cells in normal physiology (**Figure 1C**). In addition to this, we examined the cellular localization of the detected proteins, which showed significant enrichment of eight cellular compartments, including cell part, organelle, macromolecular complex, membrane, extracellular region, cell junction, synapse, and extracellular matrix. (**Figure S1**, Supporting Information). Collectively, our quantitative proteomic analysis identified a comprehensive list of proteins in all cellular components and illustrated the cellular functions of highly expressed proteins in normal bladder epithelial cells.

3.2. Whole Proteome in Bladder Epithelial Cells Perturbed by Caffeine Treatment

We determined which proteins were differentially expressed after caffeine treatment. DEPs were selected for if they had an absolute \log_2 -fold change greater than 0.58 and p -value less than 0.05. In total, we identified 32 upregulated and 25 downregulated proteins between the control versus caffeine groups (Table 1 and 2; Figure 2A). As shown in the volcano plot, some DEPs, including PSMC6 (proteasome 26S subunit ATPase 6), RUFY1 (RUN and FYVE domain containing 1), IARS (isoleucyl-tRNA synthetase), MCU (mitochondrial calcium uniporter), NAV1 (neuron navigator 1), RARG (retinoic acid receptor, gamma), etc., were significantly increased with caffeine treatment, while ST13P4 (ST13, Hsp70 interacting protein pseudogene 4), EIF5AL1 (eukaryotic translation initiation factor 5A-like 1), WASH2P (WAS protein family homolog 2 pseudogene), RBMS3 (RNA binding motif single stranded interacting protein 3), etc. decreased (Figure 2B).

Next, to understand the function of the perturbed proteins, we performed gene set enrichment analysis (GSEA) using the hallmark gene sets from the Molecular Signature Database.^[28] As a result, we found that the “glycolysis” and “PI3K/AKT/MTOR signaling” gene sets were significantly enriched for by the differentially expressed proteins (Figure 2C). We also checked the enrichment of Kyoto Encyclopedia of Genes and Genomes (KEGG) pathways in the same context and found that the “neurotrophin signaling pathway” and “purine metabolism” were significantly enriched for in caffeine-treated cells (Figure 2D). These results suggest that caffeine may be stimulating the bladder epithelium by altering the activation of the PI3K/AKT/MTOR pathway, neurotrophin signaling, and purine metabolism.

In addition, we conducted separate functional enrichment analyses on each of the 32 up- and 25 downregulated proteins using DAVID.^[25] The results suggest that upregulated DEPs were significantly enriched for “actin-myosin filament sliding,” “muscle contraction,” “purine nucleotide metabolic process,” “ATP metabolic process,” “autophagy,” “response to external biotic stimulus,” and “response to other organism.” Downregulated DEPs were significantly enriched for “chromatin assembly,” “DNA packaging,” and “cellular macromolecular complex assembly” (Figure 3A). From this, we extracted the list of most significantly upregulated DEPs belonging to “purine nucleotide metabolic process,” “autophagy,” “muscle contraction”, and “response to external biotic stimulus”. Additionally, significantly downregulated DEPs for “chromatin assembly” are also listed (Figure 3B and C).

3.3. Biological Effects of Caffeine Treatment on Immortalized Normal Bladder Epithelial Cells

To evaluate the direct effects of caffeine on bladder epithelial cells in vitro, we used TRT-HU1 cells in our study as described in Section 2. After incubating the TRT-HU1 cells in varying concentrations of caffeine (0.005, 0.05, and 0.1 mM) for 24, 48, or 72 h, we sought to determine if caffeine affects or controls cell proliferation and metabolism. We found that the cell proliferation rate of caffeine-treated TRT-HU1 cells was not significantly altered, compared to controls (Figure 4A and B).

Table 1. List of upregulated proteins in bladder epithelial cells perturbed by caffeine treatment.

Symbol	Full name	Fold change (log ₂)	p -value
S100A8	S100 calcium binding protein A8	4.17759	0.000112
ST13	ST13, Hsp70 interacting protein	3.918705	0.000224
SERPINB3	Serpin family B member 3	3.553147	0.000559
SERPINB4	Serpin family B member 4	3.553147	0.000559
WASH3P	WAS protein family homolog 3 pseudogene	2.327444	0.001342
POTEKP	POTE ankyrin domain family member K, pseudogene	2.210099	0.001565
RBMS1	RNA binding motif single stranded interacting protein 1	2.032904	0.001789
KPRP	Keratinocyte proline rich protein	1.526693	0.002124
S100A7	S100 calcium binding protein A7	1.4274	0.002236
TGM1	Transglutaminase 1	1.214751	0.002572
MYH7B	Myosin heavy chain 7B	0.970592	0.003131
MYH3	Myosin heavy chain 3	0.970592	0.003131
MYH1	Myosin heavy chain 1	0.970592	0.003131
MYH7	Myosin heavy chain 7	0.970592	0.003131
MYH8	Myosin heavy chain 8	0.970592	0.003131
MYH2	Myosin heavy chain 2	0.970592	0.003131
MYH13	Myosin heavy chain 13	0.970592	0.003131
MYH4	Myosin heavy chain 4	0.970592	0.003131
MYH7B	Myosin heavy chain 7B	0.970537	0.004025
MYH3	Myosin heavy chain 3	0.970537	0.004025
MYH1	Myosin heavy chain 1	0.970537	0.004025
MYH7	Myosin heavy chain 7	0.970537	0.004025
MYH8	Myosin heavy chain 8	0.970537	0.004025
MYH2	Myosin heavy chain 2	0.970537	0.004025
MYH13	Myosin heavy chain 13	0.970537	0.004025
MYH4	Myosin heavy chain 4	0.970537	0.004025
H2BFS	H2B histone family member S	0.895712	0.005255
S100A9	S100 calcium binding protein A9	0.871394	0.005367
UVRAG	UV radiation resistance associated	0.738812	0.00559
SULT1A4	Sulfotransferase family 1A member 4	0.665067	0.005814
SULT1A1	Sulfotransferase family 1A member 1	0.665067	0.005814
UCHL1	Ubiquitin C-terminal hydrolase L1	0.622981	0.006261
MAG13	Membrane-associated guanylate kinase, WW and PDZ domain containing 3	0.615023	0.006373
KRT74	Keratin 74	0.598941	0.006485
KRT73	Keratin 73	0.598941	0.006485
ACTA2	Actin, alpha 2, smooth muscle, aorta	0.598824	0.006708
LRRC8E	Leucine rich repeat containing 8 VRAC subunit E	0.594574	0.00682
KRT74	Keratin 74	0.594473	0.006932
KRT73	Keratin 73	0.594473	0.006932
KRT74	Keratin 74	0.594472	0.007156

(Continued)

Table 1. Continued.

Symbol	Full name	Fold change (log ₂)	p-value
KRT73	Keratin 73	0.594472	0.007156
FLCN	Folliculin	0.592834	0.007379
KRT74	Keratin 74	0.589943	0.007491
KRT73	Keratin 73	0.589943	0.007491
CPNE6	Copine 6	0.587267	0.007715
CPNE4	Copine 4	0.587267	0.007715

To examine the effects of caffeine on cell metabolism, we performed Seahorse respirometry analysis. Caffeine treatment over a 12-h period did not alter the OCR (mitochondrial respiration) or ECAR (glycolysis) in TRT-HU1 cells (Figure 4C). Briefly, basal OCR and ECAR measurements (first three time points) were monitored before caffeine (0.05 mM) or vehicle (methanol) was administered. OCR and ECAR continued to be monitored up to 12 h post treatment. Nontreated cells (media administration only) were included to control for any effects of the cells being in the analyzer for an extended period (Figure 4C). We could not detect any changes in both the OCR and ECAR, even after a 12-h treatment with 0.05 mM caffeine. Additional western blot analysis demonstrated that expression of ACTG2 and HIST1H2BM was reduced in the 0.05 mM caffeine-treated cells, while expression of ACTA2, MYH2, and MYH7B was upregulated. The expression of histone H2B and ACTB remained unchanged (Figure 4D).

4. Discussion

Approximately 60% of adults in the United States consume coffee or some other caffeinated beverage. Caffeine, a methylxanthine derived from coffee, is known to affect biological and physiological responses. Low to moderate levels of caffeine intake have been shown to benefit liver function, diabetes, neurological diseases, such as Alzheimer's and Parkinson's, and certain types of cancers. Caffeine is also known to increase urine calcium excretion via translocation of annexin A1 from the apical surface of cells into the cytoplasm. Therefore, caffeine intake is considered to be associated with lower risk of kidney stones.^[29] A previous prospective study on the effects of caffeine in coffee suggested that coffee reduction can be a strategy in preventing urinary symptoms, such as frequency, urgency, and bladder pain syndrome.^[9]

The aim of this study was to evaluate if caffeine consumption is associated with changes to protein expression in the normal bladder using semiquantitative proteomic analysis. While there are reports about antilipid accumulation via gene expression suppression of proliferator-activated receptor γ and CCAAT/enhancer binding protein α in 3T3-L1 adipocytes,^[30] or apoptosis induction in various cell lines, the direct effects of caffeine on the bladder remains elusive. Although the amount of caffeine in a cup of coffee varies, it is typically 300–600 mg. Using caffeine concentrations equivalent to typical coffee

Table 2. List of downregulated proteins in bladder epithelial cells perturbed by caffeine treatment.

Symbol	Full name	Fold change (log ₂)	p-value
ST13P4	ST13, Hsp70 interacting protein pseudogene 4	−4.06184	0.000224
EIF5AL1	Eukaryotic translation initiation factor 5A-like 1	−3.14456	0.000559
LOC102723897	–	−2.27955	0.001453
WASH2P	WAS protein family homolog 2 pseudogene	−2.27955	0.001453
RBMS3	RNA binding motif single-stranded interacting protein 3	−2.22487	0.001565
POTEI	POTE ankyrin domain family member I	−1.25276	0.004137
POTEJ	POTE ankyrin domain family member J	−1.25276	0.004137
HIST1H2BM	Histone cluster 1 H2B family member m	−1.07852	0.00436
DES	Desmin	−0.97497	0.004584
TENM1	Teneurin transmembrane protein 1	−0.87939	0.004919
ACTG2	Actin, gamma 2, smooth muscle, enteric	−0.82627	0.005255
HIST1H2BD	Histone cluster 1 H2B family member d	−0.78302	0.006708
HIST1H2BC	Histone cluster 1 H2B family member c	−0.78302	0.006708
HIST2H2BF	Histone cluster 2 H2B family member f	−0.78302	0.006708
HIST1H2BH	Histone cluster 1 H2B family member h	−0.78302	0.006708
HIST1H2BN	Histone cluster 1 H2B family member n	−0.78302	0.006708
RPL29	Ribosomal protein L29	−0.73583	0.007044
RNF175	Ring finger protein 175	−0.71108	0.007267
TFAP2B	Transcription factor AP-2 beta	−0.65122	0.007715
DLG2	Discs large MAGUK scaffold protein 2	−0.64864	0.007826
RAB3A	RAB3A, member RAS oncogene family	−0.62645	0.00805
ZDHHC13	Zinc finger DHHC-type containing 13	−0.60304	0.009951
EPHA6	EPH receptor A6	−0.60218	0.010063
PRC1	Protein regulator of cytokinesis 1	−0.59503	0.010174
MRPL34	Mitochondrial ribosomal protein L34	−0.5944	0.010286

consumption (one to two cups), we performed unbiased proteomic analysis using LC–MS/MS on bladder epithelial cells treated with caffeine and identified 32 upregulated and 25 downregulated DEPs (log₂-fold change > 0.58; p-value < 0.05; Figure 1B; Table 1 and 2). These DEPs were enriched for functions such as actin–myosin filament sliding, muscle contraction,

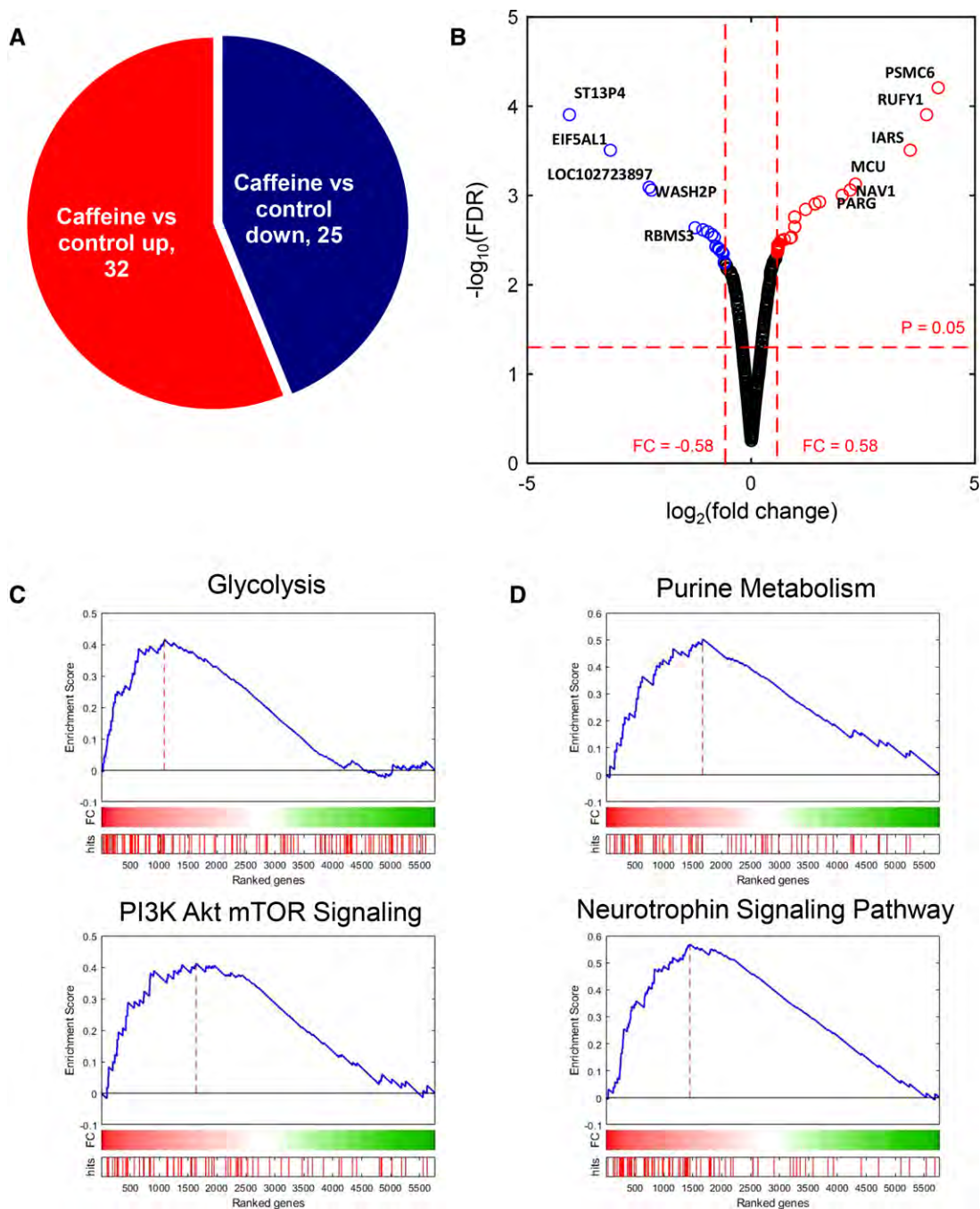
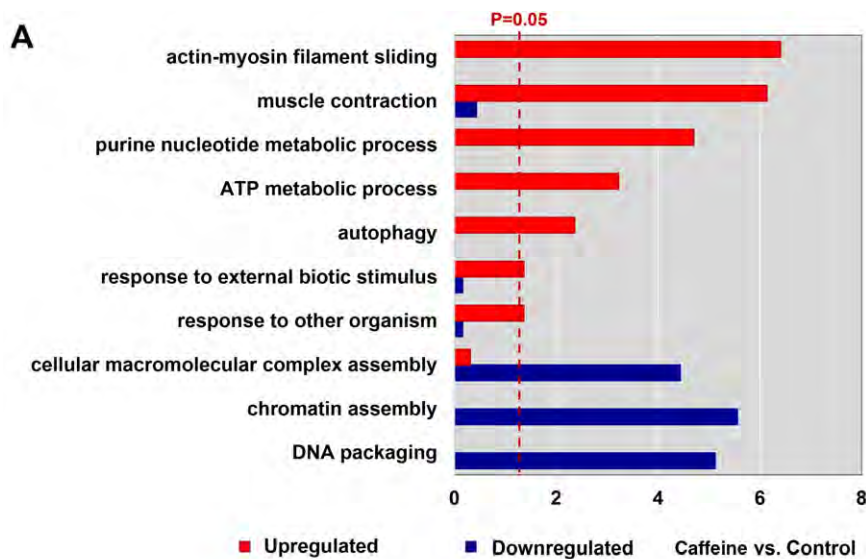


Figure 2. Differentially expressed proteins (DEPs) perturbed by caffeine treatment. A) Pie chart showing the DEPs in presence of caffeine. B) A volcano plot showing the up- or downregulated DEPs due to caffeine in bladder epithelial cells. Up- or downregulated DEPs are marked as red or blue dot. C) GSEA plot of Hallmark gene set MsigDB (Glycolysis and PI3K/AKT/mTOR signaling). D) GSEA plot of KEGG pathway gene sets (Purine Metabolism and Neurotrophin signaling pathway).

and chromatin assembly proteins (Figure 3A). Alterations to the cytoskeleton and the proteins that interact with it have been linked to a wide range of diseases.^[31] Caffeine has similar actions with 5' adenosine monophosphate-activated protein kinase (AMPK), an enzyme whose roles include contraction during energy deprivation in skeletal muscles.^[32] Among the proteins involved in the enriched cellular functions, ACTG2, also known as

alpha smooth muscle actin, is associated with multiple functions in cell motility, structure, integrity, and intercellular signaling.^[33] However, caffeine did not change any of the muscle-associated stabilizing proteins, which regulate the number, or the length, of microtubules.^[34] This suggests that increased expression of ACTG2 by caffeine in the bladder may enhance the contractility of bladder and may also be associated with urinary symptoms.



B

Biological process	Upregulated proteins in caffeine treated sample
Purine nucleotide metabolic process	MYH3, MYH4, MYH7, MYH8, SULT1A1, FLCN, MAGI3, SULT1A4
Autophagy	S100A8, S100A9, UCHL1, UVRAG, FLCN
Muscle contraction	ACTA2, MYH1, MYH2, MYH3, MYH4, MYH7, MYH8, MYH13
Response to external biotic stimulus	ACTA2, S100A7, S100A8, S100A9, H2BFS

C

Biological process	Downregulated proteins in caffeine treated sample
Chromatin assembly	HIST1H2BD, HIST1H2BN, HIST1H2BM, HIST1H2BH, HIST1H2BC, HIST2H2BF

Figure 3. Differential enrichment of cellular processes by up- and downregulated proteins perturbed by caffeine. A) Bar plot showing enriched cellular processes in up- or downregulated DEPs. B) List of proteins involved in the enriched cellular processes by upregulated DEPs. C) List of proteins involved in the enriched cellular processes by downregulated DEPs. Proteins reported with cancer are in bold.

Our experimental data suggested that these proteins, such as ACTG2 and HIST1H2BM, become more redundant in bladder epithelial cells upon exposure to caffeine. Although the function of HIST1H2BM as a regulator of caffeine and its effects has not been studied well, it is originally known to be associated with epigenetic regulation in response to DNA methylation.^[35]

In this study, we also found that the protein expression level of membrane-associated guanylate kinase inverted 3 (MAGI3) was upregulated in presence of caffeine in normal bladder cells. This was further validated using western blot experiments. MAGI3 localizes to the tight junction in epithelial cells and has originally been identified as a scaffolding protein and tumor suppressor in gliomas and breast cancers. The previous investigations on the role and molecular mechanism revealed that MAGI3 plays a role in phospholipid signaling pathways and suppresses cancer cell proliferation via upregulation of phosphatase and tensin homolog (PTEN), a well-known tumor suppressor.^[36] MAGI3 has been found to interact with PTEN, via the PDZ domain of MAGI3, and together contribute to regulation of the kinase

activity of AKT/PKB and tumor cell survival. Interestingly, MAGI3 has been reported to be involved in the reduced cell proliferation, arrests of the cell cycle, and inhibition of the migration of glioma cells. Overexpression of MAGI3 resulted in a suppression of β -catenin's transcriptional activity and inhibition the expression of target genes such as Cyclin D1 in glioma cells.^[36] More interestingly, misregulated or modified MAGI3 demonstrated its different roles in cell proliferation and cancer. For example, when MAGI3 is found fused with AKT3, MAGI3-AKT3 contributes to a constitutive phosphorylation and activation of AKT kinase and its downstream targets, such as GSK3b, in breast cancer.^[37] Premature cleavage and polyadenylation of MAGI3, MAGI3pPA, was identified to result in an oncogenic protein in breast cancer.^[38] Given that overexpressed MAGI3 has a functional link to the suppressed oncogenic characteristics, our data support the hypothesis that caffeine might benefit in the prevention of cancer, which is consistent with previous reports showing that coffee consumption is inversely associated with risk for various cancers, including prostate.^[39]

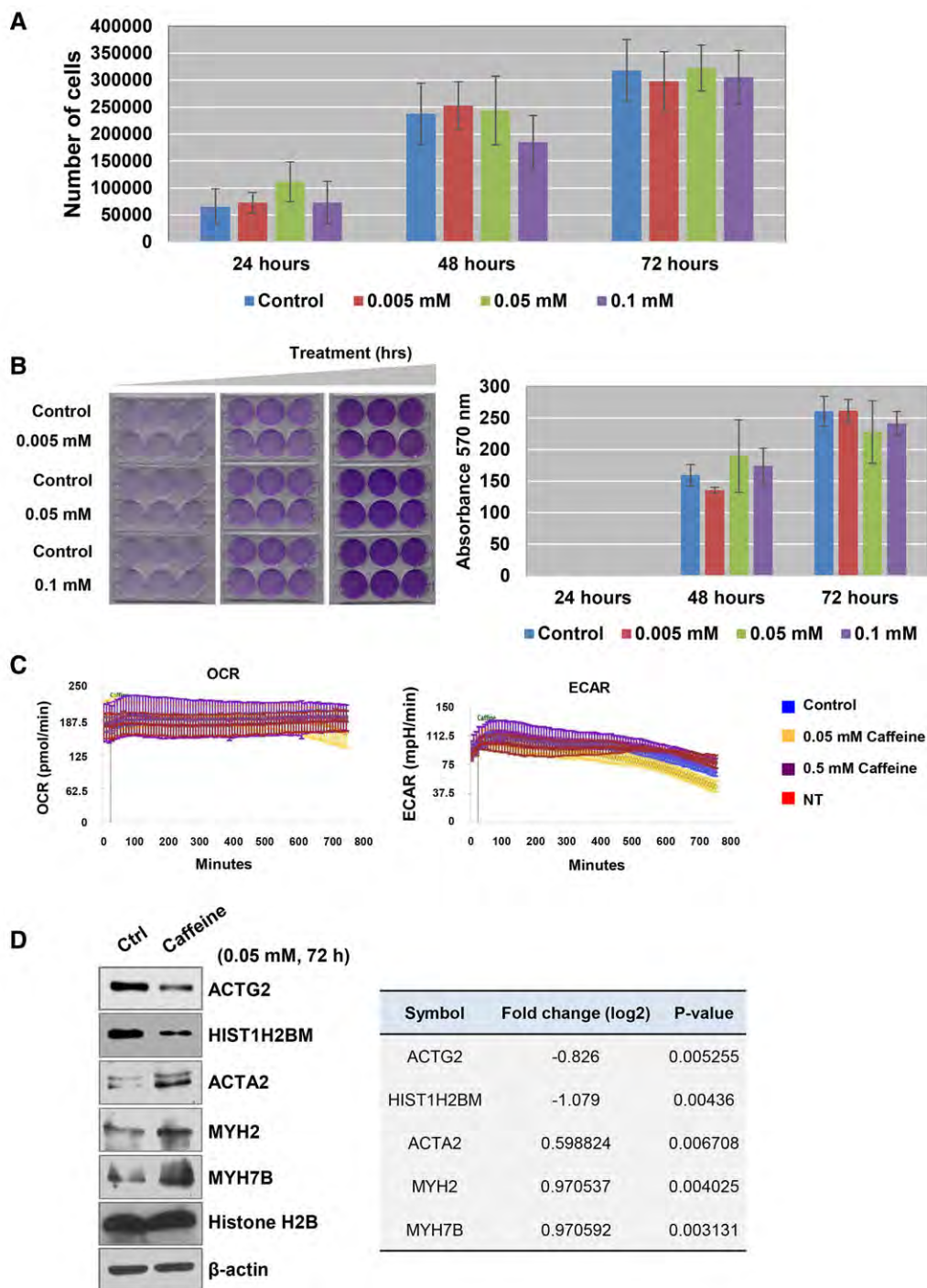


Figure 4. Cell proliferation was suppressed in response to caffeine treatment. (A and B) TRT-HU1, immortalized normal bladder epithelial cells, were treated with 0.005, 0.05, and 0.1 mM caffeine for 24, 48, or 72 h. A) Cell counting and B) crystal violet proliferation assay were conducted as described in Methods. * $p < 0.05$ (two-sided Student's t -test) compared with the control group. Representative images of TRT-HU1 cells treated with caffeine (lower panels). C) Seahorse data showed that caffeine treatment did not alter metabolism of normal bladder epithelial cells. Top, oxygen consumption rate (OCR) chart * $p < 0.05$. Bottom, extracellular acidification rate (ECAR) chart ** $p < 0.05$. D) Quantification results from western blot analysis to measure the expression levels of ACTG2, HIST1H2BM, ACTA2, MYH2, MYH7B, and histone H2B proteins in the presence or absence of caffeine. β -actin was used loading control. The differentially expressed protein levels obtained from proteomics analysis were shown in table (right).

There are several limitations in this study. We are aware that a single proteomic study conducted on one cell line and MS platform is not enough for conclusive statements on whether in vitro protein perturbation due to caffeine can represent the same perturbation in vivo. Urinary caffeine levels can be quantified by ultra high performance LC–MS/MS, and those levels are positively associated with consumption frequency of coffee (area under the curve = 0.849, 95% confidence interval [0.808;0.891]).^[40] Also, we conducted two biological replicates under each condition. In general, a small number of replicates has low statistical power. However, we identified DEPs using an empirical null distribution estimated by randomly permuted samples, which should reflect distribution of detected proteins. Furthermore, expression of some DEPs was confirmed using western blot analysis (Figure 4C). Despite these limitations, our experimental findings provide evidence for the potential mechanisms through which caffeine intake is associated with LUTS, suggesting that the restriction of caffeine may benefit muscle contraction and functional gene expression through impaired epigenetic regulation.

Supporting Information

Supporting Information is available from the Wiley Online Library or from the author.

Acknowledgements

M.S. and A.Y. were involved in and performed most of the experiments. S.Y. and M.K. performed proteomics analysis and helped to draft paper. A.A. performed metabolic and biochemical analyses in vitro. J.K. designed and conceived the study and wrote the paper. All authors discussed the results and commented on the manuscript at all stages, and read and approved the manuscript. The authors acknowledge support from National Institutes of Health grants (1U01DK103260, 1R01DK100974, U24 DK097154, NIH NCATS UCLA CTSI UL1TR000124), Department of Defense grants (W81XWH-15-1-0415), Centers for Disease Controls and Prevention (1U01DP006079), IMAGINE NO IC Research Grant, the Steven Spielberg Discovery Fund in Prostate Cancer Research Career Development Award, and the U.S.-Egypt Science and Technology Joint Fund (to J.K.). J.K. is former recipient of Interstitial Cystitis Association Pilot Grant, a Fishbein Family IC Research Grant, New York Academy of Medicine, and Boston Children's Hospital Faculty Development. The funders had no role in the experimental design, data collection, analysis, preparation of the manuscript, or decision to publish. In addition, this article is derived from the Subject Data funded in whole or part by National Academies of Sciences, Engineering, and Medicine (NAS) and The United States Agency for International Development (USAID). Any opinions, findings, conclusions, or recommendations expressed in this article are those of the authors alone, and do not necessarily reflect the views of USAID or NAS.

Conflict of Interest

The authors declare no conflict of interest.

Keywords

biological network, bladder epithelial cells, caffeine, global proteome, lower urinary tract symptoms

Received: May 3, 2018
Revised: August 6, 2018
Published online: October 11, 2018

- [1] D. E. Irwin, Z. S. Kopp, B. Agatep, I. Milsom, P. Abrams, *BJU Int.* **2011**, *108*, 1132.
- [2] K. S. Coyne, A. J. Wein, A. Tubaro, C. C. Sexton, C. L. Thompson, Z. S. Kopp, L. P. Aiyer, *BJU Int.* **2009**, *103*, 4.
- [3] J. Silva, C. M. Silva, F. Cruz, *Curr. Opin. Urol.* **2014**, *24*, 21.
- [4] K. S. Coyne, A. Wein, S. Nicholson, M. Kvasz, C. I. Chen, I. Milsom, *J. Manag. Care Pharm.* **2014**, *20*, 130.
- [5] D. Robinson, I. Giarenis, L. Cardozo, *Maturitas* **2014**, *79*, 8.
- [6] Q. He, Y. Yang, M. Xia, N. Zhang, S. Wu, Y. Xiao, G. Li, S. Zhan, L. Liu, H. Xiao, J. Zhao, *Zhonghua Yi Xue Za Zhi* **2014**, *94*, 428.
- [7] M. J. Wells, K. Jamieson, T. C. Markham, S. M. Green, M. J. Fader, *J. Wound Ostomy Continence Nurs.* **2014**, *41*, 371.
- [8] B. L. Anderson, L. M. Juliano, J. Schulkin, *J. Women's Health* **2009**, *18*, 1457.
- [9] A. Staack, B. Distelberg, A. Schlaifer, J. Sabate, *Neurourol. Urodyn.* **2017**, *36*, 432.
- [10] N. N. Maserejian, C. G. Wager, E. L. Giovannucci, T. M. Curto, K. T. McVary, J. B. McKinlay, *Am. J. Epidemiol.* **2013**, *177*, 1399.
- [11] F. Turati, C. Bosetti, J. Polesel, A. Zucchetto, D. Serraino, M. Montella, M. Libra, A. Galfano, C. La Vecchia, A. Tavani, *Urology* **2015**, *86*, 1179.
- [12] A. M. Bode, Z. Dong, *Cancer Lett.* **2007**, *247*, 26.
- [13] Z. He, W. Y. Ma, T. Hashimoto, A. M. Bode, C. S. Yang, Z. Dong, *Cancer Res.* **2003**, *63*, 4396.
- [14] Y. S. Cho, I. G. Ko, S. E. Kim, L. Hwan, M. S. Shin, C. J. Kim, S. H. Kim, J. J. Jin, J. Y. Chung, K. H. Kim, *Mol. Med. Rep.* **2014**, *10*, 2931.
- [15] R. Kershen, T. Mann-Gow, J. Yared, I. Stromberg, P. Zvara, *J. Urol.* **2012**, *188*, 1986.
- [16] J. S. Hockey, C. Wu, C. H. Fry, *BJU Int.* **2000**, *86*, 531.
- [17] J. Kim, M. Ji, J. A. DiDonato, R. R. Rackley, M. Kuang, P. C. Sadhukhan, J. R. Mauney, S. K. Keay, M. R. Freeman, L. S. Liou, R. M. Adam, *In Vitro Cell. Dev. Biol. Anim.* **2011**, *47*, 2.
- [18] D. Y. Choi, S. You, J. H. Jung, J. C. Lee, J. K. Rho, K. Y. Lee, M. R. Freeman, K. P. Kim, J. Kim, *Proteomics* **2014**, *14*, 1845.
- [19] Y. Qu, B. Zhou, W. Yang, B. Han, Y. Yu-Rice, B. Gao, J. Johnson, C. N. Svendsen, M. R. Freeman, A. E. Giuliano, D. Sareen, X. Cui, *Sci. Rep.* **2016**, *6*, 32007.
- [20] A. Rinas, J. A. Espino, L. M. Jones, *Anal. Bioanal. Chem.* **2016**, *408*, 3021.
- [21] M. Niu, J. H. Cho, K. Kodali, V. Pagala, A. A. High, H. Wang, Z. Wu, Y. Li, W. Bi, H. Zhang, X. Wang, W. Zou, J. Peng, *Anal. Chem.* **2017**, *89*, 2956.
- [22] B. Zhang, M. C. Chambers, D. L. Tabb, *J. Proteome Res.* **2007**, *6*, 3549.
- [23] H. Lee, S. Chae, J. Park, J. Bae, E. B. Go, S. J. Kim, H. Kim, D. Hwang, S. W. Lee, S. Y. Lee, *Mol. Cell. Proteomics* **2016**, *15*, 3461.
- [24] J. D. Storey, R. Tibshirani, *Proc. Natl. Acad. Sci. U. S. A.* **2003**, *100*, 9440.
- [25] W. Huang da, B. T. Sherman, R. A. Lempicki, *Nat. Protoc.* **2009**, *4*, 44.
- [26] T. Hashimoto, Z. He, W. Y. Ma, P. C. Schmid, A. M. Bode, C. S. Yang, Z. Dong, *Cancer Res.* **2004**, *64*, 3344.
- [27] H. Mi, X. Huang, A. Muruganujan, H. Tang, C. Mills, D. Kang, P. D. Thomas, *Nucleic Acids Res.* **2017**, *45*, D183.
- [28] A. Liberzon, C. Birger, H. Thorvaldsdottir, M. Ghandi, J. P. Mesirov, P. Tamayo, *Cell Syst.* **2015**, *1*, 417.
- [29] a) P. Peerapen, V. Thongboonkerd, *Sci. Rep.* **2016**, *6*, 38536; b) P. M. Ferraro, E. N. Taylor, G. Gambaro, G. C. Curhan, *Am. J. Clin. Nutr.* **2014**, *100*, 1596.
- [30] T. Mitani, T. Nagano, K. Harada, Y. Yamashita, H. Ashida, *J. Nutr. Sci. Vitaminol.* **2017**, *63*, 331.

- [31] L. Cicchillitti, R. Penci, M. Di Michele, F. Filippetti, D. Rotilio, M. B. Donati, G. Scambia, C. Ferlini, *Mol. Cancer Ther.* **2008**, *7*, 2070.
- [32] T. Egawa, T. Hamada, N. Kameda, K. Karaike, X. Ma, S. Masuda, N. Iwanaka, T. Hayashi, *Metab. Clin. Exp.* **2009**, *58*, 1609.
- [33] B. Hinz, G. Celetta, J. J. Tomasek, G. Gabbiani, C. Chaponnier, *Mol. Biol. Cell* **2001**, *12*, 2730.
- [34] J. L. Franklin, M. Mirzaei, T. A. Wearne, J. Homewood, A. K. Goodchild, P. A. Haynes, J. L. Cornish, *J. Proteome Res.* **2016**, *15*, 1455.
- [35] W. E. Ek, E. W. Tobi, M. Ahsan, E. Lampa, E. Ponzi, S. A. Kyrtopoulos, P. Georgiadis, L. H. Lumey, B. T. Heijmans, M. Botsivali, I. A. Bergdahl, T. Karlsson, M. Rask-Andersen, D. Palli, E. Ingelsson, A. K. Hedman, L. M. Nilsson, P. Vineis, L. Lind, J. M. Flanagan, A. Johansson, C. Epigenome-Wide Association Study, *Hum. Mol. Genet.* **2017**, *26*, 3221.
- [36] Q. Ma, Y. Zhang, R. Meng, K. M. Xie, Y. Xiong, S. Lin, Z. L. He, T. Tao, Y. Yang, J. Z. Zhao, J. Q. He, *Biomed. Environ. Sci.* **2015**, *28*, 502.
- [37] S. Banerji, K. Cibulskis, C. Rangel-Escareno, K. K. Brown, S. L. Carter, A. M. Frederick, M. S. Lawrence, A. Y. Sivachenko, C. Sougnez, L. Zou, M. L. Cortes, J. C. Fernandez-Lopez, S. Peng, K. G. Ardlie, D. Auclair, V. Bautista-Pina, F. Duke, J. Francis, J. Jung, A. Maffuz-Aziz, R. C. Onofrio, M. Parkin, N. H. Pho, V. Quintanar-Jurado, A. H. Ramos, R. Rebollar-Vega, S. Rodriguez-Cuevas, S. L. Romero-Cordoba, S. E. Schumacher, N. Stransky, K. M. Thompson, L. Uribe-Figueroa, J. Baselga, R. Beroukhi, K. Polyak, D. C. Sgroi, A. L. Richardson, G. Jimenez-Sanchez, E. S. Lander, S. B. Gabriel, L. A. Garraway, T. R. Golub, J. Melendez-Zajgla, A. Toker, G. Getz, A. Hidalgo-Miranda, M. Meyerson, *Nature* **2012**, *486*, 405.
- [38] T. K. Ni, C. Kuperwasser, *eLife* **2016**, *5*, e14730.
- [39] a) G. Pounis, C. Tabolacci, S. Costanzo, M. Cordella, M. Bonaccio, L. Rago, D. D'Arcangelo, A. Filippo Di Castelnuovo, G. de Gaetano, M. B. Donati, L. Iacoviello, F. Facchiano, i. Moli-sani study, *Int. J. Cancer* **2017**, *141*, 72; b) J. Sado, T. Kitamura, Y. Kitamura, T. Sobue, Y. Nishino, H. Tanaka, T. Nakayama, I. Tsuji, H. Ito, T. Suzuki, K. Katanoda, S. Tominaga; Three-Prefecture Cohort Study Group, *Cancer Sci.* **2017**, *108*, 2079.
- [40] D. Petrovic, S. Estoppey Younes, M. Pruijm, B. Ponte, D. Ackermann, G. Ehret, N. Ansermot, M. Mohaupt, F. Paccaud, B. Vogt, A. Pechere-Bertschi, P. Y. Martin, M. Burnier, C. B. Eap, M. Bochud, I. Guessous, *Nutr. Metab.* **2016**, *13*, 81.

RESEARCH ARTICLE

Open Access



Epidermal growth factor expression as a predictor of chemotherapeutic resistance in muscle-invasive bladder cancer

Ahmed M. Mansour^{1,2}, Mona Abdelrahim¹, Mahmoud Laymon¹, Mamdouh Elsherbeen¹, Mohammed Sultan¹, Ahmed Shokeir¹, Ahmed Mosbah¹, Hassan Abol-Enein¹, Amira Awadalla¹, Eunho Cho³, Vikram Sairam³, Taeun D. Park⁴, Muhammad Shahid⁵ and Jayoung Kim^{3,5*}

Abstract

Background: Epidermal growth factor receptor (EGFR) overexpression is believed to be associated with bladder cancer (BC) progression and poor clinical outcomes. In vivo studies have linked EGFR subcellular trafficking and chemo-resistance to cisplatin-based chemotherapies. This has not been studied in the clinical adjuvant setting. We aimed to investigate the prognostic significance of EGFR expression in patients receiving cisplatin-based adjuvant chemotherapy following radical cystectomy for advanced BC.

Methods: The database from the Urology and Nephrology Center at Mansoura University was reviewed. BC patients who were treated with radical cystectomy and adjuvant chemotherapy for adverse pathological features or node positive disease were identified. Patients who underwent palliative cystectomy, had histological diagnoses other than pure urothelial carcinoma, or received adjuvant radiotherapy were excluded from the study. Immunohistochemical staining for EGFR expression was performed on archived bladder specimens. The following in vitro functional analyses were performed to study the relationship of EGFR expression and chemoresponse.

Results: The study included 58 patients, among which the mean age was 57 years old. Majority of patients had node positive disease ($n = 53$, 91%). Mean follow up was 26.61 months. EGFR was overexpressed in 25 cystectomy specimens (43%). Kaplan-Meier analysis revealed that EGFR over-expression significantly correlated with disease recurrence ($p = 0.021$). Cox proportional hazard modeling identified EGFR overexpression as an independent predictor for disease recurrence ($p = 0.04$). Furthermore, in vitro experiments demonstrated that inhibition of EGFR may sensitize cellular responses to cisplatin.

Conclusions: Our findings suggest that EGFR overexpression is associated with disease recurrence following adjuvant chemotherapy for advanced BC. This may aid in patient prognostication and selection prior to chemotherapeutic treatment for BC.

Keywords: EGFR, Bladder cancer, Survival, Adjuvant chemotherapy

* Correspondence: Jayoung.kim@csmc.edu

³University of California Los Angeles, Los Angeles, CA, USA

⁵Departments of Surgery and Biomedical Sciences, Samuel Oschin Comprehensive Cancer Institute, Cedars Sinai Medical Center, 8700 Beverly Blvd, Los Angeles, CA 90048, USA

Full list of author information is available at the end of the article



Background

Bladder cancer (BC) is the second most common genitourinary malignancy and the fourth most common cancer in the United States (U.S.). Over an estimated \$4 billion/year is spent on BC treatment annually in the U.S., making BC one of the most expensive cancer treatments to date [1–3]. Currently, BC is also the most common cancer in Egyptian males, representing about 30% of all cancer types [4]. Thus, BC is a major burden on the health services and economic resources at an international level [5]. Despite the drastic decrease in the prevalence of schistosomiasis in Egypt due to nationwide anti-bilharzial campaigns, there has been an increase in incidences of bladder urothelial carcinoma. This could possibly be due to smoking and carcinogenic chemical exposure [6, 7].

The gold standard therapy for patients with muscle-invasive bladder cancer (MIBC) is radical cystectomy with regional lymphadenectomy. Despite local aggressive therapy, nearly half of patients eventually develop metastasized tumors and, ultimately, die from the disease [8]. In an attempt to improve survival, integration of systemic chemotherapy with surgical management has been suggested to control micrometastasis [9]. However, around 40% of patients receiving neoadjuvant chemotherapy are termed “non-responders”, with a complete pathological down-staging rate of only 14–38% [10, 11]. MIBC patients who do not respond to adjuvant chemotherapy generally have a poor prognosis [12]. The incidence of BC recurrence following chemotherapy remains high with a modest survival advantage of 5–15%. Thus, there is an important and urgent need to identify prognostic marker(s) that will identify patients who are at risk and to better understand the functional contribution of potential predictive markers in aggressive BC.

Prior research has shown that epidermal growth factor receptor (EGFR) overexpression has been associated with BC progression and poor clinical outcomes [13, 14]. In vivo studies have linked EGFR subcellular trafficking and chemo-resistance in many tumor types [15, 16]. However, this has not yet been studied in the clinical adjuvant setting.

In this study, we aimed to investigate the prognostic significance of EGFR expression in patients receiving adjuvant chemotherapy. Our study was conducted on an Egyptian cohort. Our findings suggest that EGFR protein expression may be indicative of aggressive BC and these expression patterns possibly involve direct action on signaling pathways in BC cells.

Methods

Patients and tissue samples

All of the enrolled patients had been treated with similar or identical regimens with at least four cycles of cisplatin-based chemotherapy. Patients previously treated

with radical cystectomy and had completed adjuvant chemotherapy for adverse pathological features or node positive diseases were selected. Exclusion criteria were applied to patients who underwent palliative cystectomy, those with histological diagnosis other than pure transitional cell carcinoma, and patients who received adjuvant radiotherapy. Bladder tumors were staged according to the 2002 TNM classification. Disease progression was defined as newly diagnosed distant metastases with a $\geq 20\%$ increment increase in tumor mass following radical cystectomy. Surgical tumor tissues were macro-dissected, typically within 15 min of surgical resection. Each BC specimen was confirmed as representative by analysis of adjacent tissue in fresh frozen sections from radical cystectomy specimens.

Reagents

Cisplatin was purchased from Sigma. Antibodies against EGFR and β -actin were obtained from Cell Signaling Technology (for Western blot analysis), Abcam (for IHC analysis) and Santa Cruz Biotechnology. The ECL detection kit was from BioRad and New England Nuclear. All other biochemical reagents were purchased from Sigma or BD Biosciences.

Immunohistochemical staining

Immunohistochemical (IHC) analysis for EGFR expression was performed on archived bladder specimens. The relationship of EGFR expression and clinical outcomes was assessed. In vitro studies were performed to determine whether EGFR expression was associated with resistance to chemotherapeutic reagents. Paraffin blocks from 58 BC cases were used for immunohistochemical analysis. Tissue sections were cut and placed on Superfrost Plus microscope slides. Using the Benchmark XT automated immunohistochemistry stainer (Ventana Medical Systems, Inc., Tucson, AZ, USA), slides were stained following typical procedure. Detection was done using the Ventana Ultraview DAB Kit (Ventana Medical Systems).

Sections were deparaffinized using EZ Prep solution. CC1 standard (pH 8.4 buffer contained Tris/Borate/EDTA) was used for antigen retrieval. DAB inhibitor (3% H_2O_2 , Endogenous peroxidase) was blocked for 4 min at 37 °C temperature. Sections were incubated with an anti-EGFR (Cat # ab32077, Abcam Inc., San Diego, CA, dilution 1/100) primary antibody for 40 min at 37 °C, and then incubated with a secondary antibody of Universal HRP Multimer for 8 min at 37 °C. Slides were then incubated with DAB + H_2O_2 substrate for 8 min, followed by hematoxylin and bluing reagent counterstain at 37 °C. Reaction buffer (pH 7.6 Tris buffer) was used as the washing solution. Staining intensity and proportion of positively-stained cells were evaluated. Staining intensity

Table 1 Baseline characteristics of the patients in this study

Variables		Incidence (SD or %)
Age mean (SD)		57 (6.6)
No. gender (%)	Male	53(91.4)
	Female	5 (8.6)
No. clinical T stage (%)	T2	7 (12.1)
	T3	30 (51.7)
	T4a	18 (31.1)
	T4b	3 (5.2)
No. pathologic T stage (%)	T1S	1 (1.7)
	T1	1 (1.7)
	T2a	7 (12.1)
	T2b	7 (12.1)
	T3a	22 (37.9)
	T3b	15 (25.9)
	T4a	5 (8.6)
No. pathologic N status (%)	N0	5 (8.6)
	N1	14 (24.1)
	N2	37 (63.8)
	N3	2 (3.4)
No. lymphovascular invasion (%)	Yes	45 (77)
	No	13 (23)
No. strong EGFR expression (%)	Yes	10 (17.2)
	No	48 (82.8)

was classified as follows: none (score 0), weak (score 1), moderate (score 2) and strong (score 3). Each specimen was examined and scored separately by two pathologists, and discrepancies were discussed until agreements were reached.

Cell culture and transfection

TCCSUP or T24 human BC cells were purchased from American Type Culture Collection (ATCC, Manassas, VA) and maintained in DMEM or RPMI1640 (Invitrogen, Carlsbad, CA) with 10% FBS and 1% Penicillin/Streptomycin at 37 °C under 5% CO₂. The day before transfection, TCCSUP or T24 cells were trypsinized and counted. Cells were plated in 6-well plate with approximately 6.25×10^5 cells per well in 2 ml of complete growth medium. When cell density reached 80–90% confluence, TCCSUP or T24 BC cells were transiently transfected with 25–50 nM of small interfering RNAs (siRNAs) targeting EGFR (SignalSilence® EGF Receptor siRNA, Cell Signaling #6482) using Lipofactamine 2000. For transfection controls, empty (Ctrl) or non-target siRNAs (siCtrl) were used.

Cell viability assay

Experiments were performed in 6-well plates after cell density reached to about 90% (2×10^3 /well). TCCSUP or T24 cells were transfected with various constructs or siRNAs and cisplatin simultaneously for 48 h (siRNA added 2 h before cisplatin). Cells were then incubated with cisplatin containing serum-free medium (RPMI1640

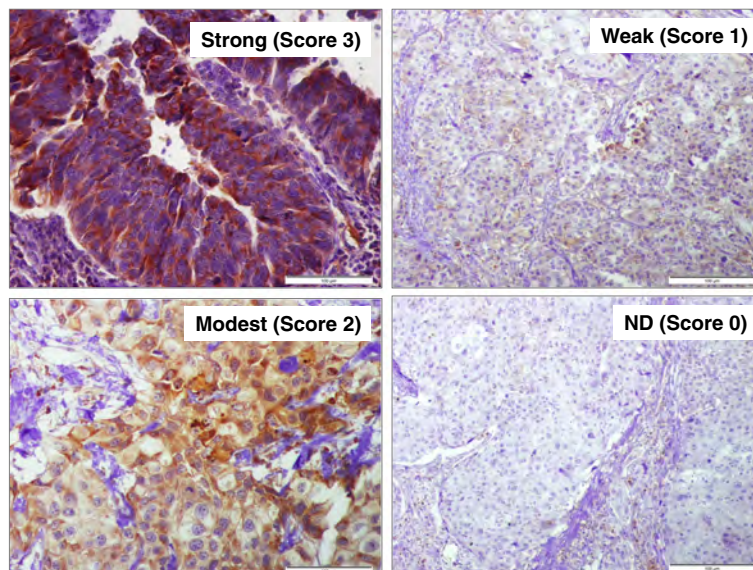


Fig. 1 Representative figures showing IHC slides with different scores. Immunohistochemical staining for EGFR in BC tissue samples. Four representative fields are shown after IHC staining with anti-EGFR (1:1000 dilution). Negative (Score 0), weak (Score 1), intermediate (Score 2), and strong (Score 3). EGFR expression was observed in the cytoplasm, membrane, and/or nucleus in our BC specimens. The intensity of EGFR staining was often heterogeneous within the same cancer tissue.

Table 2 Cox proportional hazard model of overall survival predictors

Covariate	Univariate		Multivariate	
	HR (95% CI)	P value	HR (95% CI)	P value
Age	1.41 (1.02–2.45)	0.029	1.34 (0.94–1.77)	0.056
Sex (M vs F)	1.88 (1.06–3.34)	0.048	1.48 (0.26–1.80)	0.479
EGFR expression (strong vs negative/weak/moderate)	1.55 (1.30–2.33)	0.002	1.38 (1.201–2.744)	0.004
Chemotherapy Regimen (MVAC vs GemCis)	1.72 (0.84–3.75)	0.159		
pT stage (T2 or less vs greater than T2)	2.88 (1.92–3.99)	0.003	3.28 (1.54–4.62)	< 0.001
pN stage (N0 vs greater than N0)	2.31 (1.88–2.93)	< 0.001	1.81 (1.23–2.74)	< 0.001

or DMEM) for the indicated time. Cell viability was determined using MTS reagents, as instructed by the company’s protocol (Promega Corporation, Madison, WI).

Statistical analysis

Univariate analysis with the Pearson chi-square was performed to analyze associations between strong EGFR expression and pT stage, pN stage, (N0 and greater than N0) and lymphovascular invasion. A Kaplan-Meier estimator curve with the log rank test and a Cox proportional hazard model were used to test whether observed

response to chemotherapy predicted disease specific survival.

Results

Baseline characteristics

The study included 58 patients. The mean age of the 57 patients who received adjuvant therapy was 57 ± 6.6 years, and the mean follow-up period was 26.61 months. A majority of patients had node positive disease (n = 53, 91%). Forty-five patients (77%) had lymphovascular invasion. Other baseline characteristics of the patients are presented in Table 1.

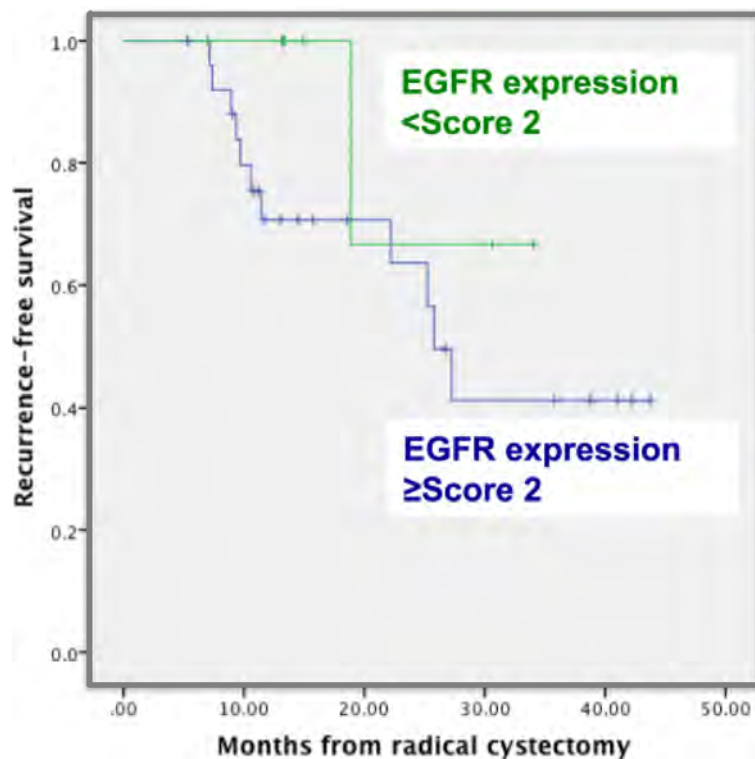


Fig. 2 Cancer-specific survival in BC patients stratified by EGFR staining

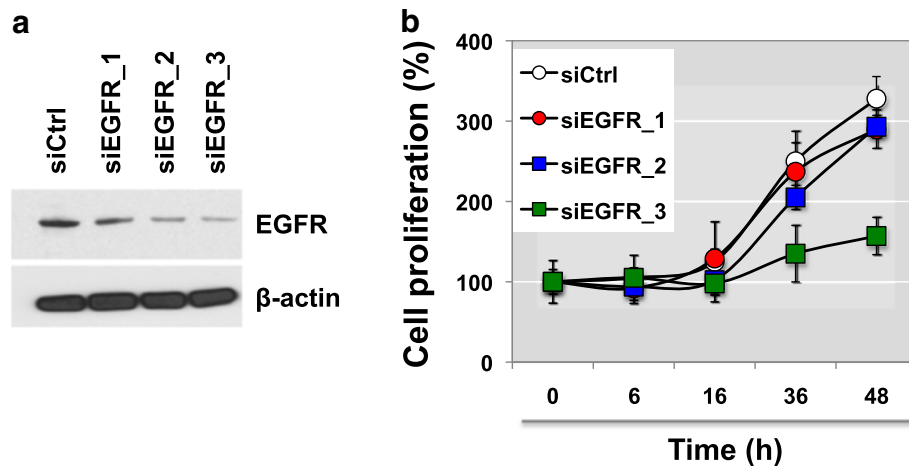


Fig. 3 EGFR expression is associated with drug sensitivity to cisplatin treatment. **a, b** TCCSUP cells were transiently transfected with varying doses of siRNA against EGFR. Knockdown of EGFR with control and EGFR-targeted siRNAs shows that proliferation in TCCSUP BC cells decreases in a dose-dependent manner (siEGFR_1, siEGFR_2, siEGFR_3). Cell proliferation assay was performed at the indicated time points (0, 6, 16, 36, or 48 h after transient transfection with siRNAs) using MTT assay at the varying time points. * $p < 0.05$ (Student's t-test)

EGFR expression is negatively correlated with survival

To measure EGFR expression in our cohort, IHC analysis was performed. IHC images were scored from 0 (negative staining) to 3 (highest staining intensity). Representative images are shown in Fig. 1. Cox proportional hazard modeling identified EGFR overexpression as an independent predictor for disease recurrence (OR, 1.38 (1.201–2.744), $p = 0.004$) in the Egyptian cohort (Table 2). Kaplan-Meier analysis revealed that EGFR overexpression (score ≥ 2)

significantly correlated with disease recurrence ($p = 0.021$) (Fig. 2).

EGFR silencing alters cell proliferation, viability and response to cisplatin-induced apoptosis

We further performed loss-of-function studies on TCCSUP human BC cells to assess the biological role of EGFR. EGFR was knocked-down using iRNAs and this was subsequently confirmed via western blot analysis (Fig. 3a). Silencing of EGFR did not induce a

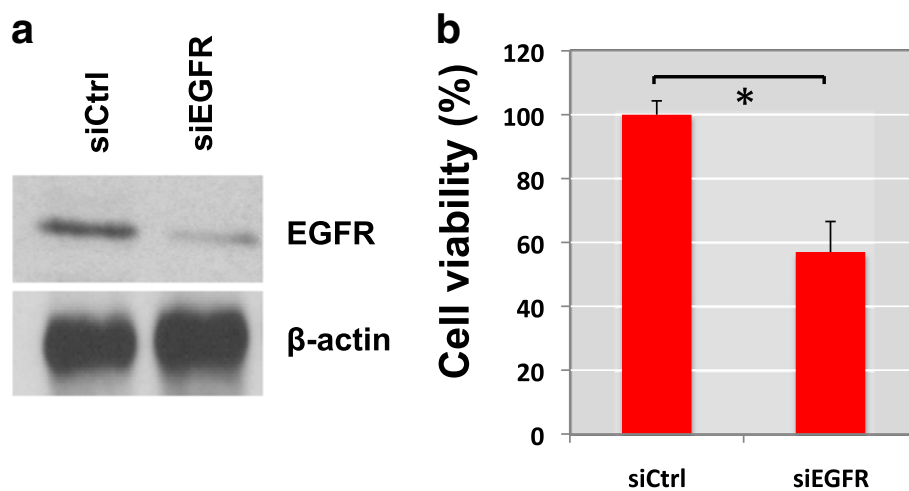


Fig. 4 Knockdown of EGFR suppresses recovery from cisplatin treatment. **a** EGFR silenced TCCSUP cells (siEGFR) or control TCCSUP cells (siCtrl) were challenged with cisplatin treatment. TCCSUP cells were incubated with cisplatin (10 μ M) and siRNAs for 48 h and then re-treated with cisplatin alone for an additional 6 h. After, the cisplatin was removed from the culture media and cells were incubated in normal growth medium for 24 h. **b** Cell viability was measured using MTT assay. Cell viability levels of three wells of transfected cells were determined. The graph was plotted as %, compared to control, no cisplatin treatment in siCtrl group (\pm SD). * $P < 0.05$ (Student's t-test). All experiments were done in at least triplicates

morphological switch. However, in vitro functional analysis demonstrated that EGFR expression levels can alter cell proliferation rates in TCCSUP BC cells. A dose dependent transfection of EGFR siRNAs (siEGFR_1, _2, or _3) revealed that EGFR deficiency evoked an approximately 50% decrease in cell proliferation (Fig. 3b). This data implicates that EGFR loss as an important mechanism through which BC cells keep proliferating.

We next assessed whether loss of EGFR expression can result in cell viability responses in relation to the effects of cisplatin and whether inhibition of EGFR can enhance the sensitivity of BC cells to cisplatin. We found that EGFR expression is associated with resistance to cisplatin-induced cytotoxicity. EGFR knockdown delayed cell recovery from 10 μM cisplatin treatment (Fig. 4).

Viability of control cells (siCtrl) in serum-free medium was compared with or without a challenge by 10 μM cisplatin. Cell viability assay revealed that silencing of

EGFR sensitized TCCSUP BC cells to cisplatin treatment. Knockdown of EGFR was validated by western blot analysis (Fig. 4a). Cells transfected with EGFR siRNAs showed around 50% viability after cisplatin treatment compared to control TCCSUP cells (siEGFR). Removal of cisplatin from the culture medium of control cells resulted in 100% recovery of cell viability (siCtrl) (Fig. 4b).

We next sought to determine whether gene silencing of EGFR might also increase drug sensitivity to cisplatin. TCCSUP BC cells were transfected with EGFR siRNAs or control siRNAs for 48 h. Immunoblotting confirmed that EGFR expression was significantly reduced in siEGFR-transfected cells (Fig. 5a). Interestingly, loss of EGFR made TCCSUP cells more sensitive to cisplatin-induced cell apoptosis, leading to reduced cell viability. TCCSUP cells were ~2x more sensitive to 5 or 10 μM cisplatin treatments (Fig. 5b). These results were further validated in T24 BC cells (Fig. 5c-d). These

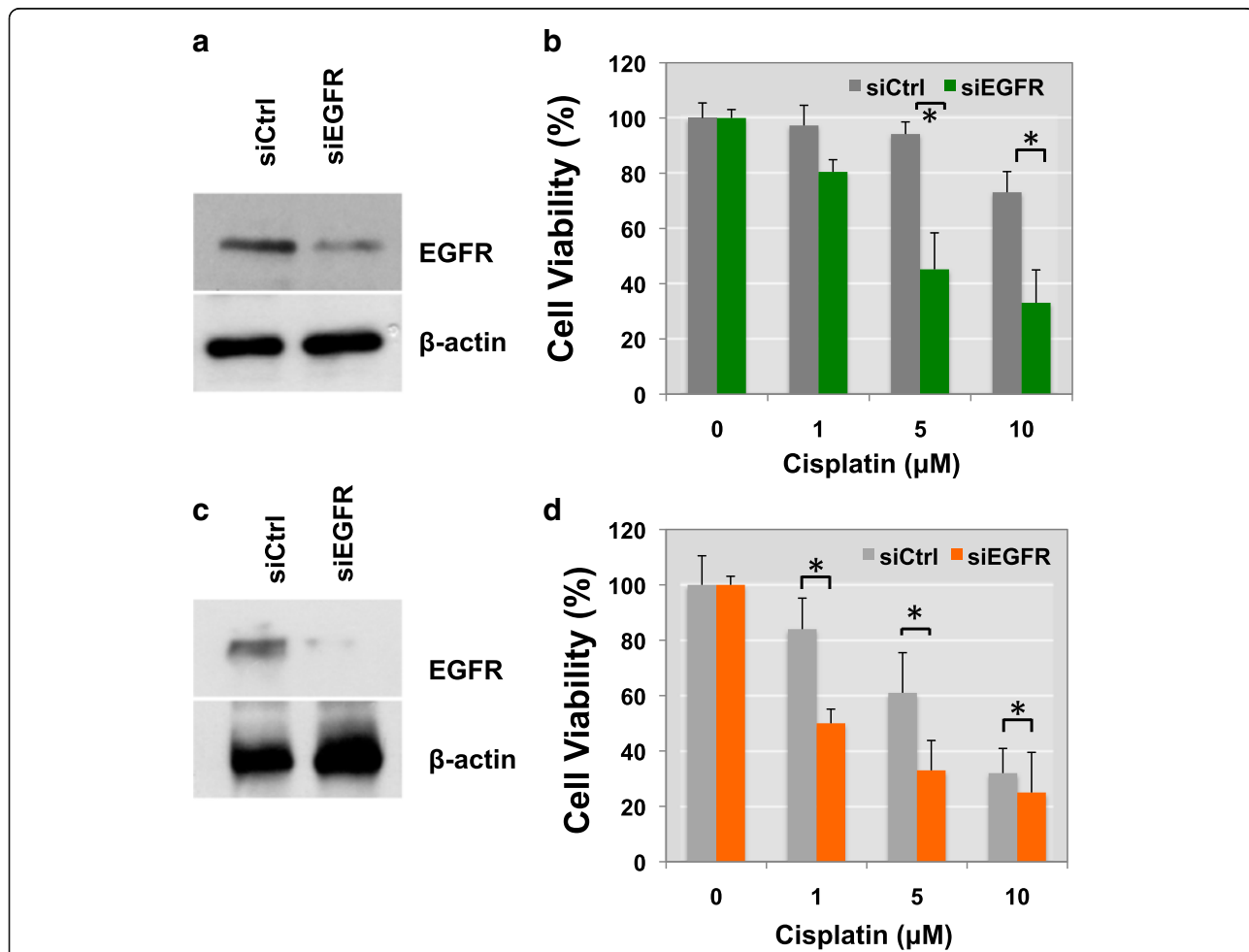


Fig. 5 Gene silencing of EGFR enhances drug sensitivity to cisplatin treatment. (a and b, TCCSUP; c and d, T24) Transiently transfected TCCSUP (a) or T24 (c) cells with siRNA of EGFR were treated with cisplatin (0, 1, 5 and 10 μM). Cisplatin was added together with siRNA for 48 h and then re-treated with cisplatin. Cell viability was measured by MTS assay after 2 days. Overexpression of siEGFR, but not a control siRNA, in TCCSUP (c) or T24 (d) cells reduced cell proliferation (Student's t-test, **p* < 0.05)

findings suggest that EGFR knockdown not only suppresses the recovery of BC cells from cisplatin-reduced cell viability but also enhances the sensitivity of BC cells to cisplatin's cytotoxicity.

Discussion

Systemic chemotherapy is currently being used as the first line of treatment in advanced stages of BC. However, it is still unclear which group of patients will benefit and which patients will be more sensitive to cisplatin-based therapy. Our findings suggest that EGFR overexpression is associated with disease recurrence following adjuvant chemotherapy for advanced BC [17, 18]. Determining EGFR expression status may help predict prognoses and assist in deciding which patients would best benefit from adjuvant chemotherapy. Our findings also suggest that patients with higher EGFR expression may have a worse prognosis than those with little to no EGFR expression. An evaluation of intratumoral molecular marker(s) could be used to identify BC patients more likely to respond to cisplatin-based chemotherapy.

These findings align with previous studies showing that approximately 50% of BC tumor tissues overexpress EGFR and that EGFR positivity indicates more invasive cells and poor differentiation [13, 14]. However, the mechanisms through which BC tumors acquire cisplatin resistance are still elusive. Our results suggest that EGFR silencing may enhance cisplatin's capability to shrink tumors. This observation highlights the potential of EGFR targeting strategies (e.g., kinase inhibitors or EGFR neutralizing antibodies such as gefitinib, erlotinib, trastuzumab, cetuximab, matuzumab, panitumumab et al.) to improve the effects of cisplatin-based chemotherapy. Recent reports have demonstrated that a subgroup of muscle-invasive bladder carcinomas with a basal-like phenotype are sensitive to EGFR kinase blockers, such as erlotinib [19, 20]. Rebouissou et al. identified a subgroup of aggressive MIBC, which shows a basal-like phenotype using their 40-gene expression classifier. In this BC subgroup, the EGFR pathway was highly activated, suggesting that anti-EGFR therapy could be used as a powerful therapeutic strategy [21, 22]. EGFR-targeted agents have only shown modest success due to acquired resistance in current ongoing clinical trials. Therefore, comprehensive clinical studies using EGFR-targeting in combination with other therapies would be more attractive.

Conclusions

Many questions regarding EGFR silencing strategies remain unanswered. For example, what signaling cascades are modulated by high EGFR expression? How can these be regulated pharmacologically? Will BC cells obtain resistance to cisplatin? Can cells become resistant to EGFR

silencing? In this study, our experimental results present EGFR as a marker of recurrence in Egyptian BC patients. Further studies are needed to better understand the regulatory mechanisms of EGFR overexpression and its downstream signaling pathways in BC, particularly in the context of squamous cell carcinoma (SCC) and transitional cell carcinoma (TCC). Our findings also suggest that elucidating some of these facets of EGFR and BC drug resistance might improve pharmacologic intervention.

Abbreviations

BC: Bladder cancer; EGFR: Epidermal growth factor receptor; MIBC: Muscle-invasive bladder cancer; siCtrl: Control cells; siRNAs: Small interfering RNAs

Acknowledgements

None

Funding

The authors acknowledge support from National Institutes of Health grants (1U01DK103260, 1R01DK100974, U24 DK097154, NIH NCATS UCLA CTSI UL1TR000124), Department of Defense grants (W81XWH-15-1-0415), Centers for Disease Controls and Prevention (1U01DP006079), IMAGINE NO IC Research Grant, the Steven Spielberg Discovery Fund in Prostate Cancer Research Career Development Award, and the U.S.-Egypt Science and Technology Joint Fund (to J.K.). J.K. is former recipient of Interstitial Cystitis Association Pilot Grant, a Fishbein Family IC Research Grant, New York Academy of Medicine, and Boston Children's Hospital Faculty Development. The funders had no role in the experimental design, data collection, analysis, preparation of the manuscript, or decision to publish. In addition, this article is derived from the Subject Data funded in whole or part by National Academies of Sciences, Engineering, and Medicine (NAS) and The United States Agency for International Development (USAID). Any opinions, findings, conclusions, or recommendations expressed in this article are those of the authors alone, and do not necessarily reflect the views of USAID or NAS.

Availability of data and materials

All of data were presented in the main paper. The data that support the findings of this study are available on request from the corresponding author [J.K.]. The data are not publicly available due to information that could compromise research participant privacy.

Authors' contributions

JK and AMM conceived of the study, designed experiments, evaluated data and wrote the paper. AMM, ML, EC, VS, TP, MS, AM, MA, AA, and ME performed experiments. MS, AS, and AM provided expertise and supervised data interpretation. JK, AMM, and HA-E have contributed conceptually and intellectually and to the writing of the manuscript. All authors have read and approved the final manuscript.

Ethics approval and consent to participate

The biospecimens used in the present retrospective study were available from Mansoura University. The Ethics Committee of Mansoura Urology and Nephrology Center approved the protocol used for this study. The Institutional Review Board of Mansoura Urology and Nephrology Center approved analysis of all samples and database reviewed retrospectively (Mansoura UNC IRB #RP-16-12-91). Consent from patients for use of the archived bladder specimens samples or their data was waived by the IRB because this study was retrospective study.

Consent for publication

Not applicable.

Competing interests

The authors declare that they have no competing interests.

Publisher's Note

Springer Nature remains neutral with regard to jurisdictional claims in published maps and institutional affiliations.

Author details

¹Urology and Nephrology Center, Mansoura University, Mansoura, Egypt. ²University of Texas Health Science Center, San Antonio, USA. ³University of California Los Angeles, Los Angeles, CA, USA. ⁴University of California, Berkeley, CA, USA. ⁵Departments of Surgery and Biomedical Sciences, Samuel Oschin Comprehensive Cancer Institute, Cedars Sinai Medical Center, 8700 Beverly Blvd, Los Angeles, CA 90048, USA.

Received: 3 January 2017 Accepted: 19 October 2018

Published online: 09 November 2018

References

- Antoni S, Ferlay J, Soerjomataram I, Znaor A, Jemal A, Bray F. Bladder Cancer incidence and mortality: a global overview and recent trends. *Eur Urol*. 2017;71(1):96–108.
- Kamat AM, Hahn NM, Efstathiou JA, Lerner SP, Malmstrom PU, Choi W, Guo CC, Lotan Y, Kassouf W. Bladder cancer. *Lancet*. 2016;388(10061):2796–810.
- Kaplan AL, Litwin MS, Chamie K. The future of bladder cancer care in the USA. *Nature reviews Urology*. 2014;11(1):59–62.
- Mahdavi N, Ghoncheh M, Pakzad R, Momenimovahed Z, Salehiniya H. Epidemiology, incidence and mortality of bladder cancer and their relationship with the development index in the world. *Asian Pac J Cancer Prev*. 2016;17(1):381–6.
- Ibrahim AS, Khaled HM, Mikhail NN, Baraka H, Kamel H. Cancer incidence in Egypt: results of the national population-based cancer registry program. *J Cancer Epidemiol*. 2014;2014:437971.
- Zaghloul MS, Nouh A, Moneer M, El-Baradie M, Nazmy M, Younis A. Time-trend in epidemiological and pathological features of schistosoma-associated bladder cancer. *J Egypt Natl Cancer Inst*. 2008;20(2):168–74.
- Mostafa MH, Sheweita SA, O'Connor PJ. Relationship between schistosomiasis and bladder cancer. *Clin Microbiol Rev*. 1999;12(1):97–111.
- Ghoneim MA, Abdel-Latif M, el-Mekresh M, Abol-Enein H, Mosbah A, Ashamalla A, el-Baz MA. Radical cystectomy for carcinoma of the bladder: 2,720 consecutive cases 5 years later. *J Urol*. 2008;180(1):121–7.
- Grossman HB, Natale RB, Tangen CM, Speights VO, Vogelzang NJ, Trump DL, deVere White RW, Sarosdy MF, Wood DP Jr, Raghavan D, et al. Neoadjuvant chemotherapy plus cystectomy compared with cystectomy alone for locally advanced bladder cancer. *N Engl J Med*. 2003;349(9):859–66.
- Mansour AM, Soloway MS, Eldefrawy A, Singal R, Joshi S, Manoharan M. Prognostic significance of cystoscopy findings following neoadjuvant chemotherapy for muscle-invasive bladder cancer. *Can J Urol*. 2015;22(2):7690–7.
- Rosenblatt R, Sherif A, Rintala E, Wahlqvist R, Ullen A, Nilsson S, Malmstrom PU, Nordic Urothelial Cancer G. Pathologic downstaging is a surrogate marker for efficacy and increased survival following neoadjuvant chemotherapy and radical cystectomy for muscle-invasive urothelial bladder cancer. *Eur Urol*. 2012;61(6):1229–38.
- Black PC, Dinney CP. Growth factors and receptors as prognostic markers in urothelial carcinoma. *Curr Urol Rep*. 2008;9(1):55–61.
- Abbosh PH, McConkey DJ, Plimack ER. Targeting signaling transduction pathways in bladder Cancer. *Curr Oncol Rep*. 2015;17(12):58.
- van Kessel KE, Zuiverloon TC, Alberts AR, Boormans JL, Zwarthoff EC. Targeted therapies in bladder cancer: an overview of in vivo research. *Nature Rev Urol*. 2015;12(12):681–94.
- Lee HH, Wang YN, Hung MC. Non-canonical signaling mode of the epidermal growth factor receptor family. *Am J Cancer Res*. 2015;5(10):2944–58.
- Tan X, Lambert PF, Rapraeger AC, Anderson RA. Stress-induced EGFR trafficking: mechanisms, functions, and therapeutic implications. *Trends Cell Biol*. 2016;26(5):352–66.
- Kim WT, Kim J, Yan C, Jeong P, Choi SY, Lee OJ, Chae YB, Yun SJ, Lee SC, Kim WJ. S100A9 and EGFR gene signatures predict disease progression in muscle invasive bladder cancer patients after chemotherapy. *Ann Oncol*. 2014;25(5):974–9.
- Symanowski JT, Kim ES. Gene expression and prognosis in bladder cancer—real progress? Editorial on 'S100A9 and EGFR gene signatures predict disease progression in muscle invasive bladder cancer patients after chemotherapy. *Ann Oncol*. 2014;25(5):919–20.
- Choi W, Czerniak B, Ochoa A, Su X, Siefker-Radtke A, Dinney C, McConkey DJ. Intrinsic basal and luminal subtypes of muscle-invasive bladder cancer. *Nature Rev Urol*. 2014;11(7):400–10.
- Shah JB, McConkey DJ, Dinney CP. New strategies in muscle-invasive bladder cancer: on the road to personalized medicine. *Clin Cancer Res*. 2011;17(9):2608–12.
- Bladder cancers respond to EGFR inhibitors. *Cancer discovery*. 2014, 4(9):980–981.
- Rebouissou S, Bernard-Pierrot I, de Reynies A, Lepage ML, Krucker C, Chapeaublanc E, Herault A, Kamoun A, Caillault A, Letouze E, et al. EGFR as a potential therapeutic target for a subset of muscle-invasive bladder cancers presenting a basal-like phenotype. *Sci Transl Med*. 2014;6(244):244ra291.

Ready to submit your research? Choose BMC and benefit from:

- fast, convenient online submission
- thorough peer review by experienced researchers in your field
- rapid publication on acceptance
- support for research data, including large and complex data types
- gold Open Access which fosters wider collaboration and increased citations
- maximum visibility for your research: over 100M website views per year

At BMC, research is always in progress.

Learn more [biomedcentral.com/submissions](https://www.biomedcentral.com/submissions)






Centromere protein F (CENPF), a microtubule binding protein, modulates cancer metabolism by regulating pyruvate kinase M2 phosphorylation signaling

Muhammad Shahid, Min Young Lee, Honit Piplani, Allen M. Andres, Bo Zhou, Austin Yeon, Minjung Kim, Hyung L. Kim & Jayoung Kim


To cite this article: Muhammad Shahid, Min Young Lee, Honit Piplani, Allen M. Andres, Bo Zhou, Austin Yeon, Minjung Kim, Hyung L. Kim & Jayoung Kim (2018) Centromere protein F (CENPF), a microtubule binding protein, modulates cancer metabolism by regulating pyruvate kinase M2 phosphorylation signaling, *Cell Cycle*, 17:24, 2802-2818, DOI: [10.1080/15384101.2018.1557496](https://doi.org/10.1080/15384101.2018.1557496)


To link to this article: <https://doi.org/10.1080/15384101.2018.1557496>

 View supplementary material [↗](#)


 Accepted author version posted online: 09 Dec 2018.
Published online: 17 Dec 2018.

 Submit your article to this journal [↗](#)

 Article views: 269

 View related articles [↗](#)

 View Crossmark data [↗](#)

 Citing articles: 2 View citing articles [↗](#)

RESEARCH PAPER



Centromere protein F (CENPF), a microtubule binding protein, modulates cancer metabolism by regulating pyruvate kinase M2 phosphorylation signaling

Muhammad Shahid^a, Min Young Lee^b, Honit Piplani^{c,d}, Allen M. Andres^{c,d}, Bo Zhou^a, Austin Yeon^a, Minjung Kim^e, Hyung L. Kim^a, and Jayoung Kim^{a,f,g,h}

^aDepartments of Surgery and Biomedical Sciences, Cedars-Sinai Medical Center, Los Angeles, CA, USA; ^bInstitute for Systems Biology, Seattle, WA, USA; ^cDepartment of Medicine, Cedars Sinai Medical Center, Los Angeles, CA, USA; ^dCedars-Sinai Heart Institute, Los Angeles, CA, USA; ^eDepartment of Cell Biology, Microbiology and Molecular Biology, University of South Florida, Tampa, FL, USA; ^fDepartment of Medicine, University of California Los Angeles, CA, USA; ^gSamuel Oschin Comprehensive Cancer Institute, Cedars-Sinai Medical Center, Los Angeles, CA, USA; ^hDepartment of Urology, Ga Cheon University College of Medicine, Incheon, South Korea

ABSTRACT

Prostate cancer (PC) is the most commonly diagnosed cancer in men and is the second leading cause of male cancer-related death in North America. Metabolic adaptations in malignant PC cells play a key role in fueling the growth and progression of the disease. Unfortunately, little is known regarding these changes in cellular metabolism. Here, we demonstrate that centromere protein F (CENPF), a protein associated with the centromere-kinetochore complex and chromosomal segregation during mitosis, is mechanically linked to altered metabolism and progression in PC. Using the CRISPR-Cas9 system, we silenced the gene for CENPF in human PC3 cells. These cells were found to have reduced levels of epithelial-mesenchymal transition markers and inhibited cell proliferation, migration, and invasion. Silencing of CENPF also simultaneously improved sensitivity to anoikis-induced apoptosis. Mass spectrometry analysis of tyrosine phosphorylated proteins from CENPF knockout (CENPF^{KO}) and control cells revealed that CENPF silencing increased inactive forms of pyruvate kinase M2, a rate limiting enzyme needed for an irreversible reaction in glycolysis. Furthermore, CENPF^{KO} cells had reduced global bio-energetic capacity, acetyl-CoA production, histone acetylation, and lipid metabolism, suggesting that CENPF is a critical regulator of cancer metabolism, potentially through its effects on mitochondrial functioning. Additional quantitative immunohistochemistry and imaging analyzes on a series of PC tumor microarrays demonstrated that CENPF expression is significantly increased in higher-risk PC patients. Based on these findings, we suggest the CENPF may be an important regulator of PC metabolism through its role in the mitochondria.

ARTICLE HISTORY

Received 20 August 2018
Revised 13 November 2018
Accepted 28 November 2018

KEYWORDS

CENP-F; prostate cancer; mitochondria

Introduction

Prostate cancer (PC) remains a major public health concern; it is the most common malignant neoplasia among men and is the 6th leading cause of cancer-related male mortality worldwide [1]. In the U.S., there are more than 200,000 newly diagnosed cases and nearly 40,000 deaths from PC annually. The current standard methods of diagnosing and monitoring PC involve testing the levels of prostate specific antigen (PSA) and digital rectal screening. However, recent studies have reported that these procedures contribute little to no reduction in overall PC mortality [2,3].

Proliferating PC cells generate the energy required to support accelerated cell division by modulating its

metabolism. These cells exhibit increased glucose uptake and lactate production [4,5]. Rapidly dividing cells are able to convert glucose into lactate, regardless of oxygen availability, a phenomenon known as aerobic glycolysis or the Warburg effect [2]. The Warburg effect has been demonstrated to be a key contributor of tumorigenesis and can be a target for cancer therapy [6]. Many oncogenes and/or tumor suppressor genes have been reported to be involved in the metabolic switch towards aerobic glycolysis. For instance, oncogenes AKT [7], c-Myc [8], Ras [9], and HIF-1 α [10] promote the Warburg effect; whereas tumor suppressors p53 and PTEN inhibit it [11,12]. Epithelial-mesenchymal transition (EMT) also plays a pivotal role in the development of metastatic castration-resistant prostate cancer (mCRPC)

[13] and chemoresistant PC [14]. However, current understandings of the dynamic metabolic changes underlying EMT are limited.

Centromere protein F (CENPF), which is located on chromosome 1q41, encodes for a protein that acts as part of the centromere-kinetochore complex and is a component of the nuclear matrix during G₂ of interphase [15]. As a regulator of chromosome segregation, CENPF is expressed in a cell cycle-dependent manner; it gradually accumulates during the cell cycle, reaches peak levels in the G₂/M phase, and then degrades upon completion of mitosis [16]. CENPF is upregulated in PC and plays an important part in malignant progression [17,18]. Interestingly, CENPF also significantly enhances chemotherapeutic sensitivity [19]. It was recently observed that CENPF and forkhead box M1 (FOXO1) cooperate together, acting as synergistic master regulators of malignancy in PC [20]. Furthermore, COUP transcription factor 2 (COUP-TFII) may be promoting metastasis in PC through the CENPF signaling pathway [21].

In this study, we aimed to determine the functional role of CENPF and its underlying mechanism in PC progression. Our experimental results showed that silencing CENPF expression significantly inhibited EMT, cell proliferation, and colony formation, while also enhancing global phosphorylation and sensitivity to anoikis-induced apoptosis. Additional proteomics and computational analysis demonstrated that CENPF may regulate cancer cell metabolism through the phosphorylation of pyruvate kinase M2 (PKM2). Moreover, Seahorse Respirometry revealed that CENPF loss leads to a general decrease in metabolic activity in PC cells, which is characterized by reduced respiration and glycolysis. In summary, we propose CENPF as a novel target protein, providing a potential effective paradigm in curing PC.

Materials and methods

Cell culture and cell lines

Human prostate cancer cell lines PC3, DU145, and 22RV1 were purchased from American Type Culture Collection (ATCC, Manassas,

VA, USA) and were cultured in 10% fetal bovine serum (FBS)/Dulbecco's Modified Eagle medium (DMEM) or RPM1640 medium. Cells were maintained in humidified incubators set at 37°C with 5% CO₂. A CENPF-knockout PC3 cell line (CENPF^{KO}) was constructed using the CRISPR/Cas9 system by ALSTEM, LLC (Richmond, CA). The combination of two gRNAs (GTTTCAGCTTGACAGTCTCG and CATTATTGACAGAGAAGTGC) targeted the deletion of an 85 bp fragment in the exon1-intron1 junction, with 32 bp of this deletion fragment in the exon1 and 54 bp deleted in intron. For transient transfection of cells with a CENPF-expressing construct or siRNA CENPF (ThermoScientific), we followed the previously established protocol using Lipofectamine 2000 (Invitrogen), according to the manufacturer's instructions [22]. All cell lines were confirmed and tested for mycoplasma every 6 months during the experimental period.

Antibodies and reagents

The following antibodies were used: β -Actin (A1978) from Sigma, E-Cadherin (610182), Phosphotyrosine (610000) from BD Transduction Laboratories, ACSS2 (PA5-52059) from ThermoFisher Scientific, ALDH7A1 (ab154218), CENPF (ab5), and OXPHOS (ab110413) from Abcam, and Tom40 (sc365467) from Santa Cruz Biotechnology, phospho-mTOR (2971), phospho- β -catenin (9564), phospho-p38 MAPK (9216), phospho-PAK1 (2601), phospho-NF- κ B (3033), TCF8/ZEB1 (3396), phospho-PKM2 (3827), PKM2 (4053), Snail (3879), N-cadherin (13116), MMP2 (13132), MMP9 (13667), Slug (9585), phospho-p70 S6 Kinase (9206), phospho-Src Family (2101), Phospho-p44/42 MAPK (Erk1/2) (Thr202/Tyr204) (4370), β -Catenin (8480), Cleaved-PARP (9541), and Fatty acid and Lipid Metabolism Antibody Kit (8335), Acetyl-Histone Antibody Kit (9933), Tight Junction Antibody Kit (8683) and HRP-conjugated secondary antibodies (7074, 7076) from Cell Signaling Technology.

Proliferation assay

Cell proliferation was analyzed using trypan blue staining. Cells were seeded onto 6-well culture plates (2×10^2 cells/well) and cultured for 24 hrs. Each well culture was maintained and incubated for 2 d. The medium was replaced every day. The results are presented as the percentage of viable cells relative to that of the control.

Two-dimensional (2D) and three-dimensional (3D) colony formation assay

The growth capability of CENPF^{KO} and control cells was examined using 2D colony formation assays. Approximately 500 controls and CENPF^{KO} cells were seeded onto separate 15 cm culture plates. After incubation at 37°C for 14 d, the cells were washed with PBS twice, fixed with methanol and then stained with 0.1% crystal violet. The number of colonies containing >30 cells was counted under the microscope. Anchorage-independent growth was measured through a 3D colonization assay. Cells were seeded at 1×10^4 in 3 ml 0.35% agar in DMEM/FBS, overlaid on 2 ml of 0.7% agar in DMEM/FBS, in six-well plates. Plates were incubated for up to 14 d and cells were fed every 3–4 d. After two weeks, the plates were stained with MTT and the number of colonies that developed within each well was counted and visualized under a microscope. Colonies that were comprised of more than 10 cells were scored as positive. Experiments were run in triplicate for each cell line and data are representative of three independent trials.

Wound-healing assay

For the wound-healing migration assay, CENPF^{KO} and control cells were seeded on 6-well plates at a density of 1×10^5 cells/well in culture medium. After 24 hrs post seeding, the confluent monolayer of the culture was scratched with a fine pipette tip and migration capacity was visualized under a microscope. The rate of wound closure was observed for an additional 24 hrs during incubation.

Anoikis assays

Cells (5×10^5) were plated onto poly-HEMA-coated six-well plates (Corning, Tewksbury, MA, USA) in growth medium to prohibit attachment. After 24, 48 and 72 hrs in suspension, cells were transferred onto regular cell culture plates in growth medium supplemented with FBS (1%) to aid attachment. Cells were incubated for 0, 1, 2, and 3 hrs prior to the MTT assay (no. G4100, Promega, Madison, WI, USA). Absorbance was read using a microplate reader (Tecan, Männedorf, Switzerland). Experiments were repeated three times.

Western blot analysis

Cells were lysed with RIPA buffer (20 mM Tris, 150 mM NaCl, 1% Nonidet, P-40, 0.1 mM EDTA) (Pierce, ThermoFisher) supplemented with a phosphatase inhibitor cocktail (ThermoFisher). The protein concentration of each sample was measured using the Bradford Protein Kit Assay, according to the manufacturer's instructions (Pierce, ThermoFisher). Equal amounts of protein extract were separated via SDS-PAGE and transferred onto a PVDF membrane. The membranes were then blocked with 5% bovine serum albumin or 5% nonfat milk in TBST buffer [2.42 g/L Tris-HCl, 8 g/L NaCl, and 1 mL/L Tween 20 (pH 7.6)] and incubated overnight at 4°C with specific primary antibodies in TBST. The membranes were then incubated with secondary antibodies conjugated with horseradish peroxidase. β -actin was used as an internal control.

Immunohistochemistry (IHC) analysis

Two independent commercial PC tissue microarrays (TMAs) were purchased from US Biomax (Derwood, MD). Detailed information was not available except sex, TMN, grade, and stages. TMAs were immunostained with mAb CENPF, according to the manufacturer's recommended protocol. Immunostaining was considered positive when more than 10% of all tumor cells were immunoreactive. For quantification, the TMAs were scored for IHC intensity by two independent

investigators. Tumors that showed no positive staining were given a score of 0, those with weak staining were given a score of 1, and tumors with strong IHC staining were given a score of 2.

Acetate measurement assay

The acetate colorimetric assay kit (BioVision, Milpitas, CA) was used according to the instructions provided. The reaction was incubated at room temperature for 40 min. Acetate fluorescence (absorbance at 450nm) was measured using a POLARstar Galazy fluorometer in a 96-well plate.

Free fatty acid (FFA) and cholesterol quantification

Quantification of FFAs and cholesterol were determined using the Free Fatty Acid Quantification Kit and Cholesterol Quantification Kit (FFA: MAK044 and Cholesterol: MAK043, Sigma MO, USA). Briefly, cells were lysed in 1% Triton X-100 in chloroform (w/v). The samples were centrifuged at $13,000 \times g$ for 10 min to remove insoluble debris. The organic phase was collected and air dried in a 50°C dry bath for 20 min. Samples were vacuum dried for 30 min to remove traces of chloroform. The dried lipids were resuspended via vortex in fatty acid assay buffer and further quantified, using the manufacturer's instructions.

Global proteomics

All chemicals used for preparation of liquid chromatography-tandem mass spectrometry (LC-MS/MS) samples were of at least sequencing grade and were purchased from Sigma-Aldrich, unless otherwise stated. Whole protein was extracted from CENPF^{KO} and control cells using 4% SDS-containing buffer. Protein concentration was measured with the Pierce 660nm Assay Kit. From each sample, 60 µg of protein was digested with trypsin, using FASP, and labeled with TMT6plex reagents in parallel. After TMT labeling, peptides were merged, desalted with C18, and fractionated by high-pH reverse phase liquid chromatography (RPLC). Peptides were sequenced and quantified by LC-MS/MS. Database searching and

quantification were performed using Proteome Discoverer (v2.1). A standard false discovery rate of 1% was applied to filter peptide-spectrum matches, peptide identifications, and protein identifications. Next, data was normalized in the Proteome Discoverer environment, assuming that the total peptide amount in each different sample was the same. In addition, TMT126-labeled samples were selected as a reference channel and ratios between samples were computed by Proteome Discoverer [23]. The fold-changes between CENPF^{KO} and parent PC3 cells were determined as the average ratios of the three TMT tags for each group. The significance of the differential abundances between the two groups was computed using Welch's t-test on the scaled abundances and Benjamini-Hochberg (BH) procedure for multiple testing corrections. Differentially expressed proteins (DEPs) were identified by applying a threshold of BH FDR ≤ 0.01 and ratio ≥ 1.5 .

Phosphoproteomics

Proteins were eluted from p-Y conjugated beads and resolved by a quick separation (5–6mm height) in a 12% SDS-PAGE gel. Upon in-gel reduction, alkylation, and trypsin digestion, the tryptic peptides were extracted and reconstituted in 0.2% formic acid. The peptides were then separated in a 15 cm EASY-Spray C18 column and analyzed on a LTQ Orbitrap Elite Mass Spectrometer (Thermo Scientific). Up to 20 collision-induced dissociation (CID) spectra were acquired per survey scan in the rapid CID scan mode. The raw MS/MS spectra were searched against the Uniprot Human Database (released on 01/22/16, including 20,985 sequences) with MaxQuant (v 1.5.2.8) and Andromeda. A stringent 1% false discovery rate was set for peptide and protein identifications [24].

Network analysis

We identified gene ontology biological processes (GOBPs) and Kyoto Encyclopedia of Genes and Genomes (KEGG) pathways represented by the DEPs using DAVID [25]. The significance of terms was determined at a BH FDR ≤ 0.1 . To delineate the associations of enriched biological functions and

DEGs, a network model was constructed using HitPredict, a database of experimentally determined protein-protein interactions [26]. The database update version, 04Jul2017, was downloaded and only high confidence interactions among genes involved in the selected terms were parsed for the network construction. Genes involved in the same biological functions were grouped into the same module, each of which was labeled by their corresponding GOBP and KEGG pathway terms. The network was visualized using Cytoscape (v. 3.2.1) [27].

Seahorse respirometry assay

CENPF^{KO} and control PC3 cells were seeded into a 24-well Seahorse culture plate at a density of 50,000 cells/well 24 hrs before the Seahorse assay. The media was then changed to a XF Base Medium (pH 7.4) supplemented with 10 mM glucose, 1mM sodium pyruvate and 1mM sodium glutamine. Cells equilibrated for 1 hour in a non-CO₂ incubator at 37°C before assay start. Chemical reagents (Sigma) were used at final concentrations as follows: 1 μM oligomycin – an ATP synthase inhibitor, 1 μM (FCCP) carbonyl cyanide 4-(trifluoromethoxy) phenylhydrazone – an uncoupling agent, and a mixture of 0.5 μM antimycin A – a cytochrome C reductase inhibitor and 0.5 μM rotenone – a complex I inhibitor. Oxygen consumption rate (OCR) and extracellular acidification rate was monitored during the duration of the assay run. Results were normalized to protein concentrations determined by a BCA assay (Thermo Scientific).

Statistical analysis

Statistical analyses were performed using a two-tailed Student's t-test. For all experiments with error bars, the standard deviation (SD) was calculated to indicate the variation within each experiment, and values represent mean ± SD. Differences were considered significant if $p < 0.05$.

Results

CENPF is associated with aggressive PC

To evaluate whether CENPF expression is associated with cancer progression, we performed two

independent IHC imaging analyses using PC TMAs, as described in Methods section. Using commercial PC TMAs, we found that CENPF was overexpressed in approximately 70% of call cases, with an upward trend in tumors of higher grades (III-IV) (Figure 1(a)). IHC analyses using 2 different commercial TMAs revealed that CENPF was expressed in approximately 60% and 50% of all cases, respectively. We also found moderate staining in the normal prostate tissues and hyperplasia. CENPF expression was considerably higher in PC tissue compared to adjacent normal prostate tissue from the same patient. Levels of CENPF expression were also positively correlated to pathological stage and grade (Figure 2(b)). This observation was consistent with previous literature demonstrating CENPF as part of a signature that distinguishes biochemical recurrence and advanced cancer [28]. Collectively, the expression levels of CENPF in PC tissue were significantly higher than that of normal prostate tissue. These results point to the notion that CENPF expression may be potentially associated with PC progression.

CENPF loss reversed EMT in PC3 cells

To elucidate the role of CENPF in PC cells, CENPF was stably knocked-out in PC3 cells using the CRISPR/Cas9 system. These CENPF-knockout

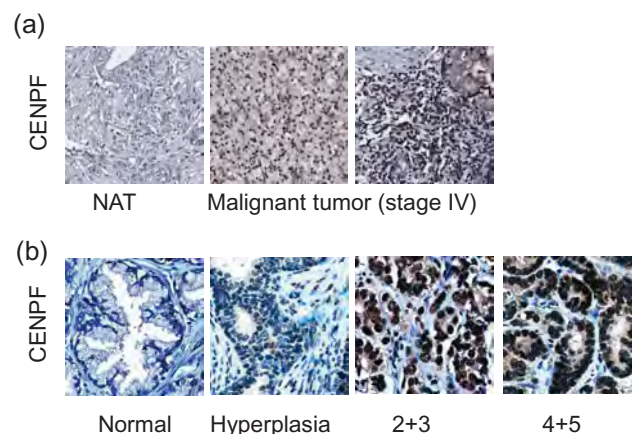


Figure 1. CENPF expression is correlated with PC progression. Two independent tissue microarrays (TMAs) were used. TMA slides were stained with CENPF specific antibody (brown) and counterstained with hematoxylin (blue). (a) The IHC images represent adjacent normal prostate tissues (NAT) or tumors from PC patients with different stages, as described in figures. (b) Representative IHC images show the differential CENPF protein levels.

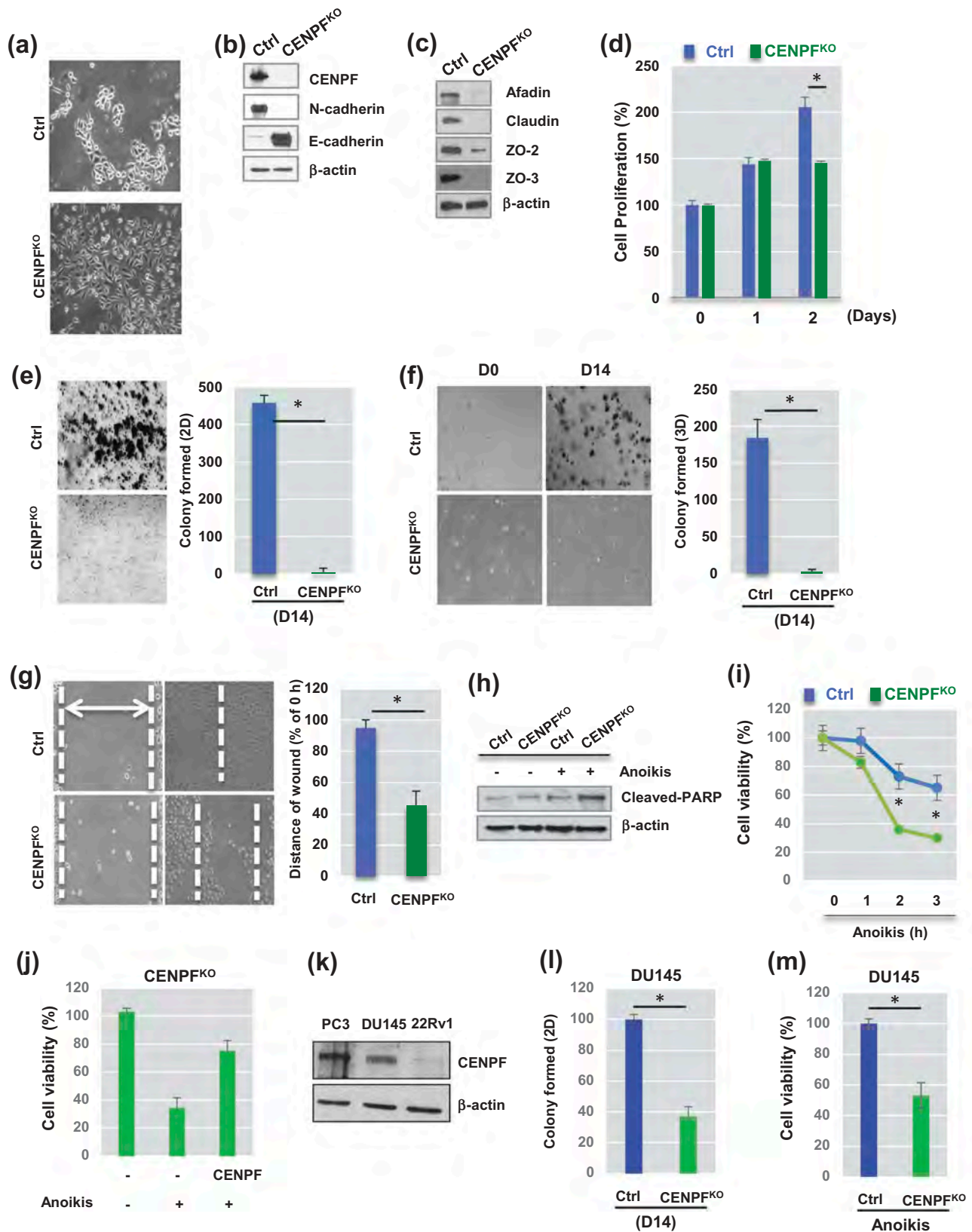


Figure 2. Knockout of CENPF reduces Epithelial-Mesenchymal transition (EMT) and slows proliferation of prostate cancer cells. (a) Morphological changes between parental PC3 cells (Ctrl) and CENPF – knockout PC3 cells (CENPF^{KO}) were observed. Representative images were shown. (b) Western blot analysis demonstrated well-known EMT markers in Ctrl and CENPF^{KO} cells. (c) Cell junction markers were assessed by Western blot analysis. (d) Cell proliferation was determined by trypan blue staining and compared in Ctrl and CENPF^{KO} cells at 0, 24 and 48hrs. (e-f) Gene knockout of CENPF reduced colony formation ability in 2D (e) or 3D (f) settings. (g)

(CENPF^{KO}) cells were then carefully characterized in the laboratory. There were some noted morphological alterations in the CENPF^{KO} cells, compared to the control PC3 cell line (Figure 2(a)). Western blot analysis demonstrated that CENPF expression was lost in the CENPF^{KO} cells (Figure 2(b)). Consistent with morphological changes, we found that protein expression of mesenchymal cell markers, including N-cadherin (Figure 2(b)), snail, slug, matrix metalloproteinase-2 (MMP2), MMP9, β -catenin (Supplementary Figure 1), was significantly reduced in CENPF^{KO} cells, compared to control cells [29,30]. E-cadherin, an epithelial marker, dramatically increased in CENPF^{KO} cells (Figure 2(b)). In addition, tight junction proteins (e.g. afadin, claudin, and zonula occludens (ZO), such as ZO-2 and ZO-3), which are involved in cell-cell contact regions [31], were also greatly reduced in CENPF^{KO} cells. This was consistent with the morphological changes observed (Figure 2(c)).

Effects of CENPF silencing on the biological outcomes of PC cells

We next sought to determine if CENPF plays any major roles in controlling cell proliferation, migration, invasion, and colony formation capability. *In-vitro* wound healing, migration, and Matrigel invasion assays were conducted on both PC3 CENPF^{KO} and control cells. Starting from day 2, the cell proliferation rate of CENPF^{KO} cells was significantly reduced compared to controls (Figure 2(d)).

We further assessed the ability of the cells to form colonies in the 2-dimensional (2D) and 3-dimensional (3D) planes. These colony formation assays revealed that CENPF^{KO} cells formed very few colonies even after 2 wk of incubation (2D, $p < 0.0001$) (Figure 2(e)). Anchorage-independent cell proliferation was measured with the 3D colony formation assay, and,

compared to control cells, CENPF^{KO} cells showed very low colony formation capacity (3D, $p < 0.003$) (Figure 2(f)).

For the cell wound healing assay, a scratch was inflicted on cell cultures once they reached 90% confluence. We found that the wound healing capability of CENPF^{KO} cells was significantly delayed than the control, suggesting that the migratory ability of CENPF^{KO} cells may be impaired (Figure 2(g)). Knockout of CENPF also increased PC3 cell death by anoikis, which is apoptosis that is induced when cells are unable to attach to the extracellular matrix (ECM) [32]. Expression levels of cleaved PARP (c-PARP), an apoptotic marker, were higher in CENPF^{KO} cells compared to controls (Figure 2(h)). This was consistent with the cell viability assay results (Figure 2(i)). Furthermore, a rescue experiment using a CENPF construct showed that the effects of CENPF knockout could be diminished by inducing overexpression of CENPF (Figure 2(j)). In addition, we found that CENPF plays the same roles in DU145 PC cells, whose CENPF expression levels were as redundant as PC3 cells (Figure 2(k)). Colony formation capability (Figure 2(l)) and viability (Figure 2(m)) were both significantly decreased when CENPF was knocked-down in DU145 cells. Collectively, these results indicate that CENPF inhibition reverses EMT and suppresses the proliferative characteristics of PC cells, while simultaneously enhancing anoikis-induced apoptosis.

CENPF silencing alters the whole proteome to promote signaling and glucose metabolism

Since there have been no previous proteomics studies showing the biological function of CENPF in the context of PC, we were prompted to understand the whole proteome alterations caused by CENPF silencing. In order to understand the mechanisms

Wound-healing assay showed the slower migration of CENPF^{KO} cells, compared to Ctrl. Knockout in prostate cancer cell line. (h-i) Anoikis-induced cell apoptosis was enhanced when CENPF was downregulated. (h) Western blot analysis showed that cleaved form of PARP, an apoptotic marker, was increased in CENPF KO. (i) Levels of cell viability were measured by MTT assay after anoikis for 0, 1, 2, or 3h. All experiments were carried out in triplicate. (j) CENPF overexpression reversed the effects of CENPF knockout on cell viability in response to anoikis. (k) The protein expression of CENPF was compared in PC3, DU145, and 22RV1 PC cells. (l-m) Downregulation of CENPF reduced colony formation (l) and decreased cell viability in response anoikis (m) in DU145 cells. For all Western blot analysis, β -actin was used as the loading control. Data are representative of at least three different experiments and are expressed as the means \pm SD.

underlying CENPF function, we performed mass spectrometry-based proteomics analysis, as described in the Methods. Whole-cell lysates in biological triplicates were digested with trypsin. Using LC-MS/MS, we determined which proteins were differentially expressed following CENPF knockout. In total, 549 DEPs were identified (adjusted p-value based on BH procedure ≤ 0.01 and ratio ≥ 1.5) (Supplementary Table 1), of which 130 were upregulated and 419 were downregulated, as shown in the volcano plot (Figure 3(a)). We next conducted a functional gene enrichment analysis of DEPs using the DAVID software to understand the most perturbed pathways based on previously reported GOBPs or KEGGs. Significantly enriched GOBPs included “negative regulation of microtubule polymerization” and “canonical glycolysis” (Figure 3(b)). CENPF silencing significantly enriched KEGG terms for “glycolysis/gluconeogenesis” and various metabolic pathways (Figure 3(c)). To further understand the changes in relationships among biological networks, network analysis was performed. Phosphorylation signaling transduction pathways, various metabolisms (carbohydrate, lipid, amino acids), adhesion, actin cytoskeleton, and endocytosis pathways were clearly marked as being highly enriched for by DEPs in CENPF^{KO} cells (Figure 3(d)). DEPs linked to fatty acid degradation were enriched as well (Figure 3(d)). Figure 3(e) shows the top 10 enriched pathways and the DEPs that belong to each term.

Silencing of CENPF impeded epigenetic modulation of histone markers and lipid synthesis in PC3 cells

We further defined the biological roles of CENPF in PC3 cells. Fatty acid and lipid metabolism play critical roles in energy maintenance and cellular nutrition in cancer, particularly in PC [33,34]. Biosynthesis of fatty acids utilizes glucose and exploits a pathway that is mainly controlled by an enzyme, fatty acid synthase (FASN). Prior studies have presented evidence showing that FASN is also associated with cell growth, survival, and drug resistance in PC [33]. To test the hypothetical link between CENPF levels and metabolic shifts in PC, cholesterol and free fatty acid levels were quantified in CENPF^{KO} and control PC3 cells. We found significant reduction in both cholesterol

and free fatty acid levels in the CENPF^{KO} cells (Figure 4(a,b)). We further measured the expression levels of genes related to fatty acid and lipid synthesis in both cell lines. Expression levels of long-chain fatty-acid-coenzyme A ligase (ACSL1) [35], FASN [36], acetyl-CoA carboxylase (ACC), and phosphorylation levels of ACC (p-ACC) [37] were significantly decreased in CENPF^{KO} cells (Figure 4(c)). This data demonstrated that knocking-out CENPF resulted in decreased expression of lipid metabolism-associated proteins, as well as intracellular concentrations of FFAs and cholesterol.

In addition, we found that expression levels of acyl-coenzyme A synthetase short-chain family members 1 and 2 (ACSS1 and ACSS2), which are key regulatory proteins for lipid synthesis and energy generation, were also downregulated when CENPF was silenced (Figure 4(d)). Western blot analysis of CENPF^{KO} cells showed that ACSS2 expression greatly decreased, while ACSS1 was modestly downregulated, compared to controls (Figure 4(d)). Interestingly, ACSS2 expression is positively correlated with PC progression [38–40]. ACSS2 has been reported to mediate acetyl modification of histone proteins (histone acetylation) and gene regulation through the generation of acetyl-CoA [41]. Thus, we speculated that CENPF is required for regulating acetate metabolism and contributes to epigenetic modification through its effects on histones via ACSS1 and/or ACSS2 (Figure 4(e)). Our acetate measurements, using a commercial kit, showed that acetate levels in CENPF^{KO} cells were almost completely diminished. We also evaluated for expression of acetylated histones in CENPF^{KO} and control cells. Western blot analysis found that expression levels of key acetylated histones, including H2A, H2B, H3 and H4, were significantly reduced in CENPF^{KO} cells (Figure 4(f)).

CENPF^{KO} cells have a distinct tyrosine phosphorylation profile

We next sought to profile the phosphorylation events that occur when CENPF is knocked-out. Just to get a general idea of the phosphorylation statuses of specific signaling pathways modulated by CENPF silencing, a series of western blot

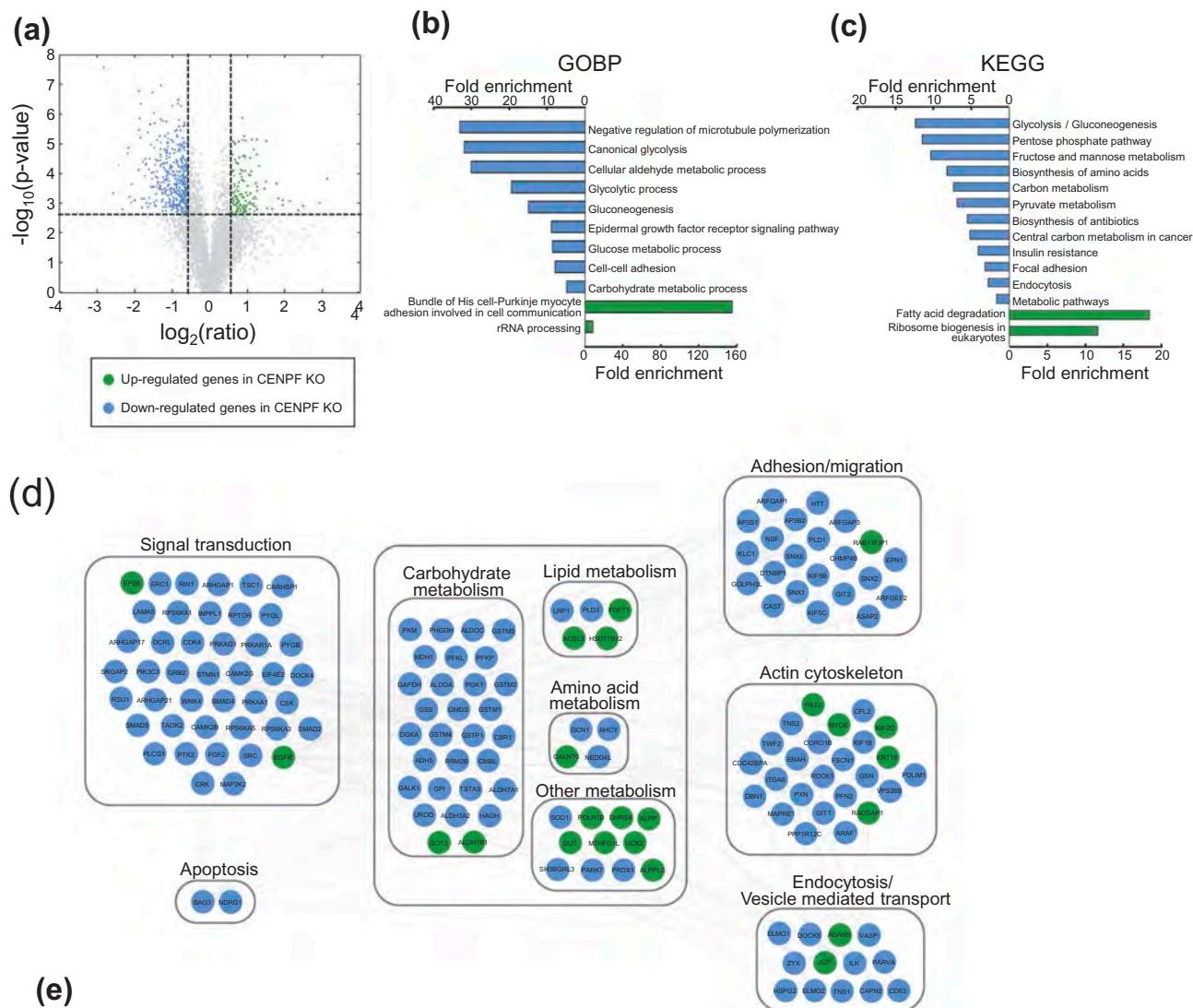


Figure 3. Silencing of CENPF perturbed proteome. (a) Unbiased global proteomics analysis was performed using CENPF^{KO} cells and Ctrl. The volcano plot shows the differentially expressed proteins. Green, upregulated; Blue, downregulated proteins in CENPF^{KO} cells, compared to Ctrl (b-c) Functional enrichment analysis of DEPs was performed using DAVID. GOBP- (b) or KEGG-based analysis (c), (d) Network modeling suggested activation of phosphotyrosine signaling in PC cells. (e) The list of DEPs who belong to the 10 most-enriched pathways.

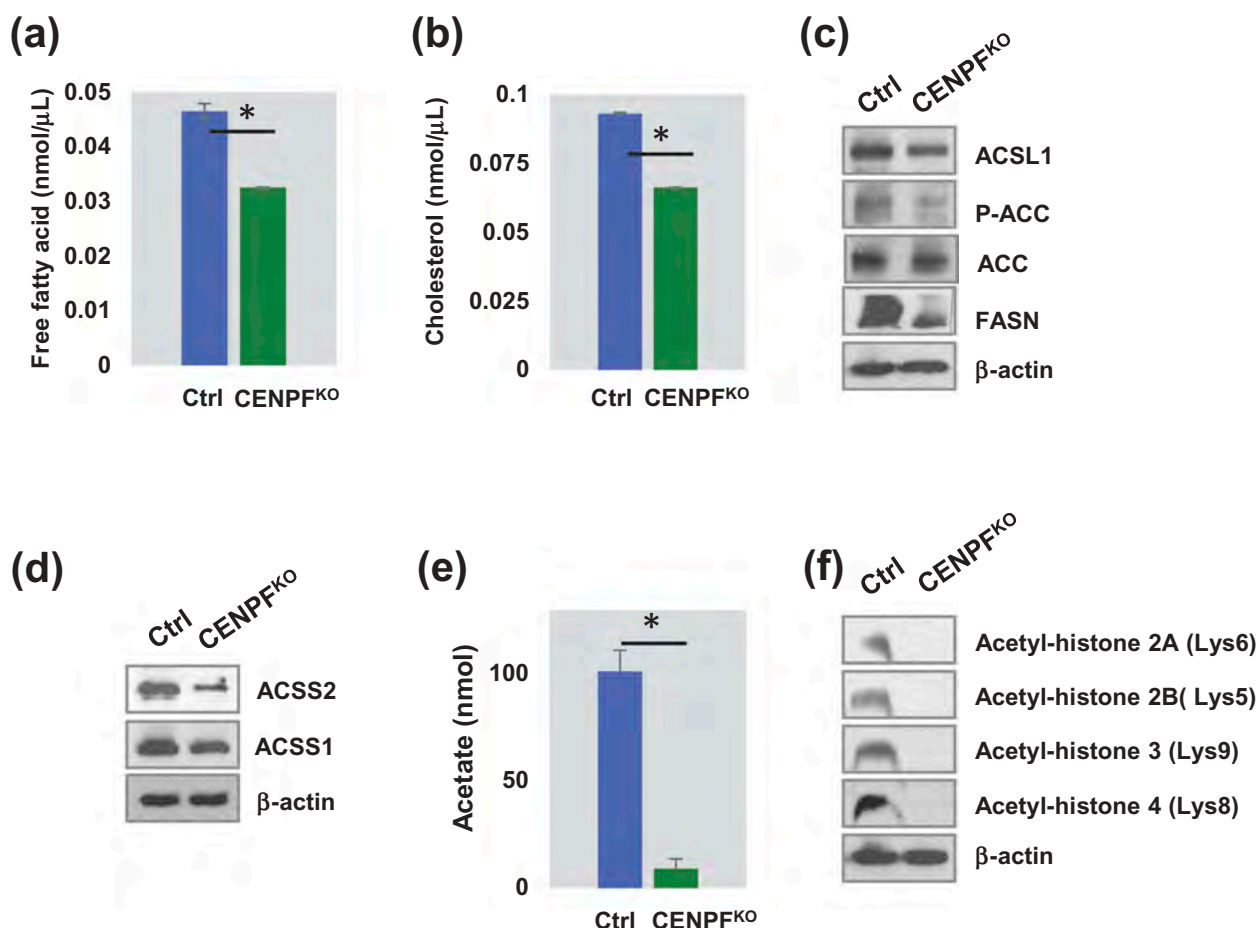


Figure 4. CENPF involved in epigenetic regulation of histone and lipid metabolism. (a) The histogram showed free fatty acid level. (b) Cholesterol level between CENPF^{KO} and Ctrl. (c) Western blot analysis showing long-chain fatty-acid-coenzyme A ligase (ACSL1), acetyl-CoA carboxylase (ACC), phosphorylation level of ACC (p-ACC) and fatty acid synthase (FASN). (d) Both ACSS1 and ACSS2 expression are reduced in CENPF^{KO}. (E) CENPF^{KO} decreased the synthesis of acetate to Ctrl. (f) Western blot analysis of key acetylated histone markers (H2A, H2B, H3, and H4) between CENPF^{KO} and Ctrl. The data represent the mean \pm standard deviation. A two-tailed Student's t-test was used to calculate statistical significance. β -actin was used as the loading control.

analyses were carried out on both CENPF^{KO} PC3 cells and controls. We found that CENPF is required for maintaining various phosphorylation events that are important for PC progression. Compared to control cells, the phosphorylation levels of Src (Tyr416), β -catenin (Ser45), p21 activated kinase 1 (PAK1) (Thr423), and NF- κ B (Ser536) were elevated in CENPF^{KO} cells (Figure 5(a)). In contrast, phosphorylation of Akt (Ser473), extracellular signal-regulated kinase 1/2 (ERK1/2) (Thr202/Tyr204), S6Kinase (Thr389), mTOR (Ser2448), and p38MAPK (Thr180/Tyr182) decreased in CENPF^{KO} cells compared to controls. However, the total protein expression levels remained unchanged (data were not shown) (Figure 5(a)). Interestingly, western blot analysis with anti-phospho-tyrosine antibodies revealed

that CENPF^{KO} cells have stronger p-Tyr intensity with distinct phosphorylation patterns (Figure 5 (b)), signifying that subduing CENPF increased or changed patterns of tyrosine phosphorylation.

Tyrosine phosphorylation levels of pyruvate kinase M2 (PKM2) were decreased in CENPF^{KO} cells

Although phosphorylation of tyrosine sites constitutes less than a few percentage of all phosphorylation events, we next attempted to specifically focus on defining tyrosine phosphorylation events. This was because previous findings have indicated that phospho-tyrosine (pTyr) based phosphoproteomics can be utilized as a tool for measuring the critical events needed for activating key kinases. In

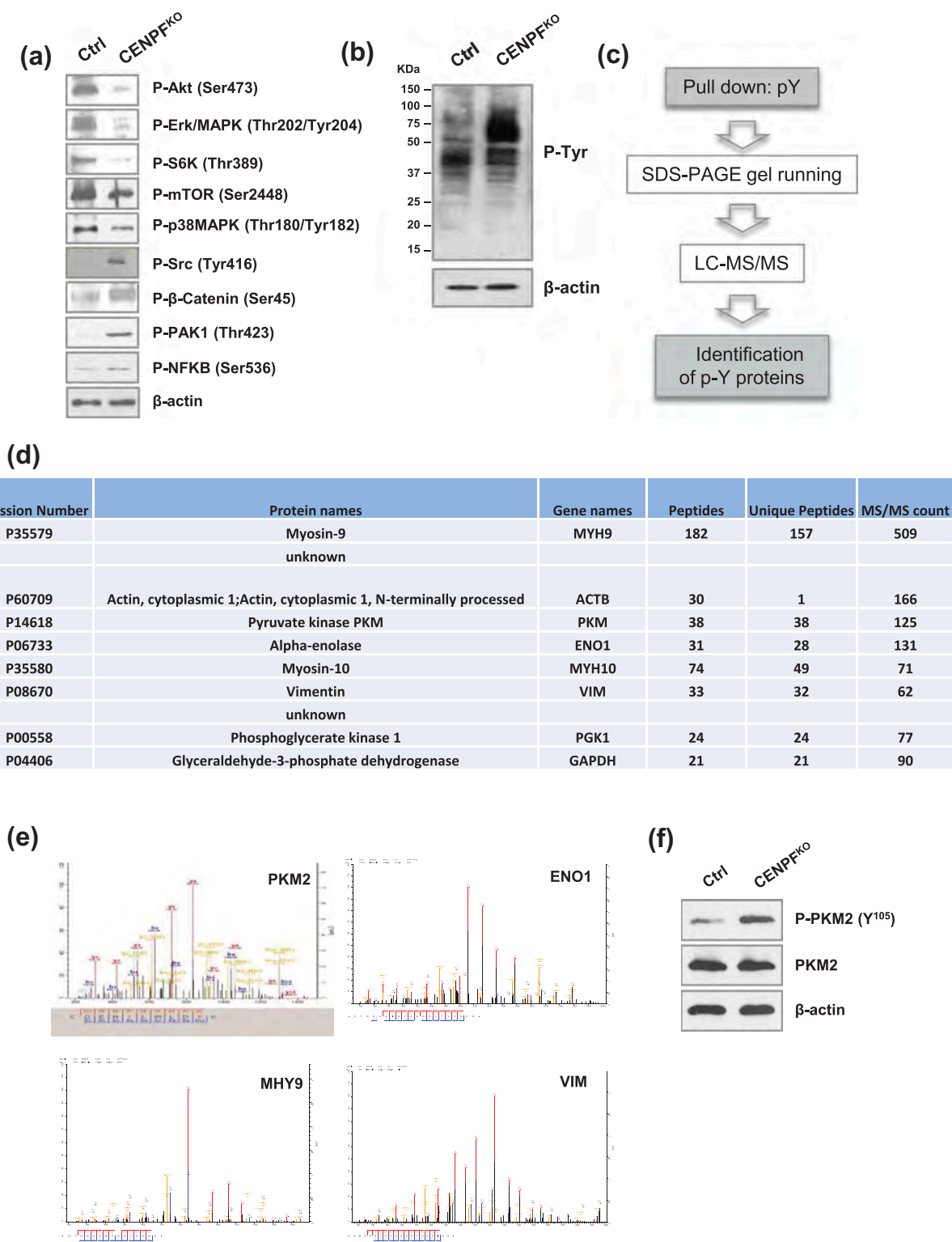


Figure 5. CENPF reduce metabolism in prostate cancer cells. (a) Western blot analysis of key signal transduction proteins. (b) Western blot analysis of phospho-tyrosine (pY) signaling was performed in CENPF^{KO} cells and Ctrl. (c) A workflow including phospho-tyrosine-enrichment by protein pull-down and LC-MS/MS illustrates the experimental design to identify the tyrosine phosphorylated proteins specifically enriched in CENPF^{KO} cells. (d) The 10 top proteins identified from B. (e) Representative MS spectrum of PKM2, ENO1, MYH9, and VIM, which were identified in this study. (f) Phosphorylation of PKM2 at Y¹⁰⁵ and non-phosphorylated form of PKM2 were assessed by western blot analysis in CENPF^{KO} cells and Ctrl. β-actin was used as the loading control.

turn, this allows for better recognizing perturbation of downstream signaling pathways [42,43]. To further define tyrosine-phosphorylated proteins in CENPF^{KO} cells and controls, proteomics profiling and bioinformatics approaches were applied. Tyrosine-phosphorylated proteins were enriched for target protein identification via mass spectrometry. This enrichment was done using p-Tyr, an anti-phospho-tyrosine antibody coupled to agarose beads. The coupled proteomic identification was then carried out using LC-MS/MS (Figure 5(c)). This procedure resulted in a list of candidate proteins that may be biologically important for PC progression. Figure 5(d) shows the top 10 proteins, which included myosin-9, actin, PKM, alpha-enolase, myosin-10, vimentin, phosphoglycerate kinase 1, glyceraldehyde-3-phosphate dehydrogenase, and 2 additional proteins without annotations.

PKM2 is known as a tumor-specific isoform of pyruvate kinase (PK), the rate-limiting enzyme during glycolysis, which catalyzes the production of pyruvate and adenosine 5'-triphosphate (ATP) from phosphoenolpyruvate (PEP) and adenosine 5'-diphosphate (ADP) [44]. The detected tandem mass spectrum of PKM2 and other proteins (e.g. Enolase 1 (ENO1), myosin, heavy chain 9 (MHY9), Vimentin (VIM)) are shown in Figure 5(e). Additional western blot analysis confirmed that phosphorylation levels of PKM2 at site Y¹⁰⁵ significantly increased in CENPF^{KO} cells, while expression of total PKM2 levels remained unchanged (Figure 5(f)). Given prior findings demonstrating that PKM2 activity is crucial for aerobic glycolysis and that phosphorylation of the Y¹⁰⁵ site may inactivate PKM2 [45], our data suggests that knockout of CENPF may be inactivating PKM2 via Y¹⁰⁵ site phosphorylation and this may be associated with the biological outcomes observed.

Both mitochondrial respiration and glycolysis are downregulated in CENPF^{KO} cells

Given that CENPF silencing leads to PKM2 inactivation, we hypothesized that CENPF can regulate cancer-associated metabolism, such as aerobic glycolysis and mitochondrial respiration. To determine the effect of CENPF knockout on

PC energy shifts, we used the Seahorse XFe24 Analyzer [46]. Mitochondrial respiration was profiled by measuring the oxygen consumption rate (OCR), which can determine the changes in levels of oxidative phosphorylation (OXPHOS)-dependent ATP generation. Compared to the control PC3 cells, CENPF^{KO} cells had a considerable decrease in OCR (Figure 6(a)). Both the basal and maximum oxygen consumption rates were significantly reduced; approximately 35% and 50%, respectively, of the control rates were observed in CENPF^{KO} cells (Figure 6(b,c)). Extracellular acidification rate (ECAR), which is an indicator of glycolysis, also decreased in CENPF^{KO} cells (Figure 6(d)). Collectively, these experimental results suggest that biogenesis was significantly reduced in CENPF^{KO} cells and that these cells were metabolically quiescent, compared to controls.

We next examined whether CENPF regulates mitochondrial quantity. Mitochondrial metabolic respiration-associated proteins, including TOM40 (a central component of the translocase of outer membrane (TOM) receptor complex in mitochondria) and a series of mitochondrial oxidative phosphorylation (OXPHOS) proteins [47], were measured via western blot analysis. The expression levels of TOM 40, C I subunit (NDUFB8), C II subunit (SDHB), C III core protein 2 (UQCRC2), C IV subunit (I MTCO1), and C V alpha subunit (ATP5A) decreased in CENPF^{KO} cells (Figure 6(e)). These findings suggest that CENPF abrogation results in attenuated metabolism evidenced by impaired mitochondrial ATP production and glycolysis. Furthermore, we tested whether the increase in PKM2 phosphorylation can be reversed when mitochondrial biogenesis is boosted by pioglitazone, a medication that is widely used for diabetes [48,49]. Western blot analysis suggested that pioglitazone treatment significantly decreased CENPF knockout-induced tyrosine phosphorylation of PKM2 (Figure 6(f)).

Discussion

Since the discovery of evidence presenting that perturbed metabolic pathways, such as oxidative phosphorylation, glycolysis, and fatty acid biosynthesis, can suppress cancer cell growth,

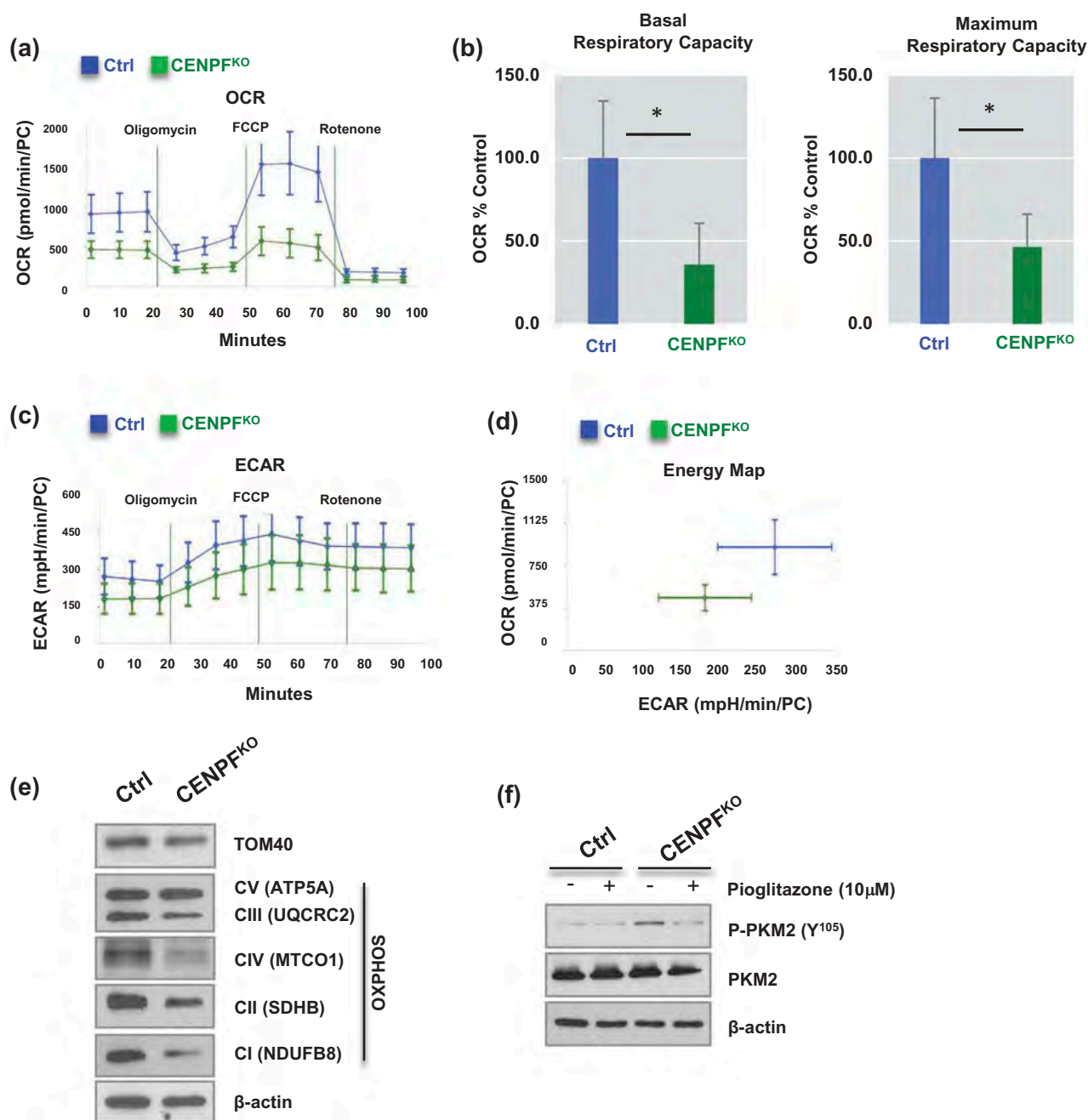


Figure 6. Silencing of CENPF decreased mitochondrial oxidative phosphorylation. The mitochondrial biogenetic activity was determined for CENPF^{KO} and Ctrl in real-time using the Seahorse extracellular flux analyzer. (a) The oxygen consumption rate (OCR) curves in CENPF^{KO} cells and Ctrl treated with oligomycin, FCCP and rotenone/antimycin A ($n = 6$ independent experiments). The OCR curves were determined by using a Seahorse XF24 Analyzer. (b) Basal and maximum respiratory capacity normalized to the cell numbers in CENPF^{KO} cells and Ctrl. (c) Extracellular acidification rate (ECAR) was determined. (d) An energy map showing difference between CENPF^{KO} cells and Ctrl. (e) Western blot analysis was performed to measure the levels of TAM20 and OXPHOS proteins. (f) Western blot data showing phospho-PKM2 (Y¹⁰⁵) and PKM2 expression in CENPF^{KO} cells and Ctrl in presence or absence of pioglitazone. Both cells were treated with 10 μ M pioglitazone for 24 h before sample preparation. The graphs shown here are representative examples of three independent experiments. The data represent the mean \pm standard deviation. A two-tailed Student's t-test was used to calculate statistical significance.

cancer metabolism has become an emerging field [50–52]. In this study, a series of unbiased proteomics and consecutive functional experiments revealed that knocking-out CENPF impaired

mitochondrial functioning and signaling activation that is required for PC growth and metastasis. We herein demonstrated that CENPF knock-out can reverse EMT and suppress

metabolic rates by reducing OXPHOS and glycolysis, possibly through its effects on PKM2.

High levels of PKM2 are expressed in a variety of human tumors, including lung, breast, and colon cancer [53], and are reported to promote the Warburg effect [44]. PKM2 exists as a low-activity dimeric or high-activity tetrameric form, and cancer cells predominantly express the low-activity dimeric form with a reduced ability to convert phosphoenolpyruvate to pyruvate [54]. Phosphorylation of PKM2 at Tyr105 is reported to disrupt its active tetrameric form [45,55] and reduce its catalytic activity. PKM2 phosphorylation at Tyr105 is known to impair PKM2's enzymatic activity and ability to catalyze the formation of ATP from ADP using a phosphate group from 2-phosphoenolpyruvate (PEP).

Our histone acetylation data suggested that metabolic reprogramming influences histone acetylation levels in PC (Figure 4(a)). Previous studies have demonstrated the correlation between histone acetylation levels and clinical outcomes, such as recurrence and patient survival, in various cancer types [56]. Other studies have shown that elevated nuclear levels of acetylated histone 2A.Z or decreased global histone acetylation in PC was correlated to poorer prognoses [52,57,58]. Although it is well-accepted that histone acetylation has important roles in gene regulation and DNA repair, the biological significance of global histone acetylation levels and its underlying effects on metabolic rewiring (e.g. how histone modification regulates PC progression and treatment response) remain elusive.

Since nuclear acetylation events are highly dependent on the availability of acetyl-CoA, we decided to survey acetate levels in our control and CENPF^{KO} PC3 cell lines. An acetate assay showed decreased acetate levels in CENPF^{KO} cells, which was consistent with their histone acetylation levels (Figure 4(b)). Lipogenic enzymes, such as ACCS, are the primary enzymatic sources of acetyl-CoA outside of the mitochondria. Several studies have demonstrated that ACLY may also be present in the nucleus and plays a crucial role in regulating histone acetylation. However, our study did not provide any evidence showing CENPF affecting ACLY's role in histone acetylation.

In summary, our study demonstrates that CENPF, a centromere protein, is required for

PC progression through its effects on signaling, glucose metabolism, and epigenetic regulation. Improved understanding of whether a perturbed metabolism precedes changes in epigenetic regulation or vice versa could provide clues on the cross talk that occurs between oncogenic metabolic reprogramming and the epigenome. The finding that the PKM2-mediated glucose metabolism pathway is a key player in maintaining mitochondrial function represents potential therapeutic strategies against PC. Future functional studies assessing the causative role of histone acetylation with altered metabolism by CENPF silencing are needed to further grasp how CENPF regulates mitochondrial functioning during metabolic and epigenetic changes in PC progression.

Acknowledgments

We would like to thank Drs. Wei Yang at the Biomarker Discovery Platform Core (Cedars-Sinai Medical Center) for guidance with proteomics studies and assistance with liquid chromatography-mass spectrometry (LC-MS/MS). The authors acknowledge support from National Institutes of Health grants (1U01DK103260, 1R01DK100974, U24 DK097154, NIH NCATS UCLA CTSI UL1TR000124), Department of Defense grants (W81XWH-15-1-0415), Centers for Disease Controls and Prevention (1U01DP006079), IMAGINE NO IC Research Grant, the Steven Spielberg Discovery Fund in Prostate Cancer Research Career Development Award, the U.S.-Egypt Science and Technology Joint Fund (to J.K.), and Florida Department of Health, Bankhead-Coley Cancer Research Program (5BC03) (to M.K.). J.K. is former recipient of Interstitial Cystitis Association Pilot Grant, a Fishbein Family IC Research Grant, New York Academy of Medicine, and Boston Children's Hospital Faculty Development. The funders had no role in the design, data collection and analysis, decision to publish or preparation of the manuscript. In addition, this article is derived from the Subject Data funded in whole or part by National Academies of Sciences, Engineering, and Medicine (NAS) and The United States Agency for International Development (USAID). Any opinions, findings, conclusions, or recommendations expressed in this article are those of the authors alone, and do not necessarily reflect the views of USAID or NAS.

Author contributions

JK and HLK designed the study. MS, AY, PL, AA, BZ, and HP carried out all biochemical experiments and

mitochondrial metabolomics analysis. ML performed bioinformatics analysis. MS and MK participated in interpretation of data and writing of the manuscript. MK and AA provided valuable insights on study design and data interpretation. JK wrote the manuscript. All authors discussed the results and commented on the manuscript at all stages.

Disclosure statement

No potential conflict of interest was reported by the authors.

Funding

This work was supported by the Centers for Disease Control and Prevention [1U01DP006079]; Foundation for the National Institutes of Health [1U01DK103260]; U.S. Department of Defense [W81XWH-15-1-0415]. The authors acknowledge support from National Institutes of Health grants (1U01DK103260, 1R01DK100974, U24 DK097154, NIH NCATS UCLA CTSI UL1TR000124), Department of Defense grants (W81XWH-15-1-0415), Centers for Disease Control and Prevention (1U01DP006079), IMAGINE NO IC Research Grant, the Steven Spielberg Discovery Fund in Prostate Cancer Research Career Development Award, the U.S.- Egypt Science and Technology Joint Fund (to J.K.), and Florida Department of Health, Bankhead- Coley Cancer Research Program (5BC03) (to M.K.). J.K. is former recipient of Interstitial Cystitis Association Pilot Grant, a Fishbein Family IC Research Grant, New York Academy of Medicine, and Boston Children's Hospital Faculty Development. The funders had no role in the design, data-collection and analysis, decision to publish or preparation of the manuscript. In addition, this article is derived from the Subject Data funded in whole or part by National Academies of Sciences, Engineering, and Medicine (NAS) and The United States Agency for International Development (USAID). Any opinions, findings, conclusions, or recommendations expressed in this article are those of the authors alone, and do not necessarily reflect the views of USAID or NAS.

References

- [1] Siegel RL, Miller KD, Jemal A. Cancer statistics, 2016. *CA Cancer J Clin.* 2016 Jan-Feb;66(1):7–30. PubMed PMID: 26742998.
- [2] Schroder FH, Hugosson J, Roobol MJ, et al. Screening and prostate-cancer mortality in a randomized European study. *N Engl J Med.* 2009 Mar 26;360(13):1320–1328. PubMed PMID: 19297566.
- [3] Andriole GL, Crawford ED, Grubb RL 3rd, et al. Mortality results from a randomized prostate-cancer screening trial. *N Engl J Med.* 2009 Mar 26;360(13):1310–1319. PubMed PMID: 19297565; PubMed Central PMCID: PMC2944770.
- [4] Cutruzzola F, Giardina G, Marani M, et al. Glucose metabolism in the progression of prostate cancer. *Front Physiol.* 2017;8:97. PubMed PMID: 28270771; PubMed Central PMCID: PMC5318430.
- [5] Mitsuzuka K, Arai Y. Metabolic changes in patients with prostate cancer during androgen deprivation therapy. *Int J Urol.* 2017 Oct 20. PubMed PMID: 29052905. DOI:10.1111/iju.13473
- [6] Levine AJ, Puzio-Kuter AM. The control of the metabolic switch in cancers by oncogenes and tumor suppressor genes. *Science.* 2010 Dec 03;330(6009):1340–1344. PubMed PMID: 21127244.
- [7] Elstrom RL, Bauer DE, Buzzai M, et al. Akt stimulates aerobic glycolysis in cancer cells. *Cancer Res.* 2004 Jun 1;64(11):3892–3899. PubMed PMID: 15172999.
- [8] Miller DM, Thomas SD, Islam A, et al. c-Myc and cancer metabolism. *Clin Cancer Res.* 2012 Oct 15;18(20):5546–5553. PubMed PMID: 23071356; PubMed Central PMCID: PMC3505847.
- [9] Smith B, Schafer XL, Ambeskovic A, et al. Addiction to coupling of the Warburg effect with glutamine catabolism in cancer cells. *Cell Rep.* 2016 Oct 11;17(3):821–836. PubMed PMID: 27732857; PubMed Central PMCID: PMC35108179.
- [10] Courtney R, Ngo DC, Malik N, et al. Cancer metabolism and the Warburg effect: the role of HIF-1 and PI3K. *Mol Biol Rep.* 2015 Apr;42(4):841–851. PubMed PMID: 25689954.
- [11] Dang CV, Kim JW, Gao P, et al. The interplay between MYC and HIF in cancer. *Nat Rev Cancer.* 2008 Jan;8(1):51–56. PubMed PMID: 18046334.
- [12] Vousden KH, Ryan KM. p53 and metabolism. *Nat Rev Cancer.* 2009 Oct;9(10):691–700. PubMed PMID: 19759539.
- [13] Matuszak EA, Kyprianou N. Androgen regulation of epithelial-mesenchymal transition in prostate tumorigenesis. *Expert Rev Endocrinol Metab.* 2011 May;6(3):469–482. PubMed PMID: 23667383; PubMed Central PMCID: PMC3648215.
- [14] Bitting RL, Schaeffer D, Somarelli JA, et al. The role of epithelial plasticity in prostate cancer dissemination and treatment resistance. *Cancer Metastasis Rev.* 2014 Sep;33(2–3):441–468. PubMed PMID: 24414193; PubMed Central PMCID: PMC4230790.
- [15] Varis A, Salmela AL, Kallio MJ. Cenp-F (mitosin) is more than a mitotic marker. *Chromosoma.* 2006 Aug;115(4):288–295. PubMed PMID: 16565862.
- [16] Liao H, Winkfein RJ, Mack G, et al. CENP-F is a protein of the nuclear matrix that assembles onto kinetochores at late G2 and is rapidly degraded after mitosis. *J Cell Biol.* 1995 Aug;130(3):507–518. PubMed PMID: 7542657; PubMed Central PMCID: PMC2120529.
- [17] Testa JR, Zhou JY, Bell DW, et al. Chromosomal localization of the genes encoding the kinetochore proteins CENPE and CENPF to human chromosomes 4q24–>q25 and 1q32–>q41, respectively, by

- fluorescence in situ hybridization. *Genomics*. 1994 Oct;23(3):691–693. PubMed PMID: 7851898.
- [18] Li P, You S, Nguyen C, et al. Genes involved in prostate cancer progression determine MRI visibility. *Theranostics*. 2018;8(7):1752–1765. PubMed PMID: 29556354; PubMed Central PMCID: PMC5858498.
- [19] Mitrofanova A, Aytes A, Zou M, et al. Predicting drug response in human prostate cancer from preclinical analysis of in vivo mouse models. *Cell Rep*. 2015 Sep 29;12(12):2060–2071. PubMed PMID: 26387954; PubMed Central PMCID: PMC4591242.
- [20] Aytes A, Mitrofanova A, Lefebvre C, et al. Cross-species regulatory network analysis identifies a synergistic interaction between FOXM1 and CENPF that drives prostate cancer malignancy. *Cancer Cell*. 2014 May 12;25(5):638–651. PubMed PMID: 24823640; PubMed Central PMCID: PMC4051317.
- [21] Lin SC, Kao CY, Lee HJ, et al. Dysregulation of miRNAs-COUP-TFII-FOXM1-CENPF axis contributes to the metastasis of prostate cancer. *Nat Commun*. 2016 Apr 25;7:11418. PubMed PMID: 27108958; PubMed Central PMCID: PMC4848536.
- [22] Jung JH, You S, Oh JW, et al. Integrated proteomic and phosphoproteomic analyses of cisplatin-sensitive and resistant bladder cancer cells reveal CDK2 network as a key therapeutic target. *Cancer Lett*. 2018 Nov 28;437:1–12. PubMed PMID: 30145203; PubMed Central PMCID: PMC6181132.
- [23] Rinas A, Espino JA, Jones LM. An efficient quantitation strategy for hydroxyl radical-mediated protein footprinting using Proteome discoverer. *Anal Bioanal Chem*. 2016 Apr;408(11):3021–3031. PubMed PMID: 26873216.
- [24] Morley S, You S, Pollan S, et al. Regulation of microtubule dynamics by DIAPH3 influences amoeboid tumor cell mechanics and sensitivity to taxanes. *Sci Rep*. 2015 Jul 16;5:12136. PubMed PMID: 26179371; PubMed Central PMCID: PMC4503992.
- [25] Huang DW, Sherman BT, Lempicki RA. Systematic and integrative analysis of large gene lists using DAVID bioinformatics resources. *Nat Protoc*. 2009;4(1):44–57. PubMed PMID: 19131956.
- [26] Patil A, Nakai K, Nakamura H. HitPredict: a database of quality assessed protein-protein interactions in nine species. *Nucleic Acids Res*. 2011 Jan 39 (Database issue): D744–9. PubMed PMID: 20947562; PubMed Central PMCID: PMC3013773. DOI:10.1093/nar/gkq897
- [27] Shannon P, Markiel A, Ozier O, et al. Cytoscape: a software environment for integrated models of biomolecular interaction networks. *Genome Res*. 2003 Nov;13(11):2498–2504. PubMed PMID: 14597658; PubMed Central PMCID: PMC403769.
- [28] Horning AM, Wang Y, Lin CK, et al. Single-cell RNA-seq reveals a subpopulation of prostate cancer cells with enhanced cell-cycle-related transcription and attenuated androgen response. *Cancer Res*. 2018 Feb 15;78(4):853–864. PubMed PMID: 29233929; PubMed Central PMCID: PMC5983359.
- [29] Sun Y, Wang BE, Leong KG, et al. Androgen deprivation causes epithelial-mesenchymal transition in the prostate: implications for androgen-deprivation therapy. *Cancer Res*. 2012 Jan 15;72(2):527–536. PubMed PMID: 22108827.
- [30] Gao F, Al-Azayzih A, Somanath PR. Discrete functions of GSK3alpha and GSK3beta isoforms in prostate tumor growth and micrometastasis. *Oncotarget*. 2015 Mar 20;6(8):5947–5962. PubMed PMID: 25714023; PubMed Central PMCID: PMC4467413.
- [31] Landers KA, Samaratunga H, Teng L, et al. Identification of claudin-4 as a marker highly overexpressed in both primary and metastatic prostate cancer. *Br J Cancer*. 2008 Aug 5;99(3):491–501. PubMed PMID: 18648369; PubMed Central PMCID: PMC2527792.
- [32] Sakamoto S, Kyprianou N. Targeting anoikis resistance in prostate cancer metastasis. *Mol Aspects Med*. 2010 Apr;31(2):205–214. PubMed PMID: 20153362; PubMed Central PMCID: PMC2988681.
- [33] Suburu J, Chen YQ. Lipids and prostate cancer. *Prostaglandins Other Lipid Mediat*. 2012 May;98(1–2):1–10. PubMed PMID: 22503963; PubMed Central PMCID: PMC3348998.
- [34] Itkonen HM, Brown M, Urbanucci A, et al. Lipid degradation promotes prostate cancer cell survival. *Oncotarget*. 2017 Jun 13;8(24):38264–38275. PubMed PMID: 28415728; PubMed Central PMCID: PMC5503531.
- [35] Gao Y, Islam MS, Tian J, et al. Inactivation of ATP citrate lyase by Cucurbitacin B: A bioactive compound from cucumber, inhibits prostate cancer growth. *Cancer Lett*. 2014 Jul 10;349(1):15–25. PubMed PMID: 24690568.
- [36] Huang M, Koizumi A, Narita S, et al. Diet-induced alteration of fatty acid synthase in prostate cancer progression. *Oncogenesis*. 2016 Feb 15;5:e195. PubMed PMID: 26878389; PubMed Central PMCID: PMC5154344.
- [37] Park HU, Suy S, Danner M, et al. AMP-activated protein kinase promotes human prostate cancer cell growth and survival. *Mol Cancer Ther*. 2009 Apr;8(4):733–741. PubMed PMID: 19372545; PubMed Central PMCID: PMC2775041.
- [38] Mews P, Donahue G, Drake AM, et al. Acetyl-CoA synthetase regulates histone acetylation and hippocampal memory. *Nature*. 2017 Jun 15;546(7658):381–386. PubMed PMID: 28562591; PubMed Central PMCID: PMC5505514.
- [39] Shi L, Tu BP. Acetyl-CoA and the regulation of metabolism: mechanisms and consequences. *Curr Opin Cell Biol*. 2015 Apr;33:125–131. PubMed PMID: 25703630; PubMed Central PMCID: PMC4380630.
- [40] Schug ZT, Vande Voorde J, Gottlieb E. The metabolic fate of acetate in cancer. *Nat Rev Cancer*. 2016 Nov;16(11):708–717. PubMed PMID: 27562461.
- [41] Gao X, Lin SH, Ren F, et al. Acetate functions as an epigenetic metabolite to promote lipid synthesis under

- hypoxia. *Nat Commun.* **2016** Jun 30;7:11960. PubMed PMID: 27357947; PubMed Central PMCID: PMC4931325.
- [42] Drake JM, Graham NA, Stoyanova T, et al. Oncogene-specific activation of tyrosine kinase networks during prostate cancer progression. *Proc Natl Acad Sci U S A.* **2012** Jan 31;109(5):1643–1648. PubMed PMID: 22307624; PubMed Central PMCID: PMC3277127.
- [43] Labots M, van der Mijl JC, Beekhof R, et al. Phosphotyrosine-based-phosphoproteomics scaled-down to biopsy level for analysis of individual tumor biology and treatment selection. *J Proteomics.* **2017** Jun 6;162:99–107. PubMed PMID: 28442448.
- [44] Christofk HR, Vander Heiden MG, Harris MH, et al. The M2 splice isoform of pyruvate kinase is important for cancer metabolism and tumour growth. *Nature.* **2008** Mar 13;452(7184):230–233. PubMed PMID: 18337823.
- [45] Hitosugi T, Kang S, Vander Heiden MG, et al. Tyrosine phosphorylation inhibits PKM2 to promote the Warburg effect and tumor growth. *Sci Signal.* **2009** Nov 17;2(97):ra73. PubMed PMID: 19920251; PubMed Central PMCID: PMC2812789.
- [46] Wu M, Neilson A, Swift AL, et al. Multiparameter metabolic analysis reveals a close link between attenuated mitochondrial bioenergetic function and enhanced glycolysis dependency in human tumor cells. *Am J Physiol Cell Physiol.* **2007** Jan;292(1):C125–36. PubMed PMID: 16971499.
- [47] Georgieva E, Ivanova D, Zhelev Z, et al. Mitochondrial dysfunction and redox imbalance as a diagnostic marker of “Free Radical Diseases”. *Anticancer Res.* **2017** Oct;37(10):5373–5381. PubMed PMID: 28982845.
- [48] Scherthaner G, Currie CJ, Scherthaner GH. Do we still need pioglitazone for the treatment of type 2 diabetes? A risk-benefit critique in 2013. *Diabetes Care.* **2013** Aug;36(Suppl 2):S155–S161. PubMed PMID: 23882041; PubMed Central PMCID: PMC4931325.
- [49] Boxall N, Bennett D, Hunger M, et al. Evaluation of exposure to pioglitazone and risk of prostate cancer: a nested case-control study. *BMJ Open Diabetes Res Care.* **2016**;4(1):e000303. PubMed PMID: 28074141; PubMed Central PMCID: PMC4931325.
- [50] Kim WJ, Kim J. Looking to the metabolic landscapes for prostate health monitoring. *Prostate Int.* **2017** Sep;5(3):85–88. PubMed PMID: 28828350; PubMed Central PMCID: PMC5551909.
- [51] Lue HW, Podolak J, Kolahi K, et al. Metabolic reprogramming ensures cancer cell survival despite oncogenic signaling blockade. *Genes Dev.* **2017** Nov 14. PubMed PMID: 29138276. DOI:10.1101/gad.305292.117
- [52] Webber LP, Wagner VP, Curra M, et al. Hypoacetylation of acetyl-histone H3 (H3K9ac) as marker of poor prognosis in oral cancer. *Histopathology.* **2017** Aug;71(2):278–286. PubMed PMID: 28326594.
- [53] Luo W, Semenza GL. Emerging roles of PKM2 in cell metabolism and cancer progression. *Trends Endocrinol Metab.* **2012** Nov;23(11):560–566. PubMed PMID: 22824010; PubMed Central PMCID: PMC4931325.
- [54] Mazurek S. Pyruvate kinase type M2: a key regulator of the metabolic budget system in tumor cells. *Int J Biochem Cell Biol.* **2011** Jul;43(7):969–980. PubMed PMID: 20156581.
- [55] Christofk HR, Vander Heiden MG, Wu N, et al. Pyruvate kinase M2 is a phosphotyrosine-binding protein. *Nature.* **2008** Mar 13;452(7184):181–186. PubMed PMID: 18337815.
- [56] Chervona Y, Costa M. Histone modifications and cancer: biomarkers of prognosis? *Am J Cancer Res.* **2012**;2(5):589–597. PubMed PMID: 22957310; PubMed Central PMCID: PMC4931325.
- [57] Ellinger J, Schneider AC, Bachmann A, et al. Evaluation of global histone acetylation levels in bladder cancer patients. *Anticancer Res.* **2016** Aug;36(8):3961–3964. PubMed PMID: 27466500.
- [58] Valdes-Mora F, Gould CM, Colino-Sanguino Y, et al. Acetylated histone variant H2A.Z is involved in the activation of neo-enhancers in prostate cancer. *Nat Commun.* **2017** Nov 07;8(1):1346. PubMed PMID: 29116202; PubMed Central PMCID: PMC5676741.

Structure Annotation of All Mass Spectra in Untargeted Metabolomics

Ivana Blaženović,[†] Tobias Kind,[†] Michael R. Sa,[†] Jian Ji,[‡] Arpana Vaniya,[†] Benjamin Wancewicz,[†] Bryan S. Roberts,[†] Hrvoje Torbašinović,[§] Tack Lee,^{||} Sajjan S. Mehta,[†] Megan R. Showalter,[†] Hosook Song,^{||} Jessica Kwok,[†] Dieter Jahn,^{⊥,#} Jayoung Kim,^{∇,○,◆,||} and Oliver Fiehn^{*,†,ⓑ}

[†]West Coast Metabolomics Center, University of California, Davis, Davis, California 95616, United States

[‡]School of Food Science, State Key Laboratory of Food Science and Technology, Jiangnan University, Wuxi, Jiangsu 330047, China

[§]Inovatus Ltd., Zagreb 10000, Croatia

^{||}Department of Urology, Inha University College of Medicine, Incheon 22212, South Korea

[⊥]Institute of Microbiology, Technische Universität Braunschweig, Braunschweig 38106, Germany

[#]Braunschweig Integrated Centre of Systems Biology (BRICS), Technische Universität Braunschweig, Braunschweig 38106, Germany

[∇]Departments of Surgery and Biomedical Sciences, Cedars-Sinai Medical Center, Los Angeles, California 90048, United States

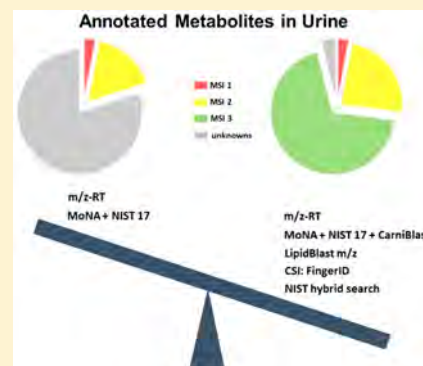
[○]Department of Medicine, University of California Los Angeles, Los Angeles, California 90095, United States

[◆]Samuel Oschin Comprehensive Cancer Institute, Cedars-Sinai Medical Center, Los Angeles, California 90048, United States

^{||}Department of Urology, Ga Cheon University College of Medicine, Incheon 22212, South Korea

Supporting Information

ABSTRACT: Urine metabolites are used in many clinical and biomedical studies but usually only for a few classic compounds. Metabolomics detects vastly more metabolic signals that may be used to precisely define the health status of individuals. However, many compounds remain unidentified, hampering biochemical conclusions. Here, we annotate all metabolites detected by two untargeted metabolomic assays, hydrophilic interaction chromatography (HILIC)-Q Exactive HF mass spectrometry and charged surface hybrid (CSH)-Q Exactive HF mass spectrometry. Over 9,000 unique metabolite signals were detected, of which 42% triggered MS/MS fragmentations in data-dependent mode. On the highest Metabolomics Standards Initiative (MSI) confidence level 1, we identified 175 compounds using authentic standards with precursor mass, retention time, and MS/MS matching. An additional 578 compounds were annotated by precursor accurate mass and MS/MS matching alone, MSI level 2, including a novel library specifically geared at acylcarnitines (CarniBlast). The rest of the metabolome is usually left unannotated. To fill this gap, we used the *in silico* fragmentation tool CSI:FingerID and the new NIST hybrid search to annotate all further compounds (MSI level 3). Testing the top-ranked metabolites in CSI:Finger ID annotations yielded 40% accuracy when applied to the MSI level 1 identified compounds. We classified all MSI level 3 annotations by the NIST hybrid search using the ClassyFire ontology into 21 superclasses that were further distinguished into 184 chemical classes. ClassyFire annotations showed that the previously unannotated urine metabolome consists of 28% derivatives of organic acids, 16% heterocyclics, and 16% lipids as major classes.



Metabolomics is used as one of the major -omics tools to tackle the complex area of personalized medicine and health.¹ Target analysis of metabolites is an integral part of clinical laboratories worldwide. Conversely, untargeted metabolomics provides comprehensive insights into complex metabolomes and allows for discovery of novel biomarkers and generating new metabolic hypothesis. Yet, untargeted metabolomics is challenged by very low identification rates.^{2,3} Since there is no single platform capable of capturing the entire metabolome of urine, we have employed two chromatographic platforms that are highly suited for untargeted metabolome

analysis: hydrophilic interaction chromatography (HILIC; for polar metabolite profiling) and charged-surface hybrid chromatography (CSH, for lipidomics profiling). While lipids are usually low abundant in (aqueous) urine samples, recent technological advancements of high-resolution mass spectrometry (MS) have largely improved the comprehensive lipid

Received: October 12, 2018

Accepted: January 2, 2019

Published: January 4, 2019

profiling of cells, tissues, and biofluids, including urine. Lipids can serve as important biomarkers even in urine samples, for example for prostate cancer⁴ or segmental glomerulosclerosis.⁵ Combined, metabolomics and lipidomics reveal biologically active metabolites in urine and provide a diagnostic chemical signature of human metabolic phenotypes. The urinary metabolome is associated with urological diseases, including bladder dysfunctions such as interstitial cystitis/bladder pain syndrome (IC).^{6–8} IC is characterized by chronic bladder and/or pelvic pain, as well as nocturia and an increase in urinary frequency and urgency.^{9–11} The work presented here investigated how many urine metabolites from IC patients could be identified, as defined by the Metabolomics Standards Initiative (MSI),¹² using freely available comprehensive metabolite annotation tools, novel databases, and libraries that were developed and used here for the first time.¹³

EXPERIMENTAL SECTION

Extraction. Subjects, urine specimen collection, and clinical and pathological features of subjects were described in a previous paper from our laboratory.¹⁴ Deidentified urine samples were stored at $-80\text{ }^{\circ}\text{C}$ until further analysis. Urinary lipids were extracted with methanol and methyl *tert*-butyl ether both containing a cocktail of lipid standards.¹⁵ Water was subsequently added for phase separation. This extraction protocol extracts all main lipid classes in urine with high recoveries, specifically phosphatidylcholines (PC), sphingomyelins (SM), phosphatidylethanolamines (PE), lysophosphatidylcholines (LPC), ceramides (Cer), cholesteryl esters (CholE), and triacylglycerols (TG).¹⁶ Lipid standards were purchased from Avanti Polar lipids (Alabaster, USA). After concentrating extracts to complete dryness, samples were reconstituted prior to LC-MS analysis as published before.¹⁷ Polar metabolites were retrieved by using the polar phase of the lipid extraction procedure. Samples were dried in a centrivap prior to a cleanup step of 50% acetonitrile and dried again. Samples were reconstituted for HILIC-MS analysis in an 80:20 acetonitrile:water solution containing internal standards from Sigma and CDN Isotopes.

Instrumentation. All measurements were carried out on a Thermo Q Exactive instrument. For lipidomics measurements, 1 μL of diluted samples was separated on a Waters Acquity UPLC CSH C18 column ($100 \times 2.1\text{ mm}$; $1.7\text{ }\mu\text{m}$) coupled to an Acquity UPLC CSH C18 VanGuard precolumn ($5 \times 2.1\text{ mm}$; $1.7\text{ }\mu\text{m}$). The column was maintained at $65\text{ }^{\circ}\text{C}$ with a flow rate of 0.6 mL/min . The positive ionization mobile phases consisted of (A) acetonitrile:water (60:40, v/v) with ammonium formate (10 mM) and formic acid (0.1%) and (B) 2-propanol:acetonitrile (90:10, v/v) with ammonium formate (10 mM) and formic acid (0.1%). The negative ionization mobile phases consisted of (A) acetonitrile:water (60:40, v/v) with ammonium formate (10 mM) and (B) 2-propanol:acetonitrile (90:10, v/v) with ammonium formate (10 mM). The separation was conducted under the following gradient: 0 min 15% B; 0–2 min 30% B; 2–2.5 min 48% B; 2.5–11 min 82% B; 11–11.5 min 99% B; 11.5–12 min 99% B; 12–12.1 min 15% B; 12.1–15 min 15% B. The Q Exactive MS instrument was operated using positive mode electrospray ionization using the following parameters: Mass range, 120–1200 m/z ; Sheath gas flow rate, 60; Aux gas flow rate, 25; Sweep gas flow rate, 2; Spray Voltage (kV) 3.6; Capillary temp, $300\text{ }^{\circ}\text{C}$; S-lens RF level, 50; Aux gas heater temp, $370\text{ }^{\circ}\text{C}$. Full MS parameters: Resolution, 60,000; AGC target, 1e6;

Maximum IT, 100 ms; Spectrum data type, Centroid. Data dependent MS2 parameters: Resolution, 15,000; AGC target, 1e5; Maximum IT, 50 ms; Loop count, 4; TopN, 4; Isolation Window, 1.0 m/z ; Fixed First Mass, 70.0 m/z ; (N)CE/stepped (N)CE, 20, 30, 40; Spectrum data type, Centroid.

For profiling polar compounds and biogenic amines, HILIC-Q Exactive MS/MS data acquisition was performed. One μL of diluted samples was separated on a Waters Acquity UPLC BEH Amide column ($150 \times 2.1\text{ mm}$; $1.7\text{ }\mu\text{m}$) coupled to an Acquity UPLC BEH Amide VanGuard precolumn ($5 \times 2.1\text{ mm}$; $1.7\text{ }\mu\text{m}$). The column was maintained at $45\text{ }^{\circ}\text{C}$ with a flow rate of 0.4 mL/min . The mobile phases consisted of (A) water with ammonium formate (10 mM) and formic acid (0.125%) and (B) acetonitrile:water (95:5, v/v) with ammonium formate (10 mM) and formic acid (0.125%). The separation was conducted under the following gradient: 0 min 100% B; 0–2 min 100% B; 2–7.7 min 70% B; 7.7–9.5 min 40% B; 9.5–10.25 min 30% B; 10.25–12.75 min 100% B; 12.75–17 min 100% B.

The Q Exactive MS instrument was operated using positive mode electrospray ionization (ESI HILIC) with the following parameters: Mass range, 60–900 m/z ; Sheath gas flow rate, 60; Aux gas flow rate, 25; Sweep gas flow rate, 2; Spray Voltage (kV) 3.6; Capillary temp, $300\text{ }^{\circ}\text{C}$; S-lens RF level, 50; Aux gas heater temp, $370\text{ }^{\circ}\text{C}$. Full MS parameters: Microscans, 1; Resolution, 60,000; AGC target, 1e6; Maximum IT, 100 ms; Number of scans, 1; Spectrum data type, Centroid. Data dependent MS2 parameters: Microscans, 1; Resolution, 15,000; AGC target, 1e5; Maximum IT, 50 ms; Loop count, 4; MSX count, 1; TopN, 4; Isolation Window, 1.0 m/z ; Isolation offset 0.0 m/z ; (N)CE/stepped (N)CE, 20, 30, 40; Spectrum data type, Centroid.

Data Processing and Compound Identification. The LC-MS/MS data was analyzed by MS-DIAL software.¹⁸ Detailed parameter settings are listed in Supplemental Table 1 (HILIC and lipidomics data processing settings). Data tables containing accurate masses, retention times, and peak heights were exported, and further analysis was performed in R and Metabox.¹⁹ Automated annotation of metabolites was performed separately for polar metabolites and lipids. Table S1 lists libraries, methods, and software used for each platform.

Metabolite annotations were achieved using a combination of different tools. On MSI level 1, we developed and used a novel HILIC-MS/MS library of 1,102 authentic standards including retention time, precursor mass, and MS/MS spectra. All spectra, retention times, and chromatography conditions are freely available at MassBank of North America (<http://massbank.us>). Search windows were used as follows: 0.1 min RT tolerance (for the alignment of peaks), 0.0001 Da tolerance for the precursor masses, and 0.05 Da tolerance for the MS/MS spectral matching. Similarly, we used lipid retention times and MS/MS spectra for lipidomics identifications.¹⁵ On MSI level 2, we annotated compounds that did not trigger MS/MS fragmentations in data dependent mode but that were still identified based on accurate mass and retention time using the HILIC-MS/MS library in addition to manually curated lipid retention times. Moreover, MSI level 2 annotations were also based on accurate mass and MS/MS annotations for spectra for which no authentic retention time library was available, such as the NIST17, HMDB,²⁰ GNPS,²¹ the new CarniBlast library, and the LipidBlast libraries.^{17,22,23} For MSI level 3 annotations, we used CSI:FingerID,²⁴ the NIST-Hybrid Search,²⁵ and LipidBlast accurate mass search services.

RESULTS AND DISCUSSION

MSI Level 1 Annotations. The number of precursors that triggered MS/MS fragmentations was sample dependent. Table S2 contains all 3,894 merged spectra for all samples that were aligned and processed by MS-DIAL software which were subsequently used for MSI level 1 and 2 annotations (Table 1). Compound identifications with the highest level of

Table 1. Results of Comprehensive Annotation of Urinary Metabolomics and Lipidomics MS/MS Spectra

chromatography and databases	type of matching	MSI level of annotation	no. of annotations
HILIC	precursor m/z , RT experimental library MS/MS	MSI level 1	103
lipidomics	m/z , RT, experimental + <i>in silico</i> library MS/MS		72
HILIC: MoNA+NIST17	precursor m/z , experimental library MS/MS	MSI level 2	440
HILIC	precursor m/z and RT		13
lipidomics: CarniBlast	m/z , <i>in silico</i> library MS/MS		18
HILIC: CarniBlast	precursor m/z , <i>in silico</i> library MS/MS		107
lipidomics: mzRT lookup	precursor m/z with RT curation	MSI level 3	96
HILIC and lipidomics: NIST17 hybrid search	MS/MS (hybrid and experimental library)		6,447
HILIC: Sirius/CSI:FingerID	precursor m/z and <i>in silico</i> predicted MS/MS		728

confidence (MSI level 1) were achieved using libraries of authentic standards. All library spectra and retention times were acquired under identical conditions as the experimental urine spectra. Specifically, a new HILIC-Q Exactive MS/MS library was established using 1,102 authentic compounds measured in positive mode. Data and metadata for this library can be downloaded from MassBank of North America (Fiehn HILIC). By matching experimental urine spectra against library retention times (RT), accurate precursor masses (m/z), and MS/MS spectra, overall 175 compounds were identified at MSI level 1. Specifically, we identified 72 lipids in CSH-Q Exactive MS/MS as members of 7 lipid classes and 103 hydrophilic compounds using HILIC-Q Exactive MS/MS as amino acids, biogenic amines, and other polar compound classes (Table S2). Detailed settings and cutoffs are listed in Table S1.

MSI Level 2 Annotations. Retention-time based libraries of authentic standards are necessarily smaller than the complement of available MS/MS spectra in public or licensed mass spectral libraries. Therefore, it is a common practice in metabolomics research to perform mass spectral similarity searches of experimental to library MS/MS spectra to increase the annotation rate. While metabolite MS/MS fragmentations are independent of chromatography conditions, spectra often show differences due to slightly different fragmentation parameters or different mass spectrometers used. In addition, many metabolites show only a few characteristic fragment ions, rendering the use of classic spectral similarity searches unreliable. To retain high confidence, we combined accurate precursor mass and MS/MS searches for all over queries, using 750 dot-product score (HILIC-MS/MS) and 400 reverse dot-product (CSH-MS/MS) as lower threshold below which no further correct match hits were expected. Subsequently, each

spectrum was manually inspected to verify spectral matches and retention time matches, where available.

MassBank of North America (MoNA; <http://massbank.us>) currently contains over 260,000 mass spectra from 15 individual mass spectral repositories such as MassBank, MassBank EU, GNPS, ReSpec, LipidBlast, MetaboBase, and HMDB, covering more than 80,000 compounds. We combined MoNA spectra with MS/MS data from the NIST17 library, the largest available licensed repository with over 550,000 experimental spectra from 13,808 chemical compounds. We merged all spectra from both resources into one.msp within MS-DIAL software for mass spectral similarity matching. In total, this approach yielded 480 identified compounds on MSI level 2.

While investigating and validating MS/MS spectra, we observed many spectra that appeared similar to 17 acylcarnitines annotated by using LipidBlast or MoNA spectra. Acylcarnitines in urine serve as biomarkers for bladder cancer,²⁶ diabetic nephropathy,²⁷ obesity,²⁸ and human kidney cancer.²⁹ The identification of acylcarnitines has to be performed either using authentic reference compounds or with reference library spectra.³⁰ However, only a few tandem mass spectra of acylcarnitines exist in commercial (NIST) and open mass spectral libraries (MassBank,³¹ METLIN,³² Respect DB³³), covering less than 50 acylcarnitine structures. Conversely, when using a structure similarity search in the CAS SciFinder literature database, we found 453 acylcarnitine-like structures of which only 62 were commercially available. Such finding indicated a high chemical diversity of acylcarnitines that could not possibly be closed by purchasing more chemical compounds. To overcome this gap and identify all urinary acylcarnitines, we developed an *in silico* tandem mass spectral library of acylcarnitines using structure templates²³ similar to our previous LipidBlast²² and FAHFA predicted MS/MS libraries.³⁴ Here, we constructed the CarniBlast library of 2,400 acylcarnitine species covering a wide range of saturated, unsaturated, -hydroxyl, -keto, -dicarboxylic, and oxidized acyl chain substituted acylcarnitines. We matched all experimental MS/MS spectra from both polar and lipidomics profiling against the new *in silico* database of acylcarnitines. After removing duplicates and manually validating each candidate spectrum, we identified 67 novel acylcarnitines through the CarniBlast library in addition to the 17 acylcarnitines obtained by LipidBlast and MoNA. Detailed settings and cutoffs are listed in Table S1.

All urinary metabolomic data were acquired by data-dependent MS/MS. Yet, we used retention-time based MS/MS libraries such as the new HILIC-Q Exactive MS/MS repository. For lipids, we have recently shown³⁵ that compound annotations can be based on accurate precursor mass and retention time alone with high confidence. Using these two orthogonal parameters (m/z and RT), six further acylcarnitines were annotated at MSI level 2. In the same manner, we assigned 201 further compounds that were too low abundant to trigger MS/MS fragmentations but that were covered in our m/z and RT libraries that were acquired under the same experimental conditions.

In combination, we identified 578 metabolites at MSI level 2 confidence (39 lipids, 85 acylcarnitines, and 454 hydrophilic compounds). Metadata such as dot product, reverse dot product scores, number of matching ions, and MS-DIAL calculated MS2 similarity have been taken into account. Detailed results are listed in Table S2.

MSI Level 3 Annotations. When combining compound annotations on MSI level 1 and 2, the 753 compound annotations only covered 19.3% of the acquired urinary MS/MS spectra (Figure 1). While this number of annotated

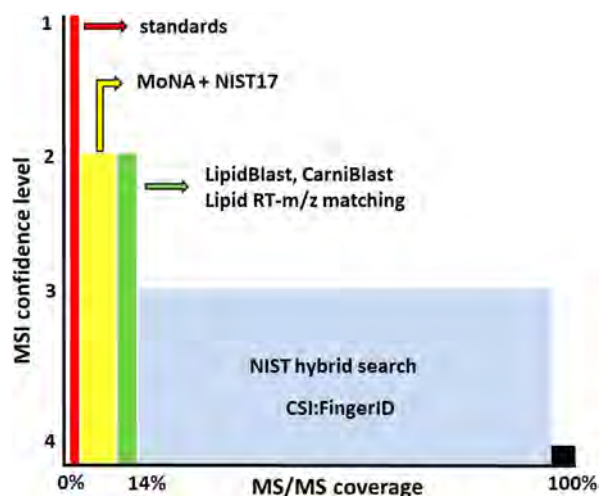


Figure 1. Categorized overview of the complete annotation of MS/MS spectra of human urine metabolomes based on MSI level 1, 2, and 3 confidence scores.

compounds is already significantly higher than most other studies on urine metabolomics,^{36,37} it is worrisome that more than 80% of all MS/MS spectra remain unannotated in metabolomics screens. Many biologists will focus their attention only on identified compounds and not even perform

statistical assessments on complete metabolome data, including unknowns. Yet, it appears very likely that the fraction of more than 80% unknowns might include very important biomarkers or signatures of diseases, food patterns, exposome compounds, or other significant chemicals. We therefore used three tools to investigate this dark matter of metabolomics³⁸ closer: (a) accurate mass search, (b) structure elucidation tools, and (c) mass spectral library hybrid search. We used the most exhaustive MS/MS files for MSI level 3 annotations, using raw MS/MS spectra from individual IC patients for each stepped collision energy to enable best-possible annotations. Spectra were exported as either mgf or msp files and used in the different software programs. For HILIC-MS/MS analyses, we used between 5,192 and 6,447 MS/MS spectra; for CSH-MS/MS lipidomics analyses, the number of spectra ranged from 5,705 to 7,050 MS/MS spectra per sample (Table 1 and Table S2). The number of raw spectra is higher than in the MS-DIAL processed file because MS-DIAL merged the stepped collision energies during data acquisition.

First, we used precursor mass lookups. In general, simple mass lookups yield many false discoveries due to a plethora of isomers and isobars at a given accurate mass level. This problem is especially pronounced in HILIC-MS for which hardly any constraint can be applied with respect to the number of possible chemicals. Yet, for lipidomics assays, lipids can already be assigned to specific lipid classes with some level of confidence based on m/z and retention time (in relation to MSI level 1 and 2 annotated lipids within the same study). Additional structure information on such lipid class annotations and their acyl chains cannot be made using accurate mass alone. We extracted m/z precursor information from the MS-

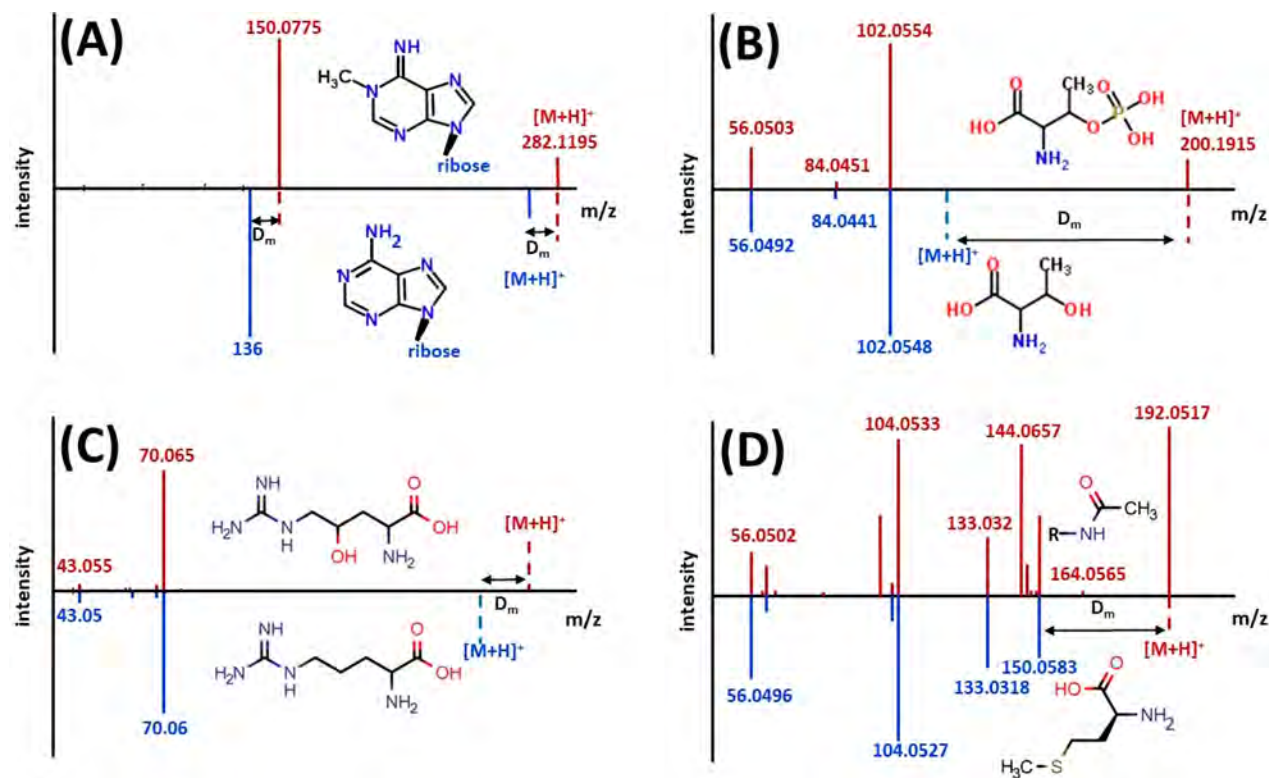


Figure 2. Head-to-tail comparison of MS/MS spectra of distinct shifts in spectra of modified versions of canonical metabolites. (A) methylation: 1-methyladenosine to adenosine, (B) phosphorylation: phosphothreonine to threonine, (C) hydroxylation: hydroxyarginine to arginine, (D): acetylation: *N*-acetylmethionine to methionine.

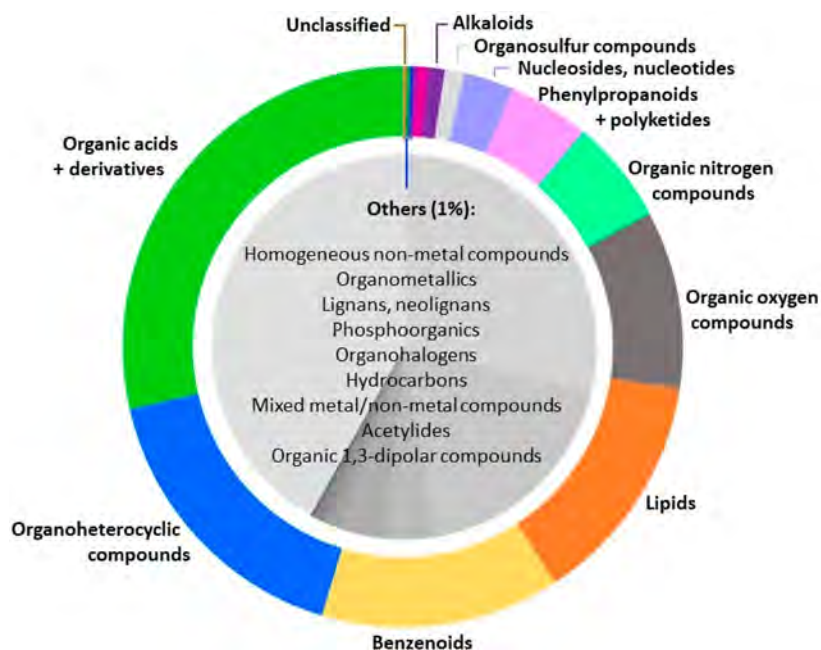


Figure 3. Structural categorization of compounds present in urine samples of 43 subjects diagnosed with interstitial cystitis. Chemicals are structured according to the “Superclass level” of the ClassyFire classification system.

DIAL output in positive ionization mode and used the m/z lookup macro within LipidBlast v49 to assign additional lipids. We used a 5 mDa mass tolerance for lipid assignments based on the mass accuracy of the Q Exactive instrument. This way, an additional 96 lipid annotations were obtained for the lipidomics data set in positive ionization mode.

Second, we used cheminformatics tools to annotate accurate mass HILIC-MS/MS spectra to likely chemical structures. A range of software tools has been published such as MS-FINDER,³⁹ Sirius, CFM-ID,⁴⁰ and others. Here, we used two programs, Sirius 4.0 with CSI:FingerID interface²⁴ and the new NIST17 hybrid-search.²⁵ Sirius/CSI:FingerID scored highly during the latest CASMI structure identification challenges^{41,42} but has never been applied to urinary metabolomics. The NIST17 hybrid-search software was released after the CASMI challenges but offers advantages by greatly expanding the utility of existing mass spectral libraries. For Sirius/CSI:FingerID, MS/MS spectra were exported as a MGF file from each raw file using the MSConvert program. The largest MGF file contained 6,447 MS/MS spectra. Formulas were assigned at 10 ppm search windows, retaining the 10 best formula candidates. Using Sirius, spectra were processed within 2 min on a 16 CPU machine, assigning formulas to a total of 6,184 features (96%). Subsequently, CSI:FingerID performed spectral fingerprint matching via a Web service to annotate isomer structures. Within 5 min processing time, 728 MS/MS spectra were assigned to chemical structures in the biodatabase, a filtered version of Pubchem containing over 270,000 structures of biological interest, and 1,557 MS/MS spectra were assigned to chemicals in the much larger PubChem database. Scored results of all isomeric structures were exported as CSV files. For structures returned by biodatabase searches, CSI:FingerID yielded up to 130 results per MS/MS scan and up to 10,000 structure candidates per MS/MS spectrum in PubChem queries. Time-consuming manual investigations have to be performed to select the most likely structures. To test CSI:FingerID accuracy, we selected 103 MS/MS spectra

from the urinary HILIC-Q Exactive MS/MS data set that were unambiguously assigned by authentic standards and tested these spectra within 5 ppm mass accuracy and a biodatabase structure query. Using our publicly available HILIC library (see above), 41 compounds (40%) were correctly annotated by CSI:FingerID as top hit, and 54 MS/MS spectra (52%) were correctly assigned within the top 3 isomer candidates. Detailed results are given in Table S3. CSI:FingerID is not optimized for use in lipidomics MS/MS spectra.

Third, we used the novel NIST17 hybrid search²⁵ that combines mass spectral library-based scoring with calculating fragment and precursor mass shifts for chemical modifications of library structures. Such a tool mimics the experience of well-trained chemists⁴³ because known biochemical modifications such as methylations or acetylations produce epimetabolites that are removed from their classic functions in canonical metabolic pathways.⁴⁴ Four examples of how the NIST17 hybrid search works are given in Figure 2 for head-to-tail MS/MS spectral comparisons of methyladenosine/adenosine, phosphothreonine/threonine, hydroxyarginine/arginine, and acetylmethionine/methionine. Spectra of modified metabolites show distinct shifts in precursor masses and fragments when comparing to nonmodified library spectra. Yet, the NIST17 hybrid search correctly associated the modified spectra with their best scoring related library spectra.

We exported all lipidomics and HILIC-MS/MS spectra from 43 interstitial cystitis patients from MS-DIAL to the NIST pepSearch software and used the NIST17 hybrid search function. The software supports batch processing, enables users to include or exclude specific MS/MS spectra, and yields quick overviews of the complement of chemical structures in mass spectral profiling studies. Results are given in Table S2. Within 10 min processing time, 95% of all spectra were assigned with structure annotations and compound names, including a set of confidence scores such as forward and reverse dot products and a probability score. Hybrid search annotations must be treated with caution as they do not

represent an identification but rather a nearest known neighbor to the unknown spectrum. While in many cases NIST17 hybrid searches give correct results (Figure 2), overall results highlight a high probability of chemical class annotations (MSI level 3) rather than exact structures. We therefore used these results for exactly this purpose, classifying the thousands of patient urinary MS/MS spectra to chemical classes. For this purpose, we implemented a batch search version of the automated chemical hierarchy classification system ClassyFire⁴⁵ (<https://cfb.fiehnlab.ucdavis.edu>). ClassyFire requires International Chemical Identifiers (InChI keys) as input.⁴⁶ Today, InChI keys are a standard tool in all chemical and biochemical databases to assign and compare chemical structures with machine-readable, unique keys. The ClassyFire Batch search utilizes the ClassyFire API to look up provided InChIKeys and, if no match is found, to query its nonstereo form. It yields a tabular CSV version of the results. We used the online tool Chemical Translation Services (CTS)⁴⁷ to convert chemical names from the NIST17 hybrid pepSearch results to InChI keys. This conversion reduced the compound list by ~1% because some NIST17 hybrid search chemical names are not yet included in PubChem or the other 200 chemical databases that support the CTS tool. Hence, of the average number of 5,250 MS/MS spectra found per patient in lipidomics and HILIC-MS/MS, about 95% of all spectra were now annotated by exact chemical structures or by chemical classes (MSI level 3, Figure 1). Results of classifications are organized into Kingdom, Superclass, Class, Subclass, and two parent levels. Detailed results are given in Table S4, with varying chemical classes present in urines of different patients. An average MSI level 3 classification is given in Figure 3 using the superclass and subclass classifications as defined by ClassyFire. Roughly one-third of the urinary metabolome was classified as chemicals containing aromatic rings or heterocycles, one-third was classified as compounds containing ketones, alcohols, or acids, while the remaining one-third consisted of lipids, phenylpropanoids, and nitrogenous- or sulfur containing organics. As expected, organic phosphates, organometallic, or other compound classes comprised less than 1% of the urinary metabolome.

CONCLUSION

Unlike proteomic MS/MS spectra assignments, the field of metabolomics currently lacks generally accepted and validated automated calculations of compound identification confidence levels with false-discovery rate assessments. As remedy, structure annotation in untargeted MS/MS metabolomics reports must be annotated with MSI confidence levels to detail which metabolites can be trusted and used for metabolic pathway annotations (MSI level 1 and 2), especially if annotated spectra use accurate mass information and manual curation. While the majority of acquired MS/MS spectra cannot be annotated with certainty to specific chemicals, Sirius/CSI:Finger ID and NIST17 hybrid search results yield many structure assignments that are worthy to be validated by acquiring spectra from corresponding authentic chemicals. In addition, MSI level 3 chemical classes can be ordered by ClassyFire and used for chemical class enrichment statistics,⁴⁸ for example, in biomarker discovery studies. Moreover, MSI level 3 classifications may yield differences in urinary chemicals that detail differences in subjects due to diet and chemical exposure in epidemiology studies.

ASSOCIATED CONTENT

Supporting Information

The Supporting Information is available free of charge on the ACS Publications website at DOI: 10.1021/acs.analchem.8b04698.

Table S1, settings used for LC-MS/MS data processing of polar metabolites and biogenic amines (XLSX)

Table S2, multilevel compound annotations (XLSX)

Table S3, HILIC library annotations of all 43 IC patients (XLSX)

Table S4, structural classification of all spectra from 43 IC patients (XLSX)

AUTHOR INFORMATION

Corresponding Author

*Phone +1-530-754-8258 (office), +1-530-752-9922 (lab), +1-530-723-4450 (cell). Corresponding author address: NIH West Coast Metabolomics Center, UC Davis Genome Center, Room 1313, 451 Health Sci Drive, Davis, CA 95616.

ORCID

Tobias Kind: 0000-0002-1908-4916

Oliver Fiehn: 0000-0002-6261-8928

Author Contributions

I.B., T.K., J.J., K.J., D.J., and O.F. designed the study. Data processing and compound ID were performed by I.B. Data analysis, figures, and tables were produced by I.B. and O.F. T.K. processed data using CSI:FingerID, B.R. and B.W. assisted in sample preparation, data preprocessing, and validation, J.K. and O.F. edited the manuscript, H.T. assisted with Java support, A.V. performed IDs using *in silico* fragmentation tools, M.S. provided assistance with the HILIC library, and K.J., T.L., and H.S. selected the cohort and provided the IC urine samples. The manuscript was written through the support of all authors. All authors have given approval to the final version of the manuscript.

Notes

The authors declare no competing financial interest.

ACKNOWLEDGMENTS

The authors acknowledge support from National Institutes of Health grant U2C ES030158 (to O.F.) and the following grants to J.K.: NIH U01 DK103260, R01 DK100974, U01 DP006079, NIH NCATS UCLA CTSI UL1 TR000124, Department of Defense grant W81XWH-15-1-0415, IMAGINE NO IC research grant, the Steven Spielberg Discovery Fund in Prostate Cancer Research Career Development Award, and the U.S.-Egypt Science and Technology Joint Fund. The funders had no role in the design, data collection, and analysis, decision to publish, or preparation of the manuscript.

REFERENCES

- (1) Jacob, M.; Lopata, A. L.; Dasouki, M.; Abdel Rahman, A. M. *Mass Spectrom. Rev.* **2017**, DOI: 10.1002/mas.21548.
- (2) Bloszies, C. S.; Fiehn, O. *Current Opinion in Toxicology* **2018**, *8*, 87–92.
- (3) Blazenovic, I.; Kind, T.; Ji, J.; Fiehn, O. *Metabolites* **2018**, *8*, 31.
- (4) Yang, J. S.; Lee, J. C.; Byeon, S. K.; Rha, K. H.; Moon, M. H. *Anal. Chem.* **2017**, *89*, 2488–2496.
- (5) Erkan, E.; Zhao, X.; Setchell, K.; Devarajan, P. *Pediatr. Nephrol.* **2016**, *31*, 581–588.

- (6) Antunes-Lopes, T.; Cruz, C. D.; Cruz, F.; Sievert, K. D. *Current opinion in urology* **2014**, *24*, 352–357.
- (7) Kuo, H. C. *Int. J. Urol.* **2014**, *21* (S1), 34–41.
- (8) Pedroza-Diaz, J.; Rothlisberger, S. *Biochemia medica* **2015**, *25*, 22–35.
- (9) Clemens, J. Q.; Clauw, D. J.; Kreder, K.; Krieger, J. N.; Kusek, J. W.; Lai, H. H.; Rodriguez, L.; Williams, D. A.; Hou, X.; Stephens, A.; Landis, J. R.; MAPP Research Network. *J. Urol.* **2015**, *193*, 1554–1558.
- (10) Naliboff, B. D.; Stephens, A. J.; Afari, N.; Lai, H.; Krieger, J. N.; Hong, B.; Lutgendorf, S.; Strachan, E.; Williams, D.; MAPP Research Network. *Urology* **2015**, *85*, 1319–1327.
- (11) Hanno, P. M.; Burks, D. A.; Clemens, J. Q.; Dmochowski, R. R.; Erickson, D.; Fitzgerald, M. P.; Forrest, J. B.; Gordon, B.; Gray, M.; Mayer, R. D.; Newman, D.; Nyberg, L., Jr.; Payne, C. K.; Wessellmann, U.; Faraday, M. M. *J. Urol.* **2011**, *185*, 2162–2170.
- (12) Schymanski, E. L.; Jeon, J.; Gulde, R.; Fenner, K.; Ruff, M.; Singer, H. P.; Hollender, J. *Environ. Sci. Technol.* **2014**, *48*, 2097–2098.
- (13) Kind, T.; Tsugawa, H.; Cajka, T.; Ma, Y.; Lai, Z.; Mehta, S. S.; Wohlgemuth, G.; Barupal, D. K.; Showalter, M. R.; Arita, M.; Fiehn, O. *Mass Spectrom. Rev.* **2018**, *37*, 513–532.
- (14) Wen, H.; Lee, T.; You, S.; Park, S. H.; Song, H.; Eilber, K. S.; Anger, J. T.; Freeman, M. R.; Park, S.; Kim, J. J. *Proteome Res.* **2015**, *14*, 541–548.
- (15) Cajka, T.; Fiehn, O.: LC–MS-Based Lipidomics and Automated Identification of Lipids Using the LipidBlast In-Silico MS/MS Library. In *Lipidomics: Methods and Protocols*; Bhattacharya, S. K., Ed.; Springer New York: New York, NY, 2017; pp 149–170, DOI: 10.1007/978-1-4939-6996-8_14.
- (16) Matyash, V.; Liebisch, G.; Kurzchalia, T. V.; Shevchenko, A.; Schwudke, D. *J. Lipid Res.* **2008**, *49*, 1137–1146.
- (17) Cajka, T.; Smilowitz, J. T.; Fiehn, O. *Anal. Chem.* **2017**, *89*, 12360–12368.
- (18) Tsugawa, H.; Cajka, T.; Kind, T.; Ma, Y.; Higgins, B.; Ikeda, K.; Kanazawa, M.; VanderGheynst, J.; Fiehn, O.; Arita, M. *Nat. Methods* **2015**, *12*, 523–526.
- (19) Wanichthanarak, K.; Fan, S.; Grapov, D.; Barupal, D. K.; Fiehn, O. *PLoS One* **2017**, *12*, No. e0171046.
- (20) Wishart, D. S.; Feunang, Y. D.; Marcu, A.; Guo, A. C.; Liang, K.; Vazquez-Fresno, R.; Sajed, T.; Johnson, D.; Li, C.; Karu, N.; Sayeeda, Z.; Lo, E.; Assempour, N.; Berjanskii, M.; Singhal, S.; Arndt, D.; Liang, Y.; Badran, H.; Grant, J.; Serra-Cayuela, A.; Liu, Y.; Mandal, R.; Neveu, V.; Pon, A.; Knox, C.; Wilson, M.; Manach, C.; Scalbert, A. *Nucleic Acids Res.* **2018**, *46*, D608–D617.
- (21) Wang, M.; Carver, J. J.; Phelan, V. V.; Sanchez, L. M.; Garg, N.; Peng, Y.; Nguyen, D. D.; Watrous, J.; Kapono, C. A.; Luzzatto-Knaan, T.; Porto, C.; Bouslimani, A.; Melnik, A. V.; Meehan, M. J.; Liu, W. T.; Crusemann, M.; Boudreau, P. D.; Esquenazi, E.; Sandoval-Calderon, M.; Kersten, R. D.; Pace, L. A.; Quinn, R. A.; Duncan, K. R.; Hsu, C. C.; Floros, D. J.; Gavilan, R. G.; Kleigrewe, K.; Northen, T.; Dutton, R. J.; Parrot, D.; Carlson, E. E.; Aigle, B.; Michelsen, C. F.; Jelsbak, L.; Sohlenkamp, C.; Pevzner, P.; Edlund, A.; McLean, J.; Piel, J.; Murphy, B. T.; Gerwick, L.; Liaw, C. C.; Yang, Y. L.; Humpf, H. U.; Maansson, M.; Keyzers, R. A.; Sims, A. C.; Johnson, A. R.; Sidebottom, A. M.; Sedio, B. E.; Klitgaard, A.; Larson, C. B.; Boya, P. C. A.; Torres-Mendoza, D.; Gonzalez, D. J.; Silva, D. B.; Marques, L. M.; Demarque, D. P.; Pociute, E.; O'Neill, E. C.; Briand, E.; Helfrich, E. J. N.; Granatosky, E. A.; Glukhov, E.; Ryffel, F.; Houson, H.; Mohimani, H.; Kharbush, J. J.; Zeng, Y.; Vorholt, J. A.; Kurita, K. L.; Charusanti, P.; McPhail, K. L.; Nielsen, K. F.; Vuong, L.; Elfeki, M.; Traxler, M. F.; Engene, N.; Koyama, N.; Vining, O. B.; Baric, R.; Silva, R. R.; Mascuch, S. J.; Tomasi, S.; Jenkins, S.; Macherla, V.; Hoffman, T.; Agarwal, V.; Williams, P. G.; Dai, J.; Neupane, R.; Gurr, J.; Rodriguez, A. M. C.; Lamsa, A.; Zhang, C.; Dorrestein, K.; Duggan, B. M.; Almaliti, J.; Allard, P. M.; Phapale, P. *Nat. Biotechnol.* **2016**, *34*, 828–837.
- (22) Kind, T.; Liu, K. H.; Lee, D. Y.; DeFelice, B.; Meissen, J. K.; Fiehn, O. *Nat. Methods* **2013**, *10*, 755–758.
- (23) Kind, T.; Okazaki, Y.; Saito, K.; Fiehn, O. *Anal. Chem.* **2014**, *86*, 11024–11027.
- (24) Duhrkop, K.; Shen, H.; Meusel, M.; Rousou, J.; Bocker, S. *Proc. Natl. Acad. Sci. U. S. A.* **2015**, *112*, 12580–12585.
- (25) Burke, M. C.; Mirokhin, Y. A.; Tchekhovskoi, D. V.; Markey, S. P.; Heidbrink Thompson, J.; Larkin, C.; Stein, S. E. *J. Proteome Res.* **2017**, *16*, 1924–1935.
- (26) Kim, W. T.; Yun, S. J.; Yan, C.; Jeong, P.; Kim, Y. H.; Lee, I. S.; Kang, H. W.; Park, S.; Moon, S. K.; Choi, Y. H.; Choi, Y. D.; Kim, I. Y.; Kim, J.; Kim, W. J. *Yonsei Med. J.* **2016**, *57*, 865–871.
- (27) Mirzoyan, K.; Klavins, K.; Koal, T.; Gillet, M.; Marsal, D.; Denis, C.; Klein, J.; Bascands, J. L.; Schanstra, J. P.; Saulnier-Blache, J. S. *Biochem. Biophys. Res. Commun.* **2017**, *487*, 109–115.
- (28) Rauschert, S.; Uhl, O.; Koletzko, B.; Hellmuth, C. *Ann. Nutr. Metab.* **2014**, *64*, 314–324.
- (29) Ganti, S.; Taylor, S. L.; Kim, K.; Hoppel, C. L.; Guo, L.; Yang, J.; Evans, C.; Weiss, R. H. *Int. J. Cancer* **2012**, *130*, 2791–2800.
- (30) Solberg, H. E.; Bremer, J. *Biochim. Biophys. Acta, Gen. Subj.* **1970**, *222*, 372–380.
- (31) Horai, H.; Arita, M.; Kanaya, S.; Nihei, Y.; Ikeda, T.; Suwa, K.; Ojima, Y.; Tanaka, K.; Tanaka, S.; Aoshima, K.; Oda, Y.; Kakazu, Y.; Kusano, M.; Tohge, T.; Matsuda, F.; Sawada, Y.; Hirai, M. Y.; Nakanishi, H.; Ikeda, K.; Akimoto, N.; Maoka, T.; Takahashi, H.; Ara, T.; Sakurai, N.; Suzuki, H.; Shibata, D.; Neumann, S.; Iida, T.; Tanaka, K.; Funatsu, K.; Matsuura, F.; Soga, T.; Taguchi, R.; Saito, K.; Nishioka, T. *J. Mass Spectrom.* **2010**, *45*, 703–714.
- (32) Zhu, Z.-J.; Schultz, A. W.; Wang, J.; Johnson, C. H.; Yannone, S. M.; Patti, G. J.; Siuzdak, G. *Nat. Protoc.* **2013**, *8*, 451–460.
- (33) Sawada, Y.; Nakabayashi, R.; Yamada, Y.; Suzuki, M.; Sato, M.; Sakata, A.; Akiyama, K.; Sakurai, T.; Matsuda, F.; Aoki, T.; Hirai, M. Y.; Saito, K. *Phytochemistry* **2012**, *82*, 38–45.
- (34) Ma, Y.; Kind, T.; Vaniya, A.; Gennity, I.; Fahrman, J. F.; Fiehn, O. *J. Cheminf.* **2015**, *7*, 53.
- (35) Blazenovic, I.; Shen, T.; Mehta, S. S.; Kind, T.; Ji, J.; Piparo, M.; Cacciola, F.; Mondello, L.; Fiehn, O. *Anal. Chem.* **2018**, *90*, 10758–10764.
- (36) Bouatra, S.; Aziat, F.; Mandal, R.; Guo, A. C.; Wilson, M. R.; Knox, C.; Bjorn Dahl, T. C.; Krishnamurthy, R.; Saleem, F.; Liu, P.; Dame, Z. T.; Poelzer, J.; Huynh, J.; Yallou, F. S.; Psychogios, N.; Dong, E.; Bogumil, R.; Roehring, C.; Wishart, D. S. *PLoS One* **2013**, *8*, No. e73076.
- (37) Zaghlool, S. B.; Mook-Kanamori, D. O.; Kader, S.; Stephan, N.; Halama, A.; Engelke, R.; Sarwath, H.; Al-Dous, E. K.; Mohamoud, Y. A.; Roemisch-Margl, W.; Adamski, J.; Kastenmuller, G.; Friedrich, N.; Visconti, A.; Tsai, P. C.; Spector, T.; Bell, J. T.; Falchi, M.; Wahl, A.; Waldenberger, M.; Peters, A.; Gieger, C.; Pezer, M.; Lauc, G.; Graumann, J.; Malek, J. A.; Suhre, K. *Hum. Mol. Genet.* **2018**, *27*, 1106–1121.
- (38) da Silva, R. R.; Dorrestein, P. C.; Quinn, R. A. *Proc. Natl. Acad. Sci. U. S. A.* **2015**, *112*, 12549–12550.
- (39) Tsugawa, H.; Kind, T.; Nakabayashi, R.; Yukihira, D.; Tanaka, W.; Cajka, T.; Saito, K.; Fiehn, O.; Arita, M. *Anal. Chem.* **2016**, *88*, 7946–7958.
- (40) Allen, F.; Pon, A.; Wilson, M.; Greiner, R.; Wishart, D. *Nucleic Acids Res.* **2014**, *42*, W94–99.
- (41) Schymanski, E. L.; Ruttkies, C.; Krauss, M.; Brouard, C.; Kind, T.; Duhrkop, K.; Allen, F.; Vaniya, A.; Verdegem, D.; Bocker, S.; Rousou, J.; Shen, H.; Tsugawa, H.; Sajed, T.; Fiehn, O.; Ghesquiere, B.; Neumann, S. *J. Cheminf.* **2017**, *9*, 22.
- (42) Blazenovic, I.; Kind, T.; Torbasinovic, H.; Obrenovic, S.; Mehta, S. S.; Tsugawa, H.; Wermuth, T.; Schauer, N.; Jahn, M.; Biedendieck, R.; Jahn, D.; Fiehn, O. *J. Cheminf.* **2017**, *9*, 32.
- (43) Nikolic, D.; Macias, C.; Lankin, D. C.; van Breemen, R. B. *Rapid Commun. Mass Spectrom.* **2017**, *31*, 1385–1395.
- (44) Showalter, M. R.; Cajka, T.; Fiehn, O. *Curr. Opin. Chem. Biol.* **2017**, *36*, 70–76.
- (45) Djoumbou Feunang, Y.; Eisner, R.; Knox, C.; Chepelev, L.; Hastings, J.; Owen, G.; Fahy, E.; Steinbeck, C.; Subramanian, S.; Bolton, E.; Greiner, R.; Wishart, D. S. *J. Cheminf.* **2016**, *8*, 61.

- (46) Heller, S. R.; McNaught, A.; Pletnev, I.; Stein, S.; Tchekhovskoi, D. *J. Cheminf.* **2015**, *7*, 23.
- (47) Wohlgemuth, G.; Haldiya, P. K.; Willighagen, E.; Kind, T.; Fiehn, O. *Bioinformatics* **2010**, *26*, 2647–2648.
- (48) Barupal, D. K.; Fiehn, O. *Sci. Rep.* **2017**, *7*, 14567.



Innovative technologies for the smart E-Healthcare system

“Oh wow, a dolphin! It looks so real and it’s swimming around me.” Calming music in the background mingles with the faint sound of ocean water and aquatic animals. Several clown fish slowly move into view and swim in a circle. A cute dolphin beckons, as if to play, and a big whale is seen leisurely swimming in the distance.

Michael, a six-year old boy with burns on his two legs due to recent car accident, is enjoying his deep-sea adventure through smart phone virtual reality (VR), a three-dimensional (3D) computer-generated virtual environment. It was only a week ago when he was living in constant fear and pain from the daily dressing of his burn wounds at the hospital. His physicians needed to prescribe heavy doses of strong intravenous pain medication during these sessions. However, a VR kit was recently recommended as an alternative for Michael’s pain management.

For severe, acute, and/or chronic pain, various painkillers, including opioids, are being used. Unfortunately, use of such powerful painkillers can often lead to financial burden and potential drug addiction. Misuse of addictive painkillers leads to the overdosing and death of about 47,000 people a year [1]. More and more physicians are starting to consider VR technologies as an alternative to painkillers. The basic idea behind using VR for pain management is that immersive environment and stimuli can distract patients from their pain and emotional states. In particular, hospitalized and/or bed-bound patients, such as women in labor and patients receiving chemotherapy, dialysis, radiation, or imaging procedures, may have biopsychosocial distress, such as depression, anxiety, and boredom due to their health condition and environment changes. Since 1996, the Harborview Burn Center in Seattle has used VR for burn patients, which has helped distract patients by providing relief and escape from painful treatments [2]. Recent studies from my institute at Cedars-Sinai Medical Center and others explored the use of VR in 100 hospitalized

patients and found that those who participated in VR therapy showed a significant reduction in pain scores [3]. This suggests that VR may offer holistic inpatient care by effectively reducing anxiety and pain perception and helping patients relax before, during, or after procedures. Additionally, VR technology is now becoming more user-friendly, cost-effective, interactive, flexible, immersive, and portable. VR is now being considered an effective, safe, and feasible intervention for a variety of disease states, such as obesity, anxiety, eating disorders, post-traumatic stress disorder, cancer, Parkinson's, nicotine/alcohol addiction, cognitive/motor rehabilitation et al. However, the challenge remains on figuring out how to incorporate VR into standard of care procedures in the everyday clinical setting.

One interesting use of VR could be in urology. Medical training using VR and/or AR (augmented reality, an interactive experience of environments where objects in the real-world are "augmented" by computer-generated perceptual information) could improve education and surgical practice, thereby increasing the speed and accuracy of certain procedures. The traditional Halstedian method of “see one, do one, teach one” in medical training could be improved by applying VR/AR-based simulators before performing live surgery. Complicated anatomy can be visualized in a 3D hologram format, and AR navigation can then facilitate the recognition and localization of anatomic structures. Using a projector beam and a see-through device, such as a smart google, physicians can see the virtual model directly projected on the patient. Furthermore, individual medical records can be reviewed, and images can be portrayed on screens during camera-based AR procedures. VR stimulation training has also been shown to result in superior speed and significant reduction of procedure-related complications. VR/AR stimulators can provide a variety of surgical scenarios that can be used during medical training to improve the overall skills required for operations, such as transurethral

resection of the prostate or prostatectomy. It can record the operative process of trainees in real-time, which can be used for evaluations. Considering how robotic surgical procedures continue to grow rapidly, a computer-derived virtual operative field with a tactile feedback system could be a new reliable standard method in robotic training programs.

A VR/AR simulator can not only be applied for surgeries, but also for personalized treatment of debilitating benign bladder dysfunctions, such as interstitial cystitis (IC)/painful bladder syndrome. IC is characterized by a need for frequent urination, typically urgent (and often uncontrollable), involuntary episodes, and flares of acute pain without any bacterial or yeast infections [4]. Along with no known etiology, IC has been challenging to urologists because there are no effective pharmacological, surgical, or behavioral treatments available. Current recommendations include exercising specific pelvic floor muscles to reduce severe urinary symptoms. To train unconscious physiological processes, a VR/AR-based biofeedback designed to visualize these exercising muscles could be applied. If patients can see the pelvic floor muscles through a head-mounted display, tablet, or hologram, they can easily understand exactly which muscles they are working and focus their efforts with more specificity; thereby, improving the overall efficacy of the therapy.

Including our own group, many scientific investigators have been developing biomarkers specific to each urological disease using biospecimens from tissues, blood, or other body fluids [5]. It is widely accepted that molecular biomarkers are useful since they can be used for prognoses and treatment response monitoring. Of note, accurate real-time monitoring can be immensely helpful for disease prevention, early diagnosis, and reduction of incidence rates. Biosensors are analytical devices designed to detect biological and physiochemical biomarkers and have been developed into smart health monitoring devices that can wirelessly sync with smartphones [6]. Data collection, storage, and analysis can be done in the connected cloud environment. The key components of potentially successful biosensors in the clinical setting include portability, rapidity, and cost-effectiveness. In particular, for efficient application in communication between urologists and patients, more effort should be placed on developing newer generations of highly sensitive molecular diagnostic biosensors with compact and user-friendly platforms.

While blood tests are currently the gold standard for noninvasive, painless, and continuous monitoring of biomarkers, urine is a particularly attractive resource in the urology field. Urine biosensors may provide real-

time levels of the patients' urinary metabolite biomarkers, electrolytes, temperature, and pH. There have been studies on developing rapid diagnoses of urinary tract infections (UTIs) in the clinical setting, which would allow for the early identification of UTI and timely antibiotic treatment. UTI is one of the most common infections in women, elders, and infants. Recently, investigators developed a small and disposable UTI biosensor embedded in a diaper. When activated upon exposure to urine, the self-powered sensor can determine the presence of chemical compounds associated with UTI [7]. The data can then be collected via a wireless smartphone app and used for further analysis by urologists and patients, allowing them to discuss the patterns of UTI. For other bladder diseases, such as IC, urinary biosensors may be able to facilitate real-time identification of flares (acute pain) and fluctuation of biomarkers, such as specific metabolites [5]; thereby enabling personalized treatment regimens for patients. Wearable wireless urinary metabolic sensors enable remote tracking of disease biomarkers and bladder health 24/7. They can replace bladder diaries (voiding diaries) and help accelerate interventions regardless of location, time, or device.

Research related to smart health devices is already changing the paradigm of the healthcare industry. Smart healthcare is characterized by eHealth, which is supported by computer-based information and communication technology, and mHealth services, a medical practice supported by mobile devices. Our healthcare system is now rapidly evolving for better patient diagnoses and treatment by establishing the personal digital assistants for electronic record management and smart remote services through biosensor platforms that are wirelessly connected between urologists and patients.

CONFLICTS OF INTEREST

The authors have nothing to disclose.

ACKNOWLEDGMENTS

The authors acknowledge support from National Institutes of Health grants (1U01DK103260, 1R01DK100974, U24 DK097154, NIH NCATS UCLA CTSI UL1TR000124), Department of Defense grants (W81XWH-15-1-0415), Centers for Disease Controls and Prevention (1U01DP006079), the US-Egypt Science and Technology Joint Fund by National Academies of Sciences, Engineering, and Medicine (NAS) and The United States Agency for International Development (USAID) (to J.K.). Any opinions, findings, conclusions, or

recommendations expressed in this article are those of the authors alone, and do not necessarily reflect the views of USAID or NAS. And this research was supported by the International Science and Business Belt Program through the Ministry of Science, ICT and Future Planning (to W.J.K.) (2015-DD-RD-0070).

Wun-Jae Kim¹, Jayoung Kim²

Corresponding Author: Wun-Jae Kim

ORCID: <https://orcid.org/0000-0002-8060-8926>

¹Department of Urology, Chungbuk National University
College of Medicine, Cheongju, Korea

²Departments of Surgery and Biomedical Sciences,
Cedars-Sinai Medical Center, Los Angeles, CA, USA

E-mail: wjkim@chungbuk.ac.kr

REFERENCES

1. Rudman W Jr, Corcoran P, Elliott K. Prescription drug monitoring programs and opioid death rates. *JAMA* 2017 Nov 28 [Epub]. <http://doi.org/10.1001/jama.2017.16300>.
2. Escudero LA, Cerutti S, Olsina RA, Salonia JA, Gasquez JA. Factorial design optimization of experimental variables in the on-line separation/preconcentration of copper in water samples using solid phase extraction and ICP-OES determination. *J Hazard Mater* 2010;183:218-23.
3. Tashjian VC, Mosadeghi S, Howard AR, Lopez M, Dupuy T, Reid M, et al. Virtual reality for management of pain in hospitalized patients: results of a controlled trial. *JMIR Ment Health* 2017 Mar 29 [Epub]. <http://doi.org/10.2196/mental.7387>.
4. McLennan MT. Interstitial cystitis: epidemiology, pathophysiology, and clinical presentation. *Obstet Gynecol Clin North Am* 2014;41:385-95.
5. Wen H, Lee T, You S, Park SH, Song H, Eilber KS, et al. Urinary metabolite profiling combined with computational analysis predicts interstitial cystitis-associated candidate biomarkers. *J Proteome Res* 2015;14:541-8.
6. Jayanthi VSPKSA, Das AB, Saxena U. Recent advances in biosensor development for the detection of cancer biomarkers. *Biosens Bioelectron* 2017;91:15-23.
7. Yu W, Seo W, Tan T, Jung B, Ziaie B. A diaper-embedded disposable nitrite sensor with integrated on-board urine-activated battery for UTI screening. *Conf Proc IEEE Eng Med Biol Soc* 2016;2016:303-6.



Application of Low-Cost, Easy-to-Use, Portable Biosensor Systems for Diagnosing Bladder Dysfunctions

Nosang V. Myung¹, Sungyong Jung², Jayoung Kim^{3,4,5,6}

¹Department of Chemical and Environmental Engineering, University of California Riverside, Riverside, CA, USA

²Department of Electrical Engineering, University of Texas at Arlington, Arlington, TX, USA

³Departments of Surgery and Biomedical Sciences, Cedars-Sinai Medical Center, Los Angeles, CA, USA

⁴Samuel Oschin Comprehensive Cancer Institute, Cedars-Sinai Medical Center, Los Angeles, CA, USA

⁵University of California Los Angeles, Los Angeles, CA, USA


⁶Department of Urology, Gacheon University College of Medicine, Incheon, Korea

To the editor

A recently published series of articles in the *International Neurourology Journal* elegantly presented the current trends in Smart Health. In particular, 3 articles by Taeg-Keun Whangbo and colleagues [1,2] and Kang et al. [3] summarized how close we are to making personalized technology-based healthcare a reality in the clinical setting. Given that the authors provided an overview of the current applications of newly emerging technologies, we thought about how they could be utilized for diagnosing and monitoring nonfatal bladder diseases, such as interstitial cystitis (IC). Because of its unknown etiology and symptomatic manifestation as urinary discomfort in the absence of other causes, diagnosing IC is dependent on clinical parameters, such as pain, urinary urgency, and frequency. Additionally, due to the lack of proper conventional markers, diagnosis involves traditional urinalysis, urine culture, cystoscopy, bladder biopsy, and bladder hydro-distention. IC can cause a multitude of symptoms that have a negative impact on sexual activity and quality of life. The most significantly reported concern is chronic pelvic pain [4], which can also create sexual dysfunctions. Although the financial and personal burden of IC is extensive on the American public [5], there is still no clear diagnostic test for IC. Although our own group and several other laboratories have identified a series of IC urinary biomarkers, it is still unknown whether they would be clinically useful. Expanding use

of this knowledge is costly and complexity of conventional analytical platforms, such as mass spectrometry, is hard to implement clinically.

Evaluating the impact duration, severity, pain localization, anxiety, and depression related to bladder dysfunctions may help identify risk factors. In addition to our own laboratory, many scientists have focused on developing biomarkers specific to each urological disease using biospecimens, such as tissue, blood, or other bodily fluids. Molecular biomarkers are widely accepted as a useful resource for prognoses and treatment response monitoring. Most importantly, accurate real-time monitoring of biomarkers may be immensely helpful for disease prevention, early diagnosing, and incidence rate reduction. Active oversight of biomarkers could be implemented using biochemical sensors, which are analytical devices designed to detect biological or physiochemical markers, that can also be integrated with other smart health monitoring devices that sync wirelessly with smartphones. This data can be collected, stored, and analyzed in a shared cloud environment between patients and physicians. In order for such internet of biosensors to be successful in the clinical setting, they need to be portable, rapid, and cost-effective. For particularly efficient application in urology, effort should be focused on developing next generations of highly sensitive diagnostic biosensors that are portable, user-friendly, and low cost.

Corresponding author: Jayoung Kim  <https://orcid.org/0000-0002-3683-4627>
Departments of Surgery and Biomedical Sciences, Cedars-Sinai Medical Center, Davis 5071, 8700 Beverly Blvd., Los Angeles, CA 90048, USA
E-mail: Jayoung.Kim@cshs.org / Tel: +1-310-423-7168 / Fax: +1-310-967-3809
Submitted: January 21, 2019 / **Accepted after revision:** January 24, 2019



This is an Open Access article distributed under the terms of the Creative Commons Attribution Non-Commercial License (<http://creativecommons.org/licenses/by-nc/4.0/>) which permits unrestricted non-commercial use, distribution, and reproduction in any medium, provided the original work is properly cited.

Biosensors are analytical devices that can selectively detect and quantitatively measure analytes interacting with biological elements, such as tissues, microorganisms, antibodies, and nucleic acids. Biosensors consist of receptor-functionalized sensing materials that react to analytes and transducers that can convert biological responses into electrical signals. It is integrated with electronic circuits to readout and process signals, including amplifying, filtering, digitizing, analyzing, interfacing, transmitting, and displaying. The readout circuits are typically implemented with an operational amplifier, an analog-to-digital converter, a microcontroller, and a communication device. The types of biosensors can be categorized based on their detection mechanisms, such as electrochemical, thermal, electrical, magnetic, optical, and piezoelectric. Among these biosensors, electrochemical sensors are the most versatile, portable, and highly developed (approximately 58% of all chemical sensors) in the market. Prime examples of commercially available portable and easy-to-use electrochemical analyzers include glucose meters and portable blood analyzer (e.g., i-Stat Blood Chemistry Analyzer, Abbott, Princeton, NJ, USA), which have clearly demonstrated their ability to cost-effectively detect multiple analytes from small sample volumes. Like blood chemistry analyzers, high density electrochemical sensor arrays can be developed to accurately identify and quantify IC biomarkers from urine.

In addition to the development of portable analyzers for biological fluids, there has been rapid developments in gas sensor technology to mimic the human olfactory system to identify and quantify various gases (odors). This artificial olfactory system (e-nose) simulates the different stages of the human olfactory system, including sampling and filtering gaseous molecule. Using artificial gas sensors that odor molecules can react with, these sensors can then amplify and treat signal responses. Integrated artificial intelligence and web-based knowledge systems can evaluate key information to finally recognize the odor. Such devices could have a significant role in the early diagnosis and detection of IC by analyzing odors from urine samples.

Research and development related to mobile health devices will provide a game-changer in Smart Health and the future healthcare industry. Smart hospitals supported by computers, wireless network-based information, and communication technology are now rapidly evolving for more personalized care and electronic management of clinical records. As innovative thinkers, how can we apply biosensor technologies for medical diag-

nostics and health monitoring, particularly in urological care?

• **Conflict of Interest:** No potential conflict of interest relevant to this article was reported.

ACKNOWLEDGEMENTS

This was supported by the Future Materials Discovery Program from the National Research Foundation of Korea (NRF). Funding was received from the Ministry of Science, ICT & Future Planning (NRF-2016M3D1A1027836), and the NAVSEA METCAL program. The authors also acknowledge support from National Institutes of Health grants (1U01DK103260, 1R01DK100974, U24DK097154, NIH NCATS UCLA CTSI UL1TR000124), Department of Defense grants (W81XWH-15-1-0415), Centers for Disease Controls and Prevention (1U01DP006079), the U.S.-Egypt Science and Technology Joint Fund by National Academies of Sciences, Engineering, and Medicine (NAS) and The United States Agency for International Development (USAID) (to J.K.). Any opinions, findings, conclusions, or recommendations expressed in this article are those of the authors alone, and do not necessarily reflect the views of USAID or NAS.

REFERENCES

1. Whangbo TK, Eun SJ, Jung EY, Park DK, Kim SJ, Kim CH, et al. Personalized urination activity recognition based on a recurrent neural network using smart band. *Int Neurourol J* 2018;22(Suppl 2):S91-100.
2. Eun SJ, Whangbo TK, Park DK, Kim KH. Development of personalized urination recognition technology using smart bands. *Int Neurourol J* 2017;21(Suppl 1):S76-83.
3. Kang M, Park E, Cho BH, Lee KS. Recent patient health monitoring platforms incorporating internet of things-enabled smart devices. *Int Neurourol J* 2018;22(Suppl 2):S76-82.
4. Katz L, Tripp DA, Carr LK, Mayer R, Moldwin RM, Nickel JC. Understanding pain and coping in women with interstitial cystitis/bladder pain syndrome. *BJU Int* 2017;120:286-292.
5. Tung A, Hepp Z, Bansal A, Devine EB. Characterizing health care utilization, direct costs, and comorbidities associated with interstitial cystitis: a retrospective claims analysis. *J Manag Care Spec Pharm* 2017;23:474-82.

Downregulation of CENPF Remodels Prostate Cancer Cells and Alters Cellular Metabolism

Muhammad Shahid, Minhyung Kim, Min Young Lee, Austin Yeon, Sungyong You, Hyung L. Kim, and Jayoung Kim*

Metabolic alterations in prostate cancer (PC) are associated with progression and aggressiveness. However, the underlying mechanisms behind PC metabolic functions are unknown. The authors' group recently reported on the important role of centromere protein F (CENPF), a protein associated with the centromere–kinetochore complex and chromosomal segregation during mitosis, in PC MRI visibility. This study focuses on discerning the role of CENPF in metabolic perturbation in human PC3 cells. A series of bioinformatics analyses shows that CENPF is one gene that is strongly associated with aggressive PC and that its expression is positively correlated with metastasis. By identifying and reconstructing the CENPF network, additional associations with lipid regulation are found. Further untargeted metabolomics analysis using gas chromatography-time-of-flight-mass spectrometry reveals that silencing of CENPF alters the global metabolic profiles of PC cells and inhibits cell proliferation, which suggests that CENPF may be a critical regulator of PC metabolism. These findings provide useful scientific insights that can be applied in future studies investigating potential targets for PC treatment.

1. Introduction

Prostate cancer (PC) is the second most commonly diagnosed cancer and the fifth leading cause of male mortality worldwide, with an estimated 1.3 million new cases and 359 000 associated deaths in 2018.^[1,2] It is now widely accepted that proliferating cancer cells alter their metabolic activities to satisfy increased needs for energy and biosynthetic precursors, such as glucose.^[3] Rather than utilizing the normal process of oxidative phosphorylation, even with the presence of oxygen and fully functioning mitochondria, these proliferating cancer cells favor aerobic glycolysis, which dramatically increases the uptake of glucose and production of lactate; a process known as the Warburg Effect.^[4] Glutamine metabolism also plays a vital role in cancer cell energy metabolism by providing Krebs cycle intermediates, which further corroborates the idea of altered

cancer cell metabolism.^[5] Most cancers depend on increased glutaminolysis to compensate for increased energy needs and fill their carbon and nitrogen pools for the biosynthesis of macromolecules.^[6] Besides the higher utilization of the glycolytic pathway, cancer cells frequently exhibit a heightened ability to synthesize lipids, and this increased lipogenesis is tightly coupled to glucose metabolism.^[7,8] Reprogrammed energy metabolism is an important hallmark of the upkeep of altered homeostasis in cancer.^[9] For instance, increased glycolysis has been observed in many cancer types, including PC.^[10,11] Several studies have shown that this dysregulated metabolism plays a crucial role in PC progression.^[12–14] These alterations in metabolic features may represent potential prognostic biomarkers.^[15] Therefore, investigating PC metabolism could be an opportunity to find new prognostic or therapeutic biological markers.

Metabolomics involves the study of metabolism and metabolite profiling and is an important analytical tool used in oncology for discovering novel biosignatures and therapeutic targets.^[16] It is widely applied as an interdisciplinary omics approach, combining pattern recognition, bioinformatics, epidemiology, analytical biochemistry, and biology.^[17] This comprehensive analysis provides a valuable opportunity to better understand the biochemical changes underlying cancer metabolism and improve early detection, progression, and therapeutic monitoring.^[18] Metabolomics can also respond to clinical challenges by providing a method of

Dr. M. Shahid, Dr. M. Kim, A. Yeon, Prof. S. You, Prof. H. L. Kim, Prof. J. Kim

Department of Surgery
Cedars-Sinai Medical Center
Los Angeles, CA, USA
E-mail: jayoung.kim@cshs.org


Dr. M. Y. Lee
Institute for Systems Biology
98109, Seattle, WA, USA

Prof. S. You, Prof. H. L. Kim, Prof. J. Kim
Samuel Oschin Comprehensive Cancer Institute
Cedars-Sinai Medical Center
Los Angeles, CA, USA

Prof. S. You, Prof. J. Kim
Department of Biomedical Sciences
Cedars-Sinai Medical Center
Los Angeles, CA, USA

Prof. J. Kim
University of California Los Angeles
CA, USA

Prof. J. Kim
Department of Urology
Ga Cheon University College of Medicine
Incheon, South Korea

 The ORCID identification number(s) for the author(s) of this article can be found under <https://doi.org/10.1002/pmic.201900038>

DOI: 10.1002/pmic.201900038

detecting vital and promising novel biomarkers.^[19,20] In terms of cancer, metabolomics can enable additional measurement of downstream activities, thereby allowing for the discovery of key oncometabolites.^[21] These metabolites are markers of biochemical activity and are closely related to clinical phenotypes.^[22] An increasing number of metabolomic studies have focused on improving the current understanding of PC. There have been several attempts at capturing metabolic PC biomarkers due to evidence suggesting that perturbed metabolism may play a crucial role in the development and progression of PC.^[14] These metabolite profiles can be distinct and could provide important prognostic information. For example, a metabolomic study of PC and healthy controls found increased choline levels in malignant tissue.^[23] PC can be a particularly attractive model for metabolomic profiling; the healthy prostate has a unique metabolism that is needed for producing prostatic fluid and alterations can be feasibly tracked.^[24]

Our group recently conducted a transcriptomic study on magnetic resonance imaging (MRI)-visible and -invisible prostate cancers to find differentially expressed genes (DEGs) between the two groups. We identified centromere protein F (CENPF) as one of four genes related to MRI visibility, progression-free survival, and metastatic deposits.^[25] We further found that CENPF is a critical regulator of cancer metabolism, potentially through pyruvate kinase M2 (PKM2). Our findings align with previous reports suggesting that CENPF is a master regulator of malignancy in PC.^[26,27] PKM2 is also well known to be a key player in PC metabolism^[28]; however, its link between CENPF and the development of PC using untargeted metabolomics profiling has not been done before. By further defining the role of CENPF in PC, we can gain a deeper mechanistic understanding of its effects in downstream events and disease development.

This study aimed to determine the metabolic profile of CENPF-knockout (CENPF^{KO}) PC cells and identify differentially expressed metabolites (DEMs) that can be used as prognostic markers. Our experimental results showed that silencing of CENPF reduced global metabolism. Additional computational analysis demonstrated that CENPF regulates PC metabolism. Our results may allow us to derive new information that could be helpful in better targeting the underlying mechanisms driving PC.

2. Experimental Section

2.1. Cell Lines and Culturing

Human PC3 cells were obtained from American Type Culture Collection (ATCC) (Manassas, VA, USA). Cells were maintained in Dulbecco's modified Eagle medium (DMEM) supplemented with 10% heat-inactivated fetal bovine serum (FBS) and penicillin–streptomycin at 37 °C with 95% air and 5% CO₂. DMEM and FBS were purchased from Life Technologies (Grand Island, NY, USA). The CENPF^{KO} PC3 cell line was constructed using the CRISPR/Cas9 system by ALSTEM, LLC (Richmond, CA) and maintained as described previously.^[29] If frozen, after thawing, cells were used under ten passages. Mycoplasma contamination was monitored for periodically.

Significance Statement

PC remains to be a worldwide public health concern. It has been accepted that proliferating PC cells satisfy elevated energy requirements needed to support accelerated cell division by modulating metabolism. However, the mechanisms behind these metabolic alterations are largely unknown. One key modulator that has been previously identified is CENPF, which is shown to be upregulated in PC cells. Despite this knowledge, there has been no detailed systematic analysis on how CENPF regulates PC cellular metabolism. In this study, we aimed to better understand the global metabolic changes mediated by CENPF in PC cells using a quantitative metabolomics approach, which includes GC-TOF-MS. The metabolites and metabolic enzymes that we identified may serve as potential biomarkers or therapeutic targets. These findings shed new light on the biochemical mechanisms and biological functions of CENPF in PC and may pave the way for novel treatment options.

2.2. Identification of DEGs

The transcriptome of 1,321 PC patient samples was obtained from the Prostate Cancer Transcriptome Atlas (PCTA; www.thepcta.org), which was then used to develop the prostate cancer subtype (PCS) classification system.^[30] PC transcriptome data was then normalized and batch corrected by median-centering and quantile scaling (MCQ). Independent PC data describing gene expression changes in multiparametric (MP)-MRI-visible and invisible tumors based on ribonucleic acid (RNA) sequencing (GSE95369) was obtained from the Gene Expression Omnibus (GEO) database.^[31] Read count data was normalized using the TMM normalization method.^[32] The integrated hypothesis testing method was applied, as previously reported.^[33] Briefly, three independent statistical tests were performed, including the T-test, median ratio test, and rank-sum test, on each gene. To compute the significance level (*p*-values) of the observed T-values, log₂-median ratios, and rank-sum differences, the empirical null hypothesis distribution was used, which was estimated by random permutation of the samples. Finally, the adjusted *p*-values were computed using Stouffer's method.^[34] DEGs between MRI visible and invisible patients in the MP-MRI data were selected for if they had adjusted *p*-values <0.05 and absolute fold-changes ≥2. DEGs between metastatic castration-resistant prostate cancer (mCRPC) and primary patients in the PCTA were selected for if they had adjusted *p*-values <0.01 and absolute fold-changes ≥1.5. Functional enrichment analyses were performed using gene set enrichment analysis (GSEA) for hallmark gene sets^[35] and DAVID (Ver. 6.8).^[36]

2.3. Selection of CENPF Network Genes

To identify genes that are differentially regulated by CENPF in PC, samples were selected from the PCTA data with high and low CENPF expression. High and low CENPF samples were defined as those with upper and lower terciles of expression, respectively. The adjusted *p*-values were then computed using the

same method, as described above. DEGs between the high- and low-CENPF groups were selected if they had adjusted *p*-values <0.05.

2.4. Identification of Hub Genes in the CENPF Network

To identify hub genes that could be potential regulator candidates of the CENPF network in PC, protein–protein interactions were collected from six different databases; the Biological General Repository for Interaction Datasets (BioGRID)^[37], the Databased of Interacting Proteins (DIP)^[38], High Confidence Protein–Protein Interactions (HitPredict)^[39], the IntAct Molecular Interaction Database (IntAct)^[40], the Molecular INterAction Database (MINT)^[12] and the Functional Protein Associations Network (STRING)^[41]. The number of interactions in the up- and downregulated genes in the high and low-CENPF samples was then counted separately. Significance of the number of the interactions was computed as enrichment *p*-values using Fisher's exact test.

2.5. Reconstruction of a Network Model

To reconstruct a network model, we first selected for lipid metabolism and pathway-associated genes from the CENPF network genes using Gene Ontology Biological Process (GOBP). Then, protein–protein interaction and transcription factor (TF)-target interaction information of the differentially expressed lipid-related genes were collected from the six interactome databases that were used for our master regulator analysis. CENPF transcriptional target information from a prior study done by Aytes et al.^[26] was also included. The network was visualized using Cytoscape (v. 3.2.1).^[42]

2.6. GC-TOF-MS Analysis

Gas chromatography-time-of-flight-mass spectrometry (GC-TOF-MS) analysis was performed on CENPF^{KO} and control PC3 cells.^[43,44] Samples were dissolved in 1 ml of 20 °C mixture of acetonitrile, isopropanol, and water (3:3:2 v/v) at a pH of 7. The solution was then vortexed at 4 °C for 5 min. Samples were centrifuged for 2 min at 14 000 rcf and 500 μL were aliquoted. The aliquots were then evaporated in a Labconco Centrivap Cold Trap to complete dryness. The methoximation step was performed using a 10 μL solution of 40 mg mL⁻¹ of O-methylhydroxylamine hydrochloride (CAS: [593-56-6]^[6]; formula: CH₃NO.HCl) and shaken for 90 min at 30 °C. Then, 90 μL of *N*-methyl-*N*-trimethylsilyltrifluoroacetamide (MSTFA) was added and the solution was shaken for 30 min at 37 °C. After that, a 1 μL mixture of fatty acid methyl ester (FAME) retention time markers was added. The mixture was transferred to amber crimp autosampler vials. Measurements were done on a Leco Pegasus IV Time of Flight Mass Spectrometer coupled to an Agilent 6890GC with an Agilent 6890 Split/Splitless Injector.

The column used was a Restek RTX-5Sil MS (95% dimethyl/5% diphenyl polysiloxane), which had 30 m length, 0.25 mm i.d., 0.25 μm film thickness, and an additional 10 m guard column. The injection volume used was 1 μL at 250 °C. The GC parameters were set to have a constant helium flow of 1 mL min⁻¹ and an oven ramp temperature of 50 °C (1 min hold) that increased to 330 °C at a rate of 20 °C min⁻¹ with a 5 min hold before cool down. The transfer line temperature was set to 280 °C, and spectra were recorded in the electron ionization mode at 70 eV with a filament temperature of 250 °C TOF and scan range of 85–500 Da.

2.7. Annotation and Identification of Compounds

Detection or deconvolution of peaks and compounds was performed using the Leco ChromaTOF software. Spectra were matched against the FiehnLib Mass Spectral and Retention Index Library.^[23] Post-curation and peak replacements were done using the in-house developed BinBase software, which was set as follows: validity of chromatogram (<10 peaks with intensities >10⁷ counts per second), unbiased retention index marker detection (MS similarity >800, validity of intensity range for high *m/z* marker ions), and retention index calculation by 5th order polynomial regression. Sample matrices with all known and unknown compounds were then exported to a Microsoft excel sheet. A total of 524 compounds were detected. Of these, 144 were annotated as known compounds with KEGG compound identifier.

2.8. Normalization and Identification of DEMs

The raw data was normalized based on mTIC, which is the sum of all peak heights for all identified metabolites for a sample.^[45] The average mTIC was calculated and a normalization factor for a sample was defined by dividing the average mTIC by the mTIC of the individual sample. The normalized intensity was then calculated by multiplying the raw intensity by the normalization factor. DEMs were selected according to the criteria of a false discovery rate (FDR) adjusted *p*-value (*q*-value) ≤ 0.05 from a two-tailed Welch's *t*-test and a fold-change ≥ 1.5.^[46]

The normalized intensities of the 524 metabolites were transformed into log₂ scale and were standardized as *z*-score, and then principal component analysis (PCA) was applied to understand variations in the metabolite profiles of different cell lines. Hierarchical clustering of the DEMs was performed using Euclidean distance and ward linkage.

2.9. Metabolite Enrichment Analysis

Metabolites Biological Role (MBROLE) 2.0 was used to identify statistically significant metabolic pathways enriched by the DEMs.^[47] MBROLE is a web-based tool containing functional annotations on chemical compounds compiled from various public databases, such as the Kyoto Encyclopedia of Genes and Genomes (KEGG) and PubChem. *P*-Values are computed based

on hypergeometric distribution by comparing the number of metabolites in the DEMs and background set, which is the annotated metabolites with KEGG compound identifiers. Pathways with P -values < 0.1 and at least 2 DEMs were selected for functional interpretation.

2.10. Proliferation Assay

Trypan blue assay was carried out to assess cell proliferation. Briefly, cells were seeded at a density of 2×10^2 cells per well onto six-well culture plates in complete medium. Following 24 h of cell growth, each well culture was maintained and incubated for 48 h. The medium was replaced every day. After 48 h, cells were trypsinized, washed, and resuspended in PBS containing 0.4% trypan blue. The number of viable cells was counted using a hemocytometer, as per standard protocol. Each experiment was done a minimum of three independent times. The results are presented as the percentage of viable cells relative to that of the control.

2.11. Branched-Chain Amino Acid/Aromatic Amino Acid Ratio

The branched-chain amino acid (BCAA)/aromatic amino acid (AAA) ratio was calculated as the ratio between the concentration of BCAAs (valine, leucine, and isoleucine) and AAAs (phenylalanine and tyrosine).^[48]

$$\text{BCAA / AAA ratio} = \frac{[\text{valine}] + [\text{leucine}] + [\text{isoleucine}]}{[\text{phenylalanine}] + [\text{tyrosine}]}$$

The concentration of each amino acid was calculated by dividing the quantified intensity by the quantified m/z .

2.12. Acetate Measurement Assay

Acetate levels were measured using an Acetate Colorimetric Assay Kit (Biovision Inc.) according to the instructions provided. Briefly, cells (1×10^6) were rapidly homogenized with 100 μL of ice-cold acetate assay buffer for 10 min on ice. The mixture was then centrifuged at 12,000 rpm for 5 min, and the resulting supernatant was collected. After that, 1–50 μL of sample (50–200 μg) was added onto a 96-well plate. The final volumes were adjusted to 50 μL with acetate assay buffer. The reaction was incubated at room temperature for 40 min, and optical reading was taken at 450 nm using a spectrophotometer. The unknown sample concentration was calculated from the standard curve.

2.13. Statistical Analysis

Results were expressed as mean \pm standard error (SE) from at least three independent experiments. To evaluate differences between two groups, statistical analysis was done using Student's t -test. Unless otherwise indicated, $p < 0.05$ was deemed

significant. MATLAB (v.9.0; Mathworks, Natick, MA, USA) and R (v.3.5) were used for bioinformatic analyses.

3. Results

3.1. Transcriptome Analysis Reveals Genes Associated With Aggressive PC

To identify genes associated with aggressive PC, we utilized two independent transcriptome datasets. One was obtained from the PCTA database, which provided 1321 PC transcriptome profiles^[30] (hereafter referred to as PCTA). The other was from a separate study that examined the gene expression differences between MP-MRI-visible and invisible tumors^[25] (hereafter referred to as MRI). The transcriptome data was produced using RNA sequencing, and the count data was deposited in the GEO database under the accession number GSE95369. Of note, survival analysis of these independent study cohorts presented four gene signatures as being significantly correlated with metastatic progression and biochemical recurrence.

With this transcriptome data, we hypothesized that DEGs between mCRPC versus primary PC and MP-MRI-visible versus invisible tumors may be potential regulator candidates of PC progression. We then performed integrative hypothesis testing on the PCTA and MRI datasets to identify 182 (mCRPC vs PC) and 457 (MRI-visible vs invisible) DEGs (Figure 1A; see Section 2 for details). Between these two compared groups, ten shared DEGs were identified (Figure 1B). SPP1 (secreted phosphoprotein 1), CENPF, MEX3A (mex-3 RNA binding family member A), NUSAP1 (nucleolar and spindle associated protein 1), and TOP2A (DNA topoisomerase II alpha) were significantly upregulated in mCRPC and MRI-visible PC, while GAS1 (growth arrest specific 1), PGM5 (phosphoglucomutase 5), CHRDL1 (chordin-like 1), PCAT4 (prostate cancer associated transcript 4), and H19 (H19, imprinted maternally expressed transcript) were significantly downregulated. Interestingly, the clinical significance of CENPF in PC was previously reported^[49] and identified as a potential master node of PC malignancy.^[26]

3.2. CENPF Expression is Correlated with PC Progression

We examined CENPF expression in tissues with five distinct disease statuses (benign, Gleason score (GS) < 6 , $GS = 7$, $GS > 7$, and mCRPC) to discern the association of CENPF with disease progression (Figure 2A). Consistent with previous studies,^[27] CENPF gene expression levels increased significantly in higher GS and mCRPC tissue (one-way ANOVA $P < 0.001$, rank-sum $p < 0.001$). A prior cross-species study^[27] and MRI study^[25] revealed a regulatory relationship between CENPF and FOXM1 in PC progression. We thus checked for a correlation between CENPF and FOXM1 expression in the PCTA data.^[30] We found that expression of CENPF and FOXM1 exhibited a significant positive correlation in all PCTA samples and individual disease states (Figure 2B). This implies that gene expression and regulation of CENPF and FOXM1 are significantly associated with PC progression.

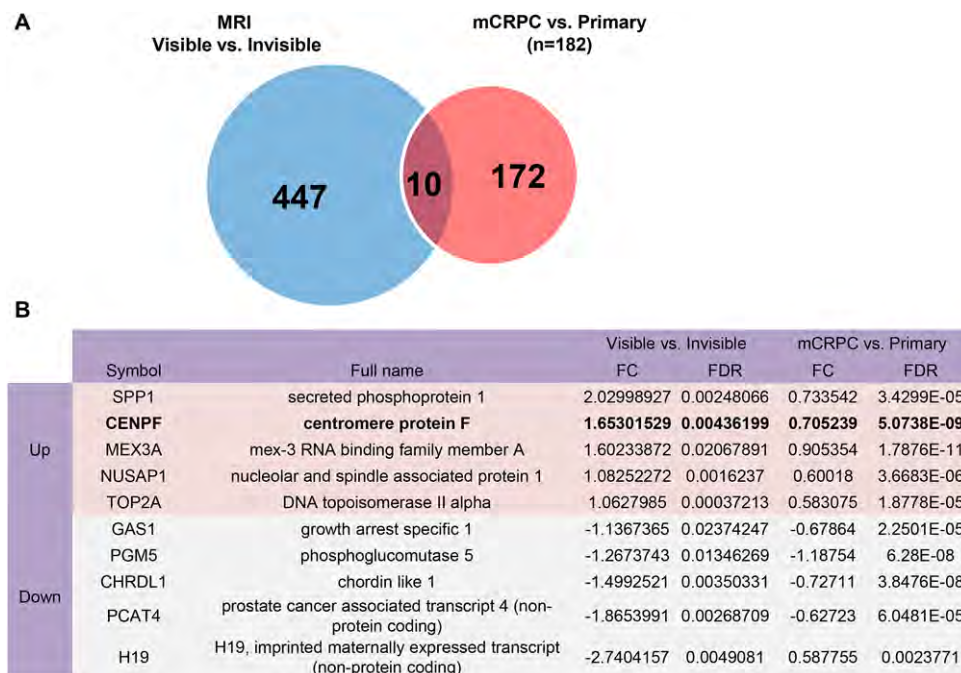


Figure 1. Selection of genes associated with aggressive PC. A) Venn diagram depicts the number of DEGs in MP-MRI-visible versus invisible tumors and mCRPC versus primary PC. Transcriptome data of MP-MRI visibility was obtained from the GEO database (GSE95369), and mCRPC and PC gene expression profiles are from PCTA. DEGs for MRI visibility were selected if they had an adjusted p -value < 0.05 and fold-change ≥ 2 . DEGs in the mCRPC and PC group were selected if they had an adjusted p -value < 0.01 and fold-change ≥ 1.5 . B) List of overlapping genes associated with both MRI visibility and metastatic progression.

3.3. Genes Involved in the CENPF Network in PC

Given the significance of CENPF expression in PC progression, investigating the downstream CENPF transcriptional network may be relevant in discovering the molecular mechanisms of PC. For this, we defined high and low CENPF-expressing groups in the PCTA by selecting for upper and lower terciles. Secondly, we identified significantly up and downregulated CENPF-associated genes in the high and low groups (Figure 3A). To identify molecular pathways and cellular processes regulated by CENPF, we then performed GSEA and functional enrichment analysis using hallmark gene sets from MsigDB and GOBP. GSEA results showed that the E2F target, G2M checkpoint, MYC target, and mitotic spindle gene sets were significantly enriched for in the high-CENPF group. However, myogenesis, TGF-beta signaling, ultraviolet (UV) response, protein secretion, apical surface, apoptosis, epithelial-mesenchymal transition, apical junction, and hypoxia gene sets were significantly enriched in the low-CENPF group (Figure 3B).

Functional enrichment analysis results from DAVID also showed consistent results with GSEA. Cell cycle-related GOBPs, like mitosis, nuclear division, organelle fission, and chromosome segregation, were enriched in the high-CENPF group. This may be reflective of the known function of CENPF as a core member of the centromere-kinetochore complex. Development-related (cell development, muscle system processes, muscle structure development), motility-related (regulation of cell migration, locomotion, and motility), and response to stimuli-related GOBPs (response to wounding and chemical stimuli) were enriched

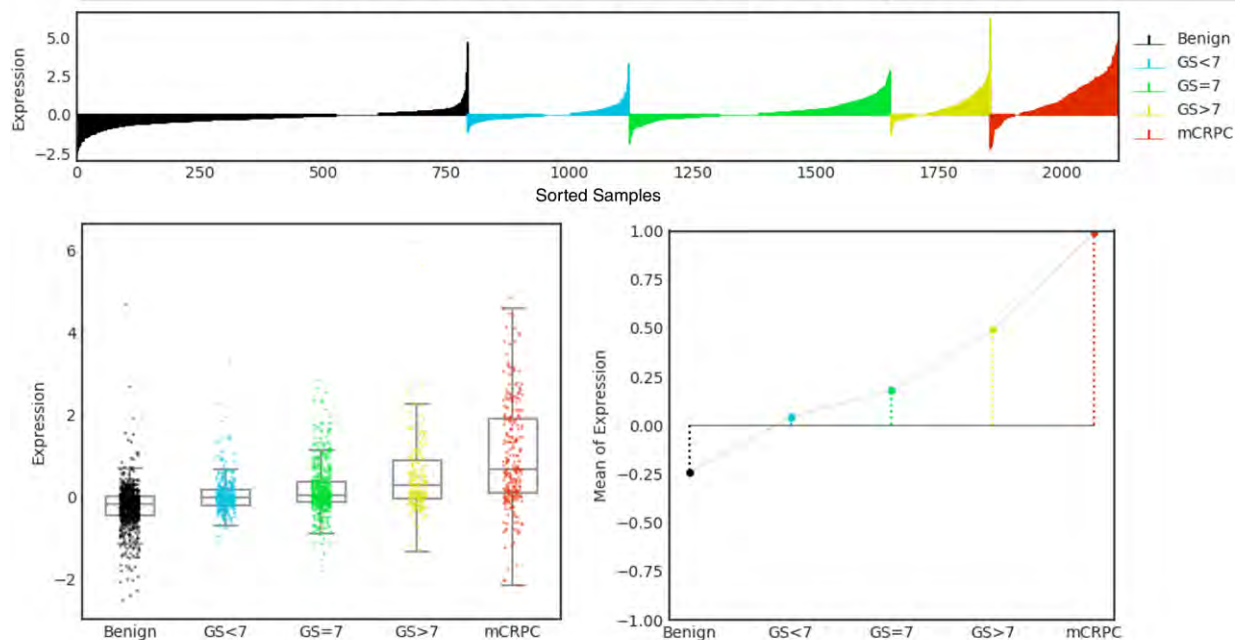
in the low-CENPF group (Figure 3C). In addition to this, we searched for hub genes among the identified DEGs that could be key regulators of the CENPF downstream transcriptional network (see Section 2 for details).

When searching for both up- and downregulated genes among the DEGs, MYC, CCDC8 (coiled-coil domain-containing protein 8), BRCA1, CDK1 (cyclin-dependent kinase 1), and PLK1 (Polo-like kinase 1) were found to be the top five genes that act as key regulator candidates in the CENPF network (Figure 3D). When performing the same analysis with only up-regulated genes, these five genes were selected with significant consistence (Figure 3E). When searching for only down-regulated genes, SMAD3 (SMAD family member 3), GSK3B (glycogen synthase kinase 3 beta), CAV1 (caveolin 1), SMAD4 (SMAD family member 4), and PRKCA (protein kinase C alpha) were identified as the top five regulator candidates (Figure 3F).

3.4. CENPF and Lipid Regulation

Lipid-related GOBPs, including positive regulation of lipid biosynthetic process, regulation of lipid metabolic process, phospholipid scrambling, lipid modification, lipid metabolic process, cellular lipid metabolic process, lipid biosynthetic process, cellular response to lipid, and response to lipid, were highly enriched by the downregulated genes in high-CENPF samples (Figure 4A). To identify genes that both regulate lipid-related functions and are CENPF-dependent, we performed hub gene analysis on

A Association of CENPF with PC progression



B Correlation of CENPF and FOXM1 with PC progression

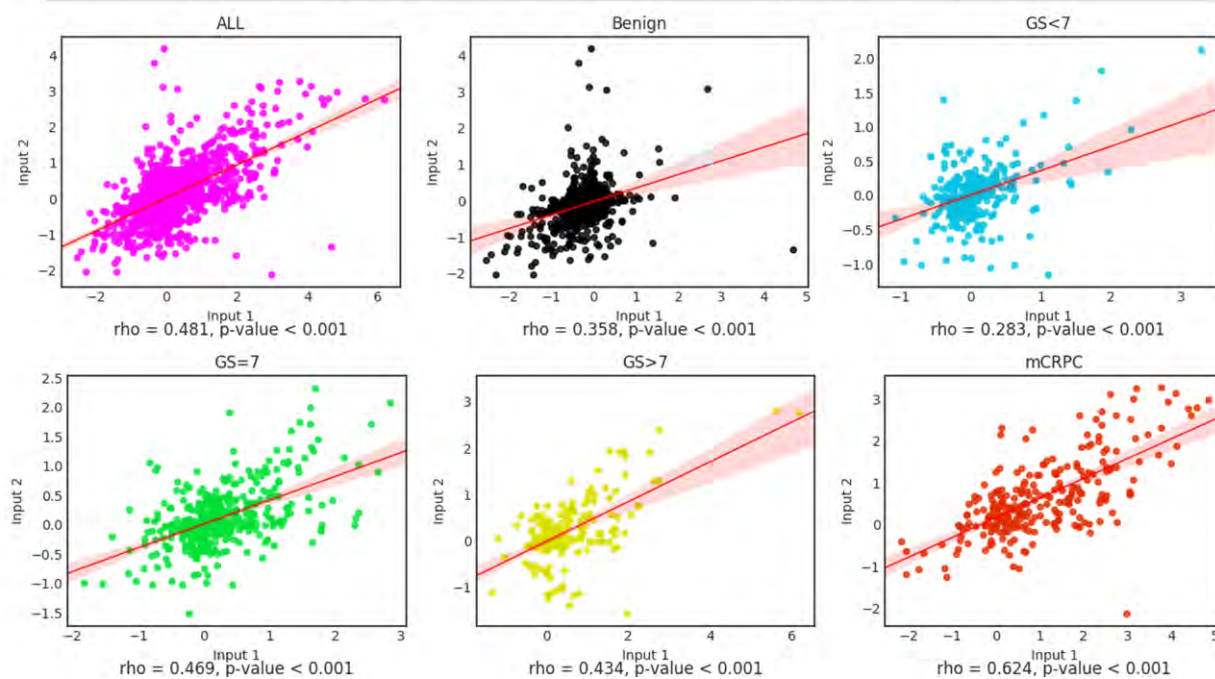


Figure 2. Gene expression of CENPF in PC progression. A) Lollipop plot (upper panel), box plot (lower left), and line plot (lower right) display CENPF gene expression patterns across disease progression from the PCTA data. Lollipop plot shows CENPF expression levels of individual samples. For each disease state, samples were sorted by CENPF expression. Whiskers on the box plot indicate interquartile range (IQR) and 1.5 times the IQR. Individual dots on the box plot represent individual samples. The line plot shows the average expression level of CENPF for each disease state. Dotted lines on the plot indicate the trend of gene expression between disease states. B) Scatter plot and regression lines were drawn to illustrate correlation between CENPF and FOXM1 in all the PCTA samples and each disease state. Input 1 and 2 represent CENPF and FOXM1, respectively.

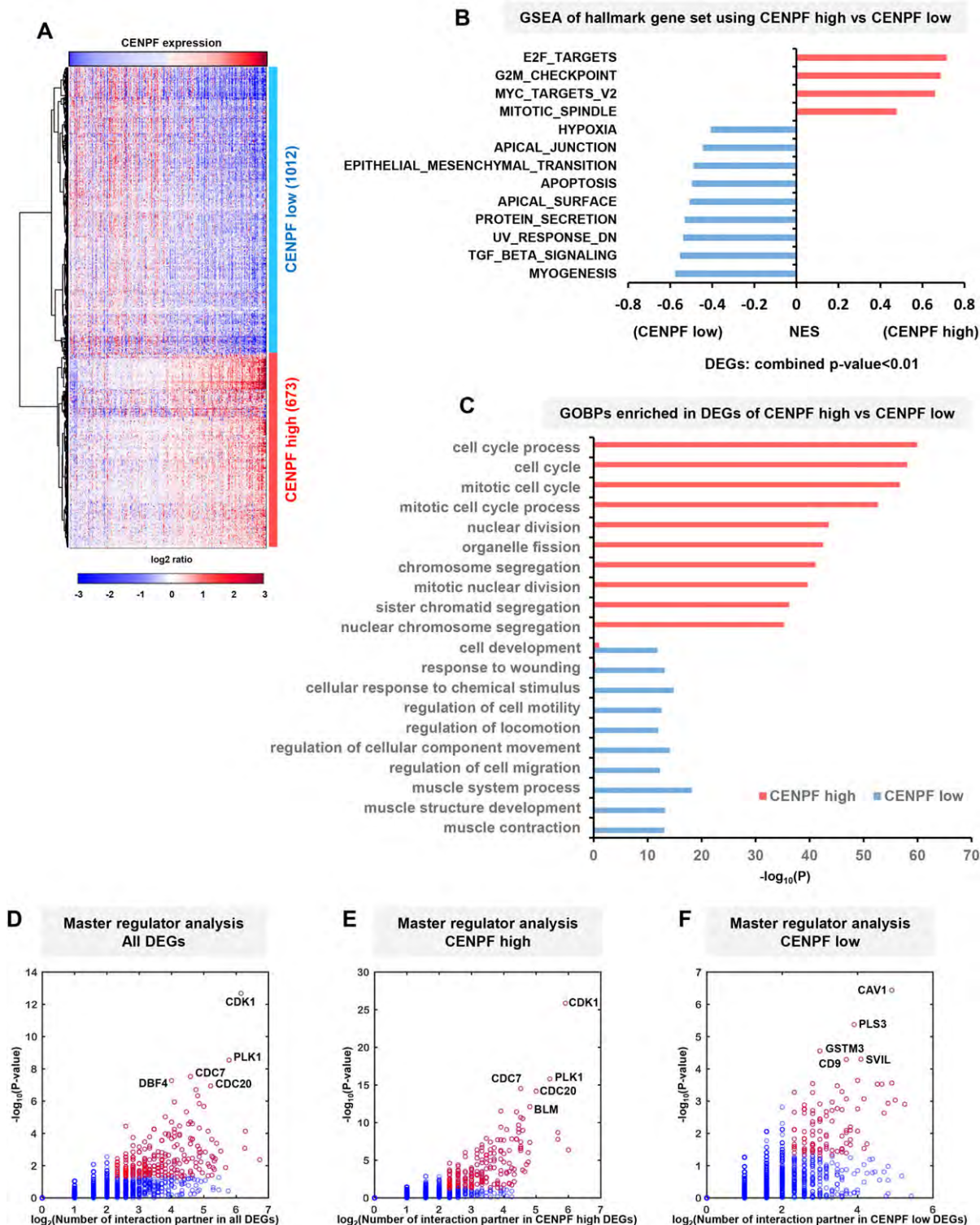


Figure 3. Identification of genes in the CENPF network. A) Heatmap depicts differential expression patterns of the genes between samples with high and low CENPF expression. Red and blue indicate up- and downregulated genes, respectively, in PC samples with high CENPF expression (CENPF high) compared with those with low expression (CENPF low). B) Bar plot displays enrichment scores of hallmark gene sets based on GSEA. All the gene sets on the plot were significantly enriched for in the CENPF-high or low groups with nominal p -value < 0.05. NES; normalized enrichment score. C) Gene Ontology Biological Processes (GOBPs) enriched by DEGs in CENPF-high versus CENPF-low with p -value < 0.05. D–F) Scatter plots illustrate up- and downregulated genes in the CENPF network (D), upregulated gene in the CENPF network (E), and downregulated genes in the CENPF network (F). Hub genes are indicated with red dots. These genes have more than three interactions in the CENPF network and p -values < 0.05.

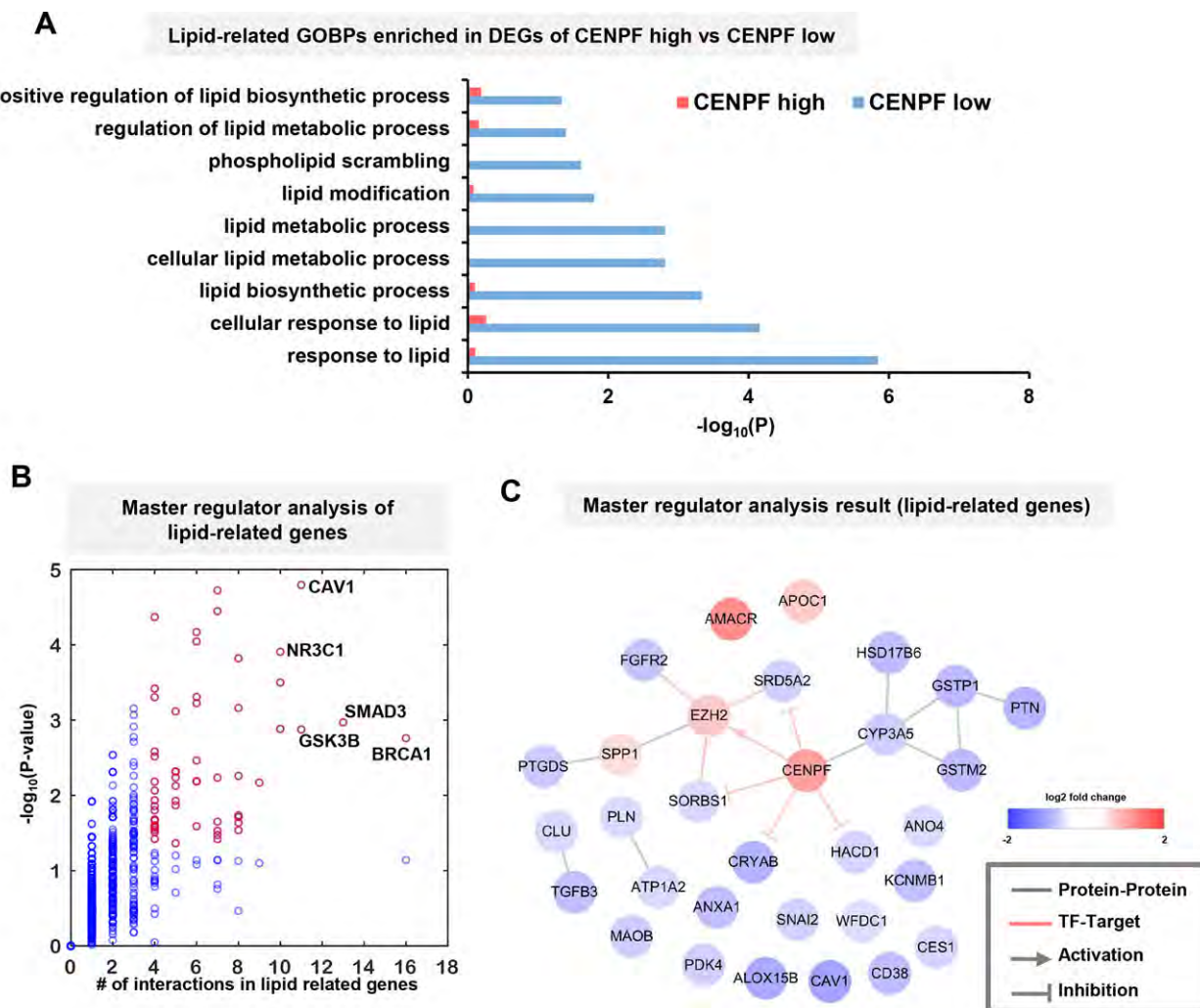


Figure 4. Association of the CENPF network with lipid regulation. A) Bar plot shows enrichment scores of the GOBPs associated with lipid metabolism and pathways in the DEGs of CENPF-high versus CENPF-low. B) Scatter plot illustrates the number of interactions among the lipid metabolism and pathway-associated genes in the CENPF network. Genes represented by red dots indicate hub genes with p -values < 0.05 . C) A network model describing interactions among the lipid-associated genes in the CENPF network. Node color represents up- and downregulation in CENPF-high versus low PCs. Edges represent interactions.

those listed to be involved in lipid-related GOBPs in Figure 4A, which resulted in BRCA1, SMAD3, CAV1, GSK3B, and NR3C1 (nuclear receptor subfamily 3 group C member 1) ($p < 0.05$) (Figure 4B). We then reconstructed a network model describing the interactions between the presence of CENPF and lipid-related genes (Figure 4C).

3.5. CENPF^{KO} Cells Show Perturbed Cellular Metabolism and Metabolic Pathways

To elucidate on the metabolite enrichment analysis between control PC3 and CENPF^{KO} cells, the annotated DEPs were further explored for their corresponding biological meaning by gene ontology annotations retrieved from the Gene Ontology Consortium and mapped against their KEGG biological pathway information. A total of 524 metabolites were profiled and quantified

from the GC-MS-based metabolomics experiment. The intensities of the 524 metabolites were normalized based on the peak sums, also called metabolite total ion chromatogram (mTIC). The normalized data was then sequentially log₂ and z-score transformed before PCA, which revealed a difference in overall metabolite expression profiles between the control and CENPF^{KO} cells (Figure 5A). Further statistical significance analysis between the two cell lines identified a total of 92 DEMs. Of these 92 DEMs, 68 were upregulated and 24 were downregulated in CENPF^{KO} cells, compared to controls. These metabolites were determined based on a fold-change ≥ 1.5 and a FDR-adjusted p -value (q -value) ≤ 0.05 (Figure 5B). Among the 92 DEMs, 23 upregulated and 12 downregulated metabolites in CENPF^{KO} cells were annotated with a KEGG compound identifier (Figure 5C). The expression profiles of the 92 DEMs were illustrated in a heatmap (Figure 5D).

The annotated metabolites were labeled with the corresponding compound names. Functional enrichment analysis

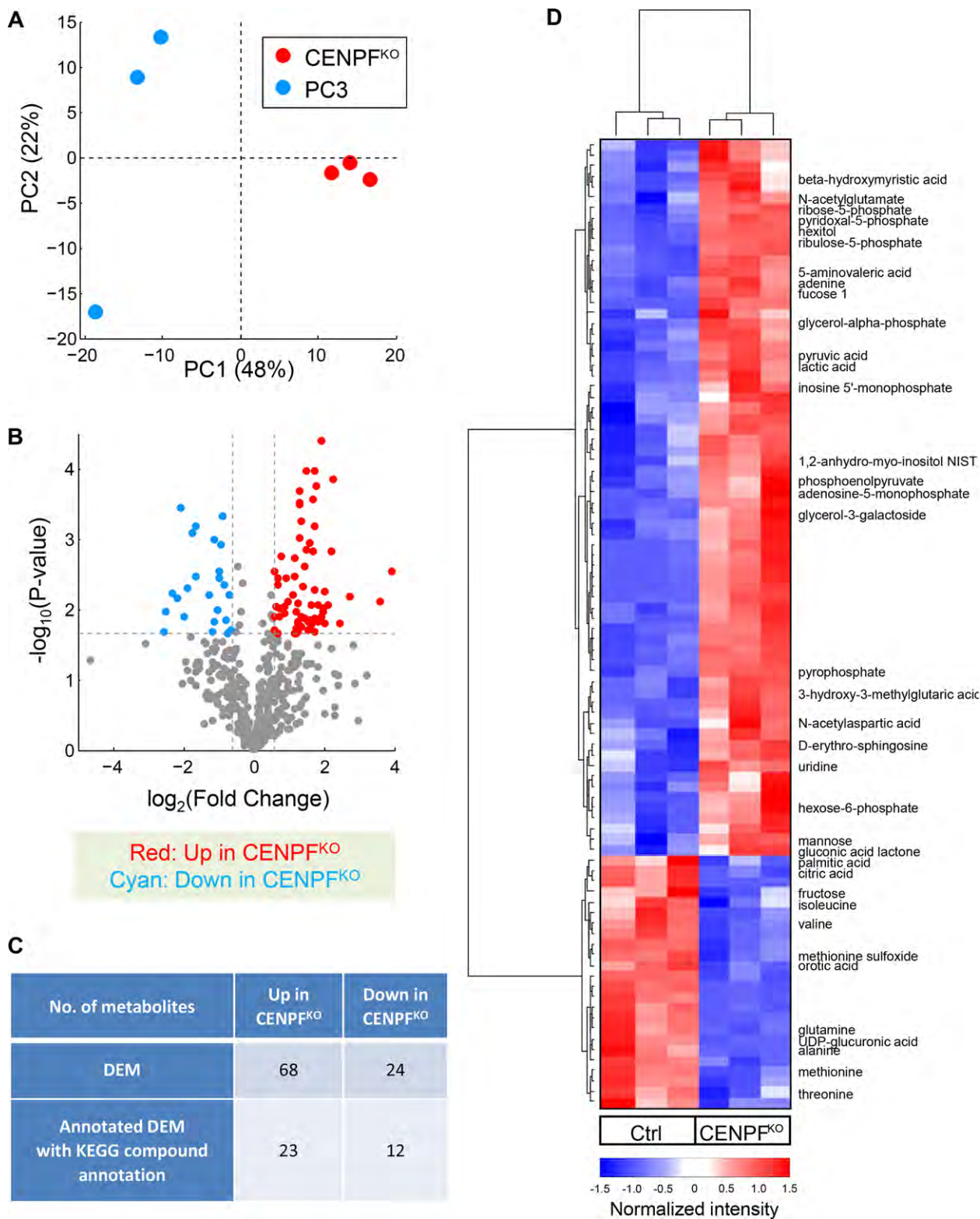


Figure 5. Metabolomic profiling of CENPF^{KO} PC3 cells. A) Principal component analysis (PCA) plot based on the 524 metabolites profiled as different between CENPF^{KO} and control PC3 cells. B) Volcano plot displaying the statistical significance (\log_{10} -based p -value) and magnitude of the changes (\log_2 -based fold-change) of the metabolites. Red and cyan indicate statistically significant up- and downregulation in CENPF^{KO} cells, respectively (fold-change ≥ 1.5 and FDR-adjusted p -value (q -value) ≤ 0.05). C) The number of DEMs identified from the statistical analyses is summarized. D) The heatmap shows the expression profiles of the 92 DEMs. The 37 annotated DEMs with compound names were marked with the corresponding identifications.

Table 1. Pathways significantly enriched for by the DEMs.

	KEGG pathway	Count	p-Value	FDR	Metabolites
Up	Carbon fixation in photosynthetic organisms	4	0.0099	0.3510	Ribulose-5-phosphate, ribose-5-phosphate, pyruvic acid, phosphoenolpyruvate
	Vitamin B6 metabolism	3	0.0108	0.3510	Ribulose-5-phosphate, pyruvic acid, pyridoxal-5-phosphate
	Pyruvate metabolism	2	0.0218	0.3770	Pyruvic acid, phosphoenolpyruvate
	Pentose phosphate pathway	4	0.0290	0.3770	Ribulose-5-phosphate, ribose-5-phosphate, pyruvic acid, gluconic acid lactone
	Phosphotransferase system (PTS)	4	0.0290	0.3770	Pyruvic acid, phosphoenolpyruvate, mannose, hexitol
	Purine metabolism	4	0.0436	0.4720	Ribose-5-phosphate, inosine 5'-monophosphate, adenosine-5-monophosphate, adenine
	Zeatin biosynthesis	2	0.0594	0.5450	Adenosine-5-monophosphate, adenine
Down	Amino-tRNA biosynthesis	6	0.0038	0.1570	Valine, threonine, methionine, isoleucine, glutamine, alanine
	Valine, leucine, and isoleucine biosynthesis	3	0.0071	0.1570	Valine, threonine, isoleucine
	Glucosinolate biosynthesis	3	0.0221	0.2930	Valine, threonine, isoleucine
	Valine, leucine, and isoleucine degradation	2	0.0266	0.2930	Valine, isoleucine
	Cysteine and methionine metabolism	3	0.0470	0.4140	Methionine sulfoxide, methionine, alanine
	ABC transporter	5	0.0642	0.4710	Valine, threonine, isoleucine, glutamine, alanine

of the annotated DEMs based on KEGG pathways identified various dysregulated metabolic pathways in CENPF^{KO} cells (Table 1). Upregulated metabolites were enriched for pathways related to carbon fixation, vitamin B6 metabolism, pyruvate metabolism, pentose phosphate pathway, phosphotransferase, purine metabolism, and zeatin biosynthesis. Downregulated metabolites were primarily enriched for pathways related to amino acid biosynthesis and metabolism (Table 1).

3.6. CENPF-Stimulated PC Proliferation

To determine whether CENPF is also required for regular cell growth, our cell proliferation assay compared growth between CENPF^{KO} and control cells. The proliferation rate of CENPF^{KO} cells was significantly reduced after 48 h (Figure 6A). We speculated that CENPF is required for regulating acetate metabolism. As expected, our results showed that acetate levels in CENPF^{KO} cells were almost completely reduced (Figure 6B). Several studies have demonstrated that significant alterations are found in the utilization of BCAAs in cancers.^[50] We then checked BCAA/AAA ratio from metabolomics data. In contrast to the control, BCAA/AAA ratio was significantly decreased (Figure 6C).

4. Discussion

The aim of this study was to determine the role of CENPF in tumor growth and aggression in both clinical PC tissue and human PC3 cells. Although CENPF is named after its association with the centromere–kinetochore protein complex, it has been reported to function in mitosis regulation and cellular proliferation as well.^[51–53] Previous studies have also shown that CENPF can potentially predict PC clinical outcome and progression.^[49] We decided to investigate if CENPF expression could stratify risk in PC patients, and if there are any resulting perturbed metabolite panels that can be used as a prognostic signature. Our study found that CENPF expression is necessary for cellular growth. Silencing of the gene resulted in significantly delayed proliferation.

Furthermore, we found that increased CENPF expression may be correlated with PC aggressiveness. PC tissue with higher clinical grades showed increased expression of CENPF, which further validates the potential use of CENPF as a prognostic marker of PC progression.

Our current study also focused on the relationship of CENPF to other genes as well. Prior studies have suggested that CENPF and FOXM1 may have a synergistic interaction that drives PC malignancy and aggressiveness.^[26],54] In addition, our previous study found that ALDH2 may be negatively correlated to CENPF.^[25] In order to validate these relationships in the context of predicting PC aggressiveness, we tested these genes in clinically graded PC samples. We found that PC samples with prediction analysis of microarray 50 (PAM50) scores >7 had higher CENPF expression and, consequently, increased FOXM1 and reduced ALDH2 levels (Figure S1, Supporting Information). This confirmed our initial speculation on the relationship of CENPF to these other genes.

To further examine the association of CENPF with various PC types, we tested for the expression of CENPF in PC tissue classified with our PCS signatures. Our prior analysis of subtype-specific gene expression patterns found that PCS1 and PCS2 tumors reflect luminal subtypes, while PCS3 tumors are basal.^[30] We found that PCS1 and PCS2 tissues had significantly higher expression of CENPF, which suggests that CENPF is elevated in luminal subtypes (Figure S2, Supporting Information). Additionally, this could mean that testing for both CENPF expression and our PCS signature could potentially identify which PC tissues are luminal. Considering how luminal subtypes are transformation-competent and, thereby, more progressive and aggressive, it would be clinically helpful to be able to accurately identify tissue subtypes.

In this study, we found that CENPF and its network may be controlling PC aggression and progression by altering cellular metabolism. BCAA metabolism is one such pathway that is regulated by CENPF, and there have been several conflicting studies regarding the relationship between BCAA metabolism and cancer progression. Loss of BCAA catabolism has been shown to lead to BCAA accumulation and activation of mTORC1 in liver and ovarian cancers^[55–57]. However, contrastingly, loss

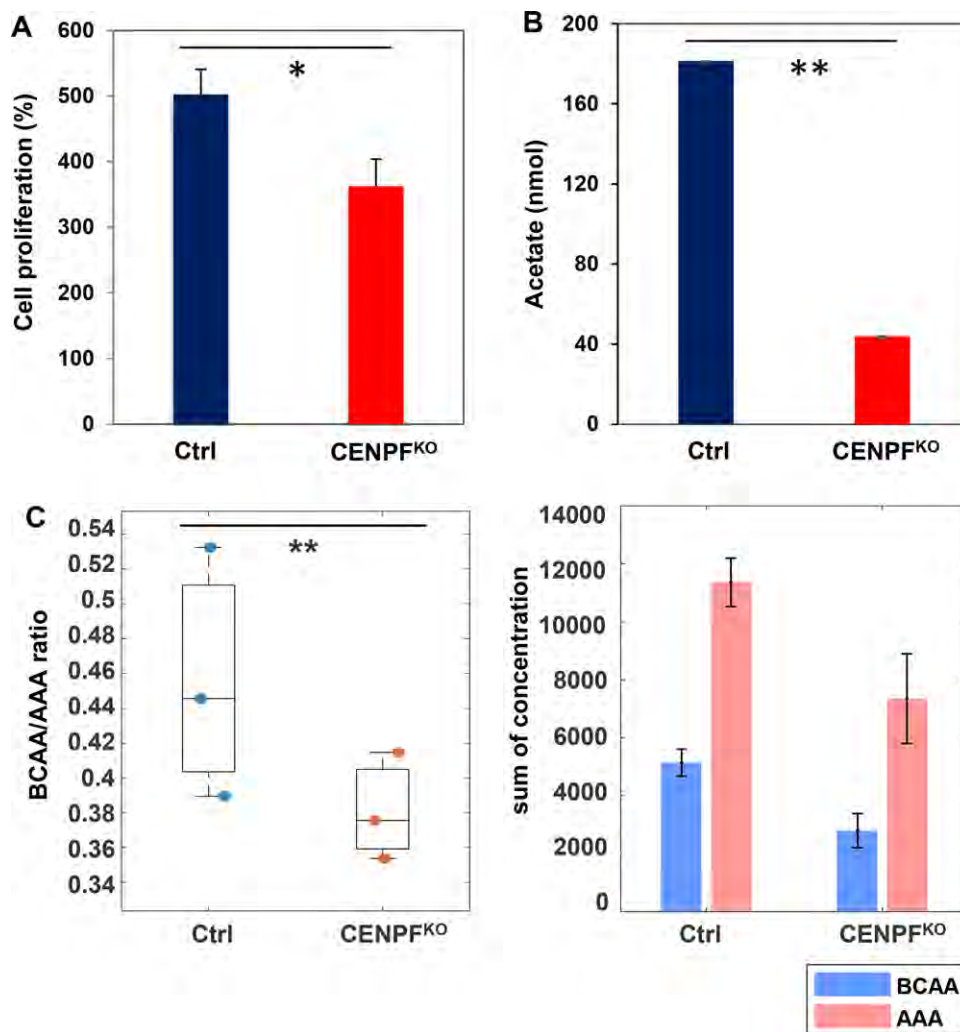


Figure 6. Perturbed metabolisms due to CENPF silencing. A) Cell growth analysis using trypan blue staining. Cell proliferation was suppressed in CENPF^{KO} cells compared to controls at 48 h. * $p < 0.05$ (two-sided Student's *t*-test). B) CENPF^{KO} cells showed decreased synthesis of acetate compared to control. C) Box plot showing BCAA/AAA ratio in Ctrl and CENPF^{KO} cells. CENPF^{KO} cells showed inhibited BCAA content compared to Ctrl. * $p < 0.05$ and ** $p < 0.01$ (two-sided Student's *t*-test). Error bars represent standard deviation ($n = 3$).

of BCAA catabolism was found to limit proliferation in glioblastoma, NSCLC, and breast cancer [58–60]. As described recently by White et al.^[61], BCAAs are also currently used as biomarker for disease pathogenesis. They have been shown to significantly involve in the development of different diseases, such as type 2 diabetes (T2D) and cardiovascular problems. Our own study found that elevated CENPF expression enhances BCAA catabolism, which leads to increased PC cell proliferation and tumor formation. Furthermore, we found that low-grade PC has limited BCAA catabolism, and this accumulation of BCAAs had no effect on mTORC1. The observed changes in CENPF-dependent acetate concentration also support the regulation of BCAA catabolism. Acetate is one of the major short-chain fatty acids and is a key substrate for cancer bioenergetics [62]. Fatty acid synthesis requires acetate and acyl-CoA synthetase short-chain family member 2 (ACSS2) [63]. Given acetate derived from glucose metabolism rewiring is elevated in cancer cells [64], it has now become apparent that acetate metabolism regulates

many different types of cancer through its role in energy or lipid production. Additionally, acetate can also affect certain cancers through regulation of histone acetylation [65].

These findings provide a basis for further studies. Despite this exciting discovery, the main limitation of our study was the lack of a large prospective patient cohort to test on. Additionally, the functional mechanisms behind CENPF that are responsible for these effects in PC patients remain elusive. However, given our previous observations^[25,29] and current human PC data bioinformatic analyses, future studies could be expanded to investigate the molecular mechanisms associated with CENPF and assess whether CENPF silencing can be a clinical biomarker for diagnosing PC or predicting aggressiveness.

The data obtained in this study will be accessible at the NIH Common Fund's Data Repository and Coordinating Center (supported by NIH grant, U01-DK097430) website, the Metabolomics Workbench, <http://www.metabolomicsworkbench.org>.

Supporting Information

Supporting Information is available from the Wiley Online Library or from the author.

Acknowledgements

M.S. and M.K. contributed equally to this work. J.K. designed the study, led the obtainment of funding, overviewed the analysis of literature, and oversaw drafting of the manuscript. M.S., A.Y., and M.L. were involved in performing metabolomics analysis and data interpretation. M.K. and M.L. performed computational analyses of metabolomics data. M.S. and A.Y. performed biochemical and functional experiments in the cell culture system. J.K. and H.L.K. carried out the analysis of references and drafted the manuscript. All authors read and approved the final manuscript. The authors thank their long-term collaborator, Dr. Oliver Fiehn, for providing guidance on this project, and the members of his lab for discussions. This work was supported by the National Institutes of Health grants (1U01DK103260, 1R01DK100974, NIH NCATS UCLA CTSI UL1TR000124), Department of Defense grants (W81XWH-15-1-0415), Centers for Disease Controls and Prevention (1U01DP006079), and the U.S.–Egypt Science and Technology Joint Fund (to J.K.). The funders had no role in the design, data collection and analysis, decision to publish, or preparation of the manuscript. In addition, this article is derived from the Subject Data funded in whole or part by National Academies of Sciences, Engineering, and Medicine (NAS) and The United States Agency for International Development (USAID). Any opinions, findings, conclusions, or recommendations expressed in this article are those of the authors alone and do not necessarily reflect the views of USAID or NAS.

Conflict of Interest

The authors declare no conflict of interest.

Keywords

CENPF, metabolomics, prostate cancer

Received: January 21, 2019

Revised: March 22, 2019

Published online: May 8, 2019

- [1] a) R. L. Siegel, K. D. Miller, A. Jemal, *Ca-Cancer J. Clin.* **2016**, *66*, 7; b) F. Bray, J. Ferlay, I. Soerjomataram, R. L. Siegel, L. A. Torre, A. Jemal, *Ca-Cancer J. Clin.* **2018**, *68*, 394.
- [2] M. G. Vander Heiden, *Drug Discovery* **2011**, *10*, 671.
- [3] P. P. Hsu, D. M. Sabatini, *Cell* **2008**, *134*, 703.
- [4] C. V. Dang, *Cancer Res.* **2010**, *70*, 859.
- [5] B. J. Altman, Z. E. Stine, C. V. Dang, *Cancer* **2016**, *16*, 773.
- [6] a) A. Baron, T. Migita, D. Tang, M. Loda, *J Cell Biochem* **2004**, *91*, 47; b) N. Zaidi, L. Lupien, N. B. Kuemmerle, W. B. Kinlaw, J. V. Swinnen, K. Smans, *Prog. Lipid Res.* **2013**, *52*, 585.
- [7] P. S. Ward, C. B. Thompson, *Cancer Cell* **2012**, *21*, 297.
- [8] a) F. Cutruzzola, G. Giardina, M. Marani, A. Macone, A. Paiardini, S. Rinaldo, A. Paone, *Front. Physiol.* **2017**, *8*, 97; b) D. Hanahan, R. A. Weinberg, *Cell* **2011**, *144*, 646.
- [9] a) A. W. Hsing, L. C. Sakoda, S. Chua, Jr., *Am. J. Clin. Nutr.* **2007**, *86*, s843; b) J. E. McDunn, Z. Li, K. P. Adam, B. P. Neri, R. L. Wolfert, M. V. Milburn, Y. Lotan, T. M. Wheeler, *Prostate* **2013**, *73*, 1547.
- [10] D. A. McGrowder, L. A. Jackson, T. V. Crawford, *Asian Pac. J. Cancer Prev.* **2012**, *13*, 1.
- [11] M. G. Vander Heiden, L. C. Cantley, C. B. Thompson, *Science* **2009**, *324*, 1029.
- [12] O. A. Aboud, R. H. Weiss, *Clin. Chem.* **2013**, *59*, 138.
- [13] J. L. Spratlin, N. J. Serkova, S. G. Eckhardt, *Clin. Cancer Res.* **2009**, *15*, 431.
- [14] N. J. Serkova, K. Glunde, *Methods Mol. Biol.* **2009**, *520*, 273.
- [15] a) L. L. Cheng, M. A. Burns, J. L. Taylor, W. He, E. F. Halpern, W. S. McDougal, C. L. Wu, *Cancer Res.* **2005**, *65*, 3030; b) A. Sreekumar, L. M. Poisson, T. M. Rajendiran, A. P. Khan, Q. Cao, J. Yu, B. Laxman, R. Mehra, R. J. Lonigro, Y. Li, M. K. Nyati, A. Ahsan, S. Kalyana-Sundaram, B. Han, X. Cao, J. Byun, G. S. Omenn, D. Ghosh, S. Pennathur, D. C. Alexander, A. Berger, J. R. Shuster, J. T. Wei, S. Varambally, C. Beecher, A. M. Chinnaiyan, *Nature* **2009**, *457*, 910.
- [16] E. Holmes, R. L. Loo, J. Stampler, M. Bictash, I. K. Yap, Q. Chan, T. Ebbels, M. De Iorio, I. J. Brown, K. A. Veselkov, M. L. Daviglus, H. Kesteloot, H. Ueshima, L. Zhao, J. K. Nicholson, P. Elliott, *Nature* **2008**, *453*, 396.
- [17] G. J. Patti, O. Yanes, G. Siuzdak, *Mol. Cell Biol.* **2012**, *13*, 263.
- [18] B. J. Trock, *Urol. Oncol.* **2011**, *29*, 572.
- [19] R. S. Kelly, M. G. Vander Heiden, E. Giovannucci, L. A. Mucci, *Cancer Epidemiol. Biomarkers Prev.* **2016**, *25*, 887.
- [20] P. Li, S. You, C. Nguyen, Y. Wang, J. Kim, D. Sirohi, A. Ziembiec, D. Luthringer, S. C. Lin, T. Daskivich, J. Wu, M. R. Freeman, R. Saouaf, D. Li, H. L. Kim, *Theranostics* **2018**, *8*, 1752.
- [21] A. Aytes, A. Mitrofanova, C. Lefebvre, M. J. Alvarez, M. Castillo-Martin, T. Zheng, J. A. Eastham, A. Gopalan, K. J. Pienta, M. M. Shen, A. Califano, C. Abate-Shen, *Cancer Cell* **2014**, *25*, 638.
- [22] S. C. Lin, C. Y. Kao, H. J. Lee, C. J. Creighton, M. M. Ittmann, S. J. Tsai, S. Y. Tsai, M. J. Tsai, *Nat. Commun.* **2016**, *7*, 11418.
- [23] T. Hitosugi, S. Kang, M. G. Vander Heiden, T. W. Chung, S. Elf, K. Lythgoe, S. Dong, S. Lonial, X. Wang, G. Z. Chen, J. Xie, T. L. Gu, R. D. Polakiewicz, J. L. Roesel, T. J. Boggon, F. R. Khuri, D. G. Gilliland, L. C. Cantley, J. Kaufman, J. Chen, *Sci. Signaling* **2009**, *2*, ra73.
- [24] M. Shahid, M. Lee, H. Piplani, A. M. Andres, B. Zhou, A. Yeon, M. Kim, H. L. Kim, J. Kim, *Cell Cycle* **2018**, *24*, 2802.
- [25] S. You, B. S. Knudsen, N. Erho, M. Alshalalfa, M. Takhar, H. Al-Deen Ashab, E. Davicioni, R. J. Karnes, E. A. Klein, R. B. Den, A. E. Ross, E. M. Schaeffer, I. P. Garraway, J. Kim, M. R. Freeman, *Cancer Res.* **2016**, *76*, 4948.
- [26] R. Edgar, M. Domrachev, A. E. Lash, *Nucleic Acids Res* **2002**, *30*, 207.
- [27] M. D. Robinson, D. J. McCarthy, G. K. Smyth, *Bioinformatics* **2010**, *26*, 139.
- [28] J. Shin, M. Kim, H. J. Jung, H. L. Cha, H. Suh-Kim, S. Ahn, J. Jung, Y. Kim, Y. Jun, S. Lee, D. Hwang, J. Kim, *Sci. Rep.* **2017**, *7*, 2826.
- [29] D. Hwang, A. G. Rust, S. Ramsey, J. J. Smith, D. M. Leslie, A. D. Weston, P. de Atauri, J. D. Aitchison, L. Hood, A. F. Siegel, H. Bolouri, *Proc. Natl. Acad. Sci. U. S. A.* **2005**, *102*, 17296.
- [30] A. Subramanian, P. Tamayo, V. K. Mootha, S. Mukherjee, B. L. Ebert, M. A. Gillette, A. Paulovich, S. L. Pomeroy, T. R. Golub, E. S. Lander, J. P. Mesirov, *Proc. Natl. Acad. Sci. U. S. A.* **2005**, *102*, 15545.
- [31] W. Huang da, B. T. Sherman, R. A. Lempicki, *Nat Protoc* **2009**, *4*, 44.
- [32] C. Stark, B. J. Breitkreutz, T. Reguly, L. Boucher, A. Breitkreutz, M. Tyers, *Nucleic Acids Res.* **2006**, *34*, D535.
- [33] L. Salwinski, C. S. Miller, A. J. Smith, F. K. Pettit, J. U. Bowie, D. Eisenberg, *Nucleic Acids Res.* **2004**, *32*, D449.
- [34] A. Patil, K. Nakai, H. Nakamura, *Nucleic Acids Res.* **2011**, *39*, D744.
- [35] S. Orchard, M. Ammari, B. Aranda, L. Breuza, L. Briganti, F. Broackes-Carter, N. H. Campbell, G. Chavali, C. Chen, N. del-Toro, M. Duesbury, M. Dumousseau, E. Galeota, U. Hinz, M. Iannuccelli, S. Jagannathan, R. Jimenez, J. Khadake, A. Lagreid, L. Licata, R. C. Lovering, B. Meldal, A. N. Melidoni, M. Milagros, D. Peluso, L. Perfetto, P. Porras, A. Raghunath, S. Ricard-Blum, B. Roehert, et al., *Nucleic Acids Res.* **2014**, *42*, D358.

- [36] D. Szklarczyk, A. Franceschini, S. Wyder, K. Forslund, D. Heller, J. Huerta-Cepas, M. Simonovic, A. Roth, A. Santos, K. P. Tsafou, M. Kuhn, P. Bork, L. J. Jensen, C. von Mering, *Nucleic Acids Res.* **2015**, *43*, D447.
- [37] P. Shannon, A. Markiel, O. Ozier, N. S. Baliga, J. T. Wang, D. Ramage, N. Amin, B. Schwikowski, T. Ideker, *Genome Res.* **2003**, *13*, 2498.
- [38] a) T. Kind, V. Tolstikov, O. Fiehn, R. H. Weiss, *Anal. Biochem.* **2007**, *363*, 185; b) T. Kind, G. Wohlgemuth, D. Y. Lee, Y. Lu, M. Palazoglu, S. Shahbaz, O. Fiehn, *Anal. Chem.* **2009**, *81*, 10038.
- [39] M. Y. Lee, A. Yeon, M. Shahid, E. Cho, V. Sairam, R. Figlin, K. H. Kim, J. Kim, *Oncotarget* **2018**, *9*, 13231.
- [40] J. D. Storey, *J. R. Stat. Soc.* **2002**, *64*, 479.
- [41] J. Lopez-Ibanez, F. Pazos, M. Chagoyen, *Nucleic Acids Res.* **2016**, *44*, W201.
- [42] J. E. Fischer, J. M. Funovics, A. Aguirre, J. H. James, J. M. Keane, R. I. Wesdorp, N. Yoshimura, T. Westman, *Surgery* **1975**, *78*, 276.
- [43] Y. J. Zhuo, M. Xi, Y. P. Wan, W. Hua, Y. L. Liu, S. Wan, Y. L. Zhou, H. W. Luo, S. L. Wu, W. D. Zhong, C. L. Wu, *Int. J. Mol. Med.* **2015**, *35*, 966.
- [44] V. E. Baracos, M. L. Mackenzie, *J. Nutr.* **2006**, *136*, 237S.
- [45] a) P. Bomont, P. Maddox, J. V. Shah, A. B. Desai, D. W. Cleveland, *EMBO J.* **2005**, *24*, 3927; b) J. Feng, H. Huang, T. J. Yen, *Chromosoma* **2006**, *115*, 320; c) S. V. Holt, M. A. Vergnolle, D. Hussein, M. J. Wozniak, V. J. Allan, S. S. Taylor, *J. Cell Sci.* **2005**, *118*, 4889.
- [46] I. Lokody, *Cancer* **2014**, *14*, 450.
- [47] a) E. A. Ananieva, A. C. Wilkinson, *Curr. Opin. Clin. Nutr. Metab. Care* **2018**, *21*, 64; b) R. E. Ericksen, S. L. Lim, E. McDonnell, W. H. Shuen, M. Vadiveloo, P. J. White, Z. Ding, R. Kwok, P. Lee, G. K. Radda, H. C. Toh, M. D. Hirschey, W. Han, *Cell Metab.* **2019**; c) Z. Q. Wang, A. Faddaoui, M. Bachvarova, M. Plante, J. Gregoire, M. C. Renaud, A. Sebastianelli, C. Guillemette, S. Gobeil, E. Macdonald, B. Vanderhyden, D. Bachvarov, *Oncotarget* **2015**, *6*, 31522.
- [48] a) M. Tonjes, S. Barbus, Y. J. Park, W. Wang, M. Schlotter, A. M. Lindroth, S. V. Pleier, A. H. C. Bai, D. Karra, R. M. Piro, J. Felsberg, A. Addington, D. Lemke, I. Weibrecht, V. Hovestadt, C. G. Rolli, B. Campos, S. Turcan, D. Sturm, H. Witt, T. A. Chan, C. Herold-Mende, R. Kemkemer, R. Konig, K. Schmidt, W. E. Hull, S. M. Pfister, M. Jugold, S. M. Hutson, C. Plass, et al., **2013**, *19*, 901; b) J. R. Mayers, M. E. Torrence, L. V. Danai, T. Papagiannakopoulos, S. M. Davidson, M. R. Bauer, A. N. Lau, B. W. Ji, P. D. Dixit, A. M. Hosios, A. Muir, C. R. Chin, E. Freinkman, T. Jacks, B. M. Wolpin, D. Vitkup, M. G. Vander Heiden, *Science* **2016**, *353*, 1161; c) L. Zhang, J. Han, *Biochem. Biophys. Res. Commun.* **2017**, *486*, 224.
- [49] P. J. White, C. B. Newgard, *Science* **2019**, *363*, 582.
- [50] T. Mashimo, K. Pichumani, V. Vemireddy, K. J. Hatanpaa, D. K. Singh, S. Sirasanagandla, S. Nannepaga, S. G. Piccirillo, Z. Kovacs, C. Foong, Z. Huang, S. Barnett, B. E. Mickey, R. J. DeBerardinis, B. P. Tu, E. A. Maher, R. M. Bachoo, *Cell* **2014**, *159*, 1603.
- [51] S. A. Comerford, Z. Huang, X. Du, Y. Wang, L. Cai, A. K. Witkiewicz, H. Walters, M. N. Tantawy, A. Fu, H. C. Manning, J. D. Horton, R. E. Hammer, S. L. McKnight, B. P. Tu, *Cell* **2014**, *159*, 1591.
- [52] H. Wen, S. Lee, W. G. Zhu, O. J. Lee, S. J. Yun, J. Kim, S. Park, *Biochim. Biophys. Acta Mol. Cell Biol. Lipids* **2019**, *1864*, 413.
- [53] Z. T. Schug, J. Vande Voorde, E. Gottlieb, *Cancer* **2016**, *16*, 708.



Published in final edited form as:

Divers Equal Health Care. 2019 ; 16(1): 1–8. doi:10.21767/2049-5471.1000185.

Effectiveness of a Tailored Colorectal Cancer Educational Seminar in Enhancing the Awareness, Knowledge, and Behavior of Korean Americans Living in the Los Angeles Koreatown Area

Sungjin Kim¹, Austin Yeon², Eunho Cho², Muhammad Shahid², and Jayoung Kim^{1,2,3,4}

¹Samuel Oschin Comprehensive Cancer Institute, Cedars-Sinai Medical Center, Los Angeles, CA, USA

²Departments of Surgery and Biomedical Sciences, Cedars-Sinai Medical Center, Los Angeles, CA, USA

³University of California, Los Angeles, CA, USA

⁴Department of Urology, Ga Cheon University College of Medicine, Incheon, South Korea

Abstract

Background: Improving rates of colorectal cancer (CRC) screening can reduce CRC-related mortality, which is estimated to cause about 50,630 deaths in the U.S. by the end of 2018. There is a noted increasing prevalence of CRC among Korean Americans. Although CRC screening has been widely implemented, Korean Americans over the age of 50 have the lowest rates of proper CRC screening, compared to those of other Asian ethnicities. Barriers, such as language and culture, may be making participation in screening procedures difficult for those with immigrant backgrounds. Thus, this study aimed to determine whether proper CRC education can enhance awareness, knowledge, and behavior in screening among Korean Americans living in the Los Angeles Koreatown area.

Design: This study was conducted among 100 self-identified Korean Americans between the ages of 45–75, who voluntarily participated in this study through local community outreach from January to June 2018. Educational brochures were provided for those in the control group, while those in the intervention group attended an additional short educational seminar. All participants were asked to complete a questionnaire after, and data were collected on site.

Results: We found that intervention had a significant effect on awareness regarding colorectal polyps (OR (odds ratio): 22.47; 95% CI: 6.42–78.62; p-value <0.001) and fecal occult blood tests (FOBTs)/stool blood test (OR, 245.37; 95% CI: 34.55–1742.75; p-value <0.001). Willingness for CRC screening in following 6 months significantly increased (OR: 87.17; 95% CI: 19.01–399.63; p-value <0.001). Knowledge on options for CRC screening (OR: 126.63; 95% CI: 23.61–679.07; p-value <0.001) and stool blood tests (OR: 157.17; 95% CI: 18.02–1370.41; p-value <0.001) were significantly enhanced. In additional univariate analysis, we found that Korean Americans with

higher level of education, birthplace in US or better general health showed better CRC awareness or knowledge.

Conclusion: There is a significant gap in our knowledge and understanding of the contributing factors that may be leading to low CRC screening rates in Korean Americans. This study suggests that well-tailored educational seminars can overcome certain barriers to screening and improve CRC knowledge and awareness, which is critical to achieving greater screening compliance. Our findings provide important references for designing effective strategies to increasing CRC screening rates among Korean Americans.

Keywords

Colorectal cancer screening; Korean Americans; Koreatown Los Angeles; Educational seminar; Inequality

Introduction

Colorectal cancer (CRC) is the third most common cancer and third leading cause of cancer-related deaths in both men and women in the United States (US) [1]. Changes in risk factors, improvements in treatment, and advancements in early detection have steadily lowered rates of CRC [2]. One of the most important factors that reduced CRC incidence and death is surveillance. A recent study found that, compared to no surveillance, one or two surveillance visits were associated with significantly lower CRC incidence [3]. While there are many options for CRC screening, including fecal occult blood testing, stool DNA analysis, and sigmoidoscopy, the gold standard remains to be colonoscopy [4]. According to statistics provided by the American Cancer Society (ACS), treatment options for CRC have greatly improved recently, resulting in more than 1 million CRC survivors in the US alone. Along with this development, early diagnosis through regular and timely screening can decrease CRC risk; however, there are certain populations that have shown a steady rise in CRC incidence. In particular, Asian communities have not only seen a higher rate of CRC, but an increasing trend as well [5].

Although there are no concrete explanations for this increase of CRC incidence among Asians, studies have shown some attribution to fatalistic attitudes, changes in diet, and education on screening [5–7]. This lapse in vigilant CRC monitoring is particularly evident in the Korean population [8]. CRC is ranked as one of the most common cancers in Korea and places an immense economic burden on patients and society at large [9]. This is not just limited to the Korean population overseas. Rates of colorectal cancer in immigrant patients have been found to be similar to those in their home countries, compared to Caucasians in the same area [10]. Additionally, studies on minority health have shown that the Korean American population has one of the lowest cancer screening rates [11]. Screening for CRC is further hindered by the socioeconomic and cultural barriers Korean Americans face [12]. A prior study found that less than 30% of Korean Americans in Los Angeles County had ever received screening for CRC [13]. Furthermore, a California Health Interview Survey found that, compared to other Asian American groups, Korean Americans had the lowest rates of CRC screening [14]. More than half of Japanese, Chinese, Filipino, and Vietnamese Americans between the ages of 50 to 64 years old received screening for CRC, while only

37% of Korean Americans in the same age range have [15]. Therefore, there is an urgent need to solve this increasing discrepancy in the Korean population.

Southern California, particularly Los Angeles (LA) and Orange County (OC), has the highest concentration of Koreans and Korean Americans in the US, making up about 25% of all Koreans residing in America. A majority of Koreans are concentrated around the LA Koreatown area. Koreatown is the most densely populated district, by population, in LA county, with an average of 42,611 people per square mile. There is an increasing burden of CRC in Korean populations. CRC is the most commonly occurring cancer in males particularly [16]. Koreans over the age of 50 had the lowest rate of proper colorectal screening compared to those of other Asian and Asian American ethnicities [17]. In addition, there is a significant knowledge gap in the comprehensive understanding of the contributing factors that affect colorectal screening in Korean Americans. Being that LA is home to such a large number of Koreans, it provides the ideal environment to study and attempt to resolve this troubling issue.

To better understand how to improve current knowledge and awareness of CRC in the Korean American immigrant population, we conducted a survey of general questions regarding CRC on two different Korean audiences in LA Koreatown. This area was ideal because it is one of the most densely populated districts in LA and is home to the largest concentrations of Koreans outside of Korea. This study broadens our knowledge of the contributing factors of low CRC screening in Korean Americans living in LA county. The questionnaire inquired about whether primary healthcare providers recommended CRC screening (lack of awareness), which CRC screening methods were preferred (screening method), and if their health insurance covered the cost of screening (access to care). The findings from this study suggest that implementing cultural and language appropriate seminars significantly increase both knowledge and interest in CRC screening among Korean Americans.

Methods and Materials

Data collection procedures

Eligible participants included men and women between the ages of 45 to 75, who self-identified as of Korean ethnicity, were Korean or English speaking, and were living or had contacts in the LA Koreatown area. Individuals with a prior history of CRC or significant medical problems that affected attendance to the educational seminar or survey were excluded. The sample size for this study was limited to 100 participants, who were all recruited from Korean churches, senior recreation centers, senior community colleges, language schools, college cultural organizations, grocery stores, coffee shops, and nail/hair salons (Cedars-Sinai Medical Center Institutional Review Board Approval number Pro00048053).

Our structured research questionnaire, Korean Community Health Survey: Colorectal Cancer, was administered in either Korean or English. It involved inquiries about demographics, general health concerns and lifestyle factors, such as age, weight, height, and

general health level (Table 1). The survey was designed to establish base information for future Korean community-based CRC epidemiologic research.

Those in the control group received an English-language brochure provided by Cedars-Sinai Medical Center. Participants in the intervention group received the brochure and an additional 30-min educational seminar with a slide presentation. American Cancer Society (ACS)-developed CRC educational materials and presentation slides were used after slight modifications and translation by a certified Korean translator. The presentation included information related to colon health and CRC (incidence rate, risk factors, diet and lifestyle recommendations, screening methods, etc.). During the seminar, participants were encouraged to ask their primary physicians about CRC and screening options.

Self-reported paper and pen-based surveys were distributed directly after intervention and confirmation of willingness to participate. Some demographic characteristics, such as sex, age range, marriage status, height, and weight (Q1-Q4) were asked. Participants' birth place, proportion of lifetime in the US, English proficiency, and education level were next questioned (Q5-Q8). Computer skills and usage of social network service were asked as well (Q10-Q11). To determine general information on healthcare utilization, participants gave responses to the three following questions; "How's your overall health?", "Do you frequently access a healthcare newsletter?", and "Where do you find health information from?" (Q9, Q12-Q13). The control group took the survey after only examining the brief brochure, while the intervention group took the survey after examining both the brochure and attending the seminar on CRC prevention, screening, and treatment.

Data analysis

Sociodemographic characteristics included age, sex, marital status, height, weight, birthplace, years lived in the US, English fluency, educational level, computer skill, and use of social networks. Health-related variables included self-perceived health status, family history of CRC, and reasons for reluctance to screen for CRC, if any. Self-reported CRC screening behavior was assessed as: 1) ever having had a fecal occult blood test (FOBT), colonoscopy, or any other test done, and 2) being up-to-date with CRC screening. Knowledge regarding CRC was assessed with 6 questions, which included knowing how many CRC screening tests exist, the age to begin screening, recommended frequency of tests, and awareness of gender differences in CRC risk. CRC awareness was measured by asking whether participants had ever heard of CRC, colon polyps, FOBT, and colonoscopy.

For statistical analysis, data are presented as frequency (percentage, %) for categorical variables and median (IQR, interquartile range) for continuous variables. Univariate associations were examined using Wilcoxon rank-sum tests for continuous variables, and chi-square test or Fisher's exact test for categorical variables, as appropriate. To avoid potential overfitting due to a large number of baseline characteristics and to balance potential confounding factors between the intervention and control groups, propensity score (PS) analysis was performed [18]. The propensity score of being in the intervention group (vs. control group) was estimated using a multivariable logistic regression model after adjusting for Q1 through Q11, Q13, and Q28-Q29 [18-20], and the estimated propensity scores were included as a covariate in the multivariable logistic regression model for each

outcome [19]. Analyses were performed using SAS 9.4 (SAS Institute, Inc., Cary, North Carolina) with two-sided tests and a significance level of 0.05.

Results

Participant characteristics

A total of 100 Korean American participants voluntarily participated in this study. Table 1 presents baseline characteristics of the participants in this study. Most of the participants (96%) were over the age of 50. There were more female participants (63%) than males (37%), and most participants were married (74%). Almost all the participants were born in the Korea (98%), and 70% had lived in the US for more than 20 years. Many participants reported not speaking English fluently or well; they self-reported their English-speaking abilities to be at a beginner's level (96%). Only 32% of participants had a high school education or higher. A majority of participants reported that their overall health levels were fair/poor (77%). Most of them find health-related information from television (85%). Nearly all participants were not familiar with social network services (97%) and lacked computer skills (84%).

Comparison of intervention and control groups

Conventional educational materials on CRC and screening methods were provided for the control group (n=50). In addition to these materials, the intervention group received a 30-min health lecture designed for seniors. Both groups were asked to complete a 1-page questionnaire, which was translated by a certified English-Korean translator. Participants were allowed to choose from either an English or Korean version.

Awareness test included four "yes or no" screening questions –

“Q14. Have you heard about colorectal cancer?”

“Q15. Have you heard about colorectal polyp?”

“Q16. Have you heard about the fecal occult blood test (FOBT) or stool blood test?”, and

“Q19. Have you heard about colonoscopy?” Behavior domain contained five questions -

“Q17. Have your doctor told you that you should be tested for colon cancer (FOBT)?” “Q18. Have you ever had a FOBT?”

“Q20. Have your doctor recommend colonoscopy?” “Q21. Have you ever had a colonoscopy?”, and

“Q30. Are you willing to undergo colon cancer testing within 6 months?”

Knowledge domain consisted of six questions –

“Q22. I believe that there is only one screening test for colon cancer”,

“Q23. There is a stool blood test using a “home” test”,

“Q24. I believe that people are supposed to start getting tested for colon cancer at age of 50”,

“Q25. Once people start having stool blood test, they should have them every 3 years”,

“Q26. In general, once people start having colonoscopy exams at age of 50, they should have them every 5 years”, and

“Q27. I believe that colon cancer is mainly a problem for men” (Table 2).

Participants in the intervention group had significantly better awareness, behavior, and knowledge on compared to the control group. Both the control and intervention groups had awareness about CRC and colonoscopies; however, participants in the intervention group were significantly more aware on colorectal polyps (90% vs. 28%) and FOBT (94% vs. 8%) than the control group (Tables 2).

Willingness to undergo CRC screening within 6 months was significantly higher in the intervention group (88% vs. 8%). In addition, participant knowledge regarding CRC screening test options were higher in the intervention group. Most participants in the control group (90%) believed that there was only one screening test for CRC. The intervention group recognized other options for CRC screening, and only 8% thought there was only one form of screening. Only 2% of participants in the control group knew that the FOBT/stool blood test could be done at home, compared to 78% of intervention group.

There was no difference in knowledge on the recommended age for CRC screening and how often it should be conducted between the control and intervention groups (Tables 2).

Univariate and multivariable analyses of awareness, behavior, and knowledge

After propensity score (PS), we found that intervention remained a significant effect on awareness of colorectal polyps (OR (odds ratio): 22.47; 95% CI: 6.42–78.62; p-value <0.001) and FOBT or stool blood test (OR: 245.37; 95% CI: 34.55–1742.75; p-value <0.001). In the intervention group, willingness to screen for CRC in the following 6 months was significantly higher than the control group (OR: 87.17; 95% CI: 19.01–399.63; p-value <0.001). Knowledge on additional screening options (OR: 126.63; 95% CI: 23.61–679.07; p-value <0.001) and stool blood test (OR: 157.17; 95% CI: 18.02–1370.41; p-value <0.001) was also significantly enhanced (Table 3).

Further univariate analyses showed that, participants who reported overall health as “very good/good” were more likely to have heard about colorectal polyps than those who reported overall health as “fair/poor” (p-value=0.009, data not shown). Participants born in the US were more likely to have ever had a FOBT compared to those born in Korea (p-value=0.040, data not shown). Participants with higher education levels were more likely to answer yes regarding the possibility of using stool blood tests at home (p-value=0.006, data not shown). Overall health status was associated with increased knowledge regarding CRC and CRC screening (Q24. I believe that people are supposed to start getting tested for colon cancer at age of 50, p-value= 0.020; Q26. In general, once people start having colonoscopy exams at

age of 50, they should have them every 5 years, p -value=0.018; Q27. I believe that colon cancer is mainly a problem for men, p -value=0.023, data not shown).

Discussion

The current study showed that a tailored CRC seminar can improve knowledge, behavior, and awareness among Korean American immigrants facing language barriers or those of lower socioeconomic status. This study examined the associations between groups (intervention vs. control), and outcomes/domains, such as knowledge, behavior and awareness in univariate and multivariable analyses. By conducting multivariable analysis of each outcome/domain, we calculated a PS. We further examined the associations between questionnaires and outcomes/domains in univariate analyses and found that better general health, higher education level, and birthplace in US were significantly associated with greater CRC awareness or knowledge.

Due to cultural and language barriers, Korean Americans in the LA Koreatown area have been a difficult population to reach when implementing cancer education and prevention programs. Our results were consistent with other studies suggesting that a lack of acculturation in the US seems to be a critical barrier in receiving preventive health services [21]. Providing culturally integrated and tailored cancer education to Korean Americans could significantly improve knowledge regarding CRC and screening; thereby, ultimately reducing CRC screening disparities in the Korean population. Our present study suggests several associated factors related to knowledge improvement of CRC after educational intervention. These results should be taken into consideration by local academic medical centers when creating culturally integrated educational programs.

Several previous reports have demonstrated that health education intervention can improve preventative cancer screening in the Asian American populations, including Vietnamese Americans, Chinese Americans, Hmong Americans, Korean Americans, Filipino Americans et al. [22–26]. Gu et al. suggested that small group-based education programs prepared by Chinese-speaking community health workers can enhance the implementation fidelity for breast cancer screening by mammography [27]. Aligned with these findings, our results strongly argue for the necessity and importance of raising self-awareness about CRC screening in Korean Americans. After health education, participants were more likely to be aware of and willing to try CRC screening options. Their own knowledge and inquiry influenced physicians who were also motivated by the specific request from their patients (action-reaction). We also found that detailed information could not be delivered efficiently or memorized by participants, particularly those were older. Considering the age range of our participants, we suggest that follow-up information via phone call, text, or voicemail regarding future CRC screenings should be considered by healthcare providers.

Findings from this pilot study indicate a strong need for education programs that are linguistically and culturally customized for the Korean American population. Although further studies should be conducted to determine the feasibility of such interventions and to ascertain their long-term impact on actual screening rates, tailored education will nevertheless be critically necessary for reducing CRC-related mortality and morbidity

among Korean Americans. However, we are aware that there are several limitations in our study. First, considering that our study was based on self-reported responses and that the extent of reliability and validity of self-reporting is somewhat limited, we believe that an additional study assessing objective and quantitative results should be designed. Second, this study was restricted to concentrated populations living in the LA Koreatown area, and it may not be generalizable to Korean American populations based in other regions. Third, the study was not able to determine the long-term effects of intervention, such as actual CRC screening rates. Fourth, our voluntary participants may be more active and self-motivated about health issues in general, so the findings from this study cannot be expected to be the same in a less motivated population. Lastly, our sample size was relatively small, so conclusive statements cannot be made.

Despite our limitations, a major strength of our study was the finding that culturally and linguistically integrated seminars by trusted community leaders in the academic field can support the wellbeing of participants. Our educational seminar included a short slide presentation and provided a point-by-point lecture on layman's terminology, to particularly assist the older or less educated participants. This approach created a friendly and informal environment to help participants clearly understand the health messages in the educational materials. Participants were encouraged to ask questions in their own languages during and after the seminar.

Conclusion

In conclusion, our tailored intervention made a significant improvement in awareness, knowledge, and behavior related to CRC and screening in Korean Americans residing in Koreatown, many of whom could be considered underserved. Although further larger scale community-based studies are required to validate this finding, the results from our current study suggest that providing culturally and linguistically integrated educational community programs may greatly improve cancer prevention in high risk subgroups of Asian Americans and reduce disparities in CRC screening.

Acknowledgement

We sincerely thank all leaders and staff from participating community organizations. The authors acknowledge support from National Institutes of Health grants (1U01DK103260, 1R01DK100974, U24 DK097154, NIH NCATS UCLA CTSI UL1TR000124), Department of Defense grants (W81XWH-15-1-0415), Centers for Disease Controls and Prevention (1U01DP006079), IMAGINE NO IC Research Grant, the Steven Spielberg Discovery Fund in Prostate Cancer Research Career Development Award, and the U.S.-Egypt Science and Technology Joint Fund (to J.K.). J.K. is a former recipient of the Interstitial Cystitis Association Pilot Grant, a Fishbein Family IC Research Grant, New York Academy of Medicine, and Boston Children's Hospital Faculty Development. The funders had no role in the experimental design, data collection, analysis, preparation of the manuscript, or decision to publish. In addition, this article is derived from the Subject Data funded in whole or part by National Academies of Sciences, Engineering, and Medicine (NAS) and The United States Agency for International Development (USAID). Any opinions, findings, conclusions, or recommendations expressed in this article are those of the authors alone, and do not necessarily reflect the views of USAID or NAS.

Reference

1. Siegel R, Desantis C, Jemal A (2014) Colorectal cancer statistics. *CA Cancer J Clin* 64: 104–117. [PubMed: 24639052]

2. Vogelaar I, van Ballegooijen M, Schrag D (2006) How much can current interventions reduce colorectal cancer mortality in the U.S? Mortality projections for scenarios of risk-factor modification, screening, and treatment. *Cancer* 107: 1624–1633. [PubMed: 16933324]
3. Atkin W, Wooldrage K, Brenner A (2017) Adenoma surveillance and colorectal cancer incidence: a retrospective, multicentre, cohort study. *Lancet Oncol* 18: 823–834. [PubMed: 28457708]
4. Schreuders EH, Ruco A, Rabeneck L (2015) Colorectal cancer screening: a global overview of existing programmes. *Gut* 64: 1637–1649. [PubMed: 26041752]
5. Deng Y (2017) Rectal Cancer in Asian vs. Western Countries: Why the Variation in Incidence? *Curr Treat Options Oncol* 18: 64. [PubMed: 28948490]
6. Jun J, Oh KM (2013) Asian and Hispanic Americans' cancer fatalism and colon cancer screening. *Am J Health Behav* 37: 145–154. [PubMed: 23026095]
7. Ng SC, Wong SH (2013) Colorectal cancer screening in Asia. *Br Med Bull* 105: 29–42. [PubMed: 23299409]
8. Lee HY, Lundquist M, Ju E (2011) Colorectal cancer screening disparities in Asian Americans and Pacific Islanders: which groups are most vulnerable? *Ethn Health* 16: 501–518. [PubMed: 22050536]
9. Jung KW, Park S, Won YJ (2012) Prediction of cancer incidence and mortality in Korea, 2012. *Cancer Res Treat* 44: 25–31. [PubMed: 22500157]
10. Lee J, Xiao YY, Sun YY (2017) Prevalence and characteristics of hereditary non-polyposis colorectal cancer (HNPCC) syndrome in immigrant Asian colorectal cancer patients. *BMC Cancer* 17: 843. [PubMed: 29237405]
11. Maxwell AE, Song H (2003) Cancer Screening of Korean Americans in Los Angeles County: Adding Pieces to the Puzzle. *Korean Am Stud Bull* 13: 59–70. [PubMed: 17057820]
12. Jo AM, Maxwell AE, Rick AJ (2009) Why are Korean American physicians reluctant to recommend colorectal cancer screening to Korean American patients? Exploratory interview findings. *J Immigr Minor Health* 11: 302–309. [PubMed: 18607728]
13. Jo AM, Maxwell AE, Wong WK (2008) Colorectal cancer screening among underserved Korean Americans in Los Angeles County. *J Immigr Minor Health* 10: 119–126. [PubMed: 17574545]
14. Hwang H (2013) Colorectal cancer screening among Asian Americans. *Asian Pac J Cancer Prev* 14: 4025–4032. [PubMed: 23991947]
15. Maxwell AE, Crespi CM, Antonio CM (2010) Explaining disparities in colorectal cancer screening among five Asian ethnic groups: a population-based study in California. *BMC Cancer* 10: 214. [PubMed: 20482868]
16. Liu L, Wang Y, Sherman RL (2016) Cancer in Los Angeles County: Trends by Race/Ethnicity 1976–2012 Los Angeles Cancer Surveillance Program, University of Southern California.
17. Maxwell AE, Crespi CM (2009) Trends in colorectal cancer screening utilization among ethnic groups in California: are we closing the gap?. *Cancer Epidemiol Biomarkers Prev* 18: 752–759. [PubMed: 19273482]
18. Rosenbaum PR (1983) The central role of the propensity score in observational studies for causal Effects. *Biometrika* 70: 41–55.
19. Rosenbaum PR (1984) Reducing bias in observational studies using subclassification on the propensity score. *J Am Stat Assoc* 79: 516–524.
20. D'Agostino RB, D'Agostino RB (2007) Sr. Estimating treatment effects using observational data. *JAMA* 297: 314–316. [PubMed: 17227985]
21. Society AC (2011) Colorectal cancer facts & figures 2011–2013
22. Carballeira NM, Shalabi F, Stefanov K (1995) Comparison of the fatty acids of the tunicate *Botryllus schlosseri* from the Black Sea with two associated bacterial strains. *Lipids* 30: 677–679. [PubMed: 7564924]
23. Cuaresma CF, Sy AU, Nguyen TT (2018) Results of a lay health education intervention to increase colorectal cancer screening among Filipino Americans: A cluster randomized controlled trial. *Cancer* 124: 1535–1542. [PubMed: 29578603]

24. Jo AM, Nguyen TT, Stewart S (2017) Lay health educators and print materials for the promotion of colorectal cancer screening among Korean Americans: A randomized comparative effectiveness study. *Cancer* 123: 2705–2715. [PubMed: 28440872]
25. Lee S, Zhai S, Zhang GY (2015) Factors Associated with Hepatitis C Knowledge Before and After an Educational Intervention among Vietnamese Americans. *Clin Med Insights Gastroenterol* 8: 45–53. [PubMed: 26561280]
26. Nguyen TT, Tsoh JY, Woo K (2017) Colorectal Cancer Screening and Chinese Americans: Efficacy of Lay Health Worker Outreach and Print Materials. *Am J Prev Med* 52: e67–e76. [PubMed: 27986352]
27. Gu J, Maxwell AE, Ma GX (2018) Evaluating the Training of Chinese-Speaking Community Health Workers to Implement a Small-Group Intervention Promoting Mammography. *J Cancer Educ*

Characteristics of Korean American Participants in Colorectal Cancer Screening Survey in Los Angeles, California: 2018

Table 1:

Variable	All participants (N=100)	Control (N=50)	Intervention (N=50)	P-value
Q1. Gender				
Female	63 (63)	30 (60)	33 (66)	0.534
Male	37 (37)	20 (40)	17 (34)	
Q2. Age (years)				
45	1 (1)	0 (0)	1 (2)	0.146
45-49	3 (3)	2 (4)	1 (2)	
50-64	45 (45)	27 (54)	18 (36)	
65 or over	51 (51)	21 (42)	30 (60)	
Q3. Marital status				
No	26 (26)	13 (26)	13 (26)	1.000
Yes	74 (74)	37 (74)	37 (74)	
Q4. Height (cm)				
Median (IQR)	153 (151 – 158)	153 (151 – 158)	154 (151 – 158)	0.206
Q4. Weight (kg)				
Median (IQR)	55 (45.5 – 61)	55 (45.5 – 61)	55 (45.5 – 61)	0.992
Q5. Where were you born?				
Korea	98 (98)	50 (100)	48 (96)	0.495
USA	2 (2)	0 (0)	2 (4)	
Q6. About how many years have you lived in the United States?				
< 11 years	12 (12)	4 (8)	8 (16)	0.184
11-20 years	18 (18)	12 (24)	6 (12)	
More than 20 years	70 (70)	34 (68)	36 (72)	
Q7. What is your level of English?				
Beginner	96 (96)	48 (96)	48 (96)	1.000
Low intermediate	2 (2)	1 (2)	1 (2)	
Intermediate	2 (2)	1 (2)	1 (2)	
Q8. What is the highest grade of education you have completed?				

Variable	All participants (N=100)	Control (N=50)	Intervention (N=50)	P-value
First through 11 th grade	68 (68)	36 (72)	32 (64)	0.293
High School graduate	25 (25)	13 (26)	12 (24)	
One to three years of college	4 (4)	1 (2)	3 (6)	
College graduate	3 (3)	0 (0)	3 (6)	
Q9. How's your overall health?				
Poor	2 (2)	0 (0)	2 (4)	0.022
Fair	75 (75)	41 (82)	34 (68)	
Good	11 (11)	7 (14)	4 (8)	
Very good	12 (12)	2 (4)	10 (20)	
Q9. How's your overall health? (combined)				
Fair/Poor	77 (77)	36 (72)	41 (82)	0.235
Very good/Good	23 (23)	14 (28)	9 (18)	
Q10. How would you rate your computer skills (your skill on the internet)?				
Great. I find most anything I search for	2 (2)	0 (0)	2 (4)	0.525
Ok, sometimes I have trouble finding information	14 (14)	6 (12)	8 (16)	
Not so great, I struggle with how to use it	69 (69)	37 (74)	32 (64)	
I have little to no experience	15 (15)	7 (14)	8 (16)	
Q11. Do you frequently use Social Network Service?				
No	97 (97)	48 (96)	49 (98)	1.000
Yes	3 (3)	2 (4)	1 (2)	
Q13. Where do you find health information from?				
Television	85 (85)	43 (86)	42 (84)	1.000
Internet	10 (10)	5 (10)	5 (10)	
Newspaper	5 (5)	2 (4)	3 (6)	
Q28. Have any of your relatives ever had colon cancer?				
No	94 (94)	47 (94)	47 (94)	1.000
Yes	6 (6)	3 (6)	3 (6)	
Q29. If you may be reluctant to have test for colon cancer, what is the reason for that?				
It is because of the cost	78 (78)	39 (78)	39 (78)	

Variable	All participants (N=100)	Control (N=50)	Intervention (N=50)	P-value
Having the tests done would be embarrassing	10 (10)	4 (8)	6 (12)	
I am worried that testing will show that I have colon cancer	12 (12)	7 (14)	5 (10)	

Data are presented as number of patients (column %) or median (IQR, interquartile range).

P-value is calculated by Wilcoxon rank-sum test for numerical variables, and chi-square or Fisher's exact test for categorical variables.

Note: All subjects answered 'Yes' to 'Q12: Do you frequently access health care newsletter?'

Table 2:

Domains stratified by group.

Domain	All participants (N=100)	Control (N=50)	Intervention (N=50)
Awareness			
Q14. Have you heard about colorectal cancer?			
No	5 (5)	2 (4)	3 (6)
Yes	95 (95)	48 (96)	47 (94)
Q15. Have you heard about colorectal polyp?			
No	41 (41)	36 (72)	5 (10)
Yes	59 (59)	14 (28)	45 (90)
Q16. Have you heard about the fecal occult blood test (FOBT) or stool blood test?			
No	49 (49)	46 (92)	3 (6)
Yes	51 (51)	4 (8)	47 (94)
Q19. Have you heard about colonoscopy?			
No	9 (9)	3 (6)	6 (12)
Yes	91 (91)	47 (94)	44 (88)
Behavior			
Q17. Have your doctor told you that you should be tested for colon cancer (FOBT)?			
No	50 (50)	47 (94)	3 (6)
Yes	50 (50)	3 (6)	47 (94)
Q18. Have you ever had a FOBT?			
No	98 (98)	49 (98)	49 (98)
Yes	2 (2)	1 (2)	1 (2)
Q20. Have your doctor recommend colonoscopy?			
No	39 (39)	37 (74)	2 (4)
Yes	61 (61)	13 (26)	48 (96)
Q21. Have you ever had a colonoscopy?			
No	87 (87)	46 (92)	41 (82)
Yes	13 (13)	4 (8)	9 (18)

Domain	All participants (N=100)	Control (N=50)	Intervention (N=50)
Q30. Are you willing to undergo colon cancer testing within 6 months?			
No	52 (52)	46 (92)	6 (12)
Yes	48 (48)	4 (8)	44 (88)
Knowledge			
Q22. I believe that there is only one screening test for colon cancer.			
No	51 (51)	5 (10)	46 (92)
Yes	49 (49)	45 (90)	4 (8)
Q23. There is a stool blood test using a "home" test			
No	60 (60)	49 (98)	11 (22)
Yes	40 (40)	1 (2)	39 (78)
Q24. I believe that people are supposed to start getting tested for colon cancer at age of 50.			
No	64 (64)	32 (64)	32 (64)
Yes	36 (36)	18 (36)	18 (36)
Q25. Once people start having stool blood test, they should have them every 3 years.			
No	68 (68)	29 (58)	39 (78)
Yes	32 (32)	21 (42)	11 (22)
Q26. In general, once people start having colonoscopy exams at age of 50, they should have them every 5 years.			
No	52 (52)	28 (56)	24 (48)
Yes	48 (48)	22 (44)	26 (52)
Q27. I believe that colon cancer is mainly a problem for men.			
No	50 (50)	43 (86)	7 (14)
Yes	50 (50)	7 (14)	43 (86)

Data are presented as number of patients (column %).

Comparison in awareness, behavior, and knowledge between Korean American participants in the post-intervention and control groups. Univariate and multivariable analyses of each domain for post-intervention vs. control are shown.

Table 3:

Domain	Univariate		Multivariable*	
	Odds Ratio (95% CI)	P-value	Odds Ratio (95% CI)	P-value
Awareness				
Q14. Heard about colorectal cancer	0.65 (0.10–4.08)	0.649	0.97 (0.11–8.30)	0.980
Q15. Heard about colorectal polyp	23.14 (7.62–70.31)	<0.001	22.47 (6.42–78.62)	<0.001
Q16. Heard about the FOBT or stool blood test	180.17 (38.20–849.83)	<0.001	245.37 (34.55–1742.75)	<0.001
Q19. Heard about colonoscopy	0.47 (0.11–1.99)	0.303	0.64 (0.12–3.32)	0.593
Behavior				
Q17. Ever been recommended for colon cancer (FOBT) test	245.44 (47.11–1278.77)	<0.001	1473.56 (68.58–31660.02)	<0.001
Q18. Ever had a FOBT	1.00 (0.06–16.44)	1.000	0.23 (0.01–9.56)	0.437
Q20. Ever been recommended for colonoscopy	68.31 (14.51–321.58)	<0.001	91.90 (15.06–560.96)	<0.001
Q21. Ever had a colonoscopy	2.52 (0.72–8.82)	0.147	2.08 (0.51–8.50)	0.309
Q30. Are you willing to undergo colon cancer testing within 6 months?	84.33 (22.28–319.14)	<0.001	87.17 (19.01–399.63)	<0.001
Knowledge				
Q22. I do not believe that there is only one screening test for colon cancer.**	158.39 (32.45–773.18)	<0.001	126.63 (23.61–679.07)	<0.001
Q23. There is a stool blood test using a “home” test.	173.73 (21.49–1404.51)	<0.001	157.17 (18.02–1370.41)	<0.001
Q24. I believe that people are supposed to start getting tested for colon cancer at age of 50.	1.00 (0.44–2.26)	1.000	0.75 (0.29–1.95)	0.561
Q25. Once people start having stool blood test, they should have them every 3 years.**	2.57 (1.07–6.15)	0.034	2.64 (0.97–7.21)	0.057
Q26. In general, once people start having colonoscopy exams at age of 50, they should have them every 5 years.**	0.73 (0.33–1.59)	0.424	0.87 (0.35–2.14)	0.761

Abbreviations: FOBT, fecal occult blood test.

Odds ratio is for the intervention group relative to the control group. 100 observations were used in the multivariable models.

* The propensity score (PS) of being in the intervention group was estimated using a multivariable logistic regression model including Q1 through Q11, Q13, and Q28–Q29. Then, the multivariable model was adjusted for the PS.

** Models were fitted with a response ‘No’ vs. ‘Yes’ as ‘No’ is the correct answer.

REVIEW

Open Access

Sexual pain and IC/BPS in women

Su Jin Kim^{1,5}, Jayoung Kim^{2,3*} and Hana Yoon^{4*}



Abstract

Interstitial cystitis/bladder pain syndrome (IC/BPS) and female sexual dysfunction (FSD) are common conditions that substantially reduce women's health. In particular, women with IC/BPS show vulvodynia, a kind of FSD that originates from consistent pain around the vulvar area. There have been many studies attempting to find the underlying mechanisms that induce the chronic pain associated with IC/BPS and vulvodynia and explain why these two conditions often coexist. Proposed theories suggest that pain hypersensitivity is being mediated by peripheral and central sensitization. However, there are still many unknown factors, such as etiologies, that can evoke pain hypersensitivity and may be linking the casual relationship between IC/BPS and vulvodynia. At present, knowledge regarding IC/BPS and vulvodynia are insufficient when considering their clinical importance. Therefore, efforts are necessary to elucidate the issues surrounding IC/BPS and vulvodynia.

Keywords: Cystitis, interstitial, Sexual dysfunction, Chronic pain, Vulvodynia, Lower urinary tract symptoms, Quality of life

Background

Female sexual dysfunction (FSD) and interstitial cystitis/bladder pain syndrome (IC/BPS) are two conditions affecting women's health. A study on the association between sexual and general well-being found that women reported better quality of life (QoL) with higher sexual satisfaction, regardless of age and/or menopausal status [1]. Both FSD and IC/BPS significantly impairs a woman's abilities to pursue and enjoy sexual relations. Approximately 40–50% of women experience FSD and 0.5–12% experience IC/BPS. Considering these incidence rates, both FSD and IC/BPS present serious challenges for patients and clinicians [2–6].

Chronic pain deteriorates not only personal health and wellness, but also QoL. Chronic pain can induce sexual dysfunction, such as arousal disorder, and relationship problems [7]. Furthermore, studies have shown that significantly more women with chronic pelvic pain (CPP) show FSD compared to those without CPP. Women with CPP and FSD reported various types of sexual dysfunctions, including hypoactive sexual desire disorder, sexual arousal disorder, orgasmic disorder, and sexual pain disorder [8].

The symptoms of IC/BPS, such as urinary frequency, urgency, and pelvic pain, can have a negative impact on sexual activity and QoL [9]. Women with overactive bladder (OAB) frequently have a risk for sexual dysfunction [10]. In the postmenopausal group, women with scores indicating severe OAB reported worse sexual function, particularly in the arousal, lubrication, orgasm, pain, and total domains [11]. Despite the known association between FSD and bladder diseases, contributing risk factors have yet to be explored. Evaluating the impact of duration, severity, pain localization, sexual trauma history, anxiety, and depression associated with sexual dysfunction may help elucidate risk factors. Increasing our knowledge about sexual dysfunction as it relates to bladder diseases may aid in clinical diagnoses, treatment strategies, and overall symptom improvement. This review will provide an overview of studies that address FSD in women with IC/BPS.

Pain in FSD

According to consensus from the 4th International Consultation on Sexual Medicine (ICSM), FSD is classified as hypoactive sexual desire dysfunction, female sexual arousal dysfunction, female orgasmic dysfunction, female-genital-pelvic pain dysfunction, persistent genital arousal disorder, postcoital syndrome, hypohedonic orgasm, or painful orgasm [2, 12]. Guidelines from the 4th ICSM also define pain-associated FSD as female-genital-pelvic pain dysfunction and include all conditions that inhibit sexual

* Correspondence: Jayoung.Kim@csmc.edu; wowhana@ewha.ac.kr

²Departments of Surgery and Biomedical Sciences, Cedars-Sinai Medical Center, Los Angeles, CA 90048, USA

⁴Department of Urology, Medical Research Center, Ewha Womans University School of Medicine, Seoul, Republic of Korea

Full list of author information is available at the end of the article



intercourse or induce negative effects on sexual functions. Female-genital-pelvic pain dysfunction is different from the previous classification characterized as pain associated with FSD, which includes sexual pain disorder including dyspareunia and vaginismus [13]. According to the ICSM, female-genital-pelvic pain dysfunction includes persistent or recurrent difficulties with at least one of the following: (1) vaginal penetration during intercourse, (2) marked vulvovaginal or pelvic pain during genital contact, (3) marked fear or anxiety about vulvovaginal or pelvic pain in anticipation of, during, or as a result of genital contact, or (4) marked hypertonicity or overactivity of pelvic floor muscles with or without genital contact [14]. Painful orgasm also falls under this category and is defined as genital and/or pelvic pain during or shortly after orgasm [2]. These recent new definitions reflect the evolving concept behind pain-associated FSD as it also now includes pain in the vulvovaginal and pelvic area and pelvic floor hypertonicity. The new categorization of female-genital-pelvic pain dysfunction has broadened the view on pain-associated FSD and has differentiated it from its previous classification, which confined symptoms to each organ or single disease. This recent change in classification by the ICSM considers pain-associated FSD as a complex condition influenced by psychological and physical factors and supports the general thought that FSD is multifactorial.

Previously, vulvodynia had been generalized under chronic vulvar pain with no precise discrimination for it. However, recent consensus has redefined chronic vulvar pain as vulvar pain associated with specific diseases, such as inflammation, neoplasm, and/or injury. This was conducted at a conference with the International Society for the Study of Vulvovaginal Disease, the International Society for the Study of Women's Sexual Health, and the International Pelvic Pain Society [15]. Vulvodynia can have diverse pain characteristics; therefore, pain-based classification helps in identification, diagnosis, and treatment. Vulvodynia can be characterized as either general (entire vulva) or localized (parts of the vulva). Additionally, based on the situation of the pain, vulvodynia can be classified as either provoked (triggered by physical contact) or unprovoked (spontaneous occurrence without specific triggers) [16]. Women of all ages can experience vulvodynia, and provoked vulvodynia is the most commonly diagnosed [17, 18]. Provoked vulvodynia is thought to be more widely diagnosed than unprovoked because its symptoms can be better recognized by doctors. Therefore, there is a great need to better identify unprovoked vulvodynia patients.

Sexual pain and IC/bps

IC/BPS is a disorder that induces chronic pain or discomfort in the bladder and surrounding pelvic organs [19, 20]. At present, IC/BPS is not a disease confined to just the

bladder and pelvic area; it is a complex disease that includes the outside of the genitourinary tract. Tripp et al. [21] investigated the pain characteristics of IC/BPS using whole-body diagram pain locators. They found that women with IC/BPS reported significantly more pain all over their body, compared to healthy women without. Only 52 of the 193 IC/BPS diagnosed women (27%) presented pain restricted to the bladder and pelvic area. Moreover, IC/BPS patients had various co-morbidities. Diseases, such as irritable bowel syndrome, fibromyalgia, vulvodynia, chronic pelvic pain, endometriosis, OAB, allergies and chronic fatigue syndrome, were found to coexist in IC/BPS patients [22–28].

In addition, there are several reports that IC/BPS can increase the risk for or worsen other diseases, including FSD. A population-based study found higher prevalence of FSD in women with IC/BPS [29]. FSD incidence also increased depending on the severity of IC/BPS symptoms, suggesting that FSD is a factor may be worsening IC/BPS. In regards to the pain associated with FSD, vulvodynia may be contributing to flare-ups of IC/BPS symptoms and could be the reason why IC/BPS patients avoid sexual activity [9, 30].

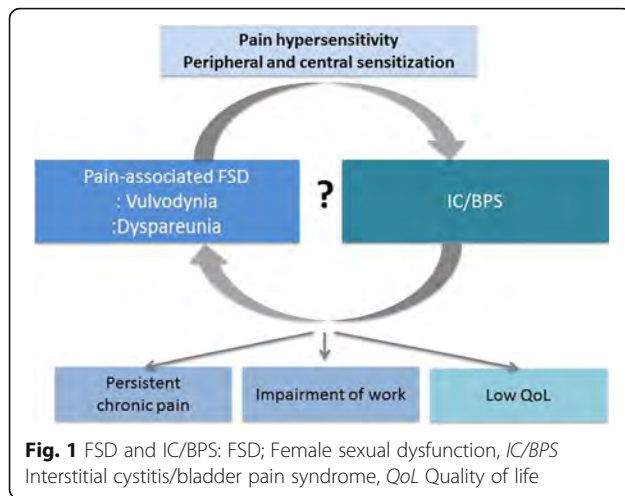
Can FSD and IC/bps be generalized as one disease?

Diseases characterized with lower urinary tract symptoms (LUTS) in females, such as incontinence and OAB, are known to have a negative impact on all domains in female sexual function. Symptoms of IC/BPS can also deteriorate patient's sexual activities and QoL. A significant number of IC/BPS patients avoid sexual activity because of pain. In addition, FSD and IC/BPS share similar clinical characteristics and comorbidities, making it difficult to discriminate between the two [31–33]. As mentioned previously, there are many clinical reports presenting an association between IC/BPS and vulvodynia, mainly due to shared FSD conditions.

Although the mechanisms of the association between IC/BPS and vulvodynia are unclear, visceral nerve cross-talking and the anatomic relationship between genital organs and the bladder offer a simple proximity explanation. Another possible mechanism behind the relationship is abnormal pain hypersensitivity induced by peripheral and central sensitization. The abnormal pain response frequently observed in vulvodynia patients is caused by central or peripheral maladaptive pain processing from local insult, injury, or trauma (Fig. 1).

Role of peripheral sensitization in the pain hypersensitivity of vulvodynia and IC/BPS

Exposure of nociceptors to repetitive pain stimulation reduces the pain threshold and amplifies the responsiveness of nociceptors. Therefore, this can abnormally increase peripheral transduction of sensitivity and lead to the



development of peripheral pain hypersensitivity [34–36]. The potential underlying mechanism of peripheral pain hypersensitivity noted in both vulvodynia and IC/BPS could be due to sensory nerve upregulation. Previous studies have shown that sensory nerve density is significantly increased in the vulva vestibule and bladder. Compared to the normal controls, patients with vulvodynia were found to have increased nociceptors in their vulvar vestibule [37–40]. Consequentially, this increased density of peripheral nociceptors results in increased sensitivity. It was also found that transient receptor potential V1 (TRPV1) exists in these nociceptive nerve endings and enhances pain signaling [37, 41, 42]. Pukall CF et al. [43] and Giesecke J et al. [44] reported increased peripheral tactile, pressure, and pain sensitivity in the patients with vulvodynia and confirmed histologic and molecular changes of peripheral nociceptors is associated with clinical manifestations. Similarly with vulvodynia, it has been reported that IC/BPS patient bladders have upregulated sensory innervation and TRPV1 expression [45–47].

Role of central sensitization in the pain hypersensitivity of vulvodynia and IC/BPS

Central sensitization is an important mechanism underlying various conditions associated with chronic pain and induces pain hypersensitivity through pathologically enhanced pathways that are not normally associated with nociception. For example, the low-threshold A δ fiber, that is mostly used for temperature and pressure signaling, can be sensitized to pain. Chronic pain induced by central sensitization is persistent even after initiation of the signal and disappearance of the peripheral cause [48]. Studies have shown that the pain characteristics of central sensitization can be found in vulvodynia patients. Foster DC et al. [49] observed that vulvar vestibulitis syndrome patients experienced hyperalgesia and allodynia more often than normal controls after intradermal foot and

forearm capsaicin injections. In addition, pelvic organ crosstalk has an important role in central sensitization because pelvic organs, such as the bladder, colon and vulva, are controlled by the same neural pathway [50]. Thus, afferent signals from other pelvic organs can provoke pain through neural crosstalk even though the initiation and peripheral causes of vulvodynia and IC/BPS have gone. Therefore, central sensitization plays an important role in the chronic pain observed in vulvodynia and IC/BPS. Clinically, similar manifestations of vulvodynia and IC/BPS have also existed. Moreover, recently, there has been an attempt to categorize various pain-associated conditions due to central sensitization as central sensitivity syndrome (CSS). Vulvodynia and IC/BPS are considered subgroups of CSS [51]. Previous studies on clinical findings support the notion that the same mechanisms associated with central sensitization are involved in the pain behind vulvodynia and IC/BPS [52–54].

Recently, evidence supporting central sensitization using functional and structural brain imaging were reported in vulvodynia and IC/BPS. Previously, Pukall et al. [55] showed that increased perception and activation of pain-related brain regions were observed in women with vulvar vestibulitis syndrome, compared to normal women, after tactile stimulation of the vulvar vestibule. Other studies have reported that vulvodynia patients show increased grey matter density in pain-modulating and stress-related regions of the brain as well as alterations in the intrinsic connectivity of regions comprising the sensorimotor, salience, and default mode resting state networks [56, 57]. Similarly, women with IC/BPS showed alterations of oscillation frequency and functional connectivity of brain regions previously reported in other chronic pain conditions [58] and various white matter (right anterior thalamic radiation, left forceps major, and right longitudinal fasciculus, right superior and bilateral inferior longitudinal fasciculi) abnormalities that correlated with severity of pain, urinary symptoms, and impaired QoL [59]. Fig. 2 shows common therapeutic approaches and points of divergence among IC/BPS, IC/BPS + vulvodynia, and vulvodynia patient groups.

Approach and management of vulvodynia and IC/bps patients

Clinically, vulvodynia and IC/BPS often coexists and differentiation between the two is not easy, especially when the patient reports LUTS combined with pain. A majority of patients also seek medical care after relatively longer periods of initially feeling pain, leading to central sensitization that has been firmly established. Furthermore, clinical manifestations of chronic pain found in various other comorbidities can mask vulvodynia and IC/BPS, making it confusing and difficult to officially diagnose.

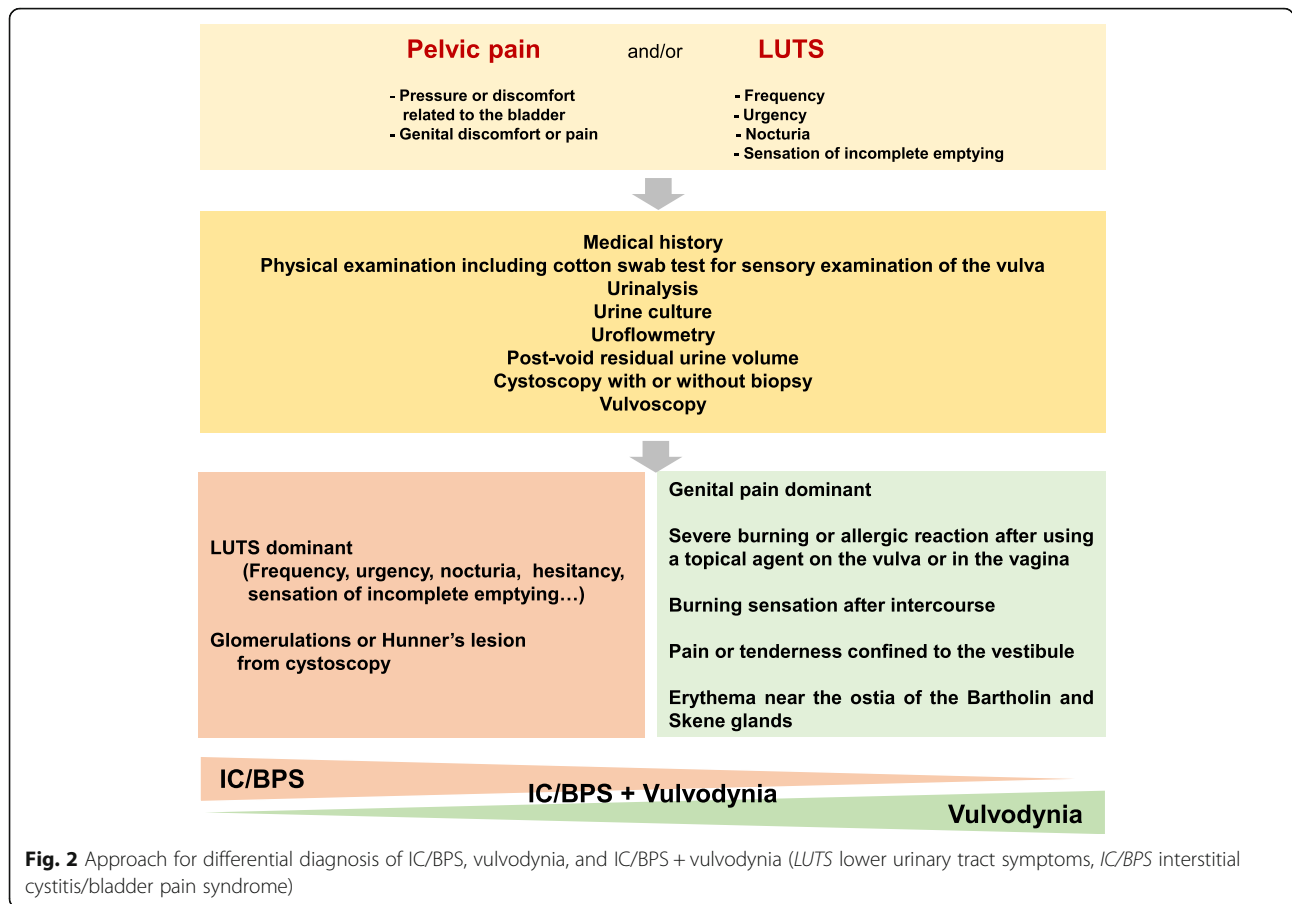


Table 1 Characteristics of FSD observed in women with IC/BPS

	Age	Types of FSD	Prevalence (%)	Other associated conditions
Verit et al. [8] ^a	34.73 ± 8.07 years	NA	67.8 (78 of 112)	NA
Gardella et al. [28]	38.7 ± 12 years	Vulvodynia Dyspareunia	Vulvodynis: 85.1 (40 of 47) Vaginal burning: 65.9 (31 of 47) Dyspareunia: 31.9 (15 of 47)	LUTS (frequency, urgency)
Carrico et al. [24]	52 years (range, 19–90)	Vulvodynia	Vulvar pain: 48.1 (91/189) Pain with intercourse: 66.9 (117/175)	Sexually transmitted infections (genital warts, positive HPV, gonorrhea, chlamydia)
Yoon et al. [9]	51.0 ± 14.7 years	Vulvodynia Dyspareunia	NA	LUTS (frequency, urgency)
Bogart et al. [27]	43.6 ± 16.7 years	NA	Women experienced with sexual dysfunction symptoms: 88 (866/985)	NA
Gardella et al. [23]	38.2 ± 11.3 years	Vulvodynia Dyspareunia	Spontaneous vulvodynia: 23.4 (11 of 47) Provoked vulvodynia: 74.5 (35/47) Localized vulvodynia: 80.9 (38/47) Generalized vulvodynia: 17 (8/47) Dyspareunia: 87.2 (41/47)	NA

^aThis study was done in the women diagnosed of chronic pelvic pain. FSD female sexual dysfunction, IC/BPS interstitial cystitis/bladder pain syndrome, LUTS lower urinary tract symptom, NA Not applicable

Many previous studies have revealed a close correlation between LUTS and impaired sexual function; IC/BPS is not an exception. Besides, it is not uncommon to have trouble differentiating sexual pain and IC/BPS-related genital pain in women. Unfortunately, despite the growing population of affected individuals, there is a lack of comprehensive studies regarding sexual dysfunction and IC/BPS (Table 1). Clinicians should take more concern regarding sexual dysfunction and pain in IC/BPS patients, and more randomized controlled studies should be conducted to better understand correlations and diagnostic differentiations.

Conclusions

Both vulvodynia and IC/BPS are common and irritable conditions that disrupt normal life and reduce QoL in women. Vulvodynia also manifests itself along with IC/BPS and there are several reports supporting an association between the two diseases. Unfortunately, knowledge concerning vulvodynia and IC/BPS is inadequate when considering the clinical impact and importance of these two conditions. Therefore, there is an essential need for further studies that delve into discovering the features of vulvodynia and IC/BPS.

Abbreviations

CPP: Chronic pelvic pain; CSS: Central sensitivity syndrome; FSD: Female sexual dysfunction; IC/BPS: Interstitial cystitis/bladder pain syndrome; ICSM: International consultation on sexual medicine; LUTS: Lower urinary tract symptoms; OAB: Overactive bladder; QoL: Quality of life; TRPV1: Transient receptor potential V1

Acknowledgements

The authors would like to thank Mr. Taeun Daniel Park and Mr. Austin Yeon for careful review and editing the manuscript.

Authors' contributions

HY and JK made substantial contributions to conception and design and involved in critically for important intellectual content. SK was involved in acquisition of data, interpretation of data, and drafting the manuscript. All authors gave final approval of the version to be published.

Funding

The authors acknowledge support from National Institutes of Health grants (1U01DK103260), Department of Defense grants (W81XWH-15-1-0415 and W81XWH-19-1-0109), Centers for Disease Control and Prevention (1U01DP006079), the Steven Spielberg Discovery Fund in Prostate Cancer Research Career Development Award, the U.S.-Egypt Science and Technology Development Fund by the National Academies of Sciences, Engineering, and Medicine, Burroughs Wellcome Fund (BWF) 2017 Collaborative Research Travel Grant (CRTG), and Southeast Center for Integrated Metabolomics (SECIM) Pilot and Feasibility Grant (to J.K.). This funding source had no role in the design of this study and will not have any role during its execution, analyses, interpretation of the data, or decision to submit results.

Availability of data and materials

Not applicable.

Ethics approval and consent to participate

Not applicable.

Consent for publication

Not Applicable.

Competing interests

The author(s) declare(s) that they have no competing interests.

Author details

¹Department of Urology, Seoul St. Mary's Hospital, The Catholic University of Korea College of Medicine, Seoul, Republic of Korea. ²Departments of Surgery and Biomedical Sciences, Cedars-Sinai Medical Center, Los Angeles, CA 90048, USA. ³Department of Medicine, University of California Los Angeles, Los Angeles, CA 90095, USA. ⁴Department of Urology, Medical Research Center, Ewha Womans University School of Medicine, Seoul, Republic of Korea. ⁵Current address: Department of Urology, Yonsei University Wonju College of Medicine, Wonju, Republic of Korea.

Received: 16 February 2018 Accepted: 22 May 2019

Published online: 06 June 2019

References

- Davison SL, Bell RJ, LaChina M, Holden SL, Davis SR. The relationship between self-reported sexual satisfaction and general well-being in women. *J Sex Med.* 2009;6:2690–7.
- McCabe MP, Sharlip ID, Lewis R, Atalla E, Balon R, Fisher AD, Laumann E, Lee SW, Segraves RT. Incidence and prevalence of sexual dysfunction in women and men: a consensus statement from the fourth international consultation on sexual medicine 2015. *J Sex Med.* 2016;13:144–52.
- Leppilähti M, Tammela TL, Huhtala H, Auvinen A. Prevalence of symptoms related to interstitial cystitis in women: a population based study in Finland. *J Urol.* 2002;168:139–43.
- Clemens JQ, Meenan RT, O'Keefe Rosetti MC, Brown SO, Gao SY, Calhoun EA. Prevalence of interstitial cystitis. *Urology* 2009 Mar;73(3):494–498. <https://doi.org/10.1016/j.urology.2008.01.053>. Epub 2009 Jan.
- Lifford KL, Curhan GC. Prevalence of painful bladder syndrome in older women. *Urology.* 2009;73:494–8.
- Clemens JQ, Link CL, Eggers PW, Kusek JW, Nyberg LM Jr, McKinlay JB; BACH Survey Investigators. Prevalence of painful bladder symptoms and effect on quality of life in black, Hispanic and white men and women. *J Urol* 2007;177:1390–1394.
- Ambler N, Williams AC, Hill P, Gunary R, Cratchley G. Sexual difficulties of chronic pain patients. *Clin J Pain.* 2001;17:138–45.
- Verit FF, Verit A, Yeni E. The prevalence of sexual dysfunction and associated risk factors in women with chronic pelvic pain: a cross-sectional study. *Arch Gynecol Obstet.* 2006;274:297–302.
- Yoon HS, Yoon H. Correlations of interstitial cystitis/painful bladder syndrome with female sexual activity. *Korean J Urol.* 2010;51:45–9.
- Juliato CRT, Melotti IGR, Junior LCS, Britto LGO, Ricetto CLZ. Does the severity of overactive bladder symptoms correlate with risk for female sexual dysfunction? *J Sex Med.* 2017;14:904–9.
- Cohen BL, Barboglio P, Gousse A. The impact of lower urinary tract symptoms and urinary incontinence on female sexual dysfunction using a validated instrument. *J Sex Med.* 2008;5:1418–23.
- Jayasena CN, Alkaabi FM, Liebers CS, Handley T, Franks S, Dhillon WS. A systematic review of randomized controlled trials investigating the efficacy and safety of testosterone therapy for female sexual dysfunction in postmenopausal women. *Clin Endocrinol.* 2019;90:391–414.
- Leiblum SR. Classification and diagnosis of female sexual disorders. In: Goldstein I, Meston CM, Davis S, Traish AM, editors. *Women's sexual function and dysfunction: study, diagnosis and treatment.* London: Taylor and Francis; 2005. p. 323–31.
- McCabe MP, Sharlip ID, Atalla E, Balon R, Fisher AD, Laumann E, Lee SW, Lewis R, Segraves RT. Definitions of sexual dysfunctions in women and men: a consensus statement from the fourth international consultation on sexual medicine 2015. *J Sex Med.* 2016;13:135e143.
- 2015 Consensus terminology and classification of persistent vulvar pain. http://www.iswsh.org/images/PDF/Consensus_Terminology_of_Vulvar_Pain.pdf
- Haefner HK. Report of the International Society for the Study of Vulvovaginal Disease Terminology and Classification of Vulvodynia. *J Low Genit Tract Dis.* 2007;11:48–9.
- Clare CA, Yeh J. Vulvodynia in adolescence: childhood vulvar pain syndromes. *J Pediatr Adolesc Gynecol.* 2011;24:110–5.
- Reed BD, Harlow SD, Sen A, Legocki LJ, Edwards RM, Arato N, Haefner HK. Prevalence and demographic characteristics of vulvodynia in a population-based sample. *Am J Obstet Gynecol.* 2012;206:170.e1–9.

19. Barr S. Diagnosis and management of interstitial cystitis. *Obstet Gynecol Clin N Am.* 2014;41:397–407.
20. Hanno P, Nordling J, van Ophoven A. What is new in bladder pain syndrome/interstitial cystitis? *Curr Opin Urol.* 2008;18:353–8.
21. Tripp DA, Nickel JC, Wong J, Pontari M, Moldwin R, Mayer R, Carr LK, Doggweiler R, Yang CC, Mishra N, Nordling J. Mapping of pain phenotypes in female patients with bladder pain syndrome/interstitial cystitis and controls. *Eur Urol.* 2012;62:1188–94.
22. Nickel JC, Tripp DA, Pontari M, Moldwin R, Mayer R, Carr LK, Doggweiler R, Yang CC, Mishra N, Nordling J. Interstitial cystitis/painful bladder syndrome and associated medical conditions with an emphasis on irritable bowel syndrome, fibromyalgia and chronic fatigue syndrome. *J Urol.* 2010;184:1358–63.
23. Chelimsky G, Heller E, Buffington CA, Rackley R, Zhang D, Chelimsky T. Comorbidities of interstitial cystitis. *Front Neurosci.* 2012;6:114.
24. Alagiri M, Chottiner S, Ratner V, Slade D, Hanno PM. Interstitial cystitis: unexplained associations with other chronic disease and pain syndromes. *Urology.* 1997;49:52–7.
25. Gardella B, Porru D, Nappi RE, Dacco MD, Chiesa A, Spinillo A. Interstitial cystitis is associated with vulvodynia and sexual dysfunction—a case-control study. *J Sex Med.* 2011;8:1726–34.
26. Carrico DJ, Sherer KL, Peters KM. The relationship of interstitial cystitis/painful bladder syndrome to vulvodynia. *Urol Nurs.* 2009;29:233–8.
27. Pontari MA. Chronic prostatitis/chronic pelvic pain syndrome and interstitial cystitis: are they related? *Curr Urol Rep.* 2006;7:329–34.
28. Elliott CS, Payne CK. Interstitial cystitis and the overlap with overactive bladder. *Curr Urol Rep.* 2012;13:319–26.
29. Bogart LM, Suttrop MJ, Elliott MN, Clemens JQ, Berry SH. Prevalence and correlates of sexual dysfunction among women with bladder pain syndrome/interstitial cystitis. *Urology.* 2011;77:576–80.
30. Gardella B, Porru D, Ferdeghini F, Martinotti Gabellotti E, Nappi RE, Rovereto B, Spinillo A. Insight into urogynecologic features of women with interstitial cystitis/painful bladder syndrome. *Eur Urol.* 2008;54:1145–51.
31. Groysman V. Vulvodynia: new concepts and review of the literature. *Dermatol Clin.* 2010;28:681–96.
32. Shah M, Hoffstetter S. Vulvodynia. *Obstet Gynecol Clin N Am.* 2014;41:453–64.
33. Dasgupta J, Tincello DG. Interstitial cystitis/bladder pain syndrome: an update. *Maturitas.* 2009;64:212–7.
34. Hucho T, Levine JD. Signaling pathways in sensitization: toward a nociceptor cell biology. *Neuron.* 2007;55:365–76.
35. Chen X, Tanner K, Levine JD. Mechanical sensitization of cutaneous C-fiber nociceptors by prostaglandin E2 in the rat. *Neurosci Lett.* 1999;267:105–8.
36. Petho G, Derow A, Reeh PW. Bradykinin-induced nociceptor sensitization to heat is mediated by cyclooxygenase products in isolated rat skin. *Eur J Neurosci.* 2001;14:210–8.
37. Bohm-Starke N, Hilliges M, Falconer C, Rylander E. Increased intraepithelial innervation in women with vulvar vestibulitis syndrome. *Gynecol Obstet Investig.* 1998;46:256–60.
38. Bohm-Starke N, Hilliges M, Falconer C, Rylander E. Neurochemical characterization of the vestibular nerves in women with vulvar vestibulitis syndrome. *Gynecol Obstet Investig.* 1999;48:270–5.
39. Tympanidis P, Terenghi G, Dowd P. Increased innervation of the vulval vestibule in patients with vulvodynia. *Br J Dermatol.* 2003;148:1021–7.
40. Goetsch MF, Morgan TK, Korcheva VB, Li H, Peters D, Leclair CM. Histologic and receptor analysis of primary and secondary vestibulodynia and controls: a prospective study. *Am J Obstet Gynecol.* 2010;202:614.e1–8.
41. Halperin R, Zehavi S, Vaknin Z, Ben-Ami I, Pansky M, Schneider D. The major histopathologic characteristics in the vulvar vestibulitis syndrome. *Gynecol Obstet Investig.* 2005;59:75–9.
42. Tympanidis P, Casula MA, Yiangou Y, Terenghi G, Dowd P, Anand P. Increased vanilloid receptor VR1 innervation in vulvodynia. *Eur J Pain.* 2004;8:129–33.
43. Pukall CF, Binik YM, Khalifé S, Amsel R, Abbott FV. Vestibular tactile and pain thresholds in women with vulvar vestibulitis syndrome. *Pain.* 2002;96:163–75.
44. Giesecke J, Reed BD, Haefner HK, Giesecke T, Clauw DJ, Gracely RH. Quantitative sensory testing in vulvodynia patients and increased peripheral pressure pain sensitivity. *Obstet Gynecol.* 2004;104:126–33.
45. Hanno P, Andersson KE, Birder L, Elnil S, Kanai A, Pontari M. Chronic pelvic pain syndrome/bladder pain syndrome: taking stock, looking ahead: ICI-RS 2011. *Neurourol Urodyn.* 2012;31:375–83.
46. Amaya F, Oh-hashi K, Naruse Y, Iijima N, Ueda M, Shimamoto G, Tominaga M, Tanaka Y, Tanaka M. Local inflammation increases vanilloid receptor 1 expression within distinct subgroups of DRG neurons. *Brain Res.* 2003;963:190–6.
47. Liu BL, Yang F, Zhan HL, Feng ZY, Zhang ZG, Li WB, Zhou XF. Increased severity of inflammation correlates with elevated expression of TRPV1 nerve fibers and nerve growth factor on interstitial cystitis/bladder pain syndrome. *Urol Int.* 2014;92:202–8.
48. Latremoliere A, Woolf CJ. Central sensitization: a generator of pain hypersensitivity by central neural plasticity. *J Pain.* 2009;10:895–926.
49. Foster DC, Dworkin RH, Wood RW. Effects of intradermal foot and forearm capsaicin injections in normal and vulvodynia-afflicted women. *Pain.* 2005;117:128–36.
50. Klumpp DJ, Rudick CN. Summation model of pelvic pain in interstitial cystitis. *Nat Clin Pract Urol.* 2008;5:494–500.
51. Yunus MB. Editorial review: an update on central sensitivity syndromes and the issues of nosology and psychobiology. *Curr Rheumatol Rev.* 2015;11:70–85.
52. Kayhan F, Kükük A, Satan Y, Ilgün E, Arslan Ş, Ilik F. Sexual dysfunction, mood, anxiety, and personality disorders in female patients with fibromyalgia. *Neuropsychiatr Dis Treat.* 2016;12:349–55.
53. Bel LG, Vollebregt AM, Van der Meulen-de Jong AE, Fidder HH, ten Hove WR, Vliet-Vlieland CW, Ter Kuile MM, de Groot HE, both S. sexual dysfunctions in men and women with inflammatory bowel disease: the influence of IBD-related clinical factors and depression on sexual function. *J Sex Med.* 2015;12:1557–67.
54. Clemens JQ, Elliott MN, Suttrop M, Berry SH. Temporal ordering of interstitial cystitis/bladder pain syndrome and non-bladder conditions. *Urology.* 2012;80:1227–31.
55. Pukall CF, Strigo IA, Binik YM, Amsel R, Khalifé S, Bushnell MC. Neural correlates of painful genital touch in women with vulvar vestibulitis syndrome. *Pain.* 2005;115:118–27.
56. Schweinhardt P, Kuchinad A, Pukall CF, Bushnell MC. Increased gray matter density in young women with chronic vulvar pain. *Pain.* 2008;140:411–9.
57. Gupta A, Rapkin AJ, Gill Z, Kilpatrick L, Fling C, Stains J, Masghati S, Tillisch K, Mayer EA, Labus JS. Disease-related differences in resting-state networks: a comparison between localized provoked vulvodynia, irritable bowel syndrome, and healthy control subjects. *Pain.* 2015;156:809–19.
58. Kilpatrick LA, Kutch JJ, Tillisch K, Naliboff BD, Labus JS, Jiang Z, Farmer MA, Apkarian AV, Mackey S, Martucci KT, Clauw DJ, Harris RE, Deutsch G, Ness TJ, Yang CC, Maravilla K, Mullins C, Mayer EA. Alterations in resting state oscillations and connectivity in sensory and motor networks in women with interstitial cystitis/painful bladder syndrome. *J Urol.* 2014;192:947–55.
59. Farmer MA, Huang L, Martucci K, Yang CC, Maravilla KR, Harris RE, Clauw DJ, Mackey S, Ellingson BM, Mayer EA, Schaeffer AJ, Apkarian AV, Research Network MAPP. Brain white matter abnormalities in female interstitial cystitis/bladder pain syndrome: a MAPP Network neuroimaging study. *J Urol.* 2015;194:118–26.

Publisher's Note

Springer Nature remains neutral with regard to jurisdictional claims in published maps and institutional affiliations.

Ready to submit your research? Choose BMC and benefit from:

- fast, convenient online submission
- thorough peer review by experienced researchers in your field
- rapid publication on acceptance
- support for research data, including large and complex data types
- gold Open Access which fosters wider collaboration and increased citations
- maximum visibility for your research: over 100M website views per year

At BMC, research is always in progress.

Learn more biomedcentral.com/submissions





Looking into the clinical application of CD47-targeted near-infrared photoimmunotherapy for human bladder cancer treatment

Jayoung Kim^{1,2,3}

¹Department of Surgery and Biomedical Sciences, Cedars-Sinai Medical Center, Los Angeles, CA, USA; ²Department of Medicine, University of California Los Angeles, CA, USA; ³Department of Urology, Ga Cheon University College of Medicine, Incheon, Republic of Korea

Correspondence to: Jayoung Kim, PhD. Department of Surgery and Biomedical Sciences, Cedars-Sinai Medical Center, 8700 Beverly Blvd., Los Angeles, CA 90048, USA. Email: Jayoung.Kim@cshs.org.

Provenance: This is an invited article commissioned by Section Editor Xiao Li (Department of Urology, Jiangsu Cancer Hospital & Jiangsu Institute of Cancer Research & Nanjing Medical University Affiliated Cancer Hospital, Nanjing, China).

Comment on: Kiss B, van den Berg NS, Ertsey R, *et al.* CD47-Targeted Near-infrared Photoimmunotherapy for Human Bladder Cancer. *Clin Cancer Res* 2019;25:3561-71.

Submitted May 20, 2019. Accepted for publication May 28, 2019.

doi: 10.21037/tau.2019.05.13

View this article at: <http://dx.doi.org/10.21037/tau.2019.05.13>

A recently published paper by a Stanford research team led by Dr. Joseph C. Liao in *Clinical Cancer Research* (1) reported on their well-designed study demonstrating the potential application of CD47-targeted near-infrared photoimmunotherapy (NIR-PIT) for human bladder cancer (BC) (Figure 1).

CD47, also known as an integrin-associated protein, is a cell surface transmembrane protein that plays a role in neutrophil migration and T-cell co-stimulation. In the context of BC, high expression levels of CD47 have been observed in BC tumor cells (in both non-muscle invasive and muscle invasive BC). However, expression was found to be absent in terminally differentiated luminal umbrella cells of the normal bladder epithelium. Thus, blocking CD47 may enable our immune system to selectively recognize BC cells, leading to the hypothesis that targeting CD47 may be the potential strategy for specifically killing cancer cells while avoiding unnecessary harm to normal bladder cells. In this paper, the authors elegantly performed a series of *in vitro* experiments using well-characterized BC cell lines. Their *in vivo* experiments used human specimens, which successfully showed that anti-CD47-IR700 may play as a molecular photosensitizer for NIR-PIT of BC. Further experimental results using a xenograft mouse model suggested that CD47-targeted NIR-PIT may effectively block BC growth.

Phototherapy, also known as light therapy, utilizes specific wavelengths of light to treat medical conditions. The inception of this idea began in the late 19th century by Ryberg Finsen, who developed phototherapy for the treatment of lupus vulgaris, a type of skin condition (2). Since then, phototherapy has been adapted and modified into various forms, such as photoimmunological, photochemical, and photodynamic therapies (3). These different phototherapies have become incredibly advantageous when it comes to treating cancer. They have diversified treatment options and are versatile enough to be combined with other therapies. For instance, photoimmunotherapy (PIT) has been shown to increase nano-drug uptake 24-fold in tumor tissues compared to normal (4). Photodynamic therapy (PDT) has been demonstrated to successfully destroy tumor cells, which leads to stimulation of anti-tumor immunity and generation of an innate immune response (5). Because treatment options for BC are mainly limited to surgery and chemotherapy, utilization of these phototherapies are of particular interest.

Unfortunately, when it comes to BC, PDT has largely been abandoned. Clinical trials of PDT lead to several noted adverse events that ultimately demonstrated toxicity and bystander effects on normal bladder cells (6). Another potential challenge of using PDT in BC is the hypoxic microenvironment in BC tissues, which limits

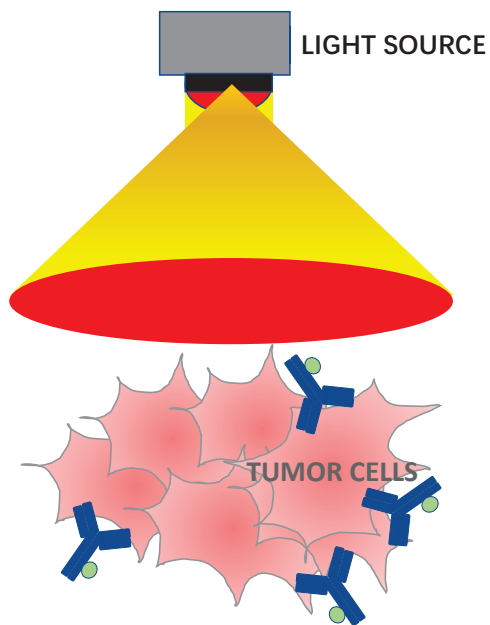


Figure 1 CD47-targeted near-infrared photoimmunotherapy.

the needed O_2 supply for creating reactive oxygen species and eventual cell death (7,8). There have been some studies that have addressed the issue of hypoxia and demonstrated potential reintroduction of PDT in BC, but clinical application remains far ahead (9). On the other hand, PIT has had promising results and is being further explored as a viable treatment option. Studies have demonstrated highly-selective targeting of BC cells by conjugating a photoabsorber dye with panitumumab, an anti-EGFR antibody (10). This strategy takes advantage of the fact that EGFR is overexpressed in BC tissue, with relatively low expression in normal bladder urothelial cells (11,12). A recent study took this a step further by targeting HER2 along with EGFR, which would allow for more effective apoptosis of BC cells across different tumor phenotypes (13).

Collectively, these promising findings by this research team was able to provide persuasive evidence that CD47-targeted NIR-PIT can be deployed endoscopically and holds the potential to augment treatment of localized BC. NIR-PIT, a localized molecular cancer therapy combining a photosensitizer-conjugated monoclonal antibody and light energy, is a particularly attractive tool to use in the urinary tract due to ease of access. One major and important concern is related to safety and therapeutic efficacy. Since it is currently being investigated in other clinical trials

for hematopoietic and solid cancers (ClinicalTrials.gov NCT02216409), I believe that we will have better idea how CD47-targeted NIR-PIT therapy can be used as a potential standard option of treatment against BC in the real clinical setting soon.

Acknowledgments

The author would like to thank Mr. Austin Yeon for careful review and editing the manuscript.

Funding: The author acknowledges support from National Institutes of Health grants (1U01DK103260), Department of Defense grants (W81XWH-15-1-0415 and W81XWH-19-1-0109), Centers for Disease Control and Prevention (1U01DP006079), the Steven Spielberg Discovery Fund in Prostate Cancer Research Career Development Award, the U.S.-Egypt Science and Technology Development Fund by the National Academies of Sciences, Engineering, and Medicine, Burroughs Wellcome Fund (BWF) 2017 Collaborative Research Travel Grant (CRTG), and Southeast Center for Integrated Metabolomics (SECIM) Pilot and Feasibility Grant (to J Kim).

Footnote

Conflicts of Interest: The author has no conflicts of interest to declare.

References

1. Kiss B, van den Berg NS, Ertsey R, et al. CD47-Targeted Near-infrared Photoimmunotherapy for Human Bladder Cancer. *Clin Clin Cancer Res* 2019;25:3561-71.
2. Grzybowski A, Pietrzak K. From patient to discoverer--Niels Ryberg Finsen (1860-1904) --the founder of phototherapy in dermatology. *Clin Dermatol* 2012;30:451-5.
3. Li Y, Li X, Zhou F, et al. Nanotechnology-based photoimmunological therapies for cancer. *Cancer Lett* 2019;442:429-38.
4. Kobayashi H, Choyke PL. Super enhanced permeability and retention (SUPR) effects in tumors following near infrared photoimmunotherapy. *Nanoscale* 2016;8:12504-9.
5. Mroz P, Hashmi JT, Huang YY, et al. Stimulation of anti-tumor immunity by photodynamic therapy. *Expert Rev Clin Immunol* 2011;7:75-91.
6. Raikar R, Agarwal PK. Photodynamic Therapy in the Treatment of Bladder Cancer: Past Challenges and

- Current Innovations. *Eur Urol Focus* 2018;4:509-11.
7. Blick C, Ramachandran A, Wigfield S, et al. Hypoxia regulates FGFR3 expression via HIF-1alpha and miR-100 and contributes to cell survival in non-muscle invasive bladder cancer. *Br J Cancer* 2013;109:50-9.
 8. Hunter BA, Eustace A, Irlam JJ, et al. Expression of hypoxia-inducible factor-1alpha predicts benefit from hypoxia modification in invasive bladder cancer. *Br J Cancer* 2014;111:437-43.
 9. Lin T, Zhao X, Zhao S, et al. O₂-generating MnO₂ nanoparticles for enhanced photodynamic therapy of bladder cancer by ameliorating hypoxia. *Theranostics* 2018;8:990-1004.
 10. Railkar R, Krane LS, Li QQ, et al. Epidermal Growth Factor Receptor (EGFR)-targeted Photoimmunotherapy (PIT) for the Treatment of EGFR-expressing Bladder Cancer. *Mol Cancer Ther* 2017;16:2201-14.
 11. Chaux A, Cohen JS, Schultz L, et al. High epidermal growth factor receptor immunohistochemical expression in urothelial carcinoma of the bladder is not associated with EGFR mutations in exons 19 and 21: a study using formalin-fixed, paraffin-embedded archival tissues. *Hum Pathol* 2012;43:1590-5.
 12. Rotterud R, Nesland JM, Berner A, et al. Expression of the epidermal growth factor receptor family in normal and malignant urothelium. *BJU Int* 2005;95:1344-50.
 13. Siddiqui MR, Railkar R, Sanford T, et al. Targeting Epidermal Growth Factor Receptor (EGFR) and Human Epidermal Growth Factor Receptor 2 (HER2) Expressing Bladder Cancer Using Combination Photoimmunotherapy (PIT). *Sci Rep* 2019;9:2084.

Cite this article as: Kim J. Looking into the clinical application of CD47-targeted near-infrared photoimmunotherapy for human bladder cancer treatment. *Transl Androl Urol* 2019;8(Suppl 3):S322-S324. doi: 10.21037/tau.2019.05.13



Utilizing machine learning to discern hidden clinical values from big data in urology

Suppose you are asked to choose the single most important information technology that has given decision-making processes a massive upgrade. Many of us would choose machine learning (ML). The application of ML is defined as “giving computers the ability to learn without being explicitly programmed”. The main purpose of ML is to introduce algorithms that ingest input data, apply computer analysis to predicting output values within an acceptable range of accuracy, identify patterns and trends in data, and to learn from previous experience. ML is often applied to complicated and poorly understood natural phenomena, such as complex biological systems, climate change, astronomy, or particle physics.

The two major pathways in ML are supervised and unsupervised learning. In supervised learning, an algorithm is often provided with data, $X_{N \times P}$ (N samples with P number of features) and a desired target y . The goal is to train a model f (e.g., a decision function), that performs prediction on for X , i.e., $f(X)=y$. Supervised learning primarily deals with classification and regression problems. In unsupervised learning, an algorithm is provided with data, X , without any labels/annotations, to find latent patterns, sometimes producing both answers and questions that may not have been conceived by the investigators. Unsupervised learning typically deals with clustering and dimensionality reduction problems. The patterns identified in unsupervised learning often need to be evaluated for utility by human interrogation or via application within a supervised learning task.

While validation of unsupervised algorithm can only be performed with a hidden ground, the performance of a supervised learning algorithm can be evaluated by various metrics based on the objective of a task. A dataset is typically divided into two independent sets, i.e., training and testing sets; where training of an algorithm is performed using the training set and then the trained model is evaluated using the testing set. In order to remove bias introduced in a single division of training/testing sets, cross validation is often used to evaluate supervised learning algorithms.

HOW IS ML APPLIED TO DEVELOP PRECISION MEDICINE?

Many of us in the healthcare and science field would agree that big data will transform medicine. In recent years, large amounts of data have been accumulated through big omics studies of genome, epigenomes, transcriptomes, proteomes, metabolomes, and other sources. This immense data needs to be analyzed, interpreted, and manipulated to provide biological meaning. Where ML shines is in handling enormous numbers of predictors. ML has become ubiquitous and indispensable for solving complex problems in most sciences. ML will become an indispensable tool for clinicians seeking to truly understand their patients. However, there are several shortcomings when it comes to applying ML to big data [1]. First, algorithms might “overfit” predictions to spurious correlations in the data; multicollinear, correlated predictors could produce unstable estimates. Second, ML algorithms often require a large number of observations to reach acceptable performance levels.

Precision medicine is one of the important developments in modern medicine. It provides clinicians with early intervention by using advanced diagnostic procedures and customizes personalized treatments for patients. Many scientists and physicians are convinced of the importance of information technology and ML in precision medicine. This includes data storage and analysis for disease outcomes, and identification of patient characteristics and optimal treatment. Utilizing ML for pattern recognition, development of statistical models, creation of knowledge bases for existing phenotype categories and diseases, organization of clinical datasets of population size, and development of open software platforms for statistical analysis of high-dimensional healthcare and multi-omics data are crucial for practical realization of precision medicine.

As one can imagine, ML will have a huge impact on disease (especially cancer) diagnostics and prognostics; in par-

ticular, on the development of novel computational tools for stratification, grading, and prognostication of patients with the overall goal of improving care. There are various ML techniques, which have been widely used in disease diagnosis, and prognosis. A series of previous studies have shown how ML can improve diagnostic performance and prediction accuracy in clinically relevant patient cohorts [2]. One study demonstrated how ML can improve on already established standards, such as Gleason scoring; thus, providing more precise prognostication. Another study engineered a ML-based system to predict microsatellite instability in patients with gastrointestinal or endometrial cancers; both accuracies were higher than prediction with molecular markers. Some studies have also shown that ML can lead to higher accuracy in drug response prediction. ML is becoming a popular tool for medical researchers and has demonstrated promising ability to effectively predict future disease outcomes.

So how is ML currently being used in clinical research? For digitalized pathology, various applications incorporating ML are developed to assist in processing pathological diagnoses. Major applications include detection of specific objects, such as cancer cells, cell nuclei, cell division, and blood vessels, classification/grading of tumors, and evaluation of immunostaining. The major obstacle in using ML in pathological imaging is inadequate image annotations. At present, there exist many technologies to address this concern [3]. For example, generative adversarial networks are used for pathological data analysis to automatically prepare image datasets necessary for subsequent deep learning. Pathologists are looking forward to this potential new gold standard technology for processing images.

Applications of ML in radiology are designed to help computers analyze medical imaging data and support diagnoses by associating clinical outcomes. These radiomic techniques can predict diseases with higher accuracy than humans. Using ML to recognize and analyze image data will fundamentally change our understanding of disease risk and treatment. ML can often extract image information that humans cannot recognize, which can lead to the discovery of novel disease patterns and predictive markers.

At present, the use of omics research to drive cancer biomarker discovery is very popular. Because of large datasets, researchers need advanced information technology, such as ML, to analyze and understand data. ML has already been applied to mass spectrometry (MS) data across different biological disciplines, including various cancers. ML can be useful in determining which proteins from MS data can be used as biomarkers to differentiate between classes. ML is also useful for interpreting large genomic datasets and annotating a

wide variety of genomic sequence elements, which has led to the identification of potentially valuable disease biomarkers.

HOW ABOUT APPLYING ML INTO UROLOGICAL RESEARCH?

When it comes to prostate cancer (PC), many technology platforms for diagnosis, prognosis, and treatment have demonstrated potential benefits of ML. The ML methods can be extended into treatment planning and intervention by augmenting surgeries with information, such as tumor localization and other image-guided options. Computer-assisted diagnosis of PC in histopathological slides can be achieved by ML to enhance accuracy. ML can also help genomics research. By identifying specific genes, ML can be used to develop diagnostic and risk stratification tools, determine the best individualized treatments, and generate targeted drug treatment schemes.

ML can be used to read radiological or pathological images of bladder cancer (BC) to provide useful information. Previous studies have used ML models to analyze magnetic resonance imaging data of BC; they were able to identify low and high-grade BC before surgery with 83% accuracy. ML-based methods have been further applied to accurately quantify tumor buds from immunofluorescence-labeled slides of muscle-invasive BC patients. ML algorithms have also been employed to create recurrence and survival predictive models from imaging and operative data. These algorithms can be used to identify genes at initial presentation that are most predictive of recurrence and can be applied as molecular signatures to predict recurrence risk within 5 years after transurethral resection of the bladder tumor [4].

ML technology has been used to analyze the clinical and imaging data of renal cell carcinoma (RCC) to provide disease diagnoses, prognostic information, and assist in treatment plans. Previous studies have shown that the ML model can accurately distinguish high-grade and low-grade RCC by analyzing computed tomography (CT) image feature [4]. In recent years, ML has been developed to identify biomarkers and multiple gene expression-based signatures to predict survival and disease prognosis in clear cell RCC. Moreover, some studies have demonstrated how noninvasive deep learning models constructed from radiomic features have comparable performance to percutaneous renal biopsy in predicting International Society of Urological Pathology grading.

ML has also been applied to various modalities of urinary stone therapy. Computer-assisted detection using image features can support radiologists in identifying stones. With large datasets, artificial neural networks (ANN) can predict

outcomes after various forms of endourologic intervention. ANN has been used to differentiate ureteral stones from phleboliths in thin slice CT volumes due to their similarity in shape and intensity. ANN also can be used for the early detection of kidney stone types and most influential parameters to provide a decision-support system. The model resulted in 97.1% accuracy for predicting kidney stone type. Recently, ML algorithms have been used to predict treatment success after a single-session shock wave lithotripsy in ureteral stone patients.

Additionally, ML can be applied to benign bladder diseases, such as overactive bladder syndrome [5]. A ML model using a random forest-based algorithm was studied to identify patients for whom anticholinergic medications are likely to fail. A validated ML prediction model can predict treatment failure in a 3-month standard anticholinergic treatment experiment with accuracy rate higher than 80%.

HOW WILL ML BE EVOLVED INTO TOMORROW'S UROLOGY?

In today's fast-moving technologically enhanced world, ML is still in its evolution. The steps needed to integrate ML into the clinic are still unknown. How the new algorithms will influence diagnosis and management of patients remains within our realm of decision. Future research should focus on the construction of larger medical databases and further development of artificial intelligence techniques. The predictive precision of ML will continue to provide and enhance personalized medicine with the further inclusion of data and model retraining. There are limitless future applications for artificial intelligence in the field of urology.

CONFLICTS OF INTEREST

The authors have nothing to disclose.

ACKNOWLEDGMENTS

We would like to thank the support from National Institutes of Health grants (1U01DK103260, 1R01DK100974, U24DK097154, NIH NCATS UCLA CTSI UL1TR000124), Department of Defense grants (W81XWH-15-1-0415 and W81XWH-19-1-0109), Centers for Disease Controls and Prevention (1U01DP006079), and the US-Egypt Science and Technology Joint Fund (to J.K.). This work has supported by the National Research Foundation of Korea (NRF) grant funded by the Korea government (MSIT) (No. 2018R1A2B22005473).

This research was supported by the Samuel Oschin Com-

prehensive Cancer Institute (SOCCI) at Cedars-Sinai Medical Center through 2019 Lucy S. Gonda Award.

AUTHORS' CONTRIBUTIONS

Research conception and design: Wun-Jae Kim and Jayoung Kim. Data acquisition: Peng Jin and Won Hwa Kim. Drafting of the manuscript: Peng Jin, Won Hwa Kim, and Jayoung Kim. Critical revision of the manuscript: Wun-Jae Kim and Jayoung Kim. Obtaining funding: Jayoung Kim. Administrative, technical, or material support: Wun-Jae Kim and Jayoung Kim. Supervision: Wun-Jae Kim and Jayoung Kim. Approval of the final manuscript: all authors.

Wun-Jae Kim¹ , Peng Jin² , Won Hwa Kim³ ,
Jayoung Kim^{2,4,5,6} 

Corresponding Author: Jayoung Kim

ORCID: <https://orcid.org/0000-0002-3683-4627>

¹Department of Urology, College of Medicine, Chungbuk National University, Cheongju, Korea, ²Departments of Surgery and Biomedical Sciences, Cedars-Sinai Medical Center, Los Angeles, CA, ³Department of Computer Science and Engineering, University of Texas at Arlington, Arlington, TX, ⁴Samuel Oschin Comprehensive Cancer Institute, Cedars-Sinai Medical Center, Los Angeles, CA, ⁵University of California Los Angeles, CA, USA, ⁶Department of Urology, Gachon University College of Medicine, Incheon, Korea
E-mail: Jayoung.Kim@cshs.org

REFERENCES

1. Obermeyer Z, Emanuel EJ. Predicting the future-big data, machine learning, and clinical medicine. *N Engl J Med* 2016;375:1216-9.
2. Kourou K, Exarchos TP, Exarchos KP, Karamouzis MV, Fotiadis DI. Machine learning applications in cancer prognosis and prediction. *Comput Struct Biotechnol J* 2014;13:8-17.
3. Komura D, Ishikawa S. Machine learning approaches for pathologic diagnosis. *Virchows Arch* 2019;475:131-8.
4. Suarez-Ibarrola R, Hein S, Reis G, Gratzke C, Miernik A. Current and future applications of machine and deep learning in urology: a review of the literature on urolithiasis, renal cell carcinoma, and bladder and prostate cancer. *World J Urol* 2019 Nov 5 [Epub]. <https://doi.org/10.1007/s00345-019-03000-5>.
5. Sheyn D, Ju M, Zhang S, Anyaeche C, Hijaz A, Mangel J, et al. Development and validation of a machine learning algorithm for predicting response to anticholinergic medications for overactive bladder syndrome. *Obstet Gynecol* 2019;134:946-57.

Classification of the urinary metabolome using machine learning and potential applications to diagnosing interstitial cystitis

Feng Tong¹, Muhammad Shahid², Peng Jin^{2,3}, Sungyong Jung⁴, Won Hwa Kim¹, Jayoung Kim^{2,5,6,7*}

¹Department of Computer Science, University of Texas at Arlington, Arlington TX 76019, USA

²Departments of Surgery and Biomedical Sciences, Cedars-Sinai Medical Center, Los Angeles, CA 90048, USA

³Shengjing Hospital of China Medical University, Shenyang 110004, Liaoning, China

⁴Department of Electrical Engineering, University of Texas, Arlington, Arlington, TX 76019, USA

⁵Samuel Oschin Comprehensive Cancer Institute, Cedars-Sinai Medical Center, Los Angeles, CA 90048, USA

⁶University of California Los Angeles, Los Angeles, CA 90095, USA

⁷Department of Urology, Gachon University College of Medicine, Incheon 13120, South Korea

*Corresponding author: Jayoung Kim, Email: jayoung.kim@cshs.org

Competing interests: The authors have declared that no competing interests exist.

Abbreviations used: ADTree, alternative decision tree; AI, artificial intelligence; ANN, artificial neural network; AUC, area under the curve; CV, cross validation; FN, false negative; FP, false positive; IC, interstitial cystitis; LR, logistic regression; ML, machine learning; NFM, neurofuzzy modelling; NMR, nuclear magnetic resonance; PCA, principal component analysis; PR, precision and recall; RBF, radial basis function; ROC, receiver operating characteristic; SVM, support vector machine; TN: true negative; TP: true positive

Received March 20, 2020; Revision Received April 30, 2020; Accepted May 12, 2020; Published June 2, 2020

ABSTRACT

With the advent of artificial intelligence (AI) in biostatistical analysis and modeling, machine learning can potentially be applied into developing diagnostic models for interstitial cystitis (IC). In the current clinical setting, urologists are dependent on cystoscopy and questionnaire-based decisions to diagnose IC. This is a result of a lack of objective diagnostic molecular biomarkers. The purpose of this study was to develop a machine learning-based method for diagnosing IC and assess its performance using metabolomics profiles obtained from a prior study. To develop the machine learning algorithm, two classification methods, support vector machine (SVM) and logistic regression (LR), set at various parameters, were applied to 43 IC patients and 16 healthy controls. There were 3 measures used in this study, accuracy, precision (positive predictive value), and recall (sensitivity). Individual precision and recall (PR) curves were drafted. Since the sample size was relatively small, complicated deep learning could not be done. We achieved a 76%–86% accuracy with leave-one-out cross validation depending on the method and parameters set. The highest accuracy achieved was 86.4% using SVM with a polynomial kernel degree set to 5, but a larger area under the curve (AUC) from the PR curve was achieved using LR with a l_1 -norm regularizer. The AUC was greater than 0.9 in its ability to discriminate IC patients from controls, suggesting that the algorithm works well in identifying IC, even when there is a class distribution imbalance between the IC and control samples. This finding provides further insight into utilizing previously identified urinary metabolic biomarkers in developing machine learning algorithms that can be applied in the clinical setting.

Keywords: interstitial cystitis; biomarker; urine; metabolomics; machine learning; artificial algorithm

INTRODUCTION

Interstitial cystitis (IC), also known as painful bladder syndrome or bladder pain syndrome, is a chronic visceral pain syndrome of unknown etiology that presents itself as a constellation of symptoms, including bladder pain, urinary frequency, urgency, and small voided volumes, in the absence of other identifiable diseases [1-3]. Urine is in direct contact with the bladder epithelial cells that could be giving

rise to IC; as a result, metabolites released from bladder cells may be enriched in urine [4].

The urinary metabolome was previously investigated by our group for potential IC diagnostic biomarkers [5-7]. We attempted to identify IC-associated metabolites from urine specimens obtained from IC patients and controls using nuclear magnetic resonance (NMR). Our findings provided preliminary evidence that metabolomics analysis of urine can potentially segregate IC patients from controls. We sought to

How to cite this article: Tong F, Shahid M, Jin P, Jung S, Kim WH, Kim J. Classification of the urinary metabolome using machine learning and potential applications to diagnosing interstitial cystitis. *Bladder* 2020;7(2):e43. DOI: 10.14440/bladder.2020.815

capture the most differentially detected NMR peaks and discern if there was a significant difference in the peak distribution between IC and control specimens. Based on multivariate statistical analysis, principal component analysis (PCA) suggested that the urinary metabolome of IC patients and controls were clearly different; 140 NMR peaks were significantly altered in IC patients ($FDR < 0.05$) compared to controls [5].

Machine learning (ML), originally described as a program that learns to perform a task or make decisions based on data, is a valuable and increasingly necessary tool for modern healthcare [8]. However, this definition is broad and could cover nearly any form of data-driven needs. ML is not a magical approach that can turn data in immediate benefits, even though many news outlets imply that it can. Rather, it is natural extension to traditional statistical approaches. In our present study, we utilized ML and automated performance metrics to evaluate the clinical value of our 140 identified NMR peaks. We used ML algorithms examine the relationship between metabolic expression and disease. We applied logistic regression (LR) [9] and support vector machine (SVM) [10,11], which are traditionally known to work well even with small sample sizes, to our metabolomics signatures and used this data together with patient clinicopathological features to diagnose IC. We used our dataset of 59 cases to train, test, and validate the model. The results showed that our ML-based algorithms were able to successfully identify IC patients from healthy subjects.

This study aimed to address the question of, “Does utilizing metabolic data in ML play a role in diagnosing IC?”. ML is a form of artificial intelligence (AI) and learns from past data in order to predict the future. Our NMR-based ML algorithm was able to collectively distinguish the IC patient urinary profile from that of controls

MATERIALS AND METHODS

Ethics statement

For this paper, we used the deposited dataset derived from the published data. This study used the publicly deposited data, which does not need IRB approval.

Dataset

There are 59 samples in total in the IC dataset. In order to acquire IC-associated metabolites, urine samples were collected from 43 IC patient group and 16 healthy control group. Each urine specimen was analyzed using NMR and biomarkers were identified with 140 NMR peaks. The 140 NMR peak feature was utilized to apply the dataset to ML algorithms for classification of IC patients in this paper [5].

Method

Due to limited sample size, we adopted two machine learning algorithms, *i.e.*, support vector machine (SVM) [10,11] and LR [9], that are traditional but work well even with small number of samples. These are supervised learning algorithms, where each data sample is represented by a number of features and comes with a label that tells which group the sample belongs to.

When data is represented as scattered data points in a feature space that consists of two clusters representing individual groups, SVM finds a decision boundary (either linear or non-linear) that separates the different groups. Training an SVM optimizes the decision boundary to maximize the margin between the clusters, and it requires a kernel

function train a kernel SVM that learns a non-linear decision boundary, *i.e.*, a non-linear classifier [12]. The model contains a user parameter known as “slack variable” that controls the width of the margin.

LR is also a classifier that learns *via* a linear model. By feeding a set of training samples with a number of features, it learns specific weights associated with features. When a data sample is input into a LR model, a classification is made by a linear combination between the weights and the data; together with a sigmoid function, the combined value is mapped to a probability between 0 and 1. The predicted label is assigned according to the probability, and by minimizing the classification error (usually formulated using cross-entropy) in the training dataset, the weights are learned. One can add additional regularization terms in the model, such as l_1 or l_2 -norm of the weights, where l_1 -norm controls the sparsity of the weights [13], which will select the most important features, while l_2 -norm controls the smoothness of the weights to make the model more robust [13,14]. Both SVM and LR were implemented using the sklearn package in Python.

Training

Because the sample size was very small, the leave-one-out cross validation (CV) [15] method was utilized to make full use of the data set and to obtain unbiased result from the classifiers. With leave-one-out, we picked one sample as a testing set while using the rest of samples as a training set to train and test the model. The same process was iterated for every sample in the dataset. An illustration of the leave-one-out CV workflow is given in the **Figure 1**.

For SVM, we performed a set of experiments with a linear model, radial basis function (RBF) kernel, polynomial kernel with degree being 3, 5 and 7. The slack variable was set to 1 for all cases. For LR, we tried l_1 and l_2 penalties with different strengths; *i.e.*, the inverse of regularization strength C was set to 1, 5, and 10.

Evaluation

After repeating training and testing the model 59 times with leave-one-out CV, each sample was assigned a predicted label. By comparing these 59 predicted labels with the true labels, we constructed a confusion matrix by counting numbers of true positive (TP), true negative (TN), false positive (FP) and false negative (FN). From these numbers, accuracy, precision and recall were calculated to evaluate the performances of the models. Receiver operating characteristic (ROC) curve and precision and recall (PR) curve were plotted, and their area under the curve (AUC) are reported in the result section. Especially when the distribution of labels in the dataset is skewed, the AUC of the PR curve is a suitable measure for evaluating to account for the imbalance.

RESULTS

Classification of IC samples with SVM

SVM was applied to the IC dataset with the leave-one-out CV scheme to classify IC samples from controls. The result varied depending on user parameters (*i.e.*, kernel type and kernel parameters) as shown in **Figure 2** and **Table 1**. Comparing the numbers, it was found that SVM with polynomial kernel resulted in the best performance when the degree of the polynomial kernel was 3 with 86.4% accuracy, 0.88 AUC of PR curve, and 0.85 AUC of ROC curve. Although the accuracy was the highest when the degree was 5, the AUCs of ROC and PR curves with

degrees set to 3 was the highest. Moreover, the degree equal to 3 has less chance of overfitting than a degree of 5

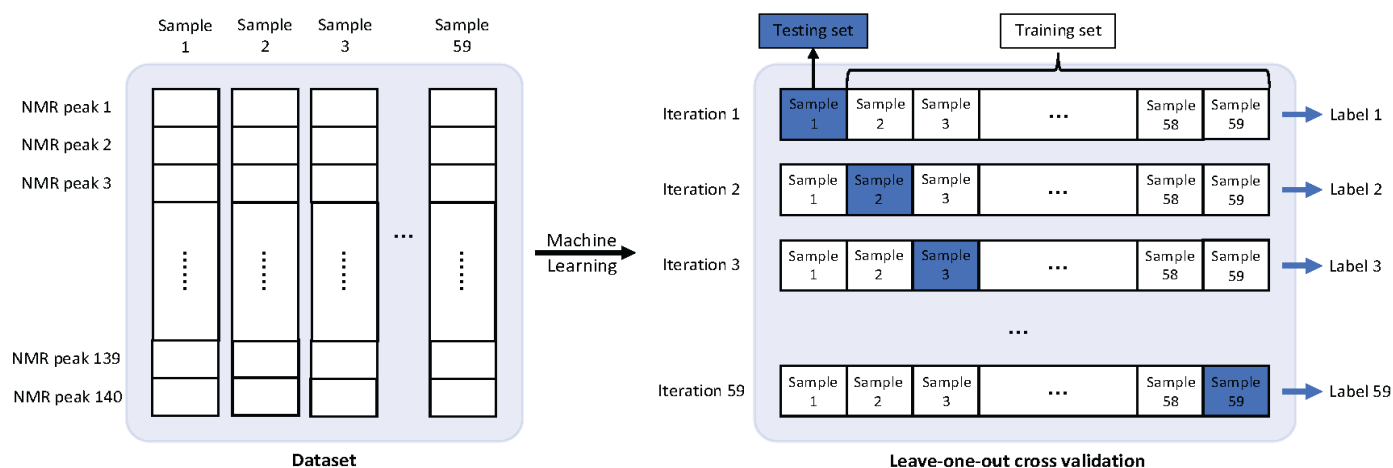


Figure 1. IC classification experimental scheme with leave-one-out cross validation.

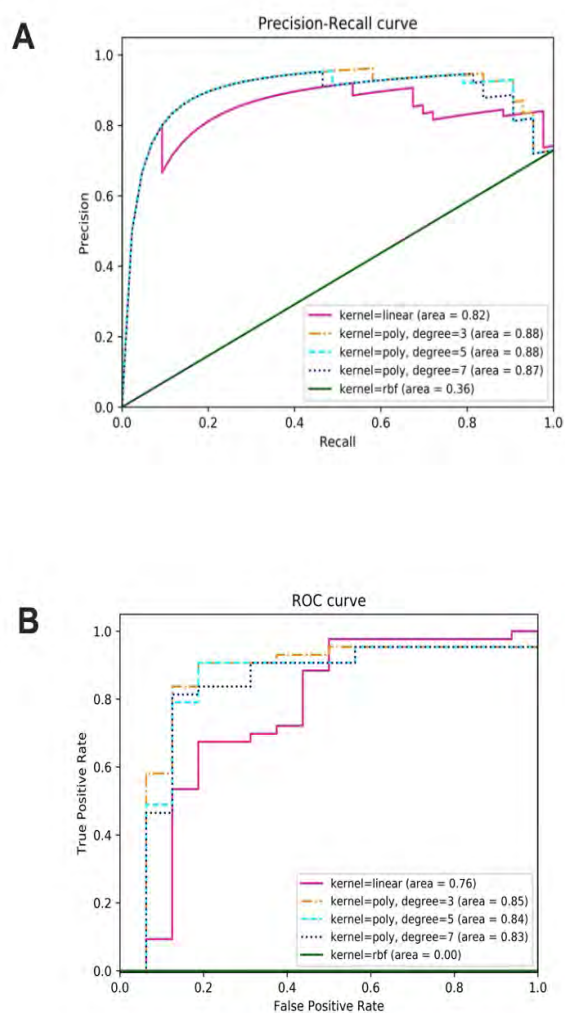


Figure 2. Classification result evaluation curves using SVM. A. Precision-Recall curve. B. ROC curve. The values of AUC are calculated for each curve and larger values indicate better performance.

Here, the usage of linear kernel did not perform well. It may be because the data were not linearly separable or simply the sample size ($N = 59$) was too small compared to the dimension of the data (*i.e.*, 140 features). Performance of RBF kernel was also poor; looking at the accuracy using RBF kernel with SVM shown in **Table 1** (*i.e.*, 72.9%), it was the same as the proportion of IC samples in the dataset (*i.e.*, 43 IC subjects out of 59 subjects) and its recall was 1. This means that the classifier was simply predicting that all the samples belong to IC group and was not able to handle the class distribution imbalance problem.

Classification of IC samples with LR

In addition to SVM experiment, LR was used to classify IC samples and the results are shown in **Figure 3** and **Table 2** with different user parameter settings. LR with l_1 -penalty yielded the best performance when its penalty parameter was set to 10 with 84.7% accuracy, 0.91 for AUC of PR curve and 0.86 for the AUC of ROC curve, which was slight better than the results from SVM. These numbers are the best among several trials because of its randomness with the initial weights being trained, and the results from other trials did not differ much from those reported in **Figure 3** and **Table 2**.

Table 1. The comparison of results from SVM with different set of parameters.

Parameters	TP	TN	FP	FN	Accuracy	Precision	Recall	AUC of PR	AUC of ROC
Kernel = linear	36	9	7	7	0.763	0.837	0.837	0.82	0.76
Kernel = poly, degree = 3	39	11	5	4	0.847	0.886	0.907	0.88	0.85
Kernel = poly, degree = 5	39	12	4	4	0.864	0.907	0.907	0.88	0.84
Kernel = poly, degree = 7	39	11	5	4	0.847	0.886	0.907	0.87	0.83
Kernel = RBF	43	0	16	0	0.729	0.729	1.000	0.36	0.00

Table 2. The comparison of results from LR with different set of parameters.

LR	TP	TN	FP	FN	Accuracy	Precision	Recall	AUC of PR	AUC of ROC
Penalty = l_1 , C = 1	39	9	7	4	0.814	0.848	0.907	0.82	0.75
Penalty = l_1 , C = 5	39	10	6	4	0.831	0.867	0.907	0.88	0.84
Penalty = l_1 , C = 10	38	12	4	5	0.847	0.905	0.884	0.91	0.86
Penalty = l_2 , C = 5	38	7	9	5	0.763	0.809	0.884	0.82	0.75
Penalty = l_2 , C = 10	38	7	9	5	0.763	0.809	0.884	0.82	0.75

It was observed that LR worked well despite being a linear model. Notice that the performance of linear SVM was poor in **Table 1**; this is because of the l_1 -norm penalty applied to the trained parameter imposing sparsity and behaving as a natural feature selector. When we checked the trained weight of features, most of the weights converged to 0 (a very small number on average of absolute values across the leave-one-out process). When the penalty parameter was 10, the average weights of 133 features was less than or equal to 0.1. This means that we only need a few critical features to predict correct label. In our experiment, feature ID = 73, 4, 129, and 35 were the most dominant features with the highest weights regardless of the random initialization. In other words, they were the four most useful NMR features. We have performed further statistical group analysis on these four NMR peaks using two-sample t-test, which resulted in P -values of 0.003, 0.001, 0.057, and 0.036 respectively. It was interesting to see that there were many other NMR peaks with even lower P -values and the peak ID = 129 had a P -value greater than 0.05. While these statistical tests are performed independently, our classification results were derived by taking all the peaks at the same time for the analysis and it demonstrates that a linear combination of the features can be more powerful to distinguish IC from controls.

The l_2 -norm constraint did not contribute much in these experiments. This is because the model can robustly operate even without the l_2 -

norm regularizer, which typically degrades performance of models in exchange for model robustness. Especially with the l_1 -norm regularizer significantly lowering the dimension of the data (with 133 redundant features), the sample size ($N = 59$) was sufficient to make robust and correct predictions for IC samples.

DISCUSSION

It comes with no surprise that medicine is awash with claims that ML applications into big healthcare data will create extraordinary revolutions [8,16,17]. Recent examples have demonstrated how big data and ML can create algorithms that can perform on par with human physicians. AI is one ML approach without prerequisites. Various AI techniques already exist, and successful metabolomics analysis has been reported in previous studies [18-20]. Conventional statistical analysis and AI-based methods were used to assess the discrimination capability of quantified metabolites. A multiple logistic regression (MLR) model, alternative decision tree (ADTree), neurofuzzy modelling (NFM), artificial neural network (ANN), and SVM machine learning methods were used [21,22].

Modern advancements in computational and data science, with its most popular implementation in ML, has facilitated novel complex data-driven research approaches. Combined with biostatistics, ML

aims at learning from data. It accomplishes this by optimizing the performance of algorithms with immediate previous knowledge. ML can be applied in either a supervised or unsupervised fashion. Supervised learning entails monitoring of the algorithm while it is being trained to learn a correct class assignment from a set of parameters, such as how to make a correct diagnosis from clinical and laboratory information [18].

Current biomarkers for IC diagnosis and prognosis are insufficiently robust for clinical practice using AI. Instead, we used AI to identify IC-related metabolites in an NMR metabolomics dataset from our previous study [5], which was able to collectively distinguish IC patient urinary profiles from that of healthy controls. The development of diagnostic tools using ML may be useful for more accurately identifying IC patients.

AI has the potential to manage the imprecision and uncertainty that is common in clinical and biological data. AI or ML-based algorithms can take several different forms. The icons in the presented figure in this paper represent typical ML methods. These include multilayer neuronal networks, decision tree-based algorithms, SVM, and related algorithms that separate classes by placing hyperplanes between them, and prototype-based algorithms, such as k-nearest neighbors that compare feature vectors carried by a case with those carried by other cases and assign classes based on similarities. ML-based algorithms are not being actively applied to IC research. Such applications could lead to a better understanding and deeper knowledge of metabolomics data, which would then provide insights into biomarker discovery.

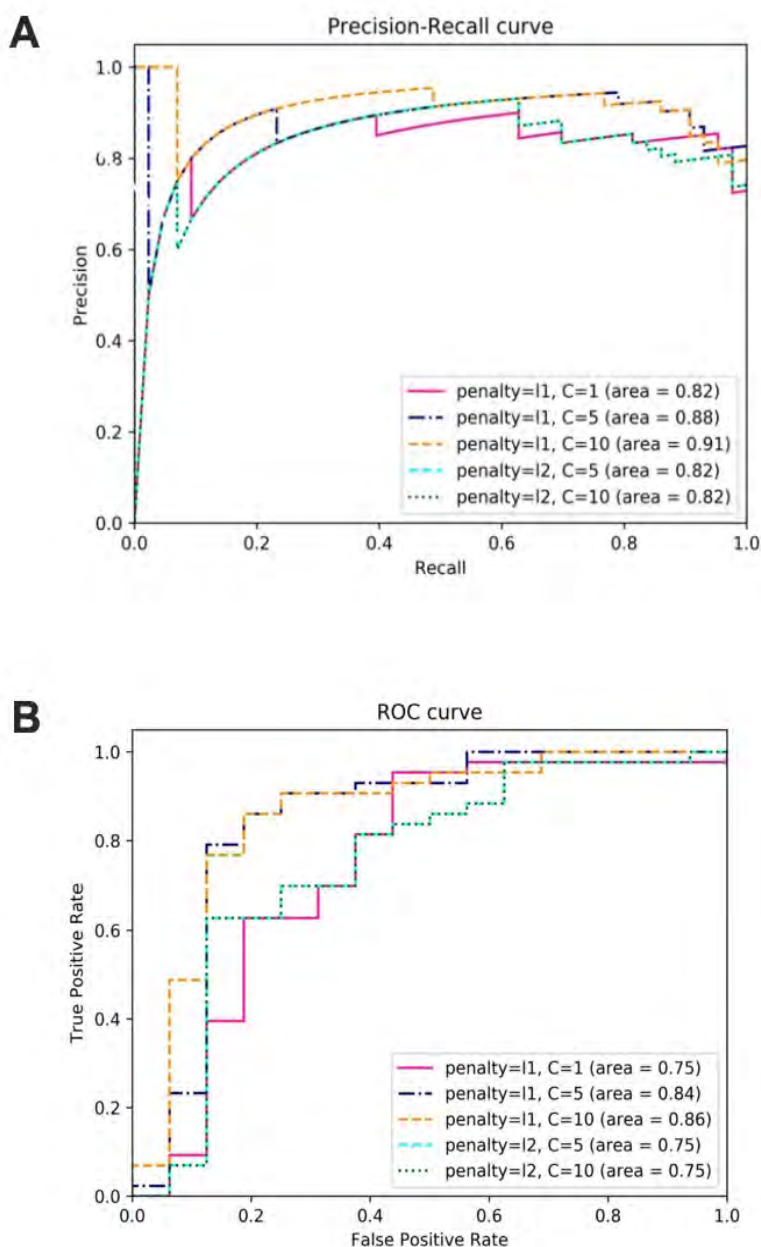


Figure 3. Classification result evaluation curves using LR. A. Precision-Recall curve. **B.** ROC curve. The values of AUC are calculated for each curve and larger values indicate better performance.

Although this is out of scope for this study, AI algorithms can be used to predict IC progression or therapeutic responses, too [23,24]. Patient clinicopathological features are commonly used to train AI algorithms to predict patient outcomes in other diseases, such as cancer [25–27]. For instance, Wong *et al.* developed a prostate cancer patient-specific ML algorithm based on clinicopathological data to predict early biochemical recurrence after prostatectomy [28]. The resulting 3 ML algorithms were trained using 338 patients and achieved an accuracy of 95%–98% and AUC of 0.9–0.94. When compared to traditional Cox regression analysis, the 3 ML algorithms had superior prediction performance. This study demonstrated how AI algorithms, trained with clinicopathological data, imaging radiomic features, and genomic profiling, outperformed the prediction accuracy of D’Amico risk stratification, single clinicopathological features, and multiple discriminant analysis, a type of conventional multivariate statistics [28]. There is also a role for AI in selecting effective drugs for cancer treatment [29]. Using an ML-based algorithm, Saeed *et al.* quantified the phenotypes of castration-resistant prostate cancer cells and tested their response to over 300 emerging and established clinical cancer drugs [30].

We are aware that one of the limitations of this study includes the novelty of using crowdsourcing in medical biomarker development. To our knowledge, there is no previous reference for comparison. Additionally, this study was limited to participants in South Korea and to a 1-time point collection. A major problem associated with medical datasets is a small sample size [5]. Given that sufficiently large datasets are important when creating classification schemes for disease modeling, a relatively larger dataset can result in reasonable validation due to sufficient partitioning of training and testing sets. On the contrary, a smaller training dataset can lead to misclassifications and may result in unstable or biased models. For our study, a major problem was the small sample size. However, the reason for this is that it takes an immense amount of time, effort, and cost to collect a larger amount of medical research data. Furthermore, medical research data is often inconsistent, incomplete, or noisy in nature; thereby, reducing sample sizes even more. Such small sample size for high-dimensional data often leads to “curse of dimensionality”, *i.e.*, failing to properly estimate necessary parameters due to lack of samples, which we also faced with only 59 samples for 140 NMR features. For the SVM used in this study, when casting its objective function as a dual form using Lagrangian multiplier, the optimization problem seeks for a sparse solution that identifies a few “support vectors” and thus greatly reduces the dimension of problem. For the LR, we used two different regularizers on the parameters to estimate, *i.e.*, l_1 and l_2 -norms, to avoid curse of dimensionality and obtain feasible solutions. As demonstrated in the results, as l_1 -norm constraint behaved as a data-driven feature selector reducing the dimension of the problem, the classifier avoided the curse of dimensionality. Although we were able to stay away from the curse of dimensionality in this study, poor analysis may lead to data overfitting and irreproducible results. ML-based algorithms may be manipulated by datasets containing dominant but irrelevant features when the sample number is limited. Also, AI cannot be used as an end-all solution to any question. There are instances where traditional statistics has outperformed AI or where additional AI does not improve results.

In summary, we have found that ML-based algorithms can be applied to developing diagnostic models for IC patients. In the current clinical setting, urologists are generally dependent on cystoscopy and questionnaire-based decisions to diagnose IC due to a lack of objective

molecular biomarkers. The purpose of this study was to develop machine learning methods for diagnosing IC and assess their performance using metabolomics data. Considering how ML techniques for analyzing omics data can play a role in predicting the diagnosis and prognosis of diseases, future studies should integrate use of a larger multidimensional and heterogeneous dataset, application of more accurate validation results, and use of different techniques for classifying and selecting features to pave a promising way toward clinical applications.

Acknowledgments

The author(s) disclosed receipt of the following financial support for the research, authorship, and/or publication of this article: This work was supported by National Institutes of Health grants (1U01DK103260, 1R01DK100974, U24 DK097154, NIH NCATS UCLA CTSI UL1TR000124), Department of Defense grants (W81XWH-15-1-0415 and W81XWH-19-1-0109), Centers for Disease Control and Prevention (1U01DP006079), IMAGINE NO IC Research Grant, the Steven Spielberg Discovery Fund in Prostate Cancer Research Career Development Award, and the U.S.-Egypt Science and Technology Joint Fund (to J.K.). This research was partly supported by the Samuel Oschin Comprehensive Cancer Institute at Cedars-Sinai Medical Center through 2019 Lucy S. Gonda Award (to J.K.). This article is derived from the Subject Data funded in whole or part by National Academies of Sciences, Engineering, and Medicine and The United States Agency for International Development. Any opinions, findings, conclusions, or recommendations expressed in this article are those of the authors alone, and do not necessarily reflect the views of USAID or NAS

Author contributions

J Kim, M Shahid, P Jin: data collection or management and manuscript drafting; F Tong, S Jung, WH Kim: data analysis and manuscript drafting; S Jung, WH Kim, J Kim: project development, manuscript writing/editing and data analysis

References

- Hanno P, Keay S, Moldwin R, Van Ophoven A (2005) International Consultation on IC - Rome, September 2004/Forging an International Consensus: progress in painful bladder syndrome/interstitial cystitis. Report and abstracts. *Int Urogynecol J Pelvic Floor Dysfunct* 16 Suppl 1: S2-S34. PMID: 15883858
- Nordling J, Anjum FH, Bade JJ, Bouchelouche K, Bouchelouche P, et al. (2004) Primary evaluation of patients suspected of having interstitial cystitis (IC). *Eur Urol* 45: 662-669. doi: 10.1016/j.eururo.2003.11.021. PMID: 15082211
- Hanno PM, Burks DA, Clemens JQ, Dmochowski RR, Erickson D, et al. (2011) AUA guideline for the diagnosis and treatment of interstitial cystitis/bladder pain syndrome. *J Urol* 185: 2162-2170. doi: 10.1016/j.juro.2011.03.064. PMID: 21497847
- Urology Think Tank Writing Group (2018) Urine: Waste product or biologically active tissue. *Neurourol Urodyn* 37: 1162-1168. doi: 10.1002/nau.23414. PMID: 29464759
- Wen H, Lee T, You S, Park S, Song H, et al. (2014) Urinary metabolite profiling combined with computational analysis predicts interstitial cystitis-associated candidate biomarkers. *J Proteome Res* 14: 541-548. doi: 10.1021/pr5007729. PMID: 25353990
- Kind T, Cho E, Park TD, Deng N, Liu Z, et al. (2016) Interstitial cystitis-associated urinary metabolites identified by mass-spectrometry based metabolomics analysis. *Sci Rep* 6: 39227. doi: 10.1038/srep39227. PMID: 27976711
- Shahid M, Lee MY, Yeon A, Cho E, Sairam V, et al. (2018) Menthol, a unique urinary volatile compound, is associated with chronic inflammation in interstitial cystitis. *Sci Rep* 8: 10859. doi: 10.1038/s41598-018-29085-3. PMID: 30022124
- Cahan EM, Hernandez-Boussard T, Thadaney-Israni S, Rubin DL (2019) Putting the data before the algorithm in big data addressing personalized healthcare. *NPJ Digit Med* 2: 78. doi: 10.1038/s41746-019-0157-2. PMID: 31453373

9. Tolles J, Meurer WJ (2016) Logistic regression: relating patient characteristics to outcomes. *JAMA* 316: 533-534. PMID: [27483067](#)
10. Cortes C, Vapnik V (1995) Support-vector networks. *Machine learning* 20: 273-97. doi: [10.1007/BF00994018](#).
11. Platt JC (1998) [Internet]. Microsoft Research. Sequential minimal optimization: A fast algorithm for training support vector machines. Available from: <https://www.microsoft.com/en-us/research/wp-content/uploads/2016/02/tr-98-14.pdf>.
12. Lin Y, Lee Y, Wahba G (2002) Support vector machines for classification in nonstandard situations. *Mach Learn* 46: 191-202.
13. Tibshirani R (1996) Regression shrinkage and selection via the lasso. *J Roy Stat Soc B* 58: 267-88. doi: [10.1111/j.2517-6161.1996.tb02080.x](#).
14. Ng AY (2004) Feature selection, L1 vs. L2 regularization, and rotational invariance. In: *Proceedings of the twenty-first international conference on Machine learning*. New York, NY: Association for Computing Machinery. doi: [10.1145/1015330.1015435](#).
15. Vehtari A, Gelman A, Gabry J (2017) Practical Bayesian model evaluation using leave-one-out cross-validation and WAIC. *Statistics and Computing* 27: 1413-1432. doi: [10.1007/s11222-016-9696-4](#).
16. Esteva A, Robicquet A, Ramsundar B, Kuleshov V, DePristo M, et al. (2019) A guide to deep learning in healthcare. *Nat Med* 25: 24-29. doi: [10.1038/s41591-018-0316-z](#). PMID: [30617335](#)
17. Miotto R, Wang F, Wang S, Jiang X, Dudley JT (2018) Deep learning for healthcare: review, opportunities and challenges. *Brief Bioinform* 19: 1236-1246. doi: [10.1093/bib/bbx044](#). PMID: [28481991](#)
18. Zampieri G, Vijayakumar S, Yaneske E, Angione C (2019) Machine and deep learning meet genome-scale metabolic modeling. *PLoS Comput Biol* 15: doi: [10.1371/journal.pcbi.1007084](#). PMID: [31295267](#)
19. Bordbar A, Monk JM, King ZA, Palsson BO (2014) Constraint-based models predict metabolic and associated cellular functions. *Nat Rev Genet* 15: 107-120. doi: [10.1038/nrg3643](#). PMID: [24430943](#)
20. Cuperlovic-Culf M (2018) Machine Learning Methods for Analysis of Metabolic Data and Metabolic Pathway Modeling. *Metabolites* 8: doi: [10.3390/metabo8010004](#). PMID: [29324649](#)
21. Angermueller C, Pärnamäa T, Parts L, Stegle O (2016) Deep learning for computational biology. *Mol Syst Biol* 12: 878. doi: [10.15252/msb.20156651](#). PMID: [27474269](#)
22. Min S, Lee B, Yoon S (2017) Deep learning in bioinformatics. *Brief Bioinform* 18: 851-869. doi: [10.1093/bib/bbw068](#). PMID: [27473064](#)
23. Vamathevan J, Clark D, Czodrowski P, Dunham I, Ferran E, et al. (2019) Applications of machine learning in drug discovery and development. *Nat Rev Drug Discov* 18: 463-477. doi: [10.1038/s41573-019-0024-5](#). PMID: [30976107](#)
24. Jing Y, Bian Y, Hu Z, Wang L, Xie XS (2018) Deep learning for drug design: an artificial intelligence paradigm for drug discovery in the big data era. *AAPS J* 20: 58. doi: [10.1208/s12248-018-0210-0](#). PMID: [29603063](#)
25. Klauschen F, Muller KR, Binder A, Bockmayr M, Hagele M, et al. (2018) Scoring of tumor-infiltrating lymphocytes: From visual estimation to machine learning. *Semin Cancer Biol* 52: 151-157. doi: [10.1016/j.semcancer.2018.07.001](#). PMID: [29990622](#)
26. Baptista D, Ferreira PG, Rocha M (2020) Deep learning for drug response prediction in cancer. *Brief Bioinform*: pii: bbz171. doi: [10.1093/bib/bbz171](#). PMID: [31950132](#)
27. Tolios A, De Las Rivas J, Hovig E, Trouillas P, Scorilas A, et al. (2020) Computational approaches in cancer multidrug resistance research: Identification of potential biomarkers, drug targets and drug-target interactions. *Drug Resistance Updates* 48: 100662. doi: [10.1016/j.drug.2019.100662](#). PMID: [31927437](#)
28. Wong NC, Lam C, Patterson L, Shayegan B (2018) Use of machine learning to predict early biochemical recurrence after robot-assisted prostatectomy. *BJU Int* 123: 51-57. doi: [10.1111/bju.14477](#). PMID: [29969172](#)
29. Madhukar NS, Khade PK, Huang L, Gayvert K, Galletti G, et al. (2019) A Bayesian machine learning approach for drug target identification using diverse data types. *Nat Commun* 10: 5221. doi: [10.1038/s41467-019-12928-6](#). PMID: [31745082](#)
30. Saeed K, Rahkama V, Eldfors S, Bychkov D, Mpindi JP, et al. (2017) Comprehensive drug testing of patient-derived conditionally reprogrammed Cells from Castration-resistant prostate cancer. *Eur Urol* 71: 319-327. doi: [10.1016/j.eururo.2016.04.019](#). PMID: [27160946](#)



This work is licensed under a Creative Commons Attribution-Non-Commercial-ShareAlike 4.0 International License: <http://creativecommons.org/licenses/by-nc-sa/4.0>

Research Paper

S-Palmitoylation as a Functional Regulator of Proteins Associated with Cisplatin Resistance in Bladder Cancer

Muhammad Shahid¹, Minhyung Kim¹, Peng Jin¹, Bo Zhou¹, Yang Wang¹, Wei Yang^{1,2}, Sungyong You¹, Jayoung Kim^{1,2}✉

1. Departments of Surgery and Biomedical Sciences, Cedars-Sinai Medical Center, Los Angeles, CA, USA.

2. Department of Medicine, University of California Los Angeles, CA 90095, USA.

✉ Corresponding author: Jayoung Kim, PhD. Departments of Surgery and Biomedical Sciences; Cedars-Sinai Medical Center, Davis 5071; 8700 Beverly Blvd., Los Angeles, CA 90048. Tel.: +1-310-423-7168; Fax: +1-310-967-3809; E-mail: Jayoung.kim@csmc.edu.

© The author(s). This is an open access article distributed under the terms of the Creative Commons Attribution License (<https://creativecommons.org/licenses/by/4.0/>). See <http://ivyspring.com/terms> for full terms and conditions.

Received: 2020.03.18; Accepted: 2020.05.02; Published: 2020.07.19

Abstract

Protein S-palmitoylation is a powerful post-translational modification that regulates protein trafficking, localization, turnover, and signal transduction. Palmitoylation controls several important cellular processes, and, if dysregulated, can lead to cancer, cardiovascular disease, and neurological disorders. The role of protein palmitoylation in mediating resistance to systemic cisplatin-based chemotherapies in cancer is currently unknown. This is of particular interest because cisplatin is currently the gold standard of treatment for bladder cancer (BC), and there are no feasible options after resistance is acquired. Using unbiased global proteomic profiling of purified S-palmitoylated peptides combined with intensive bioinformatics analyses, we identified 506 candidate palmitoylated proteins significantly enriched in cisplatin-resistant BC cells. One of these proteins included PD-L1, which is highly palmitoylated in resistant cells. Pharmacological inhibition of fatty acid synthase (FASN) suppressed PD-L1 palmitoylation and expression, which suggests the potential use of FASN-PD-L1-targeted therapeutic strategies in BC patients. Taken together, these results highlight the role of protein palmitoylation in mediating BC chemoresistance.

Key words: S-palmitoylation; lipid; lipidation; post-translational modification; tumor

Introduction

Systemic cisplatin-based chemotherapy is the current gold standard of treatment for metastatic bladder cancer (BC) [1-3]. However, acquired chemoresistance is common; thereby, limiting the usage of cisplatin. Patients who acquire chemoresistance ultimately have no further viable treatment options and their cancer usually recurs. The 5-year survival rate for BC after recurrence is approximately 15% [4-6]. As of now, there is a lack of comprehensive understanding behind the mechanisms driving cisplatin resistance. Thus, there is an unsolved and urgent need to identify a method of distinguishing which BC patients are at a higher risk of developing chemoresistance.

Metabolic reprogramming has been accepted as a hallmark of cancer [7-10]. These changes in metabolic activities may also be involved in

cisplatin-induced cell death. As a result, metabolic studies on cisplatin resistance may potentially lead to new clues for improving therapies against refractory BC. Several prior metabolomic studies found that BC may have abnormalities in metabolites involved in lipid usage [11,12]. It has also been suggested that perturbed metabolism may be implicated in cancer drug-resistance, aggressiveness, or progression [13]. Consistent with these earlier findings, our recent study suggested that alterations in acetate and lipid metabolism, which is mediated by acetyl-CoA synthetase 2 (ACSS2), an enzyme that converts acetate to acetyl-CoA, plays a role in cisplatin resistance [14]. By performing unbiased data-driven analysis, as described below, our real-time live metabolomics identified metabolic reprogramming in a series of isogenic cisplatin-sensitive and resistant BC cell lines.

In a previous study, we also found that glucose-derived endogenous acetate contributes to cell viability and increased de novo synthesis of lipids via ACS2 [15]. However, the role of these bioactive metabolites in influencing lipid metabolism in BC cisplatin resistance is not fully understood.

Lipid modification of proteins at the post-translational level mostly occurs on cysteine thiols through the covalent addition of long-chain fatty acids (predominantly 16-carbon palmitic acid) [16,17]. This is called protein palmitoylation and can lead to an increase in hydrophobicity of cytoplasmic proteins and an affinity to cytosolic membrane surfaces [18]. Palmitoylation is an attractive mechanism for modulating protein activity, stability, interactions, localization, signaling transduction, apoptosis, and carcinogenesis [19-24]. It has been shown that palmitoylation is particularly important for protein stability; it suppresses degradation by preventing ubiquitylation [19]. The role of palmitoylation in protein stability has been demonstrated in a wide variety of targets and diseases, including c-Met, TEAD transcription factor, progressive rod-cone degeneration, and Huntington's disease [16,25-27]. Based on the critical role of palmitoylation in protein function and disease, investigating its impact on acquired chemoresistance in BC presents a promising opportunity. From our original palmitoyl-protein identification and site characterization (PalmPISC) method [28], we previously developed a low-background acyl-biotinyl exchange (LB-ABE), a significantly improved method for successful purification and identification of hydrophobic palmitoylated proteins [28,29]. By largely eliminating the co-isolation of non-palmitoylated proteins, LB-ABE minimizes the "ratio compression" issue and substantially improves quantification accuracy [29,30].

Fatty acid synthase (FASN) is a multifunctional enzyme that is involved in the de-novo synthesis of lipids [31]. Its main function is catalyzing the synthesis of 16-C palmitate [32]. Overexpression of FASN has been noted in a variety of different tumor types, including non-muscle invasive BC (NMIBC), and is significantly associated with poorer prognoses [33]. Studies have shown that FASN is a particularly informative prognostic predictor in BC; expression was found to be positively correlated with tumor aggressiveness, histologic grade, recurrence, and poor survivability in patient cohorts [34,35]. Additionally, inhibition of FASN via siRNA increased apoptosis and decreased proliferation in BC cells [36]. The primary product of FASN, palmitate, plays an especially important in protein palmitoylation by attaching to and regulating protein localization,

stability, and function [17]. Consequently, FASN is directly involved in the palmitoylation of proteins.

Current understanding of protein palmitoylation (more accurately termed S-acylation) status and its role in cisplatin resistance remains very limited. In this paper, our proteome-scale analysis of adipocyte S-acylated proteins in cisplatin-sensitive vs resistant BC cells suggest 506 putative palmitoylated proteins associated with cisplatin resistance. We also tested the hypothesis that lipid metabolism changes in cisplatin-resistant BC cells may be mediated by the S-palmitoylation of FASN. Our experimental results demonstrated that protein palmitoylation of FASN contributes to cisplatin resistance in BC cells. This study also provides evidence suggesting that FASN inhibition alters the palmitoylation of programmed death ligand-1 (PD-L1).

Materials and Methods

Cell culture

Parental T24 human BC cells were procured from American Type Culture Collection. Cisplatin-sensitive (T24S) and resistant T24 (T24R) BC cells were developed and characterized in the laboratory [37]. Cells were cultured in Dulbecco's modified eagle medium (DMEM) supplemented with 10% fetal bovine serum, 2% glutamine, and 1% antibiotics (Invitrogen, Carlsbad, CA). All BC cells used for this paper were maintained under a humidified atmosphere of 5% CO₂ at 37 °C.

Antibodies and reagents

The following antibodies and dilutions were used according to manufacturer's instructions: β -actin (A1978) from Sigma; PD-L1 (13684) (1:1000), FASN (3180) (1:1000) and HRP-conjugated secondary antibodies, rabbit (7074) (1:3000), mouse (7076) (1:3000), from Cell Signaling Technology.

Palmitoyl-protein enrichment using LB-ABE

Palmitoyl proteins were enriched using our LB-ABE method [30]. Briefly, after cell lysis, 0.7 mg of protein from each replicate was reduced by 50 mM tris(2-carboxyethyl)phosphine (TCEP) and alkylated sequentially by 50 mM N-ethylmaleimide and 50 mM 2,2'-dithiodipyridine (DTDP). Palmitoyl proteins were converted into biotinylated proteins using 2 M neutral hydroxylamine and 1 mM biotin-N-[6-(biotinamido) hexyl]-3'-(2'-pyridyldithio) propionamide (HPDP), enriched by streptavidin affinity purification, and eluted by 50 mM TCEP.

CAPTUREome™ S-Palmitoylated Protein Kit Assay

Confirmation of S-palmitoylated proteins in BC cells was conducted using the commercially available CAPTUREome™ S-Palmitoylated Protein Kit (cat # K010-311, Badrilla, UK). Following the indicated 2-bromopalmitate (2-BP) treatments, cells were collected and washed in phosphate-buffered saline (PBS). The methodology for acyl-RAC, including blocking of free thiols, cleavage of thioester linkages, and capture of nascent thiols on Sepharose, was carried out according to the manufacturer's instructions. In particular, equal amounts of protein (1-2 mg) were diluted in 500 µl of blocking buffer (buffer A and thiol blocking reagent) and incubated at 40 °C for 4 hours with constant shaking. Three volumes of cold acetone were added, and proteins were allowed to precipitate at -20°C for 20 min. Following centrifugation of the solution at 16,000 g for 5 min, the pellet was extensively washed with 70% acetone five times and air-dried completely after the final wash. Pellet was re-dissolved in 300 µl binding buffer and incubated in a shaking heat block at 40°C for 1 hour. The homogenates were centrifuged at 16,000 × g for 5 min to remove insoluble debris. Approximately 20 µl of each supernatant was saved as the "total input." The pre-washed capture resin slurry (50 µl) was added to the remaining lysates, and 19 µl of thioester cleavage reagent was then added. Binding reactions were carried out on a rotator at room temperature for 2.5 hours. Resins were washed at least five times with binding buffer. Supernatants were removed and mixed with 2× Laemmli loading buffer, heated to 60 °C for 10 min, and separated via SDS-PAGE. All kits were used following the manufacturer's instructions.

Palmitoyl protein digestion and label-free proteomic analysis

Enriched palmitoyl proteins were digested by trypsin, using filter-aided sample preparation (FASP) [38,39]. Label-free proteomic analysis was performed using an EASY-nLC 1000 connected to an LTQ Orbitrap Elite Hybrid Mass Spectrometer, as previously described [29]. Tryptic peptides were loaded onto a 2 cm trap column and separated on a 50 cm EASY-Spray Analytical Column heated to 55 °C, using a gradient of 2-34% B in 174 min, 34-60% B in 10 min, 60-100% B in 2 min, and 100% B in 14 min at the flow rate of 150 nL/min. Mass spectra were acquired in a data-dependent manner, with automatic switching between mass spectrometry (MS) and tandem mass spectrometry (MS/MS) scans. In the MS scans, a lock mass at m/z 445.120025 was applied to provide internal mass calibration. The full scan was

performed using a 240,000 resolution at m/z 400 Th, with an ion packet setting of 1×10⁶ for automatic gain control and maximum injection time of 500 ms. The 20 most intense peptide ions with charge state ≥2 were automatically selected for MS/MS fragmentation by rapid collision-induced dissociation (rCID), using a resolution of 7,500, 1×10⁴ automatic gain control, 50 ms maximum injection time, 10 ms activation time, and 35% normalized collision energy. Dynamic exclusion was enabled with a repeat count of 1, an exclusion duration of 30 s, and a repeat duration of 90 s.

Database searching for protein identification and quantification

The acquired MS data was searched against the Uniprot_Human Database (released on 01/22/2016, containing 20,985 sequences) using the Andromeda [40] algorithm in the MaxQuant [41] (v1.5.5.1) environment. The searching parameters were set as follows: trypsin/P as the protease; oxidation (M), acetyl (protein N-term), NEM(C), and carbamidomethyl (C) as variable modifications; up to two missed cleavages; minimal peptide length as 7; mass tolerance for MS1 was 4.5 ppm for main search and for MS2 was 0.5 Da; identification of second peptides enabled; label-free quantification (LFQ) enabled, and match-between-runs within 2 min were enabled. A stringent 1% FDR was used to filter PSM, peptide, and protein identifications.

Identification of differentially palmitoylated proteins (DPPs)

LFQ intensities were normalized using the quantile normalization method [42] to compare different conditions. To filter out low-quality proteins, selected proteins were detected in at least two samples under each condition. DPPs between T24S and T24R cells were identified using a previously reported statistical test [43]. Briefly, log₂ intensities of each protein from T24R cells were compared to those in T24S cells using the Student's t-test and log₂-median ratio test. We estimated empirical null distributions of t-values and log₂-median ratio values by randomly permuting 6 samples 1,000 times and calculating the t-test and log₂-median ratio test. These two p-values were then integrated into an overall p-value using Stouffer's method [44]. DPPs were identified as proteins with overall P<0.05 and absolute log₂-fold-change ≥ 0.58.

Functional enrichment analysis

Enrichment analysis of gene ontology biological process (GOBPs) and Kyoto Encyclopedia of Genes and Genomes (KEGG) pathways for DPPs was

performed using DAVID [45]. The functional classification analysis of GOBPs, gene ontology cellular components (GOCCs), and gene ontology molecular functions (GOMFs) was performed using PANTHER (Ver. 11) [46].

Reconstruction of a network model

To reconstruct a network model describing cisplatin resistance in BC cells, a subset of genes that are involved in metabolic processes was selected. Interaction information of the genes from the STRING database (Ver. 10.5) [47] was then collected and used to reconstruct a network model. Finally, the network model was visualized using Cytoscape [48]. The nodes in the network model were distributed according to the metabolic pathways that they are involved in.

Western blot analysis

Whole-cell lysates for western blot analysis were prepared as described in a previous paper [49]. T24R and T24S BC cells were cultured on 10 cm plates and treated with 2-BP or orlistat at varying doses. Cells were lysed with RIPA buffer (20 mM Tris, 150 mM NaCl, 1% Nonidet P-40, 0.1 mM EDTA) (Pierce, ThermoFisher) supplemented with a phosphatase inhibitor cocktail (ThermoFisher), homogenized, and centrifuged at 13,000 \times g and 4°C for 20 min. Afterwards, 25 μ g of protein lysates per lane was run on a 4-15% gradient SDS-PAGE gel. Following protein transfer onto polyvinylidene fluoride (PVDF), the membranes were blocked with either 5% bovine serum albumin (BSA) or 5% nonfat milk in Tris-buffered saline with 0.1% Tween 20 (TBST [2.42 g/L Tris-HCl, 8 g/L NaCl, and 1 mL/L Tween 20 (pH 7.6)]) for 1 hour at room temperature. This was followed by incubation with specific primary antibodies at 4 °C overnight and 3 X 10 min washes with TBST solution. The membranes were further incubated with HRP-conjugated secondary antibodies at room temperature for 1 hour. β -actin was used as a loading control. Experiments were performed in at least triplicates for each western blot analysis.

Measurement of palmitate and cholesterol

Levels of palmitate in T24S and T24R cells were determined by targeted metabolomics analysis through the University of Florida Metabolomics Core using mass spectrometry-based targeted metabolomics analysis. Levels of cholesterol in the BC cells were determined using the commercially available Cholesterol Quantification Kit (cat #MAK043, Sigma, MO, USA). Cells were lysed in 1% (w/v) Triton X-100 in chloroform. The homogenates were centrifuged at 13,000 \times g for 10 min to remove insoluble debris, and the organic phase (lower phase)

was collected and dried in a 50°C dry bath for 20 min. Samples were vacuum dried for 30 min to remove traces of chloroform. The dried lipids were resuspended via vortex in an assay buffer and further quantified. All kits were used in accordance with the manufacturer's instructions.

Cell proliferation assay

Cells were seeded at a density of 2×10^6 cells/well in 12-well plates. Cells were then incubated with standard growth medium and treated with varying doses of 2-BP or orlistat, as described in the figures. Cells were stained with 0.05% crystal violet solution after removing the medium. After incubation at room temperature for 15 min, the wells were washed thoroughly with PBS, and cells were fixed with 4% paraformaldehyde at room temperature for 5 min. For quantitative analysis, the stained cells were dissolved in 10% acetic acid solution for reading absorbance at 570-590 nm [50]. All experiments were run in at least triplicates.

Statistical analysis

Student's t-tests were performed to evaluate differential expression of the proteins between two groups. Variables with normal distribution were expressed as mean \pm standard deviation (SD). All reported p-values are two-tailed, with $P < 0.05$ being considered as statistically significant.

Results

Palmitoyl-proteomics analysis identified DPPs associated with cisplatin resistance in BC cells

Our group previously developed and characterized isogenic human BC cell lines, cisplatin sensitive (T24S) and resistant T24 BC cells (T24R) [51]. In this study, we coupled LB-ABE enrichment with label-free proteomics to identify the potential link between protein palmitoylation and cisplatin resistance in BC. Briefly, we isolated palmitoyl-proteins from whole cell lysates by LB-ABE, digested them into peptides with trypsin using FASP, analyzed peptides by liquid chromatography-tandem mass spectrometry (LC-MS/MS), and performed database searching analysis and LFQ using MaxQuant. Our proteomics analysis workflow is summarized in **Figure 1A**. A total of 4,188 putative palmitoylated proteins were identified with a false discovery rate of $\leq 1\%$. Representative MS spectrum of FASN is shown in **Figure 1B**.

After filtering out the low-quality proteins, which are detected less than two replicates from T24S or T24R BC cells, we found that most of the palmitoylated proteins overlap in T24S and T24R cells (3,315 proteins: 89.71% of total) (**Figure 1C**). We also

identified 184 proteins that were palmitoylated only in T24R cells, not in T24S, and 196 proteins that were palmitoylated only in T24S cells, not in T24R (Figure

1C). The heatmap shows that the palmitoylation levels of most proteins in T24S and T24R cells were not significantly different (Figure 1D).

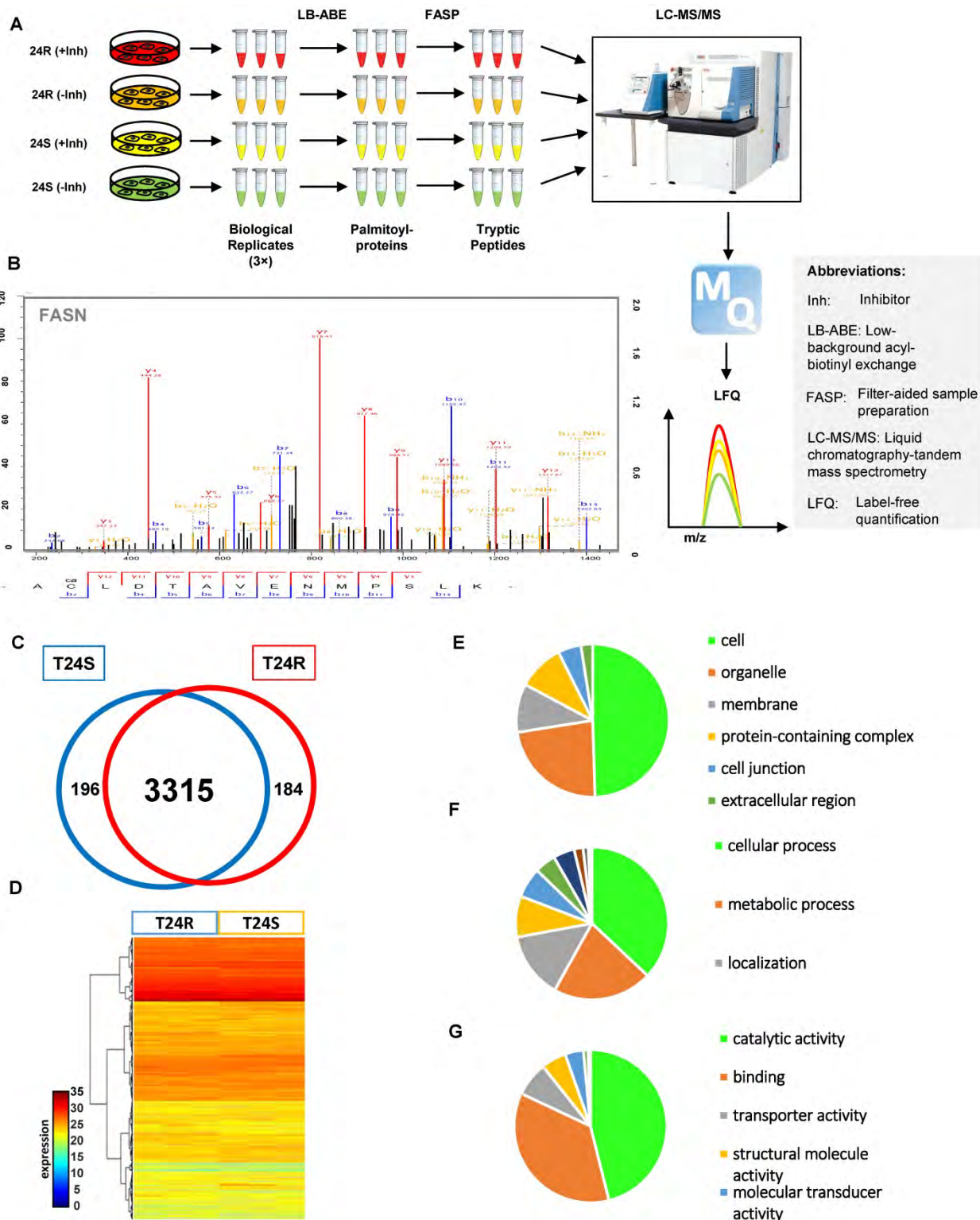


Figure 1. (A) Workflow for quantitative palmitoyl-proteomic comparison of two isogenic BC cells, T24R and T24S, using LFQ LC-MS/MS analysis following LB-ABE. After LB-ABE, a total of 16 samples (4 samples × 4 conditions) were digested in parallel into tryptic peptides by FASP, followed by LC-MS/MS. (B) Representative tandem mass spectrum of candidate palmitoyl peptide. LB-ABE-enriched proteins were separated by SDS-PAGE and digested in gel, followed by the extraction of tryptic peptides, which were analyzed by LC-MS/MS. Free cysteines in the purified peptides are candidate palmitoylation sites. (C-G) The detected palmitoylated proteins from T24R and T24S cells were classified by gene ontology categories. (C) Venn diagram shows the number of identified proteins in T24R and T24S cells. (D) Heatmap depicts abundance of commonly identified proteins in both T24R and T24S. Red and blue indicate high and low abundance of the proteins, respectively. (E-G) Pie chart visualizes the proportion of the number of proteins involved in the enriched gene ontology categories including cellular compartment (E), biological processes (F), and molecular functions (G).

Supplementary table 1 shows the 3,695 palmitoylated proteins identified in both T24S and T24R BC cells. To assess the functions of these 3,695 palmitoylated proteins, we performed functional classification analysis using PANTHER [46]. The location and function of these proteins are summarized in **Figures 1E-1G**. The identified palmitoylated proteins are functionally highly diverse; however, 35.1% of the classified proteins are

related to metabolic processes and localization (**Figure 1F**).

DPPs between T24R and T24S cells. Among the 3,695 identified proteins, at least 2,581 (70%) were previously reported to be palmitoylated in other human cells [29,52], confirming successful enrichment of palmitoyl-proteins in this study. Most of the 2,581 putative palmitoylated proteins were not reported in normal human bladder or BC cells (**Figure 2A**).

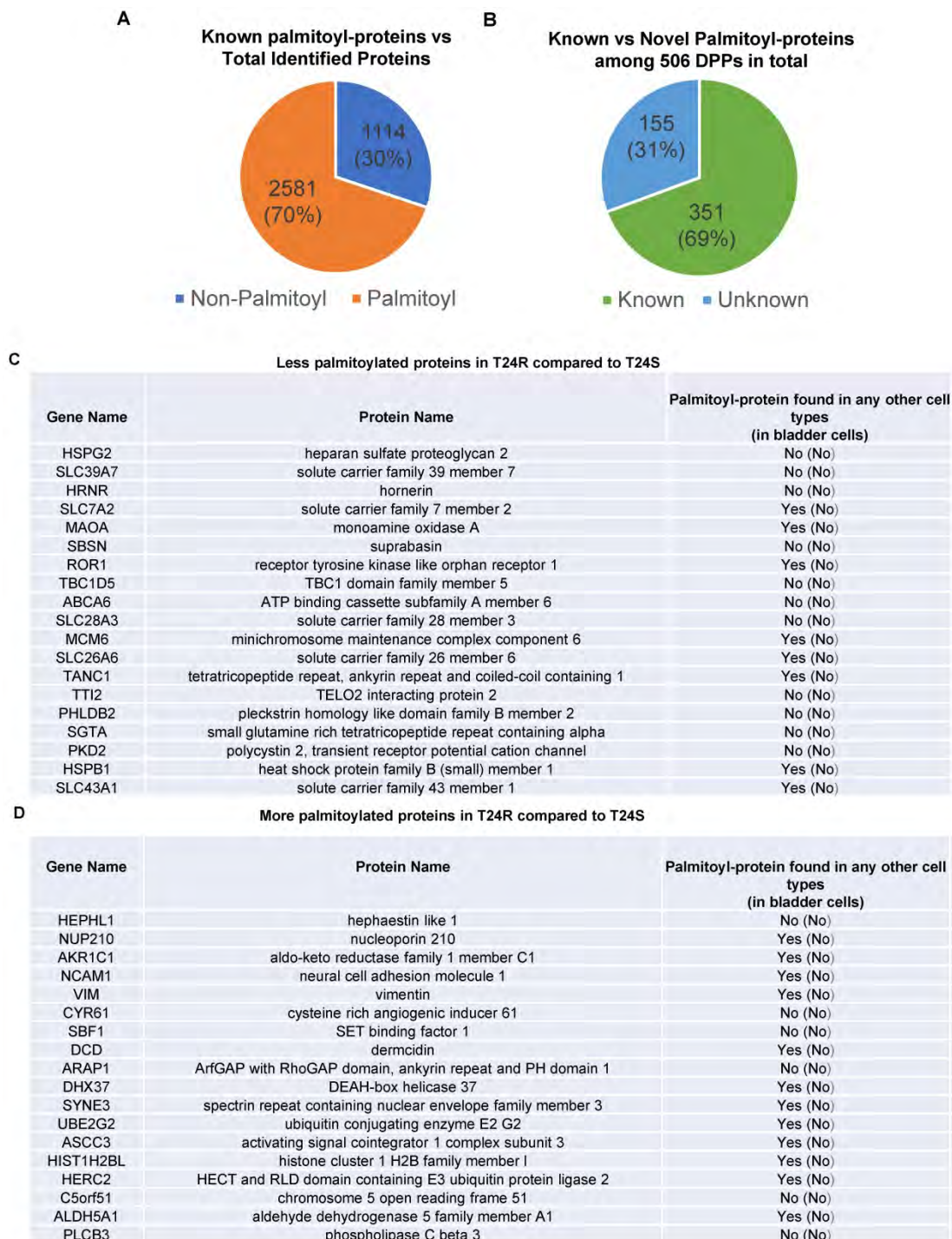


Figure 2. Known and novel palmitoylated proteins from T24R and T24S cells. (A) Pie chart depicts the proportion of palmitoylated and non-palmitoylated proteins from the total identified proteins. **(B)** Pie chart shows proportion of known and novel candidate palmitoyl-proteins. **(C-D)** Known and novel palmitoylated proteins in other cancer cells and bladder cells.

Next, we sought to identify DPPs in T24R cells compared to T24S. To further understand cisplatin resistance-associated protein palmitoylation changes, we aimed to identify DPPs between T24R and T24S cells. A statistical hypothesis test using an empirical null model was conducted (see **Methods**). From the total 3,315 putative palmitoylated proteins, 506 proteins were identified as DPPs based on the criteria of a combined $P < 0.05$ and \log_2 -transformed fold-change of 0.58 (**Figure 2B**). Furthermore, we found only 506 proteins as being differentially abundant in T24R cells compared to T24S after extensive statistical analysis. Among those identified 506 DPPs, at least 351 (69%) were identified as known palmitoyl proteins [29,52] (**Figure 2B**). To construct the database of known palmitoylated proteins, we combined the 3,593 human palmitoyl proteins compiled in the SwissPalm (v2), a compendium of palmitoyl proteins, with the 2,895 high-confidence candidate human palmitoyl proteins identified from LNCaP cells using LB-ABE to generate the currently most comprehensive palmitoyl-proteome database, containing 4,669 known palmitoyl proteins. Then, by comparing the 506 differentially abundant palmitoyl proteins with the 4,669 known human palmitoyl proteins, 351 DPPs were identified as known palmitoyl-proteins. The remaining 155 (31%) DPPs are novel putative palmitoyl-proteins and not reported in any type of cells (**Figure 2B**). A few examples of known and novel DPPs were shown in **Figures 2C and 2D**.

Cisplatin resistance-associated protein palmitoylation changes

These 506 DPPs included 180 upregulated and 326 downregulated DPPs in T24R cells, compared to T24S (**Figure 3A**). A volcano plot displays DPPs between the T24R vs. T24S cells (**Figure 3B**). Among these DPPs, NCAM1, VIM, ROR1, MAOA, and SLC7A2 are known to be palmitoylated in other types of cells[52]. **Figure 3C** summarizes the most altered known palmitoylated proteins in T24R compared to T24S cells.

Biological and mechanistic meaning of DPPs associated with cisplatin resistance

The top 10 significantly enriched biological processes suggest that carboxylic acid transport, cell-cell adhesion, and biological adhesion were enriched for by DPPs in T24R cells (**Figure 4A**). Further functional enrichment analysis of the 180 upregulated DPPs in T24R cells revealed that oxidation-reduction or lipid metabolic processes were enriched, while the 326 downregulated DPPs were enriched for anion/ion transport and apoptosis (5 out

of top 7 biological processes) (**Figure 4B**). The following doughnut charts exhibit the proportion of the numbers of up (outside) and downregulated DPPs (inside) for enriched molecular functions (**Figure 3B**) and cellular compartments (**Figure 4C**). In terms of molecular functions, those related to catalytic activity or binding were enriched for in both up and downregulated DPPs, suggesting that palmitoylation functions in membrane anchoring, trafficking, and cellular localization-associated enzymatic activity (**Figure 4D**). Cellular compartments, such as the organelles and membrane, were also enriched for by DPPs (**Figure 4E**).

Table 1 shows the enriched biological processes of DPPs between T24R and T24S cells. Functional analysis suggested that proteins related to oxidation-reduction and lipid metabolism pathways are highly palmitoylated in T24R cells. In contrast, those related to ion and anion transport were significantly downregulated in T24R cells. Collectively, our data imply that protein palmitoylation may be involved in a wide range of biological processes and aggressiveness of cancer, which can be further associated with cisplatin resistance.

Inhibition of palmitoylation differently perturbed protein palmitoylation in T24S and T24R cells

A lipid-based protein palmitoylation inhibitor, 2-BP, was used to test how palmitoylation of identified DPPs are regulated in T24R and T24S cells. In T24S cells, 165 DPPs were identified as being downregulated in response to 2-BP (\log_2 -fold-change > 0.58 , combined p-value < 0.05) (**Figure 5A**). A volcano plot exhibits the DPPs significantly altered by palmitoylation inhibition (**Figure 5B**). The enriched biological processes among downregulated DPPs indicated protein localization (**Figure 5C**), while those upregulated include intermediate filament, skin development, and fatty acid beta-oxidation. (**Figure S1A**).

In T24R cells, 75 DPPs were upregulated and 132 were downregulated by palmitoylation inhibition (\log_2 -fold-change > 0.58 , combined p-values < 0.05) (**Figure 5D**). A volcano plot exhibits up or downregulated DPPs after 2-BP treatment (**Figure 5E**). The enriched biological processes among the 132 processes downregulated by palmitoylation inhibition indicated the glycosaminoglycan metabolomic process, hippo signaling, and protein localization to the plasma membrane (**Figure 5F**); while those upregulated include epidermis development, skin development, cell junction

organization, and fatty acid beta-oxidation. (Figure S1B).

There were several clustered patterns of palmitoylation changes among DPPs. For example, palmitoylation levels of DDPs, such as AGPAT1 (1-acylglycerol-3-phosphate O-acyltransferase 1), PKP2 (plakophilin 2), TMEM231 (transmembrane protein 231), SLC7A2 (solute carrier family 7 member 2), CLCN2 (chloride voltage-gated channel 2), and F2R (protease-activated receptors), decreased in both T24S and T24R cells after 2-BP treatment (Figure 5G). In

contrast, DPPs, like PPP2R1B (protein phosphatase 2 scaffold subunit A beta), CSRP1 (cysteine and glycine rich protein 1), SHB (SH2 domain containing adaptor protein B), were decreased only in T24R cells following 2-BP treatment (Figure 5G). Collectively, these findings suggest that a variety of palmitoylation mechanisms may play a role in the regulation of protein palmitoylation. In both T24S and T24R cells, there were noticeable common biological processes affected by palmitoylation inhibition, including protein localization and fatty acid beta-oxidation.

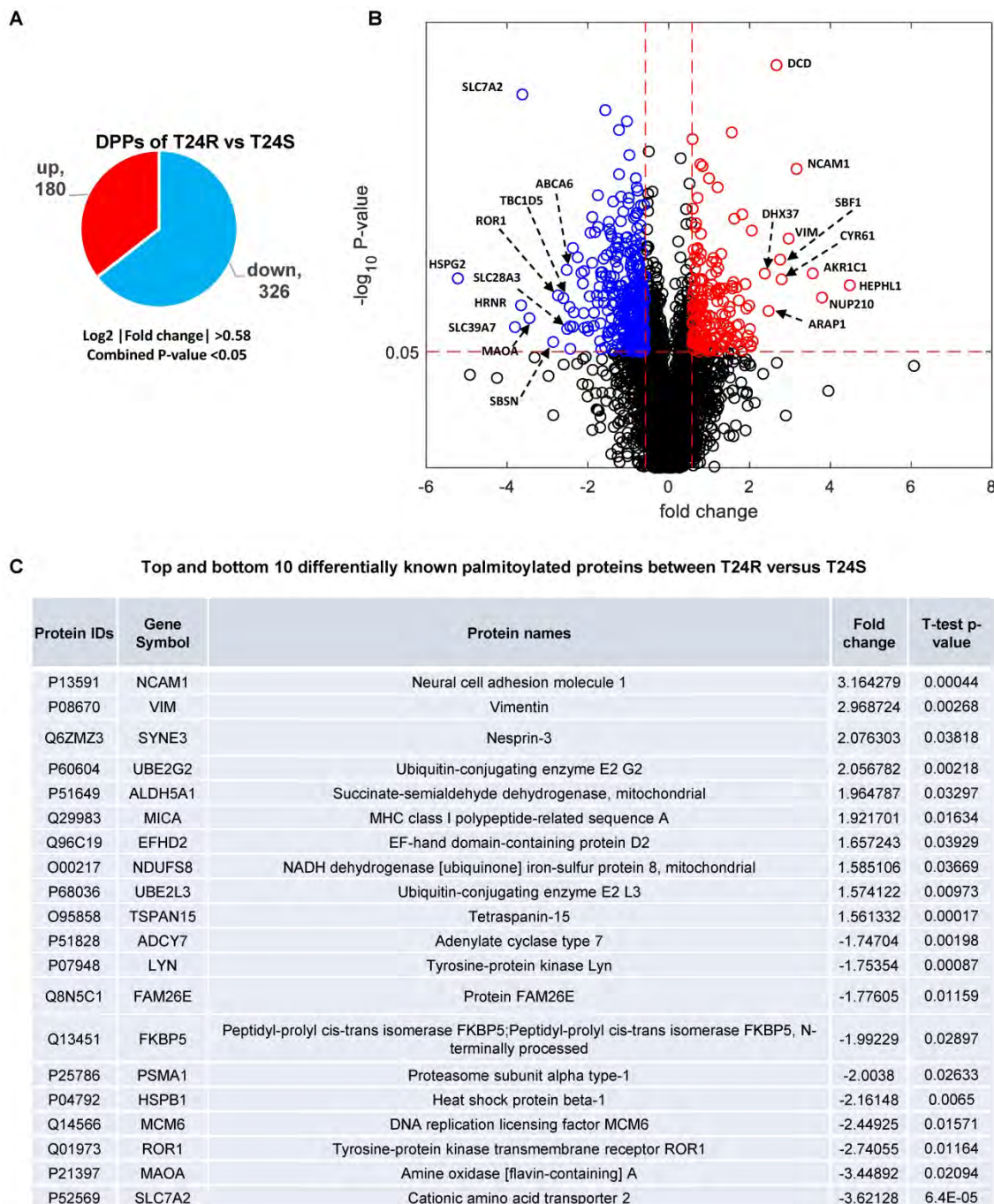


Figure 3. Identification of differentially palmitoylated proteins (DPPs). (A) Diagram showing 180 up and 326 downregulated DPPs in T24R cells. (B) Volcano plot shows all putative palmitoylated proteins. Red, upregulated DPPs in T24R cells compared to T24S (n=180). Blue, downregulated DPPs in T24R cells compared to T24S (n=326). (C) Top 10 most and least DDPs among known palmitoylated proteins.

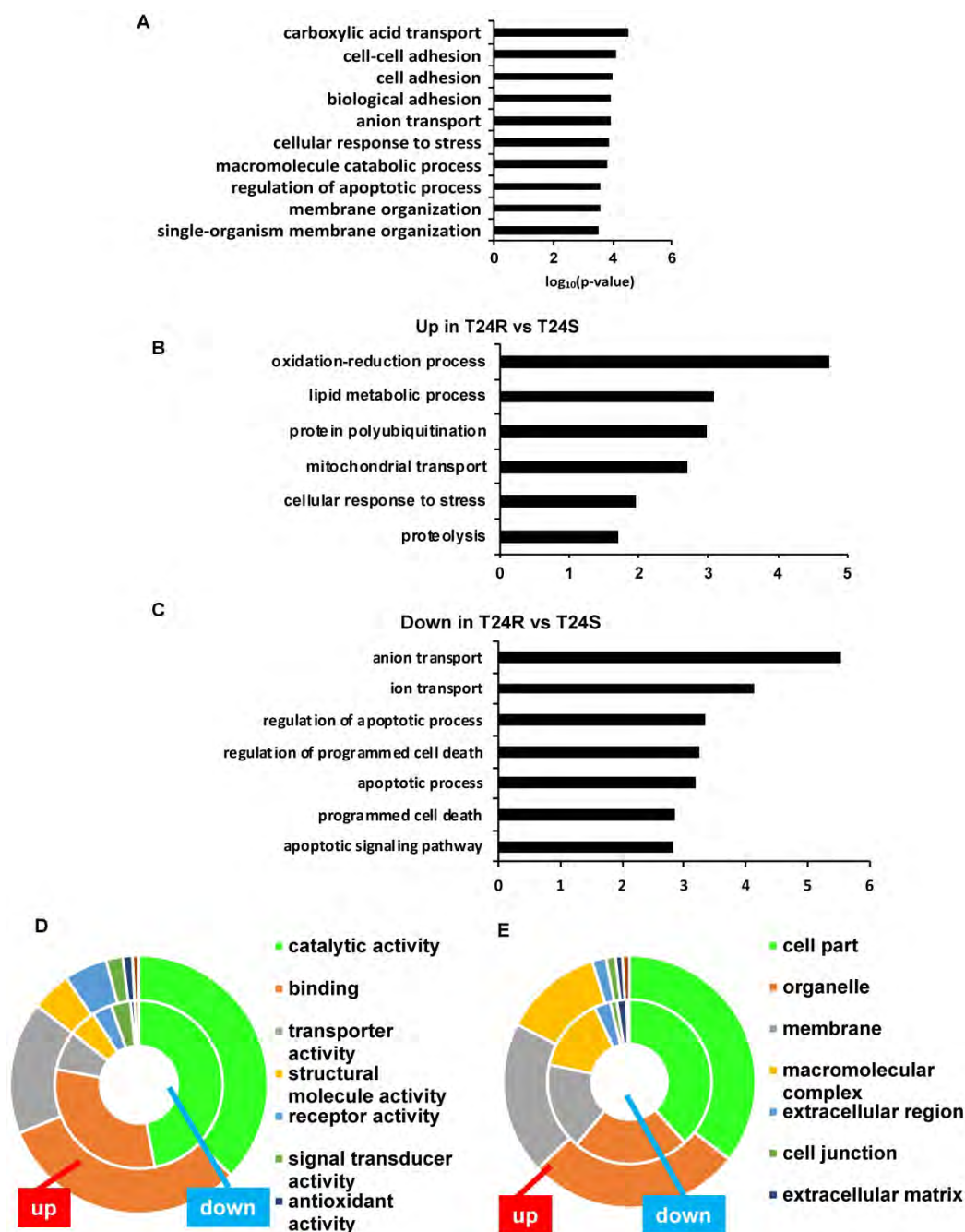


Figure 4. Biological enrichment of DPPs between T24R and T24S cells. (A) Bar graph shows top 10 biological processes enriched by DPPs in T24R cells compared to T24S. **(B-C)** Bar graphs show enriched biological processes upregulated **(B)** and downregulated by DPPs in T24R cells **(C)**. **(D-E)** Doughnut charts visualize the proportion of the numbers of up (outside donut) and downregulated (inside donut) DPPs in the enriched molecular functions **(D)** and cellular compartments **(E)**.

ACSS2 inhibition decreases fatty acid synthesis and changes palmitoylation of proteins in BC cells

Our previous study extensively investigated and demonstrated the link between lipid production and cisplatin resistance. The total lipid levels in T24R cells were significantly higher than those in T24S cells (~170%) [52]. In T24R cells, expression of several lipid metabolism-related proteins, such as ACC (acetyl-CoA carboxylase), FASN, and ACSS2 (acyl-CoA

synthetase short chain family member 2), was found to be increased. Since FASN is a key player in palmitate synthesis, the influence of palmitate levels and cholesterol concentration was examined in the context of cisplatin resistance. Experimental results from our previous [53] and current study show increased palmitate, cholesterol, and lipid production in T24R cells compared to T24S **(Figure 6A and 6B)**. Our group previously found that ACSS2 inhibition decreased the *de novo* synthesis of fatty acid by more than 60% in T24R cells, but not in T24S [51].

Table 1. Enriched biological process of DPPs

	GOBPs	Gene count	P-value	Genes
	cell adhesion	29	0.006294	ARHGAP5, ATP1B1, CASP8, CSRP1, DSP, CYR61, LDHA, BCAM, ME1, NCAM1, NEO1, PKP2, PLCB3, PLXNB3, PSMB10, SHB, SHC1, STK10, TPBG, SCARF1, NRP2, ME3, TMOD3, OLA1, ERBIN, ESYT2, EFHD2, VASN, MICA.
T24R vs T24S Up	lipid metabolic process	27	0.000834	ACAA1, ACACA, ALDH1A3, ALDH3A2, CREBBP, AKR1C1, DHCR7, GM2A, HMGS1, CYR61, PTPNA, PLCB3, ABCD3, SCD, ALDH5A1, SCARF1, ACAA2, AGPAT1, DDX20, PTGR1, ACSL5, NANS, DOLP1, MBOAT7, PTPMT1, CERS6, IAH1.
	oxidation-reduction process	26	0.000018	ACAA1, ALDH1A3, ALDH3A2, ALDOC, COX15, AKR1C1, DHCR7, LDHA, ME1, NDUFS8, PGD, ABCD3, PYGB, SCD, SPR, ALDH5A1, ACAA2, ME3, PTGR1, PRDX5, KDM3A, SQOR, NXN, VKORC1L1, QSOX2, HEPHL1.
	cell adhesion	45	0.005795	CD59, CLPTM1, COL6A1, DNM2, DSC3, HDLBP, HSPB1, JUP, LAMC1, LGALS1, LRP6, LYN, TACSTD2, MCAM, NCAM2, PDPK1, PNN, PODXL, PRKCD, PSEN1, RANGAP1, ROBO1, RPL22, S100A11, SLC9A1, ZEB1, TGFB1, TGFB2, MAD1L1, RIPK2, TJP2, FLOT1, PACSIN2, CLASP2, MPRIIP, ICOSLG, NECTIN3, TES, BAIAP2L1, JAM2, EPS8L2, VMP1, CD99L2, ANTXR1, PHLDB2.
T24R vs T24S Down	ion transport	47	0.000072	ABCD1, CLCN2, CLCN7, CLN3, COX4I1, DNM2, DPYSL2, STOM, F2R, GLS, LYN, ABCC1, P2RX4, PDPK1, PKD2, PLP2, PSEN1, PSEN2, SLC6A9, SLC7A2, SLC9A1, SLC12A2, SLC25A1, SNAP25, TGFB1, SLC39A7, SLC43A1, SLC5A6, SLC16A3, TMEM63A, SLC12A7, SERINC3, SLC39A14, CALHM2, TRPV2, SLC38A2, MCOLN1, SERINC1, SLC26A6, TTYH3, SLC38A1, MCU, ORAI3, SLC46A1, NIP1, SLC9B2, CALHM5.
	anion transport	25	0.000003	ABCD1, CLCN2, CLCN7, CLN3, DPYSL2, GLS, ABCC1, P2RX4, PSEN1, SLC6A9, SLC7A2, SLC12A2, SLC25A1, SNAP25, SLC43A1, SLC5A6, SLC16A3, SLC12A7, SERINC3, SLC38A2, SERINC1, SLC26A6, TTYH3, SLC38A1, SLC46A1.

Given these findings, we speculated that increased palmitate and cholesterol production via ACSS2 in T24R promotes changes in palmitoylation status of specific proteins; thereby, contributing to cisplatin resistance. An LC-MS/MS approach was used to determine if ACSS2 inhibition perturbs palmitoylation status of proteins in T24S and T24R cells. In T24S cells, bioinformatic analysis revealed 255 DPPs, of which 80 were upregulated and 175 were downregulated (Figure 6C). The volcano plot in Figure 6D shows the downregulated proteins and their palmitoylation levels following ACSS2 inhibition treatment. The biological processes of these DPPs include ion transport, cellular homeostasis, cell adhesion, cell migration, and proliferation (Figure 6E). In T24R cells, ACSS2 inhibition led to 98 downregulated DDPs (Figure 6F and 6G). The downregulated DDPs are involved in immune response related biological processes, such as regulation of response to external stimulus, homeostatic process, inflammatory response, chemotaxis, leukocyte migration, and regulation of cell proliferation (Figure 6H).

FASN palmitoylation and PD-L1 expression in BC

The palmitoylation of FASN was first validated because its link to lipid metabolism is well established in many cancer types, including BC [33,36,54,55]. FASN was found to be more palmitoylated in T24R cells compared to T24S. Because palmitoylation often contributes to increased protein stability and eventual upregulated expression, FASN expression could be associated with BC cisplatin resistance. We next tested a possible link between increased lipid production and palmitoylation with cisplatin resistance in BC.

At baseline, T24R cells were found to express modest but greater levels of FASN expression than

T24S (Supplementary Figure 2). The LB-ABE method was used to validate whether FASN was palmitoylated in BC cells. FASN palmitoylation levels were increased in T24R cells compared to T24S (Figure 7A). There were more palmitoylated FASN proteins detected as well. Palmitoylation inhibition by 2-BP repressed FASN expression in a dose-dependent manner in both T24S and T24R cells (Figure 7B). This implies that FASN is palmitoylated in BC cells, and the increase in palmitoylation of FASN is likely associated with cisplatin resistance in BC.

Additional experiments were conducted to support the FASN palmitoylation data using commercial palmitoylation protein assay kits, as described in the Methods. These kits are based on similar enrichment principles as our own. After palmitoylation enrichment, the total palmitoylation levels were almost identical in T24R and T24S cells. However, after treatment with 2-BP, the total palmitoylated proteins were significantly reduced in T24S cells compared to T24R, which had partial remaining palmitoylated proteins. Further data using western blot analysis showed that palmitoylated FASN was increased in T24R cells compared to T24S (Figure 7C, palmitoylated FASN panel). PD-L1 was also found to be palmitoylated in both T24S and T24R cells. Palmitoylation levels of PD-L1 were greater in T24R cells with or without 2-BP treatment (Figure 7C, palmitoylated PD-L1 panel). PD-L1 expression was determined to be approximately 15-fold greater in T24R cells compared to T24S (Figure 7D). When palmitoylation was inhibited by 2-BP, PD-L1 expression was significantly reduced in both T24R and T24S cells (Figure 7D). Although 2-BP abolished PD-L1 palmitoylation completely, it was not able to effectively suppress PD-L1 palmitoylation in T24R cells.

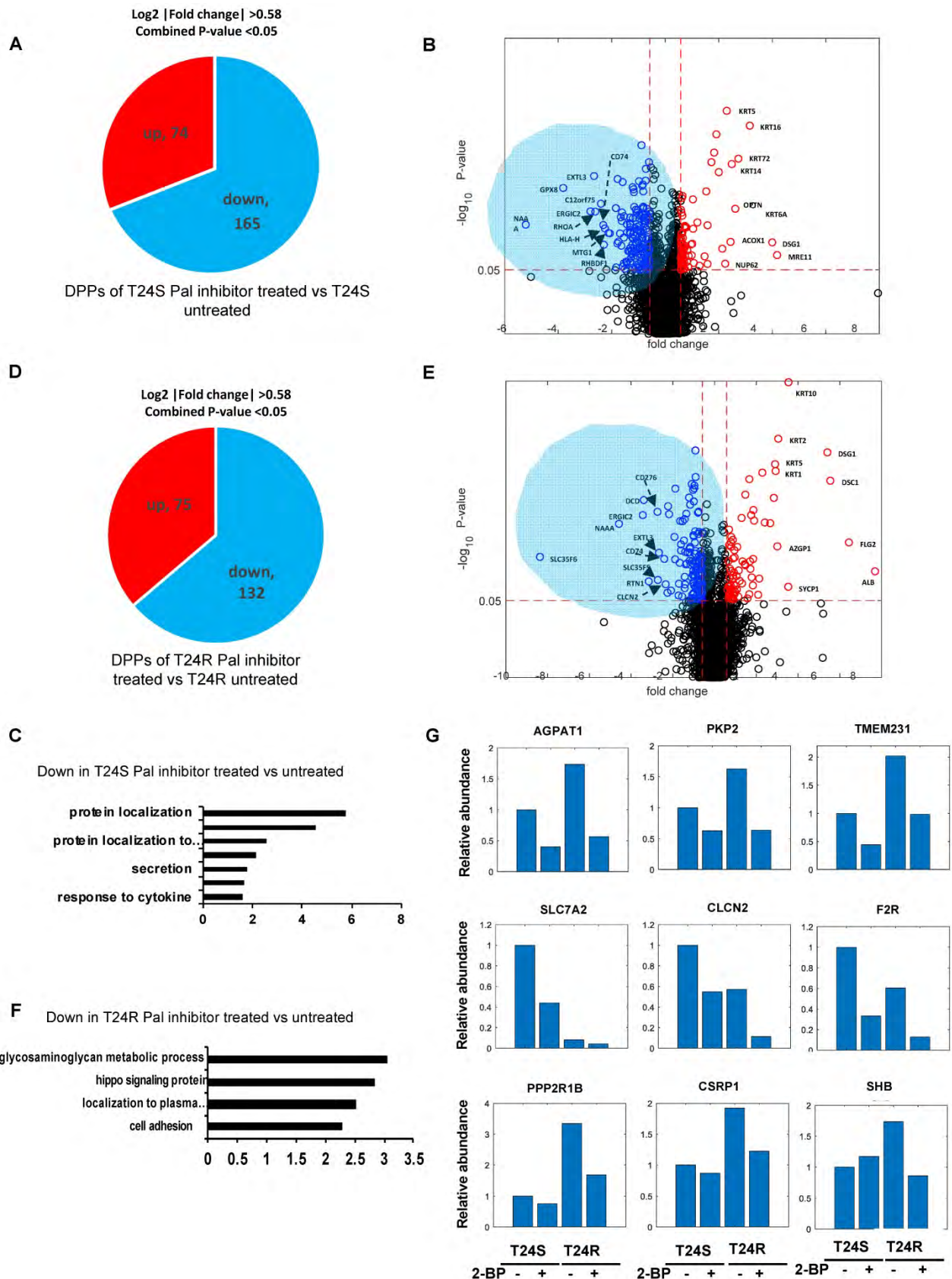


Figure 5. Effects of palmitoylation inhibition in T24S and T24R cells (A) Pie chart depicts the number of up and downregulated DPPs by palmitoylation inhibitor treatment in T24S cells. **(B)** Volcano plot shows the distribution of the DPPs with \log_2 ratio of palmitoylation inhibitor treated and untreated T24S cells (x-axis) and statistical significance (y-axis). **(C)** Bar plot shows downregulated biological processes in T24S cells in response to the inhibitor treatment. **(D)** Pie chart depicts the number of up and downregulated DPPs by palmitoylation inhibitor treatment in T24R cells. **(E)** Volcano plot shows the distribution of the DPPs with \log_2 ratio of inhibitor treated and untreated T24R cells (x-axis) and statistical significance (y-axis). **(F)** Bar plot shows downregulated biological processes in T24R cells in response to the inhibitor treatment. **(G)** Palmitoylated protein abundance with or without palmitoylation inhibitor in T24S and T24R cells. Examples of palmitoyl-proteins that have different effects on the treatment of

palmitoylation inhibitor are shown. **(Top)** Three proteins exhibit higher expression in T24R cells compared to T24S and have significant downregulation after inhibitor treatment in both. **(Middle)** Three proteins are significantly higher in T24S cells compared to T24R and have significant downregulation in both. **(Bottom)** Three proteins are significantly higher in T24R cells compared to T24S and have significant downregulation only in T24R.

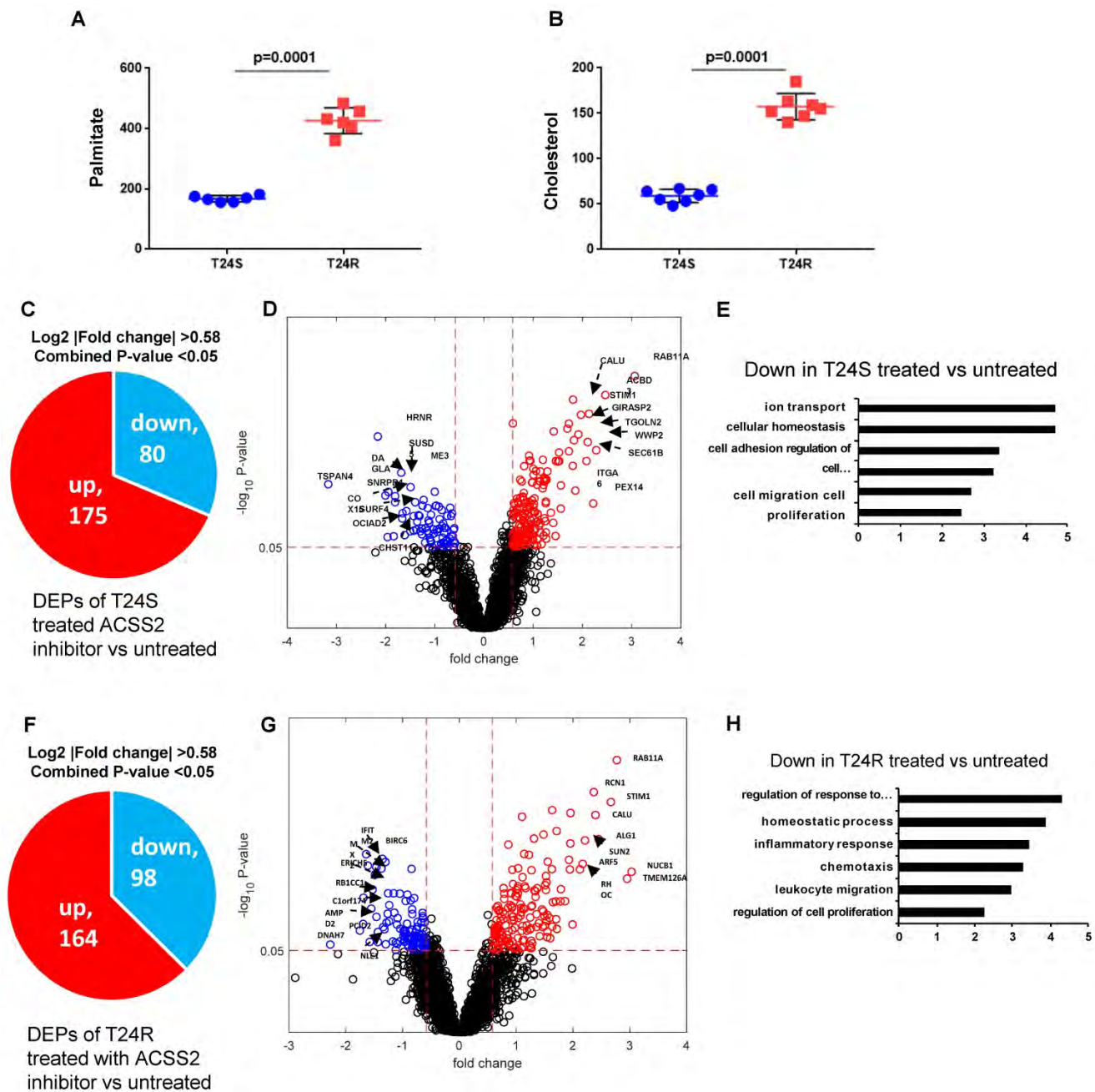


Figure 6. Effects of ACSS2 inhibitor in T24S and T24R cells. **(A)** Palmitate concentration in T24S and T24R cells. **(B)** Cholesterol levels were compared in T24S and T24R cells. **(C)** Pie chart depicts the number of up (n=175) and downregulated DPPs (n=80) following ACSS2 inhibitor treatment in T24S cells. **(D)** Volcano plot shows the distribution of the DPPs with log₂ ratio of ACSS2 inhibitor treated and untreated T24S cells (x-axis) and statistical significance (y-axis). **(E)** Bar plot shows downregulated biological processes in T24S cells in response to ACSS2 inhibitor treatment. **(F)** Pie chart depicts the number of up (n=164) and downregulated DPPs (n=98) following ACSS2 inhibitor treatment in T24R cells. **(G)** Volcano plot shows the distribution of the DPPs with log₂ ratio of ACSS2 inhibitor treated and untreated T24R cells (x-axis) and statistical significance (y-axis). **(H)** Bar plot shows downregulated biological processes in T24R cells in response to ACSS2 inhibitor treatment.

Next, the effects of FASN inhibition on BC-specific palmitoylated proteins was examined. T24S and T24R cells were treated with orlistat. This reduced PD-L1 protein expression in both T24R and T24S cells (**Figure 7E**), suggesting that FASN activity likely regulates PD-L1 palmitoylation and stability. It

was confirmed that there were no cytotoxic effects of orlistat within the conditions used, based on additional analysis showing that there were no observed changes in cell viability in response to orlistat in both T24S and T24R cells (**Figure 7F**).

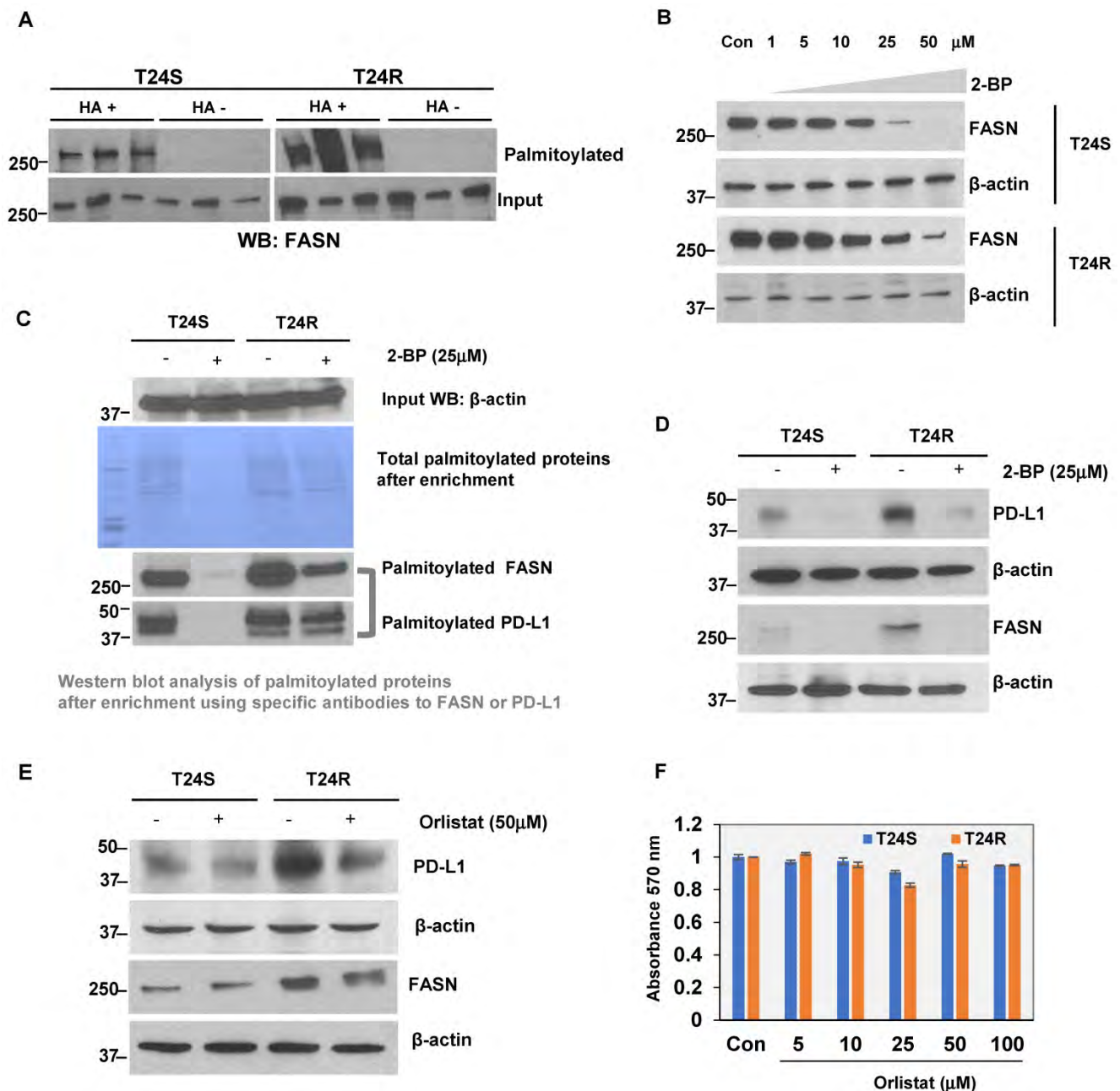


Figure 7. (A) Validation of FASN palmitoylation in T24S and T24R cells. Western blot analysis was performed using palmitoylation-enriched proteins. The same amount of proteins was used as starting materials (input). (B) FASN protein expression is downregulated by palmitoylation inhibition. Vehicle-treated cells acted as controls. (C) Further validation of FASN palmitoylation using a commercial kit. PD-L1 was also palmitoylated both in T24S and T24R cells. (D) Palmitoylation inhibition by 25 μM 2-BP treatment dramatically reduced protein expression of PD-L1 and FASN. Western blot analysis of FASN and PD-L1 protein expression from cells exposed to either 2-BP or vehicle control. (E) Expression of PD-L1 decreased in response to 50 μM orlistat treatment. (F) Cell viability assays on the effects of orlistat at varying time points or concentrations did not show any significant difference. Differences in cell viability, in which vehicle acted as control, was determined by t-test. Data are representative of at least three different experiments. Error bars denote SEM. *, **, and n.s. stand for $p < 0.01$, $p < 0.05$, and $p \geq 0.05$, respectively.

Discussion

S-palmitoylation (S-acylation) is the enzymatic addition of a fatty acid (acyl) group, such as palmitate, onto cysteine residues of a protein via thioester linkage, which is catalyzed by palmitoyltransferases and depalmitoyltransferases [56]. Many protein substrates can be palmitoylated by more than one DHHC enzyme with certain DHHC-substrate

specificity. DHHCs may act as a functional heterodimer, which may affect their enzymatic activities. S-palmitoylation is a powerful regulatory mechanism for a number of cellular processes, including signal transduction, protein turnover, vesicle fusion, and cell-cell interactions. Dysfunctions can lead to cancer, cardiovascular disease, and neurological disorders [57-59]. The reversible modification of cysteine residues by thioester formation with palmitate by the addition of a C16:0

carbon palmitoyl moiety is an abundant lipid post-translational modification. This addition of palmitate enhances a protein's affinity to the membrane, directs its distribution in membrane micro-domains, and mediates protein-protein interactions, trafficking, stability, and aggregation state. There is an intriguing potential connection between alterations in the metabolome and mitochondrial regulation. In addition, post-translational lipid modification targets and shuttles proteins between the cytosol and lipid raft within the plasma and mitochondrial membranes. Palmitoylation is known to play active roles in the sorting and trafficking of many proteins, and fluctuations in palmitoylation may contribute to signaling outcomes. S-palmitoylation has been observed in many ER and mitochondrial proteins, suggesting an intriguing potential connection between metabolic lipids and mitochondrial regulation [60]. However, it is unknown whether or how mitochondrial S-palmitoylation is regulated in the context of resistance against chemotherapy [16,61-63].

Our palmitoyl-proteomics approach detected a total of 25,598 peptides and 3,695 putative palmitoylated proteins in either T24S or T24R BC cells. The further defined 506 DDPs included 180 upregulated and 326 downregulated palmitoylated proteins in T24R cells. Our results also uncovered a novel molecular mechanism of palmitoylation, which demonstrates that protein palmitoylation of putative candidate proteins, is linked with responsiveness to chemotherapy, such as cisplatin. In this study, our palmitoylated protein-enriched proteomics profiling comparing cisplatin-resistant and sensitive BC cells showed that FASN is critical for protein palmitoylation in cisplatin-resistant cells. FASN plays an important role in synthesis of palmitate, which is both a precursor for fatty acids and the acyl group that is added to cysteine residues during palmitoylation [64]. Therefore, it is logical to infer that overexpression of FASN is associated with increased protein palmitoylation, which then contributes to worse prognoses in certain cancers [65]. Furthermore, a recent study found that FASN mediates EGFR palmitoylation in EGFR-mutated chemo-resistant non-small cell lung cancer [32].

We found that FASN expression and palmitoylation may lead to increased PD-1 expression and palmitoylation. PD-L1, a T cell regulatory molecule that is expressed on the surface of tumor and tumor-infiltrating immune cells, was also found to be highly palmitoylated in cisplatin-resistant BC cells, compared to isogenic control cells [66]. Activation of the pathway inhibits the activation of cytotoxic T lymphocytes and is one of the main

methods through which tumor cells evade immune responses [67]. Antibodies targeting PD-L1 are known to benefit overall survival in BC, and several agents have received accelerated approval from the FDA for treatment [68]. In addition to being a clinical target, PD-L1 has also been shown to be a significant clinical predictor for stage and treatment response in BC [69]. It has been previously shown that PD-L1 is palmitoylated via a covalent attachment of palmitic acid to its 272 cysteine residue for stability [70]. Although the effects of PD-L1 palmitoylation has not been thoroughly examined in the context of BC, previous studies have shown that palmitoylation stabilizes PD-L1 and promotes tumor growth in other cancer types, such as breast cancer [71], melanoma, and BC. Based on this prior evidence, exploring the influence of PD-L1 palmitoylation in BC progression and aggression presents a promising opportunity.

There are limitations in this study. Although there are ongoing studies in our laboratory, this study did not provide evidence to demonstrate whether inhibition of both FASN and PD-L1 may have synergistic inhibitory effects on cancer progression. These alternative hypotheses await further investigation. Currently, the most widely used palmitoylation inhibitor, 2-BP, a non-metabolizable palmitate analog, elicits pleiotropic effects. However, no inhibitory drugs targeting palmitoylation with high-affinity and specificity are available. There is an urgent need to identify specific, high-affinity inhibitors of protein palmitoylation for basic research and therapeutic intervention based on palmitoylation. Thus, much work remains to be developed on the specific and high affinity inhibitors of protein palmitoylation that can be applied as therapeutic strategies designed for overcoming cisplatin resistance in BC. In this study, we did not focus on the specific enzymes that catalyze palmitoylation of PD-L1. Further analysis on how palmitoylases and depalmitoylases, such as ZDHHC and APT/PPT, control PD-L1 palmitoylation and activity and contribute to activation of oncogenic pathways is warranted. Additional exploration of these mechanisms is necessary to clarify how PD-L1 is trafficked in the cell and how its activity is controlled in the context of cisplatin resistance.

Supplementary Material

Supplementary figures and tables.

<http://www.ijbs.com/v16p2490s1.pdf>

Competing Interests

The authors have declared that no competing interest exists.

References

- Noon AP, Catto JW. Bladder cancer in 2012: Challenging current paradigms [Review]. *Nat Rev Urol*. 2013 Feb;10(2):67-8.
- Kirkali Z, Chan T, Manoharan M, et al. Bladder cancer: epidemiology, staging and grading, and diagnosis [Review]. *Urology*. 2005; 66(6 Suppl 1):4-34.
- Kim J, Jahng WJ, Di Vizio D, et al. The phosphoinositide kinase PIKfyve mediates epidermal growth factor receptor trafficking to the nucleus [Research Support, N.I.H., Extramural Research Support, Non-U.S. Gov't]. *Cancer Res*. 2007 Oct 1;67(19):9229-37.
- Kamat AM, Hegarty PK, Gee JR, et al. ICUD-EAU International Consultation on Bladder Cancer 2012: Screening, diagnosis, and molecular markers [Consensus Development Conference Practice Guideline Review]. *Eur Urol*. 2013 Jan;63(1):4-15.
- Gakis G, Efstathiou J, Lerner SP, et al. ICUD-EAU International Consultation on Bladder Cancer 2012: Radical cystectomy and bladder preservation for muscle-invasive urothelial carcinoma of the bladder [Consensus Development Conference Practice Guideline Review]. *Eur Urol*. 2013 Jan;63(1):45-57.
- Sternberg CN, Bellmunt J, Sonpavde G, et al. ICUD-EAU International Consultation on Bladder Cancer 2012: Chemotherapy for urothelial carcinoma-neoadjuvant and adjuvant settings [Consensus Development Conference Practice Guideline Review]. *Eur Urol*. 2013 Jan;63(1):58-66.
- Masui K, Cavenee WK, Mischel PS. mTORC2 in the center of cancer metabolic reprogramming [Review]. *Trends Endocrinol Metab*. 2014 May 21.
- Masui K, Cavenee WK, Mischel PS. mTORC2 dictates Warburg effect and drug resistance [Editorial]. *Cell Cycle*. 2014 Apr 1;13(7):1053-4.
- Phan LM, Yeung SC, Lee MH. Cancer metabolic reprogramming: importance, main features, and potentials for precise targeted anti-cancer therapies [Review]. *Cancer Biol Med*. 2014 Mar;11(1):1-19.
- Kroemer G, Pouyssegur J. Tumor cell metabolism: cancer's Achilles' heel [Research Support, Non-U.S. Gov't Review]. *Cancer Cell*. 2008 Jun;13(6):472-82.
- Huang Z, Lin L, Gao Y, et al. Bladder cancer determination via two urinary metabolites: a biomarker pattern approach. *Mol Cell Proteomics*. 2011 Oct;10(10):M111 007922.
- Jin X, Yun SJ, Jeong P, et al. Diagnosis of bladder cancer and prediction of survival by urinary metabolomics. *Oncotarget*. 2014 Mar 30;5(6):1635-45.
- Amoedo ND, Obre E, Rossignol R. Drug discovery strategies in the field of tumor energy metabolism: Limitations by metabolic flexibility and metabolic resistance to chemotherapy. *Biochim Biophys Acta*. 2017 Aug;1858(8):674-685.
- Schug ZT, Peck B, Jones DT, et al. Acetyl-CoA synthetase 2 promotes acetate utilization and maintains cancer cell growth under metabolic stress. *Cancer Cell*. 2015 Jan 12;27(1):57-71.
- Huang Z, Zhang M, Plec AA, et al. ACS2 promotes systemic fat storage and utilization through selective regulation of genes involved in lipid metabolism. *Proc Natl Acad Sci U S A*. 2018 Oct 2;115(40):E9499-E9506.
- Linder ME, Deschenes RJ. Palmitoylation: policing protein stability and traffic. *Nat Rev Mol Cell Biol*. 2007 Jan;8(1):74-84.
- Resh MD. Palmitoylation of proteins in cancer. *Biochem Soc Trans*. 2017 Apr 15;45(2):409-416.
- Tabaczar S, Czogalla A, Podkalicka J, et al. Protein palmitoylation: Palmitoyltransferases and their specificity. *Exp Biol Med (Maywood)*. 2017 Jun;242(11):1150-1157.
- Valdez-Taubas J, Pelham H. Swf1-dependent palmitoylation of the SNARE Tlg1 prevents its ubiquitination and degradation. *EMBO J*. 2005 Jul 20;24(14):2524-32.
- Levental I, Grzybek M, Simons K. Greasing their way: lipid modifications determine protein association with membrane rafts. *Biochemistry*. 2010 Aug 3;49(30):6305-16.
- Sophasan S, Chatsudthipong V, Kraisaewekwisai S. Kidney pressures after the release of 24 hours of bilateral ureteral ligation in the rat. *J Urol*. 1982 Nov;128(5):1081-6.
- Akimzhanov AM, Boehning D. Rapid and transient palmitoylation of the tyrosine kinase Lck mediates Fas signaling. *Proc Natl Acad Sci U S A*. 2015 Sep 22;112(38):11876-80.
- Cao N, Li JK, Rao YQ, et al. A potential role for protein palmitoylation and zDHHCl6 in DNA damage response. *BMC Mol Biol*. 2016 May 10;17(1):12.
- Chen X, Ma H, Wang Z, et al. EZH2 Palmitoylation Mediated by ZDHHCl5 in p53-Mutant Glioma Drives Malignant Development and Progression. *Cancer Res*. 2017 Sep 15;77(18):4998-5010.
- Coleman DT, Gray AL, Kridel SJ, et al. Palmitoylation regulates the intracellular trafficking and stability of c-Met. *Oncotarget*. 2016 May 31;7(22):32664-77.
- Murphy J, Kolandaivelu S. Palmitoylation of Progressive Rod-Cone Degeneration (PRCD) Regulates Protein Stability and Localization. *J Biol Chem*. 2016 Oct 28;291(44):23036-23046.
- Noland CL, Gierke S, Schnier PD, et al. Palmitoylation of TEAD Transcription Factors Is Required for Their Stability and Function in Hippo Pathway Signaling. *Structure*. 2016 Jan 5;24(1):179-186.
- Yang W, Di Vizio D, Kirchner M, et al. Proteome scale characterization of human S-acylated proteins in lipid raft-enriched and non-raft membranes. *Mol Cell Proteomics*. 2010 Jan;9(1):54-70.
- Zhou B, Wang Y, Yan Y, et al. Low-Background Acyl-Biotinyl Exchange Largely Eliminates the Coisolation of Non-S-Acylated Proteins and Enables Deep S-Acylproteomic Analysis. *Anal Chem*. 2019 Aug 6;91(15):9858-9866.
- Zhou B, Wang Y, Yan Y, Mariscal J, et al. Low-background acyl-biotinyl exchange largely eliminates the co-isolation of non-S-acylated proteins and enables deep S-acylproteomic analysis. *bioRxiv*. 2009;588988
- Li J, Dong L, Wei D, et al. Fatty acid synthase mediates the epithelial-mesenchymal transition of breast cancer cells. *Int J Biol Sci*. 2014;10(2):171-80.
- Ali A, Levantini E, Teo JT, et al. Fatty acid synthase mediates EGFR palmitoylation in EGFR mutated non-small cell lung cancer. *EMBO Mol Med*. 2018 Mar;10(3).
- Abdelrahman AE, Rashed HE, Elkady E, et al. Fatty acid synthase, Her2/neu, and E2F1 as prognostic markers of progression in non-muscle invasive bladder cancer. *Ann Diagn Pathol*. 2019 Apr;39:42-52.
- Chen Q, Chong T, Yin J, et al. Molecular events are associated with resistance to vinblastine in bladder cancer. *Cell Mol Biol (Noisy-le-grand)*. 2015 May 8;61(2):33-8.
- Sugino T, Baba K, Hoshi N, et al. Overexpression of fatty acid synthase in human urinary bladder cancer and combined expression of the synthase and Ki-67 as a predictor of prognosis of cancer patients. *Med Mol Morphol*. 2011 Sep;44(3):146-50.
- Jiang B, Li EH, Lu YY, et al. Inhibition of fatty-acid synthase suppresses P-AKT and induces apoptosis in bladder cancer. *Urology*. 2012 Aug;80(2):484 e9-15.
- Kim WT, Kim J, Yan C, et al. S100A9 and EGFR gene signatures predict disease progression in muscle invasive bladder cancer patients after chemotherapy. *Annals of oncology : official journal of the European Society for Medical Oncology*. 2014 May;25(5):974-9.
- Wisniewski JR, Zougman A, Nagaraj N, et al. Universal sample preparation method for proteome analysis. *Nat Methods*. 2009 May;6(5):359-62.
- Zhou B, Yan Y, Wang Y, et al. Quantitative proteomic analysis of prostate tissue specimens identifies deregulated protein complexes in primary prostate cancer. *Clin Proteomics*. 2019;16:15.
- Cox J, Neuhauser N, Michalski A, et al. Andromeda: a peptide search engine integrated into the MaxQuant environment. *J Proteome Res*. 2011 Apr 1;10(4):1794-805.
- Cox J, Mann M. MaxQuant enables high peptide identification rates, individualized p.p.b.-range mass accuracies and proteome-wide protein quantification. *Nat Biotechnol*. 2008 Dec;26(12):1367-72.
- Bolstad BM, Irizarry RA, Astrand M, et al. A comparison of normalization methods for high density oligonucleotide array data based on variance and bias. *Bioinformatics*. 2003 Jan 22;19(2):185-93.
- Shin J, Kim M, Jung HJ, et al. Characterization of developmental defects in the forebrain resulting from hyperactivated mTOR signaling by integrative analysis of transcriptomic and proteomic data. *Sci Rep*. 2017 Jun 6;7(1):2826.
- Hwang D, Rust AG, Ramsey S, et al. A data integration methodology for systems biology. *Proc Natl Acad Sci U S A*. 2005 Nov 29;102(48):17296-301.
- Huang da W, Sherman BT, Lempicki RA. Systematic and integrative analysis of large gene lists using DAVID bioinformatics resources. *Nat Protoc*. 2009;4(1):44-57.
- Mi H, Huang X, Muruganujan A, et al. PANTHER version 11: expanded annotation data from Gene Ontology and Reactome pathways, and data analysis tool enhancements. *Nucleic Acids Res*. 2017 Jan 4;45(D1):D183-D189.
- Szklarczyk D, Morris JH, Cook H, et al. The STRING database in 2017: quality-controlled protein-protein association networks, made broadly accessible. *Nucleic Acids Res*. 2017 Jan 4;45(D1):D362-D368.
- Shannon P, Markiel A, Ozier O, et al. Cytoscape: a software environment for integrated models of biomolecular interaction networks. *Genome research*. 2003 Nov;13(11):2498-504.
- Shahid M, Lee MY, Yeon A, et al. Menthol, a unique urinary volatile compound, is associated with chronic inflammation in interstitial cystitis. *Sci Rep*. 2018 Jul 18;8(1):10859.

50. Choi DY, You S, Jung JH, et al. Extracellular vesicles shed from gefitinib-resistant nonsmall cell lung cancer regulate the tumor microenvironment. *Proteomics*. 2014 Aug;14(16):1845-56.
51. Wen H, Lee S, Zhu WG, et al. Glucose-derived acetate and ACS2 as key players in cisplatin resistance in bladder cancer. *Biochim Biophys Acta Mol Cell Biol Lipids*. 2019 Mar;1864(3):413-421.
52. Blanc M, David FPA, van der Goot FG. SwissPalm 2: Protein S-Palmitoylation Database. *Methods Mol Biol*. 2019;2009:203-214.
53. Lee MY, Yeon A, Shahid M, et al. Reprogrammed lipid metabolism in bladder cancer with cisplatin resistance. *Oncotarget*. 2018 Mar 29;17(1):13231-13243.
54. Kim J, Kim WJ, Liu Z, et al. The ubiquitin-specific protease USP2a enhances tumor progression by targeting cyclin A1 in bladder cancer. *Cell Cycle*. 2012 Mar 15;11(6):1123-30.
55. Tao T, Su Q, Xu S, et al. Down-regulation of PKM2 decreases FASN expression in bladder cancer cells through AKT/mTOR/SREBP-1c axis. *J Cell Physiol*. 2019 Mar;234(3):3088-3104.
56. Shen LF, Chen YJ, Liu KM, et al. Role of S-Palmitoylation by ZDHHC13 in Mitochondrial function and Metabolism in Liver. *Sci Rep*. 2017 May 19;7(1):2182.
57. Yeste-Velasco M, Linder ME, Lu YJ. Protein S-palmitoylation and cancer. *Biochim Biophys Acta*. 2015 Aug;1856(1):107-20.
58. Fuller W, Reilly L, Hilgemann DW. S-palmitoylation and the regulation of NCX1. *Channels (Austin)*. 2016;10(2):75-7.
59. Napoli E, Song G, Liu S, et al. Zdhhc13-dependent Drp1 S-palmitoylation impacts brain bioenergetics, anxiety, coordination and motor skills. *Sci Rep*. 2017 Oct 16;7(1):12796.
60. Dallavilla T, Abrami L, Sandoz PA, et al. Model-Driven Understanding of Palmitoylation Dynamics: Regulated Acylation of the Endoplasmic Reticulum Chaperone Calnexin. *PLoS Comput Biol*. 2016 Feb;12(2):e1004774.
61. Ko PJ, Dixon SJ. Protein palmitoylation and cancer. *EMBO Rep*. 2018 Oct;19(10).
62. Wang W, Runkle KB, Terkowski SM, et al. Protein Depalmitoylation Is Induced by Wnt5a and Promotes Polarized Cell Behavior. *J Biol Chem*. 2015 Jun 19;290(25):15707-16.
63. Levental I, Lingwood D, Grzybek M, et al. Palmitoylation regulates raft affinity for the majority of integral raft proteins. *Proc Natl Acad Sci U S A*. 2010 Dec 21;107(51):22050-4.
64. Menendez JA, Lupu R. Fatty acid synthase and the lipogenic phenotype in cancer pathogenesis. *Nat Rev Cancer*. 2007 Oct;7(10):763-77.
65. Piyathilake CJ, Frost AR, Manne U, et al. The expression of fatty acid synthase (FASE) is an early event in the development and progression of squamous cell carcinoma of the lung. *Hum Pathol*. 2000 Sep;31(9):1068-73.
66. Gao Y, Li S, Xu D, et al. Prognostic value of programmed death-1, programmed death-ligand 1, programmed death-ligand 2 expression, and CD8(+) T cell density in primary tumors and metastatic lymph nodes from patients with stage T1-4N+M0 gastric adenocarcinoma. *Chin J Cancer*. 2017 Jul 29;36(1):61.
67. Huang Y, Zhang SD, McCrudden C, et al. The prognostic significance of PD-L1 in bladder cancer. *Oncol Rep*. 2015 Jun;33(6):3075-84.
68. Aggen DH, Drake CG. Biomarkers for immunotherapy in bladder cancer: a moving target. *J Immunother Cancer*. 2017 Nov 21;5(1):94.
69. Wu CT, Chen WC, Chang YH, et al. The role of PD-L1 in the radiation response and clinical outcome for bladder cancer. *Sci Rep*. 2016 Jan 25;6:19740.
70. Gu W, Wang L, Wu Y, et al. Undo the brake of tumour immune tolerance with antibodies, peptide mimetics and small molecule compounds targeting PD-1/PD-L1 checkpoint at different locations for acceleration of cytotoxic immunity to cancer cells. *Clin Exp Pharmacol Physiol*. 2019 Feb;46(2):105-115.
71. Yang Y, Hsu JM, Sun L, et al. Palmitoylation stabilizes PD-L1 to promote breast tumor growth. *Cell Res*. 2019 Jan;29(1):83-86.



Advances in urinary biomarker discovery in urological research

Jayoung Kim^{1,2} , Won Tae Kim^{3,4} , Wun-Jae Kim^{3,4}

¹Departments of Surgery and Biomedical Sciences, Cedars-Sinai Medical Center, Los Angeles, CA, ²Department of Medicine, University of California Los Angeles, CA, USA, ³Department of Urology, Chungbuk National University College of Medicine, Cheongju, ⁴Department of Urology, Chungbuk National University Hospital, Cheongju, Korea

A disease-specific biomarker (or biomarkers) is a characteristic reflecting a pathological condition in human body, which can be used as a diagnostic or prognostic tool for the clinical management. A urine-based biomarker(s) may provide a clinical value as attractive tools for clinicians to utilize in the clinical setting in particular to bladder diseases including bladder cancer and other bladder benign dysfunctions. Urine can be easily obtained by patients with no preparation or painful procedures required from patients' side. Currently advanced omics technologies and computational power identified potential omics-based novel biomarkers. An unbiased profiling based on transcriptomics, proteomics, epigenetics, metabolomics approaches et al. found that expression at RNA, protein, and metabolite levels are linked with specific bladder diseases and outcomes. In this review, we will discuss about the urine-based biomarkers reported by many investigators including us and how these biomarkers can be applied as a diagnostic and prognostic tool in clinical trials and patient care to promote bladder health. Furthermore, we will discuss how these promising biomarkers can be developed into a smart medical device and what we should be cautious about toward being used in real clinical setting.

Keywords: Biomarkers; Cystitis, interstitial; Urinary bladder; Urinary bladder neoplasms; Urine

This is an Open Access article distributed under the terms of the Creative Commons Attribution Non-Commercial License (<http://creativecommons.org/licenses/by-nc/4.0>) which permits unrestricted non-commercial use, distribution, and reproduction in any medium, provided the original work is properly cited.

INTRODUCTION

The bladder is a hollow, soft muscular organ located in the lower abdomen, which stores urine until it is ready to excrete. In urological diseases, the incidence of bladder diseases is quite high. The common bladder diseases include bladder cancer (BC), bladder dysfunction (cystitis, urinary incontinence, overactive bladder, etc.) and other bladder problems. BC is the sixth most common cancer in the United States, accounting for 4.7% of cancer cases [1]. About 45,000 men and 17,000 women in the United States are diagnosed

as BC every year.

Interstitial cystitis (IC) is the most common disease in bladder dysfunction. According to the International Continence Society, the definition of IC is "the complaint of suprapubic pain related to bladder filling, accompanied by other symptoms such as increased daytime and nighttime frequency, in the absence of proven urinary infection or other obvious pathology." [2] The morbidity of IC in the general population is 0.26% to 12.6% [3,4]. The estimated morbidity of IC in women is 45/100,000, which is 4 to 5 times than that in men, with the morbidity of 8/100,000 [5]. In the United

Received: 27 August, 2019 • **Accepted:** 22 October, 2019

Corresponding Author: Wun-Jae Kim <https://orcid.org/0000-0002-8060-8926>

Department of Urology, Chungbuk National University College of Medicine, 1 Chungdae-ro, Seowon-gu, Cheongju 28644, Korea
TEL: +82-43-269-6371, FAX: +82-43-269-6144, E-mail: wjkim@chungbuk.ac.kr

States, 3.3 million women are diagnosed as IC every year [6]. At present, one of the most important methods to diagnose bladder diseases is cystoscopy, but this technique is invasive and may lead to urinary tract infection. Compared to cystoscopy, urine testing is easier to perform in clinical practice. Urine can be obtained non-invasively and shows increased stability over serum or blood, which allows for easy multiple sampling. With the direct contact between urine and bladder diseases, the use of urinary biomarkers detection in bladder diseases becomes more and more important.

WILL IT BE USEFUL THE URINE-BASED DIAGNOSTIC BIOMARKERS TO DETECT AND MONITOR THE BLADDER DISEASES?

Urinary biomarkers are particularly attractive due to the direct contact of the urine with the urothelial tumor cells and the ease of sample collection. Urine-based diagnostic biomarkers are reviewed in our paper from the following aspects: gene mutations and gene expression-based biomarkers, proteomic biomarkers, metabolomic biomarkers, and DNA methylation biomarkers.

1. Gene mutations associated with BC

The exact cause of BC is still unclear. There are several risk factors related to BC, including environment, smoking, toxic industrial chemicals and gases, bladder inflammation, and gene mutations. As a noninvasive method, detecting mutant genes in urine plays an important role in the diagnosis of BC.

A study of Zhu et al. [7] indicated 14 important mutation genes related to BC by searching the Catalogue Of Somatic Mutations In Cancer (COSMIC) database. The mutation genes included P53, fibroblast growth factor receptor 3 (FGFR3), TSC complex subunit 1 (TSC1), stromal antigen 2 (STAG2), HRas proto-oncogene (HRAS), phosphatidylinositol-4,5-bisphosphate 3-kinase catalytic subunit alpha (PIK3CA), Erb-B2 receptor tyrosine kinase 3 (ERBB3), neurofibromatosis type 1 (NF1), ERBB2, FGFR1, cyclin-dependent kinase inhibitor 2A (CDKN2A), AT-rich interaction domain 1A (ARID1A), histone-lysine *N*-methyltransferase 2D (KTM2D), and CREB binding protein (CREBBP). Several studies showed that the development of BC is associated with the mutations of P53 gene [8-11]. Sidransky et al. [12] first described the mutations of P53 gene in the urine of BC patients in 1991. They found that alterations in P53 gene were associated with poor differentiation, advanced urothelial cell carcinoma and poor prognosis [8,9]. Traczyk-Borszynska et al. [13] showed that the mutations of P53 gene were more com-

mon in clinically and histologically advanced carcinoma, and were the negative prognostic factor in BC. FGFR3 mutations also participated in the development of BC. A study showed that mutations of the FGFR3 gene were surrogate markers for the detection of genome stable bladder tumors [14]. Another study indicated that FGFR3 mutations were the feature of well-differentiated BC but not the prognostic marker in BC [13]. In other studies, van Rhijn et al. [15] showed that the combination of FGFR3 with MIB-1 (Ki67) had a more accurate prediction of the progression and survival in BC. Ploussard et al. [16] found that the progression and recurrence of FGFR3 mutations in disease depended on allele loss of 9p22. Also, Rebouissou et al. [17] found that the progression of FGFR3 mutations in non-muscle-invasive disease depended on the homozygous deletion of 9p21. HRAS is a proto-oncogene, which may promote tumorigenesis in several organs including the bladder. HRAS gene mutations in bladder cells were associated with BC, but the mutation rate was low. A study showed that the mutation rate of HRAS gene varies greatly in BC (0%–30%) [18]. Beukers et al. [19] indicated that HRAS gene mutations were more likely to occur in young BC patients (<20 years) compared with older patients. It suggested that mosaicism of oncogenic HRAS mutations may increase the risk of developing BC at a young age.

Several studies showed that TSC1 had inactive point mutations on 9q34 in 10% to 15% of BC patients, resulting in complete loss of function of TSC1 [20-22]. Also, the deletion of a single TSC1 allele may promote the growth of bladder epithelial cells and therefore promote the development of BC [23]. STAG2 mutations were recently identified in BC patients. However, the significance of STAG2 mutations remains controversial. Solomon et al. [24] showed that loss of STAG2 promoted the lymph node metastases in BC and increased the risk of recurrence and mortality. However, different subtypes of BC may exhibit different mutations [25]. In several studies, loss of STAG2 was reported to be associated with BC in low stage and low grade [26-28]. Lelo et al. [29] found that STAG2 mutations were much more common in non-muscle invasive BC (32%) than in muscle invasion BC (12%). These studies suggested that STAG2 could be a potentially useful biomarker for predicting recurrence and progression in non-muscle invasive BC. BRCA1-associated protein 1 (BAP1) is a nuclear ubiquitin carboxy-terminal hydrolase or deubiquitinating enzyme which can regulate several cellular functions, including cell cycle, differentiation, proliferation, and DNA damage response [30]. The recent research indicated that BAP1 mutations were related to BRCA pathway alterations in BC. Lin et al. [31] indicated that patients carrying BAP1 genetic variant al-

leles of rs12163565 had an increased risk of developing BC, although the increased risk was not statistically significant (odds ratio, 1.17; $p=0.070$). There were studies showed that PIK3CA gene alterations, including mutations, copy gains or amplifications, were associated with non-muscle invasive BC [32,33]. Dueñas et al. [33] showed that PIK3CA gene alterations were frequent and associated with low recurrence and low progression in non-muscle invasive BC, which indicated that PIK3CA may be a potential biomarker for predicting recurrence and progression in non-muscle invasive BC. Collectively, many genes mutations have been found in BC patients. Further studies are required to discover more gene mutations and new biomarkers in BC before they can be used in clinical practice.

2. Gene expression-based BC biomarkers

Gene expression-based urinary biomarkers have good sensitivity and specificity in the detection of BC. They are less likely to be affected by inflammatory and other benign conditions. Several important genetic changes in BC have been identified in the past two decades. Based on the technology of rapid nucleic acid extraction and the proven stability of DNA and RNA in urine, gene expression-based biomarkers play an important role in the detection of BC.

A study from Beukers et al. [34] showed that FGFR3, telomerase reverse transcriptase (TERT), and orthodenticle homeobox 1 (OTX1) were significant in the diagnosis of BC. They acted as a urinary biomarker combination with a sensitivity of 57% in low grade primary BC patients and 83% in pT1 or muscle invasive BC. In a study of Holyoake et al. [35], the researchers used microarray data from BC patients and healthy controls to generate a panel of genes that were differentially expressed in various stages and grades of BC patients and normal controls. They tested the markers in voided-urine samples to generate an mRNA panel, including cyclin-dependent kinase-1 (CDK1; also known as CDC2), midkine (MDK), insulin like growth factor binding protein 5 (IGFBP5), and homeobox A3 (HOXA3), which could predict the presence of BC with a sensitivity of 48% to 100% and a specificity of 85%. Park et al. [36] examined aurora kinase A (AURKA) gene amplification in exfoliated cells in urine samples. They concluded that AURKA could be a biomarker for the detection of BC with a specificity of 96.6% and a sensitivity of 87%, and the degree of gene amplification was also associated with high grade BC. Urquidi et al. [37] used Affymetrix arrays of 92 patients (52 BC and 40 controls) and derived a 14 gene panel that could predict the presence of BC, with high sensitivity and specificity (90% and 100%, respectively) and AUC (area under the receiver operat-

ing curve) of 0.98. The 14 genes were: carbonic anhydrase 9 (CA9), transmembrane protein 45A (TMEM45A), C-C motif chemokine ligand 18 (CCL18), matrix remodeling associated 8 (MXRA8), matrix metalloproteinase 9 (MMP9), semaphorin 3D (SEMA3D), ERBB2, vascular endothelial growth factor A (VEGFA), desmocollin 2 (DSC2), Ras-related protein Rab-1A (RAB1A), angiotensinogen (AGT), synaptogyrin 1 (SYNGR1), deleted in malignant brain tumors 1 (DMBT1), angiogenin (ANG). The first seven genes were upregulated and the last seven genes were down-regulated in the urines of BC patients. Bongiovanni et al. [38] found that the expression levels of septin 4 (SEPT4) were up-regulated in the urine of BC patients, with a sensitivity of 93%, a specificity of 65%, and AUC of 0.798. All these studies have shown promise in the diagnosis of BC. However, the majority of them remain in the discovery phase.

MicroRNAs (miRNAs) are a class of small, endogenous, noncoding RNA. They regulate gene expression by affecting mRNA translation and stability or by modulating promoter activity of their target genes. In oncology, miRNAs are considered as promising biomarkers for early diagnosis, prognosis evaluation and therapeutic response prediction of the tumor. A large number of studies showed that miRNAs acted as diagnostic biomarkers in urine samples of BC patients [36,39-42]. Some miRNAs were down-regulated such as miR-125b, miR-140-5p, miR-141, miR-200a, miR-200c, and others were up-regulated such as miR-18a, miR-92a, miR-96. Other studies indicated that miR-126, miR-152, miR-222, and miR-452 were up-regulated in BC [43-45]. However, miR-200 family, miR-155, miR-192, miR-205, and miR-143 were found to be down-regulated in studies [44,46]. Eissa et al. [47] found that the levels of miR-324-5p, miR-4738-3p, and FOSB mRNA were up-regulated in the urine of BC patients, whereas lncRNA miR-497-HG and RCAN1 mRNA were down-regulated in BC patients, compared with patients with benign lesions and healthy controls. The sensitivities and accuracies of the RNAs were significantly higher than those of cytology. In the urinary ceRNA: lncRNA-miRNA-mRNA network, 2 mRNAs (FOS B and RCAN1) displayed the highest accuracy for the diagnosis of BC. A study of Chen [48] showed that miR-101 was decreased in BC patients, and was negatively associated with aggressive clinical characteristics, with a sensitivity of 82.0% and a specificity of 80.9% in BC.

Most of the studies on miRNAs were different in methodology, with little overlap, and no results were fully validated. At present, there are no valid conclusions about urinary miRNAs in the detection of BC patients. Multicenter prospective validation studies in large clinical settings are needed in the future.

3. Proteomics profiling revealed urinary biomarkers for BC

The urinary proteome enriched in proteins reflects the development and invasion of the tumor through direct contact with BC. The study of urinary proteomic biomarkers has been mainly used to help diagnose primary and recurrent BC and to assess the aggressiveness of the disease.

Nuclear matrix protein 22 (NMP22) is one urinary biomarker approved by the U.S. Food and Drug Administration (FDA) using enzyme-linked immunosorbent assay (ELISA) test and BladderChek point-of-care test [49,50]. However, in a meta-analysis of 19 studies for the detection of BC, the sensitivity of NMP22 was 52% to 59% and the specificity was 87-89%, with an AUC of 0.83 [51]. Another biomarker approved by FDA is the bladder tumor antigen (BTA), also known as human complement factor H related protein (hCFHrp). In a meta-analysis of 13 studies using BTA STAT test, the sensitivity of BTA was 64% to 69% and the specificity was 73% to 77% [52]. In a meta-analysis of 5 studies using BTA STAT test, the sensitivity of BTA was 62% to 71% and the specificity was 45% to 81% [53]. Both of the two markers above were not good in sensitivities and specificities.

An ideal protein biomarker should be the one with high sensitivity, specificity, positive predictive value (PPV), negative predictive value (NPV), and AUC values [54]. Several studies showed that Apo-A1, BLCA-4, and hyaluronidase in urine were independently validated in BC with high sensitivities and specificities [55-60]. Apo-A1 is the primary protein component of high-density lipoprotein, which may improve tumor angiogenesis through kinase activation [61,62]. But the association between lipoproteins and BC progression is still not very clear. Studies showed that Apo-A1 was independently validated in BC with the sensitivity of 89% to 95% and the specificity of 85% to 92% [55-57]. BLCA-4 is a nuclear transcription factor found in the early stages of BC. Cai et al. [58] found that BLCA-4 was independently validated with the sensitivity of 93% and the specificity of 97% through an analysis of nine studies. Hyaluronidase could improve cellular proliferation and motility through hyaluronic acid [63]. Studies of Eissa et al. [59] and Pham et al. [60] showed the sensitivity and specificity of hyaluronidase ranged from 87% to 100% and 89% to 98% respectively. Besides the three proteins, there were several additional urine proteins that exhibited with high sensitivities and specificities, but they have not yet been independently validated, including ANG, apolipoprotein E (APOE), CA-9, interleukin-8 (IL-8), MMP, MMP10, plasminogen activator inhibitor 1 (PAI-1), VEGF [63,64]. Goodison et al. [63] found that the eight-biomarker panel above achieved a sensitivity of 92% and a specificity

of 97%, while the BTA TRAK ELISA test achieved a sensitivity of 78% and a specificity of 83% in the same cohort for BC detection. Another study of Urquidi et al. [65] showed that urine CCL18 achieved a sensitivity of 88% and a specificity of 86%, while BTA TRAK ELISA achieved a sensitivity of 80% and a specificity of 84% in the same cohort for BC detection. All of the biomarkers above had better sensitivities and specificities than BTA. These head-to-head studies compared the biomarkers with the FDA-approved test in the same patient cohort, increasing the validity of the studies.

4. Proteomics profiling revealed urinary biomarkers for IC

IC/bladder pain syndrome (BPS) is the most common disease in bladder dysfunction. At present, the etiology of IC/BPS is still not fully understood. There are several possible mechanisms, including infection, inflammation, toxic substances absorption, mucus layer with deficient glycosaminoglycan, hypoxia, and genetics. So far there are no gold standards in the diagnosis of IC/BPS. Some invasive testing including biopsy, urodynamic, and cystoscopy are applied to help diagnose the disease. However, there is still a lack of tools to facilitate accurate diagnosis and objective follow-up. Therefore, it is significant to investigate urinary biomarkers that can be used in clinical practice.

A study by Magalhaes et al. [66] reviewed the urinary biomarkers associated with IC/BPS. They found potential biomarkers investigated in urine specimens included macrophage inhibitory factor (MIF), nerve growth factor (NGF), methylhistamine, histamine, IL-6, antiproliferative factor (APF), epithelial growth factor (EGF), heparin-binding (HB)-EGF, glycoprotein G5P1, and a chemokine profile. Tonyali et al. [67] detected urinary NGF and nerve density in the bladder mucosa. They found that urinary NGF/Cr was significantly increased in IC/BPS patients comparing to control groups, which was similar to nerve density. Corcoran et al. [68] assessed both urine samples and bladder biopsy samples to determine the profile of 23 chemokines in 10 IC/BPS patients and 10 controls. The results indicated that univariate analysis showed no significant differences in any of the urinary proteins assessed, but multivariate analysis showed that VCAM-1 and ICAM-1 in urine were significantly different between IC/BPS and controls. A study of Vera et al. [69] studied urinary MIF concentrations in subgroups of BPS with and without Hunner lesions and control groups. They verified that urinary MIF was significantly higher in BPS patients with Hunner lesion compared with patients without Hunner and with controls, with a sensitivity of 74.4%, a specificity of 71.8%, and AUC 0.718. For the urinary

MIF/Cr ratio, the sensitivity was 47%, the specificity was 91% and AUC was 0.730 in identifying patients with IC/BPS and Hunner lesions. Lamale et al. [70] investigated urinary histamine, IL-6, and methylhistamine in IC/BPS patients and controls. They found that urinary concentrations of histamine and IL-6 were increased in IC/BPS patients. However, methylhistamine levels had no significant differences between IC/BPS patients and controls. Further logistic regression analysis demonstrated that the best predictor for IC/BPS was a combined model with IL-6 and methylhistamine, with an AUC of 0.788. Furthermore, Keay et al. [71] found that APF was increased in IC/BPS patients compared to controls, but HB-EGF concentrations were decreased in IC/BPS patients. Byrne et al. [72] demonstrated that glycoprotein G5P1 concentration in urine was lower in IC/BPS patients than that in controls.

In general, urine proteomic biomarkers of bladder diseases have great promise, but the best biomarkers with the highest clinical utility remain to be discovered. There is still a need for more comprehensive screening of urine proteomic markers through extensive multi-institution validation. Table 1 shows the urinary biomarkers suggested for BC and IC diagnosis [51-53,55-60,63,65,67-72].

5. Metabolomic biomarkers for BC

At present, urinary metabolomic biomarker studies are primarily conducted either by NMR-based or mass spectrometry (MS)-based identification. Three metabolites (2,5-furandicarboxylic acid, ribitol, and ribonic acid) were found to be lower in the urine of BC patients than in healthy controls [73-75]. Taurine is the metabolite known as a free-radical scavenger that can prevent cell damage. Studies showed that taurine was elevated in the urine of BC patients than in healthy controls [75,76]. Several studies showed that urinary citrate, succinate, and hippurate were reduced in BC patients compared with control groups, which suggested that citrate changes were related to an altered tricarboxylic acid (TCA) cycle in BC metabolism [73-77]. On the study of glycolysis-related metabolites, decreased fructose levels and increased lactate levels were showed in BC patients [73,75]. Urinary acetylcarnitine and adipate in BC patients were elevated, which were the results of disturbed fatty acid transportation, altered mitochondrial TCA cycle, and energy metabolism processes or an excess of acetyl-CoA production [74,75,77].

Wittmann et al. [75] identified between 178 and 233 discriminating metabolites (depending on the respective comparison) in a retrospective MS study. They compared current BC patients with three different control groups: patients

with haematuria, controls with BC in the past but without the current disease, and a mixed group of patients with haematuria, those with BC in the past and some healthy subjects. They found that 3-hydroxybutyrate and gluconate were the most highly increased in BC patients, while anserine, 3-hydroxyphenylacetate and pyridoxate showed the lowest values in BC patients. In another high-resolution liquid chromatography (LC)-MS study, glycolysis and acylcarnitines were increased in BC than a combined control group (patients with haematuria and healthy controls) [78]. Besides, amino acid metabolism and fatty acid oxidation were also important factors in BC pathology. A study showed that the acylcarnitines, decanoylcarnitine, decenoylcarnitine, hydroxynonanoylcarnitine and hydroxybutyrylcarnitine were all increased in BC patients [79]. These urinary metabolomic biomarkers may have potential significance in the diagnosis of BC.

6. Metabolomic biomarkers for IC

In the research of IC/BPS, Parker et al. [80] used LC-MS in urine samples of 40 women with IC/BPS and 40 controls to determine metabolomic profiles. They found six metabolites were closely associated with IC/BPS. One of them was etiocholan-3 α -ol-17-one (Etio-S). The elevated Etio-S was a good predictor of IC/BPS, with a sensitivity of 91.2%, a specificity of 87.4%, and AUC of 0.92. Longitudinal analysis of women in this cohort showed that the differences in Etio-S persisted, indicating that these changes could last long.

The results from these early studies on metabolomic biomarkers suggest that urine may act as a potential tool on screening or monitoring bladder diseases in the clinical field, but it is still in the discovery phase. More large multicenter studies with independent validation cohorts are needed to advance the field. Table 2 shows the urinary biomarkers suggested for IC diagnosis [73-80].

7. DNA methylation biomarkers for BC

DNA methylation has been recognized to be important in developmental biology and cancer etiology [81]. Aberrant DNA methylation is a major characteristic of BC and it plays an important role in tumor occurrence and progression [82-84]. Compared to RNA or protein, DNA is inherently stable, so it is more powerful in cancer detection. Chan et al. [85] examined the DNA methylation of seven genes (the retinoid acid receptor- β [RAR β]), death associated protein kinase 1 (DAPK1), Ecadherin, CDKN2A (p16), p15^{INK4b} (p15), glutathione S-transferase Pi 1 (GSTP1), and O-6-methylguanine-DNA methyltransferase (MGMT) in voided urine of BC patients and age and sexmatched controls. Four biomarkers

Table 1. Proteomics-based urinary biomarkers

Bladder diseases	Biomarkers	Study	Sample size	Method	Sensitivity (%)	Specificity (%)	AUC	Notes
BC	NMP22	Wang et al., 2017 [51]	5,291 patients total (meta-analysis of 19 studies)	NMP22 BladderChek, ELISA	52–59	87–89	0.83	FDA-approved
	BTA	Guo et al., 2014 [52]	3,462 patients total (meta-analysis of 13 studies)	BTA stat test	64–69	73–77	0.75	FDA-approved
	BTA	Glas et al., 2003 [53]	829 patients total (meta-analysis of 5 studies)	BTA TRAK test	62–71	45–81	NO	FDA-approved
	Apo-A1	Li et al., 2011 [55]	107 BC and 49 OUC	ELISA	83.7–91.6	85.7–89.7	0.875–0.928	
		Li et al., 2014 [56]	223 BC and 153 controls	ELISA	89	85	0.948	
		Chen et al., 2010 [57]	126 specimens	ELISA	95	92	0.982	
	BLCA-4	Cai et al., 2015 [58]	1,119 subjects total (meta-analysis of 9 studies)	ELISA (8 studies), qPCR (1 study)	93	97	0.9607	
	Hyaluronidase	Eissa et al., 2015 [59]	94 BC, 60 OUC, and 56 HC	Zymography	89	91	0.948	PPV=89%
		Pham et al., 1997 [60]	22 G1 BC, 9 G2 BC, 40 G3 BC, 48 OUC, and 20 HC	ELISA-like assay	100	89	NO	
	ANG, APOE, CA9, IL-8, MMP9, MMP10, PAI-1, VEGF	Goodison et al., 2012 [63]	64 BC and 62 HC	ELISA	92	97	NO	
IC/BPS	CCL18	Urquidi et al., 2012 [65]	64 BC and 63 controls	ELISA	88	86	0.919	PPV=86%, NPV=87%
	NGF	Tonyali et al., 2018 [67]	15 women with BPS, 18 male and female controls	ELISA	NO	NO	NO	NGF/Cr was increased (p<0.001)
	VCAM-1, ICAM-1 and MCP-3	Corcoran et al., 2013 [68]	10 men and women with BPS, 10 male and female controls	Immuno-assay	NO	NO	NO	VCAM-1 and ICAM-1 was increased; MCP-3 was decreased (p<0.05)
	MIF	Vera et al., 2018 [69]	55 women with BPS without Hunner lesions, 43 women with BPS with Hunner lesions, and 100 female controls	ELISA	MIF 74.4, MIF/Cr 47	MIF 71.8, MIF/Cr 91	MIF 0.718, MIF/Cr 0.730	MIF, MIF/Cr was increased in BPS with Hunner lesion
	Histamine, IL-6, and methyl-histamine	Lamale et al., 2006 [70]	40 women with BPS, and 29 female controls	RIA, ELISA	70.00	72.40	0.788	Histamine and IL-6 was increased (p<0.05). Best predictor: combined model with IL-6 and methylhistamine
	APF and HB-EGF	Keay et al., 2004 [71]	24 men with BPS, 36 male controls	3H-thymidine incorporation in cell cultures, ELISA	94	95	NO	APF was increased, HB-EGF was decreased (p<0.00001)
	G5P1	Byrne et al., 1999 [72]	36 patients with BPS and 23 controls	ELISA	NO	NO	NO	G5P1/Cr was decreased (p<0.0001)

AUC, area under the receiver operating curve; BC, bladder cancer; NMP22, nuclear matrix protein 22; ELISA, enzyme-linked immunosorbent assay; FDA, U.S. Food and Drug Administration; BTA, bladder tumor antigen; NO, not reported; OUC, controls with other urinary conditions; qPCR, quantitative polymerase chain reaction; HC, healthy controls; PPV, positive predictive value; ANG, angiogenin; APOE, apolipoprotein E; CA9, carbonic anhydrase 9; IL, interleukin; MMP, matrix metalloproteinase; PAI-1, plasminogen activator inhibitor 1; VEGF, vascular endothelial growth factor; CCL18, C-C motif chemokine ligand 18; NPV, negative predictive value; IC/BPS, interstitial cystitis/bladder pain syndrome; NGF, nerve growth factor; MIF, macrophage inhibitory factor; APF, antiproliferative factor; HB-EGF, heparin-binding epithelial growth factor.

Table 2. Metabolomics urinary biomarkers

Bladder diseases	Biomarkers	Study	Sample size	Method	Sensitivity (%)	Specificity (%)	AUC	Notes
BC	2,5-furandicarboxylic acid, ribitol, and ribonic acid	Pasikanti et al., 2013 [73]	38 BC and 61 controls	GC×GC-TOFMS	71	100	NO	Decreased
	Taurine	Pasikanti et al., 2010 [74] Wittmann et al., 2014 [75]	24 BC and 51 controls 95 BC and 345 controls	GC-TOFMS UHPLC-MS/MS and GC-MS	100 NO	NO NO	0.9 NO	Decreased Increased
		Srivastava et al., 2010 [76]	33 BC and 37 healthy	1H NMR spectroscopy	NO	NO	NO	Increased
	Citrate	Pasikanti et al., 2013 [73] Pasikanti et al., 2010 [74]	38 BC and 61 controls 24 BC and 51 controls	GC×GC-TOFMS GC-TOFMS	71 100	100 NO	NO 0.9	Decreased Decreased
	Succinate and hippurate	Pasikanti et al., 2010 [74] Huang et al., 2011 [77]	24 BC and 51 controls 27 BC and 32 controls	GC-TOFMS LC-MS	100 92.60	NO 68.80	0.9 0.867 (hippurate)	Decreased Decreased
	Fructose and lactate	Pasikanti et al., 2013 [73]	38 BC and 61 controls	GC×GC-TOFMS	71	100	NO	Fructose decreased and lactate increased
	Acetylcarnitine and adipate	Pasikanti et al., 2010 [74] Huang et al., 2011 [77]	24 BC and 51 controls 27 BC and 32 controls	GC-TOFMS LC-MS	100 NO	NO NO	0.9 0.598 (acetylcarnitine)	Increased Increased
	Component I and Carnitine C9:1	Huang et al., 2011 [77]	27 BC and 32 controls	LC-MS	90.50	96.90	0.9 and 0.88, respectively	Increased
	3-hydroxybutyrate and gluconate	Wittmann et al., 2014 [75]	95 BC and 345 controls	UHPLC-MS/MS and GC-MS	NO	NO	NO	Increased
	Anserine, 3-hydroxyphenylacetate and pyridoxate	Wittmann et al., 2014 [75]	95 BC and 345 controls	UHPLC-MS/MS and GC-MS	NO	NO	NO	Decreased
	Glycolysis and acylcarnitines	Jin et al., 2014 [78]	138 BC, 52 haematuria, and 69 healthy	high-resolution LC-MS	85–91.3	85–92.5	0.937	Increased
	Acylcarnitines, decanoylcarnitine, decenoylcarnitine, hydroxynonanoylcarnitine and hydroxybutyrylcarnitine	Liu et al., 2018 [79]	53 BC, 6 benign lesions, and 203 healthy controls	high-resolution LC-MS	NO	NO	0.8	Increased
IC/BPS	Etio-S	Parker et al., 2016 [80]	40 women with BPS and 40 controls	liquid chromatography-MS	91.20	87.40	0.92	Increased

AUC, area under the receiver operating curve; BC, bladder cancer; GC×GC-TOFMS, two-dimensional gas chromatography time-of-flight mass spectrometry; NO, not reported; UHPLC-MS/MS, ultra-high-performance liquid chromatography/tandem mass spectrometry; GC-MS, gas chromatography-mass spectrometry; LC-MS, liquid chromatography-mass spectrometry; Etio-S, etiocholan-3 α -ol-17-one.

Table 3. Epigenetic urinary biomarkers

Bladder diseases	Biomarkers	Study	Sample size	Method	Sensitivity (%)	Specificity (%)	AUC	Notes
BC	A combination of FGFR3, TERT, and OTX1	Beukers et al., 2017 [34]	977 BC	RT-PCR	57–83	59	NO	
	A combination of CDC2, MDK, IGFBP5, and HOXA3	Holyoake et al., 2008 [35]	75 BC and 77 controls	RT-PCR	48–100	85	NO	
	AURKA	Park et al., 2008 [36]	23 BC and 7 controls	FISH	87	96.60	0.939	
	A 14 gene panel: CA9, TMEM45A, CCL18, MXRA8, MMP9, SEMA3D, ERBB2, VEGFA, DSC2, RAB1A, AGT, SYNGR1, DMBT1, ANG	Urquidí et al., 2012 [37]	52 BC and 40 controls	Affymetrix arrays	90	100	0.98	The first 7 genes were upregulated and the last 7 genes were down-regulated
	SEPT4	Bongiovanni et al., 2012 [38]	41 BC and 17 controls	RT-PCR	93	65	0.798	Upregulated
	miR126 and miR152	Hanke et al., 2010 [43]	18 BC and 18 controls	RT-qPCR	72 (the RNA ratio of miR-126:miR-152)	82 (the RNA ratio of miR-126:miR-152)	0.768 (the RNA ratio of miR-126:miR-152)	Upregulated
	miR222 and miR452	Puerta-Gil et al., 2012 [44]	37 BC and 57 controls	RT-qPCR			0.718 and 0.848	Upregulated
	miR96 and miR183	Yamada et al., 2011 [45]	100 BC and 498 controls	RT-qPCR	71 and 74	89.2 and 77.3	0.831 and 0.817	Upregulated
	miR-200 family, miR-155, miR-192, miR-205	Wang et al., 2012 [46]	51 BC and 24 controls	RT-qPCR	NO	NO	NO	Downregulated
	miR-324-5p, miR4738-3p, and FOSB mRNA	Eissa et al., 2019 [47]	98 BC, 48 benign diseases, and 50 controls	RT-qPCR	87.7, 84.7, and 99	86.7, 80.6, and 98.9	NO	Upregulated
	lncRNA miR497-HG and RCAN1 mRNA	Eissa et al., 2019 [47]	98 BC, 48 benign diseases, and 50 controls	RT-qPCR	90.5 and 99	83 and 98.9	NO	Downregulated
	DNA methylation biomarkers							
	DAPK, RARβ, E-cadherin, and p16	Chan et al., 2002 [85]	22 BC and 17 controls	MSP	91	76	NO	
	DAPK, TERT, and BCL2	Friedrich et al., 2004 [86]	37 BC and 20 controls	MSP	78	100	NO	
	CDKN2A, p14ARF, MGMT, and GSTP1	Hoque et al., 2006 [87]	160 BC and 94 controls	qMSP	69	100	NO	
	TWIST1 and NID2	Renard et al., 2010 [88]	496 urine samples	qMSP	90 and 48, respectively	93 and 96, respectively	NO	
	A 4-marker panel (ZNF154, HOXA9, POU4F2, and EOMES)	Abern et al., 2014 [89] Fantony et al., 2015 [90] Reinert et al., 2011 [91]	111 patients 209 patients 119 BC and 59 controls	qMSP qMSP MSP	79 (a combination) 67 (a combination) 84	63 (a combination) 69 (a combination) 96	NO NO NO	

Table 3. Continued

Bladder diseases	Biomarkers	Study	Sample size	Method	Sensitivity (%)	Specificity (%)	AUC	Notes
	A 6-marker panel (EOMES, HOXA9, POU4F2, TWIST1, VIM, and ZNF154)	Reinert et al., 2012 [92]	184 BC and 35 controls	MS-HRM	82–89	94–100	NO	
	A 3-marker panel (SOX1, IRAK3, and L1-MET)	Su et al., 2014 [93]	90 non-muscle invasive BC	MSP	86 in BC with recurrence and 80 in BC with no recurrence	89 in BC with recurrence and 97 in BC with no recurrence	NO	
	A combination of CFTR, SALL3, and TWIST1	van der Heijden et al., 2018 [96]	111 BC and 57 controls	MSP	85	68	0.874	
IC/BPS	CpG-sites, MCP-3, G5P1, and HB-EGF	Magalhaes et al., 2019 [66]	478 records total	A systematic review	NO	NO	NO	Hypomethylation
	CpG sites	Bradley et al., 2018 [97]	19 IC BPS and 17 controls	Illumina Infinium MethylationEPIC BeadChip	NO	NO	NO	86% of MARK pathway sites with hypomethylation

AUC, area under the receiver operating curve; BC, bladder cancer; EGFR3, fibroblast growth factor receptor 3; TERT, telomerase reverse transcriptase; OTX1, orthodenticle homeobox 1; RT-PCR, reverse transcriptase-polymerase chain reaction; NO, not reported; MDK, midkine; IGFBP5, insulin like growth factor binding protein 5; HOXA3, homeobox A3; AURKA, aurora kinase A; FISH, fluorescence *in situ* hybridization; CA9, carbonic anhydrase 9; TMEM45A, transmembrane protein 45A; CCL18, C-C motif chemokine ligand 18; MXRA8, matrix remodeling associated 8; MMP9, matrix metalloproteinase 9; SEMA3D, semaphorin 3D; ERBB2, Erb-B2 receptor tyrosine kinase 2; VEGFA, vascular endothelial growth factor A; DSC2, desmocollin 2; RAB1A, Ras-related protein Rab-1A; AGT, angiotensinogen; SYNGR1, synaptogyrin 1; DMBT1, deleted in malignant brain tumors 1; ANG, angiogenin; SEPT4, septin 4; RT-qPCR, quantitative reverse transcriptase-polymerase chain reaction; DAPK, death associated protein kinase; RARβ, retinoid acid receptor-β; MSP, methylation-specific polymerase chain reaction; CDKN2A, cyclin dependent kinase inhibitor 2A; MGMT, O-6-methylguanine-DNA methyltransferase; GSTP1, glutathione S-transferase Pi 1; qMSP, specific high-resolution melting; TWIST1, Twist family BHLH transcription factor 1; NID2, nidogen 2; ZNF154, zinc finger protein 154; HOXA9, homeobox protein Hox-A9; POU4F2, POU class 4 homeobox 2; EOMES, eomesodermin; VIM, vimentin; MS-HRM, methylation-specific high-resolution melting; SOX1, SRY-box transcription factor 1; IRAK3, interleukin 1 receptor associated kinase 3; CFTR, cystic fibrosis transmembrane conductance regulator; SALL3, spalt like transcription factor 3; HB-EGF, heparin-binding epithelial growth factor.

DAPK1, RAR β , E-cadherin, and p16) achieved a sensitivity of 91% and a specificity of 76% for detecting BC. And cytology achieved a sensitivity of 46% and a specificity of 100% by comparison. Friedrich et al. [86] examined DNA methylation of apoptosis-associated genes (DAPK, TERT, and apoptosis regulator [BCL2]) in the urine of BC patients. They found that combined methylation analyses achieved both high sensitivity and specificity (78% and 100%, respectively) for detecting BC. In another study, Hoque et al. [87] examined the DNA methylation of nine genes (adenomatous polyposis coli (APC), ARF tumor suppressor (p14ARF), cadherin-1 (CDH1), GSTP1, MGMT, cyclin dependent kinase inhibitor 2A (CDKN2A), retinoic acid receptor beta (RAR β 2), ras association domain family member 1 (RASSF1A), and TIMP metalloproteinase inhibitor 3 (TIMP3). They found that combined methylation analysis based on four genes (CDKN2A, p14ARF, MGMT, and GSTP1) achieved a sensitivity of 69% and a specificity of 100%. Recently there were some studies on Twist family BHLH transcription factor 1 (TWIST1) and nidogen 2 (NID2) genes. Renard et al. [88] reported that TWIST1 and NID2 genes were frequently methylated in BC patients in a total of 496 urine samples collected from three urology clinical sites. The sensitivity of this 2 gene panel was significantly better than that of cytology (90% and 48%, respectively), with the specificity of 93% and 96%, respectively. The PPV and NPV of the 2 gene panel was 86% and 95%, respectively. However, the sensitivities of these two genes were poor in the studies of Abern et al. [89] and Fantony et al. [90]. In other studies, Reinert et al. [91] found a 4marker panel (zinc finger protein 154 [ZNF154], homeobox protein Hox-A9 (HOXA9), POU class 4 homeobox 2 (POU4F2), and eomesodermin (EOMES) achieved a sensitivity of 84% and a specificity of 96% for detecting BC in urine samples from 119 BC patients and 59 controls. Another study of Reinert et al. [92] found a 6-marker panel (EOMES, HOXA9, POU4F2, TWIST1, vimentin (VIM), and ZNF154) had a sensitivity of 82% to 89% and a specificity of 94% to 100% for detecting BC in urine samples from 184 BC patients and 35 controls.

In a study of 368 urine samples collected from 90 non-muscle invasive BC patients, Su et al. [93] reported that a panel of 3 markers (SRY-box transcription factor 1 [SOX1], interleukin 1 receptor associated kinase 3 [IRAK3], and L1-MET) discriminated between patients with recurrence and with no recurrence, with a sensitivity of 86% and a specificity of 89% of patients with recurrence, compared with the sensitivity of 80% and specificity of 97% of patients with no recurrence in validation sets. The results demonstrated that the combination of SOX1, IRAK3, and L1MET could detect disease recurrence with high sensitivity and specificity. Another study selected seven DNA methylation biomarkers (CDH13, cystic fibrosis transmembrane conductance regulator [CFTR], NID2, spalt like transcription factor 3 (SALL3), transmembrane protein with EGF like and two follistatin like domains 2 [TMEFF2], TWIST1, and VIM2) from four recently published BC studies [81,94,95]. They found that the best possible combination to discriminate against BC from controls was the combination CFTR, SALL3, and TWIST1 [96]. The three-gene methylation classifier achieved an AUC of 0.874, with a sensitivity of 85% and a specificity of 68%. The discovery of highly sensitive methylation biomarkers may allow us to lower the number of follow-up cystoscopies in patients with BC, which can improve the life quality of the patients.

8. DNA methylation biomarkers for IC

In the research of IC/BPS, Magalhaes et al. [66] concluded that DNA methylation in urine samples was associated with IC/BPS. Bradley et al. [97] determined DNA methylation profiles in IC/BPS and controls. After Bonferroni correction, there was no genome-scale significantly different methylation in CpG sites. Among the methylated CpG sites, the most prominent enrichment pathway was the mitogen-activated protein kinase (MAPK) pathway. This pathway had 86% of sites with hypomethylation in IC/BPS patients compared to the controls.

There is evidence that DNA methylation biomarkers

Table 4. Commercially available biomarker kits

Biomarker kits	Study	Sensitivity (%)	Specificity (%)	Notes
Cytology	Liou, 2006 [99]	16–89	81–100	FDA-approved
Hematuria dipstick	Liou, 2006 [99]	40–93	51–97	FDA-approved
NMP22	Wang et al., 2017 [51]	52–59	87–89	FDA-approved
BTA stat test	Guo et al., 2014 [52]	64–69	73–77	FDA-approved
BTA TRAK test	Glas et al., 2003 [53]	62–71	45–81	FDA-approved
Immuno Cyt	Liou, 2006 [99]	39–100	73–84	Approved only for BC surveillance
FGFR3	Beukers et al., 2017 [34]	57–83	59–82.7	FDA-approved

FDA, U.S. Food and Drug Administration; NMP22, nuclear matrix protein 22; BTA, bladder tumor antigen; FGFR3, fibroblast growth factor receptor 3.

are more sensitive than cytology although there were biomarkers tested on cohorts that varied between studies. And some markers showed specificity comparable with that of cytology. A highly selective panel of methylation biomarkers may increase the sensitivity and specificity of urine analysis in the clinical studies [98]. Standardized assays and cutoff values should be used in a large and well-designed cohort in future studies. Table 3 summarizes urine epigenetics-based biomarkers for BC and IC [34,38,43-47,66,85-93,96,97].

CONCLUSIONS

Many studies have shown that urinary-based biomarkers have high sensitivity and specificity in the diagnosis of bladder diseases (such as BC and IC), which confirms the feasibility of using urinary exfoliated epithelium as an analyzer to diagnose bladder diseases. As shown in Table 4 [34,51-53,99], commercially available biomarker kits for diagnosis of bladder disease such as BC have been introduced in market. If this method is accurate and reliable enough, it can be used not only for the diagnosis of bladder diseases but also for the screening of diseases in the population. However, further researches are needed to apply urinary biomarkers to clinical practice. More efforts should be made to improve and validate the biomarker panel and promote the progress of urine-based biomarker analysis, which will be applied to clinical work as soon as possible.

CONFLICTS OF INTEREST

The authors have nothing to disclose.

ACKNOWLEDGMENTS

The authors acknowledge support from National Institutes of Health grants (1U01DK103260), Department of Defense grants (W81XWH-15-1-0415), Centers for Disease Controls and Prevention (1U01DP006079). The research was supported by the International Science and Business Belt Program through the Ministry of Science, ICT and Future Planning (2017K000490) Basic Science Research Program through the National Research Foundation of Korea (NRF) funded by the Ministry of Education (2017R1D1A3B03031486), and the National Research Foundation of Korea (NRF) grant funded by the Korea government (MSIT) (2018R1A2B2005473).

AUTHORS' CONTRIBUTIONS

Research conception and design: Wun-Jae Kim. Data acquisition: Jayoung Kim. Data analysis and interpretation: Jayoung Kim. Drafting of the manuscript: Jayoung Kim. Critical revision of the manuscript: Won Tae Kim. Administrative, technical, or material support: Won Tae Kim. Supervision: Wun-Jae Kim. Approval of the final manuscript: all authors.

REFERENCES

1. Siegel RL, Miller KD, Jemal A. Cancer statistics, 2018. *CA Cancer J Clin* 2018;68:7-30.
2. Abrams P, Cardozo L, Fall M, Griffiths D, Rosier P, Ulmsten U, et al. The standardisation of terminology of lower urinary tract function: report from the Standardisation Sub-committee of the International Continence Society. *Am J Obstet Gynecol* 2002;187:116-26.
3. Choe JH, Son H, Song YS, Kim JC, Lee JZ, Lee KS. Prevalence of painful bladder syndrome/interstitial cystitis-like symptoms in women: a population-based study in Korea. *World J Urol* 2011;29:103-8.
4. Temml C, Wehrberger C, Riedl C, Ponholzer A, Marszalek M, Madersbacher S. Prevalence and correlates for interstitial cystitis symptoms in women participating in a health screening project. *Eur Urol* 2007;51:803-8; discussion 809.
5. Patnaik SS, Laganà AS, Vitale SG, Buttice S, Noventa M, Gizzo S, et al. Etiology, pathophysiology and biomarkers of interstitial cystitis/painful bladder syndrome. *Arch Gynecol Obstet* 2017;295:1341-59.
6. Berry SH, Elliott MN, Suttorp M, Bogart LM, Stoto MA, Eggers P, et al. Prevalence of symptoms of bladder pain syndrome/interstitial cystitis among adult females in the United States. *J Urol* 2011;186:540-4.
7. Zhu F, Zhang Y, Shi L, Wu CL, Chen SQ, Zheng H, et al. Gene mutation detection of urinary sediment cells for NMIBC early diagnose and prediction of NMIBC relapse after surgery. *Medicine (Baltimore)* 2019;98:e16451.
8. van Rhijn BW, van der Kwast TH, Vis AN, Kirkels WJ, Boevé ER, Jöbsis AC, et al. FGFR3 and P53 characterize alternative genetic pathways in the pathogenesis of urothelial cell carcinoma. *Cancer Res* 2004;64:1911-4.
9. Ecke TH, Sachs MD, Lenk SV, Loening SA, Schlechte HH. TP53 gene mutations as an independent marker for urinary bladder cancer progression. *Int J Mol Med* 2008;21:655-61.
10. Goebell PJ, Groshen SG, Schmitz-Dräger BJ; International Study-Initiative on Bladder Cancer (ISBC). p53 immunohistochemistry in bladder cancer--a new approach to an old ques-

- tion. *Urol Oncol* 2010;28:377-88.
11. Malats N, Bustos A, Nascimento CM, Fernandez F, Rivas M, Puente D, et al. P53 as a prognostic marker for bladder cancer: a meta-analysis and review. *Lancet Oncol* 2005;6:678-86.
 12. Sidransky D, Von Eschenbach A, Tsai YC, Jones P, Summerhayes I, Marshall F, et al. Identification of p53 gene mutations in bladder cancers and urine samples. *Science* 1991;252:706-9.
 13. Traczyk-Borszynska M, Borkowska E, Jablonowski Z, Jedrzejczyk A, Pietrusinski M, Kaluzewski B, et al. Genetic diversity of urinary bladder cancer and the risk of recurrence based on mutation analysis. *Neoplasma* 2016;63:952-60.
 14. Junker K, van Oers JM, Zwarthoff EC, Kania I, Schubert J, Hartmann A. Fibroblast growth factor receptor 3 mutations in bladder tumors correlate with low frequency of chromosome alterations. *Neoplasia* 2008;10:1-7.
 15. van Rhijn BW, Zuiverloon TC, Vis AN, Radvanyi F, van Leenders GJ, Ooms BC, et al. Molecular grade (FGFR3/MIB-1) and EORTC risk scores are predictive in primary non-muscle-invasive bladder cancer. *Eur Urol* 2010;58:433-41.
 16. Ploussard G, Soliman H, Dubosq F, Méria P, Vérine J, Desgrand-Champs F, et al. The prognostic value of FGFR3 mutational status for disease recurrence and progression depends on allelic losses at 9p22. *Am J Cancer Res* 2011;1:498-507.
 17. Rebouissou S, Hérault A, Letouzé E, Neuzillet Y, Laplanche A, Ofualuka K, et al. CDKN2A homozygous deletion is associated with muscle invasion in FGFR3-mutated urothelial bladder carcinoma. *J Pathol* 2012;227:315-24.
 18. Fernández-Medarde A, Santos E. Ras in cancer and developmental diseases. *Genes Cancer* 2011;2:344-58.
 19. Beukers W, Hercegovic A, Zwarthoff EC. HRAS mutations in bladder cancer at an early age and the possible association with the Costello Syndrome. *Eur J Hum Genet* 2014;22:837-9.
 20. Knowles MA, Habuchi T, Kennedy W, Cuthbert-Heavens D. Mutation spectrum of the 9q34 tuberous sclerosis gene TSC1 in transitional cell carcinoma of the bladder. *Cancer Res* 2003;63:7652-6.
 21. Knowles MA, Platt FM, Ross RL, Hurst CD. Phosphatidylinositol 3-kinase (PI3K) pathway activation in bladder cancer. *Cancer Metastasis Rev* 2009;28:305-16.
 22. Pymar LS, Platt FM, Askham JM, Morrison EE, Knowles MA. Bladder tumour-derived somatic TSC1 missense mutations cause loss of function via distinct mechanisms. *Hum Mol Genet* 2008;17:2006-17.
 23. Goebell PJ, Knowles MA. Bladder cancer or bladder cancers? genetically distinct malignant conditions of the urothelium. *Urol Oncol* 2010;28:409-28.
 24. Solomon DA, Kim JS, Bondaruk J, Shariat SF, Wang ZF, Elkahloun AG, et al. Frequent truncating mutations of STAG2 in bladder cancer. *Nat Genet* 2013;45:1428-30.
 25. Aquila L, Ohm J, Woloszynska-Read A. The role of STAG2 in bladder cancer. *Pharmacol Res* 2018;131:143-9.
 26. Guo G, Sun X, Chen C, Wu S, Huang P, Li Z, et al. Whole-genome and whole-exome sequencing of bladder cancer identifies frequent alterations in genes involved in sister chromatid cohesion and segregation. *Nat Genet* 2013;45:1459-63.
 27. Balbás-Martínez C, Sagrera A, Carrillo-de-Santa-Pau E, Earl J, Márquez M, Vazquez M, et al. Recurrent inactivation of STAG2 in bladder cancer is not associated with aneuploidy. *Nat Genet* 2013;45:1464-9.
 28. Taylor CF, Platt FM, Hurst CD, Thygesen HH, Knowles MA. Frequent inactivating mutations of STAG2 in bladder cancer are associated with low tumour grade and stage and inversely related to chromosomal copy number changes. *Hum Mol Genet* 2014;23:1964-74.
 29. Lelo A, Prip F, Harris BT, Solomon D, Berry DL, Chaldeckas K, et al. STAG2 is a biomarker for prediction of recurrence and progression in papillary non-muscle-invasive bladder cancer. *Clin Cancer Res* 2018;24:4145-53.
 30. Carbone M, Yang H, Pass HI, Krausz T, Testa JR, Gaudino G. BAP1 and cancer. *Nat Rev Cancer* 2013;13:153-9.
 31. Lin M, Zhang L, Hildebrandt MAT, Huang M, Wu X, Ye Y. Common, germline genetic variations in the novel tumor suppressor BAP1 and risk of developing different types of cancer. *Oncotarget* 2017;8:74936-46.
 32. Segovia C, Martínez-Fernández M, Dueñas M, Rubio C, López-Calderón FF, Costa C, et al. Opposing roles of PIK3CA gene alterations to EZH2 signaling in non-muscle invasive bladder cancer. *Oncotarget* 2017;8:10531-42.
 33. Dueñas M, Martínez-Fernández M, García-Escudero R, Villacampa F, Marqués M, Saiz-Ladera C, et al. PIK3CA gene alterations in bladder cancer are frequent and associate with reduced recurrence in non-muscle invasive tumors. *Mol Carcinog* 2015;54:566-76.
 34. Beukers W, van der Keur KA, Kandimalla R, Vergouwe Y, Steyerberg EW, Boormans JL, et al. FGFR3, TERT and OTX1 as a urinary biomarker combination for surveillance of patients with bladder cancer in a large prospective multicenter study. *J Urol* 2017;197:1410-8.
 35. Holyoake A, O'Sullivan P, Pollock R, Best T, Watanabe J, Kajita Y, et al. Development of a multiplex RNA urine test for the detection and stratification of transitional cell carcinoma of the bladder. *Clin Cancer Res* 2008;14:742-9.
 36. Park HS, Park WS, Bondaruk J, Tanaka N, Katayama H, Lee S, et al. Quantitation of Aurora kinase A gene copy number in urine sediments and bladder cancer detection. *J Natl Cancer Inst* 2008;100:1401-11.
 37. Urquidi V, Goodison S, Cai Y, Sun Y, Rosser CJ. A candidate molecular biomarker panel for the detection of bladder cancer.

- Cancer Epidemiol Biomarkers Prev 2012;21:2149-58.
38. Bongiovanni L, Pirozzi F, Guidi F, Orsini M, Chiurazzi P, Bassi PF, et al. Bradeion (SEPT4) as a urinary marker of transitional cell bladder cancer: a real-time polymerase chain reaction study of gene expression. *J Urol* 2012;187:2223-7.
 39. Friedrich MG, Toma MI, Hellstern A, Pantel K, Weisenberger DJ, Noldus J, et al. Comparison of multitarget fluorescence in situ hybridization in urine with other noninvasive tests for detecting bladder cancer. *BJU Int* 2003;92:911-4.
 40. Sarosdy ME, Schellhammer P, Bokinsky G, Kahn P, Chao R, Yore L, et al. Clinical evaluation of a multi-target fluorescent in situ hybridization assay for detection of bladder cancer. *J Urol* 2002;168:1950-4.
 41. Bollmann M, Heller H, Bánkfalvi A, Griefingholt H, Bollmann R. Quantitative molecular urinary cytology by fluorescence in situ hybridization: a tool for tailoring surveillance of patients with superficial bladder cancer? *BJU Int* 2005;95:1219-25.
 42. Kipp BR, Karnes RJ, Brankley SM, Harwood AR, Pankratz VS, Sebo TJ, et al. Monitoring intravesical therapy for superficial bladder cancer using fluorescence in situ hybridization. *J Urol* 2005;173:401-4.
 43. Hanke M, Hoefig K, Merz H, Feller AC, Kausch I, Jocham D, et al. A robust methodology to study urine microRNA as tumor marker: microRNA-126 and microRNA-182 are related to urinary bladder cancer. *Urol Oncol* 2010;28:655-61.
 44. Puerta-Gil P, García-Baquero R, Jia AY, Ocaña S, Alvarez-Múgica M, Alvarez-Ossorio JL, et al. miR-143, miR-222, and miR-452 are useful as tumor stratification and noninvasive diagnostic biomarkers for bladder cancer. *Am J Pathol* 2012;180:1808-15.
 45. Yamada Y, Enokida H, Kojima S, Kawakami K, Chiyomaru T, Tatarano S, et al. MiR-96 and miR-183 detection in urine serve as potential tumor markers of urothelial carcinoma: correlation with stage and grade, and comparison with urinary cytology. *Cancer Sci* 2011;102:522-9.
 46. Wang G, Chan ES, Kwan BC, Li PK, Yip SK, Szeto CC, et al. Expression of microRNAs in the urine of patients with bladder cancer. *Clin Genitourin Cancer* 2012;10:106-13.
 47. Eissa S, Safwat M, Matboli M, Zaghoul A, El-Sawalhi M, Shaheen A. Measurement of urinary level of a specific competing endogenous RNA network (FOS and RCAN mRNA/ miR-324-5p, miR-4738-3p, /lncRNA miR-497-HG) enables diagnosis of bladder cancer. *Urol Oncol* 2019;37:292.e19-292.e27.
 48. Chen X. MiR-101 acts as a novel bio-marker in the diagnosis of bladder carcinoma. *Medicine (Baltimore)* 2019;98:e16051.
 49. Soloway MS, Briggman V, Carpinito GA, Chodak GW, Church PA, Lamm DL, et al. Use of a new tumor marker, urinary NMP22, in the detection of occult or rapidly recurring transitional cell carcinoma of the urinary tract following surgical treatment. *J Urol* 1996;156(2 Pt 1):363-7.
 50. Miyake M, Goodison S, Giacoia EG, Rizwani W, Ross S, Rosser CJ. Influencing factors on the NMP-22 urine assay: an experimental model. *BMC Urol* 2012;12:23.
 51. Wang Z, Que H, Suo C, Han Z, Tao J, Huang Z, et al. Evaluation of the NMP22 BladderChek test for detecting bladder cancer: a systematic review and meta-analysis. *Oncotarget* 2017;8:100648-56.
 52. Guo A, Wang X, Gao L, Shi J, Sun C, Wan Z. Bladder tumour antigen (BTA stat) test compared to the urine cytology in the diagnosis of bladder cancer: a meta-analysis. *Can Urol Assoc J* 2014;8:E347-52.
 53. Glas AS, Roos D, Deutekom M, Zwinderman AH, Bossuyt PM, Kurth KH. Tumor markers in the diagnosis of primary bladder cancer. a systematic review. *J Urol* 2003;169:1975-82.
 54. Chakraborty A, Dasari S, Long W, Mohan C. Urine protein biomarkers for the detection, surveillance, and treatment response prediction of bladder cancer. *Am J Cancer Res* 2019;9:1104-17.
 55. Li H, Li C, Wu H, Zhang T, Wang J, Wang S, et al. Identification of Apo-A1 as a biomarker for early diagnosis of bladder transitional cell carcinoma. *Proteome Sci* 2011;9:21.
 56. Li C, Li H, Zhang T, Li J, Liu L, Chang J. Discovery of Apo-A1 as a potential bladder cancer biomarker by urine proteomics and analysis. *Biochem Biophys Res Commun* 2014;446:1047-52.
 57. Chen YT, Chen CL, Chen HW, Chung T, Wu CC, Chen CD, et al. Discovery of novel bladder cancer biomarkers by comparative urine proteomics using iTRAQ technology. *J Proteome Res* 2010;9:5803-15.
 58. Cai Q, Wu Y, Guo Z, Gong R, Tang Y, Yang K, et al. Urine BLCA-4 exerts potential role in detecting patients with bladder cancers: a pooled analysis of individual studies. *Oncotarget* 2015;6:37500-10.
 59. Eissa S, Matboli M, Essawy NO, Kotb YM. Integrative functional genetic-epigenetic approach for selecting genes as urine biomarkers for bladder cancer diagnosis. *Tumour Biol* 2015;36:9545-52.
 60. Pham HT, Block NL, Lokeshwar VB. Tumor-derived hyaluronidase: a diagnostic urine marker for high-grade bladder cancer. *Cancer Res* 1997;57:778-83.
 61. Gourin CG, Zhi W, Adam BL. Proteomic identification of serum biomarkers for head and neck cancer surveillance. *Laryngoscope* 2009;119:1291-302.
 62. Yang HH, Chen XF, Hu W, Lv DQ, Ding WJ, Tang LJ, et al. Lipoprotein(a) level and its association with tumor stage in male patients with primary lung cancer. *Clin Chem Lab Med* 2009;47:452-7.
 63. Goodison S, Chang M, Dai Y, Urquidi V, Rosser CJ. A multi-

- analyte assay for the non-invasive detection of bladder cancer. *PLoS One* 2012;7:e47469.
64. Frantzi M, Vlahou A. Ten years of proteomics in bladder cancer: progress and future directions. *Bladder Cancer* 2017;3:1-18.
 65. Urquidi V, Kim J, Chang M, Dai Y, Rosser CJ, Goodison S. CCL18 in a multiplex urine-based assay for the detection of bladder cancer. *PLoS One* 2012;7:e37797.
 66. Magalhaes TF, Baracat EC, Doumouchtsis SK, Haddad JM. Biomarkers in the diagnosis and symptom assessment of patients with bladder pain syndrome: a systematic review. *Int Urogynecol J* 2019 Aug 13 [Epub]. <https://doi.org/10.1007/s00192-019-04075-9>.
 67. Tonyali S, Ates D, Akbiyik F, Kankaya D, Baydar D, Ergen A. Urine nerve growth factor (NGF) level, bladder nerve staining and symptom/problem scores in patients with interstitial cystitis. *Adv Clin Exp Med* 2018;27:159-63.
 68. Corcoran AT, Yoshimura N, Tyagi V, Jacobs B, Leng W, Tyagi P. Mapping the cytokine profile of painful bladder syndrome/interstitial cystitis in human bladder and urine specimens. *World J Urol* 2013;31:241-6.
 69. Vera PL, Preston DM, Moldwin RM, Erickson DR, Mowlazadeh B, Ma F, et al. Elevated urine levels of macrophage migration inhibitory factor in inflammatory bladder conditions: a potential biomarker for a subgroup of interstitial cystitis/bladder pain syndrome patients. *Urology* 2018;116:55-62.
 70. Lamale LM, Lutgendorf SK, Zimmerman MB, Kreder KJ. Interleukin-6, histamine, and methylhistamine as diagnostic markers for interstitial cystitis. *Urology* 2006;68:702-6.
 71. Keay S, Zhang CO, Chai T, Warren J, Koch K, Grkovic D, et al. Antiproliferative factor, heparin-binding epidermal growth factor-like growth factor, and epidermal growth factor in men with interstitial cystitis versus chronic pelvic pain syndrome. *Urology* 2004;63:22-6.
 72. Byrne DS, Sedor JF, Estojak J, Fitzpatrick KJ, Chiura AN, Mulholland SG. The urinary glycoprotein GP51 as a clinical marker for interstitial cystitis. *J Urol* 1999;161:1786-90.
 73. Pasikanti KK, Esuvaranathan K, Hong Y, Ho PC, Mahendran R, Raman Nee Mani L, et al. Urinary metabotyping of bladder cancer using two-dimensional gas chromatography time-of-flight mass spectrometry. *J Proteome Res* 2013;12:3865-73.
 74. Pasikanti KK, Esuvaranathan K, Ho PC, Mahendran R, Kamaraj R, Wu QH, et al. Noninvasive urinary metabonomic diagnosis of human bladder cancer. *J Proteome Res* 2010;9:2988-95.
 75. Wittmann BM, Stirdivant SM, Mitchell MW, Wulff JE, McDunn JE, Li Z, et al. Bladder cancer biomarker discovery using global metabolomic profiling of urine. *PLoS One* 2014;9:e115870.
 76. Srivastava S, Roy R, Singh S, Kumar P, Dalela D, Sankhwar SN, et al. Taurine-a possible fingerprint biomarker in non-muscle invasive bladder cancer: a pilot study by 1H NMR spectroscopy. *Cancer Biomark* 2010;6:11-20.
 77. Huang Z, Lin L, Gao Y, Chen Y, Yan X, Xing J, et al. Bladder cancer determination via two urinary metabolites: a biomarker pattern approach. *Mol Cell Proteomics* 2011;10:M111.007922.
 78. Jin X, Yun SJ, Jeong P, Kim IY, Kim WJ, Park S. Diagnosis of bladder cancer and prediction of survival by urinary metabolomics. *Oncotarget* 2014;5:1635-45.
 79. Liu X, Cheng X, Liu X, He L, Zhang W, Wang Y, et al. Investigation of the urinary metabolic variations and the application in bladder cancer biomarker discovery. *Int J Cancer* 2018;143:408-18.
 80. Parker KS, Crowley JR, Stephens-Shields AJ, van Bokhoven A, Lucia MS, Lai HH, et al. Urinary metabolomics identifies a molecular correlate of interstitial cystitis/bladder pain syndrome in a Multidisciplinary Approach to the Study of Chronic Pelvic Pain (MAPP) research network cohort. *EBioMedicine* 2016;7:167-74.
 81. Esteller M. Epigenetics in cancer. *N Engl J Med* 2008;358:1148-59.
 82. Kim WJ, Kim YJ. Epigenetic biomarkers in urothelial bladder cancer. *Expert Rev Mol Diagn* 2009;9:259-69.
 83. Besaratinia A, Cockburn M, Tommasi S. Alterations of DNA methylation in human bladder cancer. *Epigenetics* 2013;8:1013-22.
 84. Kandimalla R, van Tilborg AA, Zwarthoff EC. DNA methylation-based biomarkers in bladder cancer. *Nat Rev Urol* 2013;10:327-35.
 85. Chan MW, Chan LW, Tang NL, Tong JH, Lo KW, Lee TL, et al. Hypermethylation of multiple genes in tumor tissues and voided urine in urinary bladder cancer patients. *Clin Cancer Res* 2002;8:464-70.
 86. Friedrich MG, Weisenberger DJ, Cheng JC, Chandrasoma S, Siegmund KD, Gonzalgo ML, et al. Detection of methylated apoptosis-associated genes in urine sediments of bladder cancer patients. *Clin Cancer Res* 2004;10:7457-65.
 87. Hoque MO, Begum S, Topaloglu O, Chatterjee A, Rosenbaum E, Van Criekinge W, et al. Quantitation of promoter methylation of multiple genes in urine DNA and bladder cancer detection. *J Natl Cancer Inst* 2006;98:996-1004.
 88. Renard I, Joniau S, van Cleynebreugel B, Collette C, Naômé C, Vlassenbroeck I, et al. Identification and validation of the methylated TWIST1 and NID2 genes through real-time methylation-specific polymerase chain reaction assays for the non-invasive detection of primary bladder cancer in urine samples. *Eur Urol* 2010;58:96-104.
 89. Abern MR, Owusu R, Inman BA. Clinical performance and

- utility of a DNA methylation urine test for bladder cancer. *Urol Oncol* 2014;32:51.e21-6.
90. Fantony JJ, Abern MR, Gopalakrishna A, Owusu R, Jack Tay K, Lance RS, et al. Multi-institutional external validation of urinary TWIST1 and NID2 methylation as a diagnostic test for bladder cancer. *Urol Oncol* 2015;33:387.e1-6.
91. Reinert T, Modin C, Castano FM, Lamy P, Wojdacz TK, Hansen LL, et al. Comprehensive genome methylation analysis in bladder cancer: identification and validation of novel methylated genes and application of these as urinary tumor markers. *Clin Cancer Res* 2011;17:5582-92.
92. Reinert T, Borre M, Christiansen A, Hermann GG, Ørntoft TF, Dyrskjøt L. Diagnosis of bladder cancer recurrence based on urinary levels of EOMES, HOXA9, POU4F2, TWIST1, VIM, and ZNF154 hypermethylation. *PLoS One* 2012;7:e46297.
93. Su SF, de Castro Abreu AL, Chihara Y, Tsai Y, Andreu-Vieyra C, Daneshmand S, et al. A panel of three markers hyper- and hypomethylated in urine sediments accurately predicts bladder cancer recurrence. *Clin Cancer Res* 2014;20:1978-89.
94. Yu J, Zhu T, Wang Z, Zhang H, Qian Z, Xu H, et al. A novel set of DNA methylation markers in urine sediments for sensitive/specific detection of bladder cancer. *Clin Cancer Res* 2007;13:7296-304.
95. Costa VL, Henrique R, Danielsen SA, Duarte-Pereira S, Eknaes M, Skotheim RI, et al. Three epigenetic biomarkers, GDF15, TMEFF2, and VIM, accurately predict bladder cancer from DNA-based analyses of urine samples. *Clin Cancer Res* 2010;16:5842-51.
96. van der Heijden AG, Mengual L, Ingelmo-Torres M, Lozano JJ, van Rijt-van de Westerloo CCM, Baixauli M, et al. Urine cell-based DNA methylation classifier for monitoring bladder cancer. *Clin Epigenetics* 2018;10:71.
97. Bradley MS, Burke EE, Grenier C, Amundsen CL, Murphy SK, Siddiqui NY. A genome-scale DNA methylation study in women with interstitial cystitis/bladder pain syndrome. *Neurourol Urodyn* 2018;37:1485-93.
98. Kim YJ, Kim WJ. Can we use methylation markers as diagnostic and prognostic indicators for bladder cancer? *Investig Clin Urol* 2016;57 Suppl 1:S77-88.
99. Liou LS. Urothelial cancer biomarkers for detection and surveillance. *Urology* 2006;67(3 Suppl 1):25-33; discussion 33-4.

Biomarker discovery and beyond for diagnosis of bladder diseases

Sungyong Jung¹, Jayoung Kim^{2,3*}

¹Department of Electrical Engineering, University of Texas at Arlington, Arlington, TX 76019, USA

²Departments of Surgery and Biomedical Sciences, Cedars-Sinai Medical Center, Los Angeles, CA 90048, USA

³Department of Medicine, University of California Los Angeles, CA 90095, USA

*Corresponding author: Jayoung Kim, Email: Jayoung.Kim@cshs.org

Competing interests: The authors have declared that the funders had no role in the experimental design, data collection, analysis, preparation of the manuscript, or decision to publish. In addition, this article is derived from the Subject Data funded in whole or part by National Academies of Sciences, Engineering, and Medicine (NAS) and The United States Agency for International Development (USAID). Any opinions, findings, conclusions, or recommendations expressed in this article are those of the authors alone, and do not necessarily reflect the views of USAID or NAS.

Abbreviations used: BPS, bladder pain syndrome; CGM, continuous glucose monitors; DID, diabetes interactive diary; IHC, immunohistochemistry; IC, interstitial cystitis; IoT, internet of things; MAPP, multidisciplinary approach to the study of chronic pelvic pain; NIH, National Institutes of Health; ROC, receiver operator characteristic; SMBG, self-monitoring of blood glucose; UI, urinary incontinence; UTI, urinary tract infection

Received January 6, 2020; Revision received March 9, 2020; Accepted March 9, 2020; Published March 24, 2020

ABSTRACT

Molecular biosignatures of altered cellular landscapes and functions have been casually linked with pathological conditions, which imply the promise of biomarkers specific to bladder diseases, such as bladder cancer and other dysfunctions. Urinary biomarkers are particularly attractive due to costs, time, and the minimal and noninvasive efforts acquiring urine. The evolution of omics platforms and bioinformatics for analyzing the genome, epigenome, transcriptome, proteome, lipidome, metabolome, etc., have enabled us to develop more sensitive and disease-specific biomarkers. These discoveries broaden our understanding of the complex biology and pathophysiology of bladder diseases, which can ultimately be translated into the clinical setting. In this short review, we will discuss current efforts on identification of promising urinary biomarkers of bladder diseases and their roles in diagnosis and monitoring. With these considerations, we also aim to provide a prospective view of how we can further utilize these bladder biomarkers in developing ideal and smart medical devices that would be applied in the clinic.

Keywords: biomarker; bladder; urine; medical device; biosensor

URINE AND URINARY BIOMARKERS FOR BLADDER DISEASES

Urine is a waste product that is readily produced by all patients and contains a wealth of information. It can be produced in high-volume and procurement of samples is noninvasive. Considering these factors alone, urine is a highly attractive potential resource. However, there are several glaring issues that make urinalysis difficult. Factors such as preanalytical reliability and data analysis can be a major challenge [1,2]. Transport and preservation of urine samples are particularly important. It has been shown that increased time gaps between sampling and analysis, lack of temperature control, and lack of preservatives for samples that cannot be analyzed within two hours after collection can lead to low-quality test results [3]. However, preservatives may also affect the chemical properties and alter the appearance of certain particles [4]. Additionally, urine contains much more complex compounds that

can be affected by a wide range of external factors, including diet and environment [5]. A comparative urinary metabolite profiling study of habitual diet discovered that 417 urinary metabolites were correlated with more than one food, beverage, or supplement [6]. Exposure to different environmental toxins and chemicals have been shown to be reflected in urine. A study of pediatric exposure to pyrethroids, an insecticide, found differing concentrations of the chemical in urine based on each child's level of risk [7]. Fortunately, recent advances in technology and standardization have made urinalysis more of a viable option for a number of clinical issues [8]. Because the uroepithelial-associated sensory web may be related to hypersensitive benign urological disorders [9], it is not always necessary that clinopathological status results in a change in urinary components. As the pathology of genitourinary diseases is being better understood, more diagnostic and prognostic biomarkers are also being identified [10]. A recent study reported that 4 urinary biomarkers were associated with kidney injury [11]. By

How to cite this article: Jung S, Kim J. Biomarker discovery and beyond for diagnosis of bladder diseases. *Bladder* 2020;7(1):e40. DOI: 10.14440/bladder.2020.813

integrating newer technologies with increased knowledge of diseases, novel biomarkers can be discovered.

MULTI-OMICS APPLICATION FOR BLADDER BIOMARKER DEVELOPMENT

Omics involves the high-throughput analysis of different domains of biological information, including the genome, transcriptome, proteome, and metabolome [12,13]. Comprehensive omics analysis of urine can be a potentially valuable source of disease biomarkers. For instance, the proteomic profile of healthy urine can be used as a standard to compare disease-state urine to identify proteins of interest [14]. Recent new types of software are being developed to create workflows that involve distinguishing biomarkers *via* integrated comparative and quantitative analysis [15]. Advanced proteomic analysis has led to high-throughput profiling of bladder cancer-related proteins with both high sensitivity and specificity, which has resulted in a wealth of informative biomarkers [16]. A similar strategy was utilized in a recent study that identified 54 potential protein biomarkers of bladder schistosomiasis by quantitatively comparing urinary samples from humans [17]. Other types of omics applications, such as genomics, epigenomics, transcriptomics and metabolomics, were also applied to determine biomarkers of bladder schistosomiasis. Metabolomic profiling using urine and plasma samples revealed that the perturbed glycerophospholipid and sphingolipid metabolisms are associated with schistosomiasis and its associated-bladder cancer pathologies [18]. Epigenetic regulation on RASSF1A and TIMP3 were found using a quantitative methylation-specific PCR assay in urine sediments of patients with schistosomiasis infection. Hypermethylation of both RASSF1A and TIMP3 shows 77.55% of area under the receiver operator characteristic (ROC) curves ($P = 0.023$) [19]. Another study profiled urinary amino acids to identify potential biomarkers for lower urinary tract symptoms in male patients [20]. As non-invasive disease biomarkers, urinary extracellular vesicles such as exosomes have been discovered to contain a variety of molecular and genetic materials including nucleotides, proteins, metabolites, miRNAs, and they function as a cargo and transfer those materials to nearby neighbor cells [21,22]. Progress in these comprehensive tests continues to increase our understanding of the complexity of biomarkers that underlie diseases and, with technology, it is becoming easier to navigate how to utilize them.

MICROBIOME STUDIES IN UROLOGICAL DISEASES

The microbiome is defined as the collective genome of all microorganisms in an environment [23]. Interest in this field has recently boomed as it has been shown that microbiota and alterations in their communities can contribute to the pathogenesis of chronic urological diseases, such as urothelial carcinoma [24]. A preliminary study found an association between urinary dysbiosis and urothelial carcinoma, suggesting that the ratio for microbiota could be used as a potential diagnostic indicator [25]. Another study observed that bacterial richness increased in the urine of patients with cancer compared to controls [26]. However, despite all the promising exploratory data surrounding microbiome's usage in urological diseases, the field is still relatively new and more comprehensive studies are needed [27]. Studies on the influence of microbiota expand beyond the genitourinary tract as well.

For instance, *Helicobacter pylori* is, well-documented, increasing the risk of duodenal and gastric ulcer disease and gastric cancer [28]. Bacterial pathogenesis is also noted to be potentially associated with colorectal cancer [29]. Based on the extensive role of microbiomes in many diseases, a better understanding of urinary microbes and their roles in urological diseases may prove to be significant.

Aside from potential utilization of the microbiome in diagnostics and prognostics, identifying present microbiota may be important when it comes to various treatments. For instance, gastrointestinal microbes are known to affect the metabolism and toxicity of various agents [30]. *Mycoplasma hyorhinis* has been shown to metabolize and inactivate gemcitabine, a chemotherapeutic drug, which can result in drug resistance [31]. Additionally, reactivation of the inactive metabolites of irinotecan, a topoisomerase I inhibitor, by gastrointestinal bacteria can lead to adverse toxicities, such as severe diarrhea [32]. For urological diseases, there are also some noted interactions between microbiota and treatment. It has been shown that D-mannose, a simple sugar, can hinder bacterial adhesion to the urothelium, thereby reducing risk of urinary tract infections and aiding in acute cystitis management [33].

The urinary microbiome is believed to play an important role in predicting disease status for many different urogenital diseases. Recently, a pilot study looking into the relationship between the urinary microbiome and bladder cancer uncovered that bacteria belonging to the genus *Fusobacterium* were significantly more abundant in urine specimens from cancer patients [34]. Another exploratory study comparatively surveyed the urine microbiota of female patients with interstitial cystitis (IC)/bladder pain syndrome (BPS) and controls who were enrolled in the National Institutes of Health (NIH) Multidisciplinary Approach to the Study of Chronic Pelvic Pain (MAPP) Research Network. It identified potential negative impacts of the presence of *Lactobacillus gasseri* and protective influence of *Corynebacterium* [35]. It should be noted that a different study on urinary incontinence (UI) found a lack of *Lactobacillus* to be associated with urgency UI and resistance to anticholinergic treatments [36]. However, being that these are two different diseases, the conflicting results are not unexpected. Furthermore, there are many species of *Lactobacillus* and some may contribute to a healthy or disease bladder. On the other hand, another study that collected urinary samples from 21 IC patients and 20 matched controls found no significant differences in urinary microbiota [37]. The conflicting conclusions between these two recent studies highlight controversy surrounding this fairly new field and the need for a more comprehensive longitudinal study.

CHALLENGES AND CONSIDERATION IN URINE BIOMARKER DEVELOPMENT

Despite the promising potential of urinary biomarkers, there are several precautions to consider. One important factor that can affect biomarker outcomes is age. Studies have shown that the maturing kidney can affect biomarker levels and interpretation, suggesting that age-specific biomarker reference ranges may be needed for certain diseases [38]. Furthermore, baseline metabolites have been shown to be different among different age-groups, which may highlight carefully establishing different age groups should be warranted when conducting urinalysis [39]. Gender is another factor to be considered when establishing reference values for urinary biomarkers [14]. Proteomic analysis of female and male urine observed different patterns and variations of proteins

[40]. Given that urine sample can have huge variation in concentration of proteins or metabolites due to the fluid consumption, special care should be taken to data normalization methods to reduce any potential artifacts [41]. Furthermore, external factors that are dependent on individuals can influence the expression of urinary biomarkers. Studies have shown differences in expression of urinary biomarkers in patients who have undergone cisplatin therapy [14]. Certain procedures can also affect urinary levels of metabolites; another study found increased urinary neurotrophin in women with stress urinary incontinence after a midurethral sling procedure [42]. This suggests that in order to effectively utilize urinalysis, there needs to be a comprehensive understanding of the fluctuations in biomarkers that can occur within each individual

BIOSENSOR FOR THE DETECTION OF URINARY BIOMARKERS

Biosensors are an arising field of great interest when it comes to detecting and monitoring markers in biofluids, such as sweat and urine. Wearable sensors are particularly garnering attention because they can be portable, convenient, non-invasive, and provide real-time evaluation of important biomarkers [43]. In addition to its detection and monitoring benefits, biosensors could also be integrated with therapeutic drugs to monitor for response to treatments [44]. The potential for sensors can extend to many different types of situations. For example, biosensors can be developed into electrochemical sensors or fluid measuring sensors [45]. These biosensors can be constructed to detect various compounds, such as antigens, biomarkers, and bacterial enzymes.

With the advent of smart technologies, there has been exciting developments in utilizing such devices in healthcare as well. In 2015, a team of biomedical engineers at the University of Arizona was able to develop a highly-sensitive and cost-efficient paper-based analytical device (μ Pad) that could monitor urine for urinary tract infection (UTI) and gonorrhea [46]. A recent study developed a similar device that quantified β -glucuronidase, an enzyme released by 95% of *E. coli*, the bacteria that causes UTI [47]. In addition to these urinalysis-based detection devices, several others have been developed to detect other compounds. A study by the Southern Taiwan University of Science and Technology developed an ultraportable microsensor-lined biosensor that can actually quantify the presence of Gal-1, a protein biomarker indicative of multiple oncological conditions, including bladder cancer [48]. These novel devices only scratch the surface of the great potential for biosensors.

The use of technology can also extend beyond detection. Taking advantage of the fact that most people use a smartphone, a study in the United Kingdom crowdsourced members of the public to grade immunohistochemistry stains of bladder cancer tumor microarrays [49]. Surprisingly, this was found to be a potentially accurate way to screen immunohistochemistry (IHC) data and speed biomarker discovery.

DIGITAL APPLICATIONS OF BIOSENSORS

The rise of digital applications of biosensors is also a rising field of great interest. There are incredible possibilities that comes from being able to use everyday technology to monitor health. Not only would this reduce risks to patients and lower healthcare costs, but it could also

lead to an immense wealth of data that can be used to pioneer science even further. The most commonly used interactive app for monitoring has been in diabetes. Currently, there are two major mobile apps that incorporate self-monitoring of blood glucose (SMBG) recording and insulin bolus calculators. These are Diabeo (Voluntis) and Diabetes Interactive Diary (DID) [50]. Studies have shown that monitoring of patients with type 1 diabetes by using Diabeo can lead to substantial improvement in metabolic control in chronic poorly controlled patients without requiring more medical time and at a lower cost than typical standard care [51]. Similar studies with DID show that it can reduce risk of moderate to severe hypoglycemia while also improving quality of life [52]. However, these apps are still a work in progress and have only shown improvements in certain areas of diabetes monitoring. With rapid technological innovation and progress, the focus on making these apps better should be continued.

In addition to real-time monitoring of chronic diseases, digital applications can lead to an enormous wealth of health data that can be used for more comprehensive studies. For instance, adding internet of things (IoT) capabilities to commercially used continuous glucose monitors (CGM) can lead to both the monitoring of patients remotely and crowdsourcing of that data [53]. As personal tech becomes increasingly embedded in the lives of patients, digital phenotypes can be captured to enhance health and wellness [54]. There is one caveat with this integration of technologies with personal health. As information is formed and sourced, careful attention must be paid to decentralizing databases and ensuring that patient health information remains private and protected. With proper cyber security, the promises of digital health monitoring are endless.

CONCLUDING REMARKS

Advances in urine-based molecular profiling technologies, the development of biosensor targeting disease-specific biomarkers and the wirelessly connected medical device would lead to smart diagnosis and monitoring for patients affected by bladder diseases. Thanks to rigorous efforts of scientists and urologists including us to define biomarkers for bladder diseases such as bladder cancer and other types of bladder dysfunction, we have better idea how to manage those bladder diseases. As we discussed in this paper, the current evidence suggests the integration of multi-omics profiling-based characterization of bladder diseases and application of urinary biomarkers into smart medical device could lead future tools for patient care.

Acknowledgments

The authors acknowledge support from National Institutes of Health grants (1U01DK103260, 1R01DK100974, U24 DK097154, NIH NCATS UCLA CTSI UL1TR000124), Department of Defense grants (W81XWH-15-1-0415 and W81XWH-19-1-0109), Centers for Disease Controls and Prevention (1U01DP006079), IMAGINE NO IC Research Grant, the Steven Spielberg Discovery Fund in Prostate Cancer Research Career Development Award, and the U.S.-Egypt Science and Technology Joint Fund (to J.K.). J.K. is a former recipient of the Interstitial Cystitis Association Pilot Grant, a Fishbein Family IC Research Grant, New York Academy of Medicine, and Boston Children's Hospital Faculty Development.

References

- Coppens A, Speeckaert M, Delanghe J (2010) The pre-analytical challenges of routine urinalysis. *Acta Clin Belg* 65: 182-189. doi: [10.1179/acb.2010.038](https://doi.org/10.1179/acb.2010.038). PMID: 20669786
- Howanitz PJ, Howanitz JH (1983) Quality control for the clinical laboratory. *Clin Lab Med* 3: 541-551. doi: [10.1016/S0272-2712\(18\)30974-0](https://doi.org/10.1016/S0272-2712(18)30974-0). PMID: 6357609
- Delanghe J, Speeckaert M (2014) Preanalytical requirements of urinalysis. *Biochem Med (Zagreb)* 24: 89-104. doi: [10.11613/BM.2014.011](https://doi.org/10.11613/BM.2014.011). PMID: 24627718
- Fogazzi GB, Verdesca S, Garigali G (2008) Urinalysis: core curriculum 2008. *Am J Kidney Dis* 51: 1052-1067. doi: [10.1053/j.ajkd.2007.11.039](https://doi.org/10.1053/j.ajkd.2007.11.039). PMID: 18501787
- Bouatra S, Aziat F, Mandal R, Guo AC, Wilson MR, et al. (2013) The human urine metabolome. *PLoS One* 8: e73076. doi: [10.1371/journal.pone.0073076](https://doi.org/10.1371/journal.pone.0073076). PMID: 24023812
- Hg DS, Siltberg-Liberles J (2016) Paralog-specific patterns of structural disorder and phosphorylation in the vertebrate SH3-SH2-tyrosine kinase protein family. *Genome Biol Evol* 8: 2806-2825. doi: [10.1093/gbe/evw194](https://doi.org/10.1093/gbe/evw194). PMID: 27519537
- Glorennec P, Serrano T, Fravallo M, Warembourg C, Monfort C, et al. (2017) Determinants of children's exposure to pyrethroid insecticides in western France. *Environ Int* 104: 76-82. doi: [10.1016/j.envint.2017.04.007](https://doi.org/10.1016/j.envint.2017.04.007). PMID: 28453973
- Filip S, Zoidakis J, Vlahou A, Mischak H (2014) Advances in urinary proteome analysis and applications in systems biology. *Bioanalysis* 6: 2549-2469. doi: [10.4155/bio.14.210](https://doi.org/10.4155/bio.14.210). PMID: 25411698
- Apodaca G, Balestreire E, Birder LA (2007) The uroepithelial-associated sensory web. *Kidney Int* 72: 1057-1064. doi: [10.1038/sj.ki.5002439](https://doi.org/10.1038/sj.ki.5002439). PMID: 17667988
- Xing J, Reynolds JP (2018) Diagnostic advances in urine cytology. *Surg Pathol Clin* 11: 601-610. doi: [10.1016/j.path.2018.06.001](https://doi.org/10.1016/j.path.2018.06.001). PMID: 30190143
- Nadkarni GN, Coca SG, Meisner A, Patel S, Kerr KF, et al. (2017) Urinalysis findings and urinary kidney injury biomarker concentrations. *BMC Nephrol* 18: 218. doi: [10.1186/s12882-017-0629-z](https://doi.org/10.1186/s12882-017-0629-z). PMID: 28683730
- Rhee EP (2018) How omics data can be used in nephrology. *Am J Kidney Dis* 72: 129-135. doi: [10.1053/j.ajkd.2017.12.008](https://doi.org/10.1053/j.ajkd.2017.12.008). PMID: 29478865
- Miyake M, Owari T, Hori S, Fujimoto K (2019) Significant lack of urine-based biomarkers to replace cystoscopy for the surveillance of non-muscle invasive bladder cancer. *Transl Androl Urol* 8(Suppl 3): S332-S334. doi: [10.21037/tau.2019.05.07](https://doi.org/10.21037/tau.2019.05.07). PMID: 31392161
- Zhao M, Li M, Yang Y, Guo Z, Sun Y, et al. (2017) A comprehensive analysis and annotation of human normal urinary proteome. *Sci Rep* 7: 3024. doi: [10.1038/s41598-017-03226-6](https://doi.org/10.1038/s41598-017-03226-6). PMID: 28596590
- Salomonis N (2018) Integrative analysis of proteomics data to obtain clinically relevant markers. *Methods Mol Biol* 1788: 89-111. doi: [10.1007/978-1-4939-9419-1_94](https://doi.org/10.1007/978-1-4939-9419-1_94). PMID: 29147916
- Zhang H, Fan Y, Xia L, Gao C, Tong X, et al. (2017) The impact of advanced proteomics in the search for markers and therapeutic targets of bladder cancer. *Tumour Biol* 39: 1010428317691183. doi: [10.1177/1010428317691183](https://doi.org/10.1177/1010428317691183). PMID: 28345451
- Onile OS, Calder B, Soares NC, Anumudu CI, Blackburn JM (2017) Quantitative label-free proteomic analysis of human urine to identify novel candidate protein biomarkers for schistosomiasis. *PLoS Negl Trop Dis* 11: e0006045. doi: [10.1371/journal.pntd.0006045](https://doi.org/10.1371/journal.pntd.0006045). PMID: 29117212
- Adebayo AS, Mundhe SD, Awobode HO, Onile OS, Agunloye AM, et al. (2018) Metabolite profiling for biomarkers in *Schistosoma haematobium* infection and associated bladder pathologies. *PLoS Negl Trop Dis* 12: e0006452. doi: [10.1371/journal.pntd.0006452](https://doi.org/10.1371/journal.pntd.0006452). PMID: 29708967
- Zhong X, Isharwal S, Naples JM, Shiff C, Veltri RW, et al. (2013) Hypermethylation of genes detected in urine from Ghanaian adults with bladder pathology associated with *Schistosoma haematobium* infection. *PLoS One* 8: e59089. doi: [10.1371/journal.pone.0059089](https://doi.org/10.1371/journal.pone.0059089). PMID: 23527093
- Mitsui T, Kira S, Ihara T, Sawada N, Nakagomi H, et al. (2018) Metabolomics approach to male lower urinary tract symptoms: identification of possible biomarkers and potential targets for new treatments. *J Urol* 199: 1312-1318. doi: [10.1016/j.juro.2017.11.070](https://doi.org/10.1016/j.juro.2017.11.070). PMID: 29175111
- De Palma G, Di Lorenzo VF, Krol S, Paradiso AV (2019) Urinary exosomal shuttle RNA: Promising cancer diagnosis biomarkers of lower urinary tract. *Int J Biol Markers* 34: 101-107. doi: [10.1177/1724600819827023](https://doi.org/10.1177/1724600819827023). PMID: 30862241
- Junker K, Heinzelmann J, Beckham C, Ochiya T, Jenster G (2016) Extracellular vesicles and their role in urologic malignancies. *Eur Urol* 70: 323-331. doi: [10.1016/j.eururo.2016.02.046](https://doi.org/10.1016/j.eururo.2016.02.046). PMID: 26924769
- Schwabe RF, Jobin C (2013) The microbiome and cancer. *Nat Rev Cancer* 13: 800-812. doi: [10.1038/nrc3610](https://doi.org/10.1038/nrc3610). PMID: 24132111
- Xu W, Yang L, Lee P, Huang WC, Nossa C, et al. (2014) Mini-review: perspective of the microbiome in the pathogenesis of urothelial carcinoma. *Am J Clin Exp Urol* 2: 57-61. PMID: 25126590
- Alfano M, Canducci F, Nebuloni M, Clementi M, Montorsi F, et al. (2016) The interplay of extracellular matrix and microbiome in urothelial bladder cancer. *Nat Rev Urol* 13: 77-90. doi: [10.1038/nrurol.2015.292](https://doi.org/10.1038/nrurol.2015.292). PMID: 26666363
- Wu P, Zhang G, Zhao J, Chen J, Chen Y, et al. (2018) Profiling the urinary microbiota in male patients with bladder cancer in China. *Front Cell Infect Microbiol* 8: 167. doi: [10.3389/fcimb.2018.00167](https://doi.org/10.3389/fcimb.2018.00167). PMID: 29904624
- Markowski MC, Boorjian SA, Burton JP, Hahn NM, Ingersoll MA, et al. (2019) The microbiome and genitourinary cancer: a collaborative review. *Eur Urol* 75: 637-646. doi: [10.1016/j.eururo.2018.12.043](https://doi.org/10.1016/j.eururo.2018.12.043). PMID: 30655087
- Wroblewski LE, Peek RM (2010) Wilson KT. *Helicobacter pylori* and gastric cancer: factors that modulate disease risk. *Clin Microbiol Rev* 23: 713-739. doi: [10.1128/CMR.00011-10](https://doi.org/10.1128/CMR.00011-10). PMID: 20930071
- Dahmus JD, Kotler DL, Kastenberg DM, Kistler CA (2018) The gut microbiome and colorectal cancer: a review of bacterial pathogenesis. *J Gastrointest Oncol* 9: 769-777. doi: [10.21037/jgo.2018.04.07](https://doi.org/10.21037/jgo.2018.04.07). PMID: 30151274
- Spanogiannopoulos P, Bess EN, Carmody RN, Turnbaugh PJ (2016) The microbial pharmacists within us: a metagenomic view of xenobiotic metabolism. *Nat Rev Microbiol* 14: 273-287. doi: [10.1038/nrmicro.2016.17](https://doi.org/10.1038/nrmicro.2016.17). PMID: 26972811
- Geller LT, Barzily-Rokni M, Danino T, Jonas OH, Shental N, et al. (2017) Potential role of intratumor bacteria in mediating tumor resistance to the chemotherapeutic drug gemcitabine. *Science* 357: 1156-1160. doi: [10.1126/science.aah5043](https://doi.org/10.1126/science.aah5043). PMID: 28912244
- Wallace BD, Wang H, Lane KT, Scott JE, Orans J, et al. (2010) Alleviating cancer drug toxicity by inhibiting a bacterial enzyme. *Science* 330: 831-835. doi: [10.1126/science.1191175](https://doi.org/10.1126/science.1191175). PMID: 21051639
- Domenici L, Monti M, Bracchi C, Giorgini M, Colagiovanni V, et al. (2016) D-mannose: a promising support for acute urinary tract infections in women. A pilot study. *Eur Rev Med Pharmacol Sci* 20: 2920-2925. PMID: 27424995
- Bucevic Popovic V, Situm M, Chow CT, Chan LS, Roje B, et al. (2018) The urinary microbiome associated with bladder cancer. *Sci Rep* 8: 12157. doi: [10.1038/s41598-018-29054-w](https://doi.org/10.1038/s41598-018-29054-w). PMID: 30108246
- Nickel JC, Stephens-Shields AJ, Landis JR, Mullins C, Bokhoven A, van , et al. (2019) A culture-independent analysis of the microbiota of female interstitial cystitis/bladder pain syndrome participants in the MAPP research network. *J Clin Med* 8. doi: [10.3390/jcm8030415](https://doi.org/10.3390/jcm8030415). PMID: 30917614
- Gvender Y, Gabriel I, Minassian V, Fichorova R (2019) The Current Evidence on the Association Between the Urinary Microbiome and Urinary Incontinence in Women. *Front Cell Infect Microbiol* 9: 133. doi: [10.3389/fcimb.2019.00133](https://doi.org/10.3389/fcimb.2019.00133). PMID: 31119104
- Bresler L, Price TK, Hilt EE, Joyce C, Fitzgerald CM, et al. (2019) Female lower urinary tract microbiota do not associate with IC/PBS symptoms: a case-controlled study. *Int Urogynecol J* 30: 1835-1842. doi: [10.1007/s00192-019-03942-9](https://doi.org/10.1007/s00192-019-03942-9). PMID: 30993388
- Greenberg JH, Parikh CR (2017) Biomarkers for diagnosis and prognosis of AKI in children: one size does not fit all. *Clin J Am Soc Nephrol* 12: 1551-1557. doi: [10.2215/CJN.12851216](https://doi.org/10.2215/CJN.12851216). PMID: 28667085
- Psihogios NG, Gazi IF, Elisaf MS, Seferiadis KI, Bairaktari ET (2008) Gender-related and age-related urinalysis of healthy subjects by NMR-based metabolomics. *NMR Biomed* 21: 195-207. doi: [10.1002/nbm.1176](https://doi.org/10.1002/nbm.1176). PMID: 17474139
- Guo Z, Zhang Y, Zou L, Wang D, Shao C, et al. (2015) A proteomic analysis of individual and gender variations in normal human urine and cerebrospinal fluid using iTRAQ quantification. *PLoS One* 10: e0133270. doi: [10.1371/journal.pone.0133270](https://doi.org/10.1371/journal.pone.0133270). PMID: 26222143
- Chen Z, Kim J (2016) Urinary proteomics and metabolomics studies to monitor bladder health and urological diseases. *BMC Urol* 16: 11. doi: [10.1186/s12894-016-0129-7](https://doi.org/10.1186/s12894-016-0129-7). PMID: 27000794
- Antunes-Lopes T, Coelho A, Pinto R, Barros SC, Cruz CD, et al. (2016) Urinary neurotrophin levels increase in women with stress urinary incontinence after a midurethral sling procedure. *Urology* 99: 49-56. doi: [10.1016/j.urology.2016.08.048](https://doi.org/10.1016/j.urology.2016.08.048). PMID: 27697460
- Kim J, Campbell AS, de Ávila BE, Wang J (2019) Wearable biosensors for healthcare monitoring. *Nat Biotechnol* 37: 389-406. doi: [10.1038/s41587-019-0045-y](https://doi.org/10.1038/s41587-019-0045-y). PMID: 30804534
- McKeating KS, Aube A, Masson JF (2016) Biosensors and nanobiosensors for therapeutic drug and response monitoring. *Analyst* 141: 429-449. doi: [10.1039/c5an01861g](https://doi.org/10.1039/c5an01861g). PMID: 26631282
- Liu X, Lillehoj PB (2017) Embroidered electrochemical sensors on gauze for rapid quantification of wound biomarkers. *Biosens Bioelectron* 98: 189-194. doi: [10.1016/j.bios.2017.06.053](https://doi.org/10.1016/j.bios.2017.06.053). PMID: 28675839
- Cho S, Park TS, Nahapetian TG, Yoon JY (2015) Smartphone-based, sensitive microPAD detection of urinary tract infection and gonorrhea. *Biosens Bioelectron*

- 74: 601-611. doi: [10.1016/j.bios.2015.07.014](https://doi.org/10.1016/j.bios.2015.07.014). PMID: [26190472](https://pubmed.ncbi.nlm.nih.gov/26190472/)
47. Noiphung J, Laiwattanapaisal W (2019) Multifunctional paper-based analytical device for *in situ* cultivation and screening of *Escherichia coli* infections. *Sci Rep* 9: 1555. doi: [10.1038/s41598-018-38159-1](https://doi.org/10.1038/s41598-018-38159-1). PMID: [30733495](https://pubmed.ncbi.nlm.nih.gov/30733495/)
48. Chuang CH, Yc, Du , Wu TF, Chen CH, Lee DH, et al. (2016) Immunosensor for the ultrasensitive and quantitative detection of bladder cancer in point of care testing. *Biosens Bioelectron* 84: 126-132. doi: [10.1016/j.bios.2015.12.103](https://doi.org/10.1016/j.bios.2015.12.103). PMID: [26777732](https://pubmed.ncbi.nlm.nih.gov/26777732/)
49. Smittenaar P, Walker AK, McGill S, Kartsonaki C, Robinson-Vyas RJ, et al. (2018) Harnessing citizen science through mobile phone technology to screen for immunohistochemical biomarkers in bladder cancer. *Br J Cancer* 119: 220-9. doi: [10.1038/s41416-018-0156-0](https://doi.org/10.1038/s41416-018-0156-0). PMID: [29991697](https://pubmed.ncbi.nlm.nih.gov/29991697/)
50. Shan R, Sarkar S, Martin SS (2019) Digital health technology and mobile devices for the management of diabetes mellitus: state of the art. *Diabetologia* 62: 877-87. doi: [10.1007/s00125-019-4864-7](https://doi.org/10.1007/s00125-019-4864-7). PMID: [30963188](https://pubmed.ncbi.nlm.nih.gov/30963188/)
51. Charpentier G, Benhamou PY, Dardari D, Clergeot A, Franc S, et al. (2011) The Diabeo software enabling individualized insulin dose adjustments combined with telemedicine support improves HbA1c in poorly controlled type 1 diabetic patients: a 6-month, randomized, open-label, parallel-group, multicenter trial (TeleDiab 1 Study). *Diabetes Care* 34: 533-539. doi: [10.2337/dc10-1259](https://doi.org/10.2337/dc10-1259). PMID: [21266648](https://pubmed.ncbi.nlm.nih.gov/21266648/)
52. Rossi MC, Nicolucci A, Lucisano G, Pellegrini F, Di Bartolo P, et al. (2013) Impact of the "Diabetes Interactive Diary" telemedicine system on metabolic control, risk of hypoglycemia, and quality of life: a randomized clinical trial in type 1 diabetes. *Diabetes Technol Ther* 15: 670-679. doi: [10.1089/dia.2013.0021](https://doi.org/10.1089/dia.2013.0021). PMID: [23844569](https://pubmed.ncbi.nlm.nih.gov/23844569/)
53. Fernández-Caramés TM, Froiz-Míguez I, Blanco-Novoa O, Fraga-Lamas P (2019) Enabling the internet of mobile crowdsourcing health things: A mobile fog computing, blockchain and IoT based continuous glucose monitoring system for diabetes mellitus research and care. *Sensors (Basel)* 19: doi: [10.3390/s19153319](https://doi.org/10.3390/s19153319). PMID: [31357725](https://pubmed.ncbi.nlm.nih.gov/31357725/)
54. Jain SH, Powers BW, Hawkins JB, Brownstein JS (2015) The digital phenotype. *Nat Biotechnol* 33: 462-3. doi: [10.1038/nbt.3223](https://doi.org/10.1038/nbt.3223). PMID: [25965751](https://pubmed.ncbi.nlm.nih.gov/25965751/)



This work is licensed under a Creative Commons Attribution-Non-Commercial-ShareAlike 4.0 International License: <http://creativecommons.org/licenses/by-nc-sa/4.0>

Article

Identification of Metabolic Alterations in Breast Cancer Using Mass Spectrometry-Based Metabolomic Analysis

Sili Fan ¹, Muhammad Shahid ², Peng Jin ², Arash Asher ³ and Jayoung Kim ^{2,3,4,5,6,*}

¹ West Coast Metabolomics Center, University of California, Davis, CA 95616, USA; slfan@ucdavis.edu

² Departments of Surgery, Cedars-Sinai Medical Center, Los Angeles, CA 90048, USA; muhammad.shahid@cshs.org (M.S.); Peng.Jin@cshs.org (P.J.)

³ Samuel Oschin Comprehensive Cancer Institute, Cedars-Sinai Medical Center, Los Angeles, CA 90048, USA; Arash.Asher@cshs.org

⁴ Departments of Surgery and Biomedical Sciences, Cedars-Sinai Medical Center, Los Angeles, CA 90048, USA

⁵ Department of Medicine, University of California, Los Angeles, CA 90095, USA

⁶ Department of Urology, Ga Cheon University College of Medicine, Incheon 461-701, Korea

* Correspondence: Jayoung.Kim@cshs.org

Received: 3 April 2020; Accepted: 21 April 2020; Published: 24 April 2020



Abstract: Breast cancer (BC) is a major global health issue and remains the second leading cause of cancer-related death in women, contributing to approximately 41,760 deaths annually. BC is caused by a combination of genetic and environmental factors. Although various molecular diagnostic tools have been developed to improve diagnosis of BC in the clinical setting, better detection tools for earlier diagnosis can improve survival rates. Given that altered metabolism is a characteristic feature of BC, we aimed to understand the comparative metabolic differences between BC and healthy controls. Metabolomics, the study of metabolism, can provide incredible insight and create useful tools for identifying potential BC biomarkers. In this study, we applied two analytical mass spectrometry (MS) platforms, including hydrophilic interaction chromatography (HILIC) and gas chromatography (GC), to generate BC-associated metabolic profiles using breast tissue from BC patients. These metabolites were further analyzed to identify differentially expressed metabolites in BC and their associated metabolic networks. Additionally, Chemical Similarity Enrichment Analysis (ChemRICH), MetaMapp, and Metabolite Set Enrichment Analysis (MSEA) identified significantly enriched clusters and networks in BC tissues. Since metabolomic signatures hold significant promise in the clinical setting, more effort should be placed on validating potential BC biomarkers based on identifying altered metabolomes.

Keywords: biomarkers; mass spectrometry; metabolomics; breast cancer

1. Introduction

Breast cancer (BC) is the most commonly diagnosed cancer in women in the U.S. and is the second leading cause of cancer-related death [1]. The American Cancer Society (ACS) predicts that there will be approximately 276,480 new diagnoses of invasive BC and 48,530 new cases of carcinoma in situ (CIS) BC in the U.S. in 2020. The ACS also estimates that 42,170 women will die from BC or BC-related complications in 2020. Early diagnosis of BC is crucial for a better prognosis. Currently, there are various ways of detecting BC, including breast exams and imaging techniques, such as mammography, magnetic resonance imaging (MRI), positron-emission tomography (PET), computed tomography (CT), and single-photo emission computed tomography (SPECT) [2]. However, these techniques have limitations, including cost, time, and suitability for different age groups [3]. In addition to these

diagnostic methods, there are different BC markers that are being clinically used. These include tissue markers, such as hormone receptors, human epidermal growth factor-2, and urokinase plasminogen activator, genetic markers, such as breast cancer 1 (BRCA1) and BRCA2, and serum markers, such as CA 15.3 and BR 27.29 [4]. However, these markers are unable to diagnose BC in its early stages and can be affected by variations in disease state or therapies [5]. Therefore, there is an urgent need for a reliable rapid method of early BC detection.

Metabolomics involves studying the entire set of metabolites in a biological system, which is reflective of cellular functions and phenotypes [6]. It is well-documented that cancer cells display significantly altered cellular processes compared to normal cells, and these differences can be key to identifying a wealth of information, including cancer progression and therapeutic response [7]. One of the most established examples of cancer metabolic reprogramming is the “Warburg effect”, which leads to increased aerobic glycolysis in cells [8]. Metabolomics is a promising approach, particularly when it comes to BC, which is known to have complex and distinct molecular characteristics [9]. Metabolites are the ultimate results of downstream genes, RNA, and proteins, which allow for a better understanding of the complex biological interactions underlying BC [10]. By profiling the metabolic landscape of BC, novel molecular signatures can be identified that can not only provide early detection but also predict therapeutic response [11].

Alterations in amino acid transporters and glutamine metabolism have recently emerged as a field of interest in BC metabolomics [12]. Amino acids are the main molecules necessary for protein synthesis; as a result, growing tumor cells have an increased demand for them [13]. Several amino acid transporters, including SLC1A5, SLC6A14, and SLC7A5, were found to have varied expression in BC tissue compared to controls based on the type of cancer (i.e., HER2+ or ER+) [14–16]. Recent studies have also looked into how amino acid radiotracers can be utilized to better image BC [17]. One study demonstrated that both primary and metastatic sites of BC can be visualized via PET using ¹¹C-methionine, a radioactively labeled amino acid [18]. Another study applied the same approach using ¹⁸F-fluciclovine, which found that uptake of the compound was 4-fold greater in malignant BC compared to normal [19]. This suggests that metabolic alterations can be used to diagnose BC, subtype the disease, and be applied in conjunction with other methods to more accurately characterize it in each patient.

There are a variety of metabolomic tools that can be applied when studying BC, including liquid chromatography-mass spectrometry (LC-MS), gas chromatography-MS (GC-MS), and nuclear magnetic resonance (NMR). Recent studies have even utilized *ex vivo* proton high-resolution magic angle spinning magnetic resonance (HR MAS MR) spectrometry on intact BC tissue samples to identify differentially expressed metabolites (DEMs), which found characterizable differences in levels of glycine, choline, and amino acid metabolism [20]. Based on these promising results, metabolomics is becoming more of an appealing and opportune avenue for future BC studies.

In this study, we aimed to identify metabolomic signatures capable of differentiating BC patients from healthy controls and to understand enriched metabolic pathways in BC. Two independent metabolomic profiling analyses found that glutamine levels were increased in BC. Further analysis using Chemical Similarity Enrichment Analysis (ChemRICH), MetaMapp, and Metabolite Set Enrichment Analysis (MSEA) found interesting BC-enriched clusters and networks.

2. Materials and Methods

2.1. Ethics Statement

The Institutional Review Board (IRB) at Cedars-Sinai Medical Center (CSMC) approved this study for metabolomics profiling and data analysis of BC samples collected through the CSMC Biobank’s central IRB (Pro00044997). All experiments were performed in accordance with relevant guidelines and regulations.

2.2. GC/TOF MS Analysis

Sample extraction and gas chromatography-time-of-flight-mass spectrometry (GC-TOF-MS) analysis was performed as described in previous papers [21,22]. Briefly, tissue samples were prepared in conical polypropylene centrifuge tubes. Then, extraction solvent (acetonitrile, isopropanol, and water in a proportion ratio of 3:3:2) was added to the samples and homogenized for 45 s to ensure the uniform suspension of samples. After samples were centrifuged at 1500× g for 5 min, the supernatant was aliquoted into two 500 µL samples, one for analysis and another as backup. To process and analyse the supernatant, the samples were evaporated in a Labconco Centrивap Cold Trap Concentrator to complete dryness and resuspended in 500 µL of 50% acetonitrile. The samples were then centrifuged for 2 min at 14,000 rcf and the resulting supernatant was transferred to new Eppendorff tubes. This supernatant was again evaporated to complete dryness in the Labconco Centrивap Cold Trap Concentrator. For quality assurance, one blank negative control extraction was performed by applying the full procedure without any true biological samples for each sequence in the sample extraction.

2.2.1. Data Acquisition

Data are acquired using the following chromatographic parameters as described with minor modifications [23]. Restek Rtx-5Sil MS Columns (30 m length × 0.25 mm internal diameter with 0.25 µm film made of 95% dimethyl/5% diphenyl polysiloxane) were used under the optimized running condition. The analytical GC column was protected by a 10 m long empty guard column, which was cut into 20 cm intervals whenever the reference mixture containing quality control (QC) samples indicated problems caused by column contaminations. This resulted in excellent retention and separation of primary metabolite classes (amino acids, hydroxyl acids, carbohydrates, sugar acids, sterols, aromatics, nucleosides, amines and miscellaneous compounds). Automatic liner exchanges, after each set of 10 injections, were done to reduce sample carryover for highly lipophilic compounds. The following MS parameters were used; Leco Pegasus IV Mass Spectrometer with a unit mass resolution at 17 spectra s⁻¹ from 80–500 Da at –70 eV ionization energy and 1800 V detector voltage with a 230 °C transfer line and a 250 °C ion source.

2.2.2. Data Processing

After data acquisition, raw data files were preprocessed using ChromaTOF vs. 2.32. Apex masses were reported for use in the BinBase algorithm and the resulting *.txt files containing absolute spectra intensities were stored in a data server for further processing. The BinBase algorithm (rtx5) was used with the following settings: validity of chromatogram (<10 peaks with intensity >10⁷ counts/second), unbiased retention index marker detection (MS similarity > 800, validity of intensity range for high *m/z* marker ions), and retention index calculation by 5th order polynomial regression. Spectra were cut to 5% base peak abundance and matched to database entries from most to least abundant spectra. The filters used included: retention index window ± 2000 units (equivalent to about ± 2 s retention time), validation of unique ions and apex masses (unique ion must be included in apex masses and present at >3% of base peak abundance), mass spectrum similarity must fit criteria dependent on peak purity and signal/noise ratios, and a final isomer filter. The failed spectra were placed into new database entries when *s/n* >25, purity <1.0 and presence in the biological study design class was >80%. The BinBase administration software, BinView, was also used for analysis. For each metabolite, the number of high-confidence peak detections and the ratio of the average height of replaced values to high-confidence peak detections were stored.

2.3. HILIC-ESI-QTOF-MS/MS Analysis

Samples extraction and hydrophilic interaction liquid chromatography-electrospray ionization quadruple time-of-flight tandem mass spectrometry (HILIC-ESI-QTOF-MS/MS) analysis was performed as described in previous papers [21,22].

2.3.1. Data Acquisition

Data were acquired using the following chromatographic parameters, established as standard procedure in the Fiehn Laboratory. Analysis was done via HILIC-QTOF-MS/MS. The Waters Acquity UPLC BEH Amide Column (1.7 μm , 2.1 \times 150 mm) and Waters Acquity and UPLC BEH Amide VanGuard Pre-Column (1.7 μm , 5 \times 2.1 mm) were used at 40 °C and under a 0.4 mL/min flow rate. The injection volume was 3 μL for ESI (+), mass resolution was 10,000 for ESI (+) on an Agilent 6530 QTOF MS, and the scan range was m/z 60–1200 Da. The analytical ultra high-performance liquid chromatography (UHPLC) column was protected by a short guard column. This chromatography method yields excellent retention and separation of metabolite classes (biogenic amines, cationic compounds) and good within-series retention time reproducibility.

2.3.2. Data Processing

The raw data were processed in an untargeted (qualitative) manner using mzMine 2.0 to find peaks in up to 300 chromatograms. Alternatively, selected peaks were collated and constrained into Agilent's MassHunter quantification method on the accurate mass precursor ion level, using the MS/MS information and the NIST14 / Metlin / MassBank libraries to identify metabolites with manual confirmation of adduct ions and spectral scoring accuracy. MassHunter enables back-filling of quantifications for peaks that were missed in the primary peak finding process, hence yielding datasets without missing values. All metabolites were identified using the Fiehn library, which is publicly available at: <http://massbank.us>.

2.4. Bioinformatics Analysis for Identification of Metabolic Marker Candidates

To identify potential metabolites as marker candidates that can discriminate BC from controls, the following steps were applied. Data were normalized and the t -test was applied to the log₂ of the processed data. The Student's t -test was performed to extract significant metabolites from the normalized MS data. After false positive correction (FDR) using the Benjamini–Hochberg procedure, none of the p -values remained significant on the chosen level of 0.05.

Significant metabolites were selected for by the volcano plot based on a fold-change threshold > 2 (or < 0.5) and t -test p -value threshold < 0.1 . MetaboAnalyst version 3.0. Log transformation and mean-centering with auto scaling was performed prior to multivariate statistical analysis. Partial least square discriminant analysis (PLS-DA) and model evaluation with permutation strategy was then carried out according to published protocols [23].

To further confirm potential metabolic markers in distinguishing BC from controls, a support vector machine (SVM)-based classifier was built using MATLAB (R2014a). Tenfold cross-validation was applied to evaluate performance. All annotated compounds were validated with authentic standards and are MSI level 1 [24,25].

2.5. Statistical Analysis

2.5.1. Univariate Analysis

To identify significant compounds comparing BC vs. controls, the Mann–Whitney U test was performed on each compound. Benjamini–Hochberg FDR correction was utilized to deal with the multiple comparison problem. Fold-changes, defined as the median average of BC divided by the median average of the control samples, were calculated. Volcano plots visualizing the univariate analysis result for each identified metabolite with adjusted p -values less than 0.05 and fold-change greater than 2 or less than 0.5 were identified.

2.5.2. Multivariate Analysis

Principal component analysis (PCA) using significant compounds are shown in Figure 1B. The 25 identified metabolites with the smallest p -values were used to construct the heatmap and hierarchical clustering analysis. Euclidean distance and Ward's method were used. Two supervised learning algorithms, PLS-DA and SVM, were built. The Q^2 was reported as a measure of the predictive performance of the PLS-DA model, whereas the cross-validated area under the curve (AUC) of the receiver operating characteristic (ROC) curve was the measure for the SVM algorithm. Permutation tests were used as validation for performance. The variable importance in projection (VIP) scores for compounds are reported, and VIP scores greater than 1 were considered as important.

2.6. Biological Interpretation

Chemical Similarity Enrichment Analysis for Metabolites (ChemRICH) was conducted to calculate metabolite cluster statistics based on chemical similarities. The Kolmogorov–Smirnov test was used on the identified clusters to evaluate whether a metabolite cluster was represented more than expected by chance. These clusters are visualized by bubble plot, where the bubble size indicates the number of metabolites in corresponding cluster and the color indicates the percentage of increased metabolites, with red being 100% and blue being 0%. To visualize the metabolite changes, MetaMapp was used. MetaMapp-encoded chemical structures of all the identified metabolites were retrieved from the PubChem Compound Database using compound identifiers and the NCBI Batch Entrez Utility. MetaMapp uses the Tanimoto chemical similarity co-efficient (range 0.0 to 1.0, where a high score means high similarity between two metabolites) to calculate the similarity among the encoded structures, which are decomposed into a substructure matrix defined by an 881 bit substructure key fingerprint (metamapp.fiehnlab.ucdavis.edu). A Tanimoto score threshold of 0.7 was used to define the similarity cut-off among metabolites. To calculate the metabolite cluster statistics based on the human metabolic pathway-associated metabolite sets, over representation analysis (ORA) was also conducted.

3. Results

3.1. Characteristics of the Study Subjects

BC was clinically diagnosed by physicians at Cedars-Sinai using standard operating procedures (SOPs). Surgical tissue samples were collected through an already established pipeline at the Cedars-Sinai Biobank. In total, 99 deidentified breast tissue samples were obtained (59 BC tumor tissues and 40 normal-adjacent BC tissues).

3.2. Primary Metabolomics Analyses Were Performed via ALEX-CIS-GC-TOF-MS and HILIC-ESI-QTOF-MS/MS

To profile the BC-specific metabolomes, two independent MS platforms were used. They were the automated liner exchange-cold injection system-gas chromatography-time-of-flight-mass spectrometry (ALEX-CIS-GC-TOF-MS) and HILIC-ESI-QTOF-MS/MS, both of which were combined with BinBase data processing. A total of 442 and 559 compounds were detected in the GC and HILIC platforms, respectively. A workflow of this study is shown in Figure 1A.

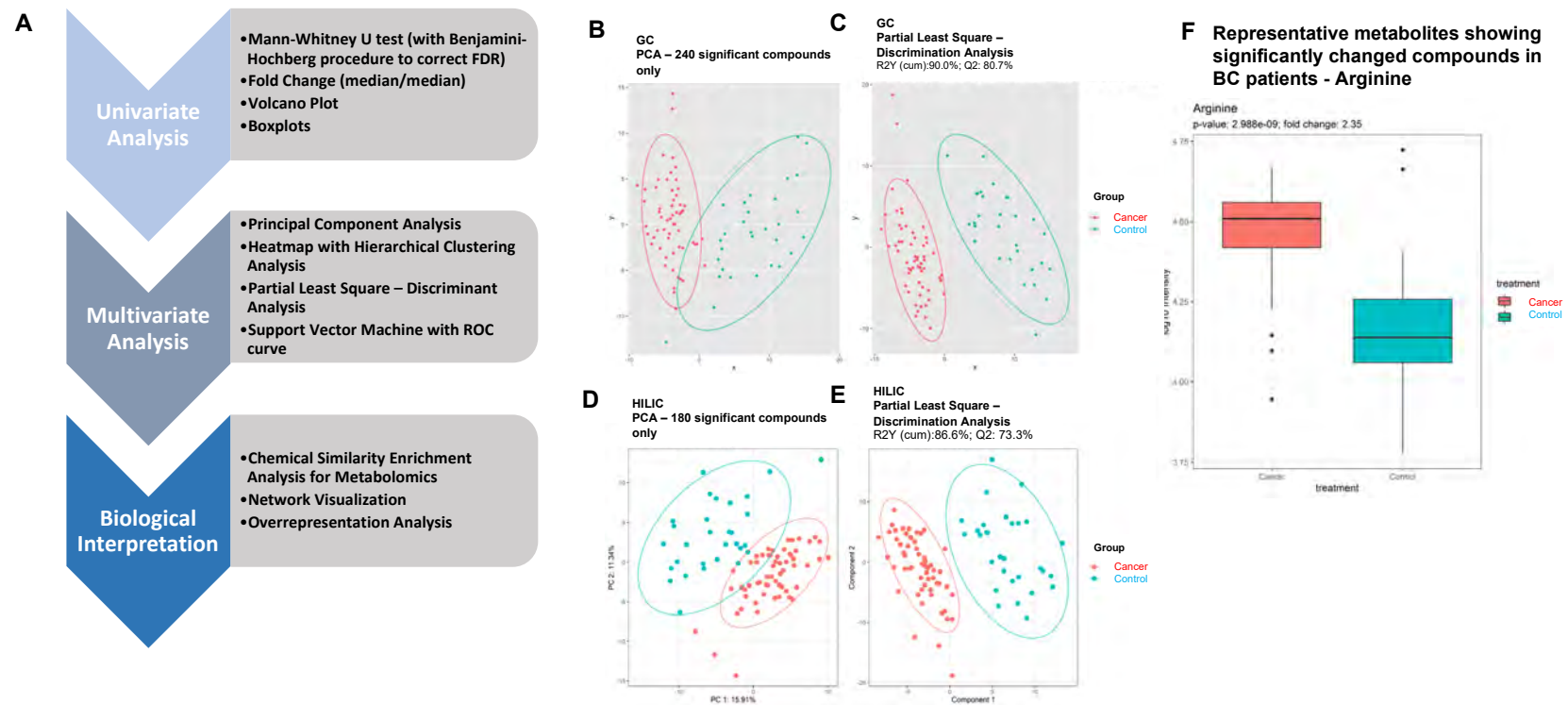


Figure 1. (A) Workflow for this study. (B) Principal component analysis (PCA) score plot visualization using 240 identified metabolites with Mann–Whitney U test raw p -values less than 0.05 in the GC platform. (C) Partial least square–discriminant analysis (PLS-DA) score plot of cancer vs. control. PLS-DA plot shows a clear separation of metabolites between BC patients and controls. Red: control samples; Green: BC patient samples. The model was established using three principal components. Cumulative R2 archived 90.0%, and Q2 achieved 80.7% with permutation test p -values less than 0.05. (D) PCA score plot visualization using 180 identified metabolites with Mann–Whitney U test raw p -values less than 0.05 in the HILIC platform. (E) PLS-DA score plot on cancer vs. control. Cumulative R2 archived 86.6%, and Q2 achieved 73.3% with permutation test p -values less than 0.05. (F) Boxplot of representative metabolite (arginine) showing significant alteration in BC patients.

GC-TOF-MS identified 203 significant differentially expressed metabolites (DEMs), as shown in Supplementary Table S1 (Mann–Whitney U test raw p -values less than 0.05, fold-change > 2 or < 0.5). PCA score plots visualized the results from PCA discrimination analysis (Figure 1B). PLS components showed differentiation of the BC samples (red) from controls (blue) with good separation and dispersion; the cumulative R2Y achieved 90.0%, and Q2 achieved 80.7% with permutation test p -values less than 0.05. (Figure 1C). Metabolomics profiling using HILIC-ESI QTOF MS/MS identified 139 compounds (Supplementary Table S2). Both the PCA score plot (Figure 1D) and PLS components showed great segregation of the BC group from controls. The cumulative R2Y was 86.6% and Q2 was 73.3% with permutation test p -values less than 0.05 (Figure 1E). A representative boxplot (arginine) shows the significantly changed compounds in BC patients compared to controls (Figure 1F).

3.3. Identification of DEMs in BC Patients

Among the 203 DEMs identified by GC-TOF-MS, only the top 25 DEMs, with fold-change > 1.20 or < 0.83 and p -values < 0.1 were selected and constructed into a heat map (Figure 2A). The heat map exhibits the distinct patterns of metabolites between BC and controls. These 25 DEMs are presented as \log_2 fold-changes against the $-\log_{10}(p)$ of the differential expression between BC and control samples.

Significantly altered metabolites distinguishing cancer and control samples were acquired based on the Mann–Whitney U test $p < 0.05$, fold-change > 2 or < 0.5 , and $VIP > 1$ (Figure 2B). A total of nine example metabolites were chosen for box-whisker plots (\log_{10} scale) to visualize differences (Figure 2D). Outliers in these boxplots are defined as those greater than the 1.5 interquartile range (IQR). The volcano plots highlight metabolites with FDR p -values < 0.05 and fold-change > 1.5 or < 0.5 . In total, there were 18 and 13 metabolites highlighted in the GC and HILIC platforms, respectively.

The levels of glycerol (fold-change of 3.10), glutamine (1.47), glucose-1-phosphate (1.44), benzoic acid (1.38), palmitic acid (1.47), urea (1.40), pyrophosphate (1.76), serotonin (1.70), docosahexaenoic acid (1.54) were significantly increased in the BC group compared to controls, with adjusted p -values < 0.001 . In contrast, levels of 2,3-bisphosphoglyceric acid (fold-change of 0.027), fructose (0.40), lactamide (0.36), N-acetylmethionine (0.34), lactic acid (0.43), maleic acid (0.60), cysteine-glycine (0.55), glycerol-alpha-phosphate (0.41), aspartic acid (0.63), pyruvic acid (0.38), and lactulose (0.20) were significantly decreased in the BC group compared to control, with adjusted p -values < 0.001 (Figure 2B).

A volcano plot (Figure 2C) and additional box plots (Figure 2D) show several representative DEMs whose expression were up- or downregulated in the BC group. The significant compounds with p -values less than 0.05 were used to conduct the PCA, with PC1 explaining 16% variance, and a PC2 of 11%. A clear separation between cancer and control samples are observed. The PLS-DA achieved a Q2 of 73.3%, with permutation test p -value less than 0.05, indicating a good predicting performance. The VIP score for each compound is reported in Figure 2B.

Given that *different* analytical instruments for metabolomics profiling each have their own advantages and disadvantages, a smarter and innovative approach is to combine datasets *across* analytical *platforms* for more comprehensive coverage. A total of 139 DEMs was identified by HILIC-ESI-QTOF-MS/MS, of which the top 25 are shown in a heatmap (Figure 3A). These DEMs include arginine (fold-change of 2.35), carnitine (1.71), cystine (1.71), betaine (1.53), urea (1.33), glutamine (1.30), alanine (0.80), and maltose (0.20) (Figure 3B). Through an independent analysis (data not shown), a total of 23 known metabolites were shared across two different MS platforms with identical direction of expression changes. A volcano plot shows the representative DEMs whose expression were significantly altered in BC compared to controls (Figure 3C). The most significant DEMs are presented as box plots in Figure 3D. The expression levels of glutamine, citrulline, and urea were commonly upregulated in BC regardless of the analytical platform (Figures 2 and 3).

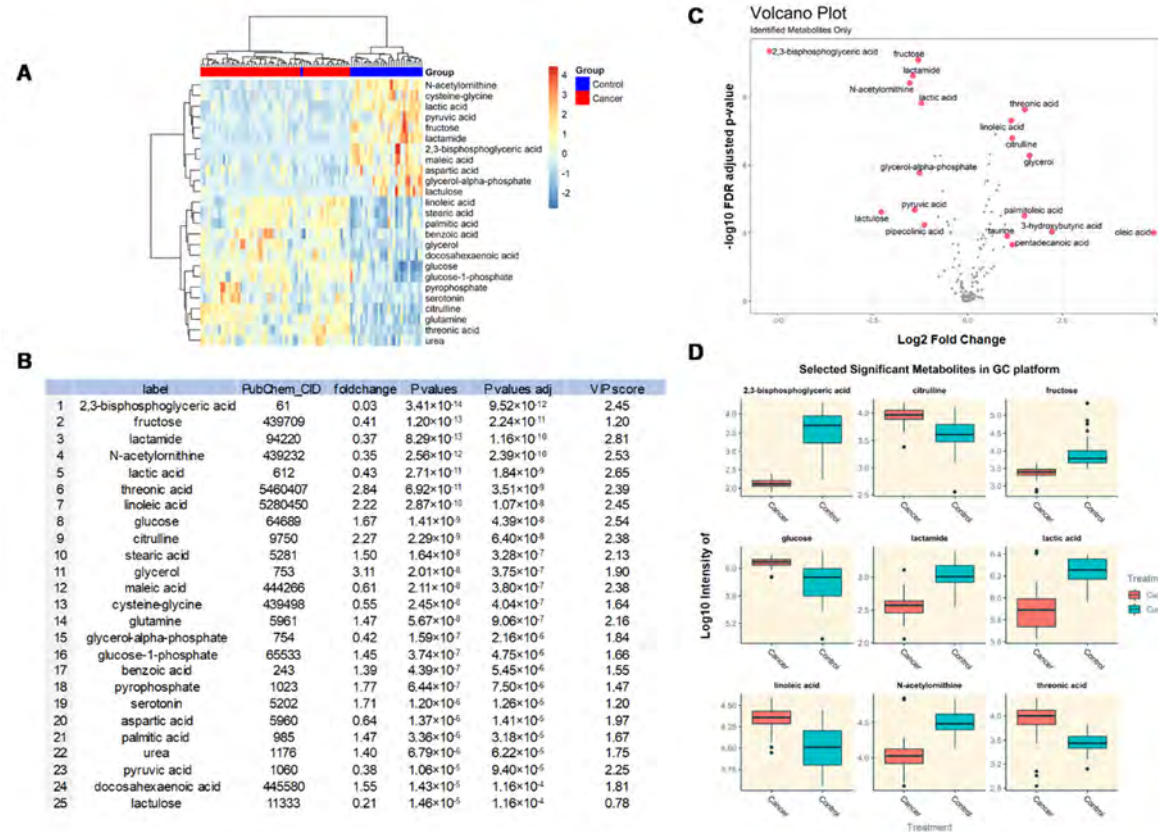


Figure 2. (A) Heatmap of identified metabolites in the GC platform showing the 25 differentially expressed metabolites (DEMs) between BC and control groups with the smallest Mann-Whitney U test *p*-values. Euclidean distance metric and Ward's clustering method was used for the hierarchical clustering of samples and compounds. (B) A table summarizing the 25 identified metabolites and their statistical values. Fold-changes are presented as median average of cancer divided by control. False discovery rate-adjusted *p*-values using the Benjamini–Hochberg procedure are reported at the last column. VIP score for each compound is reported in Figure 3B (VIP > 1 highlighted as red). (C) Volcano plot with annotated metabolites that were significantly altered in BC patients compared to controls. The red dots represent metabolites above the threshold. The further the metabolite's position away from the (0, 0), the more significant the metabolite is. Volcano plot visualizes the $-\log_{10}$ adjusted *p*-values and \log_2 fold-changes. Metabolites with adjusted *p*-values less than 0.05 and a fold-change greater than 2-fold or less than 1/2-fold are highlighted and labeled. (D) Selected boxplots of metabolites showing the most significant changes in the GC platform.

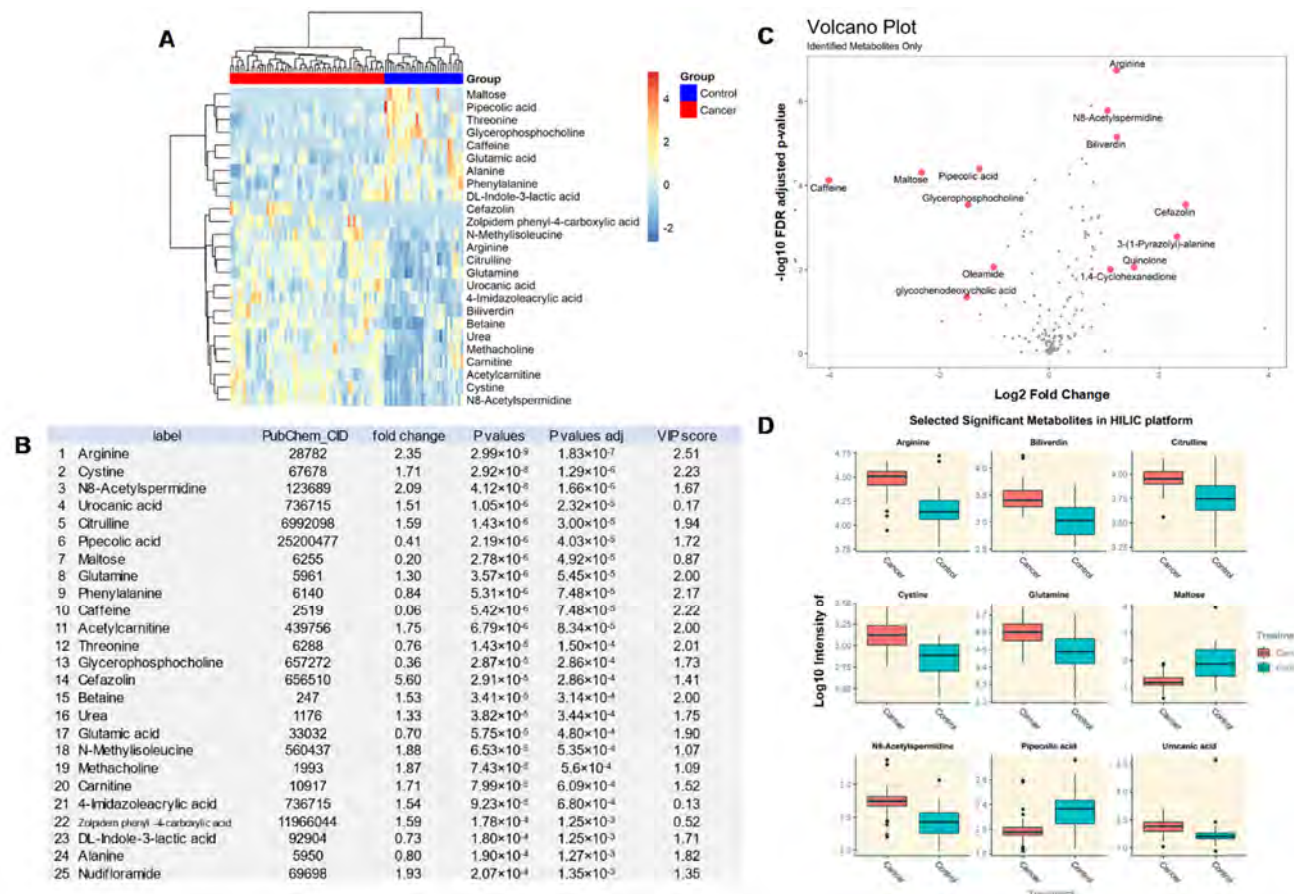


Figure 3. (A) Heatmap of identified metabolites in HILIC platform with the top 25 DEMs with the smallest Mann–Whitney U test *p*-values, comparing BC to control. Euclidean distance metric and Ward’s clustering method was used for the hierarchical clustering of samples and compounds. (B) The 25 identified metabolites are listed. Fold-changes are presented as the median average of cancer divided by control. False discovery rate-adjusted *p*-values using the Benjamini–Hochberg procedure are reported at the last column. VIP score for each compound is reported in Figure 3B (VIP > 1 highlighted as red). (C) Volcano plot visualizes the $-\log_{10}$ adjusted *p*-values and \log_2 fold-changes. Metabolites with adjusted *p*-values less than 0.05 and fold-change greater than 2-fold or less than 0.5 fold are highlighted and labeled. (D) Select example metabolite boxplots from the HILIC platform showing significant differences between BC and control.

3.4. ROC Curves of SVM.

To predict the probability of a binary outcome, ROC curves of SVM were used with leave-one-out cross-validation. SVM was applied to distinguish cancer and control using significant compounds. To avoid the overfitting issue, the leave-one-out procedure was used when calculating the AUC of the ROC curve. The AUC was calculated using metabolites with adjusted p -values less than 0.05 from both the GC-TOF-MS and HILIC-ESI-QTOF-MS/MS platforms. The calculated AUCs were 1 and 0.927 for GC-TOF-MS and HILIC-ESI-QTOF-MS/MS, respectively (Figure 4). These data suggest that our model has a strong predicting power and reflects great differentiation capability. The permutation test returned a p -value less than 0.0001, showing that the model is validated and further guaranteed for non-overfitting.

3.5. ChemRICH Plots of BC-Associated Metabolites

Next, we aimed to understand the biological meaning of the BC-specific metabolomes. Since biological interpretations of metabolic regulation in metabolomic datasets can be limited due to incomplete pathway definitions and enrichment statistics, ChemRICH, a newly developed pathway mapping tool, was applied [22]. Instead of traditional MSEA, which is determined by pre-defined compound cluster database, ChemRICH uses chemical ontologies and structure similarities to group metabolites. p -values in ChemRICH are calculated using a self-contained Kolmogorov–Smirnov (KS) test and clusters metabolites into non-overlapping chemical groups rather than sparse biochemical knowledge annotations [26].

The plot in Figure 5A shows the ChemRICH enrichment results with the most significantly impacted metabolite clusters of BC-specific DEMs ($p < 0.05$). The most significantly altered clusters were the trimethyl ammonium compounds (p -value = 5.1×10^{-13} ; false discovery rate = 1.3×10^{-11}), which are located on the top of the plot y-axis in Figure 5A. The cluster colors give the proportion of increased or decreased compounds (red = increased, blue = decreased, purple = the most decreased). Several clusters, including the saturated fatty acid (FA) cluster (stearic acid as key component), unsaturated FA cluster (linoleic acid as key component), sugar alcohols (glycerol as key component), and carnitine (acetylcarnitine as key component), were found to be greatly increased in BC (Figure 5B). There were 11 metabolite clusters enriched with false discovery rate p -values less than 0.05. They include trimethyl ammonium compounds, saturated FA, sugar acids, disaccharides, histidine, unsaturated FA, basic amino acids, basic carnitine, sugar alcohols, diamino, and hexoses (Figure 5B).

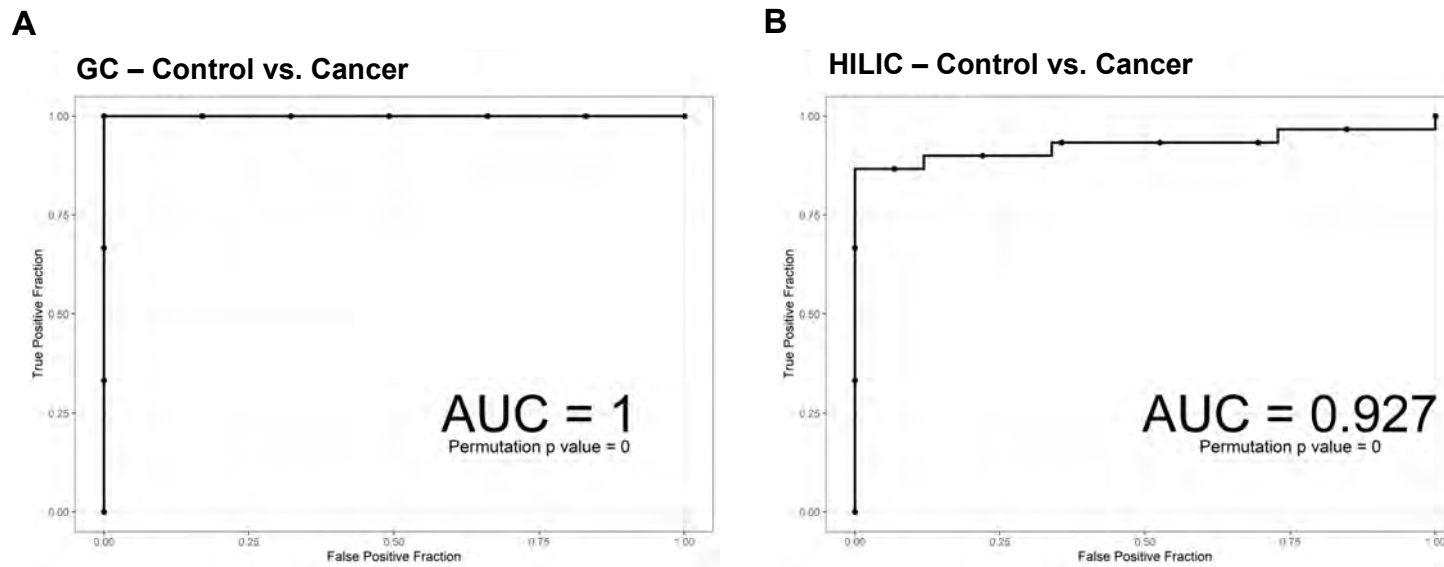


Figure 4. (A, B) Receiver operating characteristic (ROC) curves of support vector machine (SVM) with leave-one-out cross-validation of the area under the curve (AUC) using metabolites with adjusted *p*-values less than 0.05 in the GC (A) or HILIC platforms (B), respectively.

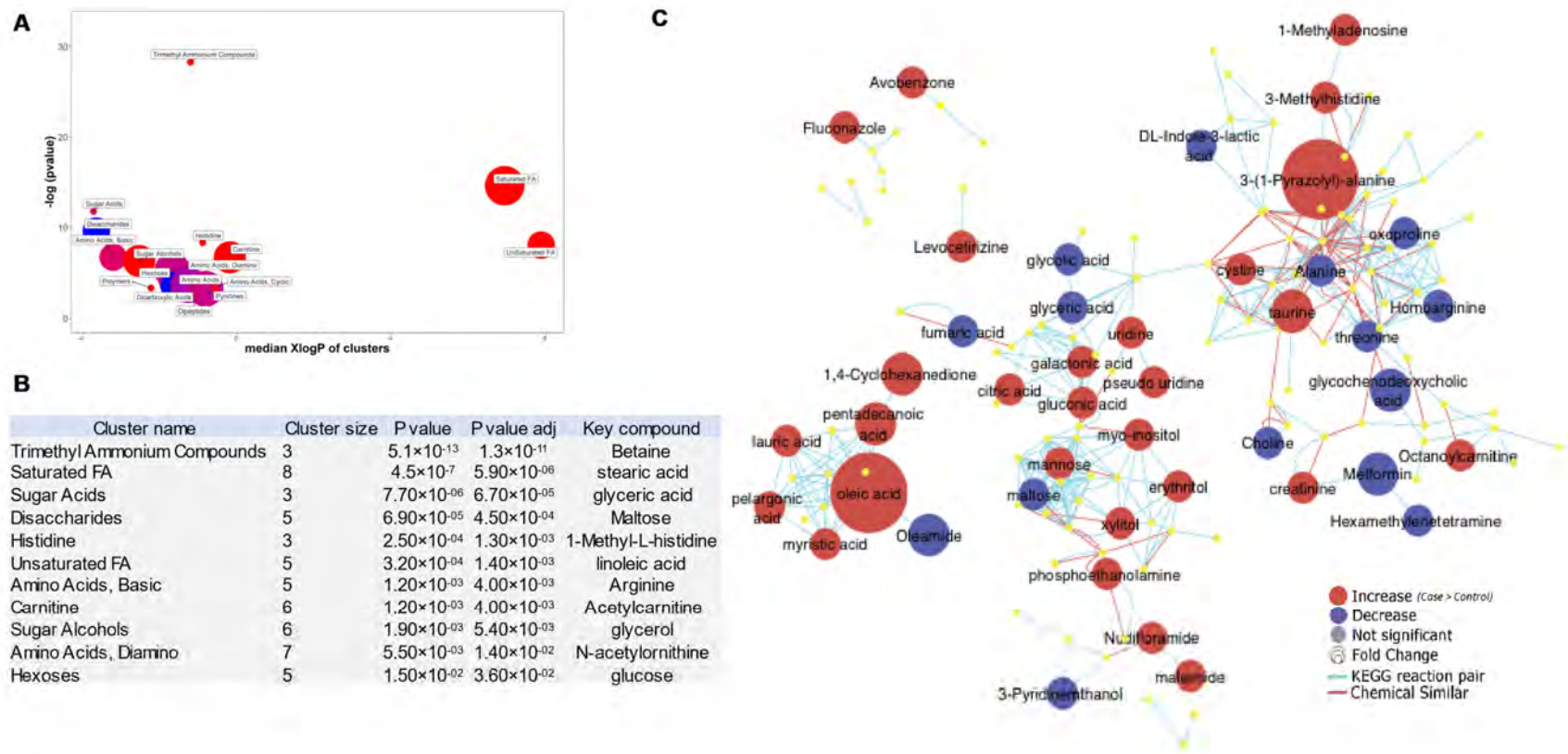
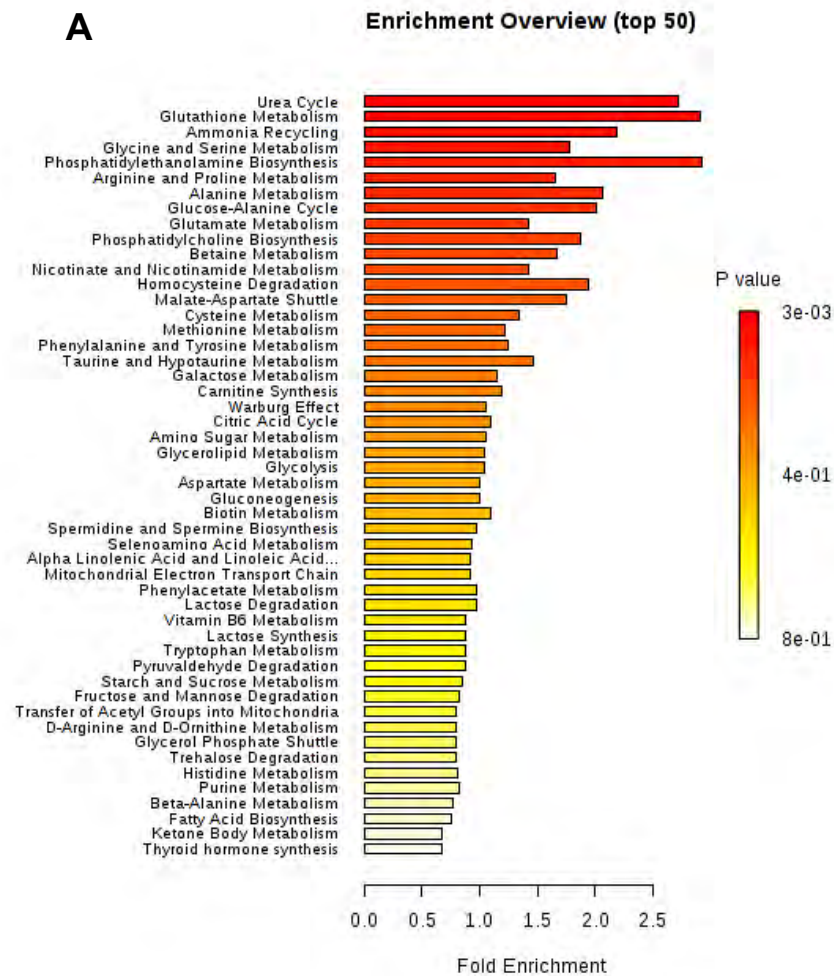


Figure 5. (A) ChemRICH analysis plot. Y-axis shows the most significantly altered clusters. Cluster color shows the proportion of increased or decreased metabolites compared to control (red = increased, blue = decreased, purple = mostly decreased). Cluster size indicates the number of compounds in each cluster. Chemical enrichment statistics were calculated by the Kolmogorov–Smirnov test. Only significantly different enrichment clusters (raw $p < 0.05$) are shown. (B) Statistics table for metabolite clusters. (C) MetaMapp metabolite network visualization. Red nodes indicate increased metabolites in BC compared to control, while the blue indicates a decrease. Node size indicates the magnitude of fold change. Compounds are connected by KEGG reaction pair (blue line), and chemical similarity (red line).

Next, to efficiently map and visualize the metabolomic data, MetaMapp, a tool for integrating information from biochemical pathways and chemical and mass spectral similarity was used [23]. MetaMapp is able to map all detected metabolites into network graphs using the KEGG reactant pair database and Tanimoto chemical and National Institute of Standards and Technology (NIST) mass spectral similarity scores. Although Cytoscape (www.cytoscape.org) has been widely used for differential network visualizations and subnetwork identification, MetaMapp graphs in Cytoscape show clearer metabolic modularity and complete content visualization compared to conventional biochemical mapping approaches (<http://metamapp.fiehnlab.ucdavis.edu>) [27]. MetaMapp analysis revealed that several metabolites act as key players in the BC-specific metabolome. Red nodes reflect the metabolites found to be significantly upregulated in BC (p -value < 0.05) while those that are downregulated are shown as blue. The node sizes correlate with fold-change. Metabolites that were not found to be differentially regulated or “unknown” were left unlabeled for visual clarity. Red edges denote KEGG reactant pair links. Blue edges denote Tanimoto chemical similarity with $T > 700$. MetaMapp uses biochemical reaction pair information (Figure 5, blue lines) and chemical similarity (Figure 5, red lines) to create an overview of metabolic regulation. It clearly visible that saturated and unsaturated FAs are most upregulated, while disaccharides are the most downregulated. Oleic acid as well as 3-(1-Pyrazolyl)-alanine are two major central metabolites linked to many other metabolites upregulated in BC (Figure 5C).

3.6. Top 50 Metabolic Pathway-Associated DEMs Sets

Over representation analysis (ORA), as shown in Figure 6, was done to detect the impact of pathways, depending on the number of changed metabolites, and to test if a group of compounds was represented more than expected by chance. In the context of pathway analysis, compounds involved in a pathway are enriched and compared by random hits as tested. Detailed results from the pathway analysis are depicted in Figure 6A. Urea cycle, glutathione metabolism, ammonia recycling, glycine and serine metabolism, phosphatidylethanolamine biosynthesis, arginine and proline metabolism were found to be significant, with p -values less than 0.1 (Figure 6B).



B

	total	expected	hits	Raw p
Urea Cycle	29	3.31	9	0.00338
Glutathione Metabolism	21	2.4	7	0.0063
Ammonia Recycling	32	3.66	8	0.0226
Glycine and Serine Metabolism	59	6.74	12	0.0288
Phosphatidylethanolamine Biosynthesis	12	1.37	4	0.0387

Figure 6. (A) Summary plot for over representation analysis (ORA) on metabolites with Mann-Whitney U test raw *p*-values less than 0.05. Top 50 metabolic pathway-associated metabolite sets are shown. (B) Five significant metabolic pathways with *p*-values less than 0.05. Top 50 metabolic pathway-associated metabolite sets are shown. (B) Five significant metabolic pathways with *p*-values less than 0.05.

4. Discussion

In this study, two independent analytic platforms combined with chemical similarity-based mapping and visualization tools revealed central clusters and network models in human BC tissue specimens. Both independent metabolomics' profiling analyses suggested that glutamine metabolism, phosphatidylethanolamine biosynthesis, urea cycle, and ammonia recycling were significantly associated with BC. In addition, ChemRICH revealed trimethyl ammonium compounds, saturated FAs, and sugar acids as being the most significantly enriched metabolite clusters (false discovery rate adjusted p -values < 0.001) in BC compared to controls.

The data from this study showed that metabolites, including glutamine, citrulline, and urea, are upregulated in BC. Alterations in metabolism in BC has been reported to be characteristic of highly diverse BC. FA and glutamine [28] metabolisms are well-known in aggressive BC types, such as triple-negative BC (TNBC), whose expression of ASCT2/SLC1A5 (alanine, serine, cysteine-preferring transporter 2) was found to be increased. Enhanced glutamine metabolism is linked with protein and nucleotide synthesis in cancer [29,30]. Glutamine provides biosynthesis substrates, such as carbon and nitrogen, and acts as an energy resource through ATP biosynthesis. The inhibition of glutaminase exhibited antitumor activity in both the *in vitro* and *in vivo* BC models [31]. The metabolic signatures were linked to BC subtypes. The ER- subtype showed reprogrammed glutamine metabolism compared to the ER+ subtype [32,33]. Additionally, the ER- subtype is a preferential target for glutaminase inhibitors.

Our results showed increased citrulline in BC patients. However, the mechanisms behind this increase in citrulline remain unclear. Citrulline is a naturally occurring non-essential amino acid and an intermediate in the urea cycle. It is also a direct precursor of arginine, and its metabolic activity is mainly a result of its close link with arginine metabolism. There are three parallel metabolic transformations of citrulline, including arginine biosynthesis and the arginine–citrulline–nitric oxide (NO) cycle [34]. Citrulline is synthesized by ornithine transcarbamylase from ornithine and metabolized by argininosuccinate synthase in the urea cycle [35]. Alterations in the expression of urea cycle enzymes in BC [36] have revealed a revolutionary mechanism to maximize nitrogen incorporation into biomass [37]. The rewiring of urea cycle enzymes and the role of citrulline in cancer notes a new and exciting era for cancer metabolic studies. Further investigation into the functions of citrulline and its alterations is warranted and could lead to the identification of more effective therapeutic strategies against BC.

The data from this study also suggest that oleic and linoleic acid are enriched in BC, which is consistent with previous observations noting that changes in lipid metabolism are established hallmarks of BC [38]. Breast epithelial cells are embedded within a fat environment, which suggests that potential metabolites or substrates that are released during adipose lipolysis may be contributing to cancer progression [39]. We found that arginine, glutathione and sugar metabolism, and polyamines are altered in BC. Interestingly, arginine is involved in polyamine synthesis, which was found to also be implicated in BC [40–42]. Free fatty acids (FFAs) are an energy source and can induce activation of signal transduction pathways in BC cells [43]. However, the mechanisms through which altered FFA metabolism drives relapse has not been addressed. Oleic acid is one of the most common monounsaturated FFA in human adipocytes and other tissues [44]. Our analysis demonstrated that oleic acid is associated with BC compared to controls. Oleic acid prompts cell proliferation and migration in metastatic cancer through various pathways, including EGFR, AKT and NF- κ B [45]. Linoleic acid is an essential and omega-6 polyunsaturated FA, which constitutes a major component of FAs in occidental diets. High fat diet intake has previously been shown to be associated with increased risk of BC [46]. Linoleic acid mediates a variety of cellular processes, including expression of plasminogen activator inhibitor-1 and cellular migration and invasion, and can induce an epithelial-to-mesenchymal transition-like process in BC [47]. Based on our metabolic observations, it could be postulated that the FFAs microenvironment might favor tumor progression, which provides novel potential targets for the chemoprevention of human cancer.

Current metabolomics biochemical knowledge/databases and mapping tools have limited coverage of detected metabolites. In order to resolve the shortcomings of mapping approaches and data visualization and to improve pathway analysis, we adopted ChemRICH and MetaMapp, which were recently developed in Fiehn laboratory. In this study, to better understand the metabolic signatures specific to BC and control groups, we performed ChemRICH and used Mann–Whitney U test p -values and median fold-changes to identify metabolites. To evaluate whether a metabolite cluster was represented more than expected by chance, the Kolmogorov–Smirnov test was performed on the identified clusters.

ChemRICH identifies enriched pathways using chemical similarity from medical subject headings and Tanimoto substructure chemical similarity coefficients. ChemRICH is useful for translating data obtained from clinical specimens, although it does not provide information regarding enzymes or diseases.

While conserving biochemical organization, the constructed MetaMapp-integrated network graph displays the key metabolites associated with BC. Significantly upregulated metabolites are denoted as red nodes and labeled with their respective BinBase names, while those downregulated are denoted as blue (p -value < 0.05). The node sizes are reflective of the amount of fold-change. Metabolites that were not differentially regulated in BC or unknown were left unlabeled for clarity. KEGG reactant pair links are reflected as red edges. Tanimoto chemical similarity, with $T > 0.7$, is reflected through blue edges. A MetaMapp-integrated network graph has several advantages. Firstly, the data are independent of the methodology used to acquire metabolomics profiles (i.e., MS or NMR). This allows for integration and visualization of data from different platforms. However, the only requirement is that all chemical structures are already encoded. Secondly, genomics is not a constraining factor when using MetaMapp. Detected metabolites can be mapped across studies or species; for instance, metabolites can be mapped from gut microbes to compounds that stem from mammalian enzymes. Lastly, the MetaMapp layout is dynamic and automatically updates based on the input of compound lists. As a result, MetaMapp graphs enable higher biochemical clarity despite having larger metabolic nodes. Since MetaMapp outputs are compatible with Cytoscape, next-generation metabolomic datasets with greater identified metabolites and integration of genomic and proteomic data can be visualized.

However, there are several shortcomings with MetaMapp. It cannot be used to compute flux or enzymatic reactions among metabolites. Although it is scalable to an extent, adding large numbers of nodes can lead to blurring. This was seen when we added a higher number of unknowns based on MS similarity. The visual clarity of MetaMapp can also decrease when statistical results are combined from further comparisons. As a result, multiple two-way graphs are recommended for displaying more complex biological studies.

We are aware there are some limitations in this study. First, subjects were not excluded based on menopausal status, so it is impossible to rule out hormone-related effects on data. Second, biospecimens were not obtained from the same patients or compared directly, although the aim of the current study was to explore potential BC biomarkers. Thus, we do not have detail clinical information such as the mutational status of collected tumours, which is a big limitation of this study. Further investigation into BC patients with different molecular characteristics will provide evidence suggesting potential prognostic and diagnostic tools for precision medicine. To further develop metabolic inhibitors as clinical regimens with existing therapies for BC patients, it is be critical to understand the heterogeneity in metabolism and targetable metabolic vulnerabilities in BC.

In summary, BC displays heterogeneous metabolic profiles similarly so unbiased global metabolomics profiling can reveal overlapped metabolic vulnerabilities in different BC types. The findings from this study provide another layer of evidence suggesting key metabolic players in BC. This can be further developed into therapeutic strategies to hinder or delay aggressive BC progression.

Supplementary Materials: The following are available online at <http://www.mdpi.com/2218-1989/10/4/170/s1>, Table S1: GC-TOF-MS identified significant differentially expressed metabolites, Table S2: Metabolomics profiling using HILIC-ESI QTOF MS/MS identified compounds.

Author Contributions: J.K., and A.A. designed the study, led obtaining funding, and overviewed the literature analysis and drafting the manuscript. S.F., M.S., and P.J. performed metabolomics analysis and sample preparation. S.F., and J.K. performed data analysis and visualize the data. S.F., M.S., P.J., and A.A. helped writing the manuscript. All authors read and approved the final manuscript.

Funding: This research was funded by National Institutes of Health (1U01DK103260, 1R01DK100974, U24 DK097154, NIH NCATS UCLA CTSI UL1TR000124), Department of Defense (W81XWH-15-1-0415 and W81XWH-19-1-0109), Centers for Disease Controls and Prevention (1U01DP006079), and the U.S.-Egypt Science and Technology Development Fund by the National Academies of Sciences, Engineering, and Medicine (all to J.K.). The funders had no role in the design, data collection and analysis, decision to publish or preparation of the manuscript.

Acknowledgments: This research was supported by the Samuel Oschin Comprehensive Cancer Institute (SOCCI) at Cedars-Sinai Medical Center through 2019 Lucy S. Gonda Award.

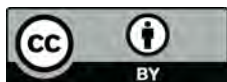
Conflicts of Interest: The authors declare that there is no conflict of interests regarding the publication of this paper.

References

1. DeSantis, C.E.; Ma, J.; Goding Sauer, A.; Newman, L.A.; Jemal, A. Breast cancer statistics, 2017, racial disparity in mortality by state. *CA Cancer J. Clin.* **2017**, *67*, 439–448. [[CrossRef](#)] [[PubMed](#)]
2. Jafari, S.H.; Saadatpour, Z.; Salmaninejad, A.; Momeni, F.; Mokhtari, M.; Nahand, J.S.; Rahmati, M.; Mirzaei, H.; Kianmehr, M. Breast cancer diagnosis: Imaging techniques and biochemical markers. *J. Cell Physiol.* **2018**, *233*, 5200–5213. [[CrossRef](#)] [[PubMed](#)]
3. Wang, L. Early Diagnosis of Breast Cancer. *Sensors* **2017**, *17*, 1572. [[CrossRef](#)] [[PubMed](#)]
4. Donepudi, M.S.; Kondapalli, K.; Amos, S.J.; Venkanteshan, P. Breast cancer statistics and markers. *J. Cancer Res. Ther.* **2014**. [[CrossRef](#)]
5. Duffy, M.J. Serum Tumor Markers in Breast Cancer: Are They of Clinical Value? *Clin. Chem.* **2006**, *52*, 345–351. [[CrossRef](#)]
6. Green, D.R.; Galluzzi, L.; Kroemer, G. Metabolic control of cell death. *Science* **2014**, *345*, 1250256. [[CrossRef](#)]
7. Hart, C.D.; Tenori, L.; Luchinat, C.; Di Leo, A. Metabolomics in Breast Cancer: Current Status and Perspectives. *Adv. Exp. Med. Biol.* **2016**, *882*, 217–234. [[CrossRef](#)]
8. Hanahan, D.; Weinberg, R.A. Hallmarks of Cancer: The Next Generation. *Cell* **2011**, *144*, 646–674. [[CrossRef](#)]
9. Network, C.G.A.; Network, T.C.G.A.; Koboldt, D.C.; Fulton, R.S.; McLellan, M.; Schmidt, H.; Kalicki-Veizer, J.; McMichael, J.F.; Fulton, L.L.; Dooling, D.J.; et al. Comprehensive molecular portraits of human breast tumours. *Nature* **2012**, *490*, 61–70. [[CrossRef](#)]
10. Bathen, T.F.; Sitter, B.; Tessem, M.-B.; Gribbestad, I.S.; Sjøbakk, T.E. Magnetic Resonance Metabolomics of Intact Tissue: A Biotechnological Tool in Cancer Diagnostics and Treatment Evaluation. *Cancer Res.* **2010**, *70*, 6692–6696. [[CrossRef](#)]
11. Coleman, W.B. Next-Generation Breast Cancer Omics. *Am. J. Pathol.* **2017**, *187*, 2130–2132. [[CrossRef](#)] [[PubMed](#)]
12. Cha, Y.J.; Kim, E.-S.; Koo, J.S. Amino Acid Transporters and Glutamine Metabolism in Breast Cancer. *Int. J. Mol. Sci.* **2018**, *19*, 907. [[CrossRef](#)] [[PubMed](#)]
13. Bhutia, Y.D.; Babu, E.; Ramachandran, S.; Ganapathy, V. Amino Acid Transporters in Cancer and Their Relevance to “Glutamine Addiction”: Novel Targets for the Design of a New Class of Anticancer Drugs. *Cancer Res.* **2015**, *75*, 1782–1788. [[CrossRef](#)] [[PubMed](#)]
14. Bernhardt, S.; Bayerlová, M.; Vetter, M.; Wachter, A.; Mitra, D.; Hanf, V.; Lantzsch, T.; Uleer, C.; Peschel, S.; John, J.; et al. Proteomic profiling of breast cancer metabolism identifies SHMT2 and ASCT2 as prognostic factors. *Breast Cancer Res.* **2017**, *19*, 112. [[CrossRef](#)]
15. Karunakaran, S.; Ramachandran, S.; Coothankandaswamy, V.; Elangovan, S.; Babu, E.; Periyasamy-Thandavan, S.; Gurav, A.; Gnanaprakasam, J.P.; Singh, N.; Schoenlein, P.V.; et al. SLC6A14 (ATB0,+) Protein, a Highly Concentrative and Broad Specific Amino Acid Transporter, Is a Novel and Effective Drug Target for Treatment of Estrogen Receptor-positive Breast Cancer. *J. Biol. Chem.* **2011**, *286*, 31830–318384. [[CrossRef](#)]
16. Furuya, M.; Horiguchi, J.; Nakajima, H.; Kanai, Y.; Oyama, T. Correlation of L-type amino acid transporter 1 and CD98 expression with triple negative breast cancer prognosis. *Cancer Sci.* **2011**, *103*, 382–389. [[CrossRef](#)]

17. Ulaner, G.A.; Schuster, D.M. Amino Acid Metabolism as a Target for Breast Cancer Imaging. *PET Clin.* **2018**, *13*, 437–444. [[CrossRef](#)]
18. Leskinen-Kallio, S.; Någren, K.; Lehtikainen, P.; Ruotsalainen, U.; Joensuu, H. Uptake of ¹¹C-methionine in breast cancer studied by PET. An association with the size of S-phase fraction. *Br. J. Cancer* **1991**, *64*, 1121–1124. [[CrossRef](#)]
19. Tade, F.I.; Cohen, M.; Styblo, T.M.; Odewole, O.A.; Holbrook, A.I.; Newell, M.S.; Savir-Baruch, B.; Li, X.B.; Goodman, M.M.; A Nye, J.; et al. Anti-3-[¹⁸F] FACBC (Fluciclovine) PET-CT of Breast Cancer An Exploratory Study. *J. Nucl. Med.* **2016**, *57*, 1357–1363. [[CrossRef](#)]
20. Haukaas, T.H.; Euceda, L.R.; Giskeødegård, G.F.; Bathen, T.F. Metabolic Portraits of Breast Cancer by HR MAS MR Spectroscopy of Intact Tissue Samples. *Metabolites* **2017**, *7*, 18. [[CrossRef](#)]
21. Kind, T.; Tolstikov, V.; Fiehn, O.; Weiss, R. A comprehensive urinary metabolomic approach for identifying kidney cancer. *Anal. Biochem.* **2007**, *363*, 185–195. [[CrossRef](#)]
22. Kind, T.; Wohlgemuth, G.; Lee, Y.; Lu, Y.; Palazoglu, M.; Shahbaz, S.; Fiehn, O. FiehnLib: Mass Spectral and Retention Index Libraries for Metabolomics Based on Quadrupole and Time-of-Flight Gas Chromatography/Mass Spectrometry. *Anal. Chem.* **2009**, *81*, 10038–10048. [[CrossRef](#)]
23. Szymańska, E.; Saccenti, E.; Smilde, A.K.; Westerhuis, J.A. Double-check: Validation of diagnostic statistics for PLS-DA models in metabolomics studies. *Metabolomics* **2012**, *8* (Suppl. 1), 3–16. [[CrossRef](#)] [[PubMed](#)]
24. Sumner, L.W.; Amberg, A.; Barrett, D.; Beale, M.H.; Beger, R.D.; Daykin, C.A.; Fan, T.W.-M.; Fiehn, O.; Goodacre, R.; Griffin, J.; et al. Proposed minimum reporting standards for chemical analysis Chemical Analysis Working Group (CAWG) Metabolomics Standards Initiative (MSI). *Metabolomics* **2007**, *3*, 211–221. [[CrossRef](#)] [[PubMed](#)]
25. Fiehn, O.; Wohlgemuth, G.; Scholz, M.; Kind, T.; Lee, Y.; Lu, Y.; Moon, S.; Nikolau, B. Quality control for plant metabolomics: Reporting MSI-compliant studies. *Plant J.* **2008**, *53*, 691–704. [[CrossRef](#)] [[PubMed](#)]
26. Barupal, D.K.; Fiehn, O. Chemical Similarity Enrichment Analysis (ChemRICH) as alternative to biochemical pathway mapping for metabolomic datasets. *Sci. Rep.* **2017**, *7*, 14567. [[CrossRef](#)]
27. Barupal, D.K.; Haldiya, P.K.; Wohlgemuth, G.; Kind, T.; Kothari, S.L.; Pinkerton, K.E.; Fiehn, O. MetaMapp: Mapping and visualizing metabolomic data by integrating information from biochemical pathways and chemical and mass spectral similarity. *BMC Bioinform.* **2012**, *13*, 99. [[CrossRef](#)]
28. Van Geldermalsen, M.; Wang, Q.; Nagarajah, R.; Marshall, A.; Thoeng, A.; Gao, D.; Ritchie, W.; Feng, Y.; Bailey, C.; Deng, N.; et al. ASCT2/SLC1A5 controls glutamine uptake and tumour growth in triple-negative basal-like breast cancer. *Oncogene* **2015**, *35*, 3201–3208. [[CrossRef](#)]
29. DeBerardinis, R.J.; Mancuso, A.; Daikhin, E.; Nissim, I.; Yudkoff, M.; Wehrli, S.; Thompson, C.B. Beyond aerobic glycolysis: Transformed cells can engage in glutamine metabolism that exceeds the requirement for protein and nucleotide synthesis. *Proc. Natl. Acad. Sci. USA* **2007**, *104*, 19345–19350. [[CrossRef](#)]
30. Duran, R.V.; Oppliger, W.; Robitaille, A.M.; Heiserich, L.; Skendaj, R.; Gottlieb, E.; Hall, M.N. Glutaminolysis Activates Rag-mTORC1 Signaling. *Mol. Cell* **2012**, *47*, 349–358. [[CrossRef](#)]
31. Gross, M.I.; Demo, S.D.; Dennison, J.B.; Chen, L.; Chernov-Rogan, T.; Goyal, B.; Janes, J.R.; Laidig, G.J.; Lewis, E.R.; Li, J.; et al. Antitumor Activity of the Glutaminase Inhibitor CB-839 in Triple-Negative Breast Cancer. *Mol. Cancer Ther.* **2014**, *13*, 890–901. [[CrossRef](#)] [[PubMed](#)]
32. Cappelletti, V.; Iorio, E.; Miodini, P.; Silvestri, M.; Dugo, M.; Daidone, M.G. Metabolic Footprints and Molecular Subtypes in Breast Cancer. *Dis. Markers* **2017**, *2017*, 7687851. [[CrossRef](#)] [[PubMed](#)]
33. Budczies, J.; Brockmüller, S.; Müller, B.M.; Barupal, D.K.; Richter-Ehrenstein, C.; Kleine-Tebbe, A.; Griffin, J.L.; Orešič, M.; Dietel, M.; Denkert, C.; et al. Comparative metabolomics of estrogen receptor positive and estrogen receptor negative breast cancer: Alterations in glutamine and beta-alanine metabolism. *J. Proteom.* **2013**, *94*, 279–288. [[CrossRef](#)]
34. Husson, A.; Brasse-Lagnel, C.; Fairand, A.; Renouf, S.; Lavoine, A. Argininosuccinate synthetase from the urea cycle to the citrulline-NO cycle. *JBIC J. Boil. Inorg. Chem.* **2003**, *270*, 1887–1899. [[CrossRef](#)] [[PubMed](#)]
35. A Barzał, J.; Szczylik, C.; Rzepecki, P.; Jaworska, M.; Anuszevska, E. Plasma citrulline level as a biomarker for cancer therapy-induced small bowel mucosal damage. *Acta Biochim. Pol.* **2014**, *61*. [[CrossRef](#)]
36. Gandhi, N.; Das, G. Metabolic Reprogramming in Breast Cancer and Its Therapeutic Implications. *Cells* **2019**, *8*, 89. [[CrossRef](#)]
37. Keshet, R.; Szlosarek, P.; Carracedo, A.; Erez, A. Rewiring urea cycle metabolism in cancer to support anabolism. *Nat. Rev. Cancer* **2018**, *18*, 634–645. [[CrossRef](#)]

38. Yoon, S.; Lee, M.-Y.; Park, S.W.; Moon, J.-S.; Koh, Y.-K.; Ahn, Y.H.; Park, S.; Kim, K.-S. Up-regulation of Acetyl-CoA Carboxylase α and Fatty Acid Synthase by Human Epidermal Growth Factor Receptor 2 at the Translational Level in Breast Cancer Cells. *J. Boil. Chem.* **2007**, *282*, 26122–26131. [[CrossRef](#)]
39. Wang, Y.; Attané, C.; Milhas, D.; Dirat, B.; Dauvillier, S.; Guerard, A.; Gilhodes, J.; Lazar, I.; Alet, N.; Laurent, V.; et al. Mammary adipocytes stimulate breast cancer invasion through metabolic remodeling of tumor cells. *JCI Insight* **2017**, *2*, e87489. [[CrossRef](#)]
40. Geck, R.C.; Foley, J.R.; Stewart, T.M.; Asara, J.M.; Casero, R.A., Jr.; Toker, A. Inhibition of the polyamine synthesis enzyme ornithine decarboxylase sensitizes triple-negative breast cancer cells to cytotoxic chemotherapy. *J. Boil. Chem.* **2020**. [[CrossRef](#)]
41. Geck, R.C.; Toker, A. Nonessential amino acid metabolism in breast cancer. *Adv. Boil. Regul.* **2016**, *62*, 11–17. [[CrossRef](#)] [[PubMed](#)]
42. Kus, K.; Kij, A.; Zakrzewska, A.; Jaształ, A.; Stojak, M.; Walczak, M.; Chlopicki, S. Alterations in arginine and energy metabolism, structural and signalling lipids in metastatic breast cancer in mice detected in plasma by targeted metabolomics and lipidomics. *Breast Cancer Res.* **2018**, *20*, 148. [[CrossRef](#)] [[PubMed](#)]
43. Navarro-Tito, N.; Guzman, A.S.; Castro-Sanchez, L.; Martinez-Orozco, R.; Salazar, E.P. Oleic acid promotes migration on MDA-MB-231 breast cancer cells through an arachidonic acid-dependent pathway. *Int. J. Biochem. Cell Biol.* **2010**, *42*, 306–317. [[CrossRef](#)]
44. Hardy, S.; Langelier, Y.; Prentki, M. Oleate activates phosphatidylinositol 3-kinase and promotes proliferation and reduces apoptosis of MDA-MB-231 breast cancer cells, whereas palmitate has opposite effects. *Cancer Res.* **2000**, *60*, 6353–6358. [[PubMed](#)]
45. Marcial-Medina, C.; Ordoñez-Moreno, A.; Gonzalez-Reyes, C.; Cortes-Reynosa, P.; Salazar, E.P. Oleic acid induces migration through a FFAR1/4, EGFR and AKT-dependent pathway in breast cancer cells. *Endocr. Connect.* **2019**, *8*, 252–265. [[CrossRef](#)] [[PubMed](#)]
46. Abel, S.; Riedel, S.; Gelderblom, W.C.A. Dietary PUFA and cancer. *Proc. Nutr. Soc.* **2014**, *73*, 361–367. [[CrossRef](#)]
47. Serna-Marquez, N.; Diaz-Aragon, R.; Reyes-Uribe, E.; Cortes-Reynosa, P.; Salazar, E.P. Linoleic acid induces migration and invasion through FFAR4- and PI3K-/Akt-dependent pathway in MDA-MB-231 breast cancer cells. *Med. Oncol.* **2017**, *34*, 45. [[CrossRef](#)]



© 2020 by the authors. Licensee MDPI, Basel, Switzerland. This article is an open access article distributed under the terms and conditions of the Creative Commons Attribution (CC BY) license (<http://creativecommons.org/licenses/by/4.0/>).

Available online at www.sciencerepository.org

Science Repository



Review Article

Development of Non-Invasive Biosensor Devices for the Detection of Bladder Cancer in Urine

Hyusim Park¹, Jayoung Kim^{2,3*} and Sungyong Jung^{1*}

¹Department of Electrical Engineering, University of Texas at Arlington, Arlington, Texas, USA

²Departments of Surgery and Biomedical Sciences, Cedars-Sinai Medical Center, Los Angeles, California, USA

³Department of Medicine, University of California Los Angeles, California, USA

ARTICLE INFO

Article history:

Received: 23 May, 2020

Accepted: 8 June, 2020

Published: 16 June, 2020

ABSTRACT

Bladder cancer (BC) is the fourth most common malignant tumor in the United States. It is the second most common cancer of the urinary system, accounting for 7% of all new cancer cases. It is also the fifth deadliest cancer, accounting for 4% of all cancer-related deaths in the United States. Our efforts to reduce costs of BC diagnosis and improve patients' quality of life by avoiding unnecessary invasive diagnostic tests resulted in findings of promising urinary biomarkers for the detection of BC. This short review article aims to provide the current status of non-invasive biosensor device development for detection of BC, in particular, in patients' urine samples.

© 2020 Jayoung Kim, Sungyong Jung. Hosting by Science Repository. All rights reserved

Bladder Cancer

Bladder cancer (BC) is the fourth most common malignant tumor in the United States. It is the second most common cancer of the urinary system, accounting for 7% of all new cancer cases. It is also the fifth deadliest cancer, accounting for 4% of all cancer-related deaths in the United States. The male to female ratio of morbidity and mortality is about 3:1 [1]. Risk factors are related to age, family history, and genetic factors, environment, diet, and lifestyle, especially smoking and exposure to aromatic amines [2-5]. Cigarette smoking is the single greatest risk factor for BC [6, 7]. Smokers are more than twice as likely to develop BC than non-smokers [8]. In muscle-invasive and metastatic bladder cancer, there is a causal relationship between tobacco exposure and cancer, of which the principal preventable risk factor for the muscle-invasive disease is active and passive smoking [6, 7]. There is a well-established relationship between schistosomiasis and squamous cell carcinoma of the bladder [6]. Exposure to chemotherapy and pelvic radiation is also considered as a risk factor for BC [6]. Other known risk

factors include the ingestion of high levels of arsenic or significant usage of pain relievers containing finazepine [3, 9].

Bladder Cancer Diagnosis

The most common symptom of BC is painless hematuria, which should be followed by physical examination, cystoscopy, urinary cytology, and imaging of the upper urinary tract (UUT). Both computed tomography (CT) and magnetic resonance imaging (MRI) may be used to detect stage T3b or higher BC. Studies suggest that FDG-PET/CT might have potential clinical use for staging metastatic BC [10, 11].

Treatment for Bladder Cancer

For treatments of non-muscle invasive BC (NMIBC, stage Ta-T1 and carcinoma in situ (CIS)), a combination of conventional surgery (transurethral resection of bladder tumor (TURBT)), intravesical chemotherapy, and immunotherapy are applied [12]. For patients with

*Correspondence to: Jayoung Kim, Ph.D., Departments of Surgery and Biomedical Sciences, Cedars-Sinai Medical Center, Davis 5071, 8700 Beverly Boulevard., Los Angeles, California 90048, USA; Tel: 13104237168; Fax: 13109673809; E-mail: Jayoung.kim@csmc.edu

Sungyong Jung, Ph.D., Department of Electrical Engineering, University of Texas at Arlington, Arlington, Texas 76248, USA; Tel: 18172721338; Fax: 18172722671; E-mail: jung@uta.edu

high-risk diseases and those whose diseases are difficult to treat, cystectomy may be necessary [12].

For the treatment of muscle-invasive BC (MIBC, stage T2 to T3 and CIS), the two principal treatment choices are radical cystectomy (RC) and TURBT, with concurrent radiation therapy using a radiosensitizer and systemic chemotherapy (multi-modality therapy) [6]. Standard treatment for patients with MIBC is radical cystectomy; however, this treatment only provides 5-year survival in about 50% of patients. The use of chemotherapy is beneficial to improving both survival and patient outcomes [6]. A paper published in 2005 demonstrated a significant 5% absolute survival benefit in favor of neoadjuvant chemotherapy (NAC) [13]. This study also showed that only cisplatin combined chemotherapy could produce significant therapeutic effects [13].

More modern chemotherapeutic regimens, such as gemcitabine/cisplatin, which are effective in metastatic disease, have also shown efficacy in the neoadjuvant setting [14, 15]. Adjuvant chemotherapy (AC) after RC can be used for high-risk M0 patients, such as those with pT3/4 and/or lymph node-positive (N+) disease [16]. A retrospective study from 2009 compared the long-term outcome of preoperative versus no preoperative radiation therapy (RT) in clinical T1-3 tumors [17]. The study showed that preoperative RT could lead to a reduction in order to prolong progression-free survival (PFS) [17]. External beam radiation therapy (EBRT) may be given preoperatively (neoadjuvant), postoperatively (adjuvant), or as radical treatment for patients with muscle-infiltrating cancer with no proven metastases to lymph nodes or distant metastases [6]. For the patients without lymph node metastasis or distant metastasis, external beam radiation therapy (EBRT) can be given before operation (neoadjuvant), after operation (adjuvant) or as radical treatment [6].

Metastatic BC is a serious disease. Before the development of effective chemotherapy, patients with the metastatic disease rarely had a median survival that exceeded 3-6 months [6]. The 5-year survival rate of patients with metastatic bladder cancer was previously estimated to be 5% [18]. The current estimated 5-year survival is 10% [2]. Chemotherapy is still the standard treatment for metastatic bladder cancer; however, patients with ineffective or poorly tolerated chemotherapy still have poor prognosis [6]. The recent discovery of innovative immunotherapies based on the programmed death ligand-1 (PD-L1) inhibitors, such as avelumab, durvalumab, nivolumab and atezolizumab, are promising for patients who are considered unsuitable for chemotherapy [19, 20].

Bladder Cancer Classification

Traditionally, BC has been classified into NMIBC or MIBC, and most of BC belong to transitional cell carcinoma (TCC) [21]. Recent efforts classifying phenotypes based on molecular characteristics reported several BC phenotypes. For example, there are University of North Carolina (UNC), MD Anderson Cancer Center (MDA), The Cancer Genome Atlas (TCGA), Lund University (Lund), and Broad Institute of Massachusetts Institute of Technology and Harvard University (Broad) classification.

Biosensors for Detection of Bladder Cancers Using Urine

Researchers' efforts to reduce costs of BC diagnosis and improve patients' quality of life by avoiding unnecessary invasive diagnostic tests resulted in findings of promising urinary biomarkers for the detection of BC such as telomerase, nuclear matrix protein 22 (NMP22), cytokeratin 19, etc. [22]. Along with the discovery of urinary biomarkers, biosensors for detecting those biomarkers have been developed, which can offer low detection limits, a wide linear response range, good stability and, good reproducibility [23].

The biosensor is a device that transforms a biological response into a quantifiable and processable signal. The key components of biosensors are a bioreceptor and a transducer. The bioreceptor is a molecule that specifically recognizes the analyte, such as enzyme, antibody, and protein, while the transducer is an element that converts the bio-recognition event into a measurable signal, which classifies the types of the biosensors. The biosensors for BC diagnosis with voided urine can be typically categorized into two groups, an optical biosensor and an electrochemical biosensor. The optical biosensor emits an optical signal which is proportional to the concentration of a measure substance (analyte) whereas electrochemical biosensor converts biological event to an electronic signal.

From early research, the optical biosensor has been the most commonly used biosensor to screen target biomarkers in urine [24-27]. Shin *et al.* developed the optical biosensor with silicon microring resonators to detect DNA biomarkers (fibroblast growth factor receptor 3 and Harvey RAS) in urine [24]. They successfully demonstrated linear wavelength shifts pattern in a different concentration range of target biomarkers. Due to the intrinsic advantage of silicon fabrication, a highly sensitive and specific platform was achieved for diagnosis and surveillance of BC. As another prominent urinary biomarker for BC diagnosis, telomerase activity's detection was conducted using a fluorescence method and a colorimetric method on the optical biosensor [25, 27].

Xu *et al.* established the label-free colorimetric optical biosensor based on the merits of hemin-graphene nanomaterial, such as easiness of synthesis, stability, and reliability. The sensor was validated its performance by changing colour from light blue to dark blue as telomerase activity increased due to chromogenic reaction. To detect telomerase activity, not only the optical biosensor but also the electrochemical biosensor can be applied with good reproducibility and selectivity [28]. The electrochemical biosensor was realized using methylene blue (MB) as a G-quadruplex binding on indium tin oxide. The large amount of MB bounded to G-quadruplexes under the activity of telomerase resulted in sharply decreasing diffusion current of MB. Ma *et al.* proved the effectiveness of the electrochemical immunosensor (affinity-biosensor) for detecting NMP22 on graphene oxide-tetraethylene pentaamine and trimetallic AuPdPt nanoparticles [29]. It achieved high accuracy in real urine sample, showing differential pulse voltammetry responses of the immunosensor towards different concentrations of NMP22. Another transducer, a high stability indium gallium zinc oxide field effect transistor (IGZO-FET), was utilized to build the electrochemical biosensor for capturing the NMP22 [30]. The IGZO-FET sensor was tested with real urine samples from BC patients,

and it was able to detect NMP22 with high sensitivity, selectivity, and detection limit.

Point-of-Care Detection Device for Bladder Cancer Using Urine

It is widely known that screening and early diagnosis of cancer are key to improving the likelihood of recovery and 5-year survival. Consequently, many studies have been conducted to develop a point-of-care (POC) device for BC detection, which responds fast and diagnoses non-invasively. The POC device should be low-cost, portable, reliable, and disposable.

To satisfy such requirements, a lab-on-a chip (LOC) technique has been investigated. It is reported that Liang *et al.* developed an integrated double-filtration microfluidic LOC device, which isolates, enriches, and quantifies urinary extracellular vesicles to assist in screening for bladder cancer at the POC [31]. The device detects the multiple biomarkers of BC and transfers diagnostic data in the patient's urine sample to the user through wireless communication using a cell phone. In addition, Geng *et al.* developed a microfluidic chip using polydimethylsiloxane (PDMS) to form a channel using a cast molding method, with a sliding glass coverslip as the substrate to detect BC biomarkers [32]. The chip converts different concentrations of biomarkers in urine to fluorescence intensity of image, which is a quantifiable signal. Chuang *et al.* have reported that an immunosensor chip as POC test device for detection of BC biomarker (Galectin-1 protein) realized with a photolithographically patterned gold microelectrode array [33]. They also designed a portable impedance measurement readout device for this chip, which transferred the data to the computer for improved monitoring.

A few commercial POC diagnosis devices are approved by FDA for BC detection and surveillance, such as UBC rapid, NMP22 BladderChek and BTA-STAT. UBC rapid detects cytokeratin fragments 8 and 18 in the urine to diagnose BC. It takes only 10 minutes to get the result and has the closest sensitivity of cytology in high-grade tumors [34]. NMP22 BladderCheck utilizes the detection of NMP22 as can be guessed from its name, and it takes 30 minutes to diagnose with high specificity. BTA Stat Test detects the presence of bladder tumor associated antigen (BTA) in 5 minutes. Some insists that it has higher potential in detection of early grade BC than cytology [35]. Much of the research has been done to evaluate the commercial test kit by ethnicity, case number, gender and so on [36-41].

As of now, cytology is the only recommended guidelines internationally for diagnosing BC. The aforementioned commercial POC devices have been used in combination with cystoscopy to improve the accuracy. To use the commercial POC as a standalone BC diagnosis devices, there should be more meta-analyses with various conditions such as age, gender, genetic factors, environment, and lifestyle.

Conflicts of Interest

None.

Funding

This research was funded by National Institutes of Health (1U01DK103260, 1R01DK100974, U24 DK097154, NIH NCATS UCLA CTSI UL1TR000124), Department of Defense (W81XWH-15-1-0415 and W81XWH-19-1-0109), Centers for Disease Controls and Prevention (1U01DP006079), and the U.S.-Egypt Science and Technology Development Fund by the National Academies of Sciences, Engineering, and Medicine (all to J.K.). This article is derived from the Subject Data funded in whole or part by National Academies of Sciences, Engineering, and Medicine (NAS) and The United States Agency for International Development (USAID). Any opinions, findings, conclusions, or recommendations expressed in this article are those of the authors alone, and do not necessarily reflect the views of USAID or NAS.

Acknowledgements

This research was supported by the Samuel Oschin Comprehensive Cancer Institute (SOCCI) at Cedars-Sinai Medical Center through 2019 Lucy S. Gonda Award.

Author Contributions

Research conception and design: JK, SJ. Data analysis and interpretation: HP, JK. Drafting of the manuscript: HP, JK. Critical revision of the manuscript: JK, SJ. Supervision: JK, SJ. Approval of the final manuscript: all authors.

REFERENCES

1. Siegel RL, Miller KD, Jemal A (2019) Cancer statistics, 2019. *CA Cancer J Clin* 69: 7-34. [[Crossref](#)]
2. Anderson B (2018) Bladder cancer: overview and management. Part 2: muscle-invasive and metastatic bladder cancer. *Br J Nurs* 27: S8-S20. [[Crossref](#)]
3. Pelucchi C, Bosetti C, Negri E, Malvezzi M, La Vecchia C (2006) Mechanisms of disease: The epidemiology of bladder cancer. *Nat Clin Pract Urol* 3: 327-340. [[Crossref](#)]
4. Mitra AP, Cote RJ (2009) Molecular pathogenesis and diagnostics of bladder cancer. *Annu Rev Pathol* 4: 251-285. [[Crossref](#)]
5. Ruder AM, Fine LJ, Sundin DS (1990) National estimates of occupational exposure to animal bladder tumorigens. *J Occup Med* 32: 797-805. [[Crossref](#)]
6. Witjes JA, Comperat E, Cowan NC, De Santis M, Gakis G et al. (2016) EAU guidelines on muscle-invasive and metastatic bladder cancer.
7. Babjuk M, Böhle A, Burger M, Capoun O, Cohen D et al. (2017) EAU Guidelines on Non-Muscle-invasive Urothelial Carcinoma of the Bladder: Update 2016. *Eur Urol* 71: 447-461. [[Crossref](#)]
8. Fankhauser CD, Mostafid H (2018) Prevention of bladder cancer incidence and recurrence: nutrition and lifestyle. *Curr Opin Urol* 28: 88-92. [[Crossref](#)]
9. Castela JE, Yuan JM, Gago-Dominguez M, Yu MC, Ross RK (2000) Non-steroidal anti-inflammatory drugs and bladder cancer prevention. *Br J Cancer* 82: 1364-1369. [[Crossref](#)]
10. Yang Z, Cheng J, Pan L, Hu S, Xu J et al. (2012) Is whole-body fluorine-18 fluorodeoxyglucose PET/CT plus additional pelvic images

- (oral hydration-voiding-refilling) useful for detecting recurrent bladder cancer? *Ann Nucl Med* 26: 571-577. [Crossref]
11. Maurer T, Souvatzoglou M, Kübler H, Opercan K, Schmidt S et al. (2012) Diagnostic efficacy of [11C]choline positron emission tomography/computed tomography compared with conventional computed tomography in lymph node staging of patients with bladder cancer prior to radical cystectomy. *Eur Urol* 61: 1031-1038. [Crossref]
 12. Vahr S, De Blok W, Love-Retinger N, Jensen BT, Turner B et al. (2015) Evidence-based guidelines for best practice in urological health care: intravesical instillation with mitomycin C or bacillus calmette-guérin in non-muscle invasive bladder cancer.
 13. Advanced Bladder Cancer Meta-analysis Collaboration (2005) Neoadjuvant chemotherapy in invasive bladder cancer: update of a systematic review and meta-analysis of individual patient data advanced bladder cancer (ABC) meta-analysis collaboration. *Eur Urol* 48: 202-205; discussion 205-206. [Crossref]
 14. Yuh BE, Ruel N, Wilson TG, Vogelzang N, Pal SK (2013) Pooled analysis of clinical outcomes with neoadjuvant cisplatin and gemcitabine chemotherapy for muscle invasive bladder cancer. *J Urol* 189: 1682-1686. [Crossref]
 15. Lee FC, Harris W, Cheng HH, Shenoi J, Zhao S et al. (2013) Pathologic Response Rates of Gemcitabine/Cisplatin versus Methotrexate/Vinblastine/Adriamycin/Cisplatin Neoadjuvant Chemotherapy for Muscle Invasive Urothelial Bladder Cancer. *Adv Urol* 2013: 317190. [Crossref]
 16. Witjes JA, Lebre T, Compérat EM, Cowan NC, De Santis M et al. (2017) Updated 2016 EAU Guidelines on Muscle-invasive and Metastatic Bladder Cancer. *Eur Urol* 71: 462-475. [Crossref]
 17. Granfors T, Tomic R, Ljungberg B (2009) Downstaging and survival benefits of neoadjuvant radiotherapy before cystectomy for patients with invasive bladder carcinoma. *Scand J Urol Nephrol* 43: 293-299. [Crossref]
 18. Carballido EM, Rosenberg JE (2014) Optimal treatment for metastatic bladder cancer. *Curr Oncol Rep* 16: 404. [Crossref]
 19. Powles T, Eder JP, Fine GD, Braiteh FS, Loriot Y et al. (2014) MPDL3280A (anti-PD-L1) treatment leads to clinical activity in metastatic bladder cancer. *Nature* 515: 558-562. [Crossref]
 20. Festino L, Botti G, Lorigan P, Masucci GV, Hipp JD et al. (2016) Cancer Treatment with Anti-PD-1/PD-L1 Agents: Is PD-L1 Expression a Biomarker for Patient Selection? *Drugs* 76: 925-945. [Crossref]
 21. Moch H, Cubilla AL, Humphrey PA, Reuter VE, Ulbright TM (2016) The 2016 WHO Classification of Tumours of the Urinary System and Male Genital Organs-Part A: Renal, Penile, and Testicular Tumours. *Eur Urol* 70: 93-105. [Crossref]
 22. Vrooman OP, Witjes JA (2008) Urinary markers in bladder cancer. *Eur Urol* 53: 909-916. [Crossref]
 23. Mehrotra, P (2016) Biosensors and their applications - A review. *J Oral Biol Craniofac Res* 6: 153-159. [Crossref]
 24. Shin Y, Perera AP, Park MK (2013) Label-free DNA sensor for detection of bladder cancer biomarkers in urine. *Sensors and Actuators B: Chemical* 178: 200-206.
 25. Lou X, Zhuang Y, Zuo X, Jia Y, Hong Y et al. (2015) Real-Time, Quantitative Lighting-up Detection of Telomerase in Urines of Bladder Cancer Patients by AIEgens. *Anal Chem* 87: 6822-6827. [Crossref]
 26. Peng C, Hua MY, Li NS, Hsu YP, Chen YT et al. (2019) A colorimetric immunosensor based on self-linkable dual-nanozyme for ultrasensitive bladder cancer diagnosis and prognosis monitoring. *Biosens Bioelectron* 126: 581-589. [Crossref]
 27. Xu X, Wei M, Liu Y, Liu Xu, Wei W et al. (2017) A simple, fast, label-free colorimetric method for detection of telomerase activity in urine by using hemin-graphene conjugates. *Biosens Bioelectron* 87: 600-606. [Crossref]
 28. Liu X, Wei M, Xu E, Yang H, Wei W et al. (2017) A sensitive, label-free electrochemical detection of telomerase activity without modification or immobilization. *Biosens Bioelectron* 91: 347-353. [Crossref]
 29. Ma H, Zhang X, Li X, Li R, Du B et al. (2015) Electrochemical immunosensor for detecting typical bladder cancer biomarker based on reduced graphene oxide-tetraethylene pentamine and trimetallic AuPdPt nanoparticles. *Talanta* 143: 77-82. [Crossref]
 30. Li Y, Zeng B, Yang Y, Liang H, Yang Y et al. (2020) Design of high stability thin-file transistor biosensor for the diagnosis of bladder cancer. *Chin Chem Lett* In Press.
 31. Liang LG, Kong MQ, Zhou S, Sheng YF, Wang P et al. (2017) An integrated double-filtration microfluidic device for isolation, enrichment and quantification of urinary extracellular vesicles for detection of bladder cancer. *Sci Rep* 7: 46224. [Crossref]
 32. Geng C, Li C., Li W, Yan W, Li J et al. (2018) A simple fabricated microfluidic chip for urine sample-based bladder cancer. *J Micromech Microeng* 28: 115011.
 33. Chuang CH, Du YC, Wu TF, Chen CH, Lee DH et al. (2016) Immunosensor for the ultrasensitive and quantitative detection of bladder cancer in point of care testing. *Biosens Bioelectron* 84: 126-132. [Crossref]
 34. Ecke TH, Weiß S, Stephan C, Hallmann S, Arndt C et al. UBC((R)) Rapid Test-A Urinary Point-of-Care (POC) Assay for Diagnosis of Bladder Cancer with a focus on Non-Muscle Invasive High-Grade Tumors: Results of a Multicenter-Study. *Int J Mol Sci* 19: 3841. [Crossref]
 35. Guo A, Wang X, Gao L, Shi J, Sun C et al. (2014) Bladder tumour antigen (BTA stat) test compared to the urine cytology in the diagnosis of bladder cancer: A meta-analysis. *Can Urol Assoc J* 8: E347-E352. [Crossref]
 36. Wang Z, Que H, Suo C, Han Z, Tao J et al. (2017) Evaluation of the NMP22 BladderChek test for detecting bladder cancer: a systematic review and meta-analysis. *Oncotarget* 8: 100648-100656. [Crossref]
 37. Hwang EC, Choi H, Jung SI, Kwon DD, Park K et al. (2011) Use of the NMP22 BladderChek test in the diagnosis and follow-up of urothelial cancer: a cross-sectional study. *Urology* 77: 154-159. [Crossref]
 38. Gleichenhagen J, Arndt C, Casjens S, Meinig C, Gerullis H et al. (2018) Evaluation of a New Survivin ELISA and UBC((R)) Rapid for the Detection of Bladder Cancer in Urine. *Int J Mol Sci* 19: 226. [Crossref]
 39. Lu P, Cui J, Chen K, Lu Q, Zhang J et al. (2018) Diagnostic accuracy of the UBC((R)) Rapid Test for bladder cancer: A meta-analysis. *Oncol Lett* 16: 3770-3778. [Crossref]
 40. Narayan VM, Adejoro O, Schwartz I, Ziegelmann M, Elliott S et al. (2018) The Prevalence and Impact of Urinary Marker Testing in Patients with Bladder Cancer. *J Urol* 199: 74-80.
 41. Kollarik B, Zvarik M, Bujdak P, Weibl P, Rybar L et al. Urinary fluorescence analysis in diagnosis of bladder cancer. *Neoplasma* 65: 234-241. [Crossref]



Teleurology and digital health app in COVID-19 pandemic

“April was death. April was hope. April was cruel.”

This was the sad title of The WaPo's (Washington Post, a major American daily newspaper) cover article, published on May 2, 2020. In the month of April 2020, more than 2,000 Americans died each day, and more than one out of every 325 Americans had confirmed infections with the newly emergent human virus, severe acute respiratory syndrome–coronavirus 2 (SARS-CoV-2). In the elegantly written recent article [1], Dr. Khae Hawn Kim at Gachon University Gil Medical Center described the early responses to the coronavirus disease 2019 (COVID-19) global health crisis. The day he wrote the article was the same day that a 17-year-old South Korean adolescent died of aggravated acute respiratory distress syndrome without a solid test result regarding COVID-19. Although the result turned out to be negative, it was news fearful enough to alert the healthcare community.

To respond to this pandemic, the healthcare system has been directly and indirectly forced to rapidly adjust to this new pandemic environment and reset clinical infrastructure for appropriate healthcare delivery, particularly regarding the elderly. Instead of the Standard-of-Care in-person consultation, “telemedicine,” communication through telephone or video connection, is being utilized for outpatients not at high risk. Since recent scientific evidence suggests that virus transmission occurs through symptomatic, pre-symptomatic, and even asymptomatic patients, as well as environmental transmission, patients and healthcare providers require extensive usage of personal protective equipment as well as well-curated decontamination procedures of the facility and instruments during procedures of individual therapies and treatment.

This is particularly evident in urological clinical settings. High percentages of urological patients belong to aged populations, who are subsequently more vulnerable to severe COVID-19 infection. Boehm et al. [2] reported that approximately 85% of urological patients are asking for telemedi-

cal consultations to avoid various possible risk factors. Bold clinical protocols are urgently needed to provide contact-free teleurological care during and after the outbreak of the COVID-19 pandemic.

To improve our understanding on the potential impacts and specific epidemiology of COVID-19, the implementation of mobile technology for digital data collection tools, such as smartphone applications, should be considered to facilitate research activities in reducing spread of disease and in improving contact-free patient care. Scientists and developers alike should be particularly aware that privacy is of the utmost importance to successfully apply the app-based data collection during this pandemic [3]. Patients want to be able to confidently trust the usage of digital health data.

As shown in mHealthHUB (<http://mhealth-hub.org/mhealth-solutions-against-covid-19>), a COVID-19 Symptom Tracker mobile application lead by Dr. Chan at Harvard Medical School and investigators at the COronavirus Pandemic Epidemiology (COPE) consortium is one good example for epidemiologic data collection to determine COVID-19 risk factors, clinical outcomes, public health planning, and the associated mechanism and therapeutic options [2]. The clinical values of another app-based symptom tracker for symptom tracking and modeling were assessed by clinical research led by Dr. Spector at King's College London [4] to determine whether loss of olfactory and gustatory functions is caused by COVID-19 among 2,618,862 individuals. The HEALTHLYNKED COVID-19 Tracker [5] and Apple's official COVID-19 app were developed based on the collaboration with the World Health Organization (WHO) and Centers for Disease Control and Prevention (CDC), respectively.

In *The Waste Land* (1922), T.S. Eliot (1888–1965) writes that “April is the cruelest month.” However, we know that his poem actually sings hope about the ending of Winter and the celebration of a new Spring. We do not yet know if we will experience another painful Spring next year, or if we will face a new normal all together coming out of this

pandemic. The preparation of teleurology training for urology healthcare providers in our medical schools starts as early as the upcoming semester. The post COVID-19 era may significantly rely on digital data collection from Smartphone applications and machine learning algorithms for clinical trials and research activities. Are we ready for this paradigm shift towards the telemedicine and digital health that lies just around the next corner?

CONFLICTS OF INTEREST

The authors have nothing to disclose.

ACKNOWLEDGMENTS

This research was funded by National Institutes of Health (1U01DK103260, 1R01DK100974, U24 DK097154, NIH NCATS UCLA CTSI UL1TR000124), Department of Defense (W81XWH-15-1-0415 and W81XWH-19-1-0109), Centers for Disease Controls and Prevention (1U01DP006079), and the U.S.-Egypt Science and Technology Development Fund by the National Academies of Sciences, Engineering, and Medicine (all to J.K.). This research was also supported by the Samuel Oschin Comprehensive Cancer Institute (SOCCI) at Cedars-Sinai Medical Center through the 2019 Lucy S. Gonda Award. This article is derived from the Subject Data funded in whole or part by National Academies of Sciences, Engineering, and Medicine (NAS) and The United States Agency for International Development (USAID). Any opinions, findings, conclusions, or recommendations expressed in this article are those of the authors alone, and do not necessarily reflect the views of USAID or NAS.

AUTHORS' CONTRIBUTIONS

Research conception and design: Jayoung Kim and Bruce Gewertz. Drafting of the manuscript: Jayoung Kim and Bruce Gewertz. Critical revision of the manuscript: Bruce Gewertz. Obtaining funding: Jayoung Kim. Approval of the final manuscript: Jayoung Kim and Bruce Gewertz.

Jayoung Kim^{1,2} , Bruce Gewertz¹ 

Corresponding Author: Jayoung Kim

ORCID: <https://orcid.org/0000-0002-3683-4627>

¹Departments of Surgery, Cedars-Sinai Medical Center, Los Angeles, CA, ²Department of Medicine, University of California Los Angeles, Los Angeles, CA, USA

E-mail: jayoung.kim@csmc.edu

REFERENCES

1. Kim KH. COVID-19. *Int Neurourol J* 2020;24:1.
2. Boehm K, Ziewers S, Brandt MP, Sparwasser P, Haack M, Willemis F, et al. Telemedicine online visits in urology during the COVID-19 pandemic-potential, risk factors, and patients' perspective. *Eur Urol* 2020 Apr 27 [Epub]. <https://doi.org/10.1016/j.eururo.2020.04.055>.
3. Gostin LO, Halabi SF, Wilson K. Health data and privacy in the digital era. *JAMA* 2018;320:233-4.
4. Menni C, Valdes AM, Freidin MB, Sudre CH, Nguyen LH, Drew DA, et al. Real-time tracking of self-reported symptoms to predict potential COVID-19. *Nat Med* 2020 May 11 [Epub]. <https://doi.org/10.1038/s41591-020-0916-2>.
5. Yasaka TM, Lechrich BM, Sahyouni R. Peer-to-peer contact tracing: development of a privacy-preserving smartphone app. *JMIR Mhealth Uhealth* 2020;8:e18936.



Letter to the Editor

Int Neurolog J 2020;24(2):180-181

<https://doi.org/10.5213/inj.2040198.099>

pISSN 2093-4777 · eISSN 2093-6931



Equality, Inclusion, and Diversity in Healthcare During the COVID-19 Pandemic

Jayoung Kim^{1,2}

¹Departments of Surgery and Biomedical Sciences, Cedars-Sinai Medical Center, Los Angeles, CA, USA

²Department of Medicine, University of California Los Angeles, CA, USA

To the editor,

Public health is a complicated issue. This has become particularly evident during this worldwide pandemic of COVID-19. On May 25, 2020, Mr. George Floyd, an African American man residing in Minneapolis was killed in police custody. For 8 minutes and 46 seconds, the arresting officer had his knee pressed on Mr. Floyd's neck, ultimately killing him through asphyxiation. This event ignited a movement of fiery protests fueled by the current status of racial discrimination and socioeconomic and healthcare disparities in America, much of which is still ongoing as I write this letter on June 2, 2020.

There is mounting evidence that suggests that minorities experience a greater incidence and worse cases of diseases compared to white Americans. The root causes of these health disparities have been heavily studied; racism and discrimination make access to healthcare resources difficult and, sometimes, impossible. When it comes to COVID-19, key risk factors, such as age, sex, and comorbidities (i.e., hypertension, diabetes, and cardiovascular disease), are linked to worse outcomes. Unfortunately, these factors are compounded with the disparities noted with race and socioeconomic status. Poorer communities and people of color experience limited access to health education, hygiene management, and healthy foods. Additionally, they live in areas with denser populations, which makes it difficult to maintain appropriate social distancing, specifically regarding COVID-19.

What Does Research Data Tell Us So Far?

More and more studies continue to demonstrate the disproportionately negative impact that COVID-19 has on African Americans [1]. Overall, black Americans have higher rates of infection and mortality. In Chicago, where African Americans make up only 30% of the population, more than 50% of COVID-19 cases and nearly 70% of deaths were African Americans [2]. In Louisiana, African Americans make up approximately 30% of the population; however, over 70.5% of COVID-19 deaths have been in African Americans [3]. This alarming disparity in numbers was similar in the state of Michigan, where African Americans make up only 14% of the population [4]. Recent data from 1,052 confirmed COVID-19 cases in Northern California showed that African Americans were 2.7 times more likely to be hospitalized than non-Hispanic whites [5]. In Los Angeles County, the average death rate from COVID-19 was estimated to be 9 per 100,000 cases. However, when accounting for race, the African American population had a death rate of 16 per 100,000. Shockingly, in denser black communities, such as West Rancho Dominguez, this rate shot up to 74 deaths per 100,000 cases.

Serious health disparities have also been noted in the Asian American communities, where COVID-19 has additionally contributed to a rise in anti-Asian sentiment, discrimination, and hate-related crimes [6]. Studies found a positive correlation between the percentage of Asian Americans and the percentage of incidence ($r=0.185$, $P<0.0001$) and death ($r=0.211$,

Corresponding author: Jayoung Kim  <https://orcid.org/0000-0002-3683-4627>
Departments of Surgery and Biomedical Sciences, Cedars-Sinai Medical Center,
Los Angeles, CA 90048, USA

E-mail: Jayoung.Kim@cshs.org

Submitted: June 4, 2020 / **Accepted after revision:** June 15, 2020



This is an Open Access article distributed under the terms of the Creative Commons Attribution Non-Commercial License (<https://creativecommons.org/licenses/by-nc/4.0/>) which permits unrestricted non-commercial use, distribution, and reproduction in any medium, provided the original work is properly cited.

$P < 0.0001$) from COVID-19 [7]. Data published on *Wellcome Open Research* analyzed the national health records of 16,272 COVID-19 patients in the United Kingdom suggested that black and Asian patients were at higher risk of death from COVID-19 compared to Caucasians.

In early May 2020, the U.S. Food and Drug Administration allowed the biotechnology firm, Moderna, to initiate an mRNA-1273-based phase II clinical trial. Several potential drugs for COVID-19 treatment and vaccination are being tested in numerous large clinical trials around the world. To minimize the health disparity from COVID-19, these clinical trials must include people from all ethnic and racial groups. Otherwise, we will see another level of repetitive health disparity issues from COVID-19 in future treatments and vaccines.

• **Grant/Fund Support:** This research was funded by National Institutes of Health (1U01DK103260, 1R01DK100974, U24DK097154, NIH NCATS UCLA CTSI UL1TR000124), Department of Defense (W81XWH-15-1-0415 and W81XWH-19-1-0109), Centers for Disease Controls and Prevention (1U01DP006079), and the U.S.-Egypt Science and Technology Development Fund by the National Academies of Sciences, Engineering, and Medicine (all to J.K.). This article is derived from the Subject Data funded in whole or part by National Academies of Sciences, Engineering, and Medicine (NAS) and The United States Agency for International Development (USAID). Any opinions, findings, conclusions, or recommendations expressed in this article are those of the authors alone, and do not necessarily reflect the views of USAID or NAS.

• **Conflict of Interest:** No potential conflict of interest relevant to this article was reported.

REFERENCES

1. Yancy CW. COVID-19 and African Americans. *JAMA* 2020 Apr 15 [Epub]. <https://doi.org/10.1001/jama.2020.6548>.
2. Reyes C, Husain N, Gutowski C, St Clair S, Pratt G. Chicago's coronavirus disparity: black Chicagoans are dying at nearly six times the rate of white residents, data show. *Chicago Tribune* [Internet]. 2020 Apr 7 [2020 Apr 12]. Available from: <http://www.chicagotribune.com/coronavirus/ct-coronavirus-chicago-coronavirus-deaths-demographics-lightfoot-20200406-77nlylhiavgjzb2wa4ckivh7mu-story.html>.
3. Deslatte M. Louisiana data: virus hits blacks, people with hypertension. *US News World Report* [Internet]. 2020 Apr 7 [2020 Apr 12]. Available from: <https://www.usnews.com/news/best-states/louisiana/articles/2020-04-07/louisiana-data-virus-hits-blacks-people-with-hypertension>.
4. Thebault R, Ba Tran A, Williams V. The coronavirus is infecting and killing black Americans at an alarmingly high rate. *Washington Post* [Internet]. 2020 Apr 7. Available from: <https://www.washingtonpost.com/nation/2020/04/07/coronavirus-is-infecting-killing-black-americans-an-alarmingly-high-rate-post-analysis-shows/?arc404=true>.
5. Azar KMJ, Shen Z, Romanelli RJ, Lockhart SH, Smits K, Robinson S, et al. Disparities in outcomes among COVID-19 patients in a large health care system in California. *Health Aff (Millwood)* 2020 May 21:101377hlthaff202000598. <https://doi.org/10.1377/hlthaff.2020.00598>. [Epub].
6. Chen HA, Trinh J, Yang GP. Anti-Asian sentiment in the United States - COVID-19 and history. *Am J Surg* 2020 May 16 [Epub]. <https://doi.org/10.1016/j.amjsurg.2020.05.020>.
7. Mahajan UV, Larkins-Pettigrew M. Racial demographics and COVID-19 confirmed cases and deaths: a correlational analysis of 2886 US counties. *J Public Health (Oxf)* 2020 May 21:fdaa070. <https://doi.org/10.1093/pubmed/fdaa070>. [Epub].

Metabolomic and lipidomic approaches to identify biomarkers for bladder cancer and interstitial cystitis (Review)

MUHAMMAD SHAHID¹, AUSTIN YEON¹ and JAYOUNG KIM¹⁻⁵

Departments of ¹Surgery and ²Biomedical Sciences; ³Oschin Comprehensive Cancer Institute, Cedars-Sinai Medical Center, Los Angeles, CA 90048; ⁴Department of Medicine, University of California, Los Angeles, CA 90024, USA; ⁵Department of Urology, Ga Cheon University College of Medicine, Incheon 13120, Republic of Korea

Received May 21, 2020; Accepted September 18, 2020

DOI: 10.3892/mmr.2020.11627

Abstract. The discovery, introduction and clinical use of prognostic and diagnostic biomarkers has significantly improved outcomes for patients with various illnesses, including bladder cancer (BC) and other bladder-related diseases, such as benign bladder dysfunction and interstitial cystitis (IC). Several sensitive and noninvasive clinically relevant biomarkers for BC and IC have been identified. Metabolomic- and lipidomic-based biomarkers have notable clinical potential in improving treatment outcomes for patients with cancer; however, there are also some noted limitations. This review article provides a short and concise summary of the literature on metabolomic and lipidomic biomarkers for BC and IC, focusing on the possible clinical utility of profiling metabolic alterations in BC and IC.

Contents

1. Bladder cancer
2. Recently reported molecular subtype classification of BC
3. Interstitial cystitis
4. Metabolomics and lipidomics
5. Emerging technologies

6. Applying metabolomics and lipidomics to BC
7. Applying metabolomics and lipidomics to IC
8. Human specimens-based metabolomics and lipidomics biomarkers for BC
9. Human specimens-based metabolomics markers in IC
10. Conclusion

1. Bladder cancer

Bladder cancer (BC) is the most common malignancy of the urinary tract. In 2018, there were ~549,000 new cases of BC and 200,000 deaths related to BC globally (1). BC is the eighth most common cancer among men in the US (2) and is reported to affect men more frequently than women, with a ratio of 3.2:0.9 (1,2). In addition, the incidence of BC increases with age (3). According to the European Association of Urology, BC can be classified into two divergent phenotypes: Non-muscle-invasive BC (NMIBC) and muscle-invasive BC (MIBC). Furthermore, BC can be categorized into the following subtypes: Urothelial carcinoma, squamous epithelial carcinoma and adenocarcinoma (1-3). Urothelial carcinomas account for an overwhelming 90% of worldwide BC cases (4). Risk factors for BC include occupational factors, age, sex, race, socioeconomic status, personal health, diet and infection by pathogens (5-7). It is well-established that the progression of a normal cell to a cancer cell is a multistep process involving the accumulation of genetic alterations, referred to as carcinogenesis. NMIBC generally involves the mutation of fibroblast growth factor receptor 3 (*FGFR3*), giving rise to low-grade cancer that frequently recurs but seldom becomes invasive or progresses. By contrast, MIBC and carcinoma *in situ* exhibit deletions or mutations of *TP53*, RB transcriptional corepressor 1 (*RBI*), erb-b2 receptor tyrosine kinase 2 or *PTEN*, leading to high-grade and metastatic cancer (8). The emergence of high-throughput transcriptome sequencing techniques has assisted in the identification of versatile BC biomarkers, including long non-coding RNAs (lncRNAs), the aberrant expression of which can contribute to tumorigenesis in bladder tissues (9). lncRNA abhydrolase-domain containing 11 antisense RNA 1 (ABHD11-AS1) and lncRNA hypoxia-inducible factor 1 α antisense RNA 2 (HIF1A-AS2) have been reported to be upregulated in BC tissues and cells,

Correspondence to: Professor Jayoung Kim, Department of Surgery, Cedars-Sinai Medical Center, Davis 5071, 8700 Beverly Blvd., Los Angeles, CA 90048, USA
E-mail: jayoung.kim@cshs.org

Abbreviations: BC, bladder cancer; ESI, electrospray ionization; FGFR3, fibroblast growth factor receptor 3; GC, gas chromatography; IC, interstitial cystitis; LC, liquid chromatography; MAPP, Multidisciplinary Approach to the Study of Chronic Pelvic Pain; MIBC, muscle-invasive BC; MS, mass spectrometry; NMIBC, non-muscle-invasive BC; NMR, nuclear magnetic resonance; TCA, tricarboxylic acid; TCGA, The Cancer Genome Atlas; UPLC, ultra-performance LC-MS

Key words: bladder cancer, interstitial cystitis, metabolomics, lipidomics, biomarkers

and their expression levels in tissues have been shown to be positively associated with advanced pathological grade and TNM classification (10,11).

2. Recently reported molecular subtype classification of BC

Classification systems for cancer are mainly based on pathological parameters, such as stage and grade. Such classification provides predictive prognostic information; however, for BC, recurrence and progression vary widely from patient to patient, greatly affecting monitoring and treatment (12). The development of advanced techniques, such as sequencing and mass spectrometry (MS), and their implementation in omics, has provided better diagnostic and therapeutic information for the treatment of BC (13-16). Molecular subtyping, which is based on genetic characteristics, has made particularly notable progress in BC and is of increasing interest (17). The current molecular subtypes of BC share various characteristics, such as molecular features. However, these classifications can also vary, with two to seven distinct subtypes (18-20). As a result of this diversity, molecular classifications are not feasible for use in the clinical setting. This also highlights the need for a consensus on a single set of molecular subtypes that is applicable to clinical use. Nevertheless, the understanding of the biology of BC has been substantially improved by key achievements in molecular classification; for example, associations have been identified between molecular subtypes and urothelial differentiation, and similarities have been noted between BC subtypes and other types of cancer.

The first study into BC subtyping using molecular signatures was conducted at the University of Lund. This previous study examined the transcriptomes from 308 BC samples, identifying five different subtypes: Urobasal A, genomically unstable, urobasal B, squamous cell carcinoma-like and infiltrated (2). In addition, two subtypes of high-grade MIBC were identified by examining published data from 262 BC samples (18). The expression levels of keratin and *CD44* were analyzed, which were found to be related to differentiation of the urinary epithelium. Owing to similarities with expression profiles in breast cancer, these two molecular subtypes were named luminal-like and basal-like. Case studies of the luminal-like subtype revealed that it had much higher disease-specific and overall survival rates compared with the basal-like subtype, and the following transcription factors were enriched: *FGFR3* and tubercular sclerosis 1. Specific changes were also noted in various pathways, including deletion mutations in the RB1 pathway and amplification of cyclin D1, E2F transcription factor 3 and cyclin E1 (18). In 2014, the MD Anderson Cancer Center analyzed mRNA expression patterns in 73 MIBC samples using molecular signatures identified from breast cancer studies. This led to the identification of three BC subtypes: Luminal, p53-like and basal (19). In addition to the aforementioned studies, The Cancer Genome Atlas (TCGA) has greatly improved biological databases and led to the updating of subtypes. Through genetic analysis of 129 patients with MIBC, TCGA identified four molecular BC subtypes: Clusters I, II, III and IV (20). This classification system was updated to include luminal, immune undifferentiated, luminal immune and basal subtypes based on genetic signatures, such as uroplakins and immune infiltration. Upon

analysis of an additional 412 MIBC cases, TCGA classification of BC was further updated and consolidated into five subtypes: Luminal, luminal-infiltrated, basal-squamous, neural and luminal-papillary (21).

3. Interstitial cystitis

Interstitial cystitis (IC) is a chronic condition of unknown etiology with long-term notable pelvic/suprapubic pain and urinary storage symptoms, such as urgency, nocturia and frequency (22). The advent of cystoscopy led to major findings in IC, including bladder glomerulations during hydrodistention and Hunner's lesions (23). Although the epidemiology of IC is difficult to monitor due to its plethora of symptoms, recent studies have suggested an estimated prevalence of 100-300 per 100,000 women, and the prevalence rate is ≥ 10 -20% lower in men (24,25).

IC is generally diagnosed through exclusion; however, several attempts have been made to define standard diagnostic criteria. Recent guidelines set by the European Society for the Study of Interstitial Cystitis and the American Urological Association are currently being used worldwide to treat IC (26). Although treatment options for IC are limited and include hydrodistention, several oral pharmaceutical drugs have been approved by the US Food and Drug Administration, including pentosan polysulfate (elmiron), antihistamines, tricyclic antidepressants and immune modulators (27).

Owing to its unknown etiology, and large variability in sites of occurrence and symptom severity, IC is difficult to subtype. However, there is still an urgent need for a well-established and precise subtyping system. A recent study revealed that IC with Hunner's lesions displayed completely different histology, gene expression and prognoses compared to other forms of IC (28). IC can also be defined as a distinct non-inflammatory disorder characterized by preservation of the urothelium layer and symptom spread beyond the bladder without lesions (29).

4. Metabolomics and lipidomics

Metabolomics. Metabolomics is defined as the large-scale study of small molecules and metabolites involved in the regulation of metabolic pathways and their networks. Compared with genomics and proteomics, metabolomics is more closely linked to phenotypes; therefore, it can detect subtle changes in biological pathways under different physiological conditions and abnormal pathological processes. For the purposes of this review, we will focus on the application of metabolomics and lipidomics to BC.

The aim of precision medicine is to create novel approaches to prevent disease and update clinical strategies to consider each individual's variability in terms of environment, lifestyle, genetics and molecular phenotypes (30). Metabolomics holds much promise for precision medicine and can be used to measure all metabolites in biological specimens (31). However, metabolomics presents significant analytical challenges over genomics and proteomics; it aims to measure molecules that range in polarity, from organic water-soluble acids to nonpolar lipids, which have disparate physical properties (32). As a complement to other omics techniques, metabolomics serves as a critical component of systems biology. Moreover, the study of

metabolites and molecules is closely related to phenotypes and can improve understanding of intracellular metabolic alterations (31). The main aim of metabolomics is to identify altered metabolic pathways and biomarkers (33). Recent developments in metabolomics and statistical capabilities have improved the ability to investigate cancer metabolism and better understand cancer-related changes in metabolism, such as the conversion of glucose into the macromolecules needed for tumor cell proliferation and vascularization (34-36).

Lipidomics. Lipids are essential building blocks in the body that have several critical cellular functions and can provide information regarding ongoing lipid metabolism. The lipidome is the total lipid content in a cell (37). The emergence of lipidomics allows for the complete characterization of the cellular metabolome. Lipidomics may be the potential key to numerous metabolic diseases and can be utilized in several research areas, as well as in the development of diagnostic tools, drugs and therapeutic strategies (38). Lipidomics combined with bioinformatics can serve as a powerful tool for better understanding the biochemical mechanisms underlying lipid-related diseases by quantifying alterations in the levels of individual lipids, subclasses and molecular species, and identifying changes in pathways and networks (37). The emergence of metabolomics and lipidomics has enabled improved definition of differential metabolites in pathological conditions. Over the past two decades, metabolomics and lipidomics have seen significant advances, facilitated by rapid developments in novel analysis strategies, approaches, instruments and techniques (39).

5. Emerging technologies

Current development of methodologies. The physicochemical properties of all metabolites add additional complexity to metabolomics studies. To overcome these restrictions, various methods have been applied to overcome this complexity and challenges. MS and nuclear magnetic resonance (NMR) are the most frequently applied analytical approaches in metabolomics studies.

NMR spectroscopy. NMR is a nondestructive, nonbiased, easily quantifiable, fast and reproducible spectroscopy technique based on the principle that nuclei absorb and emit electromagnetic signals based on changes in the external magnetic field. NMR has several unique advantages in metabolomics (40). Metabolomics profiling by NMR is a powerful tool that can be used to diagnose a variety of diseases. NMR is based on the fact that nuclei, such as ^1H , ^{13}C and ^{31}P , have nuclear spins and are able to exist at different energy levels in a magnetic field. Thus, these nuclei can generate valuable and identifiable information about metabolites. ^1H NMR is the most commonly used technique in metabolomics since ^1H is naturally abundant in biological samples. ^{13}C and ^{31}P NMR are used less frequently but can provide additional information on specific metabolites (40).

MS. MS-based metabolomics offers quantitative analysis of metabolites, ranging from measurement of a single molecule to thousands, with high selectivity and sensitivity. The combination of MS with separation techniques reduces the

complexity of mass spectra by separating metabolites based on time, providing isobar separation and delivering additional information regarding physicochemical properties. To calculate the mass-to-charge ratio (m/z), MS acquires spectral data and relative intensity of the measured compounds. One potential drawback of MS-based techniques is the need for sample preparation, which can lead to potential loss of metabolites, changes in experimental conditions, discrimination of specific metabolite classes and other consequences (41,42).

MS can effectively analyze small molecules separated by techniques, such as gas chromatography (GC), liquid chromatography (LC) and capillary electrophoresis. LC-MS and GC-MS can provide large amounts of chemical information for metabolomics studies. GC-MS uses the gaseous phase and achieves better metabolite separation than LC; however, unlike LC, GC typically requires chemical derivatization of the metabolic species prior to analysis. GC-MS is widely used in metabolomics studies as it can detect a wide range of intact metabolites with no need for chemical modification. For the separation of nonpolar to slightly polar molecules, traditional reverse-phase chromatography is used. Hydrophilic interaction LC is the technique of choice for separating strongly to slightly polar metabolites (41,42).

Advantages and disadvantages. For metabolomics studies, each analytical technique has its own advantages and limitations. No single instrument or method can detect all metabolites accurately. Therefore, multiple methods and instruments are recommended to detect the greatest number of metabolites. For example, the Phenome Centre Birmingham utilizes LC-MS and NMR spectroscopy for metabolomic profiling and is able to detect a higher number of metabolites compared with using a single method alone (<https://www.birmingham.ac.uk/research/activity/phenome-centre/about/index.aspx>). Owing to the complexity of the metabolome, no single analytical method can fully discern the metabolome. NMR and MS each have their own strengths and weaknesses, which are described in previous publications (41-43).

6. Applying metabolomics and lipidomics to BC

Applying metabolomics to BC. To diagnose initial or recurrent BC, two standard diagnostic procedures are used: Cystoscopy and urine cytology. However, there are several limitations (43). As a result, there is an urgent need for a noninvasive, highly-sensitive, specific and convenient method for BC diagnosis. Urine is particularly suited for diagnostic purposes due to its availability, easy sample collection and storage in the malignant bladder (42,44).

Both MS and NMR are used to analyze the metabolic profile and have become critical techniques for quantitatively and qualitatively measuring the metabolome. Both techniques allow for extensive and rapid analysis of small-molecule metabolites (45). Metabolomics can be useful in cancer research, demonstrating its potential for not only identifying candidate biomarkers but also elucidating the mechanisms underlying cancer pathogenesis. Metabolomics has already been applied to several cancer types with encouraging results, including breast, prostate, lung and liver cancer (46-50). Sahu *et al* (51) identified metabolic signatures, including those

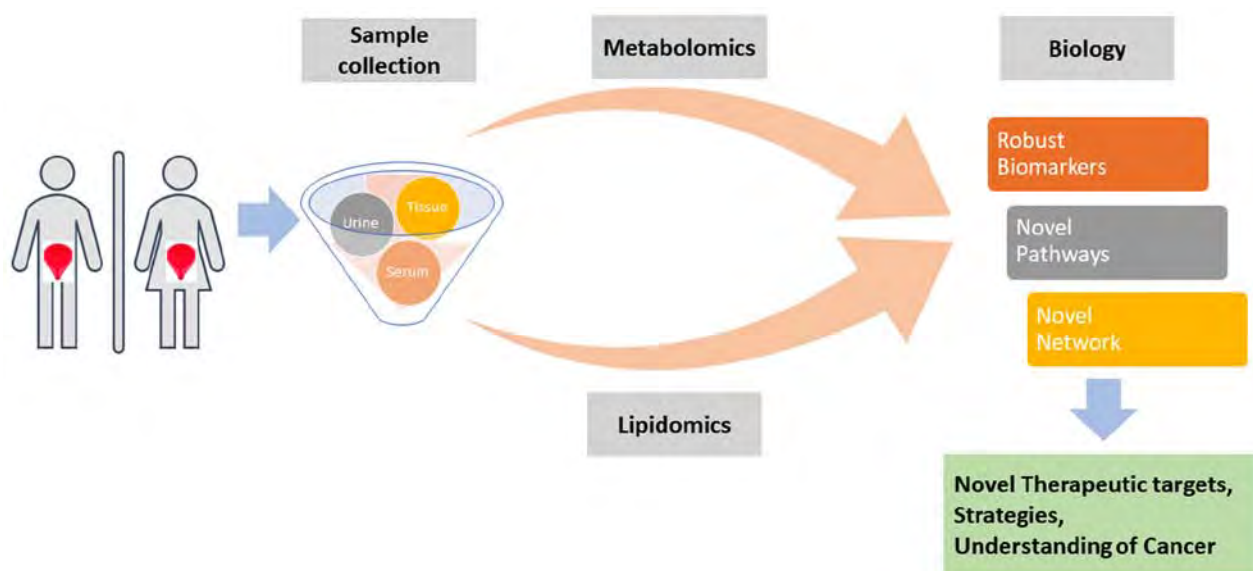


Figure 1. Biomarker discovery in the clinical setting. The field of metabolomics and lipidomics has advanced with respect to technological development. Large-scale datasets can help provide systems-scale information regarding diseases with inputs from metabolomics- and lipidomics-based analyses, which provide insightful biological data. This data can lead to robust and valid individual specific biomarkers for novel disease-specific pathways and networks. The application of new analytical technologies in omics studies should provide new information about promising drug therapeutics and improve understanding of the diseases.

for glucose, the tricarboxylic acid (TCA) cycle, lipids, amino acids and nucleotide pathways, by profiling the global metabolome using GC-MS and LC-MS. The results of this previous study revealed alterations in numerous pathways between normal urothelium and high-grade urothelial carcinoma at different stages. Recently, novel analytical methods have been developed using reverse-phase-high performance LC coupled with triple quadrupole MS for quantitatively determining and validating previously identified BC metabolites (52,53). Clinical validation has previously been performed using urine samples from 40 patients with BC and matched controls, and suggested that the recovery and precision values were within the ranges set by FDA guidelines (52). Jin *et al* (53) performed LC-MS-based profiling of metabolites and identified distinctive metabolites in 138 BC samples and 121 controls. This previous study identified 12 putative glycolysis- and β -oxidation-related markers. Multivariate regression analysis was then applied to confirm the association between the metabolic profiles and survival.

Applying lipidomics to BC. Current technologies allow for lipidomic analysis of a wide variety of biological specimens derived from animal models and clinical samples (54). The most appropriate analytical technique is selected based on the characteristics of the biological sample and the chemical properties of the targeted lipids. NMR and MS are accepted as the most powerful tools for phospholipid structure identification (55). Owing to structural diversity across phospholipid classes, analytical methods for lipidomics are continuously being improved. Notable progress has been made in lipid research by coupling MS with chromatographic separations. Soft ionization techniques, including matrix-assisted laser desorption/ionization and electrospray ionization (ESI), are good examples (56). Dill *et al* (57) used desorption ESI-imaging MS to investigate lipid species as diagnostic

biomarkers of human BC compared to adjacent normal bladder tissue samples. The results revealed significant differences in the levels of glycerophosphoinositols, glycerophosphoserines, and fatty acids in tumor tissues compared with those in normal samples. Our group previously used ultra-performance LC-MS (UPLC-MS) to identify 1,864 differentially expressed lipids in cisplatin-resistant BC cells (58). Another of our lipidomics studies on cisplatin resistance of BC demonstrated that acyl-CoA synthetase short chain family member 2 inhibition perturbed lipid metabolism, suggesting that cisplatin-resistant BC may have a specific lipidomic profile (58). Previously reported metabolomic biomarker candidates are summarized in Table I.

7. Applying metabolomics and lipidomics to IC

Applying metabolomics to IC. Chronic bladder pain is a hallmark of IC. Metabolomics studies can be used to analyze the characteristics of the disease state and identify novel approaches for reducing symptoms (41). Kind *et al* (59) performed global metabolomics profiling using various platforms, including NMR and LC-MS. Utilizing urine from patients with IC, this previous study profiled 490 metabolites, including histidine, erythronic acid and tartaric acid, and identified those with the highest fold changes. The identified metabolites were found to be associated with IC, suggesting its possible clinical use in urinary IC diagnosis. Using an MS-based metabolomics approach, the central clinical protocol of the Multidisciplinary Approach to the Study of Chronic Pelvic Pain (MAPP) Research Network, the Trans-MAPP Epidemiology and Phenotyping discovered urinary biomarkers in female patients with IC who underwent extensive urologic and non-urologic phenotyping (60). Parker *et al* (61) used LC-MS to identify molecular correlates of IC from urine obtained from female patients. This previous study identified a novel biomarker, etiocholan-3 α -ol-17-one sulfate (Etio-S), a steroid metabolite,

Table I. List of metabolomic biomarkers in BC.

First author, year	Biomarker	Method	Sample size	Sensitivity (%)	Specificity (%)	AUC	Notes	(Refs.)
Pasikanti <i>et al</i> , 2013	2,5-furandicarboxylic acid, ribitol and ribonic acid	GCxGC/TOFMS	38 BC, 61 Controls	71	100	-	Decreased	(70)
Wittmann <i>et al</i> , 2014	Taurine	MS	95 BC, 345 Controls	-	-	-	Increased	(68)
Srivastava <i>et al</i> , 2010	Taurine	NMR spectroscopy	33 BC, 37 Controls	-	-	-	Increased	(65)
Jin <i>et al</i> , 2014	Glycolysis and acylcarnitines	LC-QTOFMS	138 BC, 121 Controls	85-91.3	85-92.5	0.93	Increased	(53)

BC, bladder cancer; AUC, area under the curve; GC, gas chromatography; MS, mass spectrometry; LC-MS, liquid chromatography-MS; NMR, nuclear magnetic resonance; GCxGC/TOFMS, two-dimensional GC time-of-flight MS; LC-QTOFMS, LC-quadrupole time-of-flight MS.

as being associated with a phenotypic subgroup of highly symptomatic IC. To the best of our knowledge, there are no reports in the literature involving the use of lipidomics to identify lipid compounds associated with IC.

8. Human specimens-based metabolomics and lipidomics biomarkers for BC

Diagnosis of BC is dependent on several variables, including sensitivity and specificity of the methods, the invasiveness of the procedures and cost. Currently, cystoscopy and urine cytology are the most commonly used methods; however, both have several critical drawbacks, the most important being their limitations for detecting early BC (62). Overall survival in BC is highly dependent on early detection (62). The discovery of clinically relevant BC biomarkers will provide clinical value for prognostication, stratification, and identification of patients at higher risk for recurrence and progression. It is only through these outcomes that better management and treatment of patients with BC can be achieved (50). Zhang *et al* (63) compiled the results of previous metabolomics studies to discover BC biomarkers using urine, blood, tissue and cell lines. However, there is still a lack of consensus surrounding the pathophysiology of BC. Thus, there is a great need for noninvasive markers to differentially diagnose BC (64).

BC biomarkers

Human urine. Numerous studies have reported that biomarkers can be identified using metabolomics, and recent studies have identified biomarkers that are capable of detecting early BC and predicting response to chemotherapy or relapse (53,65-70). Some diagnostic biomarker studies have already compared the metabolic profiles of urine samples from patients with BC and healthy controls. Using ¹H NMR, Srivastava *et al* (65) revealed significant differences in the urine concentrations of hippurate, citrate and taurine in patients with BC compared with those in healthy controls. Jin *et al* (53) hypothesized that patients with BC could be distinguished from healthy controls

based on metabolic profiles. This previous study revealed that the metabolic components of glycolysis and acylcarnitines were increased in MIBC compared with those in NMIBC. Citrate levels, a key metabolite of the TCA cycle, are altered in BC (66). Other urinary metabolites, including citrate, succinate and hippurate, have also been shown to be reduced in BC compared with those in healthy controls (67,68). Shen *et al* (69) also identified three upregulated and downregulated metabolites in BC: Nicotinuric acid, trehalose and AspAspGlyTrp were upregulated, whereas inosinic acid, ureidosuccinic acid and GlyCysAlaLys were downregulated. Several other studies have confirmed these results (70). The major findings from these studies are listed in Table I.

Tissue samples. Putluri *et al* (71) identified LC-MS-based metabolomic signatures using BC tissue samples, benign adjacent tissues and healthy controls. This previous study aimed to identify potential biomarker candidates and identify biology-related processes in BC carcinogenesis. A total of 50 metabolites with significant differences between BC and healthy controls were detected. Tripathi *et al* (72) performed high-resolution magic angle spinning NMR analysis of benign and BC tissues. The results revealed that BC exhibited more metabolic abnormalities compared with benign or healthy samples. These results identified 22 clearly differentiated metabolites. Using the same tissue samples, these results were cross-validated via targeted GC-MS analysis, demonstrating the potential of these biomarkers in clinically diagnosing BC. Yang *et al* (73) examined 48 BC tissue samples treated with gemcitabine as well as adjacent normal tissues from 12 of those patients. Based on UPLC-Q-Exactive-MS analysis, 34 significantly altered metabolites were found to be associated with BC.

Blood serum samples. Blood serum-based studies have established ways of distinguishing patients with BC from healthy controls. Cao *et al* (74) examined the serum profiles of patients with high- or low-grade BC; in addition, patients with urinary calculi (hematuria) were included in the control group.

Table II. List of metabolomic biomarkers in IC.

First author, year	Biomarker	Method	Sample size	Sensitivity (%)	Specificity (%)	AUC	Notes	(Refs.)
Parker <i>et al</i> , 2016	Etiocholan-3 α -ol-1 7-one sulfate	MS	40 IC, 40 Controls	87.4	0.92	0.92	Increased	(61)
Kind <i>et al</i> , 2016	Erythronic acid, histidine and tartaric acid	GC/MS	42 IC, 21 Controls	-	-	0.9	Increased	(59)
Wen <i>et al</i> , 2015	tyramine and 2-oxoglutarate	NMR	43 IC, 21 Controls	-	-	-	Increased	(76)
Shahid <i>et al</i> , 2018	Menthol	GC-TOF-MS	10 IC, 10 Controls	-	-	-	Decreased	(79)

IC, interstitial cystitis; AUC, area under the curve; GC, gas chromatography; MS, mass spectrometry; NMR, nuclear magnetic resonance; GC-TOFMS, GC time-of-flight MS.

Statistical analysis revealed that the serum profiles of patients with BC differed from those of healthy controls and those of patients with calculi. Serum metabolic profiles also allowed for classification of low- and high-grade BC. The levels of isoleucine/leucine, tyrosine, phenylalanine, choline, lactate, glycine and citrate were also shown to be significantly lower in patients with BC compared with those in healthy controls, whereas lipid and glucose levels were higher in patients with BC. Notably, additional comparisons of metabolite levels between patients with low- and high-grade BC revealed that the levels of tyrosine, phenylalanine, lactate and glycine were comparatively higher in low-grade patients, whereas glucose levels were lower. In addition, Bansal *et al* (75) used blood serum samples from patients with low-grade and high-grade BC and healthy controls. A total of six metabolites, dimethylamine, malonate, lactate, glutamine, histidine and valine, were significantly altered in BC samples compared with those in controls. Notably, external validation via a double-blind study consisting of 106 patients with suspected BC confirmed the utility of these metabolites for early diagnosis of BC.

9. Human specimens-based metabolomics markers in IC

IC can present as a long continuum of mild to severe symptoms. In recent years, novel metabolomic techniques have been applied to gain a better understanding of disease mechanisms and uncover novel biomarkers (76). A previous study applied UPLC-MS-based metabolomics to examine urine samples from 10 patients with IC and 10 healthy controls. Phenylacetylglutamine was identified as a urinary marker of IC and was revealed to be elevated in the urine of patients with mild-to-moderate IC (77). In a separate study, Parker *et al* (61) used LC-MS to profile the metabolomes of urine samples from 40 patients with IC and matched controls. The results identified six metabolites as being closely associated with IC pathogenesis; one of which was Etio-S. Further analysis demonstrated that elevated Etio-S was a good predictor of IC, with sensitivity of 91.2%, specificity of 87.4%, and area under the curve of 0.92. Longitudinal analysis of women

in this cohort demonstrated that the differences in Etio-S persisted, indicating that these changes were long-lasting.

Taking an untargeted comprehensive metabolomic profiling approach, Kind *et al* (59) performed GC-MS analysis on urine specimens from patients with IC and healthy donors, and identified a total of 490 differentially expressed metabolites. Furthermore, Lamale *et al* (78) used urine samples from 40 women with IC and 29 healthy controls collected within a 24-h time frame. They discovered higher expression of three inflammatory markers, histamine, methylhistamine and IL-6, in patients with IC compared with those in the controls. In our previous biomarker discovery study, NMR-based global metabolomics analysis was applied to urine samples obtained from female patients with IC and matched healthy controls. The levels of tyramine and 2-oxoglutarate were significantly elevated in the IC urine specimens (76). Furthermore, in another of our previous studies, comprehensive solid-phase microextraction-GC-time-of-flight-MS profiling combined with bioinformatics analysis revealed that levels of volatile urinary metabolites, including menthol, were significantly reduced in patients with IC compared with those in normal controls (79). Previously reported metabolomics-based IC biomarker candidates are presented in Table II.

10. Conclusion

The present review aimed to understand the current development of biomarkers for bladder diseases based on various bioresources. In recent years, metabolomics and lipidomics has been widely used to understand the clinicopathology of the bladder and to discover the key differentially expressed metabolites or lipids specifically associated with bladder diseases. To determine the biological implications of metabolomic lipidomic signatures, bioinformatics tools, such as network and pathway enrichment analyses have been applied. The present review provided an overall summary of the metabolomics and lipidomic-based biomarker candidates for IC and BC (Fig. 1).

Acknowledgements

Not applicable.

Funding

The authors acknowledge support from National Institutes of Health grants (grant nos. 1U01DK103260, 1R01DK100974, U24DK097154 and NIH NCATS UCLA CTSI UL1TR000124), Department of Defense grants (grant nos. W81XWH-15-1-0415 and W81XWH-19-1-0109), Centers for Disease Controls and Prevention (grant no. 1U01DP006079), IMAGINE NO IC Research Grant, the Steven Spielberg Discovery Fund in Prostate Cancer Research Career Development Award, and the U.S.-Egypt Science and Technology Joint Fund. This research was partly supported by the Samuel Oschin Comprehensive Cancer Institute at Cedars-Sinai Medical Center through 2019 Lucy S. Gonda Award (to J.K.). In addition, this article is derived from the Subject Data funded in whole or part by National Academies of Sciences, Engineering, and Medicine (NAS) and The United States Agency for International Development (USAID). Any opinions, findings, conclusions, or recommendations expressed in this article are those of the authors alone, and do not necessarily reflect the views of USAID or NAS.

Availability of data and materials

Not applicable.

Authors' contributions

Research conception and design: JK. Data acquisition, data analysis and interpretation: MS and AY. Drafting of the manuscript: MS and AY. Critical revision of the manuscript: JK. Supervision: JK. All authors read and approved the final manuscript.

Ethics approval and consent to participate

Not applicable.

Patient consent for publication

Not applicable.

Competing interests

The authors declare they have no competing interests.

References

- Bray F, Ferlay J, Soerjomataram I, Siegel RL, Torre LA and Jemal A: Global cancer statistics 2018: GLOBOCAN estimates of incidence and mortality worldwide for 36 cancers in 185 countries. *CA Cancer J Clin* 68: 394-424, 2018.
- Sjodahl G, Lauss M, Lovgren K, Chebil G, Gudjonsson S, Veerla S, Patschan O, Aine M, Fernö M, Ringnér M, *et al*: A molecular taxonomy for urothelial carcinoma. *Clin Cancer Res* 18: 3377-3386, 2012.
- Ferlay J, Soerjomataram I, Dikshit R, Eser S, Mathers C, Rebelo M, Parkin DM, Forman D and Bray F: Cancer incidence and mortality worldwide: Sources, methods and major patterns in GLOBOCAN 2012. *Int J Cancer* 136: E359-E386, 2015.
- European Association of Urology (EAU): EAU Guidelines on Urological Infections. EAU Guidelines Office, Arnhem, 2018. <https://uroweb.org/wp-content/uploads/EAU-Guidelines-on-Urological-Infections-2018-large-text.pdf>.
- Czerniak B, Dinney C and McConkey D: Origins of bladder cancer. *Annu Rev Pathol* 11: 149-174, 2016.
- Gruber K: Coffee consumption and bladder cancer are linked, analysis shows. *BMJ* 350: h1477, 2015.
- Markowski MC, Boorjian SA, Burton JP, Hahn NM, Ingersoll MA, Maleki Vareki S, Pal SK and Sfanos KS: The microbiome and genitourinary cancer: A collaborative review. *Eur Urol* 75: 637-646, 2019.
- Knowles MA and Hurst CD: Molecular biology of bladder cancer: New insights into pathogenesis and clinical diversity. *Nat Rev Cancer* 15: 25-41, 2015.
- Zhang Q, Su M, Lu G and Wang J: The complexity of bladder cancer: Long noncoding RNAs are on the stage. *Mol Cancer* 12: 101, 2013.
- Chen M, Li J, Zhuang C and Cai Z: Increased lncRNA ABHD11-AS1 represses the malignant phenotypes of bladder cancer. *Oncotarget* 8: 28176-28186, 2017.
- Chen M, Zhuang C, Liu Y, Li J, Dai F, Xia M, Zhan Y, Lin J, Chen Z, He A, *et al*: Tetracycline-inducible shRNA targeting antisense long non-coding RNA HIF1A-AS2 represses the malignant phenotypes of bladder cancer. *Cancer Lett* 376: 155-164, 2016.
- Lopez-Beltran A, Henriques V, Montironi R, Cimadamore A, Raspollini MR and Cheng L: Variants and new entities of bladder cancer. *Histopathology* 74: 77-96, 2019.
- Boormans JL, Zwarthoff EC, Black PC, Goebell PJ, Kamat AM, Nawroth R, Seiler R, Williams SB and Schmitz-Dräger BJ: New horizons in bladder cancer research. *Urol Oncol*: March 7, 2019 (Epub ahead of print).
- Kim S, Kim Y, Kong J, Kim E, Choi JH, Yuk HD, Lee H, Kim HR, Lee KH, Kang M, *et al*: Epigenetic regulation of mammalian Hedgehog signaling to the stroma determines the molecular subtype of bladder cancer. *Elife* 8: e43024, 2019.
- Chen LM, Chang M, Dai Y, Chai KX, Dyrskjøt L, Sanchez-Carbayo M, Szarvas T, Zwarthoff EC, Lokeshwar V, Jeronimo C, *et al*: External validation of a multiplex urinary protein panel for the detection of bladder cancer in a multicenter cohort. *Cancer Epidemiol Biomarkers Prev* 23: 1804-1812, 2014.
- Loras A, Suarez-Cabrera C, Martinez-Bisbal MC, Quintás G, Paramio JM, Martínez-Mañez R, Gil S and Ruiz-Cerdá JL: Integrative metabolomic and transcriptomic analysis for the study of bladder cancer. *Cancers (Basel)* 11: 686, 2019.
- Sjodahl G, Jackson CL, Bartlett JM, Siemens DR and Berman DM: Molecular profiling in muscle-invasive bladder cancer: More than the sum of its parts. *J Pathol* 247: 563-573, 2019.
- Damrauer JS, Hoadley KA, Chism DD, Fan C, Tiganelli CJ, Wobker SE, Yeh JJ, Milowsky MI, Iyer G, Parker JS and Kim WY: Intrinsic subtypes of high-grade bladder cancer reflect the hallmarks of breast cancer biology. *Proc Natl Acad Sci USA* 111: 3110-3115, 2014.
- Choi W, Porten S, Kim S, Willis D, Plimack ER, Hoffman-Censits J, Roth B, Cheng T, Tran M, Lee IL, *et al*: Identification of distinct basal and luminal subtypes of muscle-invasive bladder cancer with different sensitivities to frontline chemotherapy. *Cancer Cell* 25: 152-165, 2014.
- Cancer Genome Atlas Research Network: Comprehensive molecular characterization of gastric adenocarcinoma. *Nature* 513: 202-209, 2014.
- Robertson AG, Kim J, Al-Ahmadie H, Bellmunt J, Guo G, Cherniack AD, Hinoue T, Laird PW, Hoadley KA, Akbani R, *et al*: Comprehensive molecular characterization of muscle-invasive bladder cancer. *Cell* 174: 1033, 2018.
- Davis NF, Brady CM and Creagh T: Interstitial cystitis/painful bladder syndrome: Epidemiology, pathophysiology and evidence-based treatment options. *Eur J Obstet Gynecol Reprod Biol* 175: 30-37, 2014.
- Fall M, Baranowski AP, Elneil S, Engeler D, Hughes J, Messelink EJ, Oberpenning F and de C Williams AC: European Association of Urology: EAU guidelines on chronic pelvic pain. *Eur Urol* 57: 35-48, 2010.
- Hanno P, Lin A, Nordling J, van Ophoven A, Ueda T and Wein A: Bladder Pain Syndrome Committee of the International Consultation on Incontinence: Bladder pain syndrome committee of the international consultation on incontinence. *Neurourol Urodyn* 29: 191-198, 2010.

25. Clemens JQ, Mullins C, Ackerman AL, Bavendam T, van Bokhoven A, Ellingson BM, Harte SE, Kutch JJ, Lai HH, Martucci KT, *et al*: Urologic chronic pelvic pain syndrome: Insights from the MAPP research network. *Nat Rev Urol* 16: 187-200, 2019.
26. van de Merwe JP, Nordling J, Bouchelouche P, Bouchelouche K, Cervigni M, Daha LK, Elneil S, Fall M, Hohlbrugger G, Irwin P, *et al*: Diagnostic criteria, classification, and nomenclature for painful bladder syndrome/interstitial cystitis: An ESSIC proposal. *Eur Urol* 53: 60-67, 2008.
27. Hanno PM, Burks DA, Clemens JQ, Dmochowski RR, Erickson D, Fitzgerald MP, Forrest JB, Gordon B, Gray M, Mayer RD, *et al*: AUA guideline for the diagnosis and treatment of interstitial cystitis/bladder pain syndrome. *J Urol* 185: 2162-2170, 2011.
28. Akiyama Y, Maeda D, Katoh H, Morikawa T, Niimi A, Nomiya A, Sato Y, Kawai T, Goto A, Fujimura T, *et al*: Molecular taxonomy of interstitial cystitis/bladder pain syndrome based on whole transcriptome profiling by next-generation RNA sequencing of bladder mucosal biopsies. *J Urol* 202: 290-300, 2019.
29. Peters KM, Killinger KA, Mounayer MH and Boura JA: Are ulcerative and nonulcerative interstitial cystitis/painful bladder syndrome 2 distinct diseases? A study of coexisting conditions. *Urology* 78: 301-308, 2011.
30. Seyhan AA and Carini C: Are innovation and new technologies in precision medicine paving a new era in patients centric care? *J Transl Med* 17: 114, 2019.
31. Clish CB: Metabolomics: An emerging but powerful tool for precision medicine. *Cold Spring Harb Mol Case Stud* 1: a000588, 2015.
32. Kuehnbaum NL and Britz-McKibbin P: New advances in separation science for metabolomics: Resolving chemical diversity in a post-genomic era. *Chem Rev* 113: 2437-2468, 2013.
33. Griffin JL and Shockey JP: Metabolic profiles of cancer cells. *Nat Rev Cancer* 4: 551-561, 2004.
34. Vander Heiden MG: Targeting cancer metabolism: A therapeutic window opens. *Nat Rev Drug Discov* 10: 671-684, 2011.
35. Pereira MM, Shori DK, Dormer RL and McPherson MA: Studies on phosphorylation of calcineurin. *Biochem Soc Trans* 18: 447, 1990.
36. Gatenby RA and Gillies RJ: Why do cancers have high aerobic glycolysis? *Nat Rev Cancer* 4: 891-899, 2004.
37. Han X: Lipidomics for studying metabolism. *Nat Rev Endocrinol* 12: 668-679, 2016.
38. Lydic TA and Goo YH: Lipidomics unveils the complexity of the lipidome in metabolic diseases. *Clin Transl Med* 7: 4, 2018.
39. Blanksby SJ and Mitchell TW: Advances in mass spectrometry for lipidomics. *Annu Rev Anal Chem (Palo Alto Calif)* 3: 433-465, 2010.
40. Emwas AH, Roy R, McKay RT, Tenori L, Saccenti E, Gowda GAN, Raftery D, Alahmari F, Jaremko L, Jaremko M and Wishart DS: NMR spectroscopy for metabolomics research. *Metabolites* 9: 123, 2019.
41. Fiehn O and Kim J: Metabolomics insights into pathophysiological mechanisms of interstitial cystitis. *Int Neurourol J* 18: 106-114, 2014.
42. Chen Z and Kim J: Urinary proteomics and metabolomics studies to monitor bladder health and urological diseases. *BMC Urol* 16: 11, 2016.
43. Zhu CZ, Ting HN, Ng KH and Ong TA: A review on the accuracy of bladder cancer detection methods. *J Cancer* 10: 4038-4044, 2019.
44. Kim J, Kim WT and Kim WJ: Advances in urinary biomarker discovery in urological research. *Investig Clin Urol* 61 (Suppl 1): S8-S22, 2020.
45. Nicholson JK, Connelly J, Lindon JC and Holmes E: Metabonomics: A platform for studying drug toxicity and gene function. *Nat Rev Drug Discov* 1: 153-161, 2002.
46. Sreekumar A, Poisson LM, Rajendiran TM, Khan AP, Cao Q, Yu J, Laxman B, Mehra R, Lonigro RJ, Li Y, *et al*: Metabolomic profiles delineate potential role for sarcosine in prostate cancer progression. *Nature* 457: 910-914, 2009.
47. Jobard E, Pontoizeau C, Blaise BJ, Bachelot T, Elena-Herrmann B and Tredan O: A serum nuclear magnetic resonance-based metabolomic signature of advanced metastatic human breast cancer. *Cancer Lett* 343: 33-41, 2014.
48. Carrola J, Rocha CM, Barros AS, Gil AM, Goodfellow BJ, Carreira IM, Bernardo J, Gomes A, Sousa V, Carvalho L and Duarte IF: Metabolic signatures of lung cancer in biofluids: NMR-based metabolomics of urine. *J Proteome Res* 10: 221-230, 2011.
49. Chen F, Xue J, Zhou L, Wu S and Chen Z: Identification of serum biomarkers of hepatocarcinoma through liquid chromatography/mass spectrometry-based metabonomic method. *Anal Bioanal Chem* 401: 1899-1904, 2011.
50. Rodrigues D, Jeronimo C, Henrique R, Belo L, de Lourdes Bastos M, de Pinho PG and Carvalho M: Biomarkers in bladder cancer: A metabolomic approach using in vitro and ex vivo model systems. *Int J Cancer* 139: 256-268, 2016.
51. Sahu D, Lotan Y, Wittmann B, Neri B and Hansel DE: Metabolomics analysis reveals distinct profiles of nonmuscle-invasive and muscle-invasive bladder cancer. *Cancer Med* 6: 2106-2120, 2017.
52. Yumba Mpanga A, Siluk D, Jacyna J, Szerkus O, Wawrzyniak R, Markuszewski M, Matuszewski M, Kaliszczak R and Markuszewski MJ: Targeted metabolomics in bladder cancer: From analytical methods development and validation towards application to clinical samples. *Anal Chim Acta* 1037: 188-199, 2018.
53. Jin X, Yun SJ, Jeong P, Kim IY, Kim WJ and Park S: Diagnosis of bladder cancer and prediction of survival by urinary metabolomics. *Oncotarget* 5: 1635-1645, 2014.
54. Yang K and Han X: Lipidomics: Techniques, applications, and outcomes related to biomedical sciences. *Trends Biochem Sci* 41: 954-969, 2016.
55. Ellis DI, Dunn WB, Griffin JL, Allwood JW and Goodacre R: Metabolic fingerprinting as a diagnostic tool. *Pharmacogenomics* 8: 1243-1266, 2007.
56. Wang C, Wang M and Han X: Applications of mass spectrometry for cellular lipid analysis. *Mol Biosyst* 11: 698-713, 2015.
57. Dill AL, Eberlin LS, Costa AB, Zheng C, Ifa DR, Cheng L, Masterson TA, Koch MO, Vitek O and Cooks RG: Multivariate statistical identification of human bladder carcinomas using ambient ionization imaging mass spectrometry. *Chemistry* 17: 2897-2902, 2011.
58. Lee MY, Yeon A, Shahid M, Cho E, Sairam V, Figlin R, Kim KH and Kim J: Reprogrammed lipid metabolism in bladder cancer with cisplatin resistance. *Oncotarget* 9: 13231-13243, 2018.
59. Kind T, Cho E, Park TD, Deng N, Liu Z, Lee T, Fiehn O and Kim J: Interstitial cystitis-associated urinary metabolites identified by mass-spectrometry based metabolomics analysis. *Sci Rep* 6: 39227, 2016.
60. Clemens JQ, Mullins C, Kusek JW, Kirkali Z, Mayer EA, Rodríguez LV, Klumpp DJ, Schaeffer AJ, Kreder KJ, Buchwald D, *et al*: The MAPP research network: A novel study of urologic chronic pelvic pain syndromes. *BMC Urol* 14: 57, 2014.
61. Parker KS, Crowley JR, Stephens-Shields AJ, van Bokhoven A, Lucia MS, Lai HH, Andriole GL, Hooton TM, Mullins C and Henderson JP: Urinary metabolomics identifies a molecular correlate of interstitial cystitis/bladder pain syndrome in a multidisciplinary approach to the study of chronic pelvic pain (MAPP) research network cohort. *EBioMedicine* 7: 167-174, 2016.
62. Mbeutcha A, Lucca I, Mathieu R, Lotan Y and Shariat SF: Current status of urinary biomarkers for detection and surveillance of bladder cancer. *Urol Clin North Am* 43: 47-62, 2016.
63. Zhang WT, Zhang ZW, Guo YD, Wang LS, Mao SY, Zhang JF, Liu MN and Yao XD: Discovering biomarkers in bladder cancer by metabolomics. *Biomark Med* 12: 1347-1359, 2018.
64. Kuo HC: Potential urine and serum biomarkers for patients with bladder pain syndrome/interstitial cystitis. *Int J Urol* 21 (Suppl 1): S34-S41, 2014.
65. Srivastava S, Roy R, Singh S, Kumar P, Dalela D, Sankhwar SN, Goel A and Sonkar AA: Taurine-a possible fingerprint biomarker in non-muscle invasive bladder cancer: A pilot study by 1H NMR spectroscopy. *Cancer Biomark* 6: 11-20, 2010.
66. Anderson NM, Mucka P, Kern JG and Feng H: The emerging role and targetability of the TCA cycle in cancer metabolism. *Protein Cell* 9: 216-237, 2018.
67. Pasikanti KK, Esuvaranathan K, Ho PC, Mahendran R, Kamaraj R, Wu QH, Chiong E and Chan EC: Noninvasive urinary metabolomic diagnosis of human bladder cancer. *J Proteome Res* 9: 2988-2995, 2010.
68. Wittmann BM, Stirdivant SM, Mitchell MW, Wulff JE, McDunn JE, Li Z, Dennis-Barrie A, Neri BP, Milburn MV, Lotan Y and Wolfert RL: Bladder cancer biomarker discovery using global metabolomic profiling of urine. *PLoS One* 9: e115870, 2014.
69. Shen C, Sun Z, Chen D, Su X, Jiang J, Li G, Lin B and Yan J: Developing urinary metabolomic signatures as early bladder cancer diagnostic markers. *OMICS* 19: 1-11, 2015.

70. Pasikanti KK, Esuvaranathan K, Hong Y, Ho PC, Mahendran R, Raman Nee Mani L, Chiong E and Chan EC: Urinary metabotyping of bladder cancer using two-dimensional gas chromatography time-of-flight mass spectrometry. *J Proteome Res* 12: 3865-3873, 2013.
71. Putluri N, Shojaie A, Vasu VT, Vareed SK, Nalluri S, Putluri V, Thangjam GS, Panzitt K, Tallman CT, Butler C, *et al*: Metabolomic profiling reveals potential markers and bioprocesses altered in bladder cancer progression. *Cancer Res* 71: 7376-7386, 2011.
72. Tripathi P, Somashekar BS, Ponnusamy M, Gursky A, Dailey S, Kunju P, Lee CT, Chinnaiyan AM, Rajendiran TM and Ramamoorthy A: HR-MAS NMR tissue metabolomic signatures cross-validated by mass spectrometry distinguish bladder cancer from benign disease. *J Proteome Res* 12: 3519-3528, 2013.
73. Yang C, Sun X, Wang H, Lu T, Wu K, Guan Y, Tang J, Liang J, Sun R, Guo Z, *et al*: Metabolomic profiling identifies novel biomarkers and mechanisms in human bladder cancer treated with submucosal injection of gemcitabine. *Int J Mol Med* 44: 1952-1962, 2019.
74. Cao M, Zhao L, Chen H, Xue W and Lin D: NMR-based metabolomic analysis of human bladder cancer. *Anal Sci* 28: 451-456, 2012.
75. Bansal N, Gupta A, Mitash N, Shakya PS, Mandhani A, Mahdi AA, Sankhwar SN and Mandal SK: Low- and high-grade bladder cancer determination via human serum-based metabolomics approach. *J Proteome Res* 12: 5839-5850, 2013.
76. Wen H, Lee T, You S, Park SH, Song H, Eilber KS, Anger JT, Freeman MR, Park S and Kim J: Urinary metabolite profiling combined with computational analysis predicts interstitial cystitis-associated candidate biomarkers. *J Proteome Res* 14: 541-548, 2015.
77. Fukui Y, Kato M, Inoue Y, Matsubara A and Itoh K: A metabolomic approach identifies human urinary phenylacetylglutamine as a novel marker of interstitial cystitis. *J Chromatogr B Analyt Technol Biomed Life Sci* 877: 3806-3812, 2009.
78. Lamale LM, Lutgendorf SK, Zimmerman MB and Kreder KJ: Interleukin-6, histamine, and methylhistamine as diagnostic markers for interstitial cystitis. *Urology* 68: 702-706, 2006.
79. Shahid M, Lee MY, Yeon A, Cho E, Sairam V, Valdiviez L, You S and Kim J: Menthol, a unique urinary volatile compound, is associated with chronic inflammation in interstitial cystitis. *Sci Rep* 8: 10859, 2018.



This work is licensed under a Creative Commons Attribution-NonCommercial-NoDerivatives 4.0 International (CC BY-NC-ND 4.0) License.



Proteomic profiling of bladder cancer for precision medicine in the clinical setting: A review for the busy urologist

Jayoung Kim^{1,2} , Peng Jin^{1,3} , Wei Yang^{1,2} , Wun-Jae Kim^{4,5} 

¹Departments of Surgery and Biomedical Sciences, Cedars-Sinai Medical Center, Los Angeles, CA, ²Department of Medicine, University of California Los Angeles, Los Angeles, CA, USA, ³Department of Urology, Shengjing Hospital of China Medical University, Shenyang, China, ⁴Department of Urology, Chungbuk National University College of Medicine, Cheongju, ⁵Institute of UroTech, Cheongju, Korea

At present, proteomic methods have successfully identified potential biomarkers of urological malignancies, such as prostate cancer (PC), bladder cancer (BC), and renal cell carcinoma (RCC), reflecting different numbers of key cellular processes, including extracellular environment modification, invasion and metastasis, chemotaxis, differentiation, metabolite transport, and apoptosis. The potential application of proteomics in the detection of clinical markers of urological malignancies can help improve patient assessment through early cancer detection, prognosis, and treatment response prediction. A variety of proteomic studies have already been carried out to find prognostic BC biomarkers, and a large number of potential biomarkers have been reported. It is worth noting that proteomics research has not been applied to the study of predictive markers; this may be due to the incompatibility between the number of measured variables and the available sample size, which has become particularly evident in the study of therapeutic response. On the contrary, prognostic correlation is more common, which is also reflected in existing research. We are now entering an era of clinical proteomics. Driven by proteomic-based workflows, computing tools, and the applicability of cross-correlation of proteomic data, it is now feasible to use proteomic analysis to support personalized medicine. In this paper, we will summarize the current emerging technologies for advanced discovery, targeted proteomics, and proteomic applications in BC, particularly in discovery of human-based biomarkers.

Keywords: Precision medicine; Review; Urinary bladder neoplasms

This is an Open Access article distributed under the terms of the Creative Commons Attribution Non-Commercial License (<http://creativecommons.org/licenses/by-nc/4.0>) which permits unrestricted non-commercial use, distribution, and reproduction in any medium, provided the original work is properly cited.

INTRODUCTION

Bladder cancer (BC) is the fourth most common malignant tumor in the United States. Traditionally, based on the degree of invasion in the bladder muscle wall, BC can be classified into either non-muscle invasive (NMIBC) or muscle invasive (MIBC) [1]. Based on the differing histology

of BC, there are several types. Transitional cell carcinoma (TCC) accounts for about 90% of all BC [2]. Other histological variants found in clinical specimens include squamous, glandular, plasmacytoid, sarcomatoid, micropapillary, and small cell carcinoma [3]. BC can also be divided pathologically into low-grade (LG) or high-grade (HG) tumors. LG tumors are usually well-differentiated, while HG tumors are poorly dif-

Received: 9 July, 2020 • **Accepted:** 6 August, 2020 • **Published online:** 27 October, 2020

Corresponding Author: Wun-Jae Kim  <https://orcid.org/0000-0002-8060-8926>

Department of Urology, Chungbuk National University College of Medicine, 1, Chungdae-ro, Seowon-Gu, Cheongju 28644, Korea
TEL: +82-43-269-6371, FAX: +82-43-269-6144, E-mail: wjkim@chungbuk.ac.kr

Table 1. Widely accepted classifications of BC based on molecular phenotypes

UNC	MDA	Lund	TCGA	Broad
Basal	Basal	UroA	Cluster I	Basal
Luminal	Luminal	UroB	Cluster II	Luminal
Claudin-low	P53-like	GU	Cluster III	Luminal immune
		SCCL	Cluster IV	Immune undifferentiated
		Infiltrated		

BC, bladder cancer; UNC, the University of North Carolina; MDA, MD Anderson Cancer Center; Lund, Lund University; TCGA, The Cancer Genome Atlas; Broad, Broad Institute of Massachusetts Institute of Technology and Harvard University; UroA, urobasal A; UroB, urobasal B; GU, genomically unstable; SCCL, squamous cell carcinoma like.

ferentiated [4].

SUBTYPE CLASSIFICATION OF BLADDER CANCER

Recent genome mRNA expression analysis demonstrated that BC can be classified into molecular subtypes. These different molecular subtypes of BC have distinct progression patterns, biological and clinical properties, and response to chemotherapies. There are currently five published classification methods; these include guidelines from the University of North Carolina (UNC), MD Anderson Cancer Center (MDA), The Cancer Genome Atlas (TCGA), Lund University (Lund), and Broad Institute of Massachusetts Institute of Technology and Harvard University (Broad) (Table 1).

The classifications by UNC define two molecular subtypes of HG BC, “luminal” and “basal”, with molecular features reflecting different stages of urothelial differentiation [5]. Luminal BC expresses terminal urothelial differentiation markers, such as those seen in umbrella cells (*uroplakin-1B* [*UPK1B*], *UPK2*, *UPK3A*, and *keratin-20* [*KRT20*]), whereas basal BC expresses high levels of genes that are typical in urothelial basal cells (*keratin-14* [*KRT14*], *KRT5*, and *KRT5B*). The UNC study created a gene signature, BASE47, that accurately discriminates intrinsic BC subtypes. Identified basal tumors had significantly decreased disease-specific and overall survival (OS). In addition, among the clinicopathological features available in from the Memorial Sloan Kettering Cancer Center dataset, only the subtypes identified by the BASE47 signature were found to be significant in disease-specific survival by univariate analysis.

Kardos et al. [6] reported the discovery of a claudin-low molecular subtype of high-grade BC that shares characteristics with the homonymous subtype of breast cancer. Although there has been much work done on the molecular phenotyping of BC, the different emphases of different classification methods have made it difficult to consolidate a widely accepted classification method. As a result, the molec-

ular phenotyping of BC remains to be further studied. The claudin-low subtype can be considered a subpopulation of the basal-like subtype (UNC classification system). Claudin-low BC tumors are rich in a variety of genetic characteristics, including increased mutation rates of *retinoblastoma transcriptional corepressor 1* (*RBI*), *E1A binding protein P300* (*EP300*), and *nuclear receptor corepressor 1* (*NCOR1*), and have increased frequency of *estimated glomerular filtration rate* (*EGFR*) amplification, decreased mutation rates of *fibroblast growth factor receptor 3* (*FGFR3*), *E74-like ETS transcription factor 3* (*ELF3*), and *lysine demethylase 6A* (*KDM6A*), and decreased frequency of *peroxisome proliferator activated receptor gamma* (*PPAR γ*) amplification. These characteristics define a molecular subtype of BC with distinct molecular features and an immunological profile that is theoretically primed for an immunotherapeutic response.

The classification system by MDA identified three molecular subtypes of MIBC: “basal”, “luminal”, and “P53-like” [7]. Basal MIBC was associated with shorter disease-specific and OS, presumably because these patients tend to have more invasive and metastatic disease at presentation. Transcription factor P63 plays a central role in controlling basal gene signatures and preliminary data suggests that EGFR, signal transducer and activator of transcription 3 (STAT3), nuclear factor kappa-light-chain-enhancer of activated B cells (NF κ B), and hypoxia-inducible factor 1-alpha (Hif-1 α) are also involved. Luminal MIBC displays active estrogen receptor/tripartite motif containing 24 (ER/TRIM24) pathway gene expression and was enriched for *forkhead box A1* (*FOXA1*), *GATA binding protein 3* (*GATA3*), *Erb-B2 receptor tyrosine kinase 2* (*ERBB2*), and *Erb-B2 receptor tyrosine kinase 3* (*ERBB3*). Luminal MIBC contains active *PPAR* gene expression and activating *FGFR3* mutations; therefore, *PPAR γ* - and *FGFR-3*-targeted agents may be therapeutic in this subtype. Because luminal MIBC responds well to neoadjuvant chemotherapy (NAC), targeted therapies should be combined with conventional chemotherapy for maximum efficacy. The P53-like MIBC responded very poorly to NAC

and was consistently resistant to frontline neoadjuvant cisplatin-based combination chemotherapy. Additionally, comparative analysis of matched gene expression profiles before and after chemotherapy revealed that all resistant tumors expressed the wild-type P53 gene expression signature. These results indicate that “P53-ness” may play a central role in BC chemoresistance.

The classification system by TCGA identified four clusters (clusters I–IV) by analyzing RNA-seq data from 129 tumors [8]. Cluster I (papillary-like) is enriched for in tumors with papillary morphology, *FGFR3* mutations, *FGFR3* copy number gain, and elevated *FGFR3* expression. Cluster I samples also had significantly lower expression of *miR-99a*, *miR-100*, *miR-145*, and *miR-125b*. Tumors with *FGFR3* alterations and those that share similar cluster I expression profiles may respond well to inhibitors of *FGFR* and its downstream targets. Clusters I and II express high levels of *GATA3* and *FOXA1*. Markers of urothelial differentiation, such as *uroplakins*, *epithelial marker E-cadherin*, and *members of miR-200* miRNAs, are also highly expressed in clusters I and II. Clusters I and II express high *human epidermal growth factor receptor 2 (HER2)* levels and an elevated estrogen receptor beta signaling signature, which suggests potential utilization of hormone therapies, such as tamoxifen or raloxifene. Cluster III (basal/squamous-like) express characteristic epithelial lineage genes, including *KRT14*, *KRT5*, *KRT6A*, and *EGFR*. Many of the samples in cluster III express *cytokeratins (KRT14 and KRT5)*. Integrated expression profiling analysis of cluster III revealed an urothelial carcinoma subtype with cancer stem-cell expression features, perhaps providing another avenue for therapeutic targeting.

The Lund classification system defines five major urothelial carcinoma subtypes: urobasal A, genomically unstable, urobasal B, squamous cell carcinoma-like (SCC-like), and infiltrated tumor class [9]. This was established using gene expression profiles from 308 tumor cases. These different molecular subtypes show significantly different prognoses.

Urobasal A had the best prognosis, whereas urobasal B and SCC-like had the worst. The prognoses of the genomically unstable and infiltrated classes were found to be moderate. Urobasal A tumors were characterized by elevated expression of *FGFR3*, *cyclin D1 (CCND1)*, *P63 (TP63)*, as well as expression of *KRT5* in cells at the tumor–stroma interface. The majority of urobasal A tumors were NMIBC and of low pathological grade. The genomically unstable subtype was characterized by expression of *ERBB2* and *cyclin E (CCNE)*, low expression of *cytokeratins*, and frequent mutations of *P53 (TP53)*. Genomically unstable cases represented a high-risk group; as close to 40% were MIBC. This subtype also

showed low *phosphatase and tensin homolog (PTEN)* expression. The SCC-like subtype was characterized by high expression of *basal keratins*, which are normally not expressed in the urothelium; these include *KRT4*, *KRT6A*, *KRT6B*, *KRT6C*, *KRT14*, and *KRT16*. SCC-like tumors also had markedly bad prognoses. Furthermore, this group showed a comparatively different proportion of female/male patients, reminiscent of the 1:1 proportion seen in patients diagnosed with bladder SCC, suggesting that females are more likely to develop urothelial carcinomas with a keratinized/squamous phenotype. Urobasal B tumors had several similarities to urobasal A tumors, such as a high *FGFR3* mutation frequency, elevated *FGFR3*, *CCND1*, and *TP63* levels, and expression of the *FGFR3* gene signature. However, this group also showed frequent *TP53* mutations and expression of several keratins specific for the SCC-like subtype. Additionally, 50% of the cases were MIBC, including 5 out of 9 that were *FGFR3*-mutated. The infiltrated subtype demonstrated a pronounced immunologic and extracellular membrane (ECM) signal, indicating the presence of immunologic and myofibroblast cells. This subtype most likely represents a heterogeneous class of tumors; immunohistochemistry (IHC) revealed the presence of tumors with genomically unstable, urobasal B, and SCC-like protein expression patterns in this group.

The Broad classification system defines four different subtypes: luminal, immune undifferentiated, luminal immune, and basal [10]. Approximately 41% of invasive BC cases were luminal, with high expression of *KRT20* and *UPKs 2/1A/1B/3A* as well as moderate to high expression of multiple pertinent transcription factors (Kruppel Like Factor 5 [KLF5], PPAR γ , and grainyhead-like 5 [GRHL5]). The luminal subtype was enriched for in male patients, BC with papillary histology, and stage II tumors. A third (29%) of invasive BC was in the basal subtype, with high expression of *KRT14*, *KRT5*, *KRT6A/B*, and *KRT16*, and low expression of *uroplakins*, which is consistent with basal or undifferentiated cytokeratin expression patterns. Consistent with prior studies, the basal subtype expressed *TP63*, *TP73*, *MYC* Proto-Oncogene, *BHLH Transcription Factor (MYC)*, *GFR*, *transglutaminase 1 (TGMI)*, and *Sciellin (SCEL)*, which is indicative of some degree of squamous differentiation. The basal subtype was enriched for in female patients and tumors with nonpapillary histology. The basal subtype also expressed many immune genes at intermediate and somewhat variable levels. These genes include *cytotoxic T-lymphocyte associated protein 4 (CTLA4)* and *CD274*, which encodes for *programmed death-ligand 1 (PD-L1)*, suggesting that there may be immune cell infiltration of tumors. A smaller per-

centage of cancers (11%) were grouped into a novel subtype called immune undifferentiated. These cancers showed very low expression of luminal markers, variable expression of basal cytokeratin, and relatively high expression of immune genes, including *CTLA4* and *CD274*, which further suggests significant immune cell infiltration and possible immune evasion. Lastly, the luminal immune subtype group constitutes about 18% of all cases and is characterized by the expression of luminal genes (cytokeratins and uroplakins) and intermediate expression of immune genes. This group was notably enriched for in stage N+ tumors. The luminal subtype was enriched for in cancers with *FGFR3* mutations and amplification events involving *PVRL4* (*nectin-4*) and *tyrosine 3-monooxygenase/tryptophan 5-monooxygenase activation protein zeta* (*YWHAZ*). The basal subtype was enriched for *nuclear factor erythroid 2 like 2* (*NFE2L2*) mutations. Both the luminal immune and immune undifferentiated subtypes had high expression levels of *zinc finger E-box binding homeobox 1* (*ZEB1*), *ZEB2*, and *twist family BHLH transcription factor 1* (*TWIST1*), which is characteristic of epithelial-mesenchymal transition (EMT).

All classification systems discussed above are widely accepted and based on molecular phenotyping. With ongoing progress in BC research, additional phenotyping classifications have been proposed. Here, we want to introduce some of these new classification systems (Table 2).

Sjödahl et al. [11] proposed five major tumor-cell phenotypes in advanced BC: urothelial-like, genomically unstable (GU), basal/SCC-like, mesenchymal-like, and small-cell/neuroendocrine-like. Urothelial-like tumors express *FGFR3* and *CCND1* and frequently demonstrate a loss of *9p21* (*cyclin dependent kinase inhibitor 2A* [*CDKN2A*]). GU tumors express *forkhead box M1* (*FOXM1*), but not *KRT5*, and frequently show loss of *RBI*. Basal/SCC-like tumors were found to express *KRT5* and *KRT14*, but not *FOXA1* and *GATA3*. The mesenchymal-like BC is a new subtype that shows a tumor-cell phenotype that starkly contrasts with previously defined subtypes and is biologically different from the basal/SCC-like cases that they are clustered with. These tumor

cells are mesenchymal-like and express typical mesenchymal genes, such as *ZEB2* and *vimentin* (*VIM*). The consensus cluster, Sc/NE-like, harbors two very distinct tumor-cell phenotypes. Half of these tumors expressed markers that are typical for neuroendocrine differentiation. This part of the Sc/NE consensus cluster also showed an absence of *PPARG*, *FOXA1*, *uroplakin*, *KRT20*, and *GATA3* expression.

Song et al. [12] explored large-scale genomic datasets encompassing NMIBC and MIBC, redefining four distinct molecular subtypes, aptly named classes 1–4. Class 1 is characterized by decreased expression of genes involved in cell proliferation, signifying the less aggressive characteristics of class 1. Class 2 included both low-grade NMIBCs and a small number of MIBCs. Class 2 displayed downregulation of immune response pathways, such as antigen processing and presentation and T cell receptor signaling pathways. All verified *human leukocyte antigen* (*HLA*) genes, which were associated with clinical prognosis in cancer patients [13], exhibited a specifically inhibited pattern in class 2. They also examined activated functions in class 2, observing increased expression of the oncogenes *FGFR3* and *CCND1* [3]. Class 3 exhibited similar involvement of high-grade NMIBC and MIBC. In particular, most T1 high-grade tumors (11 out of 16, 69%) were classified into class 3, indicating that class 3 might be capable of detecting high-risk NMIBC with progressive disease. Class 3 displayed activation of cell cycle-associated functions and the inhibition of genes involved in the Notch signaling pathway. These processes are associated with tumor progression [14–16]. Increased expression of cell cycle-related genes (*E2F1*, *FOXM1*, *CCNB1*, and *CCNE1*) [16–18] in class 3 was observed in both the NMIBC and MIBC cases. Finally, class 4, which contained the most MIBC cases, exhibited clear upregulation of genes implicated in extracellular matrix organization along with strong activation of immune response. Additionally, class 4 tumors exhibited overexpression of genes associated with EMT or myofibroblasts, which is a shared feature with the Lund infiltrated subtype [9].

Tan et al. [19] identified six molecular subtypes with differing OS and molecular features by analyzing 2,411 urothe-

Table 2. Recently developed new classifications of bladder cancer (BC) based on molecular phenotypes

Sjödahl et al. [11]	Song et al. [12]	Tan et al. [19]	Robertson et al. [20]	Kamoun et al. [23]
Urothelial-like	Class 1	Neural-like	Luminal-papillary	Luminal papillary
Genomically unstable	Class 2	HER2-like	Luminal-infiltrated	Luminal nonspecified
Basal/SCC-like	Class 3	Papillary-like	Luminal	Luminal unstable
Mesenchymal-like	Class 4	Luminal-like	Basal-squamous	Stroma-rich
Small-cell/neuroendocrine-like		Mesenchymal-like	Neuronal	Basal/squamous
		Squamous-cell carcinoma-like		Neuroendocrine-like

SCC, squamous cell carcinoma; HER2, human epidermal growth factor receptor 2.

lial BC tumors. These subtypes are neural-like, HER2-like, papillary-like, luminal-like, mesenchymal-like, and squamous cell carcinoma-like. The neural-like subtype (median OS, 87 mo) was prevalently MIBC and characterized by high WNT/ β -catenin signaling. HER2-like (median OS, 107.7 mo) evenly consisted of NMIBC and MIBC, with higher ERBB2 amplification and signaling. Papillary-like (median OS, >135 mo), an NMIBC subtype enriched in urothelial differentiation genes, showed a high frequency of actionable *FGFR3* mutations, amplifications, and *FGFR3-TACC3* fusion. Luminal-like (median OS, 91.7 mo), which was predominantly NMIBC, had higher mitogen-activated protein kinase (MAPK) signaling and more KRAS proto-oncogene, *GTPase (KRAS)*, and *lysine methyltransferase 2 C/D (KMT2 C/D)* mutations than other subtypes. Mesenchymal-like (MES; median OS, 86.6 mo) and SCC-like (median OS, 20.6 mo) were predominantly MIBC. MES is high in AXL receptor tyrosine kinase (AXL) signaling, whereas SCC has elevated programmed death 1 (PDI), CTLA4 signaling, and macrophage M2 infiltration.

Robertson et al. [20] studied the mRNA expression of BC and identified five subtypes: luminal-papillary, luminal-infiltrated, luminal, basal-squamous, and neuronal. These subtypes were associated with OS. Luminal-papillary tumors had papillary shape, low stage, and high purity. It was characterized by *FGFR3* mutations, fusion with *Tacc3*, and/or amplification. The risk of tumor progression and possibility of response to cisplatin-based NAC was very low [21]. The features of the luminal-infiltrated subtype included lowest purity, high expression of EMT, myofibroblast markers, and *miR-200s*, and moderate expression of *CD274* and *CTLA4*. Simultaneously, this subtype was also characterized by wild type p53 [7]. These tumors were found to be possibly resistant to cisplatin. Several uroplakins (*UPK1A*, *UPK2*) and genes (*krt20*, *snx31*) had the highest gene expression levels in the luminal subtype tumors. The basal-squamous subtype was characterized by high expression of *CD44*, *KRT5*, *KRT6A*, *KRT14*, *TGM1*, *DSC3*, *PI3*, *CD274*, and *CTLA4*. The incidence rate of this tumor was high in females. Cisplatin-based NAC and immunological checkpoint therapy were both suitable treatments for this subtype [22]. The neuronal subtype was characterized by expression of both neuroendocrine and neuronal genes and elevated cell cycle signals reflective of proliferation status. Small cell neuroendocrine cancer was characterized by loss of *TP53* and *RBI*. This subtype had the worst survival.

Kamoun et al. [23] identified six molecular subtypes of MIBC: luminal papillary, luminal non-specified, luminal unstable, stroma-rich, basal/squamous, and neuroendocrine-like. The three luminal subtypes were found to overexpress fea-

tures of urothelial differentiation, such as *PPARG/GATA3/FOXAI*. The characteristics of luminal papillary subtype included high expression of non-invasive TA pathway signal [24] and was closely related to *FGFR3* transcription activity. Luminal papillary tumors were abundantly T2 or T3-4 tumors, and the proportion of patients under 60 years old was much higher. The luminal non-specified subtype displayed elevated stromal infiltration signatures, mainly fibroblastic. This was the only luminal subtype associated with immune infiltration signals, which were mainly for B and T lymphocytes. Luminal non-specified tumors were abundant in *Elf3* gene mutations and was common in elderly patients. The luminal unstable subtype had higher cell cycle activity than other luminal tumors, and also contained frequent *PPARG* alterations and high-level amplification of *E2F3* and *SOX4*. The stroma-rich subtype presented a moderate degree of urothelial differentiation. It is mainly manifested by stromal infiltration and overexpression of genes in smooth muscle, endothelial cells, fibroblasts, and myofibroblasts, and contains higher levels of non-tumor cells. Immune infiltration was mainly seen in stroma-rich tumors (mostly T cells and B cell markers). The basal/squamous subtype was characterized by overexpression of genes related to basal cell differentiation. Immune infiltration is also found in this subtype (mainly cytotoxic lymphocytes and natural killer cells) with high levels of nontumorous cells. Basal/squamous tumors were strongly related to *STAT3* and *EGFR* regulon activity and *HIF1A*. Mutations in *TP53* and *RBI* were the most common in this subset of tumors. Basal/squamous tumors are more common in women, with a higher clinical stage and poorer prognosis. The neuroendocrine-like subtype was characterized by high expression of genes related to neuroendocrine differentiation. *TP53* and *RBI* inactivation was common, but no immune infiltration was detected in these tumors. Neuroendocrine-like tumor was the worst prognosis subtype.

PROTEOME AND PROTEOMICS

Proteins are effector molecules that mediate the functions of genes and their deregulation contributes to the pathogenesis and therapeutic resistance of many diseases, such as cancer and neurodegenerative disorders. They represent an enormously valuable resource for personalized diagnosis, prevention, monitoring, and treatment. Therefore, protein properties, such as abundance, post-translational modification, stability, localization, transportation, and interaction with other molecules, have been intensively studied. Historically, proteins were previously studied on an indi-

Table 3. A summary of discovery and targeted proteomics technologies

Category	Group	Quantification technology	Typical protein number	Typical sample size	Emerging technology
Discovery proteomics	DDA-MS	Label-free (LFQ)	1,000–15,000	10s	BoxCar
		Metabolic labeling (SILAC)			
		Chemical labeling (TMT)			
Targeted proteomics	DIA-MS	Label-free (LFQ)	1,000–5,000	10s–100s	TOMAHAQ
	MS-based	SRM/MRM	10s	10s–100s	
		PRM			
	MS-independent	Antibody-based (RPPA)	100s	100s–1,000s	
		Aptmer-based (SOMAscan)	1,000s	100s–1,000s	

DDA, data-dependent acquisition; MS, mass spectrometry; DIA, data-independent acquisition; LFQ, label-free quantification; SILAC, stable isotope labeling by amino acids in cell culture; TMT, tandem mass tag; SRM, selected reaction monitoring; MRM, multiple reaction monitoring; PRM, parallel reaction monitoring; RPPA, reverse-phase protein array.

vidual basis.

In the mid-90's, Wilkins et al. [25] coined the term “proteome” to describe the “PROTein complement of a genOME”. Of note, proteomics is highly complementary to genomics and transcriptomics, which can only indirectly, and, often inconclusively, measure the aforementioned protein properties. Mainly owing to the rapid advancement of proteomics technologies, the past 25 years have witnessed an explosive growth of proteomics studies, reaching a staggering number of over 11,000 proteomics-related publications in PubMed in 2019, alone.

THE PROTEOME IS A COMPLEX AND INFORMATION-RICH RESOURCE

The human genome contains about 20,000 protein-coding genes. In comparison, the human proteome is much more complex and may contain over 6 million proteoforms (i.e., individual molecular forms of an expressed protein) [26]. The major sources of proteoform diversity include: (a) single-nucleotide polymorphisms and mutations at the DNA level, (b) alternative splicing and RNA editing at the RNA level, and (c) errors in translation and post-translational modifications (PTMs) at the protein level [27]. Among these, the biggest contributor of proteoform diversity is PTMs. Currently, over 200 PTMs, such as phosphorylation, ubiquitination, and glycosylation, have been characterized according to the UniProt database (https://www.uniprot.org/help/post-translational_modification). Of note, PTMs are highly important for the regulation of protein function, activity, stability, localization, and interaction in both physiological and disease states.

DISCOVERY AND TARGETED PROTEOMICS

Proteomics can be broadly classified into discovery and targeted proteomics, which are highly complementary to each other. Discovery proteomics is generally used in hypothesis-free and comprehensive profiling studies to identify novel protein complexes as well as differentially expressed, modified, and/or localized proteins. It is a powerful tool for identifying novel candidate biomarkers and therapeutic targets and for providing fresh biological insights. In comparison, targeted proteomics is generally used to quantify candidate proteins of interest in a much larger cohort of samples with higher quantification accuracy and precision. Currently, a typical discovery proteomics study quantifies thousands of proteins in tens of samples, whereas a typical targeted proteomics study quantifies tens of proteins in hundreds of samples. A summary of the techniques for discovery and targeted proteomics is shown in Table 3.

Discovery proteomics is predominantly conducted using mass spectrometry (MS)-based technologies, which allows comprehensive analysis of protein abundance and PTMs without the required generation of target-specific antibodies [28]. Due to technical challenges, comprehensive analysis of intact proteins by MS (i.e., top-down proteomics) is still in its infancy. Hence, the vast majority of MS-based discovery proteomics studies are conducted using a bottom-up proteomics workflow, where proteins are extracted and digested into peptides by a sequence-specific enzyme (eg, trypsin) prior to liquid chromatography-tandem mass spectrometry (LC-MS/MS) analysis. The classical and preferred MS method for discovery proteomics is data-dependent acquisition (DDA), where a full spectrum of the peptides is acquired at the MS1 level, followed by the collection of as many fragmentation spectra at the MS2 level as possible, all of which is done in

a cycle time of about 3 seconds. The newer and growing MS method for discovery proteomics is data-independent acquisition (DIA), where a mixture of peptides within a relatively wide window (eg, 25 m/z units at the MS1 level) is selected and fragmented, followed by the acquisition of fragments at the MS2 level.

For peptide/protein quantitation, DDA can be coupled with different quantification strategies such as label-free quantification (LFQ), stable isotope labeling by amino acids in cell culture (SILAC), and isobaric tag-based quantification, such as tandem mass tag (TMT), and isobaric tag for relative and absolute quantitation (iTRAQ) [29]. Of note, with the recent release of the TMTpro™ 16plex label reagents (Thermo Scientific, Waltham, MA, USA), up to 16 samples can be analyzed in a single analysis, offering high-throughput analytical capabilities. In comparison, DIA is almost exclusively coupled with LFQ, where samples have to be analyzed one by one. Nevertheless, for multi-batch sample analysis, the TMT method suffers from the “missing value” problem, which aggravates with increasing batch numbers. In comparison, the DIA method is less prone to the “missing value” issue and is thus more suitable for larger sample sizes. However, DIA suffers from limitations such as the requirement of pre-existing high-quality spectral libraries and the complexity of the resulting data [30].

Targeted proteomics can be performed using MS-based and MS-independent methods [31]. At present, the most widely used MS-based targeted proteomics methods include selected reaction monitoring (SRM) [32], also called multiple reaction monitoring (MRM), and parallel reaction monitoring (PRM) [33]. The most popular MS-independent targeted proteomics methods include antibody-based reverse-phase protein array (RPPA) [34] and more recently aptamer-based SOMAScan [35].

Both SRM and PRM assays monitor transitions, i.e., specific pairs of mass-to-charge (m/z) values associated with the peptide precursor and fragment ions, over elution time for specific, sensitive and precise quantification of peptides. SRM and PRM assays are typically conducted in triple quadrupole mass spectrometers (eg, QTRAP) and high-resolution quadrupole-orbitrap mass spectrometers (eg, Q Exactive), respectively. The major difference between SRM and PRM assays is that the former requires a predefined series of transitions, whereas the latter selects the best transitions in a post-acquisition step. Generally speaking, SRM offers higher sensitivity, whereas PRM provides higher specificity and is easier to set up.

The RPPA method was first introduced in 2001 [36] and has since become increasingly popular in targeted proteomic

and phosphoproteomic analysis of small amounts of clinical specimens. RPPA contains hundreds of spots, of which each contains only one test sample. As such, each RPPA can contain hundreds of different samples in serial dilution. For protein quantification, an RPPA is probed with one single antibody that can be detected using fluorescent, colorimetric, or chemiluminescent assays. Therefore, the robustness, reproducibility, and sensitivity of the RPPA measurements are high. RPPA has been used to analyze 166 total proteins and 56 phosphoproteins across nearly 8,000 patient samples from 31 cancer types [37].

The SOMAScan assay relies on the distinctive protein-binding properties of SOMAmer (slow off-rate modified aptamer) reagents, which consist of a short single-stranded DNA sequence with “protein-like” appendages that allow tight and specific binding to its protein target [38]. Recently, SOMAScan has been used to measure about 5,000 proteins across nearly 17,000 participants with multiple different health states, demonstrating that protein expression patterns reliably encode for many health issues [35].

EMERGING TECHNOLOGIES FOR ADVANCED DISCOVERY AND TARGETED PROTEOMICS

In the past few years, many exciting proteomics techniques were developed to improve the LC-MS dynamic range (eg, BoxCar), speed of targeted proteomics (eg, trigger by offset, multiplexed, accurate mass, high-resolution, absolute quantification, TOMAHAQ), ion resolving capability (eg, ion mobility MS), sensitivity (eg, single cell proteomics), and data analysis (eg, machine learning for MS identification), to name a few [39]. To be more concise, we will only summarize the BoxCar and TOMAHAQ techniques.

1. BoxCar extends the dynamic range by an order of magnitude

The abundance of human proteins spans a large dynamic range: about 7 orders of magnitude in cells and up to 12 orders of magnitude in plasma [40]. In comparison, the typical dynamic range of detection for LC-MS is 4–6 orders of magnitude [41]. Therefore, a fast and deep profiling of the proteome requires a significant improvement in the dynamic range of peptide sampling. Recently, the Mann group developed a novel data-acquisition method, termed BoxCar, which improves the quality of MS1 signals and the dynamic range by an order of magnitude [42]. BoxCar can be coupled with both DDA and DIA for improved proteomic profiling. However, similar to DIA-MS, BoxCar analysis also requires a

pre-existing high-quality spectral library [42].

2. TOMAHAQ increases the speed of targeted proteomics analysis by an order of magnitude

SRM and PRM are predominantly coupled with label-free analysis and, thus, lack multiplexing capabilities. Recently, a novel targeted proteomics method termed TOMAHAQ was developed by the Gygi group [43]. By combining sample multiplexing with targeted proteomics, TOMAHAQ increases the throughput by an order of magnitude, compared to SRM/PRM. Using TOMAHAQ, the Gygi group was able to accurately quantify 131 peptides at the speed of 90 cell lysate samples per day [43]. Nonetheless, TOMAHAQ analysis requires highly expensive tribrid mass spectrometers, limiting its widespread adoption in research and clinical applications.

APPLYING PROTEOMICS TO BC RESEARCH

1. *In vitro* research

Based on the hypothesis that urinary biomarkers of BC are secreted from tumors, proteomic methods have been applied in investigating the secretome of tumor cells. Lin et al. [44] investigated the secretome of malignant U1 and pre-malignant U4 BC cells. They identified some differences, including laminin alpha-5 chain, ADP-ribosylation factor guanine nucleotide-exchange factor 2, and urokinase-type plasminogen activator (u-PA). Further studies on u-PA found that loss was associated with malignant transformation. Makridakis et al. [45] compared the secretome from T24 and aggressive T24M BC cells. Several proteins were identified as being associated with metastatic tumor transformation, including secreted protein acidic and cysteine rich (SPARC), tissue-type plasminogen activator (tPA), and clusterin. All of them were further validated by western blot analysis. Elevated SPARC levels in the urine of BC patients was found to be associated with tumor stage [46]. Additionally, the biological relevance of SPARC in BC was suggested when blocking SPARC with specific antibodies resulted in reduced cell motility *in vitro*.

2. The clinical setting

Given that patient response rates to the drugs reach only 25% efficiency in cancer, the demand for developing precision medicine is increasing [47]. It appears that there is no study demonstrating successful application of proteomics or other -omics technology in personalized medicine. However, as outlined in recently published review articles [48-50], sub-

stantial progress has been made in identifying proteomics-derived BC biomarkers as well as putative targets for therapeutic intervention to support patient management (diagnosis, monitoring, stratification, and treatment). Urinary proteome profiling can be used to support diagnosis/monitoring and stratification of personalized diseases; while tissue proteomics can address personalized therapeutic intervention by identifying new therapeutic targets.

3. Diagnosis and monitoring of BC

Up to now, several urinary biomarkers have been described, including FDA-approved immunoassays, which detect the urinary levels of BC-associated antigen (BTA stat) and nuclear matrix protein 22 (NMP22) with moderate performance (NMP22: 68% sensitivity, 79% specificity [51]; BTA stat: 61% sensitivity, 78% specificity [52]). In addition, several single protein biomarkers have been thoroughly investigated, including matrix metalloproteinases (matrix metalloproteinase-9 and matrix metalloproteinase-10), angiogenic factors (plasminogen activator inhibitor 1, vascular endothelial growth factor, and angiogenin), apolipoproteins (apolipoprotein A-I, apolipoprotein A-II, and apolipoprotein E), interleukin-8, and carbonic anhydrase 9, all of which are usually assessed through immunoassays (ELISA) [49].

MRM has been used to validate previously reported biomarkers, including complement C4 gamma chain, apolipoprotein A-II precursor, ceruloplasmin, and prothrombin, in a set of 76 BC patients and 23 disease-related controls (including patients with urinary tract infections and hematuria) [53]. Theodorescu et al. [54] found that fibrinopeptide was capable of detecting BC in healthy controls. Schiffer et al. [55] found that progesterone receptor membrane component 1 (PGRMC1), collagen type I alpha 1 chain (COL1A1), uromodulin (UMOD), and collagen type III alpha 1 chain (COL3A1) were capable of discriminating between muscle-invasive and NMIBC BC. Frantzi et al. [56] found that collagen fragments, hemoglobin subunit alpha (HBA), apolipoprotein A1 (APOA1), fibrinogen α (FIBA), β -2-microglobulin (B2M), and small proline-rich protein 3 (SPRR3), insulin (INS), histidine-rich glycoprotein (HRG) could detect primary BC. Collagen fragments, APOA1, heparan sulfate proteoglycan 2 (HSPG2), ADAM metalpeptidase (ADAMTS1) with thrombolytic protein type 1 parent 1, ADAM metalpeptidase domain 22 (ADAM22) was able to detect relapsed BC.

4. Identification of novel drugs/drug targets

Although there were initially no clear reports of potential drug targets from proteomic analysis of BC, a study by Peng et al. [57] found that phosphoglycerate mutase 1

(PGAM1) was significantly upregulated in BC compared to adjacent normal tissues. Using shRNA to silence PGAM1 reduced tumor growth and cell proliferation and increased apoptosis *in vivo*.

Several recent studies highlight the potential use of a tissue proteomics-based approach in identifying novel drug targets for BC. Using high-resolution LC-MS/MS, 144 proteins associated with BC invasion were identified [58], including multiple proteins previously associated with BC. These proteins include, but are not limited to, some annexins, alpha actinins, cathepsin E, hydroxyprostaglandin dehydrogenase 15(NAD), thymidine phosphorylase, and others. Importantly, eukaryotic translation initiation factor 3 subunit D (EIF3D) was identified as a promising intervention target through computer analysis, and its functional correlation was investigated using *in vitro* and *in vivo* disease models. Specifically, it showed that stable knockdown of EIF3D using lentivirus-mediated RNA interference in a metastatic BC cell line (T24M) resulted in decreased cell proliferation, migration capacity, and colony formation. Subsequent studies in xenograft models showed reduced tumor growth.

Xu et al. [59] performed pull-down assays using recombinant progranulin and protein extracts from 5637 BC cells. Proteomic analysis showed that the F-actin-binding protein, drebrin, was a novel progranulin-binding partner. Interestingly, it has been shown that drebrin depletion in tumorigenic BC cells inhibits motility, anchorage-independent growth, and tumor formation through the threonine kinase (AKT) and MAPK signaling pathways. This indicates that drebrin plays an important functional role in regulating progranulin action and may constitute a novel target for therapeutic intervention in BC. Chen et al. [60] particularly emphasized the potential significance of nucleophosmin (NPM), which is a protein associated with cell proliferation, migration, and anti-apoptotic effects in bladder carcinogenesis. NPM was ubiquitously expressed in all uroepithelial cell lines examined, suggesting its role in the development of human BC. Upregulation of NPM also seemed to be dose and time-dependent following treatment. Since soy isoflavones are capable of inhibiting NPM expression *in vitro*, soybean-based foods may potentially suppress NPM-related tumorigenesis.

Jiang et al. [61] confirmed that peroxiredoxin-I (Prx-I), which has rarely been previously linked directly to BC, was significantly downregulated following BI-TK/GCV treatment. Silencing of Prx-I significantly inhibited growth, promoted apoptosis, and regulated the cell cycle in T24 BC cells. These findings give new insights into the treatment of BC and indicate Prx-I as a new therapeutic target.

Proteome analysis has been used to study the effects and molecular mechanisms of novel potential drugs for BC. Using the 5637 urinary BC cell line, Li et al. [62] evaluated the effect of five heat shock protein 90 (HSP90) inhibitors (AUY922, ganetespib, SNX2112, AT13387, and CUDC305) *in vitro*, followed by quantitative proteome analysis at the global and histone post-translational modification levels. HSP90 inhibitors suppress cell proliferation and growth in a dose and time-dependent manner. LC-MS/MS analysis identified 518 over two-fold upregulated and 811 more than two-fold downregulated proteins, which were commonly downregulated upon treatment with AUY922 and ganetespib. These include proteins involved in cell cycle regulation (several cyclins, cyclin-dependent kinases, cullin-1, and DNA replication licensing factor MCM 5 (minichromosome maintenance complex component 5), apoptosis (BAX, caspase-14, calpalin-7, and apoptosis inducing factor 1), DNA damage repair (DNA ligase 3 and DNA repair protein XRCC1 (X-ray repair cross complementing 1), as well as the generation of reactive oxygen species (glutathione peroxidases, glutathione S-transferases, and superoxide dismutase).

HUMAN SPECIMENS-BASED PROTEOMICS BIOMARKERS

1. Identification of proteomic markers in human urine

In hematuria patients, aurora A kinase (AURKA) can distinguish low-grade BC patients from normal healthy subjects [63]. After adjusting for patients, clinical characteristics, and treatment with Bacillus Calmette-Guerin, activated leukocyte cell adhesion molecule (ALCAM) was positively correlated with tumor stage and OS [64]. Nicotinamide N-methyltransferase was elevated in BC patients and was correlated with histological grade [65]. Levels of apurinic/apyrimidinic endonuclease 1/redox factor-1 (APE/Ref-1) was also elevated in BC compared to normal controls and was correlated with grade and stage. Additionally, APE/Ref-1 has been shown to be significantly increased in patients with a history of BC recurrence [66]. The urinary cytokeratin-20 (CK20) RT-PCR assay showed that the sensitivity of urothelial BC detection was 78% to 87%, the specificity was 56% to 80%, and the diagnostic accuracy improved with tumor progression [67]. However, its performance in low-grade tumors was relatively poor. Measurements of the urinary levels of CK8 and CK18 using the UBC Rapid Test were shown to be greater in high-grade BC than in low-grade BC [68].

There are a variety of markers that can potentially be used for BC detection. Elevated urinary levels of apolipo-

proteins A1, A2, B, C2, C3, and E (APOA1, APOA2, APOB, APOC2, APOC3, and APOE) were found in BC compared to healthy controls [53,69]. A study showed that urinary fragments of uromodulin, collagen α -1 (I), collagen α -1 (III), and membrane-associated progesterone receptor component 1 could distinguish MIBC from NMIBC [55]. Other panels used IL-8, MMP-9/10, angiogenin (ANG), APOE, SDC-1, α 1AT, PAI-1, VEGFA, and CA9 to identify BC in urine samples. The advantage of these multi-urinary protein biomarkers is evident in high and low-grade diseases [70]. Some urine markers, including midkine (MDK), synuclein G, CEA cell adhesion molecule 1 (CEACAM1), zinc-alpha-2-glycoprotein (ZAG2) [71], clusterin (CLU), and ANG, showed improved sensitivity and specificity in diagnosing NMIBC when used in immunoassays and urine cytology [72]. Levels of CK20 and insulin-like growth factor II (IGF-II) were increased in the urine sediments of NMIBC patients compared to controls [73]. Increased urinary levels of HAI-1 and epithelial cell adhesion molecule (EpCAM) are prognostic biomarkers of high-risk in NMIBC patients [74]. Urinary survivin has been shown to be a potential biomarker for BC, and was further related to tumor stage, lymph node metastasis, and distant metastasis [75]. Overexpression of urinary levels of SNAIL were shown to be an independent prognostic factor for tumor recurrence in NMIBC [76]. Urinary CD44 was elevated in high-grade MIBC based on glycan-affinity glycoproteomics nanoplateforms [77].

2. Identification of proteomic markers in tissue samples

Several studies have reported that the results of urine analysis using proteomics can be further verified at the tissue level. Using two-dimensional electrophoresis (2DE), Peng et al. [57] found that PGAM1 was significantly upregulated in BC compared to adjacent tissue. In a parallel approach, cystatin B was found to be a prognostic biomarker at the tissue level; increased expression levels of the protein were correlated with stage, grade, recurrence, and progression [78].

Barboro et al. [79] studied invasive BC tissue to identify prognostic biomarkers. Using 2DE, they found significant upregulation of lamin B1 and fibrinogen beta chain and reduction of actin, desmin and VIM in MIBC tissue specimens compared to normal and non-tumor sections. They also found that protein p54 was correlated with vascular invasion and survival. Moreira et al. [80] studied the prognostic value of BC-associated protein (BLCAP) in 2,108 BC tissue specimens from archival datasets. According to the protein expression levels and cell localization, cancer cells could be divided into 4 categories, and decreased staining intensity of BLCAP was

correlated with tumor grade ($p < 0.0001$) and stage ($p < 0.0001$). Orenes-Piñero et al. [81] used protein arrays to identify serum proteins that were associated with BC. Two identified candidate biomarkers, dynamin and clusterin, were further evaluated using IHC in tissue arrays. Reduced levels of CLU was found to be associated with MIBC, while reduced dynamin was associated with adverse outcomes. Chung et al. [82] identified 12 proteins including cofilin that were differentially expressed in MIBC, compared to NMIBC.

Grau et al. [83] performed comparative proteomics on the human T24 BC cell line and its aggressive derivative, T24T. They identified cullin-3 (Cul3), a protein involved in ubiquitination, as being overexpressed in T24T cells. Silencing of this protein reduced proliferation and migration of T24T. Along the same lines, the IHC expression levels of Cul3 in tissue microarrays were associated with tumor stage, metastasis, and disease-specific survival. Srinivasan et al. [84] used antibody microarrays to identify proteins that were differentially expressed between patients with and without local recurrence. They identified 255 proteins and found that prelamin-A/C (LMNA), transcription factor AP-1 (JUN), and nuclease-sensitive element-binding protein 1 (YBOX1) were significantly upregulated; whereas L-selectin (LYAM1), cyclin-dependent kinase inhibitor 1 (CDN1A), and mothers against decapentaplegic homolog 3 (SMAD3) were significantly downregulated. Hemdan et al. [85] studied stathmin 1 in the context of BC and found that increased expression in tissue was associated with adverse outcomes. Decreased expression of stathmin 1 reduced growth and migration of T24 cells. Chen et al. [86] used laser microdissection to compare the proteome of BC and adjacent non-tumorous tissue. The levels of 4F2 cell-surface antigen heavy chain (SLC3A2), stathmin (STMN1), and transgelin-2 (TAGLN2) were elevated in cancer cells. STMN1 and TAGLN2 were both found to be significantly increased in the urine of BC patients. Wu et al. [87] used IHC to identify the association of galectin-1 overexpression (previously identified by the group) with BC pathology and prognosis in a set of 185 primary cases. Increased expression of galectin-1 was significantly associated with tumor grade, vascular invasion, nodal status, and significantly predicted disease specific survival.

3. Identification of proteomic markers in blood samples

Compared to urinalysis, there are relatively few studies on blood-based BC proteomics. Bansal et al. [88] examined the serum of patients with low-grade and high-grade BC and healthy controls; they found that there were differences in the expression of five proteins, among which S100 calcium

binding protein A8 (S100A8) and S100A9 could distinguish low-grade and high-grade BC. The authors further confirmed the findings in a later study by analyzing serum samples from 108 patients with BC (55 before and 53 after surgery) and 52 healthy patients. They found that the expression of S100A8, S100A9, S100A4 and carbonic anhydrase-1 (CA-1) decreased in BC, and the expression of annexin V increased significantly after surgery compared to patients before [89].

Lemańska-Perek et al. [90] analyzed BC plasma samples and found three groups of proteins with different expression levels compared with normal samples. The first group were proteins that should not exist in normal plasma, including fibrinogen γ , plasma transferrin, and C3b. The second group of proteins had high expression in cancer plasma, including vitamin D binding protein, α -2-macroglobulin, pigment epithelium derived factor, and binding globin. The third group of proteins had low expression in cancer plasma, including three molecular forms of immunoglobulin M (IgM).

4. Identification of proteomic markers in saliva samples

Like serum, saliva is a complex mixture of proteins with concentrations in excess of 10 orders of magnitude. The process of getting saliva is the least invasive and simplest. The saliva proteome is constantly changing from birth to adolescence, so age must be considered in the reference data [91]. At present, the study of salivary proteomics is mainly focused on oral diseases, such as oral cancer. There are also several reports about the relationship between salivary proteomics and gastric, breast, and lung cancers. However, there are no reports on salivary proteomics in BC. Therefore, the potential of proteomic BC markers in saliva samples remains to be confirmed.

Proteomics markers identified in different human samples are summarized in Table 4 [53,55,57,63-90].

DIAGNOSTIC AND PROGNOSTIC VALUES OF PROTEOMIC MARKERS IN BC

Many potential biomarkers from proteomic analysis have been reported, suggesting that proteomics can identify new biomarkers for diagnosis and prognosis. There are some FDA-approved immunoassays for diagnosing BC, including BTA stat and NMP22 [52]. Proteomic biomarkers can assist in stratifying patient prognoses in BC. There has been initial data indicating the substantial value of proteomic biomarkers and supporting the idea of using proteomics for patient stratification. In a study by Frantzi et al. [56], CE-MS urinary profiling data was able to reflect disease progression in

MIBC, which was indicated by the gradual changes in the abundance of the urinary peptides and cancer progression. Preliminary results support the use of urinary peptide profiling as a tool for stratifying non-invasive patients.

In addition, proteomics can evaluate the biological process behind BC, determine the molecular subtype of BC, improve our understanding of BC classification and prognosis, and improve the diagnosis and treatment of patients. de Velasco et al. [92] found two different molecular groups for BC using proteomic data; each of which have different functional characteristics and may provide new insight for the treatment of BC. In addition, they also defined a six-protein signature that can predict the prognosis of patients with MIBC and identified a functional node that can provide prognostic information, which provides a further means of evaluating BC.

CONCLUSIONS

Recent genomic studies to phenotype BC suggest that molecular subtypes of BC and their phenotypes can predict clinical outcomes to various therapies. However, recent findings also suggest that clinical parameters outperformed subtypes for predicting patient outcomes [93], and molecular subtype-based diagnostics applied to a population-based modern cystectomy series were not able to predict cancer-specific survival [94]. Thus, it would be worthy to consider the rapid advancement of existing and emerging proteomics technologies to molecular classification based on genomics phenotypes.

Proteomics is expected to improve personalized medical treatment by better assessing disease risk, more accurately monitoring disease, and improving targeted treatment. Although it is still in its infancy, the past few years have witnessed the emergence of single-molecule proteomic technologies [95,96]. These unbiased protein sequencing approaches, with a dynamic range that covers the full range of protein concentrations in proteomes, can potentially revolutionize the proteomics field. The addition of proteomics profiling-based biosignatures will provide tremendous benefit to the existing molecular phenotyping of BC patients in deciding treatment protocols, monitoring responses to therapies and recurrence or screening of high-risk individuals.

For successful clinical application, prospective multi-center based randomized trials should be considered to develop and assess the value of combined genomic and proteomic biomarker tests with the purpose of reducing costly cystoscopy checks during surveillance of BC patients. We are very optimistic that the utility of proteomic phenotyping

Table 4. Proteomics markers in different samples

Sample source	Proteomics marker	Expression	Function	Literature	
Urine	AURKA		Distinguish between low-grade BC patients and normal patients	de Martino et al. [63]	
	ALCAM		Positively correlate with tumor stage and OS	Arnold Egloff et al. [64]	
	NNMT	Increase	Correlate with histological grade	Pozzi et al. [65]	
	APE/Ref-1	Increase	Correlate with the grade and stage of BC	Choi et al. [66]	
	CK20		Improve diagnostic accuracy in tumor progression	Mi et al. [67]	
	CK8 and CK18	Increase	Differentiate between high-level and low-level BC	Ecke et al. [68]	
	APOA1, APOA2, APOB, APOC2, APOC3, APOE	Increase	BC detection	Chen et al. [53,69]	
	Uromodulin, collagen α -1 (I), collagen α -1 (III), mPR		Distinguish MIBC from NMIBC51	Schiffer et al. [55]	
	IL-8, MMP-9/10, ANG, APOE, SDC-1, α 1AT, PAI-1, VEGFA, CA9		BC detection	Masuda et al. [70]	
	MDK, synuclein G, CEACAM1, ZAG2		NMIBC detection	Soukup et al. [71]	
	CLU and ANG		NMIBC detection	Shabayek et al. [72]	
	CK20 and IGF-II	Increase	NMIBC detection	Salomo et al. [73]	
	HAI-1 and EpCAM	Increase	NMIBC prognosis detection	Snell et al. [74]	
	Survivin		Relate to tumor stage, lymph node metastasis, and distant metastasis	Yang et al. [75]	
	Snail	Increase	Prognostic factor for tumor recurrence in NMIBC	Santi et al. [76]	
	CD44	Increase	High-grade MIBC detection	Azevedo et al. [77]	
	STMN1 and TAGLN2	Increase	BC detection	Chen et al. [86]	
	Tissue	PGAM1	Increase	BC detection	Peng et al. [57]
		Cystatin B	Increase	Correlated with stage and grade, recurrence and progression	Feldman et al. [78]
		Lamin B1 and fibrinogen beta chain	Increase	Identify prognostic	Barboro et al. [79]
Actin, desmin and vimentin		Decrease	Identify prognostic	Barboro et al. [79]	
p54			Correlate with vascular invasion and survival	Barboro et al. [79]	
BLCAP		Decrease	Correlate with tumor grade and stage	Moreira et al. [80]	
Clusterin		Decrease	Associate with muscle invasive bladder cancer	Orenes-Piñero et al. [81]	
Dynamin		Decrease	Associated with adverse outcomes	Orenes-Piñero et al. [81]	
Cofilin		Increase	BC detection	Chung et al. [82]	
Cul3		Increase	Associate with tumor stage, metastasis and disease-specific survival	Grau et al. [83]	
LMNA, JUN, YBOX1		Decrease	Identify local recurrence	Srinivasan et al. [84]	
Stathmin 1		Increase	Associate with adverse outcomes	Hemdan et al. [85]	
SLC3A2, STMN1 and TAGLN2		Increase	BC detection	Chen et al. [86]	
Galectin-1		Increase	Associate with tumor grade, vascular invasion, nodal status, and significantly predicted disease specific survival	Wu et al. [87]	
Blood		S100A8, S100A9, S100A4, CA-1 and annexin V	Decrease	Distinguish low-grade and high-grade bladder cancer from healthy people	Bansal et al. [88,89]
		Fibrinogen γ , plasma transferrin and C3b	Not exist in normal plasma	BC detection	Lemańska-Perek et al. [90]
		DBP, α 2M, PEDF and binding globin	Increase	BC detection	Lemańska-Perek et al. [90]
	Three molecular forms of IgM	Decrease	BC detection	Lemańska-Perek et al. [90]	

α 1AT, alpha-1-antitrypsin; α 2M, α 2-macroglobulin; ALCAM, activated leukocyte cell adhesion molecule; ANG, angiogenin; APO, apolipoproteins; APR/Ref-1, apurinic/aprimidinic endonuclease 1/redox effector factor-1; AURKA, aurora A kinase; BLCAP, BC-associated protein; CA, carbonic anhydrase; CEACAM1, CEA cell adhesion molecule 1; CK, cytokeratin; CLU, clusterin; Cul3, cullin-3; DBP, vitamin D binding protein; EpCAM, epithelial cell adhesion molecule; HAI-1, hepatocyte growth factor activator inhibitor type 1; IGF-II, insulin-like growth factor II; IgM, immunoglobulin M; IL, interleukin; JUN, transcription factor AP-1; LMNA, prelamin-A/C; MDK, midkine; MMP, matrix metalloproteinases; mPR, membrane progesterone receptors; NNMT, nicotinamide N-methyltransferase; PAI-1, plasminogen activator inhibitor-1; PEDF, pigment epithelium-derived factor; PGAM1, phosphoglycerate mutase 1; S100A, S100 calcium binding protein A; SDC-1, syndecan 1; SLC3A2, 4F2 cell-surface antigen heavy chain; STMN1, stathmin 1; TAGLN2, transgelin-2; VEGFA, vascular endothelial growth factor A; YBOX1, nuclease-sensitive element-binding protein 1; ZAG2, Zinc-alpha-2-glycoprotein.

combined with genomic phenotyping will play an increasingly important role in research and clinical management in conjunction with standard diagnostic procedures and act as an additional supplement to clinical judgment.

CONFLICTS OF INTEREST

The authors have nothing to disclose.

ACKNOWLEDGMENTS

This research was supported by Osong Medical Innovation foundation funded by Chungcheongbuk-do (AG200902001). The authors acknowledge support from National Institutes of Health grants (1U01DK103260, 1R01DK100974, U24 DK097154, NIH NCATS UCLA CTSI UL1TR000124), Department of Defense grants (W81XWH-15-1-0415 and W81XWH-19-1-0109), Centers for Disease Controls and Prevention (1U01DP006079), and the U.S.-Egypt Science and Technology Joint Fund (to J.K.). In addition, this article is derived from the Subject Data funded in whole or part by National Academies of Sciences, Engineering, and Medicine (NAS) and The United States Agency for International Development (USAID). Any opinions, findings, conclusions, or recommendations expressed in this article are those of the authors alone, and do not necessarily reflect the views of USAID or NAS.

AUTHORS' CONTRIBUTIONS

Research conception and design: Jayoung Kim and Wun-Jae Kim. Data acquisition: Peng Jin and Wei Yang. Data analysis and interpretation: Peng Jin and Wei Yang. Drafting of the manuscript: Peng Jin and Wei Yang. Critical revision of the manuscript: Jayoung Kim. Supervision: Jayoung Kim and Wun-Jae Kim. Approval of the final manuscript: all authors.

REFERENCES

- Moch H, Cubilla AL, Humphrey PA, Reuter VE, Ulbright TM. The 2016 WHO classification of tumours of the urinary system and male genital organs-part A: renal, penile, and testicular tumours. *Eur Urol* 2016;70:93-105.
- Kirkali Z, Chan T, Manoharan M, Algaba F, Busch C, Cheng L, et al. Bladder cancer: epidemiology, staging and grading, and diagnosis. *Urology* 2005;66(6 Suppl 1):4-34.
- Sanli O, Dobruch J, Knowles MA, Burger M, Alemozaffar M, Nielsen ME, et al. Bladder cancer. *Nat Rev Dis Primers* 2017;3:17022.
- Reuter VE. The pathology of bladder cancer. *Urology* 2006;67(3 Suppl 1):11-7; discussion 17-8.
- Damrauer JS, Hoadley KA, Chism DD, Fan C, Tiganelli CJ, Wobker SE, et al. Intrinsic subtypes of high-grade bladder cancer reflect the hallmarks of breast cancer biology. *Proc Natl Acad Sci U S A* 2014;111:3110-5.
- Kardos J, Chai S, Mose LE, Selitsky SR, Krishnan B, Saito R, et al. Claudin-low bladder tumors are immune infiltrated and actively immune suppressed. *JCI Insight* 2016;1:e85902.
- Choi W, Porten S, Kim S, Willis D, Plimack ER, Hoffman-Censits J, et al. Identification of distinct basal and luminal subtypes of muscle-invasive bladder cancer with different sensitivities to frontline chemotherapy. *Cancer Cell* 2014;25:152-65.
- Cancer Genome Atlas Research Network. Comprehensive molecular characterization of urothelial bladder carcinoma. *Nature* 2014;507:315-22.
- Sjödahl G, Lauss M, Lövgren K, Chebil G, Gudjonsson S, Veerla S, et al. A molecular taxonomy for urothelial carcinoma. *Clin Cancer Res* 2012;18:3377-86.
- Kim J, Akbani R, Creighton CJ, Lerner SP, Weinstein JN, Getz G, et al. Invasive bladder cancer: genomic insights and therapeutic promise. *Clin Cancer Res* 2015;21:4514-24.
- Sjödahl G, Eriksson P, Liedberg F, Höglund M. Molecular classification of urothelial carcinoma: global mRNA classification versus tumour-cell phenotype classification. *J Pathol* 2017;242:113-25.
- Song BN, Kim SK, Mun JY, Choi YD, Leem SH, Chu IS. Identification of an immunotherapy-responsive molecular subtype of bladder cancer. *EBioMedicine* 2019;50:238-45.
- Hirohashi Y, Torigoe T, Mariya T, Kochin V, Saito T, Sato N. HLA class I as a predictor of clinical prognosis and CTL infiltration as a predictor of chemosensitivity in ovarian cancer. *Oncoimmunology* 2015;4:e1005507.
- Nowell CS, Radtke F. Notch as a tumour suppressor. *Nat Rev Cancer* 2017;17:145-59.
- Rampias T, Vgenopoulou P, Avgeris M, Polyzos A, Stravodimos K, Valavanis C, et al. A new tumor suppressor role for the Notch pathway in bladder cancer. *Nat Med* 2014;20:1199-205.
- Song BN, Kim SK, Chu IS. Bioinformatic identification of prognostic signature defined by copy number alteration and expression of CCNE1 in non-muscle invasive bladder cancer. *Exp Mol Med* 2017;49:e282.
- Lee JS, Leem SH, Lee SY, Kim SC, Park ES, Kim SB, et al. Expression signature of E2F1 and its associated genes predict superficial to invasive progression of bladder tumors. *J Clin Oncol* 2010;28:2660-7.
- Kim SK, Roh YG, Park K, Kang TH, Kim WJ, Lee JS, et al. Expression signature defined by FOXM1-CCNB1 activation

- predicts disease recurrence in non-muscle-invasive bladder cancer. *Clin Cancer Res* 2014;20:3233-43.
19. Tan TZ, Rouanne M, Tan KT, Huang RY, Thiery JP. Molecular subtypes of urothelial bladder cancer: results from a meta-cohort analysis of 2411 tumors. *Eur Urol* 2019;75:423-32.
 20. Robertson AG, Kim J, Al-Ahmadie H, Bellmunt J, Guo G, Cherniack AD, et al. Comprehensive molecular characterization of muscle-invasive bladder cancer. *Cell* 2018;174:1033.
 21. Seiler R, Ashab HAD, Erho N, van Rhijn BWG, Winters B, Douglas J, et al. Impact of molecular subtypes in muscle-invasive bladder cancer on predicting response and survival after neoadjuvant chemotherapy. *Eur Urol* 2017;72:544-54.
 22. Sharma P, Callahan MK, Bono P, Kim J, Spiliopoulou P, Calvo E, et al. Nivolumab monotherapy in recurrent metastatic urothelial carcinoma (CheckMate 032): a multicentre, open-label, two-stage, multi-arm, phase 1/2 trial. *Lancet Oncol* 2016;17:1590-8.
 23. Kamoun A, de Reyniès A, Allory Y, Sjödaahl G, Robertson AG, Seiler R, et al. A consensus molecular classification of muscle-invasive bladder cancer. *Eur Urol* 2020;77:420-33.
 24. Biton A, Bernard-Pierrot I, Lou Y, Krucker C, Chapeaublanc E, Rubio-Pérez C, et al. Independent component analysis uncovers the landscape of the bladder tumor transcriptome and reveals insights into luminal and basal subtypes. *Cell Rep* 2014;9:1235-45.
 25. Wilkins MR, Sanchez JC, Gooley AA, Appel RD, Humphery-Smith I, Hochstrasser DF, et al. Progress with proteome projects: why all proteins expressed by a genome should be identified and how to do it. *Biotechnol Genet Eng Rev* 1996;13:19-50.
 26. Ponomarenko EA, Poverennaya EV, Ilgisonis EV, Pyatnitskiy MA, Kopylov AT, Zgoda VG, et al. The size of the human proteome: the width and depth. *Int J Anal Chem* 2016;2016:7436849.
 27. Aebersold R, Agar JN, Amster IJ, Baker MS, Bertozzi CR, Boja ES, et al. How many human proteoforms are there? *Nat Chem Biol* 2018;14:206-14.
 28. Aebersold R, Mann M. Mass-spectrometric exploration of proteome structure and function. *Nature* 2016;537:347-55.
 29. Ankney JA, Muneer A, Chen X. Relative and absolute quantitation in mass spectrometry-based proteomics. *Annu Rev Anal Chem (Palo Alto Calif)* 2018;11:49-77.
 30. Ludwig C, Gillet L, Rosenberger G, Amon S, Collins BC, Aebersold R. Data-independent acquisition-based SWATH-MS for quantitative proteomics: a tutorial. *Mol Syst Biol* 2018;14:e8126.
 31. Yang W, Freeman MR, Kyprianou N. Personalization of prostate cancer therapy through phosphoproteomics. *Nat Rev Urol* 2018;15:483-97.
 32. Lange V, Picotti P, Domon B, Aebersold R. Selected reaction monitoring for quantitative proteomics: a tutorial. *Mol Syst Biol* 2008;4:222.
 33. Peterson AC, Russell JD, Bailey DJ, Westphall MS, Coon JJ. Parallel reaction monitoring for high resolution and high mass accuracy quantitative, targeted proteomics. *Mol Cell Proteomics* 2012;11:1475-88.
 34. Liotta LA, Espina V, Mehta AI, Calvert V, Rosenblatt K, Geho D, et al. Protein microarrays: meeting analytical challenges for clinical applications. *Cancer Cell* 2003;3:317-25.
 35. Williams SA, Kivimaki M, Langenberg C, Hingorani AD, Casas JP, Bouchard C, et al. Plasma protein patterns as comprehensive indicators of health. *Nat Med* 2019;25:1851-7.
 36. Pawletz CP, Charboneau L, Bichsel VE, Simone NL, Chen T, Gillespie JW, et al. Reverse phase protein microarrays which capture disease progression show activation of pro-survival pathways at the cancer invasion front. *Oncogene* 2001;20:1981-9.
 37. Zhang Y, Kwok-Shing Ng P, Kucherlapati M, Chen F, Liu Y, Tsang YH, et al. A pan-cancer proteogenomic atlas of PI3K/AKT/mTOR pathway alterations. *Cancer Cell* 2017;31:820-32.e3.
 38. Rohloff JC, Gelinis AD, Jarvis TC, Ochsner UA, Schneider DJ, Gold L, et al. Nucleic acid ligands with protein-like side chains: modified aptamers and their use as diagnostic and therapeutic agents. *Mol Ther Nucleic Acids* 2014;3:e201.
 39. Yates JR 3rd. Recent technical advances in proteomics. *F1000Res* 2019;8:F1000 Faculty Rev-351.
 40. Zubarev RA. The challenge of the proteome dynamic range and its implications for in-depth proteomics. *Proteomics* 2013;13:723-6.
 41. Angel TE, Aryal UK, Hengel SM, Baker ES, Kelly RT, Robinson EW, et al. Mass spectrometry-based proteomics: existing capabilities and future directions. *Chem Soc Rev* 2012;41:3912-28.
 42. Meier F, Geyer PE, Virreira Winter S, Cox J, Mann M. BoxCar acquisition method enables single-shot proteomics at a depth of 10,000 proteins in 100 minutes. *Nat Methods* 2018;15:440-8.
 43. Erickson BK, Rose CM, Braun CR, Erickson AR, Knott J, McAlister GC, et al. A strategy to combine sample multiplexing with targeted proteomics assays for high-throughput protein signature characterization. *Mol Cell* 2017;65:361-70.
 44. Lin CY, Tsui KH, Yu CC, Yeh CW, Chang PL, Yung BY. Searching cell-secreted proteomes for potential urinary bladder tumor markers. *Proteomics* 2006;6:4381-9.
 45. Makridakis M, Roubelakis MG, Bitsika V, Dimuccio V, Samiotaki M, Kossida S, et al. Analysis of secreted proteins for the study of bladder cancer cell aggressiveness. *J Proteome Res* 2010;9:3243-59.
 46. Critselis E, Rava M, Marquez M, Lygirou V, Chatzicharalam-

- bous D, Liapi P, et al. Diagnostic and prognostic performance of secreted protein acidic and rich in cysteine (SPARC) assay for detecting primary and recurrent urinary bladder cancer. *Proteomics Clin Appl* 2019;13:e1800148.
47. Spear BB, Heath-Chiozzi M, Huff J. Clinical application of pharmacogenetics. *Trends Mol Med* 2001;7:201-4.
 48. Frantzi M, Latosinska A, Flühe L, Hupe MC, Critselis E, Kramer MW, et al. Developing proteomic biomarkers for bladder cancer: towards clinical application. *Nat Rev Urol* 2015;12:317-30.
 49. Frantzi M, Vlahou A. Ten years of proteomics in bladder cancer: progress and future directions. *Bladder Cancer* 2017;3:1-18.
 50. D'Costa JJ, Goldsmith JC, Wilson JS, Bryan RT, Ward DG. A systematic review of the diagnostic and prognostic value of urinary protein biomarkers in urothelial bladder cancer. *Bladder Cancer* 2016;2:301-17.
 51. Mowatt G, Zhu S, Kilonzo M, Boachie C, Fraser C, Griffiths TR, et al. Systematic review of the clinical effectiveness and cost-effectiveness of photodynamic diagnosis and urine biomarkers (FISH, ImmunoCyt, NMP22) and cytology for the detection and follow-up of bladder cancer. *Health Technol Assess* 2010;14:1-331, iii-iv.
 52. Yafi FA, Brimo F, Steinberg J, Aprikian AG, Tanguay S, Kassouf W. Prospective analysis of sensitivity and specificity of urinary cytology and other urinary biomarkers for bladder cancer. *Urol Oncol* 2015;33:66.e25-31.
 53. Chen YT, Chen HW, Domanski D, Smith DS, Liang KH, Wu CC, et al. Multiplexed quantification of 63 proteins in human urine by multiple reaction monitoring-based mass spectrometry for discovery of potential bladder cancer biomarkers. *J Proteomics* 2012;75:3529-45.
 54. Theodorescu D, Wittke S, Ross MM, Walden M, Conaway M, Just I, et al. Discovery and validation of new protein biomarkers for urothelial cancer: a prospective analysis. *Lancet Oncol* 2006;7:230-40.
 55. Schiffer E, Vlahou A, Petrolekas A, Stravodimos K, Tauber R, Geschwend JE, et al. Prediction of muscle-invasive bladder cancer using urinary proteomics. *Clin Cancer Res* 2009;15:4935-43.
 56. Frantzi M, van Kessel KE, Zwarthoff EC, Marquez M, Rava M, Malats N, et al. Development and validation of urine-based peptide biomarker panels for detecting bladder cancer in a multi-center study. *Clin Cancer Res* 2016;22:4077-86.
 57. Peng XC, Gong FM, Chen Y, Qiu M, Cheng K, Tang J, et al. Proteomics identification of PGAM1 as a potential therapeutic target for urothelial bladder cancer. *J Proteomics* 2016;132:85-92.
 58. Latosinska A, Mokou M, Makridakis M, Mullen W, Zoidakis J, Lygirou V, et al. Proteomics analysis of bladder cancer invasion: targeting EIF3D for therapeutic intervention. *Oncotarget* 2017;8:69435-55.
 59. Xu SQ, Buraschi S, Morcavallo A, Genua M, Shirao T, Peiper SC, et al. A novel role for drebrin in regulating progranulin bioactivity in bladder cancer. *Oncotarget* 2015;6:10825-39.
 60. Chen SH, Wang YW, Hsu JL, Chang HY, Wang CY, Shen PT, et al. Nucleophosmin in the pathogenesis of arsenic-related bladder carcinogenesis revealed by quantitative proteomics. *Toxicol Appl Pharmacol* 2010;242:126-35.
 61. Jiang L, Xiao X, Ren J, Tang Y, Weng H, Yang Q, et al. Proteomic analysis of bladder cancer indicates Prx-I as a key molecule in BI-TK/GCV treatment system. *PLoS One* 2014;9:e98764.
 62. Li QQ, Hao JJ, Zhang Z, Krane LS, Hammerich KH, Sanford T, et al. Proteomic analysis of proteome and histone post-translational modifications in heat shock protein 90 inhibition-mediated bladder cancer therapeutics. *Sci Rep* 2017;7:201.
 63. de Martino M, Shariat SF, Hofbauer SL, Lucca I, Taus C, Wiener HG, et al. Aurora A Kinase as a diagnostic urinary marker for urothelial bladder cancer. *World J Urol* 2015;33:105-10.
 64. Arnold Egloff SA, Du L, Loomans HA, Starchenko A, Su PE, Ketova T, et al. Shed urinary ALCAM is an independent prognostic biomarker of three-year overall survival after cystectomy in patients with bladder cancer. *Oncotarget* 2017;8:722-41.
 65. Pozzi V, Di Ruscio G, Sartini D, Campagna R, Seta R, Fulvi P, et al. Clinical performance and utility of a NNMT-based urine test for bladder cancer. *Int J Biol Markers* 2018;33:94-101.
 66. Choi S, Shin JH, Lee YR, Joo HK, Song KH, Na YG, et al. Urinary APE1/Ref-1: a potential bladder cancer biomarker. *Dis Markers* 2016;2016:7276502.
 67. Mi Y, Zhao Y, Shi F, Zhang M, Wang C, Liu X. Diagnostic accuracy of urine cytokeratin 20 for bladder cancer: a meta-analysis. *Asia Pac J Clin Oncol* 2019;15:e11-9.
 68. Ecke TH, Weiß S, Stephan C, Hallmann S, Barski D, Otto T, et al. UBC[®] Rapid Test for detection of carcinoma in situ for bladder cancer. *Tumour Biol* 2017;39:1010428317701624.
 69. Chen YT, Chen CL, Chen HW, Chung T, Wu CC, Chen CD, et al. Discovery of novel bladder cancer biomarkers by comparative urine proteomics using iTRAQ technology. *J Proteome Res* 2010;9:5803-15.
 70. Masuda N, Ogawa O, Park M, Liu AY, Goodison S, Dai Y, et al. Meta-analysis of a 10-plex urine-based biomarker assay for the detection of bladder cancer. *Oncotarget* 2018;9:7101-11.
 71. Soukup V, Kalousová M, Capoun O, Sobotka R, Breyt Z, Pešl M, et al. Panel of urinary diagnostic markers for non-invasive detection of primary and recurrent urothelial urinary bladder carcinoma. *Urol Int* 2015;95:56-64.
 72. Shabayek MI, Sayed OM, Attaia HA, Awida HA, Abozeed H.

- Diagnostic evaluation of urinary angiogenin (ANG) and clusterin (CLU) as biomarker for bladder cancer. *Pathol Oncol Res* 2014;20:859-66.
73. Salomo K, Huebner D, Boehme MU, Herr A, Brabetz W, Heberling U, et al. Urinary transcript quantitation of CK20 and IGF2 for the non-invasive bladder cancer detection. *J Cancer Res Clin Oncol* 2017;143:1757-69.
 74. Snell KIE, Ward DG, Gordon NS, Goldsmith JC, Sutton AJ, Patel P, et al. Exploring the roles of urinary HAI-1, EpCAM & EGFR in bladder cancer prognosis & risk stratification. *Oncotarget* 2018;9:25244-53.
 75. Yang Y, Xu J, Zhang Q. Detection of urinary survivin using a magnetic particles-based chemiluminescence immunoassay for the preliminary diagnosis of bladder cancer and renal cell carcinoma combined with LAPTM4B. *Oncol Lett* 2018;15:7923-33.
 76. Santi R, Cai T, Nobili S, Galli IC, Amorosi A, Comperat E, et al. Snail immunohistochemical overexpression correlates to recurrence risk in non-muscle invasive bladder cancer: results from a longitudinal cohort study. *Virchows Arch* 2018;472:605-13.
 77. Azevedo R, Soares J, Gaiteiro C, Peixoto A, Lima L, Ferreira D, et al. Glycan affinity magnetic nanoplatfoms for urinary glycobiomarkers discovery in bladder cancer. *Talanta* 2018;184:347-55.
 78. Feldman AS, Banyard J, Wu CL, McDougal WS, Zetter BR. Cystatin B as a tissue and urinary biomarker of bladder cancer recurrence and disease progression. *Clin Cancer Res* 2009;15:1024-31.
 79. Barboro P, Rubagotti A, Orecchia P, Spina B, Truini M, Repaci E, et al. Differential proteomic analysis of nuclear matrix in muscle-invasive bladder cancer: potential to improve diagnosis and prognosis. *Cell Oncol* 2008;30:13-26.
 80. Moreira JM, Ohlsson G, Gromov P, Simon R, Sauter G, Celis JE, et al. Bladder cancer-associated protein, a potential prognostic biomarker in human bladder cancer. *Mol Cell Proteomics* 2010;9:161-77.
 81. Orenes-Piñero E, Barderas R, Rico D, Casal JI, Gonzalez-Pisano D, Navajo J, et al. Serum and tissue profiling in bladder cancer combining protein and tissue arrays. *J Proteome Res* 2010;9:164-73.
 82. Chung H, Kim B, Jung SH, Won KJ, Jiang X, Lee CK, et al. Does phosphorylation of cofilin affect the progression of human bladder cancer? *BMC Cancer* 2013;13:45.
 83. Grau L, Luque-Garcia JL, González-Peramato P, Theodorescu D, Palou J, Fernandez-Gomez JM, et al. A quantitative proteomic analysis uncovers the relevance of CUL3 in bladder cancer aggressiveness. *PLoS One* 2013;8:e53328.
 84. Srinivasan H, Allory Y, Sill M, Vordos D, Alhamdani MS, Radvanyi E, et al. Prediction of recurrence of non muscle-invasive bladder cancer by means of a protein signature identified by antibody microarray analyses. *Proteomics* 2014;14:1333-42.
 85. Hemdan T, Lindén M, Lind SB, Namuduri AV, Sjöstedt E, de Ståhl TD, et al. The prognostic value and therapeutic target role of stathmin-1 in urinary bladder cancer. *Br J Cancer* 2014;111:1180-7.
 86. Chen CL, Chung T, Wu CC, Ng KF, Yu JS, Tsai CH, et al. Comparative tissue proteomics of microdissected specimens reveals novel candidate biomarkers of bladder cancer. *Mol Cell Proteomics* 2015;14:2466-78.
 87. Wu TF, Li CF, Chien LH, Shen KH, Huang HY, Su CC, et al. Galectin-1 dysregulation independently predicts disease specific survival in bladder urothelial carcinoma. *J Urol* 2015;193:1002-8.
 88. Bansal N, Gupta A, Sankhwar SN, Mahdi AA. Low- and high-grade bladder cancer appraisal via serum-based proteomics approach. *Clin Chim Acta* 2014;436:97-103.
 89. Bansal N, Gupta AK, Gupta A, Sankhwar SN, Mahdi AA. Serum-based protein biomarkers of bladder cancer: a pre- and post-operative evaluation. *J Pharm Biomed Anal* 2016;124:22-5.
 90. Lemańska-Perek A, Lis-Kuberka J, Lepczyński A, Dratwa-Chałupnik A, Tupikowski K, Kątnik-Prastowska I, et al. Potential plasma biomarkers of bladder cancer identified by proteomic analysis: a pilot study. *Adv Clin Exp Med* 2019;28:339-46.
 91. Messana I, Cabras T, Iavarone F, Manconi B, Huang L, Martelli C, et al. Chrono-proteomics of human saliva: variations of the salivary proteome during human development. *J Proteome Res* 2015;14:1666-77.
 92. de Velasco G, Trilla-Fuertes L, Gamez-Pozo A, Urbanowicz M, Ruiz-Ares G, Sepúlveda JM, et al. Urothelial cancer proteomics provides both prognostic and functional information. *Sci Rep* 2017;7:15819.
 93. Morera DS, Hasanali SL, Belew D, Ghosh S, Klaassen Z, Jordan AR, et al. Clinical parameters outperform molecular subtypes for predicting outcome in bladder cancer: results from multiple cohorts, including TCGA. *J Urol* 2020;203:62-72.
 94. Kollberg P, Chebil G, Eriksson P, Sjö Dahl G, Liedberg F. Molecular subtypes applied to a population-based modern cystectomy series do not predict cancer-specific survival. *Urol Oncol* 2019;37:791-9.
 95. Timp W, Timp G. Beyond mass spectrometry, the next step in proteomics. *Sci Adv* 2020;6:eaax8978.
 96. Callahan N, Tullman J, Kelman Z, Marino J. Strategies for development of a next-generation protein sequencing platform. *Trends Biochem Sci* 2020;45:76-89.

Challenges in Urology during the COVID-19 Pandemic

Peng Jin^{a, b} Hyusim Park^c Sungyong Jung^c Jayoung Kim^{a, d}

^aDepartments of Surgery and Biomedical Sciences, Cedars-Sinai Medical Center, Los Angeles, CA, USA; ^bDepartment of Urology, Shengjing Hospital of China Medical University, Shenyang, China; ^cDepartment of Electrical Engineering, University of Texas at Arlington, Arlington, TX, USA; ^dDepartment of Medicine, University of California, Los Angeles, CA, USA

Keywords

COVID-19 pandemic · Test methods · Clinical challenges · Urological diseases · Urologists

Abstract

The COVID-19 pandemic has caused a global health threat. This disease has brought about huge changes in the priorities of medical and surgical procedures. This short review article summarizes several test methods for COVID-19 that are currently being used or under development. This paper also introduces the corresponding changes in the diagnosis and treatment of urological diseases during the COVID-19 pandemic. We further discuss the potential impacts of the pandemic on urology, including the outpatient setting, clinical work, teaching, and research.

© 2020 S. Karger AG, Basel

Introduction

Coronaviruses are enveloped, positive-sense, and single-stranded RNA viruses that can be subdivided into 4 different classes, i.e., α , β , γ , and δ . In recent years, sev-

eral coronaviruses have caused epidemics in various regions of the world (in 2002–2003 there was the SARS-Cov epidemic in China and in 2012 there was the MERS-CoV epidemic in Saudi Arabia). The appearance of the new viral SARS-CoV-2 (COVID-19) strain in 2019 that originated in the Chinese region of Wuhan started a global pandemic, afflicting over a million people and causing over 50,000 deaths [1]. COVID-19 belongs to the β -coronavirus family, and it is thought to have originated in bats. There is a noted similarity between the genomic sequence of human COVID-19 and that of HKU9-1 in bats; however, the intermediate host between bats and humans has yet to be identified. COVID-19 is highly contagious and it has 3 main routes for transmission, i.e., person-to-person contact, aerosol, and touch. In addition to infecting the respiratory system, the virus also infects the blood, digestive, and urinary systems. As a result, the presence of the virus has been detected in fecal, blood, and urine samples. COVID-19 can cause a variety of symptoms, such as fever, dry cough, shortness of breath, loss of appetite, and fatigue. Furthermore, hidden transmission can occur from asymptomatic individuals. The incubation period for COVID-19 ranges between 2 and 14 days.

How will life change during and after the COVID-19 pandemic from the point of view of a urologist? In this short article, we will discuss the COVID-19 pandemic and its effects on the field of urology.

Discussion

COVID-19 Examination

Common Test Methods

The general structure of coronaviruses includes spike glycoproteins, membrane proteins, nucleoproteins, and genomic RNA [2]. To detect the novel SARS-CoV-2, nucleic acid testing is the main technique for laboratory diagnoses [3]. Sample sources include sputum, throat swabs, and lower respiratory system secretions. Other methods, such as virus antigen or serological antibody testing, are valuable assays for detecting infection. The main sample source for these tests is blood. As with other emerging viruses, the development of methods was only able to begin after identification of the viral genome.

Real-time reverse transcription-polymerase chain reaction (RT-PCR) has become the standard method for diagnosing COVID-19 due to its specificity, sensitivity, and simplicity. Zhang et al. [4] used RT-PCR to detect COVID-19 from throat and rectal swab samples from patients. The virus was detected in both types of samples. Throat swabs are suggested to be more applicable in the early stages of infection, while rectal swabs are better for detecting late-stage infections [4].

Unfortunately, RT-PCR detection kits have many limitations, such as long turnaround times, complex operational procedures, expensive equipment, technical personnel requirements, false negatives, and so on [2]. As a result, these limitations make RT-PCR unsuitable for rapid and simple diagnosis and screening of patients [5, 6]. On the other hand, the COVID-19 IgG-IgM combined antibody test can generate results within 15 min and it can determine whether the viral infection occurred recently. It is easy to use, has a high sensitivity, and does not require additional equipment [4]. This rapid detection method has great potential benefits for the mass screening of COVID-19 infections [7, 8].

The COVID-19 IgG-IgM combined antibody test kit detects antibodies in the blood that are produced by the body's immune system for a prolonged period of time after infection. However, further studies of IgG-IgM tests are needed in order to validate that it provides a high enough specificity and sensitivity to be widely used [9]. RT-PCR has more benefits when diagnosing patients ini-

tially, while IgG-IgM is very useful in monitoring confirmed patients or identifying late-stage patients for the prevention of spread. As of May 17, 2020, there were 75 different COVID-19 test kit products that were Emergency Use Authorization (EUA) approved [9].

Table 1 shows a list of clinically evaluated test kits approved by EUA with results from positive percent agreement and negative percent agreement.

Routine Blood Test for COVID-19

COVID-19 can cause serological abnormalities. Some studies have shown that the levels of lymphocytes, platelets, hemoglobin, and albumin in COVID-19 patients are decreased while levels of glucose, lactate dehydrogenase, interleukin-6, serum ferritin, C-reactive protein, ESR, alanine aminotransferase, aspartate aminotransferase, creatine kinase, D-dimer, and serum procalcitonin are increased [10, 11]. However, these routine serological examinations can only indicate infection and have poor specificity, which means that they cannot be used to confirm any diagnoses of COVID-19.

Expression of ACE2 and TMPRSS2 in the Urinary System and COVID-19

The human angiotensin-converting enzyme 2 (ACE2) gene is located on chromosome Xp22 and includes 18 exons [12]. Functioning as a typical zinc metallopeptidase, the ACE2 protein contains 805 amino acids and is a type I integral membrane glycoprotein containing a single catalytic domain. In the renin-angiotensin system, ACE2 degrades angiotensin II, which is potent in vasoconstriction, proinflammation, and pro-fibrosis, converting it into Ang (1-7) which contributes to vasodilation, antiproliferation, and apoptosis. Besides its systemic effects on blood pressure regulation, ACE2 also regulates amino acid absorption in the kidneys and gut and modulates the expression of amino acid transporters.

COVID-19 has a specific spike protein 3-D structure that is characterized by a strong binding affinity to ACE2 receptors [13]. As a result, human cells that express ACE2 may act as target cells for COVID-19. Since COVID-19 must bind with ACE2 first before entering the human host cells, the distribution and expression of ACE2 may be critical for the target organ of infection [14]. It is known that ACE2 is enriched in the heart, kidneys, and testes, and it is also broadly distributed in the lungs, liver, intestine, and brain [15]. Therefore, COVID-19 mainly infects the respiratory system. In addition to respiratory symptoms, the common complications found in patients infected with COVID-19 include acute cardiac and kidney injuries.

Table 1. EAU-approved COVID-19 test kits

Test kit	Detection type	Manufacturer	PPA (%) / NPA (%)
Xpert Xpress SARS-CoV-2 test	RT-PCR	Cepheid	98.3/100 [105]
ePlex SARS-CoV-2	RT-PCR	GenMark Diagnostics	91.4/100 [105] 94.4/100 [106]
Allplex™ 2019-nCoV	RT-PCR	Seegene	100/94 [107]
Anti-SARS-CoV-2 rapid test	IgG-IgM	AutoBio	88.15/99.04 [108]

The transmembrane serine proteinase 2 (TMPRSS2) gene was first identified on human chromosome 21 in 1997 [16]. The full-length cDNA encodes a predicted 492 amino acid protein, which is anchored to the plasma membrane and belongs to the TTSPs family (type II transmembrane serine proteases). In humans, TMPRSS2 is mainly expressed on prostate, pancreatic, and colon cells, but it can also be found in lung, liver, and kidney cells [17]. The entry of SARS-CoV-2 into host cells depends on the serine protease activity of TMPRSS283-87. Cells overexpressing TMPRSS2 are susceptible to SARS-CoV-2 infection [18]. The process by which SARS-CoV-2 enters the host cell can be divided into 2 steps. In the first step the viral hemagglutinin protein attaches to ACE-2, and in the second step the hemagglutinin is cleaved to activate the internalization of the virus. This second step depends on the expression of TMPRSS2 [19].

Fecal/Urine/Semen Test for COVID-19

COVID-19 is primarily transmitted through the respiratory tract [19]. However, ACE2 expression patterns across different tissue types suggest the possibility of extrapulmonary viral transmission through bodily fluids [20]. The current focus has been placed mainly on viral clearance from respiratory secretions and little is known about the possible concurrent presence and clearance through bodily fluids.

At present, the virus is mainly detected by nasopharyngeal/oropharyngeal swabs. In addition to nasopharyngeal/oropharyngeal swabs, the presence of COVID-19 RNA has also been reported in fecal, urine, and blood samples. Feces appear to contain a high percentage of viral RNA, and the percentage of patients with viral RNA in urine and blood appears to be low. However, some studies have been contradictory; no COVID-19 RNA was found in the urine of infected patients [21].

Although this represents pertinent information related to reproductive medicine, the presence of COVID-19

in semen has not been investigated [21]. There have been few studies investigating the presence of SARS-CoV-2 in semen, and no solid reports on virus presence in semen are available. The small studies that have been done have found no viruses in semen. The sample sources came from patients with acute infection and convalescence, as well as testicular biopsies from deceased patients [21, 22]. Moreover, a recent paper published in August 2020 showed no COVID-19 viral transmission during sexual contact or assisted reproductive techniques [23]. Only one study detected the presence of SARS-CoV-2 in semen; however, the sample size was small and the possibility that the virus came from urine could not be ruled out [24]. The virus may persist in the prostate or urethra and be carried away by semen during ejaculation. Moreover, patients with severe COVID-19 infection may have contaminated specimens when collecting semen. So far, there has been no report of SARS-CoV-2 RNA in the expressed prostatic secretions of COVID-19 patients [25].

Gender and COVID-19

So far, most countries with available data have reported that men with COVID-19 have a greater severity of illness and a higher mortality rate than women across all age groups [26]. Possible reasons for this disparity include gender-related differences in ACE2 receptors, immune function, sex hormones, hygiene, habits, etc. [27]. In previous cases of pathogenic coronaviruses, this difference between men and women also existed. In the 2002–2003 SARS outbreak and the 2012 MERS outbreak, the mortality rate was comparatively higher in men [28].

The relationship between COVID-19 and ACE2 has been described before. Studies have shown that men have more ACE2 receptors than women and they have a greater expression of ACE2 in the lungs and heart, which may explain why men tend to have more serious disease [29]. Differences in immune defense abilities may also lead to differences in COVID-19 outcomes between men and

women. Compared to males, females usually produce more robust innate and adaptive immune responses and respond more strongly to most invading pathogens [30].

Sex hormones play a role in regulating the immune system and they can cause differences in immune response between men and women. Generally speaking, testosterone has an immunosuppressive effect, while estrogen tends to enhance the immune response [31]. Endogenous testosterone makes men more likely to have more serious complications related to SARS-CoV-2 infection. On the other hand, SARS-CoV-2 infection can lead to hypogonadism in men, and the reduction of androgens may cause serious complications [32]. Given that estrogen activates the immune system, higher estrogen levels can potentially have a protective effect [33]. Studies have shown that exogenous estrogen therapy can eliminate inflammation and reduce virus titers, thus improving survival [34]. The differences in hygiene and habits provide another explanation for the gender-related differences in SARS-CoV-2 infection. Studies have shown that women wash their hands more frequently than men [35], and men wear masks less than women [36]. These factors may explain the noted differences in COVID-19 rates and mortality between the sexes.

The higher smoking rate among men may also be responsible for gender-related differences in COVID-19 mortality. Smokers seem to have a higher risk of respiratory infections. A study found that the expression of ACE2 in Asian smokers is significantly higher than that in nonsmokers [37]. However, the current literature does not support smoking as a predisposing factor for SARS-CoV-2 infection. Gender differences are also reflected in men's underutilization of medical services and participation in unhealthy habits, such as alcohol use and smoking. These behaviors can cause a high blood pressure, cardiovascular disease, and other comorbidities associated with increased mortality from SARS-CoV-2. Because cells overexpressing TMPRSS2 are susceptible to SARS-CoV-2 infection, and the expression of TMPRSS2 is regulated by androgen/androgen receptor (AR) signals, the expressions of AR and TMPRSS2 are significantly positively correlated [38]. This may be a reason why there are more male patients than female patients [19].

Assisted Reproductive Technology and COVID-19

In light of the current COVID-19 pandemic and the uncertainty of its impact on pregnant women, the Society of Human Reproduction published recommendations for the management of patients undergoing infertility treatment through assisted reproductive technology

(ART) [39]. ART includes intrauterine insemination, in vitro fertilization (IVF) injection, ovum collection, implantation, transplantation, and tracking. This process could expose infertile individuals to COVID-19 infection [40]. In addition to the risk of infection, the World Health Organization (WHO) published data showing that pregnant women with COVID-19 are at greater risk of serious complications [41]. There are no clear answers as to whether there is a risk of vertical transmission of COVID-19 from mother to fetus. At present, no such cases have been reported. In a case in China, newborns were infected with the SARS-CoV-2 virus 36 h after birth [42]. However, it is unclear whether this was due to vertical transmission between mother and child [42].

At present, most reports indicate that the symptoms of pregnant women infected with COVID-19 are similar to those of others, and there is no evidence showing that pregnant women or fetuses are at a higher risk [43]. However, considering the initial data and the lack of comprehensive understanding of the pathogenesis of SARS-CoV-2 during pregnancy, most human reproduction societies have proposed postponing embryo transfer and delay of new treatment cycles.

The European Society of Human Reproduction and Embryology (ESHRE) issued a statement regarding COVID-19 and pregnancies on March 14, 2020. So far, only a few cases of COVID-19 infection during pregnancy have been reported. Therefore, there is not enough information available about the potential impact of COVID-19 infection in the early stages of pregnancy. Additionally, drug treatment for severe COVID-19 cases may include drugs that are dangerous or prohibited for use during pregnancy. The ESHRE recommends that all patients considering or planning to receive ART treatment, regardless of whether they are diagnosed with or suspected to have COVID-19 infection, should avoid pregnancy at this time and consider delaying pregnancy by freezing oocytes or embryos to delay embryo transfer [44].

In the latest guidelines updated in October 2020, the ESHRE divides the guidelines for ART services during a viral pandemic into 2 core steps. The first step is to assess the impact of the current pandemic based on epidemiological factors. The second step is to take corresponding measures based on this assessment [45]. See Table 2 for specific guidelines.

On March 17, 2020, the American Society for Reproductive Medicine (ASRM) released a new document titled "Patient Management and Clinical Recommendations during the Coronavirus (COVID-19) Pandemic" [46]. The main recommendations are as follows:

Table 2. ESHRE guidance for safe ART services during the third phase of the COVID-19 pandemic

14-day COVID-19 case notification rate per 100,000	Impact on ART services	Recommended mitigation measures
Reported cases, <i>n</i>	Insignificant	<ul style="list-style-type: none"> – Continue as per routine – Follow regional and country-specific guidance
<20	Minor	<ul style="list-style-type: none"> – Triage recommended for all patients – SARS-CoV-2 testing for triage-positive patients – Follow regional and country-specific guidance
20.0–59.9	Moderate	<ul style="list-style-type: none"> – Routine triage for patients and staff and SARS-CoV-2 testing for triage-positive patients/staff – Routine implementation of the code of conduct for staff and patients – Follow regional and country-specific guidance
60.0–119.9	Major	<ul style="list-style-type: none"> – Routine triage for patients and staff, and SARS-CoV-2 testing for triage-positive patients/staff – Routine implementation of the code of conduct for staff and patients – Remote consultation and counselling (telemedicine) – Reduction of visits to the ART clinic – Routine use of PPE for staff – Face mask recommended for patients – No accompanying persons allowed – Follow regional and country-specific guidance
≥120.0	Critical	<ul style="list-style-type: none"> – Routine implementation of the code of conduct for staff and patients – SARS-CoV-2 testing of all patients and staff – Remote medical advice and counselling (telemedicine) – Reduced clinic visits – Staff: routine use of PPE – Patients: face masks recommended – No accompanying persons allowed – Laboratory: freeze-all policy to be considered – Follow regional and country-specific guidance

- Suspend the start of new treatment cycles, including ovulation induction, intrauterine insemination, IVF, retrieval and frozen-embryo transfer, and nonemergency gamete cryopreservation.
- Strongly consider canceling all embryo transfers, whether fresh or frozen.
- Continue to care for patients who are currently “in cycle” or in need of emergency stimulation and cryopreservation.
- Suspend the selection of surgery and nonemergency diagnostic procedures.
- Minimize interpersonal interaction and increase the utilization of telemedicine.

In June 2020, the ASRM published the fifth update of patient management and clinical recommendations during the viral pandemic [47]. For details, please refer to Table 3.

However, each organization has also stressed that treatment should be carried out in certain cases, such as those in which women are required to retain fertility due

to tumor causes and in cases where delayed treatment may be more harmful than continued treatment (i.e., patients with a low ovarian reserve).

During the pandemic, the IVF department should encourage male patients to collect semen samples at home and send them to the laboratory. However, semen samples must also be considered as potential sources of infection during this process. Assessment of the presence of SARS-CoV-2 in semen is particularly important for semen cryopreservation because storage in liquid nitrogen retains the pathogenic properties of the virus [48]. Therefore, it is necessary to conduct large-scale studies on currently infected patients to confirm or exclude the risk of male gametes. These risks need to be assessed for cryopreservation in liquid nitrogen or ART. It should be noted that a vast majority of published reports so far suggest that there is no SARS-CoV-2 in semen. Only 1 article mentioned the presence of the virus in semen, but the report itself has some questionable factors.

Table 3. ASRM patient management and clinical recommendations during the coronavirus (COVID-19) pandemic: 5th update

Third-party reproduction	Do not start a cycle where the intended parents and the pregnant carrier do not live in the same country.
Fertility services for healthcare workers	Take routine precautions; there is no data to support the need for medical staff to avoid infertility treatment or pregnancy.
Having partners present when providing care	The number of people in the ward must be limited, and partners are encouraged to use telephone or video methods to participate in the escort.
Travel restrictions	Where feasible, avoid using public transportation; if there is an emergency trip, you need to know the new infection rate in the local area and destination; self-isolation should continue to be practiced as much as possible.
Resumption of reproductive surgery	Reproductive surgery can be resumed in areas where the prevalence of the disease should be low (<12%). Before any surgery that requires anesthesia, the patient should be checked for COVID-19 symptoms. Preoperative SARS-CoV-2 virus detection should also be strongly considered. If the virus test is positive, the patient needs to be rechecked for negativity before scheduling surgery.
Aerosol-generating procedures	If aerosol-generating procedures must be performed urgently during the operation, except for the anesthesiologist and the technical or circulatory nurse, the operation team should consider leaving the room immediately. Staff can wear appropriate, fully enhanced PPE. These precautions should be taken regardless of whether the patient has a negative preoperative test result, is asymptomatic, or has no test result at all.
IVF cycles	During the oocyte retrieval process, all patients should wear medical-grade surgical masks. Any planned embryo transfer should be delayed until the patient is SARS-CoV-2 negative.
Urgent surgical procedures	Staff should use enhanced respiratory PPE.

The ASRM and the ESHRE provide differing opinions on whether to perform SARS-CoV-2 testing on patients and providers [49]. The ASRM points out that, based on existing evidence, nucleic acid amplification testing-based testing should be considered before reproductive surgery or other aerosol-generating procedures. However, for antibody testing, ASRM believes that antibody testing should not be used in the decision-making of patients or providers, and it should not change compliance with personal protective equipment (PPE) guidelines. On the other hand, ESHRE relies more on serological testing. It is recommended that, if either party develops symptoms within 2 weeks before ovarian stimulation, the SARS-CoV-2 IgM/IgG test can be used to decide to continue or postpone treatment until it is negative or negative. ASRM believes that the detection of SARS-CoV-2 antibodies is currently not part of the routine workflow of infertile patients, but the ESHRE believes this is critical.

In addition to COVID-19 infection from the provider, semen samples can become a potential source of infection. There may also be a 1-way infection. Four main areas of potential 2-way infection have been identified, i.e., patient-staff, staff-staff, staff-cell, and cell-cell. The results of a failure modes and effect analysis conducted by a multi-

disciplinary IVF team showed that, except for cell-cell contamination, which is considered extremely unlikely, patient-employee, employee-employee, and employee-cell interaction periods are estimated to have a moderate to high infection risk [50]. Therefore, routine SARS-CoV-2 tests for patients and providers are necessary.

Because SARS-CoV-2 is an enveloped RNA virus, it can maintain its viability even at low temperatures, which can lead to cross-contamination between samples [51]. In assessing potential cross-contamination during cryopreservation and storage, the single recorded case of cross-contamination in tissue samples was hepatitis B in bone marrow, which was transmitted to the recipient [52]. The only known cross-contamination of tissues stored in IVF was experimental. Bielanski et al. [53] found that liquid nitrogen intentionally contaminated with bovine viral diarrhea virus spread to 21.3% of nearby open storage devices. However, all sealed straws and freezing tubes were not contaminated. In another similar study, mouse embryos were stored with murine virus vials and no cross-contamination was observed even after a year in storage [54]. These studies have shown that the risk of cross-contamination in liquid nitrogen is indeed negligible, especially when samples are stored and sealed properly.

Due to the COVID-19 pandemic, medical institutions worldwide recommend performing surgical operations for only high-priority or emergency cases. Low priority cases, such as diagnostic semen analysis, sperm banks, elective surgery for sperm retrieval, and related fertility procedures, have been delayed for 6 months or longer and pose no increased health risks to individuals [55]. However, this pandemic may last longer than expected – potentially years. During this period, the average age of women trying to conceive will increase and ovarian reserve indicators will worsen. Contrastingly, male infertility is usually related to progressive testicular damage, such as varicocele. The adverse effects of delayed future ART treatments are a growing concern. With the suspension of treatments, patients feel more anxious and fearful of impairments in possible future pregnancies [56].

Studies have shown that patients with reduced ovarian reserves starting IVF treatment up to 180 days after the first visit will not have their pregnancies affected [57]. For high-risk patients with a poor response to ovarian stimulation, this observation still applies. Providers and patients should rest assured that, if short-term treatment needs to be delayed for medical, logistical, or economic reasons, the treatment results will not be affected [58]. When treating varicocele, surgery is not the only method. Only when progressive testicular growth retardation and/or semen quality is severely impaired should clinical varicocele surgery be performed to maintain fertility [59].

Recently, 27 experts from 15 different countries expressed that postponing andrology services and male infertility treatments during the pandemic may permanently damage the chances of having children for “time-sensitive” patients [60]. This can have devastating psychological effects. The birth window for time-sensitive patients is short and any delay can be impactful. Such patients can be grouped into the following categories:

- Those with cancer and/or undergoing chemotherapy, radiotherapy, or immunosuppressive therapy
- Old age (>50 years)
- Those with severe male infertility (e.g., men with azoospermia/cryptospermia undergoing medical or post-surgical treatment to improve sperm quantity/quality)
- Those with inflammatory and systemic autoimmune diseases.

For such patients, the provision of andrology services cannot be regarded as a low priority [56]. Therefore, some experts believe that ART treatment can be carried out if the patient is considered high priority and has signed informed consent, agreeing to receive treatment and freezing procedures during a pandemic.

Urological Diseases and COVID-19

Guidelines Office of the European Association of Urology

The European Association of Urology (EAU) established a rapid reaction group after the virus outbreak to develop adaptive guidelines to deal with various situations and priorities. They divided urological diseases and conditions into the following 4 priority levels [55]:

- Low priority: clinical harm very unlikely if postponed for 6 months
- Intermediate priority: clinical harm possible, but unlikely, if postponed for 3–4 months
- High priority: clinical harm very likely if postponed for >6 weeks
- Emergency: life-threatening situation – cannot be postponed for >24 h.

Evidence from Wuhan shows that the mortality rate of asymptomatic patients who tested positive for COVID-19 after surgery was 20% [61]. Therefore, in the process of treating patients, doctors should choose the appropriate treatment plan according to the priority level. The latest guidelines provide some suggestions; for instance, surgery can be performed on high-priority and emergency patients during the COVID-19 pandemic, but surgery is not recommended for intermediate-priority patients. Next, we will introduce specific treatment plans for several common diseases in urology during the COVID-19 pandemic.

Kidney Injury

Since ACE2 is expressed in kidney cells, changes in the kidney due to COVID-19 need to have a point of focus [17]. Renal functioning needs to be monitored regularly, especially in patients with elevated plasma creatinine levels. In the event of early signs of acute kidney injury (AKI), interventions, such as continuous renal replacement therapy, should be implemented to protect renal functioning as early as possible. A study by Pei et al. [62] observed that COVID-19 patients have a high frequency of renal abnormalities, including 75.4% of patients with renal involvement, 65.8% with proteinuria, and 41.7% with hematuria.

The risk factors and causes of AKI in COVID-19 patients are diverse. The severity of pneumonia is the most important factor in the development of AKI in COVID-19 patients. The basic pathophysiology of patients with pneumonia is severe acute respiratory distress syndrome, which has been identified as an independent risk factor related to AKI [63]. This data indicates that it is necessary to provide in-depth support and careful moni-

toring of COVID-19 patients with severe pneumonia to improve their complications. However, in a study of 116 COVID-19 hospitalized patients, Wang et al. [64] found that all patients without chronic kidney disease showed no obvious abnormality of renal function, and none of these patients showed AKI. Patients with chronic kidney disease who underwent CRRT were stable, without exacerbation of chronic kidney disease throughout the course of treatment of COVID-19.

Renal Cancer

The current COVID-19 pandemic is forcing medical staff to adapt their clinical practice, especially for the management of life-threatening diseases, such as malignant urological tumors. It is important to weigh the risk of contamination related to treatment and the risk of delaying treatment.

The CCAFU recommendations for the treatment of renal cancer during the COVID-19 pandemic are as follows [65]:

- Small T1a tumors, cystic tumors (Bosniak III and IV), and T1b tumors: surgery should be postponed under supervision
- CT2 tumors: surgery can be postponed under quarterly supervision
- T3 tumors, thrombus of the renal vein, vena cava thrombus, macroscopic lymphadenopathy without other secondary lesions, signs of locoregional invasion, and symptomatic tumors (pain, hematuria), for which no endoscopic or vascular treatment is possible: surgery must be maintained as a priority
- Indications of cytoreductive nephrectomy: favor according to the prognostic stage, monitoring, or medical treatment
- Metastatic renal cancer with a good prognosis: favor a tyrosine kinase inhibitor by encouraging telephone follow-up or teleconsultations
- Metastatic renal cancer with a poor or intermediate prognosis: the benefits of current standard treatments based on a ipilimumab-nivolumab combination must be weighed against the risk of severe toxicity in the context of reduced access to an intensive care unit. The use of sunitinib by default is suboptimal but can be discussed in this context. Patients who have an intermediate prognosis with a low tumor load and are asymptomatic can be treated with tyrosine kinase inhibitor. For patients with a poor prognosis and in poor general condition (PS \geq 2), exclusive palliative treatment may be preferred.

Bladder Cancer

Patients with high-risk non-muscle-invasive bladder cancer need to be revisited to receive Calmette-Guérin Bacillus (BCG) intravesical instillation to reduce progression and recurrence after transurethral resection of the bladder [66]. It has been reported that nearly 30% of patients over 65 years of age may develop acute respiratory distress syndrome after infection with COVID-19 [66]. Most patients with non-muscle-invasive bladder cancer have a higher risk of severe forms of COVID-19 and may need to enter the intensive care unit for invasive ventilation because the median age of these patients is greater than 70 years [67].

In confirmed COVID-19 cases, due to the lack of data on the tolerance of intravesical BCG, the recommended and cautious approach is to delay additional instillation of BCG. Based on the infection status of COVID-19, it is recommended to delay the installation of BCG for at least 3 weeks after initial symptoms appear to improve. When dealing with side effects related to intravesical BCG infusion, attention should be paid to persistent fever by isolating and testing for COVID-19 [11]. Additionally, although side effects should be specifically treated according to current EAU guidelines, nonsteroidal anti-inflammatory drugs should only be used in patients with no COVID-19 infection because these drugs may lead to a higher risk of hospitalization and intensive care unit admission [66].

Prostate Cancer

Surgery is recognized as the gold-standard treatment for several malignancies, including prostate cancer (PCa). With all healthcare systems and resources focused on controlling and treating COVID-19, oncologic surgery has been reduced worldwide. Surgery is associated with a higher overall and cancer-specific survival compared to radiation therapy alone. Apart from the theoretical advantage of radiation therapy in eliminating local micrometastases, clinical evidence shows that a real multimodal approach is best for patients choosing to undergo radical prostatectomy [68]. Delay in the detection or treatment of PCa can lead to impaired functional outcomes and higher rates of biochemical recurrence [69].

Surgery should only be performed in sterile COVID-19-free facilities; otherwise, according to reports from Wuhan, postoperative mortality can reach 20% [61]. Unfortunately, the preservation of such facilities is impossible. According to the Italian experience, both asymptomatic caregivers and patients can be a source of infection, causing further spread within the hospital [70]. To

maintain a truly COVID-19-free facility, preoperative isolation and laboratory testing are needed to ensure that staff and patients have no infections.

Recently, studies have pointed out that there may be a potential link between PCa and COVID-19 [71]. A study showed that PCa patients who received androgen deprivation therapy had a 4-fold risk of SARS-CoV-2 infection than those who did not receive androgen deprivation therapy [71]. So far, there are 2 main genes related to the entry of the COVID-19 virus into host alveolar epithelial cells, i.e., ACE2 and TMPRSS2. The expression of TMPRSS2 is regulated by androgen/AR signaling. In primary and metastatic castration-resistant PCa, the expressions of AR and TMPRSS2 were significantly positively correlated [72]. These findings indicate that more androgens may mean an increased expression of TMPRSS2, which may increase the susceptibility to SARS-CoV-2. Interestingly, a recent study showed that ACE2 expression is higher in men and may be regulated by androgen/AR signaling [73]. Therefore, androgen deprivation therapy can have a potential curative effect on COVID-19.

Effects on the Testes

The testes may be affected by COVID-19. A study reported that 19% of COVID-19 men suffer from scrotal discomfort, suggesting viral orchitis [74]. Orchitis has not been confirmed as a possible complication of SARS-CoV-2 infection. The virus may not directly infect the testes, but it may trigger a secondary autoimmune response that can cause autoimmune orchitis. COVID-19 is related to abnormal blood clotting, so orchitis could also be the result of segmental vasculitis. A recent study provided insight into impaired male gonadal function after COVID-19 infection [75]. That study showed that the testosterone-to-luteinizing hormone ratio in 81 patients with COVID-19 was dramatically decreased in comparison to 100 age-matched healthy counterparts [76]. The serum testosterone-to-luteinizing hormone ratio could be a potential marker of impairment of reproductive health caused by COVID-19. Another study also confirmed that the serum LH level of patients with COVID-19 was significantly higher than that of healthy men with normal fertility, while the ratio of serum testosterone to luteinizing hormone was significantly decreased, which is indicative of subclinical hypogonadism [77].

Effects of the COVID-19 Pandemic on Urologists Outpatient Care

Due to the increased spread of the pandemic over time, in-person visits in the outpatient setting have decreased

or even been canceled. The latest EAU guidelines recommend the implementation of telemedicine during this time [55]. The development of telemedicine has been a pragmatic approach to reducing the risk of further transmission. Nonemergency patients, such as those with follow-up tumors, benign conditions (such as moderate lower urinary tract symptom and prostate enlargement), and urinary tract infections, can be given a consultation over the telephone. Clinical priority should be given to patients with a suspected relapse or new malignant tumors, severe lower urinary tract syndromes, or potential obstructive/purulent urinary tract stones and those needing an immediate postoperative examination [78].

If a face-to-face interview is needed, both the provider and the patient need to wear masks and maintain social distancing [79]. Patients should also answer questions about their COVID-19-related exposure history or symptoms [80]. Patients with a positive screening are referred to isolated treatment. In the case of a negative screening, clinicians and patients must be provided with infection control procedures throughout the length of care.

Due to technological improvements and cost reductions as well as the widespread popularity of high-speed internet and smartphones, patients can quickly deploy telemedicine consultation from home [81]. The benefits of telemedicine include convenience, access to care from a distance, and lower medical costs. At the same time, it can reduce contact with patients and potential infection. Providers in quarantine or isolation can also continue to work [82]. One of the main disadvantages of telemedicine is that consumers lack awareness of its use, services, and costs. In addition, the lack of physical contact between patients and doctors also poses challenges when conducting remote physical examinations. Most countries lack a regulatory framework to authorize, integrate, and reimburse telemedicine care for all patients, especially in emergencies and outbreak situations [83].

When it comes to face-to-face medical consultations, the effects of facial coverings by masks can have a significant negative impact on patients [84]. The “distance” effect produced by maintaining social distancing requires a louder voice for communication, which in turn may harm patient privacy and reduce patient satisfaction [85].

Urological Surgery

Most benign urological surgeries, including surgeries for incontinence, benign prostatic hyperplasia, reconstruction, infertility, erectile dysfunction, and genitourinary prolapse [86], should be postponed until the pandemic is over.

Ficarra et al. [86] and Stensland et al. [87] proposed excellent recommendations for urological practice during the COVID-19 pandemic. With regard to urinary tract obstruction or infection, ureteral stents or nephrostomy tubes under local anesthesia should be firstly considered. If this is not possible, stents under general anesthesia should be the next option. Acute urinary retention can be managed through insertion of a urethral or suprapubic catheter under local anesthesia. In cases of clot retention due to bladder cancer or PCa, a cystoscopic evacuation should be considered and transurethral hemostasis of the tumor should be done to avoid the need for blood transfusions. Additionally, interventions should only be considered for pediatric urological emergencies, such as acute torsion (implement scrotal exploration and orchidopexy) and genitourinary obstruction (consider a Foley catheter and a suprapubic tube). In patients with a genitourinary trauma, surgical exploration is recommended only in hemodynamically unstable patients [87]; otherwise, procedures that can be performed with local anesthesia may be used. Lastly, the authors recommend immediate intervention for patients with refractory priapism (consider shunting), a scrotal abscess or Fournier gangrene (consider drainage and debridement, respectively), and an infected artificial urethral sphincter or penile prosthesis (removal of the infected device) [86, 87].

Aerosol transmission of COVID-19 cannot be ignored because it can survive in the environment for 3 h [88]. Because of this, it is recommended to use the lowest intra-abdominal pressure on the pneumoperitoneum during robotic or laparoscopic surgery to reduce the risk of medical staff aerosol infection. Zheng et al. [89] recommend using lower power settings on electrocautery since ultrasonic scalpels or electrical devices may produce a large amount of surgical smoke. Additionally, adequate and complete deflation of the pneumoperitoneum may reduce the risk of infection. All console surgeons should wear goggles or sealed sunshades and carefully disinfect the console's head support between shells. Furthermore, it is recommended that endoscopic procedures and urethral catheterization be performed with caution, and surgeons should be completely protected against infection if the patient has suspected or confirmed COVID-19 [86].

In the latest EAU guidelines [55], there is some guidance on preoperative management, general surgery, and surgery for COVID-positive patients during the COVID pandemic. For example, in the preoperative stage, patients with clinical symptoms and/or those who have been in contact with COVID-19-positive individuals

should receive a preoperative COVID-19 test. For patients without any clinical symptoms and no history of contact with COVID-19-positive patients, it is recommended that they undergo a COVID-19 test within 48 h before surgery. In general, medical staff should use complete PPE regardless of the patient's COVID-19 status. Patients also need to wear a full set of PPE if they are found to be positive for COVID-19. The operation should be performed by experienced surgeons and all unnecessary personnel should remain outside the operating room. Electrocautery devices should be used on reduced power settings to decrease the generation of surgical smoke. Flushing fluid should be collected through a closed system during the urological procedure. Elderly patients with comorbidities, even in high-priority cases, should be carefully considered for surgery. If a surgical patient is diagnosed with COVID-19, a special operating room must be prepared.

Organ Transplantation in Urology

Patients with end-stage kidney disease are at a higher risk of contracting infectious diseases due to their intrinsic fragility caused by their defective immune system [90]. Although there is no evidence that COVID-19 is transmitted through organ donations, this cannot be ignored because the virus has been detected in approximately 15% of patients [91]. The Transplant Association recommends COVID-19 testing of donors suspected of having the virus, coming from endemic areas, or having a history of possible contact [92]. Special care should be given solid organ transplant recipients as they are usually under chronic immunosuppression, which puts them at a higher risk of COVID-19 infection. On the other hand, the safety of the transplantation team is another concern; they can be exposed to transplant recipients who may potentially harbor higher viral loads than that of normal contact [91]. Therefore, the transplantation team must be cautious in areas with widespread community diffusion of COVID-19. In such situations, the US Organ Procurement and Transplantation Network suggests following CDC recommendations when evaluating suspected COVID-19 patients (mask the patient, place the patient in an isolation room, medical personnel must take airborne and contact precautions when contacting the patient, and inform the local authorities about the case) [93].

Training for Urologists

The COVID-19 pandemic has influenced residency training programs and medical graduate education. Most clinical rounds are canceled in many countries. Medical

training programs and teaching activities have switched to online platforms. For instance, in Singapore, interhospital staff movement among hospitals has been put on hold, while residents training in other hospitals will stay there indefinitely [94]. However, efforts are being made to ensure that these actions do not harm the long-term needs of medical trainees. Attention must be focused on how the COVID-19 pandemic and its effects, including the suspension of all nonemergency elective procedures, delay of inpatient examinations, and cessation of clinical rounds, may have a stressful impact on residents and students [95].

Clinical and Lab-Based Urological Research

During the first stages of the COVID-19 outbreak, many researchers focused on researching the treatment and prevention of the virus. Currently, there are no approved therapies or vaccines. Several national and international research groups are working collaboratively on a variety of preventative and therapeutic interventions. Some potential antiviral drugs, including nucleoside analogs, chloroquine, and protease inhibitors, are being urgently administered to patients with COVID-19 [3].

Favipiravir (T-705) is a guanine analog. A recent study suggested that favipiravir is a potential candidate for treating COVID-19, showing effective antiviral activities in Vero E6 cells [96]. Remdesivir (GS-5734) is an adenine analog. Remdesivir has emerged as the most promising candidate for the treatment of COVID-19 infection [96]. Both lopinavir and ritonavir are protease inhibitors and have been reported to have antiviral activities against SARS and MERS [97, 98]. For treatment of COVID-19, clinical trials (ChiCTR2000029539) have been initiated to test the antiviral activity of these protease inhibitors in patients [99]. However, the antiviral efficacy of HIV protease inhibitors in coronavirus proteases is controversial.

Vaccines are the most effective strategy for preventing infectious diseases because they are more cost-effective than treatments and can reduce morbidity and mortality without long-lasting effects. However, there are still no approved vaccines for human coronaviruses. Research groups around the world are accelerating the development of COVID-19 vaccines using various approaches, including vaccination based on subunit, DNA, and mRNA [100].

Clover Biopharmaceuticals is conducting preclinical testing of a recombinant subunit vaccine based on the trimeric S protein (S-Trimer) of SARS-CoV-2 [101]. The University of Queensland is developing subunit vaccines

using the “molecular clamp,” a transformative technology [102]. Inovio Pharmaceuticals, in collaboration with Beijing Advaccine Biotechnology, has started preclinical trials for a DNA vaccine (INO-4800) against SARS-CoV-2 [103]. Moderna, Inc., has started phase I clinical trials for mRNA-1273, an mRNA vaccine, encoding the viral spike (S) protein of SARS-CoV-2 [104].

Conclusions

The COVID-19 pandemic is the biggest modern challenge facing the global healthcare system. After the pandemic, how will COVID-19 transform urological practice and research? Due to the limited supply of ventilators, manpower, and hospital resources, there is an urgent need to establish a new set of systems to meet demands in emergencies, such as replacing traditional outpatient services with telemedicine, reducing the number of nonnecessary operations, and implementing network teaching. In relation to urology, it is necessary to strengthen the safety training of medical staff. Since exposure to patients and bodily fluids presents potential increased risks of viral transmission, medical staff must be adequately protected. The concern of renal damage in patients from COVID-19 also requires much attention. Lastly, it is imperative to channel international resources into high-quality clinical trials with robust scientific rationale and vigorous statistical rigor to overcome this pandemic.

Acknowledgement

This research was supported by the Samuel Oschin Comprehensive Cancer Institute (SOCCI) at Cedars-Sinai Medical Center through the 2019 Lucy S. Gonda Award.

Conflict of Interest Statement

The authors have nothing to disclose.

Funding Source

This research was funded by the National Institutes of Health (1U01DK103260, 1R01DK100974, U24 DK097154, and NIH NCATS UCLA CTSI UL1TR000124), the Department of Defense (W81XWH-15-1-0415 and W81XWH-19-1-0109), the Centers for Disease Control and Prevention (1U01DP006079), and the US-Egypt Science and Technology Development Fund by the National Academies of Sciences, Engineering, and Medicine (all to J.K.).

This article is derived from the subject data funded in whole or part by the National Academies of Sciences, Engineering, and Medicine (NAS) and the United States Agency for International Development (USAID). Any opinions, findings, conclusions, or recommendations expressed in this article are those of the authors alone and do not necessarily reflect the views of the USAID or the NAS.

Author Contributions

Research conception and design: J.K. Data analysis and interpretation: P.J. and H.P. Drafting of this paper: P.J., S.J., and J.K. Supervision: J.K. Approval of the final version of this work: all of the authors.

References

- Center for Systems Science Engineering at Johns Hopkins University. [Coronavirus COVID-19 global cases](#) [Internet]. [cited 2020 Apr 3]. Available from: <https://coronavirus.jhu.edu/map.html>.
- Masters PS. The molecular biology of coronaviruses. *Adv Virus Res.* 2006;66:193–292.
- Ahn DG, Shin HJ, Kim MH, Lee S, Kim HS, Myoung J, et al. Current Status of Epidemiology, Diagnosis, Therapeutics, and Vaccines for Novel Coronavirus Disease 2019 (COVID-19). *J Microbiol Biotechnol.* 2020 Mar;30(3):313–24.
- Zhang W, Du RH, Li B, Zheng XS, Yang XL, Hu B, et al. Molecular and serological investigation of 2019-nCoV infected patients: implication of multiple shedding routes. *Emerg Microbes Infect.* 2020 Feb;9(1):386–9.
- Ozma MA, Maroufi P, Khodadadi E, Kose S, Esposito I, Ganbarov K, et al. Clinical manifestation, diagnosis, prevention and control of SARS-CoV-2 (COVID-19) during the outbreak period. *Infez Med.* 2020 Jun;28(2):153–65.
- Tahamtan A, Ardebili A. Real-time RT-PCR in COVID-19 detection: issues affecting the results. *Expert Rev Mol Diagn.* 2020 May;20(5):453–4.
- Li Z, Yi Y, Luo X, Xiong N, Liu Y, Li S, et al. Development and clinical application of a rapid IgM-IgG combined antibody test for SARS-CoV-2 infection diagnosis. *J Med Virol.* 2020 Feb;92(9):1518–24.
- Xie J, Ding C, Li J, Wang Y, Guo H, Lu Z, et al. Characteristics of patients with coronavirus disease (COVID-19) confirmed using an IgM-IgG antibody test. *J Med Virol.* 2020 Apr;92(10):2004–10.
- US Food and Drug Administration. [Emergency use authorizations for medical devices](#) [Internet]. Available from: <https://www.fda.gov/medical-devices/emergency-situations-medical-devices/emergency-use-authorizations#ivdnote2>.
- Chen N, Zhou M, Dong X, Qu J, Gong F, Han Y, et al. Epidemiological and clinical characteristics of 99 cases of 2019 novel coronavirus pneumonia in Wuhan, China: a descriptive study. *Lancet.* 2020 Feb;395(10223):507–13.
- Guan WJ, Ni ZY, Hu Y, Liang WH, Ou CQ, He JX, et al.; China Medical Treatment Expert Group for Covid-19. Clinical characteristics of coronavirus disease 2019 in China. *N Engl J Med.* 2020 Apr;382(18):1708–20.
- Hamming I, Cooper ME, Haagmans BL, Hooper NM, Korstanje R, Osterhaus AD, et al. The emerging role of ACE2 in physiology and disease. *J Pathol.* 2007 May;212(1):1–11.
- Xu X, Chen P, Wang J, Feng J, Zhou H, Li X, et al. Evolution of the novel coronavirus from the ongoing Wuhan outbreak and modeling of its spike protein for risk of human transmission. *Sci China Life Sci.* 2020 Mar;63(3):457–60.
- Hoffmann M, Kleine-Weber H, Schroeder S, Krüger N, Herrler T, Erichsen S, et al. SARS-CoV-2 Cell Entry Depends on ACE2 and TMPRSS2 and Is Blocked by a Clinically Proven Protease Inhibitor. *Cell.* 2020 Apr;181(2):271–280.e8.
- Li Y, Zhou W, Yang L, You R. Physiological and pathological regulation of ACE2, the SARS-CoV-2 receptor. *Pharmacol Res.* 2020 Jul;157:104833.
- Paoloni-Giacobino A, Chen H, Peitsch MC, Rossier C, Antonarakis SE. Cloning of the TMPRSS2 gene, which encodes a novel serine protease with transmembrane, LDLRA, and SRCR domains and maps to 21q22.3. *Genomics.* 1997 Sep;44(3):309–20.
- Dong M, Zhang J, Ma X, Tan J, Chen L, Liu S, et al. ACE2, TMPRSS2 distribution and extrapulmonary organ injury in patients with COVID-19. *Biomed Pharmacother.* 2020 Nov;131:110678.
- Matsuyama S, Nao N, Shirato K, Kawase M, Saito S, Takayama I, et al. Enhanced isolation of SARS-CoV-2 by TMPRSS2-expressing cells. *Proc Natl Acad Sci USA.* 2020 Mar;117(13):7001–3.
- Stopsack KH, Mucci LA, Antonarakis ES, Nelson PS, Kantoff PW. TMPRSS2 and COVID-19: Serendipity or Opportunity for Intervention? *Cancer Discov.* 2020 Jun;10(6):779–82.
- Chen Y, Guo Y, Pan Y, Zhao ZJ. Structure analysis of the receptor binding of 2019-nCoV. *Biochem Biophys Res Commun.* 2020 Feb;525(1):S0006-291X(20)30339-9.
- Paoli D, Pallotti F, Colangelo S, Basilico F, Mazzuti L, Turriziani O, et al. Study of SARS-CoV-2 in semen and urine samples of a volunteer with positive naso-pharyngeal swab. *J Endocrinol Invest.* 2020 Dec;43(12):1819–22.
- Song C, Wang Y, Li W, Hu B, Chen G, Xia P, et al. Absence of 2019 novel coronavirus in semen and testes of COVID-19 patients. *Biol Reprod.* 2020 Apr;103(1):4–6.
- Holtmann N, Edimiris P, Andree M, Doehmen C, Baston-Buest D, Adams O, et al. Assessment of SARS-CoV-2 in human semen—a cohort study. *Fertil Steril.* 2020 Aug;114(2):233–8.
- Li D, Jin M, Bao P, Zhao W, Zhang S. Clinical Characteristics and Results of Semen Tests Among Men With Coronavirus Disease 2019. *JAMA Netw Open.* 2020 May;3(5):e208292.
- Zhang S, Wang X, Zhang H, Xu A, Fei G, Jiang X, et al. The absence of coronavirus in expressed prostatic secretion in COVID-19 patients in Wuhan city. *Reprod Toxicol.* 2020 Jun;96:90–4.
- Global Health 5050. [COVID-19 sex-disaggregated data tracker](#) [Internet]. 2020. Available from: <http://globalhealth5050.org/covid19>.
- Lipsky MS, Hung M. Men and COVID-19: A pathophysiologic review. *Am J Men Health.* 2020 Sep–Oct;14(5):1557988320954021.
- Karlberg J, Chong DS, Lai WY. Do men have a higher case fatality rate of severe acute respiratory syndrome than women do? *Am J Epidemiol.* 2004 Feb;159(3):229–31.
- Cascella M, Rajnik M, Cuomo A, Dulebohn SC, Di Napoli R. [Features, Evaluation, and Treatment of Coronavirus \(COVID-19\)](#). Treasure Island (FL): StatPearls; 2020.
- Schurz H, Salie M, Tromp G, Hoal EG, Kinnear CJ, Möller M. The X chromosome and sex-specific effects in infectious disease susceptibility. *Hum Genomics.* 2019 Jan;13(1):2.
- Klein SL, Marriott I, Fish EN. Sex-based differences in immune function and responses to vaccination. *Trans R Soc Trop Med Hyg.* 2015 Jan;109(1):9–15.
- Salonia A, Corona G, Giwercman A, Maggi M, Minhas S, Nappi RE, et al. SARS-CoV-2, testosterone and frailty in males (PROTEG-GIMI): A multidimensional research project. *Andrology.* 2020 May;andr.12811.
- Robinson DP, Hall OJ, Nilles TL, Bream JH, Klein SL. 17 β -estradiol protects females against influenza by recruiting neutrophils and increasing virus-specific CD8 T cell responses in the lungs. *J Virol.* 2014 May;88(9):4711–20.
- Suba Z. Prevention and therapy of COVID-19 via exogenous estrogen treatment for both male and female patients. *J Pharm Pharm Sci.* 2020;23(1):75–85.
- Suen LK, So ZY, Yeung SK, Lo KY, Lam SC. Epidemiological investigation on hand hygiene knowledge and behaviour: a cross-sectional study on gender disparity. *BMC Public Health.* 2019 Apr;19(1):401.

- 36 Chu DK, Akl EA, Duda S, Solo K, Yaacoub S, Schünemann HJ, et al.; COVID-19 Systematic Urgent Review Group Effort (SURGE) study authors. Physical distancing, face masks, and eye protection to prevent person-to-person transmission of SARS-CoV-2 and COVID-19: a systematic review and meta-analysis. *Lancet*. 2020 Jun;395(10242):1973–87.
- 37 G C. Bulk and single-cell transcriptomics identify tobacco-use disparity in lung gene expression of ACE2, the receptor of 2019-nCoV. *medRxiv*. 2020.
- 38 Yu J, Yu J, Mani RS, Cao Q, Brenner CJ, Cao X, et al. An integrated network of androgen receptor, polycomb, and TMPRSS2-ERG gene fusions in prostate cancer progression. *Cancer Cell*. 2010 May;17(5):443–54.
- 39 Souza MD, Nakagawa H, Taitson PF, Cordts EB, Antunes RA. Management of ART and COVID-19: infertility in times of pandemic. What now? *JBRA Assist Reprod*. 2020 Jul;24(3):231–2.
- 40 Liang H, Acharya G. Novel corona virus disease (COVID-19) in pregnancy: what clinical recommendations to follow? *Acta Obstet Gynecol Scand*. 2020 Apr;99(4):439–42.
- 41 World Health Organization. *World Health Organization report of the WHO-China Joint Mission on Coronavirus Disease 2019 (COVID-19)* [Internet]. 2020. Available from: <https://www.who.int/docs/default-source/coronaviruse/who-china-joint-mission-on-covid-19-final-report.pdf>.
- 42 Wang S, Guo L, Chen L, Liu W, Cao Y, Zhang J, et al. A Case Report of Neonatal 2019 Coronavirus Disease in China. *Clin Infect Dis*. 2020 Jul;71(15):853–7.
- 43 Maleki Dana P, Kolahdooz F, Sadoughi F, Moazzami B, Chaichian S, Asemi Z. COVID-19 and pregnancy: a review of current knowledge. *Infez Med*. 2020 Jun;28 suppl 1:46–51.
- 44 European Society of Human Reproduction and Embryology. *ESHRE statement on pregnancy and conception* [Internet]. 2020. Available from: <https://www.eshre.eu/Press-Room/ESHRE-News#CoronaStatement27feb>.
- 45 European Society of Human Reproduction and Embryology. *Safe ART services during the third phase of the COVID-19 pandemic* [Internet]. Available from: https://www.eshre.eu/-/media/sitecore-files/Guidelines/COVID19/ESHRE-guidance_Safe-ART-services-during-the-third-phase-of-the-COVID19-pandemic.pdf.
- 46 American Society for Reproductive Medicine. American Society for Reproductive Medicine patient management and clinical recommendations during the coronavirus (COVID-19) pandemic [Internet]. 2020. Available from: <https://www.asrm.org/news-and-publications/covid-19/statements/patient-management-and-clinical-recommendations-during-the-coronavirus-covid-19-pandemic>.
- 47 American Society for Reproductive Medicine. *American Society for Reproductive Medicine patient management and clinical recommendations during the coronavirus (COVID-19) pandemic: update #5* [Internet]. Available from: <https://www.asrm.org/globalassets/asrm/asrm-content/news-and-publications/covid-19/covidtaskforceupdate5.pdf>.
- 48 De Paoli P. Bio-banking in microbiology: from sample collection to epidemiology, diagnosis and research. *FEMS Microbiol Rev*. 2005 Nov;29(5):897–910.
- 49 La Marca A, Nelson SM. SARS-CoV-2 testing in infertile patients: different recommendations in Europe and America. *J Assist Reprod Genet*. 2020 Aug;37(8):1823–8.
- 50 Maggiulli R, Giancani A, Fabozzi G, Dovele L, Tacconi L, Amendola MG, et al. Assessment and management of the risk of SARS-CoV-2 infection in an IVF laboratory. *Reprod Biomed Online*. 2020 Sep;41(3):385–94.
- 51 Bielanski A. A review of the risk of contamination of semen and embryos during cryopreservation and measures to limit cross-contamination during banking to prevent disease transmission in ET practices. *Theriogenology*. 2012 Feb;77(3):467–82.
- 52 Tedder RS, Zuckerman MA, Goldstone AH, Hawkins AE, Fielding A, Briggs EM, et al. Hepatitis B transmission from contaminated cryopreservation tank. *Lancet*. 1995 Jul;346(8968):137–40.
- 53 Bielanski A, Nadin-Davis S, Sapp T, Lutze-Wallace C. Viral contamination of embryos cryopreserved in liquid nitrogen. *Cryobiology*. 2000 Mar;40(2):110–6.
- 54 Kyuwa S, Nishikawa T, Kaneko T, Nakashima T, Kawano K, Nakamura N, et al. Experimental evaluation of cross-contamination between cryotubes containing mouse 2-cell embryos and murine pathogens in liquid nitrogen tanks. *Exp Anim*. 2003 Jan;52(1):67–70.
- 55 Ribal MJ, Cornford P, Briganti A, Knoll T, Gravas S, Babjuk M, et al.; GORRG Group; EAU Section Offices and the EAU Guidelines Panels. European Association of Urology Guidelines Office Rapid Reaction Group: An Organisation-wide Collaborative Effort to Adapt the European Association of Urology Guidelines Recommendations to the Coronavirus Disease 2019 Era. *Eur Urol*. 2020 Jul;78(1):21–8.
- 56 Esteves SC, Lombardo F, Garrido N, Alvarez J, Zini A, Colpi GM, et al. SARS-CoV-2 pandemic and repercussions for male infertility patients: A proposal for the individualized provision of andrological services. *Andrology*. 2020 May;andr.12809.
- 57 Romanski PA, Bortoletto P, Rosenwaks Z, Schattman GL. Delay in IVF treatment up to 180 days does not affect pregnancy outcomes in women with diminished ovarian reserve. *Hum Reprod*. 2020 Jul;35(7):1630–6.
- 58 Reřuchová M, Březinová J, Filipčiková R, Oborná I. [Influence of the length of cultivation of no early cleavage embryos on the IVF success rate]. *Ceska Gynekol*. 2013 Jan;78(1):68–72.
- 59 Jensen CF, Østergren P, Dupree JM, Ohl DA, Sonksen J, Fode M. Varicocele and male infertility. *Nat Rev Urol*. 2017 Sep;14(9):523–33.
- 60 Hallak J, Esteves SC. Concise practice recommendations for the provision of andrological services and assisted reproductive technology for male infertility patients during the SARS-CoV-2 in Brazil. *Int Braz J Urol*. 2020 Nov-Dec;46(6):1082–9.
- 61 Lei S, Jiang F, Su W, Chen C, Chen J, Mei W, et al. Clinical characteristics and outcomes of patients undergoing surgeries during the incubation period of COVID-19 infection. *EClinicalMedicine*. 2020 Apr;21:100331.
- 62 Pei G, Zhang Z, Peng J, Liu L, Zhang C, Yu C, et al. Renal Involvement and Early Prognosis in Patients with COVID-19 Pneumonia. *J Am Soc Nephrol*. 2020 Jun;31(6):1157–65.
- 63 Darmon M, Clec'h C, Adrie C, Argaud L, Allaouchiche B, Azoulay E, et al. Acute respiratory distress syndrome and risk of AKI among critically ill patients. *Clin J Am Soc Nephrol*. 2014 Aug;9(8):1347–53.
- 64 Wang L, Li X, Chen H, Yan S, Li D, Li Y, et al. Coronavirus Disease 19 Infection Does Not Result in Acute Kidney Injury: An Analysis of 116 Hospitalized Patients from Wuhan, China. *Am J Nephrol*. 2020;51(5):343–8.
- 65 Méjean A, Roupřet M, Rozet F, Bensalah K, Murez T, Game X, et al.; le comité de cancérologie de l'Association française d'urologie (CCAFU). [Recommendations CCAFU on the management of cancers of the urogenital system during an epidemic with Coronavirus COVID-19]. *Prog Urol*. 2020 Apr;30(5):221–31.
- 66 Lenfant L, Seisen T, Lorient Y, Roupřet M. Adjustments in the Use of Intravesical Instillations of Bacillus Calmette-Guérin for High-risk Non-muscle-invasive Bladder Cancer During the COVID-19 Pandemic. *Eur Urol*. 2020 Jul;78(1):1–3.
- 67 American Cancer Society. *Cancer Facts & Figures 2020*. Atlanta: ACA; 2020.
- 68 Wang Z, Ni Y, Chen J, Sun G, Zhang X, Zhao J, et al. The efficacy and safety of radical prostatectomy and radiotherapy in high-risk prostate cancer: a systematic review and meta-analysis. *World J Surg Oncol*. 2020 Feb;18(1):42.
- 69 Moschovas MC, Sighinolfi MC, Rocco B, Bhat S, Onof F, Rogers T, et al. Balancing the Effects of COVID-19 Against Potential Progression and Mortality in High-risk Prostate Cancer. *Eur Urol*. 2020 Jul;78(1):e14–5.
- 70 Coccolini F, Perrone G, Chiarugi M, Di Marzo F, Ansaloni L, Scandroglio I, et al. Surgery in COVID-19 patients: operational directives. *World J Emerg Surg*. 2020 Apr;15(1):25.
- 71 Montopoli M, Zumerle S, Vettor R, Rugge M, Zorzi M, Catapano CV, et al. Androgen-deprivation therapies for prostate cancer and risk of infection by SARS-CoV-2: a population-based study (N = 4532). *Ann Oncol*. 2020 Aug;31(8):1040–5.

- 72 Lucas JM, Heinlein C, Kim T, Hernandez SA, Malik MS, True LD, et al. The androgen-regulated protease TMPRSS2 activates a proteolytic cascade involving components of the tumor microenvironment and promotes prostate cancer metastasis. *Cancer Discov.* 2014 Nov;4(11):1310–25.
- 73 Wei X, Xiao YT, Wang J, Chen R, Zhang W, Yang Y, et al. **Sex differences in severity and mortality among patients with COVID-19: evidence from pooled literature analysis and insights from integrated bioinformatic analysis.** 2020. doi: arXiv:2003.13547.
- 74 Pan F, Xiao X, Guo J, Song Y, Li H, Patel DP, et al. No evidence of severe acute respiratory syndrome-coronavirus 2 in semen of males recovering from coronavirus disease 2019. *Fertil Steril.* 2020 Jun;113(6):1135–9.
- 75 Wang S, Zhou X, Zhang T, Wang Z. The need for urogenital tract monitoring in COVID-19. *Nat Rev Urol.* 2020 Jun;17(6):314–5.
- 76 Ma L ea. Effect of SARS-CoV-2 infection upon male gonadal function: a single center-based study. *medRxiv.* 2020.
- 77 Pozzilli P, Lenzi A. Commentary: Testosterone, a key hormone in the context of COVID-19 pandemic. *Metabolism.* 2020 Jul;108:154252.
- 78 Puliatti S, Eissa A, Eissa R, Amato M, Mazzone E, Dell'Oglio P, et al. COVID-19 and urology: a comprehensive review of the literature. *BJU Int.* 2020 Jun;125(6):E7–14.
- 79 Lotfi M, Hamblin MR, Rezaei N. COVID-19: Transmission, prevention, and potential therapeutic opportunities. *Clin Chim Acta.* 2020 Sep;508:254–66.
- 80 Luciani LG, Mattevi D, Cai T, Giusti G, Proietti S, Malossini G. Teleurology in the time of Covid-19 pandemic: here to stay? *Urology.* 2020 Jun;140:4–6.
- 81 Ohannessian R, Duong TA, Odone A. Global Telemedicine Implementation and Integration Within Health Systems to Fight the COVID-19 Pandemic: A Call to Action. *JMIR Public Health Surveill.* 2020 Apr;6(2):e18810.
- 82 Miller A, Rhee E, Gettman M, Spitz A. The Current State of Telemedicine in Urology. *Med Clin North Am.* 2018 Mar;102(2):387–98.
- 83 Smith AC, Thomas E, Snoswell CL, Haydon H, Mehrotra A, Clemensen J, et al. Telehealth for global emergencies: implications for coronavirus disease 2019 (COVID-19). *J Telemed Telecare.* 2020 Jun;26(5):309–13.
- 84 Wong CK, Yip BH, Mercer S, Griffiths S, Kung K, Wong MC, et al. Effect of facemasks on empathy and relational continuity: a randomised controlled trial in primary care. *BMC Fam Pract.* 2013 Dec;14(1):200.
- 85 Ghosh A, Sharma K, Choudhury S. COVID-19 and physician-patient relationship: potential effects of 'masking', 'distancing' and 'others'. *Fam Pract.* 2020 Sep; cmaa092.
- 86 Ficarra V, Novara G, Abrate A, Bartoletti R, Crestani A, De Nunzio C, et al.; Research Urology Network (RUN). Urology practice during the COVID-19 pandemic. *Minerva Urol Nefrol.* 2020 Jun;72(3):369–75.
- 87 Stensland KD, Morgan TM, Moinedzadeh A, Lee CT, Briganti A, Catto JW, et al. Considerations in the Triage of Urologic Surgeries During the COVID-19 Pandemic. *Eur Urol.* 2020 Jun;77(6):663–6.
- 88 van Doremalen N, Bushmaker T, Morris DH, Holbrook MG, Gamble A, Williamson BN, et al. Aerosol and surface stability of SARS-CoV-2 as compared with SARS-CoV-1. *N Engl J Med.* 2020 Apr;382(16):1564–7.
- 89 Zheng MH, Boni L, Fingerhut A. Minimally Invasive Surgery and the Novel Coronavirus Outbreak: lessons Learned in China and Italy. *Ann Surg.* 2020 Jul;272(1):e5–6.
- 90 Xiao Y, Qian K, Luo Y, Chen S, Lu M, Wang G, et al. Severe Acute Respiratory Syndrome Coronavirus 2 Infection in Renal Failure Patients: A Potential Covert Source of Infection. *Eur Urol.* 2020 Aug;78(2):298–9.
- 91 Kumar D, Manuel O, Natori Y, Egawa H, Grossi P, Han SH, et al. COVID-19: A global transplant perspective on successfully navigating a pandemic. *Am J Transplant.* 2020 Jul;20(7):1773–9.
- 92 The Transplantation Society. **An update and guidance on 2019 novel coronavirus (COVID-19) for transplant clinicians.** Available from: <https://tts.org/23-tid/tid-news/657-tid-update-and-guidance-on-2019-novel-coronavirus-2019-ncov-for-transplant-id>.
- 93 US Department of Health and Human Services. **Information for transplant programs and OPOs regarding 2019 novel coronavirus: OPTN** [Internet]. 2019. [cited 2020 Mar]. Available from: <https://optn.transplant.hrsa.gov/news/information-for-transplant-programs-and-opos-regarding-2019-novel-coronavirus/>.
- 94 Chan MC, Yeo SE, Chong YL, Lee YM. Stepping Forward: Urologists' Efforts During the COVID-19 Outbreak in Singapore. *Eur Urol.* 2020 Jul;78(1):e38–9.
- 95 Rimmer A. Trainees and COVID-19: your questions answered. *BMJ.* 2020 Mar;368:m1059.
- 96 Wang M, Cao R, Zhang L, Yang X, Liu J, Xu M, et al. Remdesivir and chloroquine effectively inhibit the recently emerged novel coronavirus (2019-nCoV) in vitro. *Cell Res.* 2020 Mar;30(3):269–71.
- 97 Chan KS, Lai ST, Chu CM, Tsui E, Tam CY, Wong MM, et al. Treatment of severe acute respiratory syndrome with lopinavir/ritonavir: a multicentre retrospective matched cohort study. *Hong Kong Med J.* 2003 Dec;9(6):399–406.
- 98 Chu CM, Cheng VC, Hung IF, Wong MM, Chan KH, Chan KS, et al.; HKU/UCH SARS Study Group. Role of lopinavir/ritonavir in the treatment of SARS: initial virological and clinical findings. *Thorax.* 2004 Mar;59(3):252–6.
- 99 Lythgoe MP, Middleton P. Ongoing Clinical Trials for the Management of the COVID-19 Pandemic. *Trends Pharmacol Sci.* 2020 Jun;41(6):363–82.
- 100 Wang J, Peng Y, Xu H, Cui Z, Williams RO 3rd. The COVID-19 Vaccine Race: Challenges and Opportunities in Vaccine Formulation. *AAPS PharmSciTech.* 2020 Aug;21(6):225.
- 101 Clover Biopharmaceuticals. **Vaccines programs.** Available from: <http://www.cloverbiopharma.com/index.php?m=content&c=index&a=lists&catid=42>.
- 102 The University of Queensland Australia. **'Significant step' in COVID-19 vaccine quest** [Internet]. [cited 2020 Feb 28]. Available from: <https://www.uq.edu.au/news/article/2020/02/significantstep%E2%80%99-covid-19-vaccine-quest>.
- 103 INOVIO. **INOVIO accelerates timeline for COVID-19 DNA vaccine INO-4800** [Internet]. [cited 2020 Mar 3]. Available from: <http://ir.inovio.com/news-andmedia/news/press-release-details/2020/Inovio-Accelerates-Timeline-for-COVID-19-DNA-Vaccine-INO-4800/default.aspx>.
- 104 Moderna. **Moderna's pipeline** [Internet]. [cited 2020 Feb 28]. Available from: <https://www.modernatx.com/pipeline>.
- 105 Zhen W, Smith E, Manji R, Schron D, Berry GJ. Clinical Evaluation of Three Sample-to-Answer Platforms for Detection of SARS-CoV-2. *J Clin Microbiol.* 2020 Jul;58(8):e00783-20.
- 106 GenMark Diagnostics. **ePlex® SARS-CoV-2 test assay manual.** Available from: <https://www.fda.gov/media/136282/download>.
- 107 Seegene. **Allplex™ 2019-nCoV assay: version 2.1; October 30th, 2020.** Available from: <https://www.fda.gov/media/137178/download>.
- 108 Hardy Diagnostics. **Instructions for use: Anti-SARS-CoV-2 rapid test.** Available from: <https://www.fda.gov/media/137367/download>.

Review

Exercise May Affect Metabolism in Cancer-Related Cognitive Impairment

Muhammad Shahid ¹ and Jayoung Kim ^{1,2,3,4,*}

¹ Departments of Surgery and Biomedical Sciences, Cedars-Sinai Medical Center, Davis 5071, 8700 Beverly Blvd., Los Angeles, CA 90048, USA; muhammad.shahid@cshs.org

² Samuel Oschin Comprehensive Cancer Institute, Cedars-Sinai Medical Center, Los Angeles, CA 90048, USA

³ Department of Medicine, University of California Los Angeles, Los Angeles, CA 90024, USA

⁴ Department of Urology, Ga Cheon University College of Medicine, Incheon 461-701, Korea

* Correspondence: Jayoung.Kim@cshs.org; Tel.: +1-310-423-7168; Fax: +1-310-967-3809

Received: 7 August 2020; Accepted: 18 September 2020; Published: 20 September 2020



Abstract: Cancer-related cognitive impairment (CRCI) is a significant comorbidity for cancer patients and survivors. Physical activity (PA) has been found to be a strong gene modulator that can induce structural and functional changes in the brain. PA and exercise reduce the risk of cancer development and progression and has been shown to help in overcoming post-treatment syndromes. Exercise plays a role in controlling cancer progression through direct effects on cancer metabolism. In this review, we highlight several priorities for improving studies on CRCI in patients and its underlying potential metabolic mechanisms.

Keywords: cancer-related cognitive impairment; therapeutic exercise intervention; metabolism; metabolomics profiling

1. Introduction

From the total global population, 13% are adults 60 years or older, which accounts for approximately 962 million people. This group is predicted to steadily increase in population to 1.4 billion, 2.1 billion, and 3.1 billion by 2030, 2050, and 2100, respectively [1]. Patients with cognitive impairment (CI) make up a large number of adults in the 60 years or older population. These patients may experience difficulties in daily functioning, decision-making, and treatment adherence; thereby, leading to reduced quality of life (QoL) and decreased survival [2,3]. In an effort to maintain independence in older adults, focusing on cognitive function is a novel target of concern, since the origins of cognitive decline may be reversible or even treatable. As a result, understanding cognitive decline in older adults is a growing field of interest. CI can also lead to increases in caregiver burdens. Prevention of CI in cancer patients is especially important for older patients, since there have been notable increases in long-term survival due to new treatments and a resulting growing number of people living with cancer as a chronic condition. The spectrum of cognitive decline between normal cognitive and mild cognitive impairment (MCI) to dementia in older adults can range from natural cognitive decline due to age to atypical cognitive impairment [1]. The prevalence rate in the group of adults older than 60 MCI showed increasing with age and lower levels of education which is approximately 6.7% to 25.2%, and is more prevalent in men [4,5].

2. CI in Cancer Patients

Cancer and treatments for it, including chemotherapy, hormone therapy, and radiation therapy, can have harmful effects on mental processes [6,7]. Previous studies reported a higher incidence of cognitive dysfunction among cancer patients compared to healthy matched controls. Up to 85% of

cancer patients receiving treatment have been found to report mild to severe cognitive complaints, which can last months to even years after finishing treatment [8]. Cancer-related CI (CRCI) can be classified as subtle, moderate, or severe based on neuropsychological testing. CRCI is the most frequent complication reported by breast cancer patients [9]. Cognitive complaints have been reported by more than 50% of breast cancer patients following chemotherapy; however, only 15%–25% of these patients have shown objective cognitive decline [10]. Demographic and other health factors, such as age, race, socioeconomic status, education, menopausal status, and body mass index, are also known to affect cognition in adults [11,12]. Since difficulties in cognitive function have a negative impact on QoL (autonomy, work balance, relationships, and self-image), there is an urgent need for more pronounced CRCI management in patients. This has fueled studies on potentially implementing cognitive rehabilitation for cancer patients [13]. In light of the prevalence and associated individual burden of CRCI, there is a clear need for strategies to manage CRCI. Currently, there are no established treatment options to reduce CRCI risk or diminish its severity [14,15]. Furthermore, advancements in hormone therapy, targeted therapy, and immunotherapy have resulted in greater survival rates for cancer patients, but at the cost of increased potential cognitive impacts [16].

The precise mechanisms underlying the pathophysiology of CRCI are unclear. Demographic factors, including age, race, socioeconomic status, and education, as well as menopausal status, health status, and body mass index, are also known to affect cognition in adults. In light of the prevalence and associated individual burden of CRCI, there is a clear need for strategies to manage CRCI. Currently, no established treatment options exist to reduce the risk of CRCI or diminish its severity. Campbell et al., performed a systematic analysis of 29 randomized controlled trials (RCTs) to better understand the relationship of exercise with CRCI. In 12 of these trials (41%) (Cohen *d* range: 0.24–1.14), they found that exercise had a significant effect on self-reported cognitive function during and after chemotherapy. These 12 trials used the EORTC QLQ-C30 exam for cognitive functioning. In 10 other trials (34%), neuropsychological testing was used to evaluate cognitive functioning; however, only 3 of these trials in breast cancer reported significant benefits from exercise (Cohen *d* range: 0.41–1.47) [17].

Another study by Witlox et al. found that physical exercise had positive effects in healthy older adults and those with mild cognitive impairment. They recruited 180 breast cancer patients with cognitive issues 2–4 years after their diagnosis with cancer and randomized them (1:1) into two groups; exercise intervention and control. The exercise intervention group underwent a 6-month course of twice weekly 1 h supervised aerobic and strength-training exercises with twice weekly 1 h power walking. They concluded that physical exercise improves cognitive functioning for breast cancer survivors [18].

To better understand CRCI's pathophysiology and the direct impact of different cancer treatments, animal models have been developed [19].

3. Biological Drivers of CRCI

Evidence from clinical and pre-clinical research suggests that many mechanisms play a role in the development of CRCI, including inflammation [20,21]. Inflammation is an important mechanism underlying cognitive impairment, especially in the elderly. Accumulating evidence has linked inflammation to cognitive decline and the risk of dementia [22]. Chemotherapy-induced pro-inflammatory cytokines levels of interleukin (IL)-1 β , IL-6, tumor necrosis factor- α (TNF- α), and IL-10 in cancer patients have been related to possible CI [23,24]. A large multicentered cohort study conducted in Singapore found that among proinflammatory plasma cytokines—including IL-1 β , IL-2, IL-4, IL-6, IL-8, IL-10, granulocyte-macrophage colony-stimulating factor, interferon- γ , and TNF- α —elevated IL-1 β and IL-6 were associated with greater self-reported cognitive impairments ($p = 0.018$ and 0.001 , respectively) [25]. However, the effects of cytokines in post-chemotherapy cognitive impairment remains in controversy; other studies have published conflicting results about the relationship between cytokine concentration and cognition [26,27]. Nonsteroidal anti-inflammatory

drugs (NSAIDs) have often been administered as a preventative measure against Alzheimer's disease (AD). The mechanism of action is believed to be through blockage of cyclo-oxygenase isoforms (e.g., COX-1 and COX-2). NSAIDs have neurotoxic and neuroprotective effects with diverse impacts on mechanisms that may influence cognitive impairment, including inflammation, release of neurotransmitters, synaptic plasticity, cerebral ischemia, and functioning of cerebral endothelial and smooth muscle [28].

Oxidative stress and its associated damage in the age-dependent cognitive loss has been previously highlighted [29]. Chemotherapy-induced oxidative stress-mediated TNF- α triggers inducible nitric oxide synthase (iNOS) production [30]. Apolipoprotein A-I (ApoA1) is possibly one of the key factors in oxidative stress and pro-inflammatory cytokine mediated CRCI. Oxidation and down-regulated expression of ApoA1 were found in a number of neurodegenerative diseases with cognitive deficits, such as Alzheimer's and Parkinson's Diseases [31]. Administration of vitamin E ameliorated memory deficit. Vitamin E-deficient rats showed decreased learning as well as memory retention ability, whereas younger rats supplemented with vitamin E displayed accelerated learning and capabilities. This could be that learning ability declined gradually with age due to chronic exposure to oxidative stress [32]. The association of DNA damage with aging is well-studied [33]. DNA lesions are accumulated in the brain during AD. Elevations in γ H2AX, a well-established marker of double-strand breaks (DSB) [34], were detected in 11 of 13 AD brains in the astrocytes of the hippocampus and cerebral cortex [35]. Studies on two independent cohorts ($n = 13$ and $n = 23$) found significant increases of γ H2AX in the astrocytes and neurons of the hippocampus and frontal cortex of AD brains; this increase was found in brains with MCI as well [36]. Other factors include reduced synaptic plasticity, altered growth factor levels, and impaired hippocampal neurogenesis [37–39].

4. The Interrelationship between CRCI and Alterations in Metabolism

In addition to powering live systems, metabolism is a complex phenomenon that is tightly linked to signaling pathways, post-translational modifications, and gene expression. In general, metabolism acts as a cellular rheostat [40]. Metabolism supports a variety of normal cell functions, including breakdown of carbohydrates, fats, and amino acids to generate energy and biosynthetic precursors needed for growth [41]. The fundamental features of metabolism are reprogrammed in cancer cells to support their aberrant growth and proliferation. This change in functioning is likely the result of genomic alterations (i.e., mutations in oncogenes and tumor suppressor genes), tumor microenvironment (compromised nutrients and oxygen availability), and other factors [42]. Metabolic alterations are a hallmark of cancer [43]. These changes favor rapidly dividing cells, inhibit the prevention of tumor initiation, and attenuates proliferation and metastasis [44]. In order to better understand cancer-specific metabolism, a systemic application of analytical techniques that can assess metabolic levels is needed.

Metabolomics combines high-throughput analysis with bioinformatics and aims to comprehensively analyze all metabolites in a given biological sample. Over the past 20 years, incredible advancements have been made in metabolomics. This has propelled its evolution into becoming a powerful tool in medicine and science, especially in the study of disease-related biomarkers, toxicology, and molecular mechanisms. Metabolomics can also provide greater detailed information regarding human biochemistry [45,46]. Metabolomics is commonly applied to discover diagnostic, prognostic, or therapeutic biomarkers [47]. For instance, early metabolomic experiments in breast cancer patients lead to the identification of positive associations between choline, glycine, and lactate with tumor grade and size [48]. Similar work has now been done in ovarian [49], prostate [50], and various other cancers. Since the efforts of metabolomics-based biomarker discovery have been well summarized in previously published review papers as described above, we will not further discuss the topic in this article.

Since its first observation 90 years ago by Dr. Otto Warburg, one of the hallmarks in cancer biology is the metabolic reprogramming such as high rates of aerobic glycolysis [51–54]. Cancer-associated metabolic alteration has been reported in many types of cancers. Amino acids, such as arginine, proline,

glutamine, and creatine, play important roles as substrates and protein synthesis in cancer cells and they have been widely studied in cancer metabolism. Specific metabolic pathways altered by cancer have also been reported, which provide therapeutical strategies. Metabolic reprogramming is considered for regimens an exploited for cancer therapy. Amino acid depletion therapies are being tested against several cancer types [55,56]. For example, metformin, an inhibitory drug of mitochondrial metabolism, has been suggested to have a synergistic effect when used with chemotherapies by inhibiting proliferation of cancer cells [57,58].

Doxorubicin (DOX) is a widely used antitumor agent for the treatment of a series of cancer types. However, DOX shows cytotoxicity to noncancer cells such as heart, skeletal muscle, liver, and kidney cells, leading to adverse effect. Recently, exercise is reported to show a beneficial adaptation to reduce the DOX-induced cellular toxicity [59]. However, the mechanisms underlying the exercise-induced protection against DOX cytotoxicity are not clear. Exercise has another benefit, reducing cognitive impairment. Brain-derived neurotrophic factor (BDNF), a key mediator of cognitive impairment in Alzheimer's dementia. A recent finding suggested that exercise-induced expression of BDNF, suggesting the potential mechanism of exercise benefit to increase cognitive function [60].

Prior studies have also provided essential information on the occurrence and association of metabolic alterations and cognitive impairment in humans. However, they have not established the molecular mechanisms behind these relationships, nor the therapeutic window that would allow for treatment before irreversible damage occurs in both systemic functionality and cognitive skills.

Different lifestyle factors are involved in the arise of diseases which may also lead increasing the risk of developing AD. Lifestyle factors are increasingly being recognized for their role in figuring out cognitive impairment, or the lack thereof, with age. Participation in recreational physical activity (PA) has been shown to be inversely related to the prevalence of age-related cognitive decline and dementia [61]. Independent studies have repeatedly shown that PA reduces cognitive decline in older age groups [62]. Similarly, several studies have also shown that due to the limited use of diet or diet restraint is resulted with the maintenance of cognitive function later in life [63].

Omega-3 fatty acids and antioxidants are specific dietary components which preserves cognitive function. Daily intake of these components works well for the eighth decade of life [64]. Glucose and insulin metabolism are key metabolic pathways and represents a metabolic spectrum with clinical thresholds for prediabetes and diabetes mellitus. Further increases in fasting glucose, with concomitant impairment of both glucose and insulin metabolism, are hallmarks of type 2 diabetes. Obesity is a known significant risk factor of AD progression for both prediabetes and diabetes [63]. Possible mechanisms underlying metabolic reserves in MCI and AD involve direct roles for insulin [65], insulin-like growth factors [66], and neurotrophic factors [67], as well as pathological changes in glucose metabolism and protein glycosylation [68]. Other components of the hormonal milieu include adipocyte cytokine leptin [69].

5. Role of Exercise in CRCI

According to the World Health Organization's definition, any bodily movement that involved skeletal muscles by utilizing energy is called PA; whereas, well planned, structured, repetitive, and intentional movement known as exercise, which is a subcategory of PA. Most observational studies assess PA rather than exercise. Based on multiple meta-analyses, physical exercise is known to be crucial for maintaining general health [70,71]. Exercise helps maintain body weight and reduces stress. People who regularly exercise are less likely to smoke tobacco or overeat. Moreover, exercise directly targets the primary aspects of health, including heart function, cholesterol, triglycerides, blood pressure, and brain function. It has been shown that regular exercise leads to enhanced maximal oxygen uptake and increases the mean lifespan of laboratory animals and humans [72]. Exercise is known to impact almost every system in the body. Benefits include improved cardiovascular health, greater bone mineral density (BMD), and decreased risk of cancer, stroke, diabetes, and cognitive impairment.

Exercise is an established safe and effective therapy for managing numerous adverse effects of cancer treatment, including fatigue, psychological distress, functional decline, and detrimental body composition changes [73]. Accumulating evidence on the positive role of exercise on improving cognitive function in healthy older adults and those with mild cognitive impairment or more severe neurocognitive impairment (i.e., AD, stroke) has sparked significant interest in the potential use of exercise as an effective management strategy for CRCI [74–76]. A variety of evidence supports the conclusion that exercise link to cancer which could lower the risk of different cancers including colon, breast, kidney, endometrial, bladder, esophageal, and stomach cancers, with moderate evidence for lung cancer. The Physical Activity Guidelines Advisory Committee determined and vigorously appreciated the conclusion [77].

Unfortunately, due to limited preclinical studies and testing of the antitumor activity of exercise is restricted. So far, only 53 studies were reported in vivo preclinical testing to assess the activity of various exercise paradigms on tumor incidence, growth, or metastasis; 35 of these studies positively reported that exercise inhibited cancer growth or progression [78]. More recently, higher-quality studies have demonstrated that paradigms of PA showed a link between exercise and epinephrine, and IL-6 to NK cell mobilization and redistribution; both of which ultimately control tumor growth [79].

Benefits of exercise were particularly noted on self-reported cognitive function in women with breast cancer [80]. RCTs have suggested that people should adopt PA and exercise to alleviate the negative impacts of aging on cognitive function. Through a meta-analysis, Heyn P. et al. found that PA and exercise had positive effects on cognition among those with cognitive decline [80].

6. The Effects of Exercise on Cancer Metabolism and Its Associated Signaling Pathways

The role of PA and exercise in the whole process of cancer from prevention to post-treatment has been extensively studied [70,81]. There is ample evidence suggesting regular PA to be related to a reduced risk for various forms of cancer [82]. Exercising at varying intensities has been found to have remarkable effects on physiologic and gene expression adaptations in mammals [83]. The role of exercise has surprisingly received little to no attention in high-risk individuals. However, recently, a larger number of groups are investigating the effects of PA and exercise on cancer; a field now called “exercise-oncology” [84]. In cancer patients, exercise is now well-documented to be a tolerable adjunct therapy associated with significant benefits across a wide range of symptoms [85].

Intratumoral signaling networks are highly modifiable and modulated by numerous extrinsic factors [86]. Vulczak et al. demonstrated that the mitochondrial activity of tumor cells in animals that exercised was lower in comparison to the tumor cells of sedentary animals, with a significant decrease in the electron transport chain capacity (E). This demonstrates lower respiratory capacity independent of mitochondrial content, measured by citrate synthase (CS) activity [87]. Kynurenine (KYN), a catabolite of the amino acid tryptophan (TRP), was found to be associated with progression and poor clinical outcome in numerous cancer types [88]. Zimmer et al. and his team investigated the influence of resistance exercise on the KYN pathway in breast cancer patients. They showed the potential exercise-induced modulation of KYN pathway metabolites in the serum and urine of healthy women and breast cancer patients undergoing radiotherapy [89]. The Akt/mTOR pathway is central for controlling growth and protein synthesis and plays a pivotal role in the muscular response to resistance training [90]. Thompson et al. reviewed several preclinical studies highlighting how the Akt/mTOR pathway is differentially regulated with exercise in many tumor types [91].

7. Conclusions

In conclusion, current evidence suggests that physical exercise shows much promise in improving cognitive impairment among cancer patients and survivors. Exercise also shows much influence on cancer incidence, lowers the risk of recurrence, and secures longer higher quality life for patients. Most of cancer patients expressed their preferences in the therapeutic potential of exercise over chemotherapeutics; this strategy may potentially alter disease pathogenesis and symptoms without the

adverse effects of conventional pharmacological agents. The positive effects of exercise are evident in large epidemiological studies, as well as controlled laboratory studies. Moreover, exercise inhibits tumor growth across cancers and at all stages of tumor development. Given these findings, future research needs to consider the type of measurements used to measure CRCI, which will further improve patient care and lead to the development of targeted therapies, preventative strategies, and cognitive rehabilitation treatment.

Author Contributions: Research conception and design: J.K. Drafting of the manuscript: M.S. Critical revision of the manuscript: J.K. Supervision: J.K. Approval of the final manuscript: All authors. All authors have read and agreed to the published version of the manuscript.

Funding: The authors acknowledge support from National Institutes of Health grants (grant nos. 1U01DK103260, 1R01DK100974, U24 DK097154 and NIH NCATS UCLA CTSI UL1TR000124), Department of Defense grants (grant nos. W81XWH-15-1-0415 and W81XWH-19-1-0109), Centers for Disease Controls and Prevention (grant no. 1U01DP006079), IMAGINE NO IC Research Grant, the Steven Spielberg Discovery Fund in Prostate Cancer Research Career Development Award, and the U.S.-Egypt Science and Technology Joint Fund. This research was partly supported by the Samuel Oschin Comprehensive Cancer Institute at Cedars-Sinai Medical Center through 2019 Lucy S. Gonda Award (to J.K.). In addition, this article is derived from the Subject Data funded in whole or part by National Academies of Sciences, Engineering, and Medicine (NAS) and The United States Agency for International Development (USAID). Any opinions, findings, conclusions, or recommendations expressed in this article are those of the authors alone, and do not necessarily reflect the views of USAID or NAS.

Acknowledgments: The authors acknowledge support from National Institutes of Health grants (1U01DK103260, 1R01DK100974, U24 DK097154, NIH NCATS UCLA CTSI UL1TR000124), Department of Defense grants (W81XWH-15-1-0415 and W81XWH-19-1-0109), Centers for Disease Controls and Prevention (1U01DP006079), IMAGINE NO IC Research Grant, the Steven Spielberg Discovery Fund in Prostate Cancer Research Career Development Award, and the U.S.-Egypt Science and Technology Joint Fund. This research was partly supported by the Samuel Oschin Comprehensive Cancer Institute at Cedars-Sinai Medical Center through 2019 Lucy S. Gonda Award (to J.K.). In addition, this article is derived from the Subject Data funded in whole or part by National Academies of Sciences, Engineering, and Medicine (NAS) and The United States Agency for International Development (USAID). Any opinions, findings, conclusions, or recommendations expressed in this article are those of the authors alone, and do not necessarily reflect the views of USAID or NAS.

Conflicts of Interest: The authors declare no conflict of interest.

References

1. Jongsiriyanyong, S.; Limpawattana, P. Mild Cognitive Impairment in Clinical Practice: A Review Article. *Am. J. Alzheimers Dis. Other Demen* **2018**, *33*, 500–507. [[CrossRef](#)] [[PubMed](#)]
2. Robb, C.; Boulware, D.; Overcash, J.; Extermann, M. Patterns of care and survival in cancer patients with cognitive impairment. *Crit Rev. Oncol. Hematol.* **2010**, *74*, 218–224. [[CrossRef](#)] [[PubMed](#)]
3. Barrios, H.; Narciso, S.; Guerreiro, M.; Maroco, J.; Logsdon, R.; de Mendonca, A. Quality of life in patients with mild cognitive impairment. *Aging Ment. Health* **2013**, *17*, 287–292. [[CrossRef](#)] [[PubMed](#)]
4. Cheng, Y.W.; Chen, T.F.; Chiu, M.J. From mild cognitive impairment to subjective cognitive decline: Conceptual and methodological evolution. *Neuropsychiatr. Dis. Treat.* **2017**, *13*, 491–498. [[CrossRef](#)] [[PubMed](#)]
5. Valenzuela, M.; Sachdev, P.; Brodaty, H. Reader response: Practice guideline update summary: Mild cognitive impairment: Report of the Guideline Development, Dissemination, and Implementation Subcommittee of the American Academy of Neurology. *Neurology* **2018**, *91*, 372. [[CrossRef](#)]
6. Tannock, I.F.; Ahles, T.A.; Ganz, P.A.; Van Dam, F.S. Cognitive impairment associated with chemotherapy for cancer: Report of a workshop. *J. Clin. Oncol.* **2004**, *22*, 2233–2239. [[CrossRef](#)]
7. Brezden, C.B.; Phillips, K.A.; Abdolell, M.; Bunston, T.; Tannock, I.F. Cognitive function in breast cancer patients receiving adjuvant chemotherapy. *J. Clin. Oncol.* **2000**, *18*, 2695–2701. [[CrossRef](#)]
8. Falletti, M.G.; Sanfilippo, A.; Maruff, P.; Weih, L.; Phillips, K.A. The nature and severity of cognitive impairment associated with adjuvant chemotherapy in women with breast cancer: A meta-analysis of the current literature. *Brain Cogn.* **2005**, *59*, 60–70. [[CrossRef](#)]
9. Schmidt, J.E.; Beckjord, E.; Bovbjerg, D.H.; Low, C.A.; Posluszny, D.M.; Lowery, A.E.; Dew, M.A.; Nutt, S.; Arvey, S.R.; Rechis, R. Prevalence of perceived cognitive dysfunction in survivors of a wide range of cancers: Results from the 2010 LIVESTRONG survey. *J. Cancer Surviv.* **2016**, *10*, 302–311. [[CrossRef](#)]

10. Lange, M.; Licaj, I.; Clarisse, B.; Humbert, X.; Grellard, J.M.; Tron, L.; Joly, F. Cognitive complaints in cancer survivors and expectations for support: Results from a web-based survey. *Cancer Med.* **2019**, *8*, 2654–2663. [[CrossRef](#)]
11. Janelsins, M.C.; Kesler, S.R.; Ahles, T.A.; Morrow, G.R. Prevalence, mechanisms, and management of cancer-related cognitive impairment. *Int Rev. Psychiatr.* **2014**, *26*, 102–113. [[CrossRef](#)] [[PubMed](#)]
12. Agrigoroaei, S.; Lachman, M.E. Cognitive functioning in midlife and old age: Combined effects of psychosocial and behavioral factors. *J. Gerontol. B Psychol. Sci Soc. Sci.* **2011**, *66 Suppl 1*, i130–i140. [[CrossRef](#)]
13. Lange, M.; Joly, F.; Vardy, J.; Ahles, T.; Dubois, M.; Tron, L.; Winocur, G.; De Ruiter, M.B.; Castel, H. Cancer-related cognitive impairment: An update on state of the art, detection, and management strategies in cancer survivors. *Ann. Oncol.* **2019**, *30*, 1925–1940. [[CrossRef](#)] [[PubMed](#)]
14. Ahles, T.A.; Root, J.C.; Ryan, E.L. Cancer- and cancer treatment-associated cognitive change: An update on the state of the science. *J. Clin. Oncol.* **2012**, *30*, 3675–3686. [[CrossRef](#)] [[PubMed](#)]
15. Gehring, K.; Roukema, J.A.; Sitskoorn, M.M. Review of recent studies on interventions for cognitive deficits in patients with cancer. *Expert Rev. Anticancer Ther.* **2012**, *12*, 255–269. [[CrossRef](#)] [[PubMed](#)]
16. Joly, F.; Heutte, N.; Duclos, B.; Noal, S.; Leger-Hardy, I.; Dauchy, S.; Longato, N.; Desrues, L.; Houede, N.; Lange, M.; et al. Prospective Evaluation of the Impact of Antiangiogenic Treatment on Cognitive Functions in Metastatic Renal Cancer. *Eur. Urol. Focus* **2016**, *2*, 642–649. [[CrossRef](#)]
17. Campbell, K.L.; Zadavec, K.; Bland, K.A.; Chesley, E.; Wolf, F.; Janelsins, M.C. The Effect of Exercise on Cancer-Related Cognitive Impairment and Applications for Physical Therapy: Systematic Review of Randomized Controlled Trials. *Phys. Ther.* **2020**, *100*, 523–542. [[CrossRef](#)]
18. Witlox, L.; Schagen, S.B.; de Ruiter, M.B.; Geerlings, M.I.; Peeters, P.H.M.; Koevoets, E.W.; van der Wall, E.; Stuiver, M.; Sonke, G.; Velthuis, M.J.; et al. Effect of physical exercise on cognitive function and brain measures after chemotherapy in patients with breast cancer (PAM study): Protocol of a randomised controlled trial. *BMJ Open* **2019**, *9*, e028117. [[CrossRef](#)]
19. Winocur, G.; Johnston, I.; Castel, H. Chemotherapy and cognition: International cognition and cancer task force recommendations for harmonising preclinical research. *Cancer Treat. Rev.* **2018**, *69*, 72–83. [[CrossRef](#)]
20. Rego, S.L.; Helms, R.S.; Dreau, D. Tumor necrosis factor-alpha-converting enzyme activities and tumor-associated macrophages in breast cancer. *Immunol. Res.* **2014**, *58*, 87–100. [[CrossRef](#)]
21. Korkaya, H.; Liu, S.; Wicha, M.S. Breast cancer stem cells, cytokine networks, and the tumor microenvironment. *J. Clin. Invest.* **2011**, *121*, 3804–3809. [[CrossRef](#)] [[PubMed](#)]
22. Sartori, A.C.; Vance, D.E.; Slater, L.Z.; Crowe, M. The impact of inflammation on cognitive function in older adults: Implications for healthcare practice and research. *J. Neurosci. Nurs.* **2012**, *44*, 206–217. [[CrossRef](#)] [[PubMed](#)]
23. Pomykala, K.L.; Ganz, P.A.; Bower, J.E.; Kwan, L.; Castellon, S.A.; Mallam, S.; Cheng, I.; Ahn, R.; Breen, E.C.; Irwin, M.R.; et al. The association between pro-inflammatory cytokines, regional cerebral metabolism, and cognitive complaints following adjuvant chemotherapy for breast cancer. *Brain Imaging Behav.* **2013**, *7*, 511–523. [[CrossRef](#)] [[PubMed](#)]
24. Lyon, D.E.; Cohen, R.; Chen, H.; Kelly, D.L.; McCain, N.L.; Starkweather, A.; Ahn, H.; Sturgill, J.; Jackson-Cook, C.K. Relationship of systemic cytokine concentrations to cognitive function over two years in women with early stage breast cancer. *J. Neuroimmunol.* **2016**, *301*, 74–82. [[CrossRef](#)] [[PubMed](#)]
25. Cheung, Y.T.; Ng, T.; Shwe, M.; Ho, H.K.; Foo, K.M.; Cham, M.T.; Lee, J.A.; Fan, G.; Tan, Y.P.; Yong, W.S.; et al. Association of proinflammatory cytokines and chemotherapy-associated cognitive impairment in breast cancer patients: A multi-centered, prospective, cohort study. *Ann. Oncol.* **2015**, *26*, 1446–1451. [[CrossRef](#)] [[PubMed](#)]
26. Ganz, P.A.; Bower, J.E.; Kwan, L.; Castellon, S.A.; Silverman, D.H.; Geist, C.; Breen, E.C.; Irwin, M.R.; Cole, S.W. Does tumor necrosis factor-alpha (TNF-alpha) play a role in post-chemotherapy cerebral dysfunction? *Brain Behav. Immun.* **2013**, *30*, S99–S108. [[CrossRef](#)] [[PubMed](#)]
27. Janelsins, M.C.; Mustian, K.M.; Palesh, O.G.; Mohile, S.G.; Peppone, L.J.; Sprod, L.K.; Heckler, C.E.; Roscoe, J.A.; Katz, A.W.; Williams, J.P.; et al. Differential expression of cytokines in breast cancer patients receiving different chemotherapies: Implications for cognitive impairment research. *Support. Care Cancer* **2012**, *20*, 831–839. [[CrossRef](#)]
28. Launer, L.J. Nonsteroidal anti-inflammatory drugs and Alzheimer disease: What's next? *JAMA* **2003**, *289*, 2865–2867. [[CrossRef](#)]

29. Aluise, C.D.; St Clair, D.; Vore, M.; Butterfield, D.A. In vivo amelioration of adriamycin induced oxidative stress in plasma by gamma-glutamylcysteine ethyl ester (GCEE). *Cancer Lett.* **2009**, *282*, 25–29. [[CrossRef](#)]
30. Tangpong, J.; Cole, M.P.; Sultana, R.; Estus, S.; Vore, M.; St Clair, W.; Ratanachaiyavong, S.; St Clair, D.K.; Butterfield, D.A. Adriamycin-mediated nitration of manganese superoxide dismutase in the central nervous system: Insight into the mechanism of chemobrain. *J. Neurochem.* **2007**, *100*, 191–201. [[CrossRef](#)]
31. Keeney, J.T.; Swomley, A.M.; Forster, S.; Harris, J.L.; Sultana, R.; Butterfield, D.A. Apolipoprotein A-I: Insights from redox proteomics for its role in neurodegeneration. *Proteomics Clin. Appl.* **2013**, *7*, 109–122. [[CrossRef](#)] [[PubMed](#)]
32. Fukui, K.; Onodera, K.; Shinkai, T.; Suzuki, S.; Urano, S. Impairment of learning and memory in rats caused by oxidative stress and aging, and changes in antioxidative defense systems. *Ann. N Y Acad. Sci.* **2001**, *928*, 168–175. [[CrossRef](#)] [[PubMed](#)]
33. Lin, X.; Kapoor, A.; Gu, Y.; Chow, M.J.; Peng, J.; Zhao, K.; Tang, D. Contributions of DNA Damage to Alzheimer’s Disease. *Int. J. Mol. Sci.* **2020**, *21*. [[CrossRef](#)] [[PubMed](#)]
34. Lin, X.; Gu, Y.; Tang, D. BMI1, ATM and DDR. *Oncoscience* **2015**, *2*, 665–666. [[CrossRef](#)] [[PubMed](#)]
35. Myung, N.H.; Zhu, X.; Kruman, I.I.; Castellani, R.; Petersen, R.B.; Siedlak, S.L.; Perry, G.; Smith, M.A.; Lee, H.G. Evidence of DNA damage in Alzheimer disease: Phosphorylation of histone H2AX in astrocytes. *Age (Dordr)* **2008**, *30*, 209–215. [[CrossRef](#)]
36. Shanbhag, N.M.; Evans, M.D.; Mao, W.; Nana, A.L.; Seeley, W.W.; Adame, A.; Rissman, R.A.; Masliah, E.; Mucke, L. Early neuronal accumulation of DNA double strand breaks in Alzheimer’s disease. *Acta Neuropathol. Commun.* **2019**, *7*, 77. [[CrossRef](#)]
37. Mody, L.; Miller, D.K.; McGloin, J.M.; Freeman, M.; Marcantonio, E.R.; Magaziner, J.; Studenski, S. Recruitment and retention of older adults in aging research. *J. Am. Geriatr. Soc.* **2008**, *56*, 2340–2348. [[CrossRef](#)]
38. Janelins, M.C.; Roscoe, J.A.; Berg, M.J.; Thompson, B.D.; Gallagher, M.J.; Morrow, G.R.; Heckler, C.E.; Jean-Pierre, P.; Opanashuk, L.A.; Gross, R.A. IGF-1 partially restores chemotherapy-induced reductions in neural cell proliferation in adult C57BL/6 mice. *Cancer Invest.* **2010**, *28*, 544–553. [[CrossRef](#)]
39. Han, R.; Yang, Y.M.; Dietrich, J.; Luebke, A.; Mayer-Proschel, M.; Noble, M. Systemic 5-fluorouracil treatment causes a syndrome of delayed myelin destruction in the central nervous system. *J. Biol.* **2008**, *7*, 12. [[CrossRef](#)]
40. Ladurner, A.G. Rheostat control of gene expression by metabolites. *Mol. Cell* **2006**, *24*, 1–11. [[CrossRef](#)]
41. DeBerardinis, R.J.; Chandel, N.S. Fundamentals of cancer metabolism. *Sci. Adv.* **2016**, *2*, e1600200. [[CrossRef](#)] [[PubMed](#)]
42. Boroughs, L.K.; DeBerardinis, R.J. Metabolic pathways promoting cancer cell survival and growth. *Nat. Cell Biol.* **2015**, *17*, 351–359. [[CrossRef](#)] [[PubMed](#)]
43. Hanahan, D.; Weinberg, R.A. Hallmarks of cancer: The next generation. *Cell* **2011**, *144*, 646–674. [[CrossRef](#)] [[PubMed](#)]
44. Nagarajan, A.; Malvi, P.; Wajapeyee, N. Oncogene-directed alterations in cancer cell metabolism. *Trends Cancer* **2016**, *2*, 365–377. [[CrossRef](#)] [[PubMed](#)]
45. Armitage, E.G.; Barbas, C. Metabolomics in cancer biomarker discovery: Current trends and future perspectives. *J. Pharm. Biomed. Anal.* **2014**, *87*, 1–11. [[CrossRef](#)]
46. Johnson, C.H.; Ivanisevic, J.; Siuzdak, G. Metabolomics: Beyond biomarkers and towards mechanisms. *Nat. Rev. Mol. Cell Biol.* **2016**, *17*, 451–459. [[CrossRef](#)]
47. Gowda, G.A.; Zhang, S.; Gu, H.; Asiago, V.; Shanaiah, N.; Raftery, D. Metabolomics-based methods for early disease diagnostics. *Expert Rev. Mol. Diagn.* **2008**, *8*, 617–633. [[CrossRef](#)]
48. Sitter, B.; Lundgren, S.; Bathen, T.F.; Halgunset, J.; Fjosne, H.E.; Gribbestad, I.S. Comparison of HR MAS MR spectroscopic profiles of breast cancer tissue with clinical parameters. *NMR Biomed.* **2006**, *19*, 30–40. [[CrossRef](#)]
49. Denkert, C.; Budczies, J.; Kind, T.; Weichert, W.; Tablack, P.; Sehouli, J.; Niesporek, S.; Konsgen, D.; Dietel, M.; Fiehn, O. Mass spectrometry-based metabolic profiling reveals different metabolite patterns in invasive ovarian carcinomas and ovarian borderline tumors. *Cancer Res.* **2006**, *66*, 10795–10804. [[CrossRef](#)]
50. Swanson, M.G.; Vigneron, D.B.; Tabatabai, Z.L.; Males, R.G.; Schmitt, L.; Carroll, P.R.; James, J.K.; Hurd, R.E.; Kurhanewicz, J. Proton HR-MAS spectroscopy and quantitative pathologic analysis of MRI/3D-MRSI-targeted postsurgical prostate tissues. *Magn Reson Med.* **2003**, *50*, 944–954. [[CrossRef](#)]
51. Masui, K.; Cavenee, W.K.; Mischel, P.S. mTORC2 in the center of cancer metabolic reprogramming. *Trends Endocrinol. Metab.* **2014**. [[CrossRef](#)] [[PubMed](#)]

52. Masui, K.; Cavenee, W.K.; Mischel, P.S. mTORC2 dictates Warburg effect and drug resistance. *Cell Cycle* **2014**, *13*, 1053–1054. [[CrossRef](#)] [[PubMed](#)]
53. Phan, L.M.; Yeung, S.C.; Lee, M.H. Cancer metabolic reprogramming: Importance, main features, and potentials for precise targeted anti-cancer therapies. *Cancer Biol. Med.* **2014**, *11*, 1–19. [[CrossRef](#)] [[PubMed](#)]
54. Kroemer, G.; Pouyssegur, J. Tumor cell metabolism: Cancer’s Achilles’ heel. *Cancer Cell* **2008**, *13*, 472–482. [[CrossRef](#)] [[PubMed](#)]
55. Phillips, M.M.; Sheaff, M.T.; Szlosarek, P.W. Targeting Arginine-Dependent Cancers with Arginine-Degrading Enzymes: Opportunities and Challenges. *Cancer Res. Treat.* **2013**, *45*, 251–262. [[CrossRef](#)]
56. Maze, I.; Noh, K.M.; Soshnev, A.A.; Allis, C.D. Every amino acid matters: Essential contributions of histone variants to mammalian development and disease. *Nature reviews. Genetics* **2014**, *15*, 259–271. [[CrossRef](#)]
57. Schulten, H.J. Pleiotropic Effects of Metformin on Cancer. *Int J. Mol. Sci.* **2018**, *19*, 2850. [[CrossRef](#)]
58. Hopkins, B.D.; Goncalves, M.D.; Cantley, L.C. Obesity and Cancer Mechanisms: Cancer Metabolism. *J. Clin. Oncol.* **2016**, *34*, 4277–4283. [[CrossRef](#)]
59. Smuder, A.J. Exercise stimulates beneficial adaptations to diminish doxorubicin-induced cellular toxicity. *Am. J. Physiol. Regul Integr. Comp. Physiol.* **2019**, *317*, R662–R672. [[CrossRef](#)]
60. Wang, R.; Holsinger, R.M.D. Exercise-induced brain-derived neurotrophic factor expression: Therapeutic implications for Alzheimer’s dementia. *Ageing Res. Rev.* **2018**, *48*, 109–121. [[CrossRef](#)]
61. Krcmery, V.; Cepcek, P. [Side effects and toxicity of new quinolones]. *Bratisl. Lek Listy* **1991**, *92*, 496–503. [[PubMed](#)]
62. Hillman, C.H.; Erickson, K.I.; Kramer, A.F. Be smart, exercise your heart: Exercise effects on brain and cognition. *Nat. Rev. Neurosci.* **2008**, *9*, 58–65. [[CrossRef](#)] [[PubMed](#)]
63. Kapogiannis, D.; Mattson, M.P. Disrupted energy metabolism and neuronal circuit dysfunction in cognitive impairment and Alzheimer’s disease. *Lancet Neurol.* **2011**, *10*, 187–198. [[CrossRef](#)]
64. Scarmeas, N.; Stern, Y.; Mayeux, R.; Manly, J.J.; Schupf, N.; Luchsinger, J.A. Mediterranean diet and mild cognitive impairment. *Arch. Neurol.* **2009**, *66*, 216–225. [[CrossRef](#)] [[PubMed](#)]
65. Craft, S. The role of metabolic disorders in Alzheimer disease and vascular dementia: Two roads converged. *Arch. Neurol.* **2009**, *66*, 300–305. [[CrossRef](#)] [[PubMed](#)]
66. Llorens-Martin, M.; Torres-Aleman, I.; Trejo, J.L. Mechanisms mediating brain plasticity: IGF1 and adult hippocampal neurogenesis. *Neuroscientist* **2009**, *15*, 134–148. [[CrossRef](#)]
67. Nagahara, A.H.; Tuszynski, M.H. Potential therapeutic uses of BDNF in neurological and psychiatric disorders. *Nat. Rev. Drug Discov.* **2011**, *10*, 209–219. [[CrossRef](#)]
68. Suji, G.; Sivakami, S. Glucose, glycation and aging. *Biogerontology* **2004**, *5*, 365–373. [[CrossRef](#)]
69. Harvey, J. Leptin regulation of neuronal excitability and cognitive function. *Curr. Opin. Pharmacol.* **2007**, *7*, 643–647. [[CrossRef](#)]
70. Friedenreich, C.M.; Neilson, H.K.; Farris, M.S.; Courneya, K.S. Physical Activity and Cancer Outcomes: A Precision Medicine Approach. *Clin. Cancer Res.* **2016**, *22*, 4766–4775. [[CrossRef](#)]
71. Lahart, I.M.; Metsios, G.S.; Nevill, A.M.; Carmichael, A.R. Physical activity, risk of death and recurrence in breast cancer survivors: A systematic review and meta-analysis of epidemiological studies. *Acta Oncol.* **2015**, *54*, 635–654. [[CrossRef](#)] [[PubMed](#)]
72. Kimura, M.; Mizuta, C.; Yamada, Y.; Okayama, Y.; Nakamura, E. Constructing an index of physical fitness age for Japanese elderly based on 7-year longitudinal data: Sex differences in estimated physical fitness age. *Age (Dordr)* **2012**, *34*, 203–214. [[CrossRef](#)] [[PubMed](#)]
73. Schmitz, K.H.; Courneya, K.S.; Matthews, C.; Demark-Wahnefried, W.; Galvao, D.A.; Pinto, B.M.; Irwin, M.L.; Wolin, K.Y.; Segal, R.J.; Lucia, A.; et al. American College of Sports Medicine roundtable on exercise guidelines for cancer survivors. *Med. Sci Sports Exerc.* **2010**, *42*, 1409–1426. [[CrossRef](#)] [[PubMed](#)]
74. Erickson, K.I.; Kramer, A.F. Aerobic exercise effects on cognitive and neural plasticity in older adults. *Br. J. Sports Med.* **2009**, *43*, 22–24. [[CrossRef](#)] [[PubMed](#)]
75. Dao, E.; Hsiung, G.R.; Liu-Ambrose, T. The role of exercise in mitigating subcortical ischemic vascular cognitive impairment. *J. Neurochem.* **2018**, *144*, 582–594. [[CrossRef](#)] [[PubMed](#)]
76. Groot, C.; Hooghiemstra, A.M.; Raijmakers, P.G.; van Berckel, B.N.; Scheltens, P.; Scherder, E.J.; van der Flier, W.M.; Ossenkoppele, R. The effect of physical activity on cognitive function in patients with dementia: A meta-analysis of randomized control trials. *Ageing Res. Rev.* **2016**, *25*, 13–23. [[CrossRef](#)] [[PubMed](#)]

77. Physical Activity Guidelines Advisory Committee Submits Scientific Report. Available online: <https://health.gov/news/blog-bayw/2018/03/2018-physical-activity-guidelines-advisory-committee-submits-scientific-report/> (accessed on 18 September 2020).
78. Ashcraft, K.A.; Peace, R.M.; Betof, A.S.; Dewhirst, M.W.; Jones, L.W. Efficacy and Mechanisms of Aerobic Exercise on Cancer Initiation, Progression, and Metastasis: A Critical Systematic Review of In Vivo Preclinical Data. *Cancer Res.* **2016**, *76*, 4032–4050. [[CrossRef](#)]
79. Pedersen, L.; Idorn, M.; Olofsson, G.H.; Lauenborg, B.; Nookaew, I.; Hansen, R.H.; Johannesen, H.H.; Becker, J.C.; Pedersen, K.S.; Dethlefsen, C.; et al. Voluntary Running Suppresses Tumor Growth through Epinephrine- and IL-6-Dependent NK Cell Mobilization and Redistribution. *Cell Metab.* **2016**, *23*, 554–562. [[CrossRef](#)]
80. Heyn, P.; Abreu, B.C.; Ottenbacher, K.J. The effects of exercise training on elderly persons with cognitive impairment and dementia: A meta-analysis. *Arch. Phys. Med. Rehabil.* **2004**, *85*, 1694–1704. [[CrossRef](#)]
81. Hojman, P.; Gehl, J.; Christensen, J.F.; Pedersen, B.K. Molecular Mechanisms Linking Exercise to Cancer Prevention and Treatment. *Cell Metab.* **2018**, *27*, 10–21. [[CrossRef](#)]
82. Moore, S.C.; Lee, I.M.; Weiderpass, E.; Campbell, P.T.; Sampson, J.N.; Kitahara, C.M.; Keadle, S.K.; Arem, H.; Berrington de Gonzalez, A.; Hartge, P.; et al. Association of Leisure-Time Physical Activity With Risk of 26 Types of Cancer in 1.44 Million Adults. *JAMA Intern. Med.* **2016**, *176*, 816–825. [[CrossRef](#)] [[PubMed](#)]
83. Sasso, J.P.; Eves, N.D.; Christensen, J.F.; Koelwyn, G.J.; Scott, J.; Jones, L.W. A framework for prescription in exercise-oncology research. *J. Cachexia Sarcopenia Muscle* **2015**, *6*, 115–124. [[CrossRef](#)] [[PubMed](#)]
84. Jones, L.W.; Alfano, C.M. Exercise-oncology research: Past, present, and future. *Acta Oncol.* **2013**, *52*, 195–215. [[CrossRef](#)] [[PubMed](#)]
85. Mishra, S.I.; Scherer, R.W.; Geigle, P.M.; Berlanstein, D.R.; Topaloglu, O.; Gotay, C.C.; Snyder, C. Exercise interventions on health-related quality of life for cancer survivors. *Cochrane Database Syst. Rev.* **2012**. [[CrossRef](#)] [[PubMed](#)]
86. Schneider, G.; Schmidt-Supprian, M.; Rad, R.; Saur, D. Tissue-specific tumorigenesis: Context matters. *Nat. Rev. Cancer* **2017**, *17*, 239–253. [[CrossRef](#)] [[PubMed](#)]
87. Vulczak, A.; Souza, A.O.; Ferrari, G.D.; Azzolini, A.; Pereira-da-Silva, G.; Alberici, L.C. Moderate Exercise Modulates Tumor Metabolism of Triple-Negative Breast Cancer. *Cells* **2020**, *9*, 628. [[CrossRef](#)] [[PubMed](#)]
88. Platten, M.; von Knebel Doeberitz, N.; Oezen, I.; Wick, W.; Ochs, K. Cancer Immunotherapy by Targeting IDO1/TDO and Their Downstream Effectors. *Front. Immunol.* **2014**, *5*, 673. [[CrossRef](#)] [[PubMed](#)]
89. Zimmer, P.; Schmidt, M.E.; Prentzell, M.T.; Berdel, B.; Wiskemann, J.; Kellner, K.H.; Debus, J.; Ulrich, C.; Opitz, C.A.; Steindorf, K. Resistance Exercise Reduces Kynurenine Pathway Metabolites in Breast Cancer Patients Undergoing Radiotherapy. *Front. Oncol.* **2019**, *9*, 962. [[CrossRef](#)]
90. Schiaffino, S.; Dyar, K.A.; Ciciliot, S.; Blaauw, B.; Sandri, M. Mechanisms regulating skeletal muscle growth and atrophy. *FEBS J.* **2013**, *280*, 4294–4314. [[CrossRef](#)]
91. Thompson, H.J.; Jiang, W.; Zhu, Z. Candidate mechanisms accounting for effects of physical activity on breast carcinogenesis. *IUBMB Life* **2009**, *61*, 895–901. [[CrossRef](#)]





Quick overview of diagnostic kits and smartphone apps for urologists during the COVID-19 pandemic: a narrative review

Hyusim Park¹, Peng Jin^{2,3}, Sungyong Jung¹, Jayoung Kim^{2,4,5}

¹Department of Electrical Engineering, University of Texas at Arlington, Arlington, TX, USA; ²Departments of Surgery and Biomedical Sciences, Cedars-Sinai Medical Center, Los Angeles, CA, USA; ³Shengjing Hospital of China Medical University, Shenyang, Liaoning, China; ⁴Departments of Surgery and Biomedical Sciences, Cedars-Sinai Medical Center, Los Angeles, CA, USA; ⁵Department of Medicine, University of California Los Angeles, CA, USA

Contributions: (I) Conception and design: J Kim; (II) Administrative support: J Kim, S Jung; (III) Provision of study materials or patients: None; (IV) Collection and assembly of data: H Park, P Jin; (V) Data analysis and interpretation: H Park, P Jin; (VI) Manuscript writing: All authors; (VII) Final approval of manuscript: All authors.

Correspondence to: Jayoung Kim, PhD. Departments of Surgery and Biomedical Sciences, Cedars-Sinai Medical Center, Davis 5071, 8700 Beverly Blvd., Los Angeles, CA 90048, USA. Email: Jayoung.kim@csmc.edu.

Abstract: The COVID-19 pandemic was an unprecedented event that has caused incredible challenges in all areas of society. However, unlike previous global pandemics, modern advancements in technology and medicine have made it possible to respond much more rapidly. Within months, countries around the world developed diagnostic kits and smartphone applications to tackle the virus. Many of these diagnostic kits vary in what they target and have different uses. Smartphone applications have been developed to provide real-time information to users regarding potential exposure, statistics, updated news, etc. Depending on the country, resources and government policies have created a wide range of products and applications. This narrative review paper focuses on providing a general overview of diagnostic kits and smartphone applications in three major countries, the U.S., South Korea, and China. Smartphone applications were used for tracing person-to-person contact and preventing the spread of COVID-19. These tools allowed public health officials to quickly identify people who may have had exposure to COVID-19 and allows them to act accordingly. In addition to discussing the mechanisms behind diagnostic kits, topics in legislation and policy for contact tracing will also be discussed. As nations enter into the next phase of the pandemic, there are serious considerations to be made about how technology can be integrated into handling future healthcare crises.

Keywords: COVID-19; urologists; diagnostic kits; smartphone applications

Submitted Jun 29, 2020. Accepted for publication Nov 12, 2020.

doi: 10.21037/tau-20-1042

View this article at: <http://dx.doi.org/10.21037/tau-20-1042>

Introduction

On March 11, 2020, severe acute respiratory syndrome-coronavirus-2 (SARS-Cov-2), which causes the COVID-19 infection, was officially declared as a pandemic by the World Health Organization (WHO). As of June 1, 2020, more than 6.26 million people have been infected and more than 380,000 lives have been lost worldwide. The mortality rate of COVID-19 differs across countries, possibly due

to differences in testing capacity, demographics, and other factors (1). Because COVID-19 can spread through asymptomatic patients, the number of confirmed cases is also in continual flux (2).

The U.S. reported its first confirmed COVID-19 case in the state of Washington. This individual had previously traveled to Wuhan, China in early January 2020 (3). Gradual increases in confirmed cases slowly rose in the U.S.,

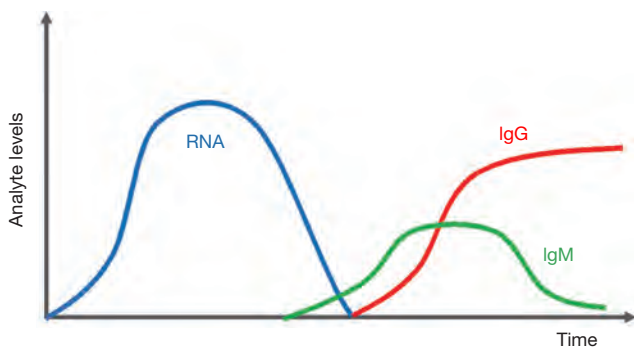


Figure 1 Changes in analyte levels following COVID-19 infection. Infection with SARS-CoV-2 leads to a building increase in viral mRNA, which peaks around 5-7 days after infection. This mRNA load begins to decrease after but is detectable up until day 14. As the viral mRNA starts to taper off, the patient's body begins to produce antibodies against the virus. The IgM antibody starts to build 5 days after the onset of symptoms and peaks around 9 days after infection. The IgG antibody is produced 14 days after infection and continues to build for a prolonged period of time, approximately 35 days. SARS-CoV-2, severe acute respiratory syndrome-coronavirus-2.

with the first COVID-19 death reported on February 29, 2020. Even with efforts to reduce spread, such as closing schools and preventing gatherings, the U.S. eventually had the most confirmed cases of COVID-19 globally, with 140,000 in March 29, 2020 (4). As of June 1, 2020, there are more than 1.79 million confirmed cases in the U.S., which accounts for almost a third of cases worldwide (5).

Fortunately, although there are consistently newly confirmed cases daily, the rate appears to be declining in some parts of the U.S. (5) However, most public health experts anticipate a second wave in the fall of 2020 (6-8). Since there are currently no effective therapies or vaccines available, the only way to prevent or mitigate a second wave is to take necessary precautions, such as social distancing and frequent hand-washing (9). The goal of this review paper is to provide an overview of trending diagnostic kits and smartphone applications against COVID-19. To this end, we searched databases and literatures available using keywords such as COVID-19, diagnostic kits, and smartphone applications. This narrative review article will summarize presently available methods for mitigating spread. Since South Korea is an established outstanding example of a country managing the COVID-19 pandemic well, the diagnostic kits and applications being widely used in that country will also be discussed.

The authors present the following article in accordance with the Narrative Review reporting checklist (available at <http://dx.doi.org/10.21037/tau-20-1042>).

COVID-19 diagnostic tests

To cope with the COVID-19 pandemic, diagnostic test kits are being evolved rapidly all over the world. Diagnostic tests can be categorized based on the analytes being measured, such as molecules or antibody. A molecular test detects certain genes, proteins, or molecules in a sample while an antibody test searches for virus-matched antibodies in the blood.

In relation to COVID-19, most molecular diagnostic tests look for the COVID-19 N gene or RdRP gene; whereas diagnostic antibody tests look for IgG or IgM antibodies (10-13). *Figure 1* shows the levels of analytes over time in samples from COVID-19-positive patients after infection. Once SARS-CoV-2 enters the human body, only the viral ribonucleic acid (RNA) can be detected for the first several days after infection. The viral load continues to increase until day 5 or 6. Around day 7, the viral RNA load starts to decrease; however, detection can be done until day 13 or 14 (14). The IgM antibody response is normally elicited 5 days after the initial onset of symptoms and hits peak levels around day 9. It is detectable until days 14-21. The IgG antibody rises after 14 days and generally peaks around or after clinical recovery, which 28-35 days after infection (15,16).

Based on the characteristics of the detected target, different COVID-19 tests kits have optimal periods of use. Molecular tests, which detect viral RNA directly, can diagnose COVID-19 within the early stages of the disease, before symptoms and antibodies form; thereby, making it ideal as a primary diagnostic tool (17,18). On the other hand, antibody tests can be used as a subsidiary diagnostic tool and is ideal for research purposes; it can be used to track potential asymptomatic patients and discover new findings behind immunity against SARS-CoV-2 (19). Diagnostic tests start with the collection of samples, such as blood or swabs collected from the throat. The presence of target analytes is then tested for in the samples and attained data is analyzed to determine whether or not the person is positive for COVID-19.

Molecular test

Molecular diagnostic tests usually utilize reverse transcription

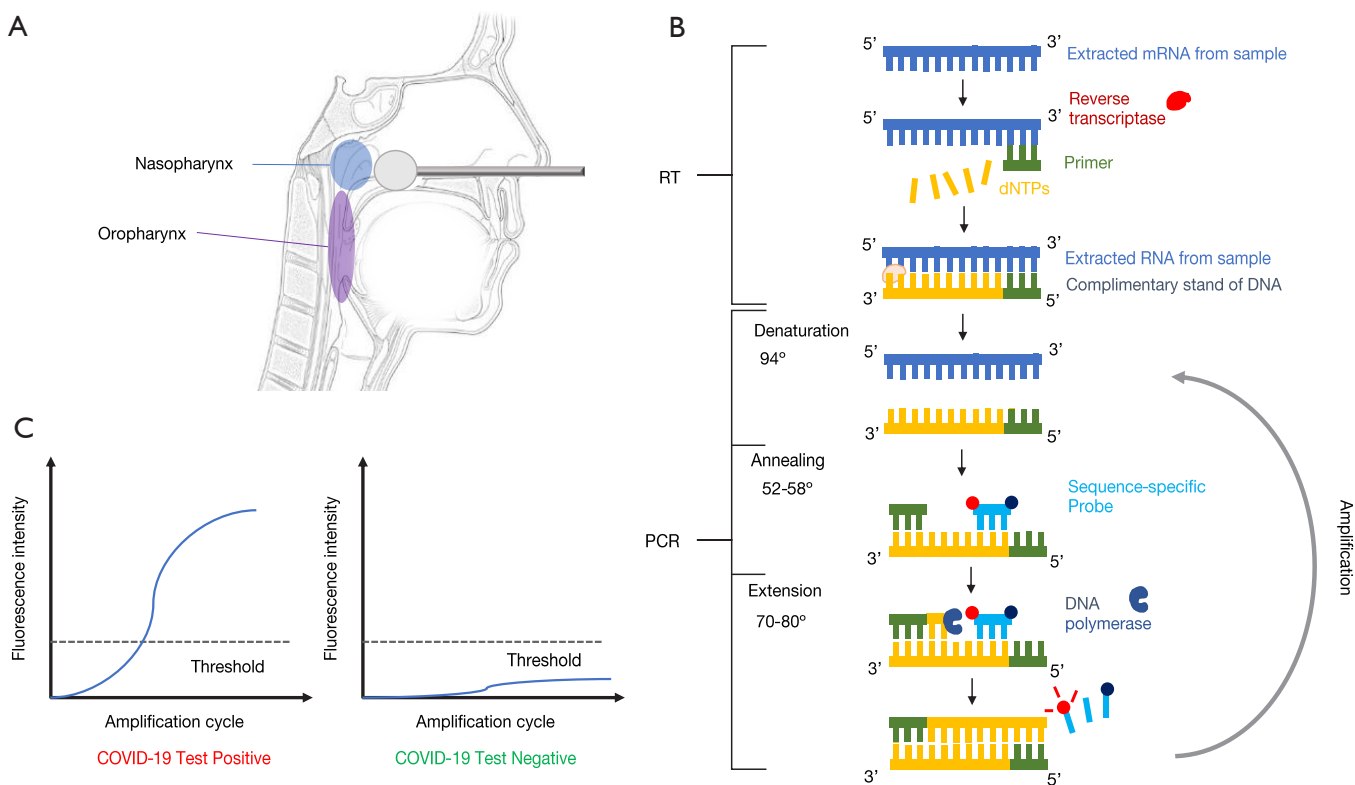


Figure 2 Example workflow for a one-step RT-PCR COVID-19 diagnostic test. (A) Collection of the sample from either the nasopharynx (upper respiratory) or oropharynx (lower respiratory) using a cotton swab. (B) Overview of RT-PCR. The mRNA is extracted from the sample and a primer attaches to the sequence of interest with reverse transcriptase. Sequence-specific probes that are conjugated with either fluorescence or color attaches and this process is amplified, leading to a detectable signal. (C) Analysis of results. A threshold for the signal intensity is established and if the fluorescence passes that threshold, then the patient is considered positive for COVID-19. RT-PCR, reverse transcription polymerase chain reaction.

polymerase chain reaction (RT-PCR) or reverse transcription loop-mediated isothermal amplification (RT-LAMP). RT-PCR takes around 90–120 minutes to complete, while RT-LAMP can be done in 30 minutes. Successful detection of SARS-CoV-2 in these two methods depends on the design of primers that bind specifically to the viral RNA and its fragments. Most molecular diagnostic tests for COVID-19 use the RT-PCR technique. *Figure 2* shows an example workflow for a RT-PCR COVID-19 diagnostic test. The first step involves collecting sputum or bronchial fluid samples from the upper or lower respiratory tract (*Figure 2A*). Upper respiratory sources are preferred due to its ease. As of April 29, 2020, the Centers for Disease Control and Prevention (CDC) recommends collecting samples from the nasopharynx (NP) rather than the oropharynx (OP) (20). It is extremely important to collect

samples as instructed by trained professionals in order to avoid false results (21).

With the collected sample, RNA is extracted using guanidinium thiocyanate-phenol-chloroform. After extraction, the sample is ready for RT-PCR, which detects specific SARS-CoV-2 mRNA (*Figure 2B*). RT synthesizes complementary deoxyribonucleic acid (cDNA) from RNA, while PCR amplifies the target cDNA. RT must be performed together (one-step) or before (two-step) PCR. From the amplification process, a fluorescent signal is emitted from sequence-specific probes or fluorescent dye, which can then be quantified using electronics or the naked eye. RT-PCR is the gold standard for detecting COVID-19 due to its high accuracy. However, the sensitivity of kits varies depending on the manufacturer and instruments used. Low sensitivity can lead to false negatives.

Additionally, training must be given in order to ensure that samples are collected and processed properly, which can make RT-PCR very labor-intensive. Furthermore, RT-PCR requires expensive equipment for proper processing (22,23) (*Figure 2C*).

Antibody test

Also known as a serological test, antibody detection is another test type to determine COVID-19 infection. This test can show whether a person is currently infected or has been infected. Unlike, RT-PCR, antibody type tests are currently not approved for use as a diagnostic tool but only for research. The antibody test has two process types, cassette-based and lab-based. The cassette-based assay includes either a lateral flow assay (LFA) or chemiluminescence immunoassay (CLIA) while the lab-based has an enzyme linked immunoabsorbent assay (ELISA), microsphere immunoassay (MIA), etc. LFA, the most common cassette-based assay, takes 10–30 minutes to complete and examines the presence of antibodies in serum. ELISA, on the other hand, is the most common lab-based assay, takes 2–5 hours to complete, and provides quantification of antibodies. Lab-based tests have several advantages over cassette-based systems because they utilize sensitive laboratory instruments and controlled test environments. However, cassette-based tests have their own advantages as well, including ease, quick response times, and cost-efficiency (24,25).

The principle behind LFA is simple: antigen-antibody binding affinity (26). *Figure 3* explains the basic procedure of a LFA-based COVID-19 diagnostic test kit. First, fluid sample is applied to a sample pad. This then migrates to the conjugate release pad, which contains antigens for either SARS-CoV-2 or control antibodies. These antigens are conjugated to colored or fluorescent particles for indication. Once the fluid reaches the conjugate release pad, if present, IgG and IgM antibodies from the fluid bind to the SARS-CoV-2 antigen conjugates. Then, the fluid moves to the test line, which has antibodies for target detection. If the migrating fluid contains the target antibodies, color or fluorescence develops to indicate the results, as shown in *Figure 3* (right). The control line is used to verify proper fluid flow and contains anti-rabbit IgG antigens to capture the rabbit IgG conjugate antibodies from the release pad. If the control line does not show positive, the results should not be trusted. The results of the LFA test kit should be analyzed as indicated from the supplier (16).

Diagnostic kits widely used in the U.S.

On January 31, 2020, the Secretary of Health and Human Services (HHS) declared a public health emergency recognizing the potential threat of SARS-CoV-2. The Federal Drug Administration (FDA) issued an emergency use authorization (EUA) to enable emergency use of the CDC 2019-nCoV Real-Time RT-PCR Diagnostic Panel, which was the first U.S. diagnostic kit. The FDA immediately issued a guidance policy specific to COVID-19 diagnostic kits on February 29, 2020 (27,28).

To be authorized for use by the FDA under EUA conditions, the performance of test kits must be verified (29). For molecular tests, analytical performance (limit of detection, reactivity/inclusivity results, specificity/exclusivity, etc.) and clinical performance should be clearly stated. The performance of antibody tests can be defined with sensitivity (PPA) and specificity (NPA). Currently, all FDA EUA issued molecular tests have more than 95% accuracy above the limit of detection. Present antibody tests show around 90% PPA and NPA (20). So far, more than 17,612,125 tests have been conducted and approximately 9.8% of total tests have been confirmed positive for COVID-19 in the U.S. (5). As of June 1, 2020, the FDA has approved 86 COVID-19 diagnostic kits (*Table 1*) (29).

Diagnostic kits widely used in South Korea

On January 20, 2020, the same day that the U.S. reported its first COVID-19 case, South Korea confirmed their own first COVID-19 patient. Within 2 weeks, South Korea approved its first diagnostic kit, the PowerCheck™2019-nCoV. In order to be authorized for use, COVID-19 diagnostic kits in South Korea must have defined limit of blank (LDB), limit of detection, limit of quantification (LoQ), strain reactivity, cross-reactivity, repeatability, cross-contamination, and clinical performance (30). As of June 1st, 2020, 6 molecular type tests have been approved for domestic use (*Table 2*). All of the approved diagnostic test kits have more than 90% accuracy (31). So far, South Korea has conducted 921,391 tests, of which 1.2% have been confirmed to be positive for COVID-19 (5).

Diagnostic kits widely used in China

SARS-CoV-2 has caused a great concern for public health and governance. The WHO held a meeting on January 30, 2020 to declare the outbreak of coronavirus in China

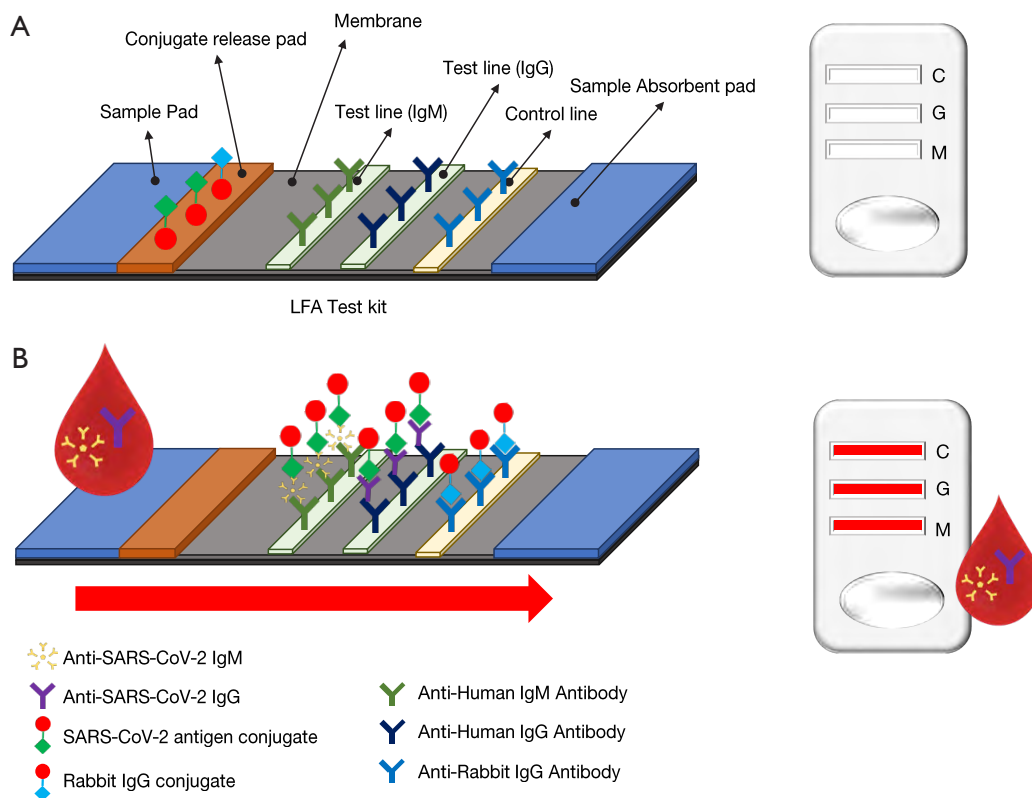


Figure 3 Example of an LFA-based COVID-19 diagnostic test (A) Inside structure of LFA-based COVID-19 diagnostic test Kit (left). Unused test kit result (right). The kit detects the antibodies (IgG, IgM) derived from COVID-19 in the sample. (B) Antigen-antibody binding affinity of test kit with COVID-19 Positive patient’s sample (left). Test kit result of COVID-19 positive patient (right). LFA, lateral flow assay.

as a public health emergency of international concern. After the outbreak of the virus, the Chinese government issued a series of effective anti-epidemic measures, and the international community recognized that China has made great progress in effectively responding epidemics. As a result, there are many lessons to be learned from the experiences of epidemic control in China. For example, many Chinese medical and biotechnology companies immediately funneled resources into developing COVID-19 test kits. Initially, test results could be generated within 6 hours; however, now the shortest tests can be done within 15 minutes. This has been incredibly useful for screening, early diagnosis, treatment, and post-treatment analysis.

As of March 27, 2020, the National Medical Products Administration (NMPA), which is the Chinese governmental agency responsible for regulating drugs and *medical devices*,

has approved 15 nucleic acid reagent test kits and 8 antibody reagent test kits. See *Table 3* for details.

Tracing person-to-person contact: current usage of smartphone applications

COVID-19 is a respiratory illness, which makes it highly contagious. SARS-CoV-2 can be transferred from person to person mainly through respiratory droplets. One of the biggest challenges to slowing down the spread of COVID-19 is the prevalence of asymptomatic patients who are unaware that they are carriers. As a result, enforcing isolation of COVID-19 patients and recommending self-quarantine for those who may have been in contact for 14 days is required (32). Contact tracing plays an essential role in determining who should be isolated or quarantined (33).

Table 1 List of U.S. COVID-19 diagnostic kits approved by the FDA under EUA

No.	Product name	Company name	Instruction for use
1	1copy COVID-19 qPCR Multi Kit (PCR)	1 drop Inc.	https://www.fda.gov/media/137935/download
2	ID NOW COVID-19 (Near)	Abbott Diagnostics Scarborough, Inc.	https://www.fda.gov/media/136525/download
3	SARS-CoV-2 IgG assay (CLIA)	Abbott Laboratories Inc.	https://www.fda.gov/media/137383/download
4	Abbott RealTime SARS-CoV-2 assay (PCR)	Abbott Molecular	https://www.fda.gov/media/136258/download
5	Alinity m SARS-CoV-2 assay (PCR)	Abbott Molecular Inc.	https://www.fda.gov/media/137979/download
6	RealStar SARS-CoV02 RT-PCR Kits U.S. (PCR)	Altona Diagnostics GmbH	https://www.fda.gov/media/137252/download
7	Linea COVID-19 Assay Kit (PCR)	Applied DNA Sciences, Inc.	https://www.fda.gov/media/138059/download
8	Assurance SARS-CoV-2 Panel (PCR)	Assurance Scientific Laboratories	https://www.fda.gov/media/138154/download
9	iAMP COVID-19 Detection Kit (LAMP)	Atila BioSystems, Inc.	https://www.fda.gov/media/136870/download
10	Anti-SARS-CoV-2 Rapid Test (LFA)	Autobio Diagnostics Co. Ltd.	https://www.fda.gov/media/137367/download
11	AvellinoCoV2 test (PCR)	Avellino Lab USA, Inc.	https://www.fda.gov/media/136453/download
12	BD SARS-CoV-2 Reagents for BD MAX System (PCR)	Becton, Dickinson & Company	https://www.fda.gov/media/136816/download
13	BioGX SARS-CoV-2 Reagents for BD MAX System (PCR)	Becton, Dickinson & Company (BD)	https://www.fda.gov/media/136653/download
14	Real-Time Fluorescent RT-PCR Kit for Detecting SARS-CoV-2 (PCR)	BGI Genomics Co. Ltd	https://www.fda.gov/media/136472/download
15	BioCore 2019-nCoV Real Time PCR Kit (PCR)	BioCore Co., Ltd.	https://www.fda.gov/media/138290/download
16	BioFire COVID-19 Test (PCR)	BioFire Defense, LLC	https://www.fda.gov/media/136353/download
17	BioFire Respiratory Panel 2.1 (RP2.1) (PCR)	BioFire Diagnostics, LLC	https://www.fda.gov/media/137583/download
18	SARS-COV-2 R-GENE (PCR)	BioMérieux SA	https://www.fda.gov/media/137742/download
19	Platelia SARS-CoV-2 Total Ab assay (EIA)	Bio-Rad Laboratories, Inc	https://www.fda.gov/media/137493/download
20	Bio-Rad SARS-CoV-2 ddPCR Test (ddPCR)	Bio-Rad Laboratories, Inc	https://www.fda.gov/media/137579/download
21	qSARS-CoV-2 IgG/IgM Rapid Test (LFA)	Cellex Inc.	https://www.fda.gov/media/136625/download
22	CDC 2019-nCoV Real-Time RT-PCR Diagnostic Panel (CDC) (PCR)	Centers for Disease Control and Prevention's (CDC)	https://www.fda.gov/media/134922/download
23	Xpert Xpress SARS-CoV-2 test (POC-PCR)	Cepheid	https://www.fda.gov/media/136314/download
24	DPP COVID-19 IgM/IgG System (LFA)	ChemBio Diagnostic System, Inc	https://www.fda.gov/media/136963/download
25	Logix Smart Coronavirus Disease 2019 (COVID-19) Kit (PCR)	Co-Diagnostics, Inc.	https://www.fda.gov/media/136687/download
26	Hymon SARS-CoV-2 Test Kit (PCR)	dba SpectronRx	https://www.fda.gov/media/138345/download
27	QuantiVirus SARS-CoV-2 Test kit (PCR)	DiaCarta, Inc	https://www.fda.gov/media/136809/download
28	LIAISON SARS-CoV-2 S1/S2 IgG	DiaSorin Inc.	https://www.fda.gov/media/137359/download
29	Simplexa COVID-19 Direct assay (PCR)	DiaSorin Molecular LLC	https://www.fda.gov/media/136286/download
30	Anti-SARS-CoV-2 ELISA (IgG) (ELISA)	EUROIMMUN US Inc.	https://www.fda.gov/media/137609/download

Table 1 (continued)

Table 1 (continued)

No.	Product name	Company name	Instruction for use
31	Everlywell COVID-19 Test Home Collection Kit (PCR)	Everlywell, Inc.	https://www.fda.gov/media/138146/download
32	FTD SARS-CoV-2 (PCR)	Fast Track Diagnostics Luxembourg S.á.r.l. (a Siemens Healthineers Company)	https://www.fda.gov/media/137690/download
33	Fosun COVID-19 RT-PCR Detection Kit (PCR)	Fosun Pharma USA Inc.	https://www.fda.gov/media/137120/download
34	Fulgent COVID-19 by RT-PCR Test (PCR)	Fulgent Therapeutics, LLC	https://www.fda.gov/media/138150/download
35	NeoPlex COVID-19 Detection Kit (PCR)	GeneMatrix, Inc.	https://www.fda.gov/media/138100/download
36	ePlex SARS-CoV-2 Test (PCR)	GenMark Diagnostics, Inc.	https://www.fda.gov/media/136282/download
37	GS™ COVID-19 RT-PCR KIT (PCR)	GenoSensor, LLC	https://www.fda.gov/media/137093/download
38	Gnomegen COVID-19 RT-Digital PCR Detection Kit (PCR)	Gnomegen LLC	https://www.fda.gov/media/136738/download
39	Gnomegen COVID-19-RT-qPCR Detection Kit (PCR)	Gnomegen LLC	https://www.fda.gov/media/137895/download
40	Gravity Diagnostics COVID-19 Assay (PCR)	Gravity Diagnostics, LLC	https://www.fda.gov/media/138530/download
41	COVID-19 IgG/IgM Rapid Test Cassette (Whole Blood/Serum/Plasma) (LFA)	Healgen Scientific LLC	https://www.fda.gov/media/138438/download
42	Panther Fusion SARS-CoV-2 Assay (PCR)	Hologic, Inc.	https://www.fda.gov/media/136156/download
43	Aptima SARS-CoV-2 assay (PCR)	Hologic, Inc.	https://www.fda.gov/media/138096/download
44	Smart Detect SARS-CoV-2 rRT-PCR Kit (PCR)	InBios International, Inc	https://www.fda.gov/media/136786/download
45	COV-19 IDx assay (PCR)	Ipsium Diagnostics, LLC	https://www.fda.gov/media/136621/download
46	Curative-Korva SARS-Cov-2 Assay (PCR)	KorvaLabs Inc.	https://www.fda.gov/media/137089/download
47	LabGun COVID-19 RT-PCR Kit (PCR)	LabGenomics Co., Ltd.	https://www.fda.gov/media/137483/download
48	COVID-19 RT-PCR Test (PCR)	Laboratory Corporation of America (LabCorp)	https://www.fda.gov/media/136151/download
49	ARIES SARS-CoV-2 Assay (PCR)	Luminex Corporation	https://www.fda.gov/media/136693/download
50	NxTAG CoV Extended Panel Assay (PCR)	Luminex Molecular Diagnostics, Inc.	https://www.fda.gov/media/136500/download
51	SARS-CoV-2 Fluorescent PCR Kit (PCR)	Maccura Biotechnology (USA) LLC	https://www.fda.gov/media/137026/download
52	Accula SARS-Cov-2 Test (PCR)	Mesa Biotech Inc.	https://www.fda.gov/media/136355/download
53	COVID-19 ELISA IgG Antibody Test (ELSIA)	Mount Sinai Laboratory	https://www.fda.gov/media/137029/download
54	NeuMoDx SARS-CoV-2 Assay (PCR)	NeuMoDx Molecular, Inc.	https://www.fda.gov/media/136565/download
55	OPTI SARS-CoV-2 RT PCR Test (PCR)	OPTI Medical Systems, Inc.	https://www.fda.gov/media/137739/download
56	VITROS Immunodiagnostic Products Anti-SARS-CoV-2 Total Reagent Pack (CLIA)	Ortho Clinical Diagnostics, Inc.	https://www.fda.gov/media/136967/download
57	VITROS Immunodiagnostic Products Anti-SARS-CoV-2 IgG Reagent Pack (CLIA)	Ortho-Clinical Diagnostics, Inc.	https://www.fda.gov/media/137363/download

Table 1 (continued)

Table 1 (continued)

No.	Product name	Company name	Instruction for use
58	GeneFinder COVID-19 Plus RealAmp Kit (PCR)	OSANG Healthcare	https://www.fda.gov/media/137116/download
59	P23 Labs TaqPath SARS-CoV-2 Assay (PCR)	P23 Labs, LLC	https://www.fda.gov/media/138297/download
60	PerkinElmer New Coronavirus Nucleic Acid Detection Kit (PCR)	PerkinElmer, Inc.	https://www.fda.gov/media/138297/download
61	Primerdesign Ltd COVID-19 genesig Real-Time PCR assay (PCR)	Primerdesign Ltd.	https://www.fda.gov/media/136823/download
62	LetsGetChecked Coronavirus (COVID-19) Test (PCR)	PrivaPath Diagnostics, Inc.	https://www.fda.gov/media/138406/download
63	QIAstat-Dx Respiratory SARS-CoV-2 Panel (PCR)	QIAGEN GmbH	https://www.fda.gov/media/136571/download
64	Quest SARS-CoV-2 rRT-PCR (PCR)	Quest Diagnostics Infectious Disease, Inc.	https://www.fda.gov/media/136231/download
65	Lyra SARS-CoV-2 Assay (PCR)	Quidel Corporation	https://www.fda.gov/media/136820/download
66	Sofia SARS Antigen FIA (FIA)	Quidel Corporation	https://www.fda.gov/media/137885/download
67	Lyra Direct SARS-CoV-2 Assay (PCR)	Quidel Corporation	https://www.fda.gov/media/138178/download
68	Rheonix COVID-19 MDx Assay (PCR)	Rheonix, Inc.	https://www.fda.gov/media/137489/download
69	Elecsys Anti-SARS-CoV-2	Roche Diagnostics	https://www.fda.gov/media/137605/download
70	cobas SARS-CoV-2 (PCR)	Roche Molecular Systems, Inc. (RMS)	https://www.fda.gov/media/136049/download
71	Rutgers Clinical Genomics Laboratory TaqPath SARS-CoV-2-Assay (PCR)	Rutgers Clinical Genomics Laboratory at RUCDR Infinite Biologics - Rutgers University	https://www.fda.gov/media/137774/download
72	Novel Coronavirus (2019-nCoV) Nucleic Acid Diagnostic Kit (PCR-Fluorescence Probing)	Sansure BioTech Inc.	https://www.fda.gov/media/137651/download
73	ScienCell SARS-CoV-2 Coronavirus Real-time RT-PCR (RT-qPCR) Detection Kit	ScienCell Research Laboratories	https://www.fda.gov/media/136691/download
74	STANDARD M nCoV Real-Time Detection Kit (PCR)	SD Biosensor, Inc.	https://www.fda.gov/media/137302/download
75	U-TOP COVID-19 Detection Kit (PCR)	SEASUN BIOMATERIALS	https://www.fda.gov/media/137425/download
76	AQ-TOP COVID-19 Rapid Detection Kit (PCR)	Seasun Biomaterials, Inc.	https://www.fda.gov/media/138307/download
77	Allplex 2019-nCoV Assay (PCR)	Seegene, Inc.	https://www.fda.gov/media/137178/download
78	Sherlock CRISPR SARS-CoV-2 Kit (CRISPR)	Sherlock BioSciences, Inc.	https://www.fda.gov/media/137746/download
79	Atellica IM SARS-CoV-2 Total (COV2T)	Siemens Healthcare Diagnostics Inc.	https://www.fda.gov/media/138442/download
80	ADVIA Centaur SARS-CoV-2 Total (COV2T)	Siemens Healthcare Diagnostics Inc.	https://www.fda.gov/media/138446/download

Table 1 (continued)

Table 1 (continued)

No.	Product name	Company name	Instruction for use
81	DiaPlexQ Novel Coronavirus (2019-nCoV) Detection Kit (PCR)	SolGent Co., Ltd.	https://www.fda.gov/media/138303/download
82	TaqPath COVID-19 Combo Kit (PCR)	Thermo Fisher Scientific, Inc.	https://www.fda.gov/media/136112/download
83	PhoenixDx 2019-CoV (PCR)	Trax Management Services Inc.	https://www.fda.gov/media/137153/download
84	New York SARS-CoV Microsphere Immunoassay for Antibody Detection (MIA)	Wadsworth Center, New York State Department of Health	https://www.fda.gov/media/137541/download
85	New York SARS-CoV-2 Real-time Reverse Transcriptase (RT)-PCR Diagnostic Panel (PCR)	Wadsworth Center, New York State Department of Public Health's (CDC)	https://www.fda.gov/media/135847/download
86	Quick SARS-CoV-2rRT-PCR Kit (PCR)	Zymo Research Corporation	https://www.fda.gov/media/137780/download

FDA, Federal Drug Administration; EUA, emergency use authorization.

Table 2 List of COVID-19 diagnostic kits approved for use in South Korea

No.	Product name	Company name	Company website	Issued date
1	PowerCheckTM2019-nCoV (PCR)	Kogene biotech	http://www.kogene.co.kr/eng/	02/04/2020
2	AllplexTM2019-nCoVAssay (PCR)	Seegene	http://www.seegene.com/	02/12/2020
3	DiaPlexQTMNovel Coronavirus (2019-nCov) Detection kit (PCR)	Solgent Co.	http://www.solgent.com/english	02/27/2020
4	STANDARD M nCoV Detection kit (PCR)	SDBiosensor	http://sdbiosensor.com/xel/	02/27/2020
5	Real-Q 2019-nCoV Detection Kit (PCR)	Biosewoom	http://www.biosewoom.com/	03/13/2020
6	BioCore 2019-nCoV Real Time PCRKit (PCR)	Bio-core	http://www.bio-core.com/	05/11/2020

This enables public health officials to quickly identify people who may have had exposure to COVID-19 and allows them to act accordingly.

South Korea's policy for tracing

Realizing the importance of contact tracing, South Korea implemented a smart city platform for contact tracing on March 26, 2020. This same approach was not successfully applied to other Western countries due to potential privacy issues. This smart city platform is a state of the art "system of systems" that integrates multiple high technologies, including information and communications, big data, and artificial intelligence, to solve burdens for high quality life in many different fields.

Once a COVID-19-positive patient is identified, the screening center reports the case to the Korea Centers for Disease Control and Prevention (KCDC). The KCDC then registers the patient on a contact tracing system linked to

the smart city data hub. Once the patient is registered, the system contacts the National Police Agency for the patient's information and requests to the Credit Finance Association (CREFIA). If the CREFIA approves, the hub requests the patient's epidemiological information from cellular service providers and credit card companies. Through this, the KCDC can collect all pertinent information regarding the patient within 10 minutes. The KCDC releases the information to the public after verification of the patient from the smart city data hub and alerts others who may have been in contact with the patient. People who receive an alert must be tested regardless of symptom manifestation. The patient information available to the public includes any public transportation that he or she took, locations visited, and time frames. This data is available for 14 days.

Meanwhile, in the U.S., once a COVID-19 patient is identified, trained public health staff manually conduct contact tracing by interrogating the patient directly. With the attained information, health officials then alert those

Table 3 List of emergency NMPA-approved COVID-19 testing kits in China

No.	Product name	company name	Company website	Registration No.
1	Nucleic acid reagent test kit for the novel coronavirus 2019-nCoV (fluorometric PCR)	Shanghai ZJ Bio-Tech Co., Ltd.	www.liferiverbiotech.com/	CFDA:20203400057
2	Nucleic acid reagent test kit for the novel coronavirus 2019-nCoV (fluorometric PCR)	Shanghai GeneoDx Biotech Co., LTD	www.geneodx.com/	CFDA:20203400058
3	Nucleic acid reagent test kit for the novel coronavirus 2019-nCoV (combinatorial probe-anchor synthesis sequencing)	BGI Biotechnology (Wuhan) Co., LTD	en.genomics.cn/	CFDA:20203400059
4	Nucleic acid reagent test kit for the novel coronavirus 2019-nCoV (fluorometric PCR)	BGI Biotechnology (Wuhan) Co., LTD	en.genomics.cn/	CFDA:20203400060
5	Nucleic acid reagent test kit for the novel coronavirus 2019-nCoV (fluorometric PCR)	Da An Gene Co., Ltd of Sun Yat-Sen University	en.daangene.com/	CFDA:20203400063
6	Nucleic acid reagent test kit for the novel coronavirus 2019-nCoV (fluorometric PCR)	Sansure Biotechnology Co., Ltd	eng.sansure.com.cn/	CFDA:20203400064
7	Nucleic acid reagent test kit for the novel coronavirus 2019-nCoV (fluorometric PCR)	Shanghai BioGerm Medical Biotechnology Co., Ltd	www.bio-germ.com/	CFDA:20203400065
8	Antibody test kit for the novel coronavirus 2019-nCoV (colloidal gold method)	Guangzhou Wondfo Biotech Co., Ltd	en.wondfo.com.cn/	CFDA:20203400176
9	Antibody test kit for the novel coronavirus 2019-nCoV (colloidal gold method)	Innovita (Tangshan) Biological Technology Co., Ltd	www.innovita.com.cn/index.html	CFDA:20203400177
10	Nucleic acid reagent test kit for six respiratory viruses (constant temperature amplification chip)	Chengdu CapitalBioPro Co., Ltd	www.capitalbio.com/	CFDA:20203400178
11	Nucleic acid reagent test kit for the novel coronavirus 2019-nCoV (fluorometric PCR)	Beijing Applied Biological Technologies Co., Ltd	www.x-abt.com/en/	CFDA:20203400179
12	IgM antibody test kit for the novel coronavirus 2019-nCoV (magnetic particle-based chemiluminescence immunoassay)	Bioscience (Chongqing) Diagnostic Technology Co., Ltd	www.bioscience-cq.com/	CFDA:20203400182
13	IgG antibody test kit for the novel coronavirus 2019-nCoV (magnetic particle-based chemiluminescence immunoassay)	Bioscience (Chongqing) Diagnostic Technology Co., Ltd	www.bioscience-cq.com/	CFDA:20203400183
14	Nucleic acid reagent test kit for the novel coronavirus 2019-nCoV (fluorometric PCR)	Maccura Biotechnology Co., Ltd.	www.maccura.com/en/	CFDA:20203400184
15	Antibody test kit for the novel coronavirus 2019-nCoV (chemiluminescence microparticle immunoassay)	Xiamen innoDx Biotech Co., Ltd	www.innodx.com	CFDA:20203400198
16	IgM antibody test kit for the novel coronavirus 2019-nCoV (colloidal gold method)	Guangdong Hecin Scientific Co., Ltd	www.hecin-scientific.cn	CFDA:20203400199
17	Nucleic acid reagent test kit for the novel coronavirus 2019-nCoV (fluorometric PCR)	Wuhan EasyDiagnosis Biomedicine Co., Ltd	www.mdeasydiagnosis.com/en/	CFDA:20203400212

Table 3 (continued)

Table 3 (continued)

No.	Product name	company name	Company website	Registration No.
18	IgM/IgG antibody test kit for the novel coronavirus 2019-nCoV (colloidal gold method)	Nanjing Vazyme Biotech Co., Ltd	www.vazymemedical.com	CFDA:20203400239
19	IgM/IgG antibody test kit for the novel coronavirus 2019-nCoV (colloidal gold method)	Zhuhai Livzon Diagnostics Co., Ltd	www.livzondiagnosics.com/en-us/	CFDA:20203400240
20	Nucleic acid reagent test kit for the novel coronavirus 2019-nCoV (Fluorescent Isothermal Amplification)	Hangzhou Ustar Biotechnology Co., Ltd	www.bioustar.com/en/index.aspx	CFDA:20203400241
21	Nucleic acid reagent test kit for the novel coronavirus 2019-nCoV (Hybrid capture immunofluorescence assay)	Anbio (Xiamen) Biotechnology Co., Ltd	www.anbio.com/en/	CFDA:20203400298
22	Nucleic acid reagent test kit for the novel coronavirus 2019-nCoV (fluorometric PCR)	Shanghai Fosun Long March Medical Science Co., Ltd	en.lm-diagnostics.com.cn/	CFDA:20203400299
23	Nucleic acid reagent test kit for the novel coronavirus 2019-nCoV (RNA capture probe method)	Shanghai Rendu Biotechnology Co., Ltd	www.rdbio.com/	CFDA:20203400300

NMPA, the National Medical Products Administration.

who may have had potential exposure. The substantial differences in contact tracing between the U.S. and South Korea arises from the levels of information disclosure and privacy.

Smartphone applications for preventing the spread of COVID-19

A multitude of researchers and companies are now striving to develop supplemental tools for preventing the spread of COVID-19. There has especially been a deluge of smartphone applications on the market due to its usefulness, affordability, and accessibility (Table 4). Smartphone applications derived from contact tracing or information sourcing has received particular attention (34,35). As mentioned previously, there are noted differences in tracing or tracking between countries due to privacy laws and attitudes.

In the U.S., tracing applications function mainly to alert exposure to SARS-CoV-2. One such application is Healthy Together by Twenty Holding Inc. The applications use Bluetooth signals and GPS location data to collect a list of people that the user has had encounters with (per the user's consent). If the user meets other users within

a certain range, the Bluetooth signal allows each user to share their encrypted serial number. GPS data is collected to understand transmission zones. If any of the users get diagnosed with COVID-19, other users who have encountered the patient will be alerted of the possible exposure with details such as the time and date. This mechanism can protect users' privacy while alerting others at risk.

Because the KCDC is already implementing a comprehensive tracing program, there are no applications with similar functionality in South Korea. Instead, there are other types of tracking applications on the market. The main function of these is alerting people when they are near COVID-19 patients using data attained from the KCDC. By informing users of potential risk, these applications can reduce infection rates. Additionally, the Korean Ministry of the Interior and Safety recently started operating an application called the Self-Quarantine Safety Protection App. This is a mandatory installation for anyone entering South Korea. It collects the users' personal information, symptoms, and GPS location in real-time and shares the data with the KCDC. Contact tracing applications are not the only informative utilities against spread. There are multiple applications that inform accurate and necessary

Table 4 Smartphone applications used in South Korea and the United States

Purpose of application	Country	Application name	Manufacturer	Characteristic
Composite	South Korea	Corona doctor	University students	Tracking, news, statistics, guideline, screening center location information are provided
		Corona 100 cine	HANDASOFT Corp.	Tracking, news, statistics, screening center location, public mask availability information are provided
		Corona map	Unknown	Tracking, statistics, guideline, screening center location information are provided
		Corona compass	Unknown	Tracking, statistics, screening site, public mask information availability are provided
		Corona now	Middle school students	News, statistics, screening site, public mask availability information are included
	United States	Healthy together	Twenty Holdings, Inc.	Tracking, self-diagnosis, guideline, screening center location information are provided. Daily checkup function is possible
		NJ COVID 19	NJ PBA	News, screening site information are provided. (Only for New Jersey)
Tracking/tracing	South Korea	Where is Corona?	Unknow	Specific date when confirmed patient tested is shown
		Coback Plus	TINA3D	Once user is near the traced place, push alarm is given to user
News feed	South Korea	Corona News	Unknown	News from 'Naver' which is one of major portal sites in South Korea are provided
	United States	CoronaFacts	Trusted Medical LLC	Preference of COVID-19 news source can be set
Statistics	South Korea	Corona World	Unknown	Global statistics is displayed
		Corona virus infection current situation	Unknown	The national statistics are shown on the map
	United States	HEALTHYNKED COVID-19 Tracker	HealthLynked Corp.	An anonymous chat room is provided
Guideline	United States	COVID Coach	US Department of Veterans Affairs	The app helps managing mental health
Screening center location Information	South Korea	Corona Screening Site	Unknown	Connects to KCDC
	United States	Apollo COVID-19	Gauss Surgical, Inc.	QR code including result of self COVID-19 assessment is given. The QR code can be used at screening center to minimize exposure during screening
Public mask availability information	South Korea	Coronapin	DBL	User can search a specific seller
		Mask Map	Unknown	3D map is provided
		Mask Alerts App	Unknown	Recommended route to chosen seller is provided
Self-quarantine control	South Korea	Self-Quarantine safety protection	Government	Installation is mandatory to people who entered South Korea

Table 4 (continued)

Table 4 (continued)

Purpose of application	Country	Application name	Manufacturer	Characteristic
Self-diagnosis	South Korea	Corona Self-diagnosis	Unknown	Questions based on self-diagnosis for staff are given
	United States	Apple COVID-19	Apple CDC	The application is available in 34 languages
		1-Check COVID	University of Nebraska	User can share the result of self-diagnosis
Symptom research	United States	COVID Symptom Study	Zoe Global Limited	Health advice is provided
		How We Feel	The How We Feel Project, Inc.	It tells user how many people have symptoms near the user

information to users, such as statistics, new guidelines, screening center locations, news updates, and face mask availability. For instance, in South Korea, there is a smartphone application for where face masks are available to purchase. This is specifically possible in South Korea because the government has allocated face masks to be sold only in assigned pharmacies.

Prospectives/future directions

When it comes to testing for COVID-19, most diagnostic tests take either a molecular or antibody approach. Within each of these, there subsets of tests that are ideal for different patients, time frames, and needs. As a result, it is essential that diagnostic test kits are utilized accordingly. For instance, mRNA-based testing kits are best utilized during the earlier stages of the infection while antibody tests are ideal for longer time frames after. These considerations must be made particularly for asymptomatic patients who may either have an active infection or recently fought off the virus. Contact tracing is another key element for preventing further spread of SARS-CoV-2. The South Korean government has taken an immensely precautionous approach with much success; however, there are some issues with privacy that can arise. In the U.S., smartphone applications are not as widely popular and entail mostly on exposure alerts.

The COVID-19 pandemic has tested the preparedness and response of each nation. These lessons are critical for moving forward and are necessary to address for potential future public health events. Advancements in science and technology has made diagnostic testing readily available;

however, the logistics, regulation, and distribution of such tests can be improved. Integration of smart technology in everyday life has also raised interesting prospects for future use in public health, but its tradeoff with privacy remains controversial. As nations continue onto the next steps of the pandemic, testing and tracing needs to evolve and adapt to meet changing demands as well.

Acknowledgments

We appreciate Dr. Heemin Rhee, a former FDA/CDER specialist and current President of Health Research International, for his scientific input on this manuscript.

Funding: This research was funded by National Institutes of Health (1U01DK103260, 1R01DK100974, U24 DK097154, NIH NCATS UCLA CTSI UL1TR000124), Department of Defense (W81XWH-15-1-0415 and W81XWH-19-1-0109), Centers for Disease Controls and Prevention (1U01DP006079), and the U.S.-Egypt Science and Technology Development Fund by the National Academies of Sciences, Engineering, and Medicine (all to J.K.). This research was also supported by the Samuel Oschin Comprehensive Cancer Institute (SOCCI) at Cedars-Sinai Medical Center through 2019 Lucy S. Gonda Award. This article is derived from the Subject Data funded in whole or part by National Academies of Sciences, Engineering, and Medicine (NAS) and The United States Agency for International Development (USAID). Any opinions, findings, conclusions, or recommendations expressed in this article are those of the authors alone, and do not necessarily reflect the views of USAID or NAS.

Footnote

Reporting Checklist: The authors have completed the Narrative Review reporting checklist. Available at <http://dx.doi.org/10.21037/tau-20-1042>

Conflicts of Interest: All authors have completed the ICMJE uniform disclosure form (available at <http://dx.doi.org/10.21037/tau-20-1042>). The authors have no conflicts of interest to declare.

Ethical Statement: The authors are accountable for all aspects of the work in ensuring that questions related to the accuracy or integrity of any part of the work are appropriately investigated and resolved.

Open Access Statement: This is an Open Access article distributed in accordance with the Creative Commons Attribution-NonCommercial-NoDerivs 4.0 International License (CC BY-NC-ND 4.0), which permits the non-commercial replication and distribution of the article with the strict proviso that no changes or edits are made and the original work is properly cited (including links to both the formal publication through the relevant DOI and the license). See: <https://creativecommons.org/licenses/by-nc-nd/4.0/>.

References

1. Mortality analyses. Available online: <https://coronavirus.jhu.edu/data/mortality>
2. Mizumoto K, Kagaya K, Zarebski A, et al. Estimating the asymptomatic proportion of coronavirus disease 2019 (COVID-19) cases on board the Diamond Princess cruise ship, Yokohama, Japan, 2020. *Euro Surveill* 2020;25:2000180.
3. Holshue ML, DeBolt C, Lindquist S, et al. First Case of 2019 Novel Coronavirus in the United States. *N Engl J Med* 2020;382:929-36.
4. US coronavirus cases surge tenfold in a week to 50,000, global infections soar past 400,000. Available online: <https://www.cnn.com/2020/03/24/global-coronavirus-cases-cross-400000-doubling-in-a-week-as-pandemic-accelerates.html>
5. Available online: <https://ourworldindata.org/coronavirus>.
6. Xu S, Li Y. Beware of the second wave of COVID-19. *Lancet* 2020;395:1321-2.
7. Chabner BA. Taking the Longer View of COVID-19. *Oncologist* 2020;25:455-7.
8. Weinstein E, Ragazzoni L, Burkle F, et al. Delayed Primary and Specialty Care: The Coronavirus Disease-2019 Pandemic Second Wave. *Disaster Med Public Health Prep* 2020;14:e19-21.
9. Qazi A, Qazi J, Naseer K, et al. Analyzing situational awareness through public opinion to predict adoption of social distancing amid pandemic COVID-19. *J Med Virol* 2020;92:849-55.
10. Kandeel M, Ibrahim A, Fayed M, et al. From SARS and MERS CoVs to SARS-CoV-2: Moving toward more biased codon usage in viral structural and nonstructural genes. *J Med Virol* 2020;92:660-6.
11. Kasibhatla SM, Kinikar M, Limaye S, et al. Understanding evolution of SARS-CoV-2: A perspective from analysis of genetic diversity of RdRp gene. *J Med Virol* 2020;92:1932-7.
12. Liu L, Liu W, Zheng Y, et al. A preliminary study on serological assay for severe acute respiratory syndrome coronavirus 2 (SARS-CoV-2) in 238 admitted hospital patients. *Microbes Infect* 2020;22:206-11.
13. Zou L, Ruan F, Huang M, et al. SARS-CoV-2 Viral Load in Upper Respiratory Specimens of Infected Patients. *N Engl J Med* 2020;382:1177-9.
14. Kim JY, Ko JH, Kim Y, et al. Viral Load Kinetics of SARS-CoV-2 Infection in First Two Patients in Korea. *J Korean Med Sci* 2020;35:e86.
15. Jacofsky D, Jacofsky EM, Jacofsky M. Understanding Antibody Testing for COVID-19. *J Arthroplasty* 2020;35:S74-81.
16. Li Z, Yi Y, Luo X, et al. Development and clinical application of a rapid IgM-IgG combined antibody test for SARS-CoV-2 infection diagnosis. *J Med Virol* 2020;92:1518-24.
17. Kuypers J, Wright N, Ferrenberg J, et al. Comparison of real-time PCR assays with fluorescent-antibody assays for diagnosis of respiratory virus infections in children. *J Clin Microbiol* 2006;44:2382-8.
18. Vinh DB, Zhao X, Kiong KL, et al. Overview of COVID-19 testing and implications for otolaryngologists. *Head Neck* 2020;42:1629-33.
19. Xie J, Ding C, Li J, et al. Characteristics of patients with coronavirus disease (COVID-19) confirmed using an IgM-IgG antibody test. *J Med Virol* 2020;92:2004-10.
20. Interim Guidelines for Collecting, Handling, and Testing Clinical Specimens for COVID-19. Available online: <https://www.cdc.gov/coronavirus/2019-ncov/lab/guidelines-clinical-specimens.html>

21. Tahamtan A, Ardebili A. Real-time RT-PCR in COVID-19 detection: issues affecting the results. *Expert Rev Mol Diagn* 2020;20:453-4.
22. Bustin SA. Quantification of mRNA using real-time reverse transcription PCR (RT-PCR): trends and problems. *J Mol Endocrinol* 2002;29:23-39.
23. Schrick L, Nitsche A. Pitfalls in PCR troubleshooting: Expect the unexpected? *Biomol Detect Quantif* 2016;6:1-3.
24. Gwyn S, Cooley G, Goodhew B, et al. Comparison of Platforms for Testing Antibody Responses against the *Chlamydia trachomatis* Antigen Pgp3. *Am J Trop Med Hyg* 2017;97:1662-8.
25. Izzo MM, Kirkland PD, Gu X, et al. Comparison of three diagnostic techniques for detection of rotavirus and coronavirus in calf faeces in Australia. *Aust Vet J* 2012;90:122-9.
26. Elif BB MK. Lateral flow assays: Principles, designs and labels. *TrAC Trends in Analytical Chemistry* 2016;82:286-306.
27. FDA Takes Significant Step in Coronavirus Response Efforts, Issues Emergency Use Authorization for the First 2019 Novel Coronavirus Diagnostic. Available online: <https://www.fda.gov/news-events/press-announcements/fda-takes-significant-step-coronavirus-response-efforts-issues-emergency-use-authorization-first>
28. Declaration Under the Public Readiness and Emergency Preparedness Act for Medical Countermeasures Against COVID-19. Available online: <https://www.federalregister.gov/documents/2020/03/17/2020-05484/declaration-under-the-public-readiness-and-emergency-preparedness-act-for-medical-countermeasures>
29. Emergency Use Authorizations for Medical Devices. Available online: <https://www.fda.gov/medical-devices/emergency-situations-medical-devices/emergency-use-authorizations#COVID19ivdTemplates>
30. Public Official's Guideline. Complainant's Guide. Available online: https://www.nifds.go.kr/brd/m_15/view.do?seq=12842
31. International Risk Information. Available online: https://www.mfds.go.kr/eng/brd/m_60/view.do?seq=74424
32. Abeler J, Backer M, Buermeyer U, et al. COVID-19 Contact Tracing and Data Protection Can Go Together. *JMIR Mhealth Uhealth* 2020;8:e19359.
33. Rubin R. Building an "Army of Disease Detectives" to Trace COVID-19 Contacts. *JAMA* 2020;323:2357-60.
34. Iyengar K, Upadhyaya GK, Vaishya R, et al. COVID-19 and applications of smartphone technology in the current pandemic. *Diabetes Metab Syndr* 2020;14:733-7.
35. Vokinger KN, Nittas V, Witt CM, et al. Digital health and the COVID-19 epidemic: an assessment framework for apps from an epidemiological and legal perspective. *Swiss Med Wkly* 2020;150:w20282.

Cite this article as: Park H, Jin P, Jung S, Kim J. Quick overview of diagnostic kits and smartphone apps for urologists during the COVID-19 pandemic: a narrative review. *Transl Androl Urol* 2021;10(2):939-953. doi: 10.21037/tau-20-1042

Research Paper

Alendronate-induced Perturbation of the Bone Proteome and Microenvironmental Pathophysiology

Jayoung Kim^{1,2,✉}, Austin Yeon¹, Sarah J. Parker³, Muhammad Shahid¹, Aissatou Thiombane¹, Eunho Cho¹, Sungyong You¹, Hany Emam⁴, Do-Gyoon Kim⁵, Minjung Kim⁶

1. Departments of Surgery and Biomedical Sciences, Cedars-Sinai Medical Center, Los Angeles, CA, USA
2. Department of Medicine, University of California Los Angeles, CA, USA
3. Smidt Heart Institute, Department of Cardiology, Cedars-Sinai Medical Center, Los Angeles, CA, USA
4. Division of Orthodontics, College of Dentistry, The Ohio State University, Columbus, OH, USA
5. Division of Oral Surgery, College of Dentistry, The Ohio State University, Columbus, OH, USA
6. Department of Cell Biology, Microbiology, and Molecular Biology, University of South Florida, Tampa, FL, USA

✉ Corresponding author: Jayoung Kim, PhD. Departments of Surgery and Biomedical Sciences, Cedars-Sinai Medical Center, Davis 5071, 8700 Beverly Blvd., Los Angeles, CA 90048. Tel: +1-310-423-7168; Fax: +1-310-967-3809; E-mail: Jayoung.kim@csmc.edu

© The author(s). This is an open access article distributed under the terms of the Creative Commons Attribution License (<https://creativecommons.org/licenses/by/4.0/>). See <http://ivyspring.com/terms> for full terms and conditions.

Received: 2021.04.14; Accepted: 2021.07.11; Published: 2021.07.23

Abstract

Objectives: Bisphosphonates (BPs) are powerful inhibitors of osteoclastogenesis and are used to prevent osteoporotic bone loss and reduce the risk of osteoporotic fracture in patients suffering from postmenopausal osteoporosis. Patients with breast cancer or gynecological malignancies being treated with BPs or those receiving bone-targeted therapy for metastatic prostate cancer are at increased risk of bisphosphonate-related osteonecrosis of the jaw (BRONJ). Although BPs markedly ameliorate osteoporosis, their adverse effects largely limit the clinical application of these drugs. This study focused on providing a deeper understanding of one of the most popular BPs, the alendronate (ALN)-induced perturbation of the bone proteome and microenvironmental pathophysiology.

Methods: To understand the molecular mechanisms underlying ALN-induced side-effects, an unbiased and global proteomics approach combined with big data bioinformatics was applied. This was followed by biochemical and functional analyses to determine the clinicopathological mechanisms affected by ALN.

Results: The findings from this proteomics study suggest that the RIPK3/Wnt/GSK3/β-catenin signaling pathway is significantly perturbed upon ALN treatment, resulting in abnormal angiogenesis, inflammation, anabolism, remodeling, and mineralization in bone cells in an *in vitro* cell culture system.

Conclusion: Our investigation into potential key signaling mechanisms in response to ALN provides a rational basis for suppressing BP-induced adverse effect and presents various therapeutic strategies.

Key words: Osteonecrosis of the jaw; bisphosphonate; GSK signaling; clinical cone beam computed tomography; bone mineral density; proteomics; biomarker

Introduction

Bone tissue undergoes continuous cycles of bone resorption by osteoclasts and bone formation by osteoblasts, which were orchestrated by osteocytes[1]. Bone tissue is also highly vascularized providing O₂, nutrients, and precursor cells for bone remodeling and serving as routes for blood and immune cells into bone tissue. Regulatory interactions between cells of these hematopoietic, immune, and skeletal (bone) systems closely regulate bone remodeling and repair processes via secreted factors such as VEGF, M-CSF,

RANKL, Wnt3a, and Osteoprotegerin, etc. and their cell surface receptors.

Several key signal pathway has been shown to play pivotal roles in bone remodeling/repair processes, enhancing osteoblast differentiation and angiogenesis and modulating immune cell functions[2]. Specifically, Wnt pathway activation via GSK3 inactivation leads to osteoblast differentiation and stimulates bone anabolism while GSK3 gain-of-function promotes osteogenesis of adipose-

derived stromal cells, making GSK3 as a possible therapeutic target for bone diseases [3-5]. Mice expressing constitutively active GSK3 β (GSK3 β S9A) mutant, exhibited a marked increase in osteogenesis, whereas ones with catalytically inactive GSK3 β (GSK3 β K85A) showed decreased osteogenic differentiation by regulating β -catenin[5]. Wnt/GSK3/ β -catenin pathway also plays important roles in angiogenesis and vasculogenesis, supporting wound healing and regeneration of oral mucosa and jaw tissue [6]. Wnt signaling activation by Wnt1, VEGF, or CHIR99021 (GSK3 β inhibitor) enhanced, while its inactivation by JW67 (targeting APC/GSK3/ β -catenin complex) or β -catenin kinase dead form suppressed, vascular differentiation of mesenchymal stem cells (MSCs) derived from dental pulp [7]. GSK3 β regulates β -catenin level in endothelial cells. Expression of β -catenin in HUVEC cells increases VEGF-A and -C level and induces capillary formation [8].

Bisphosphonates (BPs) have been suggested to modulate the proliferation and differentiation rates of osteoblasts and trigger survival signaling leading to bone homeostasis and antiresorptive effect [9-11]. First approved by the FDA in 1995, alendronate (ALN) is currently one of the most used BPs in the medical field[12]. ALN has been used successfully for the treatment of osteoporosis [13]. Several pieces of evidence indicate that there is a strong association between ALN and lower risk of bone metastases in postmenopausal women with early breast cancer [14, 15]. Cancer patients undergoing BPs-based treatments are at a 10-fold greater risk of developing bisphosphonate-related osteonecrosis of the jaw (BRONJ) [16], which is suggested to be a result of osteoclast inhibition and apoptosis[17]. Due to the prevalent usage of BPs in many bone-related diseases, more understanding on underlying mechanisms of adverse effect caused by BPs is crucial in providing better care and improving patient quality of life [18]. In oncology patients, incidence of BRONJ has been estimated to be as high as 18.6%[19], and risk of developing BRONJ increases with longer duration or higher dosages of BPs-based therapy[20].

This study sought to understand the pathogenesis of BP-associated adverse effects by looking into proteome perturbation and potential molecular biomarkers and mechanisms using an *in vitro* cell culture system.

Materials and Methods

Reagents and cell culture

Several cell lines, including MG-63, SCC-9, SCC-15, and HUVEC cells, were obtained from the

American Type Culture Collection (ATCC) (Manassas, VA). Culture condition, antibodies and reagents used for this study are available in Supplementary Materials.

Quantitative proteomics

Sample preparation methods for this study are available in Supplementary Materials. For protein quantification and statistical analysis, mapDIA was used. Data was analyzed based on the established workflows previously described [21, 22]. Briefly, peptides were identified using the openSWATH workflow [23], searched against the pan human library [24] with decoy sequences appended for false discovery rate calculation using the pyprophet algorithm [25]. Peptides with no greater than 5% identified false discovery rate (FDR) across all samples were compiled into the final experimental results using the TRIC alignment algorithm [26]. Following removal of non-proteotypic peptides (e.g., sequences matching more than one gene product from the Pan Human Library), the final aligned results were analyzed using mapDIA to select only high-quality performing fragments for quantification and to compile fragment level data into peptide and protein level abundance estimates [27]. The mapDIA software was also used to perform pairwise comparisons between ALN and control groups, including adjustment for multiple testing effects to produce a comparison FDR, which filtered proteins with significant or non-significant differential abundance in response to ALN treatment. The MS proteomics data has been deposited to the PRIDE repository with the dataset identifier, PXD024585.

Identification of differentially expressed proteins (DEPs)

Proteins with more than 3 nonredundant peptides in each sample were selected. Further selection of proteins detected in at least 2 samples in the same group was performed for statistical testing. A median difference test and Welch's t-test were performed separately, and the resulting two p-values were combined to compute adjusted p-values using Stouffer's method. The DEPs were identified based on an adjusted p-values<0.05 and absolute log₂ fold-change (FC) \geq 0.58.

VEGF ELISA assay

To determine vascular endothelial growth factor (VEGF-A) levels of conditioned medium from MG-63 cells incubated with ALN, supernatants from cell cultures were analyzed using the Human VEGF Quantikine ELISA Kit (R&D Systems, Minneapolis, Mass).

Cytokine array

Cell lysates and conditioned media from RAW 264.7 macrophages were collected and analyzed using a cytokine array, per standard provided protocols (R&D Systems, Minneapolis, MN, USA). ImageJ was used to measure the signal intensities.

Mineralization assay using Alizarin Red-S staining

The formation of calcium phosphate was quantified in MG-63 bone cells via Alizarin Red-S mineralization assay. Optical density was detected at an absorbance of 562 nm.

Statistical analysis

Most of the experiments were repeated at least six (6) times with independent treatments, while all the cases were repeated at least three times. Each of the experiments did not show significantly different results across replications. Statistical analyses were conducted using GraphPad Prism, version 7.03 (GraphPad Software Inc., La Jolla, CA). Mean values from technical replicates were used for statistical analyses, and all data were presented as the mean \pm standard deviation (SD). A one-way analysis of variance (ANOVA) or Student's t-test was conducted to compare the groups of data. Differences were considered statistically significant when $P < 0.05$.

Results

Comprehensive analysis with large unbiased global proteomic assays suggested perturbed proteins in response to BP in bone cells

Mass spectrometry (MS) has several important attributes that make it amenable to providing reproducible and accurate assays for proteins and metabolites. It provides a scalable number of analytes quantified in a single assay and absolute quantification, which leads to a standardized path from assay development to validation of new candidate biomarkers applicable in any clinical chemistry laboratory. To understand the molecular mechanisms underlying specific diseases, an unbiased and global omics approach combined with big data analysis using bioinformatics is critical.

As described in the Materials and Methods, a proteomics approach was implemented (Fig 1A). The top 10 most abundant protein classes are shown in Fig 1B. Global proteomics analysis identified a highly confident and comprehensive list of perturbed proteins in MG-63 bone cells treated with ALN. Protein quantification and statistical analysis using mapDIA identified perturbed proteins in MG-63 cells treated with 10 μ M ALN. A total of 2,865 proteins

with UniProtKB IDs were identified. Further analysis with the PANTHER Protein Classification Tool revealed that the most abundant top 10 proteins classes included extracellular matrix, metabolite interconversion, nucleic acid metabolism, protein modification, translational regulation, cytoskeletal, transporter, protein-binding activity modulator, membrane traffic, and scaffold/adaptor[28]. To identify DEPs, the integrated hypothesis testing method was applied. Briefly, the median difference test and Welch's t-test was performed on high confidence proteins, which in the case of this experiment, were proteins detected with more than 3 non-redundant peptides encompassing at least 2 samples in the same group. The median test p-value and Welch's t-test p-value were then combined to adjust for multiple testing errors. Finally, 27 up- and 31 downregulated DEPs were selected for based on adjusted p-values < 0.05 and \log_2 FC ≥ 0.58 . Significant expression was assessed using a volcano plot (Fig 1C and Fig 1D) and heatmap (Fig 1E). The DEPs are listed in Table 1.

Angiogenesis alteration in response to ALN treatment

When verifying proteins associated with angiogenesis-related Gene Ontology Biological Processes (GOBPs), several proteins were identified, including ETS proto-oncogene 1 (ETS1) (\log_2 FC, 1.1566), integrin subunit alpha 5 (ITGA5) (\log_2 FC, 0.6102), and milk fat globule-EGF factor 8 (MFG8) (\log_2 FC, -0.7468) (Table 1). To further investigate these findings, the effects of ALN on several well-known angiogenic factors were investigated. Secretion of VEGF-A, a potent angiogenic factor, was examined in bone cells after stimulation with ALN. Consistent with similarly designed work from previous trials [29], treatment of MG-63 cells with ALN led to a statistically significant but modest decrease (approximately 30%) of VEGF secretion into the conditioned medium compared to control (Fig 2A). Furthermore, HUVEC stimulation in the collected culture medium also exhibited modest but meaningful suppression of proliferation (Fig 2B). Collectively, the reduction of VEGF secretion and HUVEC proliferation by ALN strongly implies angiogenic signals to vessel cells from bone cells. This finding suggests the potential microenvironment-level regulation of bone remodeling in ONJ. For proteomics profiling, necrotic and apoptotic conditions were avoided to fully investigate the effects of ALN on bone cells. Additional analysis confirmed that there was no induced cell death with ALN treatment in MG-63 cells. Cell viability and proliferation rates, which were determined using

MTT (Fig 2C) and crystal violet staining assays (Fig 2D), showed no cytotoxicity.

Table 1. List of differentially expressed proteins (DEPs) with corresponding statistics.

Uniprot ID	Gene Symbol	Full Name	Log2 FC (ALN/ Ctrl)	Median P-Value	T Test P-Value	Adj. P
Q86VN1	VPS36	Vacuolar protein-sorting-associated protein 36	2.3697	0.0191	0.3002	0.0332
Q9BXR6	CFHR5	Complement factor H-related protein 5	1.5412	0.0306	0.0824	0.0106
Q8N350	CBARP	Voltage-dependent calcium channel beta subunit-associated regulatory protein	1.23	0.0776	0.0415	0.0129
P48163	ME1	NADP-dependent malic enzyme	1.2145	0.1359	0.0149	0.0103
Q9ULH7	MRTFB	Myocardin-related transcription factor B	1.1752	0.1301	0.0877	0.0397
P14921	ETS1	Protein C-ets-1	1.1566	0.1653	0.0497	0.0319
Q9H0V9	LMAN2L	VIP36-like protein	1.1446	0.013	0.1852	0.0136
Q15427	SF3B4	Splicing factor 3B subunit 4	1.0902	0.3234	0.0296	0.0487
Q9H223	EHD4	EH domain-containing protein 4	0.8995	0.113	0.1213	0.0463
Q07021	C1QBP	Complement component 1 Q subcomponent-binding protein, mitochondrial	0.8848	0.1071	0.1049	0.0388
Q9UJW2	TINAG	Tubulointerstitial nephritis antigen	0.8833	0.0976	0.1428	0.0474
P56192	MARS1	Methionine--tRNA ligase, cytoplasmic	0.8772	0.0039	0.1283	0.0037
P08579	SNRNPB2	U2 small nuclear ribonucleoprotein B	0.8721	0.0322	0.2438	0.0361
Q9H4B7	TUBB1	Tubulin beta-1 chain	0.8644	0.0467	0.0944	0.0172
Q9H2H8	PPIL3	Peptidyl-prolyl cis-trans isomerase-like 3 (PP1ase)	0.8257	0.1129	0.1055	0.0408
P00439	PAH	Phenylalanine-4-hydroxylase (PAH)	0.8024	0.0475	0.1114	0.0206
Q5JTZ9	AARS2	Alanine--tRNA ligase, mitochondrial	0.7071	0.0877	0.0325	0.0118
Q9UKN8	GTF3C4	General transcription factor 3C polypeptide 4	0.6861	0.0038	0.1761	0.0055
Q92747	ARPC1A	Actin-related protein 2/3 complex subunit 1A (SOP2-like protein)	0.6813	0.1877	0.0156	0.0158
P99999	CYCS	Cytochrome c	0.664	0.0456	0.1572	0.0283
Q7Z2W4	ZC3HAV1	Zinc finger CCCH-type antiviral protein 1	0.6468	0.1397	0.0465	0.0254
Q9Y5M8	SRPRB	Signal recognition particle receptor subunit beta	0.645	0.0983	0.1459	0.0486
P62191	PSMC1	26S proteasome regulatory subunit 4	0.6447	0.1717	0.0328	0.0243
P43251	BTD	Biotinidase (Biotinase)	0.6273	0.1495	0.0734	0.0392
P08648	ITGA5	Integrin alpha-5	0.6102	0.0891	0.1285	0.0398
Q07955	SRSF1	Serine/ arginine-rich splicing factor 1	0.6084	0.0123	0.0315	0.0018
P18754	RCC1	Regulator of chromosome condensation	0.5984	0.1047	0.008	0.0048
P62140	PPP1CB	Serine/ threonine-protein phosphatase PP1-beta catalytic subunit	-0.6001	0.1545	0.0111	0.0097
Q9NX40	OCIAD1	OCIA domain-containing protein 1	-0.601	0.0912	0.1301	0.041
Q14244	MAP7	Microtubule-associated protein 7	-0.6115	0.0198	0.1806	0.0178
Q9Y572	RIPK3	Receptor-interacting serine/ threonine-protein kinase 3	-0.6157	0.0717	0.0554	0.0153
Q06187	BTK	Bruton tyrosine kinase	-0.6434	0.2767	0.0165	0.027
Q8IW35	CEP97	Centrosomal protein of 97 kDa	-0.6669	0.0989	0.1153	0.0394
Q969G5	CAVIN3	Caveolae-associated protein 3	-0.6891	0.0308	0.0337	0.0045
O96033	MOC52	Molybdopterin synthase sulfur carrier subunit	-0.6914	0.0731	0.0987	0.0262
P13798	APEH	Acyl-peptide hydrolase	-0.6929	0.0508	0.239	0.0485
Q9H3H3	C11orf68	UPF0696 protein C11orf68	-0.7029	0.0819	0.1651	0.0471
Q08431	MFG8	Milk fat globule-EGF factor 8	-0.7468	0.1464	0.0932	0.0466
Q9NYJ8	TAB2	TGF-beta-activated kinase 1	-0.7572	0.1619	0.0095	0.0092
O95218	ZRANB2	Zinc finger Ran-binding domain-containing protein 2	-0.8387	0.1273	0.054	0.0261
Q93074	MED12	Mediator of RNA polymerase II transcription subunit 12	-0.91	0.0239	0.2422	0.0291
Q15047	SETDB1	Histone-lysine N-methyltransferase SETDB1	-0.9105	0.2702	0.0382	0.0459
P33241	LSP1	Lymphocyte-specific protein 1	-0.9375	0.0021	0.242	0.0058
Q9H3M7	TXNIP	Thioredoxin-interacting protein	-0.9387	0.0348	0.086	0.0123
P22307	SCP2	Sterol carrier protein X	-1.0061	0.1877	0.0682	0.0465
Q96A49	SYAP1	Synapse-associated protein 1	-1.0203	0.0638	0.0634	0.0155
Q5T1M5	FKBP15	FK506-binding protein 15	-1.0953	0.0796	0.135	0.0379
Q9NR77	PXMP2	Peroxisomal membrane protein 2	-1.1041	0.397	0.0075	0.0284
Q6P4R8	NFRKB	Nuclear factor related to kappa-B-binding protein	-1.131	0.0431	0.1973	0.0347
A6ND91	ASPDH	Aspartate dehydrogenase domain-containing protein	-1.2357	0.0503	0.2253	0.0451
Q9Y320	TMX2	Thioredoxin-related transmembrane protein 2	-1.3223	0.1468	0.0342	0.0211
Q9BRK0	REEP2	Receptor expression-enhancing protein 2	-1.3431	0.0303	0.0738	0.0094
Q9UHK6	AMACR	Alpha-methylacyl-CoA racemase	-1.3986	0.0022	0.2013	0.0046
P49407	ARRB1	Beta-arrestin-1 (Arrestin beta-1)	-1.4064	0.1261	0.016	0.01
Q92630	DYRK2	Dual specificity tyrosine-phosphorylation-regulated kinase 2	-1.4443	0.0139	0.0418	0.0027
Q9BRU9	UTP23	rRNA-processing protein UTP23 homolog	-1.8162	0.0833	0.0247	0.009
O14617	AP3D1	AP-3 complex subunit delta-1	-1.9901	0.0471	0.0127	0.0029
Q9C073	FAM117A	Protein FAM117A (C/EBP-induced protein)	-3.5266	0.0051	0.308	0.015

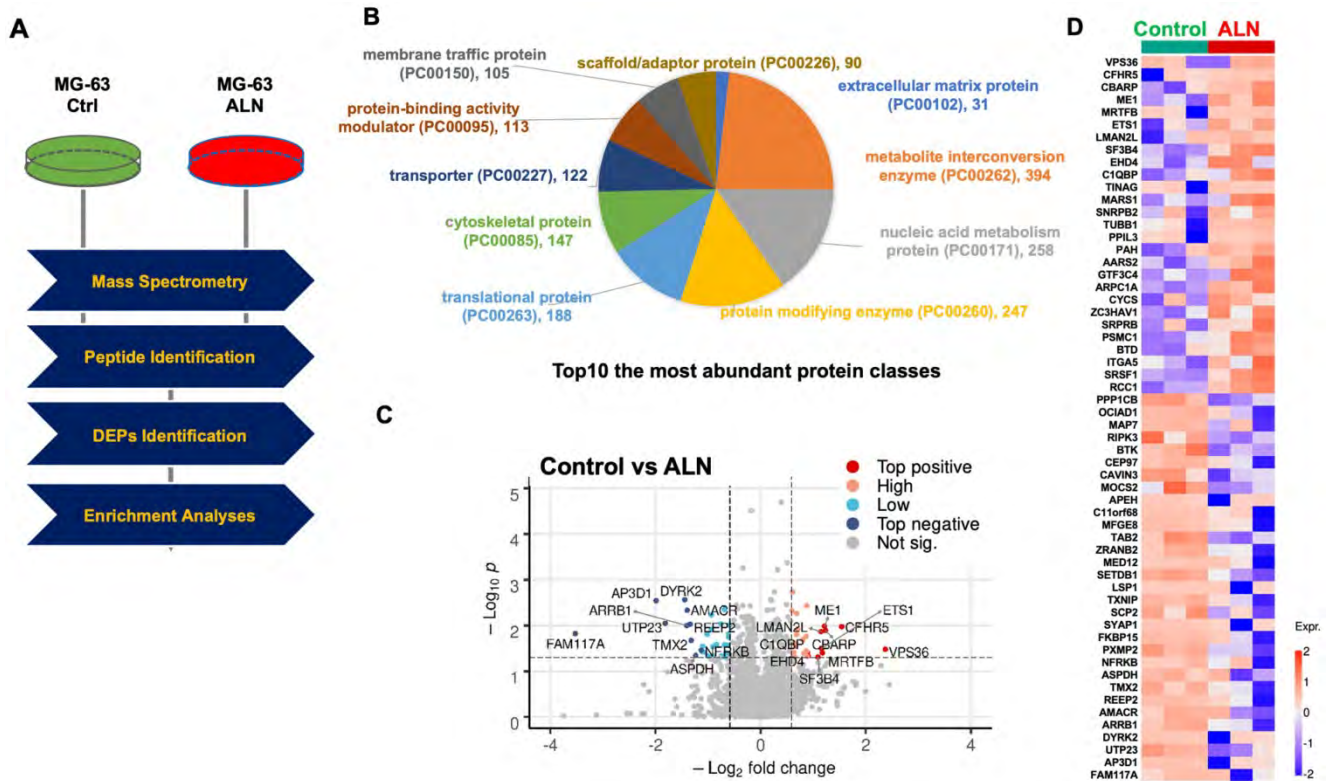


Figure 1. Proteomics profiling revealing alendronate (ALN)-induced protein alteration in the global proteome of MG-63 bone cells. (A) Experimental mass spectrometry (MS) workflow for this study. **(B)** Top 10 most abundant protein classes. **(C)** Volcano plot shows DEPs. **(D)** Heatmap depicts the differential expression patterns of proteins in response to ALN. Red and blue dots represent upregulated and downregulated proteins, respectively. Per row z-score of protein intensity is calculated. Each dot represents one protein. Proteins used are identical with those in the volcano plot. Experiments were done in triplicate.

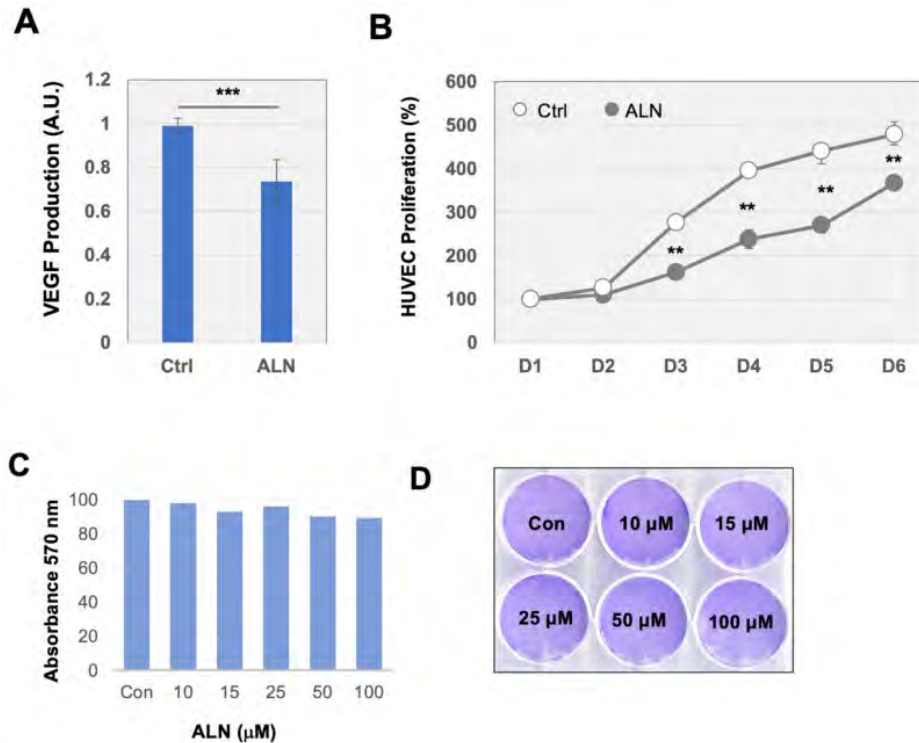


Figure 2. Angiogenic pathways may be upregulated by ALN treatment. (A) Secretion of VEGF in MG-63 bone cells treated with ALN. Effect of ALN treatment on the secreted VEGF levels into conditioned medium by MG-63 cells. Values (mean and standard deviation (SD)) are expressed as fold-changes compared to untreated cells (Ctrl, control). **(B)** Proliferation of HUVEC in the collected media of MG-63 cells. $^{***}p < 0.001$, compared to control (Student's t-test). **(C-D)** No apoptosis was observed within the treatment period of 6 h. **(C)** Cell viability of MG-63 cells. MTT assay revealed no viability changes by ALN treatment. **(D)** Crystal violet staining assay showed no cell mass changes in response to varying concentration of ALN for 6 days. Experiments were done 6 times. Representative images were shown.

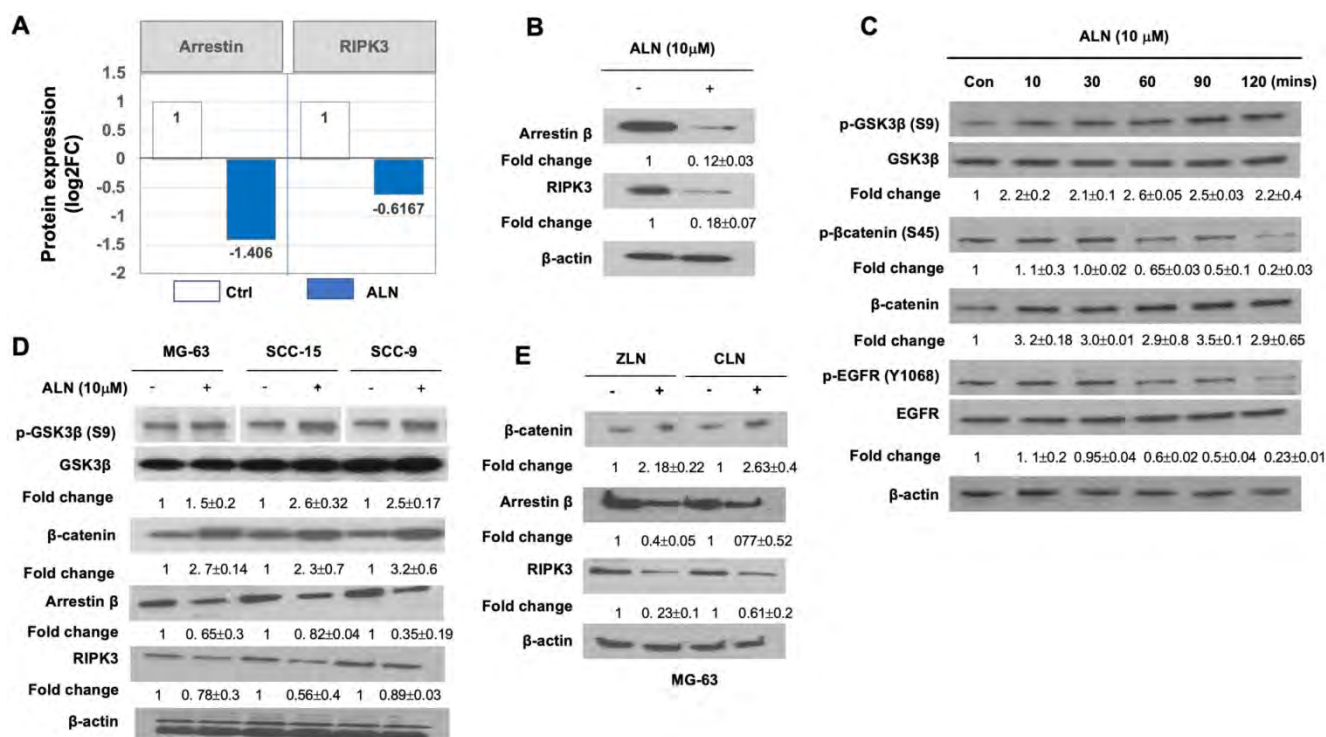


Figure 3. The RIPK3/arrestin/GSK3β/β-catenin/VEGF pathway is altered by ALN treatment. (A-B). Quantification results showed that arrestin β and RIPK3 are significantly suppressed with ALN treatment. **(A)** Data from proteomics profiling, DEP levels obtained from proteomics analysis are shown in Table 1. **(B)** Western blot analysis to measure the expression levels of arrestin β and RIPK3 proteins in the presence or absence of ALN. β-actin was used as the loading control. **(C)** ALN-induced phosphorylation of GSK3β (S9) and β-catenin (S45) led to stabilization of β-catenin in MG-63 cells. **(D)** Comparison of phosphorylation of GSK3β and expression of β-catenin, arrestin β, and RIPK3 in MG-63, SCC-15, and SCC-9 cells after treatment with ALN. **(E)** Effects of several BPs (ZLN and CLN) on β-catenin, arrestin β, and RIPK3 in MG-63 cells. After stimulation with 10 μM of ALN, ZLN, or CLN at various times, cells were harvested for protein extraction and western blot analysis. Representative western blot images were selected after experiments were repeated 6 times.

Receptor-interacting protein kinase 3 (RIPK3), a necroptosis factor, is altered in the ALN-treated proteome

Among the DEPs regulated by ALN treatment, proteins involved in angiogenesis, inflammation, and necrosis were of particular interest due to their relevance in ONJ. Proteomics profiling revealed downregulation of RIPK3 in MG63 cells treated with ALN (Fig 3A). RIPK3 has recently been reported as a mediator of necroptosis, programmed non-apoptotic cell death, and necroinflammation in response to immune signaling and cytokines, such as TNF-α [30]. The inhibition of RIPK3 activity suppressed *Enterococcus faecalis* infection-induced cell death in MG-63 cells [31]. RIPK3 expression is inhibited by hypoxia, which contributes to angiogenesis [32]. Loss of RIPK3 leads to the activation of the Wnt/β-catenin signaling pathway in the *ripk3*^{-/-} colon cancer mouse model, and enhances inflammation, immune cell infiltration, and angiogenesis [33].

Western blot analysis was able to validate that the protein expression levels of arrestin β1 (ARRB1) was significantly diminished by ALN treatment (Fig 3B), which was consistent with proteomics analysis. Given that ARRB1 is reported as a necessary

component for Wnt/β-catenin signaling and as a regulator of GSK-3β activation/inactivation [34], the effects of ALN and ARRB1 on the Wnt/GSK3/β-catenin signaling cascades were another point of interest. Proteomics profiling and biochemical analysis revealed the downregulation of RIPK3 and ARRB1 by ALN treatment, which suggests that the effects of ALN on MG-63 cells are likely to be mediated by the Wnt/GSK3/β-catenin signaling pathway.

The glycogen synthase kinase 3 (GSK3) network is an ALN regulatory signaling pathway

To understand the activation of signaling cascades in response to BP treatment in bone cells, the phosphorylation of important signaling proteins in MG-63 cells treated with ALN was assessed. The involvement of Wnt/GSK3/β-catenin signaling aberration was first determined, and the downstream secreted effectors of the Wnt pathway were evaluated as a part of the ALN signaling pathway.

Based on previous findings in literature, the Wnt/GSK3/β-catenin pathway has been shown to play a pivotal role in bone remodeling/repair processes, enhancement of osteoblast differentiation,

angiogenesis, and modulation of immune cell functions[2]. This evaluation further suggests that the Wnt/GSK3/ β -catenin pathway may play a key role in the biological effects of response to ALN treatment in MG-63 cells.

After treatment with ALN at varying incubation times (0, 20, 30, 60, 90, and 120 min), the phosphorylation status of a series of crucial signaling molecules was evaluated using western blot analysis. The phosphorylation of GSK-3 β (S9) increased with ALN treatment (Fig 3C). GSK-3, a serine/threonine protein kinase that phosphorylates and inactivates glycogen synthase, is a key downstream regulator of the PI3K/Akt pathway. GSK-3 signaling is inactivated by phosphorylation of Ser9 in GSK-3 β . Since the phosphorylation of GSK-3 β (S9) increased, this suggests that ALN treatment inactivates GSK-3 signaling in MG-63 cells.

As an important downstream effector of the Wnt signaling pathway, β -catenin is phosphorylated at S45 by a complex of axin and casein kinase I (CKI), which initiates the β -catenin phosphorylation–degradation cascade [35]. While the phosphorylation of GSK-3 β (S9) increased with ALN treatment, phosphorylation of β -catenin (S45) and EGFR (Y1068) decreased (Fig 3C). The decreased phosphorylation of β -catenin may increase protein stability and protein expression (Fig

3B). Increased phosphorylation of GSK-3 β (S9) was consistently observed in other cells, including SCC-9 and SCC-15, with ALN, zoledronic acid (ZLN), or clodronate (CLN) treatment (Fig 3D and Fig 3E). These results suggest that ANL suppresses ARRB1, inactivates GSK-3 β , and stabilizes β -catenin. The RIPK3/arrestin/Wnt/GSK/ β -catenin network may be a potential molecular regulatory network whose activation is altered upon ALN therapy.

Cytokine production and secretion in RAW 264.7 macrophages may be enhanced by ALN treatment

To test the effects of ALN on the immune system, a commercially available cytokine array was used to screen for potentially stimulated cytokines. RAW 264.7 macrophages were incubated with ALN both with and without the presence of lipopolysaccharides (LPS) (100 ng/ml) for 24 h. As shown in figure 4A, the production of tumor necrosis factor alpha (TNF- α) was stimulated by LPS and the levels of TNF- α were significantly increased with ALN. Western blot analysis also supported these findings (Fig 4B). The secretion of IL-6 also greatly increased with ALN (Fig 4C). However, there were no dramatic additional effects across other cytokines.

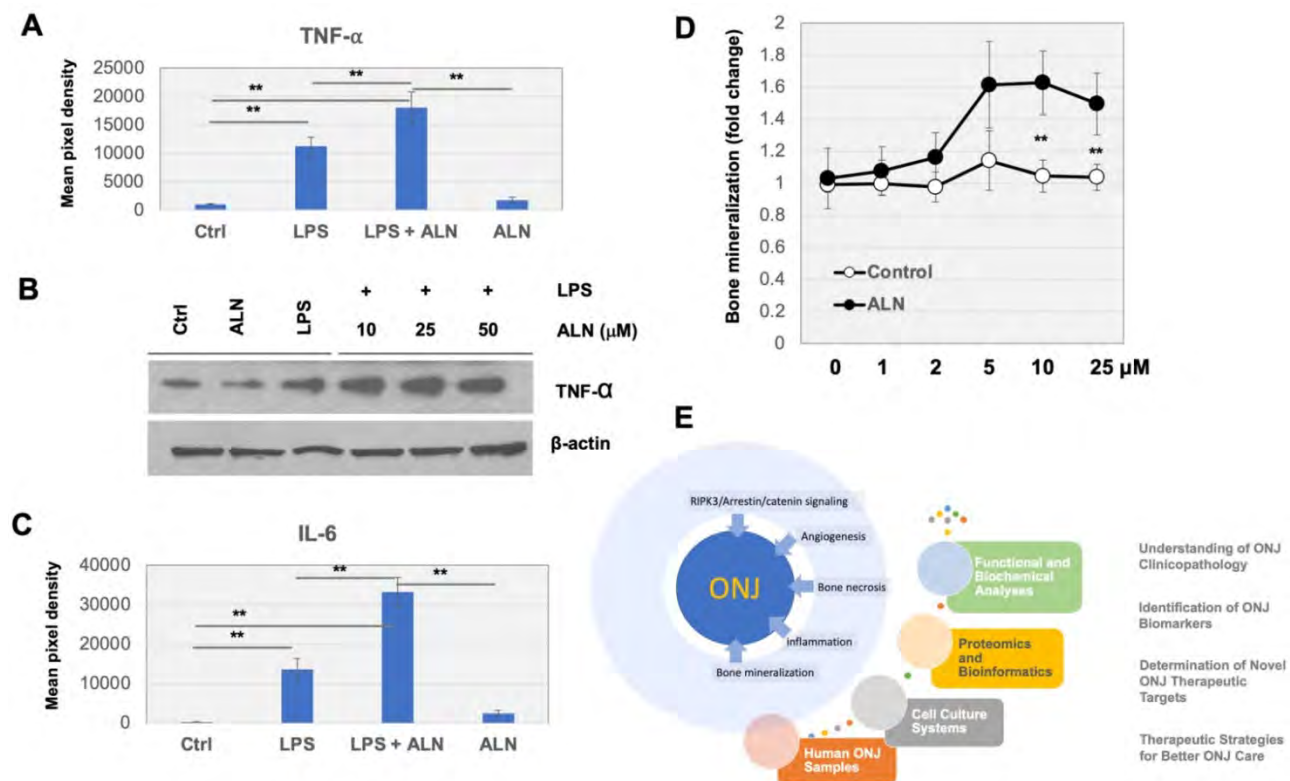


Figure 4. Pro-inflammatory cytokines are produced and secreted in response to ALN treatment in RAW 264.7 macrophage cells. (A-B) Cytokine array was conducted as described in Materials and Methods. Production of TNF- α (A) and secretion of IL-6 (B) increased with ALN treatment. (C) Western blot analysis for further validation. *** $p < 0.001$ and ** $p < 0.001$, compared to control (Student's t-test). Representative images are shown. (D) ALN treatment impaired homeostasis in bone mineralization. Quantification of mineral deposition by Alizarin Red-S staining shown as a graph. Data represent average \pm SD (n= 6). Statistical analysis was compared between ALN and vehicle only (ctrl) (p-value<0.05).

Abnormalities in calcium phosphate formation in bone cells and bone mineral density (BMD) distribution in ONJ-associated osteonecrosis

ALN is regularly used to help osteoporosis patients with bone mineralization loss. To test the effects of ALN on the quantification of mineral deposition, Alizarin Red-S staining assays were used to further assess mineralization levels after treatment. MG-63 cells were incubated with ALN or vehicle control (0, 1, 5, 10, and 25 μ M) for 2 days. Incubation of cells with ALN led to a marked increase in mineralization (to ~1.6 fold) compared to controls (Fig 4D).

Discussion

Our proteomics profiling revealed the downregulation of RIPK3 in response to ALN treatment in MG-63 bone cells. RIPK3 has been reported to play a fundamental role in inhibiting inflammation and mediating necroptosis and necroinflammation through the RIPK3-MLKL (mixed lineage kinase domain-like protein) pathway [30]. Inhibitors of RIPK3 and MLKL suppressed cell death from *Enterococcus faecalis* infection in MG-63 cells[31]. Although not encompassed in the current study, the role, and mechanisms of RIPK3 and its downstream signaling cascades in ALN-induced bone biology are under further investigation by our group. In addition, this study showed that the presence of ALN enhanced production or secretion of inflammatory cytokines in LPS-activated macrophage cells. A previous study found that ZLN, a potent BP, stimulated and increased inflammatory osteoclastic mediators [36]. Furthermore, ZLN was found to suppress proliferation and migration of vascular endothelial cells [37]. Expression of VEGF receptor 2 in vascular endothelial cells was also reported in response to treatment with ZLN[38]. In our experimental system, we observed modest decreases in VEGF secretion in response to ALN treatment.

The experimental data further suggested the potential role of the Wnt/GSK3/ β -catenin signaling pathway in the BP-perturbed proteome and its effects on bone homeostasis. This study demonstrated that the Wnt/GSK3/ β -catenin signaling pathways may play a fundamental role in bone metabolism, homeostasis, and remodeling. Multifaceted roles of GSK3 under each cellular context have been reported. In cytotoxic T lymphocytes (CTL), GSK3 inhibition blocks programmed cell death protein-1 (PD-1) transcription; thereby, enhancing CTL functioning [39]. GSK3 is a serine/threonine kinase that regulates Wnt/ β -catenin, PI3K/PTEN/AKT, RAS/RAF/MAPK, hedgehog, Notch, and other signaling

pathways and has been implicated in multiple diseases [40, 41]. Phosphorylation of GSK-3 α/β at multiple serine and threonine sites inactivates the kinase, while Tyr279/216 phosphorylation (pY) activates the kinase. GSK3 is reported to have both tumor promoting (glioblastoma, pancreatic, ovarian, and blood cancers) and tumor suppressive (breast and skin cancers) roles[42]. GSK3 stabilizes anti-apoptotic Bcl2, Bcl2L12A, c-Myb, Mcl-1, and VEGF, promoting tumors. On the other hand, GSK3 phosphorylates and destabilizes β -catenin leading to the downregulation of c-Myc and cyclin D1. GSK3 also phosphorylates T286 on cyclin D1, leading to its nuclear export and degradation[43]. Consistent with this study, previous findings have suggested an important role for the Wnt/GSK-3 signaling pathway in osteogenesis; inhibition of Wnt/GSK-3 activity induced osteoblast differentiation and significantly increased BMD in an ovariectomized rat model [44].

Experimental observation from this study suggests that a systematic overview of changes in the microenvironmental landscape is important for understanding ALN-induced pathophysiology in bone cells (Fig 4E). Treatment with ALN also leads to alterations in bone mineralization, which may further impair bone biology. In ONJ patients, our previous studies quantifying bone density and mineralization found that cone-beam computed tomography (CBCT) and micro-computed tomography image-based histomorphometric evaluation may be an efficient method to check bone health[45]. Abnormal BMD distribution in ONJ-associated osteonecrosis was observed by clinical CBCT imaging[46]. It would be worthwhile to determine if the patterns and severity of abnormal mineralization densities within jaw-bone biopsy samples can be implemented in ONJ patient care.

Collectively, the main innovative deliverables from this study are expected to lead to a better understanding of the mechanisms underlying ALN-induced pathological effects on bone and immune cells. The findings in this paper are promising but have several limitations; (1) the effects of BPs on osteoblast function are throughout the skeleton, and (2) ALN targets osteoclasts, not osteoblasts. In conjunction with standard diagnostic procedures, the more mechanistic data related to the adverse effects of ALN can also act as an applicable supplement for clinical judgment.

Supplementary Material

Supplementary methods.

<http://www.medsci.org/v18p3261s1.pdf>

Acknowledgments

This research was supported by the Samuel Oschin Comprehensive Cancer Institute (SOCCI) at Cedars-Sinai Medical Center through 2019 Lucy S. Gonda Award. We appreciate technical support from the Cedars-Sinai Proteomics and Metabolomics Core.

Kim J: Contributed to conception or design, drafted the manuscript, and critically revised the manuscript.

Yeon A: Contributed to analysis, drafted the manuscript, and critically revised the manuscript.

Parker SJ: Contributed to analysis, drafted the manuscript, and critically revised the manuscript.

Shahid M: Contributed to analysis, and critically revised the manuscript.

Thiombane A: Contributed to analysis, and critically revised the manuscript.

Cho E: Contributed to analysis, and critically revised the manuscript.

You S: Contributed to analysis, drafted the manuscript, and critically revised the manuscript.

Emam H: Contributed to analysis, drafted the manuscript, and critically revised the manuscript.

Kim D-G: Contributed to conception or design, drafted the manuscript, and critically revised the manuscript.

Kim M: contributed to conception or design, drafted the manuscript, and critically revised the manuscript.

Funding

This research was funded by National Institutes of Health (1U01DK103260, 1R01DK100974, U24 DK097154, NIH NCATS UCLA CTSI UL1TR000124), Department of Defense (W81XWH-15-1-0415 and W81XWH-19-1-0109), Centers for Disease Controls and Prevention (1U01DP006079), and the U.S.-Egypt Science and Technology Development Fund by the National Academies of Sciences, Engineering, and Medicine (all to J.K.). This article is derived from the Subject Data funded in whole or part by National Academies of Sciences, Engineering, and Medicine (NAS) and The United States Agency for International Development (USAID). Any opinions, findings, conclusions, or recommendations expressed in this article are those of the authors alone, and do not necessarily reflect the views of USAID or NAS.

Competing Interests

The authors have declared that no competing interest exists.

References

1. Florencio-Silva R, Sasso GR, Sasso-Cerri E, Simoes MJ, Cerri PS. Biology of Bone Tissue: Structure, Function, and Factors That Influence Bone Cells. *Biomed Res Int.* 2015; 2015: 421746.

2. Issack PS, Helfet DL, Lane JM. Role of Wnt signaling in bone remodeling and repair. *HSS J.* 2008; 4: 66-70.
3. Bertacchini J, Magaro MS, Poti F, Palumbo C. Osteocytes Specific GSK3 Inhibition Affects In Vitro Osteogenic Differentiation. *Biomedicines.* 2018; 6.
4. Schoeman MA, Moester MJ, Oostlander AE, Kaijzel EL, Valstar ER, Nelissen RG, et al. Inhibition of GSK3beta Stimulates BMP Signaling and Decreases SOST Expression Which Results in Enhanced Osteoblast Differentiation. *J Cell Biochem.* 2015; 116: 2938-46.
5. Huh JE, Ko R, Jung HJ, Lee SY. Glycogen synthase kinase 3beta promotes osteogenic differentiation of murine adipose-derived stromal cells. *PLoS one.* 2013; 8: e54551.
6. Pabst AM, Kruger M, Blatt S, Ziebart T, Rahimi-Nejdat R, Goetze E, et al. Angiogenesis in the Development of Medication-Related Osteonecrosis of the Jaws: An Overview. *Dent J (Basel).* 2016; 5.
7. Zhang Z, Nor F, Oh M, Cucco C, Shi S, Nor JE. Wnt/beta-Catenin Signaling Determines the Vasculogenic Fate of Postnatal Mesenchymal Stem Cells. *Stem Cells.* 2016; 34: 1576-87.
8. Skurk C, Maatz H, Rocnik E, Bialik A, Force T, Walsh K. Glycogen-Synthase Kinase3beta/beta-catenin axis promotes angiogenesis through activation of vascular endothelial growth factor signaling in endothelial cells. *Circ Res.* 2005; 96: 308-18.
9. Bellido T, Plotkin LI. Novel actions of bisphosphonates in bone: preservation of osteoblast and osteocyte viability. *Bone.* 2011; 49: 50-5.
10. Plotkin LI, Manolagas SC, Bellido T. Dissociation of the pro-apoptotic effects of bisphosphonates on osteoclasts from their anti-apoptotic effects on osteoblasts/osteocytes with novel analogs. *Bone.* 2006; 39: 443-52.
11. Plotkin LI, Weinstein RS, Parfitt AM, Roberson PK, Manolagas SC, Bellido T. Prevention of osteocyte and osteoblast apoptosis by bisphosphonates and calcitonin. *J Clin Invest.* 1999; 104: 1363-74.
12. Wilkins Parker LR, Preuss CV. *Alendronate*. StatPearls. Treasure Island (FL); 2021.
13. Weinstein RS, Roberson PK, Manolagas SC. Giant osteoclast formation and long-term oral bisphosphonate therapy. *N Engl J Med.* 2009; 360: 53-62.
14. Rouach V, Goldshtein I, Wolf I, Catane R, Chodick G, Iton A, et al. Exposure to alendronate is associated with a lower risk of bone metastases in osteoporotic women with early breast cancer. *J Bone Oncol.* 2018; 12: 91-5.
15. Jackson C, Freeman ALJ, Szlamka Z, Spiegelhalter DJ. The adverse effects of bisphosphonates in breast cancer: A systematic review and network meta-analysis. *PLoS one.* 2021; 16: e0246441.
16. Dodson TB. The Frequency of Medication-related Osteonecrosis of the Jaw and its Associated Risk Factors. *Oral Maxillofac Surg Clin North Am.* 2015; 27: 509-16.
17. George EL, Lin YL, Saunders MM. Bisphosphonate-related osteonecrosis of the jaw: a mechanobiology perspective. *Bone Rep.* 2018; 8: 104-9.
18. Zymperdikas VF, Yavropoulou MP, Kaklamanos EG, Papadopoulos MA. Bisphosphonates as Supplement to Dental Treatment: A Network Meta-Analysis. *J Dent Res.* 2021; 100: 341-51.
19. Khan A, Morrison A, Cheung A, Hashem W, Compston J. Osteonecrosis of the jaw (ONJ): diagnosis and management in 2015. *Osteoporos Int.* 2016; 27: 853-9.
20. Fung P, Bedogni G, Bedogni A, Petrie A, Porter S, Campisi G, et al. Time to onset of bisphosphonate-related osteonecrosis of the jaws: a multicentre retrospective cohort study. *Oral Dis.* 2017; 23: 477-83.
21. Parker SJ, Venkatraman V, Van Eyk JE. Effect of peptide assay library size and composition in targeted data-independent acquisition-MS analyses. *Proteomics.* 2016; 16: 2221-37.
22. Parker SJ, Stotland A, MacFarlane E, Wilson N, OroSCO A, Venkatraman V, et al. Proteomics reveals Rictor as a noncanonical TGF-beta signaling target during aneurysm progression in Marfan mice. *Am J Physiol Heart Circ Physiol.* 2018; 315: H1112-H126.
23. Rost HL, Rosenberger G, Navarro P, Gillet L, Miladinovic SM, Schubert OT, et al. OpenSWATH enables automated, targeted analysis of data-independent acquisition MS data. *Nat Biotechnol.* 2014; 32: 219-23.
24. Rosenberger G, Koh CC, Guo T, Rost HL, Kouvonon P, Collins BC, et al. A repository of assays to quantify 10,000 human proteins by SWATH-MS. *Sci Data.* 2014; 1: 140031.
25. Teleman J, Rost HL, Rosenberger G, Schmitt U, Malmstrom L, Malmstrom J, et al. DIANA--algorithmic improvements for analysis of data-independent acquisition MS data. *Bioinformatics.* 2015; 31: 555-62.
26. Rost HL, Liu Y, D'Agostino G, Zanella M, Navarro P, Rosenberger G, et al. TRIC: an automated alignment strategy for reproducible protein quantification in targeted proteomics. *Nat Methods.* 2016; 13: 777-83.
27. Teo G, Kim S, Tsou CC, Collins B, Gingras AC, Nesvizhskii AI, et al. mapDIA: Preprocessing and statistical analysis of quantitative proteomics data from data independent acquisition mass spectrometry. *J Proteomics.* 2015; 129: 108-20.
28. Mi H, Ebert D, Muruganujan A, Mills C, Albuo LP, Mushayamaha T, et al. PANTHER version 16: a revised family classification, tree-based classification tool, enhancer regions and extensive API. *Nucleic Acids Res.* 2021; 49: D394-D403.
29. Ishtiaq S, Edwards S, Sankaralingam A, Evans BA, Elford C, Frost ML, et al. The effect of nitrogen containing bisphosphonates, zoledronate and alendronate, on the production of pro-angiogenic factors by osteoblastic cells. *Cytokine.* 2015; 71: 154-60.

30. Chen H, Fang Y, Wu J, Chen H, Zou Z, Zhang X, et al. RIPK3-MLKL-mediated necroinflammation contributes to AKI progression to CKD. *Cell Death Dis.* 2018; 9: 878.
31. Dai X, Deng Z, Liang Y, Chen L, Jiang W, Zhao W. Enterococcus faecalis induces necroptosis in human osteoblastic MG63 cells through the RIPK3 / MLKL signalling pathway. *Int Endod J.* 2020; 53: 1204-15.
32. Moriwaki K, Bertin J, Gough PJ, Orłowski GM, Chan FK. Differential roles of RIPK1 and RIPK3 in TNF-induced necroptosis and chemotherapeutic agent-induced cell death. *Cell Death Dis.* 2015; 6: e1636.
33. Bozec D, Iuga AC, Roda G, Dahan S, Yeretssian G. Critical function of the necroptosis adaptor RIPK3 in protecting from intestinal tumorigenesis. *Oncotarget.* 2016; 7: 46384-400.
34. Li H, Sun X, LeSage G, Zhang Y, Liang Z, Chen J, et al. beta-arrestin 2 regulates Toll-like receptor 4-mediated apoptotic signalling through glycogen synthase kinase-3beta. *Immunology.* 2010; 130: 556-63.
35. Amit S, Hatzubai A, Birman Y, Andersen JS, Ben-Shushan E, Mann M, et al. Axin-mediated CKI phosphorylation of beta-catenin at Ser 45: a molecular switch for the Wnt pathway. *Genes Dev.* 2002; 16: 1066-76.
36. Tamari T, Elimelech R, Cohen G, Cohen T, Doppelt O, Eskander-Hashoul L, et al. Endothelial Progenitor Cells inhibit jaw osteonecrosis in a rat model: A major adverse effect of bisphosphonate therapy. *Sci Rep.* 2019; 9: 18896.
37. Lang M, Zhou Z, Shi L, Niu J, Xu S, Lin W, et al. Influence of zoledronic acid on proliferation, migration, and apoptosis of vascular endothelial cells. *Br J Oral Maxillofac Surg.* 2016; 54: 889-93.
38. Basi DL, Lee SW, Helfman S, Mariash A, Lunos SA. Accumulation of VEGFR2 in zoledronic acid-treated endothelial cells. *Mol Med Rep.* 2010; 3: 399-403.
39. Taylor A, Harker JA, Chanthong K, Stevenson PG, Zuniga EI, Rudd CE. Glycogen Synthase Kinase 3 Inactivation Drives T-bet-Mediated Downregulation of Co-receptor PD-1 to Enhance CD8(+) Cytolytic T Cell Responses. *Immunity.* 2016; 44: 274-86.
40. McCubrey JA, Steelman LS, Bertrand FE, Davis NM, Abrams SL, Montalto G, et al. Multifaceted roles of GSK-3 and Wnt/beta-catenin in hematopoiesis and leukemogenesis: opportunities for therapeutic intervention. *Leukemia.* 2014; 28: 15-33.
41. McCubrey JA, Steelman LS, Bertrand FE, Davis NM, Sokolosky M, Abrams SL, et al. GSK-3 as potential target for therapeutic intervention in cancer. *Oncotarget.* 2014; 5: 2881-911.
42. Beurel E, Jope RS. The paradoxical pro- and anti-apoptotic actions of GSK3 in the intrinsic and extrinsic apoptosis signaling pathways. *Prog Neurobiol.* 2006; 79: 173-89.
43. Alao JP. The regulation of cyclin D1 degradation: roles in cancer development and the potential for therapeutic invention. *Mol Cancer.* 2007; 6: 24.
44. Kulkarni NH, Onyia JE, Zeng Q, Tian X, Liu M, Halladay DL, et al. Orally bioavailable GSK-3alpha/beta dual inhibitor increases markers of cellular differentiation in vitro and bone mass in vivo. *J Bone Miner Res.* 2006; 21: 910-20.
45. Kim DG. Can dental cone beam computed tomography assess bone mineral density? *Journal of bone metabolism.* 2014; 21: 117-26.
46. Nye SN CE, Emam H, Kim D-G. Heterogeneity of Bone Mineral Density in Osteonecrosis of the Jaw. 2018 AADR/CADR Annual Meeting (Fort Lauderdale, Florida). 2018.